AD-A129 433 GROUND/FLIGHT TEST TECHNIQUES AND CORRELATION(U) 1/6
ADVISORY GROUP FOR AEROSPACE RESEARCH AND DEVELOPMENT
NEUILLY-SUR-SEINE (FRANCE) FEB 83 AGARD-CP-339
UNCLASSIFIED F/G 1/3 NL

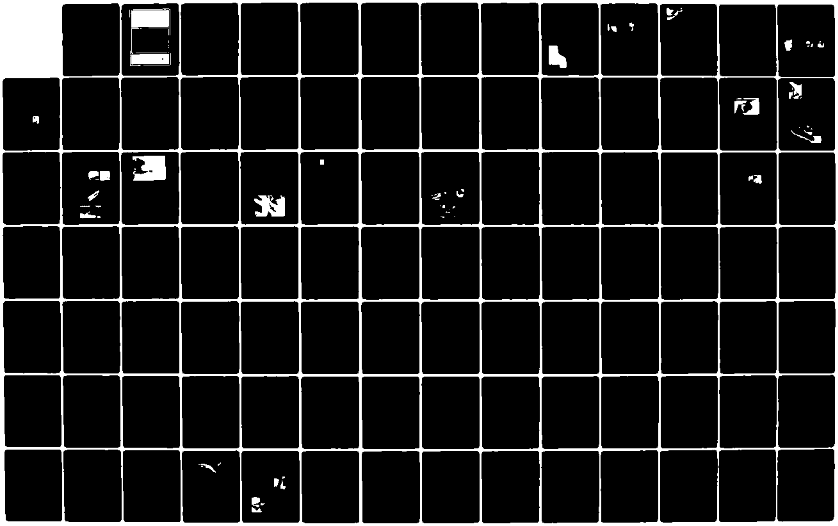

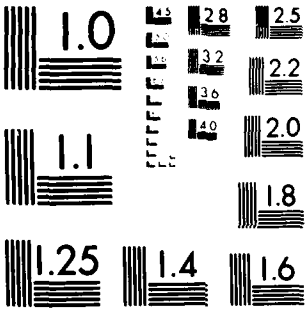
1.0
1.1
1.25
1.4
1.6
1.8
2.0
2.2
2.5
2.8
3.2
3.6
4.0
4.5

MICROCOPY RESOLUTION TEST CHART
NATIONAL BUREAU OF STANDARDS 1963 A

AGARD-CP-339

AGARD-CP-339

AD A129433

AGARD

ADVISORY GROUP FOR AEROSPACE RESEARCH & DEVELOPMENT

7 RUE ANCELLE 92200 NEUILLY SUR SEINE FRANCE

AGARD CONFERENCE PROCEEDINGS No. 339

Ground/Flight Test Techniques and Correlation

This document has been approved
for public release and sale; its
distribution is unlimited.

S
JUN 1 7 1983
A

NORTH ATLANTIC TREATY ORGANIZATION

DTIC FILE COPY

DISTRIBUTION AND AVAILABILITY
ON BACK COVER

83 06 16 067

AGARD-CP-339

NORTH ATLANTIC TREATY ORGANIZATION

ADVISORY GROUP FOR AEROSPACE RESEARCH AND DEVELOPMENT

(ORGANISATION DU TRAITE DE L'ATLANTIQUE NORD)

AGARD Conference Proceedings No.339

GROUND/FLIGHT TEST TECHNIQUES AND CORRELATION

Papers presented at the Flight Mechanics Panel Symposium on Ground/Flight Test
Techniques and Correlation held in Çeşme, Turkey, 11–14 October 1982.

THE MISSION OF AGARD

The mission of AGARD is to bring together the leading personalities of the NATO nations in the fields of science and technology relating to aerospace for the following purposes:

- Exchanging of scientific and technical information;
- Continuously stimulating advances in the aerospace sciences relevant to strengthening the common defence posture;
- Improving the co-operation among member nations in aerospace research and development;
- Providing scientific and technical advice and assistance to the North Atlantic Military Committee in the field of aerospace research and development;
- Rendering scientific and technical assistance, as requested, to other NATO bodies and to member nations in connection with research and development problems in the aerospace field;
- Providing assistance to member nations for the purpose of increasing their scientific and technical potential;
- Recommending effective ways for the member nations to use their research and development capabilities for the common benefit of the NATO community.

The highest authority within AGARD is the National Delegates Board consisting of officially appointed senior representatives from each member nation. The mission of AGARD is carried out through the Panels which are composed of experts appointed by the National Delegates, the Consultant and Exchange Programme and the Aerospace Applications Studies Programme. The results of AGARD work are reported to the member nations and the NATO Authorities through the AGARD series of publications of which this is one.

Participation in AGARD activities is by invitation only and is normally limited to citizens of the NATO nations.

The content of this publication has been reproduced
directly from material supplied by AGARD or the authors.

Published February 1983

Copyright © AGARD 1983
All Rights Reserved

ISBN 92-835-0328-7

Printed by Specialised Printing Services Limited
40 Chigwell Lane, Loughton, Essex IG10 3TZ

PREFACE

The use of simulation techniques in some form to represent conditions in flight has been one of the cornerstones of aeronautical research and development from its inception. Initially the wind-tunnel was the primary tool in such testing, but in recent times ground- and in-flight- simulation, flight demonstrators including piloted aircraft and remotely piloted vehicles, and analytical prediction methods have all been used to represent in-flight conditions in order to predict flight behaviour in advance of actual flight of the simulated project.

The question of the extent to which the simulation, in whichever form it is performed, truly represents the condition which it is intended to simulate, has consequently always been of primary concern, and it has been addressed many times. Until now this consideration has been directed primarily to comparison of wind-tunnel and flight data, and this focussed attention on the need to improve wind-tunnel simulation. A Flight Mechanics Panel meeting at Valloire in 1975 dealt primarily with wind-tunnel/flight comparisons, and this could be said to have raised as many problems as it solved, in both wind-tunnel and flight test techniques. The Flight Mechanics Panel decided in 1980 that the time was ripe for a further review of progress, this time on a wider basis than the Valloire meeting and addressing the spectrum of simulation techniques now in use. This led to the symposium, held in Turkey in October 1982, which is reported in these Proceedings.

The Symposium noted that there have been major improvements in predictive capabilities in the last decade. Large advances in wind-tunnel and flight test instrumentation and data processing have provided better confidence in the data and, consequently, improved comparison bases. Even larger advances have been made in computational aerodynamics and this has provided the basis for an efficient design tool for transport aircraft. New wind tunnels on both sides of the Atlantic have significantly enhanced prediction capabilities. Improved flight test techniques and measurement accuracy have provided a powerful tool in support of prediction. However, in spite of all these improvements there is still a problem in providing accurate and satisfactory performance predictions. Examples were cited which noted that for twelve American commercial aircraft, the drag prediction was just as apt to be high as low. Concern was also expressed that with the increasing sophistication of test and prediction techniques, engineers may lose "track" of the physics of the process of prediction and comparison.

Future symposia and/or specialist meetings should be conducted on a regular basis to ensure an adequate exchange of information.

P.POISSON-QUINTON
Member, FMP

F.STOLIKER
Member, FMP

CONTENTS

Page

PREFACE iii

Reference

CONCLUSIONS OF THE FMP SYMPOSIUM IN VALLOIRE (1975) AND PROGRESS ON GROUND/FLIGHT CORRELATION
by Ph.Poisson-Quinton 1

PROGRESS IN WIND TUNNEL TEST TECHNIQUES AND IN THE CORRECTIONS AND ANALYSIS OF THE RESULTS
by T.W.Binion, Jr., X.Vaucheret and X.Bouis 2

GROUND/FLIGHT CORRELATION ON THE SPACE SHUTTLE ORBITER FROM RE-ENTRY TO LANDING

Aerothermodynamic Flight Envelope Expansion for a Manned Lifting Re-Entry Vehicle (Space Shuttle)
by J.K.Hodge, D.R.Audley, P.W.Phillips and E.K.Hertzler 3A

Predicted and Flight Test Results of the Performance and Stability and Control of the Space Shuttle from Re-Entry to Landing
by P.W.Kirsten and D.F.Richardson 3B

GROUND/FLIGHT CORRELATION ON THE ALPHA-JET EXPERIMENTAL AIRCRAFT WITH A TRANSONIC WING

A Comparison Between Wind Tunnel and Flight Results for Aerodynamic Performance
by D.Jacob, D.Welte and H.Wünnenberg 4A

A Comparison of the Wing Pressure Distribution and Local Wake Survey from Analytical, Wind Tunnel and Flight Results
by H.Buers, V.Schmitt and J.Lerat 4B

FLIGHT AND WIND-TUNNEL CORRELATION OF BOUNDARY-LAYER TRANSITION ON THE AEDC TRANSITION CONE
by D.F.Fisher and N.S.Dougherty, Jr. 5

EXPERIMENTAL INVESTIGATIONS OF TRANSPORT AIRCRAFT LOW SPEED ENGINE INTERFERENCE EFFECTS AND FLIGHT TEST CORRELATION
by B.Ewald and W.Burgsmüller 6

COMPARISON OF PREDICTION, WIND TUNNEL AND FLIGHT TEST DATA FOR THE CANADAIR CHALLENGER TURBOFAN AIRCRAFT
by F.Mavriplis 7

LESSONS FROM TORNADO AFTERBODY DEVELOPMENT
by D.C.Leyland 8

BRIEF PREPARED COMMENTS ON PERFORMANCE CORRELATION
by R.A.Wood 9A
J.M.Hardy 9B

COMPORTEMENT A GRANDE INCIDENCE D'UN AVION DE COMBAT: CORRELATION ENTRE LES PREVISIONS ET LE VOL
par P-L.Mathe 10

THE USE OF FREE-FLIGHT MODELS FOR THE PREDICTION OF DEPARTURE CONTROL
by G.F.Moss, A.J.Ross, G.F.Edwards and E.B.Jefferies 11

COMPARISON OF FLIGHT AND WIND TUNNEL BUFFETING MEASUREMENTS ON THE SAAB 105 AIRCRAFT
by S.H.Teige, B.S.A.Nilsson, S.J.Boersen and A.N.Kraan 12

Reference

SOME MEASUREMENTS OF BUFFETING ON A FLUTTER MODEL OF A TYPICAL STRIKE AIRCRAFT
by D.G.Mabey and B.E.Cripps 13

AERODYNAMIC MODEL IDENTIFICATION FROM DYNAMIC FLIGHT TEST DATA AND WIND TUNNEL EXPERIMENTS
by J.A.Mulder, J.G. Den Hollander and H.Binkhorst 14

HELICOPTER SIMULATION VALIDATION USING FLIGHT DATA
by *D.L.Key, R.S.Hansen, W.B.Cleveland and W.Y.Abbott* 15

CORRELATION ASPECTS OF ANALYTICAL, WIND TUNNEL AND FLIGHT TEST RESULTS FOR A HINGELESS ROTOR HELICOPTER
by J.Kaletka and H.-J.Langer 16

CORRELATION ASPECTS IN THE IDENTIFICATION OF DYNAMIC EFFECTS USING COMPLEMENTARY TECHNIQUES

Flight In Turbulence – Gust Alleviation
by K.Wilhelm and R.Verbrugge 17A

Evolution aux Grands Angles
par D.Tristrant 17B

DYNAMIC STRUCTURAL AEROELASTIC STABILITY TESTING OF THE XV-15 TILT ROTOR RESEARCH AIRCRAFT
by L.G.Schroers 18

STRUCTURAL ASPECTS OF GROUND/FLIGHT CORRELATION ON THE VARIABLE SWEEP WING AIRCRAFT TORNADO

Ground and Flight Test Techniques Used for Proof of Structural Integrity of the Tornado Combat Aircraft
by K.Knauer and O.Sensburg 19A

Comparison of Flight Loads Measurements Results and Prediction for Tornado
by J.R.Dovey and G.Moretti 19B

Correlation Problems Between Flutter Flight Test Data and Ground Tests/Calculation Results for a Variable Sweep Wing Aircraft
by G. De Ferrari, A.Lotze and R.Pyrah 19C

REAL-TIME FLUTTER ANALYSIS OF AN ACTIVE FLUTTER-SUPPRESSION SYSTEM ON A REMOTELY PILOTED RESEARCH AIRCRAFT
by G.B.Gilyard and J.W.Edwards 20

FLIGHT FLUTTER TESTING WITH EMPHASIS ON THE TIP VANE METHOD
by *H.Zimmermann and R.Destuynder* 21

A THEORETICAL/EXPERIMENTAL TECHNIQUE TO EVALUATE STORE SEPARATION CHARACTERISTICS
by F.Porrato and V.Mo 22

ENTREES D'AIR D'HELICOPTERES: CONCEPTION, ESSAIS EN SOUFFLERIE, CORRELATIONS AVEC LES RESULTATS DE VOL
HELICOPTER AIR INLETS: DESIGN PROCESS, WIND TUNNEL TESTING AND CORRELATIONS WITH FLIGHT DATA
par F.Toulmay 23

SYNTHESIS OF RESPONSES TO AGARD-FMP QUESTIONNAIRE ON "PREDICTION TECHNIQUES AND FLIGHT CORRELATION"
by J.Williams 24

CONCLUSIONS OF THE FMP SYMPOSIUM IN VALLOIRE (1975)
AND PROGRESS ON GROUND/FLIGHT CORRELATION

by Ph. POISSON-QUINTON, ONERA, Fr.

More than seven years have elapsed since our first Flight Mechanics Panel Symposium focused on the review of test techniques available at that time both on the ground and in flight for the development of new aircraft (ref. 1).

I) The major conclusions and recommandations derived from a large number of informative papers and from discussions are summarized below:

- Difficulty in defining the lowest test Reynolds number in a wind-tunnel which gives flow conditions adequatly representing those of actual flight conditions: that is why there is a strong need for tunnel testing at Reynolds numbers as close as possible to the flight values;
- Many of the problems ascribed to Reynolds number effect are probably the result of inadequacies in the modeling techniques: wall and support effects, flow quality, detailed and precise model representation, aeroelastic deformation of the model under large loads, choice of adequate roughness for boundary layer transition tripping, etc.;
- The computer will play an over-increasing role:
  - for monitoring and on-line data processing and analysis in ground facilities and in flight;
  - for interpretation, correction and extrapolation of wind-tunnel data;
  - and for theoretical predictions used to reduce testing time and cost.
- There is a need for more direct communication between the design team and wind-tunnel/flight personnel...

...that is why, 7 years later, we are again together to review our progress on these various statements, which are still valid.

However, I shall try, in this short introduction, to show you some typical advances we have made everywhere in the AGARD community to improve our techniques for a better prediction of performance and flying qualities.

On the other hand, we shall conclude this Symposium by a Round Table discussion centred on the answers to a five-items questionnaire sent by the Technical Programme Committee to well known specialists in the AGARD community:

1 - What are the advantages/disadvantages of different prediction techniques?

2 - What portions of the flight regime cannot/should not be addressed by ground based techniques?

3 - Are there areas where analytical predictions can be better than wind- tunnel and/or simulation results, and vice versa?

4 - Are there methods of reducing differences between predictions and flight test results?

5 - Are there new prediction techniques that should be emphasized?

The analysis of a great number of answers will be presented by Dr. John Williams, who is also in charge of writing the Technical Evaluation Report of our Symposium (ref. 2).

II) Now, let's see some examples of progress we have made in the major test centers represented in this symposium:

II.1) A BETTER DUPLICATION OF THE REYNOLDS NUMBER IN WIND-TUNNEL TESTING:

On Figure 1, we have given the various methods to increase the test Reynolds number in a wind-tunnel and on Figure 2, we have listed the various facilities recently developed for that purpose:

A) Tunnels with very large test-sections:

- NASA has found that the size limitation of their Ames 40 x 80 foot wind-tunnel primarily constrained fixed-wing Aircraft investigations, while the existing speed limitation primarily constrained rotary-wing testing; to meet these requirements (ref. 3), modification of the 40 x 80 ft tunnel includes:

  . repowering the existing tunnel (27 MW to 100 MW) to attain higher speed in the existing closed test section (100 m/s to 150 m/s)

  . and adding a new and larger test section (80 x 120 ft = 24 x 36 m²) able to reach a speed of 50 m/s and utilizing the same power installation.

  The modified tunnel with its new open circuit is sketched on Fig 3; furthermore the background noise in the test-sections have been minimized by an acoustic treatment to perform aeroacoustic research.

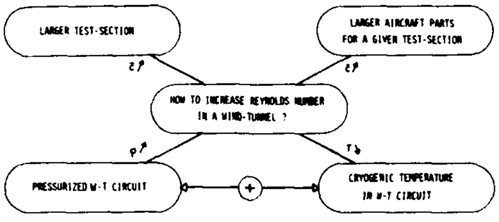
LARGER TEST-SECTION
LARGER AIRCRAFT PARTS FOR A GIVEN TEST-SECTION
c̄ ↗
c̄ ↗
HOW TO INCREASE REYNOLDS NUMBER IN A WIND-TUNNEL ?
ρ ↗
T ↘
PRESSURIZED W-T CIRCUIT
+
CRYOGENIC TEMPERATURE IN W-T CIRCUIT

$$Re = \frac{\text{INERTIA FORCE}}{\text{VISCOUS FORCE}} = \frac{\rho . V^2 . \bar{c}^2}{\mu . V . \bar{c}} = \frac{\rho . V . \bar{c}}{\mu} = \frac{\rho . M . a . \bar{c}}{\mu} \text{, WITH : } \left\{ \begin{matrix} \rho \sim T^{-1} \\ V \sim T^{0.5} \\ \mu \sim T^{0.9} \end{matrix} \right\} \text{ FOR A GIVEN MACH N°}$$

Figure 1

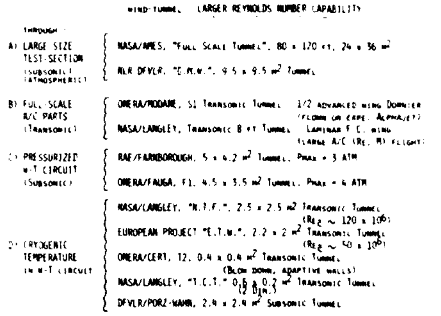

WIND-TUNNEL LARGER REYNOLDS NUMBER CAPABILITY

THROUGH :	
A) LARGE SIZE TEST-SECTION (SUBSONIC) (ATMOSPHERIC)	NASA/AMES, "FULL SCALE TUNNEL", 80 x 120 FT, 24 x 36 m² NLR DFVLR, "D.N.W.", 9.5 x 9.5 m² TUNNEL
B) FULL-SCALE A/C PARTS (TRANSONIC)	ONERA/MODANE, S1 TRANSONIC TUNNEL 1/2 ADVANCED WING DORNIER (FLOWN ON CAPE. ALPHAJET?) NASA/LANGLEY, TRANSONIC 8 FT TUNNEL LAMINAR F.C. WING (LARGE A/C (RE, M) FLIGHT)
C) PRESSURIZED W-T CIRCUIT (SUBSONIC)	RAE/FARNBOROUGH, 5 x 4.2 m² TUNNEL, PMAX = 3 ATM ONERA/FAUGA, F1, 4.5 x 3.5 m² TUNNEL, PMAX = 4 ATM
D) CRYOGENIC TEMPERATURE IN W-T CIRCUIT	NASA/LANGLEY, "N.T.F.", 2.5 x 2.5 m² TRANSONIC TUNNEL ($Re_{\bar{c}} \sim 120 \times 10^6$) EUROPEAN PROJECT "E.T.W.", 2.2 x 2 m² TRANSONIC TUNNEL ($Re_{\bar{c}} \sim 50 \times 10^6$) ONERA/CERT, T2, 0.4 x 0.4 m² TRANSONIC TUNNEL (BLOW DOWN, ADAPTIVE WALLS) NASA/LANGLEY, "T.C.T." 0.6 x 0.2 m² TRANSONIC TUNNEL (2 DIM.) DFVLR/PORZ-WAHN, 2.4 x 2.4 m² SUBSONIC TUNNEL

Figure 2

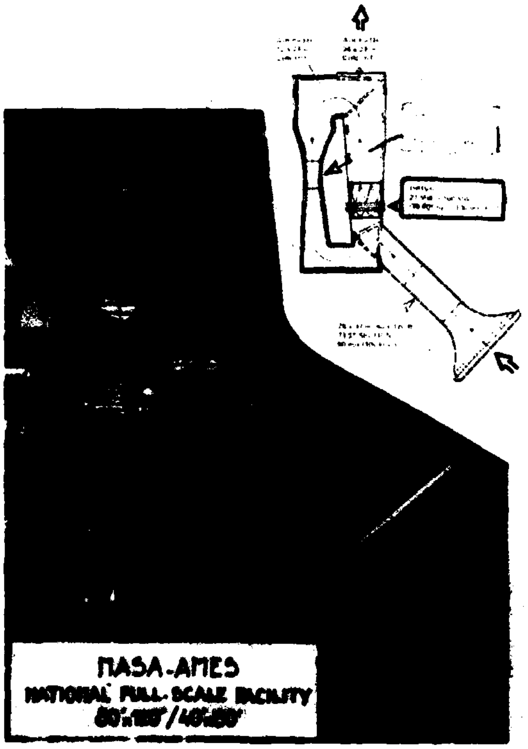
NASA-AMES
NATIONAL FULL-SCALE FACILITY
80'x120'/40'x80'

Figure 3

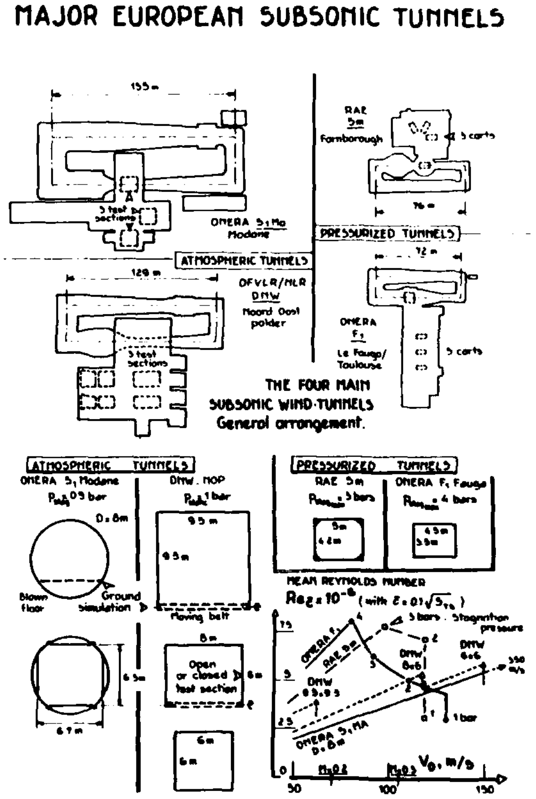
MAJOR EUROPEAN SUBSONIC TUNNELS
155 m
ONERA S1 Ma
Modane
3 test sections
ATMOSPHERIC TUNNELS
129 m
DFVLR/NLR
DNW
Noord Oost polder
3 test sections
RAE
5m
Farnborough
3 carts
76 m
PRESSURIZED TUNNELS
72 m
ONERA
F1
Le Fauga/
Toulouse
3 carts
THE FOUR MAIN
SUBSONIC WIND-TUNNELS
General arrangement.
ATMOSPHERIC TUNNELS
ONERA S1 Modane
P = 0.9 bar
D = 8m
Blown floor
Ground simulation
DNW. NOP
P = 1 bar
9.5 m
9.5 m
Moving belt
8 m
Open or closed test section
6 m
6.5 m
6.7 m
6 m
6 m
PRESSURIZED TUNNELS
RAE 5m
Pmax = 3 bars
5m
4.2m
ONERA F1 Fauga
Pmax = 4 bars
4.5m
3.5m
MEAN REYNOLDS NUMBER
Rec̄ x 10⁻⁶ (with c̄ = 0.1√S)
7.5
5
2.5
0
ONERA F1
RAE 5m
3 bars . Stagnation pressure
4
3
2
1 bar
DNW 6x6
DNW 8x6
DNW 9.5x9.5
ONERA S1 MA D=8m
350 m/s
M=0.2
M=0.3
V0, m/s
50
100
150

Figure 4

- A large Dutch-German subsonic tunnel (DNW) has been recently built in the Polders and is operated since 1980 by NLR and DFVLR; 3 interchangeable test sections are available: 9,5 x 9,5 - 8 x 6 and 6 x 6 m^2 with speeds ranging from 60 to 150 m/s (Fig. 4).

B) Testing of Full-Scale Aircraft parts (half wing-fuselage, fuselage- engine, etc.) are often tested in the ONERA S1 Modane sonic tunnel (D = 8 m); thus flight conditions can be duplicated on an actual wing before flight testing with the full instrumentation, as shown on Figure 5 for a DORNIER/ONERA research programme on an advanced wing, fitted on the Alphajet Trainer (see paper Nr. 4 in this Symposium).

Another interesting example of the Flight Reynolds number duplication (20 x 10^6) is given by a special rig installed in the 8 ft transonic tunnel at *NASA-Langley, where a large wing is* tested between area ruled walls to validate the laminar flow control concept at full-scale (Figure 6 and ref. 4).

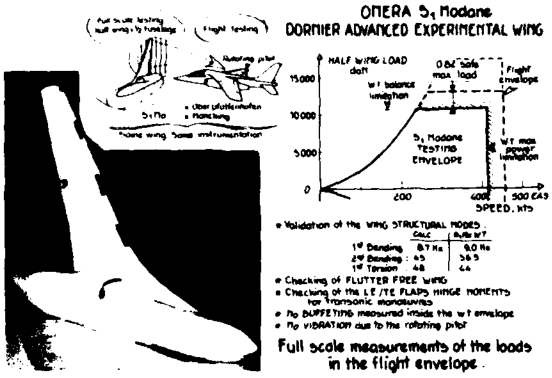
Full scale testing half wing+½ fuselage
Flight testing
Rotating pilot
S1 Ma
• Uber pfattenhafen
• Manching
Same wing Same instrumentation
ONERA S1 Modane
DORNIER ADVANCED EXPERIMENTAL WING
HALF WING LOAD daN
15000
10000
5000
0
0.8£ safe max load
Flight envelope
W.T balance limitation
S1 Modane TESTING ENVELOPE
W.T max power limitation
200
400
500 EAS
SPEED. KTS
• Validation of the WING STRUCTURAL MODES.
CALC
1st Bending
2nd Bending
1st Torsion
8.7 Hz
45
48
9.0 Hz
56.5
44
• Checking of FLUTTER FREE WING
• Checking of the LE/TE FLAPS HINGE MOMENTS for transonic manoeuvres
• No BUFFETING measured inside the w.t envelope
• No VIBRATION due to the rotating pilot
Full scale measurements of the loads in the flight envelope.

Figure 5

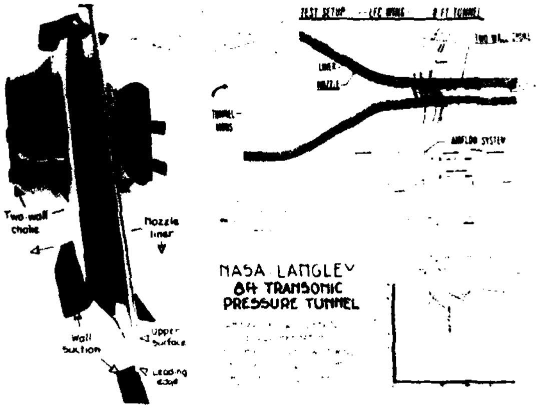
Two-wall choke
Nozzle liner
Wall suction
Upper surface
Leading edge
TEST SETUP — LFC WING — 8 FT TUNNEL
LINER
NOZZLE
TUNNEL WALLS
AIRFLOW SYSTEM
NASA LANGLEY
8ft TRANSONIC PRESSURE TUNNEL

Figure 6

C) New Pressurised Subsonic Tunnels have been recently put in operation by *ONERA* at *Toulouse-Le* Fauga (4,5 x 3,5 m^2, $p_{stag.}$ = 4 bars) and by RAE at Farnborough (5 x 4,2 m^2, $p_{stag.}$ = 3 bars) which permit to reach more than $Re_c = 7.10^6$ on a complete model with high lift systems and to analyse separately Reynolds and Mach numbers effect (Fig. 4).

D) Finally, cryogenic temperatures in the return circuit can be obtained by liquid nitrogen injection which permit to multiply the Reynolds number by a factor of 4 for given stagnation pressure and Mach number (ref. 6). This cryogenic technology have been recently developed both in US and in Europe, at first on several transonic pilot tunnels (NASA-TCT, ONERA-T2), and then for the new large transonic NTF tunnel at NASA/Langley (test-section: 2,5 x 2,5 m^2, Re_c = 120 x 10^6 at M = 1, see Fig. 7 and ref. 5) and for a modified subsonic tunnel at DFVLR/Porz-Wahn (test-section: 2,4 x 2,4 m^2, $Re_c \simeq 8 \times 10^6$); an European Transonic Cryogenic ETW tunnel is under study by a NLR/ONERA/RAE/DFVLR team (test-section 2,2 x 2 m^2, $Re_c \simeq 50 \times 10^6$ at M = 0,9).

It is interesting to see, on Figure 8, *that the strong influence* of the Reynolds number variation, up to 40 x 10^6, has been already demonstrated by a 2Dim. supercritical wing testing (NASA/DFVLR) in the Langley cryogenic pilot tunnel and in other facilities.

But it must be reminded some new problems, unique to cryogenic tunnels, with their very cold testing environment (120°K instead of 300°K!):

- New testing techniques and procedures;
- New model fabrication techniques (metal, composite...)
- *New model equipment (forces, pressures, accelerometers...).*

Sophisticated instrumentation must be developed for:

. a precise detection of the boundary layer transition, and
. precise model thermal conditioning and control.

It remains also some old problems in such pressurized tunnels:

. interference corrections for huge model-support systems;
. precise on-line measurement of model deformations.

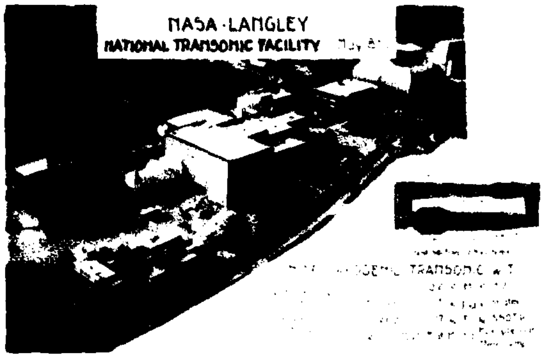
NASA-LANGLEY
NATIONAL TRANSONIC FACILITY

Figure 7

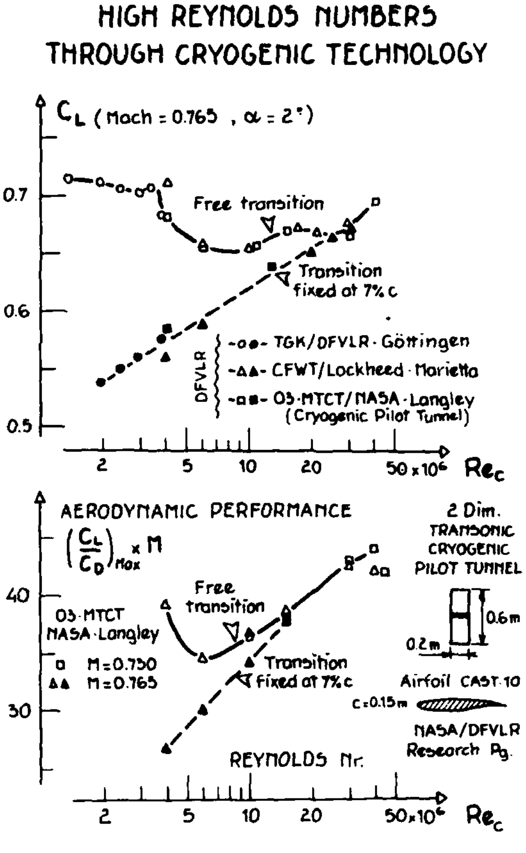

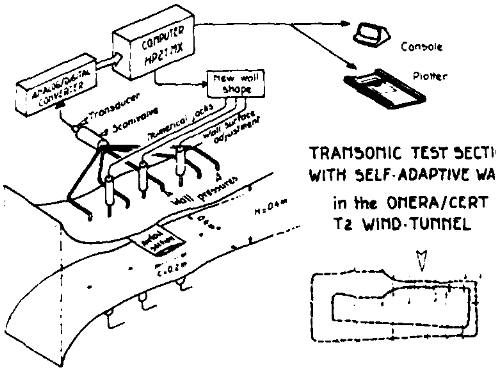
COMPUTER HP21MX
ANALOG/DIGITAL CONVERTER
Transducer
Scanivalve
Numerical jacks
Wall surface adjustment
New wall shape
Console
Plotter
Wall pressures
Airfoil
H=0.4m
c=0.2m
TRANSONIC TEST SECTION WITH SELF-ADAPTIVE WALLS
in the ONERA/CERT
T2 WIND-TUNNEL

Figure 9

Figure 8

II.2) BETTER APPROACHES TO REMOVE THE WIND-TUNNEL WALLS CONSTRAINTS:

- Better wall corrections are now calculated for both plain and transonic perforated/slotted test sections (see next paper Nr. 2, by AEDC/ONERA);
- But another approach is the development of "adaptive walls" with a computer in the loop to monitor the wall deformation giving an "infinite" environment around the model (ref. 6), thus avoiding wall correction; furthermore a larger model chord can be used for a given test section; such a concept is already operational in the ONERA/CERT T2 tunnel for 2Dim. transonic testing, (Figure 9) and will be combined with the cryogenic technology in the near future (blow-down operation with cold model injection in the test section).

II.3) INTEGRATION OF COMPUTATIONAL FLUID DYNAMICS AND WIND-TUNNEL TESTING

The increasing role of the computer is certainly the most important fact in the last few years. As shown on the table of Figure 10, the computer is already used for improving the test operations, and to correct wind-tunnel data; in the near future, its role will be extended for CFD codes assessment and as a guide during testing (interactive CFD).

The spectacular improvement of wind-tunnel efficiency (measured in millions of informations given to the customers every year) is illustrated on Figure 11 for the two major tunnels of the ONERA/Modane Center, thanks to a better computer integration for data acquisition/reduction during the last ten years.

II.4) PROGRESS IN COMPUTATIONAL FLUID DYNAMICS (C.F.D.):

The exponential progress in both hardware and software since twenty years will certainly open the way to very powerful "super-computers" dedicated to CFD in the next twenty years (ref. 7).

This trend is illustrated on Figure 12, where we have plotted the capability of Computational Fluid Dynamics to solve more and more sophisticated equations for a theoretical approach of *Aircraft Design, as a function* of the computer development since 1960 and for the future (approximatly scaled in computational speed, in Mflop).

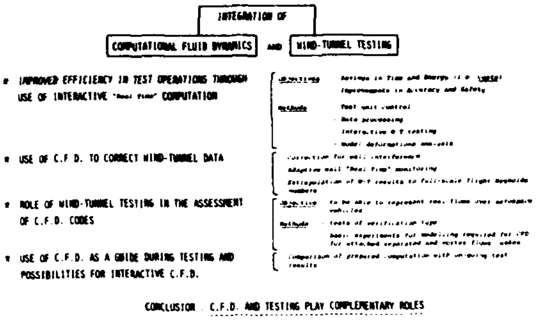
INTEGRATION OF
COMPUTATIONAL FLUID DYNAMICS
AND
WIND-TUNNEL TESTING
• IMPROVED EFFICIENCY IN TEST OPERATIONS THROUGH USE OF INTERACTIVE "Real time" COMPUTATION
Objectives
Savings in Time and Energy (i.e. costs)
Improvements in Accuracy and Safety
Methods
Test unit control
Data processing
Interactive W-T testing
Model deformations analysis
• USE OF C.F.D. TO CORRECT WIND-TUNNEL DATA
Correction for wall interference
Adaptive wall "Real Time" monitoring
Extrapolation of W-T results to full-scale flight Reynolds numbers
• ROLE OF WIND-TUNNEL TESTING IN THE ASSESSMENT OF C.F.D. CODES
Objective
to be able to represent real flows over aerospace vehicles
Methods
tests of verification type
basic experiments for modelling required for CFD for attached separated and vortex flows
• USE OF C.F.D. AS A GUIDE DURING TESTING AND POSSIBILITIES FOR INTERACTIVE C.F.D.
Comparison of prepared computation with on-going test results
CONCLUSION : C.F.D. AND TESTING PLAY COMPLEMENTARY ROLES

Figure 10

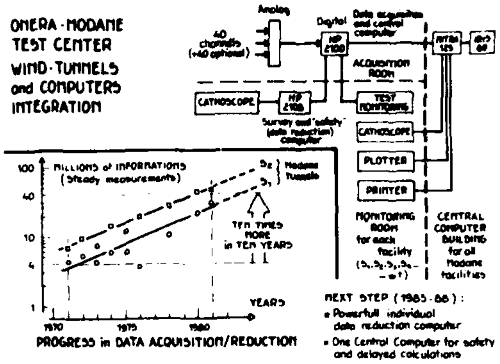
ONERA-MODANE TEST CENTER
WIND-TUNNELS and COMPUTERS INTEGRATION
Analog
Digital
40 channels (+40 optional)
HP 2100
Data acquisition and control computer
ACQUISITION ROOM
CATHOSCOPE
HP 2108
Survey and "safety" (data reduction) computer
TEST MONITORING
CATHOSCOPE
PLOTTER
PRINTER
MONITORING ROOM for each facility (S1,S2,S3,S4 ...)
CENTRAL COMPUTER BUILDING for all Modane facilities
100
40
10
4
1
MILLIONS of INFORMATIONS (Steady measurements)
S2
S1
Modane Tunnels
TEN TIMES MORE in TEN YEARS
YEARS
1970
1975
1980
PROGRESS in DATA ACQUISITION/REDUCTION
NEXT STEP (1985-88):
• Powerfull individual data reduction computer
• One Central Computer for safety and delayed calculations

Figure 11

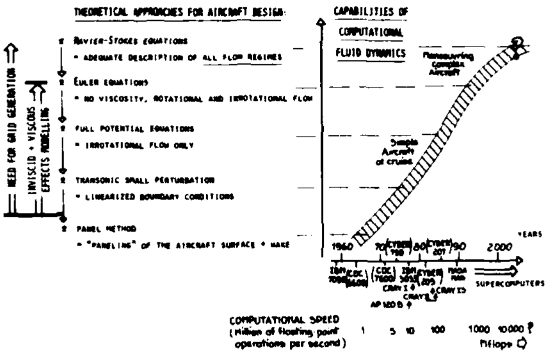

Figure 12

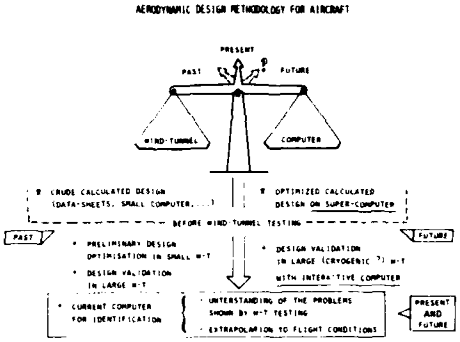
AERODYNAMIC DESIGN METHODOLOGY FOR AIRCRAFT
PRESENT
PAST
FUTURE
WIND-TUNNEL
COMPUTER
• CRUDE CALCULATED DESIGN (DATA-SHEETS, SMALL COMPUTER,...)
• OPTIMIZED CALCULATED DESIGN ON SUPER-COMPUTER
BEFORE WIND-TUNNEL TESTING
PAST
FUTURE
• PRELIMINARY DESIGN OPTIMISATION IN SMALL W-T
• DESIGN VALIDATION IN LARGE W-T
• DESIGN VALIDATION IN LARGE (CRYOGENIC ?) W-T WITH INTERACTIVE COMPUTER
• CURRENT COMPUTER FOR IDENTIFICATION
- UNDERSTANDING OF THE PROBLEMS SHOWN BY W-T TESTING
- EXTRAPOLATION TO FLIGHT CONDITIONS
PRESENT AND FUTURE

Figure 13

But there are some important conditions for progress in CFD:

- Increasing storage capacity of the computers available on the market.
- Better ability to generate coordinate systems for complex Aircraft configurations.
- Development of sophisticated algorithms to solve the flow field equations, including discontinuities (shock-waves, vortex sheets, strong separations,...) by finite difference, finite element, spectral methods,...
- Capability for modelling turbulent flow to be introduced in future Navier-Stokes approaches (Reynolds averaged, large eddy simulation)

...and better ability to visualize the computed results (quick analysis, decision to reorient a costly programme,...).

II.5) TOWARDS A NEW AERODYNAMIC DESIGN METHODOLOGY FOR AIRCRAFT:

Up to now, with the present computer capability, the Aircraft design work is limited to the study of simplified models before extensive wind-tunnel evaluation of various shapes of a new project; and the computer is extensively used for "identification", i.e. to understand the problems shown by the wind-tunnel results and to extrapolate them to flight conditions.

In the future, with the availability of some "supercomputer" the manufacturer will certainly be able to calculate an "optimized" design before wind-tunnel testing, for validation, on a sophisticated large model in the best facility available (cryogenic capability?).

This trend is illustrated on Figure 13; but wind-tunnel and computer approaches will still remain balanced and complementary to develop an optimized new Aircraft during the next decade.

II.6) PROGRESS ON EXPERIMENTAL METHODS FOR ACTIVE CONTROL SYSTEMS EVALUATION

To conclude this introduction, it seems mandatory to review the various tools recently developed to help the designer for active control technology integration in a new Aircraft project; as shown on Figure 14, both ground testing and flight testing approaches are used for basic research and for validation of the various applications of ACS on military and civil Aircraft projects:

- Relaxed stabilities
- Manoeuvre enhancing or limiting
- Airframe configuration management
- Load alleviation
- Structural modes control.

This includes a very different cockpit installation with new pilot controls and better displays, to be evaluated on sophisticated ground and flight simulators; such recent ground simulators developed by NASA-Ames and by the French Flight Test Center are illustrated on Figures 15a and b.

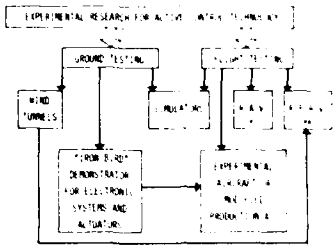
EXPERIMENTAL RESEARCH FOR ACTIVE CONTROL TECHNOLOGY
GROUND TESTING
FLIGHT TESTING
WIND TUNNELS
SIMULATORS
"IRON BIRD" DEMONSTRATION FOR ELECTRONIC SYSTEMS AND ACTUATORS
EXPERIMENTAL AIRCRAFT OR MODIFIED PRODUCTION A/C

Figure 14

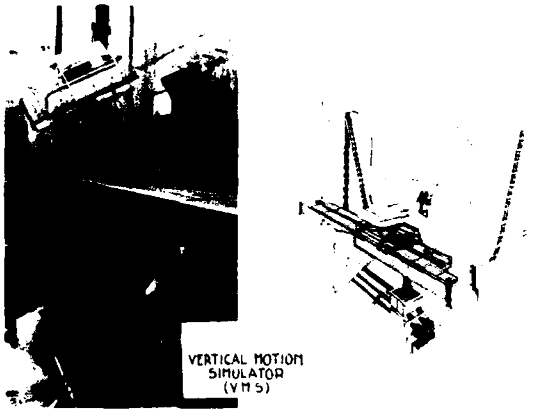
VERTICAL MOTION SIMULATOR (VMS)

Figure 15a

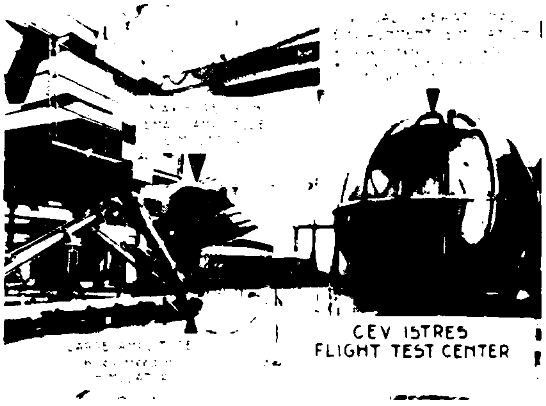
CEV ISTRES FLIGHT TEST CENTER

Figure 15b

- On the Flight Research side, NASA-Dryden Center has recently operated very sophisticated Remote Piloted Research Vehicle (RPRV "HIMAT" for example) and Remotly Augmented Vehicle (Experimental RAV/F-8 Aircraft) to study flying qualities and adaptive control with Active Control Systems (Figure 16).

But another very efficient way for ACT evaluation is the modification of an existing production Aircraft with adequate "fly-by-wire", computers and electro hydraulic controls: this was opened by US-Air Force with the B-52/CCV, the F-4 CCV and the F-16 CCV programmes in the seventies; more recently several sophisticated Flight Research programmes have been launched in several countries:

. F-104/MBB and Alphajet/KEL in Germany

. Experimental "fly-by-wire" Jaguar in UK

. F-111/AFTI, L-1011 and F-16/AFTI in US

. Reduced Stability Airbus and Relaxed Stability Concorde in Europe.

- On the Wind-Tunnel side, Figure 17 illustrates the main methods used for ACT Research:

  . Tests on "rigid" models with active control surfaces to generate a comprehensive data base on unsteady aerodynamics, mandatory for an ACT Aircraft project; such a programme recently performed by ONERA/ MBB/VFW/AEROSPATIALE in the large S1 Modane Tunnel is illustrated on Figure 18.

  . Two other approaches: free-flying Aircraft model catapulted through a local jet (to simulate vertical or lateral gust, French IMFL Laboratory), or semi-free model behind a gust generator in the test-section (DFVLR-Braunschweig) will be described in paper Nr. 17 during this Symposium; at ONERA, we have recently validate a gust generator system in a pilot-tunnel for future application in the large S1 Modane tunnel in view of generating, in the front of big models, some prescribed gusts up to transonic cruise regime.

  . Another approach is used by NASA/Langley with remotly piloted free- flying ACT model in their full scale tunnel open section.

  . Finally, aeroelastic models with active flutter control system are used since several years in the NASA/Langley TDT tunnel and in the ONERA/Modane S2 tunnel to validate adequate flutter control laws for military Aircraft (with dangerous external stores) or civil Aircraft project (with flexible high aspect-ratio wings). This approach is also used in flight on RPRV by NASA-Dryden (see paper Nr. 20 during this Symposium).

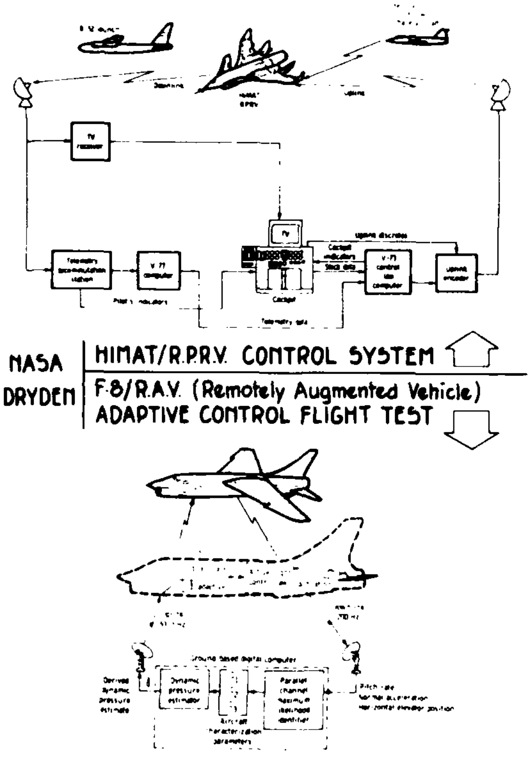
HiMAT RPRV
Downlink
Uplink
TV receiver
TV
Uplink discretes
Cockpit indicators
Stick data
V-71 computer
V-71 control law computer
Uplink encoder
Cockpit
Telemetry data
NASA
DRYDEN
HIMAT/R.P.R.V. CONTROL SYSTEM
F-8/R.A.V. (Remotely Augmented Vehicle)
ADAPTIVE CONTROL FLIGHT TEST
Ground based digital computer
Derived dynamic pressure estimate
Dynamic pressure estimator
Aircraft characterization parameters
Parallel channel maximum likelihood identifier
Pitch rate
Normal acceleration
Horizontal elevator position

Figure 16

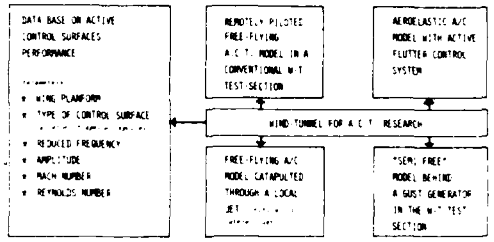
DATA BASE ON ACTIVE CONTROL SURFACES PERFORMANCE
WING PLANFORM
TYPE OF CONTROL SURFACE
REDUCED FREQUENCY
AMPLITUDE
MACH NUMBER
REYNOLDS NUMBER
REMOTELY PILOTED FREE-FLYING A.C.T. MODEL IN A CONVENTIONAL W-T TEST-SECTION
AEROELASTIC A/C MODEL WITH ACTIVE FLUTTER CONTROL SYSTEM
WIND-TUNNEL FOR A.C.T. RESEARCH
FREE-FLYING A/C MODEL CATAPULTED THROUGH A LOCAL JET
"SEMI FREE" MODEL BEHIND A GUST GENERATOR IN THE W-T TEST SECTION

Figure 17

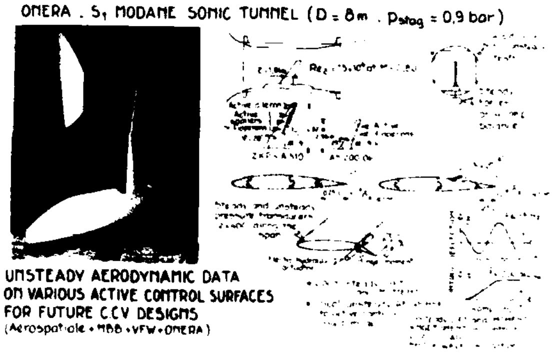
ONERA . S1 MODANE SONIC TUNNEL (D = 8m . Pstag = 0,9 bar)
Active spoilers
UNSTEADY AERODYNAMIC DATA
ON VARIOUS ACTIVE CONTROL SURFACES
FOR FUTURE C.C.V DESIGNS
(Aerospatiale + MBB + VFW + ONERA)

Figure 18

REFERENCES

(1) —— Flight/Ground Testing Facilities Correlation. 46th Meeting of the Flight Mechanics Panel, Valloire, France, 9-13 June 1975. AGARD CP-187, (1976).

(2) —— Technical Evaluation Report on the AGARD/FMP Symposium on "Ground/Flight Test Techniques and Correlation" by Dr. John Williams, AGARD AR-191

(3) —— K.W. MORT et al. - Status and Capabilities of the National Full-Scale Facility 40 by 80 foot Wind-Tunnel Modification. AIAA Paper Nr. 82-0607, (March 1982).

(4) —— W.D. HARVEY and J.D. PRIDE - The NASA-Langley Laminar Flow Control Airfoil Experiment. AIAA Paper Nr. 82-0567, (March 1982).

(5) —— L.W. McKINNEY and B.B. GLOSS - Status of the National Transonic Facility. AIAA Paper Nr. 82-0604.

(6) —— AGARD/FDP Sub-Committee - Wind-Tunnel Capability Related to Test-Section, Cryogenics, and Computer Wind-Tunnel Integration. AGARD-AR-174.

(7) —— AGARD/FDP - Applied Computational Transonic Aerodynamics. AGARDograph Nr. 266, (August 1982).

PROGRESS IN WIND TUNNEL TEST TECHNIQUES AND IN THE CORRECTIONS AND ANALYSIS OF THE RESULTS*

by
T. W. Binion, Jr.
Calspan Field Services, Inc.
Arnold Air Force Station, Tennessee 37389 USA
and
X. Vaucheret and X. Bouis
Office National d'Etudes et de Recherches Aerospatiales
Châtillon sous-Bagneux
Hauts-de-Seine, France

SUMMARY

In response to the increased complexity and cost of testing, wind tunnel operators are doing many things to improve test effectiveness. This paper describes several recent innovations designed to increase the amount of information obtained during a test, to reduce information unit cost, and to improve data quality.

INTRODUCTION

During the past few years the complexity of wind tunnel tests has increased dramatically. In the larger facilities, it is exceptional to conduct a test with only a single six-component balance and a base pressure measurement. It is not now uncommon to install a wind tunnel model with two or more balances and make a few hundred pressure measurements at the same time. It is not surprising that ONERA's experience, Fig. 1, shows that the amount of steady-state data acquired in ONERA tunnels S1MA and S2MA has increased by 1000 percent in the past decade. As a result of this activity, wind tunnel operators have been encouraged by their customers to improve test effectiveness. The operators are responding along three fronts (1) increasing the amount of information, as opposed to data, which can be obtained in ground test facilities, (2) reducing test costs per data unit, and (3) improving data quality. These goals are interrelated, but their evaluation is generally difficult because a good measure of test effectiveness applicable to a wide range of test types has not been found. However, the lack of an effective measure is not a deterrent to progress. Efforts to increase the amount of information have led to improved test techniques, improved model and environmental simulation, and new and improved instrumentation systems. Efforts to reduce costs have taken several approaches: developing methods of (a) obtaining only the required information rather than full data matrices, (b) taking data faster, (c) testing at the lowest possible Reynolds number, and (d) using computations to plan, correct, verify, extrapolate, interpolate, and interpret test data. Efforts to improve the data quality are being directed toward (a) improving tunnel flow uniformity, (b) reducing and correcting for support interference, (c) reducing and correcting for wall interference, (d) improving simulation techniques, and (e) improving measurement techniques and accuracy. A potpourri of the results from several of these efforts chosen either from AEDC or ONERA experience are discussed herein.

PROPULSION SYSTEM SIMULATION FOR TRANSPORT CONFIGURATIONS

Today about half of the direct operating costs of civilian transport aircraft are spent for fuel. This fact has induced the aerodynamicist to embark upon a tremendous effort to reduce cruise drag. A large drag contributor, and one which can be reduced, is the engine "installation" drag which depends upon the shape of the engine nacelle and pylon, its placement with respect to the wing, and the interaction of the jet efflux with the surrounding flow field. Two methods are being used currently at ONERA to simulate engines and their jets - blown nacelles and turbine-powered simulators (TPS). A typical TPS installation is shown in Fig. 2.

The force accounting system used by ONERA with the two techniques is depicted in Fig.3. A flowthrough configuration must be tested with the blown nacelle technique to obtain the inlet drag increment between the flowthrough and faired inlet configurations as well. The TPS eliminates the main part of this increment by simulating the fan inlet mass flow and the total exhaust flow. In that case, flowthrough configurations are still used to measure the smaller difference between the drag of the TPS inlet (adapted to the fan mass flow) and the drag of the real aircraft inlet (adapted to the total engine mass flow).

There are two factors that are critical to the success of each technique. First, the thrust calibrations must be done accurately at the altitude pressure of the wind tunnel tests. Second, the high-pressure air must be ducted around the balance to provide repeatable interactions which can be removed through calibrated correction tares. Because of the piping/balance interactions, the techniques are generally used with half-span models and external balances wherein sufficient space exists external to the model to duct the high-pressure air around the balance. A typical installation is shown in Fig. 4, which is an illustration of a transport aircraft configuration in the SIMA tunnel at Modane. Figure 5 gives two examples of data repeatability within a test program. The quality of these results, improved by repeating some tests and statistical surveys, allows the ranking of model configurations differing by less than one percent of drag at the cruise condition.

---

* The research reported herein was performed by the Arnold Engineering Development Center, Air Force systems Command and by Office National d'Etudes et de Recherches Aérospatiales (FRANCE).(U.S. work and analysis for this research were done by personnel of Calspan Field Services, Inc., operating contractor of the aerospace flight dynamics facilities at AEDC). Further reproduction is authorized to satisfy needs of the U.S. and French Governments.

ENGINE AIRFRAME INTEGRATION TESTING FOR COMBAT AIRCRAFT

Dassault and ONERA have worked out a combat aircraft model design and measuring system to give reliable determination of improvements to (1) internal duct performance and stability, especially at high incidence and transonic conditions, and (2) thrust-minus-drag at supersonic conditions. Both kinds of tests are done on the same model (about 1/4-scale) in SIMA at high incidence and in S2MA for the supersonic conditions. Figure 6 shows the principle of the model design. The forebody including the inlet is metric; the loads are measured by a six-component balance. The forebody is linked to the rear portion of the model by rubber seals that provide the necessary air tightness. Mass flow and pressure recovery are measured at the compressor face and are used in an engine math model to calculate thrust. Thus, it is possible to compare forebody configurations on the basis of thrust-minus-drag. This procedure reduces the amount of testing previously needed for such comparisons and improves the reliability of the results. The drag coefficient repeatability is approximately ±0.0002.

CONSTANT PARAMETER TESTING

One of the most obvious ways to reduce testing costs is to reduce the amount of data required to obtain the desired information. A method of doing this is to place a model and support system under computer control such that the model may be tested at a constant value of some aerodynamic parameter.[2] The advantage of such a test technique is shown by the example in Fig. 7. The traditional method for determining optimum cruise Mach number entails taking as many as 180 data points per configuration to establish the incidence versus Mach number at constant lift coefficient from which the cruise drag coefficient versus Mach number is derived. However, under computer control, one may test at a constant value of lift coefficient and obtain the same information with only 20 points; Mach number is varied manually or by the computer if the tunnel is automated. In addition, if the model contains remotely movable control surfaces, the constant lift coefficient data can easily be obtained at trimmed conditions corresponding to one or more center-of-gravity locations. With the use of the online plotting capability available in many tunnels, the optimum cruise Mach number can be identified almost immediately, saving all the posttest data analysis time required when using the traditional method. Thus, using the constant parameter method, configuration variables can be evaluated much more economically. Of course, once a configuration is found which satisfies the design requirements a complete set of static stability data can be obtained for the final configuration.

The constant parameter technique has been very effectively employed in full-scale[3] tests with operating engines such as the one shown in Fig. 8. Data were desired at five flight conditions, each spanning the flight vehicle weight and center-of-gravity range. A schematic of the control system is shown in Fig. 9. The vehicle contained a six-component balance and five remotely controlled parameters: the engine throttle and four control surfaces. The PDP-15 computer serves as the data acquisition system that passes engineering unit data to the facility computer. The facility computer contains the trim control algorithms and computes the command functions for the independent variables which are passed either to the PDP-15 or an independent controller which sets model attitude. The constant parameter system was set up so that all moments were held at zero about a specified center of gravity. The engine throttle was automatically controlled so that vehicle thrust-minus-drag was either zero or some specified value. Corrections for strut interference and tunnel flow angularity were included in the control algorithm. After the computer had set a point which corresponded to steady flight at a given Mach number, attitude, vehicle weight, and center-of-gravity location, a full set of data was automatically taken to define completely the vehicle performance at that point. It was estimated the cost of the program was between 15 and 25 percent of that required by traditional methods.

OPTIMIZING PARAMETERS

A natural outgrowth of constant parameter testing is the development of a technique to optimize a given aerodynamic parameter by computer manipulation of the available control surfaces. The optimization concept consists of automatically adjusting a model configuration parameter (wing flap or slat deflection, horizontal tail angle, canard angle, etc.) to maximize a designated merit function (lift, drag, etc.) subject to various, imposed constraints (constant lift, constant drag, structural limits, etc.). A program to demonstrate the technique[4] utilized four independent model variables - leading- and trailing-edge flap angles, horizontal tail angle, and angle of attack - to minimize drag for a constant value of lift coefficient, to maximize lift for a given value of drag, and to maximize lift-to-drag ratio for a given drag.

The optimization program operates in two distinct modes termed "incremental" and "simultaneous." The optimization process indicated in Fig. 10 begins with the incremental mode wherein at a given Mach number and altitude condition each independent variable is perturbed from its initial setting to generate gradient influence vectors of the function to be optimized and any specified constraints, for example, optimize lift-to-drag ratio and constrain drag coefficient. After the gradient vectors are established, the gradient projection algorithm calculates the independent variable directions for either minimizing the specified merit function or satisfying the constraint. The simultaneous mode then systematically drives all independent variables in the proper direction at relative increments for a sequence of 11 test points. The sequence is aborted if any of the constraints is violated by more than a prescribed tolerance. Upon completion of the sequence, the computer selects the best of the simultaneous mode points, repositions the independent variables to that condition, and repeats the incremental mode. The incremental-simultaneous cycle continues to convergence. An example of a convergence sequence is shown in Fig. 11 in which lift-to-drag ratio is maximized, constraining drag coefficient to 0.22 ± 0.006. The optimization used three independent variables: pitch angle, leading-edge flap angle, and trailing-edge flap angle.

The most complicated optimization done to date was accomplished on the Self-Optimizing Flexible Technology (SOFT) wing program.[5] The SOFT wing model, Fig. 12, had 12 independent variables which controlled the wing camber, thickness and twist distributions along the span, pitch angle, and tail angle in a manner to optimize specified merit functions while satisfying specified constraints as a function of flight conditions. The wing was constructed using a steel center span and a flexible steel and fiberglass skin attached to 12 individually controlled hydraulic actuators. The 12 actuators were designed to vary the leading-edge radius and the wing contour at the 15-, 25-, 65-, and 80-percent chord lines. However, in practice the leading-edge radius was not changed to avoid excessive stress in the skin. A hydraulic actuator was also used to control the horizontal tail so that tests could be conducted with the vehicle continually trimmed. An example of a series of iterations to minimize drag with lift coefficient constrained to 0.25 and pitching moment to zero is shown in Fig. 13 along with the drag polars of the basic and optimum wing contours. A drag reduction of 0.0026 was achieved at the lift coefficient value of 0.25.

PHOTOGRAMMETRIC DEVELOPMENT AND APPLICATION

Airfoil deflections caused by airloads were expected to be larger than normal for the SOFT wing model because of designed flexibility of the wing. In addition, proper interpretation of the data required that the wing contour be measured under load. The only practical means to accomplish this was through the use of a photogrammetric technique wherein stereophotographs of the model were taken of the optimum contours during testing and processed offline to obtain the actual airfoil shape, wing twist, and dihedral.

The photogrammetric analysis system developed at AEDC[6] uses 70-mm Hasselblad cameras and a Keffel & Esser DSC-3/80® analytical stereocompiler interfaced to the AEDC computer system. A light system has been devised which will project an orthogonal grid onto a featureless model to aid in reading the film. A photograph of a body used in verification of the system, illuminated with the orthogonal grid, is shown in Fig. 14. The model was photographed from eight positions. The data were read, merged into a three-dimensional representation of the model and displayed on an interactive graphics system, Fig. 15, which is used for quickly checking the results. As part of the system verification, the stereophotographs were read by three operators and compared with precise measurements of the body. A measurement accuracy which varied from ±0.13 to ±0.25 mm was obtained.

A portable-computer interfaced digital theodolite system, Fig. 16, is being developed which will be used to measure control point locations on a given test article. Control points are points of known locations which are used to ensure data accuracy. When the theodolites, which are a known distance apart, are vectored to a given point in space, a computer program will compute its location with respect to the mounting bar and transform the coordinates into any other desired axis system.

In addition to use in the SOFT wing program, the stereophotographic system has been used to measure twist and dihedral of a full-scale cruise missile wing, deflection of a cryogenic space shuttle tank under airload, and ice buildup on the leading edge of an airfoil. The icing test posed a peculiar problem. At some test conditions glaze ice (clear) formed which did not have enough opacity to cause the projected orthogonal grid to be visible at the ice surface. Fortunately, however, the ice buildup was very irregular and contained enough features so that good results could be obtained by a skilled operator.

Two future applications appear very promising. The stereophotographic system can be used to obtain as-built, test model coordinates which can be fed directly to a computational fluid-dynamics grid generation program. Work is underway to develop the software for this application. The second application is to obtain coordinates of ablating or eroding reentry vehicles under test in either ballistic ranges or arc heaters.

CONTINUOUS CAPTIVE TRAJECTORY SYSTEM

The captive trajectory system (CTS) installed in the AEDC 4-ft transonic Aerodynamic Wind Tunnel (4T) provides the capability to determine the separation trajectory of a store as it moves away from its aircraft. The system uses a computer-controlled six-degree-of-freedom mechanism to position the store at the appropriate place in the flow field. A typical CTS installation is shown in Fig. 17. The store model contains a five- or six-component balance with balance diameters as small as 4.8 and 7.6 mm, respectively. Trajectories beginning from the captive position are generated by the computer solving the equations of motion to predict a position change based on the measured store loads. The "move and pause" technique based upon position control has been used at AEDC since

1968. The system automatically moves the store to the predicted position, pauses, compares the new position with the predicted value and, if within tolerance, makes a new prediction.

In 1978, motivated by increased testing costs, a research program was undertaken at AEDC to speed the trajectory generation process. That effort has produced a velocity-controlled system that provides continuous store motion and a significant decrease in test time. The increased productivity was accomplished by moving from a single-user, single-task computer system (circa 1955) to a multilevel, hierarchial, distributed processing system,[7] shown in Fig. 18, which applies processing power at the point it is needed. The distributed process network is attractive because of the decrease in cost and the increase in processing power of small computer systems. In the generic system depicted in Fig. 18 the center computer (level 1) provides archival data storage, data editing, and analysis capability through interactive graphics and a large processing capability for mathematical modeling of aerodynamic phenomena. The facility computer (level 2) is a medium-size machine whose function is to provide the management, coordination, and direction of testing events and to perform the primary data calculations and display functions. The third and fourth level machines are various mini- and microcomputer systems dedicated to a single function. The typical minicomputer at the third level is a small-to-medium-size machine with perhaps 256K bytes of 16-bit main memory and 10M bytes of remote disk storage. These systems have multichannel analog and digital input systems through which raw data are obtained. Information can be output through digital-to-analog converters for test article or test environmental control functions. The third level computers, through computational speed and restricted functions, provide essentially real-time control and data display functions. The fourth level of the distributed network utilizes 8-bit microprocessors. They provide instrumentation and process status, alarm monitoring, dedicated control, and data acquisition functions.

That portion of a distributed processing network concerned with trajectory generation is shown in Fig. 19. The complete data set for a given test is kept on file in the central computer until the final test report is completed. During that time the data are available for editing, recomputation, and plotting through the interactive graphics terminals. The facility computer contains the test management software required to coordinate the testing process and all of the initialization information required for the trajectories. In addition, it performs some post-trajectory data processing and passes the total data information, online, to the central archival storage.

The trajectory generation processor performs the real-time trajectory generation function. Test conditions, updated twice per second, are obtained upon request from the Digital Multiplexer and Control System, which also contains operator-selected parameters and serves as the aircraft controller. The Digital Data Acquisition System provides engineering unit store loads and position information acquired at 100 Hz and passed through an autoregression digital filter that maintains a continuous average (over one-half second) of the data. The real-time graphics system allows the progress of the trajectory to be monitored as it is generated and provides near-real-time transfer of the data to the facility computer. The system is interactive which allows local selection of parameters to be displayed. The CTS control system is a network of seven dedicated microprocessors that accept position or velocity commands for each of the six-degree-of-freedom mechanisms and controls the drive motors to maintain the commanded parameters.

Implementation of velocity control required modifications to the software previously used to control position. Trajectory positions have been predicted by integrating the acceleration vectors determined from the measured store forces and moments. Of course, the component velocity vectors can be calculated from the same information. The calculated velocity components are modified so that (1) the CTS rig movement in the six directions is in a coordinated time scale and (2) one of the six drive motors is operating near its maximum speed. In the maximum efficiency mode, the time scale is changed along the length of the trajectory so that both of the above constraints are always satisfied. Some of the other program options available are pivoting two-stage fuel tank release, missile rail launch; aircraft pull-up or push-over maneuvers; aircraft banked and/or diving flight attitudes; calculated add-on aerodynamic coefficients, to simulate drogue chute deployment, for example; and active autopilot guidance and control system simulation.

The data acquisition cycle is initiated when the store passes through the last predicted trajectory position. The trajectory calculations and communication requirements between the several processors require a finite amount of time, Fig. 20. The time required depends upon which of various program options are exercised, but ranges between 0.1 and 0.5 sec. During that time the CTS rig will have moved some distance, ΔS, from the last predicted position. In order to compensate for the error that could be introduced, the new position vector is calculated from the actual position at the time the command is given, S_x, rather than the old predicted value, S_i, $i = 1,2,3,\ldots$ in Fig. 20. This procedure tends to eliminate an accumulated position error in the system.

Verification tests have been conducted by comparing trajectories obtained at the same conditions utilizing both the continuous and move-pause modes. Figure 21 shows such a comparison. In most instances, the parameters describing the trajectories, particularly the distance coordinates, are identical as shown in Fig. 21a. Discrepancies which do occur are generally in the angular directions. Figure 21b shows one of the worst agreements, which is approximately 0.5 deg in store pitch angle over a small portion of the trajectory. Although the full-scale time for the two trajectories is, of course, identical, the actual time required for the continuous mode is up to a factor of seven shorter (depending upon the trajectory) than that required for the move-pause mode. The decrease in time for a trajectory translates into an average increase in trajectories per air-on hour from 4.5 in 1977 to 16 in 1981. In one instance, a rate of almost 29 trajectories per air-on hour was obtained, indicating the potential for additional improvements in the average.

FLOW-FIELD MEASUREMENTS

Improvements to calculation methods and research on new wing shapes require a better knowledge of the flow fields about aerodynamic configurations than is provided by measurements of surface pressures and gross loads. The computer-controlled CTS mechanisms provide an excellent tool to obtain the desired information. An installation of a five-degree-of-freedom mechanism in S1MA is shown in Fig. 22. Various sensing probes from standard wake rakes to hot wires to five-hole directional sensors may be attached to the mechanism and measurements taken at precise locations under computer control. Figure 23 shows an example of a cross-flow velocity vector map obtained in essentially real time in S2MA using a five-hole probe. The probe gave at each location a very accurate measure of the flow magnitude and direction. The data were used for comparison with theoretical calculations.

In other instances, flow-field measurements outside the range of classical tools may be obtained with laser anemometry. Figure 24 shows the vorticity distribution just downstream of a two-dimensional profile obtained in S3MA.[8] These data were also used for comparison with theoretical calculations.

INSTRUMENTATION IMPROVEMENTS

Store Position - The quality of CTS trajectories has been increased by an improvement in the alignment of the store in the captive position. The previous technique used a touch wire contained in the carriage device to indicate when the store was in the carriage position. The disadvantage of the touch wire is that it only provides alignment in the vertical direction and the touch wire load into the store causes an error in the initial (carriage position) loads. Recent developments have replaced the touch wire with a diode light source and a phototransistor detector shown in Fig. 25. The diode emits infrared radiation whose reflection from the store is detected by the sensor. The strength of the reflected radiation is inversely proportional to the separation distance. A typical calibration curve is shown in Fig. 26. Because of the double-valued calibration function, software is used to detect the sign change in the rate of change of voltage with position as a safety feature in addition to the normal electrical "grounding" safety feature which stops all rig movement if any part of the CTS rig or store encounters the aircraft model. The maximum useful working distance between the store and sensor is about 5 mm. The minimum working distance can be as small as 0.5 mm if the sensor is recessed a millimeter or so into the pylon. The primary advantages of the optical sensor are (1) there is no carriage preload into the store, (2) the sensor size is small (approximately 4 x 5 mm), (3) the sensor has good stability and repeatability, (4) the infrared detector is insensitive to the tunnel environment, and (5) the sensor cost is low ($4 each).

Recently, alignment has been improved by adding a small torous target on the store to provide axial (x) and lateral (y) alignment. The target consists of a black annulus which absorbs the infrared and a silver center which provides sufficient reflected radiation for the detector. A typical calibration curve is shown in Fig. 27. It should be possible to improve the 1-mm x,y position accuracy by reducing the size of the target's reflective center. Tests demonstrating the effectiveness of the device and thus the improved accuracy in setting the store to the carriage position have been conducted.

Electro-Optical Interferometer - The application of electro-optical devices to the measurement of model angle of attack or component deformation has also been demonstrated. The technique does require small retroreflectors to be mounted flush with the model surface. The measurements are made with a two-beam laser interferometer[9] shown schematically in Fig. 28. Linearly polarized light from a 5-mw helium-neon laser is passed through a half-wave plate to adjust the polarization angle for efficient transmission through the downstream prisms. The light beam then passes through a 34-MHz Bragg cell where it is split by diffraction into two nearly equal intensity beams. In addition, the first-order beam is increased in frequency by 34 MHz while the zeroth-order beam remains unchanged in frequency. Both beams are reflected to a beam-separating lens system. The first-order beam is passed through a birefringement (Wollaston) prism and reflected onto a retroreflector located on the model or onto a stationary surface that is used as the reference beam. The zeroth-order beam is passed through a 49-MHz Bragg cell to provide an object beam which has been shifted 15 MHz from the reference beam and which still has nearly half its original intensity. Using two Bragg cells to obtain the desired 15-MHz optical carrier provides sufficient separation between the optical carrier frequency and the RF signals driving the Bragg cells to allow the signal band (carrier ± signal frequency) to be processed without disturbing crosstalk from the Bragg cell drivers. The beam which has been shifted 49 MHz is reflected to a Glan-Air prism and onto a second retroreflector. The two pairs of quarter-wave length plates and the birefringement prisms separate the outgoing beams from the returning beams. The returning beams are deflected to the variable beam splitter where they are combined and reflected to the photodiode.

Optical heterodyning the two beams at the photodiode can be considered as establishing moving virtual interference fringes of period $\lambda/2$ normal to the propagation vector of the beams incident on the retroreflectors. Thus, if the retroreflectors are stationary the photodiode will output a 15-MHz carrier signal. As a retroreflector moves, its velocity will cause the virtual fringe frequency to increase or decrease depending upon the direction of motion. Thus, the frequency change can be integrated with respect to time, applying appropriate constants, to obtain a displacement or differentiated with respect to time to obtain an acceleration.

Application of the technique has been demonstrated in the AEDC Transonic Wind Tunnel (16T).[10] The laser optics and detection electronics were housed in a special environmental box bolted to the top of the test section. The environmental box was isolated from the acoustic and vibration conditions of the tunnel and cooled with a nitrogen purge to dissipate the heat from the laser and electronics. As indicated in Fig. 29 the model rotation point is some distance behind the retroreflector location, causing the retroreflector to move downstream up to 10 cm as the model is pitched. To compensate for this movement and provide maximum signal strength, the optics package within the environmental box was rotated by a precision, computer-controlled actuator as a function of sting angle. Although not demonstrated, the ±2-deg rotation of the optics package would theoretically allow tracking of the model up to 51 deg.

Data processing is accomplished with a microprocessor which also corrects for the movement of the optics package as it tracks the retroreflectors. For the demonstration experiment, retroreflectors 5 mm in diameter and about 5 mm deep were imbedded in the fuselage of a 1.2-m-long model operating over a pitch range from -4 to 35 deg. The retroreflectors were 9 cm apart. The resolution of the system is 0.001 deg. Shown in Fig. 30 is the difference between offline measurements with the interferometer and a precision inclinometer and between the interferometer and the conventional angle-of-attack calculation using sting and balance readings. The inclinometer and interferometer readings agree to within +0.002 to -0.005, whereas comparison of the values from the interferometer and the conventional method is worse by a factor of up to 20. During the online demonstration, the interferometer experienced a signal interruption which, because the interferometer provides a relative rather than absolute measurement, in essence rezeroes the measurement. Since the model did not contain a bubble pack there was no way to establish a known reference without coming offline.

The deficiency of signal loss has not been easily overcome. Nevertheless, the instrument has been successfully used in two other testing applications. In the first instance, the dynamic displacement of a sample of the thermal protective tile on the Space Shuttle was measured during a wind tunnel test. The tile samples were subjected to a dynamic environment by the flow over the cavity around the liquid oxygen line into the Shuttle. The interferometer can measure displacements as low as 0.1 micron at a maximum frequency of 30 MHz.

The second application was the measurement, during the separation dynamics, of the first 50 msec of a missile staging event in the 12-ft vacuum chamber. The two stages were mounted on an I-beam system, Fig. 31, which permitted each to move at the initiation of separation. Two interferometers were used, each measuring the displacement of the respective stage center of mass from a stationary reference point on the optics package. Simulation of the separation event indicated that the reference point moved less than 0.013 mm during the event. Cornercube retroreflectors 1 cm in diameter were used on each stage. The separation event was initiated by firing a short duration solid-propellant rocket motor in the upper stage.

Typical data from the upper stage are shown in Fig. 32. The sharp slope change in the velocity and acceleration data occurring at 40 msec was caused by the stage encountering honeycomb deceleration material. Thirty tests were accomplished without a single instrument failure. Additional applications for the laser interferometer are limited only by the imagination of the users.

Inlet Distortion Instrumentation and Data Requirements - Both the steady and unsteady pressure recovery and distortion patterns of the airflow intakes are normally measured with rakes containing about 40 pressure probes. The unsteady pressure transducers used in this application are necessarily small to minimize duct blockage. However, they are also highly temperature sensitive which, while not affecting their ability to measure the dynamic pressure component, does make them unsuitable to measure the steady pressure component. As a result, either dual probes must be installed in the inlet, which doubles the blockage, or tests must be conducted twice,[11,12] once for the mean pressure and once for the dynamic component. This problem has been alleviated at ONERA by temperature compensating the dynamic transducers following an original method worked out in cooperation with the Kulite Corporation. A photograph of a 20-cm-diam, 43-inlet duct dynamic probe array (37 totals, 6 statics) showing some of the 43 temperature compensation networks is presented in Fig. 33. The quality of the compensation brings the transducers to an accuracy comparable with steady-state transducers used with Scanivalves®.

In the mid-1970's engineers concerned with inlet-engine compatibility were asking for time-dependent pressure maps showing maximum instantaneous distortion patterns. An example is shown in Fig. 34. Frequencies of interest corresponded to the compressor rpm, i.e., about 1 kHz for 0.25-scale models. Today, frequencies of 16 kHz sampled for several seconds are being requested. For a typical 50-channel system this leads to data acquisition rates of 800,000 measurements per second. Two minutes of data recorded at this rate yield as many data words as are recorded for steady-state tests in a whole year of tunnel operation. A recording and pulse-coded modulation coding system to satisfy this need is in service at the ONERA facilities. However, not all of the problems raised by handling such enormous amounts of data have been solved.

AUTOMATIC MODEL/DATA/TUNNEL CONTROL

In the last decade development of mini- and microcomputers and progress in data acquisition systems have provided very efficient tools to improve wind tunnel efficiency to reduce costs in spite of energy cost increases. In most of the large test centers, a wide range of methods has been worked out to accelerate wind tunnel runs and very often increase the quality of the data.[13]

One technique, which has been in operation for more than 10 years, consists of acquiring data while the model is continuously moving, generally through a pitch polar. Taking some care with analog and/or digital filtering, one gets polars at pitch rates of several degrees per second in supersonic wind tunnels and between 0.2 and 0.6 degrees per second in large transonic wind tunnels. That method requires that every measurement (strain gage, pressure orifice, probe, etc.) be connected to an independent measurement channel. That is not possible at the moment for large models having more than several tens of pressure orifices. A recently developed multiport, semiconductor pressure transducer will probably remove this limitation. Experiments have been made in this way in S2MA with a 32-channel multiport transducer which has given correct pressure distributions during a pitch polar at a rate of 0.2 degree per second.

A second technique, strongly associated with minicomputer development, is indicated in Fig. 35. Evolving from the "pitch-pause" method, automated data systems began in 1971 at AEDC with the Automatic Model Attitude Positioning and Data Acquisition System. The system became rather sophisticated at ONERA's S3MA by 1973 with the addition of angle-of-attack positioning, pressure rake position control, and some measurement quality checking. Automatic control of all wind tunnel activities is still improving with the ultimate aim of complete automation of the entire tunnel operation, model operation, and data acquisition processes. The system depicted in Fig. 35 functions as follows:

- The wind tunnel run program is stored in advance in a dedicated computer in the form of a series of interactive tables specifying model attitude, control surface deflection, Mach number, Reynolds number, etc. However, the operator is allowed to intervene to modify any table at any time from an interactive keyboard.

- Permissible deviations of all set parameters are also specified, for example, $\Delta M = 0.002$, and automatically checked by the computer before each data point is acquired. In addition, allowable rates of change of dependent parameters may be specified to ensure that steady-state data are being acquired, for example, $\Delta p/\Delta t = \pm 10$ Pa/sec.

- The sequence is begun by the operator who selects the beginning table and starts the cycle. The automatic system reads the first table values, adjusts the aerodynamic and mechanical parameters, initiates the data acquisition cycle when all specified parameters are within tolerance, checks the validity of some measurements before they are acquired, displays enough engineering unit information in real time to allow the test team to stay informed of the status of critical parameters, transfers the data to another, generally larger, computer for complete processing, and cycles to the next value of the independent test variable.

- Safety of the system is also ensured by the minicomputer which monitors critical parameters, e.g., forces, moments, angles, etc., to ensure that specified limits are not exceeded.

The automation of testing has two major benefits. First, the automatic system operates at maximum speed all the time, whereas a human operator can sustain such speed for only a few minutes. Time and energy savings for a complete tunnel run is between 10 and 40 percent. In some particular tests, such as an ONERA power plant simulation which is limited by air storage capacity, as much data are realized in one run as were previously acquired in two runs. Second, the data are much more repeatable because the computer is able to hold much tighter tolerances on all independent parameters and ensure steady-state values of many dependent measurements.

AUTOMATIC CHECKING OF MEASURING UNITS

The improvement of testing techniques and the appearance of powerful digital means for data acquisition has resulted in a regular increase in the number of measuring channels used during tests.[15] For example, within 10 years the number of channels in the S1MA and S2MA tunnels has increased from an average of 20 to 45 to over 100. Although it is possible for an operator to check rather rapidly, once a day, the quality of a few tens of measuring channels, the operation is quite lengthy for a hundred channels if an accuracy of a few parts in ten thousand is required as well. Moreover, experience has shown that some failures of analog-to-digital converters would lead to isolated unrealistic readings that would be difficult to detect without the help of computer tools. Thus, with a view toward improving the measurement accuracy, accelerating the tests, and detecting errors or failures in measuring units, hardware and software have been implemented in the main facilities at AEDC and ONERA.

The problem of checking measurement devices is that of rapid detection of a possible difficulty in a system composed of several hundred instruments (Fig. 36). An overall checking method which consists of applying known physical values, whether static or dynamic (forces, pressures, etc.), to the measurement device is obviously effective and frequently used, but it is often difficult to implement and, consequently, limited most of the time to a few elementary tests: pressure steps on transducers, polars without wind, and verification of the zeros on the balances. These tests have, however, the merit of revealing most of the failures occurring at the level of transducers and their wiring.

With consideration for the extent of the instrumentation implemented, the technique discussed below is more restricted in purpose but more ambitious in the precision sought: the point is to provide rapidly the written proof that the fixed parts of the measuring units, viz, amplifiers, filters, multiplexer-converter(s), various connections and wirings, are in the correct state required by the test and provide an overall accuracy of $\pm 2 \times 10^{-4}$ of full scale. As the transducer supply voltage is automatically checked by other means, the search for failure is shorter, being restricted to only the transducers and their wiring. Furthermore, any doubts that may appear concerning the state of the measuring unit long after a test has been completed will have no foundation if the checks described below are made.

Figure 37 presents a diagram of the general principle of the ONERA checking method illustrated with a standard analog channel. In addition to the most direct "path" between the transducer and the computer and the decoupling amplifiers, there are voltage and function generators controlled by the data acquisition minicomputer and capable, via a "low level switch", of sending calibration signals instead of transducer signals through the amplifiers and other data acquisition components. A simplified channel, without amplifier or filter, allows direct access to the multiplexer-converter. The general principle of the checks consists in comparing a theoretical signal controlled by the minicomputer with the signal measured by the multiplexer-converter with an accuracy on the order of 1×10^{-4}. This is made possible by the quality of the instruments, and above all by that of the "low level switch" which does not introduce any contact voltages higher than one microvolt.

The checking method presently functions as follows:

- A/D multiplexer-converter - The device is calibrated by automatically applying voltages in 100 steps between ±10 volts. Ten of the steps occur very close to zero. Not only do these fine increments ensure that zero crossing occurs properly, but they also ensure that the low order bits are functioning properly at the higher voltage values. A mean value is calculated from 32 readings at each step. The entire process requires about four minutes.

- Correct gain and cutoff frequency - Both the amplifier gain and filter cutoff frequency, which are set manually, are rapidly checked by applying a step voltage to the measuring channel and monitoring the instantaneous signal value at several chosen times after the step initiation. The complete procedure takes about one minute.

- Zero, gain, and linearity of the measuring unit - Eight voltages are applied to the measuring unit. After allowing time for the filters to respond, an average value is calculated from the 32 samples at each step and compared with expected values. The value is considered correct if it does not deviate from the expected value by more than ±2 mv (10 v full scale) except around zero where only ±1 mv is allowable. Because 32 samples are taken it is also possible to have an idea of the noise on each channel. An error message is emitted if the peak-to-peak deviation reaches 5 mv. The duration of this check depends upon the filter cutoff frequency. For a 1-Hz low-pass filter, the check lasts about six minutes.

The complete checking procedure takes nearly 15 minutes or longer if heavy filtering is required. It has been proposed to have the checking procedure initiated automatically by the clock before the arrival of the wind tunnel staff. Subsequent checks would be performed during the operating shift if any doubt appears during the test unit operation.

REPEATABILITY OF THE TESTS DATA

Wind tunnel operators must constantly strive to privide test data that is not only accurate but also more reliable. At first, the repeatability of polars during the same test period is essential. But during the development of an aircraft family, the manufacturer often uses a calibration model as a reference during several testing programs which can extend over several years : wind tunnel tests data must then satisfy a long term repeatability.

Some improvements of the data repeatability have been obtained in the transonic test section in the ONERA S2 Modane wind tunnel. The horizontal walls of the test section are perforated and equiped with perforated sliding plates inside the plenum chamber (figure 38) which allows for porosity adjustement.

Chiefly in the subsonic range and for the maximum porosity (geometrical porosity 6 %), the repeatability of the data was deficient. For example, four contiguous polar curves at Mach 0.5 gave deviations of $5.3\ 10^{-4}$ for CD (figure 39). Such discrepancies are too large for transport aircraft project evaluation which requires about 2.10^{-4} for CD as typical specification.

In the closed wall configuration, the repeatability is clearly better (figure 39) : $1.5\ 10^{-4}$ for CD. Such walls perform to the above specification but, unfortunately, involve too large a wall interference as opposed to the perforated configuration giving negligible constraints.

Spectral analysis of both CN and CA coefficients recorded during four minute intervals shows a large disparity for the two wall configurations (figure 40), increasing towards low frequency end of the spectrum. For the closed walls, the amplitudes of CN and CA are very near those recorded without wind. Thus the repeatability deficiences were due to very low frequency phenomena induced by a non-linear characteristic of the perforated walls : static pressures on the walls and total pressures inside the perforations exhibited pressure variations (with long periods) when the difference between test section and plenum chamber pressures were negligible.

For the case of the maximum porosity walls, a numerical filtering, at very low cutting frequency, was applied to the data. This method improved the repeatability by a factor of two (figure 39) but still does not meet the criteria. As a result the angle of attack sweeping speed during the tests must be reduced.

But thanks to a reduction of the porosity, by sliding the translation plates, the CL variances are quickly improved (figure 41). For the value of the geometrical porosity 2.9% the CL variation is reduced to the value obtained for closed walls. Under these conditions, the repeatability for four contiguous polar curves are now 1.5 10^{-4} for CD. The lift gradient deviations are reduced by 5times (figure 42); the wall interference is tolerable (2.5 % in CL_α).

This example shows the effects of improvements in the flow quality on the repeatability of the data provided to the customers.

CORRECTIONS APPLIED TO WIND TUNNEL DATA

Generaly, the model size is chosen as large as possible to obtain large Reynolds number. On the other hand, the support system size increases with the aerodynamic loads; accordingly the determination of equivalent data corresponding to "unconfined" flow, without support needs some corrections.

The sting interferences can be deduced from measurements of local pressures, at the fuselage location, with and without the sting to take account into the flow quality. Figure 43 shows the pressures induced by a "Z" sting used in the S2 Modane wind tunnel for a transport aircraft model in longitudinal configuration. Theoretical calculations can give the overall field of the support (intensity and orientation). For this purpose, Aerospatiale [16] has developed computer programs based on subcritical potentiel calculation in inviscid flow using a method of singularities distributed on panels with compressibly correction. Such theoritical data are in good agreement with experimental measurements (figure 43).

The current computer capacity allows caculations of sophisticated mounting schemes , as illustrated on figure 44, for the analysis of the drag interference due to a "Z" sting on a fuselage afterbody. By comparison with the K_p distribution, without the "Z" sting, such calculations allow an optimization of the mounting for minimum interference. The interference of the two-stings on the fuselage shown on figure 45 are very small ($\Delta K_p < 0.01$).

Another example is relative to the study of the longitudinal location of the "Z" sting in the rear part of the fuselage : a rearward location gives a small interaction localized on the afterbody, whereas a forward location of the sting modifies the whole fuselage field.

Even with the optimized sting location, the buoyancy correction remains important : for the configurations shown on figure 43 the CD for Mach 0.8 must be corrected by 16.10^{-4}.

The downwash at the horizontal tail, due to the sting effect must be known to obtain the true tail setting; Up to now this correction is obtained by a theoritical approach.

Wall interferences usually involve corrections for conventional test sections. The knowledge of the perturbation velocities (axial and vertical) induced by the walls gives the corrected Mach number and local angle of attack distributions along wing, tail and fuselage. By integration, these local corrections give the overall corrections to the aerodynamic coefficients and α. Much better wall corrections can be applied since the development of sophisticated computer programs. A recent AGARD/FDP meeting, in London (may 1982) has devoted two sessions for the wall effects in conventional test sections and one session for the new adaptive walls concept [17].

At ONERA, new approches are in progress [18] to increase the accuracy of the wall corrections, especially for large transport aircraft models in the transonic S1 and S2MA wind tunnels. The mathematical description of the model has been improved by increasing the number of singularities and by taking into account their exact location inside the test section : this parameter is more important for large angles of attack of fighter models. Moreover, the mathematical modeling includes the model support system.

A sufficient theoritical description is verified by measurements of the wall pressures for closed wall testing : the comparison between measured and calculated distributions shows (figure 45) a poor agreement with only one doublet representing the model volume; a good agreement is limited to the first part of the fuselage with 20 doublets representing the model volume; but with 15 more doublets for the sting, the agreement becomes satisfactory all along the walls in front of the model. For the lifting term, described by a vortex sheet, the comparison deals with the measured and calculated gradient of Mach number between top and bottom walls versus CL. Figure 46 shows the good agreement obtained on two orthogonal sections (X, Y = 0).

Formerly, the porosity factor laws were deducted, for a test section from reference tests in a closed wall section or in a very large tunnel, with the same model; but now, the porosity distributions, along the walls, are obtained "in situ" from a comparison between measured and calculated pressure distributions.

For 2 Dim. testings, the wall corrections are calculated directly from the model "signature" on the walls, avoiding the using of porosity factor [19].

For 3 Dim. testings, the formulation of the same method exists, but is not yet applied for routine tests; an indirect method is studied through the explicite evaluation of the porosity factor distribution on the walls. Some investigations on uniform porosity concept are in progress in S1 and S2MA tunnels. Using a parametric calculation of the blockage and lift "signatures" on the walls, versus the porosity factor, a comparison with the measured distributions has been obtained in the S3MA wind tunnel equiped with perforated walls. The above assumption of the uniform porosity concept is confirmed as shown on figure 47 and 48, at least for this case.

The corrected data accuracy depends directly on the sophistication of this mathematic modeling.

Up to now, some parts of the model, like nacelles, separated regions for ventilated walls, etc.., are not taken into account in the mathematical description of the aircraft model, due to computing difficulties and/or excessive time requirements.

TEST DATA COMPARISONS

The usual way to evaluate test data accuracy remains the comparisons of various test, obtained from:

- data on the same model in the same wind tunnel with various configurations (plain, slotted, perforated)
- data on the same model in several wind tunnels with various test section sizes,
- data on similar models in several wind tunnels.

Of course, a correlation between wind tunnel and flight data will be the ultimate objective.

In this view, a program was initiated in 1969 by ONERA [20] to test a serie of similar calibration models, representative of a transport aircraft in various transonic tunnels in seven countries. A paper, limited to the results obtained with the largest model (M5) in six establishments (AEDC, NAE, NASA Ames, NLR, ONERA, RAE) was presented at the AGARD/FMP Meeting in Paris in 1977 [21]. Figures 49, 50 recall some of these comparisons on the aerodynamic forces and on mean chord pressure distributions.

For development tests, ONERA has in operation : three tunnels at Modane (S1, S2, S3MA), one at FAUGA (F1) and one at TOULOUSE (T2); thus many correlations are available between data obtained in these tunnels on the same or similar models.

In two-dimensional flow, the recent operation of the T2 tunnel with adaptive walls [22] allows an interesting comparison with the data on the same supercritical CAST 7 wing section obtained in S3MA tunnel equiped with conventional perforated or plain walls. The C_L, α curves, obtained at S3MA with closed and perforated walls are very different before wall corrections. Applying these corrections, a good agreement is obtained. Furthermore those S3MA results (figure 51) correlated very well with the T2 data. Although the wall signatures are very different for the three test section configurations, the pressure distributions on the profile are very quite similar (figure 52). The advantage of adaptive walls is obvious, because the ratio between the profil chord and the tunnel height in T2 is twice the value used in S3MA.

In three dimensional flow, a comparison of data obtained in F1 and S1MA tunnels on a fighter model (figure 53) shows a good agreement even at very large angles of attack, up to 35 degrees. Some other correlations are not so encouraging, especially with separated flow (figure 54) even before the vortex bursting [23].

Figure 55 gives a comparison between the F1 tunnel data on a 1/10th scale model of the MERCURE 100 aircraft and the flight data provided by the DASSAULT company. For cruise and take-off configurations, the agreement is very good. For the landing configuration tests were made with the undercarriage up in F1 and down in flight : but the trimmed polar curves are still parallel for the take-off configuration as indicated.

Such correlations give confidence in wind tunnel predictions but they need a permanent effort from wind tunnel operator to improve the test methodologies and specific contributions from the manufacturers.

CONCLUDING REMARKS

This paper does not give an exhaustive review of recent innovations in wind-tunnel operation. For exemple, Acroelasticity and Active control, to be discussed by other authors in their symposium, have been omitted as well as discussions of cryogenics and adaptive walls tunnels and on-line wall interference assessment in conventional tunnels which are today not ready for customers. Progress in test effectiveness has taken so many approaches that a full survey would look like a windtunnel operator handbook. However the authors endeavoured to illustrate the trends along the "three fronts" :

- increasing the amount of information,
- reducing test costs per data unit, and
- improving data quality.

These permanent challenges arise from the evolutionary requirements of flying vehicles. Figure 56 sketches some of the relations between customers needs and test improvements. These improvements make up a fundamental aspect of wind-tunnel work, strongly supported... and seldom challenged... by computer programs. Future progress will continue the integration of computational power with improved test techniques to yield and optimal wind tunnel system to maximize test effectiveness.

REFERENCES

[1] Bécle, J.P., ONERA, et Perin, R., AEROSPATIALE, "Essais en soufflerie de maquettes motorisees. Comparaison de deux méthodes de simulation des jets des reacteurs, "AGARD FDP Symposium, Toulouse, France, 11-14 Mai 1981, T.P. ONERA No. 1981-42.

[2] Palko, R. L. and Lohr, A. D., ARO, Inc., "A Constant Aerodynamic Parameter Testing Technique with Automatic Wind Tunnel Control," AIAA Paper 78-784, 10th Aerodynamic Testing Conference, April 19-21, 1978.

[3] Palko, R. L., ARO, Inc., "A Computer-Controlled Closed-Loop Vehicle Trim System Developed in the PWT at AEDC," Proceedings AIAA 9th Aerodynamic Testing Conference, June 7-9, 1976.

[4] Palko, Richard L. and Crawford, Margaret Ann, Calspan Field Services, Inc., "Aerodynamic Parameter Optimization during Wind Tunnel Testing," AIAA Paper 82-0600, 12th Aerodynamic Testing Conference, March 22-24, 1982.

[5] Levinsky, Ely S., General Dynamics Corp., and Palko, Richard L., Calspan Field Services, Inc., "Tests of a Computer-Controlled Self-Optimizing Variable Geometry Wing," AIAA Paper 82-599, 12th Aerodynamic Testing Conference, March 22-24, 1982.

[6] Palko, Richard L. and Cassady, Patrick L., Calspan Field Services, Inc., "Photogrammetric Development and Application at AEDC," AIAA Paper 82-0610, 12th Aerodynamic Testing Conference, March 22-24, 1982.

[7] Chapman, R. G., Calspan Field Services, Inc., "A Computer Network for Continuous Control of a Captive Trajectory System," ISA International Instrumentation Symposium, Seattle, Washington, May 1981.

[8] Boutier, A., ONERA, "Velocimétrie laser a' S3 Modane," La Recherche Aerospatiale, 1981, No. 6, pp. 611-615.

[9] Bomar, B. W., Goethert, W. H., Belz, R. A., and Bentley, H. T., ARO, Inc., "The Development of a Displacement Interferometer for Model Deflection Measurements," AEDC-TR-76-116 (AD-A034384), January 1977.

[10] Goethert, W. H., ARO, Inc., "A Direct Model Pitch Measurement with a Laser Interferometer Using Retroreflectors," AEDC-TR-79-87 (AD-A090722), October 1980.

[11] Bazin , M., Grandjacques, M., Regard, D., et Bion, J. R., ONERA, "Mesures instationnaires dans les prises d'air," T. P. ONERA No. 1981-119.

[12] Grandjacques, M., ONERA, "Mesures instationnaires" dans une prise d'air," T. P. ONERA No. 1979-50.

[13] Bouis, X., Gavet, G., et Combaz, R., ONERA, "Automatic Checking of Measuring Units in the Modane Wind Tunnels," T. P. ONERA No. 1982-10.

[14] Tisseau, R., ONERA, "Wind-Tunnel Model Support Controlled by Four Microprocessors," IMEKO/IFAC Symposium, London, England, 17-20 Novembre 1980, T. P. ONERA No. 1980-169.

[15] Grenat, G., ONERA, "Utilisation des ordinateurs associés aux souffleries du Centre de Modane," AGARD/VKI, 23-24 Juin 1978, T. P. ONERA No. 1976-110.

[16] Le Gall, G., Bousquet, J., et Yermia M., Aerospatiale, "Une méthode numérique pour l'étude de l'interaction nacelle-jet-voilure en écoulement tridimensionnel non visqueux", AGARD A.R.173, Toulouse 1981.

[17] "Wall interference in wind tunnels", AGARD CP à paraître, Londres, 1982.

[18] Vaucheret, X., ONERA, "Améliorations des calculs des effets de parois dans les souffleries industrielles de l'ONERA", AGARD/FDP, Londres, 1982. TP ONERA 1982-34.

[19] Capelier C., Chevallier J.P., Bouniol F., ONERA, "Nouvelle méthode de correction des effets de parois en courant plan", La Recherche Aérospatiale n° 1978-1.

[20] Vaucheret X., Bazin M., Armand C., ONERA, "Comparaison d'essais transoniques bi et tridimensionnels effectués dans diverses grandes souffleries", AGARD C.P. 187, Valloire, 1975.

[21] Poisson-Quinton Ph., Vaucheret X., ONERA, "Prévision des caractéristiques aerodynamiques d'un avion d'après la comparaison des résultats sur une maquette étalon dans diverses grandes souffleries transoniques", AGARD CP 242, Paris, 1977 - TP ONERA 1978-22.

[22] Archambaud J.P., Chevallier J.P., ONERA, "Use of Adaptive walls in 2-D tests", AGARD/FDP Londres, 1982

[23] Vaucheret X., ONERA, "Améliorations envisagées pour résoudre les problèmes rencontrés au cours d'essais à grande incidence de maquettes en souffleries", AGARD Report N° 692, Munich, 1980.

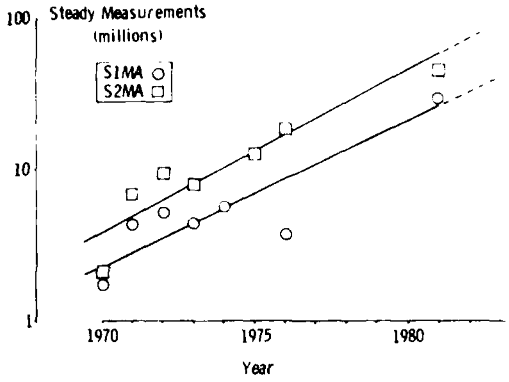

Figure 1. Trends in Measurement Requirements

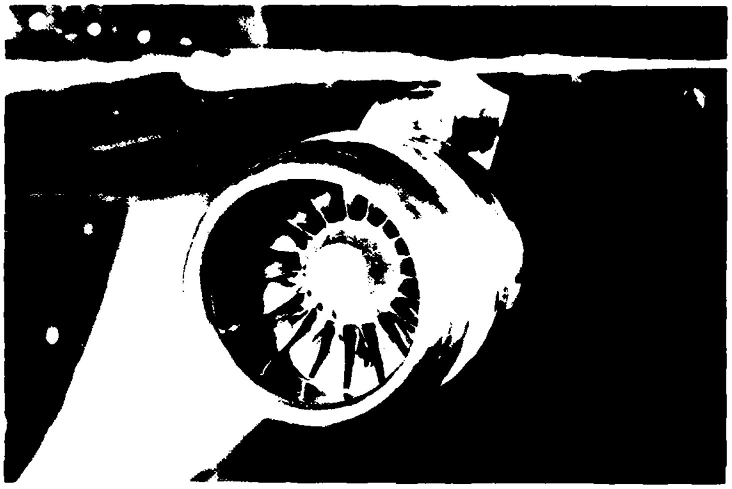

Figure 2. Turbine Powered Simulator Installed on Transport Aircraft Model

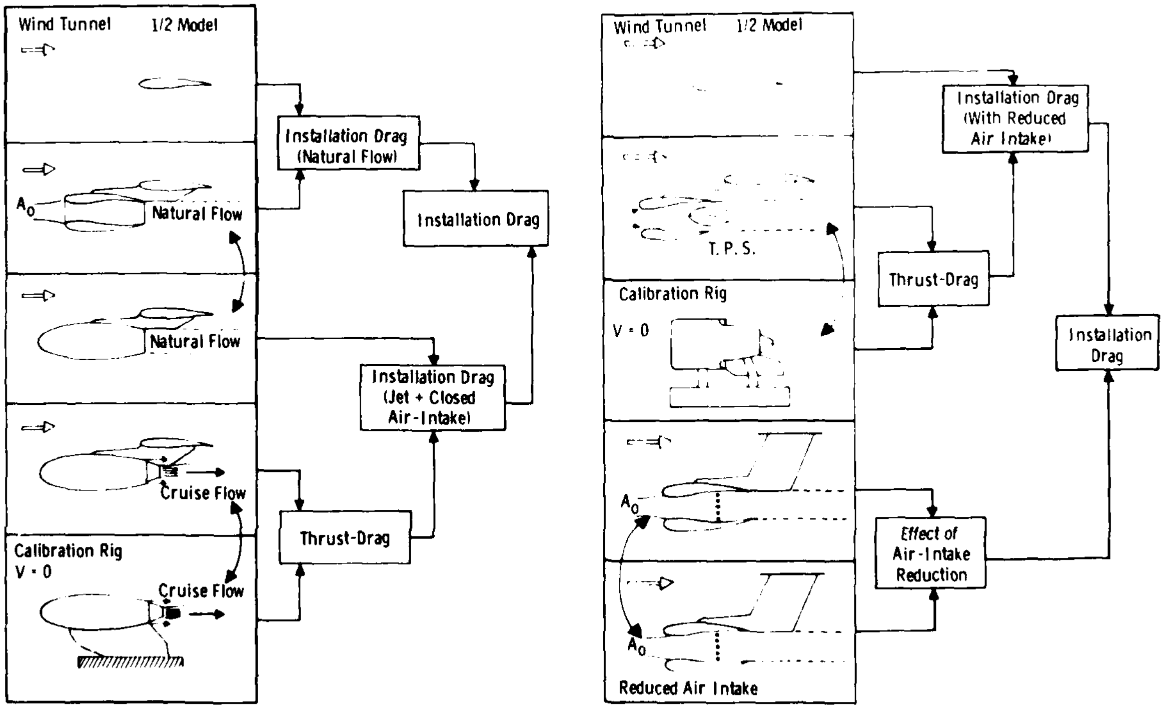
Wind Tunnel
1/2 Model
Installation Drag
(Natural Flow)
A_0
Natural Flow
Installation Drag
Natural Flow
Installation Drag
(Jet + Closed
Air-Intake)
Cruise Flow
Thrust-Drag
Calibration Rig
V = 0
Cruise Flow
Wind Tunnel
1/2 Model
Installation Drag
(With Reduced
Air Intake)
T. P. S.
Thrust-Drag
Calibration Rig
V = 0
Installation
Drag
A_0
Effect of
Air-Intake
Reduction
A_0
Reduced Air Intake

a. Blown Nacelle

b. Turbine Powered Simulator

Figure 3. Force Accounting System for Installed Drag

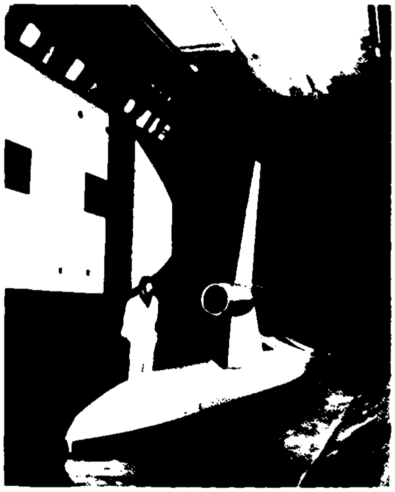

Figure 4. Reflection Plane Model in S1MA Tunnel

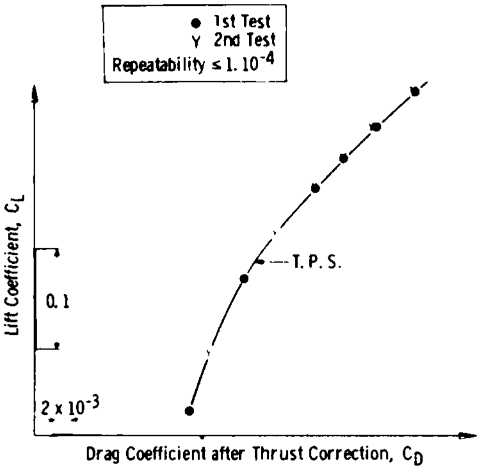

Figure 5. Example of Data Repeatability

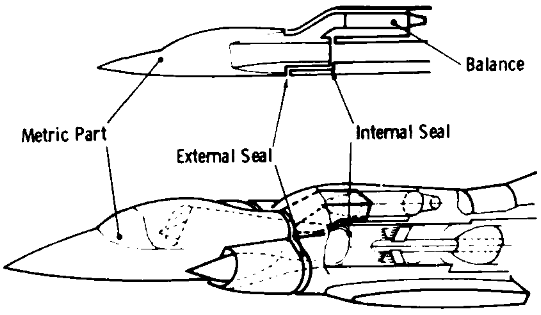
Balance
Metric Part
Internal Seal
External Seal

Figure 6. Inlet and Forebody Drag Measurements

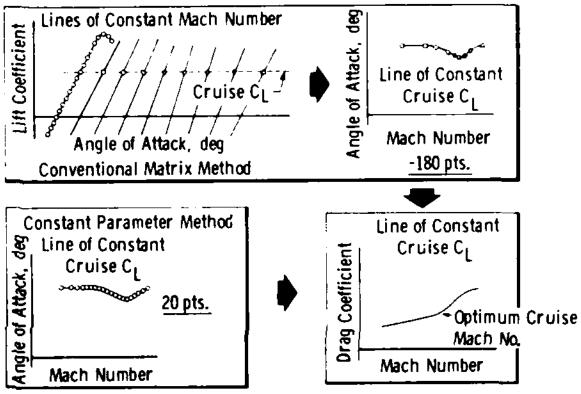
Lines of Constant Mach Number
Lift Coefficient
Cruise C_L
Angle of Attack, deg
Conventional Matrix Method
Angle of Attack, deg
Line of Constant Cruise C_L
Mach Number
-180 pts.
Constant Parameter Method
Angle of Attack, deg
Line of Constant Cruise C_L
20 pts.
Mach Number
Line of Constant Cruise C_L
Drag Coefficient
Optimum Cruise Mach No.
Mach Number

Figure 7. Test Reduction via Constant Parameter Method

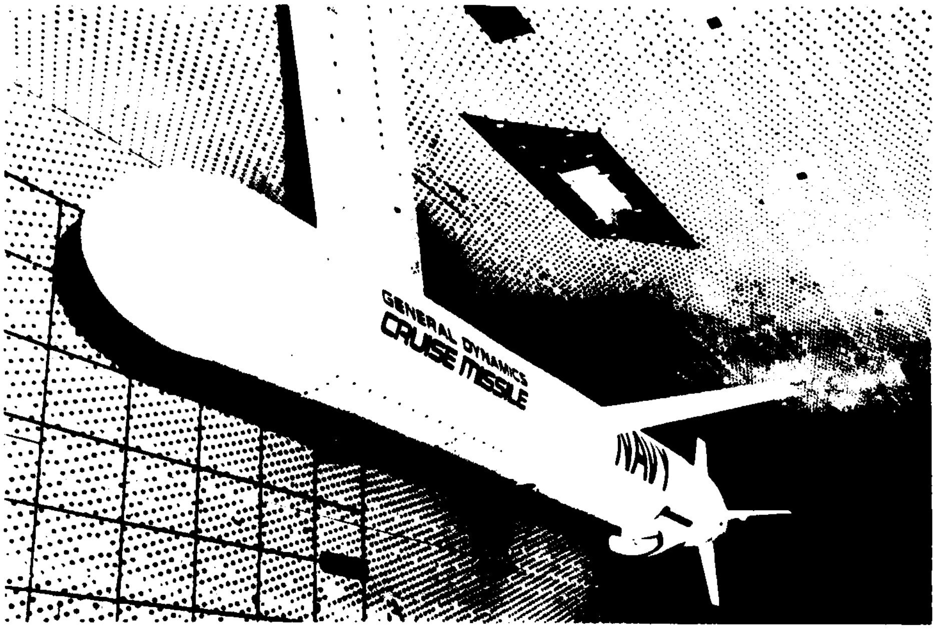
GENERAL DYNAMICS
CRUISE MISSILE
NAVY

Figure 8. General Dynamics Cruise Missile Installed in the PWT-16T

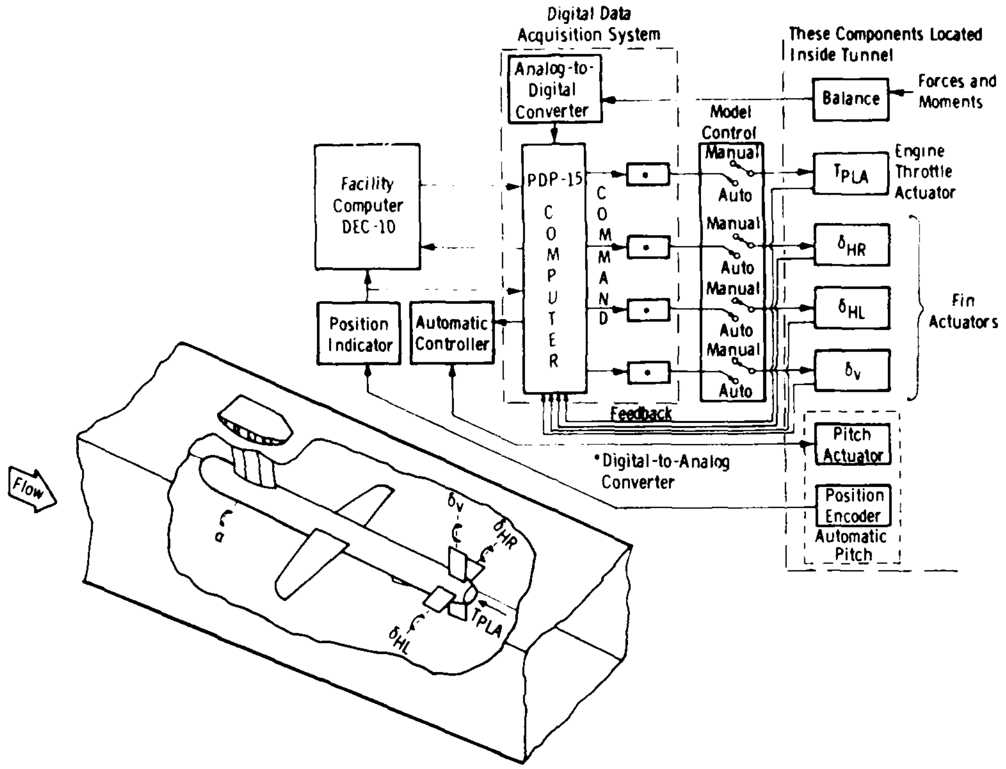
Digital Data
Acquisition System
Analog-to-Digital Converter
These Components Located Inside Tunnel
Balance
Forces and Moments
Model Control
Facility Computer DEC-10
PDP-15 COMPUTER
COMMAND
Manual
Auto
Engine Throttle Actuator
T_{PLA}
δ_{HR}
δ_{HL}
δ_V
Fin Actuators
Position Indicator
Automatic Controller
Feedback
Pitch Actuator
Position Encoder
Automatic Pitch
*Digital-to-Analog Converter
Flow
α
δ_V
δ_{HR}
δ_{HL}
T_{PLA}

Figure 9. Cruise Missile Test Control System

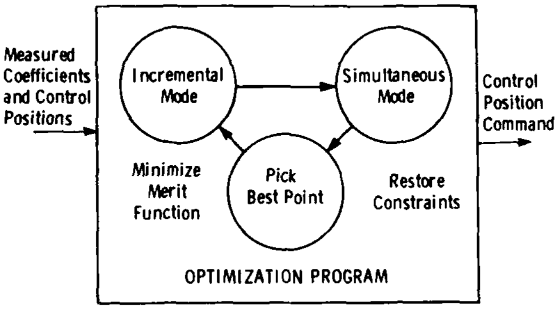
Measured Coefficients and Control Positions
Incremental Mode
Simultaneous Mode
Pick Best Point
Minimize Merit Function
Restore Constraints
Control Position Command
OPTIMIZATION PROGRAM

Figure 10. Flow Chart for Optimization Procedure

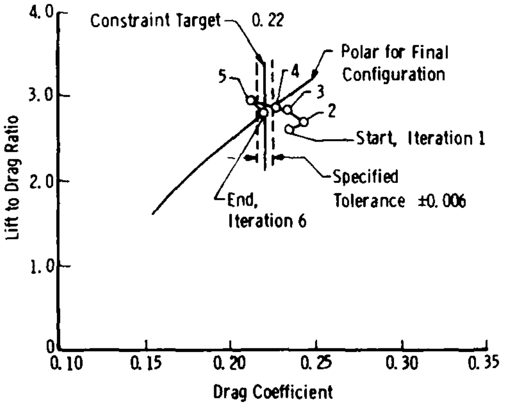

Figure 11. Convergence Process to Maximize Lift-to-Drag Ratio

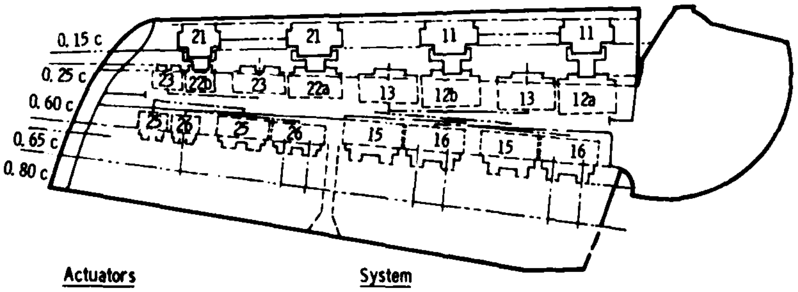
0.15 c
0.25 c
0.60 c
0.65 c
0.80 c
21
21
11
11
23
22b
23
22a
13
12b
13
12a
25
26
25
26
15
16
15
16

Actuators	System
11, 21	Leading-Edge Radius System
12a, 12b, 13, 22a, 22b, 23	Front Spar Leading-Edge Deflection System
15, 16, 25, 26	Rear Spar Trailing-Edge Deflection System

a. Planview Showing Locations of the Wing Hydraulic Actuators

Figure 12. Self-Optimizing Flexible Technology Wing

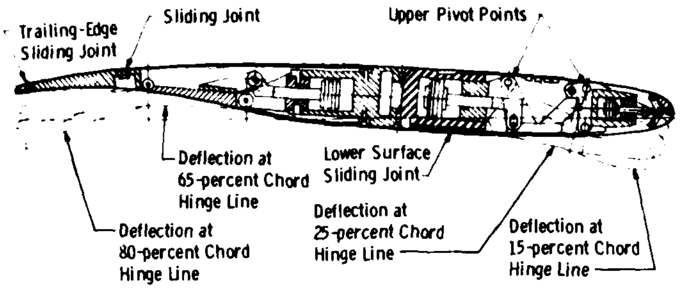
Trailing-Edge Sliding Joint
Sliding Joint
Upper Pivot Points
Deflection at 65-percent Chord Hinge Line
Lower Surface Sliding Joint
Deflection at 80-percent Chord Hinge Line
Deflection at 25-percent Chord Hinge Line
Deflection at 15-percent Chord Hinge Line

b. Typical Cross Section through Leading- and Trailing-Edge Systems Showing Leading-Edge Lower Surface and Trailing-Edge Sliding Skin Joints

Figure 12. Concluded

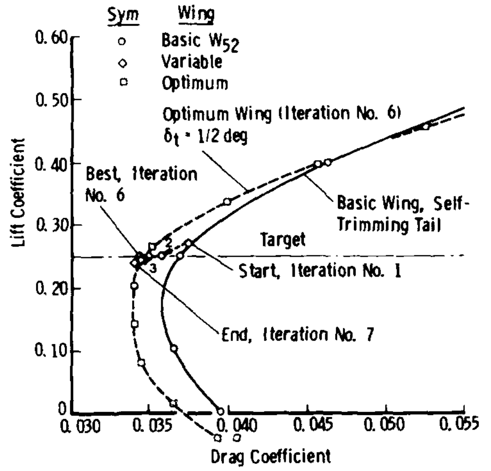

Figure 13. Convergent Process to Minimize Drag, Specified Lift

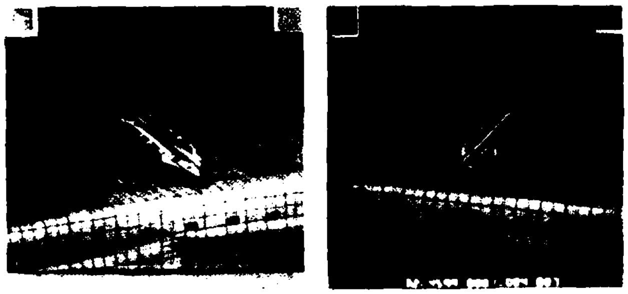

Left

Right

Figure 14. Stereo Photographic Pair of Calibration Body and Grid Overlay

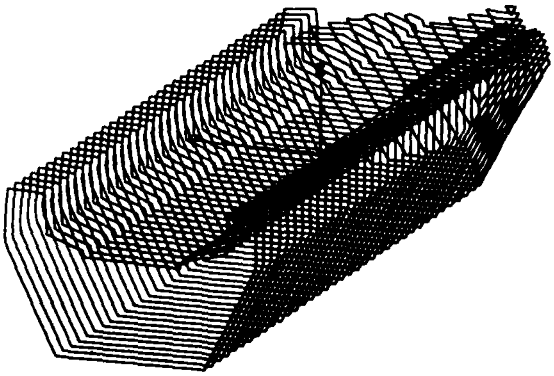

Figure 15. Computer Graphic Display of Calibration Body

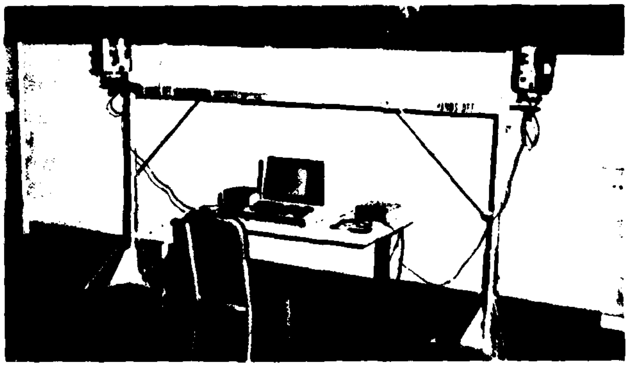

Figure 16. Digital Theodolite Measurement System

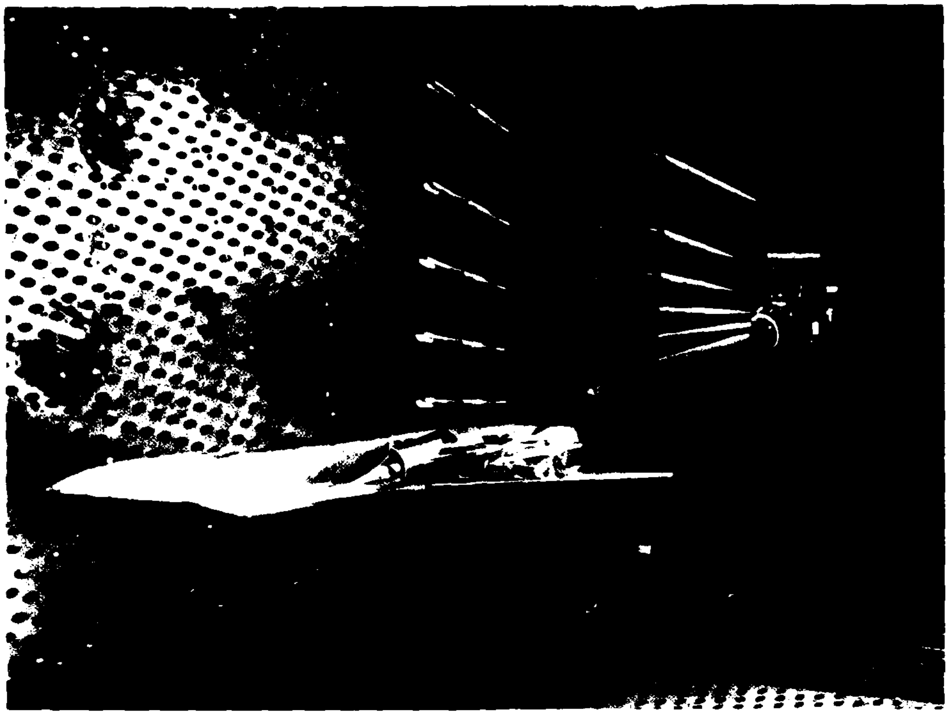

Figure 17. CTS Installation Photograph Showing Multiple Locations of the Released Store

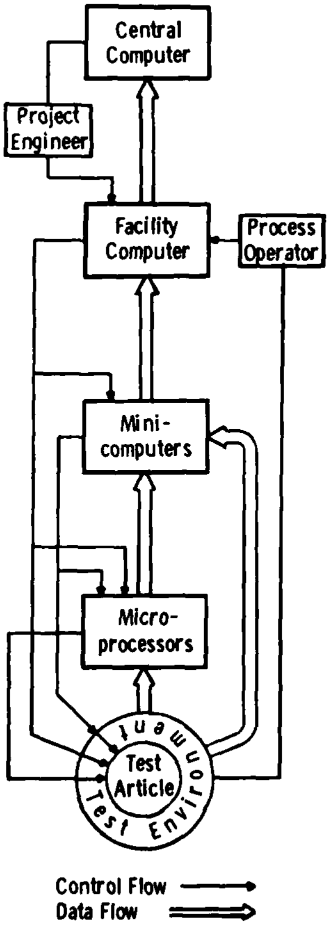
Central Computer
Project Engineer
Facility Computer
Process Operator
Mini-computers
Micro-processors
Test Article
Test Environment
Control Flow
Data Flow

LEVEL 1

- 10- to 100-sec Response Time
- Extended Analytical Support
- Data Edit and Rerun
- Math Modeling
- Archival Data Storage

LEVEL 2

- 10-msec to 10-sec Response Time
- Test Management and Direction
- Primary Performance Data Calculations
- On-Line Data Display

LEVEL 3

- 1-µsec to 10-msec Response Time
- Data Acquisition and Control
- Numerical Filtering and Preprocessing
- Test Environment and Test Article Control

LEVEL 4

- 1-µsec to 1-sec Response Time
- Status and Alarm Monitoring
- Message Output and Logging
- Dedicated Control Functions

Figure 18. Four-Level Hierarchical Distributed Computing System

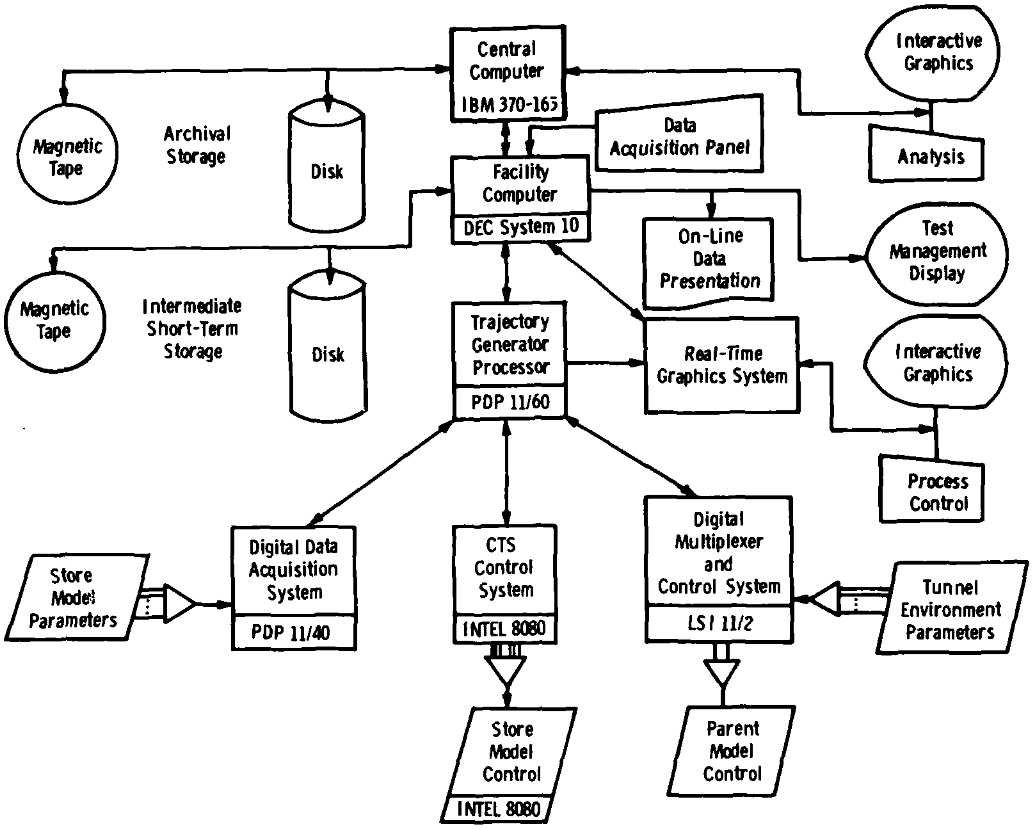
Central Computer
IBM 370-165
Magnetic Tape
Archival Storage
Disk
Data Acquisition Panel
Interactive Graphics
Analysis
Facility Computer
DEC System 10
On-Line Data Presentation
Test Management Display
Magnetic Tape
Intermediate Short-Term Storage
Disk
Trajectory Generator Processor
PDP 11/60
Real-Time Graphics System
Interactive Graphics
Process Control
Store Model Parameters
Digital Data Acquisition System
PDP 11/40
CTS Control System
INTEL 8080
Digital Multiplexer and Control System
LSI 11/2
Tunnel Environment Parameters
Store Model Control
INTEL 8080
Parent Model Control

Figure 19. Distributed Computer System Configuration for the Captive Trajectory

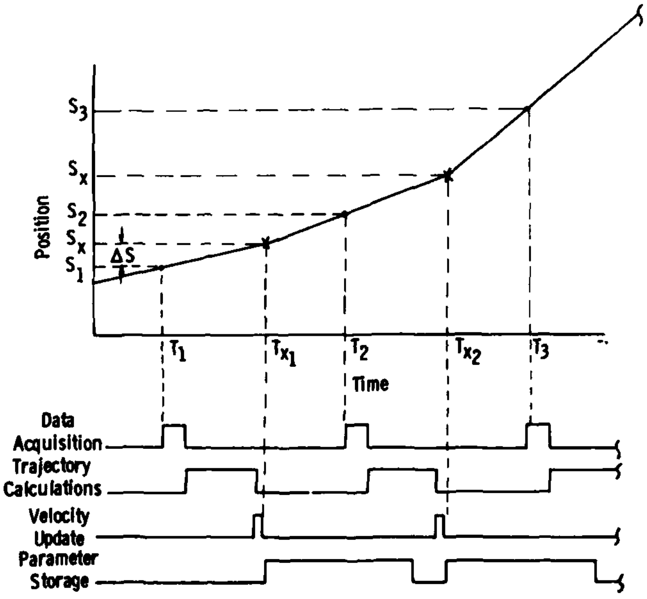

Figure 20. Timing Diagram for Trajectory Generation via Velocity Control

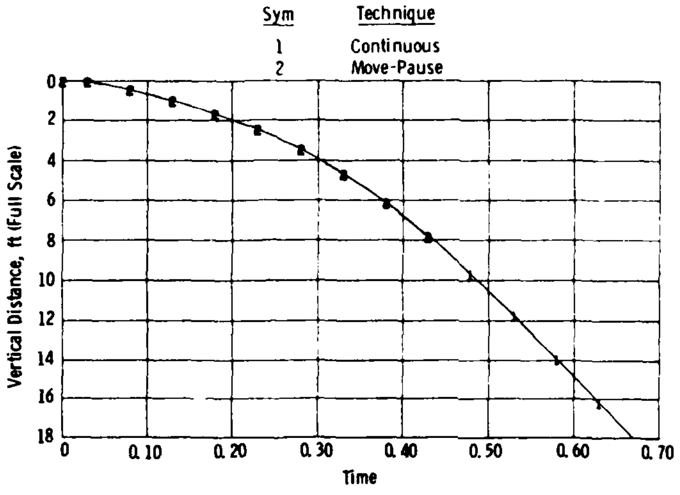

a. Vertical Distance

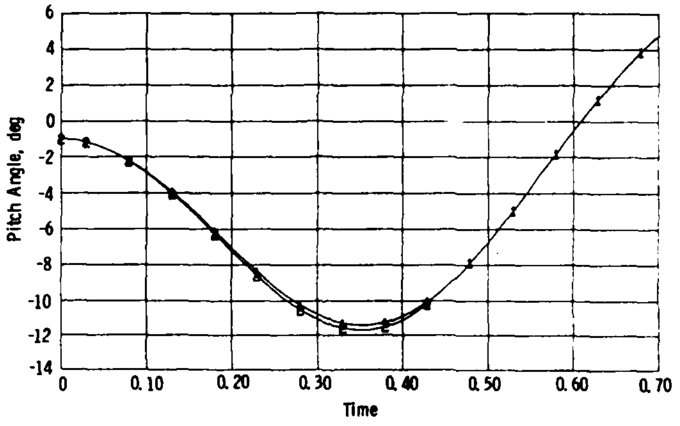

b. Pitch Angle

Figure 21. Comparison of Trajectories from Continuous and Move-Pause Operating Mode

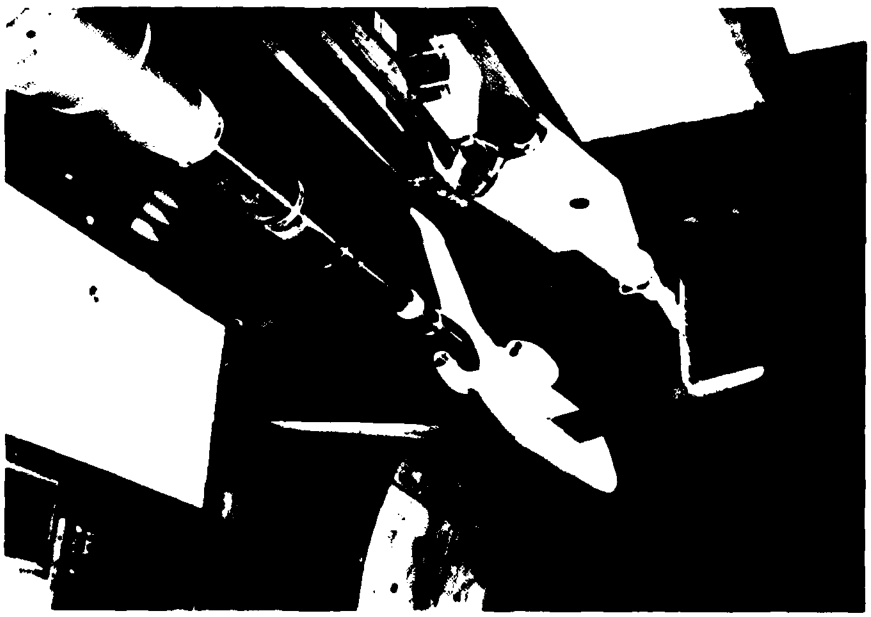

Figure 22. Flow Field Survey Mechanism in S1MA

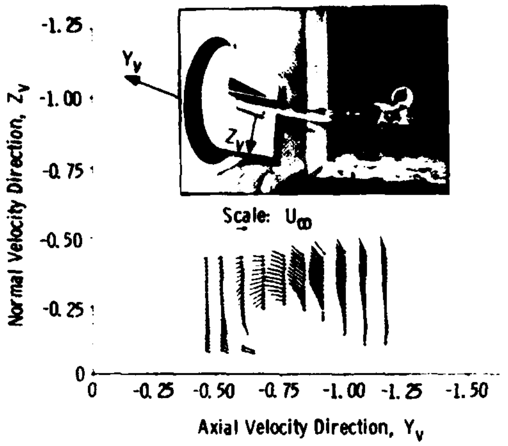

Figure 23. Typical Crossflow Velocity Vector Measurements in S2MA, $M_\infty = 0.274$, $\alpha = 19$ deg, $Re = 2.3 \times 10^6$

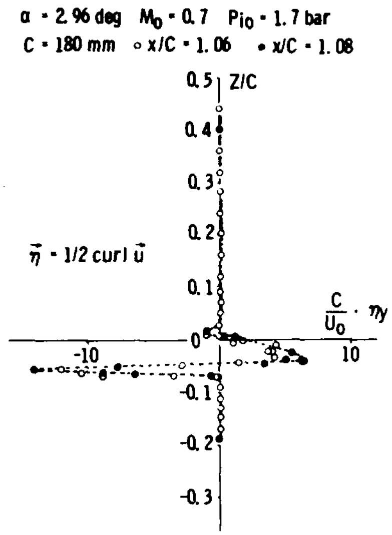

Figure 24. Vorticity in the Wake of a 2-D Profile Obtained by Laser Anemometry, S3MA

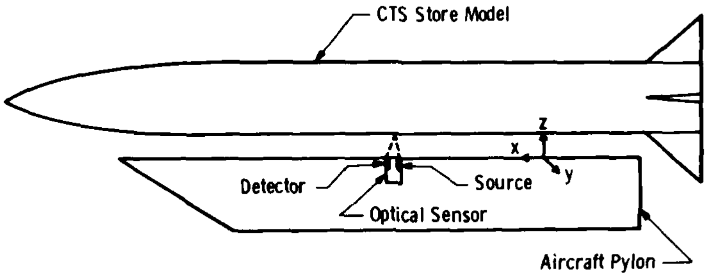
CTS Store Model
z
x
y
Detector
Source
Optical Sensor
Aircraft Pylon

Figure 25. Illustration of CTS Store Model in Carriage Position and Optical Sensor in Pylon

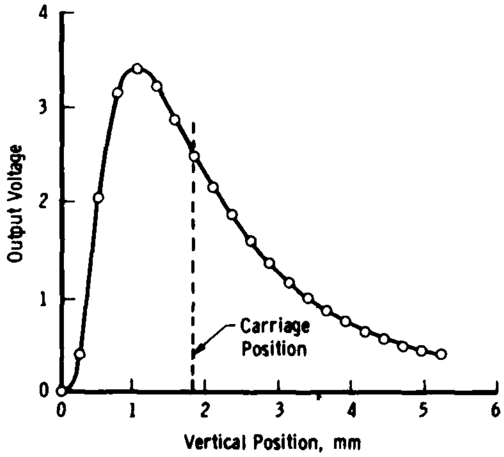

Figure 26. Typical Optical Sensor Output Signal with Variations in Vertical Position of Store

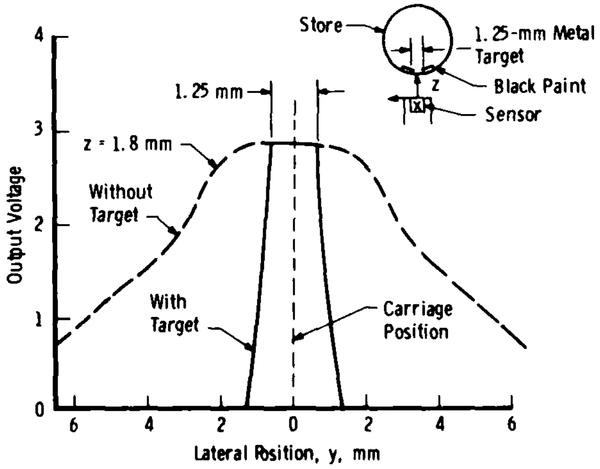

Figure 27. Typical Optical Sensor Signal with Lateral Variations in the Store Position

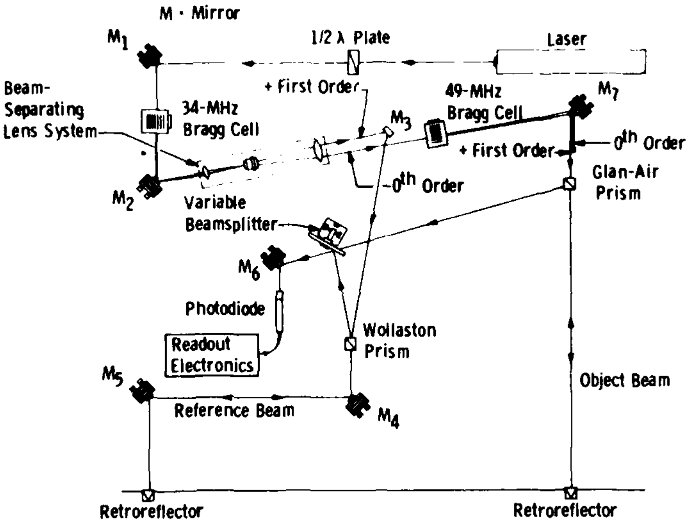
M · Mirror
M1
1/2 λ Plate
Laser
Beam-
Separating
Lens System
34-MHz
Bragg Cell
+ First Order
49-MHz
Bragg Cell
M7
M3
0th Order
+ First Order
M2
-0th Order
Glan-Air
Prism
Variable
Beamsplitter
M6
Photodiode
Readout
Electronics
Wollaston
Prism
M5
Reference Beam
M4
Object Beam
Retroreflector
Retroreflector

Figure 28. Two-Beam Interferometer Optical System

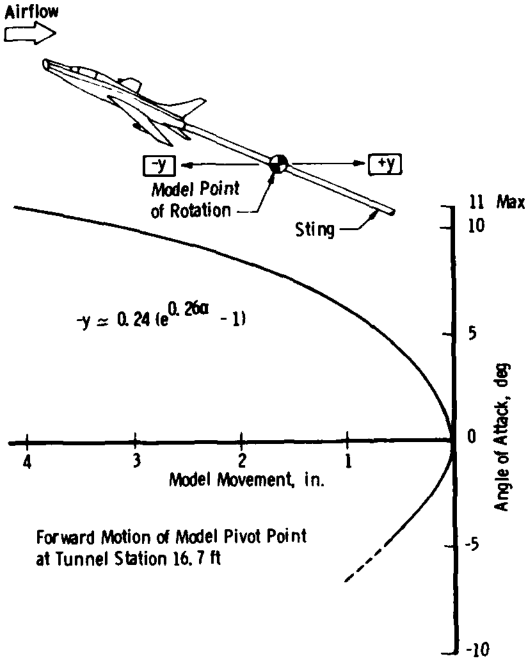

Figure 29. Model Pivot Point Forward Motion with Angle Setting of Sting Support System

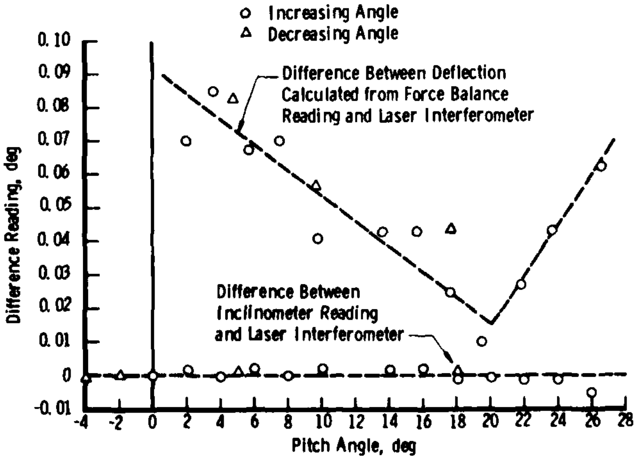

Figure 30. Comparison Between Interferometer Inclinometer and Computed Deflection, Air-Off

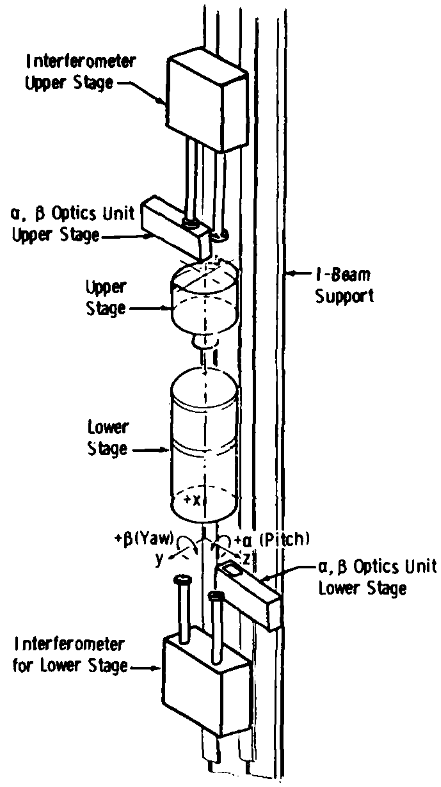
Interferometer Upper Stage
α, β Optics Unit Upper Stage
I-Beam Support
Upper Stage
Lower Stage
+x
+β(Yaw)
+α (Pitch)
y
z
α, β Optics Unit Lower Stage
Interferometer for Lower Stage

Figure 31. Interferometer Arrangement for Missile Staging Test

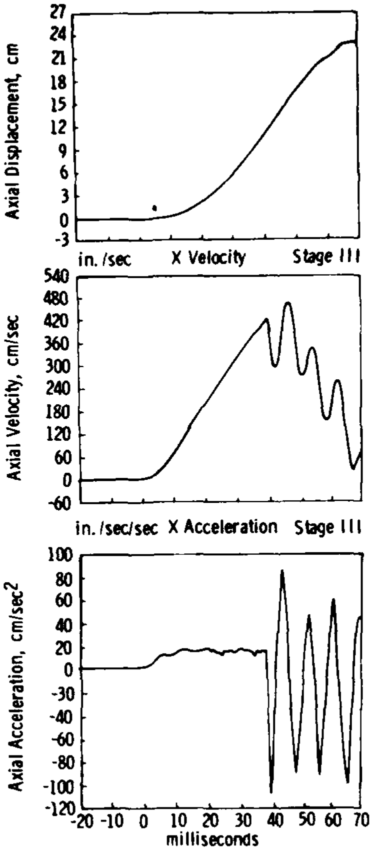

Figure 32. Typical Model Displacement, Velocity and Acceleration

Figure 33. Inlet Duct Dynamic Pressure Rake with Transducer Temperature Compensation Network

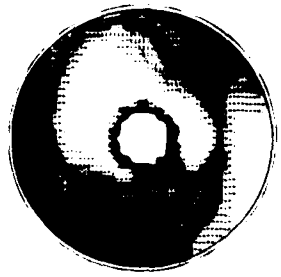

Dark Areas:
Low Total Pressure

Figure 34. Instantaneous Pressure Distortion in Inlet Duct

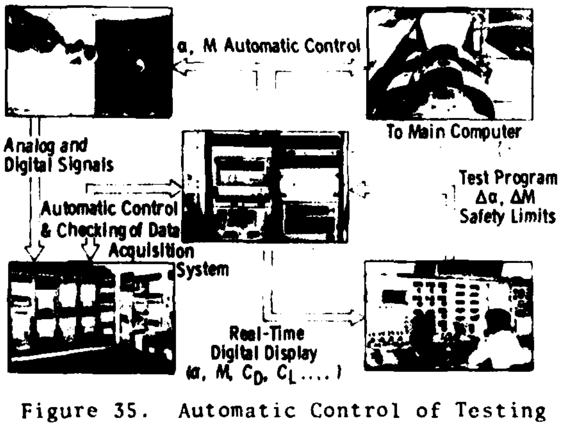
α, M Automatic Control
To Main Computer
Analog and Digital Signals
Automatic Control & Checking of Data Acquisition System
Test Program
Δα, ΔM
Safety Limits
Real-Time Digital Display
(α, M, C_D, C_L ....)

Figure 35. Automatic Control of Testing

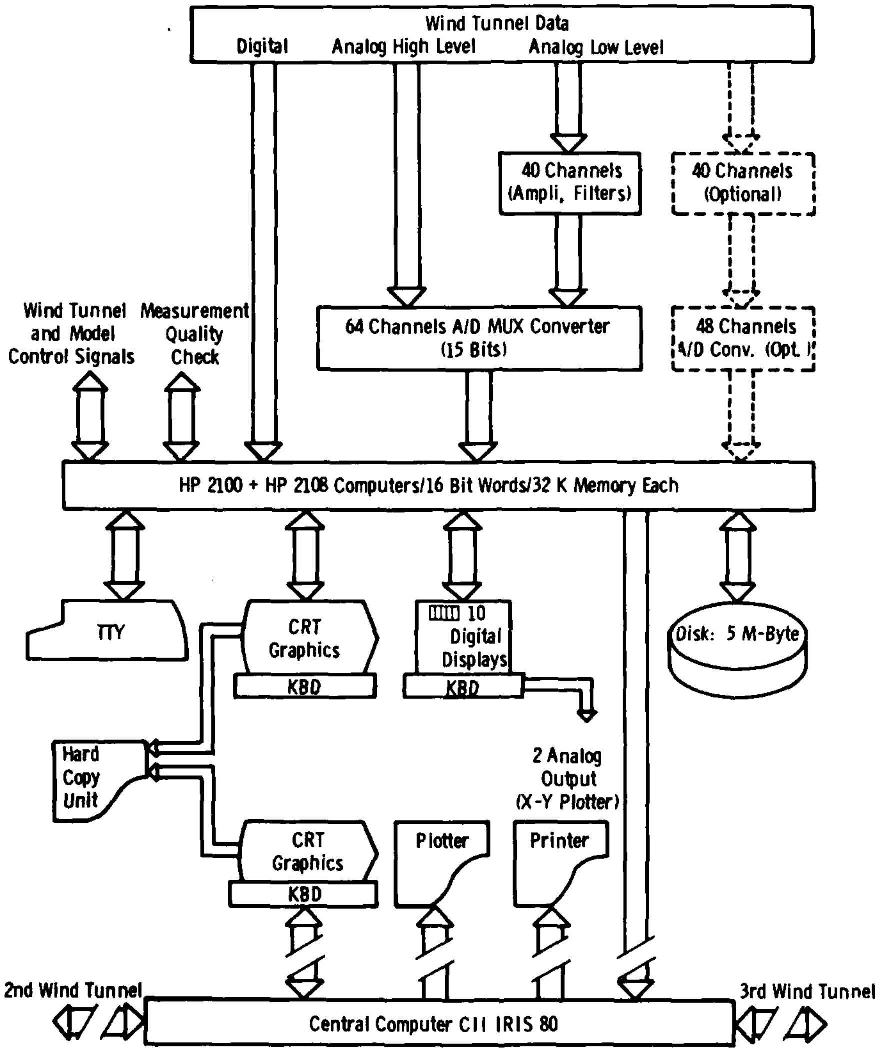
Wind Tunnel Data
Digital
Analog High Level
Analog Low Level
40 Channels (Ampli, Filters)
40 Channels (Optional)
64 Channels A/D MUX Converter (15 Bits)
48 Channels A/D Conv. (Opt.)
Wind Tunnel and Model Control Signals
Measurement Quality Check
HP 2100 + HP 2108 Computers/16 Bit Words/32 K Memory Each
TTY
CRT Graphics
KBD
10 Digital Displays
KBD
Disk: 5 M-Byte
Hard Copy Unit
2 Analog Output (X-Y Plotter)
CRT Graphics
KBD
Plotter
Printer
2nd Wind Tunnel
Central Computer CII IRIS 80
3rd Wind Tunnel

Figure 36. Typical Data Acquisition (1981)

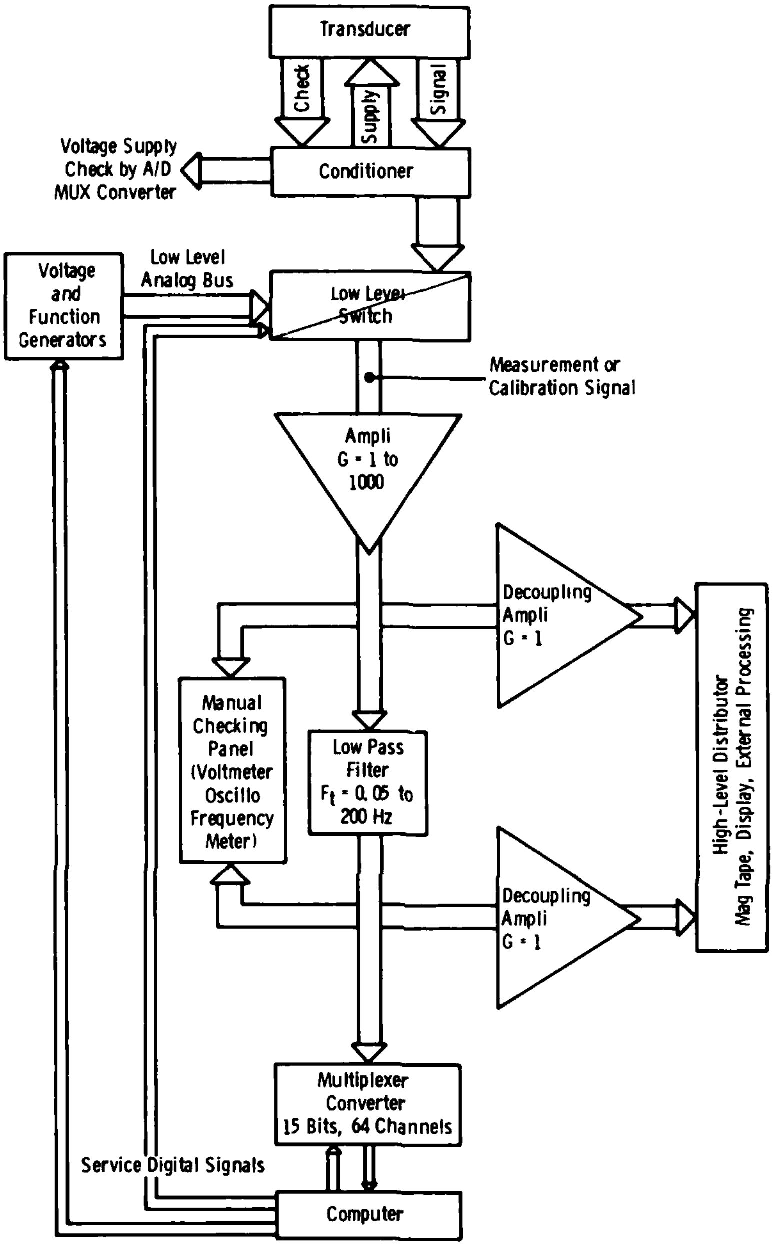
Transducer
Check
Supply
Signal
Voltage Supply Check by A/D MUX Converter
Conditioner
Voltage and Function Generators
Low Level Analog Bus
Low Level Switch
Measurement or Calibration Signal
Ampli G = 1 to 1000
Decoupling Ampli G = 1
High-Level Distributor Mag Tape, Display, External Processing
Manual Checking Panel (Voltmeter Oscillo Frequency Meter)
Low Pass Filter Ft = 0.05 to 200 Hz
Decoupling Ampli G = 1
Multiplexer Converter 15 Bits, 64 Channels
Service Digital Signals
Computer

Figure 37. Typical Analog Channel with Automatic Calibration Instrumentation

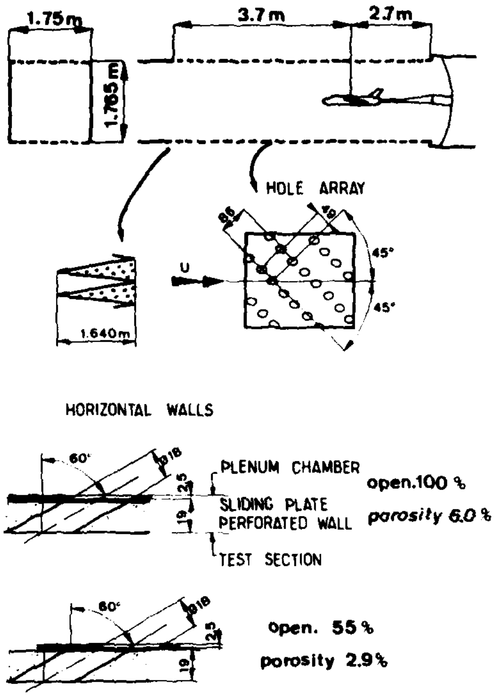
1.75m
3.7m
2.7m
1.765m
HOLE ARRAY
88
40
45°
45°
U
1.640m
HORIZONTAL WALLS
60°
Ø18
2.5
19
PLENUM CHAMBER
open.100 %
SLIDING PLATE
PERFORATED WALL
porosity 6.0 %
TEST SECTION
60°
Ø18
2.5
19
open. 55 %
porosity 2.9%

Figure 38 - S2MA wind tunnel, perforated walls

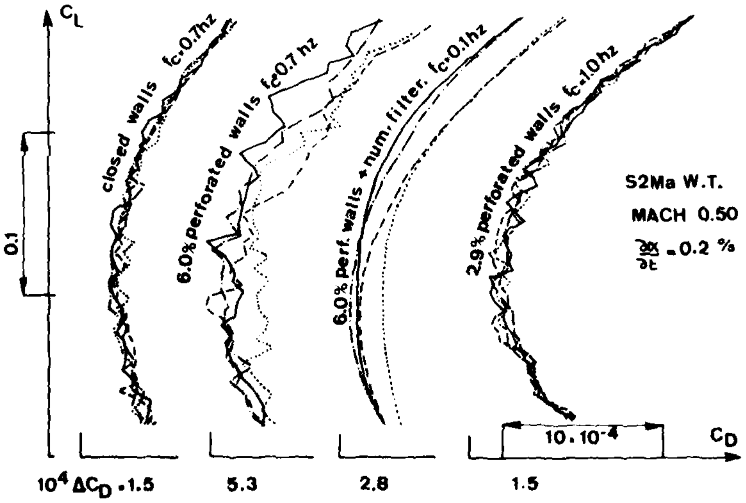

Figure 39 - Repeatability of polar curves

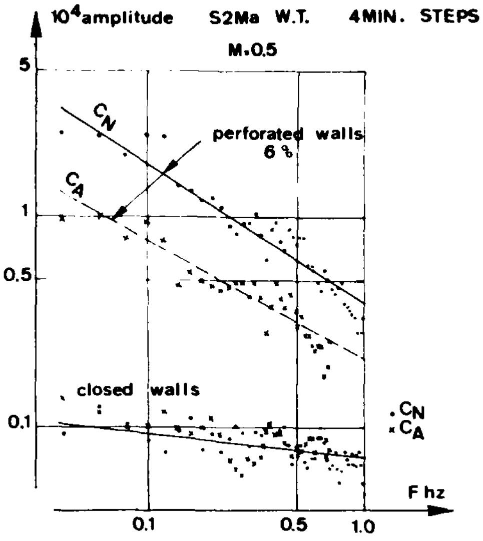

Figure 40 - Spectral analysis of CA,CN coefficients

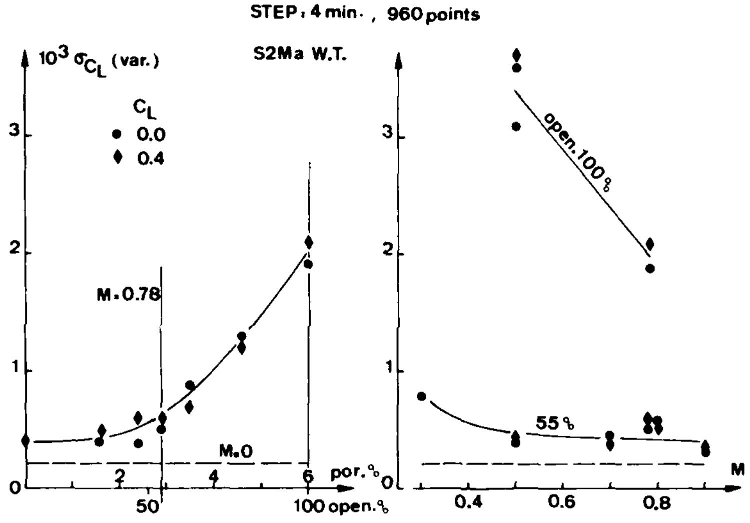

Figure 41 - Deviation reduction of CL variance versus porosity

Figure 42 - Wall effect and porosity effect on lift gradient

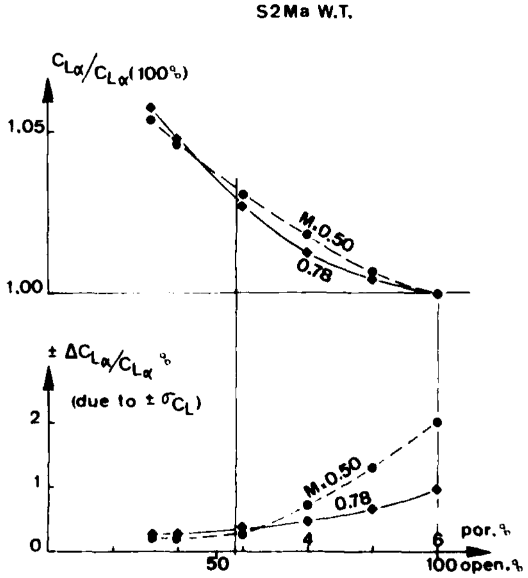

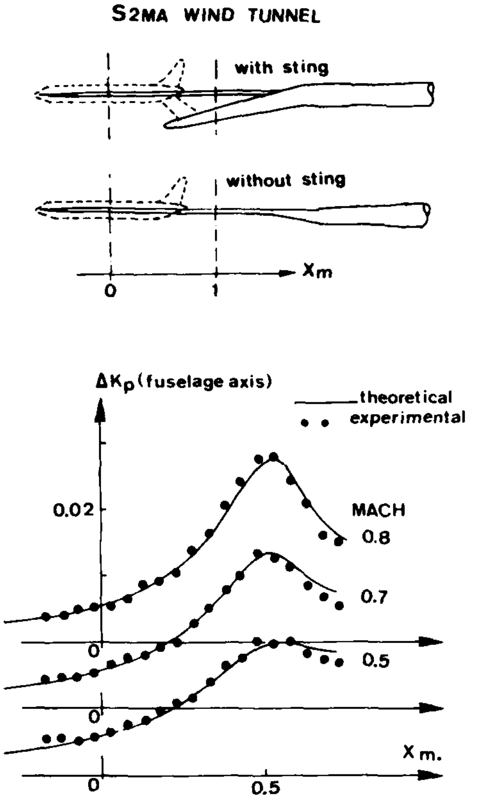

Figure 43 - Sting interference - Comparison theory-experiment

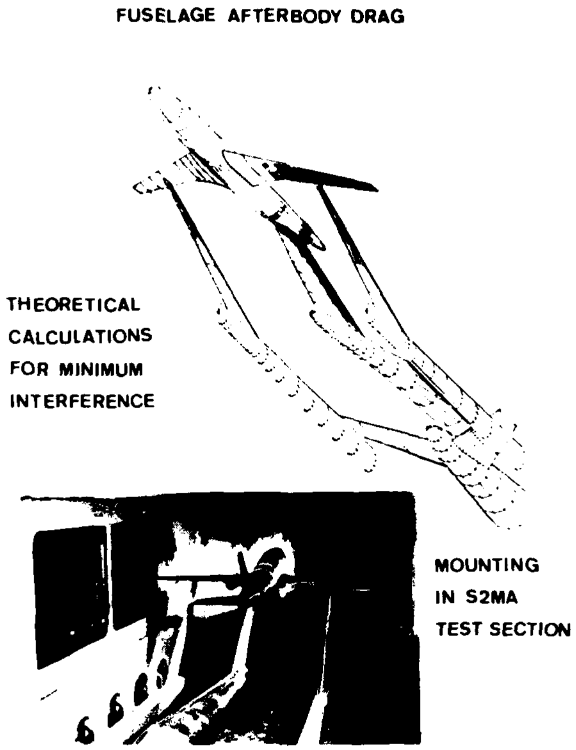
FUSELAGE AFTERBODY DRAG
THEORETICAL CALCULATIONS FOR MINIMUM INTERFERENCE
MOUNTING IN S2MA TEST SECTION

Figure 44 - Support interference

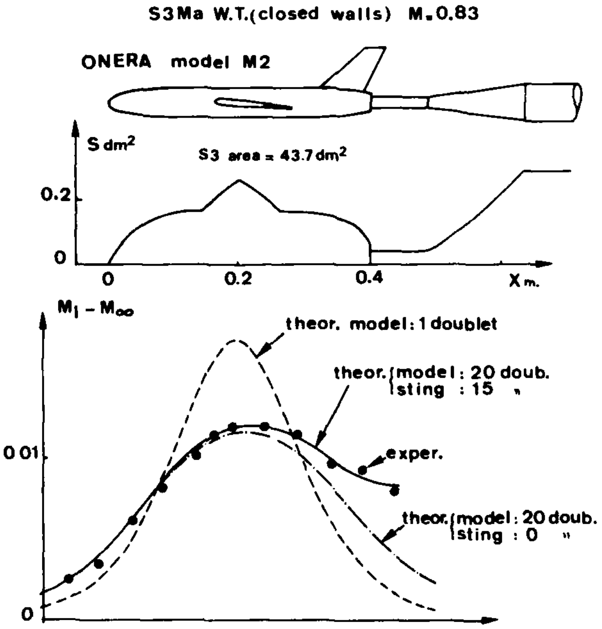

Figure 45 - Model and sting signatures on the test section walls, blockage terms

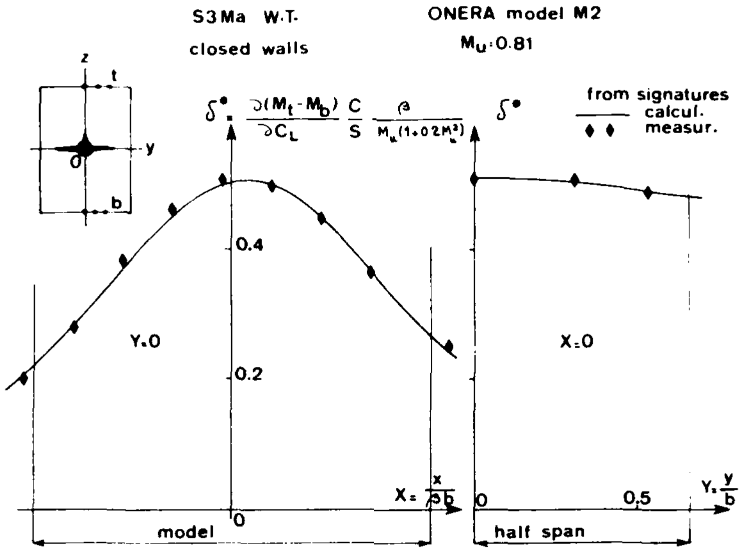

Figure 46 - Model signatures on the test section walls, lifting terms

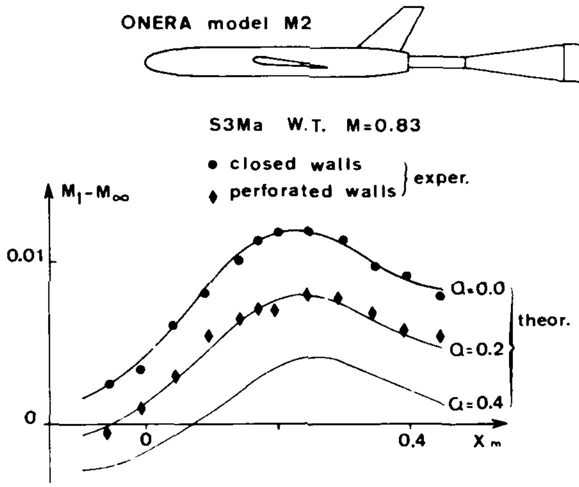

Figure 47 - Porosity factor Q determination from wall signatures, blockage terms.

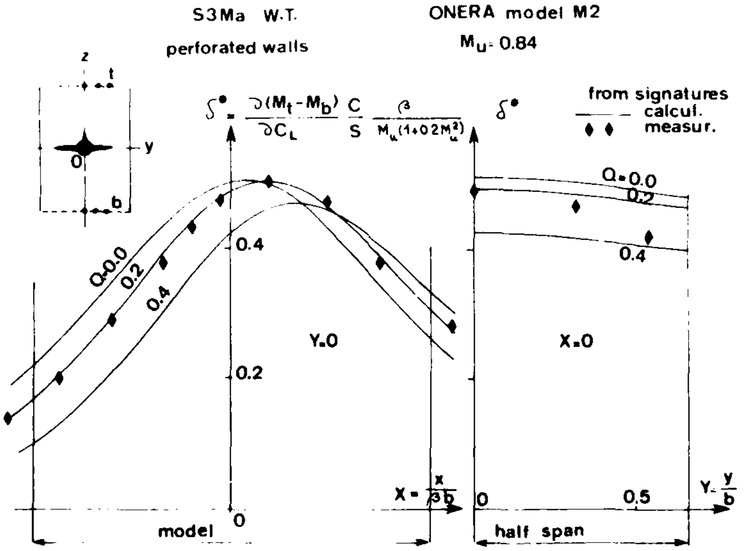

Figure 48 - Porosity factor Q determination from wall signatures, lifting terms

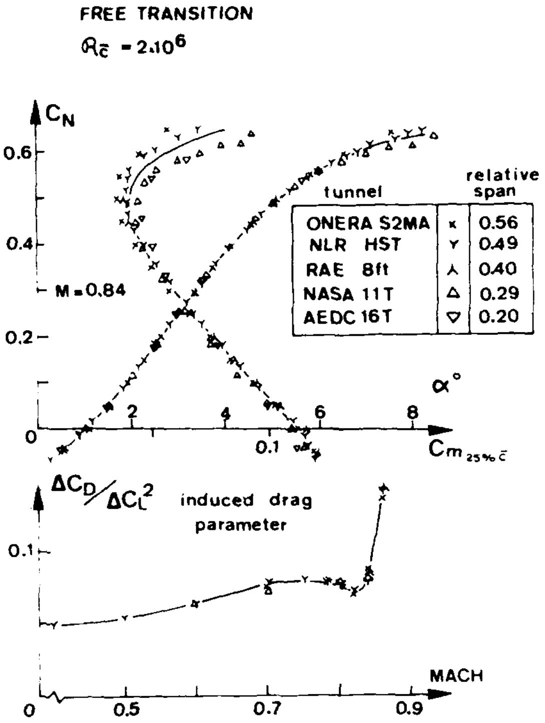

Figure 49 - Wind tunnel comparison - ONERA calibration model M5, aerodynamic coefficients

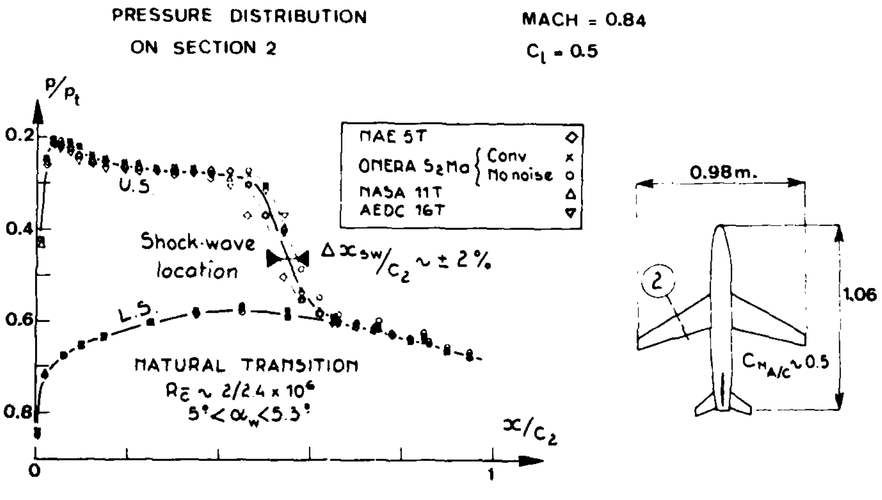

Figure 50 - Wind tunnel comparison - ONERA calibration model M5, mean chord pressure distribution

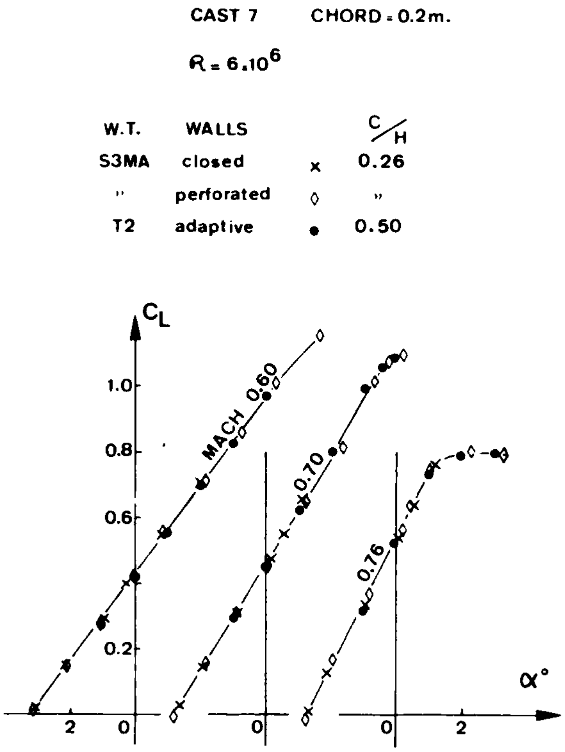

Figure 51 - 2D wind tunnel comparison :
CAST 7 profile, lift curves.

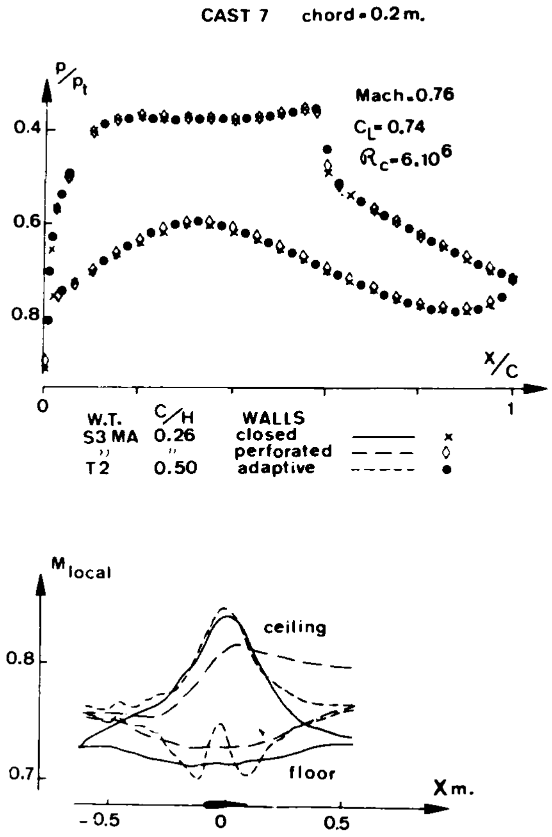

Figure 52 - 2D wind tunnel comparison : CAST 7 profile, pressure distribution and wall signatures

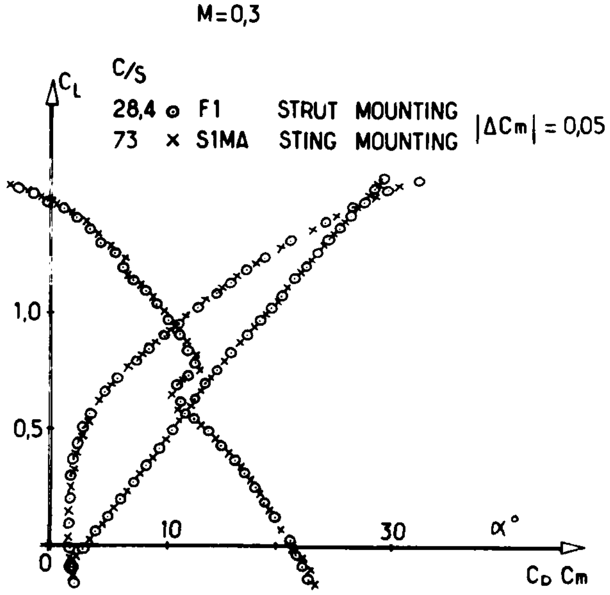

Figure 53 - 3D wind tunnel comparison - fighter model

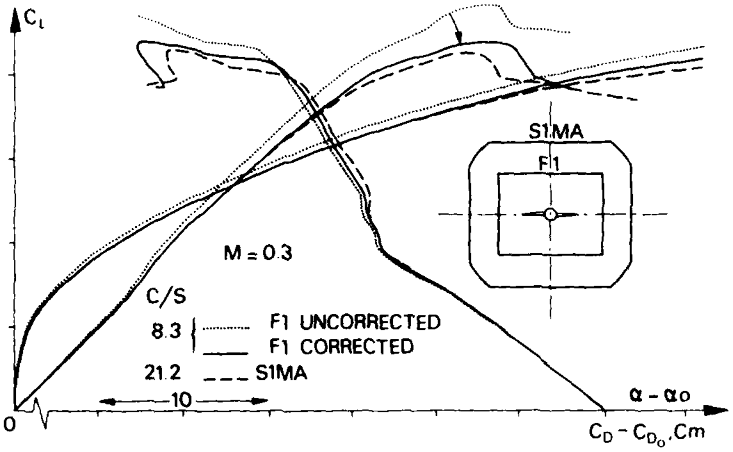

Figure 54 - 3D wind tunnel comparison - fighter model

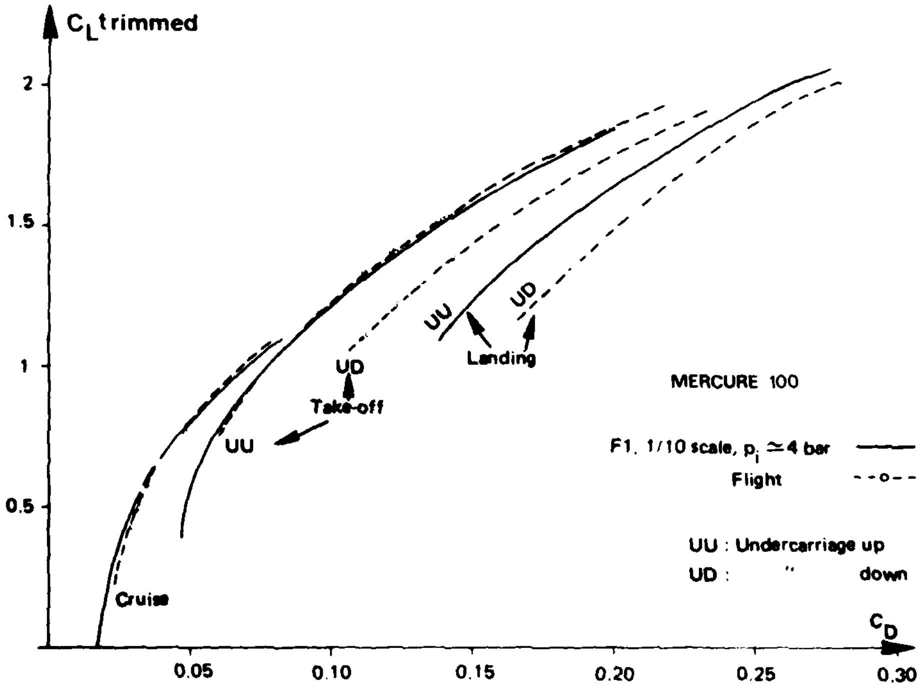

Figure 55 - 3D comparison between flight and wind tunnel data

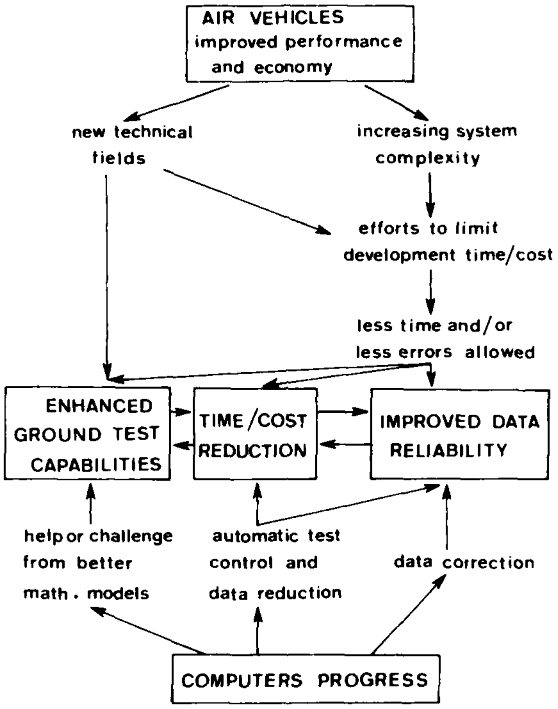
AIR VEHICLES
improved performance and economy
new technical fields
increasing system complexity
efforts to limit development time/cost
less time and/or less errors allowed
ENHANCED GROUND TEST CAPABILITIES
TIME/COST REDUCTION
IMPROVED DATA RELIABILITY
help or challenge from better math. models
automatic test control and data reduction
data correction
COMPUTERS PROGRESS

Figure 56 - concluding remarks

AEROTHERMODYNAMIC FLIGHT ENVELOPE EXPANSION
FOR A MANNED LIFTING REENTRY VEHICLE (SPACE SHUTTLE)

by

J.K. Hodge and D.R. Audley
Air Force Institute of Technology
AFIT/ENY
Wright-Patterson Air Force Base
Ohio 45433
USA

P.W. Phillips and E.K. Hertzler
Air Force Flight Test Center
6510 TESTW/TEG/Stop 236
Edwards Air Force Base
California 93523
USA

SUMMARY

A systematic approach of integrating the best of ground tests, flight simulators, and flight tests was developed and used for aerothermodynamic flight envelope expansion for the Space Shuttle Orbiter. Equations and parameters were selected which were appropriate for the flight simulator at the Air Force Flight Test Center (AFFTC) and also for the reduction of flight data from imbedded thermocouples. Transient flight test maneuvers were designed using the simulator and suggested to the National Aeronautics and Space Administration (NASA) at the Johnson Space Center. Parameters were estimated from flight thermocouple data during the maneuvers by a new data reduction technique. The parameters were compared with simulator parameters which were based on ground test data and theory. The objective, however, was envelope expansion and not data comparison. Simulator parameters were appropriately and quickly updated before the next flight test. The new flight data reduction technique could also be valuable in analyzing wind tunnel thermocouple data to reduce test time.

INTRODUCTION

A systematic approach of integrating ground tests, flight simulators, and flight tests is described. The first step in this approach consists of integrating predictions and ground test data for the heat transfer to critical points on the Orbiter Thermal Protection System (TPS) into the flight simulator. The data must be scaled to flight conditions and appropriate simulator equations and parameters selected prior to use in a real time man-in-the-loop simulator. Next, the simulator is used for flight planning, parametric studies, and design of transient flight test maneuvers which will enhance flight test data reduction and envelope expansion. After the flight test, best estimates of simulator parameters are obtained by a new data reduction technique for imbedded thermocouples which is based on systems identification theory.

Time history comparisons or comparisons at a particular time often result in difficulty. The parameters that caused variations between predicted and flight time histories can not be identified readily by comparing time histories. With the new technique, parameters which would cause variations are estimated during transients and compared directly with simulator parameters, which were based on predictions and ground test data. If appropriate, simulator parameters are updated with perhaps some conservatism in mind. These steps are repeated with subsequent flights, and the data base is enhanced by flight data. Envelope expansion may be accomplished with transient test maneuvers, while never committing the Orbiter to a more severe environment for any significant duration.

Predictions and ground test data from various sources must be incorporated into one simulator data base. Ground tests are normally not exactly at flight conditions, and data must be corrected and extrapolated. Methods of accomplishing this are often numerous and vary in complexity, and is not a topic for this paper. The best available data was used and was often constrained by timeliness and by conservatism to insure flight safety. Simplified equations for the aerodynamic heat rate to the Orbiter TPS, which were used for flight planning by NASA, were used for some locations.[1,2] Wind tunnel data for the ratio of the film transfer coefficient to a reference coefficient on a sphere were used directly for the upper surface especially. A data base evolved with improvements for the ratio of heat rate to a reference heat rate on a sphere with the variables of angle of attack, sideslip, Reynolds number, elevon deflection, flap deflection, and Mach number.

The simulator equations for aerodynamic heat rate were essentially based on linear interpolation of the tabulated ratios. This data base can be related to the aerodynamic data base where, for example, stability and control derivatives are assumed to be linear locally, and tabulated as functions of the appropriate variables. A similar assumption for the heating results in derivatives for the heat rate with respect to each variable which are referred to as heating parameters.

Since the TPS is an excellent insulator and radiator, the surface temperature could be approximated by assuming that the radiation is in equilibrium with the forced convective heating.[1,2] Equilibrium is not assumed, however. The heat rate is assumed to be independent of the wall temperature, and a one-dimensional assumption through the tile from the surface to the structure accounts for conduction. The temperatures at discrete nodes or elements through the TPS are obtained from the solution of differential equations which result from an energy balance. An implicit finite difference or finite element solution technique is used.[3] The one-dimensional assumption is also appropriate for the flight data reduction method and for simulating the response of imbedded thermocouples.

The simulator at AFFTC was used to study the response of existing thermocouples which were imbedded in the TPS. Numerous thermocouples were located near the surface of the TPS just beneath the surface coating, as well as others through the TPS to the structure. During some maneuvers which are normally used for performance, the simulated responses of the thermocouples were significant. Transient maneuvers were then designed which would enhance data reduction and envelope expansion.[4] Estimation of stability and control derivatives from data during transient maneuvers is a standard technique at the AFFTC.[5,6] The technique has also been used for the Orbiter.[7] Aerodynamic instrumentation is designed specifically for parameter estimation, and provides a measurement for each state variable.

The estimation of heating parameters is more difficult, but is possible with current methods from systems identification theory.[8] Other parameters in the one-dimensional thermal equations can also be estimated, and are referred to as thermal parameters. Thus, the thermocouple installation and thermal equations can be verified and possibly corrected. Confidence will be higher in the heating parameters than in conventional methods which do not take advantage of transients.[9,10] In addition, only data during the maneuvers have to be analyzed.

The primary purpose of the transient maneuvers, however, is safe envelope expansion. The ranging capability of a lifting reentry vehicle such as the Orbiter varies considerably with angle of attack. Current constraints are based primarily on heating. The angle of attack can be varied during a transient maneuver of approximately thirty seconds duration which is referred to as a Push-Over-Pull-Up (POPU). The angle of attack envelope can be expanded or placards identified from analysis of a POPU. Limits on the aft center of gravity are also based on heating constraints for the deflection of the elevon and flap. A similar transient maneuver during which the flap deflection is varied is referred to as a flap maneuver. The elevon deflects in an opposing direction to maintain vehicle trim. Limits on the lateral center of gravity are also based on heating constraints for sideslip, but a maneuver of sufficient duration has not been designed. The data reduction method has been developed to take advantage of the transients, as opposed to other techniques which do not.[9,10]

The data reduction method is referred to as HEATEST for HEATing ESTimation. A digital computer has been programmed for HEATEST. One-dimensional differential equations are solved numerically to propagate the temperature, the sensitivity of the temperature to each parameter, and the covariance of the temperature to the next discrete time at each discrete node through the TPS. Whenever a thermocouple sample is available, the temperature, sensitivity, and covariance are updated by an extended Kalman filter. At the end of the transient maneuver, or for any time segment, parameters are updated by a gradient algorithm to maximize a maximum likelihood function for each parameter. These parameters may be the magnitude of the heating rate ratio, heating derivatives or variations, and thermal parameters such as effective thermocouple depth, emissivity, and conductivity factor. Selected parameters are estimated for each sequential time segment, thus allowing nonlinearity in heating parameters over longer durations.

Originally, feasibility of HEATEST was demonstrated with simulated thermocouple data, wind tunnel thermocouple data, and limited first flight thermocouple data with no maneuvers.[4,8] Some of these results are presented. Further development and modifications have been made in HEATEST to improve capability and efficiency. The present HEATEST program was used to reduce thermocouple data from the second Space Shuttle flight (STS-2) in which a POPU was performed at Mach 20. Three flap maneuvers were performed at Mach 21, 17, and 14. Results from the first two maneuvers, at Mach 21-20, are presented. Variations in the heat rate ratio and temperatures are emphasized and not magnitudes. Although heat rate magnitudes did not agree always with simulator data or ground test data, derivatives or variations did agree at many locations.

SIMULATOR EQUATIONS

Both the flight simulator and the data reduction program (HEATEST) require suitable simulation equations for the aerothermodynamic performance of the TPS. These equations and their parameters are referred to in systems identification theory as the model. Since the Orbiter TPS has a low conductivity and most of the heat is radiated from the TPS, the heating rate at the surface is assumed to be independent of the surface temperature. Therefore, the heat rate or heating model can be calculated and then input to the one-dimensional equations or thermal model.

The heating rate depends upon the vehicle trajectory and the atmosphere. This dependence is partially accounted for by nondimensionalizing the heat rate by a reference heating rate on a one foot radius sphere.[1,2] The reference heating (q_r) for the Orbiter is given emperically by

$$q_r = 17700 \sqrt{\rho_\infty}\,(V_\infty/10^4)^{3.07}(1-h_w/h_o) \tag{1a}$$

$$h_w = .24\,[q_r/(\sigma\varepsilon)]^{.25} \tag{1b}$$

$$h_o = .24\,T_\infty + V_\infty^2/50063 \tag{1c}$$

where σ is the Stefan-Boltzmann constant (4.761×10^{-13}), ε is emissivity, ρ_∞ is the atmospheric density, V_∞ is the relative velocity, and T_∞ is the atmospheric temperature. The English Engineering System of units is used where the heat rate is in British Thermal Units per second per foot squared. Other choices for reference heating could be used.

The ratio of the heating rate (q) to the reference heating rate (q_r) was assumed locally to be a linear function of the form

$$\bar{q} = q/q_r = \bar{q}_o + \bar{q}_\alpha(\alpha-\alpha_o) + \bar{q}_\beta(\beta-\beta_o)$$

$$+ \bar{q}_{\log(RE)} \left[\log(RE) - \log(RE_o)\right]$$

$$+ \bar{q}_{\delta e}(\delta_e - \delta_{eo}) + \bar{q}_{\delta_{bf}}(\delta_{bf} - \delta_{bfo})$$

$$+ \bar{q}_{M_\infty}(M_\infty - M_{\infty o}) \tag{2a}$$

$$\Delta\bar{q} = \bar{q} - \bar{q}_o \tag{2b}$$

where $\bar{q}_o$ is the magnitude or intercept at the reference conditions specified by the zero subscript on each variable. The subscripts on the heating ratio ($\bar{q}$) represent partial derivatives or slopes with respect to each variable. The variables are angle of attack (α), sideslip (β), logarithm to the base ten of the Reynolds number (RE) based on characteristic length, elevon deflection angle (δ_e), flap deflection angle (δ_{bf}), and Mach number (M_∞). The variation in heat rate ratio ($\Delta\bar{q}$) from the reference conditions is given by Eq. (2b) where the magnitude is subtracted. To emphasize a comparison with trends and not magnitude during a maneuver, $\Delta\bar{q}$ and the variations in temperature are used for comparisons. For a short time duration or time segment, these parameters or derivatives are assumed constant. The heating ratio $\bar{q}$ can be tabulated as a function of all the variables, or each parameter can be tabulated as a function of appropriate variables. The simple form of Eq. 2 allows flexibility and generality to allow corrections or updates to an aerothermodynamic data base, as well as being similar to wind tunnel data formats. The derivatives are also appropriate for estimation techniques.

Once the heat rate to the TPS surface is specified, temperature through the tile can be calculated by solving the system of ordinary differential equations which result from a one-dimensional energy balance (similar to the partial differential heat equation). A typical TPS cross section for Reusable-Surface-Insulation (RSI) is shown in Fig. 1. The TPS was split into small elements of length (Δx) for a total of L node points. Blocks A through D represent different materials with thermal properties which vary with local temperature and pressure.[11] The convective heat rate (q) is input to the surface node (i=1). The surface radiates heat away and conducts a small amount into the TPS through the thin coating of thickness Δx_A or Δx_1. The surface thermocouple is normally located at the second node (i=2). The interior of block B with effective thickness (Δx_B) is divided into elements of equal thickness (Δx_i). If additional thermocouples are embedded, the distance between each is divided into elements of equal thickness so that a node corresponds to the thermocouple location. In block C, the RSI is bonded by Room-Temperature-Vulcanizing (RTV) adhesive to a nomex felt Strain-Isolation-Pad (SIP) which is bonded to the structure by RTV. In block D, the effective structural thickness and heat sink complete the one-dimensional cross section where an adiabatic wall is assumed.

An ordinary differential equation for the temperature (U_i) at the ith node point was obtained from an energy balance for each element. A system of L nonlinear differential equations results and is of the following form

$$(C_{i+}\rho_{i+}\Delta x_i + C_{i-}\rho_{i-}\Delta x_{i-1})/2\ \dot{U}_i = K_{i-\frac{1}{2}}/\Delta x_{i-1}U_{i-1} - (K_{i-\frac{1}{2}}/\Delta x_{i-1} + K_{i+\frac{1}{2}}/\Delta x_i)U_i + K_{i+\frac{1}{2}}/\Delta x_i\ U_{i+1}$$

$$- \sigma\,\varepsilon_{i-}(U_i^4 - U_{i-1}^4) - \sigma\,\varepsilon_{i+}(U_i^4 - U_{i+1}^4) + q_i \tag{3}$$

where C is the material specific heat, ρ is material density, and K is the material conductivity. Coefficients with subscripts which are less than one or greater than L are zero. The radiation and heat rate terms are also zero except at the surface and backface nodes. The radiation sink temperature (U_0 and U_{L+1}) must be specified at the surface and backface node. The emissivities on the plus or minus side of the element (ε_{i+} and ε_{i-}) were zero except at the surface, backface, and honeycomb nodes.

Given an initial condition (U_I), Eq. (3) can be solved numerically by approximating the time derivative with a first order backward difference given by

$$\dot{U}_i = \left[U_i(t_n) - U(t_{n-1})\right]/\Delta t \tag{4}$$

where Δt is the time step. The resulting system of implicit difference equations or matrix equation must be solved simultaneously. The surface node equation with the highly nonlinear radiation term was solved with a Newton-Ralphson iteration and extrapolation scheme.[3] A tridiagonal algorithm was used for the simultaneous solution of the remaining difference equations.

Numerical solution of Eq. (3) resulted in an accurate simulation of surface and bondline temperatures. Time steps and spatial step sizes were reduced to investigate accuracy. A spatial step of .00125 ft (.25cm) insured accuracy. Time steps up to one second were acceptable. Larger time steps could be used if transients were not significant.

FLIGHT TEST MANEUVERS

Flight test maneuvers which began on the second Space Shuttle flight were designed primarily for envelope expansion and placard removal.[7] The AFFTC simulator was used to evaluate test maneuvers and propose changes which enhance aerothermodynamic data reduction for envelope expansion. Two types of transient maneuvers for angle of attack and center of gravity envelope expansion were optimized for aerothermodynamics, and integrated with requirements or concerns of other disciplines.

A transient maneuver in angle of attack (POPU) is normally performed to obtain lift, drag, and vehicle trim as a function of angle of attack. The maneuver consists of manually pitching the Orbiter down at a prescribed pitch rate to a selected minimum angle of attack, pitching up to a selected maximum angle of attack, and then pitching down to the original or commanded angle of attack. The original trajectory is essentially uncharged if the time duration is short enough or the drag error is small due to the balanced maneuver. Predicted trends and variations in heat rate are verified by flight test data, or updated before committing to lower or higher angles of attack for long duration during future operational missions, especially from the Western Test Range.

Simulator studies of the maneuvers confirmed that most surface thermocouples in high-temperature and low-temperature RSI (HRSI and LRSI respectively) would respond during maneuvers. The response for a surface thermocouple in the nomex felt flexible RSI (FRSI) on the upper surface needed a longer duration maneuver because of a difference in coating properties. Five second duration holds at the selected minimum and maximum angles of attack were proposed to improve FRSI thermocouple response. Variations in heat rate with angle of attack (heating derivative, $\bar{q}_\alpha$) can be estimated from thermocouple measurements while other variables are nearly constant. Rapid and safe envelope expansion is accomplished over several flights by gradually decreasing and increasing the selected angles of attack.

A flap maneuver is similar except the flap and elevon deflection angles are varied instead of angle of attack. Variations of heat rate with flap and elevon deflection angles ($\bar{q}_{\delta bf}$, $\bar{q}_{\delta e}$) can be identified from the thermocouple measurements while other variables are nearly constant. The angle of attack does vary some during the flap maneuver, and it may be possible to identify $\bar{q}_\alpha$ simultaneously. Although the derivative ($\bar{q}_\alpha$) can be identified, envelope expansion to lower or higher angles is not accomplished. A roll doublet can also be performed while the flap is down and elevon is up to estimate aileron control derivatives. Since flap and elevon deflections depend on the center of gravity, envelope expansion to forward and aft center of gravity limits can possibly be verified without changing the center of gravity.

A flap maneuver, roll doublet, pitch doublet, and POPU were integrated into one sequence. This integrated maneuver is advantageous since most heating, stability, and control derivatives can be estimated at a fairly constant Mach number or Reynolds number. Several integrated maneuvers would ideally be performed at approximately Mach 21, 18, 14, and 8. Each Mach number corresponds to a Reynolds number on a given flight. Therefore variations in the derivatives with Reynolds number, not the derivative $\bar{q}_{\log(RE)}$, are obtained from a set of maneuvers.

The derivative $\bar{q}_{\log(RE)}$ can be estimated between maneuvers or during maneuvers, but normally requires a long time duration because of the small change in Reynolds number during a maneuver. Flow transition causes a dramatic increase in this derivative, and then a dramatic decrease when fully turbulent. This transient phenomenon should not be misinterpreted. If transition occurs during a maneuver, it causes problems in interpreting results. If interpreted correctly, it indicates sensitivity to transition in one of the variables, especially if the flow returns to a laminar state. For envelope expansion, the understanding of transition onset is improved however.

Estimation of thermal parameters *also becomes possible during a transient maneuver.* Although numerous parameters could be selected, only parameters which affect the heating derivatives were selected. These thermal parameters currently include an effective thermocouple depth or coating thickness (Δx_A), the surface emissivity (ϵ), and a conductivity factor (Φ_B) for the RSI conductivity in block B. A vector of all parameters (θ) is chosen to be $\theta = [\bar{q}_o\ \bar{q}_\alpha\ \bar{q}_\beta\ \bar{q}_{\log(RE)}\ \bar{q}_{\delta e}\ \bar{q}_{\delta bf}\ \bar{q}_{M_\infty}\ \Delta x_A\ \epsilon\ \Phi_B]$ (5)

The vector in general is of length K. In subscript form, each parameter is referred to as θ_k where $k=1,2,\ldots,K$. The primary purpose of the data reduction program is to obtain best estimates of these simulator parameters during transient flight test maneuvers.

FLIGHT TEST DATA REDUCTION

The next requirement of the systematic approach is to estimate from flight data the same parameters which are inherent in the simulator equations. Systems identification theory was used.[12] Since all states (temperatures at nodes) are not measured, best estimates of the temperature at each node are obtained by an extended Kalman filter or estimator. Best estimates of parameters are then obtained by maximizing a maximum likelihood function. The solution algorithm and program, which was originally developed by the authors at the AFFTC, is referred to as HEATEST. A simplified flow diagram for HEATEST is shown in Fig. 2. Each of the blocks will be summarized.

Initial conditions (IC) for HEATEST are required for the solution of Eq. (3) in the MODELS block. In addition, initial conditions for the sensitivity and covariance of the temperatures are required. These may be specified in several ways.

An initial condition for the temperature vector (U) at a maneuver start time t_o (or time segment start time) is given by

$$U(t_o) = U_I + \tau_I(x) \qquad (6)$$

where U_I is the initial temperature vector and the initial error (τ_I) was assumed to be a zero mean Gaussian process with an initial covariance matrix P with components

$$P_{ij} = \Phi_{ic}^{\ 2}\, U_i(t_o)\, U_j(t_o)\, \bar{R}_{ij} \qquad (7)$$

The error model for the stochastic process (τ) was assumed to be stationary and spatially distributed with zero mean and covariance and given by

$$\bar{R}_{ij} = \exp(-\sum_{\ell=i}^{j} RC_\ell/\Phi_{tr}) \tag{8a}$$

$$RC_\ell = \rho_\ell \, C_\ell \, \Delta x_\ell^2/K_\ell \tag{8b}$$

where RC is a time constant analogous to circuit theory. The initial model error covariance matrix (Q), which will be used later, uses the same spatial correlation and is given by

$$Q_{ij} = \begin{cases} (\phi_{me}^2 + \phi_{bn}^2)\, \bar{R}_{ij}\, U_{EQ}^2 & i=j=1 \\ \phi_{me} \sqrt{\phi_{me}^2+\phi_{bn}^2}\; \bar{R}_{ij}\, U_{EQ}^2 & i=1;\ j\neq 1 \\ \phi_{me}^2\, \bar{R}_{ij}\, U_{EQ}^2 & i\neq j\neq 1 \end{cases} \tag{9}$$

where U_{EQ} is an equilibrium temperature calculated from q assuming no conduction. The constants ϕ_{tr}, ϕ_{ic}, ϕ_{bn}, and ϕ_{me} are related respectively to the spatial correlation between nodes, to deviation in initial temperatures, to deviation in heating rate at the boundary, and to deviation in heat flux in the TPS due to model error. If conduction dominates at the surface instead of radiation, perhaps q should replace U_{EQ}.

The initial temperature vector U_I is specified by one of three ways. The temperature distribution is specified by some profile such as a constant based on on-orbit conditions. Initial conditions at the beginning of a time segment may be specified from the output of a previous sequential time segment. The third way, which is more efficient, is based on the radiation equilibrium assumption and an empirically determined RC time constant. The circuit analogy is used to calculate an equilibrium temperature

$$U_{EQ}(t_n) = g\, Y_1 - (g-1)\, U_{EQ}(t_{n-1}) \tag{10a}$$

$$g = 1/\left[1-\exp(-\Delta t/RC)\right] \tag{10b}$$

where Y_1 is the surface thermocouple measurement. The heat rate is calculated from U_{EQ} assuming radiation equilibrium and input to the same algorithm used to propagate temperatures on the simulator (Eq. 3). This procedure works well for the TPS for the purpose of generating an approximate initial condition for temperature.

The initial condition for the sensitivity (U_θ) of the temperature to each parameter (θ_k) is assumed to be zero. The subscript denotes partial differentiation. For sequential time segments the sensitivities at the end of the previous segment are used.

The temperature, covariance, and sensitivities are propagated to the next time step using differential equations for the TPS in the MODELS block. The temperature is propagated by Eq. (3) using the same numerical solution technique as the simulator to obtain an apriori expectation, $U(t_n^-)$. The minus denotes the expected temperature prior to availability of a measurement, whereas a plus denotes an updated temperature after comparison with a measurement. Differential equations for the sensitivities were derived by taking partial derivatives of Eq. (3) with respect to each parameter (θ_k), and quasilinearizing nonlinear terms. The resulting equations are of the form

$$\dot{U}_{\theta k} = C_k\, U_{\theta k} + D_k \tag{11}$$

where C_k is a coefficient matrix (LxL) and D_k a vector.

Eq. (11) is solved readily for each parameter since C_k is a tridiagonal matrix. For the covariance, Eq. (3) was first quasilinearized to the form

$$\dot{U} = A\, U + B + W(t) \tag{12}$$

where A is a coefficient matrix (LxL) and B a vector. The white stationary Gaussian process W(t) has zero mean and a covariance matrix Q. The propagated or a priori covariance $P(t_n^-)$ was approximated by the difference equation

$$P(t_n^-) = \Phi(\Delta t)\, P(t_{n-1}^+)\, \Phi^T(\Delta t) + \int_{t_{n-1}}^{t_n} \Phi(\lambda-t_{n-1}) Q\, \Phi^T(\lambda-t_{n-1})\, d\lambda \tag{13a}$$

$$\Phi(\Delta t) = \exp(A\Delta t) \tag{13b}$$

The transition matrix Φ and integral were calculated by Taylor series expansion and is perhaps the most inefficient part of HEATEST which needs improvement.

The temperature, covariance, and sensitivities are propagated in the MODELS block until a thermocouple measurement is available. The temperature, covariance, and sensitivities are then updated based on the measurements by the Kalman filter in the KALMAN UPDATE block. The location of the total of M thermocouples is identified by the measurement equation

$$Y(t_n) = H\, U(t_n) + \mu_n \tag{14}$$

where Y is the vector of M measurements and H is an MxL matrix defined by

$H_{mi} = 1$ if U_i corresponds to Y_m and

$H_{mi} = 0$ if U_i does not correspond to Y_m.

The error μ_n was assumed to be a white stationary process with zero mean and covariance

$$R_m = \Phi_{meas}^{\ 2}\, Y_m^{\ 2} \qquad (15)$$

for each measurement. The constant Φ_{meas} is related to the deviation in the thermocouple measurement. The updated temperature or a posteriori expectation $U(t_n^+)$ is calculated by

$$U(t_n^+) = U(t_n^-) + G\, E(t_n) \qquad (16a)$$

$$G = P(t_n^-)\, H^T[H\, P(t_n^-)H^T + R_m]^{-1} \qquad (16b)$$

$$E = Y(t_n) - H\, U(t_n^-) \qquad (16c)$$

where G is the Kalman gain and E the residual error. The updated covariance and sensitivities are calculated by

$$P(t_n^+) = [I-GH]\, P(t_n^-)\, [I-GH]^T + G\, R_m\, G^T \qquad (17)$$

$$U_{\theta_k}(t_n^+) = [I-GH]\, U_{\theta_k}(t_n^-) \qquad (18)$$

In summary, the expected temperature, covariance, and sensitivities are propagated in the MODELS block for each trajectory and thermocouple sample time as the TIME LOOP. Updates occur in the KALMAN UPDATE only when a thermocouple measurement is available. This TIME LOOP is continued until the end of the maneuver or time segment.

At the end of a time segment, the parameters (θ_k) are updated in the PARAMETER UPDATE block. A maximum likelihood criteria was preferred because of experience in estimation of stability derivatives.[6] The likelihood function (F) was specified to be the natural logarithm of the joint probability density function of the temperature which is dependent on θ and the measurements Y. The maximum of F was satisfied by equating the gradients to zero. The maximum with respect to U is satisfied by the best estimated temperature

$$U* = U(t_n^+) \qquad (19)$$

if $U(t_n^+)$ is the temperature generated with best estimates of the parameters (θ*). θ* is obtained by the gradient algorithm

$$\theta* = \theta-[\partial^2F/\partial\theta^2]^{-1}\ \partial F/\partial\theta = \theta+J^{-1}S \qquad (20)$$

where J is an approximation for the Jacobian ($\partial^2F/\partial\partial^2$) which is referred to as the (KxK) conditional information matrix and is given in component form by

$$J_{jk} = \sum_{n=1}^{N} U_{\theta j}(t_n^-)\, H^T[H\, P(t_n^-)H^T + R_m]H\, U_{\theta_k}(t_n^-) \qquad (21)$$

which corresponds to an ensemble average over the time interval of the maneuver. The gradient of F is approximated by

$$S_k = \sum_{n=1}^{N} U_{\theta_k}(t_n^-)\, H^T[H\, P(t_n^-)H^T + R_m]^{-1}\, [Y(t_n)-H\, U(t_n^-)] \qquad (22)$$

where S is referred to as the "score".

After selected parameters are updated, the ITERATION LOOP is continued for a fixed number of iterations to obtain best estimates of the parameters. The Cramer-Rao bound is calculated from J^{-1} and provides a measure of the uncertainty in the parameter estimate. After the last PARAMETER UPDATE, both the apriori temperatures and the best estimated temperature are obtained by completing the TIME LOOP again. Deviation in the temperature is obtained from the covariance. The average residual error is also computed as an indicator of the "match" with the thermocouple data.

RESULTS

Results with three data sources are presented. During initial development, thermocouple measurements during transient maneuvers were simulated by the AFFTC and distorted with noise and known parameter variations to demonstrate feasibility. Transient maneuvers were also performed in a Mach 14 wind tunnel test by Air Force Wright Aeronautical Laboratories (AFWAL) in cooperation with AFFTC with TPS test articles and flight thermocouples. Limited telemetry data were available from the first Space Shuttle test flight (STS-1), and no maneuvers were performed. One integrated maneuver and two flap maneuvers were performed on the second flight (STS-2). No maneuvers of interest to aerothermodynamics were performed on the third flight (STS-3). One case from the simulated data and one from the wind tunnel data are presented. Results from the first integrated flight test maneuver at Mach 21 during STS-2 are presented from three locations on the Orbiter. These locations included lower centerline, lower outboard elevon, and Orbital-Maneuvering-System (OMS) pod on the upper surface and include flight surface thermocouples only.

Simulated Thermocouple Data

Thermocouple data were first simulated on the AFFTC simulator. A location on the lower surface centerline at seventy-five percent characteristic length ($X/L = .75$) was chosen. A POPU at Mach 18 and Reynolds number (RE) of two million was simulated. The flow was predicted to be laminar and the heat rate only a function of α. Data were distorted with eight bit word resolution and sampled once per second corresponding to the flight recorder.

The simulated thermocouple samples along with the best estimated temperature from HEATEST at that node are shown in Fig. 3 corresponding to case 1. The estimated heating ratio, as computed from parameter estimates, is compared to the actual simulator model in Fig. 4. The derivative with respect to the angle of attack ($\bar{q}_\alpha$) is changed in the simulator model in case 2, and the heating ratio successfully estimated as shown. A bias in the magnitude ($\bar{q}_o$) in case 3 was correctly estimated. Another POPU, to a lower angle of attack in case 8 was also estimated correctly.

Other cases were also simulated.[4] Thermocouple depth was estimated correctly with very little error. Emissivity was estimated correctly only if two thermocouples were near the surface. Random noise with large deviation caused little difficulty. A thermal conductivity factor was also estimated in one case.

Four cases with initial condition error, heating model nonlinearity, atmospheric density error, and time skew between angle of attack and thermocouple samples were of concern.[4] A new method for an approximate IC is used now. Model error was investigated with a simulated POPU at Mach 8. The heating model assumed turbulent flow and the simulated heating varies with Reynolds number. The estimated derivative in angle of attack was correct as shown in Fig. 5 although a "model error" due to Reynolds number change is present. A derivative for Reynolds number is now available and can also be estimated. Heating model nonlinearity must be handled, however, on a case by case basis by time segmentation which has been added to HEATEST, or by model changes. In systems identification, "model error" is a major concern and problem. Atmospheric density error causes a bias in the heating ratio as in other techniques, and can not be identified by HEATEST. Therefore, a Best-Estimated-Trajectory (BET) and atmosphere from NASA Langley Research Center was used when available and for results presented in this paper. The time skew concern has not been resolved and causes major difficulty in estimation of thermal parameters. For a thermocouple sample leading by one second, estimates for effective thermocouple depth are negative, physically unrealistic, and the numerical solution of Eq. (3) divergent. A lag of one second results in a large estimate for the depth and larger heating derivatives, but fortunately, deviations, bounds, and residual error are larger than in other cases. A time skew of less than a quarter second caused no difficulty and is probably related to the time constant of the coating depth.

Wind Tunnel Data

Thermocouple data was also obtained during a wind tunnel test conducted by AFWAL just prior to STS-1. Three test articles consisted of a thin skin stainless steel plate, a HRSI tile, and FRSI material. The deflection angle of a flat plate with these articles was varied to simulate flight test maneuvers. A shock generator was also used to simulate flow attachment or shock interaction for a short time duration. A water cooled plate in the top of the test section maintained at least a partially known radiation sink temperature. Data from numerous steady state and transient runs were obtained. Unfortunately, because of the availability of flight data, only one case has been analyzed presently.

Wind tunnel data for one long transient maneuver with the HRSI tile were input to HEATEST. Time histories of the deflection angle, thermocouple samples, and best estimated temperature are shown in Fig. 6. Due to tunnel start and limited run time, achieving equilibrium similar to flight conditions was difficult and conduction effects are large. An initial condition error at the beginning of the time history resulted since the initial condition generation and sequential time segment options in HEATEST were not available then. Therefore, only one time segment could be analyzed. The film transfer coefficient ratio from parameter estimates is compared with theory and thin skin results from three steady state runs in Fig. 7. The reference coefficient is based on Eckert flat plate theory at zero deflection. The HEATEST results for HRSI from a transient maneuver has the same slope or derivative, but is lower in magnitude. Since equilibrium was apparently reached at four degrees deflection, the heating magnitude was verified to be correct. Two equilibrium calculations using first the temperature of the water cooled plate and then absolute zero for the radiation sink temperature agree with HEATEST results. The equilibrium calculations should be slightly lower due to conduction. A nonisothermal wall could be the cause of the lower magnitude, similar to error in calorimeters. The steel plate leading edge has a cold wall and the HRSI has a discontinuous increase in wall temperature. Eckert[13] reported that such a discontinuity could cause as much as a forty percent decrease. Further investigation of the wind tunnel data and the nonisothermal wall effect is required.

Lower Centerline Flight Thermocouple Data

STS-2 flight thermocouple data at numerous locations on the lower surface were input to HEATEST. A centerline location at $X/L=.7$ was typical of lower surface locations. A time history of the angle of attack, thermocouple measurements, and apriori temperature during the POPU at Mach 20 and flight Reynolds number of approximately 1.5 million is shown in Fig. 8. The thermocouple response was similar to the response in Fig. 3. Only variations in the temperature and heat rate due to the maneuver are presented. For purposes of envelope expansion, the variations are more important. Any discrepancy in magnitude between flight and ground data is outside the scope of this paper.

Experience has shown that a comparison with the apriori temperature instead of the best estimated temperature demonstrates more sensitivity or error to incorrect parameter estimates, and is therefore used in comparisons. As seen in Fig. 8, a good "match" was obtained. The variation in the heating rate ($\Delta\bar{q}$) from the reference angle of attack ($\alpha_0=40$ degrees) with the best estimated parameters is compared in Fig. 9 with simulator model variations which were based on wind tunnel data . Estimated parameters and uncertainty bounds are given in Table 1. The best estimated derivative or slope is slightly higher between 40 and 45 degrees angle of attack, but lower between 35 and 40 due to a small nonlinearity. When the uncertainty bound in the derivative is shown, there is good agreement.

The thermal parameter estimate for effective thermocouple depth ($\Delta x_A=.00167$ ft. or .05 cm) is higher than the simulator and data book value (.001 ft or .03 cm). The conductivity factor ($\Phi_B=.904$) is lower than the simulator value (1). The estimate for Φ_B was sensitive to the spatial correlation constant (ϕtr) and should be disregarded. Due to the five second duration holds, ϕ_B does not significantly affect results. This was confirmed by a parametric study.

Control Surface Flight Thermocouple Data

Analysis of locations on the control surfaces presents a difficult problem due to numerous variables, trading between derivatives, and nonlinearity. All parameters could not be estimated simultaneously as hoped for. Time segments had to be chosen appropriately to limit the range of a variable. In some cases, a variable changes rapidly and nonlinearity can not be avoided. The elevon falls in this category. The change in heat rate for negative deflection angles is smaller than for large positive deflection angles for example.

The lower outboard elevon near the edge is one of the more critical heating locations on the elevon. STS-2 flight thermocouple measurements on the elevon during the POPU and flap maneuvers were input to HEATEST. Time histories of the flap deflection, elevon deflection, angle of attack, thermocouple measurements, and a-priori temperature are shown in Fig. 10. The derivative, $\bar{q}_{\delta_e}$, was fixed at .0045 during the POPU because of trading with $\bar{q}_\alpha$. Parameter estimates and uncertainty bounds are given in Table 1. The variation in heating ratio ($\Delta\bar{q}$) with angle of attack and elevon deflection at the reference conditions (α_o=40, δ_{eo}=0) is shown in Fig. 11. The change with elevon deflection is apparently nonlinear around five degrees and zero degrees. Time segment 1 between approximately three to seven degrees deflection has a large uncertainty. Another time segment avoids most of the nonlinearity and has a lower uncertainty. The agreement with the simplified model is good up to five degrees deflection. One data point for the heat rate variation between STS-3 and STS-2 tends to confirm the results also.

STS-2 flight thermocouple measurements on the flap during the POPU and flap maneuver were input to HEATEST also. Parameters which have been estimated include Δx_A, $\bar{q}_\alpha$, $\bar{q}_{\log(RE)}$, $\bar{q}_{\delta e}$, and $\bar{q}_{\delta bf}$. The heating varies with angle of attack, Reynolds number, elevon deflection, and flap deflection. The parameters could not be identified simultaneously apparently because of nonlinearity in angle of attack, flap deflection, and even elevon deflection. The Reynolds number derivative must be estimated over a large time segment in which the Reynolds number changes significantly. The derivatives in angle of attack and flap deflection were considerably higher than the simplified model. Further analysis is required for the flap.

Upper Surface Flight Thermocouple Data

The most significant result of the POPU was on the side of the OMS pod which is on the upper surface. A time history of a thermocouple mounted in FRSI on the OMS pod is shown in Fig. 12. The large and unexpected increase in temperature above the design temperature limit was not predicted by the simulator models at this Reynolds number. Flow impingement on the OMS pod was expected around thirty degrees instead of thirty-seven degrees as shown by the large negative slope in Fig. 13. Because of nonlinearity, the POPU maneuver and a bank reversal following the POPU were divided into four time segments as shown in Fig. 12. A three second lag in the thermocouple samples was assumed since no data correlation could be obtained otherwise and was not consistent with other OMS pod thermocouples. This was also the only way to eliminate hysteresis even when the effective thermocouple depth (Δx_A) was estimated. The depth was estimated in both time segments 2 and 3 to be approximately .00167 ft (.05 cm). A thick coating was anticipated because of repairs in this area. The sideslip derivative was estimated in time segments 3 and 4. These parameter estimates were then used in time segments 1 and 2 to refine angle of attack derivatives for example. Uncertainty bounds are fairly large because of nonlinearity. The uncertainty in the angle of attack derivative in time segment 4 is smaller because of the smaller change in angle of attack. Confidence in these estimates would be very high if there were no time skew.

Although there was concern for the OMS pod before the maneuver, results from the POPU confirm it. The value of the transient maneuvers for envelope expansion is demonstrated even without data reduction by examining Fig. 12. With data reduction, a basis for either a placard or redesign of this small area is established. More maneuvers are needed to estimate the variations at lower angles of attack and at other Reynolds numbers.

ACKNOWLEDGEMENTS

Special thanks go to Mr. R. G. Hoey and the AFFTC who supported this new technique. Cooperation with AFWAL who is also currently supporting further data reduction is appreciated. Mr. J. R. Hayes of AFWAL also provided Mach 14 wind tunnel data and thin skin results. Application of this technique to the Space Shuttle has also depended upon cooperation with NASA subsystem managers, especially Ms. D.B. Lee.

REFERENCES

1. Evans, M.E., "Thermal Boundaries Analysis Program Document", NASA-CR-151025, April 1975.
2. Space Shuttle Orbiter Entry Aerodynamic Heating Data Book, Rockwell International Space Division, Document Number SD73-SH-0184 C Revision, Books 1 and 2, October 1978.

3. Williams, S.D. and Curry, D.M., "An Implicit-Iterative Solution of the Heat Conduction Equation with a Radiation Boundary Condition", International J. for Numerical Methods in Engineering, Vol. II, 1605-1619 (1977).

4. Hodge, J.K., Phillips, P.W., and Audley, D.R., "Flight Testing a Manned Lifting Reentry Vehicle (Space Shuttle) for Aerothermodynamic Performance", AIAA Paper 81-2421, AIAA/SETP/SFTE/SAE/ITEA/IEEE 1st Flight Testing Conference, November 1981.

5. "Parameter Estimation Techniques and Applications in Aircraft Flight Testing", NASA TN D-76-47, April 1974.

6. Nagy, C.J., "A New Method for Test and Analysis of Dynamic Stability and Control", AFFTC-TR-75-4, May 1976.

7. Cooke, D.R., "Space Shuttle Stability and Control Flight Test Techniques", AIAA Paper 80-1608, 7th Atmospheric Flight Test Mechanics Conference, August 11-13, 1980.

8. Audley, D.R. and Hodge, J.K., "Identifying the Aerothermodynamic Environment of the Space Shuttle Orbiter, Columbia", 6th IFAC Symposium on Identification and System Parameter Estimation, June 1982.

9. Williams, S.E. and Curry, D.M., "An Analytical and Experimental Study, Using a Single Embedded Thermocouple", NASA TM-58204, 1977.

10. Williams, S.D. and Curry, D.M., "An Analytical and Experimental Study Using a Single Embedded Thermocouple", J. of Spacecraft and Rockets, Volume 14, October 1977, pp. 632-637 (See Technical Comments, J. of Spacecraft and Rockets, Vol. 15, Nov-Dec 1978, pp. 381-383).

11. Space Shuttle Program Thermodynamic Design Data Book, Thermal Protection Acreage, Rockwell International Space Division, Document Number SD73-SH-0226, Vol. 2C, January 1981.

12. Maybeck, P.S., Stochastic Models, Estimation and Control, Academic Press, 1979.

13. Eckert, E.R.G., "Survey of Boundary Layer Heat Transfer at High Velocities and High Temperatures", WADC TR 59-624, 1960.

Table 1. Heating and Thermal Parameters Best Estimates and Bounds for STS-2 Flight Test Maneuvers

Location	Mach	RE x 10^{-6}	Maneuver	$\bar{q}_\alpha$ per deg	$\bar{q}_\beta$ per deg	$\bar{q}_{\delta_e}$ per deg	Δx_A ft	Φ_B
X/L=.7	20.5	1.5	POPU	.0023 ±.0004	0	0	.0016 ±.0004	.90 ±.03
OUTBOARD ELEVON	21.5	1.3	FLAP MANEUVER (Segment 1)	.0078	0	.0116 ±.0012	.0023	1.
	21.0	1.4	FLAP MANEUVER (Segment 2)	.0078	0	.0050 ±.0006	.002	1.
	20.5	1.5	POPU	.0078 ±.0015	0	.0045	.0023 ±.0006	1.
OMS POD	20.5	1.5	POPU (Segment 1)	−.00494 ±.0013	−.0053	0	.00167	1.
	20.0	1.6	POPU (Segment 2)	−.0004 ±.0007	−.0063	0	.00167	1.
	20.0	1.6	AFTER POPU (Segment 3)	−.00035	−.0128 ±.058	0	.00167 ±.00087	1.
	19.5	1.65	BANK REVERSAL (Segment 4)	−.0034 ±.0015	−.0064 ±.0015	0	.00167	1.

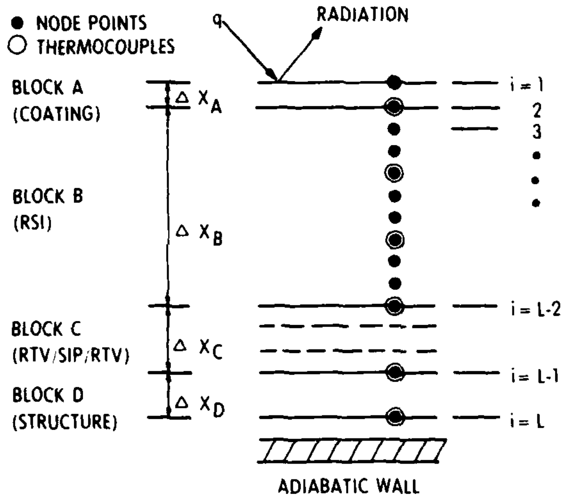
● NODE POINTS
○ THERMOCOUPLES
q
RADIATION
BLOCK A (COATING)
Δ X_A
BLOCK B (RSI)
Δ X_B
BLOCK C (RTV/SIP/RTV)
Δ X_C
BLOCK D (STRUCTURE)
Δ X_D
i = 1
2
3
i = L-2
i = L-1
i = L
ADIABATIC WALL

Figure 1. TPS Model Cross Section

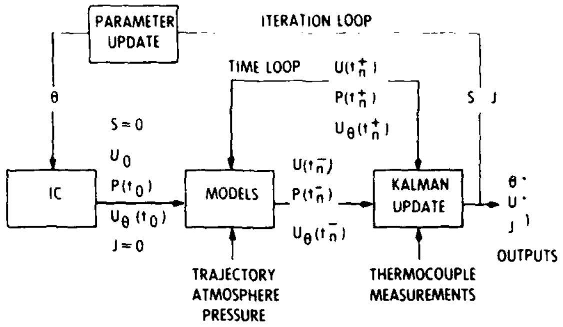
PARAMETER UPDATE
ITERATION LOOP
TIME LOOP
θ
S = 0
U_0
P(t_0)
U_θ(t_0)
J = 0
IC
MODELS
U(t_n^-)
P(t_n^-)
U_θ(t_n^-)
U(t_n^+)
P(t_n^+)
U_θ(t_n^+)
KALMAN UPDATE
S J
θ*
U*
J
OUTPUTS
TRAJECTORY ATMOSPHERE PRESSURE
THERMOCOUPLE MEASUREMENTS

Figure 2. Simplified Heatest Flow Diagram

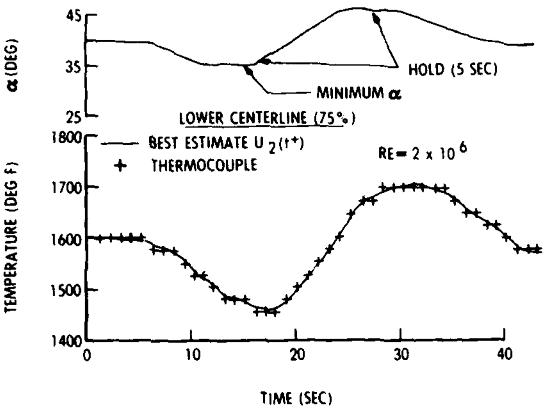

Figure 3. Simulated Thermocouple Data with 8 Bit Word (Mach 18 Pushover-Pullup Maneuver)

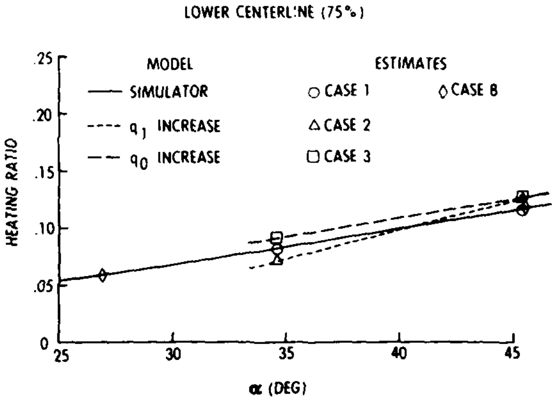

Figure 4. Heating Estimates for Simulated Thermocouple Data at Mach 18

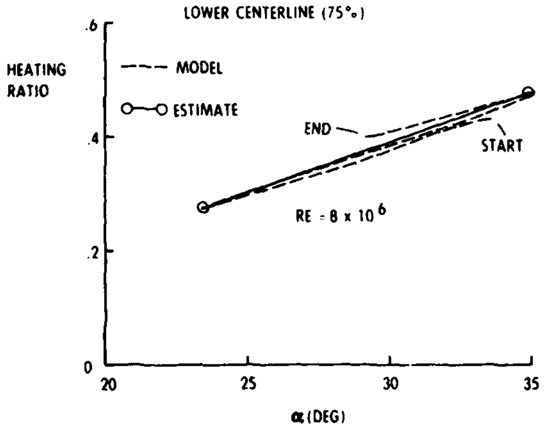

Figure 5. Heating Estimates for Simulated Thermocouple Data at Mach 8 Pushover-Pullup Maneuver

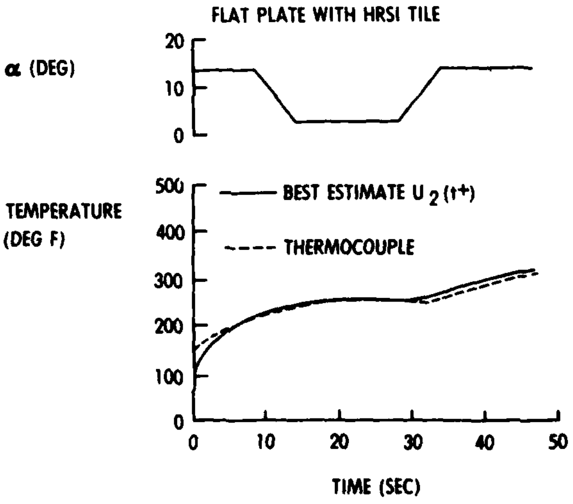

Figure 6. Wind Tunnel Thermocouple Data for Transient Maneuver (Mach 14.25)

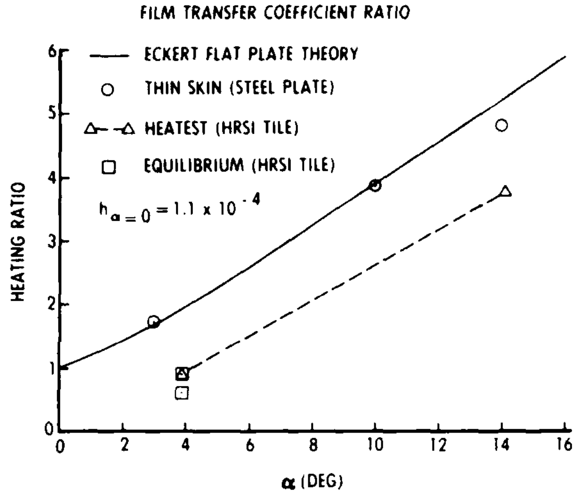

Figure 7. Heating Estimate for Wind Tunnel Thermocouple Data (Transient Maneuver)

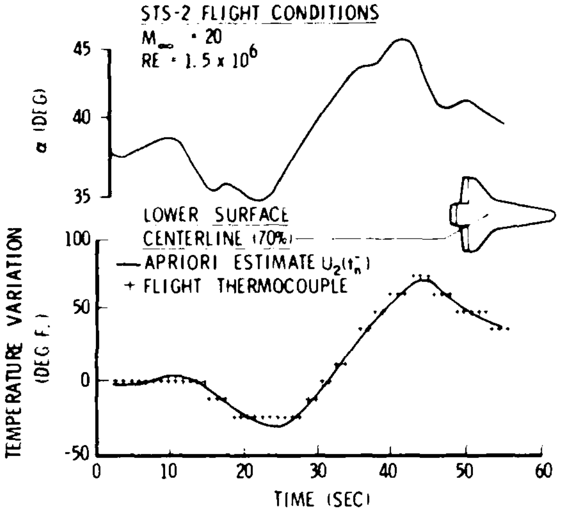

Figure 8. Lower Centerline (x/L = .7) Flight Thermocouple Data (Mach 20 Pushover-Pullup Maneuver)

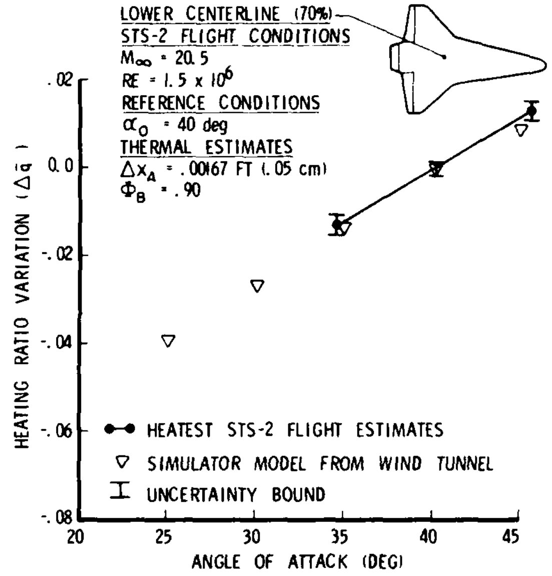

Figure 9. Heating Estimates for Lower Centerline (x/L = .7) from STS-2 Flight Thermocouple Data (Mach 20 Pushover-Pullup Maneuver)

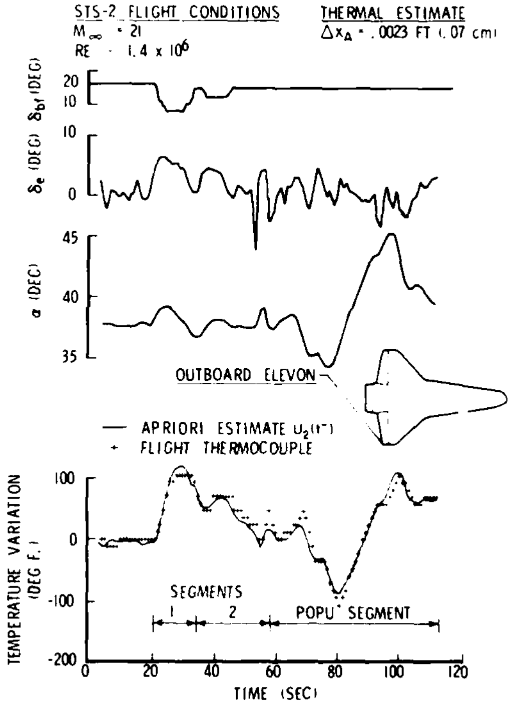

Figure 10. Elevon Tip STS-2 Flight Thermocouple Data (Mach 21 Flap and Pushover-Pullup Maneuver)

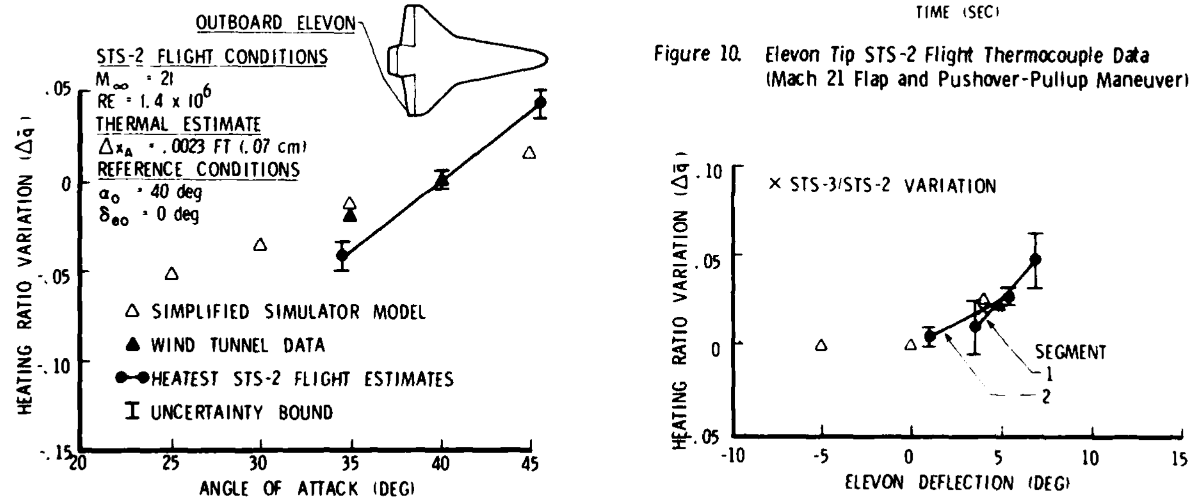

Figure 11. Heating Estimates for Outboard Elevon from STS-2 Flight Thermocouple Data (Mach 21 Flap and Pushover-Pullup Maneuver)

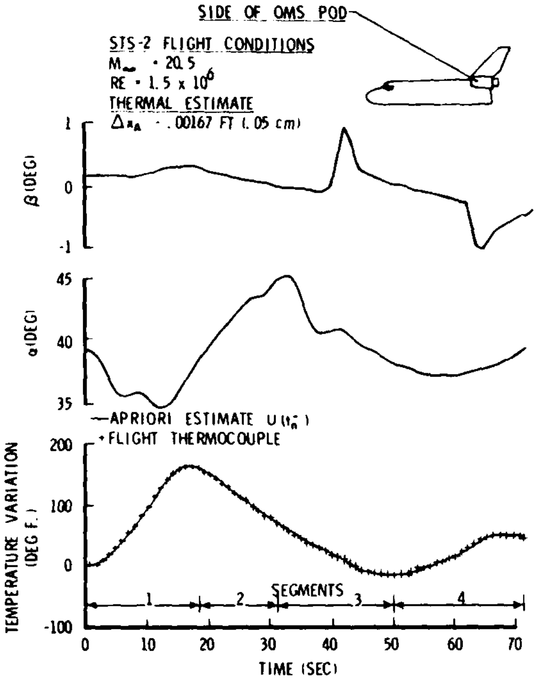

Figure 12. OMS POD STS-2 Flight Thermocouple Data (Mach 20.5 Pushover-Pullup Maneuver)

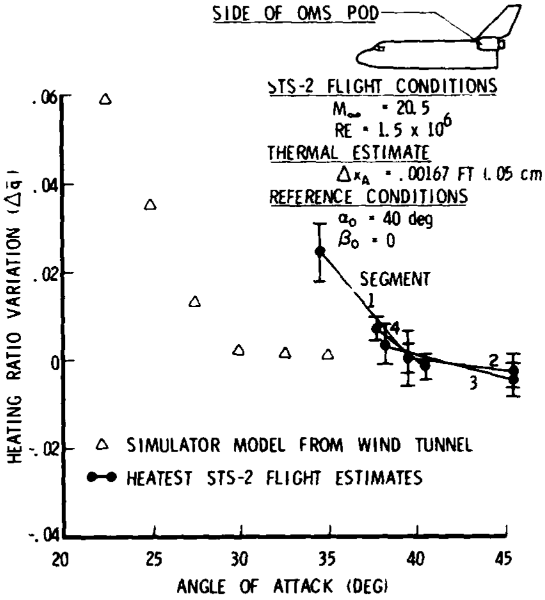

Figure 13. Heating Estimates for OMS POD from STS-2 Flight Thermocouple Data (Mach 20.5 Pushover-Pullup Maneuver)

PREDICTED AND FLIGHT TEST RESULTS OF THE PERFORMANCE AND STABILITY AND CONTROL OF THE SPACE SHUTTLE FROM REENTRY TO LANDING

by
Paul W. Kirsten, Aerospace Engineer
David F. Richardson, Aerospace Engineer
Air Force Flight Test Center
6510 Test Wing/TEG, Stop 236
Edwards Air Force Base, California 93523
USA

SUMMARY

This paper presents aerodynamic performance and stability data obtained from the first three reentries of the Space Shuttle Orbiter. Flight results are compared to predicted data from Mach 25 to Mach 0.4. Differences between flight and predicted data as well as probable causes for the discrepancies are given. Comparisons between simulator and flight results are also presented.

LIST OF ABBREVIATIONS AND SYMBOLS

AFFTC	Air Force Flight Test Center
C_A	axial force coefficient
C_D	drag force coefficient
C_L	lift force coefficient
C_ℓ	rolling moment coefficient
C_m	pitching moment coefficient
C_{m_o}	basic pitching moment coefficient
C_N	normal force coefficient
C_n	yawing moment coefficient
fps	feet per second
IMU	Inertial Measurement Unit
L/D	lift-to-drag ratio
MMLE	modified maximum likelihood estimator
m_j/m_∞	yaw jet mass flow ratio ($8.296 \times 10^{-6}\ V_\infty/\bar{q}_\infty$)
NASA	National Aeronautics and Space Administration
PJI	pitch jet interaction effects

psf	pounds per square foot
q	pitch rate, deg/sec
$\bar{q}$, $\bar{q}_\infty$	dynamic pressure, lbs/ft^2
RJI	roll jet interaction effects
STS-1,2,3	Shuttle flights 1, 2, and 3
$\bar{V}_\infty$	viscous interaction parameter
YJI	yaw jet interaction effects
α	angle of attack, degrees
β	sideslip angle, degrees
δa	aileron deflection, degrees
δBF	bodyflap deflection, degrees
δe	elevator deflection, degrees
δr	rudder deflection, degrees
ϕ_j/ϕ_∞	roll jet mass flow ratio ($.1543/\bar{q}$)
Δ	prefix meaning increment

Subscripts:

q, RJI, YJI, α, β, δa, δBF, δe, δr	partial derivatives with respect to the subscripted variables

INTRODUCTION

The United States Space Shuttle Orbiter offers a unique opportunity to correlate ground and flight test data for a manned maneuvering aerodynamic vehicle over a wide range of hypersonic velocities. Thus for the first time ground aerodynamic prediction techniques can be evaluated for extremely high velocities. In addition, the evaluation can be conducted using state-of-the-art ground and flight techniques. The Shuttle wind tunnel test program was one of the largest ever conducted, incorporating high-fidelity test facilities and wind tunnel models. Instrumentation sensors and reentry flight test maneuvers were specifically designed for the Orbiter to obtain high quality flight results. Analytical computer programs which have been proven reliable on numerous flight test programs in the past were used to extract the flight data. It is therefore felt that a meaningful comparison of predicted and flight aerodynamic data can be made throughout the Orbiter's reentry envelope.

In addition to verifying ground test facilities and analytical prediction techniques, flight-derived aerodynamic data can be used to update the predicted data base, expand the flight envelope, update crew training and engineering simulators, and improve the flight control system design. The flight data can also be used to verify aerodynamic and center of gravity placards, which, for the Orbiter, have been based on predicted data using rather large uncertainties. Hopefully, some of these placards can be removed or made less restrictive.

This paper compares flight-determined lift, drag, and stability and control derivatives to preflight predicted data for the initial three reentries of the Space Shuttle Orbiter. Data from Mach 24.6 (328,000 feet altitude) to Mach 0.4 (3,000 feet altitude) are presented. Estimated uncertainties will be given for both predicted and flight data. Differences between predicted and flight data, and the resulting effect upon the Orbiter's performance and stability, will be described. Comparisons between ground based simulator and flight data will also be given.

SYSTEM DEFINITION

The Space Shuttle Orbiter is a highly maneuverable vehicle with a double delta planform which performs a gliding reentry from orbital velocities to a horizontal landing on conventional runways. The dimensions of the Orbiter are given in Figure 1. A blend of reaction control jets and aerodynamic control surfaces are used during reentry to maintain stability and control. Above an altitude of 400,000 feet (defined as entry interface), stability and control in the pitch, roll, and yaw axes is provided by forward reaction control jets located in the nose of the vehicle and aft jets located in the orbital maneuvering system pods at the base of the vertical tail and above the wing. The forward jets are deactivated shortly before 400,000 feet, while the aft jets remain active. The aft roll axis jets are deactivated early in the reentry as the dynamic pressure increases through 10 psf (Mach = 24.5, Altitude = 260,000 feet). The aft pitch axis jets are deactivated at 20 psf. The aft yaw axis jets remain active throughout the reentry until Mach 1 to provide additional lateral-directional stability and control. Aerodynamic control surfaces consist of full span elevons at the trailing edge of the wing which move symmetrically for pitch control and differentially for roll control, a bodyflap at the aft centerline of the lower surface which is used for longitudinal trim, and a split rudder on the vertical tail which moves symmetrically for yaw control and differentially as a speedbrake for energy modulation. The elevons are activated at a dynamic pressure of 2 psf (290,000 feet) for pitch and roll control. The rudder is not activated until Mach 3.5 for transonic yaw control.

The Orbiter's aluminum substructure is covered with a reusable, lightweight insulating material to protect it from the high aerodynamic heating experienced during reentry.

REENTRY PROFILE

Figure 2 shows time histories of various parameters for the reentry of the second Orbiter flight (STS-2). The reentry profile was similar for the first and third flights. The most notable exception was the elevator bias which was deflected more downward on STS-3 to obtain elevator and aileron effectiveness as a function of bias position.

The high Mach number portion of the reentry is flown at a constant 40 degrees angle of attack to minimize upper surface aerodynamic heating. Energy modulation is performed by changing bank angle rather than angle of attack. The bank angle is reversed periodically to minimize crossrange error.

WIND TUNNEL PROGRAM

The uniqueness of the Shuttle's first flight was that it encompassed the entire Mach and altitude envelope without the benefit of a flight test buildup program. It was therefore mandatory that the best possible aerodynamic predictions be obtained prior to the first flight so that the uncertainty in the aerodynamics, and associated effects upon flight safety, be minimized.

One of the largest wind tunnel programs in history was conducted for the Space Shuttle (Reference 1). Over 27,000 occupancy hours were spent obtaining performance and stability and control characteristics for the Orbiter from virtually every major wind tunnel facility in the United States (Figure 3). A significant amount of this time was spent testing the final flight configuration. Two high fidelity wind tunnel models were constructed and tested to permit accurate modeling of all aerodynamic surfaces and simulation of all aerodynamically relevant cavities, gaps, and protuberances.

Figure 4 depicts the range of Mach and Reynolds numbers tested in the various facilities. Most testing was performed at Mach 8 and below. There were a few tests conducted above Mach 8 from which viscous interaction effects were obtained. Theoretical estimates at high altitudes (above 300,000 feet) were added to the basic wind tunnel data base to account for low density effects. Also, theoretical estimates of aeroelastic effects were incorporated at higher dynamic pressures, primarily in the transonic and subsonic regions. Real gas effects, which would primarily occur in the 150,000 to 270,000 feet altitude range, were not accounted for in the predicted data. Thus, the data referred to as "predicted" data in this report consists primarily of an extensive wind tunnel data base up to Mach 8, a limited number of wind tunnel tests above Mach 8 to obtain viscous interaction effects and high Mach effects, and theoretical estimates of low density and aeroelastic effects (Reference 2). None of the flight data contained in this report were obtained above 300,000 feet, therefore, low density effects were not applicable. Also, aeroelastic effects for most of the data presented were small in relation to the rigid wind tunnel data. Nevertheless the data must be referred to as "predicted" rather than wind tunnel data due to the extensive engineering interpretation that was applied to the basic wind tunnel data to account for such things as extrapolation of Reynolds number effects, differences between tunnels and models, inaccuracies in models, and linear interpolation between test conditions.

SIMULATOR MECHANIZATION

The U.S. Air Force at the Air Force Flight Test Center (AFFTC) developed an Orbiter simulation to aid in its flight test evaluation. The simulator consists of a six-degree-of-freedom, fixed-base, man-in-the-loop system designed to perform engineering analyses of the Orbiter's reentry and landing flight phase. The simulation was designed to be as simple and flexible as possible without incurring loss of accuracy. It was structured to allow rapid updates so that system changes, aerodynamic updates, and flight-derived data could be implemented and evaluated in a short time period. The enormous aerodynamic data base of the Orbiter was reduced as much as possible without losing accuracy at trim flight conditions. In fact, care was taken to include nonlinear effects representing small displacements about trim. Orbiter systems were also simulated in the most simplified and flexible manner possible without loss of accuracy. Simplification was acceptable for the AFFTC simulation since it was used to perform an independent Air Force analysis and was not part of the official Shuttle verification or training process.

The AFFTC simulator was used to perform numerous preflight and postflight aerodynamic performance, handling qualities, aerothermodynamics, and systems analyses. Results of these studies were made available to NASA Shuttle project personnel as "off-line" simulator analyses. It was also used to develop and design the flight test maneuvers performed during reentry to obtain aerodynamic performance, stability and control, and heating data from flight. The results obtained from these maneuvers will be the main topic of this report.

The unique nature of the Shuttle mission required that the first flight be performed without the benefit of a flight test buildup program. For this reason, preflight simulator studies conducted by the National Aeronautics and Space Administration (NASA) and the vehicle contractor were performed using rather severe uncertainties in the predicted aerodynamics to establish flight "placards" for the Orbiter. These uncertainties were referred to as "variations" in the Shuttle program, and were obtained by comparing the differences between flight and predicted data on previous aircraft and lifting body flight test programs. They are referred to as "predicted data uncertainties" in this report. One of the main objectives for obtaining accurate aerodynamic data from flight is to verify, and hopefully reduce, the flight placards based on "variations".

In the official verification process of the Orbiter design, aerodynamic differences obtained between the numerous wind tunnel tests which have been conducted were used to flight qualify the vehicle. These differences were referred to as "tolerances" in the Shuttle program. In some instances, the magnitude of these tolerances approached the magnitude of the variations. It is therefore hopeful that the acquisition of accurate flight data could also reduce the tolerance values used in the official flight verification of the Orbiter.

FLIGHT DATA SOURCES

The Orbiter flight data presented in this report were obtained from measurements made in the onboard instrumentation system. This system contains high sample rate and high resolution linear accelerometers, rate gyros, angular accelerometers, and rudder and elevon surface position indicators. The system also computes the parameters required to define flight conditions and vehicle Euler angles.

There are presently no external sources on the Orbiter for measuring the standard air data parameters at hypersonic speeds. At velocities greater than 2500 fps, velocity, angle of attack, and angle of sideslip are computed from linear accelerations and angular displacements measured by an Inertial Measurement Unit (IMU). Mach number is computed as velocity divided by 1000. Dynamic pressure is computed using a predicted estimate of drag coefficient and the measured value of drag acceleration from the IMU.

Below Mach 3.5, external side probes were deployed and measured the pressures required to compute Mach number, dynamic pressure, angle of attack, and angle of sideslip.

Vehicle weights and longitudinal and lateral center of gravity values for STS-1 and STS-2 were based on measurements obtained at the AFFTC Weight and Balance Facility shortly after landing. A post flight weighing was not performed for STS-3. Moments of inertia and vertical center of gravity values were obtained by analytical "bookkeeping" methods.

FLIGHT TEST MANEUVERS

Three types of test maneuvers specifically designed for obtaining aerodynamic data were performed during Orbiter reentries: (1) pushover-pullup maneuvers to obtain longitudinal performance data as a function of angle of attack, (2) bodyflap sweeps to obtain bodyflap effectiveness, and (3) longitudinal and lateral-directional control pulses to obtain stability and control derivatives. All three maneuvers were designed on ground based simulators and practiced extensively by the flight crews prior to flight. In addition to providing longitudinal performance and surface effectiveness data, the pushover-pullup maneuver and bodyflap sweeps provided aerodynamic heating data as a function of angle of attack and control surface position. This data was analyzed through the use of a special program developed at the AFFTC and is the subject of another report in this symposium.

The Orbiter lift, drag, and longitudinal trim data were obtained from both quasi-steady state and dynamic flight test conditions. The quasi-steady state data were obtained for all flights at constant Mach and angle of attack conditions throughout the reentry profile. The dynamic performance test maneuver (pushover-pullup) had been used successfully on previous unpowered glide vehicle research programs and was preferred over other maneuvers because it provided a significant amount of data in a relatively short time. The maneuver allows longitudinal performance data to be obtained as a function of angle of attack under transient conditions before committing to a steady state flight profile. This maneuver was performed manually and consisted of a sweep in angle of attack of ±5 to 10 degrees above and below the normal angle of attack. The piloting task was to perform the maneuver slow enough to avoid large pitch accelerations and consequently remain near trim, but fast enough to minimize the change in Mach number. Typically this maneuver took approximately 30-40 seconds to complete and resulted in a minimal perturbation of the reentry trajectory.

The most effective maneuver for obtaining accurate stability and control derivatives from flight data is a pulse doublet maneuver. In this maneuver, control inputs are executed at the highest rate possible that provides sufficient vehicle motion. The control doublet is followed by a few seconds of "free" oscillation. The control derivatives are extracted primarily from the initial control input and the stability derivatives are obtained during the "free" oscillation. The principle of the maneuver is to perform the control inputs quickly so that the effects of the control derivatives and stability derivatives are isolated. This provides unique information to the derivative extraction program and allows more accurate estimations to be obtained.

FLIGHT DATA ANALYSIS METHODS

Lift, drag, and longitudinal trim data were computed from flight test through the use of a Flight Test Performance Data Extraction program. This program required high resolution body axis accelerometers to compute performance data. Since the Orbiter is a gliding vehicle, there were not any thrust terms that had to be considered.

During a pushover-pullup maneuver, the pitch rate is sustained by an elevator deflection which also contributes to lift and drag. Therefore, the flight-derived lift, drag, and elevator deflection were corrected to zero pitch rate and pitch acceleration to obtain trimmed (equilibrium flight) data. These data were also corrected to a standard center of gravity position for comparison with the predicted data.

The performance data were corrected and standardized using predicted values for elevator effectiveness ($C_{m_{\delta e}}$, $C_{N_{\delta e}}$, and $C_{A_{\delta e}}$) and predicted pitch damping coefficient data (C_{m_q}).

Stability and control derivatives were extracted from flight data through the use of a Modified Maximum Likelihood Estimator (MMLE) program (Reference 3). This program has been extensively used on numerous aircraft and lifting body vehicles in the past, and has produced reliable and accurate results. The program models a vehicle's characteristics through the use of an appropriate set of aerodynamic equations of motion, containing unknown derivatives. The flight derivatives of the vehicle are obtained by varying the unknown derivatives until the error between the analytical and flight response is minimized.

In addition to providing an estimate of the value of the derivatives, the program also computes an estimation of the accuracy of each derivative. These accuracy estimations can be invaluable in assessing the quality of the results. However, the final assessment of accuracy should be obtained from the repeatability of the results as a function of a particular flight parameter such as Mach number or angle of attack.

There was originally some concern as to whether the Orbiter's derivatives could be accurately extracted from flight data due to the sluggish nature and slow response characteristics of the vehicle to control stimuli. These concerns were dismissed during the Approach and Landing Test program which was conducted from 1977 to 1978 with the Orbiter Vehicle. Figure 5 compares Orbiter flight data for two major derivatives obtained during this program with wind tunnel data. The solid line shown in the Figure is an average value of several wind tunnel tests conducted prior to the start of the program, and represents the best estimate of each derivative at that time. The circles represent the results of the MMLE program. The triangles represent wind tunnel results obtained after the program at the precise flight conditions and vehicle configuration at which the MMLE results were obtained. As can be seen, the MMLE results agree extremely well with these wind tunnel results (Reference 4).

COMPARISON OF FLIGHT AND PREDICTED DATA

Aerodynamic data obtained from flight are compared to "predicted" data in this section. Performance and longitudinal trim data were obtained from pushover-pullup maneuvers, bodyflap sweeps and quasi-steady state flight conditions over a Mach number range of 0.38 to 24.0. A pushover-pullup maneuver was performed during the second Orbiter flight (STS-2) at an average Mach number of 20 and provided data encompassing an angle of attack range of 34.8 to 45.7 degrees. Also, during this flight, a guidance-induced pitch maneuver at 0.4 Mach number provided excellent subsonic data covering an angle of attack range of 4.6 to 12.9 degrees. A speedbrake sweep at 0.5 Mach number provided surface effectiveness data.

The performance and longitudinal trim data are presented as a function of angle of attack at an average Mach number during the dynamic maneuver and/or average value of the viscous interaction term (V_∞) when applicable. The speedbrake effectiveness data are plotted as a function of surface deflection. The data from the bodyflap sweeps are presented as trim elevator deflection as a function of bodyflap position. These data will show the combined effectiveness of these two pitch control surfaces. (A pitch pulse was performed to isolate the elevator effectiveness.)

The predicted performance and longitudinal trim data are for a rigid Orbiter and are presented in the Figures of this report as solid lines. Uncertainties in the predicted data are presented as dashed lines above and below the predicted data.

Flight and predicted stability and control derivatives are presented primarily as a function of Mach number. Some data are presented as a function of dynamic pressure or reaction control jet mass flow ratio at high velocities where Mach number does not change rapidly. This form of presentation is for convenience only and can be misleading in some instances when other variables such as angle of attack are also changing. Since the Orbiter's reentry profile for the parameters which affect derivative results was very similar for the first three flights, predicted data for STS-2 only will be presented in the Figures. Estimations of uncertainties for the flight derivatives and predicted data are presented. Flight data uncertainties are presented as vertical bars about the derivative value. Predicted data uncertainties are presented as dashed lines about the solid line representing the predicted value.

Maneuvers have been performed and derivative results obtained down to approximately Mach 1 in the program thus far. Subsonic maneuvers have not been performed because this data was obtained in the Approach and Landing Test program conducted in 1977 with the Orbiter Vehicle launched from a 747 carrier aircraft. Subsonic results obtained from this program are contained in Reference 5.

Since the effects of rotary derivatives were small for the maneuvers presented in this report, their values were held at predicted values in all analyses and are not presented. All stability derivative data are presented at the flight center of gravity.

LONGITUDINAL PERFORMANCE

The supersonic and hypersonic lift-to-drag ratio (L/D) data obtained from the first two Orbiter flights are compared with predictions in Figure 6. The data are presented as a function of Mach number because the angle of attack at any particular Mach number during the reentry was constant (except for the pushover-pullup at Mach 20). However, the increase in L/D between Mach 15 and 5 was due to the angle of attack decrease from 40 degrees to 20 degrees rather than the Mach number change. (The predicted L/D curve does not change as a function of Mach number in this Mach regime.) Note the close agreement between flight and predicted L/D for Mach numbers greater than 1.0.

The L/D data extracted from the pushover-pullup at Mach number of 20 are shown in Figure 7. These data also showed excellent agreement with predictions. The lift and drag coefficient data obtained from this maneuver are presented in Figure 8. Both C_L and C_D are slightly less than predicted but within the uncertainty of the predicted data. The good correlation between flight and predicted C_D was not surprising because the onboard computation of dynamic pressure ($\bar{q}$) used in the performance program contains an estimation of the C_D curve. The uncertainty in determining $\bar{q}$ will remain a problem until a hypersonic air data system is installed in later versions of the Orbiter. The excellent correlation in L/D is not an issue as far as $\bar{q}$ is concerned since L/D is independent of $\bar{q}$.

The subsonic L/D data computed from the guidance-induced pitch maneuver are presented in Figure 9. The higher than predicted L/D out of ground effect is due primarily to the lower than predicted drag coefficient (Figure 10). The flight data values of C_L in Figure 10 were very close to predictions. Preliminary flight test data also indicated that the L/D in ground effect is also higher than predicted. The higher subsonic performance required some refinements to the landing approach (revised glide slope aim points) in order to touch down at the desired point on the runway.

The trimmed flight data from the speedbrake sweep at 0.5 Mach number were corrected to a common elevator deflection (6 degrees) to obtain the normal and axial force coefficient (C_N and C_A) increments due solely to the speedbrake. This correction accounted for the contribution of C_N and C_A due to elevator which was deflected to counteract the longitudinal trim change from the speedbrake. These data were corrected to a common angle of attack (6 degrees). The resultant corrected increments were plotted as a function of speedbrake deflection in Figure 11. These data indicate that the speedbrake effectiveness was slightly greater than predicted for deflections above 50 degrees. The normal force decrement due to speedbrake was less than predicted. Note that both of these increments are dependent upon the values for the longitudinal derivatives that were used to correct the flight data to the standard elevator and angle of attack. Predicted values were used for these derivatives and will be updated whenever flight test data become available.

The Orbiter flight control software logic contains a bodyflap-elevator interconnect designed to maintain the elevator on a predefined schedule as a function of Mach number by automatic trimming of the bodyflap. A significant error in longitudinal trim in the hypersonic Mach regime was apparent on all three Orbiter reentries. For example, during STS-1 the trim bodyflap was 16 degrees rather than 7 degrees at velocities greater than 17,000 fps (Figure 12). Analysis of the bodyflap sweeps and the pitch pulse performed during the second Orbiter reentry established that the major contributor to the trim error was an error in the basic pitching curve, C_{m_o}, rather than an error in elevator or bodyflap effectiveness. Figure 13 contains trim data obtained during the bodyflap sweep at a Mach number of 21. Note that the slope of the flight test data is similar to, or slightly greater than predicted. Also, the data obtained from the pitch pulse at Mach 20.6 indicated that the elevator effectiveness $C_{m_{\delta e}}$, was close to predicted (refer to Longitudinal Derivatives section). The trim elevator data obtained from the pushover-pullup at Mach 20 showed that the Orbiter was statically stable and the slope indicated that the combined elevator effectiveness/pitch static stability was close to predictions (Figure 14). Thus, the foregoing tends to confirm that the mispredicted longitudinal trim at high Mach number is attributable to an error in basic pitching moment.

The subsonic longitudinal trim data in Figure 15 extracted from the guidance-induced pitch maneuver confirm the negative static margin that was predicted at Mach numbers less than 0.8 for a center of gravity of 66.7 percent. These data also show more positive elevator deflections than predicted and the slope appears to be slightly more negative. This could be due to a small error in the basic pitching moment, the elevator effectiveness or the static stability predictions. Additional flight tests will be required to identify the error source.

In summary, at the angles of attack tested so far in the Orbiter program, the supersonic/hypersonic lift-to-drag ratio is the same as predicted. The subsonic L/D is greater than predicted due to a misprediction in drag coefficient. The hypersonic longitudinal trim was significantly different from predictions due to an error in the basic pitching moment curve. The static longitudinal stability was the same as predicted at the hypersonic Mach numbers where test data were available. Based on the limited flight test data, the static stability at subsonic Mach numbers may be slightly less than predicted.

LATERAL-DIRECTIONAL DERIVATIVES

Lateral-directional derivative results obtained from pulse doublet maneuvers during STS-2 and STS-3 are contained in Figures 16 through 21. Uncertainty estimates for the predicted and flight data are also shown. The predicted data is represented by a solid line, while the short dashed line represents a fairing of the flight data.

The dihedral effect (C_{ℓ_β}) is presented in Figure 16. The consistency of the flight results as a function of Mach number, and the flight uncertainty estimates, were considerably smaller than the uncertainty of the predicted data for most maneuvers, indicating high confidence in the flight results. Flight data showed a tendency to vary with Mach number above Mach 10, which was inconsistent with the predicted data. The flight results were considerably lower than predicted at very high Mach numbers. Note that even though the uncertainty estimates computed by the MMLE program were large for the first two maneuvers at high Mach numbers, the derivative values were reasonable and consistent with other results. These maneuvers were performed at very low dynamic pressures of 4 and 8 psf. Below Mach 3, flight results for C_{ℓ_β} were more negative than predicted. Although results were fairly consistent with Mach number, an important criterion for assessing accuracy, the uncertainty estimates were quite large. Possible causes for these large uncertainties are nonlinear effects with control surface deflection, rapidly changing Mach number/derivative value in this flight regime, and wind shears which are not modeled in the MMLE program. The Orbiter has exhibited a small amplitude lateral-directional oscillation in the transonic region on its first three flights, and it is felt that the higher than predicted dihedral effect is a contributor to this oscillation. This oscillation will be discussed further through this report.

Flight results for the directional stability derivative (C_{n_β}) were close to predicted throughout the Mach range. Results obtained on flight 3 using high resolution instrumentation were extremely consistent with Mach number and indicated a slightly more stable value above Mach 8. (High resolution instrumentation was not available on STS-2 due to an onboard tape recorder failure.) The irregular shape in the predicted data between Mach 8 and 3 represents results obtained from wind tunnel tests conducted at small amplitude sideslip deflections. Flight results (also at small sideslip deflections) agree very well with these predictions.

Aileron derivatives are shown in Figures 17 and 18. Aileron derivatives are a strong function of elevator bias position. The first three reentries were made with different elevator schedules at high Mach numbers: approximately -1, 1, and 3 degrees for STS-1, STS-2, and STS-3 respectively. Therefore for uniformity and ease of presentation, STS-3 derivative results shown in Figure 17 have been corrected to the STS-2 reentry elevator position using predicted values for these effects. In order that these effects may be evaluated, aileron derivatives are presented as a function of elevator position in Figure 18.

Flight values for the aileron effectiveness derivative ($C_{\ell_{\delta a}}$) were slightly higher than predicted above Mach 12. In addition, the slope of $C_{\ell_{\delta a}}$ versus elevator position also appears to be higher than predicted. The MMLE program could not extract aileron derivatives accurately for the maneuver performed at the highest Mach number shown (dynamic pressure = 4 psf). Their values were therefore held constant during the analysis of this maneuver. Flight values for $C_{\ell_{\delta a}}$ were generally lower than predicted between Mach 3 and 1. Low aileron effectiveness is felt to be another cause of the small amplitude lateral-directional oscillation which occurs in this flight regime. When this oscillation was analyzed with the MMLE program, the $C_{\ell_{\delta a}}$ value obtained at Mach 1.6 was considerably lower than predicted (.00075 per degree) if atmospheric wind shears were not accounted for. Wind shears were then accounted for in the MMLE program using the sideslip angle obtained from differential pressure measurements of the external side probes and the inertially computed sideslip angle. The difference between these two measurements was differentiated and programmed into the MMLE program as a forcing function in the rate of change of sideslip equation. When wind effects were included, the resulting value of $C_{\ell_{\delta a}}$ increased and was much closer to predicted. The results of this analysis should not be considered conclusive however. Accurate results are often difficult to obtain for this type of maneuver. Values of other derivatives (especially $C_{\ell_{\delta r}}$) obtained from this analysis remain questionable. Pressure lags associated with the side probe system were not accounted for and could have significant impact on the results. Nevertheless, the analysis does indicate that wind shears need to be accounted for and could be a contributing factor to the low frequency oscillation observed in flight.

Flight values of $C_{n_{\delta a}}$ agreed well with predictions for most STS-2 maneuvers. A few values below Mach 3 were more positive than predicted, but their uncertainty estimates were large. STS-3 values, obtained for a more downward elevator deflection and using the higher resolution instrumentation, were more negative than predicted at high Mach numbers. Flight values of $C_{n_{\delta a}}$ are difficult to obtain accurately for most airplanes. The large uncertainty estimates shown indicate the potential inaccuracies in the values of $C_{n_{\delta a}}$ for the Orbiter.

Rudder derivatives are shown in Figure 19. The rudder is only active from Mach 3.5 to landing. Flight results agreed very well with predicted data for the pulse doublet maneuvers.

Since the aft reaction control jets are located above the wing at the base of the vertical tail of the Orbiter, the plume produced when the jets are fired can interact with the flow field over the vehicle and alter the basic aerodynamic forces and moments. These effects are referred to as jet interaction effects, and are presented in derivative form in this report. Jet interaction effects are presented as a function of mass flow ratio, a parameter used to extrapolate Mach 10 wind tunnel data to higher Mach numbers. (Jet interaction effects were not obtained at Mach numbers greater than 10 in wind tunnel tests.) The derivative values presented are a measure of the jet plume interaction with the aerodynamic flow only, and do not contain the basic thrust and moment components of the jets.

Interaction effects for the yaw jets are presented as a function of Mach number below Mach 12 and as a function of yaw jet mass flow ratio above Mach 12 in Figure 20. Flight values of the roll due to yaw jet interaction effect ($C_{\ell_{YJI}}$) were significantly less than predicted at high values of mass flow ratio. The flight results are very consistent as a function of mass flow ratio, and the scatter in the data is much smaller than the uncertainty levels of the predicted data. The uncertainty levels of the flight results are also small. Thus a high degree of confidence is placed in the flight results. The error in the predicted value of $C_{\ell_{YJI}}$ was the major cause of a large amplitude, lightly damped lateral-directional oscillation which occurred during the initial bank maneuver performed on STS-1 at a mass flow ratio of .015 (dynamic pressure of 14 psf). This oscillation will be discussed further in the following sections of this report. Flight results obtained for the yaw due to yaw jet interaction effect ($C_{n_{YJI}}$) were somewhat greater (more negative) than predicted. The difference is much smaller than what was obtained for $C_{\ell_{YJI}}$ however. STS-3 results were more consistent as a function of mass flow ratio than STS-2 results. Therefore, more emphasis was placed on the STS-3 results when fairing the flight data.

Roll jet interaction derivatives are presented in Figure 21 as a function of roll jet mass flow ratio. Results were obtained from two pulse maneuvers performed on STS-2 prior to deactivation of the roll jets at a dynamic pressure of 10 psf. The MMLE program is modeled to obtain independent values for up and down firing jet interaction effects. However, simultaneous firing of up and down jets to produce roll during the flight maneuvers prevented the extraction of separate interaction effects. The results are therefore presented as a total rolling and yawing moment coefficient produced by one up and one down firing jet. Flight uncertainty estimates are not presented since they are not computed by the MMLE program for the total interaction effect. Flight roll due to roll jet interaction effects ($C_{\ell_{RJI}}$) were less than predicted, while yaw due to roll jet interaction effects ($C_{n_{RJI}}$) were about the same value as predicted.

LONGITUDINAL DERIVATIVES

Longitudinal pulse doublet maneuvers have been performed at high Mach numbers only in the program thus far. Elevator and angle of attack derivatives, and pitch jet interaction effects were obtained from these maneuvers. Bodyflap effectiveness data were obtained from bodyflap sweeps performed on STS-2 above Mach 10.

Elevator and angle of attack derivatives are shown in Figure 22. Elevator effectiveness is very nonlinear as a function of elevon deflection angle. The flight value of the derivative obtained is a linear average for the deflection range traversed by the surface during the maneuver. The irregular shape of the predicted data reflects the nonlinearity of the derivative and the different surface deflection range during each maneuver. Flight values of elevator effectiveness were close to predicted for all maneuvers analyzed. Elevator effectiveness derivatives were obtained with some degree of certainty at a dynamic pressure as low as 2 psf. Flight angle of attack derivatives were much more difficult to obtain at low dynamic pressures due to the small and sluggish attitude response of the Orbiter to pulse stimuli at these flight conditions. They were held at predicted values during the analyses of the three maneuvers at the lowest dynamic pressures.

Pitch jet interaction derivatives are plotted in Figure 23 as a function of the pitch jet mass flow ratio. The pitch jets are deactivated at dynamic pressures greater than 20 psf, and were therefore not fired during the Mach 20.6 doublet on STS-2 and the Mach 21.5 doublet on STS-3. The derivative values shown are a measure of the jet plume interaction with the aerodynamic flow only and do not contain the basic thrust and moment component of the jets. For reasons similar to those presented in the roll jet discussion, only the total interaction effect for up and down firing jets was obtained. Flight uncertainty estimates are not presented since they are not computed by the MMLE program for the total interaction effect. Pitch jet interaction effects were close to predicted values for the two maneuvers at the lowest mass ratios (highest dynamic pressures), but were lower than predicted at the two highest mass flow ratio maneuvers. Results obtained at the high mass flow ratios were felt to be degraded due to the loss of the high resolution instrumentation on STS-2.

Bodyflap derivatives are presented in Figure 23. Bodyflap effectiveness was slightly greater than predicted over the hypersonic Mach range analyzed. Bodyflap derivatives were obtained from slow moving bodyflap sweeps. (The maximum rate at which the bodyflap can move is three degrees per second.) The slow nature of the maneuver is not desirable for derivative extraction, and the accuracy of the bodyflap derivatives is therefore somewhat uncertain. In order to improve the accuracy of the bodyflap results, elevator derivatives were held fixed at values obtained from pulse maneuvers during the analysis of the bodyflap sweeps.

FLIGHT AND PREDICTED DATA DIFFERENCES

This section summarizes the major differences found to date between the flight and predicted data base of the Orbiter. Possible causes for the differences will be presented.

HYPERSONIC LONGITUDINAL TRIM

The flight longitudinal trim of the Orbiter was significantly different than predicted above Mach 8. Flight values of elevator and bodyflap effectiveness ($C_{m_{\delta e}}$ and $C_{m_{\delta BF}}$) obtained from pulse maneuvers and bodyflap sweeps were close to predictions in this region. The reason for the trim discrepancy is therefore an error in the predicted value of the basic pitching moment (C_{m_o}) of the vehicle rather than an error in control surface effectiveness. A pitch up C_{m_o} increment of +.023 must be applied to the predicted data to duplicate the flight longitudinal trim characteristics above Mach 18.

The primary cause of the error in the predicted hypersonic values of C_{m_o} is felt to be real gas effects. Real gas effects are the aerodynamic effects resulting from deviations of real air thermodynamic properties from ideal gas with constant specific heat. These effects were not fully simulated in wind tunnel tests and were not accounted for in the predicted aerodynamic data base of the Orbiter. Real gas effects are most significant between 150,000 and 270,000 feet. Recent analytical studies (currently unpublished) performed by the Arnold Engineering Development Center indicate real gas effects could produce a pitch up increment of .024 above Mach 18, which is very close to the difference between flight and predicted results. Real gas effects would also produce less lift force, which is consistent with flight results.

The remaining small difference between flight and predicted values of C_{m_o} could be caused by viscous interaction and high Mach number effects. These effects are thought to be small in comparison to real gas effects however, and tend to cancel each other.

The most significant effect of the error in the prediction of hypersonic trim will be increased heating on the bodyflap and/or elevon due to the more downward deflection required. Additional downward deflection, and increased heating, would be required for more aft longitudinal centers of gravity. However, it appears that heating margins are adequate to achieve the most aft center of gravity required in the Shuttle program.

REACTION CONTROL JET INTERACTION EFFECTS

The larger than predicted lateral-directional oscillation during the first bank maneuver on STS-1 was the result of over predicting the rolling moment produced by the interaction of the exhaust plume of the yaw reaction control jets with the aerodynamic flow over the upper surface of the wing. Reaction control jet plume interaction effects were obtained from three wind tunnel tests (Reference 6). Yaw jet interaction data were found to be primarily a function of the mass flow ratio of the jet plume to freestream air (m_j/m_∞), and angle of attack. Mass flow ratio is a function of freestream velocity and dynamic pressure. Flight angle of attack conditions were duplicated in the wind tunnel but mass flow ratios were not. The lowest dynamic pressure possible during wind tunnel testing was 75 psf at Mach 10.3. The dynamic pressure during the first bank reversal was 14 psf at Mach 24.4. Therefore jet interaction effects as a function of mass flow ratio measured in the tunnel were extrapolated to high Mach, low dynamic pressure flight conditions. The extrapolation proved to be invalid due to differences between the wing wake boundaries at the wind tunnel and flight test conditions. The wing wake boundary of the model was stronger and more confining due to the high static pressure levels that must be maintained in the wind tunnel. The stronger wake boundary was more resistant to jet gas diffusion, which tended to produce more of a rolling moment interaction effect than what was experienced at high altitude, low dynamic pressure flight conditions. Jet interaction effects obtained from flight were close to predicted values at Mach 20 (dynamic pressure = 48 psf) and below.

The first bank maneuver on STS-1 was performed in the automatic flight control system mode. On subsequent flights, the maneuver was performed manually by the commander at a slower roll rate to avoid the large oscillation. A flight control system modification will be made on STS-5 which should provide adequate control in both the automatic and manual modes during the first bank maneuver.

SUBSONIC PERFORMANCE

The subsonic lift-to-drag ratio data obtained from flight test at subsonic Mach numbers was greater than predicted. The major contributor to this increased L/D was a reduction in drag coefficient. The primary cause of this error in C_D is thought to be an overprediction of the drag due to surface irregularities in Thermal Protection System (TPS). The drag increment (.0038) to account for TPS gaps and steps was based on theoretical calculations and was not verified with wind tunnel tests.

TRANSONIC STABILITY

The small amplitude lateral-directional oscillation which has occurred near Mach 1.6 during the first three reentries may be the result of decreased lateral-directional stability due to lower than predicted aileron effectiveness ($C_{\ell_{\delta a}}$), higher than predicted dihedral effect (C_{ℓ_β}), and more positive yaw due to aileron ($C_{n_{\delta a}}$). Atmospheric wind shears may also have been a contributing factor to the oscillation. The uncertainty of the flight derivatives obtained in this region thus far has been large. Recent post flight wind tunnel tests have been conducted in which data for small sideslip angles and control surface deflections have been obtained to check for nonlinear effects. The data obtained was linear, and the preflight predictions were substantiated.

The bodyflap was deflected to its upper limit at Mach 1.6 during flight. Thus more forward longitudinal center of gravity movement would require the elevator to be deflected further up to maintain the desired trim angle of attack. An increased up elevator deflection would decrease $C_{\ell_{\delta a}}$ somewhat, which could in turn degrade the lateral-directional stability. The transonic oscillation could therefore restrict the forward center of gravity limit of the Orbiter until it is eliminated by a flight control system modification or other means.

HIGH MACH NUMBER DERIVATIVES

Two primary lateral-directional aerodynamic derivatives, C_{ℓ_β} and $C_{\ell_{\delta a}}$, have been inaccurately predicted above Mach 12. Predicted results estimated these derivatives to be essentially invariant with Mach number above Mach 12. Flight results for C_{ℓ_β} decreased with increasing Mach number and were considerably lower than predicted at Mach 24. Flight results for $C_{\ell_{\delta a}}$ were higher than predicted at high Mach numbers. Thus it appears that Mach number, viscous interaction, real gas, or low density effects have not been properly accounted for in the prediction of these derivatives. The cause of the discrepancy is not known at the time of this writing.

The differences in C_{ℓ_β} and $C_{\ell_{\delta a}}$ at high Mach numbers have had little effect on the Orbiter's stability thus far. One reason for this is that the Orbiter's high gain, command augmentation flight control system, which presently relies heavily on reaction control jets for stability, tends to mask most variations which may occur in aerodynamic derivatives. If the flight control system is redesigned in the future to rely less on reaction control jets (to reduce fuel and weight requirements), these aerodynamic differences will be more evident. If lower angle of attack reentries are performed in the future to achieve higher lift-to-drag ratios, the reduced value of C_{ℓ_β} and corresponding decreased value of dynamic directional stability, could be of concern.

SIMULATOR UPDATES AND ANALYSES

This section presents updates made to the AFFTC Orbiter simulation to incorporate the major differences found between flight and predicted aerodynamic data. As such, it contains a summary of the differences between flight and predicted data which have had the most significant effect upon the Orbiter's aerodynamic performance and stability and control characteristics.

In the hypersonic Mach regime, a significant error in longitudinal trim was observed during each of the Orbiter reentries. The major contributor to this error was a shift in the basic pitching moment curve. The simulator at the AFFTC was updated with a C_{m_o} shift based on STS-1 and STS-2 flight data. The magnitude of this shift was 0.023 for velocities greater than 18,000 fps. Figure 24 compares the trim elevator and bodyflap deflections from the updated simulator with STS-3 flight data. The close agreement between flight and simulator predicted data confirms the validity of the pitching moment correction.

The lightly damped lateral-directional oscillation during the first bank maneuver on STS-1 occurred at a Mach number of 24.4, a dynamic pressure of 14 psf, and an angle of attack of 40 degrees. Figure 25 contains time histories of the preflight predicted response and the flight response for this maneuver. Initially, the AFFTC simulator was used to determine the cause of the oscillation by manually varying the significant stability and control derivatives until a reasonable representation of the flight test history was obtained. Within hours after the flight data was received, results obtained from this manual matching technique concluded that an error in the prediction of the roll due to yaw jet interaction effect was the primary cause of the oscillation. These conclusions were later confirmed by results obtained from the MMLE derivative matching program. A simulator time history of the first bank maneuver using flight results obtained from the MMLE program is contained in Figure 25.

A control system modification which incorporates an inertially computed sideslip feedback will be made on STS-5 to improve the Orbiter's lateral-directional characteristics during the first bank maneuver. A simulator time history of this maneuver using the sideslip feedback modification and flight-derived stability and control derivatives is contained in Figure 26.

Figure 27 compares a time history of flight data obtained during the second bank maneuver (first bank reversal) with a simulator time history using predicted aerodynamic data. The maneuver was performed at a Mach number of 18.3, dynamic pressure of 58, and an angle of attack of 40 degrees. The flight and simulator results match well, indicating the predicted data adequately represented the flight data at these conditions. Flight data extracted during this maneuver using the MMLE program indicated that the value of the roll due to yaw jet interaction effect was indeed close to predictions.

Stability derivatives extracted from flight in the region where the small lateral-directional oscillation has occurred (Mach 1.4 to 2.0) have contained a considerable amount of uncertainty. The exact cause of the oscillation is therefore uncertain at this time. A study was conducted on the AFFTC simulator to attempt to duplicate the transonic oscillation seen in flight. No tendency to oscillate was seen using predicted derivatives, even when the simulator was pulsed (Figure 28). When the simulator was updated using the flight fairings of Figures 16 and 17, a tendency to oscillate at the same frequency which occurred in flight was observed. However, the oscillation was not sustained. When $C_{\ell_{\delta a}}$ was reduced further to a value of .00075 per degree (low confidence value obtained by analyzing the STS-1 oscillation without including wind shears), the simulator oscillated at a frequency and amplitude which was similar to the flight oscillation.

The oscillation appears to be caused by low lateral-directional stability. External disturbances such as wind shears are probably driving the oscillation. Primary cause of the oscillation is felt to be a low total roll axis gain ($C_{\ell_{\delta a}}$ plus roll axis flight control system gain). Some proof of this is provided by the fact that the oscillation always damps out in flight at a Mach number of 1.4 where the value of $C_{\ell_{\delta a}}$ increases rapidly (Figure 17). Thus is appears that the oscillation may be damped by increasing the roll axis gain of the flight control system.

The AFFTC simulator was used to evaluate the effects of a roll axis flight control system gain increase. The simulator was altered using the flight fairings of Figures 16 and 17 for C_{ℓ_β} and $C_{n_{\delta a}}$, and a value .00075 per degree for $C_{\ell_{\delta a}}$ to provide a steady oscillation. The simulator was operated in the five-degree-of-freedom mode (velocity and altitude held constant). The yaw jets were deactivated in the simulator, and a slightly divergent oscillation resulted (Figure 29). When the roll axis flight control system gain was doubled, the oscillation damped. An increased roll axis flight control system gain is being strongly considered to improve the transonic flight characteristics of the Orbiter.

CONCLUDING REMARKS

Aerodynamic performance and stability data have been successfully obtained from the first three reentries of the United States Space Shuttle Orbiter. Generally good correlation was achieved between flight results and the Orbiter's predicted data base. Some differences did occur, primarily at high Mach numbers and altitudes. The basic longitudinal pitching moment of the Orbiter was significantly different than predicted above Mach 8. The difference is thought to be caused by real gas effects at high altitudes. The interaction of the yaw reaction control jets with the aerodynamic flow field was overpredicted at low dynamic pressures, and caused a lightly damped oscillation during a bank maneuver performed early in the reentry. The overprediction was due to incorrect extrapolation from wind tunnel test conditions to very low dynamic pressure flight conditions.

It is hoped that this report has provided a meaningful comparison of flight and predicted aerodynamic data over an extremely large flight envelope. The intent has not been to critique or criticize ground test facilities, but rather to feed back information which might be useful in improving the overall data prediction and acquisition process.

REFERENCES

1. Underwood, Jimmy M. and Cooke, Douglas R., A Preliminary Correlation of the Orbiter Stability and Control Aerodynamics from the First Two Space Shuttle Flights (STS-1 and 2) with Preflight Predictions, AIAA Paper 82-0564, March 1982.

2. Aerodynamic Design Data Book, Orbiter Vehicle 102, SD2-SH-0060, Volume 1L, October 1978, plus Revisions 1, 2, and 3, Rockwell International, Space Division, Downey, California.

3. Maine, Richard E. and Iliff, Kenneth W., User's Manual for MMLE-3, A General Fortran Program for Maximum Likelihood Parameter Estimation, NASA Technical Paper 1563, November 1980.

4. Freeman, Delma C., Jr. and Spencer, Bernard Jr., Comparison of Space Shuttle Orbiter Low-Speed Stability and Control Derivatives Obtained from Wind-Tunnel and Approach and Landing Flight Tests, NASA Technical Paper 1779, December 1980.

5. Hoey, Robert G., et al, AFFTC Evaluation of the Space Shuttle Orbiter and Carrier Aircraft - NASA Approach and Landing Test, AFFTC-TR-78-14, Air Force Flight Test Center, Edwards AFB, CA, May 1978.

6. Orbital Flight Test Aerodynamic Data Analysis - Space Transportation System, Orbiter Vehicle, Volume 1, STS81-0558, Volume 1A, Rockwell International, Space Division, Downey, California.

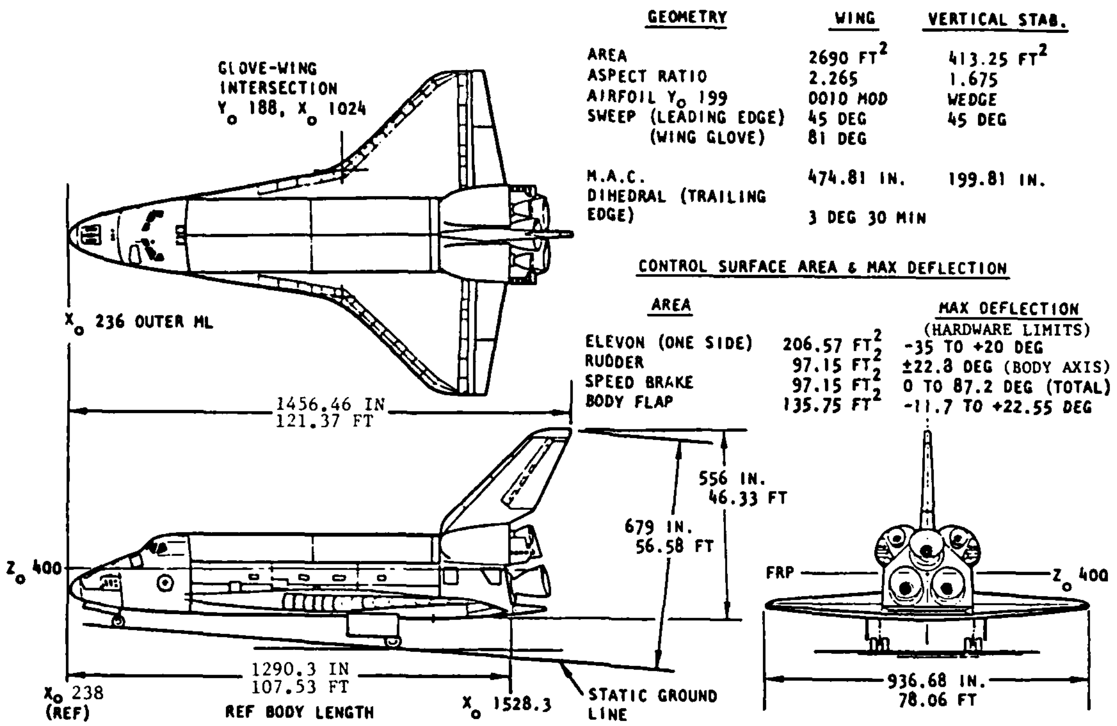

GEOMETRY	WING	VERTICAL STAB.
AREA	2690 FT^2	413.25 FT^2
ASPECT RATIO	2.265	1.675
AIRFOIL Y_o 199	0010 MOD	WEDGE
SWEEP (LEADING EDGE)	45 DEG	45 DEG
(WING GLOVE)	81 DEG	
M.A.C.	474.81 IN.	199.81 IN.
DIHEDRAL (TRAILING EDGE)	3 DEG 30 MIN	

CONTROL SURFACE AREA & MAX DEFLECTION

	AREA	MAX DEFLECTION (HARDWARE LIMITS)
ELEVON (ONE SIDE)	206.57 FT^2	-35 TO +20 DEG
RUDDER	97.15 FT^2	±22.8 DEG (BODY AXIS)
SPEED BRAKE	97.15 FT^2	0 TO 87.2 DEG (TOTAL)
BODY FLAP	135.75 FT^2	-11.7 TO +22.55 DEG

GLOVE-WING INTERSECTION
Y_o 188, X_o 1024
X_o 236 OUTER ML
1456.46 IN
121.37 FT
556 IN.
46.33 FT
679 IN.
56.58 FT
Z_o 400
FRP
Z_o 400
1290.3 IN
107.53 FT
X_o 238 (REF)
REF BODY LENGTH
X_o 1528.3
STATIC GROUND LINE
936.68 IN.
78.06 FT

FIGURE 1 - ORBITER THREE VIEW DRAWING

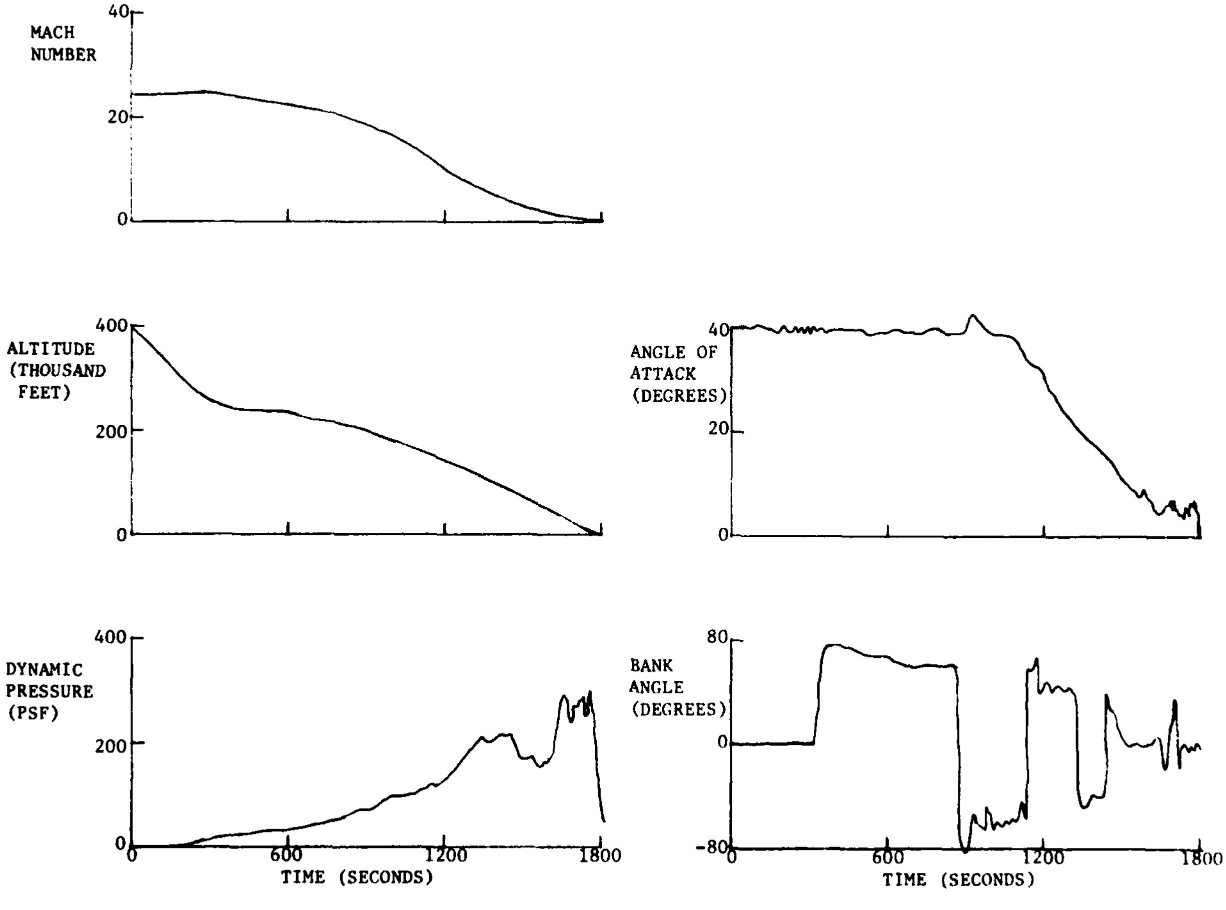

FIGURE 2 - STS-2 REENTRY PROFILE

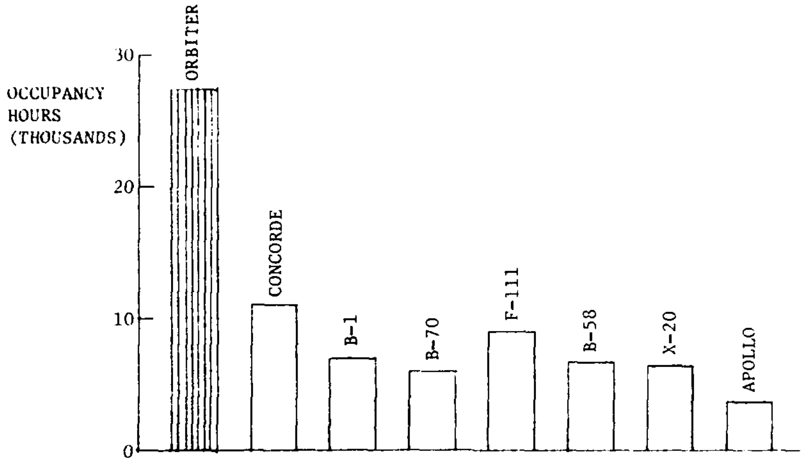

FIGURE 3 - COMPARISON OF ORBITER AERODYNAMIC WIND TUNNEL HOURS WITH OTHER PROJECTS

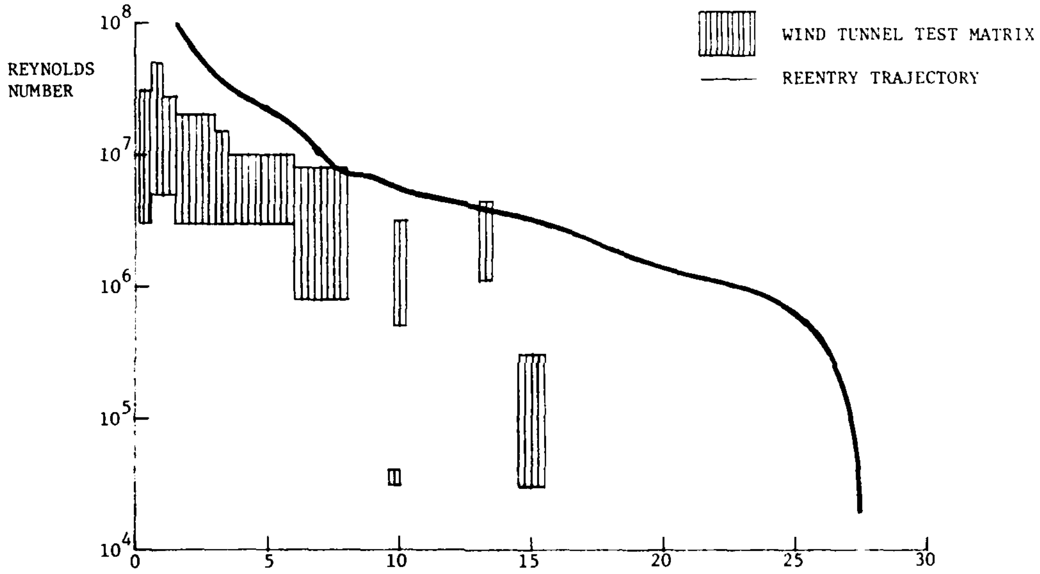

FIGURE 4 - ORBITER WIND TUNNEL DATA BASE

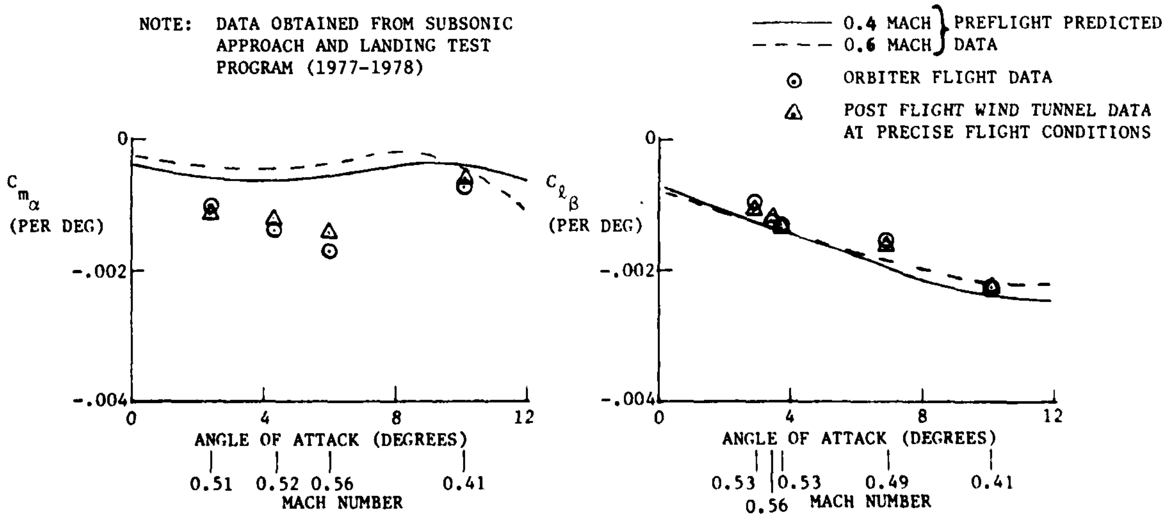

NOTE: DATA OBTAINED FROM SUBSONIC APPROACH AND LANDING TEST PROGRAM (1977-1978)

FIGURE 5 - COMPARISON OF FLIGHT RESULTS AND POST FLIGHT WIND TUNNEL DATA

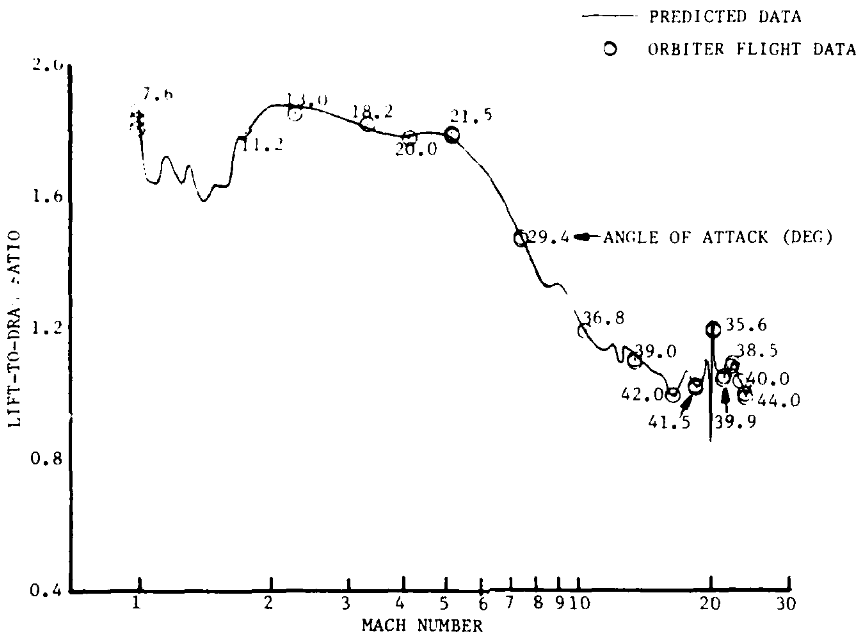

FIGURE 6 - SUPERSONIC/HYPERSONIC LIFT-TO-DRAG RATIO

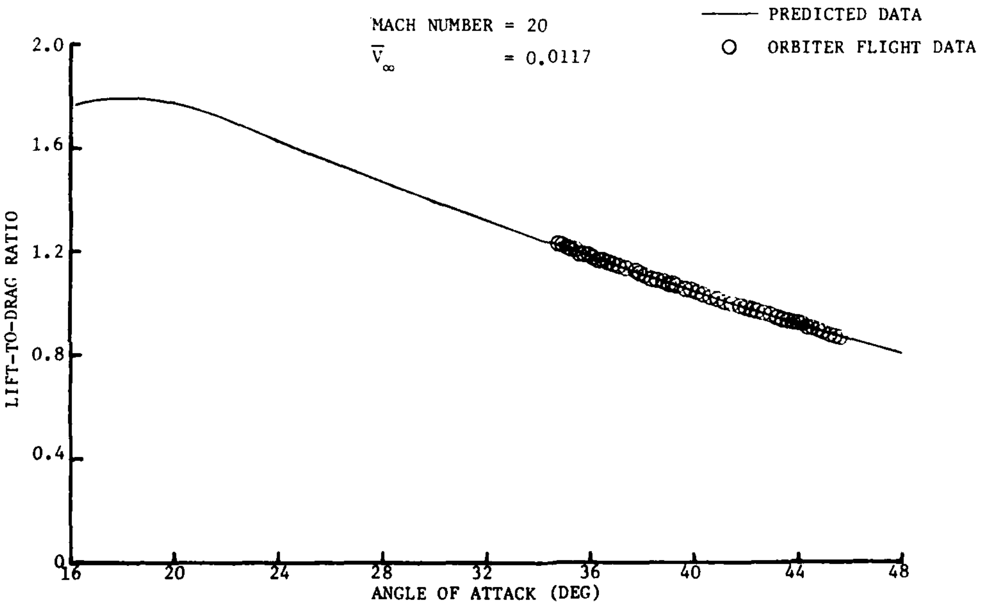

FIGURE 7 - LIFT-TO-DRAG RATIO AT MACH 20

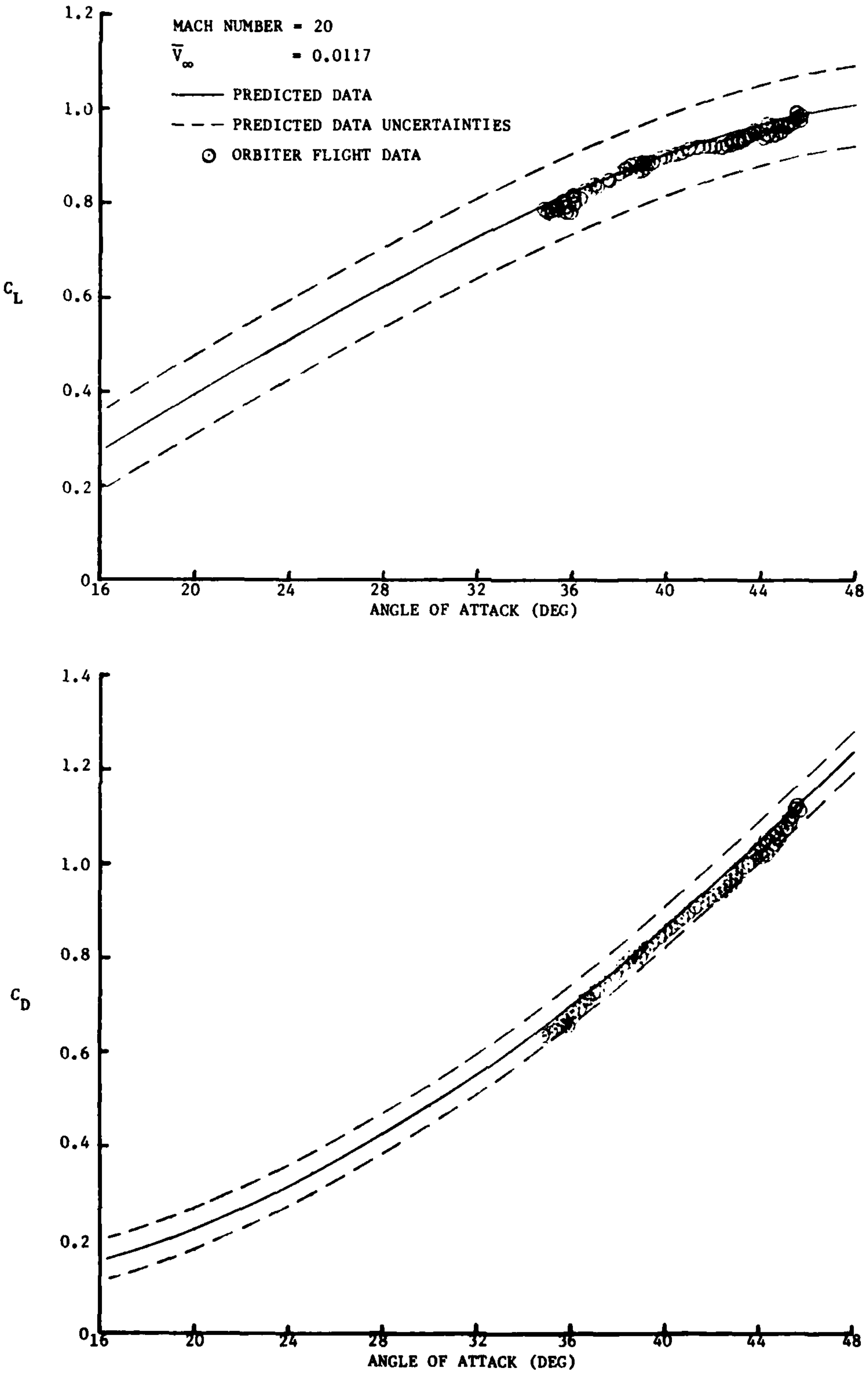

FIGURE 8 - PERFORMANCE DATA AT MACH 20

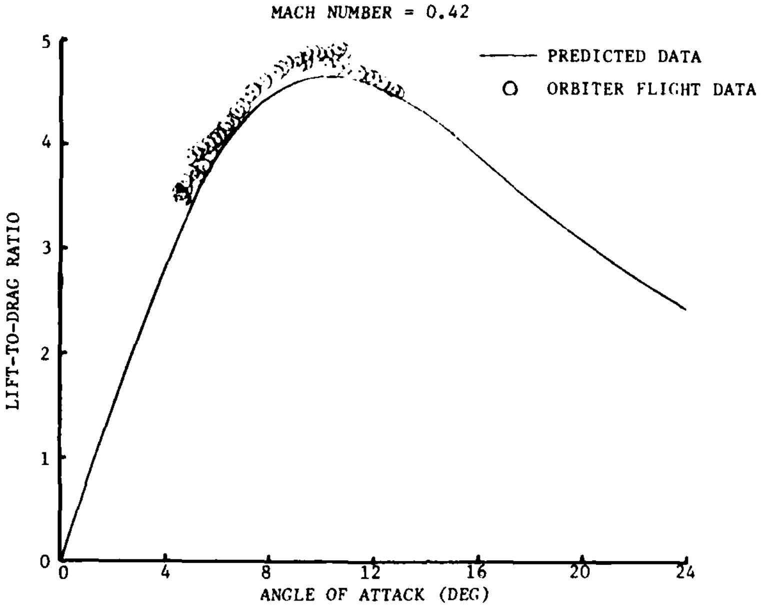

FIGURE 9 - SUBSONIC LIFT-TO-DRAG RATIO

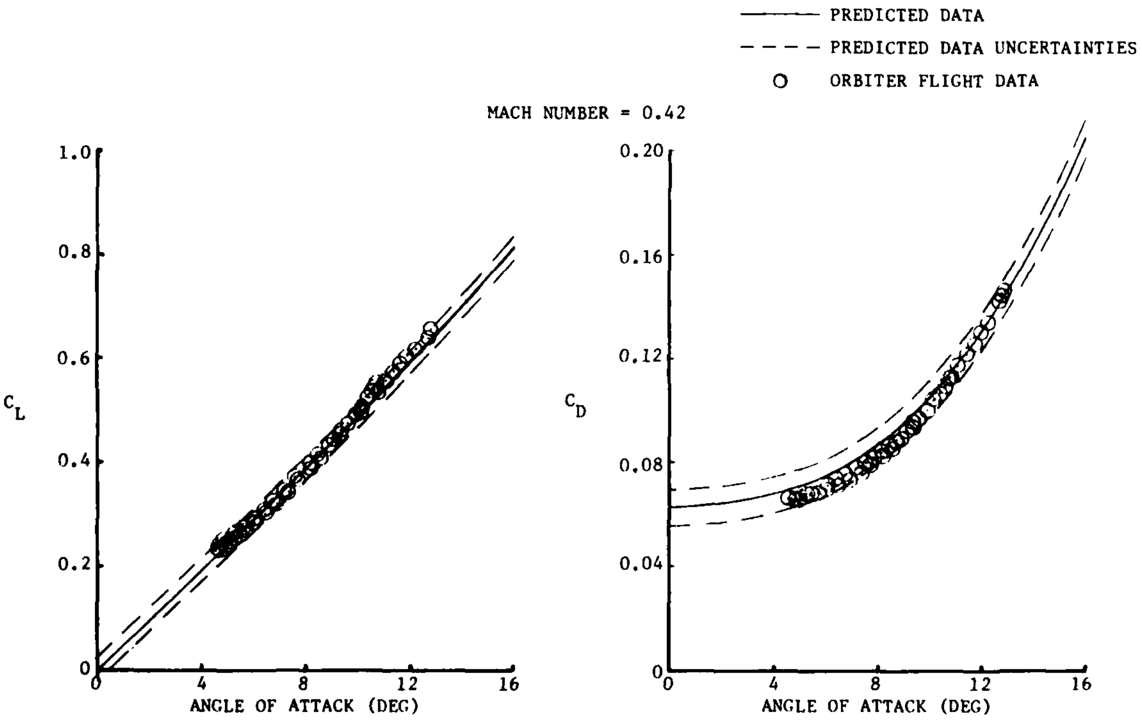

FIGURE 10 - SUBSONIC PERFORMANCE DATA

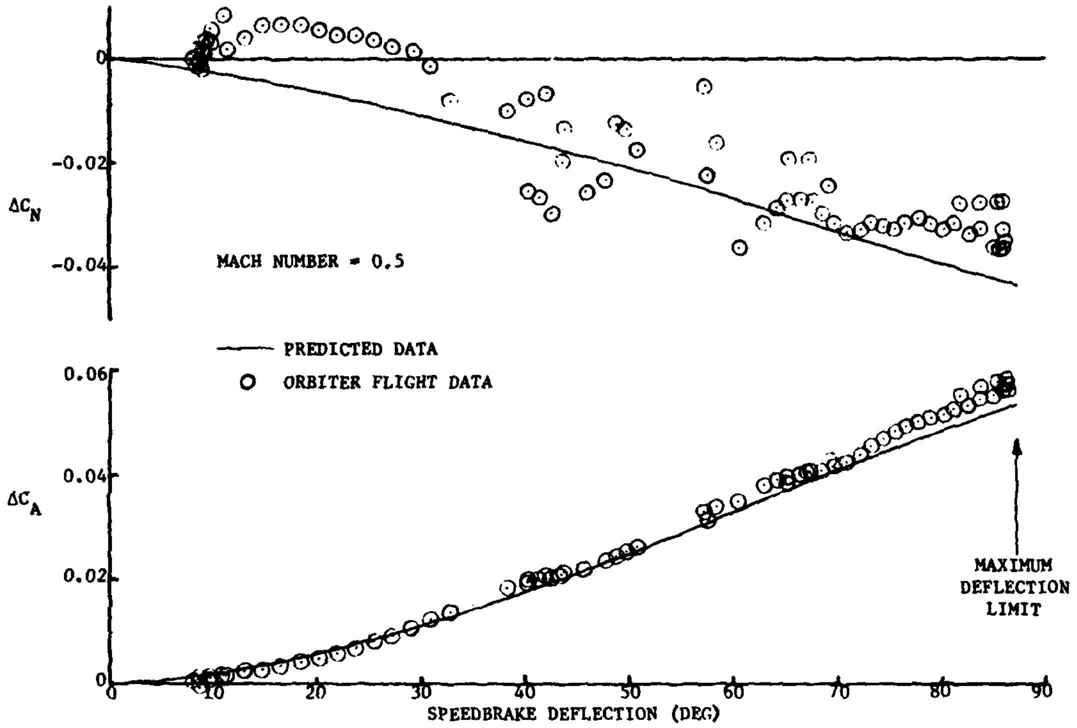

FIGURE 11 - SUBSONIC SPEEDBRAKE EFFECTIVENESS

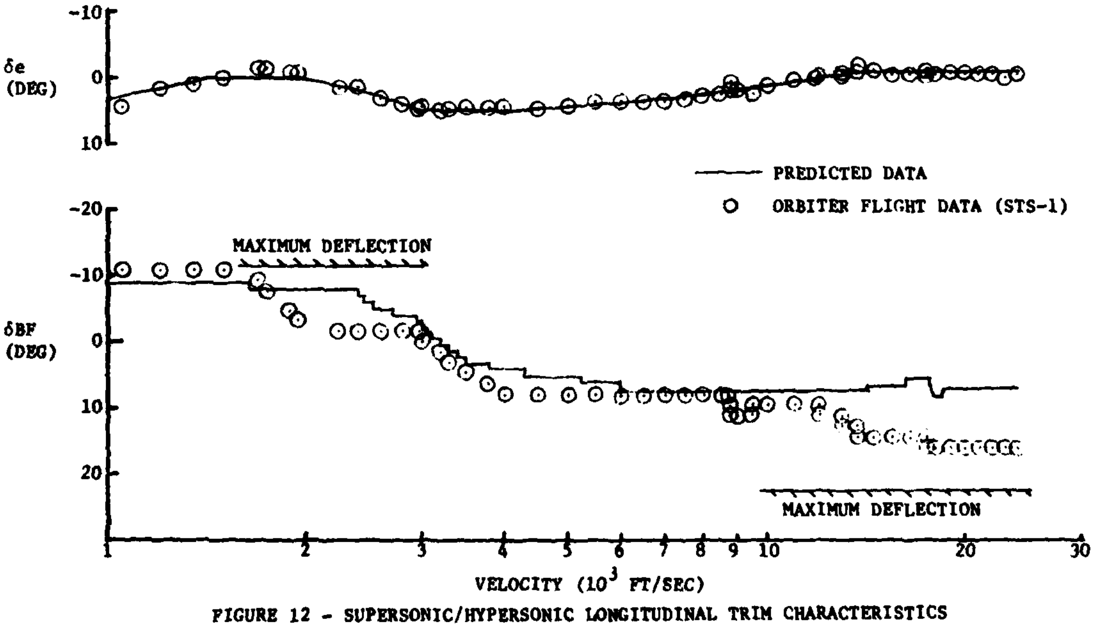

FIGURE 12 - SUPERSONIC/HYPERSONIC LONGITUDINAL TRIM CHARACTERISTICS

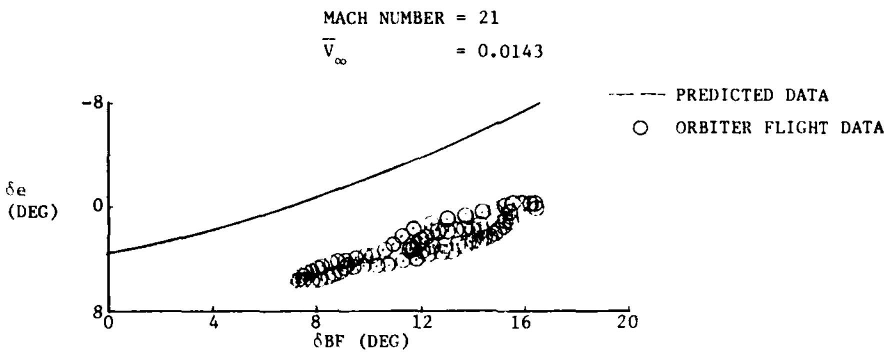

FIGURE 13 - BODYFLAP LONGITUDINAL TRIM CHARACTERISTICS

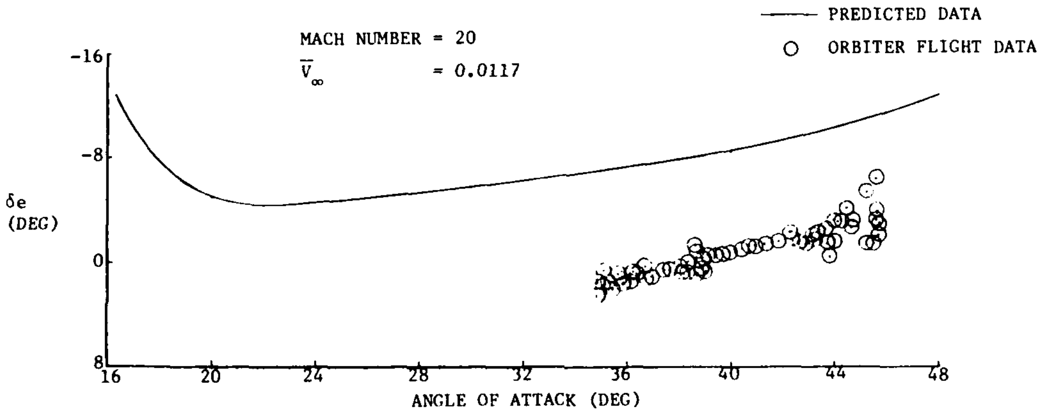

FIGURE 14 - LONGITUDINAL TRIM CHARACTERISTICS AT MACH 20

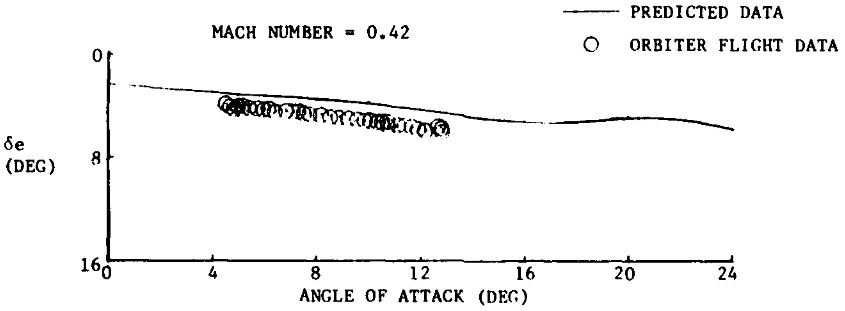

FIGURE 15 - SUBSONIC TRIM CHARACTERISTICS

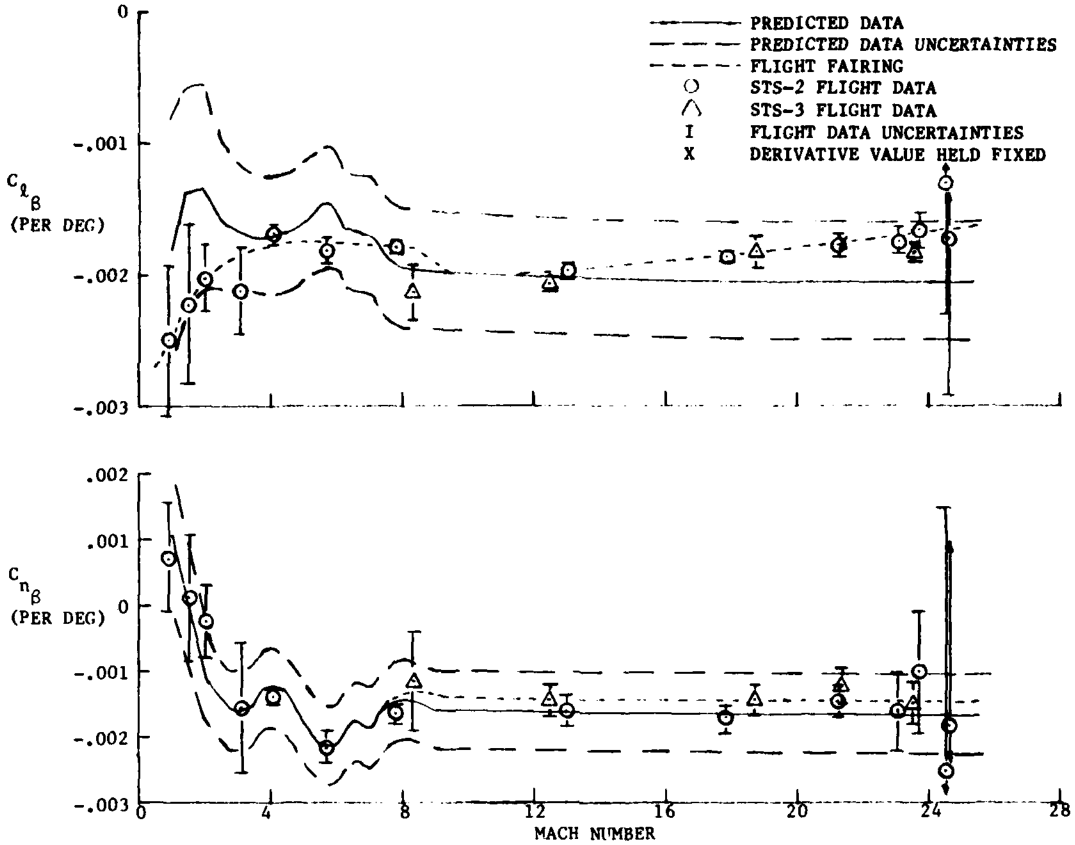

FIGURE 16 - SIDESLIP DERIVATIVES

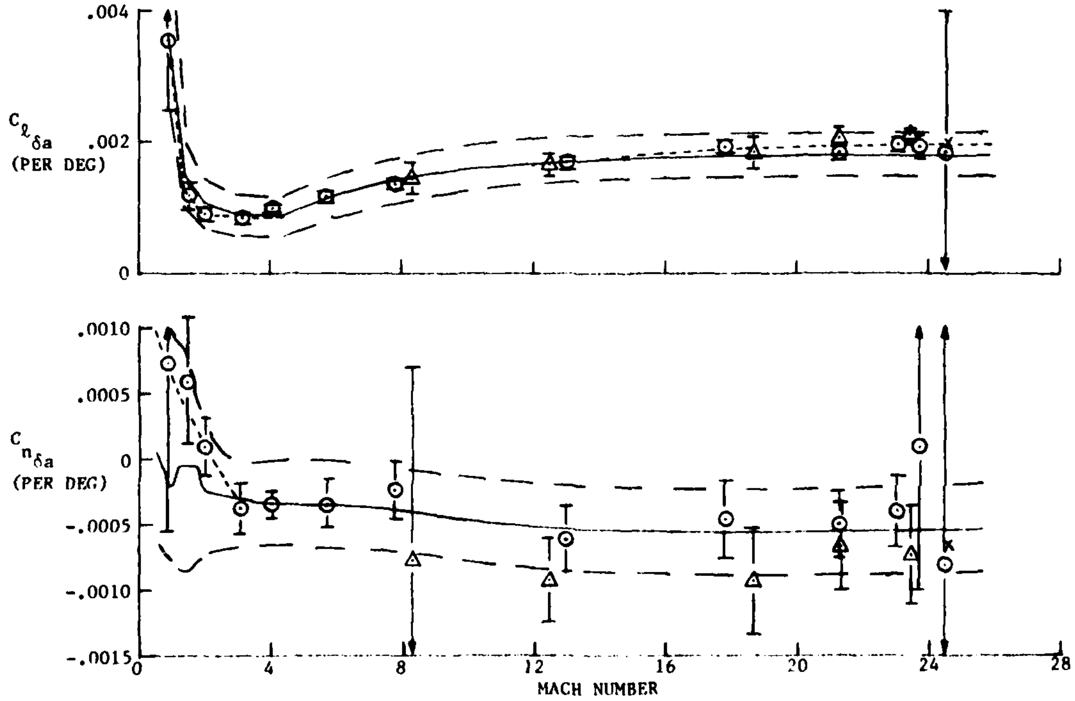

FIGURE 17 - AILERON DERIVATIVES

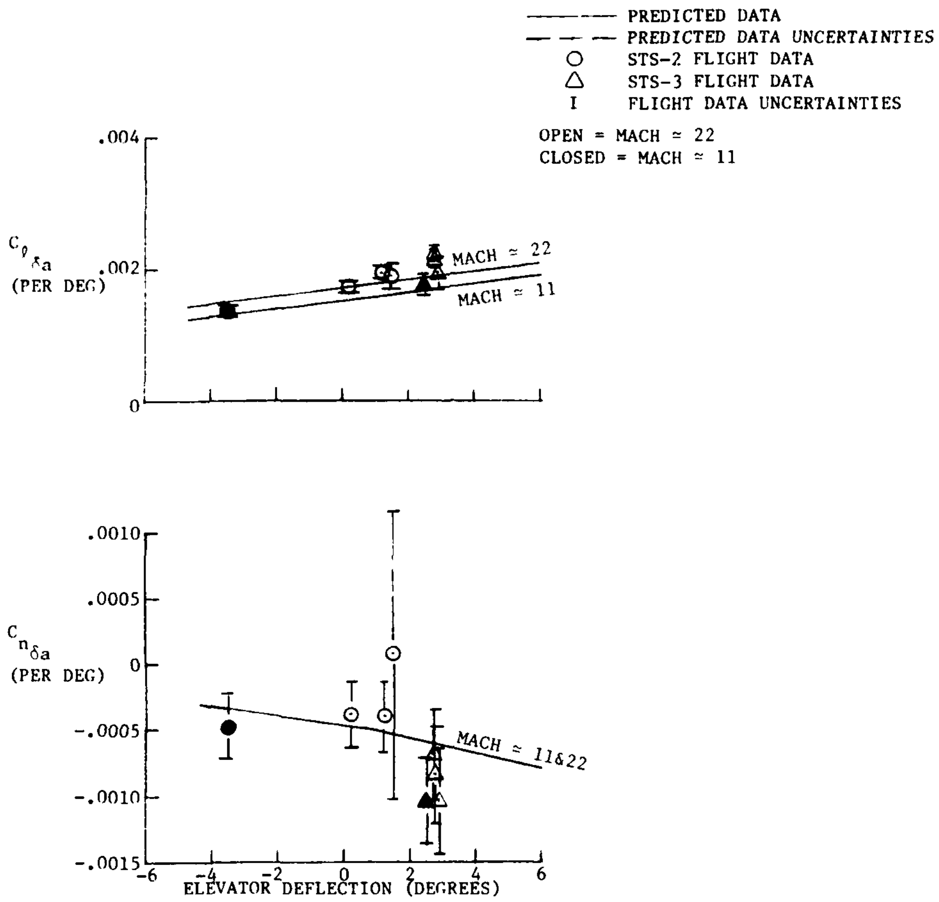

FIGURE 18 - ELEVATOR EFFECTS ON AILERON DERIVATIVES

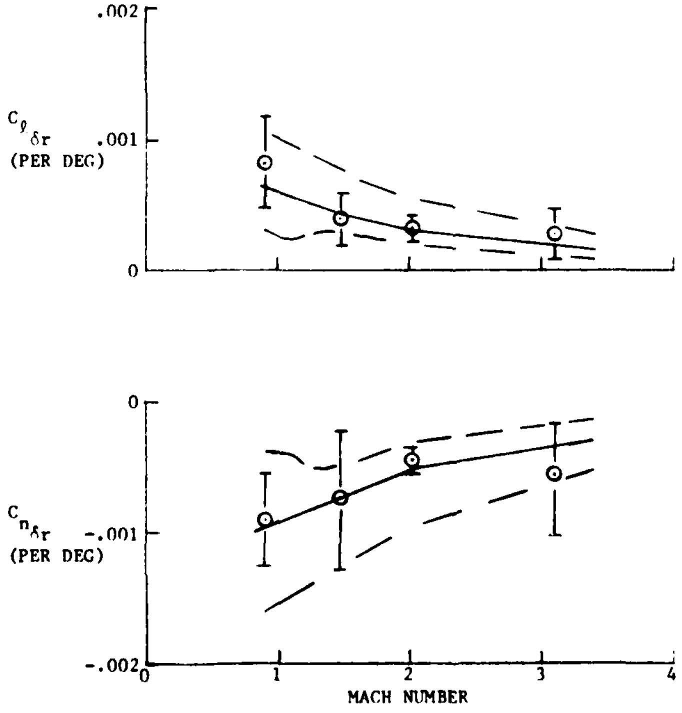

FIGURE 19 - RUDDER DERIVATIVES

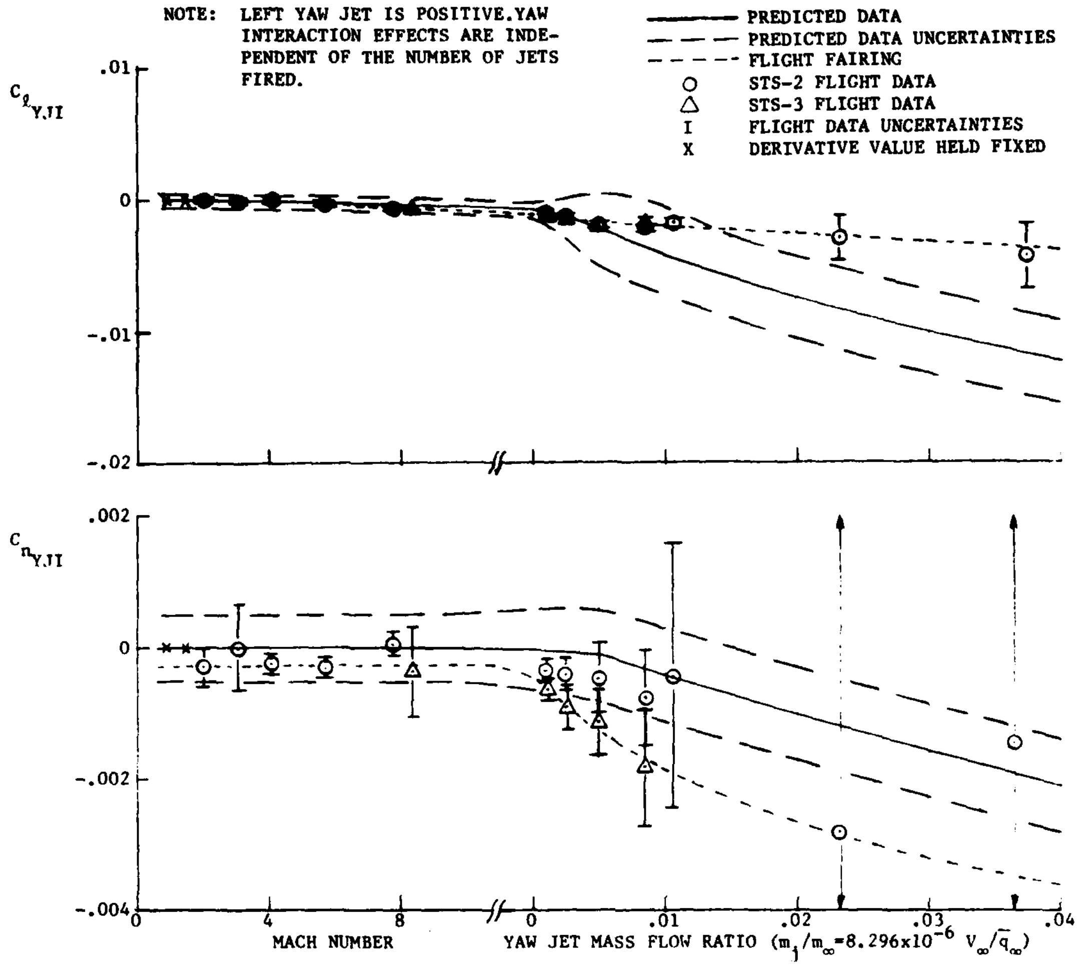

FIGURE 20 - YAW JET INTERACTION DERIVATIVES

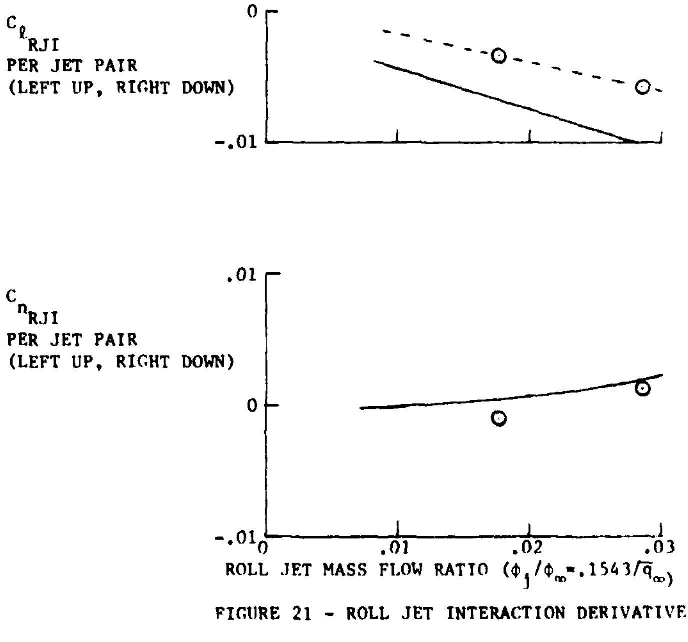

FIGURE 21 - ROLL JET INTERACTION DERIVATIVES

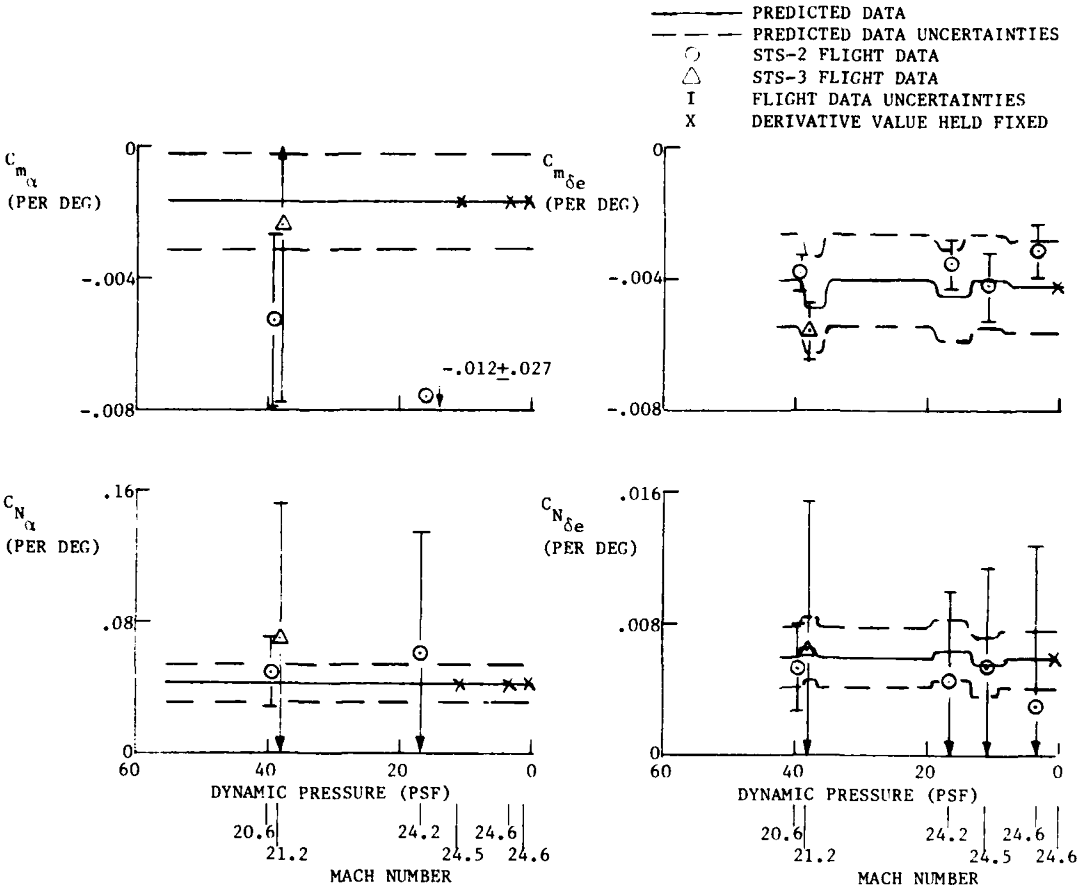

FIGURE 22 - ANGLE OF ATTACK AND ELEVATOR DERIVATIVES

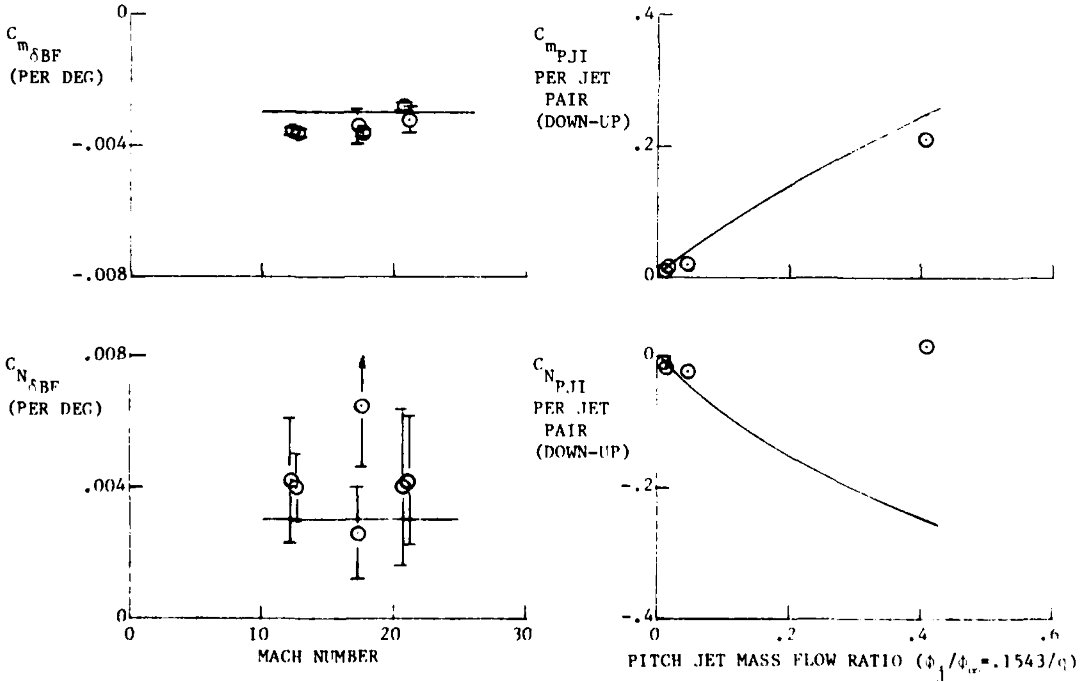

FIGURE 23 - PITCH JET INTERACTION AND BODYFLAP DERIVATIVES

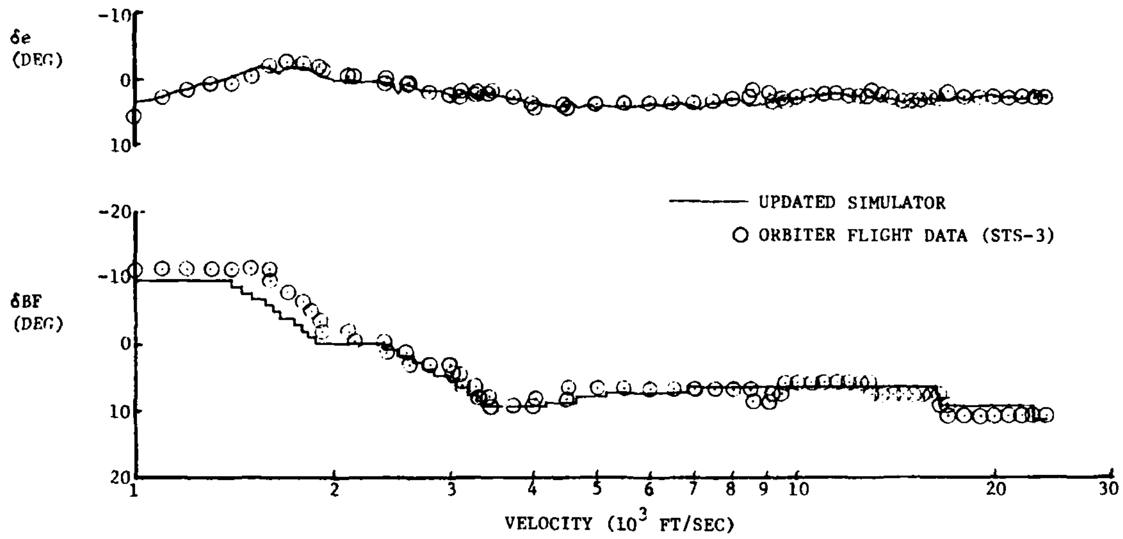

FIGURE 24 - LONGITUDINAL TRIM COMPARISONS

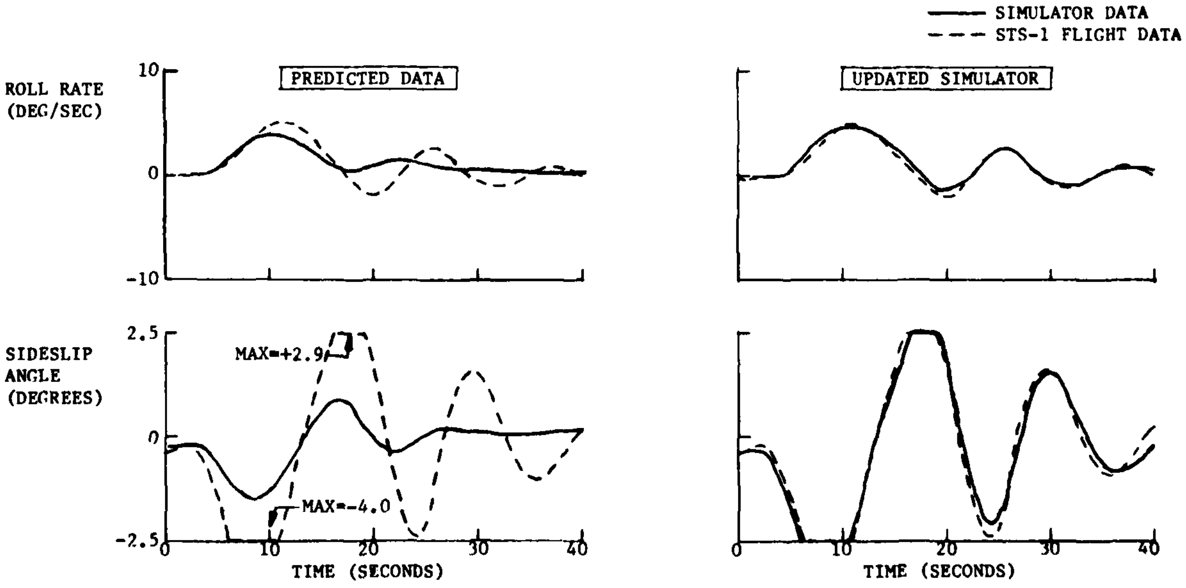

FIGURE 25 - MACH 24 BANK MANEUVER

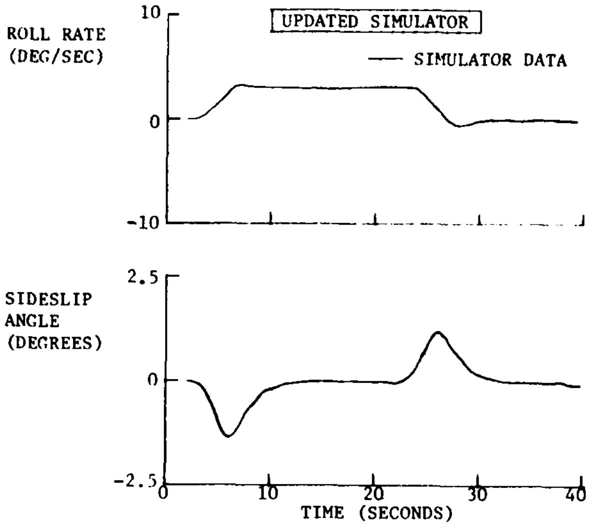

FIGURE 26 - MACH 24 BANK MANEUVER WITH PROPOSED MODIFICATIONS

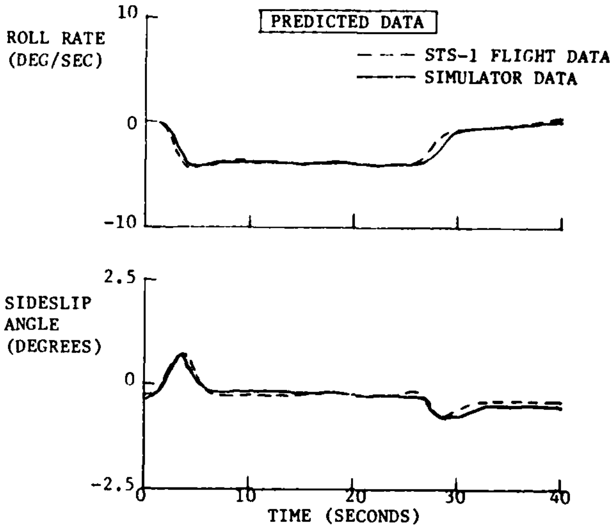

FIGURE 27 - MACH 18 BANK REVERSAL

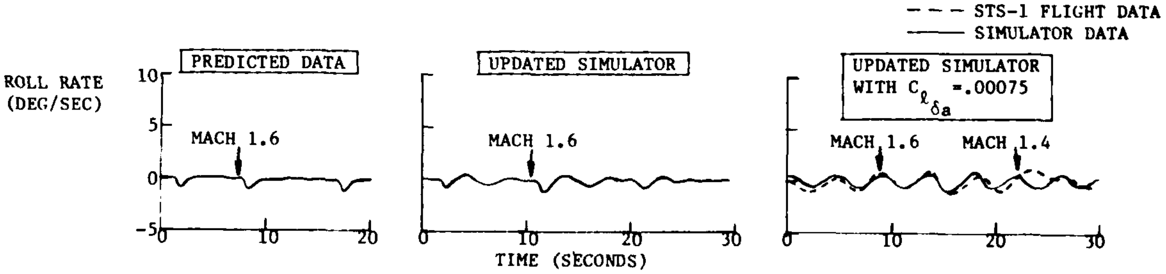

FIGURE 28 - TRANSONIC OSCILLATION

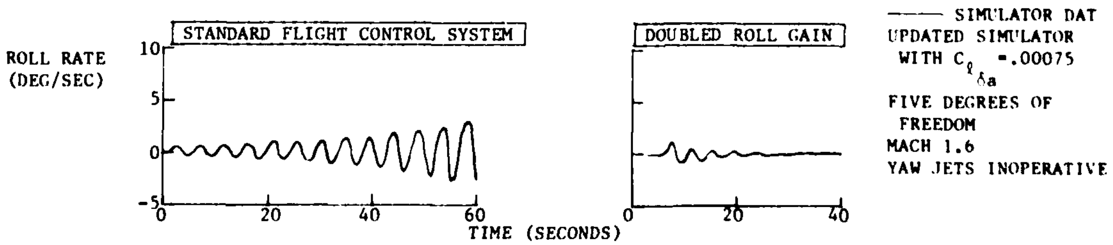

FIGURE 29 - FLIGHT CONTROL SYSTEM MODIFICATION FOR TRANSONIC OSCILLATION

GROUND / FLIGHT CORRELATION ON THE ALPHA-JET EXPERIMENTAL AIRCRAFT WITH A TRANSONIC WING

A Comparison between Wind Tunnel and Flight Results for Aerodynamic Performance

by

D. JACOB, D. WELTE, H. WONNENBERG

DORNIER GMBH
Postfach 1420
7990 Friedrichshafen

SUMMARY:

The paper compares wind tunnel and flight results obtained in an experimental program with a transonic wing (TST) on an Alpha-Jet as test vehicle. The comparison is concentrated on lift, drag and buffet data.

In addition to the analysis of ground and flight data for the TST flight data for the transonic wing and the standard wing are briefly compared.

1. INTRODUCTION

At Dornier an experimental flight test program is currently being completed, which consists of the design, manufacturing and flight testing of a transonic wing with manoeuvre flaps on the Alpha-Jet as test vehicle (Fig. 1). The purpose of this TST-program (Transsonischer Tragflügel = Transonic Wing) is:

- to show the improvements in performance and manoeuvrability obtainable by a transonic wing on a subsonic/transonic fighter aircraft,
- to develop and assess the theoretical and experimental methods required for the design of future transonic aircraft.

As pointed out in previous publications (/1/, /2/) the following main points of interest had to be investigated:

- 3-D-effects on moderate aspect-ratio wings
- performance of a transonic wing in a broad C_L-M-region
- effectiveness of manoeuvre flaps on a transonic wing
- the behaviour at and beyond the buffet boundary.

The program is sponsored by the German Ministry of Defense (BMVg). It started 1974 with a first contract within the BMVg-KEL-program to Dornier as prime contractor and VFW-Fokker as subcontractor. In 1975 it was joined by ONERA. The DFVLR supported the program by a series of wind tunnel tests. The agencies participating in the program and their main contributions are shown in Fig. 2.

After the design and manufacturing of the wing and its installation in an Alpha-Jet were completed flight testing began in December 1980 as a joint effort of Dornier and the German Flight Test Center (E-Stelle 61 and BWB AFB LG IV at Manching). Approximately 110 flights have been performed so far and the flight test program is essentially finished.

Due to its character as an experimental program the TST-program allowed the generation of ground and flight data, which are considerably more detailed than the data obtainable during standard project developments. Before a correlation of these data is discussed in the following chapters and in the next paper /3/ a brief description of the TST design and the differences to the standard wing of the Alpha-Jet will be repeated from reference /2/.

2. DESIGN DESCRIPTION

The choice of the wing design parameters (sweep angle, planform, thickness) was limited by the following restrictions:

- Cost and airplane availability considerations allowed only a replacement of the wing and no further modifications. Since the tail could not be modified, the wing planform (sweep angle) had to be kept constant (Fig. 3).
- An increased drag-rise Mach number could not be fully utilized for stationary manoeuvres due to thrust restrictions. Therefore, a thicker profile was selected which could be generated without changing the existing wing spar. (This profile leads to approximately the same drag-rise at small lift coefficients as the standard profile).

Based on these considerations, the TST experimental wing shows the following differences to the wing of the standard Alpha-Jet:

- o Transonic profiles
  (thickness, approximately 20 % increased)
- o Extended wing leading edge
  (to improve area distribution)
- o Manoeuvre flaps
  (consisting of slats and 25 % single-slotted fowler-flaps)

Fig. 4 shows a comparison of the new TST-profile with the profile (modified RAE 103) of the standard Alpha-Jet. With a thickness of 12,4 % at the root and 10,3 % at the tip it is approximately 20 % thicker than the standard profile. It is designed such that the drag-rise Mach number is not decreased at low lift coefficients and increased at high C_L-values.

The various slat and flap positions are described in Figures 5 and 6. The standard Alpha-Jet has no slat and 30 % single-slotted landing flaps with a fixed hinge-line. In the $\eta_K = 32^o$-position both flaps have the same extension of the wing planform. (η_V = slat deflection, η_K = flap deflection).

On the current experimental flight tested wing the flaps and slats cannot be moved in flight. Due to funding restrictions it was decided to use fixed flap positions, which can be changed on the ground corresponding to the five positions shown in Figures 4 - 6.

3. THEORETICAL CALCULATIONS

The transonic wing was developed by a combined theoretical and experimental procedure which utilized the following theoretical methods:

- o 2-D viscous calculations based on direct and inverse transonic small disturbance (TSP) methods combined with 2D-integral boundary layer methods.
- o 2-D and 3-D subsonic panel methods.
- o 3-D transonic small perturbation (TSP) and full potential equations (FPE) methods and 3D-boundary layer analysis.

After the design freeze of the TST improved transonic computational techniques were developed consisting of mesh generators for complex shapes and accurate full potential and Euler solvers.

A major part of the progress can be attributed to a considerably more detailed and realistic representation of the body geometry.

A comparison of theoretical pressure distributions with wind tunnel and flight test data will be presented in the following paper /3/.

4. WIND TUNNEL TESTS

Figures 7 and 8 present an overview of the wind tunnel tests performed with TST-models. Following tests with 2D profile models a 1:5 low speed model and a 1:10 high speed model were tested in different test periods with certain model modifications between the tests.

After the design of the configurations was frozen in 1977 additional wind tunnel tests were carried out which added significantly to the body of data available for comparison with flight data.

In 1980 the original half-wing of the TST mounted on a partial dummy of the Alpha-Jet fuselage was tested by ONERA in the S1 wind tunnel in Modane at flight Reynolds numbers (Fig. 9). These tests were performed in order to reduce the uncertainty about the effects of high Reynolds numbers on the aerodynamic coefficients and thus reduce the required amount of flight testing. The "model" was equipped with the same instrumentation as the identical wing on the test aircraft, which is described in more detail in section 5. The pressure distributions and wake measurements obtained in the S1 tunnel are compared with flight data in reference /3/. A direct comparison of total force coefficients is not possible because only the wing was attached to the wall-balance. However local load measurements on the wing with manoeuvre flaps were performed up to the structural limit of the wing.

Further tests with the 1:10 model in the 16T-AEDC-tunnel are part of a data exchange agreement.

The comparison of wind tunnel and flight total force coefficients will therefore be based mainly on the results obtained with the 1:10 high speed model in the ONERA S2 and NLR HST wind tunnels at a Reynolds number (based on aerodynamic mean chord) of $Re = 2,5 \cdot 10^6$ (S2) and $Re = 2,8 \cdot 10^6$ (HST) with a wind tunnel blockage (cross section of model divided by cross section of test section) of 1,2 % in both cases. In the HST-test transition was free, whereas in the S2-test free transition and a transition fixed at 10 % chord on the upper and lower surface (with 0,1 mm Ballotini) were investigated. In both wind tunnels the model was supported by a rear sting which was straight in the S2 (Fig. 10) and cranked in the HST. The inlets of the model were open and allowed a given mass flow corresponding to a typical flight condition.

In addition to total forces pressure distributions in 5 wing sections and for buffet analysis, in particular, wing root bending moments, unsteady pressures (kulites) and accelerations were measured during the S2 tests.

5. FLIGHT TESTS

As already mentioned in section 1 flight testing with the TST began in December 1980. Today the flight program is essentially completed with approximately 110 flights flown by 5 pilots. The flight testing was a joint effort of Dornier and the German Flight Test Center E-61 at Manching. After the flight envelopes were opened by Dornier the aircraft was transferred to E-61 where 70 % of the flights were performed. The flights (Fig. 11) were concentrated on the five configurations shown in Fig. 4 - 6 and a single additional flight for the configuration $\gamma_V = 0$ retracted, $\gamma_K = 5^o$ (② in Fig. 11).

Test Instrumentation

The right-hand wing of the experimental aircraft, which was already tested in the S1-tunnel, is equipped with the following devices:

- static pressure tubes at 4 sections
  (48 pressures in each section)
- 20 kulite dynamic pressure probes in 4 sections (Fig. 12)
  (Due to restrictions of the FM-unit only 7 kulites could be operated in flight (Fig. 30). The positions were selected on the basis of the S1-tunnel-results).
- 22 strain gages for buffet and load analysis
  (2 additional strain gages were installed at the horizontal stabilizer) (Fig. 13)
- 5 accelerometers for buffet and structural analysis (Fig. 13)
- a rotating ONERA-Pitot rake for wake measurements at the trailing edge (discussed in /3/)
  (This rake was not permanently installed).

An additional accelerometer was mounted at the pilot seat in some of the flights.

The data described above and the complete flight conditions of the aircraft were registered on a magnetic tape on board of the aircraft. In addition the data most important for controlling and monitoring the flight were transferred to the ground by telemetry.

Drag Polars (based on /4/ - /7/)

The main interest of the flight testing was directed towards the performance of the new wing especially in comparison to the standard Alpha-Jet. Wing performance evaluation from flight tests is a delicate problem and needs large effort in test instrumentation, calibration, data acquisition and reduction.

The evaluation procedure used at Dornier is prescribed in Fig. 14. Due to the required high accuracy of the results special preparations have been carried out to be sure of the quality of the flight test and engine data. The basic data for the performance evaluation were generated by sets of stationary, quasi-stationary and instationary manoeuvres, which lead directly to performance characteristics as maximum stationary horizontal speeds and load factors, climb rates and specific range values directly computed with the aid of the measured fuel consumption. The evaluation process was directed towards the lift and drag polar curve as the most general result, which can easily be compared with other data.

To have the best approximation of all evaluated values the individual results have been used to define the typical parameters of a mathematical description of the polar curves in the following form:

$$\text{Lift Polar:}\quad \underbrace{C_L = C_{Lo} + \frac{dC_L}{d\alpha} \cdot \alpha}_{|\leftarrow \text{normal state} \rightarrow|} \qquad \underbrace{+ \Delta C_{L\,sep}(\alpha)}_{|\leftarrow \text{separation corr.} \rightarrow|}$$

$$\text{Drag Polar:}\quad C_D = C_{Dmin} + K_1\left(C_L - C_{LC_{Dmin}}\right)^2 + K_2\, \Delta C_{L_{sep}}(\alpha)$$

(C_L = lift coefficient, C_D = drag coefficient, α = angle of attack)

Fig. 15 gives an example of the correlation of the flight test data with the mathematical approximation of the lift curve for the configuration with retracted flaps and slats. Fig. 16 to 20 show the same comparison in the case of the drag polars for all flown flap configurations. These results are based on stationary manoeuvres.

Another important aspect to the performance of the wing is the maximum attainable lift coefficient (C_{Lmax}), which is depending on the deceleration rate, altitude, cg-position and power setting. Furthermore it is important to properly define the flight characteristics, which have to be used to find the exact instant, when the maximum lift is reached. In our case this was defined as the moment, where the pilot firstly used the rudder to keep the aircraft on course. The reference deceleration rate was averaged between this point and the instant of 1.1 V_{Stall}.

Fig. 21 shows the results of the $C_{L_{max}}$-evaluation as a function of the deceleration rate, the influence of which is higher for the flap configurations. The reference values to be used are those for 1 kts/sec deceleration.

Parallel to Dornier the German Flight Test Center (BWB AFB LG IV) did their own evaluation using comparable /8/ and special methods as the MCA (mass consumption acceleration) method /9/. Also parallel to this effort the DFVLR tried to investigate the polar data by evaluating the dynamic roller coaster manoeuvres with the aid of a Maximum Likelihood Estimation Technique /10/. Fig. 22 shows a comparison of the investigations done by Dornier, AFB LG IV and DFVLR for two typical Mach numbers. It can be seen, that the results are nearly identical. Therefore it can be concluded that the flight test results have a high level of accuracy.

Buffet Results (based on /11/ - /13/)

The buffet criteria used in evaluating the flight test results are summarized in Fig. 23. They will be explained by discussing the following figures for the clean configuration (flaps and slats retracted).

At buffet onset the pilot feels the onset of flow disturbances which, however, do not impair the flight. The pilot's "top" based on this definition is compared in Fig. 24 with the 0.2 g rms-value of the wing tip accelerometer (acceleration normal to the wing surface) and in Fig. 25 with the beginning of the oscillation of the rms-signal of the BRX-accelerometer (acceleration in x direction measured at aircraft center of gravity). Both sets of data agree well with the pilot's tops.

The pilot's tops for "moderate buffet" are related to light roll oscillations of the aircraft which affect tracking without constituting a tracking limit. An evaluation of the recorded data showed that the best correlation could be reached by comparing the pilot's statements with ± 10°/sec roll oscillation (Fig. 26).

For "heavy buffet" relatively few flight data are available and a definite correlation of pilot's impression and a simple evaluation of the recorded flight data was not possible. The pilot's top for "heavy buffet" means here that control inputs are required for stabilizing the aircraft and that tracking is nearly impossible.

The mean values of the different buffet levels for the clean configuration are summarized in Fig. 27.

At the end of the flight test program some additional flights were carried out in the clean configuration with an accelerometer installed at the pilot's seat. Between these tests and the first tests in the clean configuration, on which the results described above are based, the pilots had logged approximately 80 hours on the TST in different configurations. The increased familarity of the pilots with the aircraft resulted in significantly higher buffet lines. In Fig. 28 the results of the first flights are compared with the results of three recent additional flights.

It shows, that the buffet onset curves are almost identical. They correlate well with the first kink in the rms-signal at the pilot's seat.

The more recent curves for moderate and heavy buffet lie at higher Mach numbers considerably above the initial curves. The heavy buffet curve is again solely based on pilot's tops whereas the moderate buffet curve is based on pilot's tops and the VRX = ± 10°/sec roll criterion. The shift of the VRX-data indicates that the influence of the pilot on the roll oscillation cannot be neglected and that it depends on the familarity of the pilot with the aircraft.

The moderate buffet level as defined above can roughly be correlated to a 0.2 g rms-value of the accelerometer at the pilot's seat (BRSZ). With increasing lift coefficient the BRSZ-signal increased at some Mach numbers but remained constant at others such that a reasonable correlation with the "heavy buffet" top of the pilots is not possible.

In summarizing the results for the clean configuration it can be stated that

- the buffet onset curve is relatively well defined and reproducible
- the curves for higher buffet levels are less well defined and more dependent on the experience of the pilot with the special aircraft and on his personal impression. Flights for the determination of higher buffet levels should therefore be performed only after the pilots had a chance to gain sufficient experience with the configuration. Especially for "heavy buffet" a reasonable correlation of pilot's impression and recorded flight data is difficult to achieve.

The observations are in general agreement with /14/.

Similar evaluations based on the same criteria were performed for the remaining four configurations. The mean values of the buffet onset results plotted in Fig. 29 clearly show the influence of flaps and slats on buffet onset.

Finally an attempt has been made to correlate the Kulite-signals with various buffet leves. For the Kulites in the shaded region of Fig. 30 a rms-signal has been recorded which increased beyond the corresponding basic level as an indication of disturbed flow. The boundaries of the disturbed region cannot be determined accurately because only a limited number of Kulites could be operated in flight due to limitations of the FM-unit. Fig. 30 has to be regarded as a preliminary result. An additional and more detailed evaluation of the Kulite-signals with increased sensitivity of the corresponding FM-channels will be carried out by ONERA.

6. COMPARISON OF FLIGHT AND WIND TUNNEL RESULTS

Lift and Drag Coefficient

In this section some of the results described in the previous two chapters will be compared.

Figs. 31 - 34 show the drag polars of the trimmed aircraft for 4 different configurations. The flight data correspond to the mean values taken from Figs. 16 - 20. The ground data were generated in the ONERA-S2 wind tunnel at a Reynolds number of Re = $2.5 \cdot 10^6$ with free transition. They are not corrected for Reynolds number- or wall interference effects. The latter is very small in the S2 for this configuration. The agreement of C_L (C_D) between ground and flight data is good.

In Fig. 35 the minimum drag coefficient is given versus Mach number. A comparison of data with fixed and free transition shows that the $C_{D_{min}}$-values measured with fixed transition are in better agreement with flight data. In both cases the drag rise Mach number is well predicted by the wind tunnel.

For free transition the coefficients obtained from S2 and HST-tests were almost identical. The S2-data plotted here are therefore also representative for the HST-results.

By comparing the ground and flight polar curves it has to be kept in mind that the plotting of both curves requires some interpolations (e.g. for constant Mach number) and that both curves have a certain scatter which is difficult to determine quantitatively.

The lift curve slopes measured in the windtunnels are lower than the flight data (Fig. 36).

In Fig. 37 the maximum lift coefficients for the clean and for the landing configuration obtained in different wind tunnels at a Reynolds number of Re = $1 \cdot 10^6$ are compared with flight data at Re = $9 \cdot 10^6$. The three wind tunnels give essentially identical results. Due to Reynolds number effects the maximum trimmed lift coefficients reached in flight are higher by approximately 8 % for the clean configuration and approximately 20 % for the landing configuration.

Buffet

The extraction of buffet data from wind tunnel tests is a difficult task which is generally limited to the determination of buffet onset as the following results will confirm.

In Fig. 38 the rms-values of the wing root bending moment C_F are plotted as function of the angle of attack α for different Mach numbers. The data were obtained in the S2-wind tunnel with the 1:10 model in clean configuration with free and fixed transition. On each curve the corresponding flight test results from Fig. 27 for various buffet levels are indicated. A comparison of C_F with the flight data shows, that the first kink of the $C_F(\alpha)$-curve agrees well with the flight test results for buffet onset, whereas a definite correlation between the wing root bending moment of the wind tunnel model and higher buffet levels observed in flight is not yet possible. The flight data show that the TST can penetrate well beyond the point where the C_F-signal reaches its maximum value before heavy buffet is reached. The discrepancy can partially be explained by the different structural response of wind tunnel model and actual aircraft.

Similar results are obtained for the configuration $\eta_V = 0^\circ$ out, $\eta_K = 5^\circ$. According to Fig. 39 the first kink of the C_F-signal again agrees well with the flight results for buffet onset.

A relatively good correlation /15/ with flight data for buffet onset is also obtained (Fig. 40) for that wind tunnel lift coefficient which corresponds to an angle of attack 0.5° beyond the break angle of attack α_{br}, where α_{br} is defined as that angle of attack where $C_L(\alpha)$ becomes non-linear.

Correlations for moderate buffet are more difficult. For the TST-configuration the flight test data for moderate buffet showed reasonable agreement with the following wind tunnel results:

- (C_L) moderate buffet = $(C_L)_{break} + 0.1$
- (C_L) moderate buffet = C_L, where the rms-value of the wing root bending moment reaches twice the value it has at small angles of attack (basic value).

However, these correlations differ for different configurations, wind tunnels and models and a general application is not justified.

7. COMPARISON TST - STANDARD WING

In this final chapter a short comparison of flight test results for the experimental TST-wing with manoeuvre flaps and the standard wing of the Alpha-Jet is discussed.

Drag Polars and Buffet

The drag polars C_L (C_D) plotted in Fig. 41 show that corresponding to the design goals of the TST the drag reduction of the TST increases with increasing lift coefficient and increasing Mach number.

From Fig. 42 the influence of the transonic wing and the manoeuvre flaps on buffet onset can be deduced. According to flight test results the increase in buffet intensity with increasing lift coefficient is considerably smaller for the transonic wing. The difference of the curves for TST and standard wing at higher buffet levels (e.g. tracking limit) is therefore larger than the difference at buffet onset shown in Fig. 42.

By assessing the results of Fig. 41 and 42 it has to be kept in mind that the TST-profile is 20 % thicker than the profile of the standard wing. Additional improvements with respect to drag and buffet could be realized by using a transonic profile with the same thickness as the standard profile. The thicker profile, however, allows larger internal fuel tanks in the wing and a correspondingly increased range.

The maximum lift coefficients of both wings are compared in Fig. 43. For the clean configuration the $C_{L,max}$-values are almost identical, whereas the configuration with fully extended flaps and slats has a considerably higher maximum lift than the standard wing with fully extended flaps. The increase in $C_{L,max}$ is mainly due to the slat on the TST. Similar to the Alpha-Jet the stall behaviour for both configurations is very good with early stall warning, symmetrical stall and full control in the stall region.

8. CONCLUSION

The comparison of wind tunnel and flight data described in the previous sections allows the following conclusions for the TST:

o The drag polars C_L (C_D) agree surprisingly well

o A reasonable prediction of buffet onset can be derived from wind tunnel tests. However, a reliable wind tunnel prediction of higher buffet levels is not yet possible.

A comparison of flight test results for TST and standard wing shows that the transonic wing with manoeuvre flaps offers substantial improvements in performance and manoeuvrability.

9. REFERENCES

(1) Lotz, M.; Monnerie, B.:
The Franco-German Experimental Program for the Evaluation of a Supercritical Wing for a Combat Aircraft Application.
ICAS-Paper No. 76-21,1976.

(2) Jacob, D.; Welte, D; Wünnenberg, H.:
Experimental Flight Test Programs for Improving Combat Aircraft Manoeuvrability by Manoeuvre Flaps and Pylon Split Flaps.
AGARD CP-319, Paper 10, 1981.

(3) Buers, H.; Schmitt, V.; Lerat, A.:
Ground/Flight Correlation on the Alpha-Jet Experimental Aircraft with a Transonic Wing.
A Comparison of Wing Pressure Distribution and Local Wake Survey from Analytical, Wind Tunnel and Flight Results.
AGARD FMP-Symposium, Cesme, Oct. 1982.

(4) Seher, H.; Charon, W.; Müller, R.:
Dornier-Aktenvermerk BM10-033/82

(5) Seher, H.; Friedel, H.:
Dornier-Aktenvermerk BM10-068/82

(6) Seher, H.; Müller, R.:
Dornier-Aktenvermerk BM10-090/82

(7) Seher, H.; Müller, R.:
Dornier-Aktenvermerk BM10-092/82

(8) Sonnenberg:
Alpha-Jet TST. Ermittlung des Widerstandskennfeldes unter Benutzung konventioneller Methodik.
BWB AFB LG IV-Teilbericht 1981.

(9) Schuck, G.:
Ermittlung von Flugleistungen mit Hilfe der MCA-Methode des Flugzeugs TST mit eingefahrenen Manöverklappen.
BWB AFB LG IV-Teilbericht 1982.

(10) Hicks, J.W.:
Development of a Technique of Parameter Identification of the Aircraft Aerodynamic Model from Dynamic Roller Coaster Maneuvers.
Internal DFVLR-Rep. No. IB 111-82/8 1982.

(11) Buers, H.:
Dornier-Aktenvermerk BF10-2164/82

(12) Buers, H.:
Dornier-Aktenvermerk BF10-2282/82

(13) Buers, H.:
Dornier-Aktenvermerk BF10-2253/82

(14) Hamilton, W.T. et al:
Manoeuvre Limitations of Combat Aircraft.
AGARD Advisory Report AR-155 A, 1979.

(15) Nickolaus, P.:
VFW-Bericht TE 122 KB 1145, 1982.

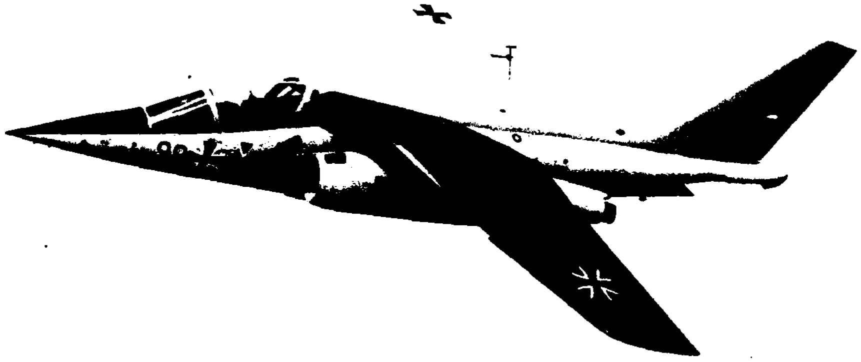

Fig. 1

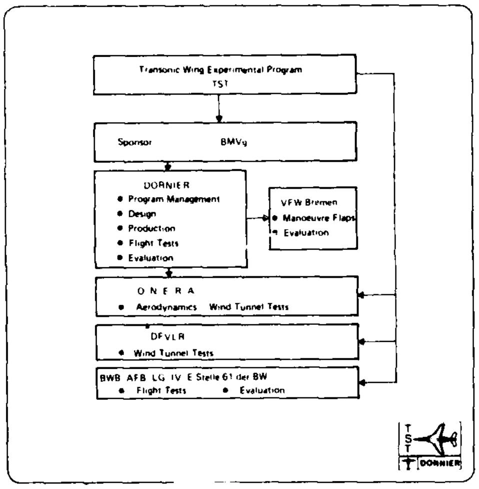

Transonic Wing Experimental Program
TST

Sponsor BMVg

DORNIER
- Program Management
- Design
- Production
- Flight Tests
- Evaluation

VFW Bremen
- Manoeuvre Flaps
- Evaluation

O N E R A
- Aerodynamics Wind Tunnel Tests

DFVLR
- Wind Tunnel Tests

BWB AFB LG IV E Stelle 61 der BW
- Flight Tests
- Evaluation

Fig. 2

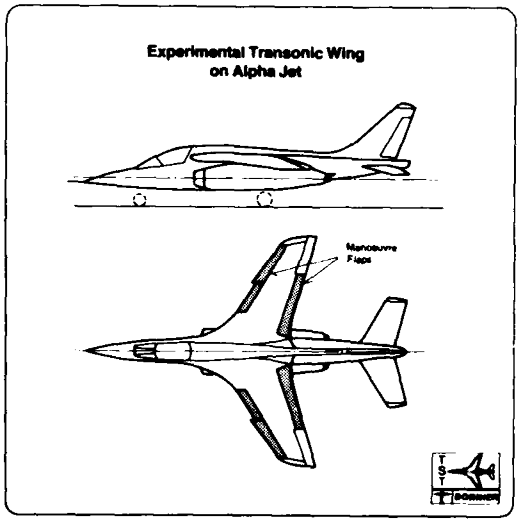

Experimental Transonic Wing
on Alpha Jet

Manoeuvre
Flaps

Fig. 3

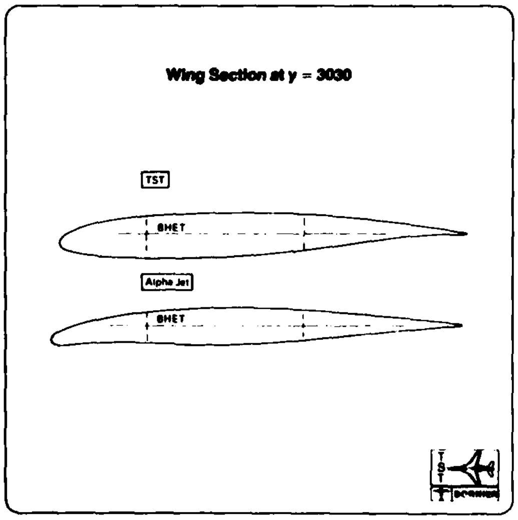

Wing Section at y = 3030

TST
BHET
Alpha Jet
BHET

Fig. 4

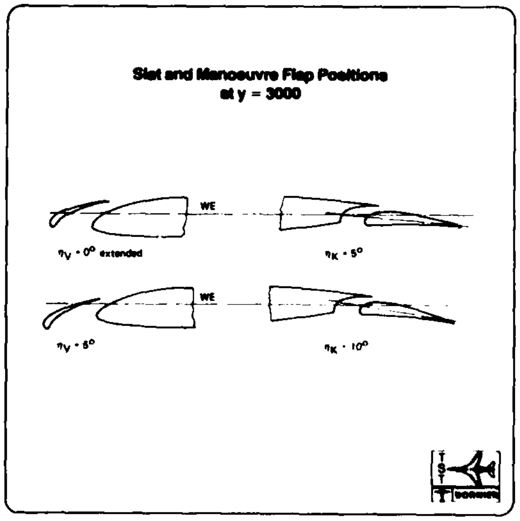

Slat and Manoeuvre Flap Positions
at y = 3000

WE
$\eta_V = 0°$ extended
$\eta_K = 5°$
WE
$\eta_V = 8°$
$\eta_K = 10°$

Fig. 5

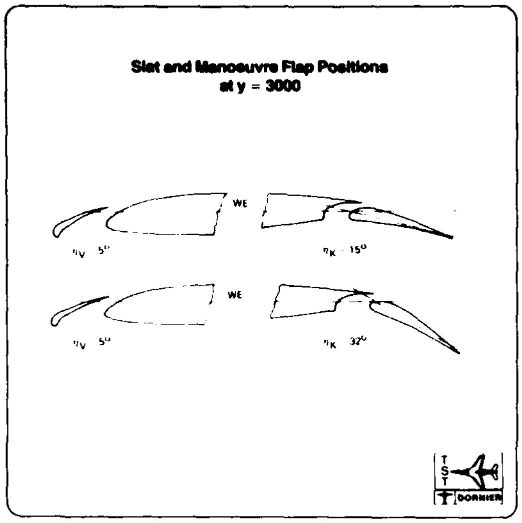

Slat and Manoeuvre Flap Positions at y = 3000

WE
$\eta_V = 5^0$
$\eta_K = 15^0$
WE
$\eta_V = 5^0$
$\eta_K = 32^0$
TST
DORNIER

Fig. 6

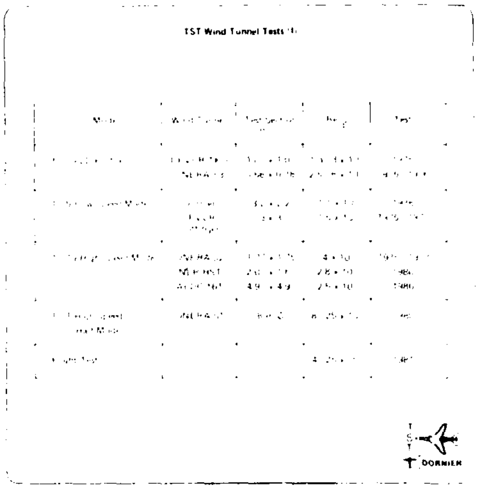

TST Wind Tunnel Tests (I)

Model	Wind Tunnel	Test Section	Re	Test
[illegible]	[illegible]	[illegible]	[illegible]	[illegible]
[illegible]	[illegible]	[illegible]	[illegible]	[illegible]
[illegible]	ONERA [illegible]	[illegible]	4 × 10	[illegible]
	NLR HST	[illegible]	2.8 × 10	1986
	AEDC 16T	4.9 × 4.9	2.5 × 10	1986
[illegible]	ONERA [illegible]	[illegible]	[illegible]	[illegible]
Flight Test			[illegible]	[illegible]

TST
DORNIER

Fig. 7

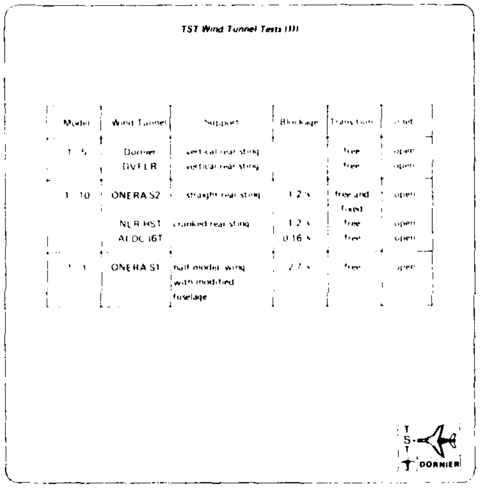

TST Wind Tunnel Tests (II)

Model	Wind Tunnel	Support	Blockage	Transition	[illegible]
1 : 5	Dornier	vertical rear sting		free	open
	DVFLR	vertical rear sting		free	open
1 : 10	ONERA S2	straight rear sting	1.2 %	free and fixed	open
	NLR HST	cranked rear sting	1.2 %	free	open
	AEDC 16T		0.16 %	free	open
[illegible]	ONERA S1	half model wing with modified fuselage	2.7 %	free	open

TST
DORNIER

Fig. 8

Fig. 9

Fig. 10

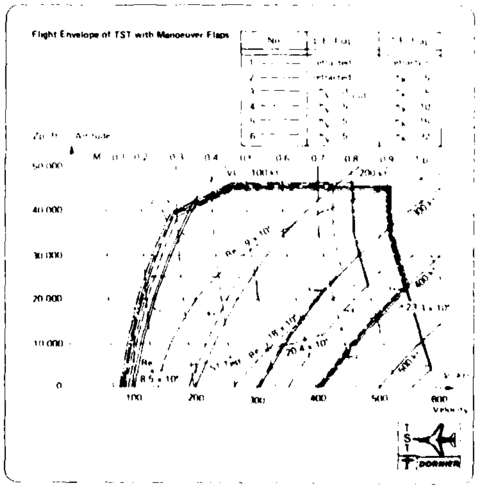

Flight Envelope of TST with Manoeuver Flaps

Fig. 11

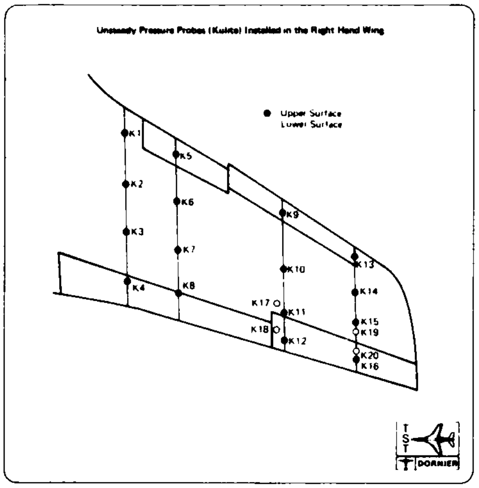
Unsteady Pressure Probes (Kulite) Installed in the Right Hand Wing
● Upper Surface
○ Lower Surface
K1
K2
K3
K4
K5
K6
K7
K8
K9
K10
K11
K12
K13
K14
K15
K16
K17
K18
K19
K20
TST
DORNIER

Fig. 12

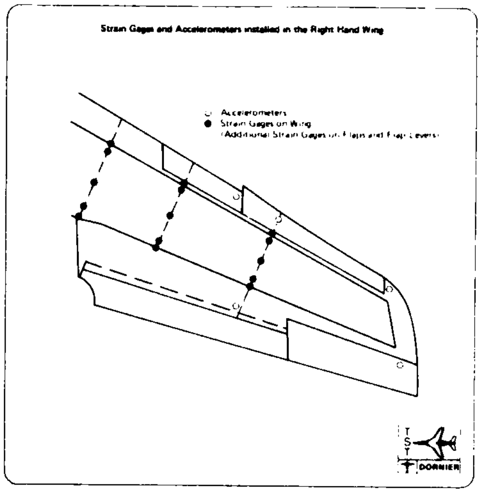
Strain Gages and Accelerometers installed in the Right Hand Wing
○ Accelerometers
● Strain Gages on Wing
(Additional Strain Gages on Flaps and Flap Levers)
TST
DORNIER

Fig. 13

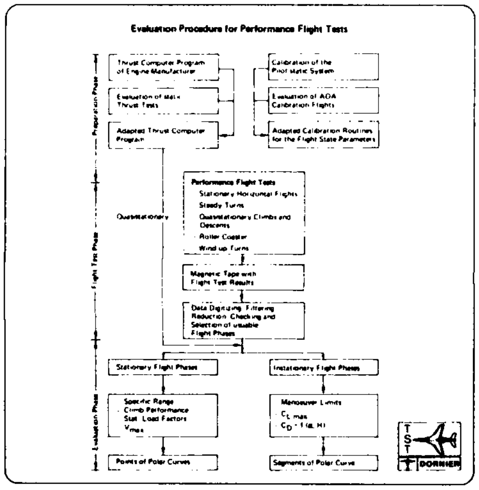
Evaluation Procedure for Performance Flight Tests
Preparation Phase
Flight Test Phase
Evaluation Phase
Thrust Computer Program of Engine Manufacturer
Evaluation of Static Thrust Tests
Adapted Thrust Computer Program
Calibration of the Pitot static System
Evaluation of AOA Calibration Flights
Adapted Calibration Routines for the Flight State Parameters
Quasistationary
Performance Flight Tests
Stationary Horizontal Flights
Steady Turns
Quasistationary Climbs and Descents
Roller Coaster
Wind up Turns
Magnetic Tape with Flight Test Results
Data Digitizing, Filtering, Reduction, Checking and Selection of usable Flight Phases
Stationary Flight Phases
Instationary Flight Phases
Specific Range
Climb Performance
Stat. Load Factors
V max
Manoeuver Limits
C L max
C D = f(α, H)
Points of Polar Curves
Segments of Polar Curve
TST
DORNIER

Fig. 14

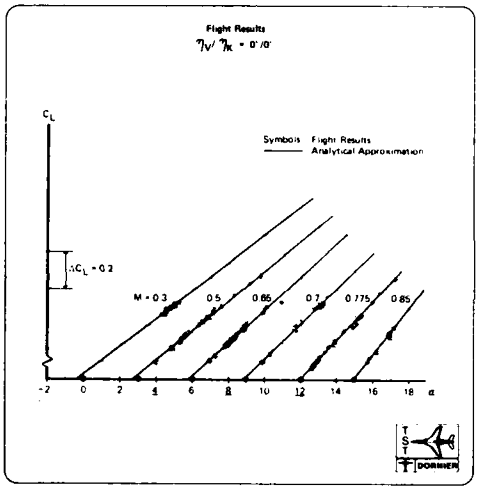

Fig. 15

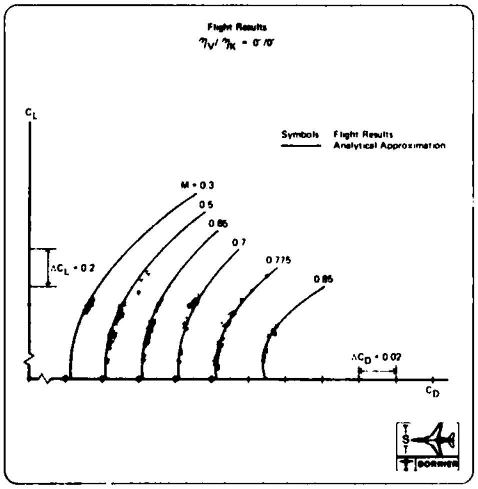

Fig. 16

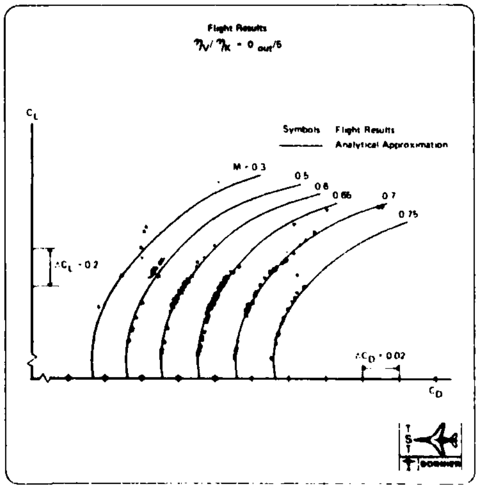

Fig. 17

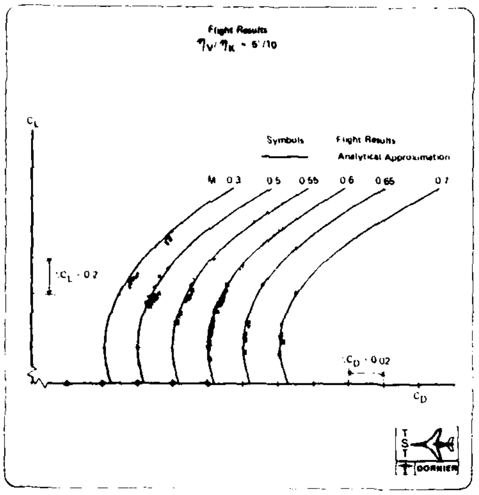

Fig. 18

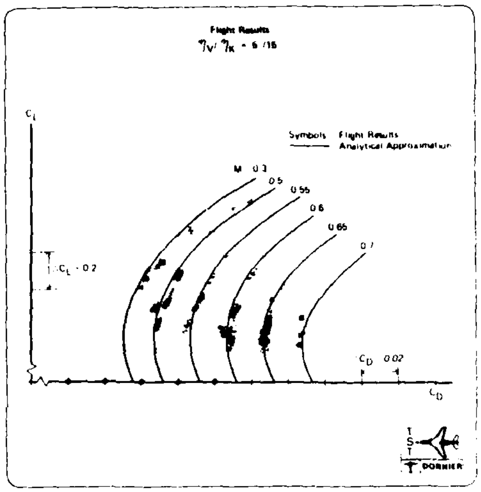

Fig. 19

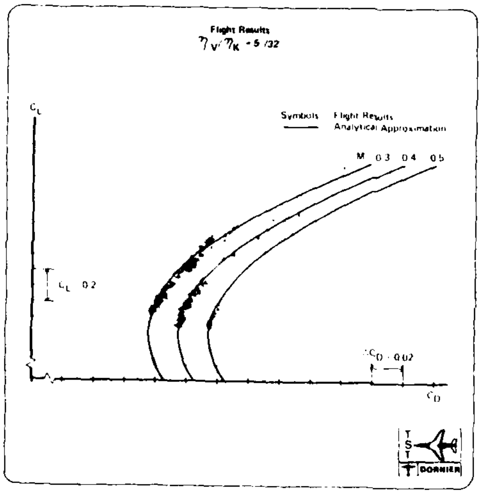

Fig. 20

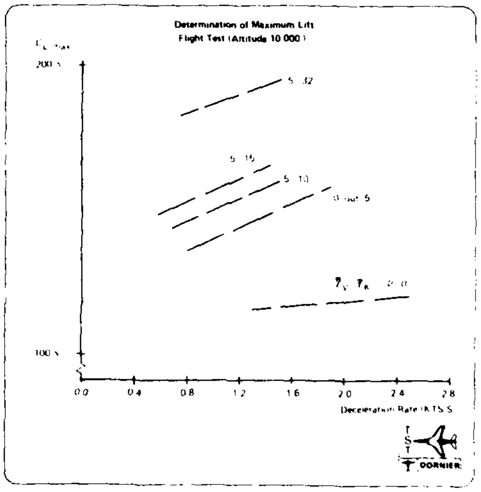

Fig. 21

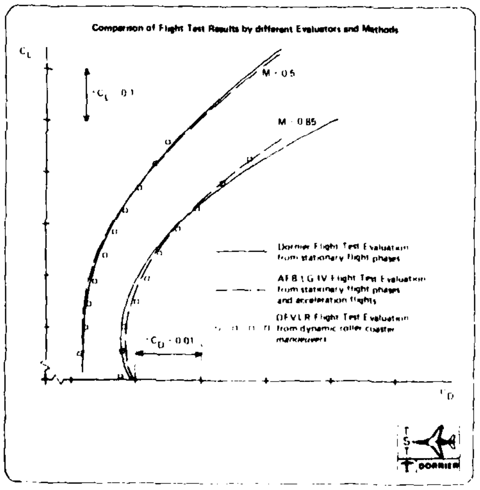

Fig. 22

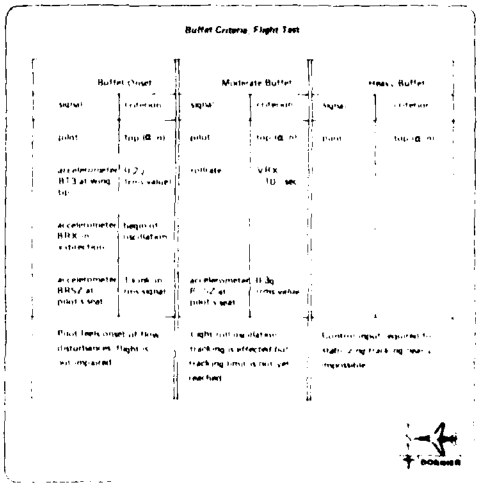

Buffet Criteria Flight Test

Buffet Onset		Moderate Buffet		Heavy Buffet	
signal	criterion	signal	criterion	signal	criterion
pilot	fup (α in)	pilot	fup (α in)	pilot	fup (α in)
accelerometer BT3 at wing tip	0.2 g (rms value)	rollrate	VRX 10 °/sec		
accelerometer BRX in x-direction	begin of oscillation				
accelerometer BRSZ at pilot's seat	1 peak in rms signal	accelerometer BRSZ at pilot's seat	0.3g rms value		
Pilot feels onset of flow disturbances, flight is not impaired		Light roll oscillation, tracking is affected but tracking limit is not yet reached		Control input required to stabilizing tracking nearly impossible	

Fig. 23

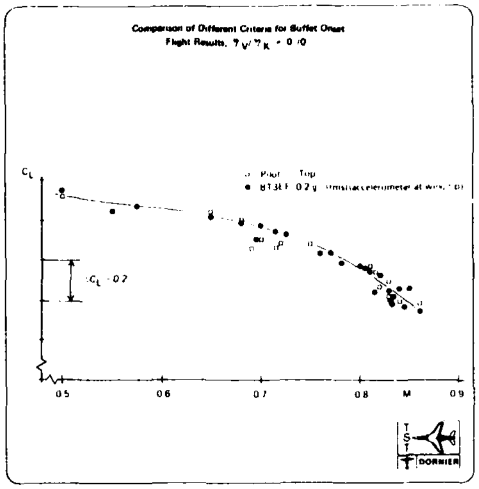

Fig. 24

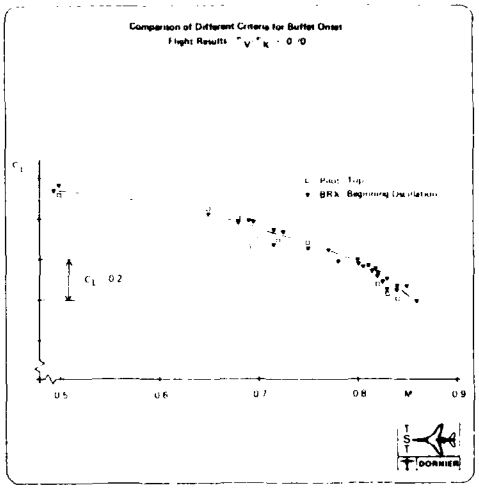

Fig. 25

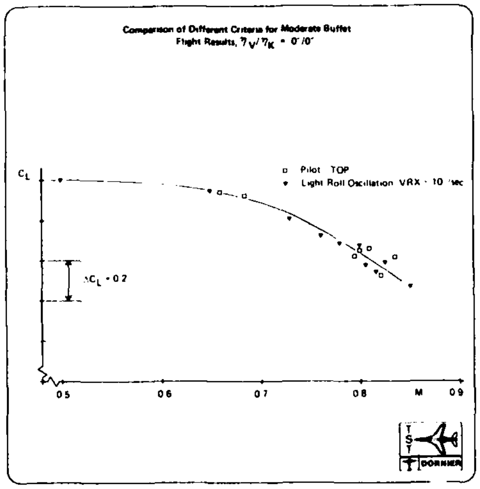

Fig. 26

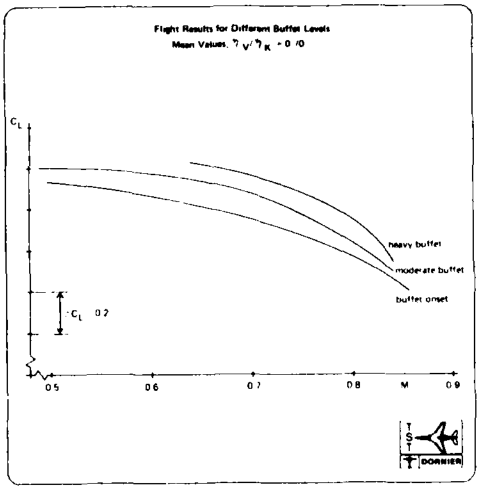

Fig. 27

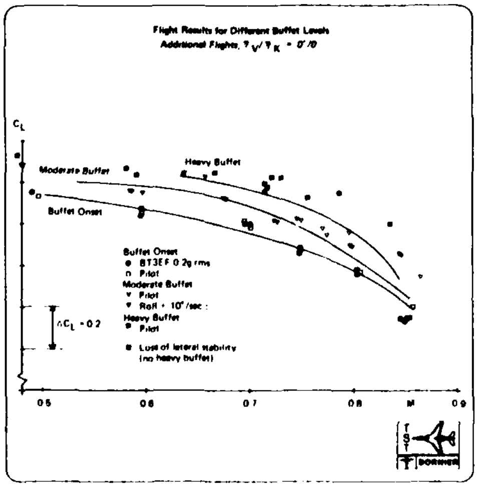

Fig. 28

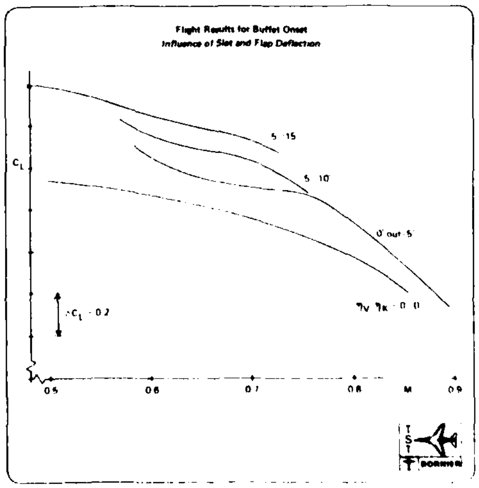

Fig. 29

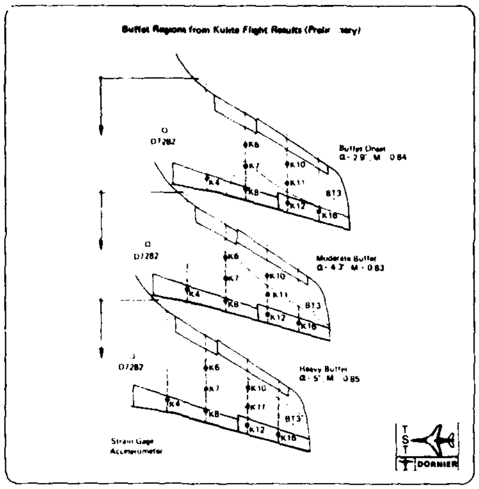
Buffet Regions from Kukta Flight Results (Prelim inary)
D7282
Buffet Onset
α = 2.9°, M 0.84
K4
K6
K7
K8
K10
K11
K12
K16
BT3
D7282
Moderate Buffet
α = 4.3° M = 0.83
D7282
Heavy Buffet
α = 5°, M 0.85
Strain Gage
Accelerometer
TST
DORNIER

Fig. 30

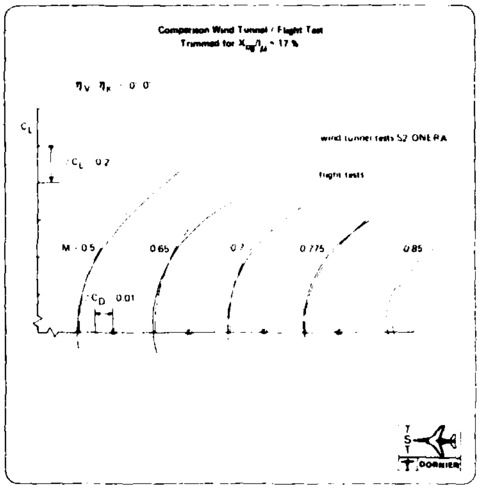

Fig. 31

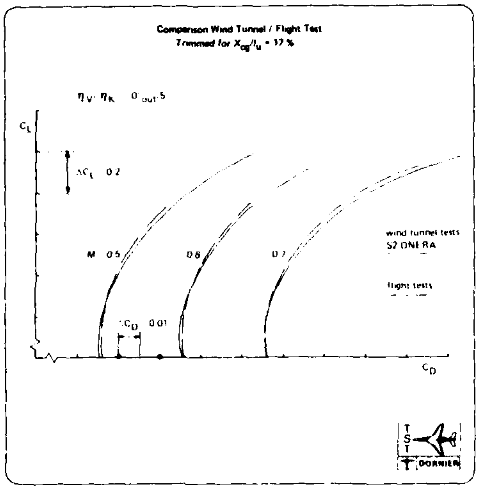

Fig. 32

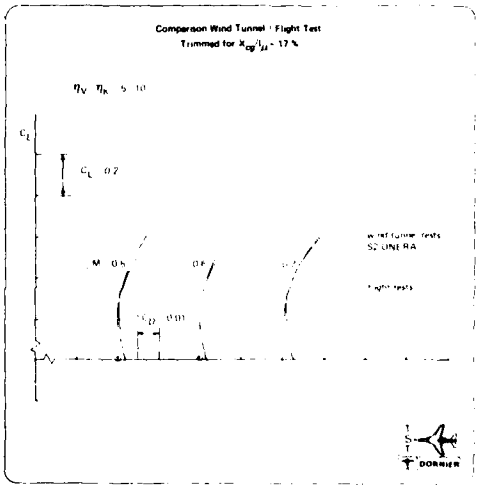

Fig. 33

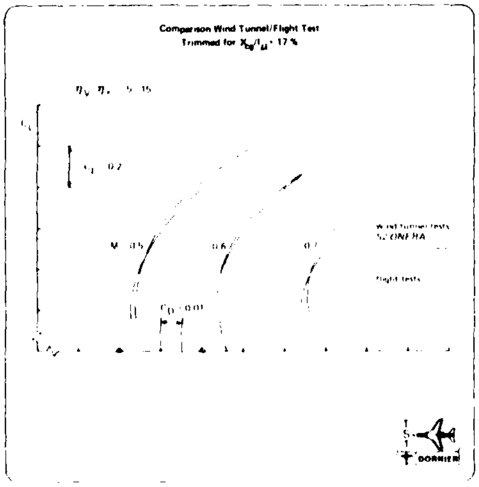

Fig. 34

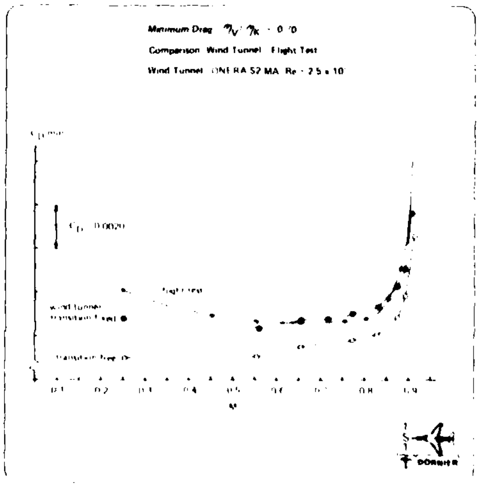

Fig. 35

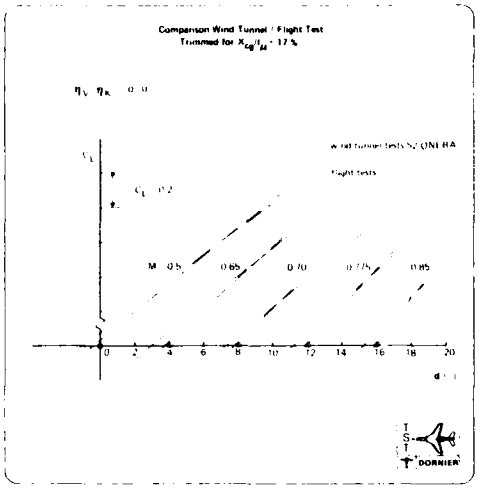

Fig. 36

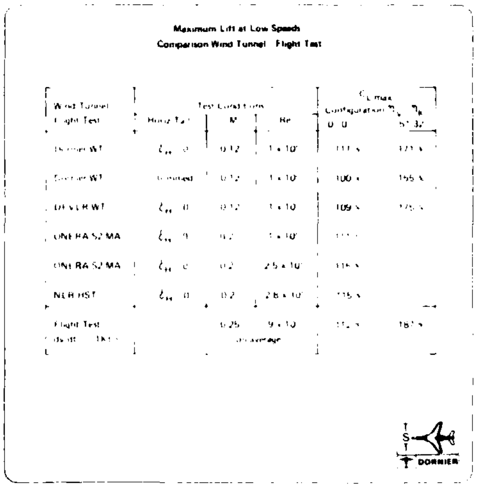
Maximum Lift at Low Speeds
Comparison Wind Tunnel Flight Test

Wind Tunnel Flight Test	Test Conditions Horiz. Tail	M	Re	$C_{L\,max}$ Configuration η_V η_K 0 0	5° 32°
[illegible] WT	ζ_H = 0	0.12	1 × 10	111 %	[illegible]
[illegible] WT	trimmed	0.12	1 × 10	100 %	155 %
DFVLR WT	ζ_H = 0	0.12	1 × 10	109 %	[illegible]
ONERA S2 MA	ζ_H = 0	0.2	1 × 10	[illegible]	
ONERA S2 MA	ζ_H = 0	0.2	2.5 × 10	116 %	
NLR HST	ζ_H = 0	0.2	2.6 × 10	115 %	
Flight Test [illegible]		0.25	9 × 10 in average	[illegible]	18[illegible] %

Fig. 37

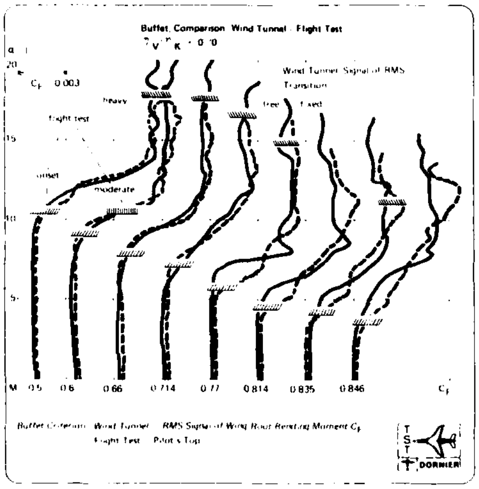

Fig. 38

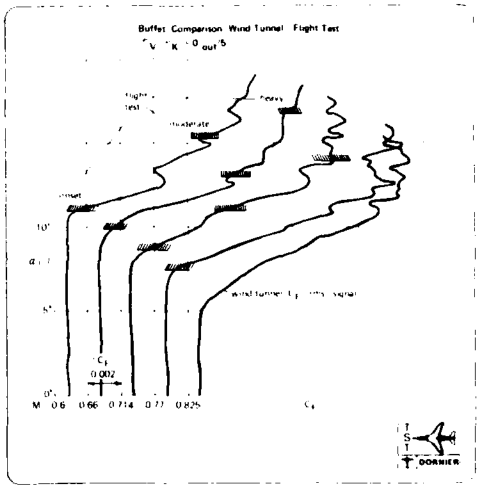

Fig. 39

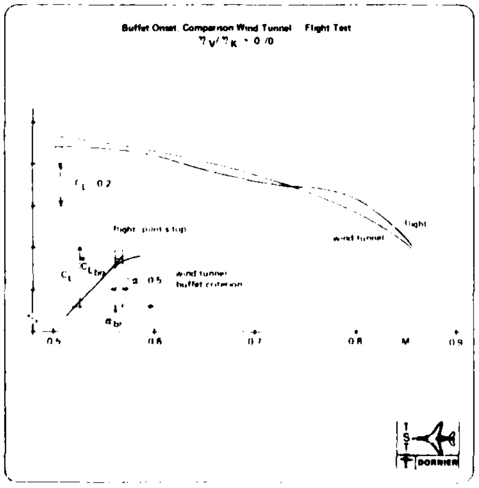

Fig. 40

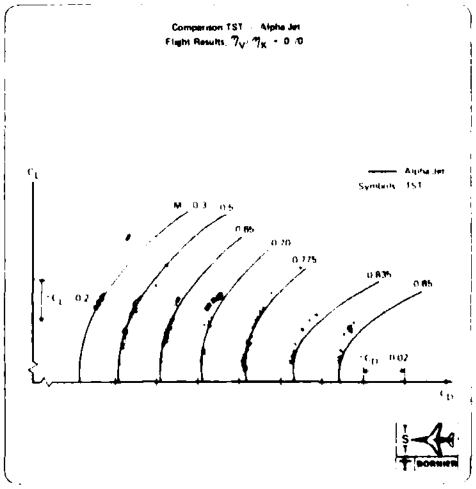

Fig. 41

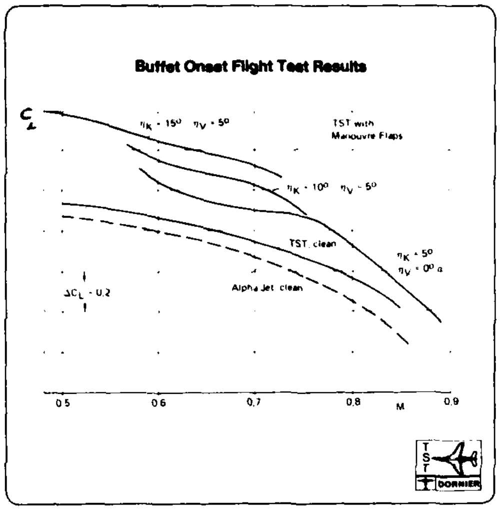

Fig. 42

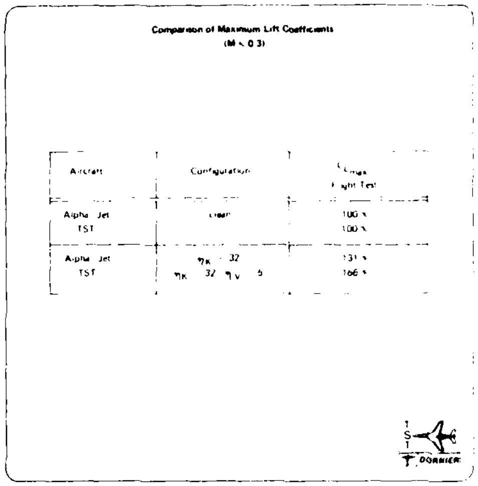

Comparison of Maximum Lift Coefficients
(M < 0.3)

Aircraft	Configuration	$C_{L_{max}}$ Flight Test
Alpha Jet TST	clean	100 % 100 %
Alpha Jet TST	$\eta_K = 32$ $\eta_K = 32$ $\eta_V = 5$	131 % 166 %

TST
DORNIER

Fig. 43

GROUND / FLIGHT CORRELATION ON THE ALPHA-JET EXPERIMENTAL AIRCRAFT WITH A TRANSONIC WING

A Comparison of the Wing Pressure Distribution and Local Wake Survey from Analytical, Wind Tunnel and Flight Results

by

H. Buers
Dornier GmbH, Germany

V. Schmitt, J. Lerat
ONERA, France

SUMMARY

Pressure Distributions at four sections of a transonic wing on a combat aircraft have been measured in different wind tunnels and in flight. The results are compared with each other and with theoretical data.

In addition, wind tunnel and flight test wake results obtained from a rotating pitot-tube are presented.

NOMENCLATURE

c	chord length
C_D	drag coefficient
C_L	lift coefficient
C_p	pressure coefficient $(p - p_\infty)/q$
C_p^*	critical pressure coefficient
p	static pressure
p_t	total pressure
q	dynamic pressure
z	vertical distance from wing reference plane
α	angle of attack
β	angle of side slip
Re	Reynoldsnumber based on aerodynamic chord
Ma	Machnumber

Subscripts

s	rotating pitot (s: sonde de silage)
w	wake

Abreviations

S1	ONERA Wind Tunnel S1 (Soufflerie 1) at Modane
S2	ONERA Wind Tunnel S2 (Soufflerie 2) at Modane

1. INTRODUCTION

The flight tests with the Dornier TST experimental aircraft are the final step of a program covering the design of a wing for a future subsonic combat aircraft with improved performance and behaviour in the transonic flight region. The main task for the new wing was the development of a new transonic basic airfoil and its modification for the tip and root sections of a real three-dimensional wing, combined with the design of a highly effective manoeuvre-flap system. Therefore great emphasis was placed on the pressure distributions of the wing during all steps of the program. The 1:10 High Speed Model as well as the right hand wing of the experimental aircraft were equipped with pressure tubes to learn as much as possible about Machnumber-, angle of attack- and Reynoldsnumber-effects on the airfoil qualities.

Reference /1/, /2/, give background information on the TST-program, the design description, the different program steps and the total aircraft performance from the flight tests.

This paper informs about pressure distributions in flight test, which reveal the influence of Machnumber and angle of attack in the transonic flight envelope. An attempt is made to show Reynoldsnumber effect. Additional wake investigations by means of an ONERA designed rotating Pitot tube are presented. The pitot delivers informations about the wake characteristics and, in particular, shows the existence of shock waves on the wing. From the wake the local drag rise boundary is determined.

Some flight test results are compared with measurements, obtained in the ONERA wind tunnel S1 and S2 (Modane). The problems involved with such a comparison are discussed.

Finally, recent progress of numerical prediction methods for complex geometries is demonstrated by a comparison of calculated pressure distribution with flight test results.

2. MEASURING EQUIPMENT AND TEST PROCEDURE

2.1 Test Set-up for Pressure Distribution and Wake Survey in Flight

For comparison with wind tunnel results the TST experimental aircraft is equipped with static pressure tubes at four wing sections. Fig. 1 shows the wing planform and gives the spanwise stations, where the pressure distributions were measured. Several flights were conducted with a rotating pitot /3/, attached close to the trailing edge flap for wake survey as shown in Fig. 2. The location of the rotating pitot is also indicated in Fig. 1. The pitot probe is installed in such a way that the local wakes of the sections 2 and 3 can be investigated. During the revolution of the pitot the total and the static pressure are measured by means of two pressure transducers. A potentiometer gives the probe position.

Fig. 3 gives the chordwise location of the pressure tubes at the four sections. All pressures of each section where led via a scanivalve to the pressure transducer. The static and dynamic reference pressure values were taken from probes at the forward fuselage. It requires 5 seconds to record a complete pressure distribution on the data tape.

2.2 Pressure Distribution in Flight Test Procedure

Of course it is more difficult to measure pressure distributions in flight than in the wind tunnel, because it is difficult to keep the flight conditions steady for a sufficiently long time. The TST-tests were complicated by the fact, that the actual configuration is a rather light aircraft without fuel storage in the wing and without external stores; therefore, to achieve higher lift coefficients, it was necessary to fly turns with higher load factors. Another point which affected the accuracy of the pressure distributions is the aircraft pitch control system, which was not optimized for the new configuration. The TST control system is rather sensitive at higher transonic Machnumbers.

In spite of these difficulties the achieved quality of the pressure distributions is rather good /4/, as demonstrated in Fig. 4 and 5. Fig. 4 shows the variation of the Machnumber and the angle of attack during the 5 seconds of one scani-run. One test point was at Mach .71 with a loadfactor of $n = 1.0$ and the other test took place at Mach .83 and was a turn with $n = 3.2$.

Fig. 5 demonstrates the effect of Machnumber and angle of attack variations on the pressure distributions. The average variations $\Delta\alpha$ of angle of attack and Δ Ma of Machnumber of the analysed pressure distributions do not exceed:

$$\left.\begin{array}{lcl}\Delta \mathrm{Ma} & = & 0.005 \\ \Delta \alpha & = & 0.15^{0}\end{array}\right\} \text{flight}$$

These values have to be compared with those from the wind tunnel tests. In 1980 for example in the S1 with the 1:1 half-model using the real TST-wing, the average Mach variation was of the same order as in the flight test. The angle of attack variation, however, was evaluated as less than .05 degrees. On the other hand, for the much more classical tests in the S2 with the 1:10 complete model in 1977, better average values were achieved:

$$\left.\begin{array}{lcl}\Delta \mathrm{Ma} & = & 0.0005 \\ \Delta \alpha & = & 0.02^{0}\end{array}\right\} \text{S2}$$

During the wind tunnel tests one scani-run took about 15 seconds.

Of course there were further parameters observed to judge the test qualities.

2.3 Wake Survey - Data Processing

The rotating pitot is operated for two or three revolutions during very well stabilized performance tests (load factor = 1.0). The angular speed of the pitot is 10^{0}/sec.

This kind of test must be performed under very steady conditions: the wake survey takes between two and ten seconds where acceptable variations must remain below:

$$\Delta \mathrm{Ma} = \pm 0.001; \; \Delta \alpha = \pm 0{,}1^{0}$$

The reliability of these measurements in flight is shown in Fig. 6, where two wakes obtained at the same Machnumber are compared.

A total of about fifty wake surveys were performed and processed in the course of these test flights.

3. FLIGHT TEST RESULTS

3.1 Pressure Distributions at the Design Point

One of the design requirements of the TST was a buffet free lift coefficient of $C_L = 0.4$ at Mach 0.83. In Fig. 7 the pressure distribution is plotted for this flight condition. Typical of the new transonic airfoil generation is the nearly constant pressure coefficient in the supersonic flow region on the upper wing surface. The pre-shock Machnumber at the four sections is about Ma = 1.2. The pressure rise is achieved by a compression shock at a chordwise location of 60 % inboard to 40 % outboard. This test point is about 1^{0} in angle of attack below the buffet onset boundary.

3.2 Off-Design Behaviour

The off-design qualities of the TST wing are demonstrated by the effects of Machnumber and angle of attack on the wing pressure distribution. Since these effects are nearly the same in all four sections, only the results for section 3 are discussed.

Fig. 8 points out the effect of Machnumber on the pressure distribution. With increasing Machnumber the supersonic flow region moves towards the trailing edge. The flat camber of the upper surface of the forward part of the wing prevents high pre-shock Machnumbers and severe dragrise.

The effect of angle of attack on the pressure distribution at design Machnumber .83 is demonstrated in Fig. 8 from $\alpha = 0.8^{0}$ up to 3.9^{0}, that is from a lift coefficient of $C_L = 0.1$ up to a lift coefficient just before buffet onset.

AD-A129 433 GROUND/FLIGHT TEST TECHNIQUES AND CORRELATION(U)
ADVISORY GROUP FOR AEROSPACE RESEARCH AND DEVELOPMENT
NEUILLY-SUR-SEINE (FRANCE) FEB 83 AGARD-CP-339

2/6

UNCLASSIFIED F/G 1/3 NL

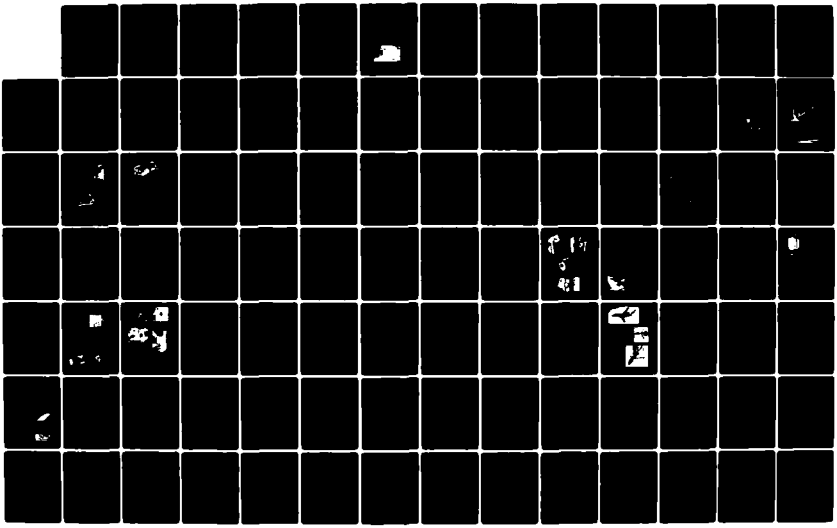

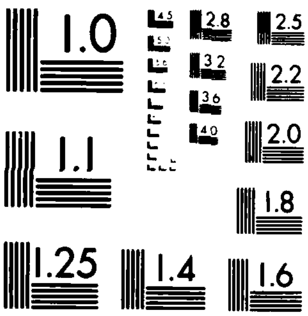
1.0
4.5
5.0
5.6
2.8
2.5
3.2
2.2
3.6
4.0
2.0
1.1
1.8
1.25
1.4
1.6

MICROCOPY RESOLUTION TEST CHART
NATIONAL BUREAU OF STANDARDS-1963 A

The rear part of the wing is hardly affected by increasing angle of attack. The supersonic region on the lower side of the wing, which is terminated by a shock wave, disappears with increasing alpha. On the upper surface there is at first an extension of the supersonic flow towards the trailing edge up to about 2° of angle of attack and for higher incidence the $C_{p_{min}}$-values grow by a nearly constant $\Delta\ C_p$ in the supercritical flow field.

3.3 Reynoldsnumber Effects in Flight Tests

In the case of transonic airfoils attention must be paid to the effect of Reynoldsnumber. Although the major effect was expected following the change from S2 wind tunnel to S1 and flight conditions, where Re changes from 2.5×10^6 to about 25×10^6, interesting differences were also discovered in Reynoldsnumber variation during the flight tests.

Of course it is not easy to separate the pure Reynolds effect in flight, because it is very difficult to achieve the same conditions at two test points. There often is an overlay of Machnumber,angle of attack and load factor influences.

Fig. 10 compares the pressure distribution at Mach 0.83 for $Re = 23 \times 10^6$ and $Re = 10.9 \times 10^6$. The subcritical flow on the lower surface is scarcely affected. Remarkable differences are detected on the upper surface of the inner part of the wing, represented by sections 1 and 2. In the supersonic flow field lower pressure coefficients are achieved at the higher Reynoldsnumber. From other tests it could be derived, that these differences are higher than those expected from the variation of the Machnumber and angle of attack during the scani-run. The outer part of the wing shows variation in C_p due to Reynoldsnumber, which is within the test accuracy. Though the difference in loadfactor between the two test points runs up to 2.5 g's, there seems to be only a little change in wing torsion, because this would lead to differences in the effective angle of attack and thus vary also the pressure on the lower surface.

3.4 Wake Measurements

Measurement of the wake total pressure is made at a loadfactor of $n = 1.0$ and the tests were performed at the same Reynolds- and Machnumbers as in the S1 wind tunnel tests.

Lift coefficients achieved in flight were very low for stable horizontal flight of the altitude corresponding to S1 tests. Therefore it was not possible to check the wake at the design point.

Fig. 11 shows the shape of the pressure distribution at section 2 and 3 at the design Machnumber, but the C_L for $n = 1.0$ is only 0.1. Shock waves on both upper and lower side can be seen, whereby the pressure loss at section 2 is bigger than at section 3. The differences in depth between the two wakes are explained by different distances between pitot and trailing edge at section 2 and 3.

Fig. 12 shows evaluation of the wakes for Machnumbers = .725, 0.835 and 0.851 at section 3. The wake thickening with increasing Machnumber indicates the growth of the shock waves, especially on the lower surface at these low angles of attack.

The drag evaluation, derived from the wake, against Machnumber is shown in Fig. 13 for both sections, following the envelope:

$$0.53 < Ma < 0.851$$
$$10.1 < Re\ .\ 10^6 < 24$$
$$0{,}10 < C_L < 0.16$$

According to this result, the section 3 profile has slightly higher drag than section 2. Nevertheless the drag divergence Machnumber is approximately the same at both sections at Mach .835.

4. COMPARISON OF FLIGHT- AND WIND-TUNNEL-RESULTS

4.1 Pressure Distribution

The comparison of the flight pressure distributions with ground test results at first requires some details about the different test conditions in flight and in the wind tunnel. The basic test series, as indicated in /1/ took place in the S2 tunnel, where the 1:10 complete model was mainly tested at a Reynoldsnumber of 2.5×10^6 with free transition. The clean model was fabricated with a perfect wing surface; there were no gaps or steps from the flap system. Flow visualization indicated very large parts with laminar boundary layer on the wing. Some tests were conducted with fixed transition at 10 % chord. In all these S2 tests wall corrections /5/ were found to be negligible.

A very important test serie was carried out in the S1 tunnel, where the original right hand wing was checked as a half-model at flight Reynoldsnumbers. Of course the surface of the original wing is not as smooth as the 1:10 wing. For example there are irregulations from rivets and metal joints, and gaps and steps from the flap system even in retracted position.

In order to reduce blockage effects to acceptable limits the fuselage dummy had to be slightly truncated in spanwise direction; nevertheless the blockage rate of 2,7 % was nearly twice that of the usual values. The calculated global wall corrections are rather small, for example at the design point:

$$\Delta Ma_c = Ma_{corrected} - Ma_{Test} = -0.005$$

$$\Delta \alpha_c = \alpha_{corrected} - \alpha_{Test} = -0.25^0$$

A recent attempt to determine local wall corrections is under progress.

An overview of Reynoldsnumbers achieved in the flight envelope and in the wind tunnel tests is given in Fig. 14.

The comparison of pressure distribution between flight and wind tunnel tests has to be made at the same Machnumber and angle of attack. Due to flight test procedure it is nearly impossible to realize that condition; more or less important differences have to be admitted and taken into account in the analysis of results.

Another point that one must consider comes from the plot presentation of the test. The distance between two pressure tubes at the wing sections is in the range of about 5 % of chord length and the measured pressure-coefficients are combined linearly. Thus smaller local effects might be overvalued.

The following figures compare flight and wind tunnel results at Mach .71 and .83.

The first result plotted in Fig. 15 a - d concerns the subcritical case at Ma .71 and angle of attack of 3^0. The flight pressure distribution was measured at a loadfactor of n = 2.8. In general the agreement between wind tunnel and flight is quite good. Main differences occur at all sections at the supercritical suction peak on the upper surface near the leading edge, where the flight exhibits higher negative C_p-values. In spite of the big differences in Reynoldsnumber between S2 and flight, there is better agreement between S2 and flight than between S1 and flight.
The differences between free and fixed transition are small and nearly limited to the location of the ballotini-strip.

At the design point, which was checked in flight with a loadfactor of n = 1.5, the results from S2 and flight agree reasonably well, as demonstrated inFig. 16 a - d. The differences are mainly located in the supersonic flow field on the upper surface. More important differences appear between flight test and S1. The local Machnumbers on the upper side in the whole supersonic region are smaller in the S1. The differences diminish from wing root to wing tip and it is supposed that they originate from the fuselage representation in the S1 together with floor boundary layer effects.

At this Machnumber the transition free tests from S2 provide better agreement with the flight test, though the interaction between shock wave and laminar boundary layer on the upper surface induces a laminar separation bubble, which leads to a light compression upstream of the shock. The principal effect of the fixed transition test is the change in shock position, which moves upstream with the fixing of the transition.

In comparison with S2 tests, the original wing test at the higher Reynoldsnumber achieved neither in S1 nor in flight significant change of rear loading. This indicates that viscous effects are not very significant on the TST wing.

4.2 Wake Shapes and Drag

Wake measurement comparison is confined to S1 wind tunnel and flight test with the full scale wing and the rotating pitot, because no wake investigations took place in the S2 wind tunnel.

Mach- and Reynoldsnumber are the same; the only difference lies in the angle of attack.

Fig. 17 shows a comparison of section 3 wake at Mach .59 and .77. The wind tunnel wakes are slightly thicker than those in flight.

Fig. 18 shows the evaluation of wake drag versus Machnumber at the same section 3 at constant angle of attack. According to the initial analysis, it seems that the drag is somewhat smallerin flight than in the wind tunnel up to the divergence point. There may be larger differences in angle of attack for this comparison, but this cannot be the reason for these differences which are still unexplained. On the other hand one notices, that the dragrise Machnumber is nearly identical in both cases.

5. COMPARISON OF CALCULATED AND FLIGHT PRESSURE DISTRIBUTION

In Fig. 19 a - b the flight test results are compared with calculated pressure distributions for two wing sections /6/, /7/. The results of two calculation methods are presented. The first method is based on the Transonic Small Disturbance (TSP) theory and was performed during the design phase. The other theoretical pressure distributions result from more recent calculations, solving the full potential equation for transonic flow in finite volume formulation, using a contour conformal mesh generation for arbitrary wing-body configurations. Details can be found in Ref. /8/ and /9/. Both calculations have been made without corrections for lift or Machnumber and without viscous effects.

The more favorable results of the recent calculations are obvious. The main improvement was found to be based on the better representation of body and wing fuselage intersection. There is reasonably good agreement with the flight results with regard to the complicated shape of the TST.

6. CONCLUSION

The comparison of ground and flight test results in the TST program showed reasonably good agreement of the pressure distributions at subsonic and transonic Machnumbers up to buffet onset boundaries. An effect of Reynoldsnumber between wind tunnel tests at $Re = 2.5 \times 10^6$ and flight tests could not be clearly identified. For this aircraft the dimension of Reynoldsnumber effect seems to be of the same order as some other effects, as there are:

- accuracy of the test results
- geometrical differences and different elastic deformation between model and real wing
- wind tunnel corrections

7. REFERENCES

/1/ JACOB, D., WELTE, D., WÜNNENBERG, H.
A Comparison between Wind Tunnel and Flight Results for Aerodynamic Performance
AGARD Symposium, Cesme, Turkey, Oct. 11 - 14, 1982

/2/ LOTZ, M., MONNERIE, B.
The Franco-German Experimental Program for the Evaluation of a Supercritical Wing for a Combat Aircraft Application
ICAS Paper No. 76-21

/3/ Explorateur de sillage d'aile
ONERA Activités 1976, p. 12

/4/ BUERS, H.
Dornier-Aktenvermerk BF10-2175/82

/5/ VAUCHERET, X.
Corrections de paroi en soufflerie transsonique - Porosité équivalente
Publication ONERA no. 1977-3

/6/ FRITZ, W.
Dornier-Aktenvermerk BF30-1281/78

/7/ LEICHER, S.
Dornier-Aktenvermerk BF30-2194/82

/8/ LEICHER, S.
Ein Finite-Volume-Verfahren zur Lösung der vollen Potentialgleichung für beliebige Flügel- und Flügel-Rumpf-Kombinationen
Dornier-FB 81/03 B, 1981

/9/ FRITZ, W., GRASHOF, J., LEICHER, S., LONGO, J.
Mesh Generation Strategies for CFD on Complex Configurations
8. International Conference on Numerical Methods in Fluid Dynamics,
June 28 - July 2, 1982
Rheinisch-Westfälische TH Aachen, West Germany

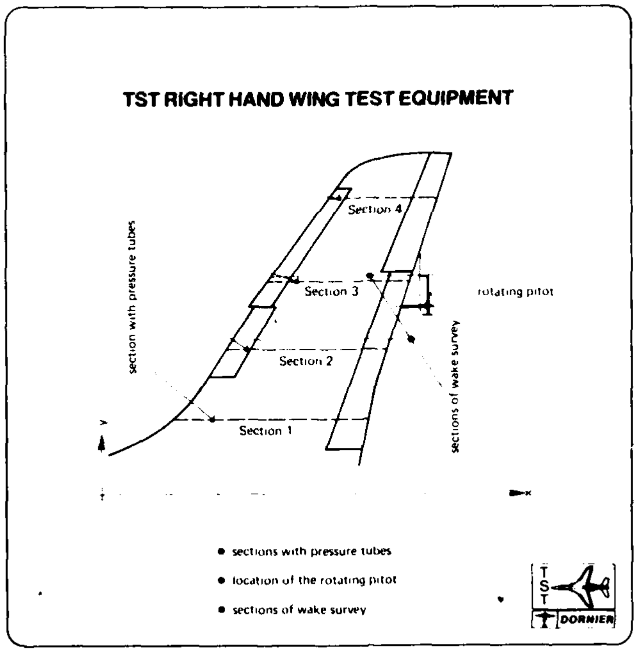
TST RIGHT HAND WING TEST EQUIPMENT
Section 4
Section 3
Section 2
Section 1
section with pressure tubes
rotating pitot
sections of wake survey
y
x
● sections with pressure tubes
● location of the rotating pitot
● sections of wake survey
TST
DORNIER

Figure 1

Figure 2

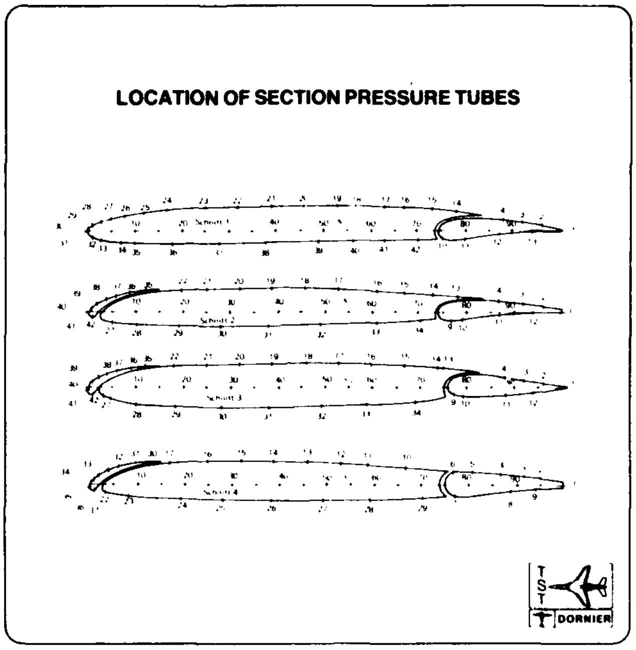

LOCATION OF SECTION PRESSURE TUBES

Figure 3

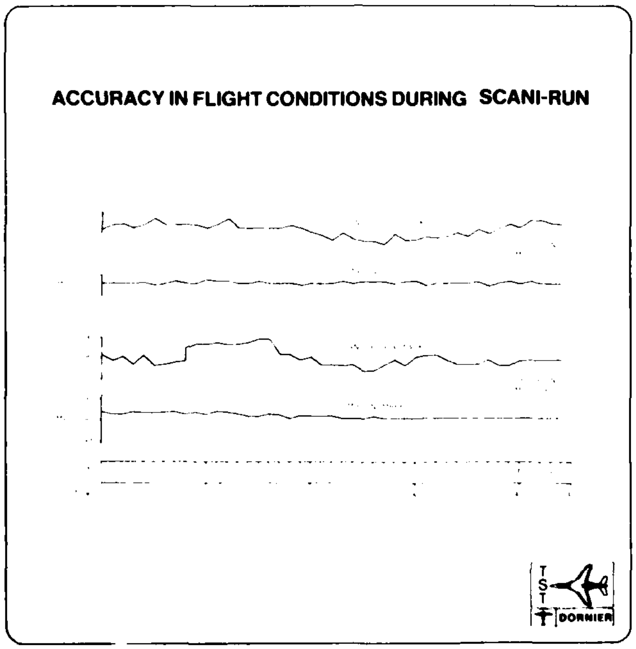

ACCURACY IN FLIGHT CONDITIONS DURING SCANI-RUN

Figure 4

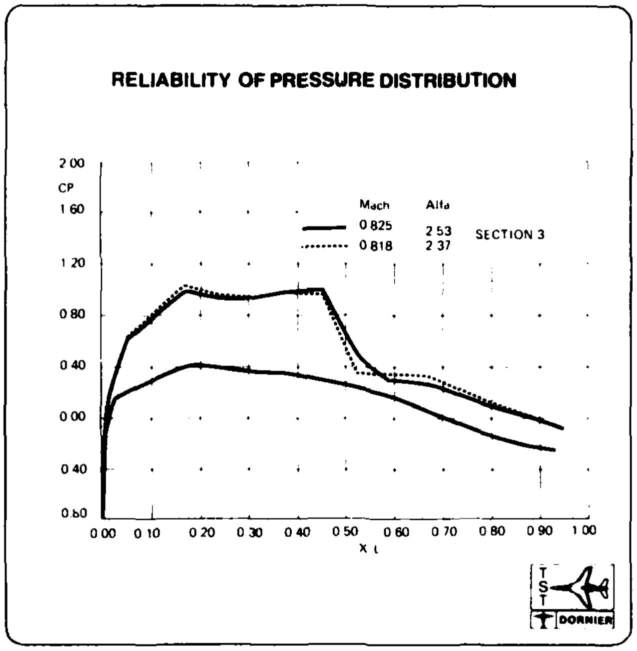

Figure 5

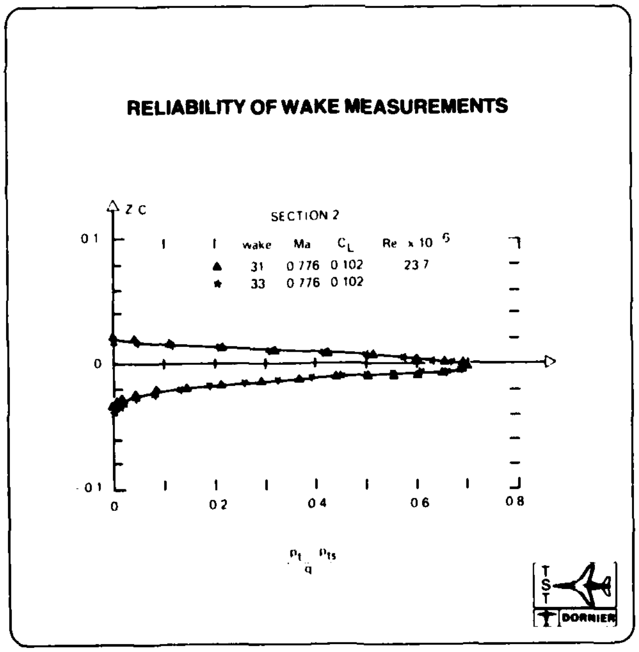

Figure 6

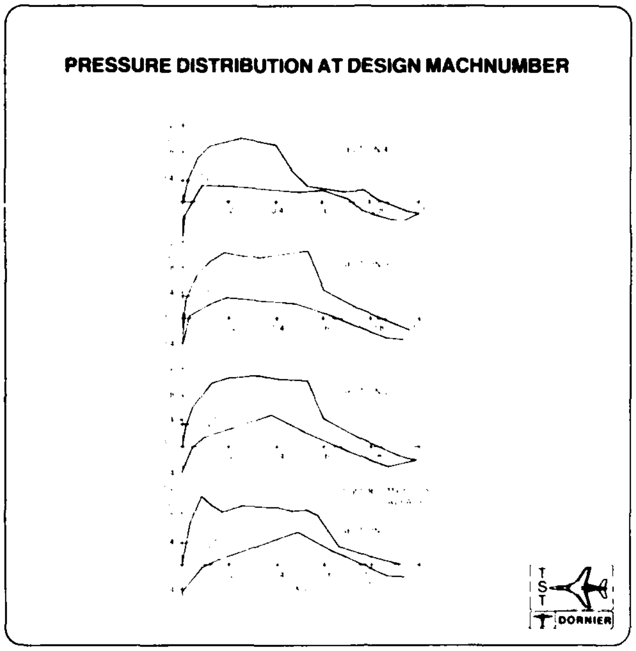

PRESSURE DISTRIBUTION AT DESIGN MACHNUMBER

Figure 7

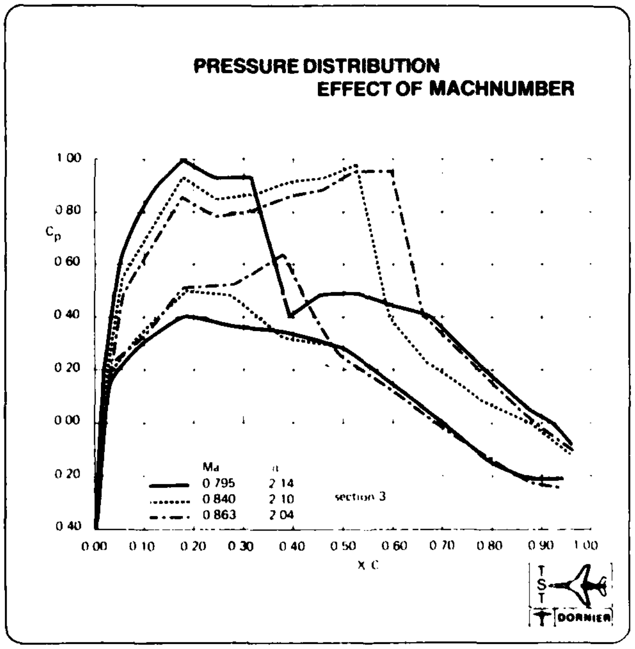

PRESSURE DISTRIBUTION
EFFECT OF MACHNUMBER

Figure 8

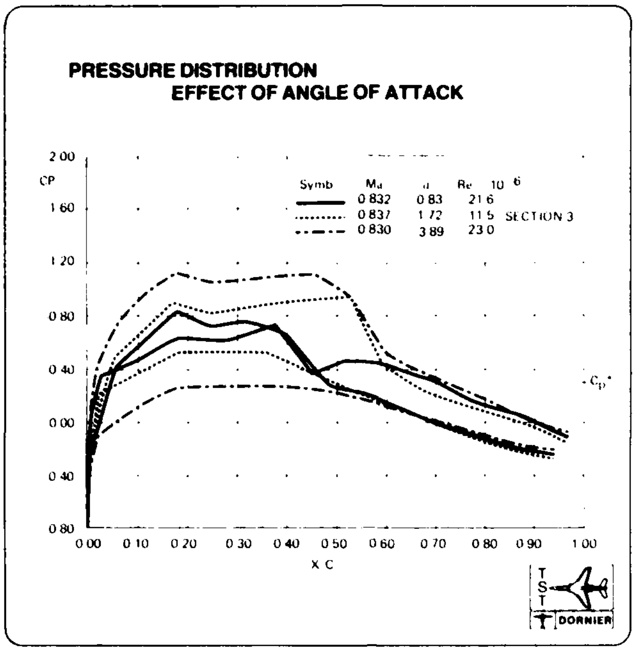

Figure 9

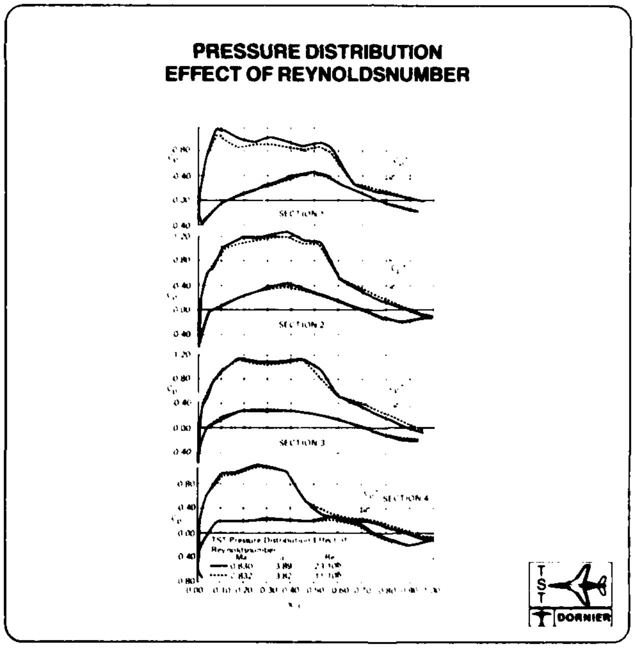

Figure 10

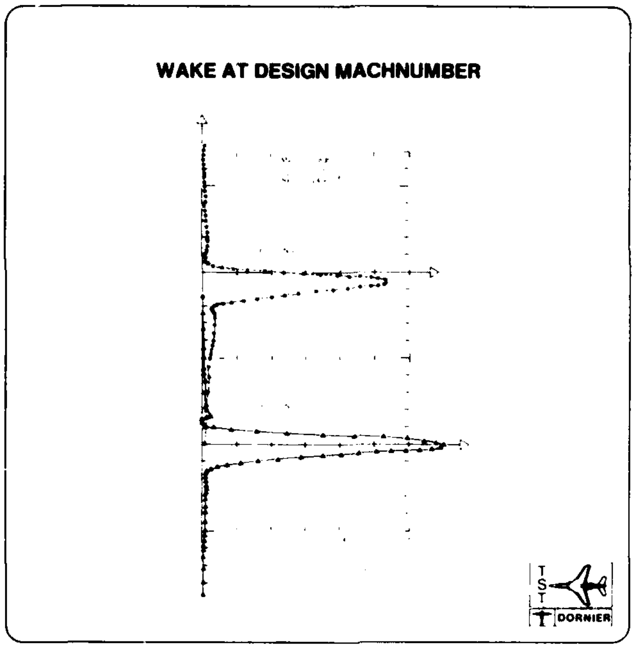

WAKE AT DESIGN MACHNUMBER

Figure 11

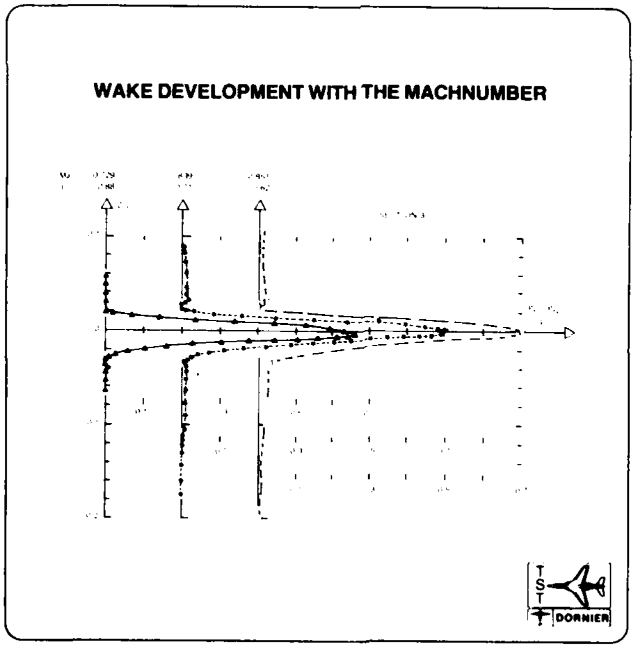

WAKE DEVELOPMENT WITH THE MACHNUMBER

Figure 12

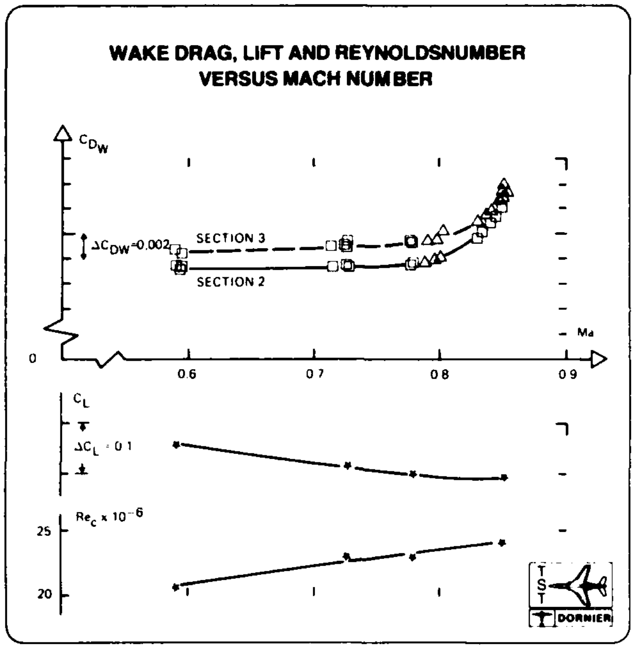

Figure 13

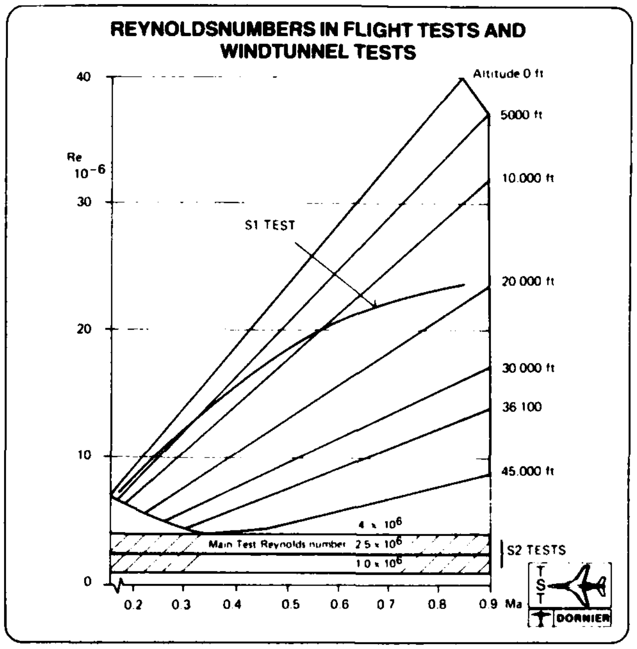

Figure 14

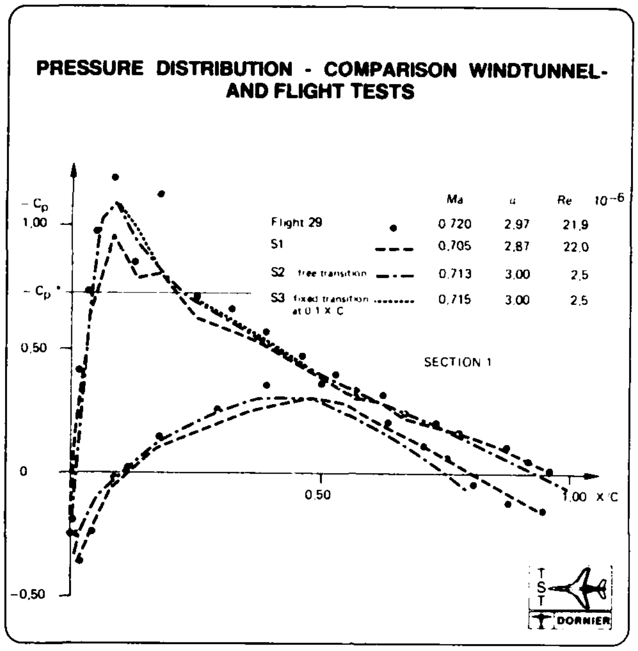

PRESSURE DISTRIBUTION - COMPARISON WINDTUNNEL- AND FLIGHT TESTS

Figure 15a

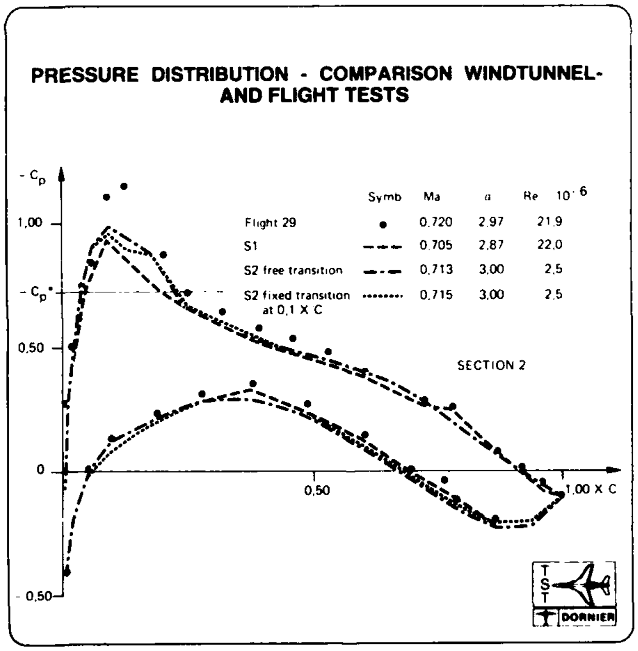

PRESSURE DISTRIBUTION - COMPARISON WINDTUNNEL- AND FLIGHT TESTS

Figure 15b

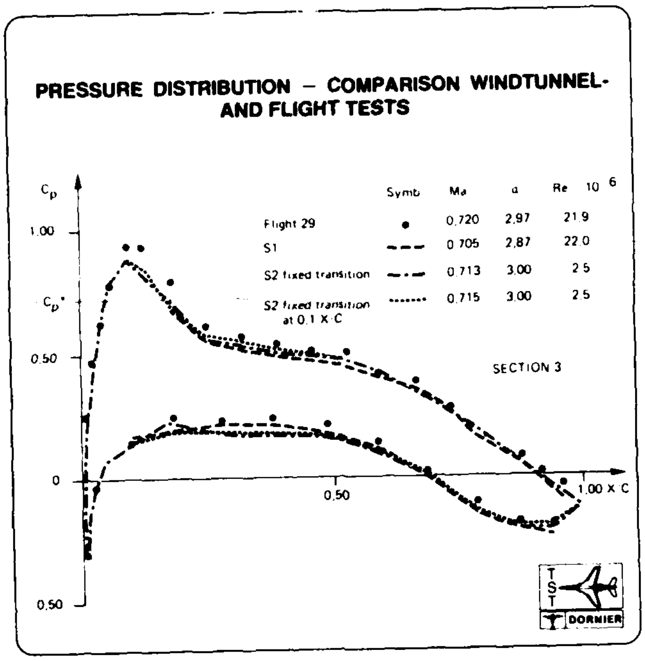

Figure 15c

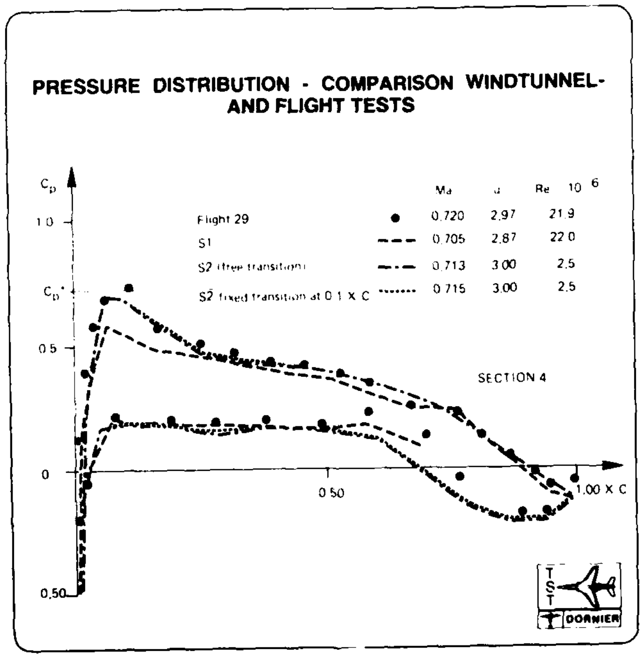

Figure 15d

PRESSURE DISTRIBUTION – COMPARISON WINDTUNNEL-AND FLIGHT TEST

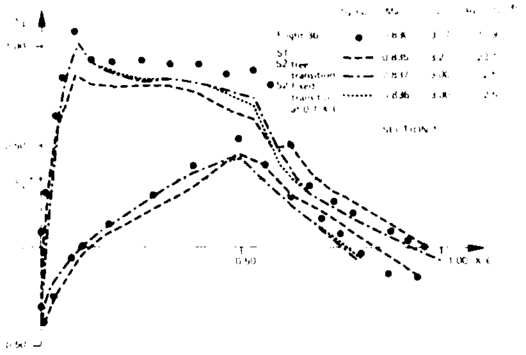

Figure 16a

PRESSURE DISTRIBUTION – COMPARISON WINDTUNNEL-AND FLIGHT TEST

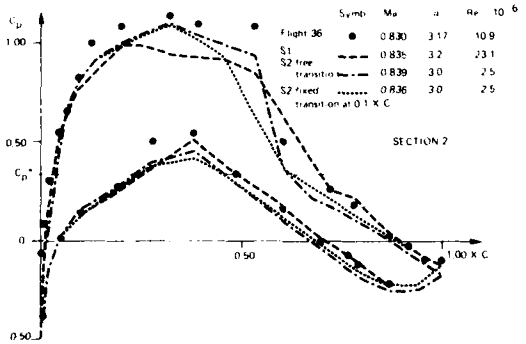

Figure 16b

PRESSURE DISTRIBUTION – COMPARISON WINDTUNNEL- AND FLIGHT TEST

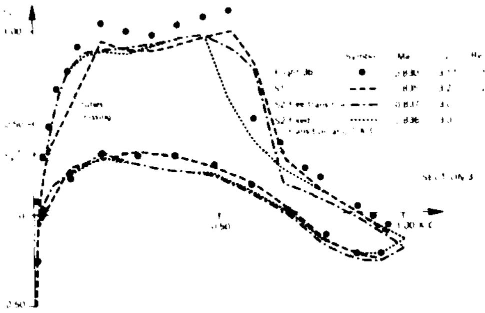

Figure 16c

PRESSURE DISTRIBUTION – COMPARISON WINDTUNNEL- AND FLIGHT TEST

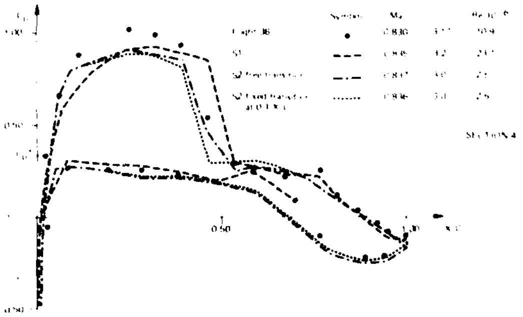

Figure 16d

WAKES-COMPARISON FLIGHT-WIND TUNNEL

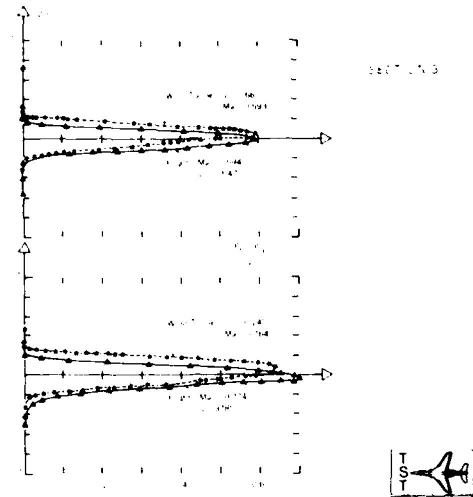

Figure 17

WAKE DRAG VERSUS MACHNUMBER
COMPARISON FLIGHT-WIND TUNNEL

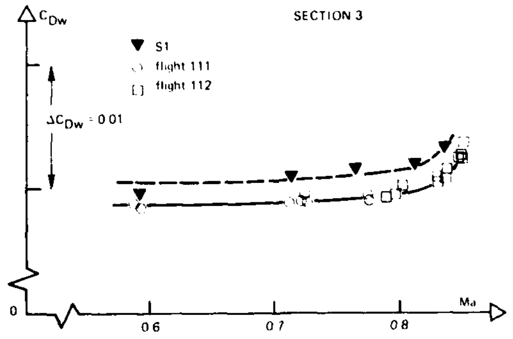

Figure 18

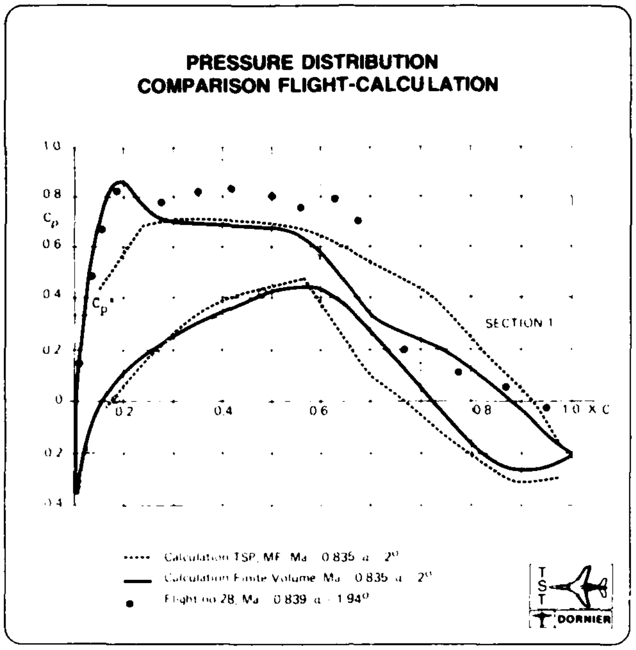

Figure 19a

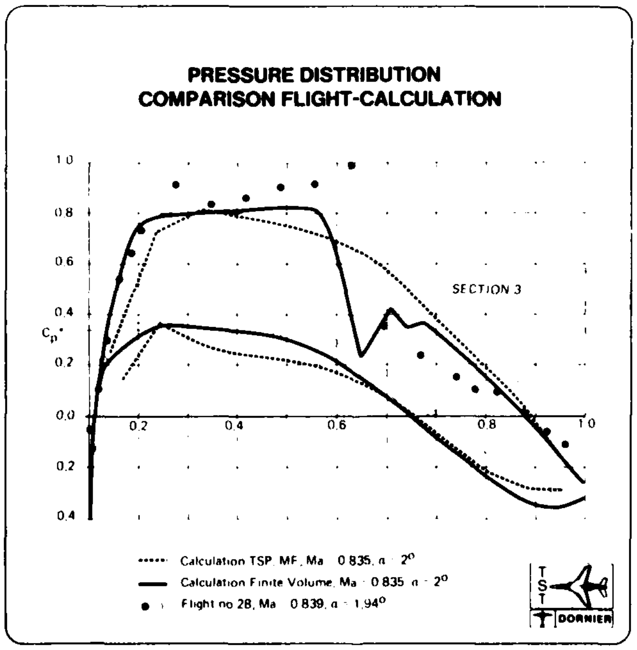

Figure 19b

FLIGHT AND WIND-TUNNEL CORRELATION OF BOUNDARY-LAYER TRANSITION ON THE AEDC TRANSITION CONE

David F. Fisher
NASA Ames Research Center
Dryden Flight Research Facility
Edwards, California 93523
U.S.A.

N. Sam Dougherty, Jr.*
Rockwell International
Huntsville, Alabama 35801
U.S.A.

SUMMARY

Transition and fluctuating surface-pressure data were acquired on a 10° included angle cone, using the same instrumentation and technique over a wide range of Mach and Reynolds numbers in 23 wind tunnels and in flight. Transition was detected with a traversing pitot-pressure probe in contact with the surface. The surface-pressure fluctuations were measured with microphones set flush in the cone surface. Good correlation of end-of-transition Reynolds number Re_T was obtained between data from the lower-disturbance wind tunnels and flight up to a boundary-layer edge Mach number, $M_e = 1.2$. Above $M_e = 1.2$, however, this correlation deteriorates, with the flight Re_T being 25 to 30% higher than the wind tunnel Re_T at $M_e = 1.6$. The end-of-transition Reynolds number correlated within ±20% with the surface-pressure fluctuations, according to the equation

$$Re_T = 3.7 \times 10^6 \left[\left(\frac{\sqrt{\overline{p_s'^2}}}{q_\infty} \right) 100 \right]^{-0.25}$$

Broad peaks in the power spectral density distributions indicated that Tollmien-Schlichting waves were the probable cause of transition in flight and in some of the wind tunnels.

NOMENCLATURE

F	nondimensional peak center frequency, $(2\pi f \nu_e)/U_e^2$
f	frequency, Hz
$G_x(f)$	power spectral density function
H	1962 standard atmosphere pressure altitude, m (ft)
L	length of cone with extension, 113.0 cm (44.5 in)
M	Mach number
p	pressure, N/m^2 (lb/ft^2)
p'	fluctuating pressure, N/m^2 (lb/ft^2)
$\sqrt{\overline{p_s'^2}}$	average static root-mean-square fluctuating pressure, N/m^2 (lb/ft^2)
q	dynamic pressure, N/m^2 (lb/ft^2)
Re_T	end-of-transition Reynolds number
Re_T'	end-of-transition Reynolds number not corrected to adiabatic temperature
Re_t	onset-of-transition Reynolds number
Re_x	Reynolds number based on length from cone apex
T	temperature, K (°R)
U	velocity, m/sec (ft/sec)
U/ν	unit Reynolds number, per m (per ft)
X_T	end-of-transition location, cm (in)
X_t	onset-of-transition location, cm (in)
x	distance along a cone ray from the cone apex, cm (in)
α	cone angle of attack with respect to airstream, deg
β	cone sideslip angle with respect to airstream, deg
ν	kinematic viscosity, m^2/sec (ft^2/sec)
φ	cone azimuthal angle relative to cone top center ray (Fig. 1(b)), deg

Subscripts:

aw	adiabatic wall
e	boundary-layer edge
max	maximum
p	traversing pitot
t	total
w	at wall

---

*Formerly with ARO, Inc., Arnold Air Force Station, Tennessee 37388, U.S.A.

α	in pitch plane
β	in sideslip plane
1	at forward microphone on cone surface (x = 45.7 cm (18 in))
2	at aft microphone on cone surface (x = 66.0 cm (26 in))
∞	free stream

1.0 INTRODUCTION

The importance of Reynolds number in scaling aerodynamic-model test results from wind tunnels to full-scale flight vehicles is well known, and the data from the small models have to be suitably adjusted for Reynolds number effects. Because these adjustments are usually based on simple extrapolations or ratios of Reynolds number, they introduce some errors. The viscous effects on the boundary-layer growth on a body are cumulative and can create boundary-layer/shock interactions or separations at transonic and supersonic speeds that differ significantly with the scale-up from model to full-scale vehicles. The location at which the boundary layer changes from laminar to turbulent flow influences boundary-layer growth and has a significant effect on these interactions and separations. Hence, the transition Reynolds number based on the point of transition and on the unit Reynolds number is a key parameter in the overall similitude of flow.

As pointed out by Potter and Whitfield (Ref. 1), one cannot expect a constant value of transition Reynolds number relative to a characteristic length Reynolds number when scaling transition-sensitive data. As noted by Morkovin (Ref. 2), there are no clear-cut rules to ensure that the transition locations predicted for general body shapes will be accurate. A common practice in wind-tunnel testing is to force transition with artificial trip devices, particularly when there is a large mismatch in model and full-scale Reynolds numbers. The fixing of transition provides a gross approximation of the flow, even though the discrete characteristics of the boundary layer on the model may not be the same as on the full-scale vehicle. The usual correction is to subtract out the skin friction of the model, using a flat-plate friction law for the wind-tunnel Reynolds number, then adding back the skin friction for the full-scale vehicle at flight Reynolds numbers.

Treon et al. (Ref. 3) have shown, however, significant differences in data for the identical model, Mach numbers, and Reynolds numbers in three different wind tunnels because of flow quality. In addition, Mabey (Ref. 4) has also shown that flow unsteadiness can affect both static and dynamic test results. Three pertinent factors are involved in wind-tunnel flow quality: uniformity of free-stream velocity, uniformity of streamlines or flow angle, and free-stream disturbance level.

During the past decade, a comprehensive series of tests in the United States and western Europe have been performed to investigate the effects of free-stream disturbances on boundary-layer transition and Reynolds number scaling. In a cooperative effort by the U.S. Air Force, National Aeronautics and Space Administration, U.S. Navy, the Calspan Corp., and the governments of the United Kingdom, France, and the Netherlands, the flow disturbance levels of 23 wind tunnels (Table 1) and in flight have been documented. A sharp, slender, smooth cone, known as the Arnold Engineering Development Center (AEDC) 10° Transition Cone, was used. Throughout the program, care was exercised to maintain the model in the same unblemished condition. The results obtained testify to the diligence exercised by the many test personnel who participated in this investigation. The flight-test program was performed by the Dryden Flight Research Facility, Edwards, California. The results of the test program were enhanced because the experiments could be repeated—sometimes as long as 8 years later—in wind tunnels (at AEDC and Ames Research Center) whose configurations were unchanged. Likewise, selected flight-test points were repeated weeks apart.

The tests reported here were conducted under the scrutiny and beneficial guidance of the U.S. Transition Study Group, Prof. Eli Reshotko, Chairman. To a great extent, the credibility of the results is attributable to the critiques, advice, and guidance sought and received on a continuous basis from this group since 1974.

The wind-tunnel data from this investigation were published by the individuals and organizations involved in Refs. 5 to 10 and are summarized in Ref. 11. The flight data were reported in Ref. 12. The correlations between wind-tunnel data and flight data were reported in Refs. 13 and 14. Many of these data were used in an independent review reported in Ref. 15.

2.0 APPROACH

Transition and pressure fluctuation data were acquired using a simple conical body and instrumentation over a wide range of Reynolds and Mach numbers at zero incidence and adiabatic wall conditions in a number of wind tunnels and in flight. The body shape chosen was the AEDC Transition Cone, a sharp, slender cone with a semi-apex angle of 5°. With the exception of the flow over a flat plate, the flow over a slender cone at zero incidence is the simplest known. At subsonic speeds, the flow experiences only a small axial favorable pressure gradient and virtually a zero pressure gradient at supersonic speeds after shock attachment. In addition, the cone does not have the end effects of a flat plate that result from the finite span of the plate, it is relatively easier to manufacture, and, because it does not generate much lift at low incidence, it is better suited to flight test.

The same instrumentation and techniques were used to detect the onset and the end of transition and to document the pressure fluctuations in the wind tunnels and in flight. A traversing pitot-pressure probe in contact with the surface was used to detect the onset and end of transition. The pressure fluctuations at the cone surface were measured with microphones set flush in the cone. The microphone-measured results approximate those of free-stream conditions only when the boundary layer is laminar.

3.0 TEST APPARATUS

The AEDC 10° Transition Cone (Fig. 1) was used for all transition and surface-pressure fluctuation measurements. The cone had a semivertex angle of 5° and an apex bluntness less than 0.10 mm (0.004 in) in equivalent diameter. The cone was made of stainless steel, highly polished, with a surface finish of 0.25 μm (10 μin) or better. It was 91.4 cm (36.00 in) long, with a cone extension that extended the length to 113.0 cm (44.50 in).

Transition was detected along the 0° ray (Fig. 1), using a traversing pitot-pressure probe (Fig. 2) in contact with the surface. A 0.238-cm- (0.094-in-) diameter semiconductor strain-gage transducer was close-coupled and mounted inside the probe.

The surface-pressure fluctuations were measured, using two flush-mounted microphones at distances of 45.7 cm (18.0 in) and 66.0 cm (26.0 in) aft of the cone apex and at azimuthal angles of $\varphi = 225°$ and 180°, respectively (Figs. 1 and 3). Condenser microphones, 0.635 cm (0.25 in) in diameter, were used for most of the wind-tunnel tests and for the low-speed portion of the flight test. For the high-speed portion of the flight tests, 0.238-cm- (0.094-in-) diameter semiconductor strain-gage-type microphones were used because of the higher recovery temperatures that were reached. Overlapping data from the two types of microphones confirmed that there was no appreciable difference in response over a bandwidth from 200 Hz to 20 kHz for the flight tests. Some corrections to the condenser microphone data at frequencies above 40 kHz were required in the wind tunnel at low ambient pressure. For the flight test only, a semiconductor strain-gage-type microphone, mounted on the knee of the traversing mechanism, measured the pressure fluctuations in the free stream, as shown in Fig. 4.

The cone temperature was determined from an iron-constantan thermocouple epoxied in a small hole on the lower centerline ray at $x/L = 0.80$. When transition was measured on the cone, the thermocouple would be in a turbulent boundary layer and a turbulent recovery factor would be applicable.

For the flight tests and for some wind-tunnel tests, a hemispherical head-sensing probe (Fig. 1) was mounted below and behind the cone apex to measure airspeed, free-stream static pressure, and flow incidence. A ring of orifices, 4.7 probe diameters aft of the probe tip, were used to determine free-stream static pressure. The free-stream static pressure was combined with the impact pressure from the orifice at the stagnation point to calculate Mach number. Two pairs of orifices in the pitch and yaw planes, 40° from the stagnation point, were used to determine angle of attack and angle of sideslip, respectively.

4.0 PROCEDURE

4.1 Flight Test

For the flight tests, the cone was mounted on the noseboom of an F-15 aircraft (Fig. 5). In order to obtain results that could be correlated, the flight and wind-tunnel data had to be obtained at flow conditions as nearly identical as possible. This required that the pilot fly the airplane at a constant airspeed and altitude, keeping the cone at zero incidence and at adiabatic conditions. An in-flight calibration of the hemispherical head-sensing probe for airspeed and altitude was made, using the pacer method (Ref. 16) at subsonic speeds and radar tracking (Refs. 17 and 18) at subsonic and supersonic speeds. The probe was calibrated for angle of attack and angle of sideslip in several wind tunnels. Both the airspeed and incidence calibrations are given in Ref. 12. The inclination of the cone sting with respect to the aircraft centerline was preset before flight to compensate for the expected aircraft trim angle of attack. Aim test-point conditions (Mach number, altitude, and trim angle of attack) were specified, and the pilot adjusted the airspeed to center the cone angle-of-attack indicator to zero.

The cone angle of sideslip was zeroed, using the rudders. Upper atmospheric temperature data from early morning radiosonde balloons were used to calculate the aim cone adiabatic wall conditions. For Mach numbers of 1.2 and above, the cone had to be preconditioned on the ground with a hot-air heater (Fig. 6). The cone was heated for about 1 hr, to a temperature of 105° C to 115° C (220° F to 240° F). The heater was removed just before takeoff, and the aircraft climb schedule was adjusted so that the cone would be at the predetermined adiabatic-wall temperature when the aircraft reached the aim test conditions. Data from the aircraft and cone were monitored continuously in real time on strip charts and video displays, and the information was relayed to the pilot. For the lower Mach numbers, it was sometimes necessary to cool the cone. This was done by flying the aircraft at a higher altitude and lower temperature than the test point until the desired cone adiabatic-wall temperature was reached.

A history of the free-stream conditions during a typical pitot-probe traverse is shown in Fig. 7. As can be seen, the conditions were quite stable, with angle of attack and angle of sideslip within ±0.2°. A pitot-probe traverse during the same test conditions is shown in Fig. 8. The onset of transition X_t was defined, as it was for the wind-tunnel data, as the location at which the minimum pitot pressure occurred. Likewise, the end of transition X_T was defined as the location at which the maximum pitot pressure occurred. Both these locations are shown in Fig. 8.

The flight-test matrix is shown in Fig. 9. The flight data are grouped by the different aircraft trim angles that were flown and correspond to nominal dynamic pressures. Test points at the same trim angle correspond approximately to the curves of constant unit Reynolds number, U/ν. Also shown in Fig. 9 is the equivalent combined envelope for the wind-tunnel data of this study. As can be seen, the flight data encompass most of the wind-tunnel test data, up to a Mach number of 2.0.

4.2 Wind Tunnel Tests

Every procedural consideration described for the flight test was present in the wind-tunnel tests, except that the problems associated with obtaining test conditions were much simpler. The cone had to be at zero incidence and adiabatic-wall temperature. No thermal preconditioning was necessary, for the temperature excursions were not nearly so severe, and there was ample time to wait for the cone to reach thermal equilibrium with the flow. Some wait between data points was necessary for T_w/T_{aw} to approach 1.0, following a large Mach number change. Usually, the sequence of test points could be planned to progress through small incremental changes in Mach number. Most wind tunnels could hold total temperature constant within ±3° C (±5° F) on a given test point. The best sequencing of points was to change U_∞/ν_∞ at constant M_∞ in a variable-density tunnel by changing p_t at constant T_t. In atmospheric tunnels, one can only change M_∞.

A bigger problem in the wind tunnels was defining the incidence angle. In some cases, negligible flow angularity was assumed and the cone was simply aligned carefully to the test section centerline. In other cases, flow angularity was known or suspected and a set of aerodynamic centering calibrations was performed at each Mach number, using the transition variation with incidence angle when the pitot probe trace was 90° relative to the windward stagnation ray. This was accomplished using the model pitch, yaw, and roll capabilities of a given wind tunnel to define vertical and horizontal components of the stream angle. The largest stream angle found was 1.5°.

In general, data were acquired for a matrix of Mach numbers and Reynolds numbers covering the full operating envelope of a given wind tunnel. The normal test-section ventilation procedures were followed for each transonic tunnel near $M_\infty = 1.0$. The minimum transonic wind-tunnel test section size was 4 by 4 ft, so wall interference attributable to transonic blockage phenomena was not considered to be a significant problem. Long sting-support systems were used in transonic tunnels to minimize support-system blockage and radiated aerodynamic noise influence. The sting-supported cone vibrations were generally at frequencies less than about 10 Hz and of amplitudes small enough that no coherent oscillations could be found in the pitot pressure that could be identified as vibratory-motion related.

Measurements of relative humidity in wind tunnels are not usually reliable. The criterion generally used for acquiring data in these experiments was not to proceed if there was visible fogging. However, in some cases when dew points were above about -23° C (-10° F) at $M_\infty \geqslant 1.8$, indicated by available instrumentation, precautions were taken to verify that the indicated M_∞ and U_∞/ν_∞ were within the wind-tunnel calibration.

5.0 RESULTS

5.1 *Laminar Instability*

Indications of laminar instabilities in the boundary layer were found in the microphone power spectral density distributions during the flight test. For purposes of illustration, the spectra obtained at two test points from all three microphone signals (free-stream impact, forward-cone, and aft-cone) are shown in Fig. 10. In Fig. 10(a), the forward-cone microphone was under transitional flow and the aft-cone microphone was under fully developed turbulent flow. In fig. 10(b), the forward-cone microphone was under laminar flow and the aft-cone microphone was under transitional flow. In all cases when the boundary layer was laminar or transitional, there was a broad peak in the pressure-fluctuation spectra, similar to those shown in Fig. 10. The nondimensional frequency at which the peak occurs is denoted by F in Fig. 10; the subscripts 1 and 2 refer to the forward- and aft-cone microphones, respectively.

Power spectral densities recorded from several flights at the same nominal Mach numbers but at different Reynolds numbers are shown in Fig. 11(a) and (b). The dominant feature in these cone boundary-layer spectra is the peak, which decreases in frequency and increases in power as Re_x increases at a given M_e. Finally, at the location near the end of transition, X_T, the peak disappears into the smooth, broadband spectrum characteristic of a turbulent boundary layer.

The spectral peaks appeared to exhibit a prescribed behavior in terms of the variation of absolute frequency f with M_e, as shown in Fig. 12 for a dynamic pressure of 14.4 kN/m^2 (300 lb/ft^2). The peak center-frequencies increase as M_e increases. A ratio of the frequencies f_1/f_2, when peaks occurred in the spectra from both microphones at a given flight condition, was approximately the inverse of the ratio of the distance from the cone apex, $(x_2/L)/(x_1/L)$, and therefore the inverse of the microphone Reynolds number, Re_{x_2}/Re_{x_1}. Hence, the peak frequencies are functions of both Re_x and M_e.

The nondimensional peak center-frequencies are shown in Fig. 13, plotted as a function of $(Re_x)^{0.50}$; they show a clear dependence on Reynolds number and Mach number. The data agree well with recent calculations by Mack, since his publication of Ref. 19 adjusted by the usual cone-planar similarity rule (where the Reynolds number on a cone is 3 times that on a flat plate). The calculations by Mack are for the first-mode laminar instability, that is, Tollmien-Schlichting waves, and the calculations agree with the characteristics of the spectra; thus, Tollmien-Schlichting waves are probably the cause of transition.

A reexamination of the wind-tunnel power spectral distributions after the flight test revealed indications of Tollmien-Schlichting instabilities in two Langley wind tunnels, the 4- by 4-ft supersonic pressure tunnel and the Unitary Plan Wind Tunnel, where the pressure fluctuation levels, $\sqrt{\overline{p_s'^2}}/q_\infty$, were the lowest measured. Microphone spectra for the 4- by 4-ft supersonic pressure tunnel at Langley Research Center for a Mach number of 1.61 are shown in Fig. 14. These data are either for a laminar or transitional boundary layer. Broad peaks in the spectra, similar to those observed in flight, are evident for the forward microphone at $Re_{x_1} = 4.41 \times 10^6$ and at $Re_{x_2} = 4.26 \times 10^6$ for the aft microphone.

5.2 Flight Transition Reynolds Number

In preparation for the flight tests, the effect of incidence on transition location was determined in various NASA wind tunnels (Fig. 15). Note that at small negative angles of attack, with the surface pitot probe on the windward ray, the effect is small for Mach numbers between 0.6 and 2.2. The effect of sideslip can be significant at angles greater than 0.25°.

During the flight tests, it was possible to control the temperature of the transition cone within ±6% of the adiabatic-wall temperature, T_{aw}, for about 90% of the test points, using the techniques described in Sec. 4.1 (Flight Test). Even this small deviation in temperature had a large influence on transition location, however, as shown in Fig. 16. The data have been grouped by Mach number and nondimensionalized by the transition Reynolds number corrected to adiabatic-wall temperature determined from fairings of the flight data for each nominal Mach number. The sensitivity of transition Reynolds number to heat transfer appears to have been essentially independent of Mach number and proportional to the temperature ratio T_w/T_{aw}. The trend of the data in Fig. 16 shows a strong heat-transfer influence on transition, delayed transition occurring when the boundary layer was cooled ($T_w/T_{aw} < 1.0$), earlier transition occurring when the boundary layer was heated ($T_w/T_{aw} > 1.0$). Also shown in Fig. 16 are data obtained during a rapid excursion of total temperature at $M = 1.2$ in the 4-ft transonic (4T) wind tunnel at AEDC. These wind tunnel results show the same trend as the flight data. According to the theoretical flat-plate e^9 method from Ref. 20, the onset of transition at a Mach number of 0.85 also follows the trend of the flight data. A curve was fitted through the flight data and used for correcting nonadiabatic data to adiabatic conditions.

The end-of-transition Reynolds numbers measured in flight, corrected to adiabatic-wall temperatures, are shown as functions of local Mach number in Fig. 17. This figure includes 82 test points (39 of which were acquired at supersonic speeds) gathered from 27 flights over 2 1/2 months. The data form a nearly linear band for both the end-of-transition and the onset-of-transition Reynolds numbers. Both were strong functions of Mach number. End-of-transition Reynolds numbers ranged from about 3.5×10^6 at a Mach number of 0.5 to above 9.0×10^6 at Mach numbers above 1.6. Actual measurements of X_t, X_T, and the corresponding flight conditions are tabulated in Ref. 12, together with the corrected values of end-of-transition Reynolds number Re_T, and onset-of-transition Reynolds number Re_t. Figure 18 shows that the ratio of onset-of-transition Reynolds number to end-of-transition Reynolds number is independent of Mach number and dynamic pressure and has a mean value of 0.86. Most of the data are within ±5% of this mean value.

Transition Reynolds number was plotted as a function of unit Reynolds number in Fig. 19 for nominal Mach numbers to determine whether the present data had the unit Reynolds number effect shown for higher Mach numbers in Refs. 11, 21, and 22. Even at Mach numbers at which there were substantial data over a wide range of unit Reynolds numbers at adiabatic conditions, the data are inconclusive.

5.3 Flight Disturbance Environment

Naturally growing Tollmien-Schlichting waves can be detected only in a low-disturbance, free-stream environment. As shown by the overall pressure fluctuations from the free-stream impact microphone (Fig. 20), the level of pressure fluctuations in the flight environment was very low. The pressure fluctuations in flight varied from about 0.16% at the lower Mach numbers to 0.017% near Mach 2, when normalized by the free-stream dynamic pressure q_∞. The different flags on the symbols, which denote flights made on different days, indicate the day-to-day variations in the atmosphere. The pressure fluctuations do not seem to be dominated by engine noise, although some discrete tones appeared randomly in the spectra, some of which may have come from the engine inlets, fans, or compressors.

The cone surface static-pressure fluctuations in the boundary layer were sensed by the surface microphones set flush in the cone. When the cone boundary layer was turbulent, the cone-surface microphones recorded pressure fluctuations in the near-field turbulent boundary layer. When the boundary layer was transitional, the amplification of the low end of the frequency spectrum during transition produced large overall values of indicated pressure fluctuation. Only under laminar conditions could the cone-surface microphones measure pressure fluctuations imposed from the free stream, and those measurements were altered by the laminar boundary-layer receptivity. As the spectral data in Figs. 10 and 11 show, the laminar boundary layer selectively amplifies certain frequencies in the spectrum, increasing some of the values sensed by the microphone.

The cone-surface static-pressure fluctuations in the laminar boundary layer $\sqrt{\overline{p_s'^2}}$ are shown normalized by q_∞ in Fig. 21 as a function of M_e. As shown, the laminar pressure fluctuations decrease with increasing M_e. A comparison of Figs. 20 and 21 shows that at the highest M_e the cone-surface pressure fluctuation is essentially the same as the free-stream impact-pressure fluctuation. The differences between the cone-surface and free-stream impact-pressure fluctuation amplitudes increase as M_e decreases. As before, the different flags on the symbols (Fig. 20) denote flights on different days to indicate day-to-day variations. The open symbols denote data acquired with the semiconductor strain-gage-type microphones used at the higher Mach numbers and higher temperatures. The solid symbols denote data acquired with condenser microphones like those used in most of the wind tunnels. The data from both types of microphones agree well. The laminar and transitional spectra measured by both sets of microphones had the same characteristics, verifying that the peaks were associated with the boundary layer and that they were not anomalies introduced by the sensors.

5.4 Correlation of Wind Tunnel and Flight Data

The wind tunnels used in these experiments were classified into four groups, based on their distinguishing geometry:

Group 1: Slotted or solid-wall transonic and subsonic tunnels
Group 2: Perforated-wall transonic tunnels
Group 3: Two-dimensional-nozzle supersonic tunnels
Group 4: Sliding-block-nozzle supersonic tunnels

The pressure fluctuation levels measured under the laminar boundary layer on the cone from the wind tunnels are shown in Fig. 22. Also shown is an envelope for the flight pressure fluctuation data from Fig. 21. The dashed curve in Fig. 22 is a relationship from Lowson (Ref. 23) for estimating the pressure fluctuations at the wall beneath an attached turbulent boundary layer. The microphones on the cone sense pressure fluctuations from all sources, including the wind-tunnel walls. As shown in Fig. 22(a), essentially all the data from the lower disturbance tunnels (groups 1, 3, and 4) are below this curve. However, the flow disturbance measured in the lower disturbance tunnels was about twice that measured in flight. For the higher disturbance tunnels (group 2, Fig. 22(b)), the flow disturbance is greater than Lowson's curve and approximately an order of magnitude greater than the flight data.

The end-of-transition Reynolds number Re_T is presented in Fig. 23 for the group 1, 3, and 4 wind tunnels. The wind-tunnel data have been extrapolated for nominal unit Reynolds numbers of 6.6×10^6/m (2.0×10^6/ft), 9.8×10^6/m (3.0×10^6/ft), and 13.1×10^6/m (4.0×10^6/ft). There is a 14% increase in Re_T for unit Reynolds numbers between 6.6×10^6/m (2.0×10^6/ft) and 13.1×10^6/m (4.0×10^6/ft) at supersonic speeds in the wind tunnels. The end-of-transition Reynolds numbers from the lower disturbance tunnels (groups 1, 3, and 4) agree well with the flight data up to $M_e = 1.2$. Above $M_e = 1.2$, the correlation deteriorates, and at $M_e = 1.6$ the flight Re_T is 25% to 30% higher than the wind-tunnel Re_T. For the higher disturbance tunnels (group 2), shown in Fig. 24, there is a very poor correlation between wind-tunnel and flight end-of-transition Reynolds numbers.

The onset-of-transition Reynolds numbers from the lower disturbance wind tunnels is shown in Fig. 25. The flight data from Fig. 17(b) are shown by the envelope. At subsonic speeds, the data from the Naval Ship Research and Development Center (NSR&DC) tunnel showed good correlation with the flight data. The onset-of-transition Reynolds numbers from the Langley 16-ft transonic dynamics tunnel (NASA/Langley 16 TDT) were lower than those of most of the flight data. Unfortunately, onset of transition from the several other lower disturbance tunnels at transonic speed was either poorly defined by the surface pitot-pressure-probe technique or lost because of poor pitot-probe contact with the cone surface.

The ratio of onset-of-transition Reynolds number to end-of-transition Reynolds numbers is shown in Fig. 26 for the wind tunnels. The flight data are represented by the fairings. The wind-tunnel ratios of onset-of-transition to end-of-transition Reynolds numbers are less than those in flight at unit Reynolds numbers of 6.6×10^6/m (2.0×10^6/ft) and 9.8×10^6/m (3.0×10^6/ft) between Mach numbers of 0.5 to 2.0. At a unit Reynolds number of 13.1×10^6/m (4.0×10^6/ft) the correlation between flight and wind tunnel data is much better. This unit Reynolds number effect was not observed in flight, even though it covered approximately the same Reynolds number range.

The end-of-transition Reynolds number as a function of the flow disturbance levels from wind tunnel and flight data are presented in Fig. 27. This figure includes data from all Mach numbers and unit Reynolds numbers. The end-of-transition Reynolds number correlated within ±20% with the surface fluctuating root-mean-square pressure level according to the equation

$$Re_T = 3.7 \times 10^6 \left[\left(\frac{\sqrt{\overline{p_s'^2}}}{q_\infty} \right) 100 \right]^{-0.25}$$

6.0 CONCLUDING REMARKS

Transition and fluctuating pressure data were acquired on a standard body (AEDC Transition Cone), using the same instrumentation and technique over a wide range of Mach and Reynolds numbers in 23 wind tunnels and in flight. The cone was held at near zero incidence and heat transfer. Transition was detected with a traversing pitot-pressure probe in contact with the surface. The pressure fluctuations at the cone surface were measured with microphones set flush in the cone surface.

There was good correlation between end-of-transition Reynolds numbers Re_T obtained in the lower disturbance wind tunnels and those obtained in flight, up to about $M_e = 1.2$. Above $M_e = 1.2$, the correlation deteriorates, with the flight Re_T being 25% to 30% higher than the wind tunnel Re_T at $M_e = 1.6$. For the higher disturbance tunnels, there was very poor correlation between tunnel and flight Re_T. The end-of-transition Reynolds number correlated within ±20% with the surface-fluctuating root-mean-square pressure level, according to the equation

$$Re_T = 3.7 \times 10^6 \left[\left(\frac{\sqrt{\overline{p_s'^2}}}{q_\infty} \right) 100 \right]^{-0.25}$$

Broad peaks in the spectra indicated that Tollmien-Schlichting waves were the probable cause of transition in flight and at least in some of the wind tunnels. The flow disturbance measured beneath the laminar boundary layer on the cone in the lower disturbance tunnels was about twice that measured in flight. In the higher disturbance tunnels, it was approximately an order of magnitude greater than the flight data.

The flight data showed a strong heat-transfer influence on transition, a delayed transition occurring when the boundary layer was cooled, and an earlier transition occurring when the boundary layer was heated.

REFERENCES

1. Potter, J. L.; and Whitfield, J. D.: Preliminary Study of the Effect of Unit Reynolds Number on Transition Sensitive Data. AEDC-TN-57-37 (AD 135338), Sept. 1957.

2. Morkovin, M. V.: Instability, Transition to Turbulence, and Predictability. AGARD-AG-236, July 1978.

3. Treon, S. L.; Steinle, F. W., Jr.; Hagerman, J. R.; Black, J. A.; and Buffington, R. J.: Further Correlation of Data from Investigations of a High-Subsonic-Speed Transport Aircraft Model in Three Major Transonic Wind Tunnels. AIAA Paper 71-291, Albuquerque, N. Mex., Mar. 1971.

4. Mabey, D. G.: Flow Unsteadiness and Model Vibrations in Wind Tunnels at Subsonic and Transonic Speeds. RAE C.P. No. 1155, Bedford, England, Oct. 1970.

5. Credle, O. P.; and Carleton, W. E.: Determination of Transition Reynolds Number in the Transonic Mach Number Range. AEDC-TR-70-218 (AD 875995), Oct. 1970.

6. Dougherty, N. S., Jr.; and Steinle, F. W., Jr.: Transition Reynolds Number Comparisons in Several Major Transonic Tunnels. AIAA Paper 74-627, Bethesda, Md., July 1974.

7. Vaucheret, X.: Acoustic Fluctuations Generated by the Ventilated Walls of a Transonic Wind Tunnel. Paper No. 25, AGARD Fluid Dynamics Panel Symposium on Wind Tunnel Design and Testing Techniques, AGARD CP-174, London, England, Oct. 6-8, 1975 (also ONERA Chatillon TP No. 1324, 1974).

8. Ross, R.; and Rohne, P. B.: The Character of Flow Unsteadiness and Its Influence on Steady-State Transonic Wind Tunnel Measurements. Paper No. 45, AGARD Fluid Dynamics Panel Symposium on Wind Tunnel Design and Testing Techniques, AGARD CP-174, London, England, Oct. 6-8, 1975 (also MLR Amsterdam TR 74128 U, Aug. 1973).

9. Mabey, D. B.: Boundary-Layer Transition Measurements on the AEDC 10° Cone in Three RAE Wind Tunnels and Their Implications. British ARC R&M 3821, RAE-TR-76077, June 1976.

10. Jordan, R.: Tests with the AEDC 10-Deg Transition Cone in the 9 X 8-Foot Transonic Tunnel. ARA, Ltd. Model Test Note Z.32, Apr. 1973.

11. Dougherty, N. S., Jr.: Influence of Wind Tunnel Noise on the Location of Boundary-Layer Transition on a Slender Cone at Mach Numbers from 0.2 to 5.5. AEDC-TR-78-44, 1980.

12. Fisher, David F.; and Dougherty, N. Sam, Jr.: In-Flight Transition Measurements on a 10° Cone at Mach Numbers From 0.5 to 2.0. NASA TP-1971, 1982.

13. Dougherty, N. Sam, Jr.; and Fisher, David F.: Boundary-Layer Transition Correlation on a Slender Cone in Wind Tunnels and Flight for Indications of Flow Quality. AEDC-TR-81-26, Feb. 1982.

14. Dougherty, N. S., Jr.; and Fisher, D. F.: Boundary-Layer Transition on a 10-Degree Cone: Wind Tunnel/Flight Data Correlation. AIAA Paper 80-0154, Jan. 1980.

15. Harvey, W. D.: Some Anomalies between Wind Tunnel and Flight Transition Results. AIAA Paper 81-1225, Palo Alto, Calif., June 1981.

16. Herrington, Russel M.; Shoemacher, Paul E.; Bartlett, Eugene P.; and Dunlap, Everett W.: Flight Test Engineering Handbook. AF Tech. Rept. No. 6273, Air Force Flight Test Center, Edwards AFB, Edwards, Calif., June 1964.

17. Larson, Terry J.; and Ehernberger, L. J.: Techniques Used for Determination of Static Source Position Error of a High Altitude Supersonic Airplane. NASA TM X-3152, 1975.

18. Webb, Lannie D.: Characteristics and Use of X-15 Air-Data Sensors. NASA TN D-4597, 1968.

19. Mack, Leslie M.: Boundary-Layer Stability Theory. NASA CR-131501, 1969.

20. Reshotko, E.: Drag Reduction by Cooling in Hydrogen Fueled Aircraft. J. Aircraft, vol. 16, Sept. 1979, pp. 584-590.

21. Beckwith, Ivan E.; and Bertram, Mitchel H.: A Survey of NASA Langley Studies on High-Speed Transition and the Quiet Tunnel. NASA TM X-1566, 1972.

22. Potter, J. Leith; and Whitfield, Jack D.: Effect of Unit Reynolds Number, Nose Bluntness, and Roughness on Boundary Layer Transition. AEDC TR-60-5, Arnold Eng. Dev. Center, Mar. 1960.

23. Lowson, M. V.: Prediction of Boundary-Layer Pressure Fluctuations. AFFDL-TR-67-167, Apr. 1968.

TABLE 1. SUMMARY OF WIND TUNNEL CHARACTERISTICS

Group	Tunnel	Mach number range	Unit Reynolds number range × 10^6 per m (per ft)	Predominant disturbances	Resonant Mach number	$\left(\sqrt{\tilde{p}_s^2}/q_\infty\right)_{max}$, percent
1	Slotted wall					
	NASA Langley 8 TPT	0.25-1.20	6.6-9.8 (2.0-3.0)	Low frequency	0.80	2.20
	NASA Langley 16 TT	0.20-1.30	4.3-12.8 (1.3-3.9)	Low frequency	0.82	3.60
	NASA Langley 16 TDT (Freon)[a]	0.30-1.15	4.9-12.1 (1.5-3.7)	Low frequency	0.85	1.40
	NSRDC 7 × 10 T	0.20-1.13	4.9-13.1 (1.5-4.0)	Low frequency	0.75	1.26
	NLR 6.55 × 5.28 HST[b]	0.15-1.30	4.9-45.9 (1.5-14.0)	Compressor	0.80	1.01
	RAE Farnborough 8 × 6[c]	0.20-1.19	1.3-8.2 (0.4-2.5)	Compressor	0.60	1.90
	Solid wall					
	NASA Ames 12 PT	0.20-0.90	6.6-9.8 (2.0-3.0)	Test Section	0.65	1.65
	RAE Bedford 8 × 8 SWT (subsonic mode)	0.20-0.80	0.8-9.8 (0.25-3.0)		None	0.80
2	Perforated wall					
	AEDC Tunnel 4T	0.40-1.30	4.9-16.4 (1.5-5.0)	Edge tones	0.80-1.30	3.75
	ONERA 6 × 6 S-2 Modane	0.25-1.30	6.6-23.6 (2.0-7.2)	Edge tones	0.80	2.77
	ONERA 2.56 × 1.83 S-3 Modane[b]	0.25-1.00	6.6-41.0 (2.0-12.5)	Stilling chamber	0.25	12.70
	AEDC Tunnel 16T	0.20-1.60	3.3-18.4 (1.0-5.6)	Edge tones	0.71	2.68
	Calspan 8 TWT	0.60-0.95	6.6-9.8 (2.0-3.0)	Wall tones	0.85	2.30
	ARA, Ltd. Bedford 9 × 8[d]	0.21-1.40	4.9-14.4 (1.5-4.4)	Wall tones	0.68	2.65
	Corrugated slot wall					
	NASA Ames 11 TWT	0.40-1.20	4.9-19.7 (1.5-6.0)	Slot organ pipe	0.75	2.00
	NASA Ames 14 TWT	0.40-1.05	8.5-13.1 (2.6-4.0)	Slot organ pipe	0.95	2.05
3	*Convergent divergent nozzle*					
	RAE Bedford 8 × 8 SWT[e]	1.40-2.40	2.0-13.1 (0.6-4.0)	Wall boundary layer	None	0.45
	NASA Langley 4 SPT	1.61-2.01	3.3-16.4 (1.0-5.0)	Wall boundary layer	None	0.12
	AEDC Tunnel 16S	1.67-2.20	3.0-7.2 (0.9-2.2)	Wall boundary layer	None	0.50
	AEDC VKF Tunnel A	1.51-5.50	7.5-22.3 (2.3-6.8)	Wall boundary layer	None	
	RAE Bedford 3 × 4 HSST	2.50-4.50	2.3-30.1 (0.7-9.2)	Wall boundary layer	None	0.20
4	Sliding block nozzle					
	NASA Ames 9 × 7 SWT	1.50-2.50	6.6-14.8 (2.0-4.5)	Wall boundary layer	None	0.18
	NASA Langley 4 SUPWT (TS No. 1)	1.60-2.86	4.9-16.4 (1.5-5.0)	Wall boundary layer	None	0.14
	NASA Langley 4 SUPWT (TS No. 2)	2.86-4.60	4.9-21.3 (1.5-6.5)	Wall boundary layer	None	0.24

[a] Tests performed using both Freon and air as tunnel working fluid

[b] Only noise data, no transition data

[c] Results affected by model surface imperfections during this test

[d] Transition data at Mach numbers from 0.2 to 0.6 only

[e] Data acquired in Mach number range from 0.2 to 0.8 also

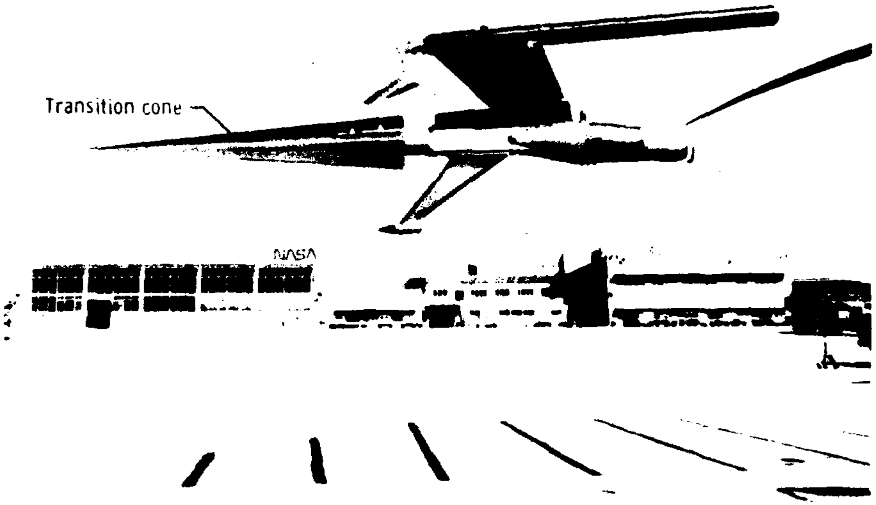

(a) Mounted on aircraft.

Figure 1. Transition cone and instrumentation.

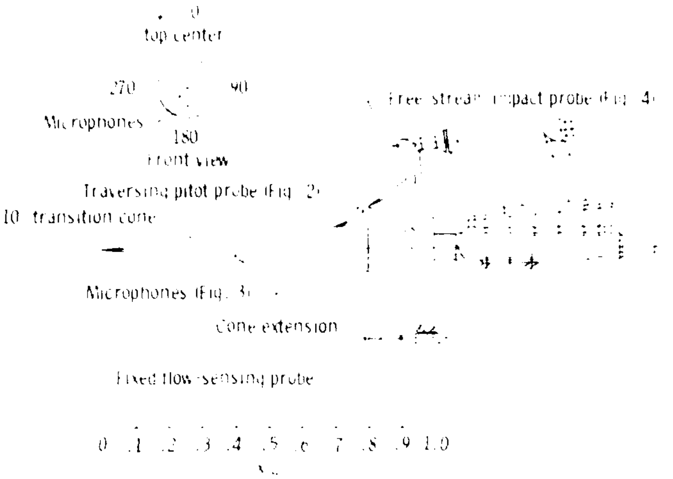
0
top center
270
90
Microphones
180
Front view
Free stream impact probe (Fig. 4)
Traversing pitot probe (Fig. 2)
10° transition cone
Microphones (Fig. 3)
Cone extension
Fixed flow-sensing probe
0
.1
.2
.3
.4
.5
.6
.7
.8
.9
1.0

(b) Location of instrumentation.

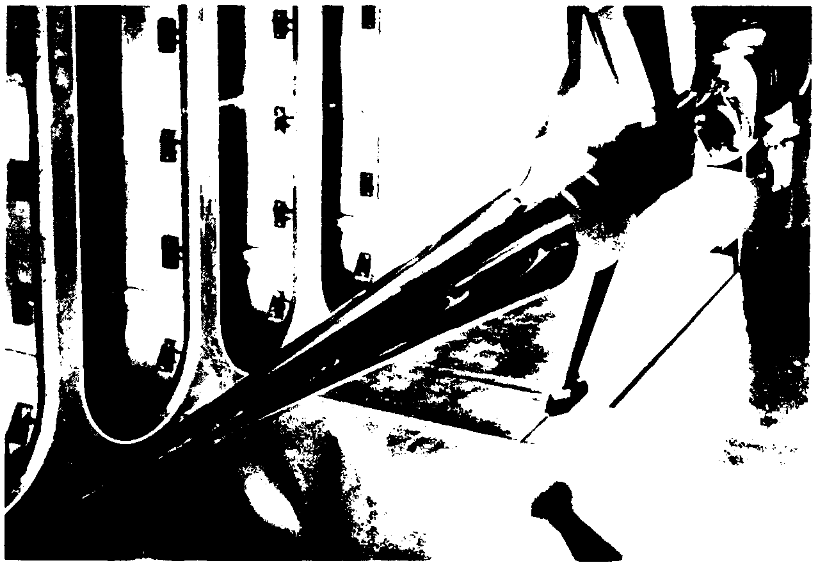

(c) Installed in AEDC VKF Tunnel A.

Figure 1. Concluded.

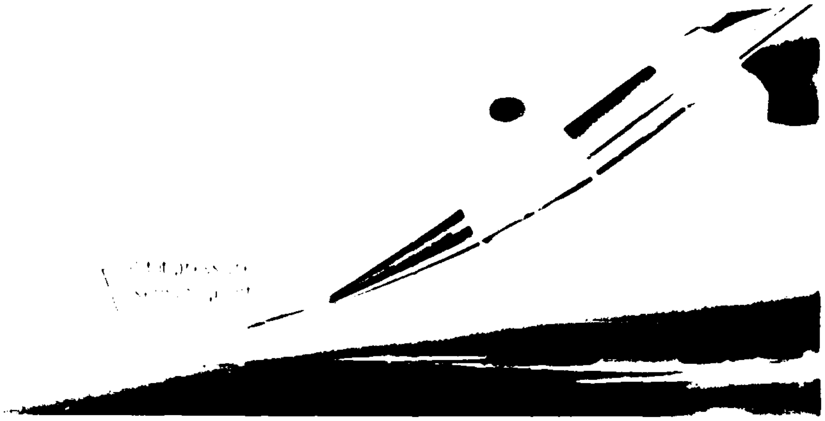

(a) Photograph.

Figure 2. Pitot pressure probe.

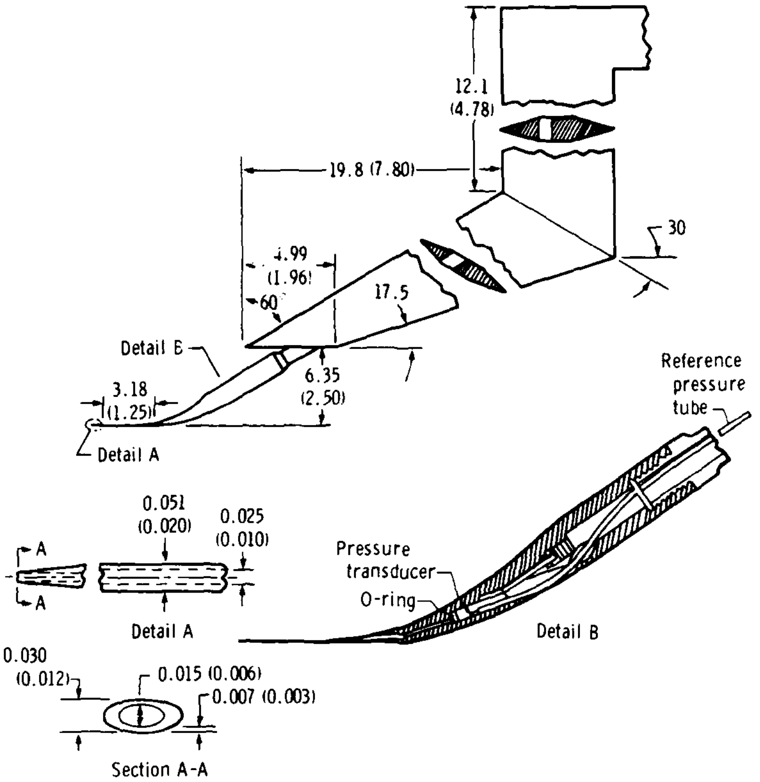
12.1
(4.78)
19.8 (7.80)
30
4.99
(1.96)
60°
17.5
Detail B
6.35
(2.50)
3.18
(1.25)
Detail A
Reference
pressure
tube
0.051
(0.020)
0.025
(0.010)
A
A
Detail A
Pressure
transducer
O-ring
Detail B
0.030
(0.012)
0.015 (0.006)
0.007 (0.003)
Section A-A

(b) Details. Dimensions are in centimeters (inches).

Figure 2. Concluded.

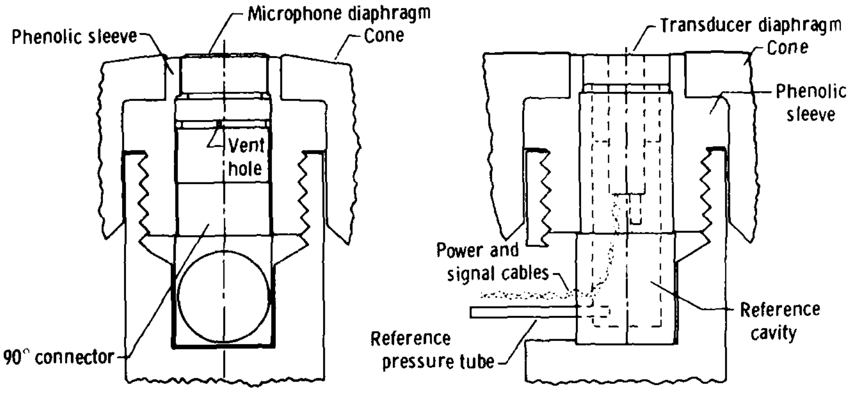
Phenolic sleeve
Microphone diaphragm
Cone
Vent
hole
90° connector
Transducer diaphragm
Cone
Phenolic
sleeve
Power and
signal cables
Reference
pressure tube
Reference
cavity

Condenser microphone
(rear view)

Semiconductor strain gage
microphone (side view)

Figure 3. Flush-mounted microphone installations.

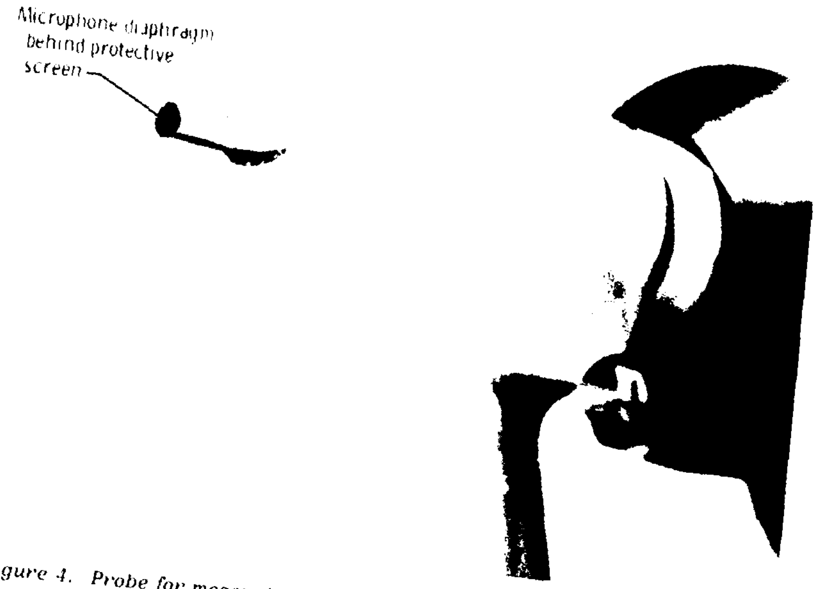
Microphone diaphragm
behind protective
screen

Figure 4. Probe for measuring fluctuating free-stream impact pressure.

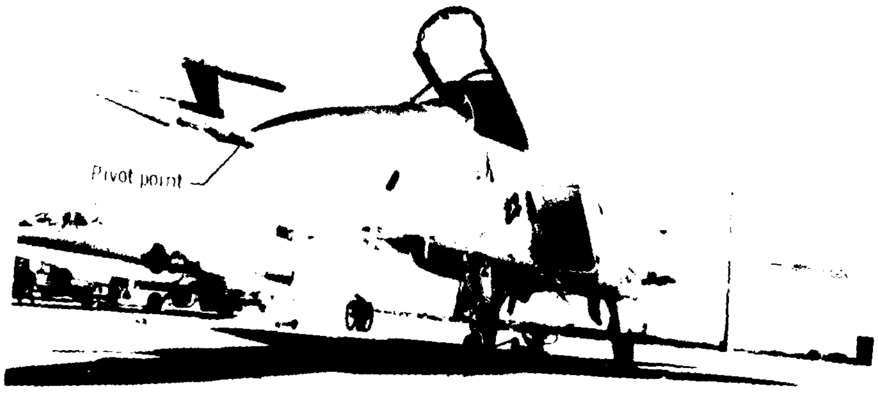
Pivot point

Figure 5. Transition cone mounted in front of test-bed aircraft.

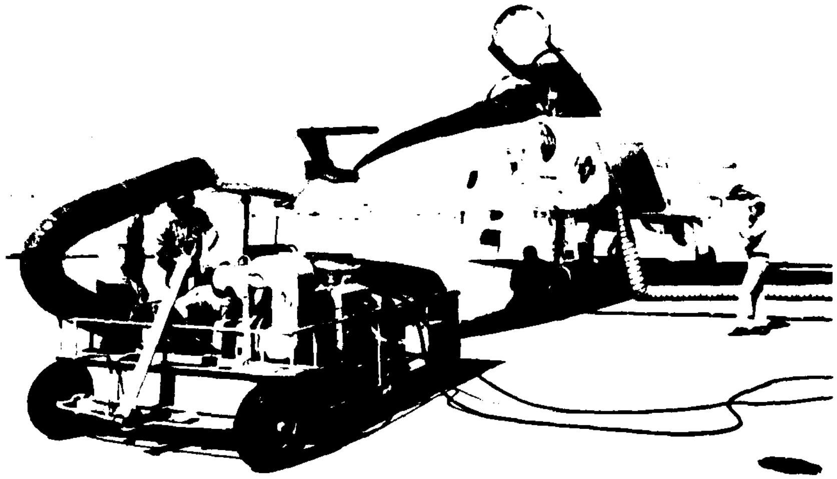

Figure 6. Transition cone being heated at end of runway before flight.

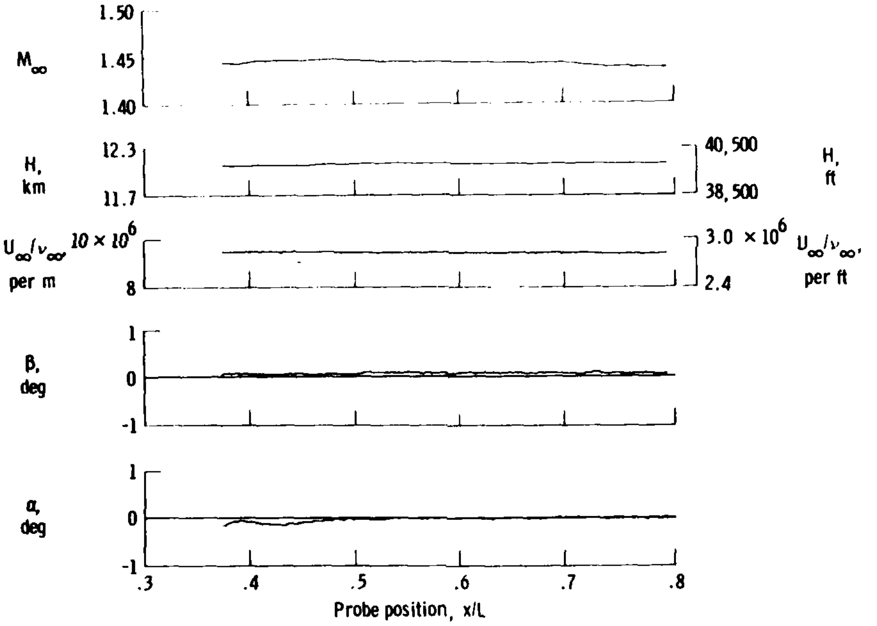

Figure 7. History of cone free-stream conditions during a typical pitot-probe traverse.

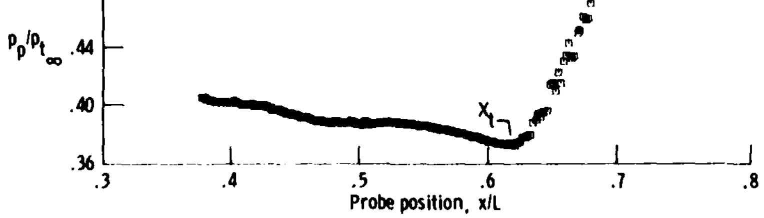

Figure 8. Typical pitot-probe pressures as a function of probe location. M_∞ = 1.44.

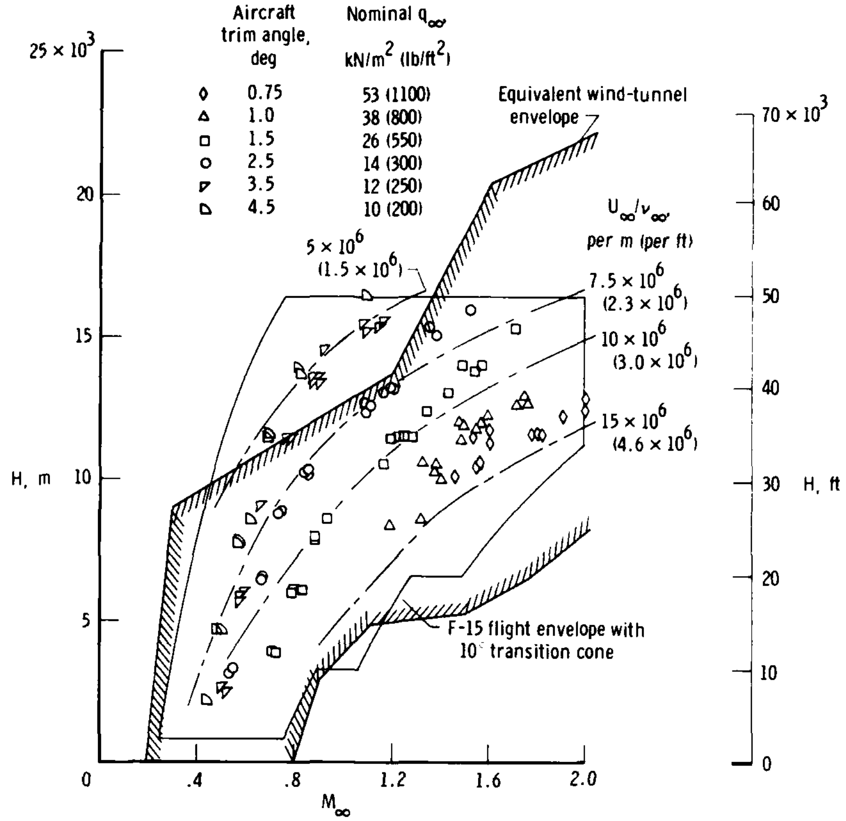

Figure 9. Transition cone flight-test matrix and equivalent wind-tunnel envelope.

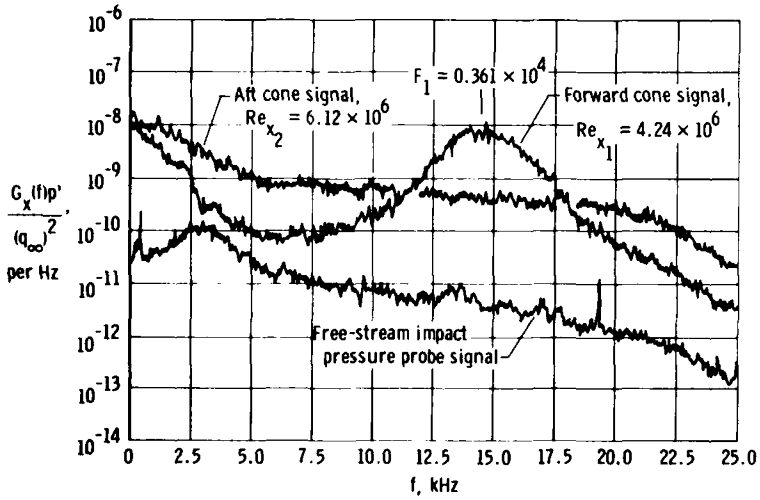

(a) $M_e = 0.84$.

Figure 10. Microphone power spectral density distribution.

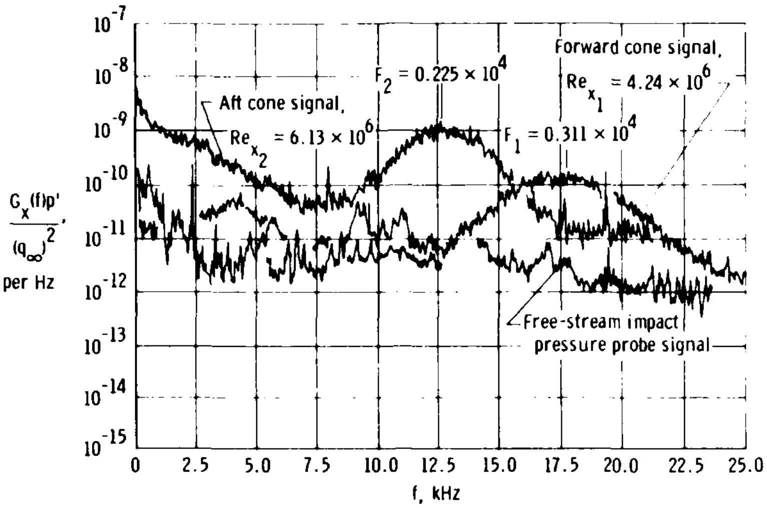

(b) $M_e = 1.31$.

Figure 10. Concluded.

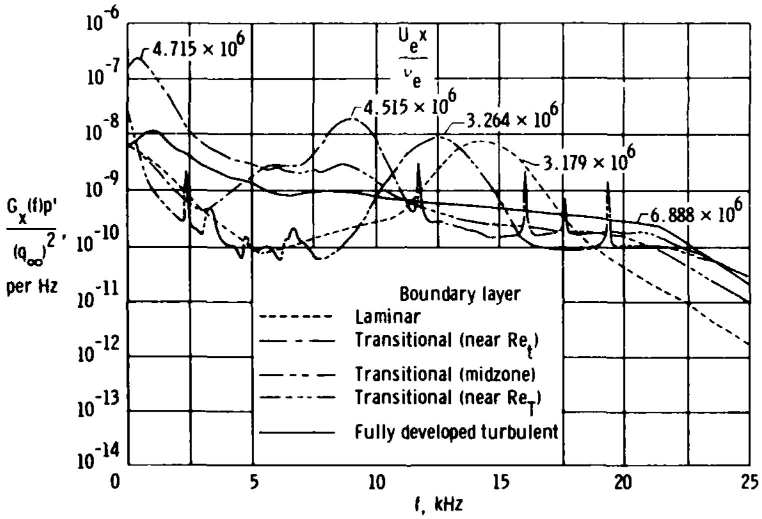

(a) $M_e \approx 0.8$.

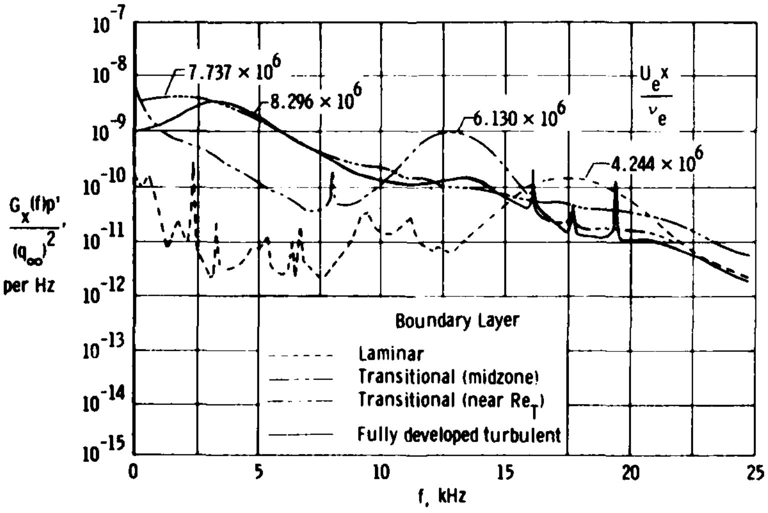

(b) $M_e \approx 1.35$.

Figure 11. Effect of Reynolds number on power spectral density distribution (spectra are smoothed).

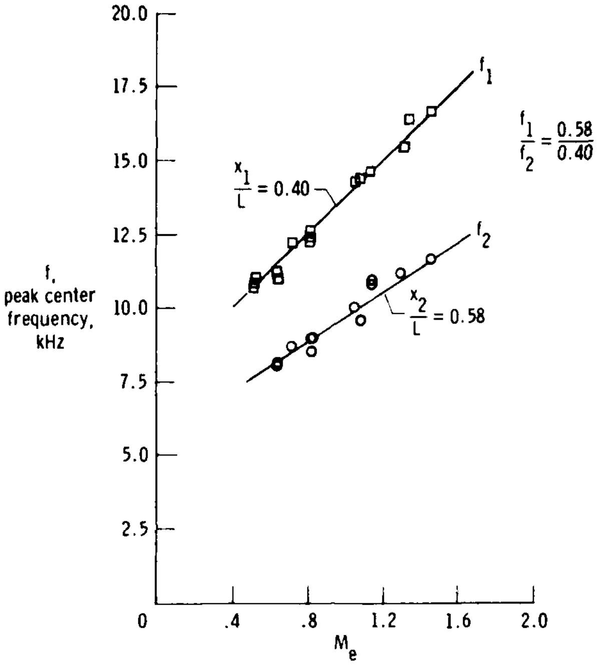

Figure 12. Variation of laminar or transitional spectral peak frequency with local Mach number; $q_\infty \approx 14.4\ kN/m^2$ (300 lb/ft^2).

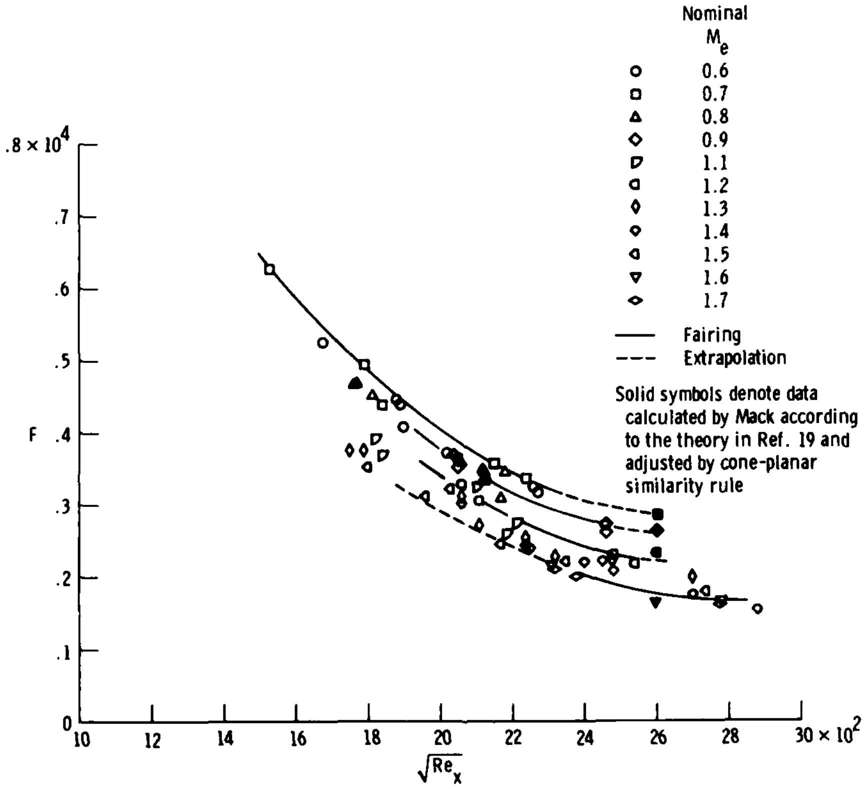

Figure 13. Variation of nondimensional frequency with Re_x.

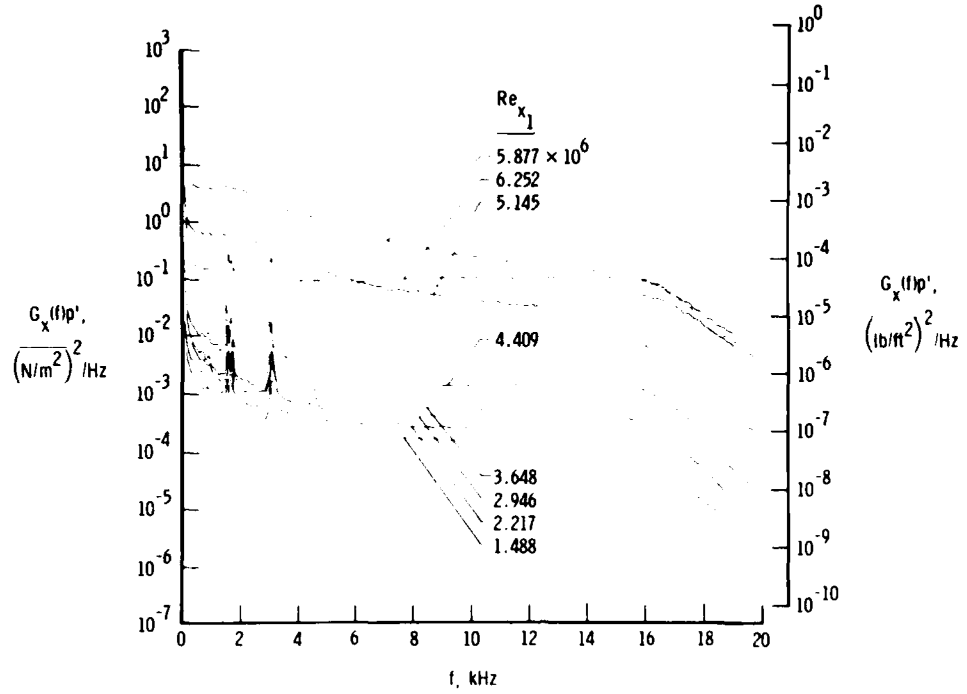

(a) Forward microphone.

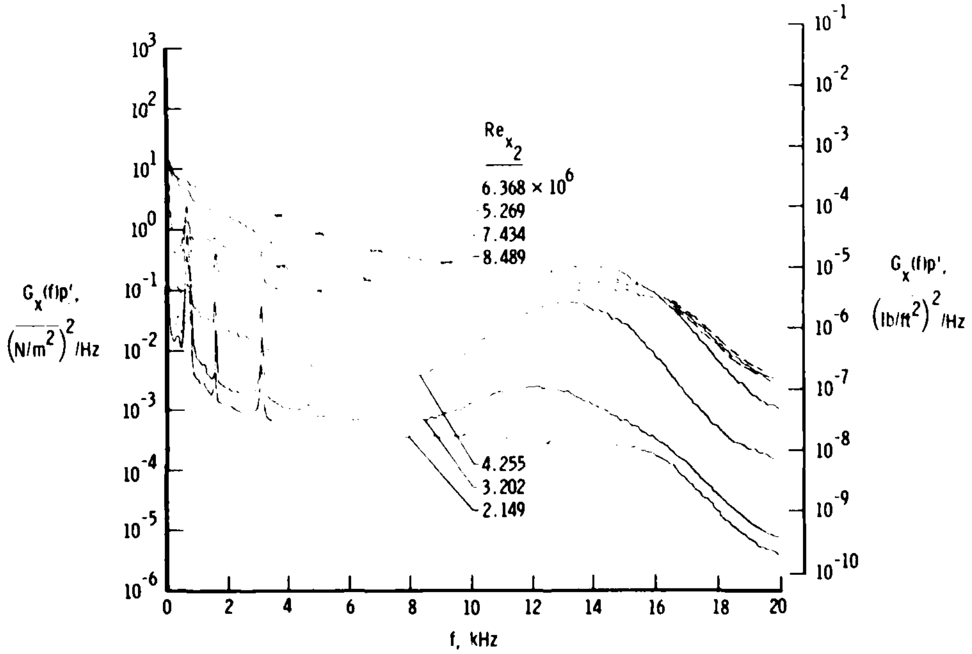

(b) Aft microphone.

Figure 14. Cone microphone spectra in the Langley 4 SPT at M_∞ = 1.61 (M_∞ = 1.57).

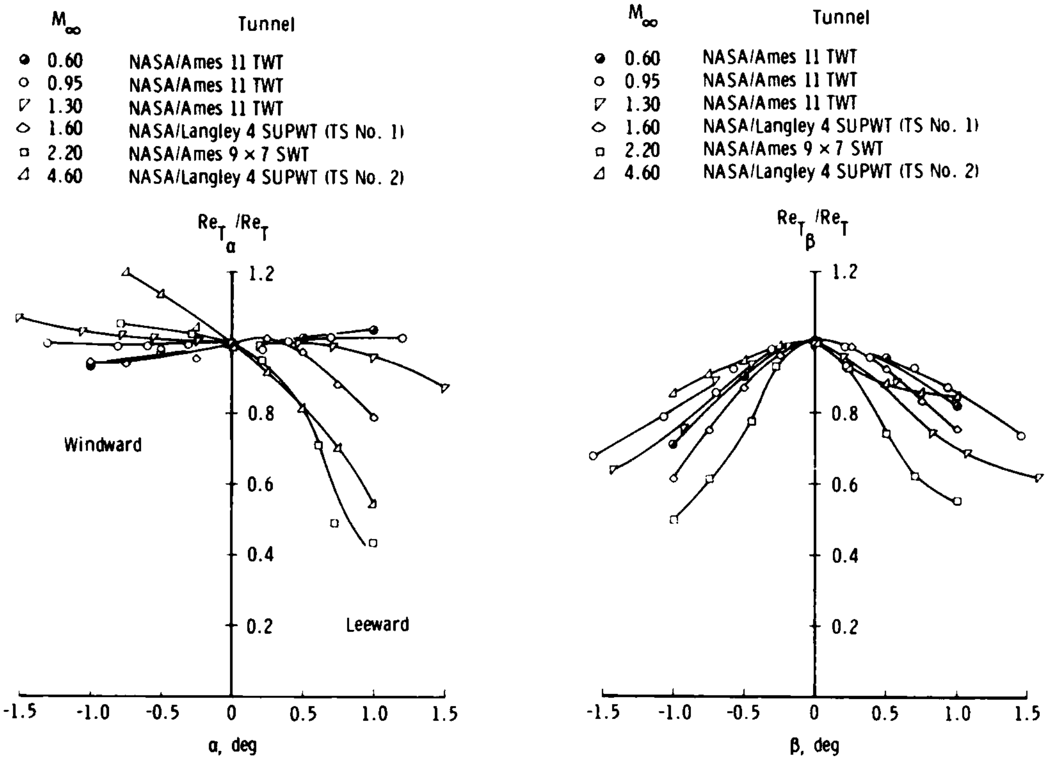

(a) Angle-of-attack influence. Re_{T_α} normalized by Re_T at $\alpha = 0°$; all data shown at $\beta = 0°$.

(b) Angle-of-sideslip influence. Re_{T_β} normalized by Re_T at $\beta = 0°$; all data shown at $\alpha = 0°$.

Figure 15. Summary of the effect of model incidence angle (α and β) on transition.

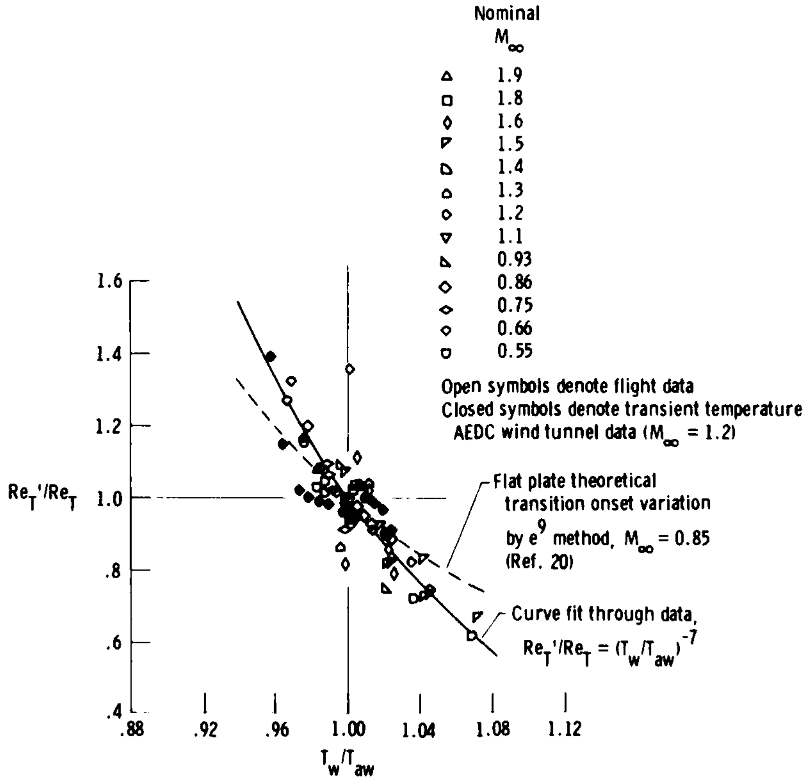

Figure 16. Variation in flight-determined transition Reynolds number with wall temperature and comparison with theoretical and wind-tunnel results.

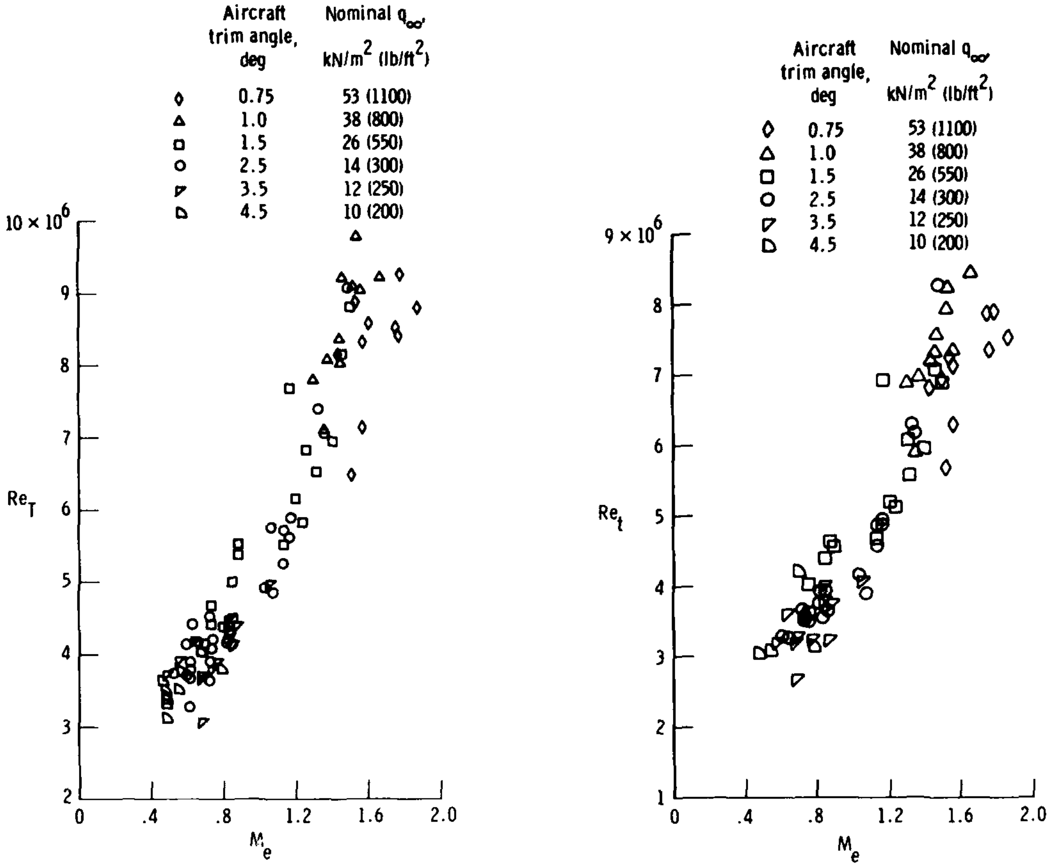

(a) *End-of-transition Reynolds number.* (b) *Onset-of-transition Reynolds number.*

Figure 17. Transition Reynolds number as a function of Mach number.

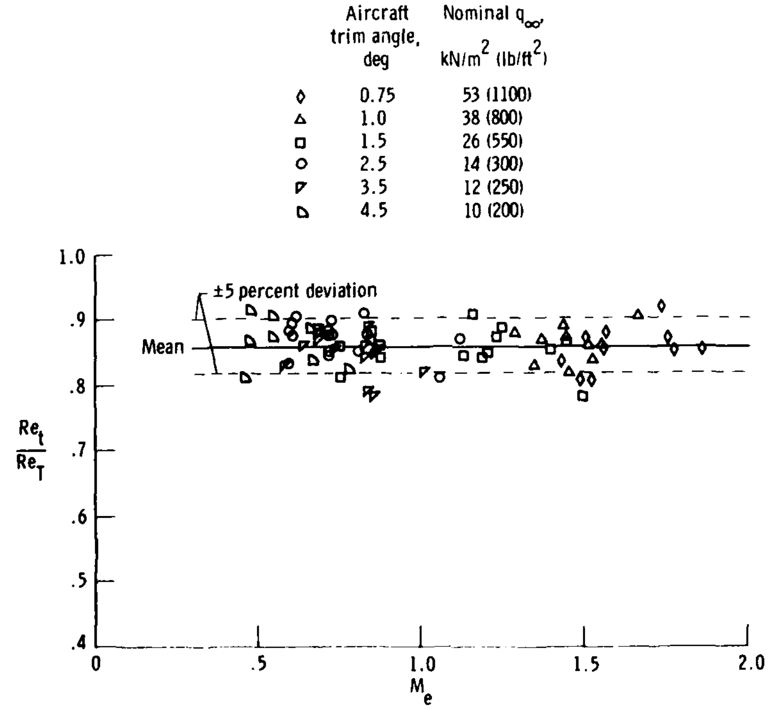

Figure 18. Ratio of onset-of-transition Reynolds number to end-of-transition Reynolds number as a function of Mach number.

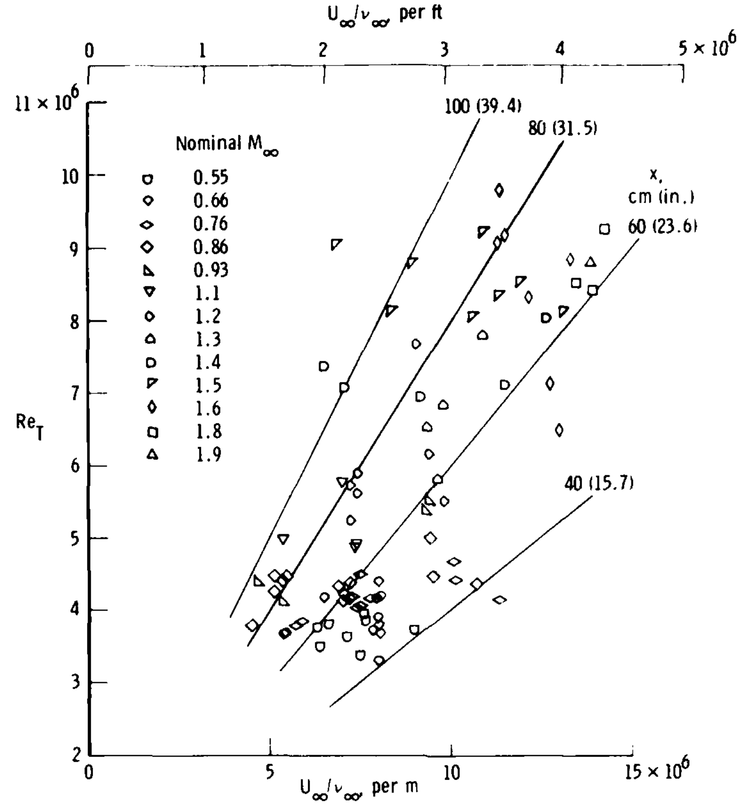

Figure 19. Transition Reynolds number as a function of unit Reynolds number.

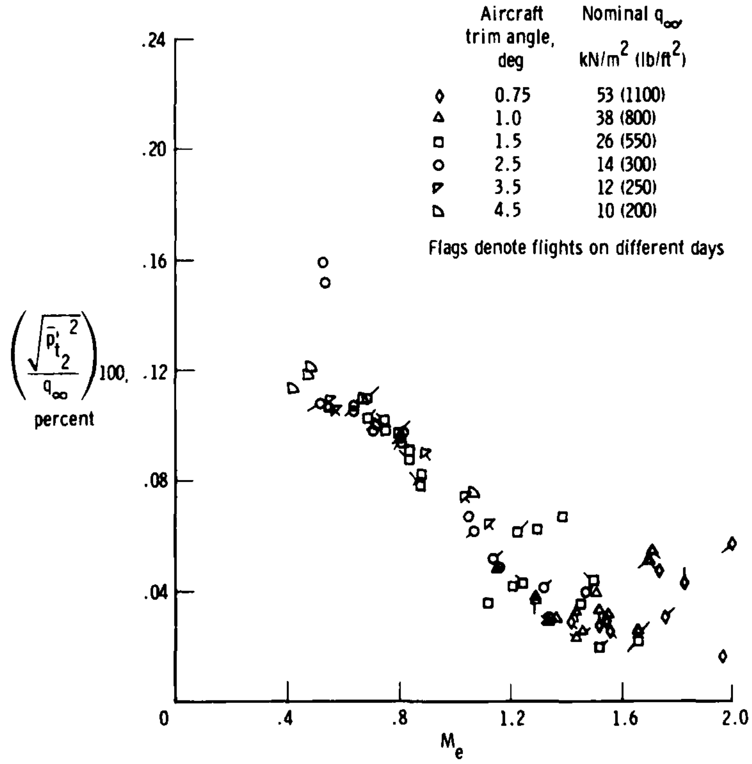

Figure 20. Fluctuating free-stream impact pressure as a function of local Mach number.

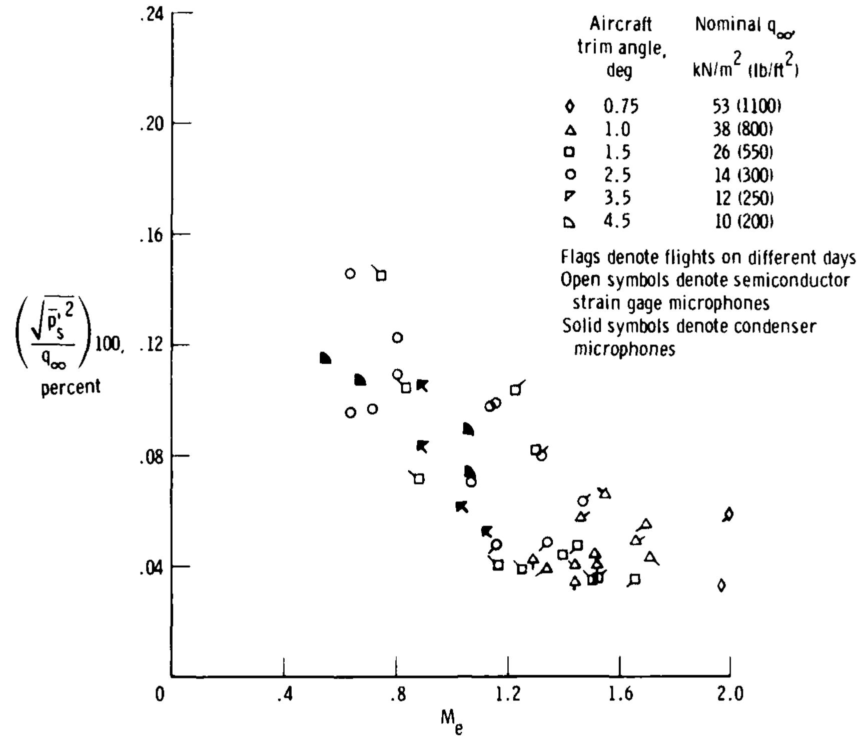

Figure 21. Fluctuating static pressure as a function of local Mach number.

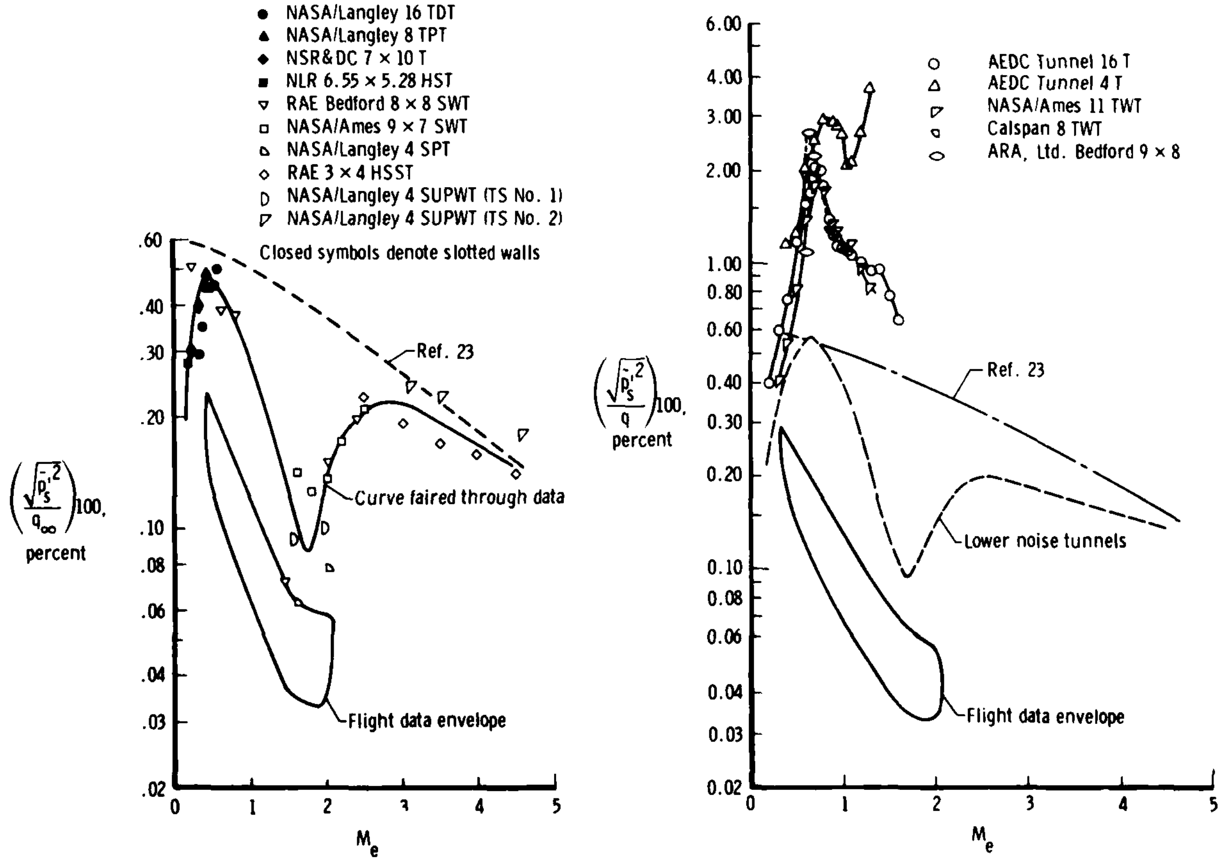

(a) Group 1, 3, and 4 wind tunnels. $U_\infty/\nu_\infty \approx 9.8 \times 10^6\ m^{-1} (3.0 \times 10^6\ ft^{-1})$.

(b) Group 2 wind tunnels. $U_\infty/\nu_\infty \approx 9.8 \times 10^6\ m^{-1}$ $(3.0 \times 10^6\ ft^{-1})$.

Figure 22. Comparison of pressure fluctuation levels measured in wind tunnels and disturbances in flight.

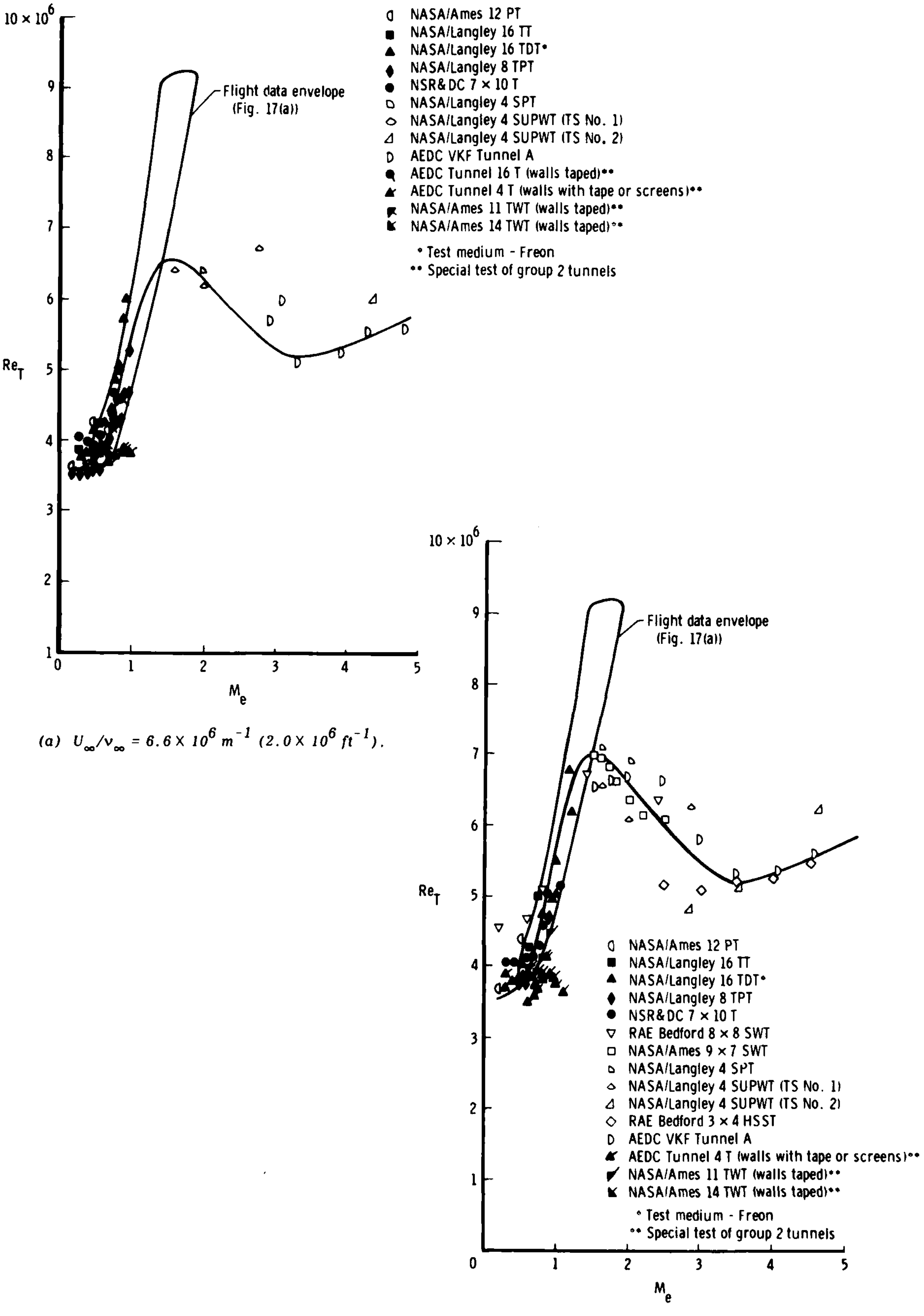

(a) $U_\infty/\nu_\infty = 6.6 \times 10^6\ m^{-1}\ (2.0 \times 10^6\ ft^{-1})$.

(b) $U_\infty/\nu_\infty = 9.8 \times 10^6\ m^{-1}\ (3.0 \times 10^6\ ft^{-1})$.

Figure 23. End-of-transition Reynolds number obtained in Group 1, 3, and 4 wind tunnels.

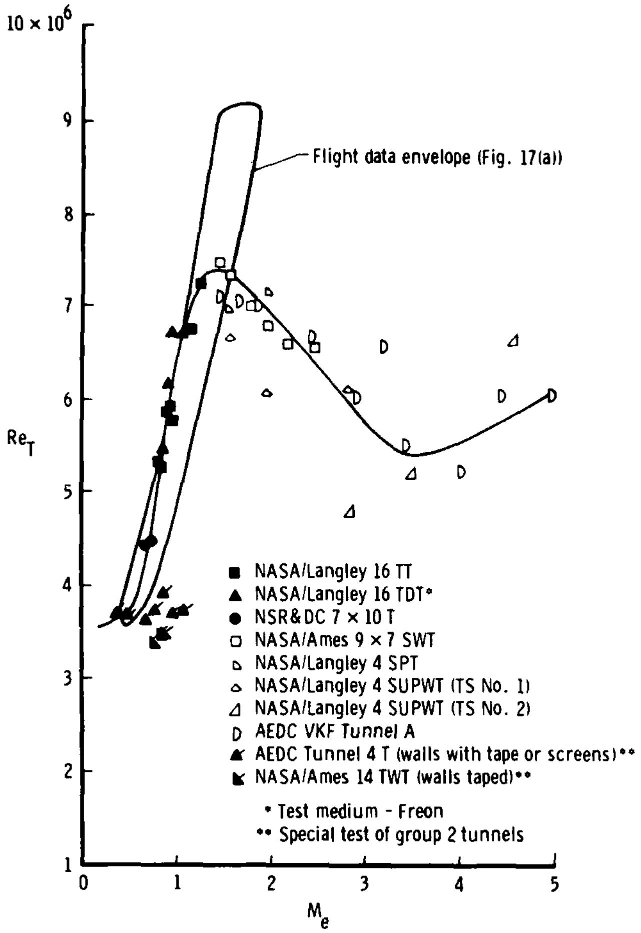

(c) $U_\infty/\nu_\infty = 13.1 \times 10^6\ m^{-1}\ (4.0 \times 10^6\ ft^{-1})$.

Figure 23. Concluded.

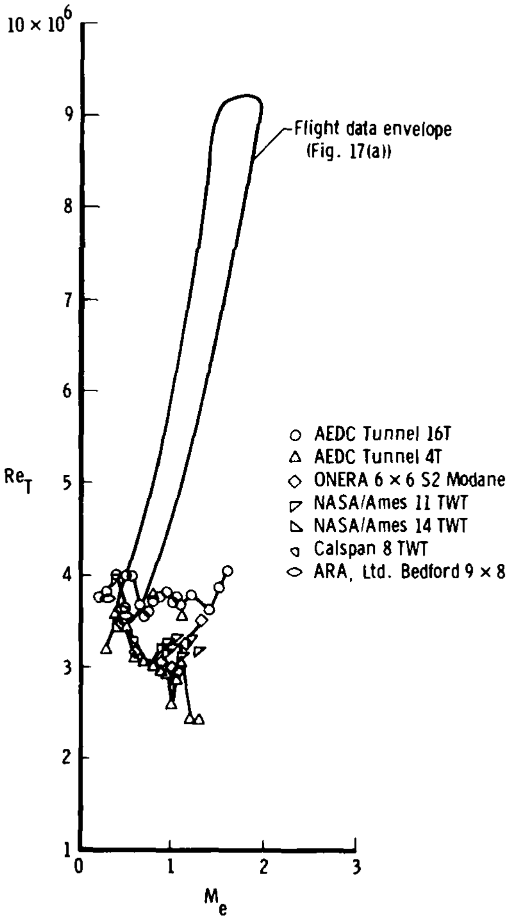

(a) $U_\infty/\nu_\infty = 6.6 \times 10^6\ m^{-1}\ (2.0 \times 10^6\ ft^{-1})$.

Figure 24. End-of-transition obtained in group 2 wind tunnels.

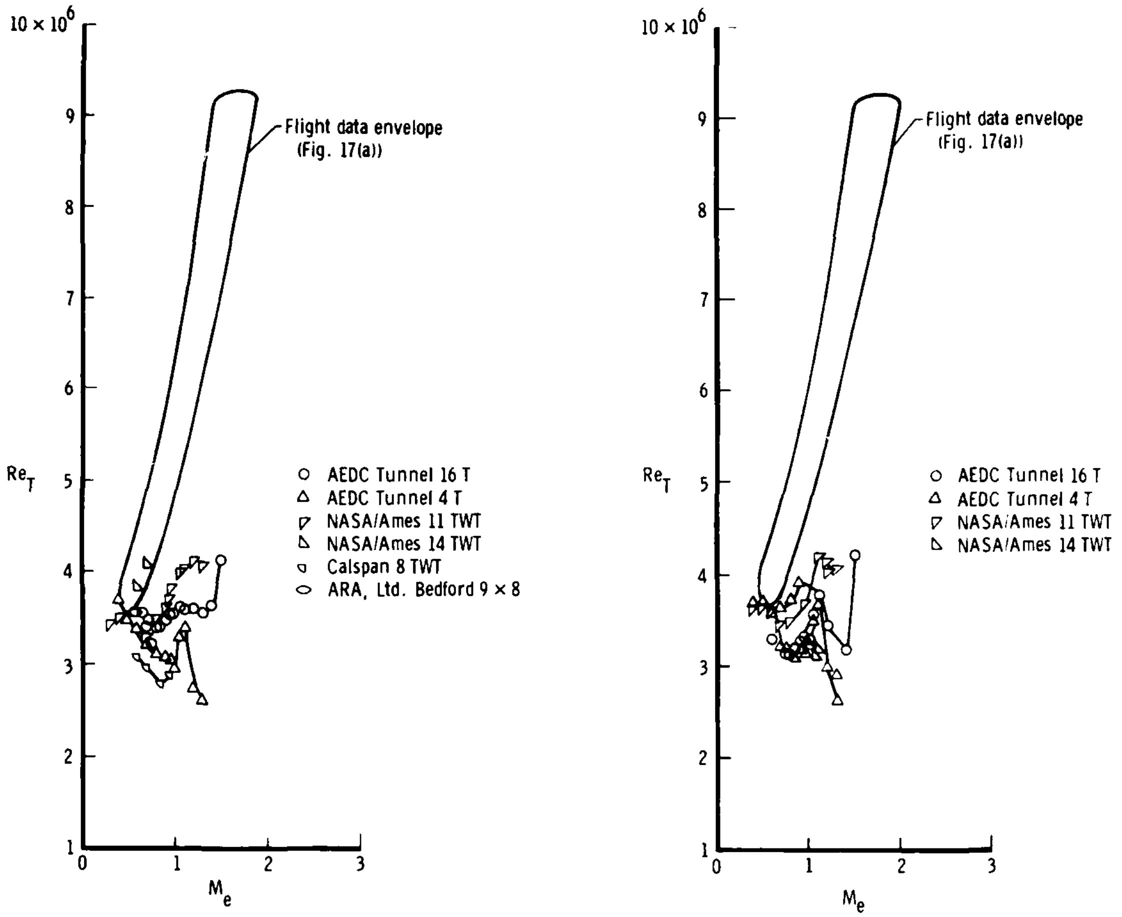

(b) $U_\infty/\nu_\infty = 9.8 \times 10^6\ m^{-1}$ ($3.0 \times 10^6\ ft^{-1}$).

(c) $U_\infty/\nu_\infty = 13.1 \times 10^6\ m^{-1}$ ($4.0 \times 10^6\ ft^{-1}$).

Figure 24. Concluded.

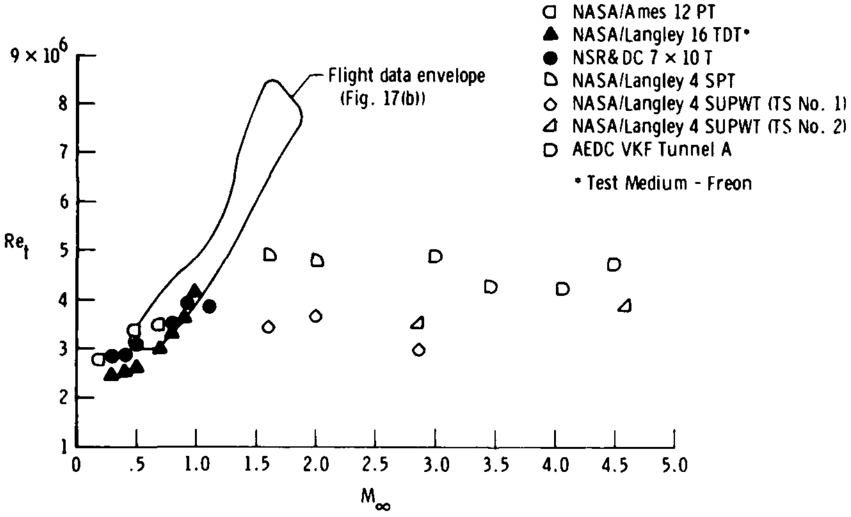

(a) $U_\infty/\nu_\infty = 6.6 \times 10^6\ m^{-1}$ ($2.0 \times 10^6\ ft^{-1}$).

Figure 25. Onset-of-transition Reynolds number from lower disturbance wind tunnels and comparison with flight data.

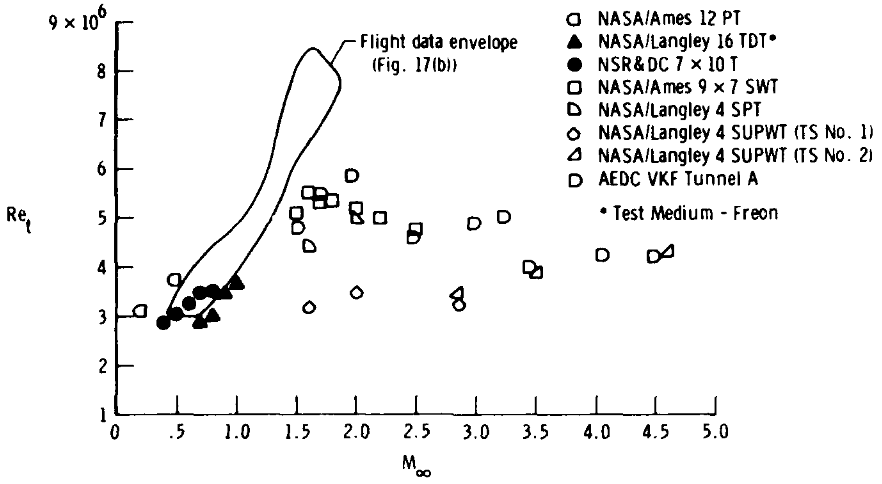

(b) $U_\infty/\nu_\infty = 9.8 \times 10^6\ m^{-1}\ (3.0 \times 10^6\ ft^{-1})$.

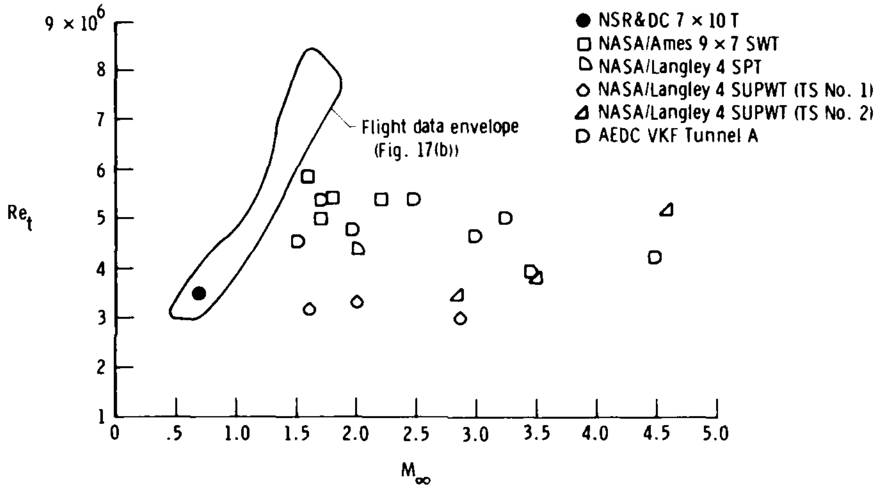

(c) $U_\infty/\nu_\infty = 13.1 \times 10^6\ m^{-1}\ (4.0 \times 10^6\ ft^{-1})$.

Figure 25. Concluded.

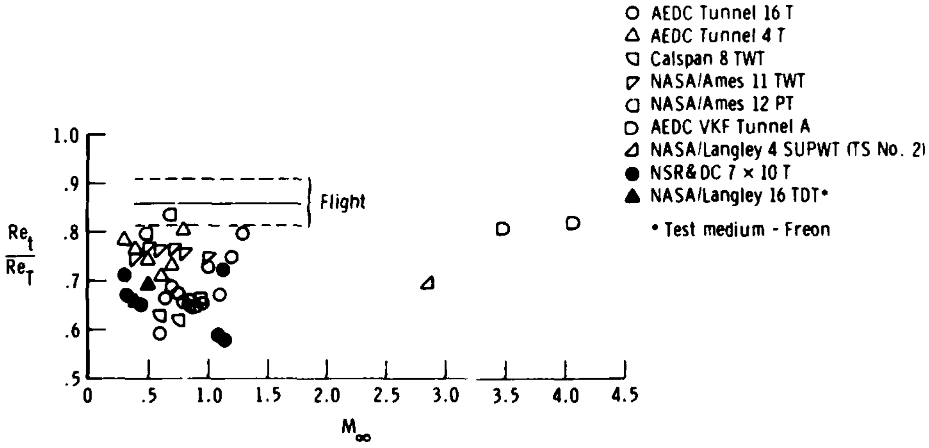

(a) $U_\infty/\nu_\infty = 6.6 \times 10^6\ m^{-1}\ (2.0 \times 10^6\ ft^{-1})$.

Figure 26. Ratio of onset- to end-of-transition Reynolds number from wind tunnels and comparison with flight data.

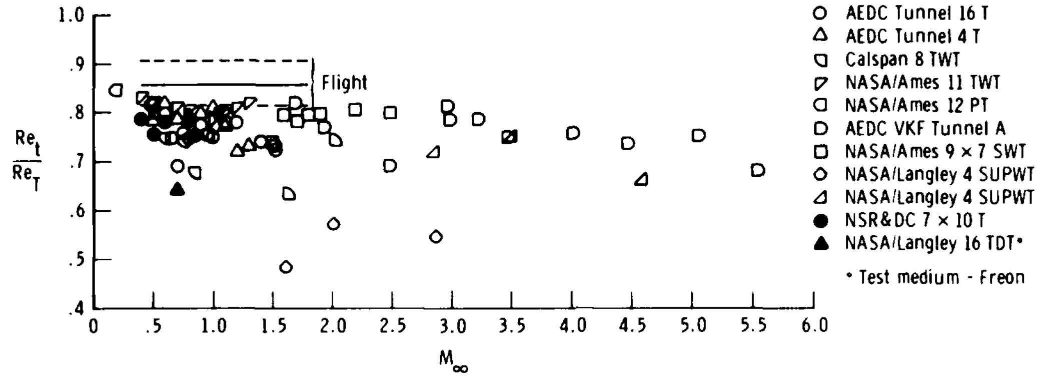

(b) $U_\infty/\nu_\infty = 9.8 \times 10^6\ m^{-1}\ (3.0 \times 10^6\ ft^{-1})$.

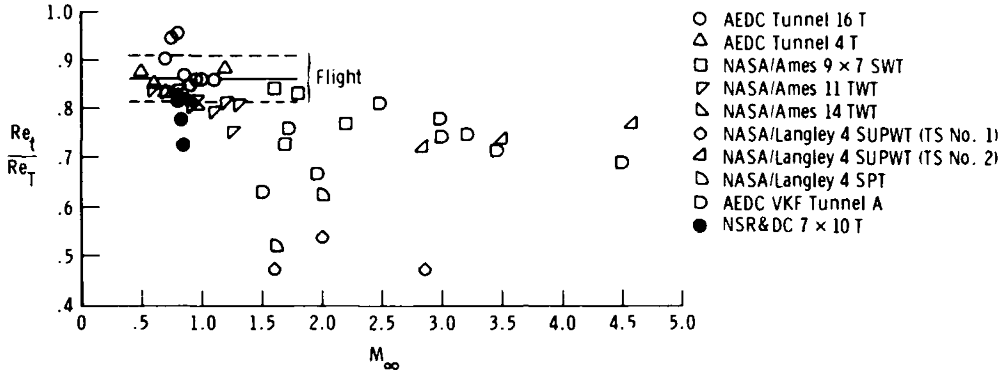

(c) $U_\infty/\nu_\infty = 13.1 \times 10^6\ m^{-1}\ (4.0 \times 10^6\ ft^{-1})$.

Figure 26. Concluded.

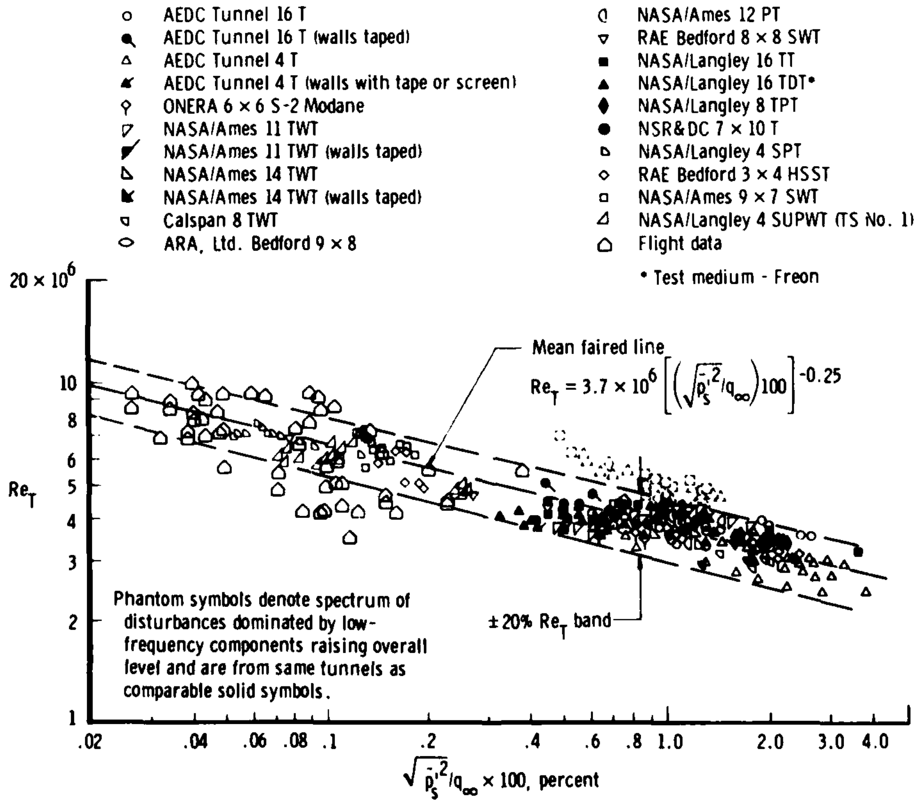

Figure 27. Correlation between Re_T and cone surface disturbance measurements.

EXPERIMENTAL INVESTIGATIONS OF TRANSPORT AIRCRAFT LOW SPEED ENGINE INTERFERENCE EFFECTS AND FLIGHT TEST CORRELATION

by

B. Ewald and W. Burgsmüller
Vereinigte Flugtechnische Werke GmbH
D 2800 Bremen
Germany

SUMMARY

Recent transport aircraft development and flight testing clearly showed important engine airframe interference effects for wing mounted engines. The tendency to reduced engine numbers - most large civil aircrafts developed during the last decade were twin engined - results in a large effect of the one engine out second segment climb on overall aircraft economy. Large development efforts are worthwhile to realize even small drag reductions in this condition.

These development efforts are successful only if a true and reliable engine simulation method in low speed wind tunnel tests is available. Conventional methods like flow through nacelles, ejector simulators or blown nacelles are inadequate. The most perfect engine simulator available today, the turbine powered simulator, TPS, was used in the high speed regime only. Quite recently VFW developed the concept of low speed TPS testing and achieved satisfactory results. The problem outlined up to here was presented in detail in Ref. 1.

Since this presentation a large number of TPS tests with different configurations was performed in the VFW wind tunnel. The TPS has proven as a reliable and valuable experimental tool also in low speed range, provided that sophisticated data acquisition and evaluation techniques are used for optimum accuracy and repeatability. Operating equipment and test methods were improved. Results and experience are described in this paper.

Several transport configurations and research configurations have been tested; results are presented together with comparable flight test results. Comparisons with isolated engine test results show the importance of precise engine interference tests.

The flight conditions, which are analyzed by such tests, are coupled with relatively large lift coefficients. So, the flow conditions are close to separation; partial separation may exist already. Such flow conditions are sensitive to Reynolds number effects, so the tests should be done at the largest available Reynolds number in order to achieve results relevant to the full scale condition. Efforts are made to increase the Reynolds number, compared with the $1.65 \cdot 10^6$ related to wing mean chord available in the VFW tunnel.

The Reynolds number available up to now in low speed TPS testing was limited by the maximum available TPS size, roughly 5 inch fan diameter. To overcome this limitation, the development of larger TPS was initiated by VFW.

9.5 inch fan diameter simulators are developed by Tech Development Inc. for the "German-Netherlands Wind Tunnel". These simulators TDI 1400 will be used with large transport models, the scale related to large civil transport aircraft in $\approx 1 : 10$. Installation of these engines into the model and the necessary equipment in the model is designed and built by VFW; details on model and simulator installation design will be given in the paper.

Even larger Reynolds numbers are available from a 16 inch fan diameter TPS (type TDI 1410), which is in development and fabrication for VFW. This simulator gives a scale of 1 : 5.4 related to full scale large fan engines and can be used with a large half model in the DNW or in the S1 MA for the high speed regime. Its physical size opens excellent possibilities for detailed nacelle-pylon-wing interference flow studies.

Another effective way to increase Reynolds number is the pressurization of the wind tunnel. With TPS tunnel pressurization was not used up to now, since blade and bearing stress problems limited the tunnel pressure to atmospheric level.

This limitation no longer exists with the 9.5 and 16 inch fan diameter simulators presented in the paper. Both engines are qualified for use at up to 3 bars tunnel pressure. The models designed for the DNW can be used with TPS in half model configuration at the Fauga F1 tunnel at pressures up to 3 bars. This corresponds to a mean chord Reynolds number of about $8 \cdot 10^6$, so these tests will clarify the Reynolds number influence on engine interference.

LIST OF SYMBOLS

C_D	drag coefficient	q	dynamic pressure
C_{D_j}	jet induced drag	I/B	inboard side
c_p	pressure coefficient $(p - p_\infty)/q$	O/B	outboard side
c	local wing chord	MTO	maximum take off power
p	local static pressure	TFN	through flow nacelle
p_∞	freestream static pressure		

1. INTRODUCTION

The strong commercial competition in the field of civil transport airplane development and fabrication not only forces the aircraft manufacturers to realize any improvement inside the present boundaries of the state of the art but even is the cause of efforts to extend these boundaries.

The efforts towards such new areas of improved technology normally have a two stage nature. In the first stage a technology area has to be identified where improvements are imaginable; in the second stage the improvement has to be realized which in many cases raises the need for new and more sophisticated experimental or theoretical methods.

Since the day of Boeing 707 development, which was the first commercial aircraft with the standard wing mounted engine position an important development potential was hidden in the aerodynamic interference between engine and wing. Several percent of total drag may be lost or gained by favourable or unfavourable flow conditions in this field. Since even today a theoretical approach has only small chances against the engine-wing configuration and the complicated effects of inlet and jet flow, only sophisticated engine effect simulation in the wind tunnel enables the development engineer to minimize unfavourable engine interference effects.

The superior engine simulation method, the turbine powered simulator (TPS) was already invented more than 10 years ago and was used since then with good success for cruise configuration testing in transonic wind tunnels. On the other side this technique was never used for testing of the low speed *configuration. The reasons for this were:*

- Engine interference effects were considered not to be very important in the low speed flight regime.
- The relation between the large simulator thrust (to be calibrated!) and the small interference drag increments (to be evaluated!) is much more unfavourable in the low speed flight region than in the case of cruise condition in the transonic tunnel. So, it is much more difficult to achive an accurate test result in low speed than in high speed.

The situation was completely changed with the development of large high performance aircraft with only two engines. The one engine out climb performance affects the overall efficiency of aircrafts like this very sensitively. So, a careful optimization of the second segment climb performance is imperative and soon it was discovered, that also in this flight condition performance uncertainties of several percent may occur due to engine interference.

So, about 3 years ago, VFW began - based on a governmental development program - to establish the TPS technique for low speed wind tunnel investigations (Ref. 1). Making use of this development and all the later governmental- and Airbus-funded tests, the additional evaluations, presented here, were derived.

2. THE VFW LOW SPEED TPS WIND TUNNEL TECHNIQUE

The basic test set-up in the VFW wind tunnel is shown in Fig. 1 and Fig. 2. The VFW Low Speed Tunnel test section size is 2.1 x 2.1 m^2, the maximum speed is about 65 m/s. The model shown in Fig. 1 is a half model of the Airbus A 300 B4, the model scale is 1 : 16. The model is mounted to the overhead mechanical balance, which is equipped with a force free air supply bridge.

The engine simulator used in this model is the TDI 441, designed and built by Tech Development Inc., Dayton, Ohio. Fan diameter is 5 inches; Fig. 3 shows the simulator without cowling. The simulator is equipped with measuring rakes behind the fan and behind the turbine which gather all data necessary for thrust calibration and evaluation.

The thrust calibration is achieved by a simple static thrust measurement; the test set-up is shown in Fig. 4. The concept of this calibration without the use of the conventional calibration tank is outlined in Ref. 1 and 2.

This test set-up is in operation since more than two years. A lot of tests have been done on various Airbus configurations. During these tests and additional basic research work test set-up, calibration and evaluation methods have been improved continuously. Since the general idea of low speed TPS testing proved to be successful, a new generation of engine simulators of various scale has been developed and partially already delivered. The aim of this paper is to report on these improvements, some results and on the new simulator and test set-up technique.

3. IMPROVEMENTS OF TEST TECHNIQUE AND EVALUATION METHODS

Generally, it should be noted here, that tests with TPS engine simulation are not even cheap, because

- more staff is needed for the operation of the engine;
- additional energy is needed to drive the TPS (for a low speed tunnel like at VFW, this is about twice the energy which is necessary to produce the required tunnel speed);
- the high loaded bearings of the TPS must be changed in certain intervals to avoid a distruction of the system.

Due to this, it is necessary, to run these tests in an optimized manner and the shortest possible time. To enable this, the following improvements of test technique, instrumentation and data evaluation system have been introduced at VFW:

- *To overcome the problem of ice build-up on the outer and inner contours of the engine due to the very low* temperatures in the primary core (a consequence of the expansioh of the compressed drive air in the turbine), the dryer for the drive air was replaced by an improved system allowing longer testing periods. Further on, the cowls for the primary core which were made of aluminium alloy were provided with heating wires or exchanged by pieces made of other materials (phenolic resin or glass fibre plastics). Further on, a purging system was installed to keep the pressure tubes in primary core and the static orifices on the outer side of the core cowl and plug free of ice and lubrication oil.

- During the first test periods, a manifolding system of pressure orifices was used on the fan rake. Three orifices on one radius (I/B or O/B-halfcircle) each were connected to one scani port at the beginning (Fig. 5). The disatvantage of that system was, that it was impossible to detect a leakage or blockage of a single orifice.
- Due to aerodynamic instabilities, oscillations of the tunnel balance and small thrust variations during the data acquisition time of one test point, a certain scatter band of test results is unavoidable. To be able to draw a mean line through the scattering data points, each point is gathered three times, before the test condition is changed (e.g. incidence angle). To shorten the time for this procedure, each orifice of the TPS pressure-rakes was connected to three different ports on one scanivalve (1 between port 1 and 16, a second between port 17 and 32 and a third between port 33 and 48). So, it is possible to registrate 3 data points with all pressure, temperature and balance signals during one turnaround of the scanivalve.
- The pressures and temperatures, which are used for the TPS thrust calculation, are shown on an on-line display in the tunnel control room. So, a failure in the data acquisition system can immediately be seen and test points can be repeated or - if necessary - a repair can be initiated.
- Additional TPS-data (static pressures behind the fan and turbine) are registrated in order to have a better control of the main data and to have a back-up system for the thrust calculation, if necessary.
- Finally, several improvements of the computer programs have been made in order to accelerate the data reduction and test analysis.

The main results of the improvements mentioned above are

- acceleration of the tests
- minimization of the data scatter band and
- acceleration of the test analysis.

4. SOME TEST RESULTS AND COMPARISON WITH FLIGHT TESTS

4.1 General

In order to get as much informations as possible from the wind tunnel tests, all available and useful test methods have been used, i. e.

- oilflow-visualizations on wing, pylon and engine
- force measurements
- measurements of static pressure distributions on wing and nacelle
- wake flow investigations behind the engine using a total pressure rake.

In the following sections, some characteristic results of these different test techniques and - as far as possible - their comparison with flight test results will be shown. Most of the tests done so far at VFW were concentrating on jet effects during take-off and second-segment climb of the aircraft, i. e. with one engine failed and one at MTO-power. These tests proved as very useful to show the areas of power effects, to predict the magnitude of modifications in these areas and to compare the jet induced drag effects of different aircrafts under similar conditions.

4.2 Oilflow visualizations

A zone of major power effects found during 2nd segment climb investigations was the upper side of the fan cowl. Fig. 6 shows the very small area of flow unsteadiness on the I/B side, while under Ground Idle conditions (Fig. 7) - which would be a typical condition, if a through flow nacelle would be used - two zones of larger dimensions I/B and O/B of the pylon can be seen. (This seems to be an area of interferences between fan and intake flow, i. e. no other jet simulation than a TPS would give the correct answers concerning drag changes.) An other zone of major jet effects are the I/B and O/B-sides of the pylon. Fig. 8 and 9 show the behaviour during a wind tunnel test.

The very good agreement between the flow visualizations in the wind tunnel and the full scale A/C are shown on Fig. 10 - 12. On Fig. 10 the cross flow over the pylon and the field of flow unsteadiness on the fan cowl at MTO-power setting can be seen which is identical with the model test (Fig. 6). The result of the W/T-test showing the pylon flowfield is the same as on Fig. 11 and Fig. 12 for the A/C.

These examples show,

- that the TPS is useful to simulate a representative flowfield and
- the use of other engine simulation techniques (e.g. through flow nacelles or blown nacelles with blocked intakes) may lead to wrong predictions for the full scale aircraft.

4.3 Force measurements

An example for the importance of a proper jet simulation even in the low speed region is shown on Fig. 13. The diagram shows the drag differences due to a modification in the pylon nacelle area for engine conditions Windmill, Ground Idle and MTO. Assuming, this test would have been done with a through flow nacelle only (mass flow ratio normally corresponding with TPS running at Ground Idle), it would have been concluded, that the modification were uneffective.

The result with MTO-power simulation by a TPS however shows the contrary. So, taking into account the second segment climb case with one engine running at MTO-power and one windmilling, the TPS-test leads to the prediction, that the modification will have a favourable effect on drag. A corresponding flight test proved not only this tendency, but also the amount of drag reduction was very similar.

An other important point is the prediction of jet induced drag effects for the second segment climb performances. To do this, at VFW the so-called "incremental"- or "delta"-method is used. This method says, that for similar aircraft configurations the differences between wind tunnel- and flight test results will be more or less the same. Using this method means, that, for example, the prediction of second segment jet interference drag for an A/C no. 2 can be made by a comparison with the wind tunnel results of A/C no. 1. An example for this is given on Fig. 14. This diagram shows the W/T-results of jet induced drag for the relevant lift coefficients and corresponding slat/flap settings for A/C no. 1, whose relation to full scale results is known. The W/T-results for the new A/C no. 2 are also shown, and the difference between these two sets of curves is used to predict the behaviour of A/C no. 2.

One more field for jet effects on drag is e. g. the influence of different engine configurations. Even here the TPS-tests at VFW showed an agreement with full scale conditions, which could not be shown with other types of engine simulation, neither with through flow nacelles nor with blown nacelles. It should be noted here however, that successful force measurements with TPS engine simulators especially in the low speed region, where the engine thrust at MTO-condition, which must be subtracted from the balance readings, is much higher than the aerodynamic drag forces, can only be achieved, if the whole data acquisition and reduction system is built up on the basis of highest possible accuracies. If this problem is solved however, no other engine simulation technique available today, gives more realistic results.

4.4 Static pressure distributions

These tests, as well as flow visualizations and the wake flow measurements, described below, mainly were done to get more details about the very complex flow field in the wing/pylon/nacelle region. Static pressure orifices were located on the wing I/B and O/B of the pylon and on the nacelle. The locations are shown on Fig. 15.

A typical result for the jet influence on the wing pressure distribution is shown on Fig. 16. From this it can be seen, that due to influence of the fan nozzle jet the static pressure on the wing l/s is increasing. This increase is more pregnant on the O/B side of the pylon than on the I/B side. This result is astonishingly on the first view, because one would expect, that the fan jet velocity is higher than the Mach number and correspondingly a suction effect should exist leading to lower pressures under the wing. This mystery found its explanation in the results of the wake flow measurements, described below, from which it can be seen, that the velocity of the fan jet close to the pylon is much closer to tunnel velocity than expected. So, there is no suction due to the jet, while the massflow in the wing/pylon/nacelle area is increasing with increasing engine thrust. These two effects together may indeed lead to increasing pressures below the wing, as the test results show.

Fig. 17 gives an example of static pressures on the core cowl of the engine at MTO-power setting. This diagram gives an impression of the influence of the fuselage and wing flowfield on the nacelle pressures. Comparing the results for $\alpha = 0$ and 11° it can be seen, that with increasing angle the static pressures on the core cowl I/B of the pylon are increasing, while those at O/B and on the bottom of the nacelle are not influenced. From this result the conclusion may be drawn, that the jet is not to be assumed as a fixed wall, like this is done if a socalled "skirted" through flow nacelle is used. Summarizing the results of the static pressure measurements, it must be stated as from the force measurements, that representative wing/pylon/nacelle interferences will not be got unless a proper jet simulation is used.

4.5 Wake flow investigations

The wake flow investigations mainly were done, to get more detailed informations about the flowfield of the model jet and its behaviour under different conditions, such as changes due to

- variation of incidence angle,
- different power settings,
- modifications of the nacelle geometry or
- increasing distance from the nozzle exit.

Comparing the TPS results with a real engine, it is to be noticed, that the temperature and hence the velocity of the primary flow are much lower for the TPS (due to expansion of pressurized air in the turbine), while the pressure ratio of the primary nozzle is comparable to full scale. The more important point however is, that the TPS can completely simulate the fan flow (i. e. pressures, temperatures, velocities, mass flow and - to a certain distinct - also swirl), which is responsible for the interferences with wing, pylon and tailplane. So, the behaviour of the fan flowfield of the TPS can also be used as an input for the development of theoretical 3-D - computer programs including jet effects.

For the wakeflow investigations in the tunnel a rake with pitot pressure orifices was used. The length of the rake was about 1.5 fan nozzle diameters. The position was in a plane normal to the engine axis (Fig. 18) and moving from I/B to O/B of the pylon, crossing the complete engine wake flow. If not other mentioned, the position downstream of the fan exit was at about 3.2 fan nozzle diameters. Only for some tests, more backward positions (about 5.2 and 7.2 D) were investigated (Fig. 19). The following examples show the behaviour of the jet under typical parametric variations, as mentioned above. Each diagram shows the isobaric lines of total pressure ratios in the measuring plane and the corresponding 3-D total pressure ratio mountain.

- The influence of incidence angle is to be seen from Fig. 20 and 21 ($\alpha = 0$ and 11°). The engine setting was MTO in both cases. As already mentioned above, these diagrams show, that the jet velocity in vicinity of the pylon is much lower than on the opposite (or lower) side. This effect is increasing with increasing incidence angle, and seems to be the explanation for the increasing pressures on the wing lower surface (see under 2.4 and Fig. 16). Further on, it can be seen from Fig. 21, that the I/B and O/B half of the jet are unsymmetrical. This may have to do with swirl of the jet and hence could not be simulated with other jet simulation techniques, available today.

- The power effect is demonstrated on Fig. 22 - 24 (incidence angle zero). The momentum loss behind the windmilling engine is clearly to be seen on Fig. 22, while Fig. 23 represents a flight idle condition and Fig. 24 stands for MTO-power. Please, note also the crater in the centre of the jet, representing the primary flow.

- An impression of the influence on the flowfield coming from engine core cowl geometry is to be seen by comparing Fig. 20 and 24, where the longer core cowl, represented in Fig. 24 leads to a more symmetrical wake flowfield than the shorter one on Fig. 20.

- To get some informations about the decay of the flowfield with increasing distance, Fig. 24 - 26 show the results for distances of about 3.2 / 5.2 / 7.2 fan nozzle diameters downstream ($\alpha = 0^{\circ}$, power setting MTO).

These diagrams show, that - except for the well known increasing size of the flowfield and the decaying pressure ratio - at a position where the tailplane may be located, the mixing of fan and primary flow has resulted in a flowfield showing no more unsymmetries, neither due to the pylon nor due to the lower pressures of the primary flow.

5. NEW TPS TESTING TECHNIQUE DEVELOPMENT

5.1 Low Speed TPS Testing in DNW

To overcome the disadvantage of low Reynolds number and lacking asymmetric effects as mentioned above, the concept of complete model TPS testing in the DNW (German/Dutch Low Speed Tunnel) was developed. The typical model scale of Airbus type aircraft in this tunnel is about 1 : 10. Fig. 27 shows the tail sting installation of an A 300 B4 model in the 6 x 8 m^2 test section of this tunnel.

For this model turbine driven simulators have been developed and delivered to DNW by TDI. Fig. 28 shows a sectional drawing of this unit, which represents a new TPS generation. The scale related to the General Electric CF6-50C is 1 : 9.5; this gives a fan diameter of 9 inches. Compared with earlier TPS design the main progresses of this engine are:

- High performance single stage fan; maximum fan pressure ratio is 1.7.
- Closed circuit bearing lubrication system; this minimizes the problem of frozen oil clogging the measuring rakes.
- Low overall length / diameter ratio; this simplifies the design of model scale cowlings around the simulator.

These units will be used for complete model tests in the DNW. Fig. 29 shows the design of the complete simulator nacelle and pylon. The simulator itself and the nacelle parts in various stages of assembly are shown in Fig. 30, 31 and 32. Apart from the internal instrumentation rakes the cowling and the pylon is instrumented with pressure distribution.

The complete Airbus model, the TPS-cowlings, pylons, the internal instrumentation and the internal air duct system were designed and built by VFW under contracts of the German Ministry of Research and Technology. The tests in DNW start with a reference test phase concerning the A 300 B4 configuration to prove the test technique and the equipment. The model will be mounted with the internal strain gage balance on the tail sting. The internal balance is bridged by a force free air supply with separate feedlines to both simulators.

The TPS nacelles are calibrated in the brand-new NLR calibration tank at the Northeastpolder. This tank closely follows the Boeing calibration tank philosophy and was especially designed and built for engines of this size and type. The calibration process started in August 1982; the facility proved to be very successful and gave accurate results. Fig. 33 shows the TPS in the calibration facility.

For the first time in the history of engine interference research this model will allow to simulate true second segment climb conditions with asymmetric flow and thrust conditions and at the same time the model scale will give a reasonably high Reynolds number. Together with the additional possibilities of DNW, e. g. moving belt ground simulation and real time ground approximation this model will launch a new era of low speed testing.

5.2 Pressurized TPS Testing

A most effective way to increase the Reynolds number is to pressurize the wind tunnel. This has not been possible with TPS operation up to now because the simulators were unable to withstand the high loads in a pressurized tunnel.

The new generation of simulators designed by TDI for DNW and VFW no longer have these limitations. Casings, blades and bearings are stressed for operation under a 3 bar environment. Together with the dimensions of the DNW Airbus model this gives a mean chord Reynolds number of $8 \cdot 10^6$. It is planned to use one half of this model for a TPS half model test set-up in the pressurized low speed tunnel ONERA F1 at Toulouse as soon as the necessary drive air facility is available at that tunnel. The DNW model is already prepared to be used as a half model and is stressed for the 3 bar environment. This test set-up will allow to study Reynolds number influence on the interference phaenomena over a wide range and so we will get a knowledge about the necessary Reynolds number for future engine interference studies.

With respect to these tests a very important problem has to be solved. Necessarily there will be a marked effect of pressure level, i. e. Reynolds number on the TPS calibration, so calibration over the total pressure range is necessary. Up to now no calibration facility is existing for this purpose; one would need something like a pressurized calibration tank. Possibly a concept may be successful which uses a Mach number range calibration from a standard calibration tank together with a Reynolds number extrapolation derived from static thrust calibrations in the pressurized wind tunnel.

5.3 New TPS development

The development of the new generation 9 inch simulators for DNW allowed simulators of other sizes to be derived from this advanced design. At the present time two very different simulators are under fabrication at TDI for VFW. An advanced small simulator with 5 inch fan diameter will be delivered early in 1983. This TPS allows the simulation of large bypass ratio turbofan engines like the GE CF6-80C at a scale of about 1 : 18 which is a very convenient half model scale for the VFW low speed tunnel and for high speed testing in some transonic tunnels as well. This TPS is very closely built to the DNW TPS design (see Fig. 29) and has the same high performance single stage fan with 1.7 pressure ratio.

The second simulator, which is under fabrication for VFW, has the remarkable scale of about 1 : 6 related to the GE CF6-80C; the fan diameter is 16 inches. Fig. 34 shows the simulator ready for acceptance tests. This engine certainly is not a toy; the power transmitted by the shaft to the fan is more than 1000 HP. Again the design is very similar to Fig. 28.

This engine will be used together with a large half model, which was already tested in the Modane S1 tunnel in the past. Fig. 35 shows this model in the tunnel ONERA S1 MA with a through flow nacelle. This model allows to do basic engine interference studies in great detail and large Reynolds number. Also very realistic thrust reserver studies are possible. For more information on this model see Ref. 3.

Both engines, the 5 inch as well as the 16 inch, have the capability to be operated in a pressurized environment up to three bars. A special utilization of the large 16 inch simulator will be intake tests in pressurized tunnels. This utilization allows intake Reynolds number pretty close to full scale and the realistic presence of an operating fan. Recent research (Ref. 4) has shown that the presence of an operating fan has an important effect on the intake flow, so the simple intake test set-up with a suction line gives different results.

6. CONCLUSIONS

The work done by VFW in the field of low speed TPS testing up to now leeds to the following conclusions:

- Low Speed engine interference testing is necessary, because interference drag dependent on the configuration are existing, which affect the second segment climb performance and can not be neglected.
- The simulation of high bypass ratio jet engines by TPS in low speed wind tunnel testing gives reliable results. If tests are done with the necessary accuracy, the repeatability of the drag measurement (including calibration errors) is inside ± 4 drag counts for an Airbus half model in the VFW tunnel.
- During several test campaigns in the VFW Low Speed Tunnel the test technique proved to be very useful
  - to describe the influence of power setting on the flow field in the region of nacelle, pylon and wing;
  - to predict the influence of modifications on A/C drag and
  - to compare different A/C concerning their jet induced drag effects.

- Independent from engine airframe interference the external flow around the engine has an effect on the engine thrust which is calibrated under static conditions.

- In some cases a predominant part of the engine-airframe interference affects the nacelle itself. So, test set-ups, where the nacelle forces are not weighed, are not suitable for low speed engine airframe interference tests.

- Good agreement was observed between wind tunnel and flight test with regard to the tendency of interference effects. In some cases the wind tunnel test resulted in smaller interference drag values than the flight test. Possible causes may be:
  - Low wind tunnel Reynolds number.
  - Asymmetric full scale effects (angle of yaw, rudder deflections) of second segment climb condition are not existing in half model wind tunnel test.
  - Accuracy of flight test.

Further on, the half model test technique is well suited for the general predevelopment and development work. The complete model test technique adopted for the DNW allows a realistic simulation of the second segment climb condition and gives more size for better Reynolds number.

The development of advanced TPS for operation in a pressurized environment up to 3 bars allows a full evaluation of Reynolds number influence on engine interference.

The fabrication of the 16 inch TPS allows a half model test set-up for detailed engine interference flow studies and realistic intake tests with Reynolds numbers close to full scale.

REFERENCES

1	B. Ewald R. Smyth	The role and implementation of different Nacelle/Engine simulation concepts for Wind-Tunnel Testing in research and development work on Transport Aircraft. AGARD-CP-301, May 1981
2	W. Burgsmüller	Halbmodellmessungen mit Triebwerkssimulation durch TPS im VFW-Niedergeschwindigkeitskanal (Grundsatzuntersuchung). VFW-Kurzbericht Ef-980, ZKP-IFAS-Bericht Nr. 10
3	G. Anders G. Giacchetto A. Gravelle	Philosophy and Results of Steady and Unsteady Test Techniques on a Large Scale Transport Aircraft Model in the ONERA Transonic Tunnel S1 MA. AGARD-CP-285, May 1980
4	B. K. Hodder	An Investigation of Engine Influence on Inlet Performance. NASA CR-166136, 1981

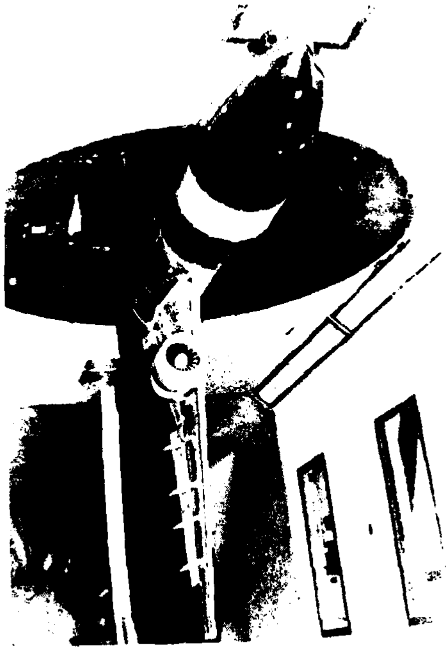

FIG. 1: Low Speed Half Model with TPS (Scale 1 : 16)

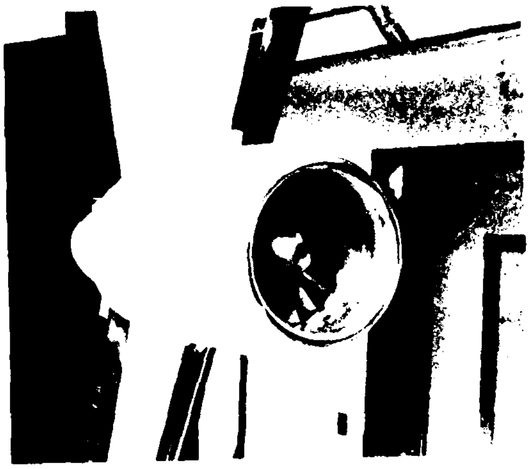

FIG. 2: TPS Nacelle

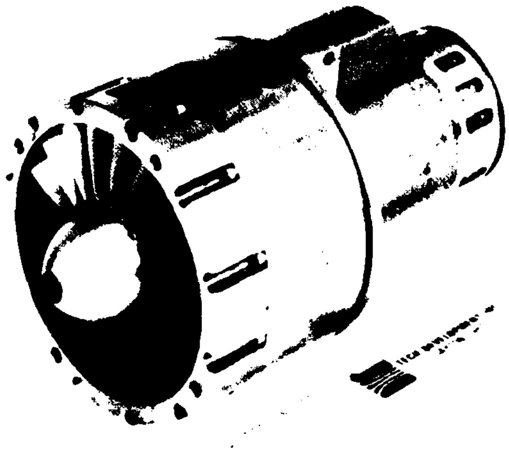

FIG. 3: Turbine Powered Simulator

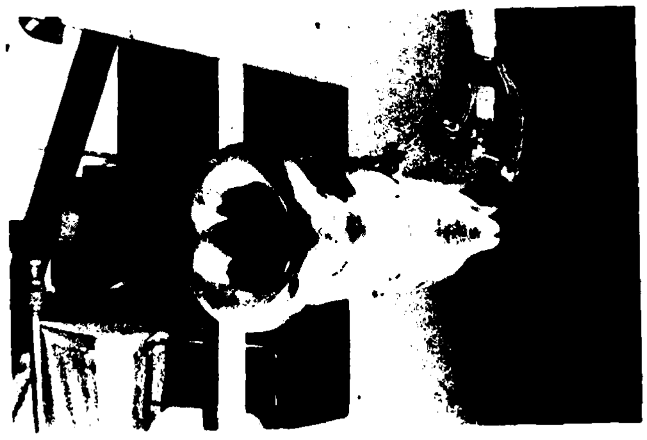

FIG. 4: Static Thrust Calibration of TPS

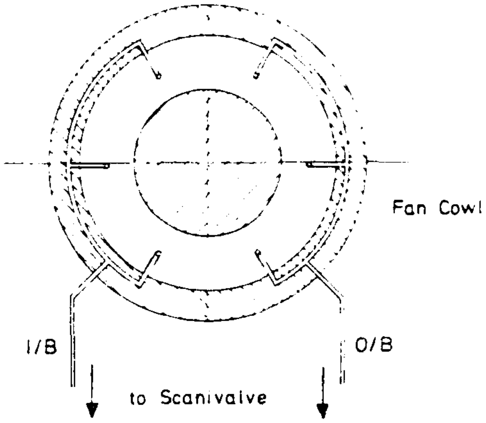

FIG. 5: Manifolding of Pressure Orifices

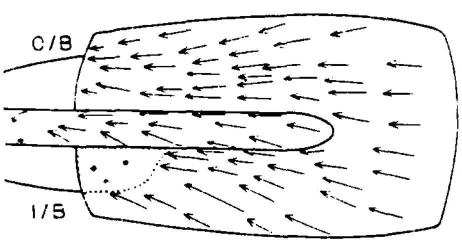

FIG. 6: Oilflow on Fan Cowl u/s at MTO-Power Cond. (W/T-Test)

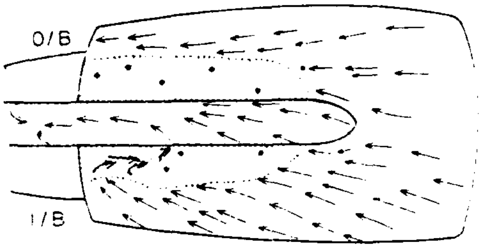

FIG. 7: Oilflow on Fan Cowl u/s at Ground-Idle Power Cond. (W/T-Test)

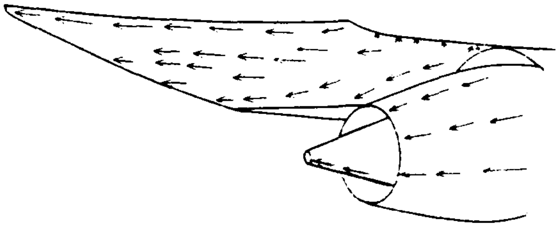

FIG. 8: Oilflow on I/B-Side of the Pylon, MTO-Power Condition (W/T-Test)

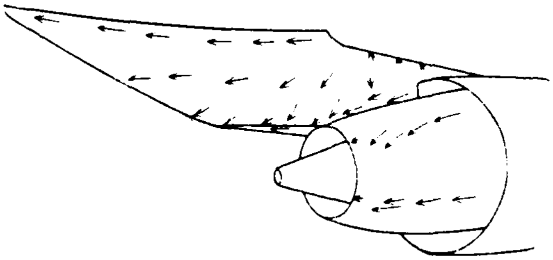

FIG. 9: Oilflow on I/B-Side of the Pylon, Windmill Cond. (W/T-Test)

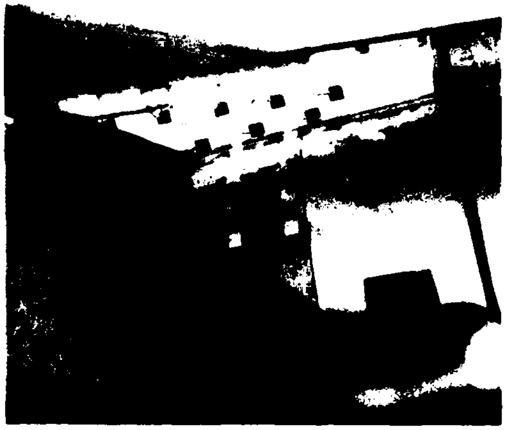

FIG. 10: Flight Test with Tufts on I/B-Side of Fan and Pylon (MTO-Power Condition)

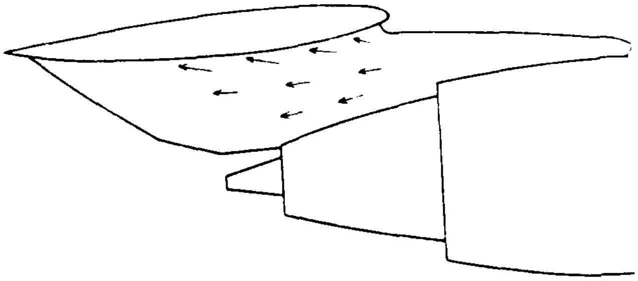

FIG. 11: Flight Test with Tufts on I/B-Side of Pylon (MTO-Power Condition)

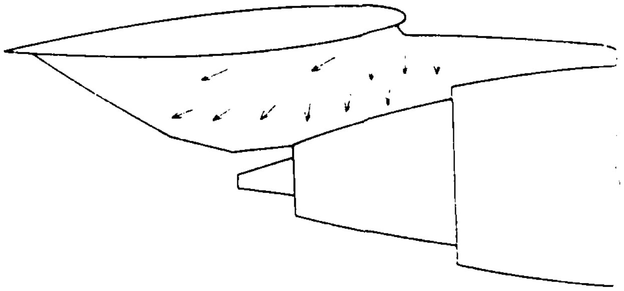

FIG. 12: Flight Test with Tufts on I/B-Side of Pylon (Windmill Condition)

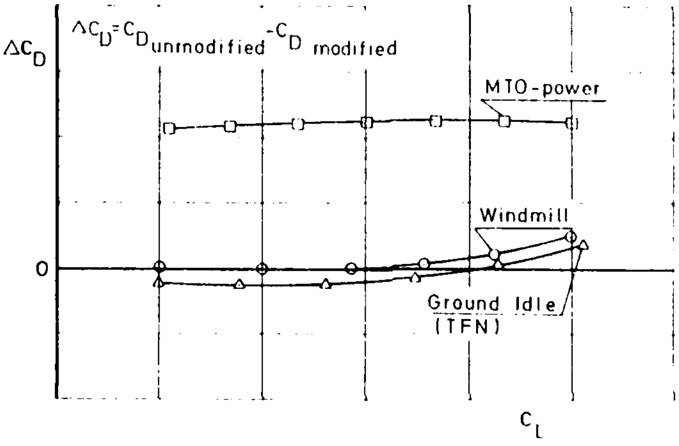

FIG. 13: Influence of Power Setting on Modification in the Wing-Pylon Area

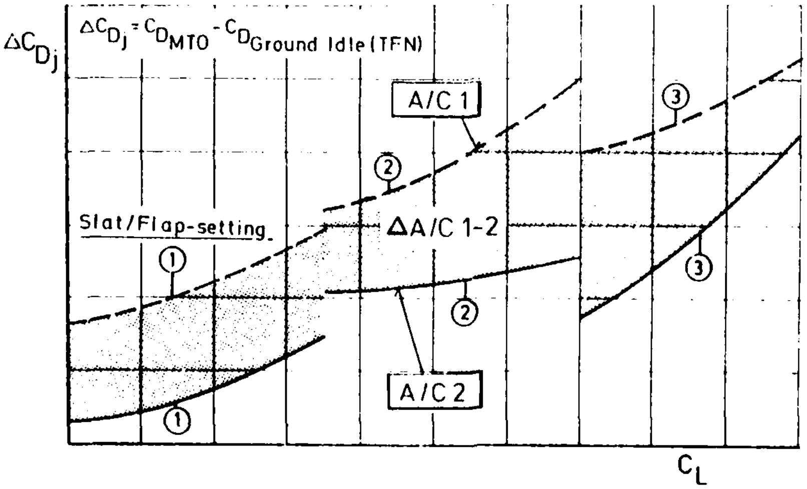

FIG. 14: Comparison of Jet Induced Drag for Similar A/C-Configurations

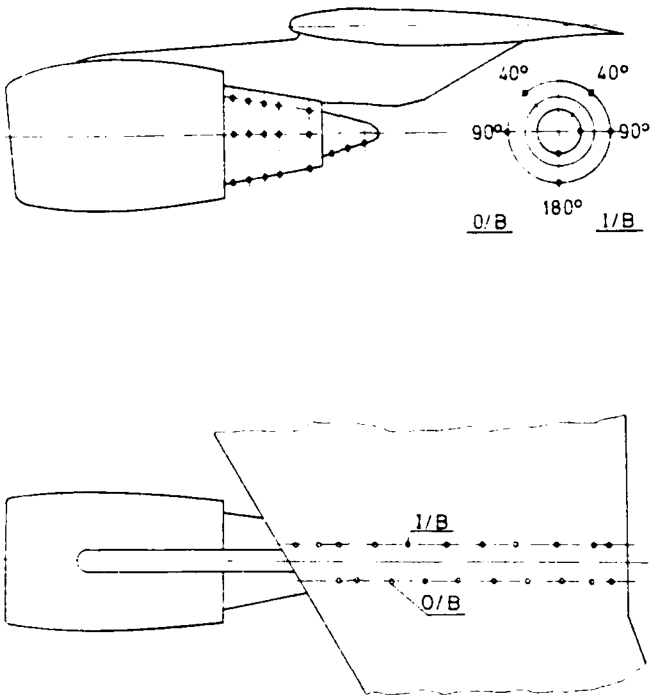

40°
40°
90°
90°
180°
O/B
I/B
I/B
O/B

FIG. 15: Pressure Points on Wing and Nacelle for W/T-test

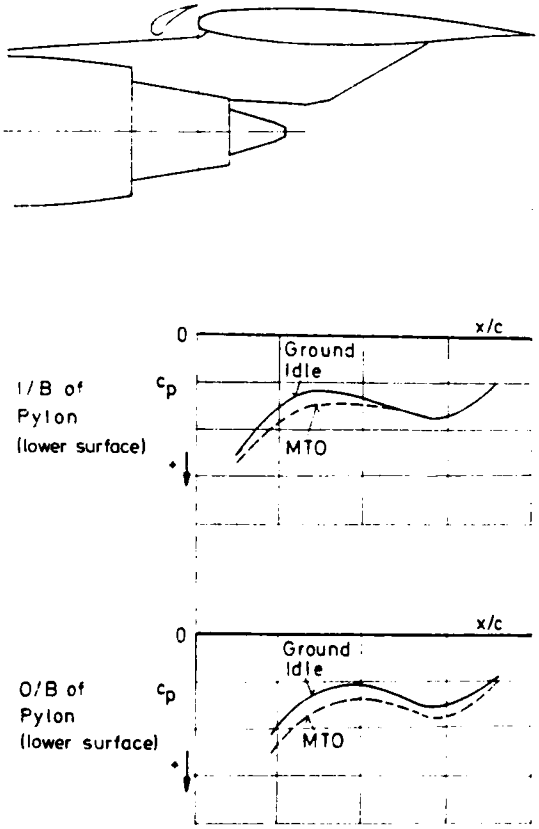

FIG. 16: Jet Effects on Wing Pressures (W/T-Test)

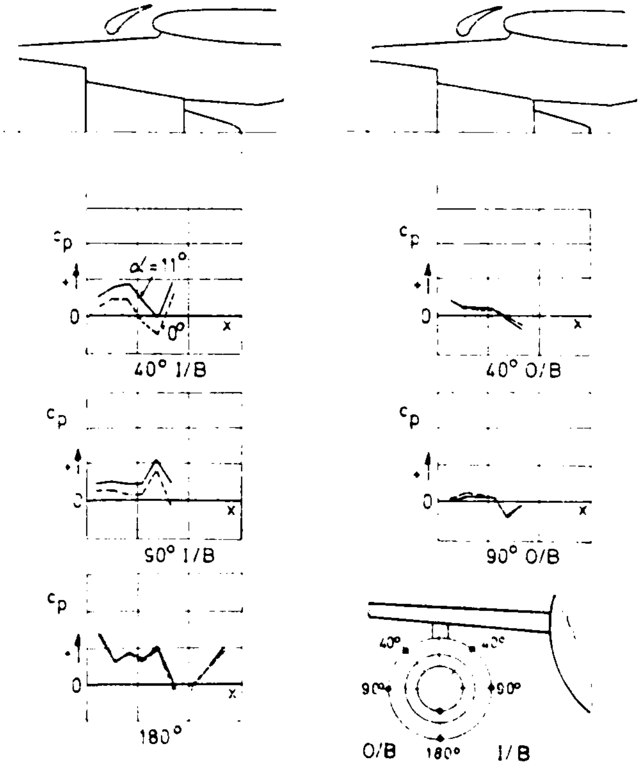

Engine condition MTO

FIG. 17: Influence of Incidence Angle on Nacelle Pressures (W/T-Test)

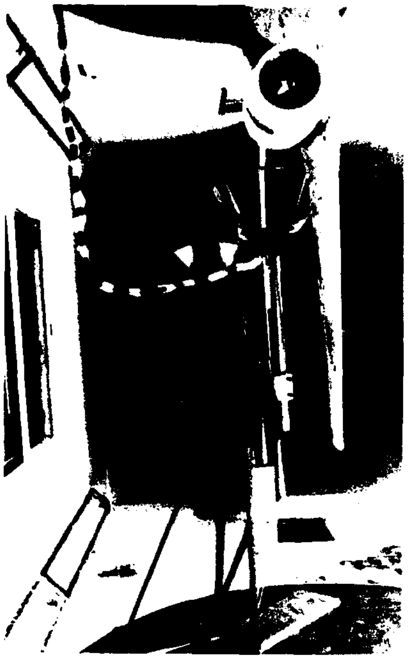

FIG. 18: Model with Wake-Flow Rake

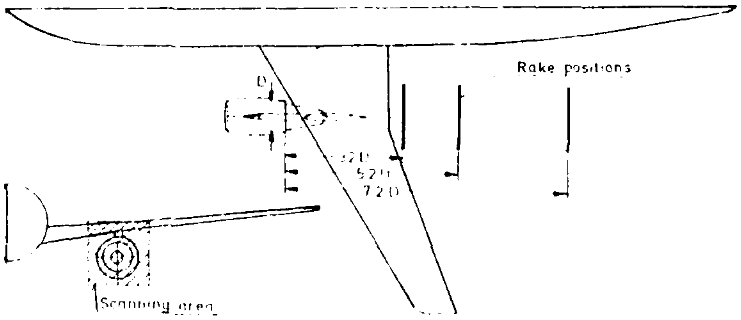
Rake positions
D
3.2D
5.2D
7.2D
Scanning area

FIG. 19: Positions of Wake-Flow Rake

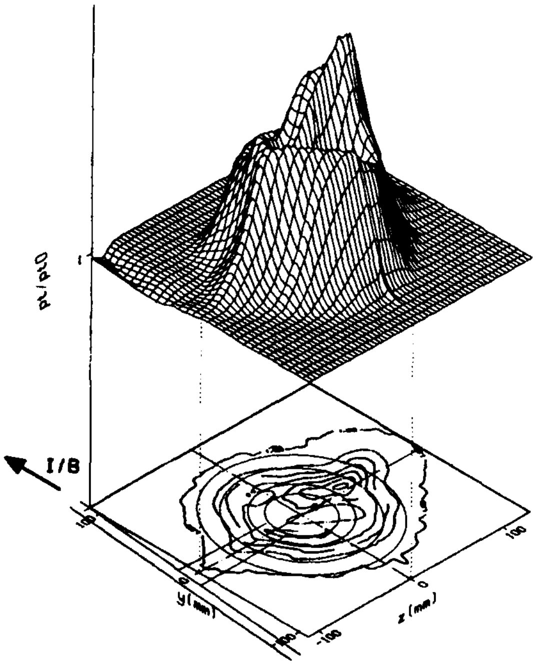

FIG. 20: Wake-Flow, MTO-Power, α = 0°
X/D = 3.2, Core Nozzle 1

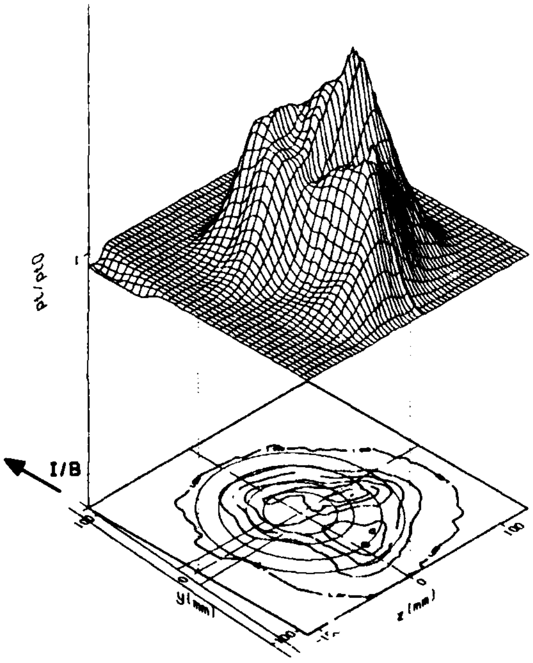

FIG. 21: Wake-Flow, MTO-Power, α = 11°
X/D = 3.2, Core Nozzle 1

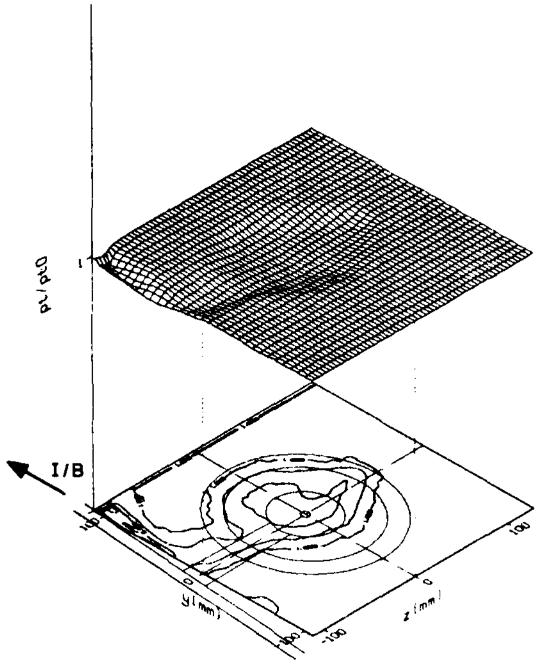

FIG. 22: Wake-Flow, Windmill, $\alpha = 0^\circ$
X/D = 3.2, Core Nozzle 2

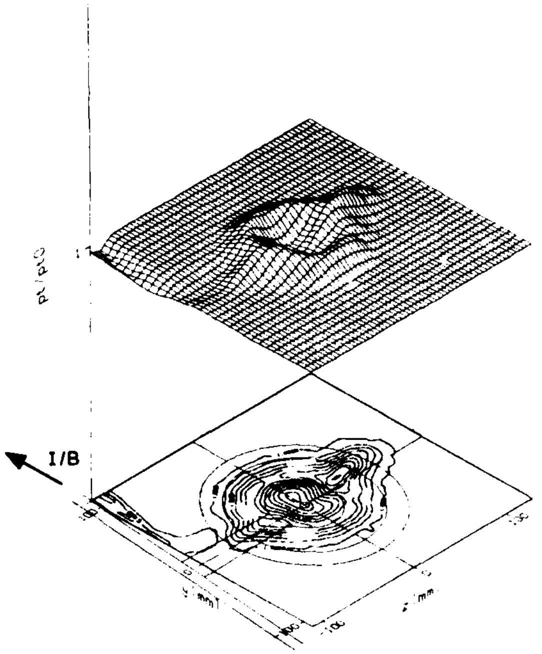

FIG. 23: Wake-Flow, Flight-Idle, $\alpha = 0^\circ$
X/D = 3.2, Core Nozzle 2

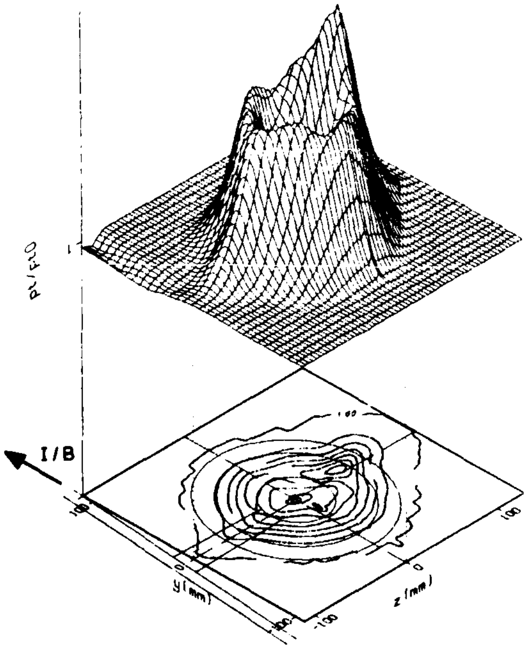

FIG. 24: Wake-Flow, MTO-Power, $\alpha = 0^\circ$
X/D = 3.2, Core Nozzle 2

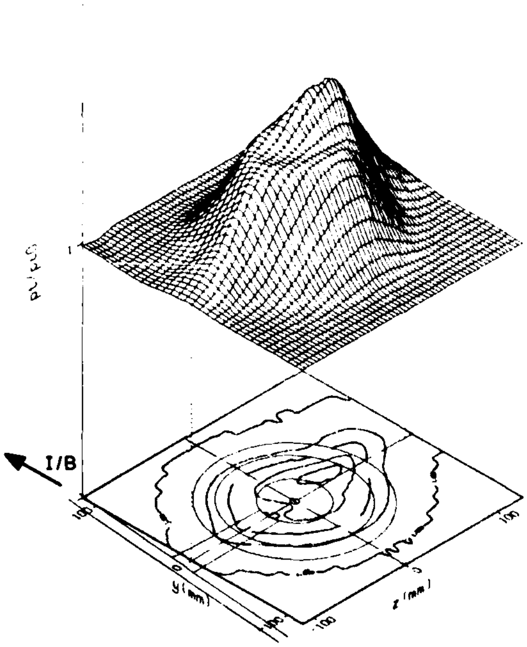

FIG. 25: Wake-Flow, MTO-Power, $\alpha = 0^\circ$
X/D = 5.2, Core Nozzle 2

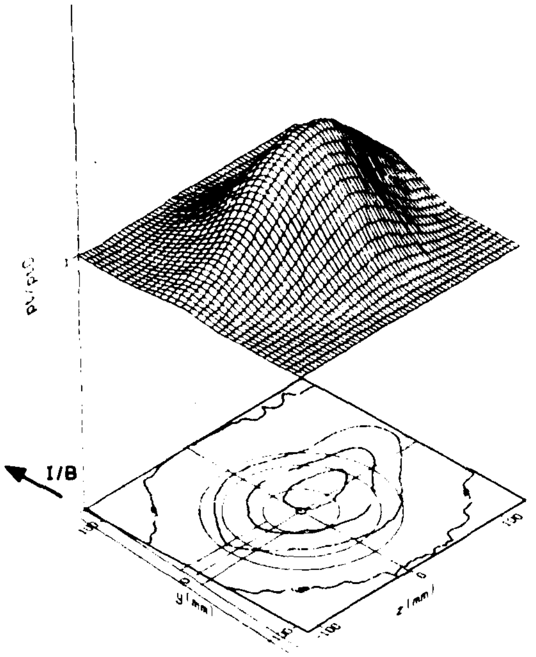

FIG. 26: Wake-Flow, MTO-Power, α = 0°
X/D = 7.2, Core Nozzle 2

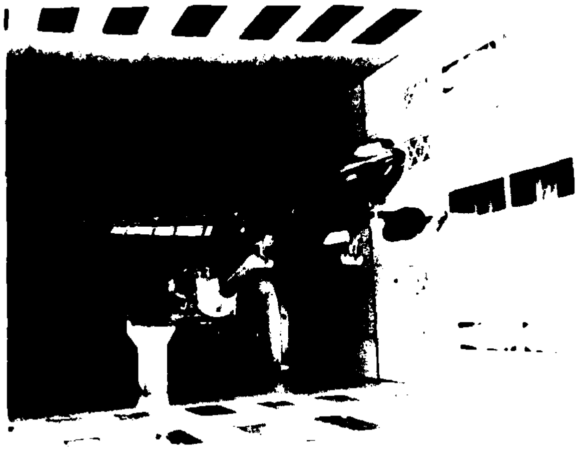

FIG. 27: A 300-B4 Model in DNW (Scale 1 : 9,5)

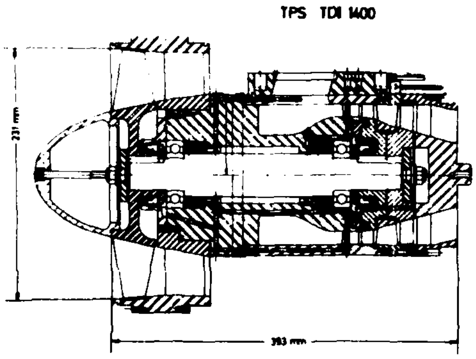
TPS TDI 1400
231 mm
393 mm

FIG. 28: Cross Section of TPS TD 1400

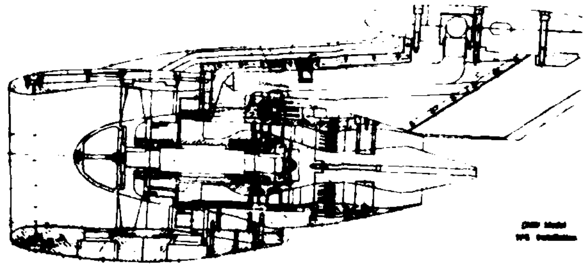
DNW Model
TPS Installation

FIG. 29: TPS Installation on DNW Model

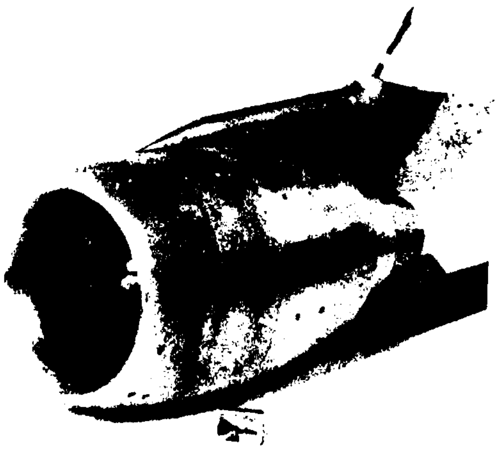

FIG. 30: TPS with Cowlings for DNW Model

FIG. 31: TPS with Fan and Core Cowl (DNW)

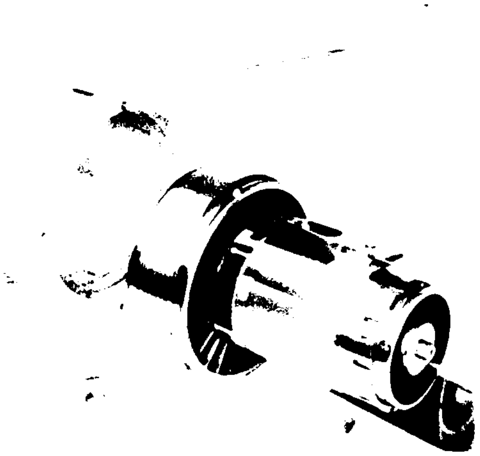

FIG. 32: TPS with Intake (DNW)

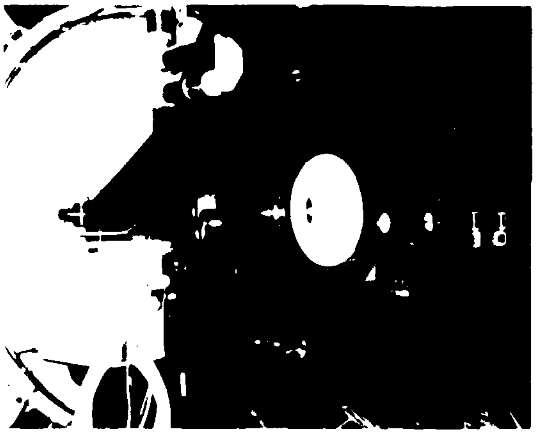

FIG. 33: TPS in the NLR Calibration Tank

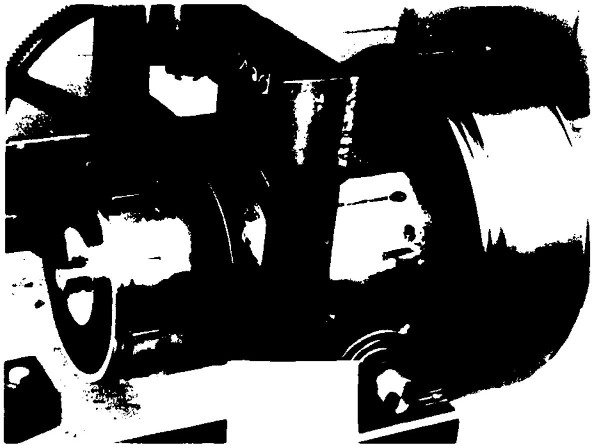

FIG. 34: TPS TD 1410 with 16 Inch Fan Diameter

FIG. 35: Half Model in ONERA S1 MA Tunnel

COMPARISON OF PREDICTION, WIND TUNNEL AND FLIGHT TEST DATA FOR THE CANADAIR CHALLENGER TURBOFAN AIRCRAFT

By: Fotis Mavriplis

Canadair Limited
Montreal, Canada

SUMMARY

Results obtained by theoretical aerodynamic methods, wind tunnel test and flight test are presented for the Challenger aircraft which features an advanced supercritical wing, a wide body and large aft mounted nacelles. These results are of interest as they represent one of the first applications of Jameson's isolated wing full potential flow transonic method to advanced wing design for an aircraft which is now in service.

The techniques used to obtain wind tunnel force and pressure distribution data at high speed and $C_{L_{max}}$ data at low speed are described. A flight wing pressure survey which provided data for comparison with wind tunnel test results is also described.

Correlations of pressure distributions between theory and wind tunnel test are presented to indicate the capabilities and limitations of the isolated wing transonic code. A modified version of this code to include the body effect shows good correlation with experiment. Wing pressure and spanwise load distributions from flight test correlate well with corresponding data from wind tunnel tests. Flight test results on $C_{L_{max}}$ and buffet onset boundary correlate also well with predictions based on wind tunnel data. Based on the above results, recommendations are made with respect to Reynolds Number and transition fixing for wind tunnel testing of supercritical wings in order to obtain good correlation with flight test.

1. INTRODUCTION

Before dealing with the actual subject of this paper, it is only appropriate to describe briefly the main features of the Challenger (Figure 1) and highlight the areas that required particular attention during the development of the aircraft.

The Canadair Challenger is a turbofan business aircraft of 40,400 lb (18,325 kg) take-off weight, capable of inter-continental flight at high subsonic cruise speeds. Its main aerodynamic features are: a rear-loaded supercritical wing, a wide-bodied fuselage, large diameter engine nacelles mounted on the rear fuselage above the wing trailing edge and a T-tail empennage configuration.

The combination of a supercritical wing with high by-pass turbofan engines provides the basis for a fuel efficient cruise at supercritical Mach Numbers. The wide-bodied fuselage was chosen in order to provide, for the first time, a comfortable cabin environment for executive air travel.

From the viewpoint of aerodynamic efficiency both the wide-bodied fuselage and the bulky rear mounted nacelles of the high by-pass turbofans are not desirable features. The proper integration of these major components with the wing to provide an acceptable configuration for high subsonic cruise was a challenging aerodynamic problem which required particular attention.

At the time the Challenger was conceived, supercritical wing technology was relatively new and there was no information available at Canadair on its application to flying aircraft. There were various transonic codes available which could be used to design airfoil sections but the 3-D transonic codes were limited in various ways and were not proven experimentally. Therefore before proceeding with the development of the Challenger, it was necessary to show experimentally that (a) the new methods could be applied with confidence to design a supercritical wing and (b) an acceptable wing-body-nacelle configuration for cruise performance could be defined within a relatively short time by wind tunnel testing.

In this paper some of the methods and techniques used for the development of the Challenger will be discussed and data will be presented to show the degree of correlation between prediction, wind tunnel, and flight test results.

2. WIND TUNNEL TESTING

Wind tunnel testing played a significant role in the development of the Challenger. Specifically the decision to go ahead with the program depended primarily on the successful outcome of one transonic wind tunnel test at the end of a seven-month preliminary study.

The purpose of this test was to verify experimentally the wing design approach which was based on the new transonic codes and to show that fuselage and nacelle interference effects were manageable. The test was conducted at the NAE 5 x 5 foot Trisonic Tunnel in Ottawa using a 0.04 scale model in 80 hours of testing. Figure 2 shows a photograph of an oil flow visualization from that test at Mach Number 0.85. By using natural transition and a Reynolds Number of 5 million, it was possible to obtain a realistic picture of the flow situation in flight.

Figure 3 shows wind tunnel test hours accumulated since the start of the preliminary study relative to some program milestones. After program go-ahead there were two significant phases of wind tunnel testing.

The first phase provided sufficient data to enable fixing of the aerodynamic configuration within six months from program go-ahead. During this phase several wing designs, empennage configurations and nacelle/pylon positions were tested with the 0.04 scale model at high speed and with a 0.08 scale model at low speed. In addition, the flap and spoiler system was developed and optimized using a 2D low-speed model.

The second phase provided all the necessary data for performance, design of flight control system, handling qualities and definition of structural loads for the final configuration. These tests were done with a 0.07 scale high-speed model at the Rockwell Trisonic and a 0.08 scale model at the NAE 6 x 9 foot Low Speed Tunnel.

All wind tunnel tests were completed before the first flight in less than two years logging a total of about 2,000 hours of testing.

3. CORRELATION OF WING PRESSURE DISTRIBUTIONS

3.1 Wind Tunnel Test Technique

Two of the main objectives of the wind tunnel test program were to obtain first, reliable data for drag estimation, and second, detailed pressure distributions, at supercritical flow conditions.

The pressure distribution data were required for the derivation of structural loads and for substantiating the flight loads at high speed for certification purposes. The latter requirement was indicated by Transport Canada early in the program since the Challenger was the first airplane with a supercritical wing seeking certification. The experimental pressure distributions were also required as feedback information to check the transonic code FLO 22 used for designing the wing, and to interpret the body and nacelle interference effects on aerodynamic performance.

For the acquisition of drag data, it was decided to use the highest possible Reynolds Number with transition fixed on all major components except on the wing where transition was allowed to occur naturally. By using a 0.07 scale model, a series of tests was conducted at the Rockwell 7 x 7 foot Trisonic Wind Tunnel at Reynolds Numbers of 6.7 million, 5.1 million and 3.75 million per mean aerodynamic chord. The airplane drag for flight at the design cruise condition ($M = 0.8$, $C_L = 0.5$) was then obtained by extrapolating the wind tunnel data to a full scale Reynolds Number of 9.3 million and correcting for laminar areas due to the difference in transition location.

Figure 4 shows the 0.07 scale Challenger model installed in the Rockwell Trisonic Tunnel facility. The model wing was made out of hardened steel and was designed to achieve in the tunnel the same spanwise twist distribution as the aircraft in level flight, when tested at the design cruise condition. The left side of the wing was plotted with 210 static pressure orifices so as to provide detailed chordwise pressure distributions at six wing sections along the span.

For the pressure measurements it was necessary to use a lower Reynolds Number than 6.7 million not only for increasing the efficiency of data acquisition but also because Rockwell was threatened with a law suit by its neighbours for disturbing the peace with a noisy tunnel operation. As described in the next paragraphs, a Reynolds Number of 3.75 million was selected after a series of comparative tests at Reynolds Numbers of 3.75 million and 5.1 million including flow visualizations and tests with fixed transition.

3.2 Effect of Reynolds Number and Transition Trip

Figures 5 and 6 show the effect of changing Reynolds Number from 3.75 million to 5.1 million with free transition, on the pressure distributions of four streamwise wing sections along the span at Mach Numbers of 0.8 and 0.85 respectively.

It can be seen that at Mach Number of 0.8, increasing the Reynolds Number from 3.7 million to 5.1 million had no noticeable effect on the wing pressure distributions and therefore no effect on spanwise loading. At Mach Number of 0.85, however, there is a noticeable effect only at the 85 percent span wing station. The shock appears to have shifted forward by a length of 8 percent chord causing a reduction in load over the outboard wing. This effect was considerably smaller at a lower lift coefficient corresponding to the high speed cruise condition.

In order to test the effect of transition trip on drag and pressure distribution, flow visualizations were first made at a Reynolds Number of 3.75 million to determine the extent of the laminar flow regions and their relative location to the shock wave. These tests showed that natural transition from laminar to turbulent flow at a Reynolds Number of 3.75 million occurred a fair distance ahead of the shock at high Mach Numbers. Using these flow visualizations as a guide, a transition trip was then placed on the wing upper surface at a distance of about 10 to 13 percent chord length forward of the shock. No trip was placed on the bottom surface because the flow visualization showed that transition was fixed at about 4 percent chord aft of the leading edge due to a coverplate joint extending from inboard to the 90 percent semispan station. The trip was a 0.1 inch (2.54 mm) wide band of 0.0032 inch (0.08 mm) diameter glass beads, based on the method of Braslow (Ref. 1).

The results from these tests are shown in Figures 7 and 8 as trip-no-trip comparisons of pressure distributions at a Reynolds Number of 3.75 million at Mach Numbers of 0.8 and 0.85 respectively.

Figure 7, shows that at Mach Number of 0.8 the transition trip had no noticeable effect on the pressure distribution and therefore no effect on spanwise loading. Figure 8, shows that a Mach Number of 0.85 the effect of transition trip was similar to that of increasing the Reynolds Number from 3.75 million to 5.1 million. Only over the 85 percent semispan station does the shock appear to have shifted forward by an 8 percent chord length.

Based on the above results a Reynolds Number of 3.75 million was selected with natural transition on the wing for all subsequent pressure measurements.

3.3 Wind Tunnel - Theory Correlations

3.3.1 Body Effect

The Challenger wing was designed with the aid of Jameson transonic wing computer code FLO 22 (Ref. 2 & 3). This method solves the full potential transonic equation in non-conservative form for an isolated wing of arbitrary thickness, twist and camber distributions and dihedral.

The first correlations of FLO 22 results with experimental pressure distributions for the Challenger wing/fuselage configuration were quite disappointing. There was poor correlation at the inboard wing stations at Mach Number 0.7 and also at the outboard stations at higher Mach Numbers. In order to provide an answer to this problem, FLO 22 was first checked with WBAERO, an inviscid subsonic panel method which can handle arbitrary complete aircraft configurations. Figure 9 shows the geometry that can be specified for WBAERO analysis.

Correlations of WBAERO with FLO 22 for an isolated wing, as used in FLO 22, at Mach Number 0.7 appeared to be in good agreement. WBAERO correlated also well with the wind tunnel data at the inboard wing stations at Mach 0.7 when the fuselage and fairing geometry were represented. It became clear therefore that the poor correlation between wind tunnel data and FLO 22 was mainly due to an inadequate representation of the fuselage and fairing in FLO 22.

An improved transonic method for analyzing the wing in combination with a wide-body like that of the Challenger was developed at Canadair as an extension of Jameson's FLO 22 incorporating the body effects. The method is based on the calculation of the flow angle on a vertical place through the wing/body junction by using WBAERO for the exact wing + body + fairing geometry. This flow angle is then used as a perturbation of the flow in the Jameson method simulating the body + fairing at the root section plane.

Figure 10 shows comparisons of calculated pressure distributions with wind tunnel data from Rockwell tests at Mach Number of 0.82 and an angle of attack of 1.5 degrees for two inboard and three outboard wing stations. It can be seen that the correlation of FLO 22 with experiment is poor especially at the inboard stations. On the other hand, the results of the new method incorporating the body effect correlate much better with the experimental data. From these data the effect of the fuselage and fairing appears to be particularly strong at the root and appears to extend to the tip.

3.3.2 Nacelle Effect

The effect of body mounted nacelles on wing pressure distributions is more complex than that of the body. To understand this effect requires both methodical wind tunnel testing and analysis with methods that can calculate the flow over complete aircraft configurations.

At subcritical flow conditions the nacelle effect can be calculated by using a panel method like WBAERO. Figure 11 shows spanwise wing loadings from WBAERO and wind tunnel pressure integrations for configurations with and without nacelles at Mach 0.7. It can be seen that WBAERO predicts well the nacelle effect which appears as a reduction of spanwise loading at the inboard wing and an increase of loading outboard.

A transonic method that can calculate the effect of nacelle interference at supercritical flow conditions has recently been developed based on small disturbance theory (Ref. 4). An exact transonic potential flow method like Jameson's to handle wing-body-nacelle configurations is still to be developed.

For the Challenger the effect of nacelle at supercritical speeds was obtained through wind tunnel testing.

Figure 12 (a) shows experimental wing pressure distributions for wing/body alone and complete aircraft configuration at Mach Number of 0.8 and constant angle of attack. The effect of the nacelle appears as a considerable loss of lift and a forward shift of the shock wave, and extends over the entire wing span.

Figure 12 (b) shows the nacelle effect at constant lift coefficient. It should be noted that an increase in angle of attack of 1.25 degrees was required to restore the loss in overall lift due to the nacelles in this case. The effect is shown as an increase in shock strength across the entire span for the nacelles-on configuration, a forward shift in shock location over most of the wing, and a rearward shift over the outboard 25 percent of wing span. In addition there is a shift in spanwise loading from inboard to outboard similar to but more pronounced than the effect at Mach 0.7 shown in Figure 11. The overall result of this effect is a loss in performance.

It is obvious that fuselage mounted nacelles dominate the performance of the inner wing and must therefore be also taken into account in the design of a wing.

In an effort to modify the inner wing to compensate for the nacelle effect, it was discovered that one cannot apply the rule, that "a wing-body combination that performs well by itself will also perform well in the presence of the nacelles". On the contrary, the modified wing that showed improved performance in the presence of the nacelles was worse than the original one when tested as a wing-body alone.

3.4 Flight Wing Pressure Survey

Two flight wing pressure surveys were conducted to collect data for comparison with wind tunnel test results.

The first survey was required for certification purposes to confirm the loads of the Challenger supercritical wing in flight, which were based on wind tunnel tests. The second pressure survey was conducted as part of an in-house development program after the aircraft was certified. In both those flight tests, chordwise pressure distributions were measured with an external flexible tubing and scanivalve installation as shown in Figure 13.

The first test using aircraft no. 3, provided pressure measurements at only three spanwise locations on the outboard wing. For the second test using aircraft no. 9, two more spanwise locations for pressure measurements were added at the inboard wing.

At each spanwise station a bank of plastic tubing of 0.096 inch (2.44 mm) inside diameter and 0.1875 inch (4.76 mm) outside diameter was installed on the upper and lower surface. There was one pressure orifice per tube, each spanwise station having a total of 33 orifices (tubes) on aircraft no. 3 and 20 orifices (tubes) on aircraft 9. The chordwise and spanwise pressure orifice locations on the aircraft were the same as on the wind tunnel model to permit direct comparison between flight and wind tunnel results.

Each bank of tubes was secured on the wing surface by means of a double-sided sticky tape after first covering the wing surface with an aluminum tape as shown in Section A-A of Figure 13. A sealant was used for aerodynamic fairing. The purpose of the aluminum tape was to provide quick and clean removal of the tubing after the test.

Three scanivalves were used on aircraft no. 3 and four on aircraft no. 9, each fitted with differential pressure transducers, to measure the wing pressures. The scanivalves were operated at 8 ports per second with one complete cycle of all 48 ports per scanivalve requiring 6 seconds.

In order to obtain an accurate measurement of the static pressure, aircraft no. 3 was fitted with a trailing cone system measuring the static pressure 124 ft. (38 m) behind the aircraft. Total pressure was provided by a nose boom mounted pitot-static system. The trailing cone static was used as a reference pressure on the scanivalves. On aircraft no. 9, the pilot's static was used as a reference pressure after the pilot's pitot-static system had been calibrated by Pacer and tower flyby tests.

Figure 14, 15 and 16 show photographs of the flexible tube installation on aircraft no. 3. Figure 14 shows the installation on the upper surface of the port wing. Figure 15 shows a close-up view of the outboard wing station at mid span of the aileron. Figure 16 shows the installation on the lower surface at the break of the wing.

The flight test points included at least three lift coefficients at each of Mach Numbers 0.7, 0.8 and 0.85, for which wind tunnel data were available.

3.5 Flight - Wind Tunnel Correlations

Both flight wing pressure surveys provided similar results. In this paper, only results from the second survey (aircraft no. 9) are presented because they include both the inboard and outboard wing.

Figure 17 shows a comparison of wing chordwise pressure distributions from flight and wind tunnel test at Mach 0.8 and a cruise lift coefficient at about 0.42. The wind tunnel test data were taken at a Reynolds Number of 3.77 million per mean aerodynamic chord with free transition on the wing. The flight Reynolds Number was about 12 million.

It can be seen that the flight test pressure distributions correlate well with the corresponding data from wind tunnel tests. There are however some noticeable differences at the root section (η = 0.135)and mid-aileron section (η = 0.85).

The irregular behaviour of the wind tunnel data near the leading edge of the root was found to be caused by model construction irregularities. Notice that the aircraft data in the same area are smooth. The higher suction peak of the flight test data near the leading edge of the mid-aileron section (η = 0.85) is due to a poor fairing of the external tubing installation. Finally, the slightly lower load on the aft part of the mid-aileron section is believed to have been caused by a 2 degree upward aileron deflection which was required to trim the aircraft during that flight.

An interesting result of these tests is a slightly more aft position of the shock wave in flight, indicating an improvement in aerodynamic performance relative to the wind tunnel data. This may be due to the fact that the model did not achieve the design twist distribution when tested at a Reynolds Number of 3.77 million.

Figure 18 shows a comparison between flight and wind tunnel spanwise loading distributions obtained by the integration of respective chordwise pressure distributions at Mach Number of 0.7 and 0.8, and C_L of 0.51 and 0.42 respectively. There is very good agreement between flight and wind tunnel data except at the root and mid-aileron stations where the disagreements reflect the differences in the test configurations discussed above.

4. C_{LMAX} CORRELATIONS

4.1 High Lift System Design

The design of the high-lift system was one of the earliest tasks. The objectives were to meet the required take-off and landing performance with a simple flap system and no leading edge device. The available space for a flap was a 27-percent chord trailing edge outboard and an average of 21-percent chord inboard.

A double-slotted flap with a fixed vane and slot was chosen for the outboard wing and an expanding type of vane-and-flap system inboard to increase the flap chord. The flaps were rotating around an external hinge. Figure 19 shows a cross-section of the outboard flap in cruise, take-off and landing positions together with the spoiler in the down position. At take-off it operates like a 20 percent chord single slotted flap.

The 2-D design and optimization of the flap and vane, including their relative position and gaps and overlaps for take-off and landing, were accomplished with the aid of MDRAG, a 2-D multi-element airfoil code developed at Canadair. MDRAG is a potential flow method combined with a boundary layer program. The potential flow method is based on the representation of the airfoil profiles by flat elements of constant vorticity distribution. A detailed description of the potential flow method is included in Ref. 5 and 6. The program provides the potential flow pressure distribution, the corrected lift coefficient due to boundary layer including small areas of separation, the drag coefficient and the transition and separation points. From separation point location versus angle of attack plots, one can estimate the angle at which stall occurs and therefore also the 2-D $C_{L_{max}}$, by using as a criterion a sudden change in forward movement of the separation point.

The estimated 2-D $C_{L_{max}}$ was then used as a basis in conjunction with DATCOM methods for the initial estimate of the full scale 3-D $C_{L_{max}}$.

A 2-D test was conducted at the NAE 6 x 9 foot Low Speed Tunnel using the Canadair 2-D Blowing Wall Facility. This facility, described in detail in Ref. 4, was designed to provide true 2-D test data for high lift systems. The purpose of this test was to verify theoretical 2-D flap design and to obtain data on spoiler characteristics. A total of only 80 hours of testing was used for these tests.

4.2 2-D Theory - Wind Tunnel Correlation

Figure 20 shows a comparison of the potential flow pressure distribution with 2-D wind tunnel data for 45 flap deflection near $C_{L_{max}}$. It can be seen that in spite of the small separation area (5 percent chord) at the flap trailing edge, the potential flow pressure distribution follows the viscous pressure distribution at somewhat lower level of suction on the top surfaces. The difference between theoretical and experimental data represents the effect of a thick boundary layer on these surfaces.

Figure 21 shows a comparison between theoretical and experimental data of 2-D lift coefficient versus angle of attack and $C_{L_{max}}$ predictions based on theoretical separation point location. Again, the prediction appears to be very good.

Because of the good agreement between 2-D theory and test, the initial estimate of full scale $C_{L_{max}}$ remained unchanged.

4.3 3-D High Lift Wind Tunnel Tests

The 3-D high lift wind tunnel tests were carried out with a 0.08 scale Challenger model at the NAE 6 x 9 foot low speed tunnel. It was realized from the beginning that this combination of scale and tunnel involved a risk due to a very low Reynolds Number but there was no alternative of using a larger tunnel and model at that time. The actual conditions were a Reynolds Number of 1.16 million per mean aerodynamic chord at Mach Number of 0.27. The flap-vane Reynolds Number under these conditions was below 100,000.

The initial tests conducted with a conventional transition trip showed a lower $C_{L_{max}}$ than predicted for the test conditions, and stalling of the flap at 45 degree deflection. The stalling of the flap at 45 degrees was assumed to be due to the very Reynolds Number of the vane, but there was no proof of it until flight testing.

An explanation for the low $C_{L_{max}}$ performance was found by testing the cruise configuration at Rockwell at a Reynolds Number of 2.16 million and a Mach Number of about 0.25. At these conditions $C_{L_{max}}$ was as expected.

An examination of Rockwell pressure distributions near the stall revealed that the problem at NAE was one of shock induced separation of the laminar boundary layer at the leading edge. Due to the blunt leading edge of the supercritical wing the pressure peaks occured forward of one percent chord with transition taking place at about one percent chord. At about mid-span of the wing leading edge, the local velocities became supercritical at a test Mach Number of 0.27 at NAE terminating with a shock that interfered with the laminar separation bubble causing it to spread over the outboard wing. This did not happen at Rockwell because at Mach 0.25 the flow was just about critical and the Reynolds Number sufficiently high to reduce the size of the bubble,thus allowing a higher angle of attack and $C_{L_{max}}$ to be achieved.

Based on the results of this investigation, the location of the upper surface transition trip for the NAE tests was moved forward from the 5-percent chord location and just below the leading edge (i.e. between stagnation point and pressure peak locations at high lifts). The lower surface trip was moved to 15 percent chord. With this trip configuration, $C_{L_{max}}$ increased by 0.2 over the initial test values.

The full scale 1-g $C_{L_{max}}$ was then obtained by applying corrections for Reynolds Number and Mach Number, based on DATCOM methods, to the NAE data with the new trip location.

4.4 Correlation with Flight Test Results

The natural stalling characteristics of the Challenger were predicted by an analysis of wind tunnel test results including pitching and rolling moments.

Flight tests showed that the stall is characterized by a sudden wing drop with no noticeable stall warning like a 'g' break or nose down moment. Recovery is accomplished by the pilot pushing the control column forward and applying power and opposite wing-down aileron.

Like most modern aircraft, the Challenger is equipped with a stall protection system consisting of a stick shaker stall warning system and a stick pusher system using angle of attack sensors and a dual channel computer. With this system the stall is characterized by a nose down moment as the stick pusher is operated at a lower angle of attack than for the natural stall.

For a correlation with wind tunnel results and prediction, it is necessary to use first the maximum lift coefficients obtained from natural stalls during flight test. According to the U.S. Federal Aviation Regulations, these are obtained by determining the minimum speed when entering the stall with a deceleration rate of 1 knot (1.85 km/hr) per second.

The $C_{L_{max}}$ obtained from such FAR stalls is higher than that corresponding to the 1-g condition, i.e. zero deceleration rate, of the wind tunnel test For this purpose the 1-g $C_{L_{max}}$ of the airplane was determined by extrapolating flight test data of various entry rates into the stall to zero deceleration rate.

Figure 22 shows FAR $C_{L_{max}}$ and 1-g $C_{L_{max}}$ from flight tests in comparison with predictions of 1-g $C_{L_{max}}$ based on wind tunnel tests, and 2-D theory and DATCOM respectively. In addition, the wind tunnel $C_{L_{max}}$ is presented to show the large gap between the model-scale and full-scale data in this case.

The agreement between flight and wind tunnel 1-g $C_{L_{max}}$ is quite good considering the large extrapolation of the wind tunnel data.

The prediction based on 2-D theory and DATCOM appears to overestimate $C_{L_{max}}$ when the flap is deflected, with the discrepancy increasing with flap angle. This is probably due to the inability of such a method to account for all three-dimensional effects and nacelle interference. Wind tunnel tests showed a loss of about 0.05 in $C_{L_{max}}$ due to the installation of the nacelles at a 40 degree flap deflection.

5. CORRELATION OF BUFFET BOUNDARY

The prediction of the buffet boundary was derived from an analysis of available wind tunnel data based on the principles established by Pearcey and Holder (Ref. 7 and 8).

According to Pearcey and Holder buffeting usually occurs when flow separation on a wing has a direct effect on the total loading. This means a change in wing circulation and therefore a change in mean trailing edge pressure. Therefore buffeting is indicated by a lift loss and a divergence of the mean trailing edge pressure compared with the linear variation with angle of attack for attached flow.

Based on these principles, kinks (defined by changes in slope) in the curves of C_L and C_M versus angle of attack were used as follows to estimate buffet boundaries for the high Mach Number range. The fist kink was used for buffet onset, the second kink for moderate buffet, and the third kink for heavy buffet. The wind tunnel data used were at a Reynolds Number of 6.7 million as compared with 10 million for full scale.

An analysis of trailing edge (100 percent chord) pressure data measured at a Reynolds Number of 3.75 million showed that at a given Mach Number separation occured first at a semi-span station of 0.675. The divergence of the trailing edge pressure of this station rather than that of the mean pressure was used to define buffet onset as an alternative method for high Mach Numbers.

For the low Mach Number range, the buffet boundary was taken to be that of $C_{L_{max}}$ derived from low speed wind tunnel tests with appropriate corrections for full scale.

Figure 23 shows the buffet boundary of the Challenger from flight tests in comparison with such predictions in terms of C_L versus Mach Number. Shown in this figure are the predicted areas of light, moderate and heavy buffet based on the method of kinks. In addition, the predicted buffet onset boundary based on trailing edge pressure divergence is shown as a solid line within the light buffet area.

The flight test data, shown by solid symbols, represent stalls characterized by wing drop. Pre-stall buffet occurred only at Mach Numbers of 0.35 and higher. The open symbols represent flight test data of buffet onset defined by an accelerometer reading of ±0.05 g at the airplane centre of gravity. This coincided also with the first perceptible buffet at the cockpit by the pilot.

The agreement between flight and prediction appears to be very good. The flight test data show buffet onset to occur rather above the predicted boundary, based on the first kink in the force data, and as high as the predicted moderate buffet boundary. The prediction based on trailing edge pressure divergence appears to represent the average of the scatter.

Figure 25 shows also that there is adequate separation between normal cruise conditions and buffet onset for maneuvers and gusts. The minimum margins are in the order of 0.05 in M and 0.5 g in C_L.

CONCLUDING REMARKS

The development of a modern transonic aircraft was accomplished in a remarkably short time by using (a) advanced aerodynamic computer methods as a design tool and (b) wind tunnel testing for configuration refinement and prediction of flight characteristics. This approach led also to a clean wing configuration requiring no modification or fixes, such as vortex generators and fences, to meet all certification requirements.

The examples presented here show that critical flight characteristics and wing pressure and load distributions are predicted well by wind tunnel tests provided the appropriate technique is used.

For models with supercritical wings it is best to test with free transition on the wing. The lowest Reynolds Number suggested for high speed tests with free transition is 5 million per mean aerodynamic chord for force data and 3.8 million for pressure data. For low speed tests for $C_{L_{max}}$ and stalling characteristics data, it is suggested to use a Reynolds Number of not less than 2 million with a Mach Number of 0.25.

Theoretical aerodynamic computer methods are valuable tools for analysis and design.

High lift systems can now be designed with the aid of a theoretical multi-element airfoil method saving considerable development in the tunnel. Subsonic panel methods show remarkable correlation with test data up to Mach 0.7 and are very useful in analyzing complete configurations in symmetric and asymmetric flight including combined rates of pitch, yaw and roll.

The Jameson isolated wing full potential flow transonic method was indispensable for the design of the Challenger wing. However, it proved to predict poorly the aerodynamic characteristics of the Challenger wing-body. A simple modification of this method using inputs from a panel method to account for the body effect was found to improve the correlation with test data.

Significant advances in the design and development of transonic configurations can be made by increasing the capability of full potential flow transonic methods to compute the flow-around complete configurations, including the effect of nacelle mass flow ratio, similar to current panel methods.

Finally the degree of correlation between prediction and flight can be significantly improved by using computational aerodynamic methods in combination with wind tunnel testing to interpret complex flow situations.

REFERENCES

1. Braslow, A.L. 'Use of Grit-Type Boundary-Layer Transition Trips on Wind Tunnel Models', NASA TN D-3579, September 1966.
2. Jameson, A. 'Interative Solution of Transonic Flows over Airfoils and Wings, Including Flows at Mach 1', Comm. Pure Appl. Math., Vol. 27, (1974) 283-309.
3. Jameson, A. and Caughey, D.A. 'Numerical Calculation of the Transonic Flow Past a Swept Wing', New York University, ERDA Report COO-3077-140, June 1977.
4. Boppe, C.W. and Aidala, P.V. 'Complex Configuration Analysis at Transonic Speeds', AGARD CP No. 285, 'Subsonic/Transonic Configuration Aerodynamics', May 1980.
5. Mavriplis, F. '*Aerodynamic Research in High Lift Systems*', *Canadian Aeronautics and Space* Journal, Vol. 17, No. 4, May 1971.
6. Mavriplis, F. 'Aerodynamic Prediction and Design Methods of Aircraft High Lift Systems', Proceedings of the Aerodynamics Seminar of Associate Committee on Aerodynamics of National Research Council of Canada, May 1974.
7. Pearcey, H.H. and Holder, D.W., 'Simple Methods for the Prediction of Wing Buffeting from Bubble Type Separation', NPL Aero Report 1024; ARC 23,884, 1962.
8. Pearcey, H.H. 'A Method for the Prediction of the Onset of Buffeting and other Separation Effects from Wind Tunnel Tests on Rigid Models'; AGARD Rep. 223, ARC Rep. 20,631, 1958.

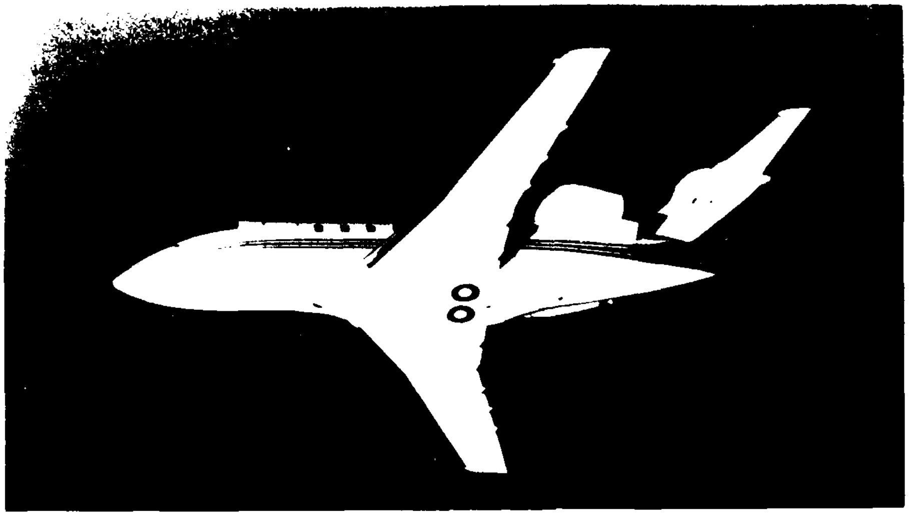

Figure 1. Canadair Challenger CL-600

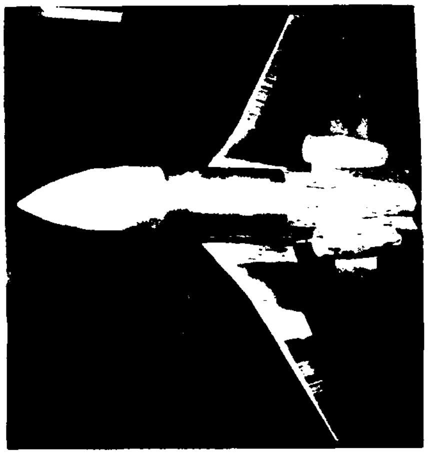

Figure 2.
0.04 Scale Wind Tunnel Model
Flow Visualization, M = 0.85

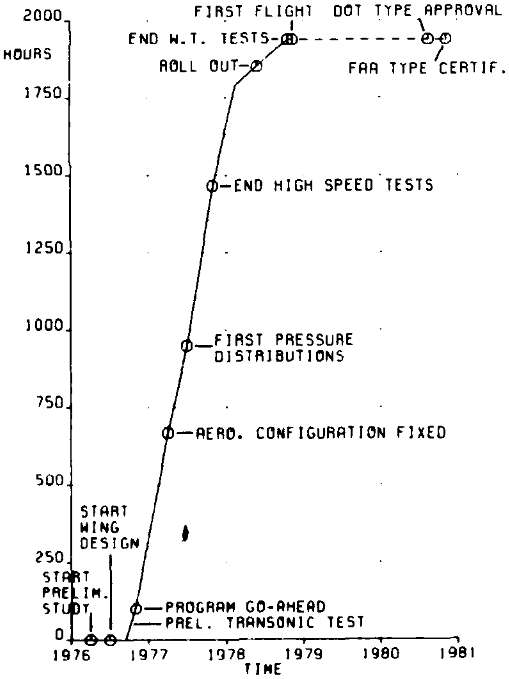

Figure 3. Wind Tunnel Test Program

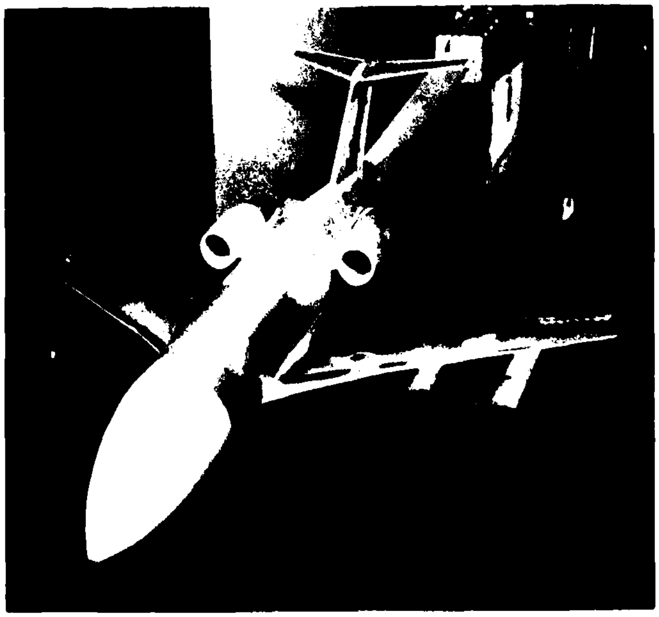

Figure 4. 0.07 Scale CL-600
at Rockwell Trisonic Wind Tunnel

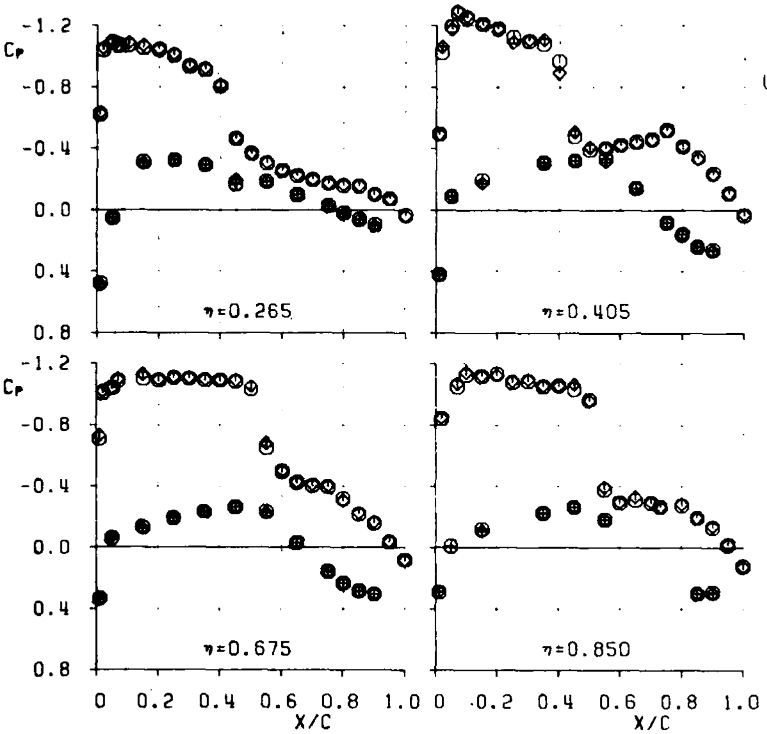

Figure 5.

Effect of Reynolds Number
on Wing Pressure Distributions
M = 0.8 $C_L \cong 0.5$

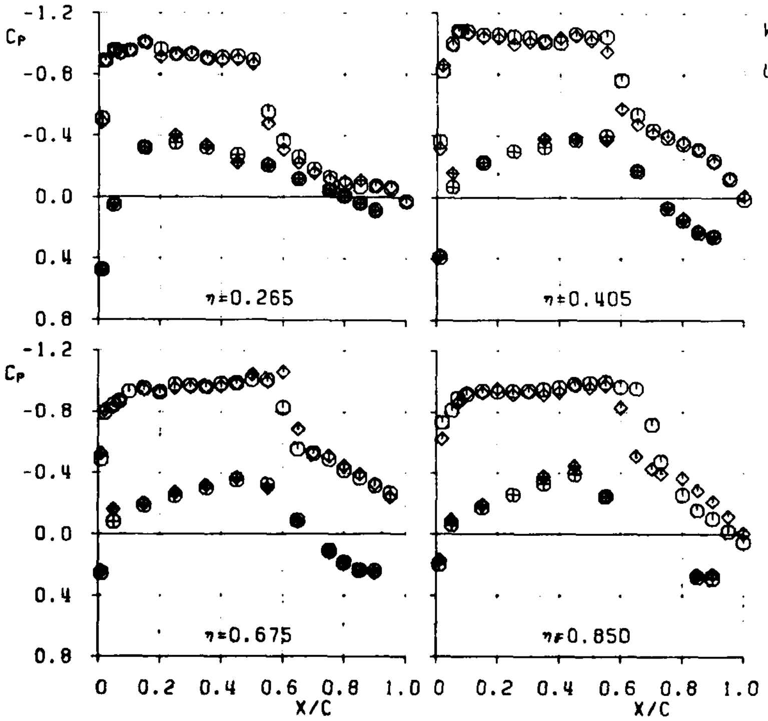

Figure 6.

Effect of Reynolds Number
on Wing Pressure Distributions
M = 0.85 $C_L \cong 0.5$

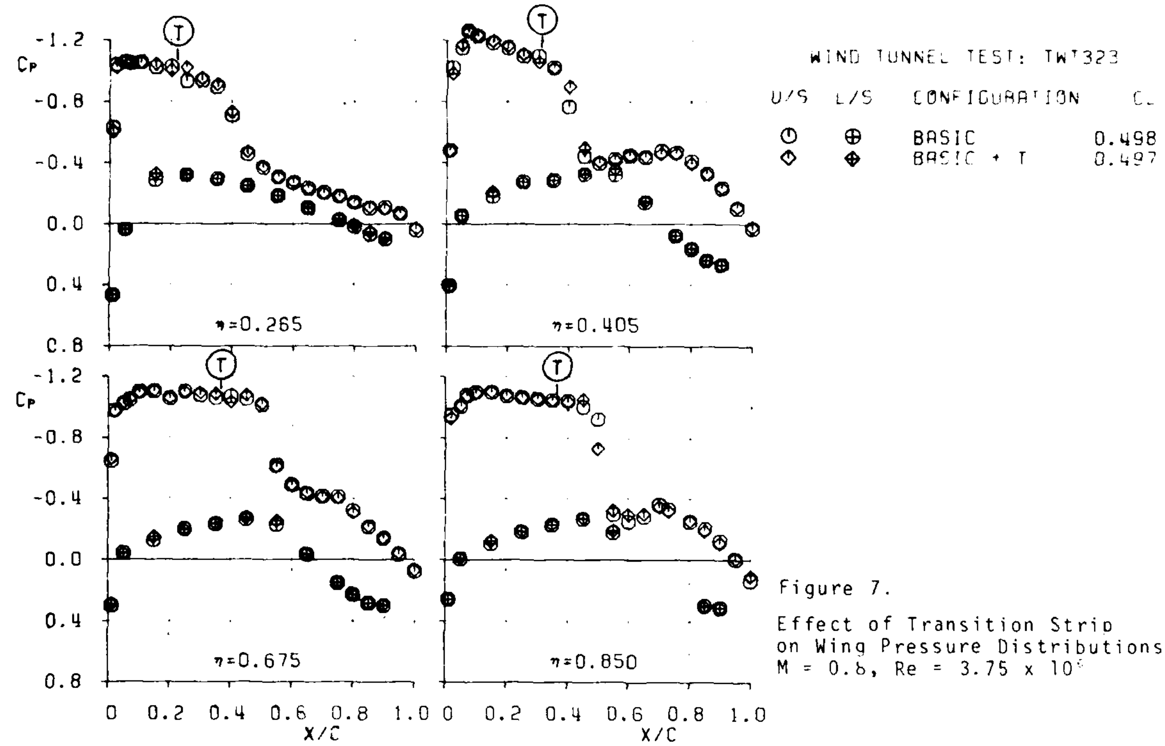

Figure 7.

Effect of Transition Strip on Wing Pressure Distributions M = 0.8, Re = 3.75 x 10^6

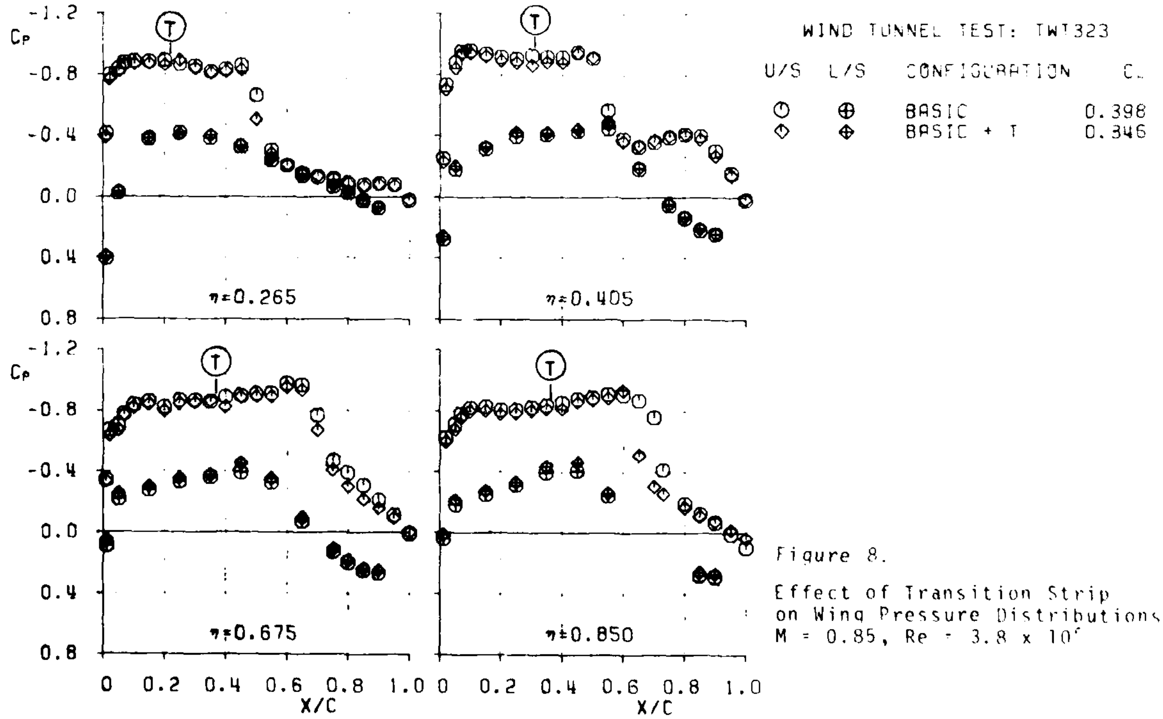

Figure 8.

Effect of Transition Strip on Wing Pressure Distributions M = 0.85, Re = 3.8 x 10^6

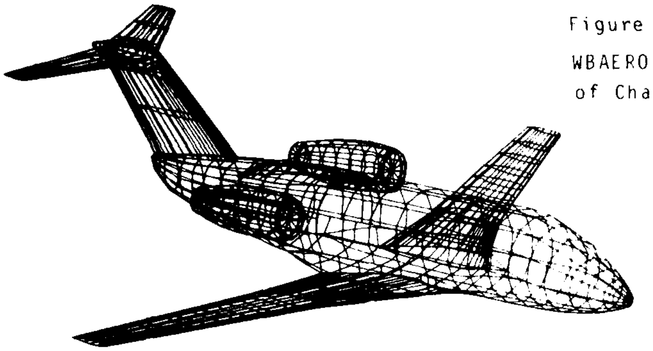

Figure 9.
WBAERO Panel Representation of Challenger CL-600

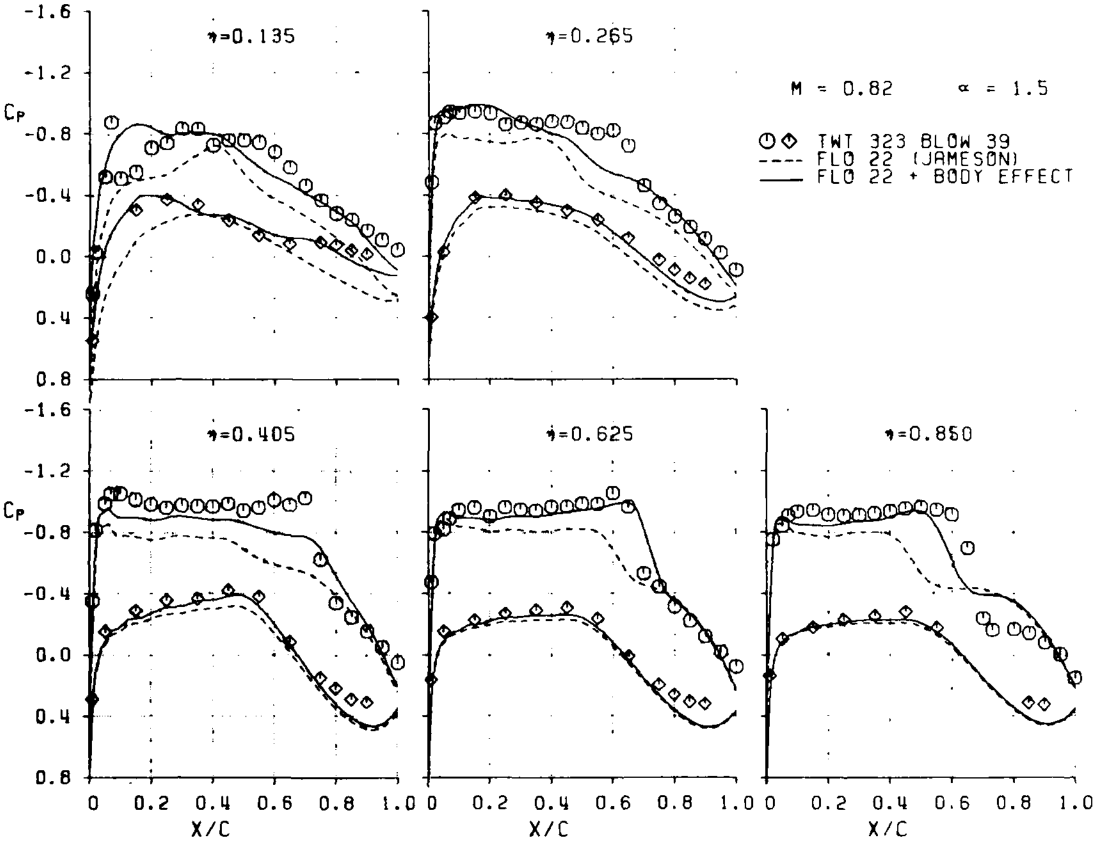

Figure 10. Effect of Body on Wing Pressure Distribution Theory (FLO 22) versus Wind Tunnel

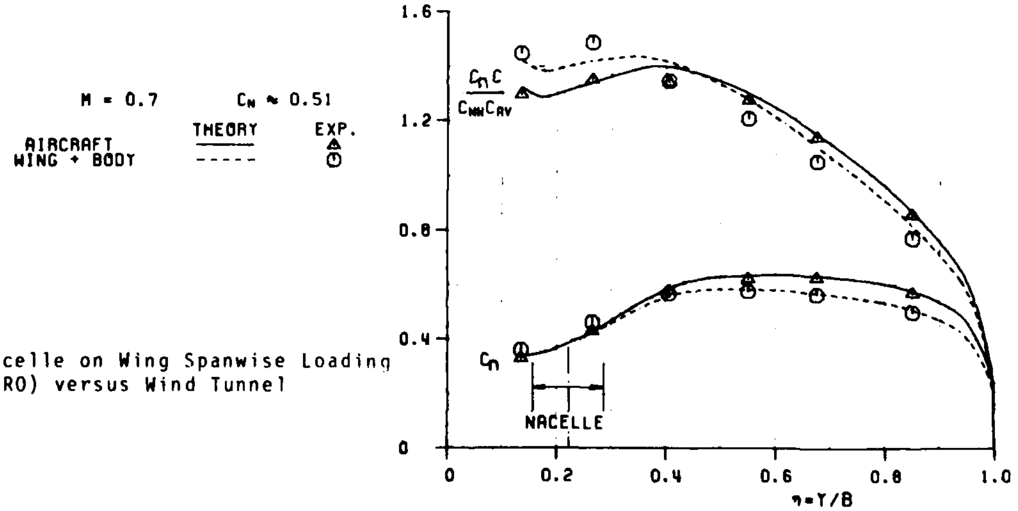

Figure 11.
Effect of Nacelle on Wing Spanwise Loading
Theory (WBAERO) versus Wind Tunnel

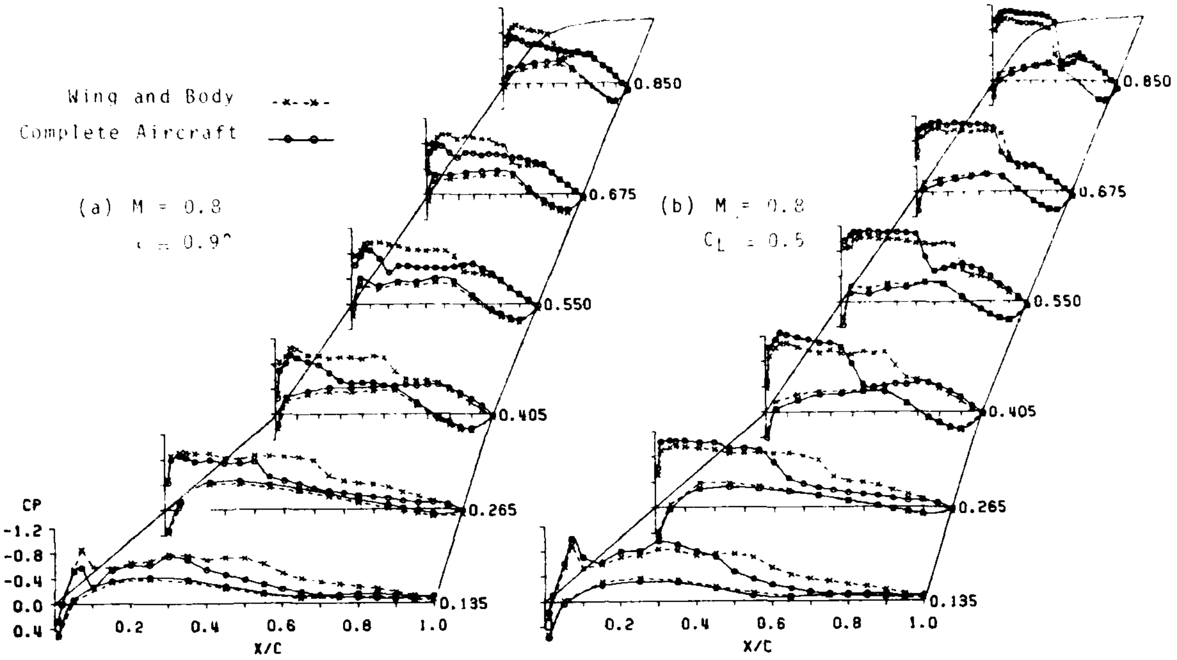

Figure 12. Nacelle Interference on Wing Pressure Distributions

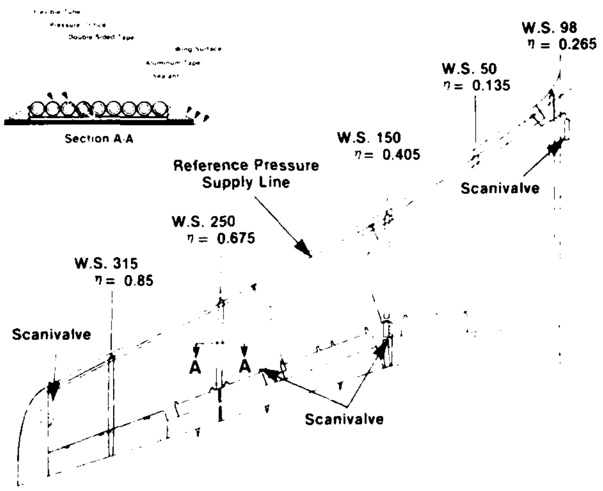
Flexible Tube
Pressure Orifice
Double Sided Tape
Wing Surface
Aluminum Tape
Sealant
Section A-A
W.S. 98
η = 0.265
W.S. 50
η = 0.135
W.S. 150
η = 0.405
Reference Pressure Supply Line
Scanivalve
W.S. 250
η = 0.675
W.S. 315
η = 0.85
Scanivalve
A
A
Scanivalve

Figure 13.
Flight Wing Pressure Survey
External Flexible Tubing Installation

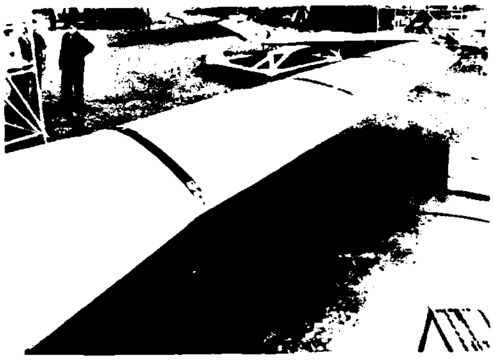

Figure 14.
Wing Pressure Tubing Installation

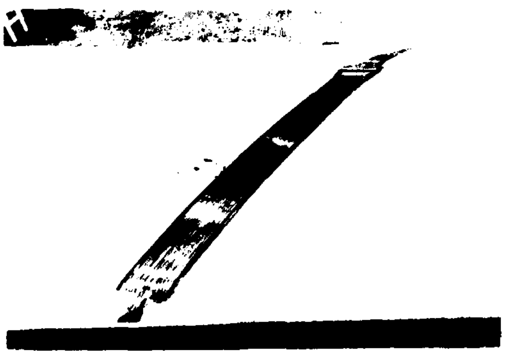

Figure 15.
Upper Surface Pressure Tubing W.S. 315

Figure 16.
Lower Surface Pressure Tubing W.S. 150

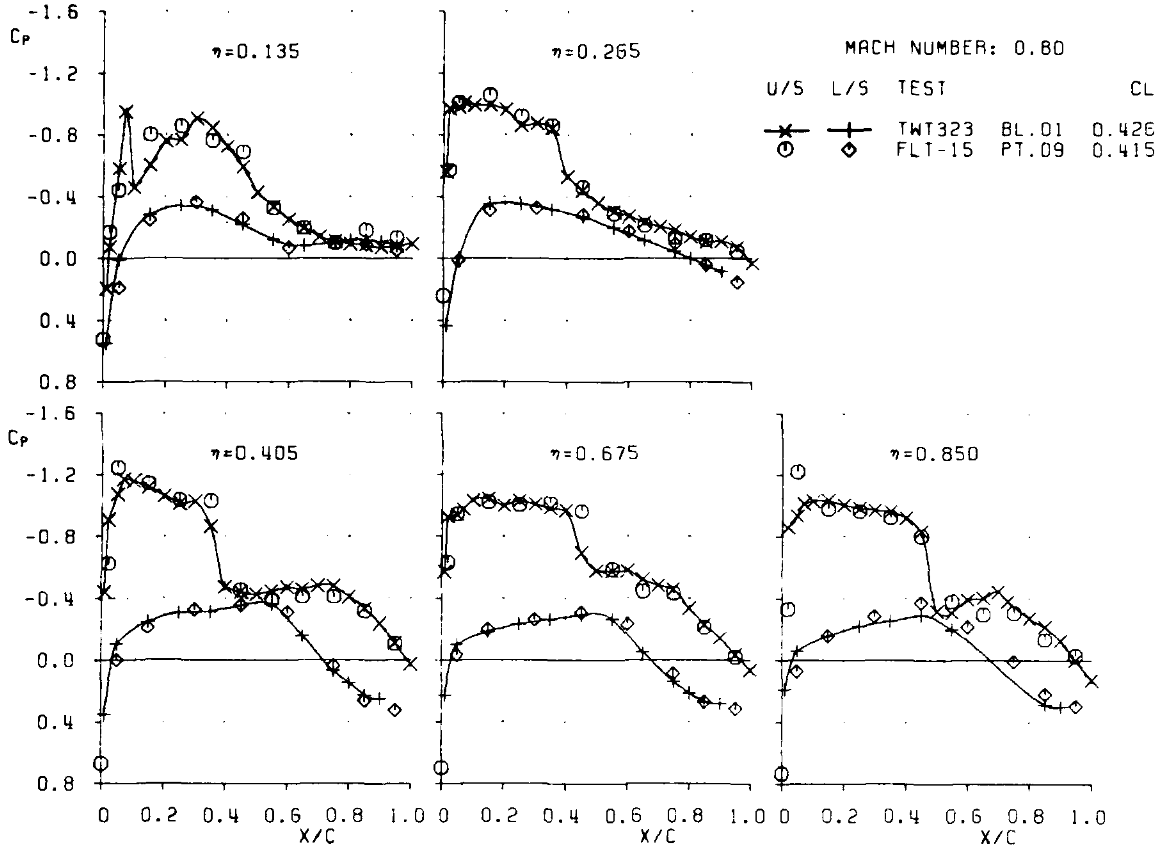

Figure 17. Wing Pressure Distributions Flight versus Wind Tunnel

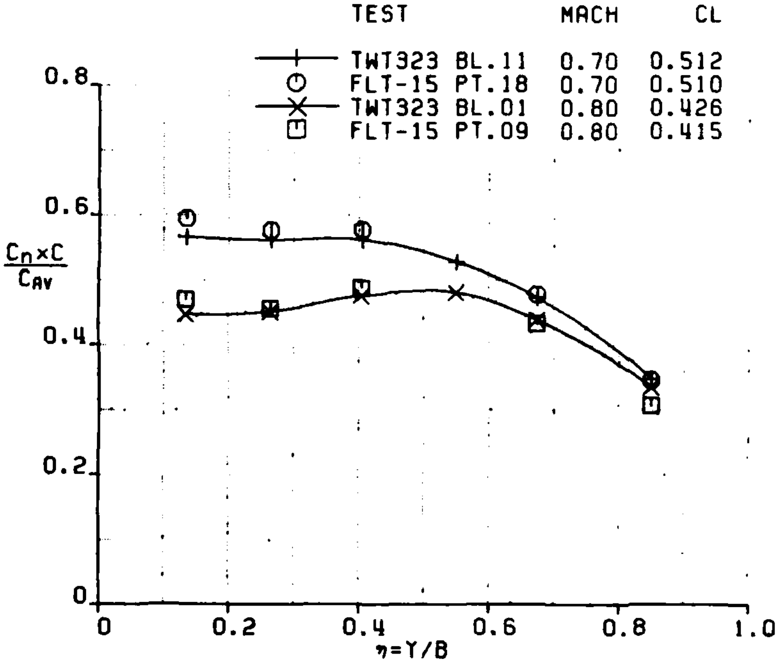

Figure 18. Wing Spanwise Load Distributions Flight versus Wind Tunnel

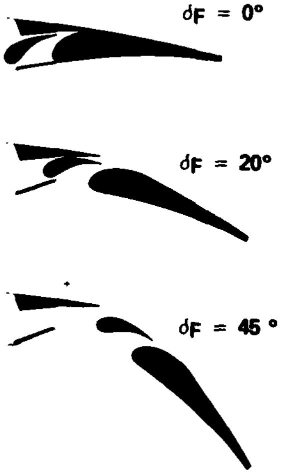

Figure 19. Outboard Flap/Spoiler Configuration

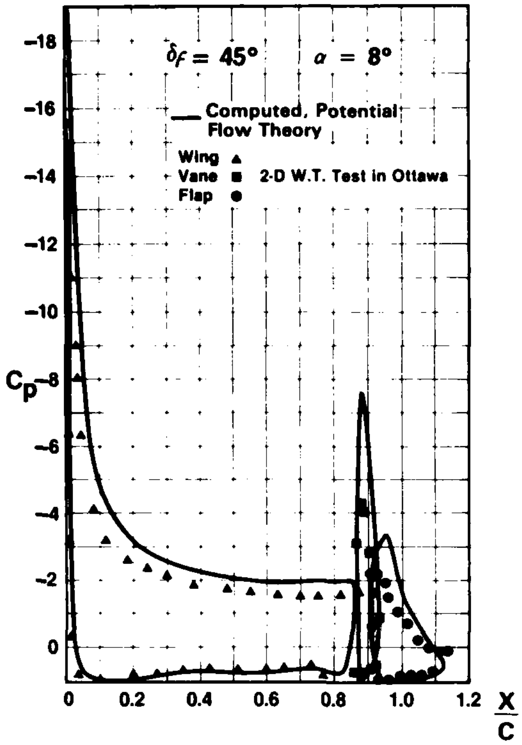

Figure 20. 2-D Pressure Distribution
of Outboard Airfoil Section
with Double Slotted Flap
Theory versus Experiment

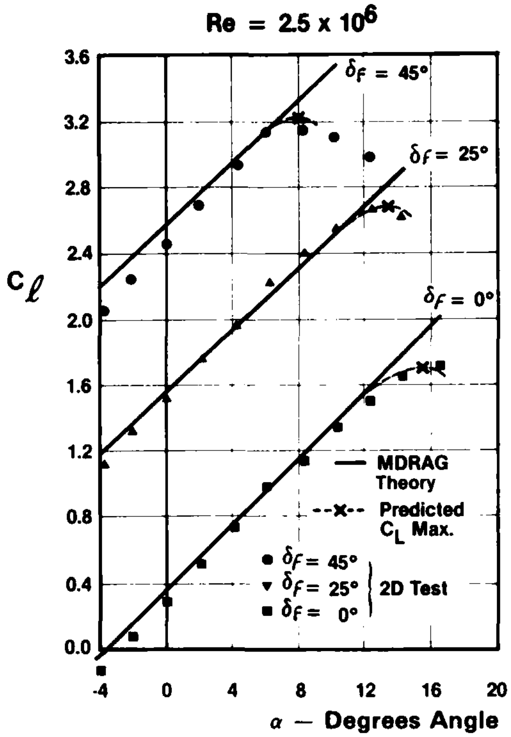

Figure 21. 2-D Lift Curves
of Outboard Airfoil Section
with Double Slotted Flap
Prediction versus Experiment

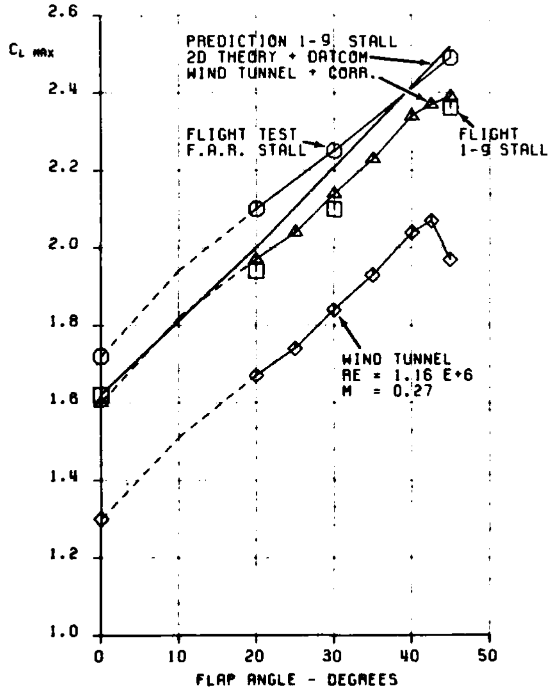

Figure 22. Maximum Lift Coefficients
Flight versus Prediction

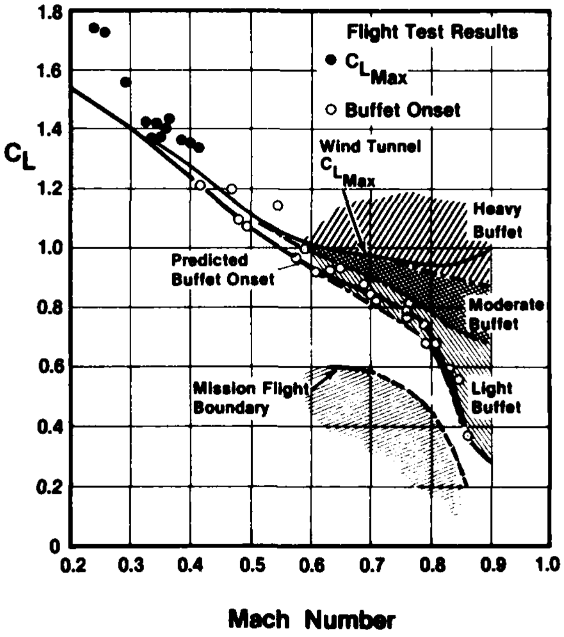

Figure 23. Buffet Boundary
Flight versus Prediction

LESSONS FROM TORNADO AFTERBODY DEVELOPMENT

by
D C Leyland
Deputy Chief Aerodynamicist
British Aerospace PLC
Warton Division
Preston PR4 1AX
England

SUMMARY

The wind tunnel model testing programme associated with Tornado aircraft design included successful development of a new afterbody test rig, which showed the benefit of measuring airframe axial force separately from nozzle forces and allowed detailed configuration development for minimum drag.

Flight testing of the aircraft showed good agreement with drag prediction but handling characteristics under certain conditions were different from predictions derived from full-model tests, as a consequence of relatively minor differences in afterbody representation. Flight and model investigations led to development of a satisfactory configuration and to conclusions as to requirements for future model test programmes.

Subsequent to the flight programme the rare opportunity was taken to compare flight and model test data by arranging additional afterbody model tests of geometric changes made during the flight programme. There was reasonably good agreement between results and, again, conclusions reached as to the requirements for future model and flight testing. Specifically, the introduction of high frequency response pressure instrumentation is proposed.

1. INTRODUCTION

The Tornado (Fig.1) was designed by the joint companies of Panavia (Aeritalia, British Aerospace and Messerschmitt Bolkow Blohm) to meet varied Italian, British and German air force requirements and was originally known as the MRCA (Multi-role combat aircraft). There was particular emphasis, however, on high speed low altitude flight where zero lift drag is dominant and therefore care needed to keep afterbody drag to a minimum. Afterbody model testing was consequently given some priority and early tests showed the initial layout to be a satisfactory configuration. In detailed engineering design there were changes made because of constraints set by the requirements for thrust reversers and for a minimum length fuselage. Second stage model testing showed a resulting increase in drag and re-definition of a satisfactory afterbody by model testing followed. Build time-scales did not allow incorporation of modifications until the sixth prototype and consequently early flight testing took place with a substandard afterbody. Afterbody drag was increased, as indicated by the model tests, but there was also a reduction in directional stability, particularly at high subsonic mach numbers. The modified sixth prototype proved to have reduced drag and increased stability but flight development was continued to further improve handling characteristics and, in the later stages, to reduce pilot-perceived vibration to a low level.

Some wind tunnel testing paralleled the flight testing but the eventual production configuration was developed on a prototype aircraft. It was later arranged, through a UK Government funded research programme, for retrospective model tests to be made of configurations for which flight data was available but which had not been included in previous model test series. There is therefore now the rare opportunity for comparing flight and model afterbody test data, and it is possible from the experience of the testing to draw clear conclusions as to procedures that should be adopted in future development programmes.

2. TORNADO AFTERBODY DESIGN

In conjunction with Turbo-Union, and based on test data, a translating shroud nozzle was chosen for the RB199 engine for Tornado. Zero base nozzles did not offer a net benefit when installation and weight penalties were taken into account, and would have given major difficulties for incorporation of the required thrust reversers. Convergent - divergent nozzles would have given too large a penalty in subsonic/transonic flight to justify the benefits at high mach number, bearing in mind that RB199 engine overall pressure ratio is relatively low and that a significant proportion of the underexpanded convergent nozzle thrust is in fact recovered on the afterbody.

Afterbody drag is primarily a function of base area and the RB199 nozzle minimises shroud base area by enveloping the operating rollers in local external fairings (Fig. 2). Additional base area is introduced, however, because of the thrust reverser operating mechanism and because of limits on the steepness of closure of the upper and lower gullies to avoid flow separation.

3. MODEL TESTING

First tests, arranged through MBB on a model at Boeing, confirmed the choice of nozzle design and nozzle separation. Tests by MBB at ARA Bedford produced basic transonic drag data but afterbody development was undertaken on the BAe twin sting afterbody rig, with transonic testing at ARA Bedford and supersonic testing in the 1.2m blow-down tunnel at Warton. The rig (Fig.3) provides independent measurements of afterbody force, nozzle thrust and combined thrust-minus-drag; the afterbody is mounted separately from the nozzles which are 'earthed' through a part of the rig's strain gauge balance.

A number of test phases were completed and care was taken to repeat a datum case for each phase. A consequence is that it is possible to check back on repeatability (Fig.4), which is probably a better measure of the quality of a rig than estimated uncertainty. It is gratifying that it is possible with this rig to discriminate reliably drag differences within 0.1 sq.ft.Do/q full scale.

4. WIND TUNNEL AFTERBODY DRAG MEASUREMENTS

Results of model drag measurements in Fig.5 show the notable difference found for the basic prototype configuration compared with the level predicted for the initial design based on early tests,changes in local lines having been made in design development. The reference model is an afterbody representative of the complete model which was used for a total aircraft drag synthesis. Stage 2 was an interim modification made to a prototype aircraft to modify handling qualities; a large base area resulted and the effect on drag is very evident. The modified prototype configuration was developed in the tunnel by eliminating areas of flow separation.

The separation (Fig. 6) had arisen on the basic prototype because detailed development of the spine and boat-tail lines had led to excessive diffusion of local area in the upper gully. Then, following improvement in the lines, it was found in the model tests that the high base pressure (positive Cp) developed by the general afterbody flow caused reverse flow in the centre base which triggered flow separation at the front of the base cavity (Fig. 7). In consequence, seals were fitted to inboard edges of the thrust reverser buckets for the modified prototype (P06), and later were also specified for the leading edges of the buckets to prevent outflow of air pressurised in the nozzle shroud and hence under the buckets.

It is evident that adequate modelling of afterbody detail must be provided in model testing and care taken to arrange an early re-test of the model if design changes are made following the basic configuration development.

5. FLIGHT TEST AFTERBODY MEASUREMENT

Special effort was made during the Tornado flight development programme to obtain best possible measurements of aircraft drag. A joint Panavia/Turbo Union working group defined procedures, altitude cell calibrated engines were used and particular care was taken in monitoring engine and aircraft testing. The recommendations made by a UK study group and published in AGARDograph 237 were largely based on Tornado planning and the success achieved proves them well justified.

Comparisons of afterbody drag measurements are limited but within the general accuracy there is broad agreement (Fig 8), especially when correction is made for the effect of imperfect representation of the base cavity on the model.

To assess the effect on drag of afterbody changes made in flight development a higher order of accuracy is required and use has been made of a base pressure correlation (Fig 9) derived from the various phases of Tornado afterbody model testing. It is not a universally applicable correlation but data available from other afterbody testing show very similar gradients and scatter bands. It would be interesting to know whether other test establishments have found and used such a correlation.

6. PROTOTYPE AIRCRAFT FLIGHT EXPERIENCE

The flow separation that had been shown to give increased drag for basic prototype aircraft was found in flight testing to also affect directional stability, the separation becoming asymmetric in sideslip (Fig.10) and reducing fin effectiveness (Fig.11). To restore stability for certain development flying the upper gully was filled on particular aircraft (Stage 2, Fig.13) as far aft as the thrust reverser bucket leading edges. That limit was necessary to allow bucket operation. A large base area resulted but the consequent higher drag was acceptable for test flying.

The design data set level of stability had been predicted from the results of tests on complete models. The models were sting supported and with some consequent distortion of the afterbody were evidently not sufficiently representative of the basic prototype configuration. It was therefore decided to re-test a model with a reduced sting and gullys introduced on the afterbody. The corrected result is shown in Fig.11 and, though not fully matched, the flight result is largely predicted. Obviously the need is indicated for proper afterbody representation in any future complete-model testing, at least as a check test for odd behaviour. If results are satisfactory then afterbody distortion, normally necessary for a flow-through model, can then probably be accepted.

Further model testing showed that some gully filling, together with a wide spine (Fig.14), could be a satisfactory configuration, and from flight testing, with the addition of vortex generators, directional stability was restored almost to original prediction (Fig.11). This solution was not desirable, however, because some variable geometry of the wide spine would be necessary to allow thrust reverser bucket operation. Flight testing therefore continued to seek a narrow spine solution. The layout of Fig. 15 was eventually developed,with the spine being narrow enough to allow bucket opening and certain vortex generators shown to be not necessary.

In the final stages of development the standard of the afterbody was judged in terms of pilot-perceived vibration. With flow separation obviously present it is not surprising that vibration was felt, but some still remained when flow separation was apparently suppressed, drag reduced and directional stability restored. It is hypothesised that with high base pressure developed there is feed forward of base pressure oscillation onto the afterbody boat-tail, not into a separated flow region, which could not be seen, but into a very thick boundary layer. The final solution for the production aircraft was the introduction in the upper gullys of part cones, which proved to be a very powerful means of reducing the vibration (Fig.16). There was little effect on drag, although base pressure was reduced, and a very satisfactory configuration was developed with drag close to that originally predicted (Fig.17).

7. FLIGHT TO WIND TUNNEL COMPARISONS

The aircraft configurations that were included in the wind tunnel research programme are indicated in Figs. 18 and 19, some variations in lower gully lines being involved as well as the filling of the upper gulley and addition of part cones. The individual arguments for each change are not relevant here but comparisons of results in Fig.20 are of interest. Drag increments from the datum (modified prototype) configuration are shown in the first row and there is a rough correlation with the measured base pressures; high Cp means low drag. There is reasonable agreement in base pressures between flight test and wind tunnel but with some dependence on configuration. There are indications (e.g. configuration 9) that discrepancies are most likely when pressure gradients exist across the base and imperfections in representation of base geometry on the model becomes significant. The upper and lower base tappings were at end of boat-tail, centre-base at the front of the recessed base.

Examples of boat-tail pressure distributions in Figs. 21 and 22 show fair agreement, but the information was generally of limited use. Where it was thought that some boat-tail separation was occurring it did not show in the usual way in the pressure distribution and hence came the hypothesis that certain characteristics were more related to a thick rather than to a separated boundary layer.

More pressure instrumentation would have allowed better assessment of configurations and fuller understanding of flow behaviour but in itself would not necessarily have given a shorter development programme. The flow is very complex and the increments involved are really quite small.

The major figure-of-merit in final development was pilot-perceived vibration and, given a Cooper type rating or measured by a cockpit accelerometer, it was used in deriving the production configuration. In the most recent model tests high response transducers have been connected to afterbody and base pressure tappings and results show a gratifying correlation with cockpit buffet. Fig.23 shows results for configurations at the start and end of the afterbody flight development programme, with buffet significantly reduced and yet base pressure increased, meaning drag reduced.It is thought that more use should be made of unsteady pressure measurement in afterbody testing, and the author would be pleased to hear from anyone who has any experience of the technique in this context.

Finally, it is interesting to see the afterbody development in terms of the afterbody drag to base pressure correlation. Fig 24 shows that, given the more comprehensive measurements available from the concluding research programme, there is a better correlation if a mean of upper and lower base pressures is used rather than a single centre base pressure. The scatter band is still as originally determined and it is notable that the production configuration lies at the lowest level. The modifications made to minimise vibration, maybe not surprisingly, also give minimum drag for that basic afterbody layout.

8. CONCLUSIONS

Experiece of Tornado afterbody development showed that:

1. Optimisation for drag can be achieved by afterbody model wind tunnel testing using the earthed nozzle technique.

2. Model drag measurements appear to be substantiated by flight drag measurements, within the accuracy of the flight data.

3. Wind tunnel and flight-measured pressures broadly agreed. Significant differences were probably due to differences in base geometry representation.

4. A correlation of drag with base pressure, obtained from model tests, gives a good monitor of drag changes in flight development.

5. Boat-tail pressures did not prove particularly useful, though model and aircraft data agreed reasonably well.

6. Major effects on drag or stability can be related to flow separation but the thick boundary layer at the end of the afterbody can give characteristics akin to flow separation.

7. Part cones fitted in boat-tail gullys proved to be a very good means for reducing vibration to low levels.

8. Vibration is a good measure of flow quality and lowest vibration gave lowest drag for a given basic geometry.

For a future programme it is concluded that:

1. Model testing for drag needs special care and repeated datum cases must be planned.

2. Detail must be well represented on the model, including any possible flow paths from the base.

3. Design modifications should be avoided subsequent to the model development programme; small changes can have large effects.

4. Matched pressure tappings on the model and the aircraft are required.

5. A check of stability derivatives is required from a complete model with a representative afterbody geometry, before testing with a distorted afterbody to allow through-flow.

6. Optimisation for stability may require flight development.

7. High response pressure instrumentation in critical regions is recommended for future wind tunnel tests and for flight development.

ACKNOWLEDGEMENT

The author acknowledges the contribution made by many members of the design and test departments of BAe (Warton) to the successful development of the Tornado afterbody and is particularly indebted to Alan Vint and Mike Briers of the Aerodynamics Department who were responsible, in succession, for the afterbody model testing and analysis. The conclusions are, however, the personal views of the author.

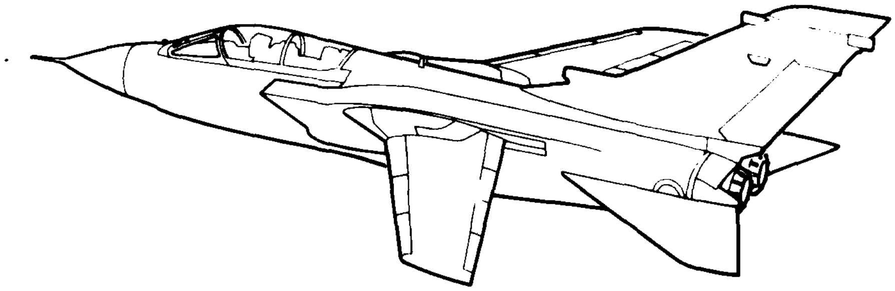

FIG 1: TORNADO

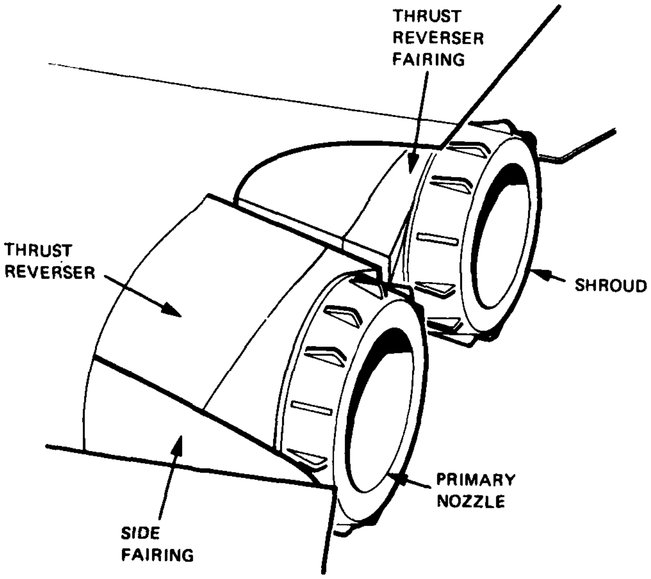
THRUST
REVERSER
FAIRING
THRUST
REVERSER
SHROUD
PRIMARY
NOZZLE
SIDE
FAIRING

FIG 2: PROTOTYPE AFTERBODY

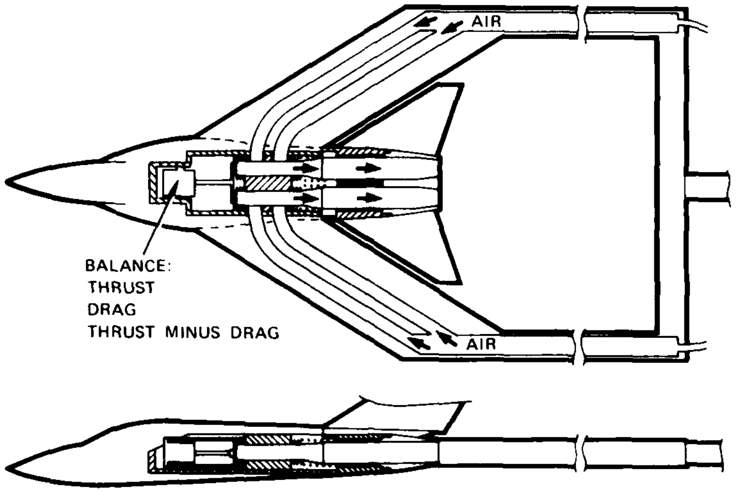
AIR
BALANCE:
THRUST
DRAG
THRUST MINUS DRAG
AIR

FIG 3: TORNADO AFTERBODY MODEL

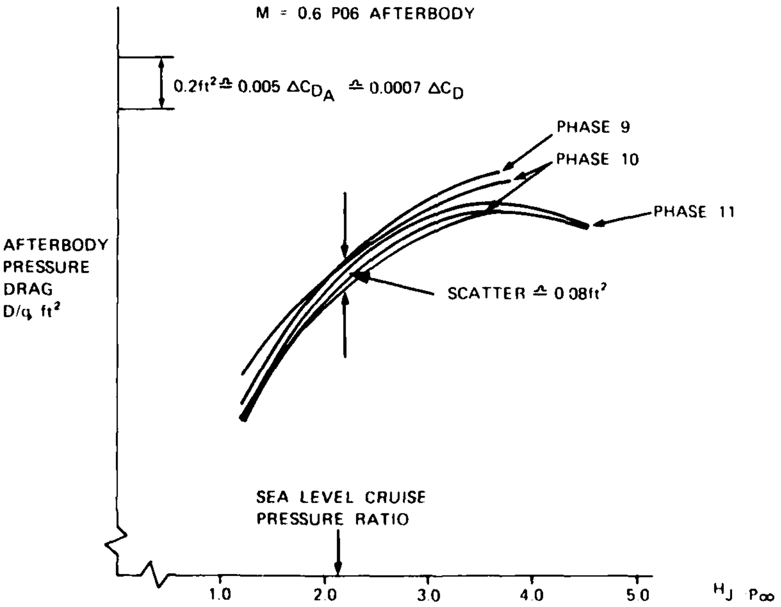

FIG 4: AFTERBODY RIG R32 PHASE TO PHASE REPEATABILITY

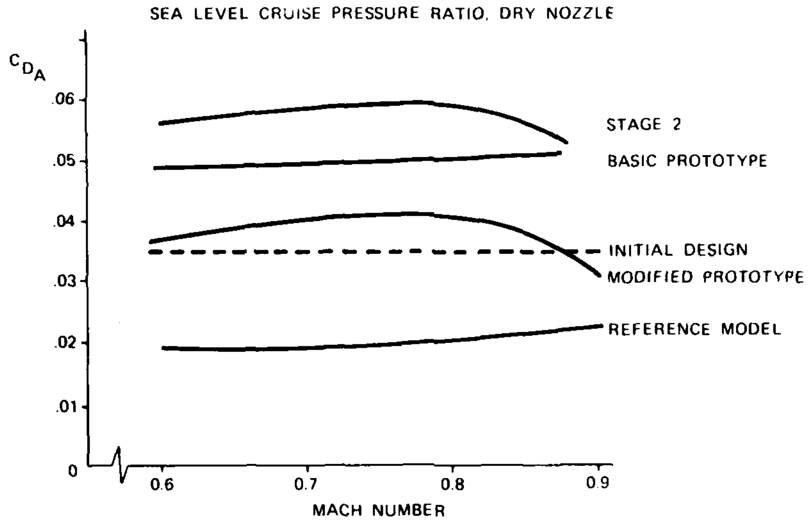

FIG 5: TORNADO AFTERBODY DRAG IN MODEL TEST DEVELOPMENT

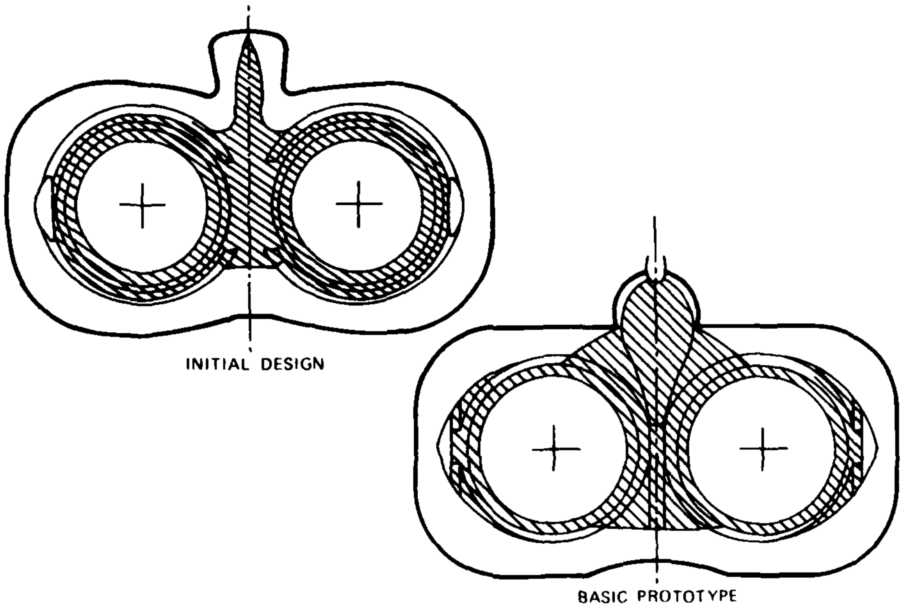
INITIAL DESIGN
BASIC PROTOTYPE

FIG 6: AFTERBODY SEPARATED FLOW

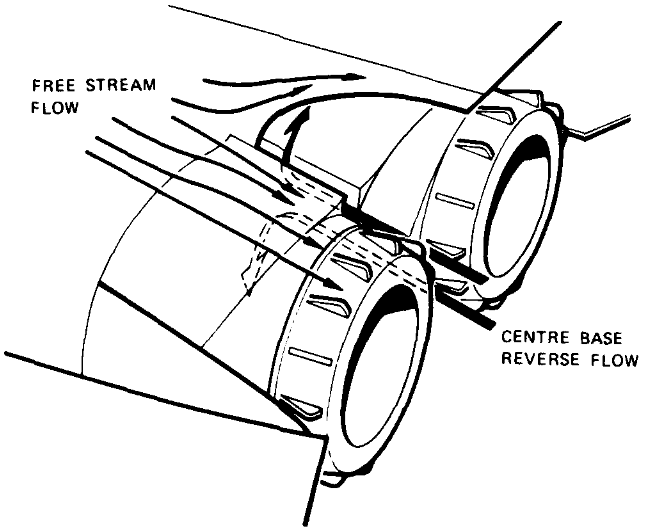
FREE STREAM
FLOW
CENTRE BASE
REVERSE FLOW

FIG 7: AFTERBODY FLOW WITHOUT SEALS

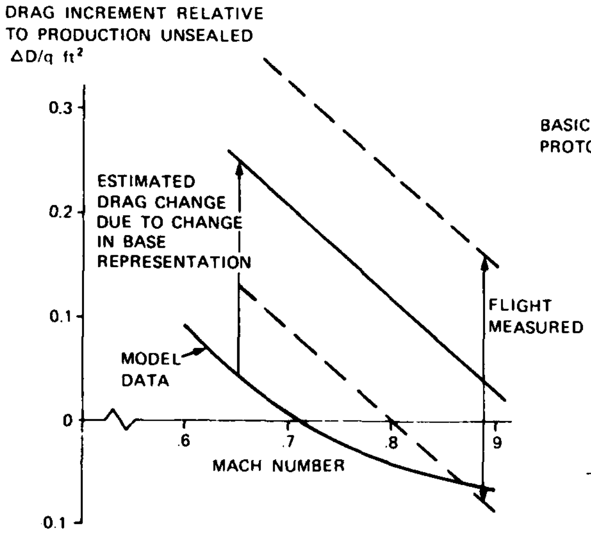

FIG 8: COMPARISON OF WIND TUNNEL AND FLIGHT DRAG INCREMENTS

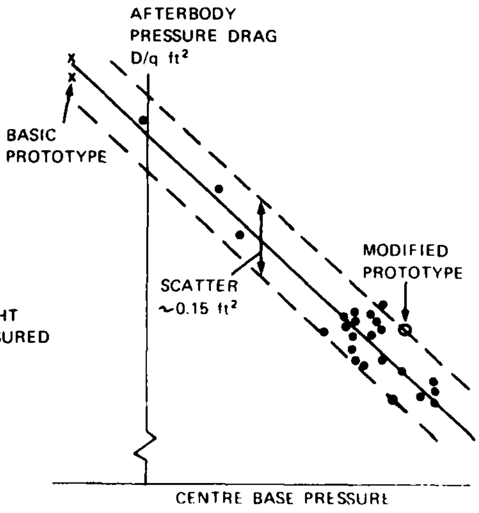

FIG 9 CORRELATION OF AFTERBODY PRESSURE DRAG WITH CENTRE BASE PRESSURE

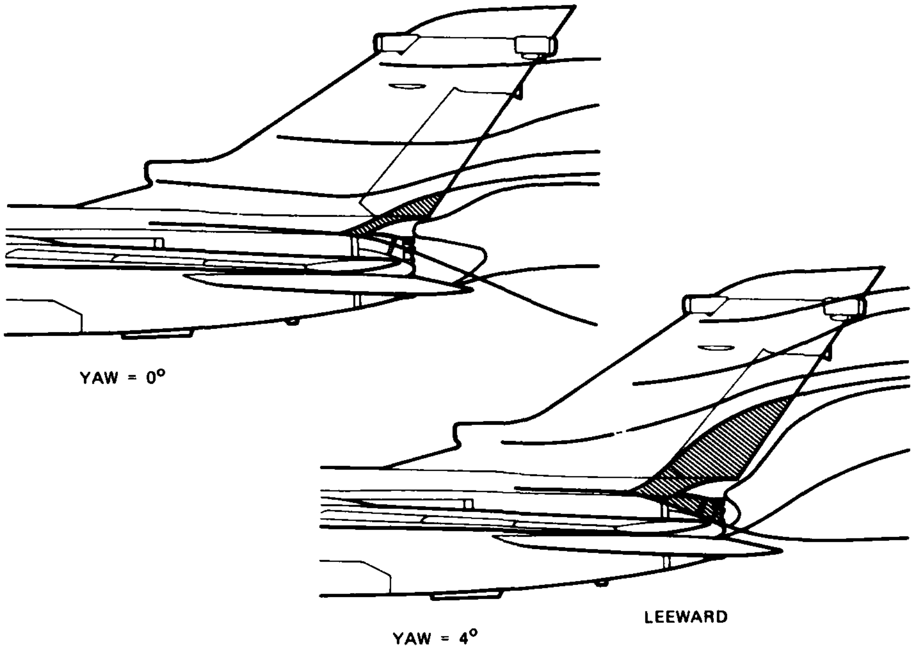
YAW = 0°
LEEWARD
YAW = 4°

FIG 10: AFTERBODY FLOW IN SIDESLIP

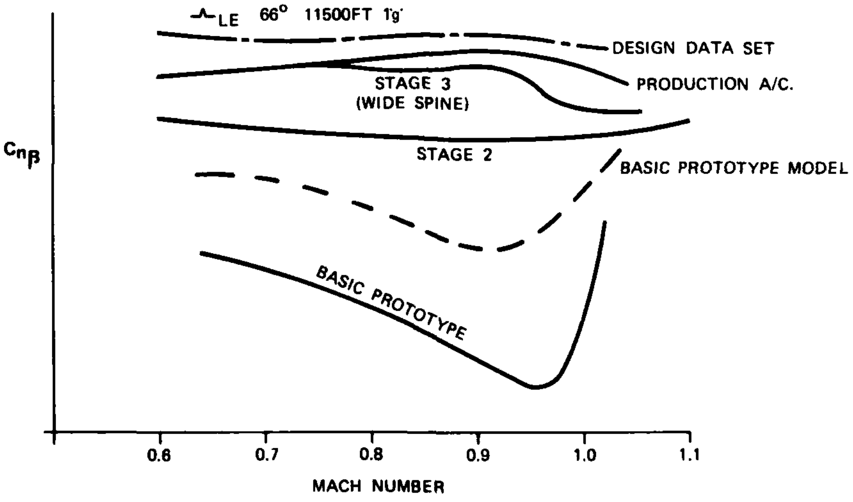

FIG 11: TORNADO DIRECTIONAL STABILITY

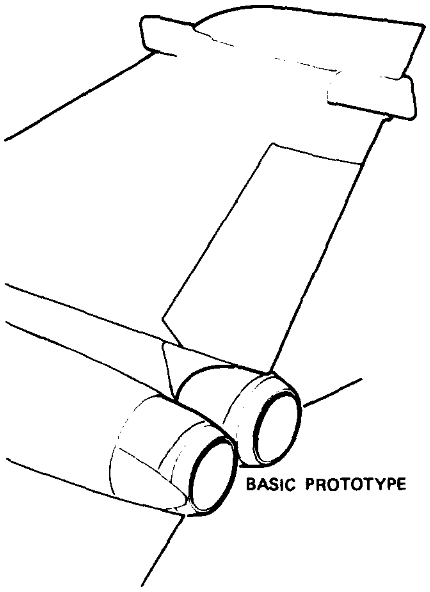
BASIC PROTOTYPE

FIG 12

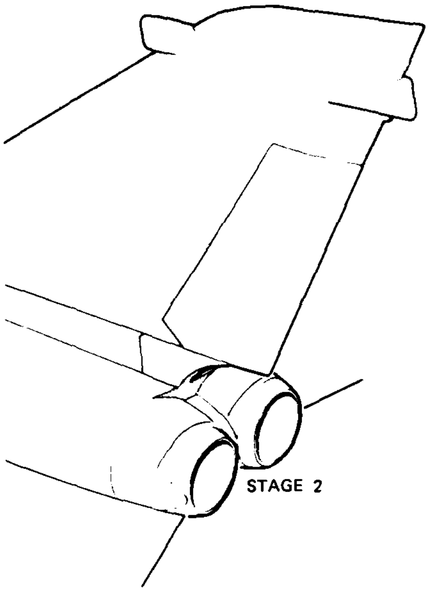

FIG 13

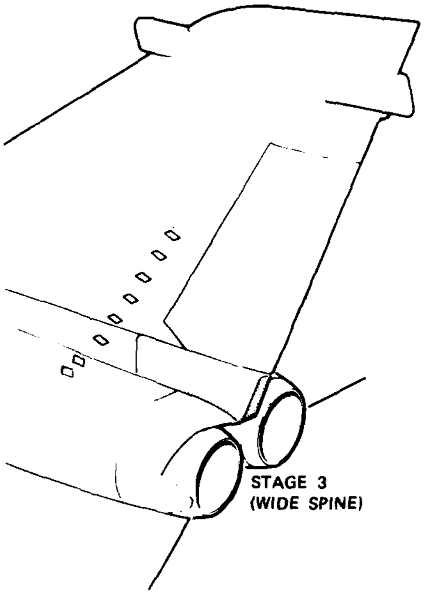
STAGE 3
(WIDE SPINE)

FIG 14

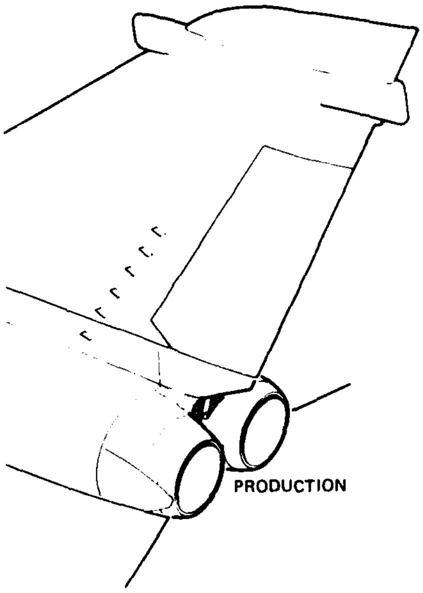
PRODUCTION

FIG 15

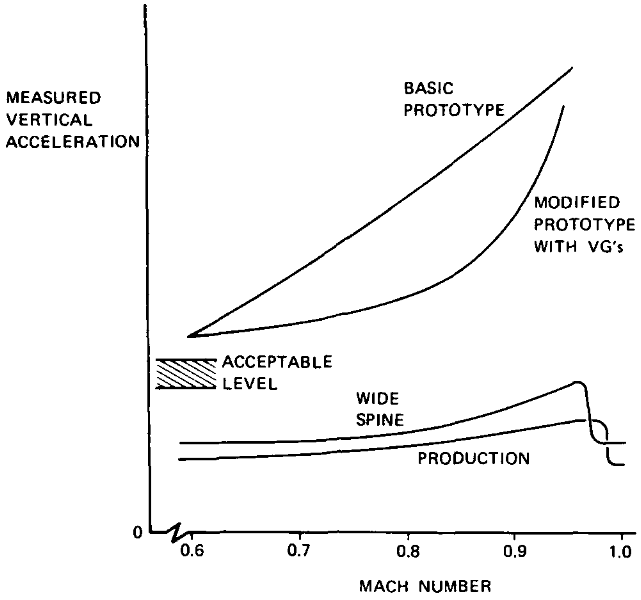

FIG 16: EFFECTS OF REAR FUSELAGE MODIFICATION ON COCKPIT VIBRATION

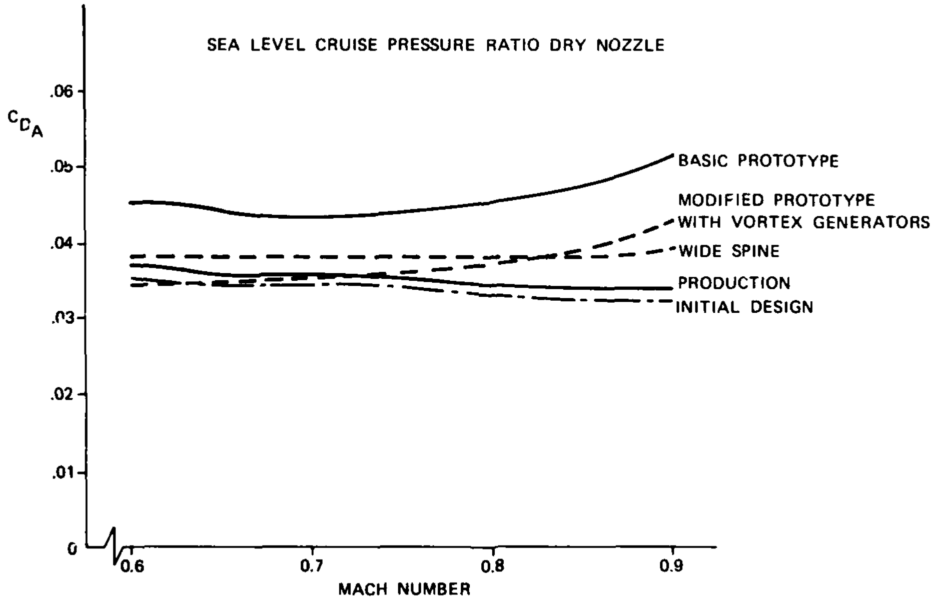

FIG 17: TORNADO AFTERBODY DRAG IN FLIGHT TEST DEVELOPMENT

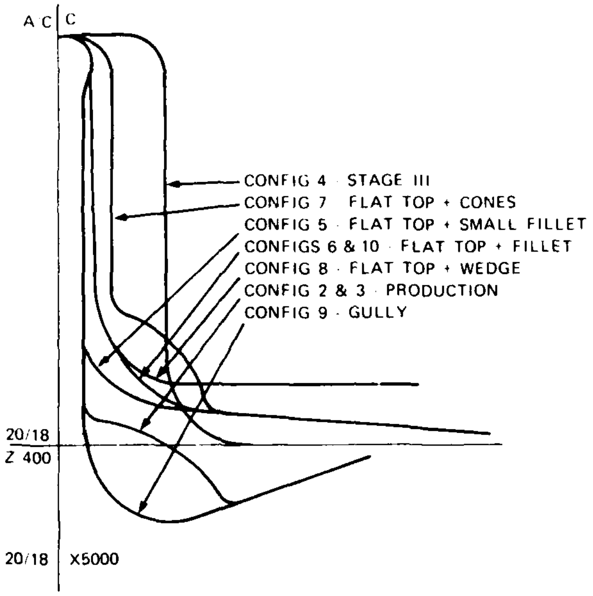
A C | C
CONFIG 4 · STAGE III
CONFIG 7 · FLAT TOP + CONES
CONFIG 5 · FLAT TOP + SMALL FILLET
CONFIGS 6 & 10 · FLAT TOP + FILLET
CONFIG 8 · FLAT TOP + WEDGE
CONFIG 2 & 3 · PRODUCTION
CONFIG 9 · GULLY
20/18
Z 400
20/18
X5000

FIG 18: AFTERBODY UPPER SURFACE PROFILE: REAR VIEW SHOWING CONFIGURATIONS TESTED DURING RESEARCH PROGRAMME

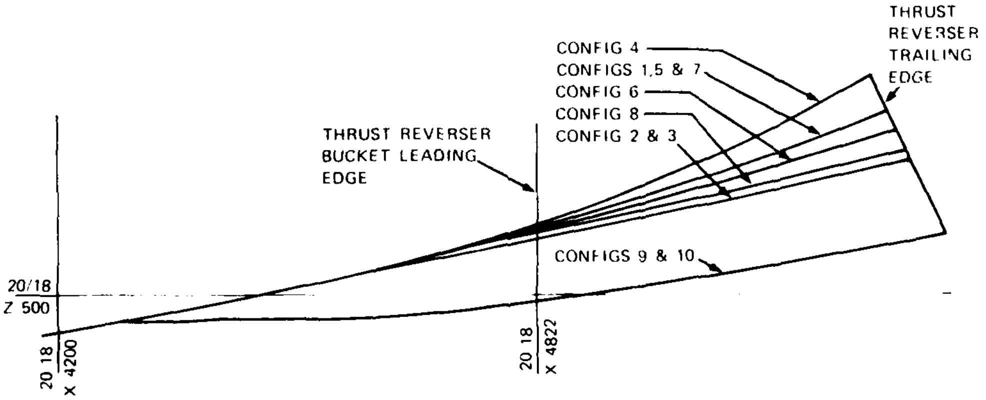
THRUST REVERSER TRAILING EDGE
CONFIG 4
CONFIGS 1,5 & 7
CONFIG 6
CONFIG 8
CONFIG 2 & 3
THRUST REVERSER BUCKET LEADING EDGE
CONFIGS 9 & 10
20/18
Z 500
20 18
X 4200
20 18
X 4822

FIG 19: AFTERBODY LOWER SURFACE PROFILE ON AIRCRAFT CENTRE LINE SHOWING CONFIGURATIONS TESTED DURING RESEARCH PROGRAMME

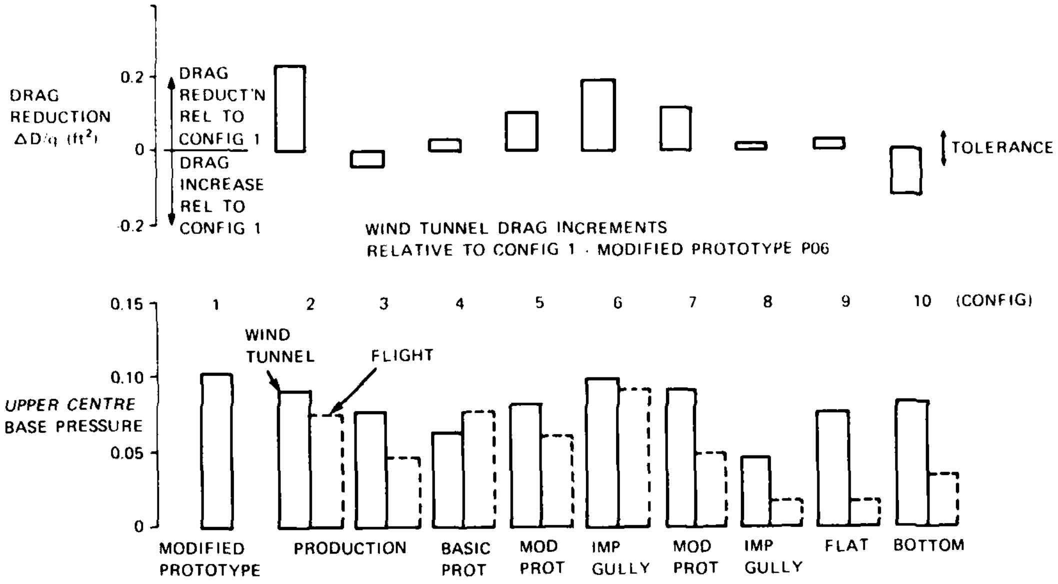

FIG 20a: COMPARISON OF IN-FLIGHT AND WIND TUNNEL CENTRE BASE PRESSURE MEASUREMENTS

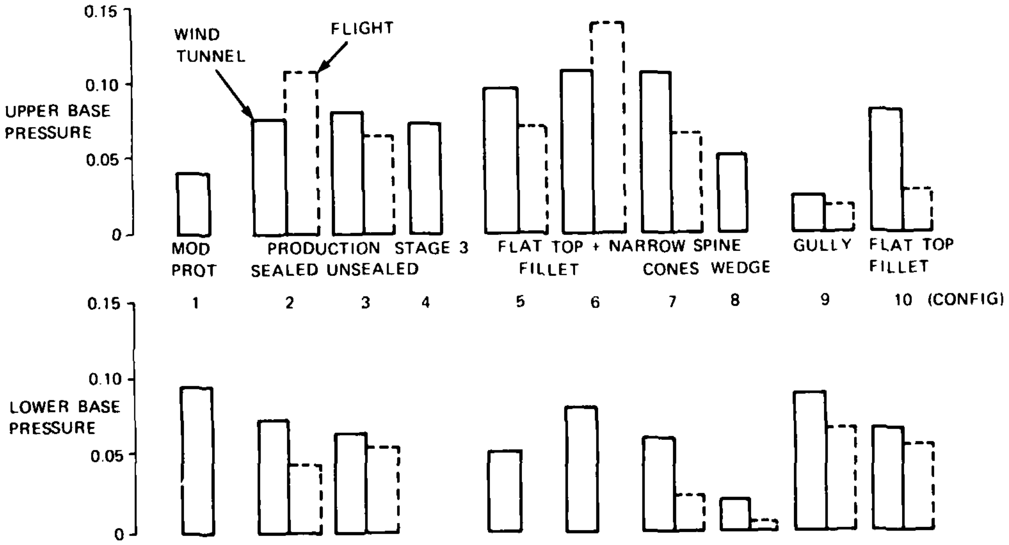

FIG 20b: COMPARISON OF IN-FLIGHT AND WIND TUNNEL BASE PRESSURE MEASUREMENTS

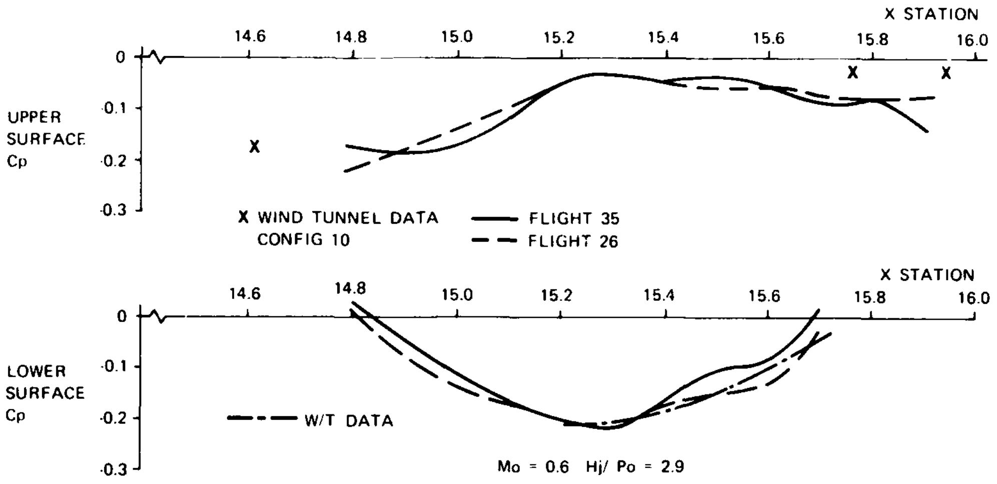

FIG 21: BOAT-TAIL SURFACE STATIC PRESSURE DISTRIBUTIONS

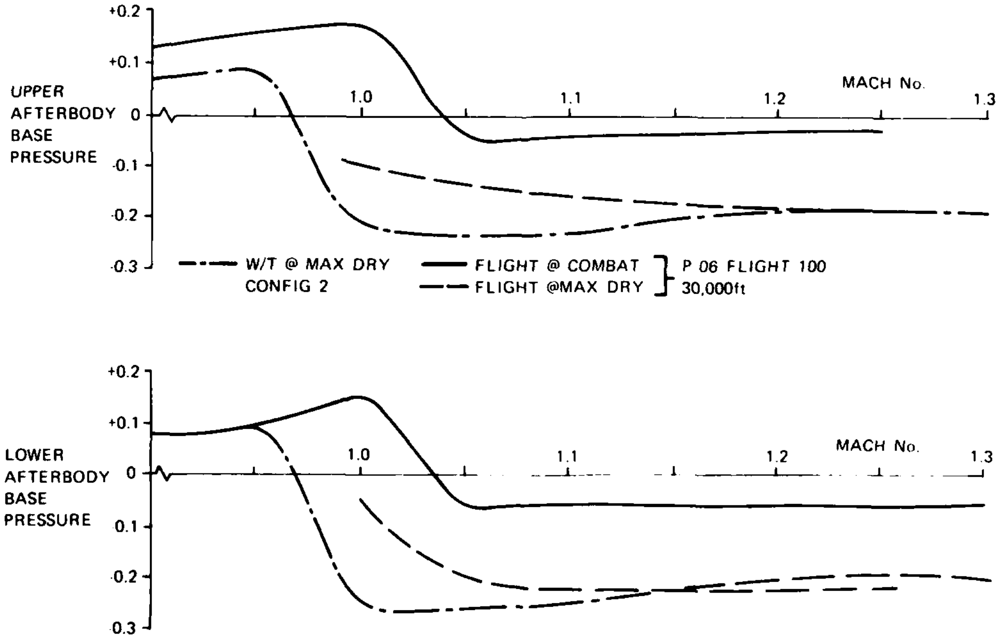

FIG 22: COMPARISON OF IN-FLIGHT AND WIND TUNNEL BASE PRESSURES AT SUPERSONIC SPEEDS FOR PRODUCTION AFTERBODY

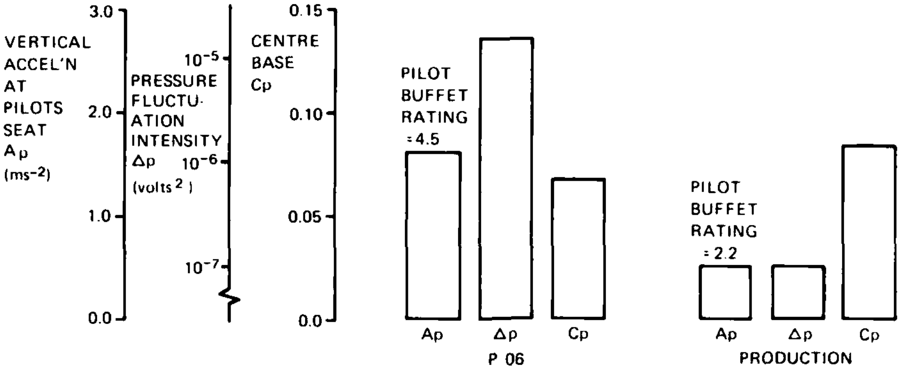

FIG 23: COMPARISON OF P06 AND PRODUCTION BUFFET, PRESSURE FLUCTUATIONS AND CENTRE BASE PRESSURES

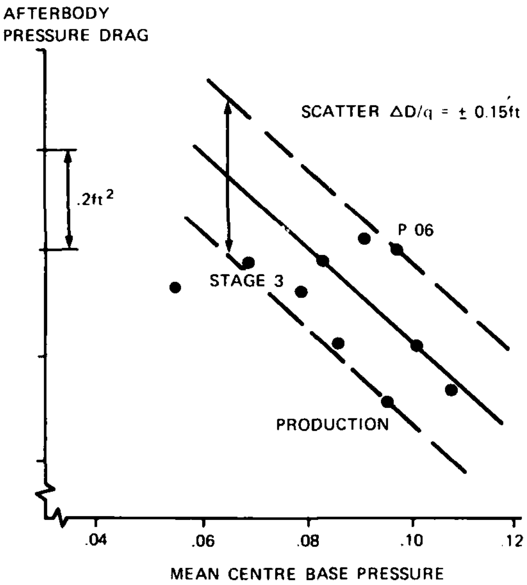

FIG 24a: CORRELATION OF AFTERBODY DRAG WITH MEAN CENTRE BASE PRESSURE

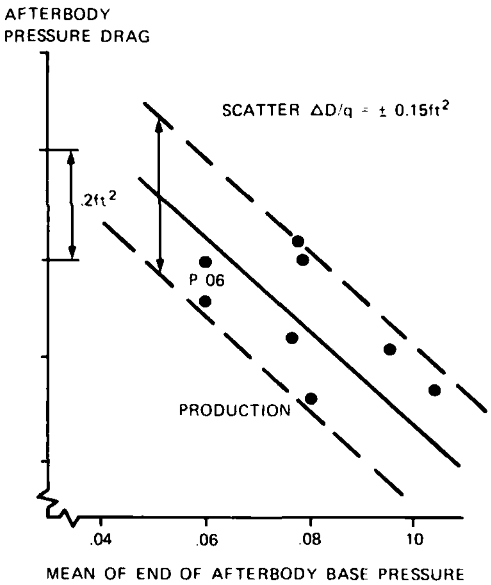

FIG 24b: CORRELATION OF AFTERBODY DRAG WITH THE MEAN END OF BOAT-TAIL BASE PRESSURE

BRIEF PREPARED REMARKS
FOR SESSION II, PERFORMANCE CORRELATION

by

Richard A. Wood
Chief, Simulator Projects Branch
Air Force Flight Test Center
6520 Test Group/ENFS, Stop 239
Edwards Air Force Base, California 93523
USA

When I was first approached to make these remarks, I felt there were four questions that I should attempt to answer. I quickly realized that I had asked myself several questions for which there were no definitive answers.

The four questions that seemed appropriate were:

1. How well do ground based estimates for drag polars and engine characteristics correlate to flight test results?

2. In what areas do performance prediction techniques work best or worst, and why?

3. What are the differences in the way various manufacturers (airframe or engine) predict drag polars and engine characteristics?

4. Are there portions of various performance prediction techniques that could or should be combined to form a better or best method?

Since the answers to these questions are subjects over which reasonable men can, and do, disagree, all I can hope to do is shed some small light on the subject. However, several important points are clear:

1. Correlation between performance estimates and flight test is reasonably good but, the ability to predict aircraft performance hasn't improved much in 20 years.

2. The ability to determine the accuracy of the predictions is a direct function of the accuracy of the flight test measurements.

3. The ability to determine the drag prediction accuracy is a direct function of the thrust accuracy. We seldom measure thrust per-se. Thrust is "calculated" from a calculation (computer) deck derived from ground based information. Therefore, the flight test determined drag is dependent on the estimated thrust.

4. Air frames can be modeled easily, pilots can not be modeled easily and,

5. An airframe manufacturer's published estimates depend on who he is negotiating with.

The answer to question 1 is "very well" if you are interested in up and away flight and plus or minus several percent is good enough. But, there are some areas where correlation is considerably poorer.

A survey of 12 commercial transport aircraft, constructed by three major American manufacturers, over a 20 year period, showed that you are just as likely to estimate too high a drag as too low a drag. Six of the twelve predictions were low, four predictions were high, and two were right on.

Number of Aircraft	Predicted C_D at Cruise Mach
6	More drag than predicted
4	Less drag then predicted
2	Right on

The drag predictions were as much as 22% low and 10% high.

This survey also showed that drag estimates on modified versions of existing aircraft were no better than the original estimates on the original aircraft. Despite having considerable flight test data from the original aircraft, aerodynamicists could not better their predictions the second time around.

Despite many years of experience in designing, testing, and analysing aircraft, several factors still inhibit the aerodynamicist's ability to predict drag. Most new aircraft incorporate new technology. Our ability to predict old technology improves with hind sight, but our ability to predict new technology does not necessarily improve with time. The available theories still make simplifying assumptions. For example, various components of the airframe are assumed to have constant skin friction; structural deflection is neglected or assumed to be some reasonably well behaved and simple function; air leaks around window frames and doors are assumed zero.

Wind tunnel models don't get around these problems. In fact, they have their own problems. Regardless of how much experience an aerodynamicist has with a wind tunnel, each model and mount system require their own unique corrections to obtain full scale numbers.

Last but not least, the aerodynamicist has no control over the quality of the workmanship on the actual aircraft. How well panels and doors fit together, and how secure the pressure seals are, are all functions of workmanship. An airframe with a lot of gaps and leaky seals will never perform as well as a tight aircraft.

If, in some flight regimes, ground based estimates correlate "very well" with flight test results specifically how well is very well? The answer becomes a subject of some controversy. It depends on what you are looking for.

The quality of performance flight test data has continually improved since the beginning of flight test. With higher quality pressure transducers, flight path accelerometers, and inertial navigation systems, better and better accuracy has been obtainable. However, under the best of conditions drag can only be measured to about ±2%. Given some typical instrumentation problems, a less than perfect thrust calculation scheme, and limited quantities of test data, ±5% is more typical and could worsen from there depending on the particular problems.

The modeling technique that is used to model the test drag polar, can effect the correlation. The type, number, and order of terms has an important effect on the shape of the polar and in what angle-of-attack and Mach number ranges the model fits the data best.

Plus or minus 2%, or 5% isn't necessarily a significant amount. However, if you are building a new commercial transport and have contractual performance guarantees, 5% is more than enough to cost you money.

In circumstances where excess thrust is limited, 5% is a big number. For example, a fighter that must meet a time-to-accelerate specification, will never meet the specification if its excess thrust is just 1% low. In a recent fighter development program, the manufacturer replaced engines three times before they identified a "good enough" engine to meet the acceleration requirement.

During a recent test program at Edwards Air Force Base, a particular airframe was flown in two separate tests to obtain an aerodynamic model. The same instrumentation system was used for both sets of tests. The second tests used the same model but newer engines than the first test. The thrust calculation scheme was the same in both cases; however, in each test somewhat different data analysis schemes were used to obtain drag. The results showed that the two sets of tests, although similar, produced drag polars of different shape, and as much as 6% different magnitude in drag coefficient.

In another example during a recent series of tests on a modified transport aircraft, two types of flight test instrumentation were available and two seperate wind tunnel analyses were conducted. Figure 1 shows the results of the overall analysis. Conclusions drawn were that the modification improved performance, and that the improvement was somewhere between two and eight percent depending on flight condition. The difference in the various analyses may not seem like enough to argue about, but when the profitability of retrofitting the fleet requires a five percent improvement in drag, the arguments are plentiful.

The answer to the second question; in what areas do performance prediction techniques work best, is fairly simple. Performance predictions are best in up-and-away flight outside of the transonic region, and they are worst in those areas where pilot technique is a big factor, like takeoff and landing; in situations where excess thrust is limited; or where significant flow separation occurs, such as high angle-of-attack.

Some very minor differences in pilot technique can be quite important and obviously it is very difficult for the aerodynamicist to control pilot technique. Some recent tests on a ground attack fighter showed a one degree change in rotation pitch attitude changed liftoff airspeed by about 5 knots and ground roll approximately 500 feet. In this case 500 feet represented 10% of the takeoff distance. The predicted takeoff performance was based on a rotation to exactly 10 degrees pitch attitude; and the rotation was commenced about 10 knots below predicted takeoff speed.

Flight test results showed on occasions where the pilot delayed rotation, several hundred feet longer ground runs resulted due to delays in the aircraft reaching a liftoff lift coefficient. On occasions where the pilot failed to achieve at least 10 degrees pitch attitude, longer ground runs also resulted due to not generating sufficient lift for takeoff until a higher speed was reached. On occasions when the pilot overrotated, the aircraft lifted off earlier due to achieving a liftoff lift coefficient at a lower speed; but then was slow and sluggish in the climb out phase. No matter what the pilot did, he would not achieve the predicted performance unless he rotated to exactly the correct pitch attitude and timed his rotation exactly right.

Landing is another area where prediction is difficult, particularly on wet runways. The actual coefficient of friction between tire and runway is difficult to determine in the best conditions. Antiskid operation is rarely modeled accurately. Most landing performance estimates assume some average effective coefficient of friction. Pilot technique during flare is extremely important with large percentages of the predicted landing distance being eaten up if the airplane is allowed to float or bounce.

A recent STOL test program graphically illustrated the differences between pilot-out-of-the-loop theoretical predictions and pilot-in-the-loop performance. The predictions showed that the aircraft could fly a 6° glide slope at a high sink rate and not exceed structural limits at touchdown. The changes in lift and drag coefficient due to ground effect resulted in the ground effect arresting the sink rate just before touchdown. Tests to confirm the analysis were flown over a dry lakebed with the auto pilot engaged. A 6° glide slope was flown until the ground effect "flared" the aircraft. The test confirmed the analysis.

However, the analysis didn't predict how the pilots would react in an operational situation. Figure 2 shows the touchdown dispersion experienced while landing on a STOL runway. Eight landings were short of the touchdown point and 26 were long. The long touchdowns resulted from several problems. The first was variable winds, the second pilot concern for the structural limits of the aircraft, and the third was high pilot workload.

In no-wind conditions the aircraft could be brought into the aim point reasonably well. With shearing or variable winds, the pilot reaction time and engine response time were long enough that if the pilot got behind the aircraft he would land at an excessive sink rate. In any event, once the aircraft was within 200 feet of the ground the pilot was completely at the mercy of the aircraft because there was insufficient time to make any corrections. In order to insure a safe landing, the pilots would often carry a little extra power and elect a long safe touchdown rather than a hard landing at the touchdown point. The net result was that most approaches were flown between 5 and 5.5°, not the predicted 6°, and touchdown sink rates never exceeded 13 feet per second even though 16 feet per second was the limit. Under such circumstances the aircraft could never achieve its designed STOL landing performance.

The theoretical 6° glide slope could be flown and the aircraft brought into a spot landing, providing the pilot had the perception and control authority to confidently maneuver the aircraft in real world conditions.

The third and fourth questions are not easily addressed. In fact, an entire symposium could be devoted to discussing drag and thrust prediction techniques and which ones are best. The simple answer is that no single methodology is best for every situation.

Most airframe manufacturers use well known techniques as a starting point and then modify the techniques according to their own experience. The aerodynamicist will start with analytical methods, then modify these estimates by wind tunnel results, and finally modify both of the previous results by his previous experience with flight test results.

The difficulty in defining a best technique lies with the fact that there are so many pieces that must be added together to develop a performance prediction. If a manufacturer is building a new, but conventional design aircraft, he will rely heavily on a perturbation analysis; that is, modify flight test results from a previous, similar design, by some predicted change. If he is building an aircraft that incorporates new or unfamiliar technology he will be forced to use more sophisticated techniques. In either case, the aerodynamicist is faced with the task of summing the drag of each component of the aircraft for example; wing, fuselage, vertical stabilizer, etc. The drag for each of these components can be made up of several components also, for example; skin friction drag, protuberance drag, drag due to lift. And then, interference drag has to be added in. There are separate analytical methods for estimating each type of drag, for each component of the aircraft, for various portions of the flight envelope.

Fortunately, in most cases, the aerodynamicist has more information on his engine. The long lead time required for engine development usally means the engine has already been developed and tested to some degree so estimating thrust requires slightly less quess work. However, the aerodynamicist is still faced with determining installation effects. What this all means is that the methodology for predicting performance is made up of many methodologies, all of which can be manipulated by the individual aerodynamicist based on his previous experience.

But this situation is still further complicated by the fact that aircraft design is an iterative process. The designer rarely knows all the details of the final configuration until the very end of the process, and will probably never know such details as where every row of rivets will be or how large the gaps in panels will be. Such an iterative process, filled with so many details, results in a tremendous bookkeeping task. The time and expense required to go through many calculations for each iteration often results in short cuts being taken.

Two important observations can be made from all this. First, the quality of the estimate is more a function of the time and care taken to include all the details and higher order terms than it is of the particular equations used. Second, no one technique covers all aircraft types, configurations, and flight regimes.

Airframe manufactures are reluctant to disclose what they have learned through extensive and expensive experience. They all feel they know something their competitors don't know and they are not about to give it away free. Several years ago the U.S. Air Force found that the numerous combinations and permutations of performance estimation methodologies made it difficult to compare proposals from different airframe manufactures. An attempt was made to standardize the methodology amongst manufacturers. The attempt failed due to both the reluctance of the manufacturers to change what each of them felt was their "best" method and, for the lack of definitive proof of what combinations of methodologies were best for any particular situation.

So the opportunity still remains, for some perceptive member of our industry, to provide us with the definitive answers to these last two questions.

IMPROVEMENT IN PERFORMANCE AT CRUISE MACH NUMBER

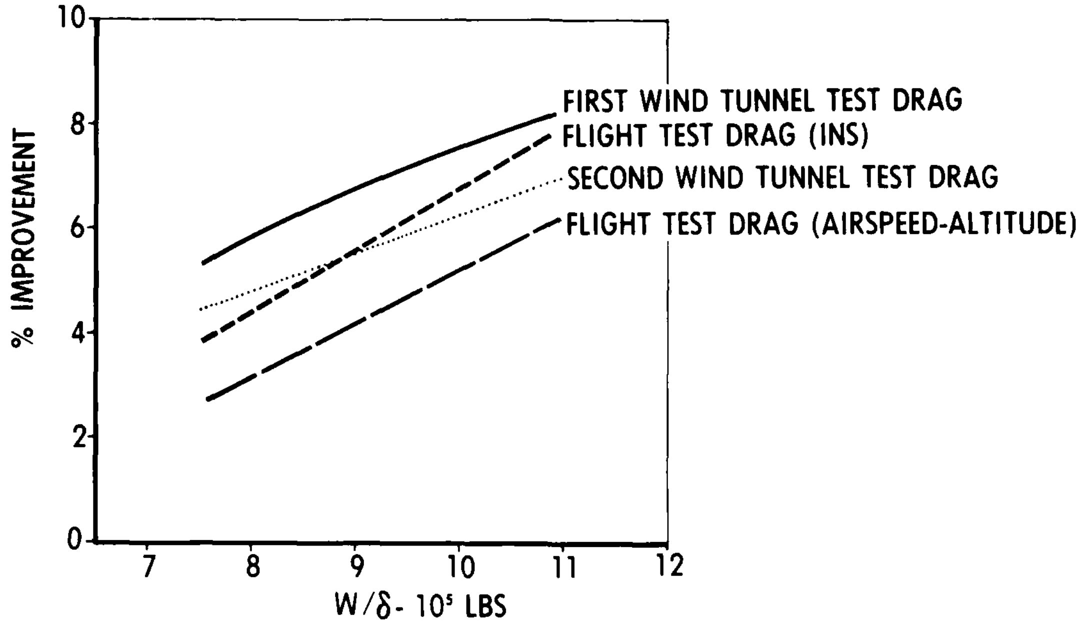

FIGURE 1

STOL LANDING TOUCHDOWN DISPERSION

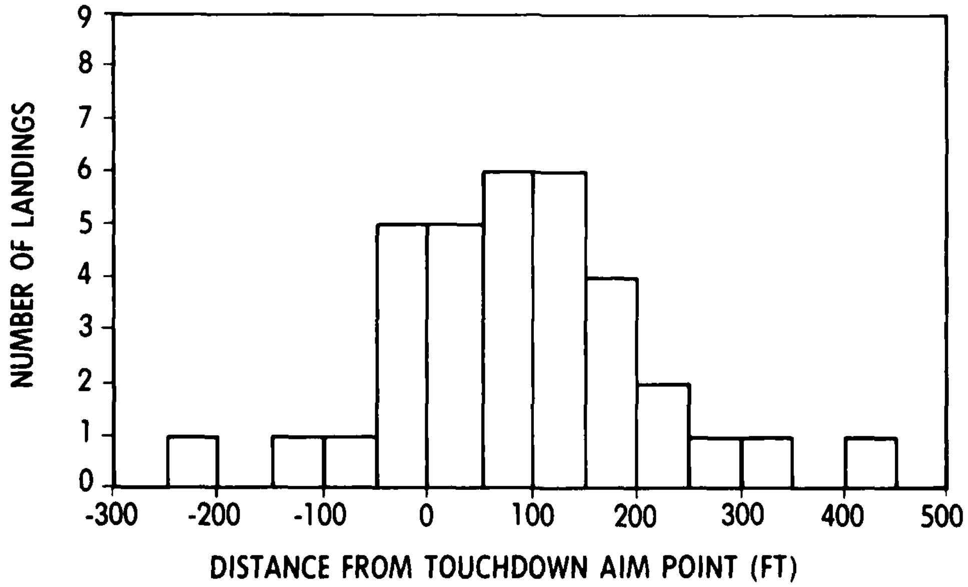

FIGURE 2

BRIEF PREPARED COMMENTS ON PERFORMANCE CORRELATION

PROPULSIVE AFTERBODY DESIGN AND PERFORMANCE PREDICTION COMPARED WITH FLIGHT RESULTS

by

J.M.Hardy
SNECMA
France

SUMMARY

The analysis of the Flight performance of propulsive afterbody schemes on several Military (Mirage 3 – 4 – F1 – 2000 – 4000) and Civil Aircraft (Mercure, Concorde, DC8/CFM-56) has given SNECMA a general philosophy on their prediction at the design stage.

This methodology is based on three principles:

(a) Synthesis of experimental results obtained on models to obtain correlations qualitatively verified in Flight;

(b) Development of sophisticated calculation methods validated in wind-tunnel (local and global aspects); these methods are used for flow analysis and for extrapolation of *model testing;*

(c) Static calibration on models of afterbodies with exhaust flow conditions (model nozzle coefficients) used for the Flight thrust calculation.

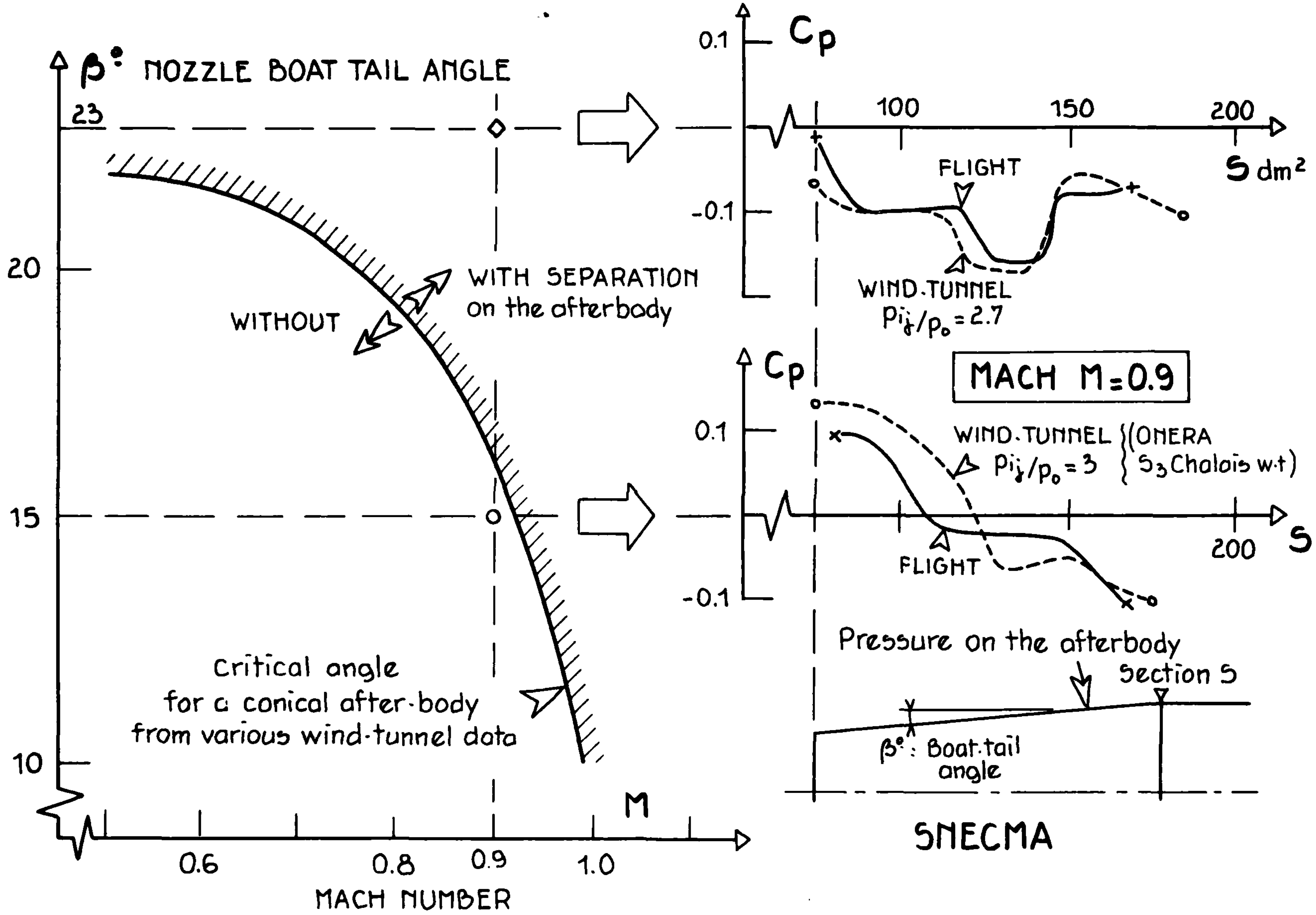
β° NOZZLE BOAT TAIL ANGLE
23
20
15
10
WITH SEPARATION on the afterbody
WITHOUT
Critical angle for a conical after-body from various wind-tunnel data
0.6
0.8
0.9
1.0
M
MACH NUMBER
Cp
0.1
-0.1
100
150
200
S dm²
FLIGHT
WIND-TUNNEL $p_{i_j}/p_o = 2.7$
MACH M=0.9
Cp
0.1
-0.1
WIND-TUNNEL $p_{i_j}/p_o = 3$ (ONERA S_3 Chalois w.t)
FLIGHT
200
S
Pressure on the afterbody
Section S
β°: Boat-tail angle
SNECMA

CORRELATION FLIGHT/WIND TUNNEL on PROPULSIVE AFTERBODIES :

Influence of the mixing length on the base pressure

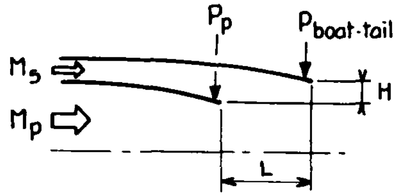
P_p
$P_{boat\text{-}tail}$
M_s
M_p
H
L

$$\mu_s = \frac{\text{Secondary flow}}{\text{Primary flow}} = \frac{M_s\sqrt{T_s}}{M_p\sqrt{T_p}}$$

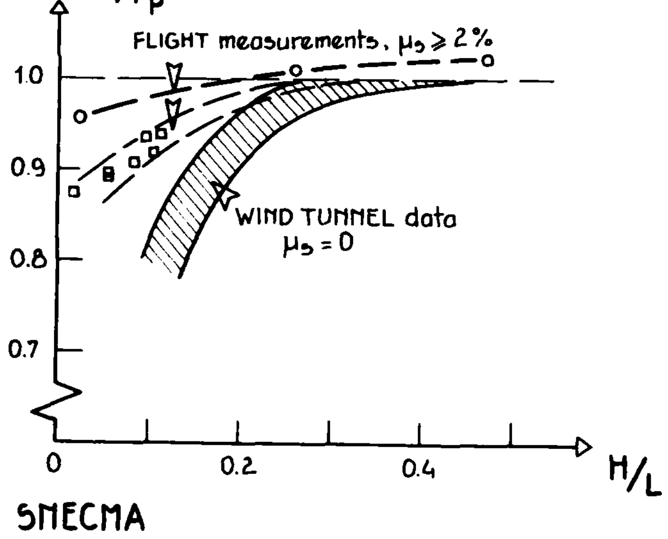

CONCORDE NOZZLE, SUPERSONIC CRUISE :

Internal flow computation

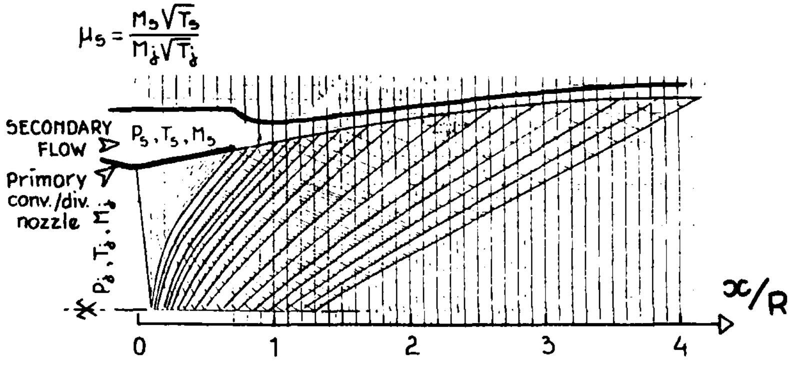
$\mu_s = \frac{M_s\sqrt{T_s}}{M_j\sqrt{T_j}}$
SECONDARY FLOW
P_s, T_s, M_s
Primary conv./div. nozzle
P_j, T_j, M_j
0
1
2
3
4
x/R

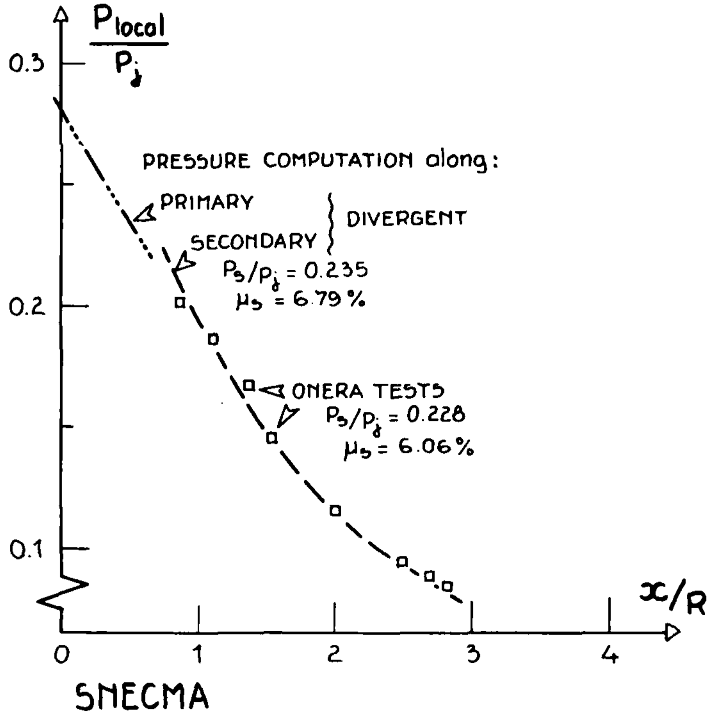

COMPUTATION of FLOW around an axisymmetric nozzle boat-tail with jet exhaust

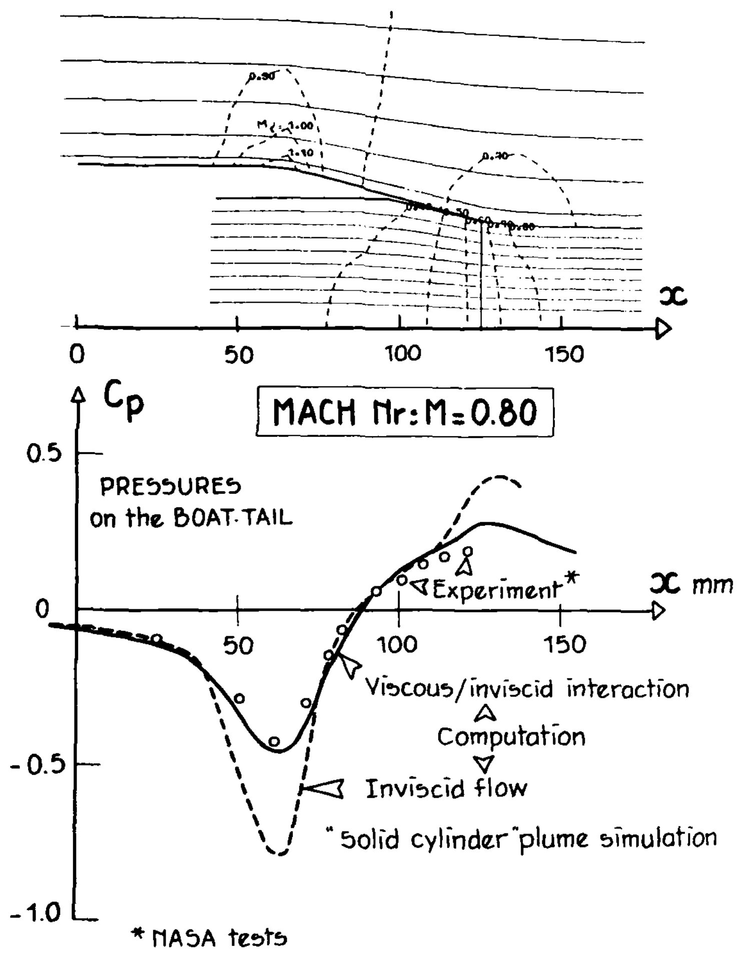

SNECMA

INTAKE for TURBO-FAN at CRUISE, Mach = 0.801 $\alpha = 0°$

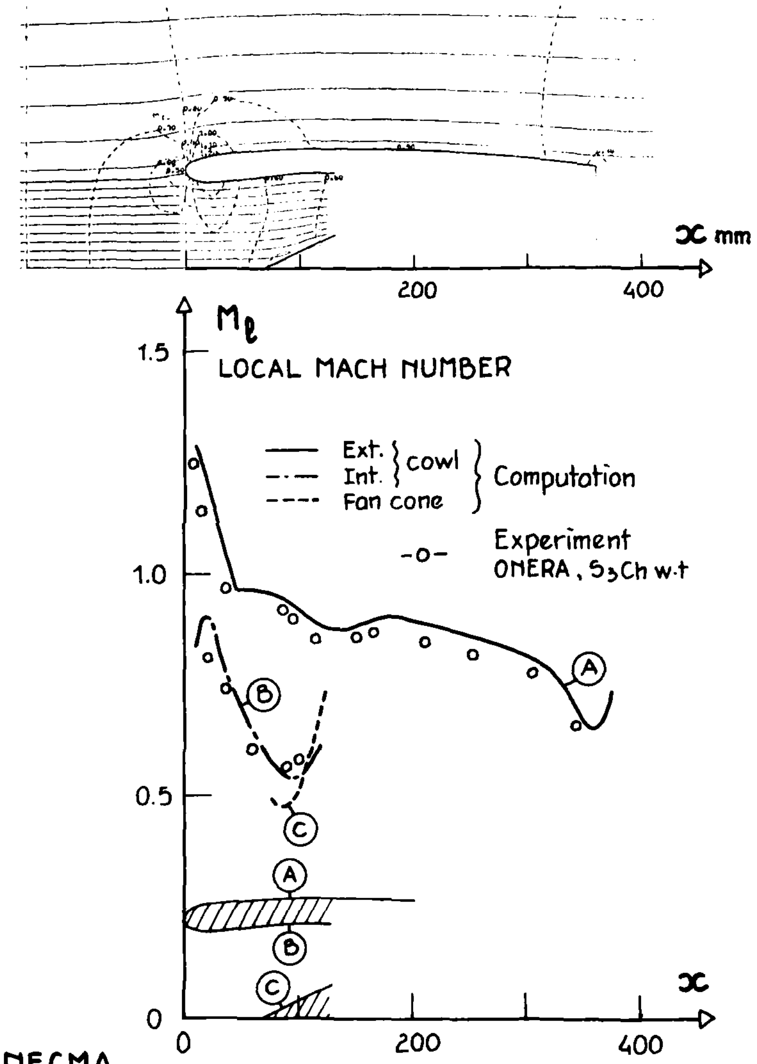

SNECMA

COMPORTEMENT A GRANDE INCIDENCE D'UN AVION DE COMBAT : CORRELATION ENTRE LES PREVISIONS ET LE VOL

par

Paul-Louis MATHE

Chef du Département Dynamique du Vol

AVIONS MARCEL DASSAULT-BREGUET AVIATION (AMD-BA)
78, Quai Carnot - 92214 ST-CLOUD - FRANCE

Le MIRAGE 2000 est un avion équipé d'un système de commandes de vol strictement électriques. Nous ne détaillerons ni les raisons fondamentales du choix d'un tel système, raisons maintenant bien connues, ni toutes les fonctions qu'il assure ; nous ne parlerons ici que de l'une de ces fonctions : celle qui assure une protection automatique de l'avion vis-à-vis de la perte de contrôle.

Cette fonction qui avait été prévue de base dans la conception du système de commandes de vol de l'avion, mais sous une forme relativement simplifiée, s'est révélée d'un tel intérêt opérationnel qu'elle a été l'objet au cours de la mise au point des prototypes de multiples perfectionnements. Sous sa forme définitive, cette fonction assure la protection vis-à-vis de la perte de contrôle de l'avion pour toutes ses configurations de combat, sans aucune consigne restrictive de pilotage, et ceci, jusqu'à vitesse nulle. La réduction de charge de travail, qui en résulte pour le pilote en cours de manoeuvres de combat, renforce singulièrement l'efficacité opérationnelle de l'avion : suppression des tâches de surveillance des paramètres critiques de vol de l'avion (en particulier de l'incidence), liberté absolue de manoeuvre du pilote. Par ailleurs, les limitations des paramètres critiques de vol étant réalisés de façon plus précise par un dispositif automatique que par de simples consignes de pilotage, il en résulte une meilleure exploitation des possibilités de l'avion. Enfin, la rapidité d'exécution des manoeuvres extrêmes de combat en est très nettement améliorée.

La protection automatique de l'avion vis-à-vis d'éventuelles pertes de contrôle est réalisée :

- Par une fonction des commandes de vol assurant une limitation automatique de l'incidence de l'avion à une valeur dépendant des conditions de vol.
- Par une adaptation soignée des fonctions de contrôle et de commandes de l'axe de roulis et de l'axe de lacet de l'avion qu'assurent le système de commandes de vol : adaptation de certains gains en fonction de l'incidence, en particulier de ceux qui régissent les couplages roulis-lacet, adaptation des efficacités des commandes de gauchissement et de palonnier en fonction de la commande de profondeur, etc... Cette adaptation permet de minimiser les dérapages induits par les manoeuvres à grande incidence, ce qui entre autres choses est une condition indispensable à une bonne efficacité de la fonction de limitation d'incidence.

Précisons ici que l'incidence maximale de contrôle d'un avion n'est pas, en général, indépendante du niveau de manoeuvrabilité transversale que l'on souhaite lui conserver à cette incidence. C'est affaire de compromis. Les réglages retenus pour le système de commande de vol du MIRAGE 2000 sont tels qu'aux incidences limites la manoeuvrabilité transversale reste notable : la vitesse de roulis disponible, dans ces conditions d'incidences limites, reste toujours supérieure à 30 % de la vitesse de roulis disponible, dans les mêmes conditions de vol, à incidence modérée.

Limitation automatique de l'incidence et contrôle rigoureux des axes transversaux sont les clés de la protection de l'avion vis-à-vis de la perte de contrôle. Encore faut-il que ces fonctions puissent être remplies correctement par le système de commandes de vol de l'avion, ce qui implique un minimum d'efficacité des gouvernes et donc un minimum de vitesse. Or des conditions de vitesse très faible voire nulle peuvent être obtenues par des manoeuvres très particulières de "chandelles" quasi verticales. Ces manoeuvres pourraient certes être évitées par application de certaines consignes de pilotage, mais il a été jugé opérationnellement très contraignant d'imposer au pilote, en combat, de telles consignes.

o ° o

Dans ces conditions le domaine en incidence de l'avion prend l'allure présentée par la figure 1. Ce domaine comprend deux parties :

- une partie dans laquelle l'incidence est strictement limitée par le système de commandes de vol,
- une partie, limitée aux basses vitesses, dans laquelle les incidences et les dérapages peuvent pratiquement être quelconques, et le système de commandes de vol du MIRAGE 2000 a été défini de façon qu'en aucun cas une incursion dans cette dernière partie du domaine, incursion volontaire ou involontaire mais de toute façon très temporaire, puisse conduire à une situation de perte de contrôle tant soit peu prolongée, et ceci quelles que soient les manoeuvres effectuées pas le pilote c'est-à-dire, en définitive, sans aucune consigne restrictive de pilotage.

Comme nous l'avons dit, le MIRAGE 2000 est un avion équipé d'un système de commandes de vol strictement électriques ; de ce fait, tant que le système de commandes de vol n'est pas saturé (butée de détecteurs, butée de gouvernes, vitesse limite de servocommandes, ...), le comportement en vol de l'avion dépend moins de ses caractéristiques particulières aérodynamiques que des lois de contrôle introduites dans le système de commandes de vol. Quelques exemples sont significatifs :

- A 150 kts, une erreur de 50 % sur le Clp (amortissement aérodynamique de roulis) ne change que de 10 % l'amortissement global de l'ensemble avion + commandes de vol sur ce même axe. Une erreur de 20 cm sur la position du foyer aérodynamique de l'avion modifie la période de l'oscillation d'incidence de moins de 10 %.
- Une erreur de 100 % (x par 2) sur le coefficient croisé Cnp de lacet dû à la vitesse de roulis ne modifie que très peu la qualité du comportement de l'avion en manoeuvre de gauchissement (modification de quelques dixièmes de degrés du dérapage maximum atteint pendant la manoeuvre).

Cette situation est évidemment très favorable à la fiabilité des prévisions que l'on peut faire quant au comportement aérodynamique en vol d'un avion équipé de commandes de vol électriques. Elle pourrait faire douter de la nécessité absolue d'effectuer pour ce type d'avion une identification prévisionnelle en soufflerie aussi fine que possible des caractéristiques aérodynamiques.

Cette nécessité s'impose cependant ; en effet :

- Il y a au moins une classe de coefficients aérodynamiques dont la connaissance est strictement nécessaire : ce sont les efficacités (directes et croisées) des gouvernes ; ce sont elles qui assurent le contrôle de l'avion et tous les réglages de base du système de commandes de vol en dépendent.
- S'il est vrai que le comportement d'un avion doté d'un système de commandes de vol électriques dépend, tant que ce système n'est pas saturé, essentiellement des lois de contrôle qu'il réalise, il est évident que les conditions dans lesquelles de telles saturations peuvent être atteintes dépendent directement des caractéristiques aérodynamiques générales de l'avion. Et le dimensionnement correct des commandes de vol exige une connaissance précise de ces caractéristiques.
- Il est "normal" que dans certaines conditions extrêmes le système de commandes de vol soit temporairement saturé (gouvernes en butée par exemple) ; s'il en était autrement, cela signifierait, soit que le système de commandes de vol est surdimensionné, soit que les possibilités maximales du système ne sont pas exploitées. Or, dans ces conditions, pour lesquelles les fonctions de contrôle du système de commandes de vol sont restreintes, l'importance des caractéristiques aérodynamiques générales de l'avion sur le comportement de celui-ci devient évidemment prépondérante.

Nous ne rentrerons pas ici dans le détail des divers moyens mis en oeuvre pour obtenir une identification avant vol aussi fine que possible des caractéristiques aérodynamiques de l'avion ; nous citerons cependant ceux qui permirent l'identification prévisionnelle de l'avion dans le domaine des grandes incidences.

Le domaine d'incidence et de dérapage pour ces essais couvre largement le domaine effectif de vol de l'avion puisque, en compressible, ils ont été menés systématiquement jusqu'à des incidences comprises entre 35 et 40° et des dérapages de l'ordre de 15°. Dans le domaine des très basses vitesses, domaine dans lequel l'avion en vol, comme nous l'avons vu précédemment, n'a plus de limitation d'incidence et de dérapage, les identifications en soufflerie ont été menées entre plus ou moins 180° d'incidence et plus ou moins 180° de dérapage à l'aide d'un montage spécial.

Ces essais, à vrai dire très classiques, furent menés dans diverses souffleries et avec des maquettes de taille relativement variée, avec de nombreux recoupements de façon à minimiser les aléas inhérents aux essais de soufflerie : effets du nombre de Reynolds, précision de la représentation de la géométrie de l'avion,...

Il y a peu à dire de ces essais sinon qu'ils furent menés de façon à laisser le moins d'incertitude possible quant à la détection d'éventuels accidents aérodynamiques dans la zone des grandes incidences, zone dans laquelle l'aérodynamique de l'avion est particulièrement non linéaire. Ceci a conduit à l'identification de très nombreuses combinaisons des paramètres de "situations aérodynamiques" et de configurations de l'avion : incidence, dérapage, braquage des diverses gouvernes, etc ... Par ailleurs, un effort particulier d'identification en soufflerie des grandeurs anémométriques, nécessaires au fonctionnement du système des commandes de vol, a été fourni : recherche de positionnements corrects des girouettes d'incidence, des prises de pressions statiques et dynamiques ; étalonnage prédictif de ces mesures.

A ces essais de soufflerie que l'on peut qualifier de statique se sont ajoutés un certain nombre d'essais particuliers et sous certains aspects moins classiques, parmi lesquels il faut citer :

- Des essais d'identification en soufflerie des coefficients aérodynamiques dynamiques "directs et croisés" par la méthode des oscillations forcées. Ces essais ont été poussés jusqu'à des incidences pour lesquelles l'avion présente des non linéarités aérodynamiques statiques qui rendent d'ailleurs l'interprétation des résultats très aléatoires.
- Des essais effectués dans une soufflerie verticale à l'aide d'un montage tournant dans une très large gamme d'incidence, de dérapages et de vitesses angulaires. Ces essais avaient pour but, évidemment, de préciser certaines caractéristiques aérodynamiques dynamiques à grande incidence, mais aussi, et surtout, à vérifier que l'aérodynamique de l'avion, dans des conditions de vol à caractère fortement dynamique impliquant des vitesses angulaires et des vitesses de variation de l'incidence et du dérapage importantes, ne présentait pas d'accident rédhibitoire susceptible de mettre en défaut le fonctionnement des commandes de vol.
- Des essais de vol libre catapulté effectués avec une maquette pilotée de l'avion, essais destinés essentiellement à recouper les résultats des identifications aérodynamiques faites classiquement en soufflerie.
- Des essais de "vrilles" réalisés en soufflerie verticale ; ces essais permettant de caractériser le comportement de l'avion en condition de vrilles et de définir les consignes à appliquer pour sortir de vrilles, ont été réalisés afin d'assurer la sécurité des vols d'ouverture du domaine en incidence des prototypes du Mirage 2000, dans le cas où des divergences importantes entre nos prévisions et la réalité auraient rendu inefficace le système de protection automatique vis-à-vis de la perte de contrôle installée sur l'avion.

Ces deux derniers types d'essais ne sont pas à proprement parler des essais d'identification. Ils peuvent cependant constituer d'excellents recoupements avec les essais classiques de soufflerie. Il est d'ailleurs intéressant de noter à ce sujet qu'il a été possible, par calculs à partir des caractéristiques aérodynamiques statiques de l'avion issus des essais de soufflerie basse vitesse effectués à très grandes incidences et très grand dérapage de retrouver les principales caractéristiques des diverses vrilles mises en évidence à la soufflerie verticale.

o°o

AD-A129 433 GROUND/FLIGHT TEST TECHNIQUES AND CORRELATION(U) 3/6
ADVISORY GROUP FOR AEROSPACE RESEARCH AND DEVELOPMENT
NEUILLY-SUR-SEINE (FRANCE) FEB 83 AGARD-CP-339
UNCLASSIFIED F/G 1/3 NL

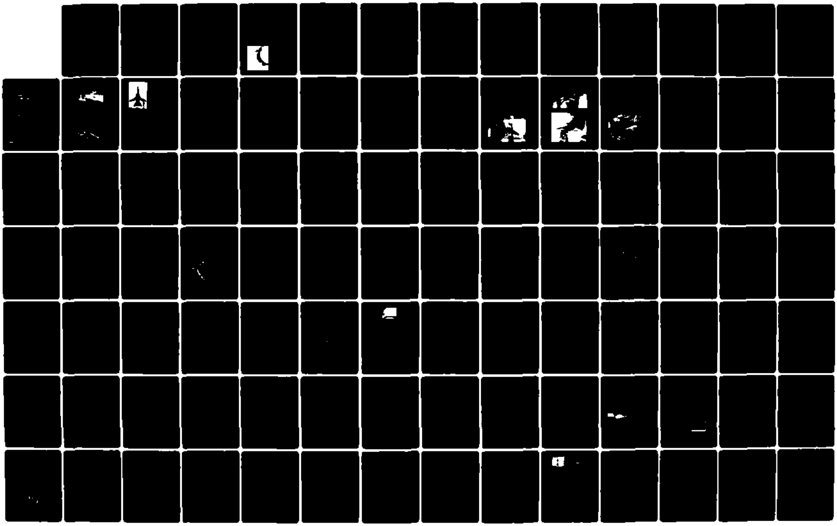

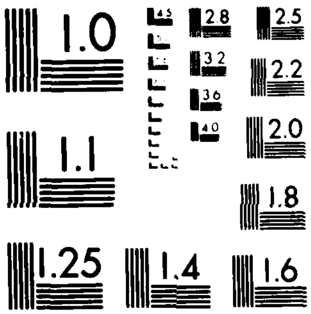
1.0
4.5
2.8
2.5
3.2
2.2
3.6
4.0
2.0
1.1
1.8
1.25
1.4
1.6

MICROCOPY RESOLUTION TEST CHART
NATIONAL BUREAU OF STANDARDS 1963 A

Avant d'aborder plus précisément l'examen de la validité des prévisions qui furent faites avant vol, quant au comportement de l'avion, il y a lieu de rappeler la méthodologie qui fut appliquée au Mirage 2000 pour "ouvrir" effectivement en vol le domaine des grandes incidences de cet avion.

Cette ouverture s'est déroulée en trois phases :

- La première de ces phases a été réalisée avec un prototype évidemment équipé de ces commandes de vol électriques mais dans lesquelles la fonction de limitation automatique d'incidence n'était pas branchée. Cette phase fut relativement courte et avait pour but de préciser les étalonnages des grandeurs anémométriques intervenant dans les réglages du système de limitation automatique d'incidence. Un premier domaine en manoeuvre symétrique, c'est-à-dire sans manoeuvre transversale, fut ainsi ouvert. Cette phase permit une première vérification des principales caractéristiques aérodynamiques, en particulier longitudinales, de l'avion.
- La deuxième phase fut la phase effective de mise au point des fonctions de protection automatique de l'avion vis-à-vis de la perte de contrôle dans son domaine "normal" de vol, c'est-à-dire hors du domaine des très faibles vitesses. C'est au cours de cette phase que put être évalué l'intérêt opérationnel de tels dispositifs de protection automatique, intérêt qui parut si important qu'un certain nombre de perfectionnements de ces fonctions furent souhaités par les pilotes et réalisés. En particulier, l'extension de la fonction de protection automatique à l'ensemble des configurations de combat de l'avion fut décidée, alors qu'initialement cette protection ne devait couvrir que les principales configurations et qu'il avait été admis qu'un certain nombre de consignes restrictives de pilotage était acceptable. C'est au cours de cette phase que le meilleur compromis entre les valeurs d'incidence maximales de l'avion et la manoeuvrabilité transversale encore disponible à ces incidences a été défini.
- Enfin, une troisième phase a permis d'ouvrir le domaine de vol de l'avion jusqu'aux vitesses très faibles, voire nulles, domaine dans lequel les incidences et les dérapages peuvent atteindre des valeurs quelconques. Il faut noter que la nécessité d'une telle ouverture de domaine n'était pas évidente a priori. En effet, ce domaine n'est accessible que par des manoeuvres très particulières de pilotage que l'on sait éviter à l'aide de consignes relativement simples à respecter par le pilote. C'est en définitive le souci de voir pour les configurations de combat toutes consignes restrictives de pilotage disparaître qui a rendu nécessaire la validation de bon fonctionnement de l'ensemble avion + commandes de vol dans ces conditions particulières. Aborder cette phase d'essais en vol exigait quelques précautions car les risques de perte de contrôle n'étaient pas a priori complètement négligeables et une campagne d'essais en soufflerie de vrille fut effectuée de façon à caractériser ces vrilles et définir les consignes à appliquer éventuellement pour en sortir. Quelques vols furent effectués afin de vérifier la validité de ces résultats : la suppression dans les commandes de vol de toutes les fonctions de protection automatique ont permis d'obtenir, effectivement en vol, quelques pertes de contrôle et de vérifier ainsi l'efficacité des consignes de sortie de vrilles définies à partir des essais en soufflerie.

Ces différentes phases d'ouverture du domaine de vol de l'avion ont été réalisées selon une procédure progressive, dont chacune des étapes comprenait successivement :

- Une "répétition" au simulateur des essais d'ouverture de domaine.
- Les essais en vol d'ouverture de domaine.
- Une comparaison systématique entre le comportement de l'avion en vol et celui qui avait été prévu.

o°o

Nous avons aujourd'hui, le recul suffisant, pour pouvoir établir un bilan très général de la qualité des prévisions concernant le comportement de l'avion que nous avons pu faire avant les vols.

L'examen de ce bilan nous permet d'affirmer que, dans leur ensemble, ces prévisions ont été excellentes.

Ce résultat est, certes en partie dû au fait, déjà cité précédement, que le comportement d'un avion équipé de commandes de vol électriques est, dans bien des conditions de vol, plus lié aux réglages adoptés pour ces commandes de vol, qu'aux caractéristiques aérodynamiques propres de l'avion ; il provient aussi du fait que les divergences, entre l'aérodynamique réelle de l'avion et celle que prévoyait la soufflerie, sont toujours restées relativement faibles.

Tout ceci ne signifie évidemment pas que la mise au point des commandes de vol électriques du MIRAGE 2000 n'ait posé aucun problème.

D'abord, et nous avons déjà eu l'occasion d'évoquer ce fait, les objectifs visés par le système de commandes de vol ont évolués au cours de la mise au point des prototypes en fonction même des possibilités nouvelles qu'offrait ce type de commandes de vol (extension et perfectionnement des limitations automatiques en particulier).

Par ailleurs, malgré l'excellente concordance d'ensemble entre l'aérodynamique réelle de l'avion et celle que nous laissait prévoir les mesures effectuées en soufflerie, quelques "surprises" ne nous ont pas été épargnées.

Je ne citerais qu'à titre anecdotique, car ne concernant pas vraiment le domaine des grandes incidences, et qu'elles n'eurent comme conséquence qu'un ajustement des réglages de la chaîne transversale de commandes de vol de l'avion, les divergences notables entre le vol et nos prévisions en ce qui concerne le lacet induit par le braquage différentiel des élevons en supersonique à faible altitude (fig. 3). Les mesures effectuées en soufflerie n'étaient pas en cause ; par contre, l'effet de l'aérodistorsion sur ces coefficients avait été évalué de façon particulièrement erronée.

Moins anecdotiques, par leur conséquence sur la définition même des commandes de vol, ont été les quelques divergences observées entre le vol et la soufflerie en ce qui concerne la stabilité longitudinale de l'avion. Ces différences restèrent toujours très faibles, mais cependant suffisantes pour remettre en cause le bilan d'équilibrage longitudinal de l'avion, aux faibles Mach, dans la gamme des incidences maximales praticables (fig. 4). Ce fait, associé au désir de ne sacrifier en aucune manière la manoeuvrabilité transversale a ces incidences, nous a conduit très rapidement au cours de l'expérimentation des prototypes à augmenter légèrement le braquage à piquer des élevons de l'avion.

Enfin, nous devons citer parmi les "surprises" aérodynamiques décelées par le vol une évolution, en fonction du nombre de mach, des caractéristiques aérodynamiques longitudinales de l'avion à grande incidence beaucoup plus brutale en transsonique que nous ne le laissait supposer la soufflerie (fig. 5). Ce fait, sans avoir eu de conséquence sur la définition de base du système de commandes de vol de l'avion, n'a certes pas simplifié la mise au point des fonctions de limitation automatique d'incidence et de facteur de charge, en particulier pour des phases de vol conduisant à des variations très rapides du nombre de Mach (décélération transsonique en butée de manche par exemple).

Telles sont les seules divergences vol/prévisions qui se soient vraiment révélées significatives quant à la définition des commandes de vol de l'avion et à son comportement.

En particulier le domaine d'incidence et de manoeuvrabilité du MIRAGE 2000 est pratiquement identique à celui qui était prévisible avant même le premier vol du premier prototype. Ceci signifie, entre autre, que les différences entre les caractéristiques aérodynamiques transversales réelles de l'avion et celles qui avait été prévues par la soufflerie (fig. 6) sont restées suffisamment faibles pour ne pas être significatives vis-à-vis du comportement de l'ensemble avion + commandes de vol.

Dans le domaine même des très faibles vitesses et donc des très grands dérapages et incidences, le comportement de l'avion, au cours des centaines d'essais réalisés en vol, s'est révélé semblable à celui qui avait été observé durant l'importante campagne de simulation qui avait précédé ces essais, simulation dont les bases aérodynamiques de représentation de l'avion étaient directement issues de soufflerie basse vitesse couvrant un domaine d'incidence et de dérapage de ± 180°. D'ailleurs, malgré les difficultés d'exploitation inhérentes à ce type très particulier d'essais en vol, il est possible de comparer les accélérations angulaires, subies par l'avion en vol à celles qu'aurait subit le modèle de simulation dans les mêmes conditions. Même dans les cas de manoeuvres particulièrement sévères, le recoupement est très satisfaisant (fig. 7).

⁂

L'excellente qualité d'ensemble de nos prévisions avant vol a été un facteur très important dans le bon déroulement de la mise au point des commandes de vol du MIRAGE 2000. Cette qualité résulte certes de milliers d'heures passées en soufflerie mais aussi de l'expérience des équipes chargées d'exploiter, et surtout d'interpréter, les données qui furent ainsi rassemblées, expérience acquise au fil des deux dernières décennies à l'occasion de réalisations aussi variées que les MIRAGES V à décollage vertical, les MIRAGES F, les MIRAGES G à géométrie variable, etc ..., dont les systèmes de commandes de vol préfiguraient déjà à plus d'un titre le système de commandes de vol strictement électriques du MIRAGE 2000.

Un autre facteur de succès, et non des moindres, est à prendre en considération : le fait que la Société AVIONS MARCEL DASSAULT-BREGUET AVIATION assure elle-même la conception, la réalisation et la production des systèmes de commandes de vol de ses avions ; il en résulte un très haut niveau d'intégration des équipes de toute discipline qui participent au développement d'un avion, depuis le stade de sa conception jusqu'au stade de sa mise en série, en passant par le stade primordial de la mise au point en vol.

⁂

Fig. I

DOMAINES D'INCIDENCE ET DE DERAPAGE

ANGLE OF ATTACK AND SIDESLIP ENVELOPES

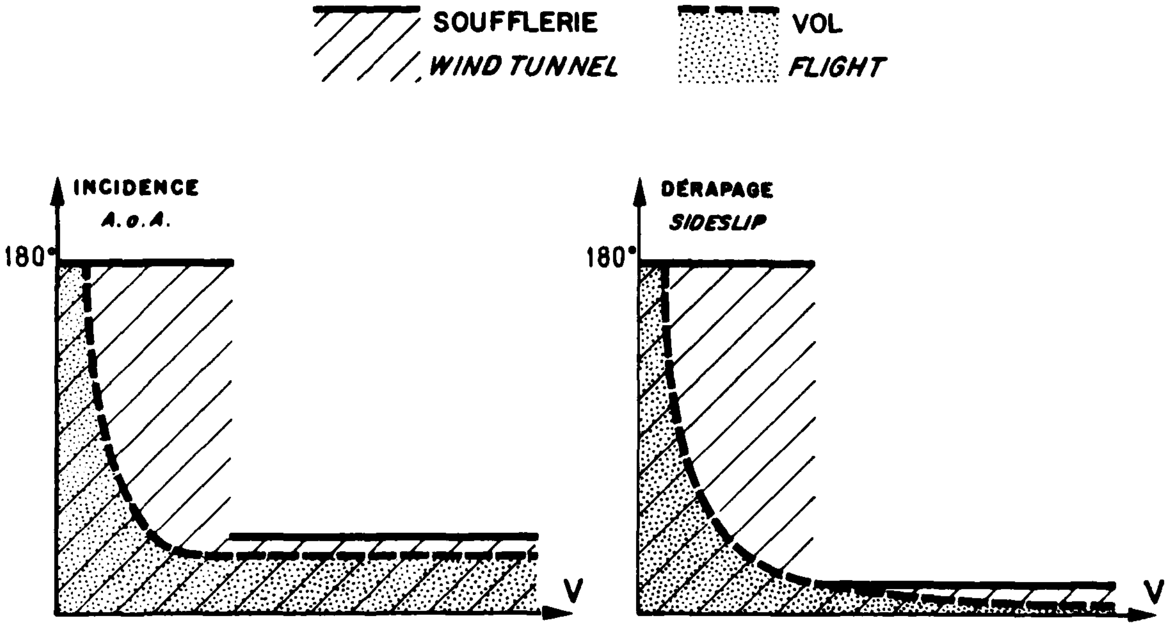
SOUFFLERIE
WIND TUNNEL
VOL
FLIGHT
INCIDENCE
A.o.A.
180°
V
DÉRAPAGE
SIDESLIP
180°
V

ESSAIS EN SOUFFLERIE
TRES GRANDES INCIDENCES
- 180° $< \alpha <$ 180°
- 180° $< \beta <$ 180°

WIND TUNNEL TESTS
AT VERY HIGH ANGLE OF ATTACK

SOUFFLERIE S4
DU C.E.A.T. TOULOUSE

Fig. 2

Fig. 3

LACET DŪ AU BRAQUAGE DIFFERENTIEL D'ELEVONS

YAWING MOMENT DUE TO DIFFERENTIAL ELEVON DEFLECTION

MACH = 1.20

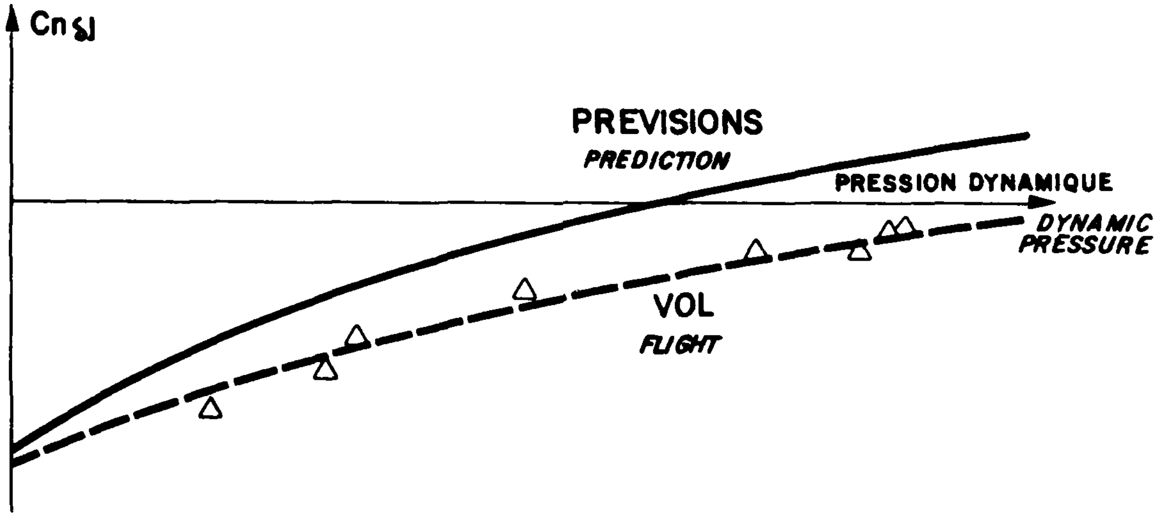

Fig. 4

STABILITE LONGITUDINALE A BASSE VITESSE

LONGITUDINAL STABILITY AT LOW SPEED

VOL / SOUFFLERIE

FLIGHT / WIND TUNNEL

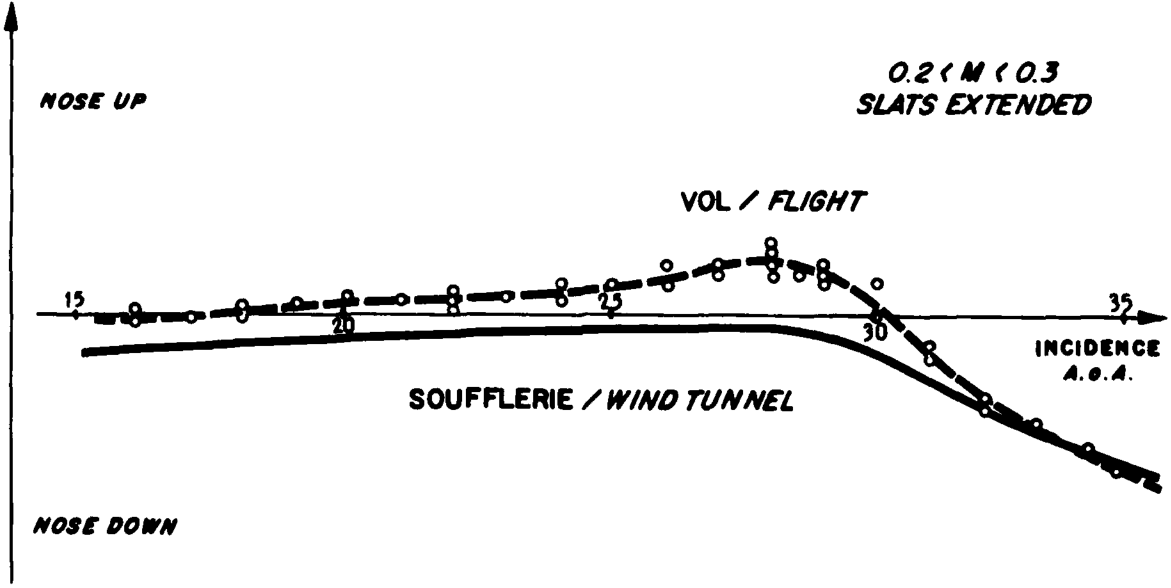

Fig.5 EVOLUTION DU MOMENT DE TANGAGE EN TRANSSONIQUE

PITCHING MOMENT VS MACH IN TRANSSONIC FLIGHT REGIME

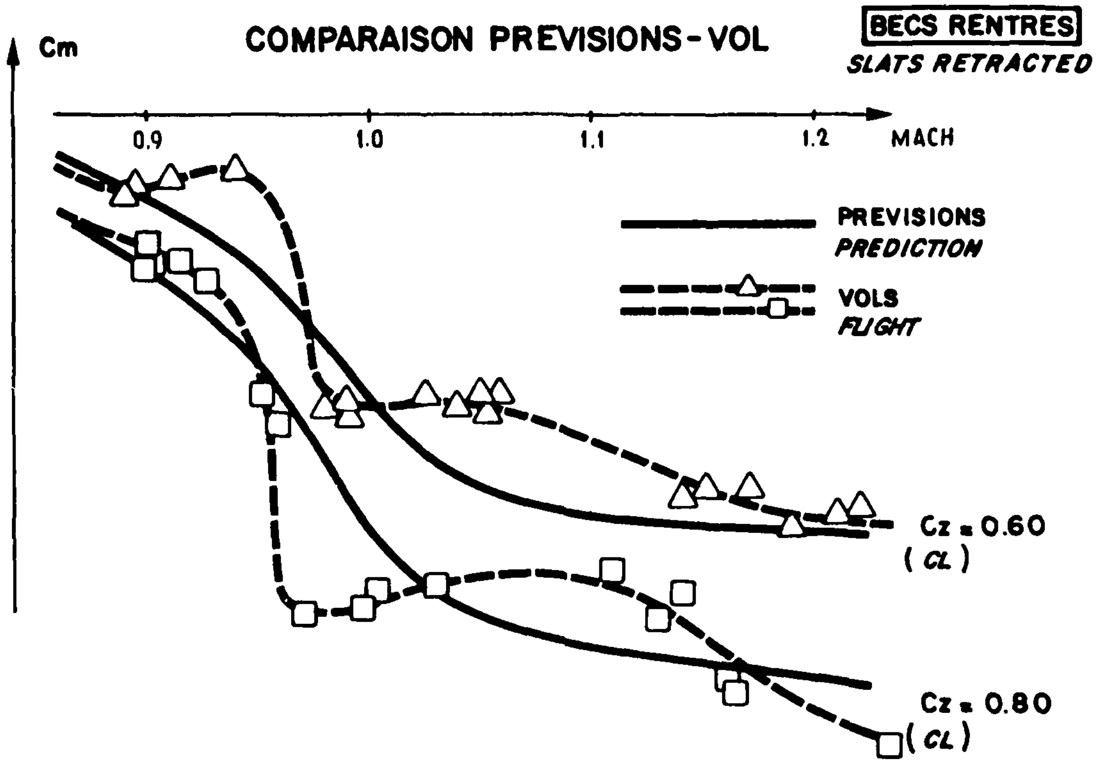

Fig.6 MOMENTS DE ROULIS ET DE LACET A GRANDE INCIDENCE

ROLLING AND YAWING MOMENT AT HIGH ANGLE OF ATTACK

COMPARAISON VOL-SOUFFLERIE

FLIGHT-WIND TUNNEL COMPARISON

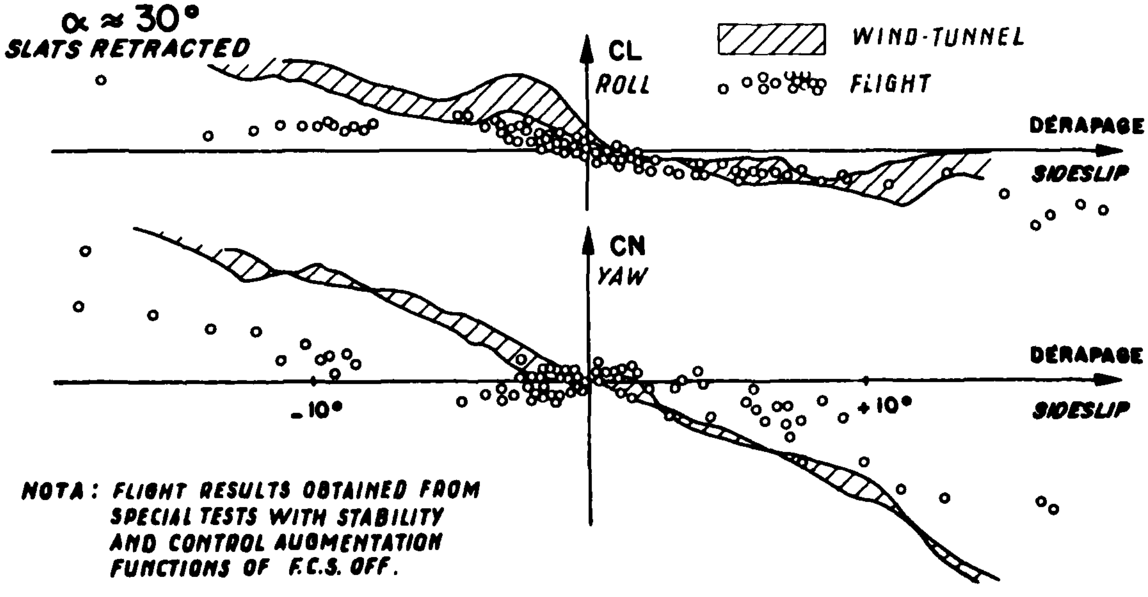

NOTA : FLIGHT RESULTS OBTAINED FROM SPECIAL TESTS WITH STABILITY AND CONTROL AUGMENTATION FUNCTIONS OF F.C.S. OFF.

Fig. 7-TONNEAUX ENCHAINES VERTICAUX JUSQU'A VITESSE NULLE

CONSECUTIVE VERTICAL ROLLS UPTO ZERO SPEED

COMPARAISON VOL / PREVISIONS

FLIGHT / PREDICTION COMPARISON

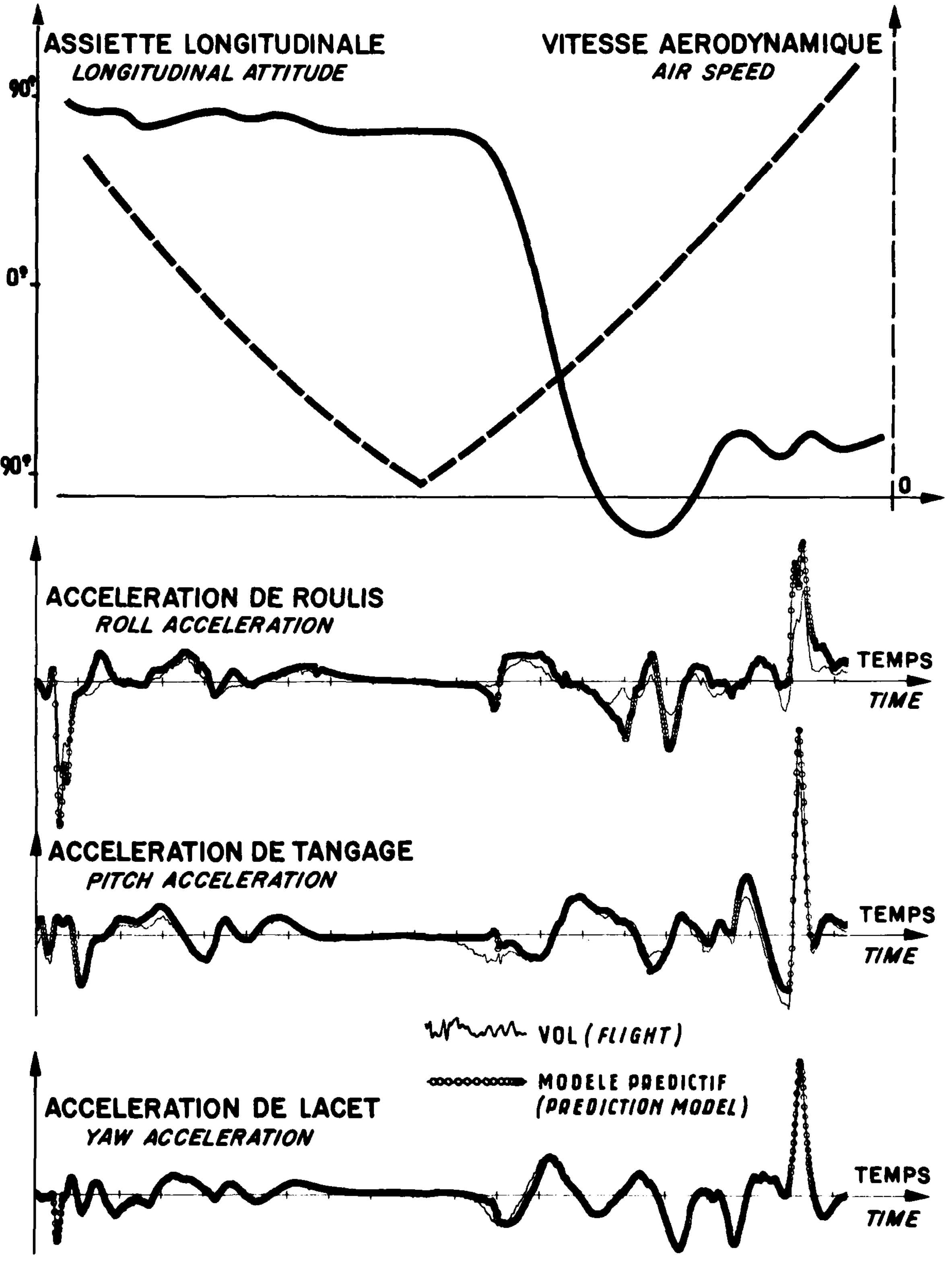

THE USE OF FREE-FLIGHT MODELS FOR THE PREDICTION OF DEPARTURE CONTROL

by

G. F. Moss, A. Jean Ross, Geraldine F. Edwards, E. B. Jefferies
Aerodynamics Department,
Royal Aircraft Establishment,
Farnborough, Hants, UK

SUMMARY

This paper discusses the importance of prediction techniques for the flight-dynamic behaviour of proposed aircraft projects and in particular the use of the free-flight model technique in this context. Such free-flight models are able to carry on-board flight-control systems and can be used to evaluate stability-augmentation and departure-prevention methods. Examples of flight records of free-flight tests are presented and comparisons made with theoretical predictions and corresponding full-scale data. A research programme using HIRM, a high incidence research model configuration, is described which has as its central objective the widening of understanding of the flight-dynamics phenomena of combat aircraft at high angles-of-attack.

1 INTRODUCTION

Techniques to predict the flight-dynamic characteristics of new combat aircraft are becoming increasingly more important as the level of technology in the design of such aircraft continues to rise. Two design trends are of particular interest in this respect: first, the use of configurations of advanced performance which are naturally unstable and which therefore rely critically on stability augmentation from a sophisticated flight-control system, and second, the developing operational requirement for a 'carefree manoeuvre' capability up to and perhaps beyond the natural aerodynamic limits, using a control system with built-in departure-prevention features. Both these trends are leading to the use of more complex control systems with sophisticated logic which are not easy to design when the aerodynamic derivatives and characteristics generally are non-linear and irregular, as is very often the case when flow separations develop at high angles-of-attack. The development of a control system which is satisfactory with respect to departure prevention at high incidence and which also enhances the ability of the pilot to make best use of his vehicle can be both costly and time consuming at the flight development stage of a new project and can carry a considerable degree of risk to the safety of both pilot and vehicle.

At the heart of this problem is the need for good prediction methods for use before and during the flight-test stage of a new project. Indeed, right from the start important decisions have to be made by the aircraft designer, for example which dynamic features of the configuration are likely to be critical and the nature of the control system which will be required, when comparatively crude theoretical predictions backed by very limited wind-tunnel test data have to be relied on. As regards the high-incidence departure characteristics in particular, these early decisions could be crucial. Over the years considerable experience from project development work has been acquired in the mathematical modelling techniques used to make predictions of aircraft dynamic behaviour and to design appropriate control systems, but the acquisition of the necessary aerodynamic derivatives and the accurate determination of the non-linear aerodynamic characteristics at high angles-of-attack can be a stumbling block. As well as extensive static wind-tunnel tests to obtain the forces, moments and control derivatives, it is necessary to make oscillatory, rotary and other time-dependent tests. At the RAE, in addition to research on mathematical modelling techniques and the development of wind-tunnel steady and unsteady experimental techniques to support this, research has also been pursued to develop a low-speed, free-flight* model technique, first to provide further data for the mathematical models themselves and then to check out the predictions of dynamic behaviour made with these mathematical models.

This paper refers to some of the recent developments in the RAE free-flight model technique, presents some data from the research work on departure characteristics carried out with this technique in recent years, and finally describes a new RAE research project on the high-incidence dynamic characteristics of combat aircraft.

2 RAE FREE-FLIGHT MODEL TECHNIQUE

The technique, which is essentially aimed at the investigation of low-speed, high incidence flight conditions, has been referred to in one or two recent papers[1,2], but development over the years has been continuous and an update at this stage is not inappropriate. Only comparatively recently has the concept of a fully-active on-board flight-control system been included and this has been useful for the purposes of high-incidence research into the design of flight systems. On direct link, *ie* without such a control system in the loop, the models are generally pre-programmed to execute a chosen sequence of control-surface positions, but some provision is now being made for an up-link from the ground to augment this simple system in some limited respects. The controls are operated by electric motors powered by batteries, other actuators required in the model recovery procedure being operated by compressed air carried in bottles. The model mass and inertias are carefully controlled in manufacture and assembly, the object being to provide a number of nominally identical models, Fig 1, which can be used in turn to obtain data in depth for a small number of selected configurations. The external lines of the models are standardised by the use of a casting-mould method of manufacture, a modular construction being used to enable damaged components to be replaced quickly and easily.

---

* No propulsion units are used.

For each drop the model is lifted from a trolley, Fig 2a, and towed to the altitude for launch by means of a helicopter, a long cable being used, Fig 2b. During this operation a small parachute is deployed from the model to avoid undue swinging on the cable, but this is jettisoned at the moment of release. The model is launched in a flying attitude at a prescribed forward speed, so usually meaningful flight data is obtained right from the time of release until the activation of the recovery procedure. Recovery is effected at low altitude by the deployment of large parachutes and the model finally lands on the ground, the shock being taken by inflated air bags on the lower surface of the fuselage, Fig 3a. Generally it is possible to re-use a model after each drop following any necessary recalibration of instruments, repair of minor damage, etc, but sometimes major repairs are required, *eg* if unexpected dynamic behaviour occurs and the recovery system is defeated, as in the case shown in Fig 3b. Recovery techniques are continually being improved and catastrophies of this kind have been rare, however. With a series of three or four identical models available a fairly continuous test programme can be conducted, weather and range facilities permitting. During the free-flight of the model, which can last up to 100 or more seconds* dependent on the nature of the test, the model transmits data to a ground receiver by telemetry and is tracked by accurate radar scanners and/or kinetheodolite cameras as required. The required sequence of control movements for each drop is set up beforehand and all systems are activated at the point of release, including the flight-control system and/or departure prevention systems that are being used. It is possible to switch such systems in and out during the flight either using the on-board programmer or by remote control. Telemetred data generally includes signals from linear and angular accelerometers, rate and attitude gyros, the position of control surfaces, pitot - static pressures, incidence and sideslip vane angles, various in-flight instrument calibration voltages, and the demand and output sides of any control systems in use. All data is recorded for off-line processing and analysis, but during the flight selected parameters are displayed on-line for on-the-spot monitoring purposes. Fig 4 shows some of the internal components which have to be carried in a typical model drop.

3 RESEARCH USING THE TORNADO CONFIGURATION

Over the last few years RAE has used the configuration of the Tornado aircraft for research purposes with respect to the development of the free-flight model technique and the derivation of mathematical models for the prediction of flight-dynamic behaviour. Both the original IDS version of this variable wing-sweep aircraft and the later ADV design have been used, the latter having in particular a longer and more slender nose, Fig 5, which was expected to aggravate the departure characteristics at high angles-of-attack. The models have all been carefully scaled to ¼ full-size by linear dimension. Three ranges have been used for these free-flight trials: the RAE Larkhill range in the UK, the Woomera range in South Australia and the NASA Dryden facilities on the USAF Edwards Base in California, USA. The large size of the latter two ranges has been essential for some of the testing carried out, *ie* where the maximum possible travel of the model has been large. Sample data from some experiments on all three ranges is presented in this paper.

Two flight-control systems have been used in conjunction with these models, an analogue system and a more 'advanced' reprogrammable digital system. Only data from tests with the analogue system, Fig 6, are presented here, and in the design of the basic Command and Stability Augmentation System (CSAS) for this, some simplifying assumptions have been made because operation was only required at low forward speeds (less than 150 kn IAS model scale, 300 kn full scale). The design comprised conventional pitch, roll and yaw dampers but with some prescribed limitation of authority in pitch and some 'wash-out' in yaw to avoid some of the pro-spin tendencies that such systems can have at high incidence. The analogue departure-prevention system took the form of a Spin Prevention Incidence Limiting System (SPILS), similar to that proposed by British Aerospace for the UK version of Tornado. Basically this system, which is designed to be put in series with the CSAS, reduced the authority of the 'stick' and 'rudder pedal' inputs by factors dependent on angle-of-attack, but with some advance determined by pitch-rate to avoid any tendency to overshoot in dynamic approaches to the stall. The above brief description gives only the basic features of the CSAS and SPILS modules: for both of these the detailed design was extremely complex.

4 COMMENTS ON THE FLIGHT RECORDS OF FIGS 7-17

In these figures, the two different configurations mentioned above, IDS and ADV, are referred to as 'I' and 'A' respectively, and in the model data of Figs 7, 10, 11, 13-17 all reference to parameters is given in terms of full-scale aircraft size rather than model size in order to facilitate comparison with the aircraft data of Figs 8, 9 and 12. For the ¼-scale model size this has meant that model test values of angular rates have been halved and the timescale has been doubled numerically. The model velocity has also been doubled (see Ref 3 for the derivation of scaling factors).

---

* Equivalent to 200 or more seconds for a full-scale aircraft of ×4 the size.

The model drop programme has included several configurations of the wing, but only data from tests with a leading-edge sweep of 25° and without manoeuvre devices deployed is presented in these figures. Also, for all these data the centre of gravity of the model was standardised at 28% and 13½% of wing geometric mean chord for the 'I' and 'A' configurations respectively. Angles of incidence and sideslip in flight have been taken from vanes mounted sometimes on a nose probe (*eg* Fig 1) and sometimes on the side of the fuselage (*eg* Fig 5). Thorough calibrations have been carried out, however, and all appropriate corrections have been applied to make the data comparable between figures for the purposes of this paper. Lastly, for ease of comparison a common format has been adopted for all the flight records quoted, but care should be taken to observe the scales of parameters quoted in different figures since it has not been possible to standardise these satisfactorily. It should be noted that pilots' input rather than control surface position has been used as standard throughout.

Fig 7:

This first record shows two separate time slices from a fairly long drop made at the Woomera range with the 'I' model configuration without any control augmentation switched in. Two levels of incidence are quoted, *circa* 25° and *circa* 30°, for the pitch-control input set at -10° and -14.6° respectively (tail-setting in this instance). At each condition a sharp rudder pulse was made to trigger a Dutch-roll type of oscillation. At the lower incidence the model response is fairly well damped, but at the higher value a divergence occurs. Records of free flight experiments of this type have been analysed to yield aerodynamic derivative data which, along with data from static and oscillatory wind-tunnel tests, has enabled a mathematical model to be set up to predict model dynamic behaviour from any given schedule of control settings.

Fig 8:

The record for the model test shown in Fig 7 may be compared with a similar record for the unaugmented full-scale aircraft, shown in Fig 8. We are extremely grateful to British Aerospace for the use of these data, and also that of Figs 9 and 12. In Fig 8 the dynamic response is triggered by combined rudder-pedal and lateral-stick movements, and at the start of the time slice even quite vigorous, if uncoordinated, pedal and stick movements are unable to trigger a divergence at incidences near 21°. This is compatible with the model record of Fig 7. However, at a higher incidence of about 24° (at $t \simeq 17$ seconds) a large coordinated movement of the two controls does result in a divergent oscillation, helped along by continued control movements as this develops. The wing in this case has manoeuvre devices deployed which makes direct comparison with the data of Fig 7 impossible, but similarities are apparent which are not without interest.

Fig 9:

When the full CSAS is switched in, as in Fig 9, the effect on the response of the same aircraft configuration of Fig 8 is dramatic. A Dutch-roll type of oscillation is excited early in the time slice by very vigorous roll-stick movements but this quickly dies away once this excitation is stopped (at t = 12 seconds) even though incidence is allowed to drift upwards from about 25°. At the end of the record similar vigorous stick movements at a somewhat higher incidence of 27° fail to cause a significant response. Thus the use of the CSAS is seen to be beneficial for such types of control movements.

Fig 10:

However, flight tests of the type shown in the records of Figs 8 and 9 are not without risk to the safety of aircraft and pilot since at the time little may be known about the nature of the departure characteristics which could follow such vigorous control movements at these high incidences. Fig 10 shows a more daring test made at the same incidence of 27° of the record of Fig 9 but with crossed 'pilot' inputs to rudder and roll control, this time made with the corresponding free-flight model fitted with a full CSAS module. This combination of maximum-control demanded inputs almost at once causes a full departure of the vehicle, leading to oscillatory spin behaviour up to very high incidences (74° maximum). It clearly would have been foolhardy to risk such a test on the full-scale aircraft.

Fig 11:

The inclusion of a control system such as CSAS can, however, cause subtle problems in the use of a free-flight technique, as Fig 11 shows. Here the incidence is being held at a comparatively low level but a rudder pulse triggers a slow but progressive wing drop in addition to the expected damped oscillation. This wing drop resulted in a large increase in bank angle which in turn caused an increase in pitch rate due to gravitation effects and thus a progressive reduction in incidence away from the natural trimmed attitude. Attempts to find aerodynamic-flow 'fixes' to avoid this non-representative sequence of events were all in vain, and this has led to a bank-angle-hold system being installed into the model control system as standard for any tests in which such effects are likely to occur.

Fig 12:

The use of the SPILS departure-prevention system on the full-scale aircraft is clearly demonstrated by the flight record of Fig 12. First, the difference between the control positions demanded by the pilot and those which actually occur is shown for the three controls. Dependent on the incidence-vane input the authority of the pilot over the controls has been reduced, this being the main function of this type of prevention system. Incidence is limited to a maximum of 28° with stick hard back and even with superimposed severe crossed inputs to rudder-pedal and roll-stick there is little or no overall adverse dynamic response or hint of departure. The aircraft with this combined CSAS and departure prevention system in use may thus be regarded as proof against even the most undesirable control movements a disorientated pilot may inadvertently make in the heat of combat. The performance of these systems in this respect is really very impressive.

Fig 13:

From a research point of view it is indeed a pity that it was not possible to repeat the pilot control inputs of the record of Fig 12 without the SPILS departure-prevention system switched in, just to clinch the matter. However, perhaps the record of the model free-flight test of Fig 13 may suffice. In this test, the unaugmented model was trimmed out at an incidence of about 28°, as at the start of the full-scale record of Fig 12, and then crossed control inputs to rudder and roll 'stick' similar (but in the opposite sense) to those of Fig 12 were applied. The flight record speaks for itself: departure is swift and complete with excursions in incidence up to 85° and strong gyrations and oscillations about all three axes.

Fig 14:

In the free-flight model research programme, the use of a departure prevention system has been investigated on the 'A' configuration in collaboration with NASA Dryden as a research study. This configuration was regarded as a more challenging case than the 'I' configuration because of the longer nose and some other features. In Fig 14 we have a record for a sequence of control changes not too far from those shown for the 'I' aircraft in Fig 12. With full-back stick (-32° tail-setting demanded) a much reduced tail-setting is apparent and incidence is limited to about 23°. The application of crossed control inputs of rudder and roll 'stick' is heavily modified by the SPILS departure-prevention system and only a small-amplitude dynamic response therefore occurs which quickly dies away. The comparison with the 'I' aircraft record of Fig 12 is quite striking and serves to demonstrate the usefulness of this free-flight model technique to predict the effectiveness of such prevention systems in advance of flight tests.

Fig 15:

The record of the fully augmented 'A' configuration model of Fig 14 may be contrasted with the corresponding record for the unaugmented model, a free-flight experiment also carried out in collaboration with NASA at the Dryden research centre. A much lower pitch 'stick' input was needed to achieve a starting incidence of 23°, *ie* about the same value as that for the augmented model trial of Fig 14. In this trial a small extra stick-back input was made as the lateral controls were moved, but even so there is no doubt of the effect of a sudden application of crossed rudder and roll-'stick' controls as was used in the record of Fig 14. Oscillations are initiated on all three axes and there is a sudden total departure at t = 4 seconds, *ie* 2 seconds (full scale) after the input of crossed control deflections.

Fig 16:

The two model trials, the data from which Figs 14 and 15 have been prepared, have been the subject of theoretical predictions using the best mathematical model we have been able to define from available sources, *ie* wind-tunnel data (static and oscillatory), free-flight control-response records and estimates. Fig 16 shows the simulated flight record thus obtained for the sequence of control deflections used in the free-flight experiment of Fig 15. The agreement between this theoretical simulation and the experiment is very encouraging to say the least, particularly in the important early stages of the departure.

Fig 17:

A similar comparison can be seen between the simulated theoretical response record of Fig 17 and the experiment of Fig 14. For this simulation the characteristics of the CSAS and SPILS control systems were modelled mathematically and added to the mathematical model used for the simulation of the unaugmented vehicle, shown in Fig 16. Once again the same sequence of control deflections has been taken as used in the free-flight experiment and comparison with Fig 16 clearly shows an overall result similar to the free-flight tests (compare Figs 14 and 15) as regards effectiveness of the departure prevention system.

Summarising this part of this paper, we can say that the free-flight technique described has been shown to be advantageous for the prediction of the effectiveness of departure-prevention-systems, and thus can be used with confidence for this purpose during full-scale development tests on new combat aircraft equipped with such systems. Also, the model data obtained has been found to be very useful in the construction of mathematical models for the development of reliable prediction methods for the dynamic behaviour of aircraft with departure-prevention systems. It is suggested that for future advanced combat aircraft, which probably will rely on a fair degree of natural longitudinal instability and an effective 'carefree manoeuvre' capability up to high angles-of-attack, the use of such a free-flight model technique could make a strong contribution to the overall design process.

5 HIRM RESEARCH PROGRAMME

After the experience obtained in the development of the free-flight model technique using the Tornado models, described in sections 3 and 4 above, we have decided to widen the scope of the research work on flight dynamics at RAE with the use of a more novel type of combat aircraft configuration. For some years RAE has been interested in the potential of 'three-surface' configurations which have a close-coupled canard as well as an aft tail, both of which can be used as controls. As other researchers have found[4-6] in addition to the lift-drag performance advantages which can be obtained by adding the extra surface, there can also be more scope for better control characteristics at high incidences, provided that a modest degree of natural longitudinal instability is assumed and that an adequate flight control system can be designed to handle the more complex control options which present themselves.

After some preliminary wind-tunnel work (and one or two false starts) the configuration of Fig 18 was established as suitable for this work, and this is now referred to as the High Incidence Research Model (HIRM). From the start the configuration has been regarded basically as a free-flight model, there being no full-scale aircraft counterpart to consider. Fig 18 shows the salient dimensions of the design in millimetres. There are five independently-driven control surfaces (two foreplanes, two tailplanes and the rudder) and the possible use of these in various ways has been investigated in a comprehensive programme of static wind tunnel tests (eg Fig 19). Also, rotary balance[7] dynamic tests have been carried out* (Fig 20) and oscillatory derivative tests[8] (Fig 21), both for a number of control-configuration options. The oscillatory-derivative measurements have included oscillations in pitch, heave, roll, yaw and sideways motion, and some cross-coupled measurements have been made in addition to the usual primary ones. Alternative leading-edge droop settings are available but no trailing-edge flaps are incorporated on the wing at present. The wind-tunnel test programme has used a range of incidence up to 90°, since of particular interest is the investigation of departure at extreme attitudes. Only a modest range of sideslip has been possible so far, however, but one of the free-flight models is to be tested in the RAE 5m tunnel soon which will allow a large range to be covered. This mass of wind-tunnel data is being used to select optimised control schedules and to design several active flight-control systems of different degrees of sophistication, bearing in mind that the free-flight models will have an adjustable range of static margin (pre-stall) from about +5% to -8% aerodynamic mean chord. The first flight in the programme is expected to occur about the end of this year (1982) with the simplest of control-systems possible carried on-board, and it is hoped that the first major free-flight trials series will be accomplished within the following year, in collaboration with NASA Dryden, with a number of more complex systems available. The design and provision of these control systems, which are such an important part of the whole project, are the concern of Flight Systems Department at RAE Farnborough.

A good deal of attention is at present being given to the establishment of a data set and the derivation of suitable mathematical models for the high-incidence dynamic characteristics of this HIRM project. Passing reference has been made to some aspects of this in a recent paper[9]. The project offers a rare opportunity to base such mathematical modelling on an entirely consistent data bank, the configuration of all wind-tunnel and free-flight models having been standardised right from the start. So often in the use of aircraft project models for this type of work complications arise from changes to the configuration detail during the flight development stage which need to be taken account of; hopefully with HIRM it should be possible to maintain a more consistent approach. The logic of the general approach to the mathematical-model development is shown in Fig 22. The model will be used to design the active control system and also to suggest free-flight experiments which need to be made with this system. As a result of these experiments more aerodynamic data will be obtained to help check on the initial form of the mathematical model and to enable predictions to be checked against actual dynamic responses. As appropriate more wind-tunnel work will be initiated to provide further data and a sensitivity analysis will be made before revising the basic model and going round the loop again. In this way it should be possible to improve the basic standard of the prediction method for dynamic behaviour at high incidence and progressively develop a flight control system able to prevent departure and give a good standard of control over a wide range of flight conditions at low speed.

The HIRM research programme is fully described elsewhere[10], but it is hoped that the brief remarks above in the context of the experience gained with the Tornado research models previously described show something of the challenge we have set ourselves with this new programme.

6 CLOSING REMARKS

It has been demonstrated by correlations with flight data and theoretical predictions that a free-flight model technique using on-board control systems, such as that described here, can be a powerful tool for the achievement of a good standard of high-incidence performance, particularly when backed by a soundly-based mathematical model to help design the necessary active-control systems. It is confidently expected that the new HIRM research programme with its greater scope will be able to take this technology further and generally widen our understanding of high-incidence control of combat aircraft.

---

* These particular tests were carried out under an extramural contract at BAe Warton.

REFERENCES

1 R. Fail. "The role of free-flight models in aircraft research and development." Paper, AGARD CP 119, April 1972

2 H.H.B.M. Thomas and Geraldine F. Edwards. "Mathematical models of aircraft dynamics for extreme flight conditions (theory and experiment)." Paper, AGARD CP 235, May 1978

3 C.O. O'Leary and H.H.B.M. Thomas. "Proposals for investigating the stalling dynamics of aircraft." RAE Technical Memorandum Aero 1188 (1970)

4 J.W. Agnew and J.R. Hess, Jr. "Benefits of aerodynamic interaction to the three-surface configuration." AIAA Paper 79-1830 (1979)

5 J.W. Agnew, G.W. Lyerla and S.B. Grafton. "The linear and non-linear aerodynamics of three-surface aircraft concepts." AIAA Paper given at the Atmospheric Flight Mechanics Conference, Danvers, Massachusetts, 1980

6 M.A. Croom, S.B. Grafton and L.T. Nguyen. "High angle-of-attack characteristics of three-surface fighter aircraft." AIAA Paper 82-0245, January 1982

7 A.W. Matthews. "Experimental determination of dynamic derivatives due to roll at British Aerospace, Warton Division." Paper 4, AGARD CP 235, May 1978

8 C.O. O'Leary. "Wind-tunnel measurement of aerodynamic derivatives using flexible-sting rigs." Paper 5, AGARD LS 114, May 1981

9 A. Jean Ross. "A comparison of analytical techniques for predicting stability boundaries for some types of aerodynamic or cross-coupling nonlinearities." Paper 17, AGARD CP 333, April 1982

10 G.F. Moss, A. Jean Ross and G.F. Butler. "A programme of work on the flight dynamics of departure using a high incidence research model (HIRM)." RAE Technical Memorandum Aero 1950 (1982)

FURTHER PUBLICATIONS IN PREPARATION:

11 P.J. Allen and D. Booker. "Large scale rolling-rig tests on the RAE Model 2130 (HIRM 2) in the BAe Warton 5.5m low speed wind tunnel." BAe Report AXR 103 (to be issued)

12 A. Jean Ross and G.E.A. Reid. "The development of mathematical models for the RAE High Incidence Research Model (HIRM). Part I: Analysis of static aerodynamic data. Part II: Analysis of oscillatory and rotary aerodynamics data." RAE Technical Reports in preparation

13 D. Pierce and G.F. Moss. "Wind tunnel tests at M = 0.60 and 0.80 of a three-surface aircraft configuration." RAE Technical Memorandum in preparation

Copyright ©, Controller HMSO, London 1983

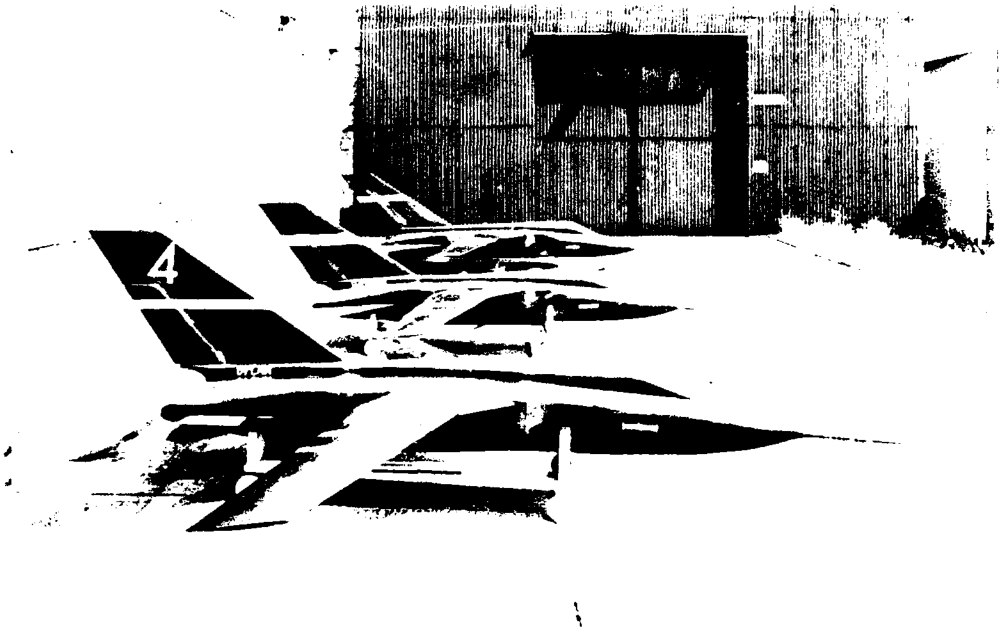

Fig 1 Three identical free-flight models ready for testing

Fig 2a Model at lift-off (NASA Dryden)

Fig 2b Model under tow (RAE Larkhill)

Fig 3a Model recovery after a free-flight trial (Woomera range)

Fig 3b "... but sometimes major repairs are required"

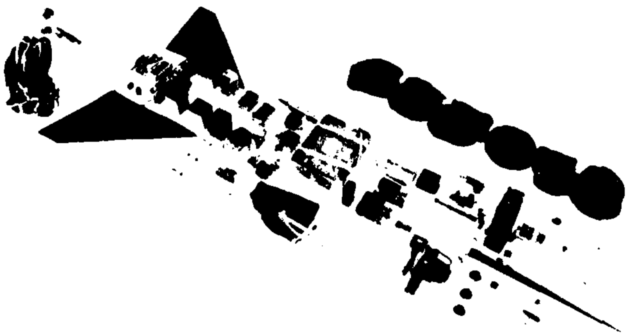

Fig 4 Display of principle free-flight model components

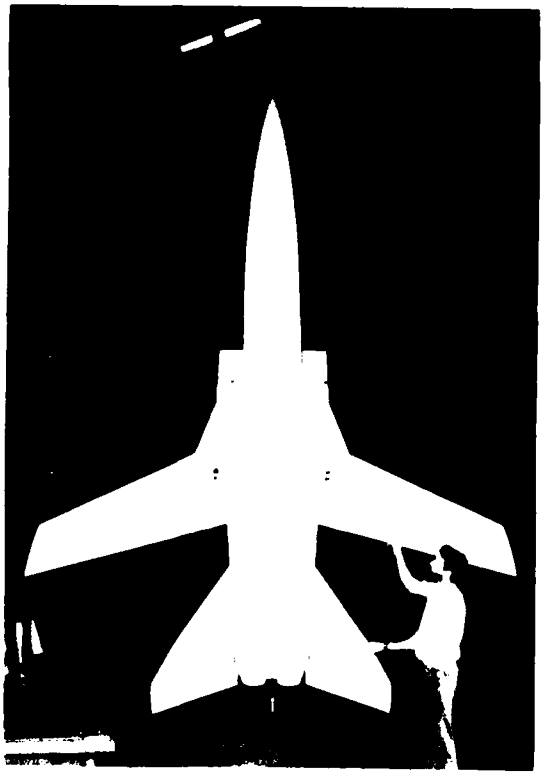

Fig 5 'A' model configuration on bi-filar rig

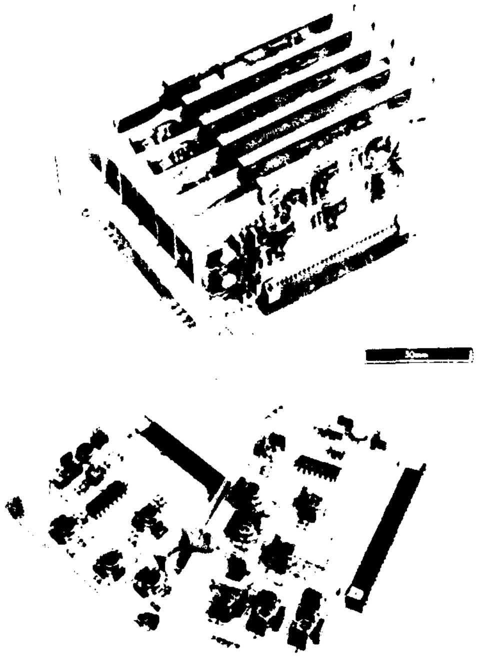

Fig 6 CSAS/SPILS flight-control and departure-prevention system

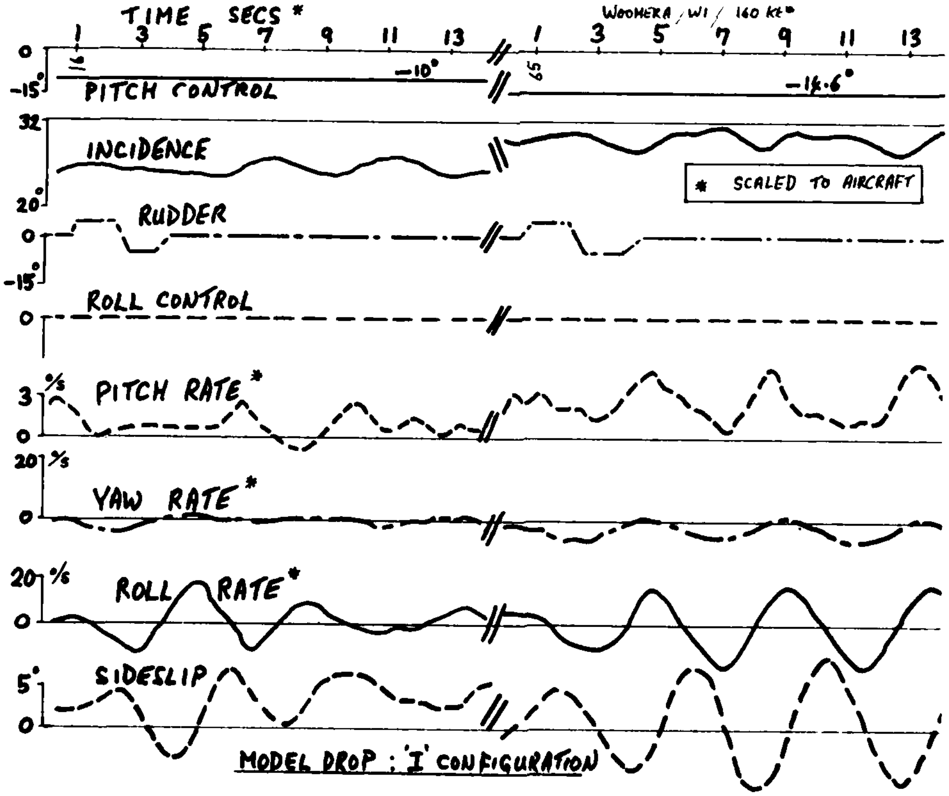

Fig 7 Excitation of Dutch-roll by means of rudder pulses

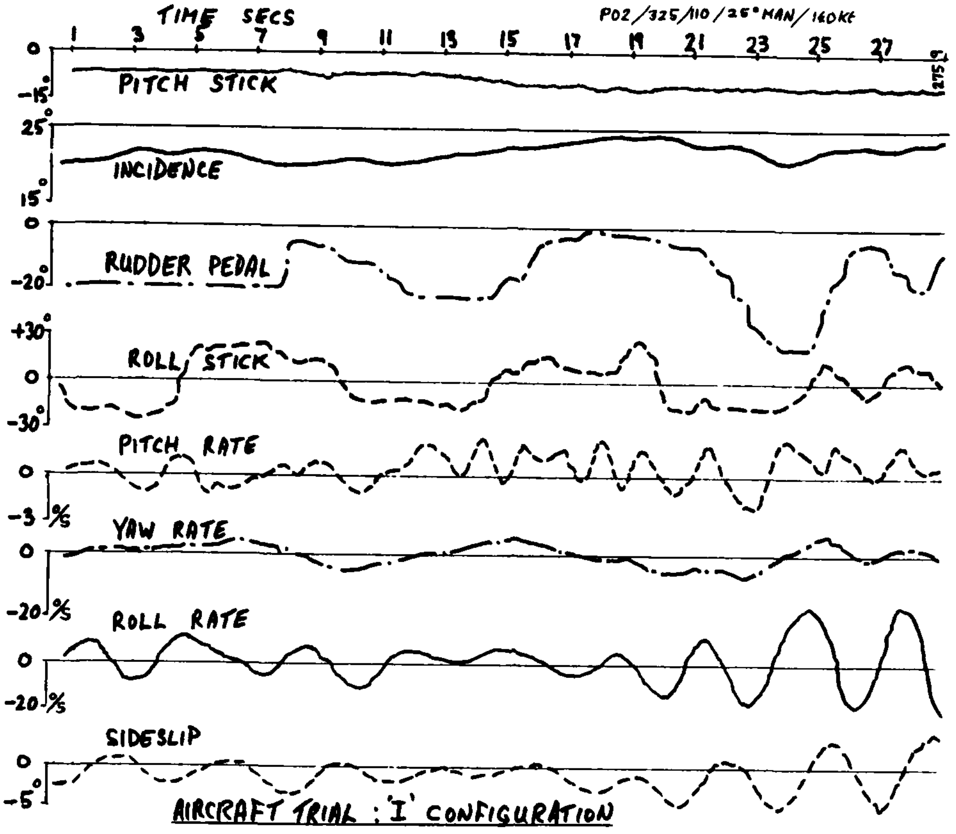

Fig 8 Excitation of Dutch-roll from rudder and taileron movements

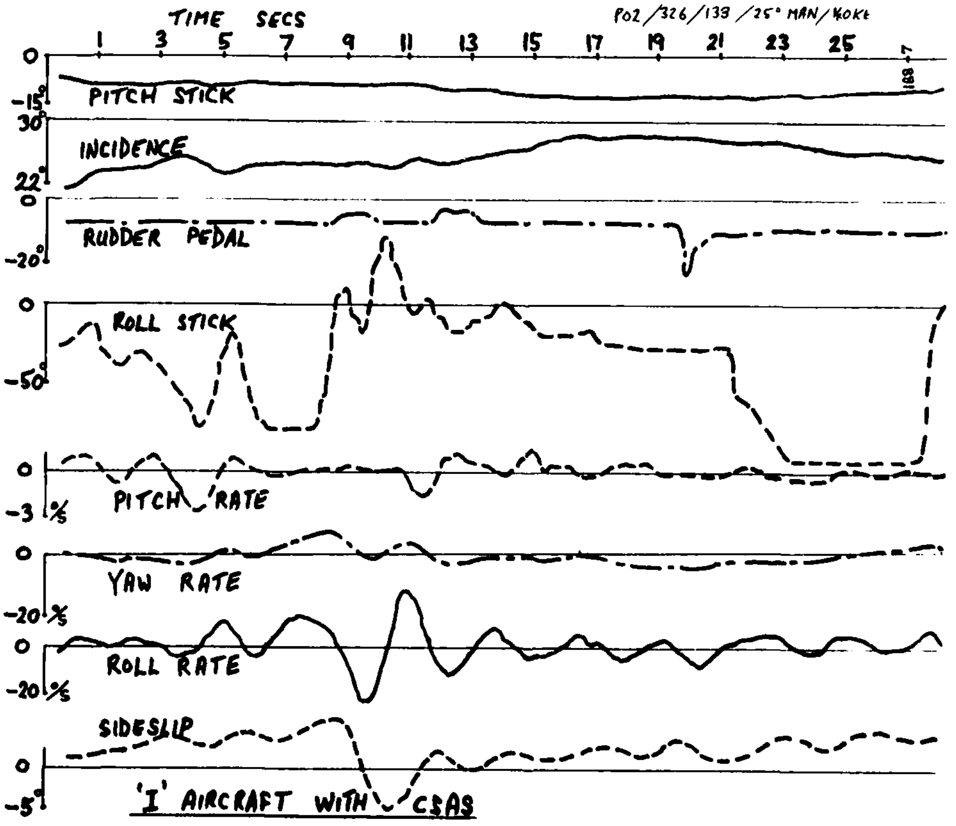

Fig 9 Benefit of stability-augmentation on Dutch-roll response

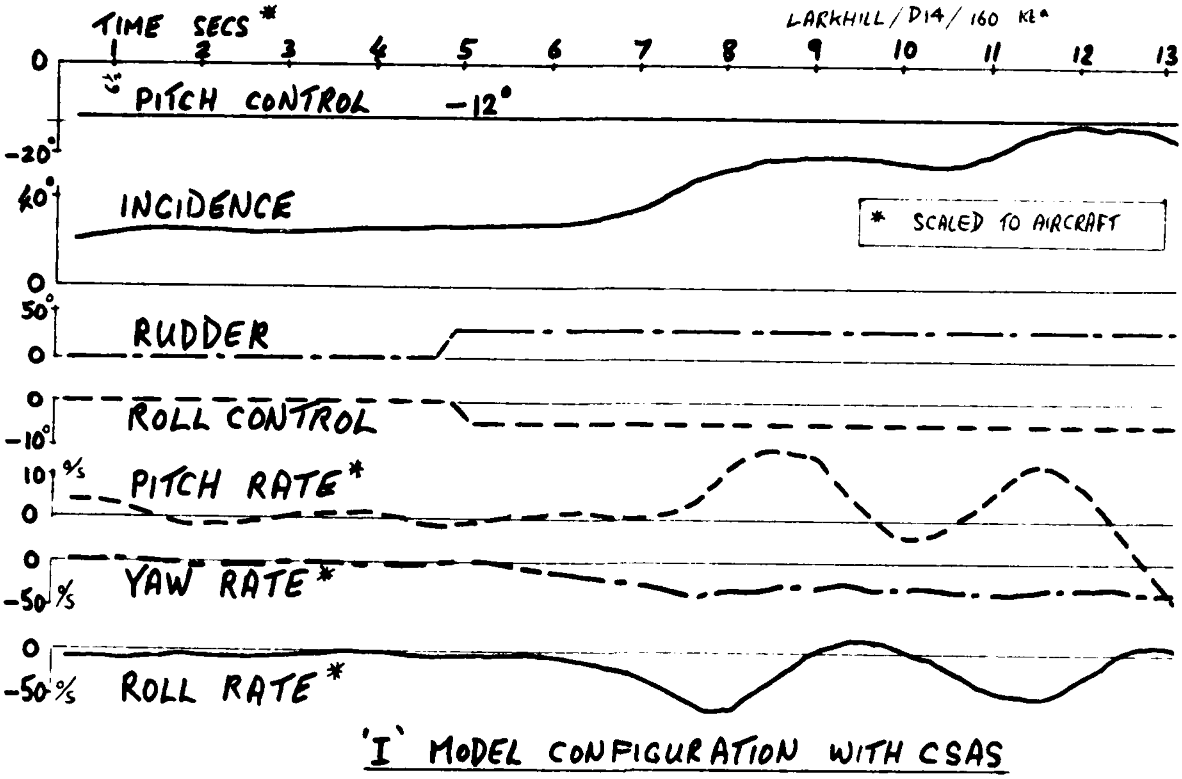

Fig 10 Departure with stability-augmentation present, crossed controls

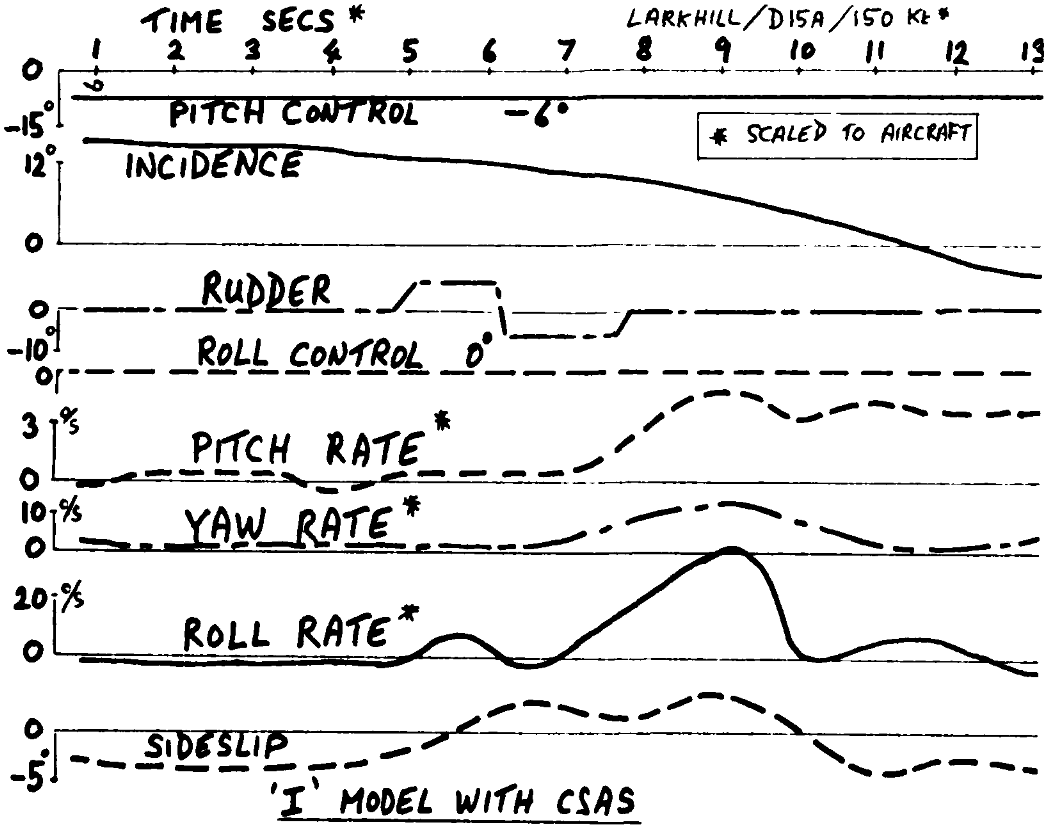

Fig 11 Roll-off due to rudder pulse at low incidence

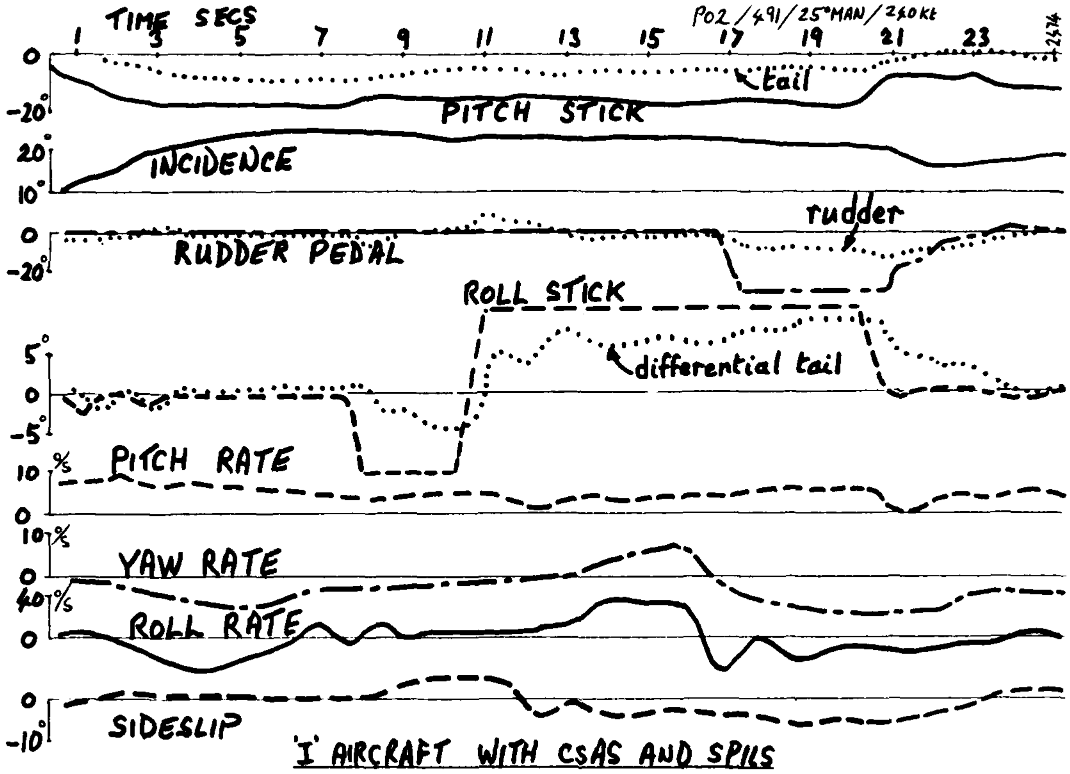

Fig 12 Effectiveness of incidence-limiting system for departure prevention

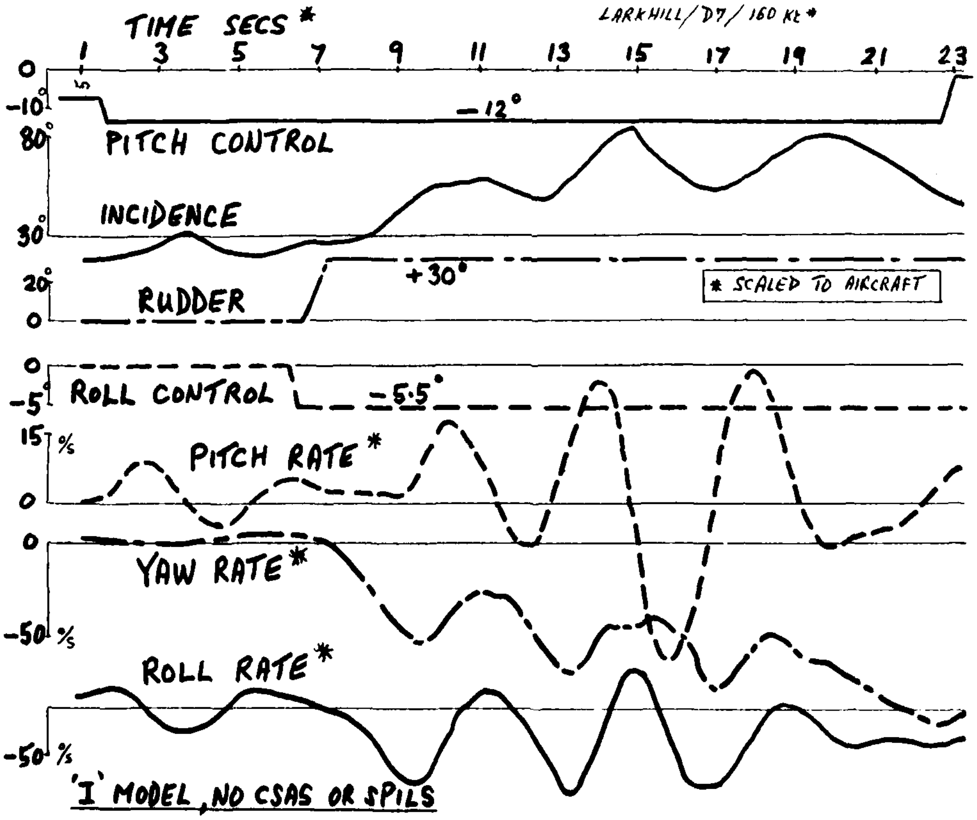

Fig 13 Departure of model with same type of control inputs as aircraft test of Fig 12

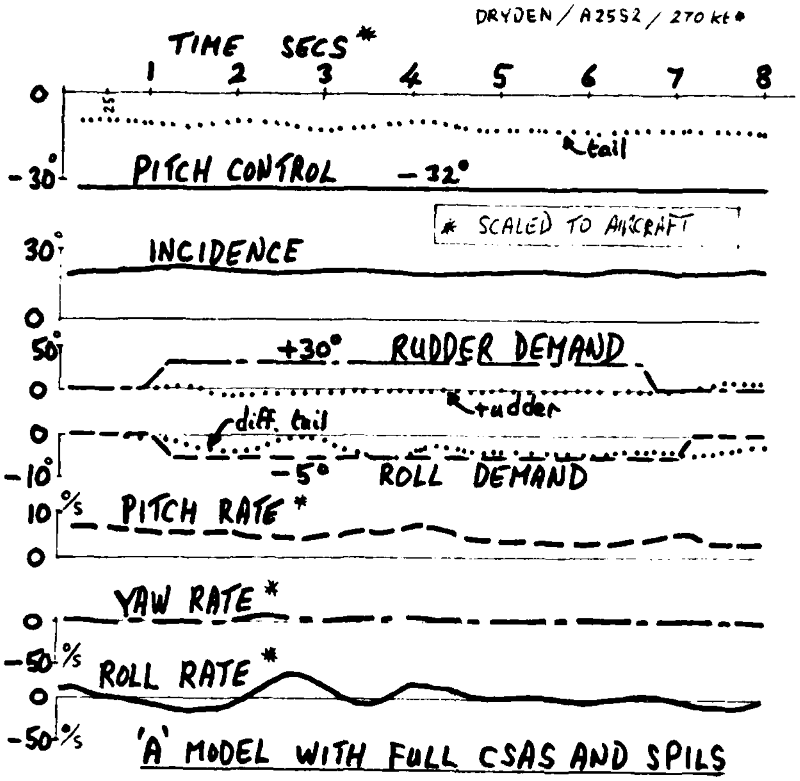

Fig 14 Use of incidence-limiting system to prevent departure for a free-flight model

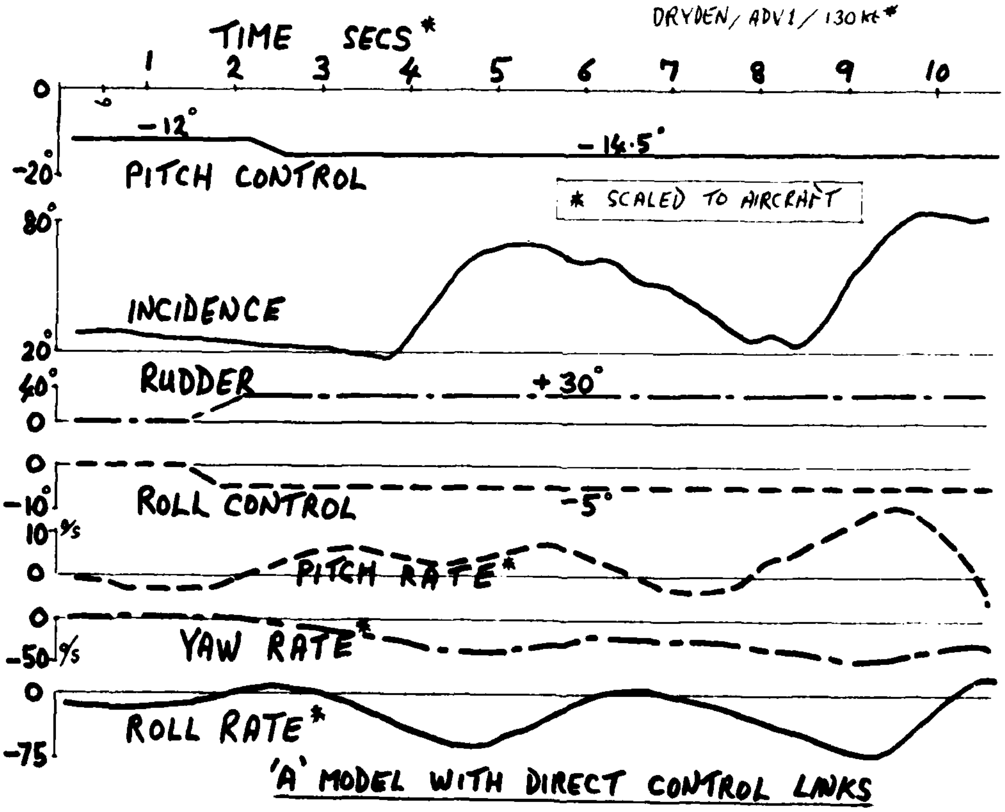

Fig 15 Departure of unaugmented model with same control inputs as used in Fig 14

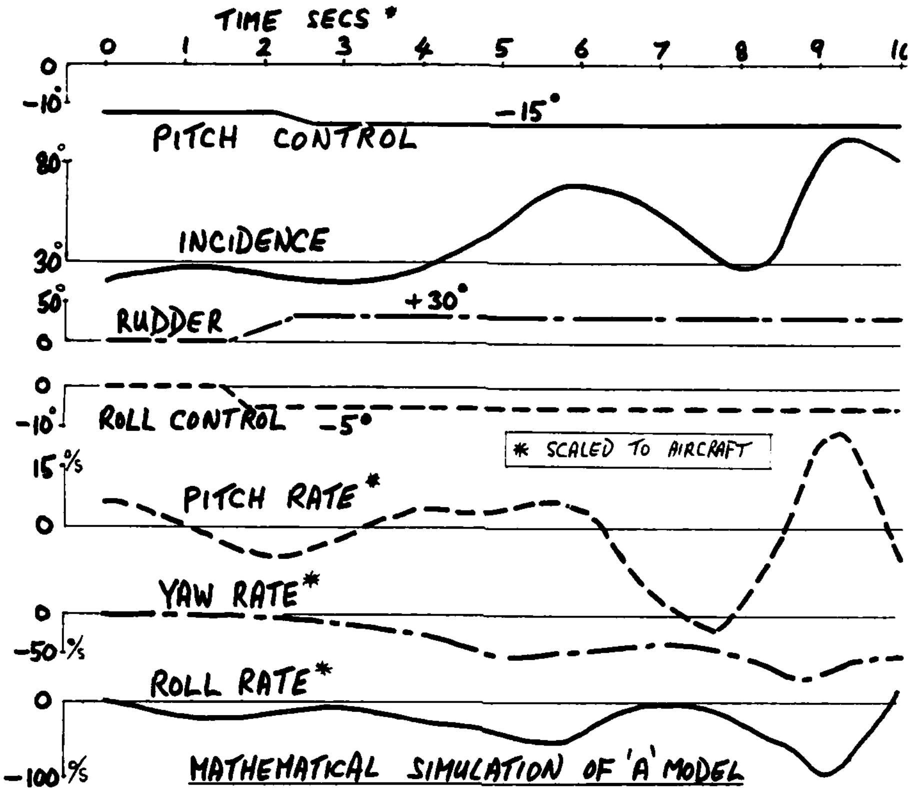

Fig 16 Prediction of departure for the control movements of Fig 15

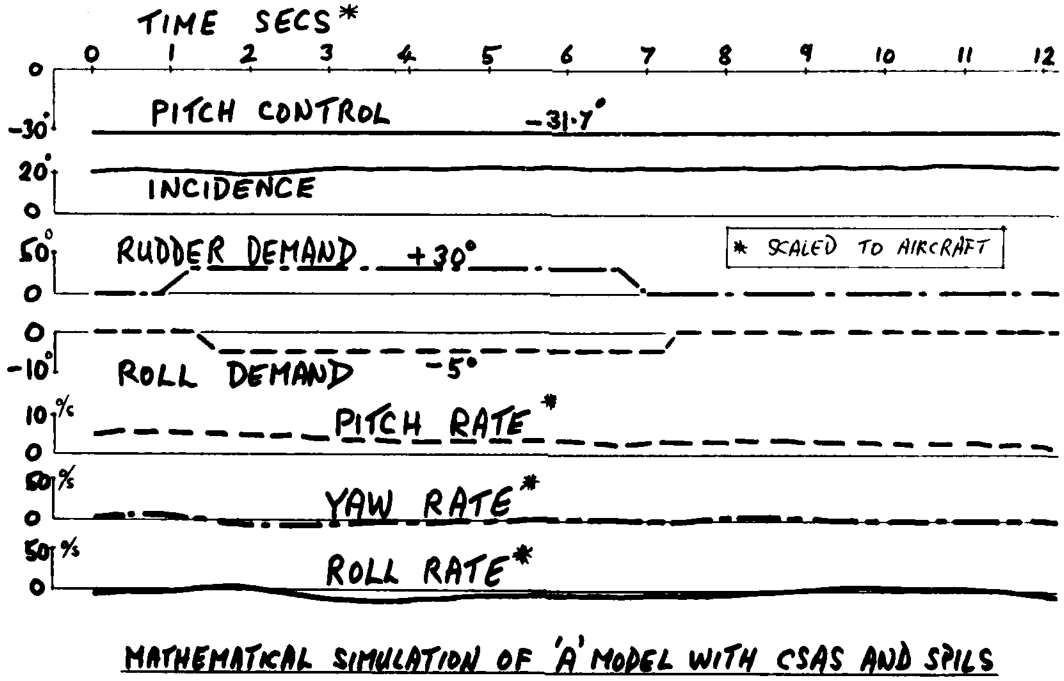

Fig 17 Prediction of effectiveness of the departure-prevention system demonstrated in Fig 14

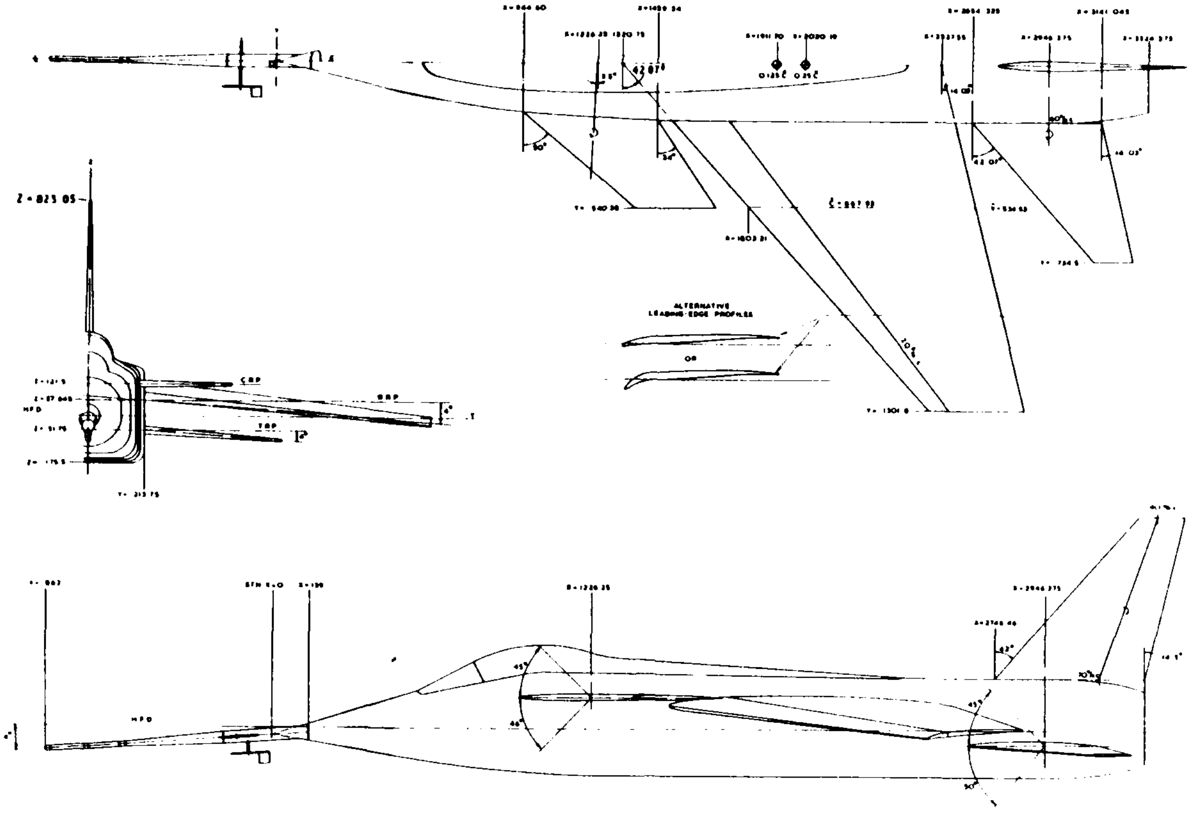
Z = 823 05
ALTERNATIVE LEADING-EDGE PROFILES
OR
CRP
TRP
HFD
STN X=O

Fig 18 General arrangement of RAE HIRM free-flight model

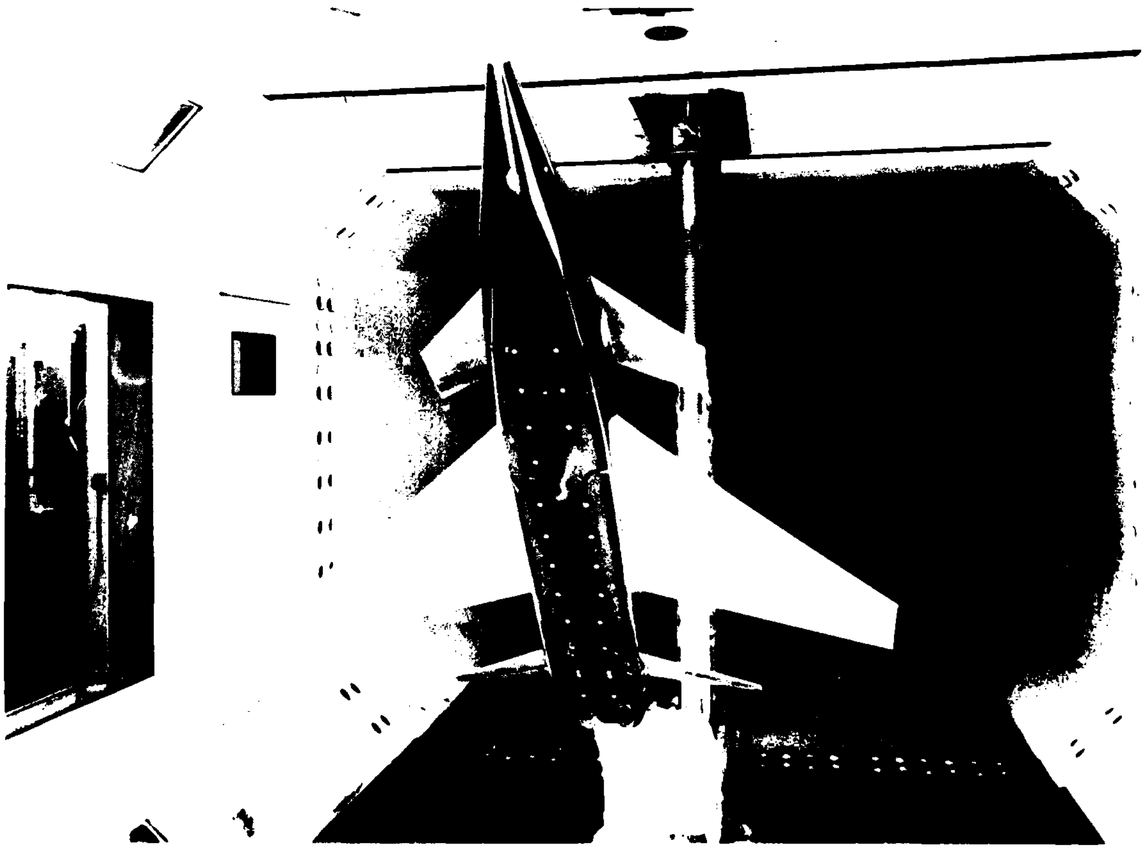

Fig 19 Static wind-tunnel tests on HIRM. RAE 11½ ft x 8½ ft low-speed tunnel

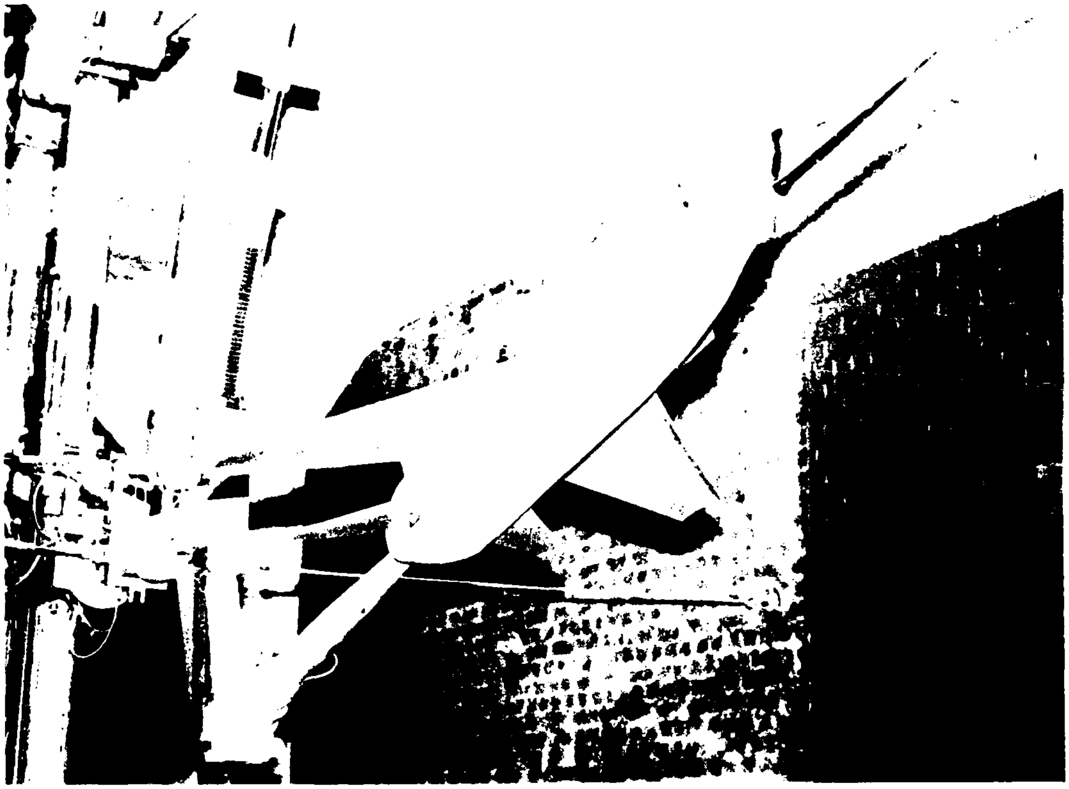

Fig 20 Dynamic wind-tunnel tests on HIRM. BAe rotary-balance rig

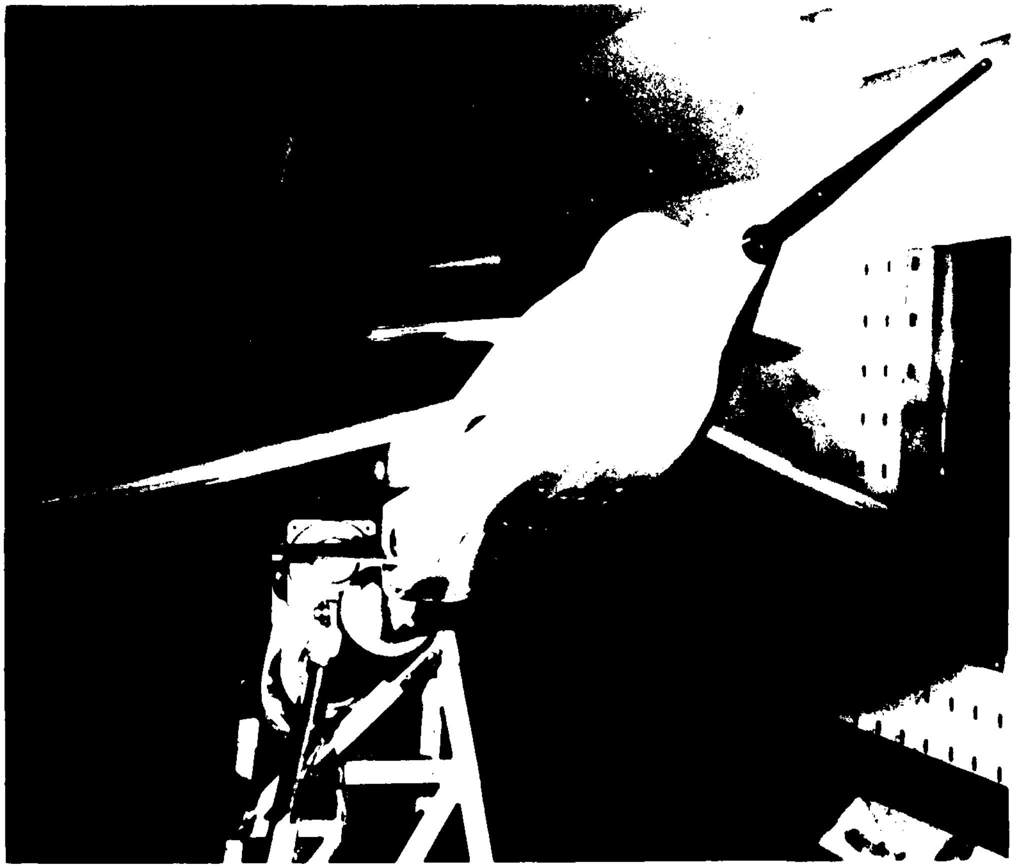

Fig 21 RAE oscillatory-derivative tests on HIRM
(triple-exposure photograph showing oscillations in roll)

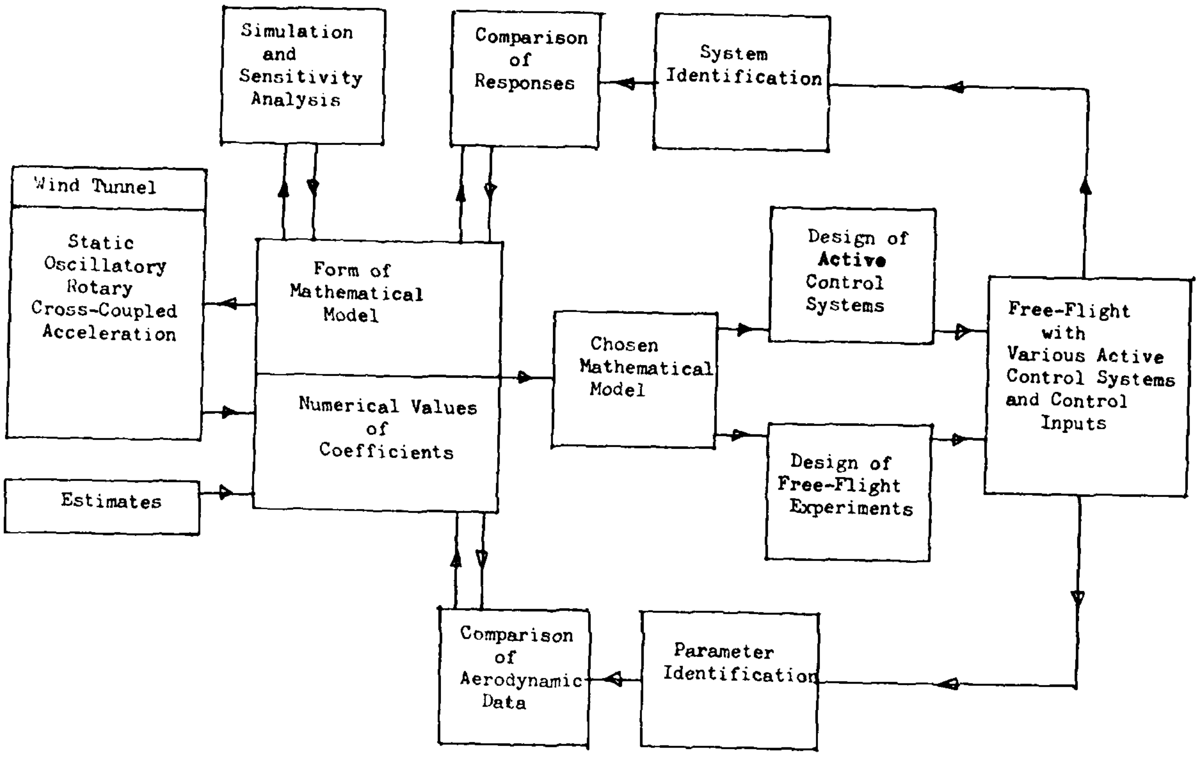
Simulation and Sensitivity Analysis
Comparison of Responses
System Identification
Wind Tunnel
Static
Oscillatory
Rotary
Cross-Coupled
Acceleration
Form of Mathematical Model
Numerical Values of Coefficients
Estimates
Chosen Mathematical Model
Design of **Active** Control Systems
Design of Free-Flight Experiments
Free-Flight with Various Active Control Systems and Control Inputs
Comparison of Aerodynamic Data
Parameter Identification

Fig 22 Application of mathematical model to RAE HIRM project

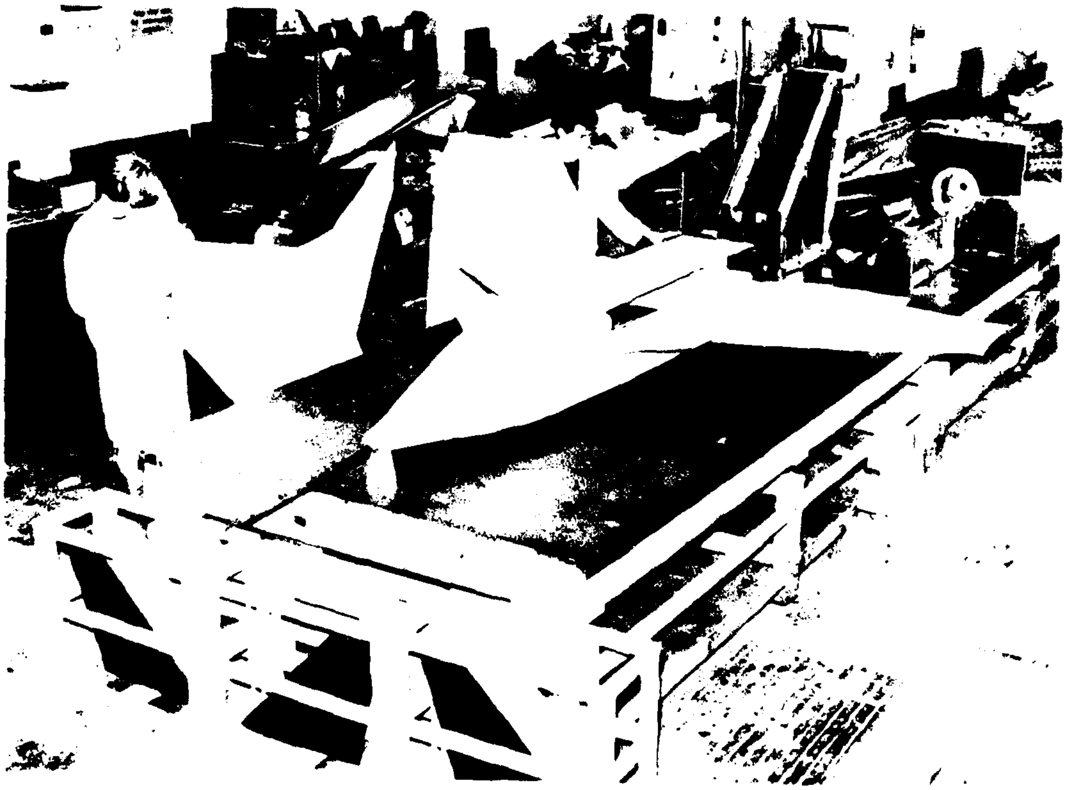

Fig 23 Assembly of one of the HIRM free-flight vehicles

COMPARISON OF FLIGHT AND WIND TUNNEL BUFFETING MEASUREMENTS ON THE SAAB 105 AIRCRAFT

by

S H Teige and B S A Nilsson
SAAB-SCANIA AB
S-581 88 Linköping
Sweden

and

S J Boersen and A N Kraan
NLR
Anthony Fokkerweg 2
1059 CM Amsterdam
Holland

SUMMARY

Buffet tests on a Saab 105 aircraft have been carried out in flight at high speed and wind tunnel measurements on a half model have been performed at the same Mach numbers and almost the same Reynolds number. Buffet levels have been derived from wind tunnel accelerometer signals using Jones' method. At Ma=.50 the flight/wind tunnel agreement is remarkably good. At Ma=.70 and in particular at Ma=.78 there are significant differences in buffet-onset and beyond. An attempt has been made to explain the discrepancies. The general conclusion is that with careful testing, this method may be used to predict flight buffet loads from wind tunnel measurements.

1 LIST OF SYMBOLS

c	chord
$\bar{c}$	mean aerodynamic chord
$C_{L_{TRIM}}$	trimmed lift coefficient
C_M	pitching moment coefficient
C_N	normal force coefficient
C_P	pressure coefficient
C_T	axial force coefficient
f	frequency
H	altitude
L_T	distance between MRP and tail 1/4-chord point
M	generalised mass
Ma	Mach number
MRP	moment reference point
n_z	load factor
p_o	W/T total pressure (Fig 8)
q	dynamic pressure
$Re_{\bar{c}}$	Reynolds number based on $\bar{c}$
S	reference area
V	free-stream velocity
W	weight
x y z	aircraft coordinate system (Fig 2)
α	incidence
ζ	total damping ratio (% crit)
ζ_a	aerodynamic damping ratio (% crit)
ζ_s	structural damping ratio (% crit)
σ	RMS acceleration

2 INTRODUCTION

An important trend in present combat aircraft programmes is the demand for improved maneuverability in the subsonic and transonic flight regime. Thus it has become increasingly important to predict the buffeting characteristics of an aircraft at an early stage in the project development programme as these characteristics may affect the choice of configuration.

Several methods have been used in order to predict buffeting from wind tunnel test. A method which has been used in the past is the study of slope changes in the normal force, pitching moment or axial force versus incidence, but if buffet level, and not only general terms such as buffet onset, moderate buffet and heavy buffet is needed, more sophisticated methods must be used. One method which has been used lately consists of measuring the fluctuating pressures on a nominally rigid model. The data are then used to calculate the response of the flexible aircraft structure. Important disadvantages of this method lie in the expensive instrumentation and complicated data handling and analysis required to determine the buffet excitation. Also, the aerodynamic damping is not measured but has to be estimated. Another method comprises the use of very expensive models with scaled structural and inertial properties. These models are too fragile to be tested at high pressure which is normally necessary in order to simulate the correct flow conditions in the wind tunnel.

In Ref. 1 G F Butler and G R Spavins presented a method originally suggested by J G Jones. The method involves the measurement of unsteady accelerations at one point on an aerodynamic surface, for instance a wing, made of solid steel or light alloy of the type normally manufactured for standard force test models. The model and instrumentation are therefore relatively simple and cheap. The method is based on the fact that a conventional wind tunnel model has modes of vibration which, for the lower and more important modes, are similar to those of the aircraft. The data reduction and analysis are similar to methods applied in flutter analysis and not unreasonably complicated or expensive. In Ref. 1 it was demonstrated that good agreement between wind tunnel test and flight test was obtained. As the method appeared to be promising, it was decided at Saab-Scania that in order to learn and gain experience in using a method that could be used for predicting the buffeting characteristics of an aircraft in the early stage of the development phase, a buffeting programme should be undertaken. The programme consisted of 1: flight test with the Saab 105 aircraft which is a military trainer/light attack aircraft and 2: wind tunnel tests on a half model of the aircraft including data reduction and prediction of full scale buffeting characteristics from the wind tunnel test data in order to compare the predicted values to the flight test results.

The wind tunnel test was performed at NLR as a joint effort between NLR and Saab-Scania. Originally it was intended to limit the wind tunnel test to Mach number 0.50 as the geometrical blockage ratio and wing surface of the model in the HST wind tunnel were rather large and this was the only Mach number at which flight test Reynolds number could be duplicated. However, as flight test data at $M_\infty=.70$ and .78 were available and as the extra cost of testing additional Mach numbers was small, it was decided to add these Mach numbers to the test programme.

The following chapters describe Jones' method, the flight test, the wind tunnel test and finally a comparison of flight/wind tunnel data is made.

3 JONES' METHOD

A more detailed description of the method is given in Ref. 1. The method makes it possible, if certain conditions and assumptions are fulfilled, to predict the full-scale buffet response of an aircraft by using wind tunnel response measurements on a semi-rigid model. The response is usually measured by accelerometers or strain-gauges. The method assumes that the shape of the lowest aircraft modes, which are the most important from the buffet point of view, are similar to those of the wind tunnel model. The method is applicable to all such modes. Further the method assumes that the modes, in buffet condition, can be described as single degree of freedom systems with negligible aerodynamic coupling. This means that the motion of the model in the wind tunnel is a measure of the aerodynamic excitation and of the total damping of each mode. The total damping is the sum of structural and aerodynamic damping. If the structural damping is measured in a ground resonance test, the aerodynamic damping can be calculated. An additional requirement is that the structural damping is small compared to the total damping.

In Jones' method the aerodynamic excitation of the model is written in nondimensional form and the excitation of the aircraft is obtained by scaling. In the same way the aerodynamic damping of the aircraft is obtained by scaling the aerodynamic damping of the wind tunnel model. Then the motion of aircraft modes under buffet condition can be calculated. The nondimensional aerodynamic excitation parameter for a mode is a function of the angle of incidence, Mach number and Reynolds number, and the nondimensional aerodynamic damping parameter is a function of the planform of the wing and the lift curve slope distribution over the wing.

In Fig. 1 the different steps in the prediction of the aircraft response under buffet condition using Jones' method are shown.

4 FLIGHT TEST

4.1 Aircraft and instrumentation

The aircraft used in the flight test was a test version of the military trainer/light attack aircraft Saab 105 (Fig. 2). The test aircraft differs from the Saab 105 used in the Swedish Air Force in the wing leading edge and in the engines. The wing was provided with underwing store pylons and 2 upper surface boundary layer fences. The wing has a 12.8° sweep-back angle at the quarter chord line and an anhedral of 6°. The thickness-to-chord ratio is 10.3 % at the wing root and 12 % at the tip.

Other Saab 105 data are:

Length	10.5 m
Span	9.5 m
Mean aerodynamic chord	1.744 m
Wing area	16.3 m^2
T.O. weight	4200 kg

The aircraft was equipped with 4 B&K accelerometers; two were mounted in the right wing tip, one in the left wing tip and one in the cockpit (Fig. 2). All accelerometers measured in the z-direction and the signals were recorded on a tape recorder.

4.2 Ground resonance test

In the ground resonance test the natural frequencies and dampings of the three lowest symmetric modes were measured with the aircraft standing on the landing gear. The aircraft was excited by 3 electrodynamic shakers and the mode shapes were measured in 7 spanwise stations on each wing half by a hand-held accelerometer. The test was made for 3 different levels of the exciting forces. Using the standard Saab procedure, the frequency, damping and generalised mass of each mode were evaluated by measuring the shaker forces and the acceleration at the shaker positions. These data are presented in the table below. As one may see, the fundamental bending mode is well separated in frequency from the higher modes.

The shape of the fundamental bending mode, 8.8 Hz, is shown in Fig. 3.

It appeared that the aircraft structure was unsymmetric, which affected the 2nd and 3rd modes. These modes are both combinations of second bending and torsion of the wing. The terms 2R and 2L in the table mean that only the right or the left wing was excited.

The generalised mass of the 1st bending mode was 212.6 kg. The mode deflection at the aft right wing tip accelerometer position (Fig. 2, no. 4) was taken as unity.

Mode	Exc.force (N)	Natural freq. (Hz)	ζ
1	30.12	8.792	1.1
1	41.16	8.785	1.2
1	57.27	8.762	1.2
2R	83.61	28.625	3.2
2L	56.64	29.073	2.2
3	12.45	34.577	2.3
3	26.49	34.385	2.3

4.3 Flight test programme

Flight tests were performed at three flight conditions:

Ma (-)	H (km)	$Re_{\bar{c}}$ (-)
0.50	6	11.4×10^6
0.70	8	13.0×10^8
0.78	8	14.1×10^6

At each flight condition, i.e. constant speed and altitude, the procedure was to increase the incidence step by step from a low value until the heavy buffet region with roll instability was reached. At each step the accelerometer signals were recorded for about 2 minutes, i.e. about 1000 cycles of the fundamental bending mode.

At high incidences it was impossible to keep both α and altitude constant. In that case α was held constant and the pilot tried to get the right mean altitude. This procedure was repeated until a total recording of 2 minutes at each α was obtained.

The aircraft incidence was measured by an α-indicator and read by the pilot. For each incidence the corresponding C_L-coefficient was calculated from $C_{LTRIM}=W.n_Z/(q.S)$ where W is the aircraft weight, n_Z the load factor, q the dynamic pressure and S the reference area.

4.4 Data reduction and results

The recorded accelerometer signals were filtered through an analog band-pass filter, bandwidth 5 Hz, centred around the fundamental bending frequency 8.8 Hz. Only this mode was used in the analysis. The filtered signals were digitized and their RMS-values calculated. Then the randomdec-method was used to determine the damping of the bending mode from the randomdec function.

In Fig. 4 the RMS-values of the filtered wing reference acceleration are drawn together with the cockpit acceleration as functions of C_{LTRIM}. The curves for Ma=.50 and Ma=.78 exhibit a gradual increase in g_{RMS} from $C_{LTRIM} \approx .3$ on and show a rather rapid growth as soon as C_{LTRIM} passes a certain limit. According to the pilot's perception, buffet onset was attained just prior to the steep g_{RMS} increase. The curves for Ma=.70 are different. The g_{RMS} is somewhat reduced as C_{LTRIM} runs from .25 to .62, and then suddenly becomes excessive. At Ma=.70 it was impossible to separate light buffeting from moderate and heavy buffeting. Attempts to increase α beyond this limit resulted in wing rock.

It is interesting to note that the cockpit acceleration has the same behaviour as the wing acceleration for all Mach numbers.

In Fig. 5 the total damping ratio of the bending mode is given as function of α for Ma=.50.

5 WIND TUNNEL TEST

5.1 Model and wind tunnel

The wind tunnel represented the Saab 105 starboard half at a 1/4.5 scale (Fig. 6). The main geometric characteristics are consequently:

Half span	1.0555 m
Mean aerodynamic chord	0.38756 m
Wing reference area	$0.40247\ m^2$

The wing was made of aluminium and consisted of one piece. The model was equipped with a flow-through nacelle, while the tail unit was not represented.

Wing and fuselage were mounted on a tang part, that was bolted on the half model balance (Fig. 7). In particular the wing-tang connection was very rigid, which is required to achieve a low structural damping. In order to locate the fuselage more or less outside the tunnel sidewall boundary layer, a 29 mm thick plate having the fuselage contour was inserted between the fuselage and the tunnel sidewall (Fig. 7a). This plate was mounted on the nonmetered turntable. A 4 mm gap was maintained between the metered fuselage and the plate; a foam seal was added to prevent flow through the gap.

The model was mounted on the half model strain gauge balance NLR 508, the heaviest balance available at NLR. Three B&K accelerometers were installed in the model; 2 in the starboard wing tip, and 1 in the fuselage. For precise wing locations one is referred to Fig. 9. The wing tip accelerometers on model and aircraft are on slightly different spanwise locations, but the difference has been accounted for.

The NLR transonic facility HST, in which the wind tunnel programme was carried out, is a closed-circuit tunnel with total pressures between 390 and 12 kPa. A performance chart is given in Fig. 8. The rectangular test section measures 2 x 1.6 m^2; top and bottom walls are slotted with an open ratio of 12.5 %; sidewalls are solid. For half model testing the main window is replaced by a nonmetered turntable, attached to the balance housing.

The Saab 105 model is fairly large for a half model configuration in terms of tunnel blockage (approx. 2.55 %). There appears to be some upstream effect (slightly higher static pressure) but the consequences on the free-stream quantities are assumed to be insignificant. Wall interference on incidence was corrected for by $\Delta\alpha = a_1 \cdot C_L$, where a_1 was scaled from previous half model/complete model comparisons. In the recent past a number of half model configurations have been tested in the HST and comparison with identical complete models has led to a correction of the above type (Ref. 2).

5.2 Ground resonance test

The ground resonance test was carried out on the model mounted in the HST test section. An electrodynamic shaker was used to excite the model. Employing a wing tip accelerometer the fundamental bending frequency was determined, 28.88 Hz. At resonance the vibration mode was measured using a separate accelerometer attached to specific points on the wing surface (Fig. 9).

The generalised mass was derived from the shift in resonance frequency due to a known mass addition (Ref. 3). As for the aircraft, the mode deflection was normalized relative to accelerometer 4. The generalised mass of the wing was 9.77 kg.

The structural damping was derived from the amplitude decay. This exercise was repeated several times, the results show slight variations of the damping ratio. In the buffet calculations ζ_s = .38 % crit. was used.

5.3 Wind tunnel test programme

The test programme was split up into 2 parts:

series 1, an α-sweep run at constant free stream conditions; the α-sweep rate was .25° per second and test results are called steady data;

series 2, in which a one-minute tape recording and simultaneous analysis at constant free-stream conditions are performed.

The Mach numbers were those of the flight test, which was carried out prior to the wind tunnel experiment. Reynolds numbers of flight and wind tunnel test were:

Ma	$Re_{\bar{c}} \times 10^{-6}$	
(-)	Flight	W/T
.50	11.4	12.2
.70	13.0	10.9
.78	14.1	9.9

The test was done at natural boundary layer transition. Some additional runs were carried out at $Re_{\bar{c}}$ 5 x 10^6 to investigate the effect of Reynolds number variations.

5.4 Data reduction and results

The steady measurements of series 1 were treated in the usual manner, the aerodynamic coefficients C_N, C_T, C_M, C_L and C_D were calculated from balance readings, the free-stream dynamic pressure and the reference quantities. As indicated above, blockage effects were small and have not been accounted for. A small correction on incidence was necessary to compensate for wall interference (see 5.1). The $C_N(\alpha)$ and $C_T(\alpha)$ results are plotted in Fig. 10.

Since the wind tunnel experiment was carried out on a model without tail surfaces, flight and tunnel results could not be compared directly. A small correction was applied to C_L. The tail lift $C_{L_T}(\alpha)$ required to counterbalance the wing C_M was estimated from:

$$C_{L_T}(\alpha) = C_M(\alpha)\,\frac{\bar{c}}{L_T} \leq .05$$

and applied to the measured wing-fuselage lift coefficient. In the above equation L_T is the distance between the MRP and the tail 1/4-chord point.

The α-sweep runs at Re ≈ 5 x 10^6 have furnished results that agree very well with those obtained at high Reynolds numbers. The C_{L_α} and buffet-onset boundaries nearly collapse; g_{RMS}, on the other hand, scales with q, as one would expect.

From the one-minute recordings of the series 2 test the accelerometer RMS-values and total damping were determined. The signals were passed through an analog band-pass filter with the filter boundaries 10 and 40 Hz. The RMS-value could be calculated readily using standard routines on a HP Fourier Analyser. For the computation of the total damping a special randomdec routine was implemented on the Fourier Analyser (Ref. 4). Once the randomdec signature was calculated, an integration routine was applied to deduce both total damping ratio and frequency.

The total damping ratios, as derived from the aft right wing tip accelerometer, are plotted in Fig. 11. The results show only little scatter and, with $\zeta_S = .38$ %, indicate that the aerodynamic damping makes up 85 to 90 % of the total damping, which is an important requirement for Jones' method to be applicable.

6 COMPARISON OF FLIGHT/WIND-TUNNEL TESTS

The buffet-onset boundaries, based on the aft right wing tip accelerometer signals from flight and wind tunnel tests, have been plotted in Fig. 12. At Ma=.50 and .70 the agreement is good. At Ma=.78, however, the buffet-onset boundaries differ considerably; $\Delta C_L \approx .09$, if one assumes this difference to be a lift effect only. This aspect will be further discussed below.

Following the prediction scheme of Ref. 1 and using measured aircraft data on mass and structural damping, the buffet response levels for the aircraft were calculated. The following expessions were arrived at:

Ma=.50 $(\zeta_a)_{A/C} = 1.16\ (\zeta_a)_{MOD}$ $\sigma_{A/C} = .408\ (\zeta_{MOD}/\zeta_{A/C})^{1/2} \cdot \sigma_{MOD}$
Ma=.70 $(\zeta_a)_{A/C} = 1.42\ (\zeta_a)_{MOD}$ $\sigma_{A/C} = .498$ -"- -"-
Ma=.78 $(\zeta_a)_{A/C} = 1.78\ (\zeta_a)_{MOD}$ $\sigma_{A/C} = .623$ -"- -"-

From this, Fig. 11 and knowing $(\zeta_S)_{A/C} = 1.1$ crit. and $(\zeta_S)_{MOD} = .38$ % crit., one may easily conclude that the predicted aircraft buffet level is approx. half that of the model value. The flight and predicted buffet results are collected in Fig. 13.

The following remarks should be made:

1 The buffet-free q_{RMS} level during flight is close to half of that of the prediction. Both in flight and in the wind tunnel the buffet-free condition could be measured rather easily, and the differences are probably caused by difference in turbulence level. An other cause may be differences in structural characteristics, in particular the mode shape, between the model mounted in the tunnel and the aircraft.

2 Buffet-onset is predicted reasonably well at Ma=.50 and Ma=.70 but the prediction fails at Ma=.78. To explain the Ma=.78 difference other information is essential; e.g. C_p-distribution and shock patterns on the aircraft as well as on the wind tunnel model.

It is also known that boundary layer transition, surface roughness and Reynolds number are extremely important for $C_{L_{MAX}}$ and buffet-onset. In 2D experiments e.g. these boundaries may easily shift .05 in C_L due to relatively small changes in $Re_{\bar{c}}$, or the state of the boundary layer in front of the shock wave. At Ma=.78 when shock location and shock-induced separation are of great importance a blockage ratio of 2.55 % could be too high for a correct simulation of the flow. It is of interest to notice that if one should predict buffet-onset at Ma=.78 from the $C_T(\alpha)$-curve in Fig. 10 the result would have been a C_L-value being $\approx .12$ lower than the predicted value using Jones' method or fairly close to the flight test value.

As mentioned before, it was impossible to keep the flight test altitude constant at this Mach number, but the scatter in the data points is similar to that occuring at Ma=.50 and .70.

Reynolds number in the wind tunnel at M=.78 is 9.9×10^6 compared to 14.1×10^6 during the flight test and this could affect the data.

3 The g_{RMS} trend after buffet-onset is predicted rather correctly at Ma=.50; at Ma=.70 the necessary flight data could not be obtained, while at Ma=.78 it is not useful to consider this aspect. The primary objective of the present exercise was to predict the buffet response level at Ma=.50, and this has been successful. A much more detailed study is needed to explain the discrepancies at the higher Mach number.

7 CONCLUSIONS

Jones' method for predicting buffet response levels from wind tunnel measurements on a rigid model has been applied to the Saab 105 aircraft. In the present case measured generalised mass and structural damping of the real aircraft were available, as opposed to only estimates in the early design phase of an aircraft.

Wing bending modes and structural dampings of aircraft and wind tunnel model met the requirements for the method to be applicable. The buffet response was predicted for an outer wing tip location (at approx. 42 % C) at Ma=.50, .70 and .78.

This limited effort has only been partly successful. At Ma=.50, where the flight Reynolds number was duplicated in the wind tunnel, the prediction method works well. The main objective of this exercise was to predict the Ma=.50 response.

At Ma=.70 the flight test has yielded incomplete data due to difficulties in flying the aircraft beyond buffet-onset, but the buffet-onset point is well predicted by the applied method. At Ma=.78 the discrepancy in buffet-onset is significant. The reason for this is not understood. Possible causes are uncertainties in the wind tunnel test technique (blockage effect, half model mounting) as well as in the flight test, in addition to differences in Reynolds number, boundary layer transition and shock-wave boundary-layer interaction.

A complete analysis of the above differences would require a study of the effect of model size as well as information on the wing pressure distribution at all relevant conditions, in particular as a function of Reynolds number.

The general conclusion is that with careful testing one should be able to obtain valuable information on the buffet response of an aircraft in the early design phase.

8 REFERENCES

1	G F Butler G R Spavins	Preliminary investigation of a technique for predicting buffet loads in flight from wind-tunnel measurements on model of conventional construction. AGARD-CP-204, Paper 24, September 1976.
2	S J Boersen	Half-model testing in the HST - A 1982 Status Report - NLR, Amsterdam (to be published)
3	P W Hansen	Structural and aerodynamic quantities of the dynamic system, similarity laws and model testing AGARD-AR-82, July 1975.
4	H A Cole, Jr	On-line failure detection and damping measurements of aerospace structures by random decrement signatures NASA CR-2205, 1973.

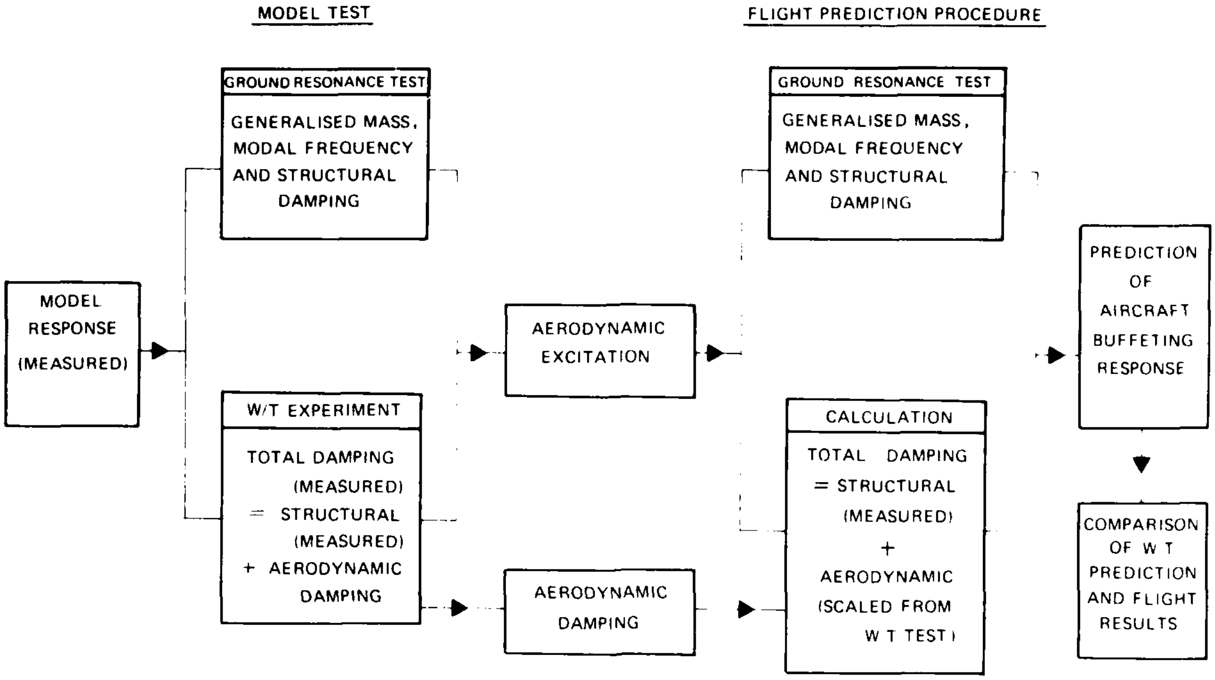
MODEL TEST
FLIGHT PREDICTION PROCEDURE
GROUND RESONANCE TEST
GENERALISED MASS, MODAL FREQUENCY AND STRUCTURAL DAMPING
GROUND RESONANCE TEST
GENERALISED MASS, MODAL FREQUENCY AND STRUCTURAL DAMPING
MODEL RESPONSE (MEASURED)
AERODYNAMIC EXCITATION
PREDICTION OF AIRCRAFT BUFFETING RESPONSE
W/T EXPERIMENT
TOTAL DAMPING (MEASURED) = STRUCTURAL (MEASURED) + AERODYNAMIC DAMPING
CALCULATION
TOTAL DAMPING = STRUCTURAL (MEASURED) + AERODYNAMIC (SCALED FROM W T TEST)
AERODYNAMIC DAMPING
COMPARISON OF W T PREDICTION AND FLIGHT RESULTS

Fig. 1 Outline of Jones' buffeting prediction method, as used in present investigation

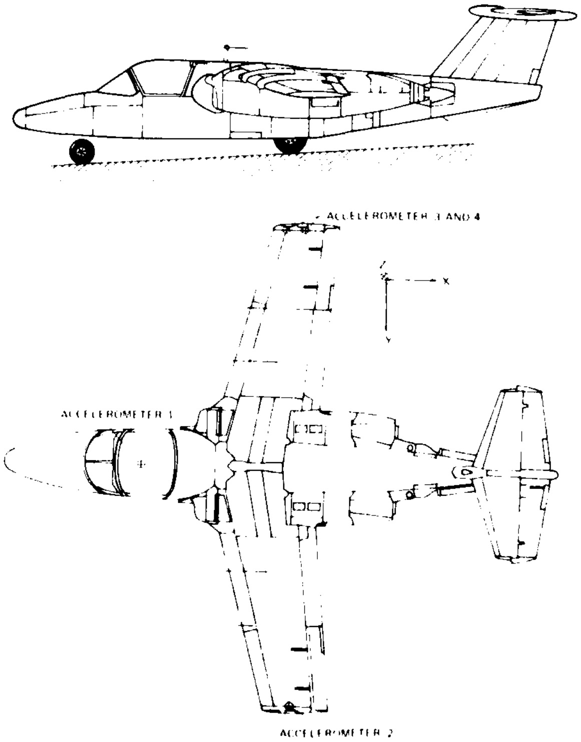
ACCELEROMETER 3 AND 4
ACCELEROMETER 1
ACCELEROMETER 2
Z
X
Y

Fig. 2 SAAB 105 aircraft with location of accelerometers

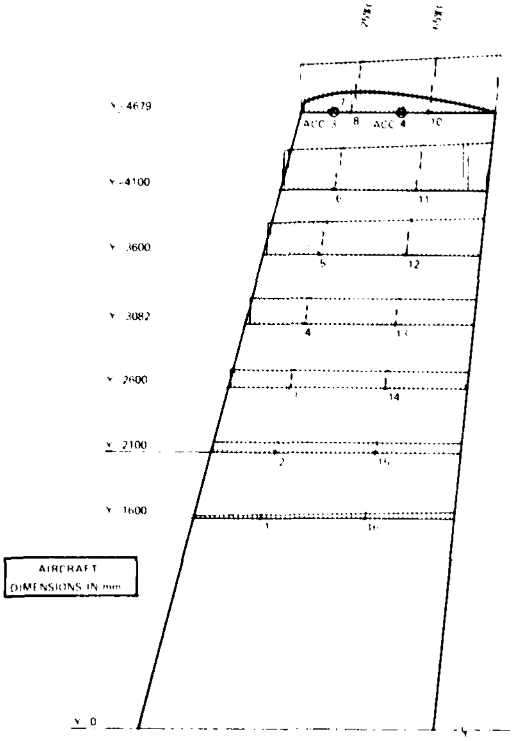
Y = 4679
ACC 3
7
8
ACC 4
10
Y = 4100
6
11
Y = 3600
5
12
Y = 3082
4
13
Y = 2600
3
14
Y = 2100
2
15
Y = 1600
1
16
AIRCRAFT DIMENSIONS IN mm
Y = 0

Fig. 3 First bending mode of SAAB 105 aircraft starboard wing

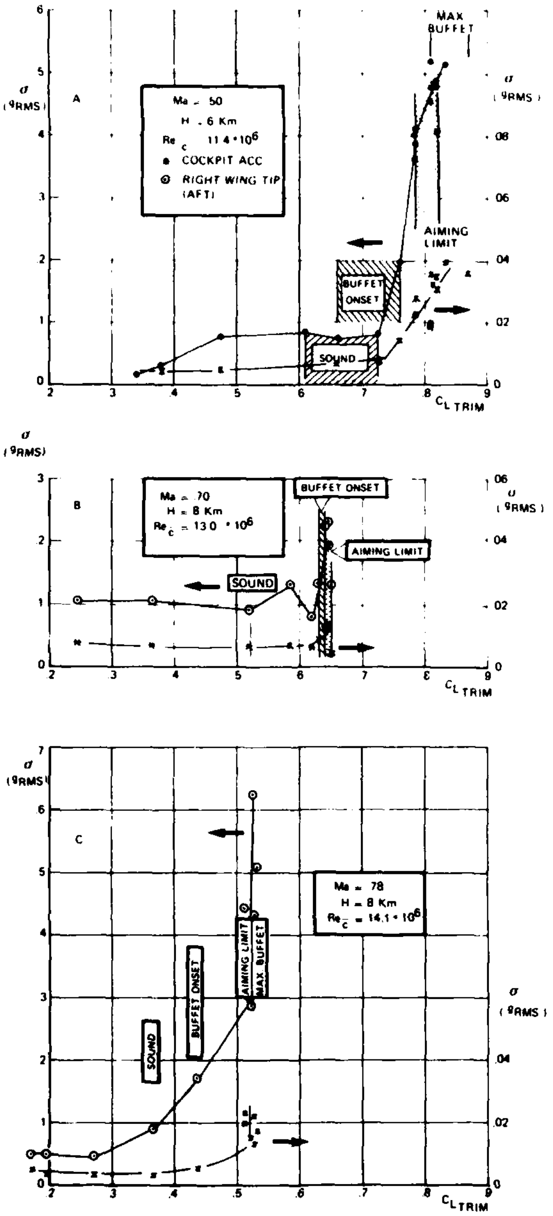

Fig. 4 RMS-value of 2 A/C accelerometers and pilot's comments

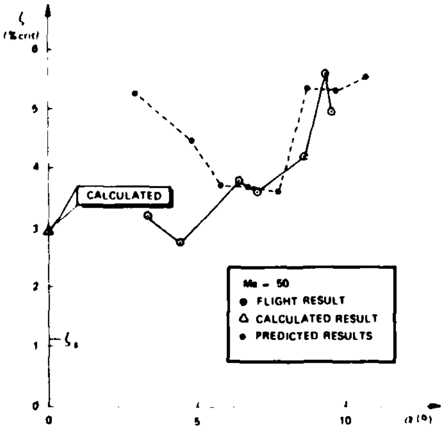

Fig. 5 Total damping ratio of aircraft from flight test at Ma = .50 and prediction

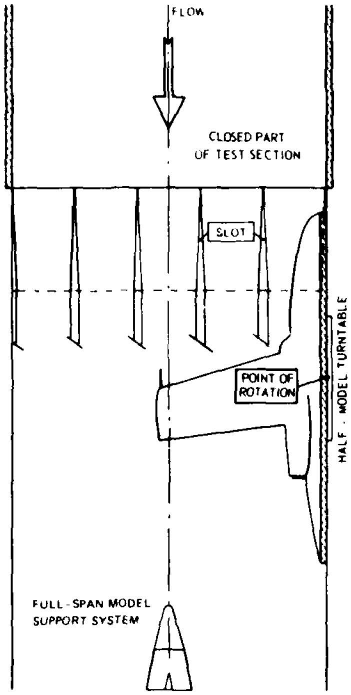
FLOW
CLOSED PART OF TEST SECTION
SLOT
POINT OF ROTATION
HALF - MODEL TURNTABLE
FULL-SPAN MODEL SUPPORT SYSTEM

Fig. 6 SAAB 105 half model in HST test section

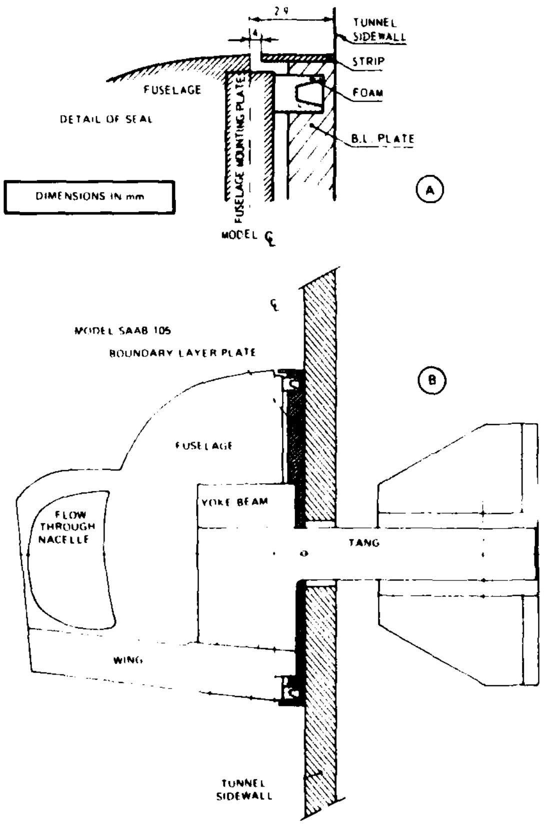
29
4
TUNNEL SIDEWALL
STRIP
FOAM
B.L. PLATE
FUSELAGE
DETAIL OF SEAL
FUSELAGE MOUNTING PLATE
DIMENSIONS IN mm
MODEL ℄
A
℄
MODEL SAAB 105
BOUNDARY LAYER PLATE
B
FUSELAGE
YOKE BEAM
FLOW THROUGH NACELLE
TANG
WING
TUNNEL SIDEWALL

Fig. 7 SAAB 105 half model mounting on HST sidewall

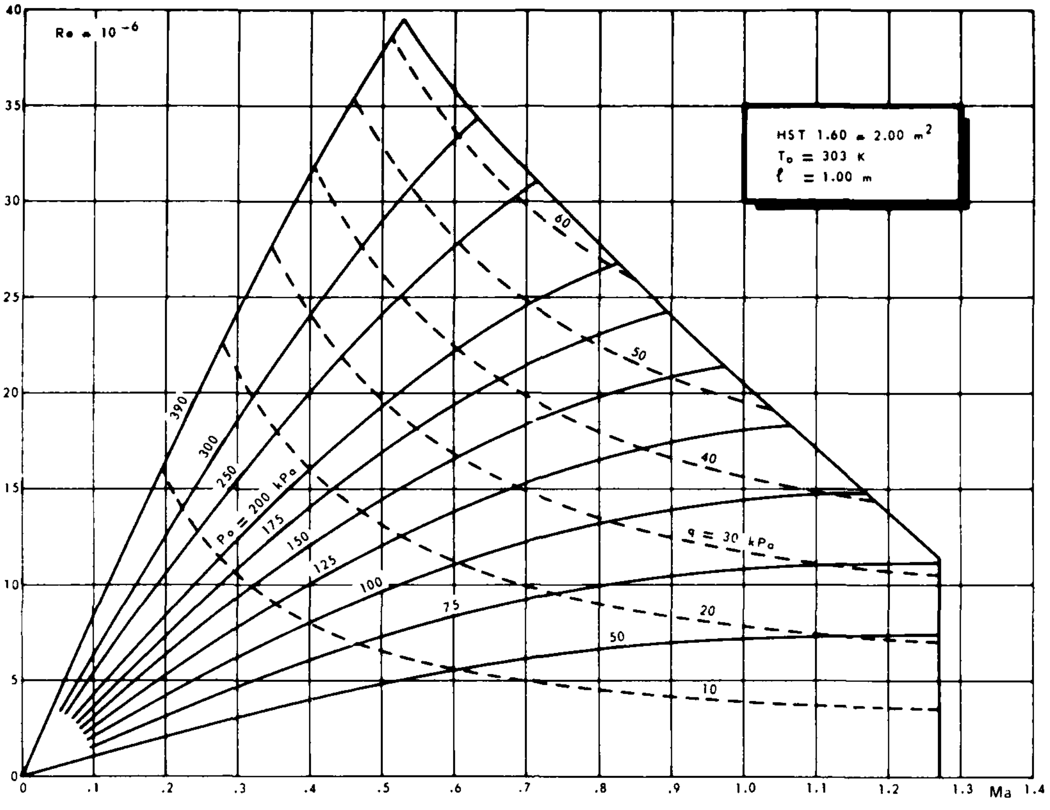

Fig. 8 HST empty test section Reynolds number as a function of Mach number

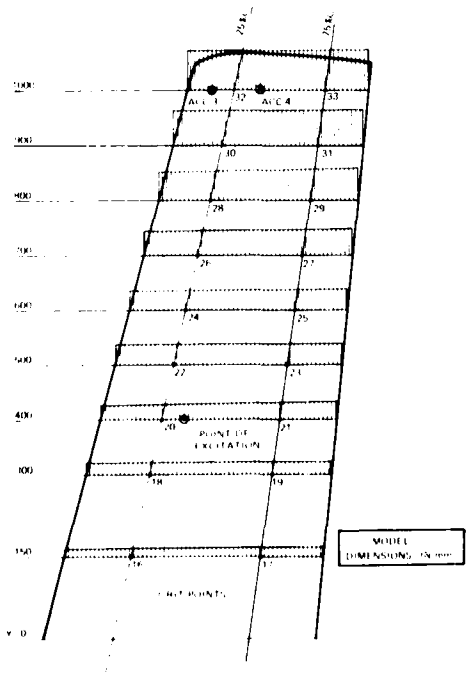
25%c
25%c
1000
ACC 3
32
ACC 4
33
900
30
31
800
28
29
700
26
27
600
24
25
500
22
23
400
20
21
POINT OF EXCITATION
300
18
19
150
16
17
MODEL DIMENSIONS IN mm
y 0

Fig. 9 First bending mode of SAAB 105 half model wing

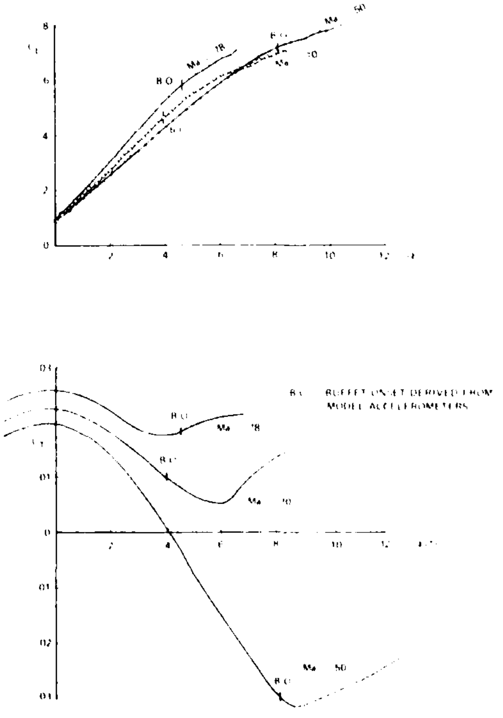

Fig.10 SAAB 105 half model aerodynamic coefficients C_L and C_T as a function of incidence

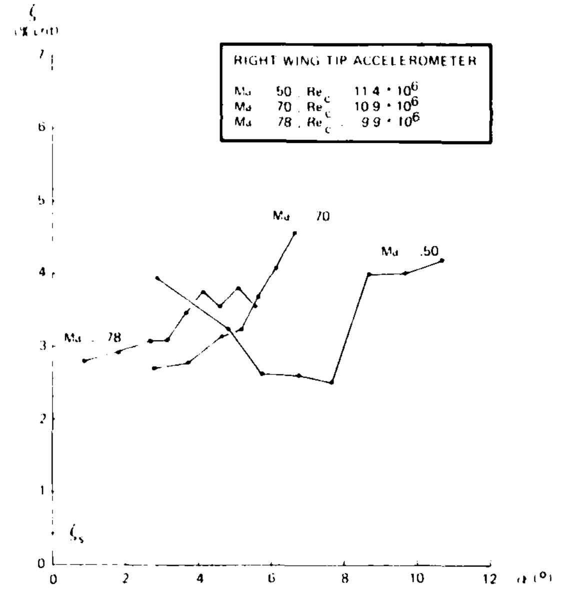

Fig. 11 Total damping ratio of model from W/T test

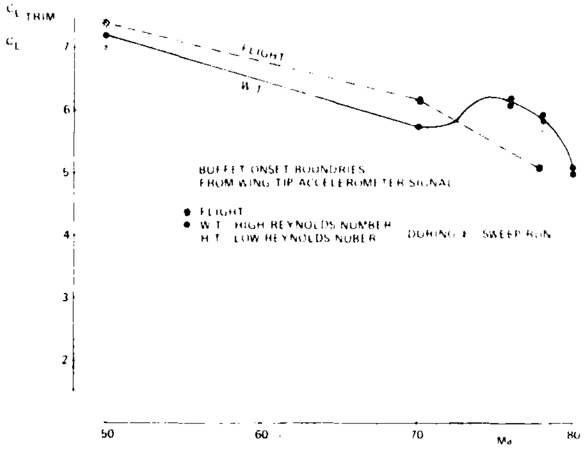

Fig.12 SAAB 105 buffet onset boundaries from flight and wind tunnel test

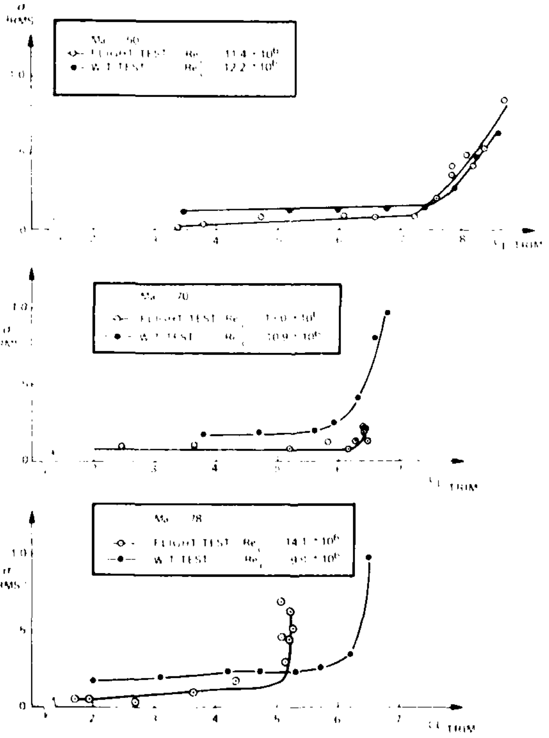

Fig.13 Comparison of right wing tip accelerometer output from flight and wind tunnel test

SOME MEASUREMENTS OF BUFFETING ON A FLUTTER MODEL OF A TYPICAL STRIKE AIRCRAFT

by

D. G. Mabey

B. E. Cripps

Aerodynamics Department,
Royal Aircraft Establishment, Bedford, UK

SUMMARY

This paper describes some buffeting measurements on a flutter model of the wing of a typical strike aircraft, and compares the results with flight experiments. New criteria for light, moderate and severe levels of buffeting are proposed, to supplement previously derived empirical criteria. The results confirm that buffet penetration in flight is not limited by the severity of buffeting, but by handling limits. The wing of this model has a rigid body freedom in the low frequency roll mode, which clearly indicates wing-rock after buffet onset. Measurements of the response in this mode indicated that the buffet excitation was bounded, and comparable with that in the first symmetric bending mode, even when the aerodynamic damping in the roll mode was falling rapidly. The rapid fall, after buffet onset, of the aerodynamic damping in this low frequency rigid body mode was accurately predicted from steady pressure measurements. In marked contrast the measured increase, after buffet onset, of the aerodynamic damping for the first symmetric bending mode could not be predicted from steady pressure measurements. These observations have important implications for the prediction of buffeting in flight from measurements on models.

NOTATION

B_1, B_2	port and starboard wing-root strain signals
b	wing span (430 mm)
c	local chord
$\bar{c}$	average chord (122 mm)
C_B	steady bending moment coefficient
C_B^{11}	buffeting coefficient (defined in Ref 11)
f	frequency (Hz)
g/2	structural damping coefficient (% crit)
k	roughness height
ℓ_p	rolling moment due to rate of roll
M	Mach number
m	generalised mass in mode
$n = f\bar{c}/U$	frequency parameter
$\sqrt{nG(n)}$	buffet excitation parameter due to wing flow separations and flow unsteadiness at zero lift
$\sqrt{nG_0(n)}$	buffet excitation parameter due to flow unsteadiness at zero lift
$\sqrt{nG_1(n)}$	buffet excitation parameter due to wing flow separations
q	kinetic pressure
R	Reynolds number based on $\bar{c}$
S	wing area
s	semi-span
U	free stream velocity
dV, V	rms and steady voltages
x	streamwise distance from leading-edge
y	spanwise distance from centre line
α	wing incidence (°)
γ	aerodynamic damping (% critical)
ϵ	rms wing-root strain
η	semi-span ratio
σ	gauge factor
ρ	free stream density

Subscript

m	model

1 INTRODUCTION

The advantages and limitations of using aeroelastic models for buffeting tests were discussed in a previous paper[1]. Two completely different aeroelastic models, of a slender wing and a typical strike aircraft, were selected for a further study of this technique. The tests of the aeroelastic model of a large slender wing transport aircraft extended into the vortex breakdown region for which no comparative flight measurements were available. The tests of the typical strike aircraft model reported here allow some limited comparison with flight measurements in well separated flows.

These tests confirm the general conclusions of the previous paper[1] that aeroelastic models can provide much more detailed and valuable information about buffeting on aircraft than can ordinary wind tunnel models. In addition the present tests show that with the provision of a freedom of rotation in roll for the wing, an aeroelastic model can give a sharp indication of the low frequency 'wing-rock' boundary, in addition to wing buffeting.

2 EXPERIMENTAL DETAILS

2.1 Model

The flutter model of the wing used for the present experiments was installed in the top and bottom slotted working section of the RAE 3ft Tunnel. The wing was mounted on a straight cylindrical body, which was totally unrepresentative of the aircraft fuselage. In particular the body included no engine nacelles, cockpit canopy or tailplane. The cylindrical body was supported on a 3° cranked sting. This could be rolled to produce either 3° body incidence over a range of sideslip, or 3° sideslip over a range of incidence, as well as a range of incidence at zero sideslip, in conjunction with the pitch variation provided by the tunnel quadrant. The wing was set at an angle of 1° to the body axis. The test results presented here relate to a clean wing, and cover a wide range of Reynolds number.

A brief description of the wing construction is appropriate, and is quoted from a report by Sowden[2]. "The wing model was structurally based on an idealised interpretation of the full scale aircraft. That is, an outer wing with three box sections welded together, the joints between adjacent boxes corresponding to the wing spars, and an inner wing with one/two box sections. The wing sections were welded to a 'rigid' fuselage spar that was 'rigidly' restrained in all freedoms except roll and this freedom was controlled by a torsion bar arrangement. Construction was of light alloy with a balsa/pine profile and a silk covering. Separate ailerons were fitted with a representative jack stiffness. Ballast weights were embedded during construction to give a representative mass distribution." The surface finish achieved by this method of construction was good, particularly in the leading-edge region (although the surface finish of the port wing was superior to the starboard wing). Hence a narrow roughness band was applied to fix transition close to the leading-edge. A slot provided in the cylindrical body allowed the wing to have a maximum roll amplitude of about ±2° on the torsion bar. For some tests a carefully fitted internal clamp suppressed this freedom in roll.

Although the modal frequencies of the wing mounted in the quadrant of the RAE 3ft Tunnel were measured 'wind off' by a frequency sweep technique, the corresponding mode shapes were not measured. However, these mode shapes should not have differed greatly from those measured in the flutter tests[2] in another wind tunnel. The symmetric and antisymmetric mode shapes, with the freedom in roll, which are of greatest interest, are reproduced in Fig 1. The frequencies quoted relate to the clean wing in the RAE 3ft Tunnel.

2.2 Instrumentation and analysis

The wing response was monitored by six uncompensated strain gauge bridges, three on each wing, provided for the original flutter tests. The static bending moments on both wings were measured by wire strain gauges. In addition the unsteady bending and torsion moments on both wings were measured by semi-conductor strain gauges for greater sensitivity.

The separate signals from the port and starboard wings could be added to give the symmetric response and subtracted to give the asymmetric response. This helped to identify the modes excited. This arrangement of separate bridges is contrary to normal practice in buffeting measurements, where pairs of gauges on each wing are wired to give only the symmetric response.

For the unsteady measurements the rms voltage, dV, the steady voltage, V, and the gauge factor, σ, give the rms strain,

$$\sigma = dV/V\sigma \ . \qquad (1)$$

A factor of $\sigma = 120$ was assumed for the semi-conductor gauges.

For the static calibration of the wing-root bending moments, known weights were applied at different points on the wings. A rough estimate of the wing normal force coefficient was obtained by assuming that the force acted at the mid-semi span (b/4). The measured bending moments were then reduced to normal force coefficients by dividing by the moment qSb/8. For the dynamic calibration, the wing was excited at the fundamental bending frequency with a vibrator, and a linear relationship was established between the rms wing-root strain signal and the rms acceleration, $\ddot{y}$, measured by a light accelerometer attached to the wing tip by double sided adhesive tape.

The experiment was controlled by monitoring the unsteady signal from the port strain gauge bridge on a Real-Time-Spectrum analyser. For a limited number of conditions the six strain gauge signals were measured on a tape recorder. Record lengths of about 120 seconds were taken, which for the wing first symmetric bending frequency at about 170 Hz gives about 21000 cycles of buffeting. With this large number of cycles of buffeting, good estimates of the total damping can be obtained, using standard methods for analysing random data[3], such as the measurement of half power points or the decay of the autocorrelation function.

2.3 Test conditions

The model was tested in the 0.91m wide × 0.64m high top and bottom slotted section of the RAE 3ft Tunnel. The Mach number range was from M = 0.45 to 0.94 and the tunnel total pressures, p_t , were 0.34, 0.67 and 0.94 bar. (The model was originally designed for flutter tests at zero incidence at $p_t = 3$ to 4 bar.) The maximum wing incidence was intended to be just above the heavy buffeting contour measured during previous tests on an ordinary wind tunnel model of a similar configuration. This heavy buffeting contour was in good agreement with the maximum flight penetration measured during steady manoeuvres. Generally this maximum incidence could be reached, even for the highest total pressure selected, without exceeding the estimated safe normal force limit of 700 N (157 lb) on each wing of the model. However, with the freedom in roll the maximum incidence (14°) could not be achieved at M = 0.60 at the highest total pressure, because of the alarming amplitude of the 'wing-rock'.

The roughness band was applied to fix transition at a streamwise distance $x_k = 5$ mm from the leading-edge of the wing. The roughness band was 2.5 mm wide and was formed by a sparse distribution of ballotini (small glass spheres) with a diameter, k = 0.1 mm. This diameter was selected to fix transition at the intermediate total pressure $p_t = 0.67$ bar, and hence to somewhat 'over-fix' transition at $p_t = 0.94$ bar. Most of the scale effect observed between $p_t = 0.67$ bar and 0.34 bar was probably due to the 'underfixing' of the boundary layer at the lower total pressure.

3 RESULTS

3.1 Steady bending moment measurements and flow visualisation

The steady bending moment coefficients measured without and with the roll freedom are generally almost the same. This indicates that the deflection between the wing and the cylindrical body is generally unchanged when the clamp is removed, permitting the roll freedom.

However, a variation of the steady bending moment coefficient with total pressure is noticeable without the roll freedom (Fig 2). Thus at M = 0.60 both the initial slope, and the level at the stall, are lower at the lowest total pressure than at the two higher pressures. In contrast, at M = 0.80 the initial slope is identical although the levels at the stall are different. These differences are unlikely to be caused by static aeroelastic distortion, because this would be expected to alter the initial slopes both at M = 0.80 and 0.86, as well as at M = 0.60. Hence the differences observed at M = 0.60 and 0.80 must be attributed to genuine adverse scale effects, particularly at the lowest Reynolds number (only about 0.5×10^6), when transition is 'under-fixed', as discussed above in section 2.3.

Fig 2 shows a significant increase in the slope from M = 0.60 to 0.80, and a further small increase at M = 0.86. These variations in the bending moment coefficient, measured with a large cylindrical fuselage, are appreciably smaller than the corresponding variations in lift curve slope measured on another model with a representative fuselage, and thus may indicate an 'interference' effect common to all the measurements, or an inboard movement of the centre of lift sensed by the moment gauges, or a combination of these effects.

Fig 2 also includes the angle of incidence for buffet onset at every Mach number, derived from the unsteady component of the wing-root bending moment. These angles of incidence do not vary significantly with total pressure, so that scale effects on buffet onset are small. The incidences for buffet onset are well within the linear range of the steady bending moment measurements. This result confirms previous findings[4] that sudden changes in lift curve slope often indicate the sudden growth of small separations (and therefore heavy buffeting), rather than the onset of separations (and light buffeting).

The development of the separation at and after buffet onset was shown by oil flow photographs taken at the highest total pressure. The separations on the port wing were a little smaller than those on the starboard wing (because of the superior finish on the port wing) and are shown in Fig 3.

For a Mach number of 0.60, buffet onset occurs at $\alpha = 9^{\circ}$. The flow separates close to the leading-edge at about 80% semi-span, forms a tiny bubble and then immediately reattaches. The flow is attached both inboard and outboard of this bubble. An increase in incidence to $\alpha = 11^{\circ}$ produces a rapid extension of this bubble, downstream towards the trailing-edge and spanwise towards the wing-tip and the wing-root. It is interesting to note that the bubble still does not extend to the trailing-edge, and that there are four discrete cells visible under the main shear layer. The span of every cell is roughly equal to its length. Well ordered structures of this kind are often observed at subsonic speeds even under nominally two-dimensional bubbles. Lateral movement at low frequencies of these cells could well excite the 'wing-rock' phenomenon discussed in Section 4. This phenomenon is much more serious at M = 0.60, when there is a well defined cellular structure under the separation, than at higher Mach numbers, when such a structure is not observed.

For a Mach number of 0.80, buffet onset occurs at $\alpha = 4^{\circ}$. The flow separates at a shock on the outboard wing (located at about $x/c = 0.25$, from about 60 to 90% of semi-span) and immediately reattaches. An increase in incidence to $\alpha = 7^{\circ}$ moves the shock forward towards the leading-edge, while the separation extends downstream towards the trailing-edge. The direction of the complex separated flow behind the shock is predominantly spanwise. Close inspection of the flow on the inboard section of the wing reveals a weak, oblique shock starting from the apex. This oblique shock is a classic feature of the transonic flow on a swept wing of finite aspect ratio, and was discussed by Rogers *et al*[5].

For a Mach number of 0.86 the separation development is similar to that described at M = 0.80, but occurs more rapidly. Buffet onset is at $\alpha = 3^{\circ}$, and by $\alpha = 5^{\circ}$ the shock induced separation is as extensive as at $\alpha = 7^{\circ}$ at M = 0.80. The oblique shock starting from the apex in the wing is stronger than at M = 0.80 and hence is more noticeable.

3.2 Dynamic strain measurements

The symmetric or antisymmetric modes excited can be found by respectively adding or subtracting the port and starboard wing-root strain signals, as discussed in section 2.2. The time histories of these combined responses may then be analysed by the Presto computer system[6], and conveniently displayed as spectra of linear rms values (Fig 4).

For a typical heavy buffeting condition ($M = 0.60$, $\alpha = 14^{\circ}$), the response in the symmetric modes is virtually the same with or without the roll freedom, and consists of first symmetric bending at 174 Hz (Fig 4a). This result is reasonable because the boundary condition for the symmetric modes is unaltered by the roll constraint. Hence the symmetric component in the excitation spectrum must excite the same response. However, for the corresponding response in the antisymmetric modes, there are inevitably large differences, because here the boundary conditions are radically different, even if the antisymmetric excitation spectrum is unaltered by the motion. Without the roll freedom the only antisymmetric mode excited significantly is the first antisymmetric bending at 155 Hz, which must involve some twisting of the sting. In marked contrast, with the roll freedom the rigid body roll at 40 Hz is excited, together with a combined antisymmetric bending and torsion mode at 251 Hz (Fig 4b). (These modes probably involve a small torsion of the sting.) For these antisymmetric modes the results for the wing with the roll freedom give a better approximation to the aircraft, which does have something like a freedom in roll. On the aircraft the Dutch Roll frequency is about 0.5 Hz, which would correspond with about 15 Hz for this 1/30 scale model. Hence the frequency parameter for the roll mode in the present tests is too high.

Two further observations can be made from Fig 4. Firstly, there is significant *forced* model response (both symmetrically, and antisymmetrically) at low frequencies (say less than 10 Hz), where there are certainly no structural modes. This observation indicates that a comparatively high level of excitation at low frequencies is provided by the flow separations on the model. (The level of response is about 5 × higher than that excited by the flow unsteadiness in the wind tunnel at zero incidence.) Secondly, because of strain gauge misalignment and differences in sensitivity, the spectrum of the symmetric modes includes a faint indication of the antisymmetric mode at 251 Hz (Fig 4a), and the spectrum of the antisymmetric modes includes a clear indication of the first symmetric bending mode at 174 Hz (Fig 4b). Further analysis of the buffeting measurements will concentrate on the large response in the first symmetric bending mode, followed by brief comments on the two antisymmetric modes.

Fig 5 shows the variation of rms unsteady wing-root strain, ε, in the first bending mode, as a function of the angle of incidence for three Mach numbers and total pressures. Buffet onset is sharply defined at M = 0.60 (with the leading-edge separation) and at M = 0.86 (with the strong shock induced separation). However, at M = 0.80 buffet onset is less well defined and caused by the slow initial extension downstream of the separation behind the shock wave. Buffet onset curves of this type, with a sudden initial rise in response, followed by a constant level before a further increase, are frequently observed on swept wings close to the boundary along which the flow changes from a leading-edge to a shock induced separation.

Early investigations[7] of the similarity laws for buffeting suggested that in the absence of scale effects:

$$\varepsilon \propto \rho^{\frac{1}{2}} \quad - \text{ for aerodynamic damping,} \qquad (2)$$

or

$$\varepsilon \propto \rho \quad - \text{ for structural damping.} \qquad (3)$$

There must be appreciable scale effects because neither of these power laws is appropriate to these measurements. In addition we shall see later (see section 3.3) that the total damping is a combination of aerodynamic and structural damping.

The strain measurements with the roll freedom are believed to correspond most closely with an aircraft in flight. Hence the damping and buffet excitation parameters subsequently presented refer to this condition.

3.3 Damping measurements

From the long signal records, well defined spectra of the buffeting measurements could be obtained (*eg* Fig 4), as discussed above in section 2.2. From these spectra total damping estimates (% critical) could be readily obtained, using the half power point method.

The buffeting spectra for the symmetric modes indicate two interesting trends in the damping measurements for the first bending mode at about 174 Hz (Fig 6):

(1) For constant Mach number and angle of incidence the damping increases with the total pressure (*ie* the stream density), as required by theory.

(2) For constant Mach number and total pressure damping increases with the angle of incidence, the increase being most marked after the onset of buffeting. This trend is most obvious at M = 0.60: its significance will be discussed in section 4. Fig 7 shows the total damping measurements at two angles of incidence: ($\alpha = 1^\circ$ and the incidence for maximum buffet penetration) plotted against the product of the free stream density x the free stream velocity. In addition to the trends shown by Fig 6, Fig 7 shows that the wind-on damping measurements are consistent with a constant structural damping coefficient of $g/2 = 0.8\%$ critical, as measured wind-off in a ground resonance test.

The total damping for the symmetric overtone bending mode at about 550 Hz is predominantly structural, ($g/2 = 2\%$ critical) and only varies a little with free stream density and velocity. The variation with angle of incidence is within the scatter of the measurements. Similar remarks apply for the first antisymmetric structural mode at about 250 Hz: this mode represents combined bending and torsion.

The roll motion was not significantly excited by the tunnel unsteadiness. Hence for attached flow conditions below the buffet boundary, no damping values could be derived from the antisymmetric wing-root strain records. However, roll motion was excited after buffet onset, and a few total damping measurements, typically about 15% critical, were obtained at high angles of incidence (Fig 8). The measurements at the higher total pressures at M = 0.60 and 0.80 are most reliable, because here the model response was largest. These measurements suggest that the total damping in this mode falls as the angle of incidence increases. This trend is consistent with that generally observed in derivative measurements and with estimates presented in section 4: the variation is directly due to the flow separations on the outboard wing section. No clear variation of total damping with stream density can be established from Fig 8, although the measurements at the highest density are consistent with a structural damping coefficient, $g/2$ about 4% critical, as measured in a previous ground resonance test.

3.4 Buffet excitation parameter

From the strain and damping measurements presented above the buffet excitation parameter, $\sqrt{nG(n)}$, can now be calculated for the modes of interest according to the relation given by Jones[8]:

$$\sqrt{nG(n)} = [2/\sqrt{\pi}]\,(m\bar{\ddot{y}}/qS)\,\zeta^{\frac{1}{2}} \tag{4}$$

where m = generalised mass in mode,
$\bar{\ddot{y}}$ = rms wing tip acceleration in mode,
q = free stream kinetic pressure,
S = wing area
and ζ = total damping in mode (fraction of critical).

A simple linear relation between the rms wing-tip acceleration measured with an accelerometer and the wing-root strain signal was obtained during a ground resonance test.

Fig 9 shows the buffet excitation parameter derived for the first bending mode for the principal test conditions. Buffet onset is sharply defined, as in the unsteady strain measurements (Fig 5). For a given Mach number the buffet excitation parameter is identical for the two highest pressures, confirming that scale effects are small when the boundary layer transition is correctly fixed. However, the buffet excitation parameter is appreciably higher at the lowest total pressure, presumably because the flow separations are larger when transition is not correctly fixed.

The level of the buffet excitation parameter (about 1.0×10^{-3} to 1.5×10^{-3}) at low angles of incidence, $\sqrt{nG_0(n)}$, before the onset of separations on the wing is a measure of the combined excitation provided by the local flow round the model and the flow unsteadiness in the wind tunnel. Since the flow unsteadiness on an ordinary wind tunnel model at transonic speeds normally produces a lower buffet excitation parameter (only about 0.5×10^{-3} to 0.7×10^{-3}), the additional excitation must be attributed to the pressure fluctuations generated by the separation on the unfaired base of the large fuselage. Thus for this model it would have been impossible to use the flow unsteadiness in the tunnel as a measure of the excitation due to buffeting[4], even at subsonic speeds. The buffet excitation parameter appropriate to the wing flow separations alone may be obtained by subtracting the contribution at low angles of incidence. It is reasonable to assume that shortly after buffet onset there is no correlation between the flow separations on the wing and the excitation at low lift, so that the buffet excitation parameter for the wing separations alone, $\sqrt{nG_1(n)}$, is given by:

$$\sqrt{nG_1(n)} = \sqrt{nG(n) - nG_0(n)} \qquad (5)$$

Equation (5) and Fig 9 show that the maximum level of $\sqrt{nG_1(n)}$ achieved during the present tests is about 3×10^{-3} at M = 0.60 and 0.80, falling to about 2×10^{-3} at M = 0.86. These levels are typical of those achieved on ordinary wind tunnel models (Fig 11), and on aircraft in flight[9,10].

In contrast to the present model, the aircraft has a streamlined rear fuselage, so that in flight the buffet excitation parameter at low angles of incidence is determined by atmospheric turbulence and the aerodynamic and mechanical excitation provided by the engines. Previous tests[9,10] suggest that the sum of these contributions is normally quite small (typically about 0.1×10^{-3} to 0.2×10^{-3}), so that correction according to equation (5) should not be necessary for flight buffeting measurements.

The buffet excitation parameter was also derived for the rigid body roll motion at high angles of incidence, for the few conditions where measurements for the total damping in roll were available. For this mode the measurements are not sufficiently numerous to establish systematic trends for the variation of buffet excitation parameter with angle of incidence, Mach number or total pressure. However the measurements indicate that the buffet excitation parameter in this very low frequency, antisymmetric rigid body mode is of the same order as that for the wing first symmetric bending mode. Further discussion of these results is deferred to section 4.

Equation (4) also provides a good correlation of the small responses in both the combined antisymmetric torsion/bending mode and the symmetric overtone bending modes (at about 250 and 550 Hz respectively).

4 DISCUSSION AND COMPARISON WITH FLIGHT MEASUREMENTS

For the prediction of the buffet characteristics of new combat aircraft from wind tunnel tests, it is important to establish how the levels of buffet excitation parameter measured in wind tunnels compare with flight measurements. In addition it must be possible to scale measured damping coefficients from tunnel to flight and to be certain that all structural modes are correctly represented.

For the present flutter model and the first symmetric bending mode the maximum penetration in the tunnel corresponds with a level of $\sqrt{nG_1(n)} = 3 \times 10^{-3}$ at M = 0.60, falling to about 2×10^{-3} at M = 0.86 (Fig 9). However for the tunnel tests the maximum incidence (Fig 10a) was restricted by the normal force on the model, whereas in flight somewhat higher angles of incidence were achieved, particularly in transient pull ups at the higher Mach numbers (Fig 10b). Hence it is reasonable to infer that if the normal force restriction had been overcome, levels of $\sqrt{nG_1(n)} = 3 \times 10^{-3}$ would have been achieved on the model over the full Mach number range from M = 0.60 to 0.86. No comparative measurements of the buffet excitation parameter are available from the flight tests of this aircraft.

For ordinary wind tunnel models the maximum level of the buffet excitation parameter in the first symmetric bending mode is again about 3×10^{-3}, and this level is comparable with that achieved in flight at much the same angles of incidence. Fig 11 illustrates this by the only measurements currently available which relate to a TACT F1-11 (for two different angles of wing sweep), a small fighter aircraft and a 65° delta wing. Hence it is reasonable to propose new criteria for the buffet excitation parameter, to supplement those derived previously from buffeting coefficients[11] (Table 1). The maximum level of the buffet excitation parameter defines the heavy buffeting criterion. The moderate and light levels are then inferred by reducing the maximum level by factors of ½ and ¼ respectively. These factors correspond with equal logarithmic decrements, as in the previously defined semi-empirical buffeting coefficients.

It is important to note that although the buffet excitation parameter, $\sqrt{nG(n)}$, attains a value of 3×10^{-3} at the heavy buffeting levels for these measurements, the parameter $\sqrt{G(n)}$ does not. This is because of variations in the frequency parameter, $n = f\bar{c}/U$, from configuration to configuration. Now the previously determined empirical buffeting coefficients[11] (for a much wider range of configurations) were directly derived from pressure fluctuation measurements. These pressure fluctuations were expressed in terms of $\sqrt{nF(n)}$, precisely analogous to $\sqrt{nG(n)}$. Thus the effects of variations in the frequency parameter within those tests were compensated and it was possible to achieve unique buffeting coefficients for a wide range of configurations.

As previously remarked[11], the correlations established between dimensionless buffet excitation parameters or buffeting coefficients and the maximum flight penetration are at first sight surprising, because it might reasonably be expected that the severity of buffeting in flight would be based on the dimensional level of vibration (either estimated by the pilot or measured with an accelerometer). However in general the severity of wing buffeting is rarely a controlling factor. The pilots of fighter or strike aircraft often fly right up to a handling boundary, such as pitch/up or stalling, irrespective of the level of buffeting. For the present tests the alarming amplitude of the 'wing-rock' at an angle of incidence of 14° at M = 0.60 and the highest total pressure, suggest that the handling boundary for this aircraft is determined primarily by a sudden fall in the derivative ℓ_p, the damping due to roll for the wing, or even to its reversal in sign. This explanation is consistent with estimated damping measurements, which are presented later (Fig 13).

Low frequency rigid body derivatives are normally measured by the forced oscillation technique[12], for both attached and separated flows. Hence the buffet excitation parameter in these modes due to the separated flows has not been measured previously. *During the present tests the buffet excitation parameter for the roll mode was measured* for the first time, and found to be of the same order of magnitude as that for the first symmetric bending mode. However the roll mode is not excited until the moderate buffeting criterion for the first symmetric bending is exceeded (Fig 12). This observation implies that somewhat larger separations, with a higher level of excitation at low frequencies, are required for the roll mode to be excited significantly. Fig 12 also suggests that the buffet excitation parameter at this low frequency remains bounded even at high angles of incidence. Hence according to equation (4), the large roll responses observed briefly at high angles of incidence at the highest pressure at M = 0.60 probably correspond with small or negative values of damping, as suggested above.

The aerodynamic damping for the low frequency rigid body roll mode at 40 Hz may be estimated by quasi-steady strip theory, using unpublished local steady lift distributions measured on a large half model. (For the roll mode the local angle of incidence is assumed proportional to the semi-span ratio, η .) With attached flow and for small angles of incidence these estimates are in excellent agreement with estimates from the constant value $\ell_p = -0.40$, obtained from data sheets (Fig 13). For large angles of incidence the strip theory predicts a sudden loss of damping about 3° to 4° above buffet onset, due to the large changes in the spanwise load distribution caused by flow separation. The incidence at which this loss of damping occurs is roughly intermediate between that for the maximum flight penetration in steady turns and transient pull-ups (Fig 10b). This incidence corresponds also with the heavy buffeting limit for the first symmetric bending mode derived from previous tunnel tests on an ordinary wind tunnel model (Fig 10a). This observation supports the previous remarks about the correspondence between traditional buffeting criteria and aircraft handling boundaries[11].

On a wind tunnel model the aerodynamic damping cannot be measured independently of the structural damping. For this aeroelastic model the structural damping, $g/2$, in the roll mode is believed to be as high as 4% critical, as in the previous flutter tests. If this value is assumed constant and subtracted from the total damping measurements (Fig 8), to give the 'measured' aerodynamic damping, these values are in fair agreement with the estimates from quasi-steady strip theory (Fig 13). In particular, the measure*ments at M = 0.60 and 0.80 confirm a loss of damping as the angle of incidence and the* area of separated flow on the wing increase.

For M = 0.60 and 0.80, Fig 13 also includes a few estimates of damping in the roll mode inferred from 1g flight at different altitudes. These are in excellent agreement with both estimates at M = 0.60, but naturally can provide no indication of the loss of damping at handling limits.

The aerodynamic damping for the higher frequency, first symmetric bending mode at 174 Hz may also be estimated by quasi-steady strip theory. Again the steady lift distribution measured on the large half model is used. (For the first symmetric bending mode the local angle of incidence is assumed proportional by η^2 .) The aerodynamic damping measurements are derived from the total damping measurements given in Fig 6, subject to the reasonable assumption derived from Fig 7 that the structural damping coefficient, $g/2$, is 0.8% critical and constant. With attached flow for small angles of incidence the estimates are in good agreement with the measurements. However, after buffet onset the estimates suggest a fairly rapid fall in aerodynamic damping (Fig 14), rather like the estimates for the aerodynamic damping in the roll mode (Fig 13). In marked contrast the measurements show a significant increase in aerodynamic damping, particularly at M = 0.60. The good agreement between the estimates and the measurements below buffet onset suggests that frequency effects on the thin attached boundary layers are small. The large discrepancy between the theory and the measurements after buffet onset suggests that frequency effects on the thick separated shear layers are large, so that the use of quasi-steady theory is no longer justified. Fig 14 suggests that these frequency effects are much larger at M = 0.60 with a large area of separated flow (from the leading-edge) than at M = 0.80 and 0.86 with a smaller area of separated flow (from the shock).

In addition to the global effect of the smaller areas of separated flow at transonic speeds, another factor probably limits the variation of aerodynamic damping with angle of incidence for aircraft structural modes. The aerodynamic damping at transonic speeds is naturally strongly influenced by the movement of shock waves. Now for inviscid transonic flows Nixon has shown[13] that although large changes of shock wave motion and phase angle occur at the very low frequency parameters appropriate to rigid body modes, frequency effects stabilise for frequency parameters appropriate to structural modes, as low as $\omega\bar{c}/U = 0.3$, or $f\bar{c}/U = 0.05$. Hence within the inviscid transonic flowfield upstream of the shock there is a powerful control applied to limit the high frequency effects produced within the area of separated flow downstream of the shock. Further evidence for the existence of this powerful control is provided by recent measurements[14] on a NACA 64A010 aerofoil pitching about its quarter chord point at a Mach number of 0.80 and a Reynolds number of 12×10^6. Comparison of the unsteady pressure measurements at $\alpha = 0^{\circ}$ (when the flow is attached) and at $\alpha = 4^{\circ}$ (when the flow is separated) show that for frequency parameters lower than about $\omega c/U = 0.5$ incidence effects due to flow separations are large, whereas above $\omega c/U = 0.5$ incidence effects are small (Ref 14, cf Figs 17 and 22). These comparisons are relevant to the present measurements shown in Figs 13b and 14b *although the thickness/chord ratio of the wing is lower than for the aerofoil, varying* from 8% at the kink to 6% at the tip.

For the higher frequencies of the symmetric overtone bending and the combined antisymmetric bending/torsion modes the damping variations with angle of incidence are negligible both at $M = 0.80$ and 0.86, consistent with the suggestions made above. In addition at these higher frequencies there is no significant influence of flow separations on the damping at subsonic speeds. This is a feature of the results which deserves investigation in a future experiment.

Returning to the problem of extrapolating from model to flight tests, aerodynamic damping measurements on a model may be extrapolated to an aircraft according to the equation given by Jones[8], if scale effects on the separations are neglected. Scale effects are generally small for the large separations associated with heavy buffeting although they are often large close to the buffet boundary. An advantage of making buffeting measurements on aeroelastic models is that they usually produce significant aerodynamic damping (eg about 3% critical for $p_t = 0.94$ bar in Fig 7). The damping ratio, γ_a/γ_m, required to extrapolate from an aeroelastic model to full scale is typically only about 3. In contrast, on an ordinary wind tunnel model the aerodynamic damping ratio is often as low as 1% critical (not measured accurately because of the difficulty of estimating the wind-on structural damping). The damping ratio, γ_a/γ_m is typically as high as 9. Hence the full scale aerodynamic damping ratio (typically about 9% critical) can be estimated more accurately from tests on aeroelastic models than on ordinary wind tunnel models.

Finally we must re-emphasise[1] that a half model can only simulate symmetric response modes of a real aircraft. A complete model must be used if antisymmetric modes are to be simulated. For buffeting measurements on a complete model it is advantageous to measure the port and starboard wing-root strain signals independently. These signals may then be added or subtracted electronically to obtain the symmetric or antisymmetric responses, as illustrated in Fig 4.

For an ordinary sting supported complete model this technique should produce rough estimates of the buffet excitation parameter both for the rigid body roll mode and good estimates for the first symmetric bending mode, even if the frequency parameters are not correct. However for higher frequency structural modes some differences are inevitable because of large differences in frequency parameter and mode shape.

5 CONCLUSIONS

Buffeting measurements on a flutter model of the wing of a typical strike aircraft suggest five main conclusions.

(1) Sufficient measurements of the buffet excitation parameter for the first symmetric bending mode having now been obtained to formulate new criteria for the severity of buffeting in flight. These new criteria supplement previously determined buffeting coefficients (Table 1).

(2) The buffeting coefficients previously determined from wind tunnel tests derive from aircraft handling boundaries, rather than from any quantitative assessment of buffeting by the pilot.

(3) On this aircraft the handling boundary at high angles of incidence is closely related with 'wing-rocking' caused by a sudden loss in the damping due to roll of the wing (Fig 13). The buffet excitation parameter in this mode remain bounded at high angles of incidence and comparable with that in the first symmetric wing bending mode (Fig 12).

(4) Significant variations on aerodynamic damping occur after the onset of flow separations. For the low frequency rigid body roll mode these variations may be explained by the spanwise changes in loading predicted by quasi-steady strip theory (Fig 13). For the higher frequency, first symmetric bending mode this method is not adequate, owing to a strong frequency effect on the separated flow (Fig 14).

(5) Although half models can predict the symmetric buffeting response of aircraft, complete models are needed to predict both symmetric and antisymmetric responses (Fig 4).

Table 1

BUFFET PENETRATION CRITERIA FOR FIRST SYMMETRIC WING BENDING

Severity of buffeting	Buffet excitation parameter $\sqrt{nG_1(n)}$	Buffeting coefficient C_B^{11} (Ref 11)
Light	0.00075	0.004
Moderate	0.00150	0.008
Heavy	0.00300	0.0160

REFERENCES

1 D.G. Mabey, Some remarks on buffeting. VKI Lecture Series on unsteady airloads and aeroelastic problems in separated and transonic flow, March 1981

2 R.A. Sowden, Utilisation of wind tunnel turbulence for model excitation, BAe unpublished, 1980

3 J.S. Bendat, A.G. Piersol, Random Data: analysis and measurement procedures, Wiley, New York (1971)

4 D.G. Mabey, Beyond the buffet boundary, J. Roy. Aero. Soc., April 1973

5 I.M. Hall, E.W.E. Rogers, The flow pattern on a tapered swept-back wing at Mach numbers between 0.6 and 1.6. ARC 19691, R&M 3271 (1957)

6 B.L. Welsh, D.M. McOwat, Presto: a system for the measurement and analysis of time-dependent signals. RAE Technical Report 79135 (1980)

7 W.B. Huston, A.G. Rainey, A. Gerald and T.F. Baker, A study of the correlation between flight and wind tunnel buffet loads. NACA RML 55E 16b, 1955

8 J.G. Jones, A survey of the dynamic analysis of buffeting and related phenomena, RAE Technical Report 72197 (1973)

9 G.F. Butler, G.R. Spavins, Preliminary evaluation of a technique for predicting buffet loads in flight from wind tunnel measurements on models of conventional construction, RAE Technical Memorandum Aero 1698, November 1976

10 G.F. Butler, G.R. Spavins, Wind-tunnel/flight comparison of the levels of buffeting response intensity for the TACT F1-11. Symposium on transonic aircraft technology, AFFDL TR 78-100, August 1978

11 D.G. Mabey, An hypothesis for the prediction of flight penetration of wing buffeting from dynamic tests on wind tunnel models, ARC CP 1171, 1971

12 C.O. O'Leary, Wind tunnel measurements of aerodynamic derivatives using flexible sting rigs, AGARD LS 114 'Dynamic stability parameters', March 1981

13 D. Nixon, On unsteady transonic shock motions, AIAA J. Vol.17, No.10, pp 1143-1145

14 S.S. Davis, G.N. Malcolm, Experiments in unsteady transonic flow, AIAA/ASME Structures, Structural Dynamics and Materials Conference, April 1979

Copyright
©
Controller HMSO London
1982

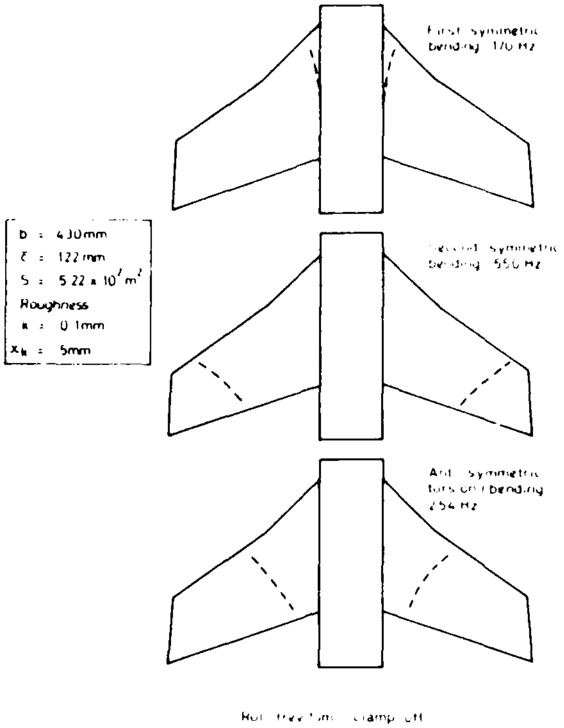
First symmetric bending 170 Hz
Second symmetric bending 550 Hz
Anti symmetric torsion / bending 254 Hz
b = 430mm
c̄ = 122mm
S = 5 22 x 10² m²
Roughness
k = 0 1mm
x_k = 5mm
Roll freedom clamped off

Fig 1 Wing modes - wind off

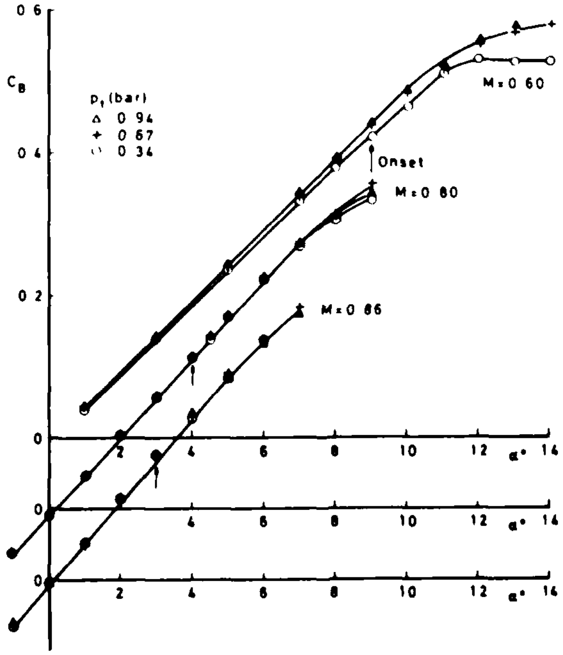

Fig 2 Steady bending moment coefficient v incidence - no roll freedom

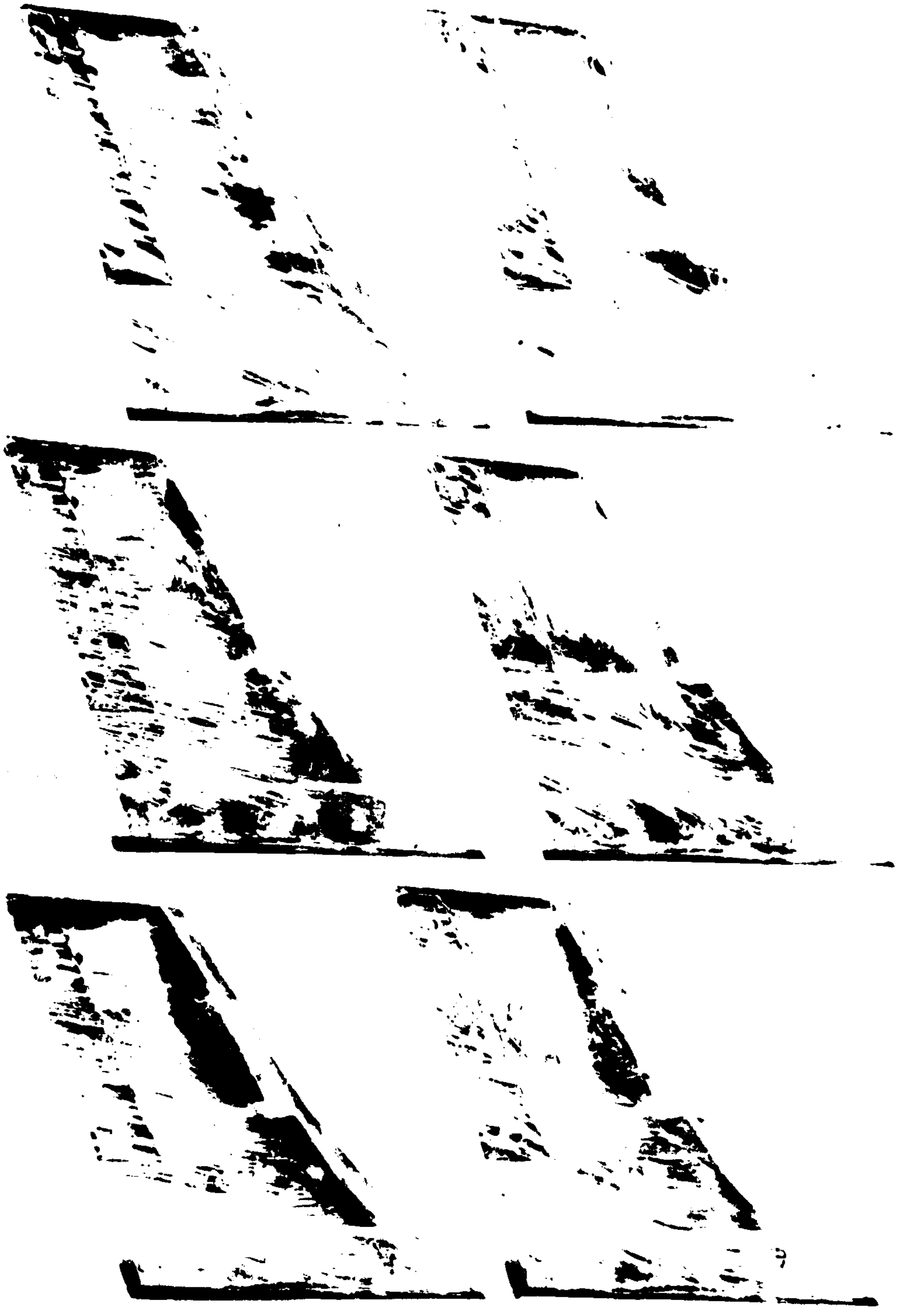

Fig 3 Typical oil flow photographs (p_t = 0.94 bar)

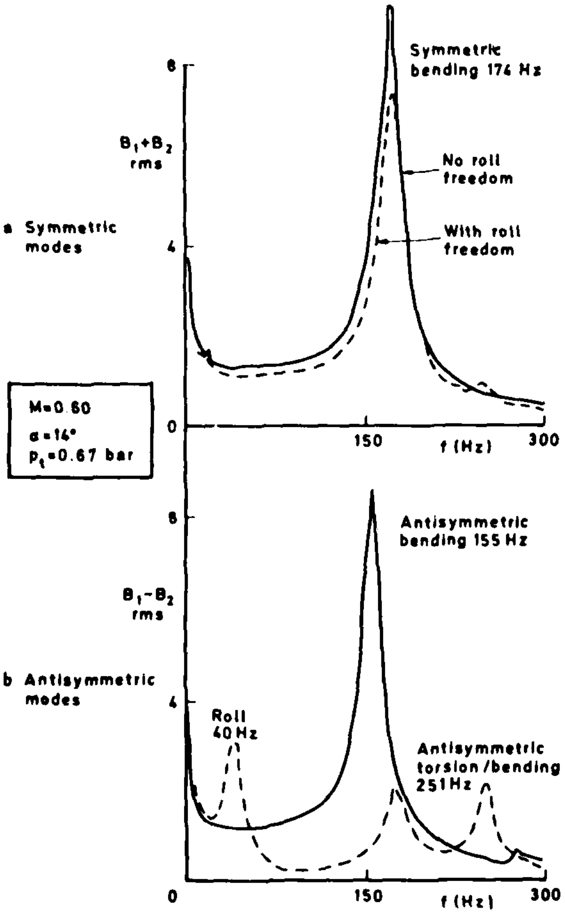

Fig 4a&b Typical spectra of combined wing-root strain signals

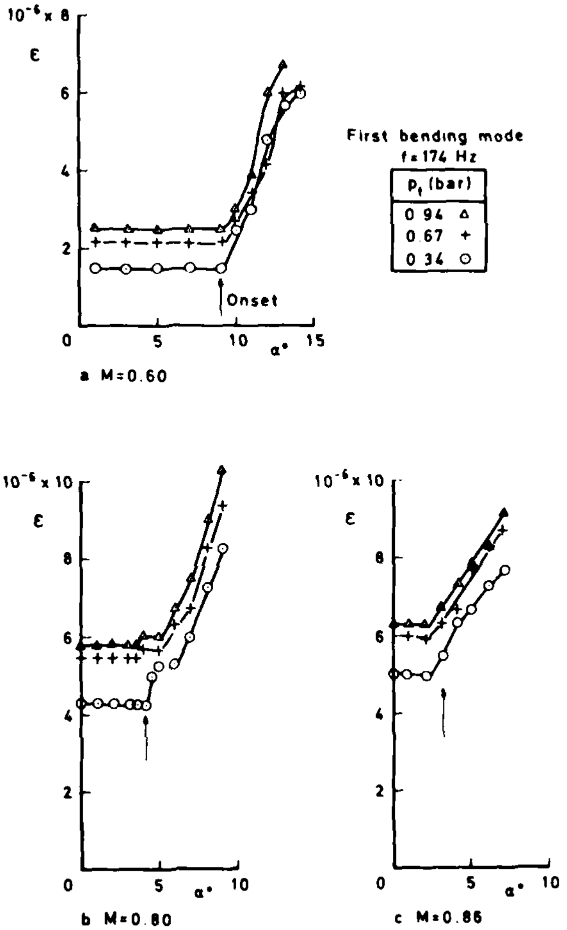

a M=0.60

b M=0.80

c M=0.86

Fig 5a-c Unsteady wing-root strain v incidence

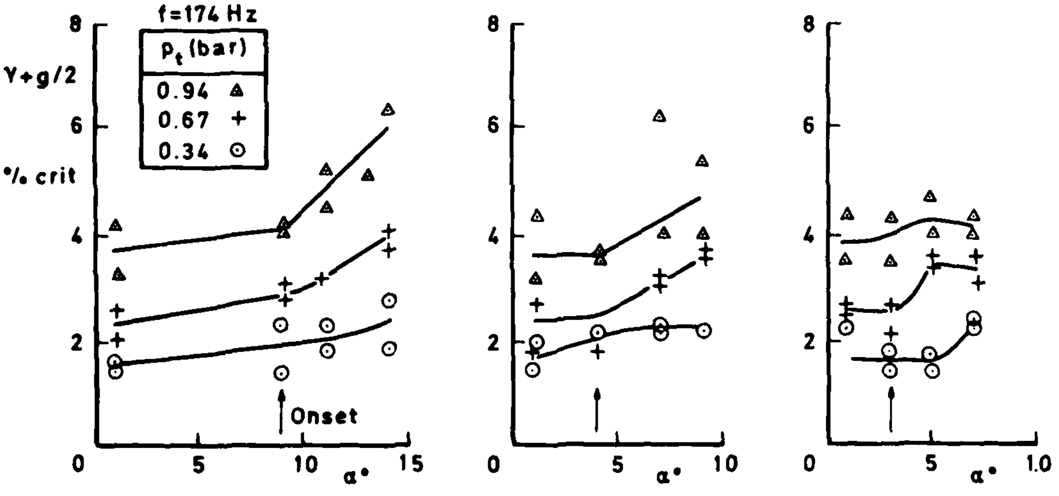

a M=0.60

b M=0.80

c M=0.86

Fig 6a-c First symmetric bending - damping - v incidence

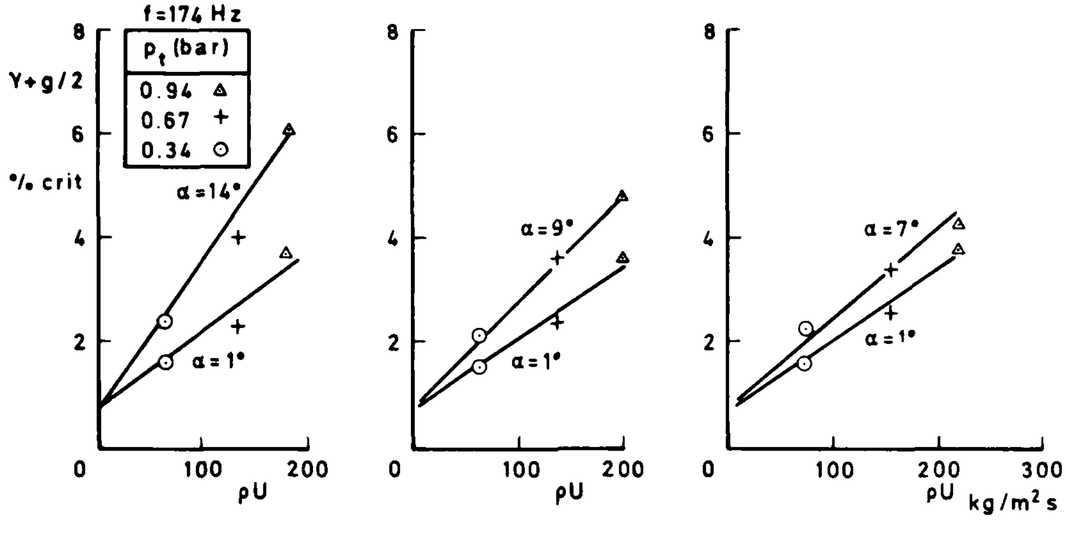

a M=0.60
b M=0.80
c M=0.86

Fig 7a-c First symmetric mode - damping v product of density × velocity

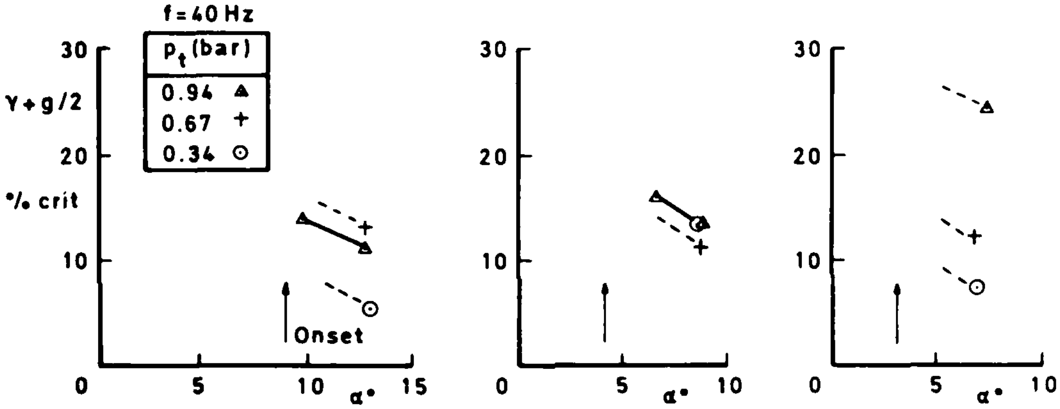

a M=0.60
b M=0.80
c M=0.86

Fig 8a-c Rigid body roll damping v incidence

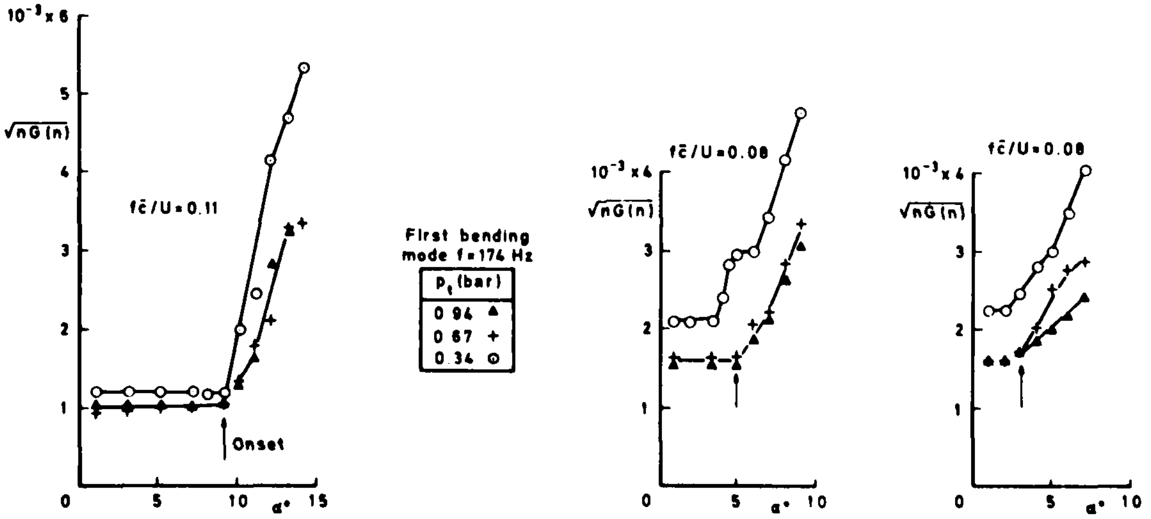

a M=0.60
b M=0.80
c M=0.86

Fig 9a-c Buffet excitation parameter v incidence

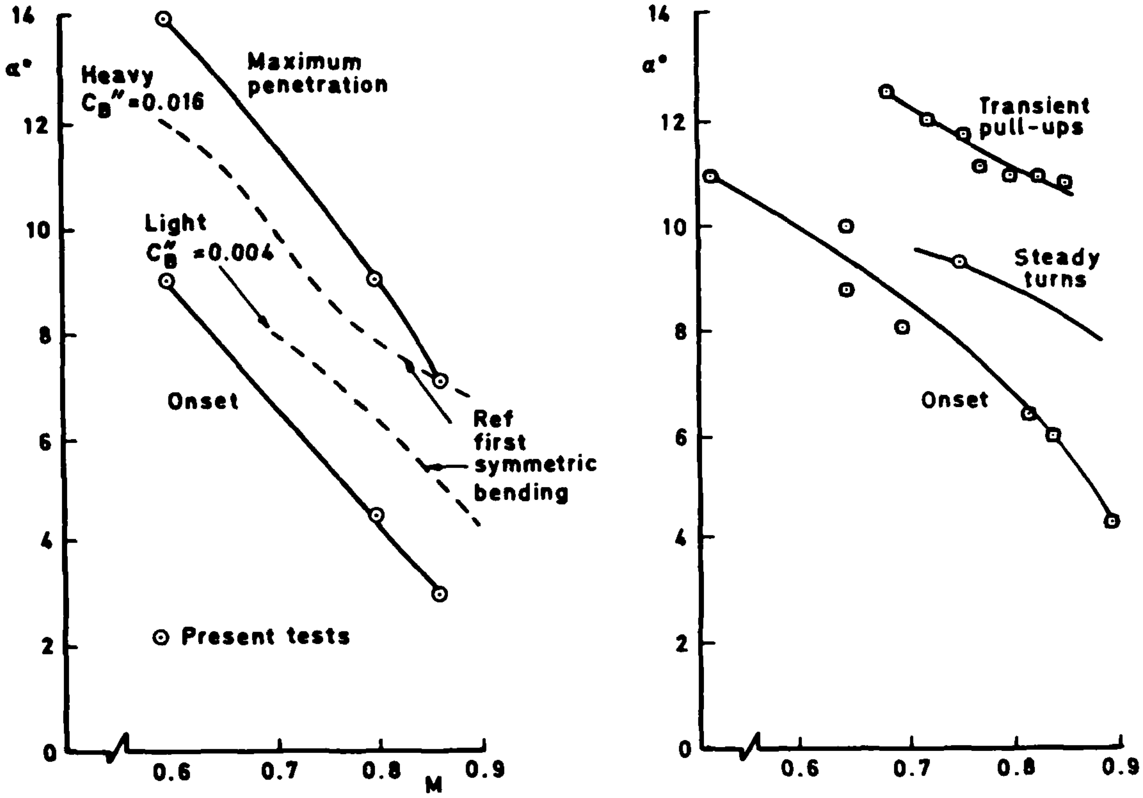

a Wind tunnel

b Flight-25000

Fig 10a&b Comparison of funnel and flight buffet boundaries

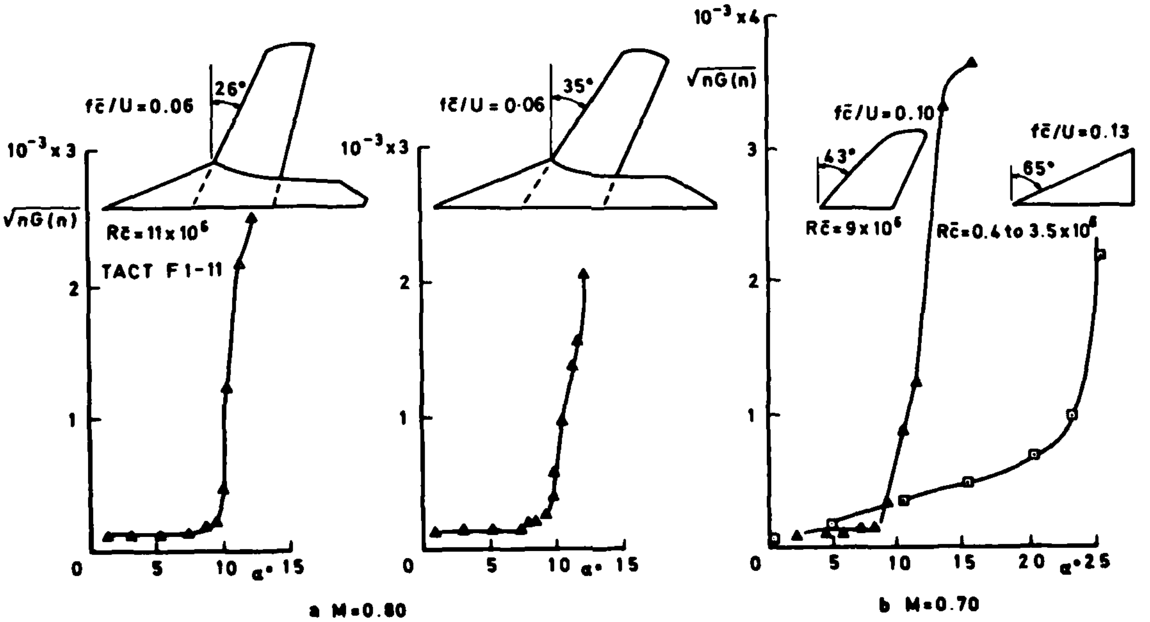

a M=0.80

b M=0.70

Fig 11a&b Buffet excitation parameters for ordinary wind tunnel models
(first bending model)

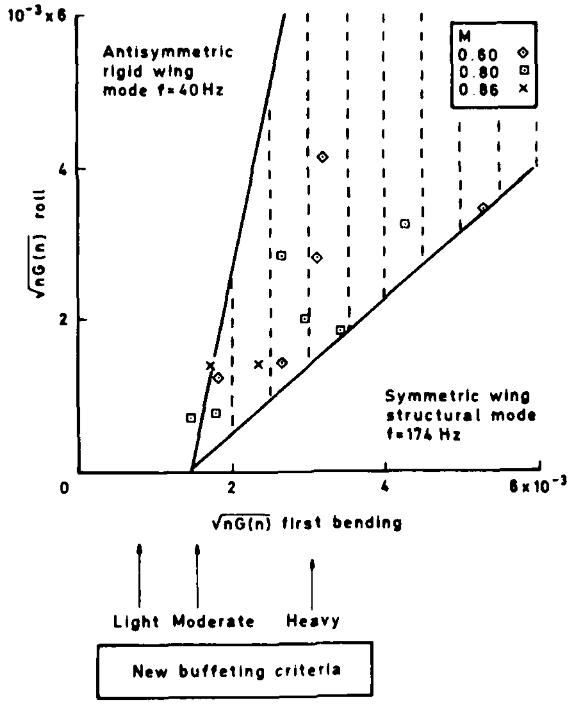

Fig 12 Relation between buffet excitation parameter in roll and bending modes

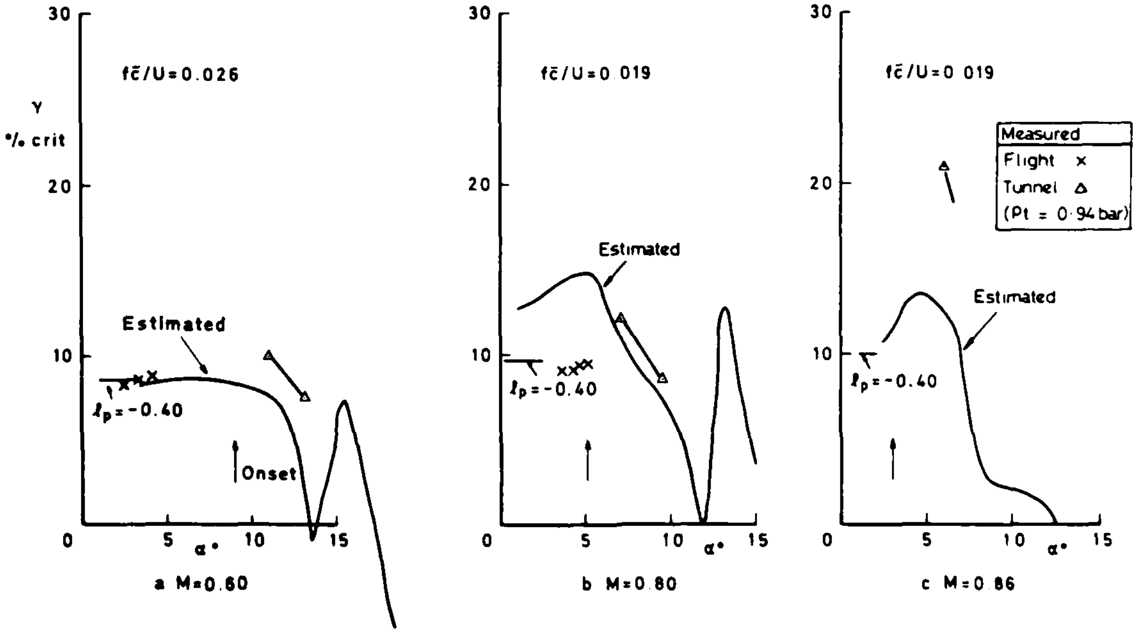

Fig 13a-c Comparison of estimated and measured aerodynamic damping in roll

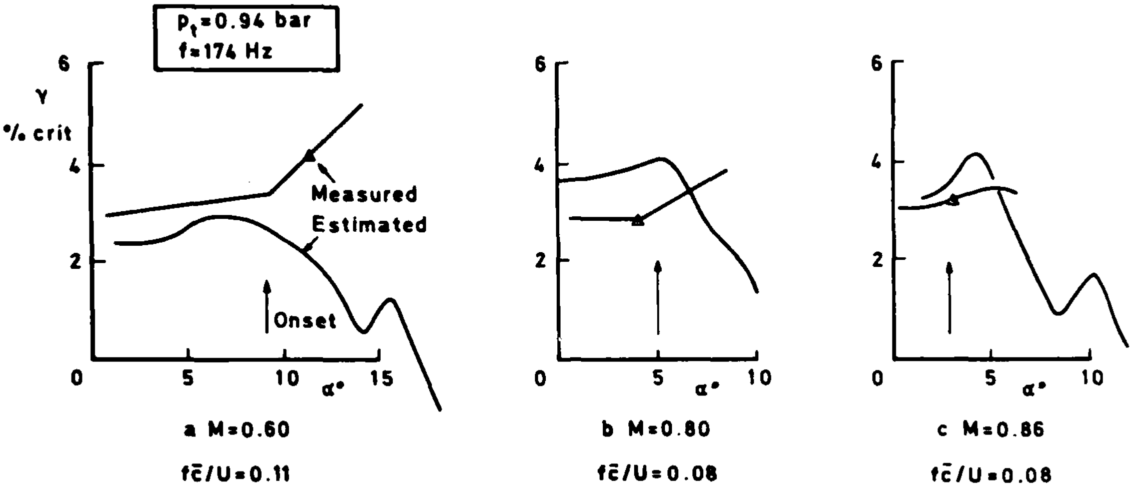

a M=0.60
$f\bar{c}/U = 0.11$

b M=0.80
$f\bar{c}/U = 0.08$

c M=0.86
$f\bar{c}/U = 0.08$

Fig 14a-c Comparison of estimated and measured aerodynamic damping in first symmetric bending

AERODYNAMIC MODEL IDENTIFICATION FROM DYNAMIC FLIGHT TEST DATA AND WINDTUNNEL EXPERIMENTS

by J.A. MULDER, J.G. DEN HOLLANDER and H. BINKHORST

Delft University of Technology
Department of Aerospace Engineering
Delft, The Netherlands

ABSTRACT

Dynamic flight test techniques may be employed for the measurement of a variety of aircraft performance characteristics as well as for the measurement of Stability and Control characteristics in the form of for instance classical Stability and Control derivatives. The present work focusses on the development of nonlinear aerodynamic models from dynamic flight test data. Several closely related characteristics of these models are discussed in detail such as goodness of fit to flight test data, the accuracy of model predictions and model complexity. Results are presented of a flight test program with the DHC-2 "Beaver" experimental aircraft of Delft University of Technology equipped with a high accuracy instrumentation system.
Different aerodynamic models are compared with results from windtunnel experiments.

1. INTRODUCTION

Techniques for the reconstruction of the actually flown flight path may be applied for assessment of approach, landing and take off performance. These techniques are also used for the creation of a database from dynamic flight test measurements for the synthesis of nonlinear aerodynamic models. The synthesis of nonlinear models from dynamic flight test data, their application for predicting aerodynamic forces and aerodynamic moments in flight conditions which are different from the set of flight conditions actually traversed in the course of some flight test maneuver and the comparison of the results of dynamic flight test data analysis with other data sources as windtunnel experiments are the subjects of the present paper. In Section 2 a short description is given of the technique for analyzing dynamic flight test data as applied here. More details are given in Ref. 2. Section 3 discusses some aspects of the identification of aerodynamic models which can from the system theoretic point of view be interpreted as multi input-single output linear static models. The characteristics are discussed of models which approximate the real physical process in a least squares sense. These models can be distinguished with respect to their potential to predict the output of the physical system in setpoints for which no actual observations are available. In Section 4 a description is given of a flight test program with the DHC-2 "Beaver" experimental aircraft of Delft University of Technology. This flight test program was carried through in cooperation with DFVLR (Deutsche Forschungs- und Versuchsanstalt für Luft- und Raumfahrt) in Braunschweig and NLR (National Aerospace Laboratory) in Amsterdam. Windtunnel experiments were carried through on a 1:11 scale model of the experimental aircraft in the low speed windtunnel of Delft University of Technology. The propellor slipstream could be simulated in these experiments, measurements were made in symmetrical (zero sideslip angle β) as well as in non symmetrical flow conditions. These experiments are described in section 5. Section 6 is used to present some of the results of the flight test program and windtunnel experiments. It is argued that dynamic flight test measurements can not as such be compared directly with the results of windtunnel experiments. A comparison requires an aerodynamic model to be identified first and consequently, differences between dynamic flight tests and windtunnel experiments cannot be attributed entirely to for example the effect of a difference in Reynolds number but depend also on which terms are included in the aerodynamic model.
It is suggested that the results of windtunnel experiments may be helpfull in synthesizing aerodynamic models for a wide range of flight conditions as required for example in mathematical models for flight simulation. Some conclusions are drawn in section 7.

2. DYNAMIC FLIGHT TEST DATA ANALYSIS

Data analysis of dynamic flight test measurements constitutes in principle a dynamical system identification problem. The system is excited by input signals as for instance elevator δ_e, rudder δ_r and aileron δ_a deflections as well as by process noise in the form of atmospheric turbulence. The system is observed via transducers such as for instance accelerometers, rate gyro's, airspeed and altitude sensors and local flow angle transducers. The art of system identification is to find estimates of the actually flown trajectory as well as of the system parameters. Some of the system parameters are already known such as aircraft mass and moments of inertia. If linear models are used the system parameters of interest are the classical so called stability and control derivatives.

Often this system identification procedure is put in the framework of maximum likelihood estimation theory. The advantage here is that as one of the transducers produces less accurate measurements, these measurements are less heavily weighted. References can be found in Ref. 7.

A disadvantage of this approach to the dynamic flight test data analysis problem is that the necessary computations are quite intricate, even more so if nonlinear system models must be used.

The approach advocated in Ref. 7 and which is also followed here divides the data analysis problem in two separate problems each of which is relatively easy to solve. This socalled two-step method starts by calculating the aircrafts flight path from very accurate accelerometer and rate gyro data and airspeed, altitude and sideslip vane or geographical position measurements. This is flight path reconstruction and constitutes the first step. The result is a set of important time histories such as angle of attack α, sideslip angle β, airspeed V as well as estimates of minuscule but nevertheless existing zero shifts of the accelerometers and rate gyro's mentioned above. Next one calculates in a straight forward manner the time histories of the aerodynamic longitudinal, lateral and vertical force coefficients C_X, C_Y and C_Z

resp. and the corresponding aerodynamic moment coefficients C_ℓ, C_m and C_n.

For the most precise results, flight path reconstruction is based on nonlinear kinematical models and is therefore probably as intricate a proces as the maximum likelihood procedure for system identification mentioned above, see Ref. 4. It needs to be done only once, however, for every flight maneuver. The resulting time histories constitute a data base for the second step which is aerodynamic model identification.

In aerodynamic model identification one developes an aerodynamic model which on the one hand can be fitted well to the available measurements but does on the other hand contain not so many parameters that parameter estimation accuracies become to low or that the model loses its capacity to predict force or moment coefficients for flight conditions different from those actually encountered in the flight test maneuver.

Aerodynamic model identification usually is a process of trial and error even if it is done in an organized way as in section 3. One may desire to investigate for instance to what extend it is possible to develop aerodynamic models for a wider range of flight conditions by joining two or more of the above mentioned data bases of different nominal flight conditions.

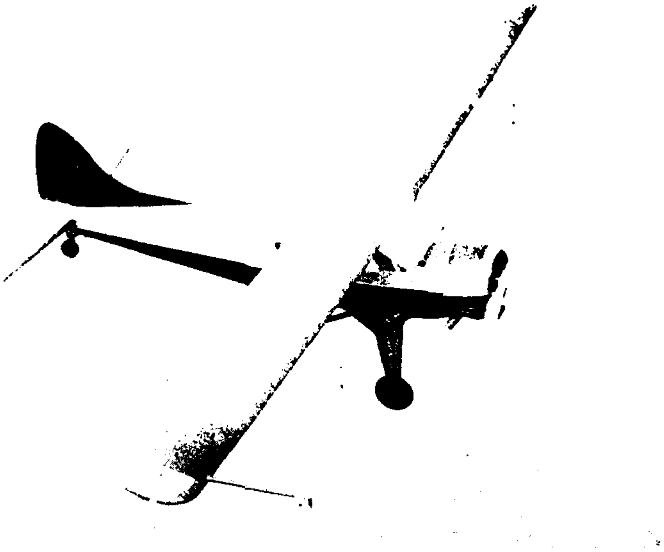

Fig. 1. DHC-2 "Beaver" experimental aircraft of Delft University of Technology.

In section 6 aerodynamic models are developed for the DHC-2 "Beaver" aircraft of Delft University of Technology, see Fig. 1. Dynamic flight tests were made with this aircraft, see section 4. In addition windtunnel experiments were made with a 1:11 scale model, see section 5.

In general, aerodynamic force and moment coefficients depend in a nonlinear way on the past and present values of variables as angle of attack α and sideslip angle β. This is clearly illustrated by Fig. 2. It is not unusual to assume that the force and moment coefficients can be expressed as functions of the present values only of a set of variables which may then include also first and higher order derivatives with respect to time. Finally, these functions are assumed to be analytic which implies they can be expanded in terms of a multiple Taylor series.

3. AERODYNAMIC MODEL IDENTIFICATION

In the present work it is assumed that aerodynamic models for the dimensionless aerodynamic force coefficients C_X, C_Y and C_Z and the dimensionless aerodynamic moment coefficients C_ℓ, C_m and C_n can be written in the following general form:

$$y(i) = \sum_{k=1}^{r} a_k x_k(i) + \varepsilon(i) \qquad (3\text{-}1)$$

$$i = 1(1)\ N$$

in which $y(i)$ denotes a scalar dependent variable, $x_k(i)$ and a_k, $k = 1(1)\ r$, represent a set of r independent variables and a set of r parameters respectively. Turbulence in the propeller slipstream and in the boundary layer, full sloshing, light atmospheric turbulence, etc. generate stochastic contributions to the force and moment coefficients. These contributions are, in a rather heuristic way, accounted for through an addition of a stochastic variable $\varepsilon(i)$ with:

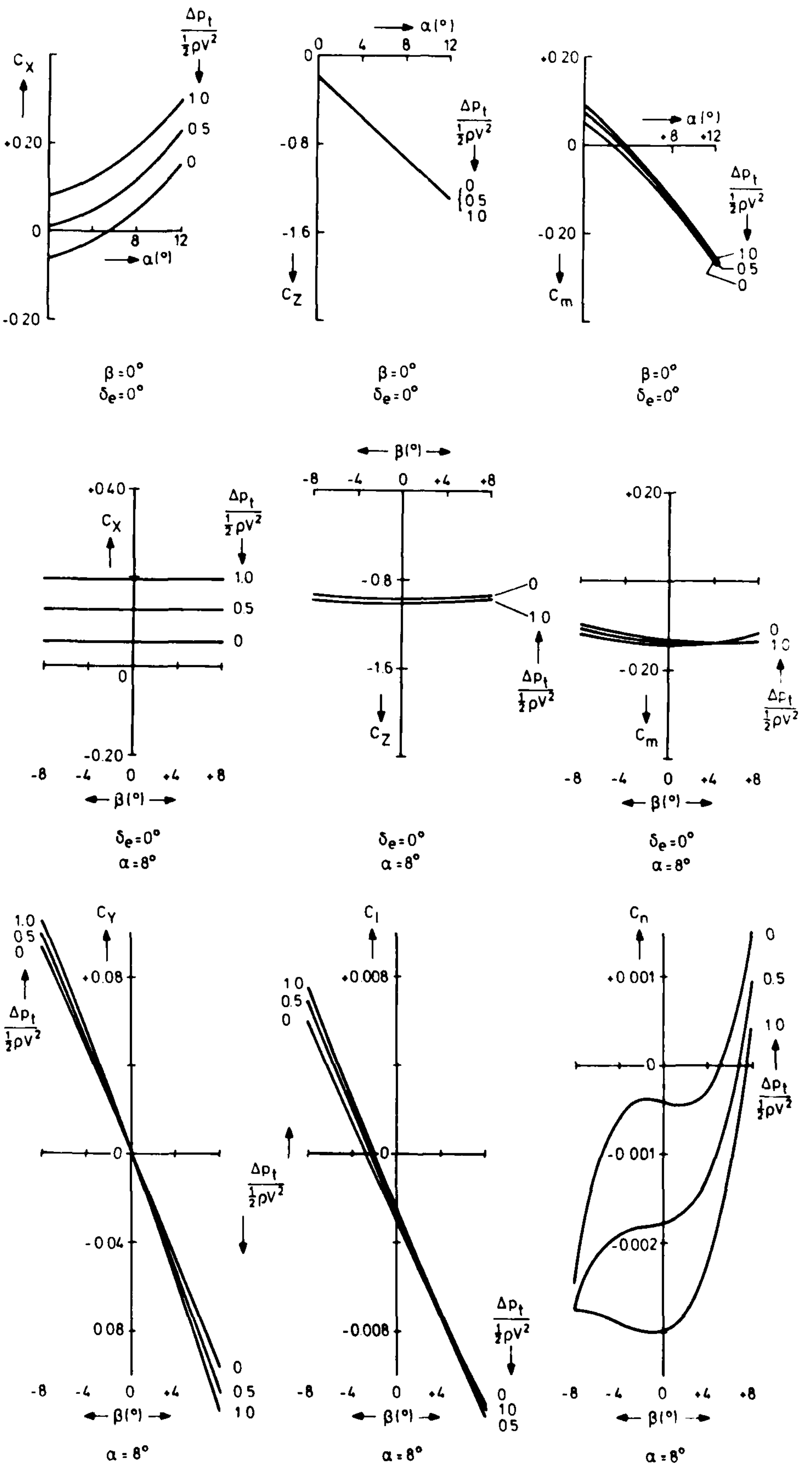

Fig. 2. DHC-2 "Beaver" aerodynamic force and moment coefficients as functions of angle of attack (α), sideslip angle (β) and $\Delta p_t/\frac{1}{2}\rho V^2$, the "strength" of the propeller slipstream. Measurements were made in the LST of Delft University of Technology at a Reynolds number of 0.47 * 10^6 using a 1:11 scale model, see section 5.

$$E\{\varepsilon(i)\} = 0$$
$$E\{\varepsilon(i)\ \varepsilon(j)\} = v_\varepsilon\ \delta_{ij} \qquad (3\text{-}2)$$

In the case of windtunnel experiments, the integer i refers to one of a set of N setpoints or to one particular time instant t_i in the case of dynamic flight test measurements.
For all i, the independent variables $x_k(i)$ are assumed to be known exactly. The dependent variable y(i) is measured with finite accuracy according to:

$$y_m(i) = y(i) + m(i) \qquad (3\text{-}3)$$

where m(i) represents a random measurement error with:

$$E\{m(i)\} = 0$$
$$E\{m(i)\ m(j)\} = v_m\ \delta_{ij} \qquad (3\text{-}4)$$

In eq. (3-1), each term $a_k x_k(i)$ corresponds to one term of the multiple Taylor series expansions of the set of non-linear functions representing the aerodynamic model. If these functions are analytic and enough terms are included, these Taylor series expansions will be perfect approximations. This may and probably will result, however, in a very large number of terms i.e. a very large value of r in (3-1).

The total number of parameters which can be estimated from a given set of N measurements $y_m(i)$ is usually much smaller than the very large value of r mentioned above. After a discussion of least squares parameter estimates, the procedure for model development and statistical tests in the following subsections, attention is focussed therefore on the estimation of the parameters in simplified models of the form:

$$y(i) = \sum_{k=1}^{r_1} a_k x_k(i) + \varepsilon(i) \qquad (3\text{-}5)$$

in which $r_1 \ll r$. The set of independent variables in (3-5) constitutes a (small) subset of the set of independent variables included in (3-1). Model identification refers to the process which leads to an optimal choice of independent variables in (3-5).

3.1. Estimation of parameters in perfect models

If the model (3-5) is perfect then $r_1 = r$ and the set of independent variables in (3-5) is identical to the set of independent variables in (3-1).

Substitution of (3-1) in (3-3) results in:

$$y_m(i) = \sum_{k=1}^{r} a_k x_k(i) + \varepsilon(i) + m(i) \qquad (3\text{-}6)$$

which can also be written as:

$$y_m(i) = x(i)\ a + \varepsilon(i) + m(i) \qquad (3\text{-}7)$$

where a denotes a column vector $a = \mathrm{col}[a_1, a_2, \ldots, a_r]$ and x(i) a row vector $x(i) = [x_1(i), x_2(i), \ldots, x_r(i)]$. Usually the set of N observations $y_m(i)$ and independent variables x(i) is written in the following compact form:

$$Y_m = X\ a + \varepsilon + m \qquad (3\text{-}8)$$

where $Y_m = \mathrm{col}[y_m(1), y_m(2), \ldots, y_m(N)$, $\varepsilon = \mathrm{col}[\varepsilon(1), \varepsilon(2), \ldots, \varepsilon(N)]$, $m = \mathrm{col}[m(1), m(2), \ldots, m(N)]$ and X denotes a matrix of independent variables $X^T = [x^T(0) \vdots x^T(1) \vdots \ldots \vdots x^T(N)]$.

When the elements of the parameter vector a are given an arbitrary value, a vector of model residuals can be calculated according to:

$$e = Y_m - X\ a \qquad (3\text{-}9)$$

Next, these values are selected such that the sum of the squares of the residuals e(i), i = 1(1) N is minimal. These values are then called the least squares estimate $\hat{a}$ of the parameter vector a:

$$\hat{a}:\ \min_{\hat{a}} \sum_{i=1}^{N} e^2(i) = \min_{\hat{a}} e^T e = \min_{\hat{a}} (Y_m - Xa)^T\ (Y_m - Xa) \qquad (3\text{-}10)$$

The necessary conditions for a minimum to exist are:

$$\frac{\partial}{\partial a}(e^T e)\Big|_{a=\hat{a}} = 0 \qquad (3\text{-}11)$$

Substitution of (3-9) then leads directly to the socalled normal equations:

$$(X^T X)\,\hat{a} = X^T\, Y_m \qquad (3\text{-}12)$$

A unique solution exists if and only if $(X^T X)$ is positive definite, i.e. its inverse exists:

$$\hat{a} = (X^T X)^{-1}\, X^T\, Y_m \qquad (3\text{-}13)$$

With (3-9) the model residuals can be estimated as:

$$\hat{e} = Y_m - X\hat{a} \qquad (3\text{-}14)$$

and an estimate can be calculated of the variance of the model residuals

$$\hat{\sigma}^2 = \hat{e}^T\hat{e}/(N - r) \qquad (3\text{-}15)$$

It is not difficult to show that the parameter estimate $\hat{a}$ is unbiased:

$$E(\hat{a}) = a$$

and that its variance matrix can be written as:

$$V(\hat{a}) = E\{[\hat{a} - E(\hat{a})]\ [\hat{a} - E(\hat{a})]^T\} = \hat{\sigma}^2[X^T X]^{-1} \qquad (3\text{-}16)$$

Now it is assumed that both ε and m are Gaussianly distributed. Then, because $\hat{a}$ is a linear estimate, see (3-13), $\hat{a}$ has also a Gaussian distribution.

3.2. Predicting the output with perfect models

Often, one is not only interested in the estimated parameter vector $\hat{a}$ but even more in the prediction $\hat{z}(j)$ at a given setpoint $x(j)$ which can be calculated with:

$$\hat{z}(j) = x(j)\ \hat{a} \qquad (3\text{-}17)$$

Typical examples are the use of aerodynamic models in real time flight simulation and the comparison of results of dynamic flight test measurements with windtunnel experiments, see section 6.

In (3-1), the physical process was assumed to be stochastic, i.e. $y(j)$ consists of a deterministic component indicated as $z(j)$ and a stochastic component $\varepsilon(j)$:

$$\begin{aligned} y(j) &= z(j) + \varepsilon(j) \\ z(j) &= \sum_{k=1}^{r} a_k x_k(j) = x(j)\ a \end{aligned} \qquad (3\text{-}18)$$

It can be shown that $\hat{z}(j)$ is an unbiased estimate of $z(j)$. The prediction error $\Delta\hat{z}(j)$ is:

$$\Delta\hat{z}(j) = \hat{z}(j) - z(j) = x(j)\ (\hat{a} - a)$$

Consequently $E\{\Delta\hat{z}(j)\} = 0$ because $\hat{a}$ is an unbiased estimate of a. This means that $\hat{z}(j)$ is an unbiased estimate of $z(j)$.

The variance $V\{\hat{z}(j)\}$ of the model prediction is:

$$V\{\hat{z}(j)\} = E\{\Delta\hat{y}(j)^2\} = E\{x(j)\ (\hat{a} - a)\ (\hat{a} - a)^T\ x(j)^T\} =$$

$$= x(j)\ V(\hat{a})\ x^T(j) \qquad (3\text{-}19)$$

in which $V(\hat{a})$ denotes the parameter estimation error variance matrix, see (3-16). The eigenvalues and eigenvectors of this matrix define a one-sigma error concentration ellipsoid of parameter estimation errors in r dimensional space. This is depicted in Fig. 3(A) for the two-dimensional case.

From (3-19) is is clear that the variance of the model prediction does not only depend on the variance matrix of parameter estimation errors but also on the particular choice of x(j). This can be depicted as in Fig. 3(B) for the two-dimensional case. For a constant model prediction variance, (3-19) represents an ellipsoid. The direction of most accurate model predictions e_1 in (B) corresponds to the direction of the smallest parameter estimation errors in (A). Conversely, for an arbitrary direction e_k in the plane of $x_1(j)$, $x_2(j)$ the model prediction accuracy depends not only on the volume of the parameter estimation error ellipsoid but also on its orientation with respect to e_k.

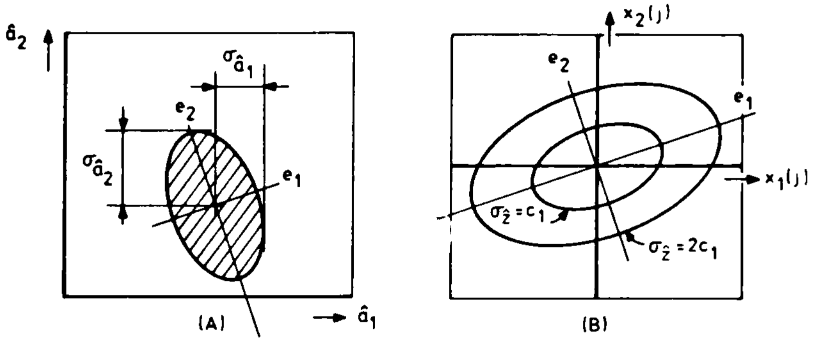

Fig. 3. One-sigma parameter estimation error concentration ellipse (A) and corresponding ellipses of constant one-sigma model prediction error.

3.3. Model development via residual analysis

In practice it is much wiser to start with a relatively simple model containing those terms which are known from experience or from theoretical considerations to be indispensable. Next, by trial and error, one adds those terms which significantly improve the fit of the model to the measurements.

A systematic, and from the computational point of view very efficient way to do this is via analysis of the residuals of a previous model.

After a given number of model extensions, let the model contain r_l parameters. For the N setpoints the model can then be written in vector-matrix form as:

$$Y = X_l\ a_l \qquad (3\text{-}20)$$

in which X_l denotes a $N x r_l$ matrix of independent variables (setpoints) and a_l denotes a parameter vector with r_l elements. The corresponding least squares parameter estimate is indicated as $\hat{a}_l{}^*$ and is equal to:

$$\hat{a}_l{}^* = (X_l{}^T X_l)^{-1}\ X_l{}^T\ Y_m \qquad (3\text{-}21)$$

The corresponding least squares model residuals are:

$$\hat{e}_l = Y_m - X_l\ \hat{a}_l{}^* \qquad (3\text{-}22)$$

From (3-22) it follows that $\hat{e}_l$ is that component of Y_m which is orthogonal to X_l. This is easily proved by showing that:

$$\hat{e}_l{}^T\ X_l = 0 \qquad (3\text{-}23)$$

Next, of a set of candicate variables one is selected to be evaluated with respect to its capability to improve the fit of the model. Let this variable be $x_h(i)$, $i = 1(1)\ N$. A column vector X_2 can then be defined as $X_2 = \text{col}[x_h(1), x_h(2), \ldots, x_h(N)]$.

If one uses X_2 as the independent variable in a model for the least squares residual e_l according to:

$$\hat{e}_l = X_2\ a_2 + e_2 \qquad (3\text{-}24)$$

the corresponding least squares estimate of a_2 is:

$$\hat{a}_2 = (X_2^T X_2)^{-1} X_2^T \hat{e}_1 \qquad (3\text{-}25)$$

and the "new" least squares residuals $\hat{e}_2$ can be written as:

$$\hat{e}_2 = \hat{e}_1 - X_2 \hat{a}_2 \qquad (3\text{-}26)$$

In general, X_2 can always be decomposed into 1) a component which is a linear combination of the columns of X_1 and 2) a component ΔX_2 which is orthogonal to all the columns of X_1:

$$X_2 = X_1 c + \Delta X_2 \qquad (3\text{-}27)$$

in which c denotes a column vector. By substituting (3-27) in (3-25) and using (3-23) it is noticed that when $\Delta X_2 = 0$ then also $a_2 = 0$. Then with (3-26) it follows that $\hat{e}_2^T \hat{e}_2 = \hat{e}_1^T \hat{e}_1$, i.e. there is no improvement in goodness of fit. In general, $a_2 \neq 0$ and $\hat{e}_2^T \hat{e}_2 < \hat{e}_1^T \hat{e}_1$. With (3-26) and (3-25) the following expression may be derived for $\hat{e}_2^T \hat{e}_2$:

$$\hat{e}_2^T \hat{e}_2 = \hat{e}_1^T \hat{e}_1 - \hat{e}_1^T \Delta X_2 (X_2^T X_2)^{-1} \Delta X_2^T \hat{e}_1$$

$$= \hat{e}_1^T \hat{e}_1 - \hat{e}_1^T \Delta X_2 \, (c^T X_1^T X_1 c + \Delta X_2^T \Delta X_2)^{-1} \Delta X_2^T \hat{e}_1 \qquad (3\text{-}28)$$

Eq. (3-28) does make clear why in residual analysis one does not use X_2 but rather its orthogonal component ΔX_2 as independent variable. In that case $e_2^T e_2$ reduces to:

$$\hat{e}_2^T \hat{e}_2 = \hat{e}_1^T \hat{e}_1 - \hat{e}_1^T \Delta X_2 \, (\Delta X_2^T \Delta X_2)^{-1} \Delta X_2^T \hat{e}_1 \qquad (3\text{-}29)$$

resulting in a smaller value because $X_1^T X_1$ is positive definite.

The orthogonal components of candidate variables can be determined according to:

$$\Delta X_2 = X_2 - X_1 c \qquad (3\text{-}30)$$

in which c is calculated as:

$$c = (X_1^T X_1)^{-1} X_1^T X_2 \qquad (3\text{-}31)$$

The model for the least squares residuals e_1 is now written as:

$$\hat{e}_1 = \Delta X_2 \, a_2^* + e_2 \qquad (3\text{-}32)$$

The least squares estimate of a_2^* is:

$$\hat{a}_2^* = (\Delta X_2^T \Delta X_2)^{-1} \Delta X_2^T \hat{e}_1 \qquad (3\text{-}33)$$

The procedure for model development via residual analysis is now to calculate of a given set of candicate variables (stored in the form of column vectors X_2) the orthogonal components with respect to the columns of X_1. Next one of the orthogonal candidates (probably the one which generates the smallest value of $\hat{e}_2^T \hat{e}_2$) is included in the model. In the subsequent step, orthogonal components are calculated with respect to the new (extended) matrix of independent variables which has the form $[X_1 \vdots \Delta X_2]$. This only requires the calculation of orthogonal components with respect to the columns of ΔX_2 since all variables already were orthogonal with respect to the columns of X_1. This procedure is continued untill there exist no longer orthogonal candidate variables which significantly contribute to the goodness of fit of the model.

Model development via residual analysis with orthogonal candidate variables is a classical technique in regression analysis, e.g. see Ref. 2.

3.4. Statistical tests for model development

The addition of new independent variables in the model as discussed above will always result in an improvement of the goodness of fit of the model to the measurements. One measure for the goodness of fit as used in section 6 is the sum of squares of residuals, the "performance index" $J_\ell = \hat{e}_\ell^T \hat{e}_\ell$ where the index ℓ refers to the ℓ-th step in the procedure for model development described above. The goodness of fit may also be expressed in terms of the simple correlation coefficient between Y_m and $\hat{Y}$. This coefficient is usually refered to as the multiple correlation coefficient R_ℓ and can be written as:

$$R_\ell^2 = 1 - \frac{\hat{e}_\ell^T \hat{e}_\ell}{\Delta Y_m^T \, \Delta Y_m} \tag{3-34}$$

in which $\Delta Y_m = \mathrm{col}[y_m(1) - \bar{y},\ y_m(2) - \bar{y},\ y_m(N) - \bar{y}]$, where $\bar{y}$ denotes the mean value of $y_m(i)$, $i = 1(1)N$. Here it is assumed that the mean value of the residuals $e_\ell(i)$, $i = 1(1)\ N$ is equal to zero which is always true if one of the columns of the X_1 matrix of the initial model has non zero but identical elements, e.g. $x_1(i) = 1$, $i = 1(1)\ N$. R_ℓ may take values between 1 (perfect fit) and 0 (no fit).

F ratio tests can be applied to test the statistical significance of each new "orthogonal parameter" estimate $\hat{a}_\ell^*$ (sequential F test) as well as to test the statistical significance of all model parameters simultaneously.

For application of the sequential F test one calculates:

$$F_{seq} = \frac{\hat{e}^T_{\ell-1}\hat{e}_{\ell-1} - \hat{e}_\ell^T \hat{e}_\ell}{\hat{e}_\ell^T \hat{e}_\ell} (N - r_\ell)$$

in which r_ℓ denotes the total number of parameters in the new rodel. F_{seq} can also be written in terms of multiple correlation coefficients according to:

$$F_{seq} = \frac{R_\ell^2 - R_{\ell-1}^2}{1 - R_\ell^2} (N - r_\ell) \tag{3-35}$$

At this stage it is convenient to introduce the partial correlation coefficient R_ℓ^* being the simple correlation coefficient between $\hat{e}_{\ell-1}$ and ΔX_ℓ. The partial correlation coefficient can be written as:

$$R_\ell^{*2} = 1 - \frac{\hat{e}^T_{\ell-1}\hat{e}_{\ell-1}}{\hat{e}^T_\ell \hat{e}_\ell} \tag{3-36}$$

The relation between the multiple correlation coefficients R_ℓ and $R_{\ell-1}$ and the partial correlation coefficient R_ℓ^* is:

$$R_\ell^2 = 1 - (1 - R_{\ell-1}^2)(1 - R_\ell^{*2}) \tag{3-37}$$

Substitution of (3-37) in (3-35) results in:

$$F_{seq} = \frac{R_\ell^{*2}}{1 - R_\ell^{*2}} (N - r_\ell) \tag{3-38}$$

The null hypothesis H_0: $a_\ell^* = 0$ is rejected in favour of the alternative hypothesis H_1: $a_\ell^* \neq 0$ when:

$$F_{seq} > F_\alpha\ (1,\ N - r_\ell) \tag{3-39}$$

in which F_α denotes the value of Fishers distribution function with 1 and $N-r_\ell$ degrees of freedom, $\alpha = \Pr\{H_1 | H_0\}$.

The combination of (3-38) and (3-39) allows to bring the sequential F test in the following form: accept H_1 when:

$$R_\ell^{*2} > \frac{k}{1 + k} \tag{3-40}$$

in which $k = \frac{1}{N - r_\ell} F_\alpha(1,\ N - r_\ell)$. This is depicted in Fig. 4.

For application of the total F test one calculates:

$$F_{tot} = \frac{\hat{e}_0^T \hat{e}_0 - \hat{e}_\ell^T \hat{e}_\ell}{\hat{e}_\ell^T \hat{e}_\ell} \frac{(N - r_\ell)}{(r_\ell - 1)} \tag{3-41}$$

in which e_0 are the residuals of the most simple model with one parameter a_0 and $x_0(i) = 1$, $i = 1(1)\ N$. F_{tot} can also be written as:

$$F_{tot} = \frac{R_\ell^2}{1 - R_\ell^2} \frac{(N - r_\ell)}{(r_\ell - 1)} \tag{3-42}$$

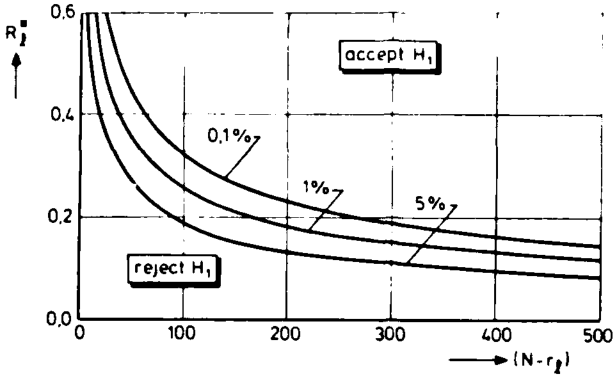

Fig. 4. F-test critical values of the partial correlation coefficient R_ℓ^* for three levels of $\alpha = \Pr\{H_1 | H_0\}$.

The null hypothesis H_0: $a_i = 0$, $i = 1(1)\ r_\ell$ is rejected and the alternative hypothesis H_1 accepted when:

$$F_{tot} > F_\alpha\ (r_\ell - 1,\ N - r_\ell) \tag{3-43}$$

in which F_α denotes the value of Fishers distribution function with r_ℓ-1 and N-r_ℓ degrees of freedom, $\alpha = \Pr\{H_1 | H_0\}$.

Combining (3-42) and (3-43) allows to bring the total F test in the following form: accept H_1 when:

$$R_\ell^2 > \frac{k}{1 + k} \tag{3-44}$$

in which $k = \frac{r_\ell - 1}{N - r_\ell} F_\alpha\ (r_\ell - 1,\ N - r_\ell)$.

For more details on statistical tests the reader is referred again to Ref. 2. The goodness of fit criteria and tests as discussed here are applied in section 6.

3.5. Characteristics of simplified models

Simplified models as considered in the present work are of the following form:

$$z(i) = \sum_{k=1}^{r_1} a_k x_k(i) \tag{3-5}$$

in which $r_1 << r$, see (3-1). No attempt is made here to model the stochastic part of the force and moment coefficients. The set of independent variables contained in (3-5) could result from a model development procedure as described in section 3.3.
With (3-5) the deterministic part of the "exact" model (3-1) can be written as:

$$Z = Xa = X_1 a_1 + X_2 a_2 \tag{3-45}$$

in which a_1 denotes a r_1 parameter vector of the simplified model and a_2 a $(r - r_1)$ vector of parameters not included in the model. It is always possible to write the matrix X_2 as:

$$X_2 = X_1 C + \Delta X_2 \tag{3-46}$$

in which C denotes a constant $r_1 \times (r - r_1)$ matrix. Eq. (3-46) is the multidimensional form of (3-27).

An estimate of the parameter vector in the simplified model $Z = X_1 a_1$ can be calculated with (3-21). Typical for simplified models is that parameter estimates are in principle always biased. This is easily proven by taking the expected value of a_1^* resulting in:

$$E\{\hat{a}_1^*\} = a_1 + Ca_2 \tag{3-47}$$

It is worth noticing here that this parameter estimation bias is not constant but rather depends on the design of the particular experiment, i.e. the structure of X.

Above it was shown that predictions $\hat{z}(j)$ made with perfect models were unbiased. Simplified models are different in this respect. If $x(j)$ is partioned as $x(j) = [x_1(j) \vdots x_2(j)]$ then the prediction error of the simpified model is:

$$\Delta\hat{z}(j) = \hat{z}(j) - z(j) = x_1(j)\,\hat{a}_1^* - x_1(j)\,a_1 - x_2(j)\,a_2 \tag{3-48}$$

The prediction bias is then:

$$E\{\Delta\hat{z}(j)\} = [x_1(j)\,C - x_2(j)]\,a_2 = -\Delta x(j)\,a_2 \tag{3-49}$$

Simplified models which are developed according to the model development procedure of section 3.3. can be expected to result in small values of $\Delta x(i)\,a_2$ for the set points $x(i)$, i.e. the rows of the matrix X of the particular experiment. If not, additional terms would have been included in the model. In general, however, when predictions are calculated for arbitrary set points $x(j)$, the bias of the prediction error estimate may become considerable.

3.6. Predict error function

Experience with the development of aerodynamic models from dynamic flight test measurements is that application of the statistical tests as discussed in section 3.5. often leads to very refined models, i.e. a relatively large number of terms is included in the model.

As mentioned above, this results in a small prediction bias for each of the set points $x(i)$ of the experiment. For arbitrary set points, however, these models often generate very large prediction errors.

It is possible to get an impression of the prediction errors generated by some model if a second data set is available. The model as developed from one data set is used to predict the measurements in the second data set. In the context of maximum likelihood estimation of stability and control derivatives from dynamic response measurements, this idea has been proposed earlier. Here the following "predict function" is used (see section 6):

$$\text{PREDICT} = \sum_{i=1}^{N} V\{\hat{z}_{21}(i)\} + \sum_{i=1}^{N} \{y_{m_2}(i) - \hat{z}_{21}(i)\}^2 \tag{3-50}$$

in which $\hat{z}_{21}(i)$ denotes the estimate of $z(i)$ of the second data set as calculated with the parameter estimates of the first data set. The first term, see (3-19), is added to take into account that the addition of terms to a model in principle always results in an increase of the prediction variance.

4. FLIGHT TESTS

As a joint effort of DFVLR (Deutsche Forschungs- und Versuchsanstalt für Luft- und Raumfahrt), NLR (National Aerospace Laboratory, Amsterdam) and DUT (Delft University of Technology) flight tests were made with the DHC-2 "Beaver" experimental aircraft, see Ref. 3.

In the course of the flight test program more than 80 dynamic longitudinal and lateral-directional dynamic flight test manoeuvers were recorded.

A high accuracy instrumentation system was used. This system, capable of measuring, digitizing and recording 400 measurements per second was a further development of an earlier system used in a Hawker Hunter mk VII dynamic flight test program, Ref. 10.

The main purpose of the flight test program was to validate different design philosophies for optimal elevator, rudder and aileron input signals. Some of the results have been presented in Ref. 9.

All together 5 different types of precalculated test signals were stored on magnetic tape and implemented via a hydraulic control system which was specially designed and constructed for that purpose.

All test signals consisted of a 10 sec elevator signal followed by a 16 sec rudder/aileron signal. Each flight test maneuver was started from a condition of approximately steady horizontal and rectilinear flight. In this stage the aircraft was flown via the hydraulic control system and controlled by the pilot via a three axes side stick and three trim knobs. After completion of the longitudinal maneuver, initiated by starting the tape recorder, the original steady straight flight condition was reestablished by means of the side stick. Finally the lateral-directional maneuver was executed by restarting of the tape recorder.

The reproducibility of the flight maneuvers flown with the hydraulic control system turned out to be very good. Those types of lateral-directional maneuvers involving relatively large roll angle excursions, however, could be reproduced to a somewhat lesser degree because of the need for the pilot to control the pitch axis by means of the side stick in order to prevent too large airspeed and altitude variations.

Of all dynamic maneuvers recorded only three were used to generate the results presented in section 6. These three maneuvers were of the "DUT type" (input signals designed by DUT, see Ref. 9) at a nominal altitude of 6000 ft and nominal true airspeeds (TAS) of 35, 45 and 55 m/sec. More results will be presented in the final report on the flight test program.

After elementary data processing and flight path reconstruction, see section 2, the variables required for aerodynamic model identification were calculated for every 0.1 sec. This results in 101 measurements ($N = 101$) in the longitudinal and 161 measurements ($N = 161$) in the lateral-directional flight test maneuver.

5. WINDTUNNEL EXPERIMENTS

All windtunnel experiments used in the present work were carried out in the Low Speed windTunnel (LST) of the Department of Aerospace Engineering of Delft University of Technology (DUT). Measurements were made with a 1:11 scale model of the DHC-2 "Beaver" experimental aircraft. The model was equiped with a 7.5 DIN-PK engine to simulate powered flight. In the following subsections brief descriptions are given of the DUT-LST, the model and the experimental program respectively.

5.1. DUT-LST

The Low Speed windTunnel of Delft University of Technology is of a conventional recirculating type. The settling chamber is provided with 8 screens, of which the first two act as expansion screens to prevent flow separation in the short wide-angle diffusor at the entry of the settling chamber. This and a high contraction ratio (17.9) ensures a very good flow quality and a low turbulence level in the test section. A specially developed speed control system for the drive prevents fluctuations of the tunnel speeds with time.

The test section is of octagonal cross section, 1.80 m wide, 1.25 m high and 2.60 m long. A system of interchangeable test sections has been developed. Exchanging the test section under test for another takes little more than 15 minutes. Turntables of 1.15 m diameter are fitted in the upper and lower walls. The maximum airspeed in the test section is 120 m/sec, corresponding to a unit Reynolds number of $8.4 * 10^6$ per m.

As mentioned above, the flow quality in the test section is very good. Over an area of 0.4 the height and 0.8 the width of the test cross section, the dynamic pressure differs less than ± 0.2% from the dynamic pressure measured in the centre. The deviations of the flow direction from a horizontal plane, measured in the area corresponding to the normal position of an aircraft model, are within ± 0.1 degrees. The longitudinal component of the turbulence ranges from 0.025% at 40 m/sec to 0.085% at 100 m/sec.

The tunnel is equiped with a six-component balance (platform type) with automatic weightbeams of high accuracy. Measurement errors are smaller than 0.005 N.

A HP-1000 computer is used for data acquisition and reduction. Measurements are stored in a core memory but can also be printed or plotted on-line.

5.2. The DHC-2 "Beaver" scale model

Structural components of the 1:11 scale model of the DHC-2 "Beaver" are shown in Fig. 5.

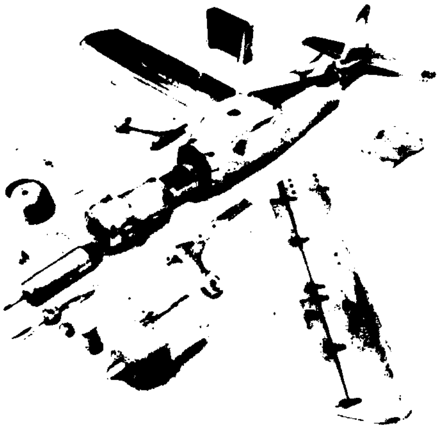

Fig. 5. Stuctural components of the DHC-2 "Beaver" 1:11 scale model.

The wing flaps, ailerons, rudder, horizontal and vertical tail planes are all adjustable. The landing gear, wing struts, air intakes as well as the horizontal and vertical tailplanes can be removed from the model. The model is equiped with a three phase induction engine of 7.5 DIN-PK driving a two-blade adjustable pitch propeller. In correspondence with the real aircraft, two interconnected total-head tubes are positioned on both sides of the NACA cowling at 0.75 R from the propeller axis and 0.16 R behind the propeller disc, R denoting the propeller radius. The NACA cowling is not vented. Small protuberances, such as the antennae, external measuring probes, the tail wheel, door steps etc. are omitted because of the expected large scale effects at low Reynolds numbers. Roughness strips have been attached to the wing and the horizontal and vertical tailplanes to prevent laminar separation of the boundary layer.

5.3. Experimental conditions

All measurements were carried out at 50 m/sec resulting in a Reynolds number of $0.47 * 10^6$. In the tunnel,

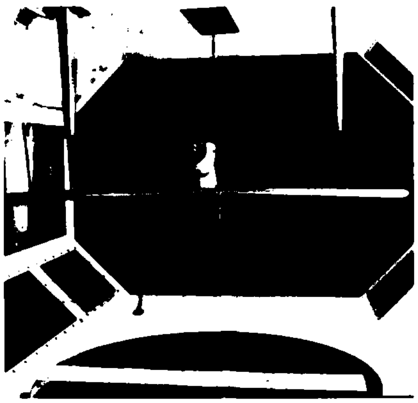

Fig. 6. Experimental configuration in the LST of Delft University of Technology.

the model is positioned upside down on a three point ceiling support system, Fig. 6. Because their effects turned out to be highly Reynolds number sensitive at this low Reynolds number, all measurements were made after removal of wing struts and landing gear. The contributions of the wing struts and landing gear were determined in separate measurements at a higher Reynolds number of $1 * 10^6$. At the relatively high airspeed corresponding to this Reynolds number representative values of $\Delta p_t/q$ cannot be attained and therefore, during these measurements, the propeller was removed from the model. These contributions were added to the results obtained at the low Reynolds number.

Tunnel wall corrections were calculated for the longitudinal aerodynamic force and moment coefficients C_X, C_Z and C_m. Application here of "classical" and "modern" (Joppa, Heyson) methods yielded approximately identical results. The lateral-directional force and moment coefficients C_Y, C_ℓ and C_n were left uncorrected for the influence of the tunnelwall. These corrections were expected to be very small because sideslip angles were kept in a relatively small range from -8 to +8 degrees.

The support system mentioned above consists of two wing struts and one tail strut. For the asymmetrical measurements, i.e. non zero sideslip angle, these struts could be made much less well streamlined compared to the struts used for the symmetrical measurements. The effect of the struts on the force and moment coefficients was considerable, in particular in the asymmetrical measurements. To determine these effects for different experimental conditions, separate measurements were made during which the model was supported by temporary struts and the original struts were replaced by dummies which could also be removed. A pitfall, which was avoided later by repositioning of the temporary struts, showed up here in the form of a non-negligible interference effect between the temporary and the dummy struts.

With the total head probes behind the propellor disc, it is possible to determine the dimensionless increase in total head $\Delta p_t/q$, $q = \frac{1}{2}\rho V^2$. This is also done in flight. In Ref 1 it is shown that $\Delta p_t/q$ is closely related to T_c, the thrust coefficient. If the dependence of the aerodynamic force and moment coefficients on variations of the rotation in the propeller slipstream is small enough as to be neglected then $\Delta p_t/q$ is left as the only parameter which determines the effect of the slipstream on the flow field around the model in the windtunnel as well as around the aircraft in flight.

In the windtunnel measurement program, the angle of attack α, the sideslip angle β, $\Delta p_t/q$, the elevator, rudder and aileron deflections δ_e, δ_r and δ_a were systematically varied to determine their effects on the aerodynamic force and moment coefficients. Some of the results are presented in Fig. 2. These results are compared with corresponding results from dynamic flight tests in section 6.

6. EXPERIMENTAL RESULTS

The windtunnel experiments were designed to systematically evaluate the influence of the angle of attack, the sideslip angle and the dimensionless increase in total-head across the propeller disc on the aerodynamic force and moment coefficients. Some of the results are shown in Fig. 2. The reason that these results are so clarifying lies in the possibility to vary each variable while keeping the remaining ones at constant values.

In a dynamic flight test maneuver, all variables of interest vary simultaneously in a way which, for a given initial flight condition, depends entirely on the time histories of the control surface deflections. To illustrate this, the relations $\Delta p_t/\frac{1}{2}\rho V^2-\alpha$ and $\beta - \alpha$ for typical longitudinal and lateral-directional flight test maneuvers are shown in Fig. 7.

In order to be able to compare the results of dynamic flight test maneuvers with windtunnel experiments mathematical models for the aerodynamic force and moment coefficients must be developed first. This is done in section 6.1. Thereafter it is possible to calculate functional relationships in a form equivalent to Fig. 2, and to compare these with corresponding windtunnel measurements. This comparison is made in section 6.2.

6.1. Development of aerodynamic models

Fig. 2 indicates that the "lateral-directional variable" β does have a (although minor) effect on the longitudinal force and moment coefficients C_X, C_Z and C_m. On the other hand the "longitudinal variable" $\Delta p_t/\frac{1}{2}\rho V^2$ affects the lateral-directional force and moment coefficients C_Y, C_ℓ and C_n. In order to take

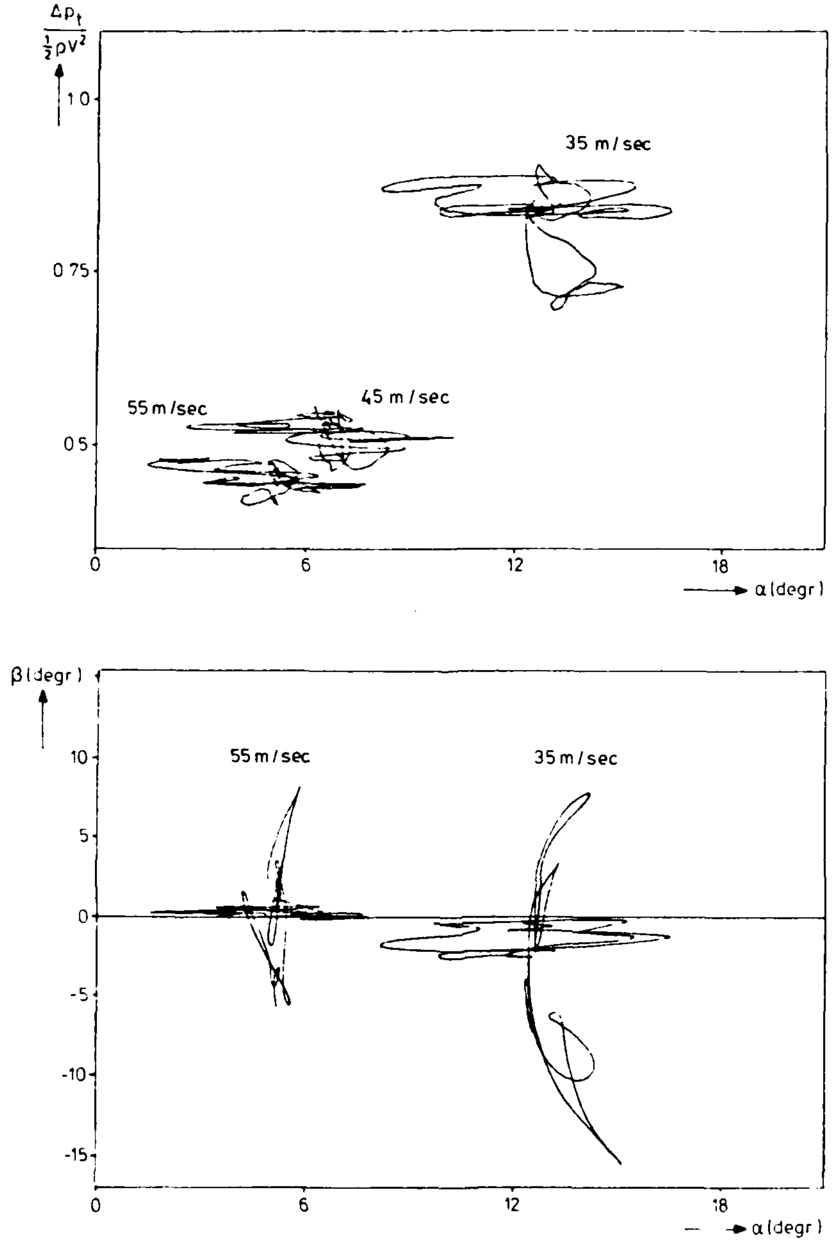

Fig. 7. Plots of $\Delta p_t/\frac{1}{2}\rho V^2$ and β versus α for dynamic flight test maneuvers a 35, 45 and 55 m/sec TAS.

these effects into account in the model development procedure the measurements of the longitudinal and the lateral-directional maneuvers must be combined. Furthermore, Fig. 7 shows that when the measurements of maneuvers at 35, 45 and 55 m/sec TAS are joined, the total range of $\Delta p_t/\frac{1}{2}\rho V^2$ and angle of attack α variations is in better agreement to the windtunnel experiments. This means that one dataset is formed consisting of 3 * 101 + 3 * 161 = 786 set points. Prior to this, differences in center of gravity locations must be corrected for.

The model development procedure starts by assuming initial models which include variables known to be non negligible. The variables in the initial models assumed here are shown in Table 1. Next, according to Section 3, a set of candidate variables must be postulated. In general, this may not be an easy task. Fig. 2 shows that the aerodynamic coefficients are in fact non linear functions of $\Delta p_t/\frac{1}{2}\rho V^2$, α and β.Following section 2, this leads to candidate variables of the form $(\Delta p_t/\frac{1}{2}\rho V^2)^i \alpha^j \beta^k$. All terms up to the third order were included in the set of candidate variables. Also included were the control surface deflections δ_e, δ_r and δ_a and their products with first and second powers of $\Delta p_t/\frac{1}{2}\rho V^2$, α and β. The possible importance of these latter variables could be deduced from windtunnel experiments not shown here. The set of candidate variables was completed by adding the body rotation rates pb/2V, $q\bar{c}/V$ and rb/2V and the time derivatives $\dot{\alpha}\bar{c}/V$ and $\dot{\beta}b/V$. This resulted in a total number of 40 candidate variables.

The above clearly illustrates that the selection of candidate variables is somewhat arbitrary, even if supported by results from windtunnel experiments as in the present case.

Two typical examples of the variation of the criteria for model development i.e. the performance index $\hat{e}_\ell^T\hat{e}_\ell$, the total F value, the partial correlation coefficient and the predict function with the number of terms added to the initial model are shown in Fig. 8. Except for the predict function, similar curves have been published in Ref. 5.

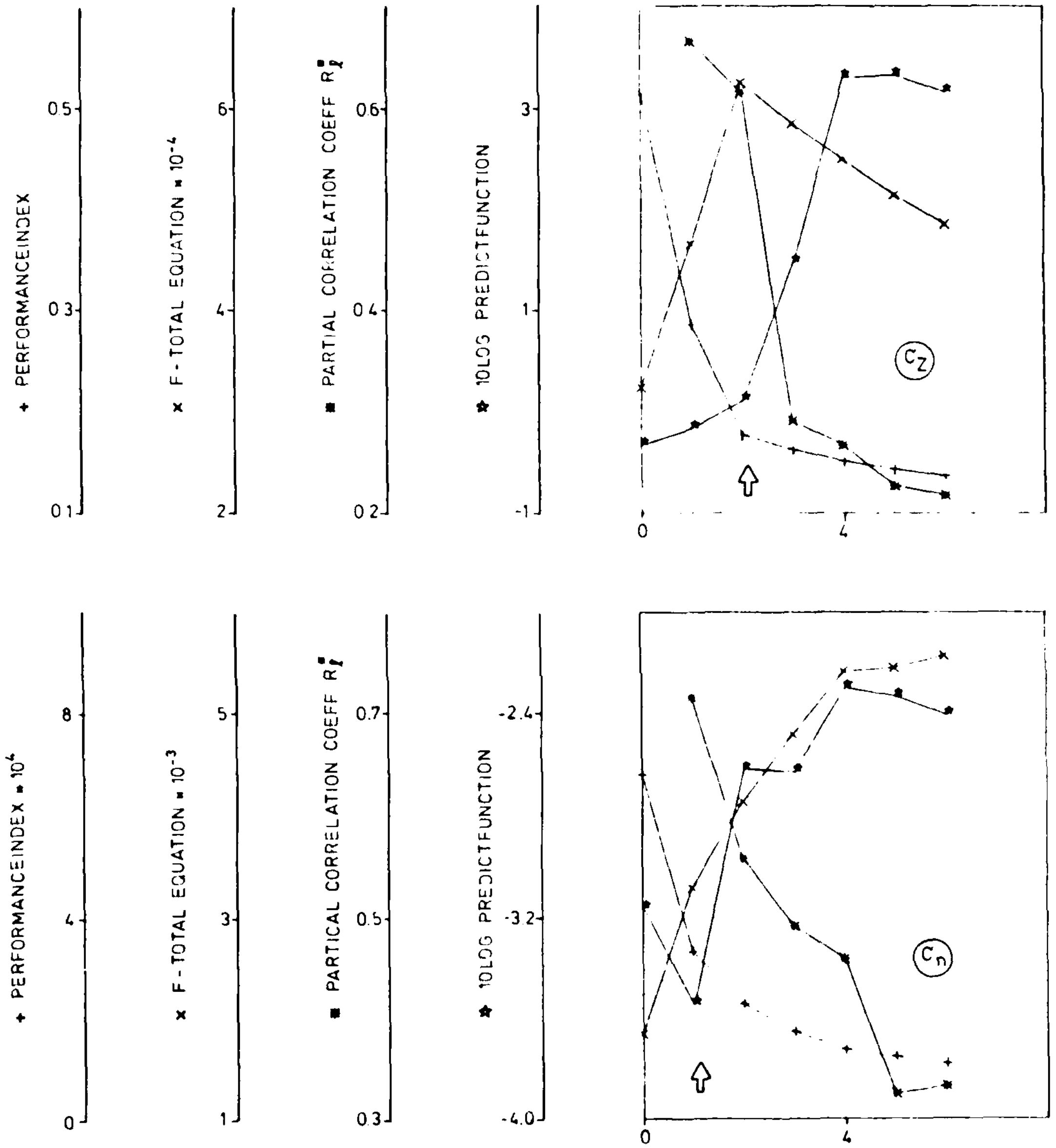

Fig. 8. Criteria for model development as a function of the number of terms added to initial models of C_Z and C_n, see also Table 2.

In these two examples, both the total (F_{tot}) as the sequential (R_ℓ^*) F tests don't reject the addition of even 6 extra terms. The predict function, however, is shown to be a much more critical criterion in this respect. Here a large increase indicates that no more than only one and two terms resp. should be added to the initial model.

Selected candidate variables and corresponding improvements of the goodness of fit are for all models shown in Table 2. With respect to goodness of fit, considerable differences exist between in particular models of aerodynamic force coefficients and models of aerodynamic moment coefficients. Rather good models could be developed for C_Y and C_Z. The fit of the models of C_n and in particular C_ℓ, however is rather poor. These results are of course not general but depend strongly on the particular type of aircraft used for the present series of flight tests. The selection of candidate variables on the basis of the partial

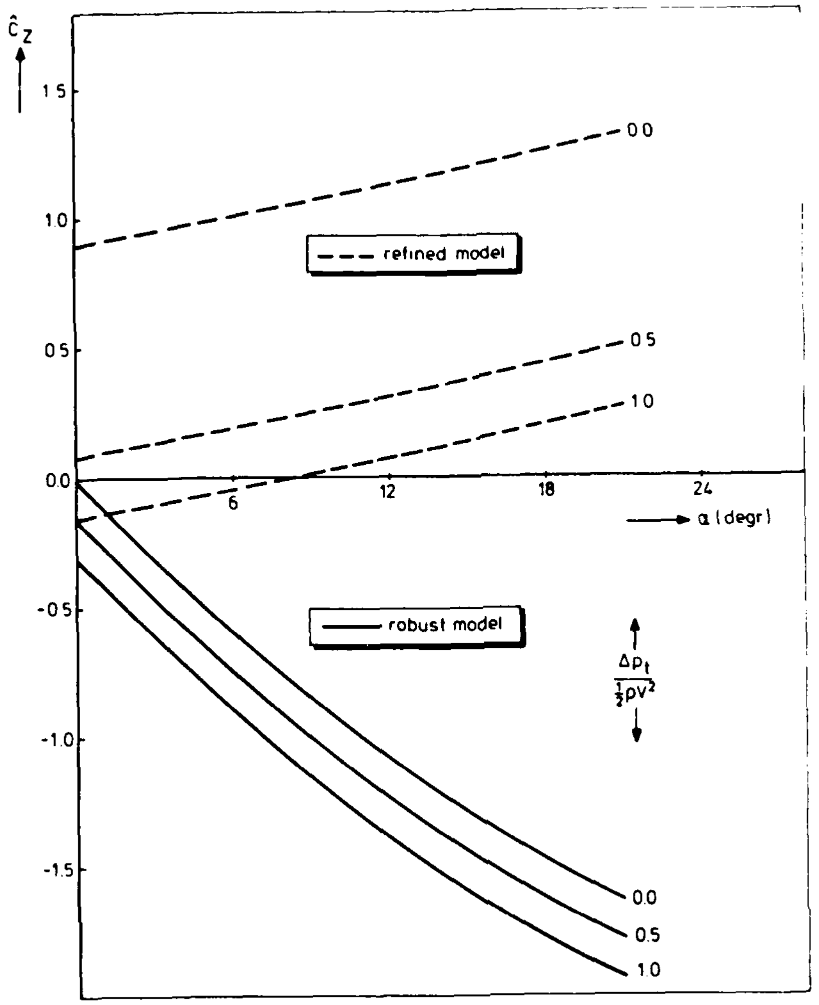

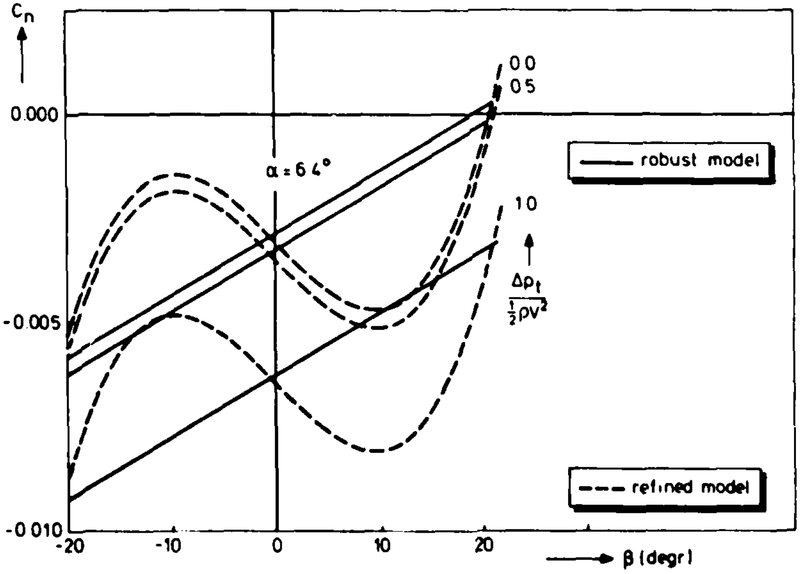

Fig. 9. Comparison of model predictions made with robust models based on the predict function criterion and refined models with 3 and 4 additional terms respectively, see Table 2.

correlation coefficient R_ℓ^* may result in models which, from the physical point of view, appear to be wrong. A typical example of this is the selection of rb/2V in the model of C_X. This is a consequence of using R_ℓ^* for the selection of candidate variables. With respect to prediction it could be better to select candidate variables on the basis of the predict function.

6.2. Comparison with windtunnel experiments

Once models have been developed for the aerodynamic force and moment coefficients it is possible to calculate curves similar to Fig. 2. The correspondence between these model predictions and the windtunnel experiments depends strongly on the number of variables added in the course of the model development procedure. To illustrate this, model predictions were calculated with "refined" and "robust" models of C_Z and of C_n, see Fig. 9.

Fig. 10 compares the predictions of the aerodynamic models as selected on the basis of the predict function, see Table 2, with the corresponding windtunnel results.

In this comparison it should be kept in mind that the windtunnel experiments were performed at a relatively low Reynolds number. So, substantial extrapolation errors may be present in the results.

In view of this a reasonable correspondence exists between the model predictions and the windtunnel results.

The most significant difference is that with respect to the results of the windtunnel, the model predictions overestimate the effect of the slipstream on C_Z and in the case of C_m predict this effect with even the wrong sign.

This may be an indication that the variable $\Delta p_t/\frac{1}{2}\rho V^2$ should have been left out of the initial models of C_Z and C_m.

If not a comparison with windtunnel experiments but rather the development of a as robust a model as possible is the aim of model identification then it is possible to join the flight test and windtunnel measurements in one data base. In this way it is possible to separate the effects of variables which could not have been separated if flight test measurements alone were used. In terms of covariance matrices of parameter estimation errors, see section 3, this means that the simple correlation coefficients of the corresponding parameters estimates decrease.

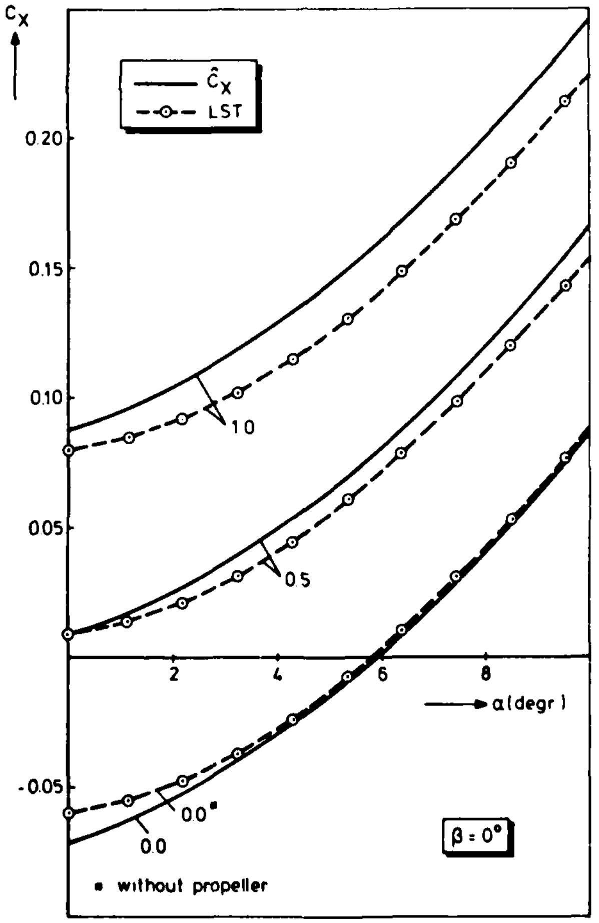

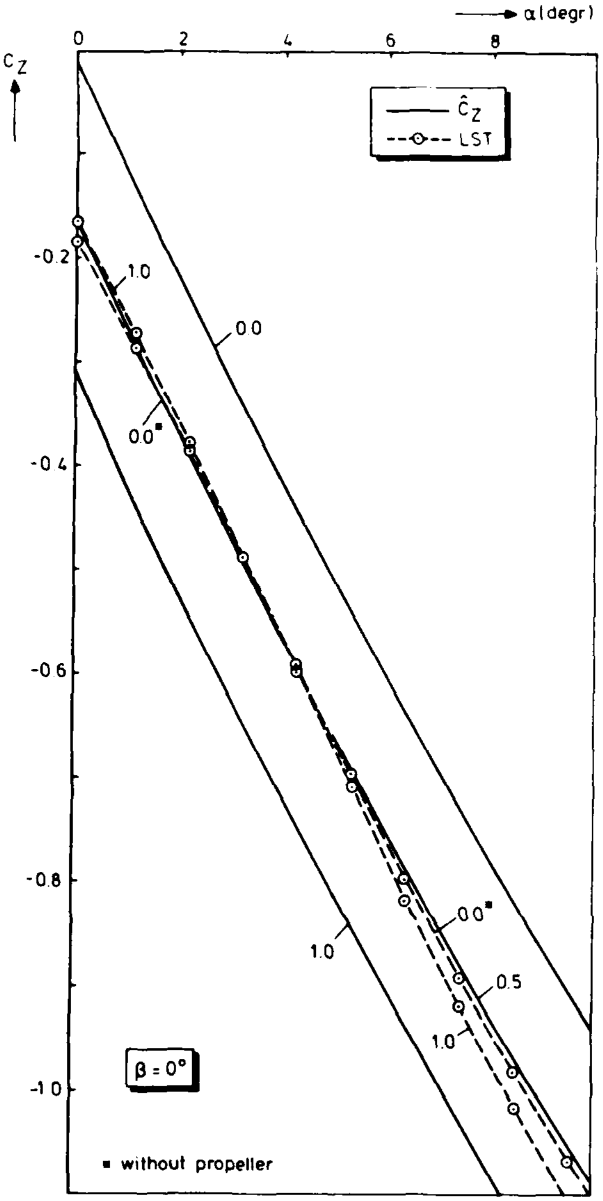
α (degr)
0
2
4
6
8
c_Z
-0.2
-0.4
-0.6
-0.8
-1.0
Ĉ_Z
LST
1.0
0.0
0.0*
1.0
0.0*
0.5
1.0
β = 0°
* without propeller

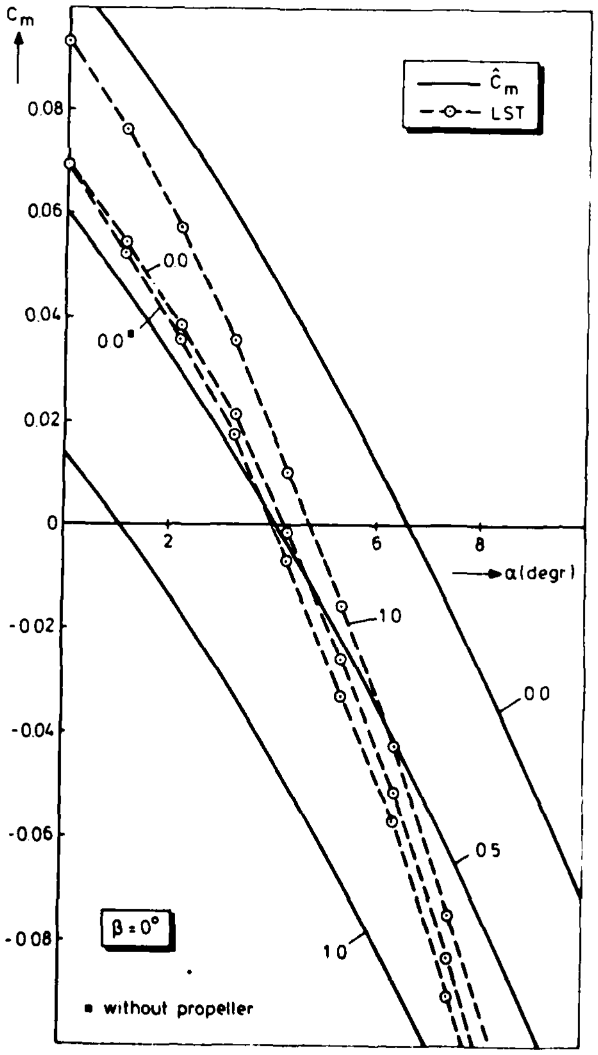
c_m
0.08
0.06
0.04
0.02
0
-0.02
-0.04
-0.06
-0.08
2
4
6
8
α (degr)
Ĉ_m
LST
0.0
0.0*
1.0
0.0
0.5
1.0
β = 0°
* without propeller

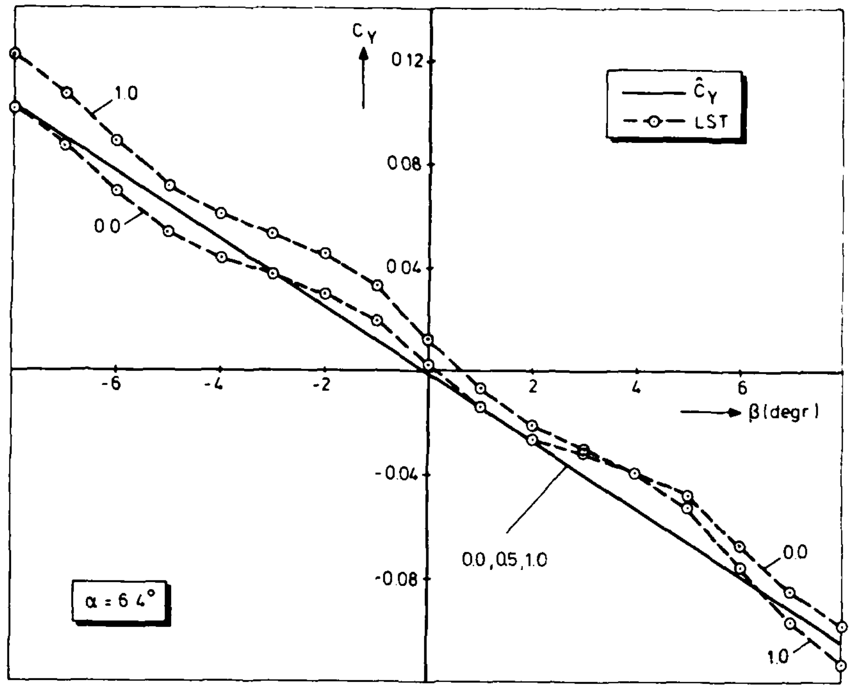

C_Y
0.12
0.08
0.04
-0.04
-0.08
-6
-4
-2
2
4
6
β (degr)
$\hat{C}_Y$
LST
1.0
0.0
0.0, 0.5, 1.0
0.0
1.0
α = 64°

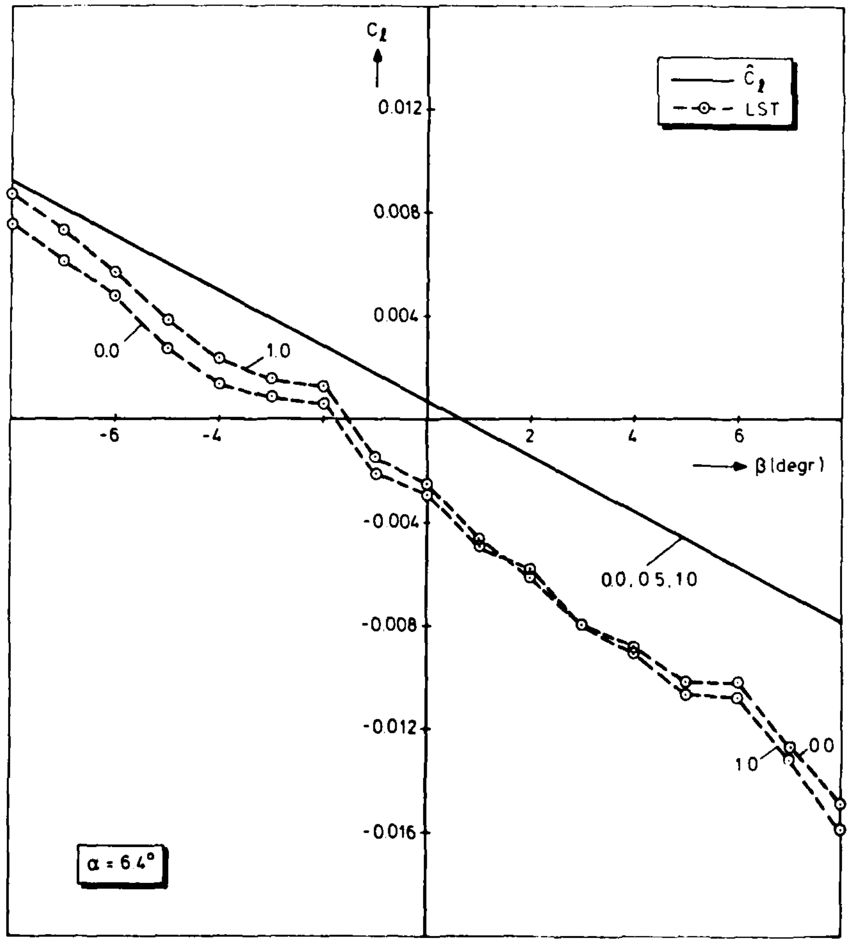

C_l
0.012
0.008
0.004
-0.004
-0.008
-0.012
-0.016
-6
-4
2
4
6
β (degr)
$\hat{C}_l$
LST
0.0
1.0
0.0, 0.5, 1.0
1.0
0.0
α = 64°

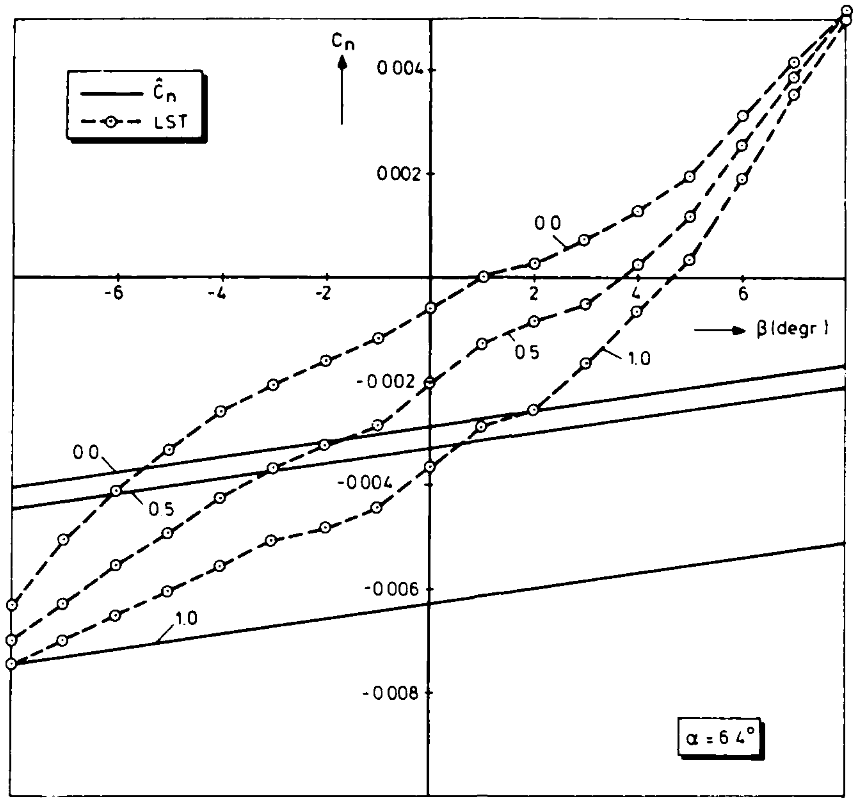

Fig. 10. Comparison of robust model predictions with corresponding windtunnel results for 3 values of $\Delta p_t/\frac{1}{2}\rho V^2$ Of 0.0, 0.5 and 1.0.

7. CONCLUSIONS

Dynamic flight test measurements can be analyzed in two steps. In the first step the flight path is reconstructed and a data base is formed for the second step in which aerodynamic models are identified. In aerodynamic model identification selections are made from a set of candidate variables for the development of models which on the one hand result in an adequate fit to the measurements but on the other hand result in statistically significant parameter estimates and good model predictions. Statistically significant models may be too refined for good model predictions. When a second set of measurements is available the predict function is a better criterion in this respect.

Comparison of the results of dynamic flight tests with windtunnel experiments depends on the development of models for the aerodynamic force and moment coefficients. In view of the relatively low Reynolds number of the windtunnel experiments a reasonable correspondence existed between the results of dynamic flight tests (model predictions) and the results of windtunnel experiments.

8. REFERENCES

1. J.J. Broek, "The use of the total-head rise across the propeller of the De Havilland Canada DHC-2 Beaver as a similarity parameter to simulate power-on flight in the windtunnel", Report VTH-190, Delft University of Technology, Department of Aerospace Engineering, Delft, The Netherlands, June 1976.

2. N.R. Draper, H. Smith, "Applied regression analysis", John Wiley & Sons, Inc., New York, 1966.

3. H.C. Garretson, III, "Beaver aircraft parameter identification - technical preparations and preliminary results", Deutsche Forschungs- und Versuchsanstalt für Luft- und Raumfahrt, DFVLR-Mitt. 78-01, 1978.

4. H.L. Jonkers, J.A. Mulder, J.J. Horsten, "Introduction to state reconstruction of dynamic flight test manoeuvres", in C.T. Leondes: "Control and dynamic systems", Volume XIX, Academic Press, 1982.

5. V. Klein, J.G. Batterson, P.C. Murphy, "Determination of airplane model structure from flight data by using modified stepwise regression", NASA Technical Paper 1916, October 1981.

6. J.A. Mulder, "Estimation of the aircraft state in non-steady flight", AGARD conference proceedings No. 172 on "Methods for aircraft state and parameter identification", Hampton, Virginia, November 1974.

7. J.A. Mulder, J.G. den Hollander, "Status of dynamic flight test technology - model identification for flight simulation", SAE paper No. 810597, April 1981, also published in the 1981 Transactions of the

SAE, September 1982.

8. J.A. Mulder, J.M. van Sliedregt, "Estimation of drag and thrust of jet-propelled aircraft by non-steady flight test manoeuvres", AGARD conference proceedings No. 223 on "Flight Test Techniques", Porz Wahn, West Germany, October 1976.

9. E. Plaetschke, J.A. Mulder, J.H. Breeman, "Flight test results of 5 input signals for aircraft parameter identification", Proceedings 6th IFAC symposium on "Identification and System Parameter Estimation", Washington DC, USA, 1982.

10. K. van Woerkom, "Design and evaluation of an instrumentation system for measurements in non-steady symmetrical flight conditions with the Hawker Hunter mk VII", Report LR-308, Delft University of Technology, Department of Aerospace Engineering, The Netherlands, January 1981.

ACKNOWLEDGEMENT

The authors wish to acknowledge the contribution of former student A.J. Blok who carried out all computations.

C_X	1	$\frac{\Delta p_t}{\frac{1}{2}\rho V^2}$	α	α^2	$\frac{q\bar{c}}{V}$	
C_Z	1	$\frac{\Delta p_t}{\frac{1}{2}\rho V^2}$	α		$\frac{q\bar{c}}{V}$	δ_e
C_m	1	$\frac{\Delta p_t}{\frac{1}{2}\rho V^2}$	α	α^2	$\frac{q\bar{c}}{V}$	δ_e
C_Y	1	β	$\frac{pb}{2V}$	$\frac{rb}{2V}$	δ_a	δ_r
C_ℓ	1	β	$\frac{pb}{2V}$	$\frac{rb}{2V}$	δ_a	δ_r
C_n	1	β	$\frac{pb}{2V}$	$\frac{rb}{2V}$	δ_a	δ_r

Table 1. Variables included in the initial models of the longitudinal and lateral-directional aerodynamic force and moment coefficients.

		R_ℓ	$\sqrt{1 - R_\ell^2}$ (%)	sel. var.
C_X		0.999415	3.41	
	1*	0.999533	3.05	$rb/2V$
	2	0.999552	2.99	$\delta_r(\Delta p_t/\frac{1}{2}\rho V^2)$
	3	0.999567	2.94	$\dot{\alpha}\bar{c}/V$
	4	0.999601	2.82	β^2
	5	0.999699	2.45	$\beta^2(\Delta p_t/\frac{1}{2}\rho V^2)$
	6	0.999712	2.39	β
C_Z		0.996999	7.74	
	1	0.998327	5.78	α^2
	2*	0.998961	4.55	$\beta^2(\Delta p_t/\frac{1}{2}\rho V^2)$
	3	0.999049	4.35	$(\Delta p_t/\frac{1}{2}\rho V^2)^2$
	4	0.999117	4.20	$(\Delta p_t/\frac{1}{2}\rho V^2)^3$
	5	0.999162	4.09	β^2
	6	0.999202	3.99	$\dot{\alpha}\bar{c}/V$
C_m		0.986308	16.49	
	1	0.991233	13.21	β^2
	2*	0.993302	11.55	$rb/2V$
	3	0.994284	10.67	β^3
	4	0.995078	9.90	β
	5	0.995479	9.49	$\beta^2(\Delta p_t/\frac{1}{2}\rho V^2)$
	6	0.995857	9.09	$\delta_e(\Delta p_t/\frac{1}{2}\rho V^2)$
C_Y		0.996551	8.29	
	1	0.997119	7.58	$\dot{\beta}b/V$
	2*	0.997571	6.96	$\delta_r\alpha$
	3	0.997740	6.71	$q\bar{c}/V$
	4	0.997895	6.48	$\dot{\alpha}\bar{c}/V$
	5	0.997993	6.33	β^2
	6	0.998323	5.78	$\delta_e\beta^2$
C_ℓ		0.954197	29.91	
	1	0.959872	28.04	α^3
	2*	0.964516	26.40	$\dot{\beta}b/V$
	3	0.967861	25.14	$\delta_a\alpha$
	4	0.969724	24.42	$(\Delta p_t/\frac{1}{2}\rho V^2)$
	5	0.972087	23.46	$\delta_r\beta^2$
	6	0.973925	22.68	$\beta(\Delta p_t/\frac{1}{2}\rho V^2)$
C_n		0.960266	27.90	
	1*	0.980841	19.48	$(\Delta p_t/\frac{1}{2}\rho V^2)^3$
	2	0.986839	16.17	$q\bar{c}/V$
	3	0.990024	14.08	β^3
	4	0.992129	12.52	$\delta_r(\Delta p_t/\frac{1}{2}\rho V^2)$
	5	0.992961	11.84	$\dot{\beta}b/V$
	6	0.993742	11.16	$(\Delta p_t/\frac{1}{2}\rho V^2)$

Table 2. Statistically significant steps in the development of models of the aerodynamic force and moment coefficients. Model development is based on the data of three longitudinal-lateral/directional dynamic flight test maneuvers at nominal true airspeeds of 35, 45 and 55 m/sec, 6000 ft pressure altitude. Asterix indicates the models as selected by the predict function criterion.

HELICOPTER SIMULATION VALIDATION USING FLIGHT DATA

David L. Key
Chief, Flight Control Division

and

Raymond S. Hansen
Aerospace Engineer
Aeromechanics Laboratory
U.S. Army Research and Technology Laboratories (AVRADCOM)

William B. Cleveland
Aerospace Engineer
National Aeronautics and Space Administration
Ames Research Center
Moffett Field, California 94035, U.S.A.

William Y. Abbott
Flight Test Engineer
U.S. Army Aviation Engineering Flight Activity
Edwards Air Force Base, California 93523, U.S.A.

SUMMARY

The paper describes a joint Army/NASA effort to perform a systematic ground-based piloted simulator validation exercise. The subject aircraft is the Army/Sikorsky UH-60A Black Hawk helicopter. The Black Hawk has recently entered service with the U.S. Army, and it is expected that many new roles and missions will evolve that require investigations of flying qualities with simulators. The helicopter has features such as elastomeric main rotor bearings, canted tail rotor, and variable incidence stabilator, all of which provide a challenge in testing, modeling, and verification.

The first step in the procedure was to obtain the best available Black Hawk math model that could be run real-time on the available simulation computer, the CDC 7600. The model is a total force, nonlinear, large angle representation; the rotor description includes rigid blade flapping, lagging, and rotational degrees of freedom. This math model has been programmed for real-time operation and will be checked against the nonreal-time version.

Flight test data were obtained to provide a basis for verifying and improving the math model. Update will be a two-step procedure: first by using engineering judgment based on a knowledge of the model generation assumptions, second by applying state estimation and parameter identification techniques.

The flight tests were performed by the Army Aviation Engineering Flight Activity (AEFA) in response to guidelines from the Aeromechanics Laboratory (AL). Since it is desired to perform analysis with parameter identification techniques, the requirements for instrumentation and calibration were extremely stringent. The tests included extensive trim and static stability points, and special system identification maneuvers as well as steps, doublets, pulses, roll reversals, pull-up and pushovers. Data on pilot performance and control activity were also recorded while performing specially defined mission-type tasks. These will be used in the simulation validation part of the exercise.

Once the math model has been shown to be an accurate representation of the UH-60A, it will be combined with NASA Ames ground-based simulator facilities. The motion base will be the VMS, and the visual system will be a four-window system using computer generated imagery (CGI). Tasks will be "flown" on the ground simulator and pilot subjective data and objective measures will be made to determine and improve the validity of the simulation.

Status of the effort is that the flight tests are complete and the math model has been developed and programmed. Efforts at updating the math model and developing the analytical techniques for assessing the simulator validity/fidelity have been initiated. The simulation portion is scheduled for early 1983.

1. INTRODUCTION

A fundamental problem in the use of simulation for aircraft development is that the pilot is required to assess an unknown aircraft. In developing this assessment, he is bound to be influenced by the quality of the simulator itself. Bray (Ref. 1) points out that a sense of realism or subjective fidelity in the simulation flight task is essential and, depending on the research task, some moderate-to-high level of objective or engineering similarity to the flight task is required to obtain this realism. There is no fundamental obstacle to obtaining high objective fidelity in aircraft simulation except in the reproduction of the visual and motion cues. At best, only a small portion of the cues present in an aircraft can be presented, and even this comes at an extremely high cost.

In the application of simulators to pilot training, the large number of facilities involved, and the tendency to maximize the realism of cues available, has led to several studies to determine just how much fidelity is required to train (Refs. 2 and 3). In the use of simulators for handling qualities research, there is a need to understand how the reduced cues influence the research results, or conversely, to define the limitations on use that the limited cues impose for obtaining valid results. The purpose of this paper is to describe a joint Army/NASA program that is making a systematic effort to address this problem.

Rotorcraft pose a particularly difficult problem for simulation technology. The mathematical model required is exceedingly complex so that it takes very large computer capacity to produce real-time solutions for man-in-the-loop simulation. Helicopter mathematical models are also very difficult to verify. The flight characteristics of helicopters tend to have low levels of stability, or be unstable, and there are large interaxis couplings; these are the characteristics which make deprivation in visual and motion cues most critical. Flight phases of particular concern to the Army involve rapid maneuvering flight at very low speed and altitude (Nap-of-the-Earth (NOE) flight). Representing this situation requires wide field-of-view and high detail, which are conflicting requirements that are very difficult to satisfy.

The helicopter chosen as a basis for this research effort is the Sikorsky UH-60A Black Hawk (Fig. 1). This is a modern-technology helicopter that can be expected to be in service with the Army (and probably also the Navy and Air Force) into the next century. It will doubtless have many modifications to satisfy new roles and to incorporate new technology. In addition, the UH-60A Black Hawk is the base helicopter for an Army Research and Development program to demonstrate modern digital flight control technology using fiberoptic components, the Advanced Digital Optical Control System (ADOCS) program. A major part of the ADOCS program involves the development and demonstration of good handling qualities through a range of day and night NOE flight phases, and generation of the appropriate control laws depends to a large extent on adequate simulation of the vehicle. Thus, in addition to the basic techniques and technology that are developed for simulation validation to be applied in general, a validated UH-60A simulation will be a useful end product of this program.

The body of the paper is divided into three main sections. The first discusses in more detail what is meant by the concept of simulator validity and the associated concept of fidelity. The second section describes the process being used to develop and validate the Black Hawk math model, and the final section discusses the approach for assessing the validity of the overall total piloted simulation.

2. SIMULATION FIDELITY

Much has been written on the subject of simulator fidelity. Defining the term has been found to be difficult; defining how much fidelity is required for a valid simulation is not currently possible.

An AGARD Working Group, AMP/FMP WG-10, was formed to address the question of how much fidelity is required for pilot training (Ref. 2). The group did not provide an answer to this question but did help clarify the concept and definition of fidelity. In that report, two types of fidelity were defined:

> "Objective fidelity (which provides an engineering viewpoint) is the degree to which a simulator would reproduce its real-life in-flight counterpart aircraft, if its form, substance, and behavior were sensed and recorded by an instrumentation system on the simulator.
>
> "Perceptual fidelity (which provides a psychological/physiological viewpoint) is the degree to which the pilot subjectively perceives the simulator to reproduce its real-life counterpart aircraft, in flight, in the operational task situation."

The point is that a distinction is being made between the real cues, which can be measured objectively, and the cues which the pilot subjectively experiences. In selected areas of equipment cues, such as cockpit instrumentation, control panel, and control system operation, the level of objective fidelity can be easily ascertained. In areas of environmental cues, such as visual scenes or motion cueing, extensive data concerning human physiology and cue perception are required. Unfortunately, the knowledge of human physiology is insufficient to determine how much objective fidelity is required to achieve a given level of perceptual fidelity.

Another aspect of fidelity has been hypothesized (Ref. 3). This is to judge the adequacy of perceptual effects by the pilot response behavior (i.e., control strategy and technique) induced by the simulator. The rationale is that if the simulator cannot induce correct technique, then presumably the fidelity is inadequate. With this concept in mind, Ref. 3 defines a concept of fidelity which is:

> "The degree to which characteristics of perceivable states induce correct psychomotor and cognitive control strategy for a given task and environment.
>
> "Correct strategy is defined in the task environment; applicable states are chosen on the basis of the specified loop structure essential for performing a task; and characteristics of the states are determined by their role in inducing correct control techniques (i.e., quantification of the loop structure adjustments)."

With this definition, then, a validated simulation could be defined as one in which the characteristics of perceivable states induce correct psychomotor and cognitive control strategy for the given task and environment. It is this concept which is being applied in the current validation effort.

3. MATH MODEL VALIDATION

The first step in the overall simulation validation procedure is development of a math model that adequately reproduces the dynamics of the flight vehicle. The approach being taken is to compare flight data with the math model output so that any discrepancies between them can be identified, and then to upgrade the math model. Two basic approaches will be used to update the math model. First, based on engineering insight, and second, by using the parameter identification techniques. This section will outline the form of the math model and the scope and nature of the flight tests, will indicate some of the correlations obtained, and will discuss the transfer of the model from a nonreal-time to a real-time operating system.

3.1 Black Hawk Math Model

The math model to be used as a basis for the real-time simulation was procured from Sikorsky Aircraft. The model is a total system free-flight representation based on the Sikorsky General Helicopter (GENHEL) flight dynamics simulation, and is described in detail in Ref. 4. It is defined at a uniform level of sophistication currently considered appropriate for handling qualities evaluations. The model is also considered to give representative performance trends but does not include the sophisticated aerodynamics necessary to define critical performance characteristics.

The overall structure of the model is presented in Figs. 2 and 3 in functional and block diagram formats, respectively. The basic model is a total force, nonlinear, large-angle representation in six rigid body degrees of freedom. In addition, rotor rigid blade flapping, lagging, and pitch/torsional degrees of freedom are represented. The total rotor forces and moments are developed from a combination of the aerodynamic, mass, and inertia loads acting on each simulated blade. The rotor aerodynamics are developed using a blade element approach where the full range of angle of attack for blade aerodynamics is represented as a function of Mach number. The fuselage is defined by six component aerodynamic characteristics from wind tunnel data which have been extended analytically to large angles. The angle of attack at the fuselage is developed from the free stream plus interference effects from the rotor. These interference effects are based on rotor loading and rotor wake skew angle. The aerodynamics of the empennage are treated separately from the forward airframe to allow good definition of nonlinear tail characteristics. The tail rotor is represented by the linearized closed-form Bailey theory solution.

The Black Hawk flight control system represented in this model covers the primary mechanical and the automatic systems. The latter incorporates the stability augmentation system (SAS), the pitch bias actuator (PBA), the flight path stabilization (FPS) system, and the stabilator mechanization. Figure 4 shows a schematic of the pitch axis. The engine/fuel control model is a linearized representation with coefficients which vary as a function of engine operating condition. The interface between the engine and the rotor module is indicated in the block diagram Fig. 5.

3.2 Real-Time Considerations

Rotorcraft math models require certain simplifications and modifications in order to run real-time in a man-in-the-loop simulation (Ref. 5). In nonreal-time the rotor can be represented by the actual number of blades, numerous blade segments, and a small azimuthal advance increment which allows for good definition of blade motion around the azimuth. The computations associated with such a representation cannot be performed real-time even with a very large computer, and an approximation has to be generated with a minimum number of blade segments and the largest rotor azimuth advance increment that will retain satisfactory static and dynamic representation. The form of real-time approximation chosen uses blade segmentation based on equal area annuli to minimize the impact of the approximation. In nonreal-time models, the maximum time step allowable is established based on the computational convergence of rotor flapping which, in turn, depends upon the complexity of blade equations and the rotor rotation rate. A considerable amount of work on the topic of simplifying rotorcraft math models and developing appropriate real-time computation techniques has been performed by McFarland (Ref. 6). These techniques were applied during programming of the Black Hawk model. For this model, a dictating consideration comes from high frequency rotor vibration effects generated by the rotor blade inertial effects in the equations, and the accuracy of the integration of those equations. Using too large a time step will result in an aliasing-like effect whereby higher harmonics of the 4/rev vibration response falls into the low-frequency handling qualities frequency region. An example of this is shown in Fig. 6, taken from some hitherto unpublished work by Mr. R. E. McFarland, NASA Ames. The low-frequency folding effects are clearly seen for $\Delta t = 0.01$ and 0.02 seconds. Such false effects can be eliminated by purging selected inertial terms. An example of the resulting spectrum is also shown in Fig. 6. Tests on the Flight Simulator for Advanced Aircraft (FSAA) show that except at very low frequency, the roll axis motion threshold is greater than the noise level with purged terms. The importance of the very low frequency noise (<0.3 rad/sec) remains to be determined.

3.3 Flight Test for Model Validation

The United States Army Aviation Engineering Flight Activity (USAAEFA) at Edwards AFB, California, performed the flight testing in response to requirements laid down by the Army Aeromechanics Laboratory. These requirements included defining the instrumentation and the test matrix required for math model verification and subsequent parameter identification efforts.

Instrumentation

Although the helicopter had been instrumented for the Army's airworthiness and flight characteristics testing, the extensive requirements for parameter identification necessitated additional instrumentation and precise calibration. Table 1 lists the instrumentation that was used. Eighty-eight parameters were measured and recorded in a serial PCM stream on magnetic tape with a sample frequency of 100 Hz. Filters of 30 Hz were used on all parameters to insure matching the dynamics and synchronizing the sampling. Some of the more unusual features of the tests are described in the following.

All 3 axes of blade motion (pitch, lead-lag, and flapping) were measured on all 4 rotor blades. Three transducers for each blade were mounted on a special fixture leased from Sikorsky, Fig. 7. Because the transducers were not mounted exactly on the axis of blade motion, a complex transformation was required to resolve the measured angles into true angles.

To assist the pilot to perform complex control inputs for the purpose of parameter identification, a real-time visual guide was developed which is similar to that used by the German Aerospace Research and Experimental Establishment, Deutsche Forschungs-und Versuchsanstalt fur Luft-und Raumfahrt (DFVLR). The system consists of an oscilloscope on which the ordinate is scaled in distance of control travel and the abscissa is scaled in time. At the start of a control sequence, a dot showing the current position of the control is superimposed on the input guide and moves right at a rate proportional to time. A trace of actual control input remains superimposed on the input guide at the end of the maneuver so that judgments may be made as to the adequacy of the input. A typical input for parameter identification is a multistep sequence, and an example is shown in Fig. 8. Although the only control inputs requiring the display are for parameter identification, it was found that the display was an excellent quality-control device for all dynamic maneuvers and the static points as well. The display showed inadvertent control movement during trim and indicated the crispness and amplitude of steps, and the timing of pulses.

Test Matrix and Methodology

Table 2 indicates the scope of the flight tests. These were accomplished in 72 flights with 123 flight hours; approximately half the data were for static points and half were dynamic. All points at a given flight condition were flown at a constant thrust coefficient C_T, constant W/δ and constant $N/\sqrt{\theta}$ (where $C_T = T/\pi R^2\rho(\omega R)^2$, $\delta = p/p_0$ and $\theta = T/T_0$); this method is described in Ref. 7. Keeping these parameters constant implied that pressure altitude was increased as fuel was burned, and rotor speed was decreased as temperature (speed of sound) was decreased. In some cases, different combinations of W/δ and $N/\sqrt{\theta}$ were used to attain the same value of C_T, thus attempting to validate the nondimensional concept for this series of tests.

To compensate for center of gravity movement as the fuel was burned, the aircraft was equipped with a movable ballast cart which could travel the length of the aft cabin on a jack screw. The electric motor drive was controlled by the co-pilot according to a predetermined schedule, and its position displayed on the console control panel.

Since the basic unaugmented Black Hawk helicopter is unstable, time histories in response to the various inputs can have very limited duration. Utilizing the SAS would facilitate longer time histories before limits were exceeded, but the SAS characteristics would dominate the response. Since it is the basic helicopter's aerodynamic characteristics that are of interest, the flight tests were flown with the augmentation systems deactivated. In particular, the stabilator was fixed in the nominal position for the test airspeed, the pitch bias actuator was centered and disabled, and the flight path stabilization system was turned off. The SAS was left on for the static points and turned off for the dynamic test points. To minimize time to establish trim, the normal procedure was to have one of the two SAS axes turned on while the pilot established trim and the co-pilot adjusted the test input fixture. As the pilot counted down to the moment of control input, either he or the co-pilot would turn off the remaining SAS axis approximately one second before input. The actual input was made by the co-pilot. Input forms were steps, pulses, doublets, and multistep inputs designed to maximally excite the helicopter without large excursions from trim. Trim was reestablished between inputs and no combined (e.g., pitch and roll) inputs were used.

3.4 Correlation with Flight Data

Correlation with two dynamic maneuvers is shown in Figs. 9 and 10. The math model response was computed using the actual flight measured control positions. In order to account for the differences in the flight measured and model predicted control positions in trim, only the deviation from trim is introduced as the forcing input. Both the flight data and the simulation data were filtered using identical zero phase shift filters in order to suppress the high frequency vibration characteristics. This enables an easier comparison of the frequencies of interest to the flight dynamicist.

In Fig. 9, the pilot's collective stick input was used to drive the math model. The first plot demonstrates a comparison of the measured collective pitch of the main rotor, and the output of the simulation, indicating some differences in the control system rigging. A comparison of the measured rotor response (coning) shows good agreement initially, but tends to diverge in the long term, indicating that the model is more unstable than the flight vehicle. The coning response can be seen to be a major contributor to the normal acceleration of the aircraft. The vertical velocity shows considerable discrepancies which are directly attributable to the errors in the predicted normal acceleration. Figure 9 illustrates a need for a systematic approach to upgrading the model, working from the input to the highest level of integration down to the lowest order state.

Figure 10 shows the response to a lateral stick input. There exists reasonably good correlation with the rotor response (lateral flapping); however, some discrepancies are evident in the roll rate which strongly affect the predicted roll attitude. It may also be noted that the trim longitudinal stick position predicted by the model does not agree with the flight value. A comparison of the responses in the off-axes (pitch and yaw) is also provided.

3.5 Parameter Identification

The motivation for the parameter identification effort is to develop a systematic and semi-automated procedure for upgrading the math model, and eliminating discrepancies such as those shown in Figs. 9 and 10. The approach being taken is somewhat different from normal because the model used for the identification is a nonlinear blade element model, and the parameters being identified are the actual physical parameters (i.e., lift curve slope, interference factors, etc.) that are present in the nonlinear equations of motion. The approach normally taken by helicopter analysts is to identify the coefficients in a model linearized about a given operating point (i.e., stability derivative extraction). The approach being taken in this project is thought to have several advantages, the most important of which is that the model is being validated over a large portion of the flight envelope rather than at one isolated operating or trim condition. This approach allows for the processing of trim and static stability data in the identification process, as well as large disturbance transient maneuvers. The approach also provides for direct correlation and improvement of an operational simulation model without the intermediate steps that would be necessary if stability derivatives were used as the basis of comparison. On the other hand, several disadvantages must be considered. The problem is a computationally complex and highly nonlinear optimization problem and, as such, requires a reasonably accurate *a priori* model to allow correct convergence. Further, use of an output error algorithm is mandatory due to the difficulties in developing an extended Kalman filter algorithm for use with a blade element type model. Use of an output error algorithm does not allow for process noise effects which implies knowledge of a perfect model structure, and does not allow for unknown external disturbances.

The number of parameters in the nonlinear parameter identification is not appreciably more than that encountered in a fully coupled rotor and body linear problem. However, the table look-up data must be parameterized in such a way as to allow for identification of errors within the tables. Further, the actual parameters identified in a given identification run must be reduced to a manageable subset that is consistent with the maneuvers and/or static data being processed.

Development of the software to perform this automated model upgrade is currently under way. The basic concept behind this computer program is shown in Fig. 11.

4. SIMULATOR VALIDATION

As defined in Section 2, the basis of assessing simulator validity will be to assess the extent to which the characteristics of the perceived states induce correct psychomotor and cognitive control strategy for the given task and environment.

The correct psychomotor and cognitive control strategies are those achieved in flight in the actual helicopter. To determine these strategies, special-mission type flight testing was performed concurrently with the parameter identification tests described in the previous section. A series of mission flight phases (Table 3) were performed. These consisted of a series of flight task segments which included basic manual regulation of flight condition (hover, cruise, descent, etc.) as well as various discrete maneuvers (takeoff, acceleration, deceleration, quick-stop, etc.). In each case the pilot was instructed to demonstrate a good representative example of the flight task execution. Generally, this was based on the existing task descriptions and performance standards given in the utility helicopter aircrew training manual.

The recording system used for the parameter identification work was also used in the mission flight tests. No additional data, such as video recording of pilots' activity or eye point of regard, was available for these tests. To provide sufficient data base with which to generalize, it was important to have maneuvers repeated both by the same pilot and by different pilots. Primary emphasis was placed on NOE point-to-point, dash-quick-stop, bob-up, sidewards mask, dolphin, and slalom. All of these tasks were flown at least twice by two pilots.

4.1 Mission Flight Test Data Analysis

The basis for data analysis is that the control strategy from the simulator should match that from flight test. A pilot strategy for controlling the task is hypothesized, and the flight data used to determine the parameters by a least squares regression fit. A closed-loop pilot aircraft model is hypothesized for each task, certain parameters in the pilot model can be assumed based on past experimental analysis, and the flight data are then used to determine the unknown parameters. This effort is being performed under contract by Systems Technology, Inc., and the approach is described in Ref. 3. Each flight task maneuver has to be modeled at its most elemental level. Thus, if the task is longitudinal in nature, the lateral portion is deleted. The model represents the pilot's control, his perception, and the helicopter plant dynamics. Figure 12 shows a block diagram comparing the situation in the simulator with that for the real aircraft. In practice, considerable skill is required to get an adequate model of these control loops. The aircraft model is obtained first by using the appropriate transfer function of aircraft response to input. Inner or high frequency loops, such as attitude control, and outer loops, such as speed and altitude control, and the appropriate cue information being used by the pilot have to be hypothesized. The parameters in these various loop closures are determined by performing linear regression fits on the actual flight time histories. By using several pilots and repeated aircraft or simulator flights, it is hoped to develop confidence in the resulting closed-loop models.

Flight test data to perform this phase of the analysis have only recently become available and so the task of generating the appropriate loop closures has only just begun; however, a preliminary analysis of a hovering turn will be described to illustrate the methodology.

4.1.1 Pilot Strategy Evaluation for Hovering Turns

Two hovering turns, one to the left and one to the right, have been analyzed to develop the pilot strategy. Time histories for the turns are shown in Fig. 13.

The pilot strategy for the hovering turns can be broken down into two segments. The first segment involves starting and maintaining the turn; the second segment involves stopping the turn, and regulating yaw rate and heading error to obtain the desired heading. In initiating the hover turn, the pilot's heading error is large (for these cases, approximately 90°), and, therefore, the feedback of this parameter is not of primary importance. Instead, the pilot puts a high priority on increasing, and subsequently maintaining, an acceptable yaw rate. As long as the heading error is greater than 10° to 15°, the pilot will try to maintain some limit yaw rate depending on the aggressiveness of the turn. As heading error is reduced to the 10° to 15° range, the pilot will shift his primary feedback emphasis back to heading error, and yaw rate will be adjusted as required to line up the nose of the helicopter with the desired heading. The control law that provided the best representation of these maneuvers is represented in Fig. 14 and has the difference equation form:

$$\delta_p = K_p \delta_p Z^{-2} + K_{\psi_e} \psi_e Z^{-1} + K_{\dot{\psi}_e} \dot{\psi}_e Z^{-1} + \text{BIAS}$$

In the first segment of the turns the heading feedback was limited to an effective constant yaw rate command, and $Y_{p_{\dot{\psi}}}$ was determined to be as indicated in Fig. 14. Frequency responses for this transfer function are shown in Fig. 15. Overall, the pilot model suggests a bandwidth requirement of approximately 0.1 rad/sec for initiation of the turn maneuver. Using these solutions for $Y_{p_{\dot{\psi}}}$ and the flight values of $\dot{\psi}$, the δ_p was computed and compared with the flight value (Fig. 16).

The pilot controller elements for the second segment of the maneuver involves closing the outer loop of heading angle as well as the use of yaw rate in the inner loop. The values obtained for the coefficients for the second segment of both turns are shown in Fig. 14. Inspection of the maneuver time histories (Fig. 13) indicates that the gain and bandwidth of the $Y_{p_{\dot{\psi}}}$ controller should be significantly greater than that required for initiation of the turn. This is further reinforced by the logical conclusion that it should be a more difficult task for a pilot to trim out on a new heading angle than for the pilot to initiate a simple heading change. Figure 17 presents a summary of the frequency response gain and phase results for the second segment of both turns. For the nose left turn, the break frequency occurs at approximately 1.1 rad/sec; the right turn break frequency is approximately 0.55 rad/sec. The difference between the two values could be partially explained by the significantly greater magnitude of control activity required by the pilot to close on the desired left turn heading when compared with the right turn. In making a left turn, the pilot must overcome the main rotor torque by increasing tail rotor thrust, whereas a right turn is produced by reducing tail rotor thrust. This puts the tail rotor into a different operating condition and may cause differences in the pilot control. Overall, the pilot model suggests an approximate bandwidth of 1.0 rad/sec for the tracking task of concluding the turn at a specified new heading. Control activity for both of these maneuvers was reconstructed using the pilot model, and the results are compared with flight in Fig. 18. As for the initiation of the turn, the results indicate that the pilot model is a realistic representation.

4.2 Simulation Evaluation

In the simulator testing, the closed-loop pilot models obtained from analysis of the flight test data will be combined with a model of the simulator that represents the perceived and used visual and motion cues (Fig. 12). It is hypothesized that differences in control strategy between the simulator and flight are due to the simulator components themselves, and the analytical approach will be to attempt to account for these differences by appropriate modeling of the visual and motion cues. The simulator testing will, therefore, consist of repeating the mission flight phases performed in flight with the simulator in its basic configuration, and also with reduced visual and motion cues.

The simulator facility to be used will consist of a helicopter cockpit having a wide field-of-view visual display with a computer generated imagery (CGI) visual scene, mounted on the NASA Ames vertical motion simulator (VMS), a large amplitude motion generator. The VMS is shown in Fig. 19, and a typical CGI scene is shown in Fig. 20 superimposed over the actual field-of-view of the Black Hawk. Table 4 shows the most pertinent performance specifications of the VMS and also lists some performance requirements (Ref. 8). The VMS capabilities are considered to be excellent for NOE flight, especially in the rotational and vertical axes, and most of the requirements of Ref. 8 have been met. Important parameters in the visual display are the field-of-view, the resolution, the level of detail, and the overall dynamics. As can be seen from Fig. 20 the four-window CGI does provide a significant field-of-view relative to the Black Hawk, and the CGI data base shown has subjectively good detail. The resolution is 6.0 arc minutes per line pair. Dynamics of the CGI system are 30 per second update rate, the picture refresh rate is 60 per second, and total delay for a scene computation change is 100 milliseconds.

The sensitivity testing portion of the simulator validation exercise will involve repeating the flight tasks with various degraded combinations of the simulator equipment. Variations in motion will be from full to 50% travel, and will also use the hexipod portion only. Use of the hexapod only is included to allow some comparison with most civil and military flight trainers which use such devices. The visual simulation parameters to be changed are field-of-view, which will be reduced from four to three to two and one windows, and display dynamics, which will be evaluated by the use of time delay compensation techniques. The technique to be used is described by Crane in Refs. 9 and 10.

It is expected that the simulator testing will be performed during the spring of 1983.

5. CONCLUSIONS

The paper describes a systematic effort to generate techniques for simulator validation. This is a complex task and involves considerable effort and the skills of several organizations.

Efforts so far have resulted in procuring and programming a basic math model, and performing flight tests to obtain the data on which to base an update. In addition, some of the parameter identification tools required to handle the data have been developed. To overcome the difficulty of quantifying perceptual fidelity, the validation effort will be based on the concept that pilot control strategy in the simulator should match the control strategy used in flight. Flight data have been obtained to use as a basis for developing models of control strategy during mission-related tasks.

Currently, work is proceeding on the model update; a contract has been issued to Sikorsky to use the flight data to identify deficiencies and make improvements in their basic math model. In-house efforts are continuing to develop and apply state and parameter identification techniques to improve the structure of the model and refine the parameters. Systems Technology, Inc. is working under contract to use the flight data to develop analytical models for control strategy and accommodate the effects of the simulator components.

The future plans are to incorporate the updated model into a NASA real-time simulator facility during 1983. At that time, data will be obtained to perform the final step in the validation assessment analysis.

6. REFERENCES

1. Bray, Richard S., "Helicopter Simulation Technology: An Ames Research Center Perspective." p. 199. NASA CP 2219, Helicopter Handling Qualities, April 1982.
2. Key, David L. (Ed.), "Fidelity of Simulation for Pilot Training." AGARD Advisory Report No. 159, October 1980.
3. Heffley, Robert K. et al., "Determination of Motion and Visual System Requirements for Flight Training Simulators." System Technology, Inc., TR 1162-1, August 1981.
4. Howlett, J. J., "UH-60A Black Hawk Engineering Simulation Program Mathematical Model." NASA CR 166309, December 1981.
5. Cooper, D. E., and Howlett, J. J., "Ground Based Helicopter Simulation." Paper presented at AHS Symposium on Status of Testing and Model Techniques for V/STOL Aircraft, October 1972.
6. McFarland, R. E., "Establishment of a Rotor Model Basis." NASA TP-2026, AVRADCOM TR-81-A-14, June 1982.
7. Boirun, B. H., "Generalizing Helicopter Flight Test Performance Data." AHS Annual National Forum, May 1978.
8. Sinacori, John B., "The Determination of Some Requirements for a Helicopter Flight Research Simulation Facility." Systems Technology, Inc., TR 1097-1, September 1977.
9. Crane, D. F., "Time Delays in Flight Simulator Visual Displays." Proceedings of the 1980 Summer Computer Simulation Conference, Seattle, Washington.
10. Crane, D. F., "Flight Simulator Visual Display Compensation." Proceedings of the 1981 Winter Simulation Conference, Atlanta, Georgia, December 1981.

TABLE 1. FLIGHT TEST INSTRUMENTATION

Inertial/ground reference	Control system	Main rotor
C.g. accelerometers (3 axes)	Pilot control positions	Blade flapping (4 blades)
Nose accelerometers (3 axes)	Swashplate position	Blade lead-lag (4 blades)
Angular rate gyros (3 axes)	Tail rotor pitch	Blade pitch (4 blades)
Vertical gyro	Stabilator position	Rotor rpm
Direction gyro	SAS servo outputs	Rotor azimuth
Angular accelerometers (3 axes)	Mixer inputs	Main rotor shaft bending
Radar altimeter	Pitch bias actuator position	Main rotor torque
Magnetic heading	Primary servos position	
Engines (both)	**Air data**	
Power turbine speed	Angle of attack	
Gas generator speed	Angle of sideslip	
Fuel flow rate	Airspeed	
Engine torque	Barometric altitude	
	Total air temperature	
	Low airspeed system	

TABLE 2. SCOPE OF TEST MANEUVERS

Static	Dynamic
Level flight – 5 longitudinal CGs, 3 lateral CGs, 4 C_Ts using 6 combinations of W/δ and $N/\sqrt{\theta}$, stabilator sweeps, and rotor speed sweeps, all at a minimum of 4 airspeeds, including hover.	Step inputs – All axes (longitudinal, lateral, pedal, and collective), both directions, 2 CGs, 4 airspeeds including hover, varying magnitude.
Low speed – Forward, rearward, and lateral at 2 CGs and 2 C_Ts to 40 knots.	Pulse inputs – All axes, both directions, 4 airspeeds including hover.
Climbs and descents – 2 CGs, 2 C_Ts with variations, 3 airspeeds, 2 rates of climb, and 2 rates of descent each.	Doublets – All axes, both directions, 2 CGs, 2 C_Ts with variation, 2 airspeeds including hover, varying magnitude.
Level turns – 3 airspeeds, 2 CGs, 2 angles of bank in both directions.	System identification inputs – All axes, both directions, 2 CGs, 3 airspeeds, varying magnitude.
Wind-up turns – 2 airspeeds, 2 g levels in both directions.	Roll reversals – Both directions, 2 airspeeds.
Hover – 5 IGE hover heights.	Sideslip reversals – One airspeed, both directions.
Static longitudinal stability – 2 CGs, 3 C_Ts with variations, 2 rotor speeds, climbs and descents, at 3 airspeeds each.	Long term response – 3 airspeeds, both directions.
Lateral-directional stability – Same as longitudinal stability.	Pushovers and pullups – 2 airspeeds, both directions, varying magnitude.

TABLE 3. MISSION FLIGHT TASKS

Takeoff/landing tasks in an airport environment

1. Takeoff to hover
2. Hover
3. Hover turns
4. Taxiway flight
5. Right sideward acceleration/deceleration
6. Left sideward acceleration/deceleration
7. Rearward acceleration/deceleration
8. Normal takeoff
9. Maximum performance takeoff
10. Traffic pattern flight
11. Approach to hover
12. Landing from hover

Level/climb/descent flight tasks

1. Straight and level flight
2. Climb at specified airspeed and rate of climb
3. Level flight turns
4. Descents at specified airspeed and rate of climb
5. Single engine approach and roll on landings
6. Autorotations to the runway followed by power recovery

NOE/contour/low level flight tasks

1. NOE terrain flight takeoff
2. Low-level flight
3. Contour flight
4. NOE flight
5. NOE pop-up
6. NOE bob-up (mask/unmask at hover)
7. NOE side unmask
8. NOE dash followed by quickstop along a straight line and with a turn
9. NOE hard break sideward
10. NOE hard turn
11. NOE slalom maneuver
12. NOE dolphin maneuver
13. Confined area approach and landing

TABLE 4. COMPARISON OF NOE SIMULATOR MOTION REQUIREMENTS AND VMS PERFORMANCE

Axis	Position rad,m		Velocity rad/sec, m/sec		Acceleration rad/sec^2, m/sec^2		Frequency response, bandwidth, rad/sec	
	Required	VMS	Required	VMS	Required	VMS	Required	VMS
Roll (ϕ)	±0.3	±0.38	±0.5	±0.26	±1	±0.87	20	0.4-20
Pitch (θ)	±0.3	±0.45	±0.5	±0.26	±1	±0.87	20	0.4-20
Yaw (ψ)	±0.4	±0.51	±0.6	±0.26	±1	±0.87	20	0.4-20
Longitudinal (X)	±1.3	±0.8	±1.3	±0.6	±3	±4.9	20	0-0.2
Lateral (Y)	±3	±6	±2.6	±3	±3	±7.3	20	0-20
Vertical (Z)	+7, -14	±9	+8, -11	±6	+14, -12	±9.8	20	0.2-12

Figure 1. UH-60A Black Hawk.

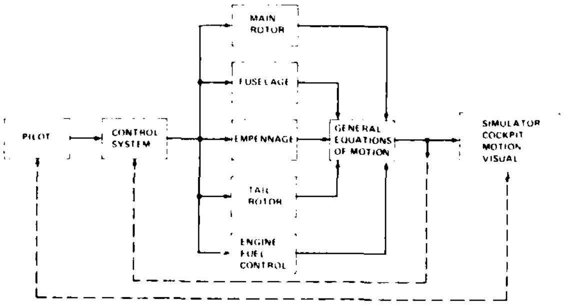
MAIN ROTOR
FUSELAGE
PILOT
CONTROL SYSTEM
EMPENNAGE
GENERAL EQUATIONS OF MOTION
SIMULATOR COCKPIT MOTION VISUAL
TAIL ROTOR
ENGINE FUEL CONTROL

Figure 3. Math model simplified block diagram.

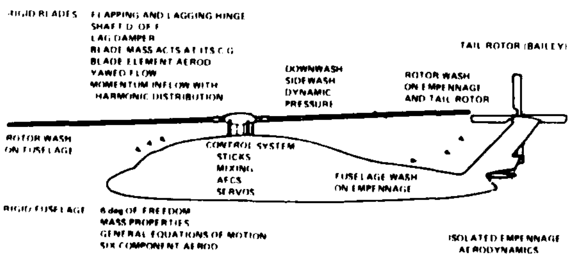
RIGID BLADES
FLAPPING AND LAGGING HINGE
SHAFT D OF F
LAG DAMPER
BLADE MASS ACTS AT ITS C G
BLADE ELEMENT AEROD
YAWED FLOW
MOMENTUM INFLOW WITH HARMONIC DISTRIBUTION
TAIL ROTOR (BAILEY)
DOWNWASH
SIDEWASH
DYNAMIC PRESSURE
ROTOR WASH ON EMPENNAGE AND TAIL ROTOR
ROTOR WASH ON FUSELAGE
CONTROL SYSTEM
STICKS
MIXING
AFCS
SERVOS
FUSELAGE WASH ON EMPENNAGE
RIGID FUSELAGE
6 deg OF FREEDOM
MASS PROPERTIES
GENERAL EQUATIONS OF MOTION
SIX COMPONENT AEROD
ISOLATED EMPENNAGE AERODYNAMICS

Figure 2. Math model features.

SWASHPLATE
PITCH BIAS ACTUATOR
SAS
2ND STAGE
1ST STAGE
SPRING
PITCH TRIM SERVO
PITCH BOOST SERVO
FWD OR AFT PRESERVO REF

Figure 4. Pitch flight controls schematic.

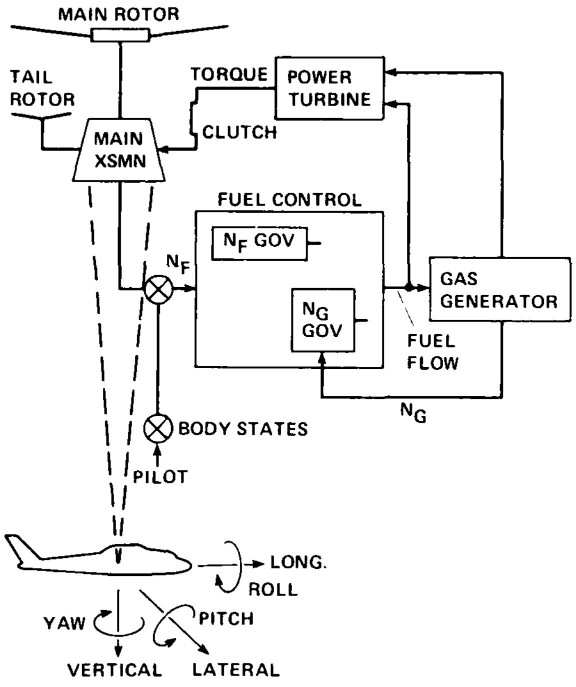
MAIN ROTOR
TAIL ROTOR
TORQUE
POWER TURBINE
MAIN XSMN
CLUTCH
FUEL CONTROL
N_F GOV
N_F
N_G GOV
GAS GENERATOR
FUEL FLOW
N_G
BODY STATES
PILOT
LONG.
ROLL
YAW
PITCH
VERTICAL
LATERAL

Figure 5. Engine integration into math model.

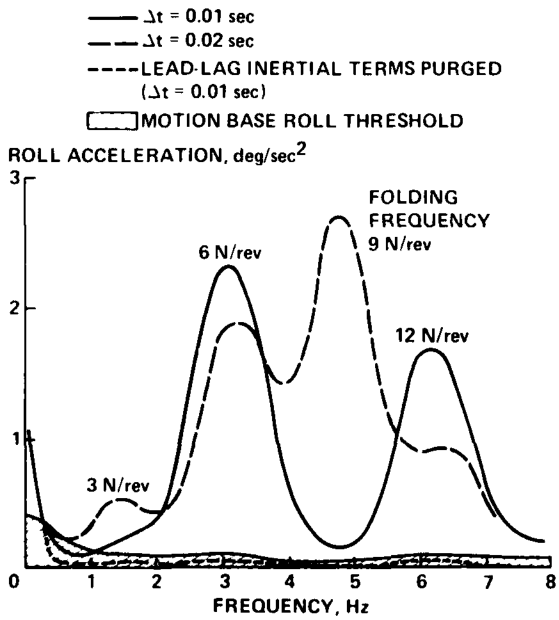

Figure 6. Power spectrum of rolling moments at 100 knots, trim.

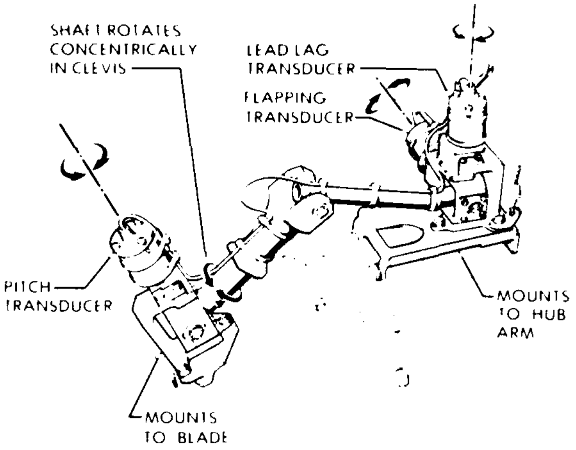
SHAFT ROTATES CONCENTRICALLY IN CLEVIS
LEAD LAG TRANSDUCER
FLAPPING TRANSDUCER
PITCH TRANSDUCER
MOUNTS TO HUB ARM
MOUNTS TO BLADE

Figure 7. Blade angle measurement fixture.

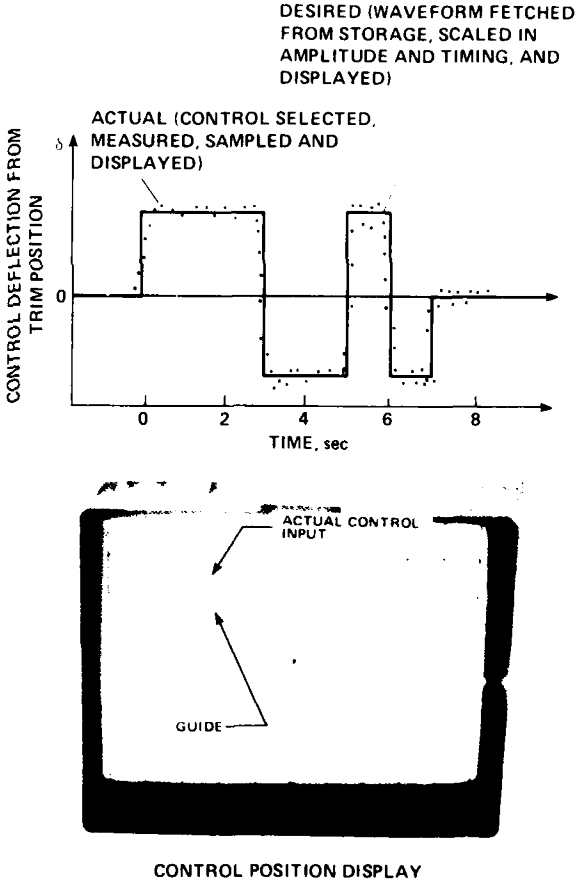

Figure 8. Input form and pilot's display.

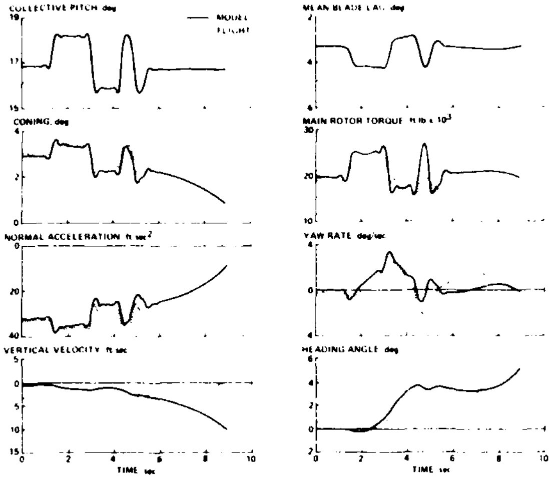

Figure 9. Collective stick input, 60 knots.

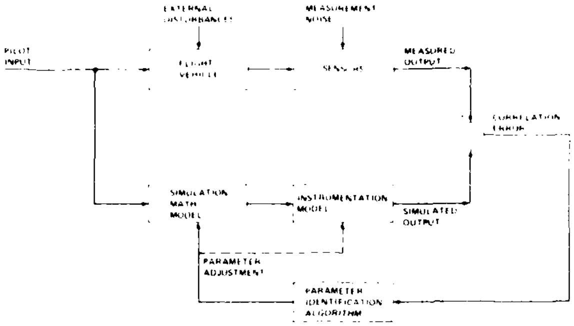
EXTERNAL DISTURBANCES
MEASUREMENT NOISE
PILOT INPUT
FLIGHT VEHICLE
SENSORS
MEASURED OUTPUT
CORRELATION ERROR
SIMULATION MATH MODEL
INSTRUMENTATION MODEL
SIMULATED OUTPUT
PARAMETER ADJUSTMENT
PARAMETER IDENTIFICATION ALGORITHM

Figure 11. Parameter identification concept.

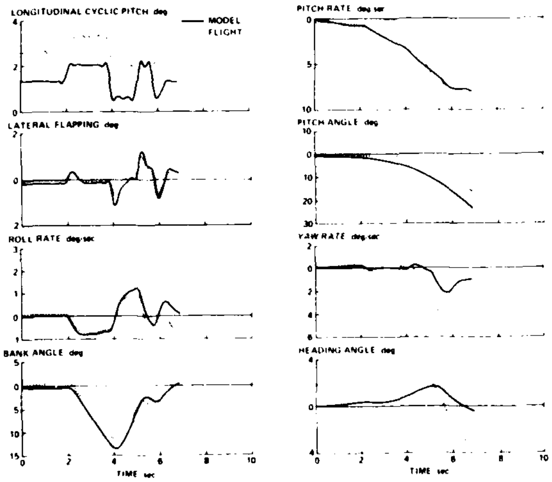

Figure 10. Lateral stick input, 60 knots.

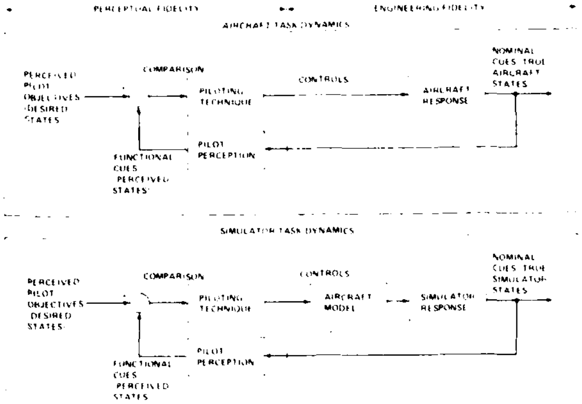
PERCEPTUAL FIDELITY
ENGINEERING FIDELITY
AIRCRAFT TASK DYNAMICS
PERCEIVED PILOT OBJECTIVES (DESIRED STATES)
COMPARISON
PILOTING TECHNIQUE
CONTROLS
AIRCRAFT RESPONSE
NOMINAL CUES (TRUE AIRCRAFT STATES)
PILOT PERCEPTION
FUNCTIONAL CUES (PERCEIVED STATES)
SIMULATOR TASK DYNAMICS
PERCEIVED PILOT OBJECTIVES (DESIRED STATES)
COMPARISON
PILOTING TECHNIQUE
CONTROLS
AIRCRAFT MODEL
SIMULATOR RESPONSE
NOMINAL CUES (TRUE SIMULATOR STATES)
PILOT PERCEPTION
FUNCTIONAL CUES (PERCEIVED STATES)

Figure 12. Flight task components in helicopter and simulator.

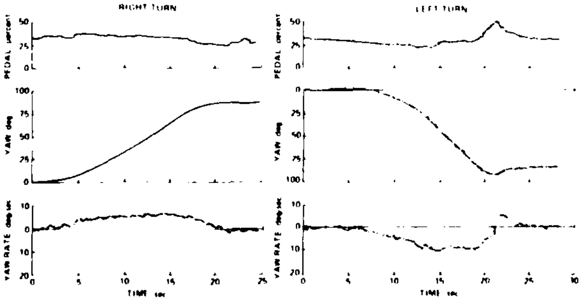

Figure 13. Time history for hovering turns.

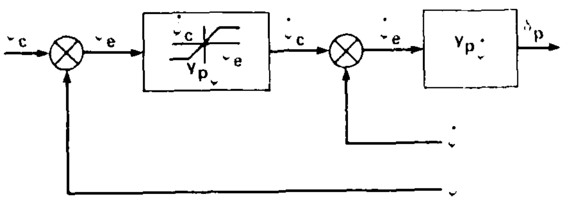

ψ_c
ψ_e
$\dot{\psi}_c$
Y_{p_ψ}
ψ_e
$\dot{\psi}_c$
$\dot{\psi}_e$
$Y_{p_{\dot{\psi}}}$
δ_p
$\dot{\psi}$
ψ

	LEFT TURN	RIGHT TURN
FIRST SEGMENT		
K_{δ_p}	0.98	0.93
$K_{\dot{\psi}_e}$ (percent-sec/deg)	0.086	0.075
SECOND SEGMENT		
K_{δ_p}	0.78	0.89
K_{ψ_e} (percent/deg)	0.55	0.12
$K_{\dot{\psi}_e}$ (percent-sec/deg)	0.32	0.25

$$Y_{p_\psi} = \frac{K_{\psi_e}}{-K_{\dot{\psi}}}$$

$$Y_{p_{\dot{\psi}}} = \frac{-K_{\dot{\psi}}}{1 - K_{\delta_p} z^{-2}}$$

Figure 14. Pilot control strategy in hovering turn.

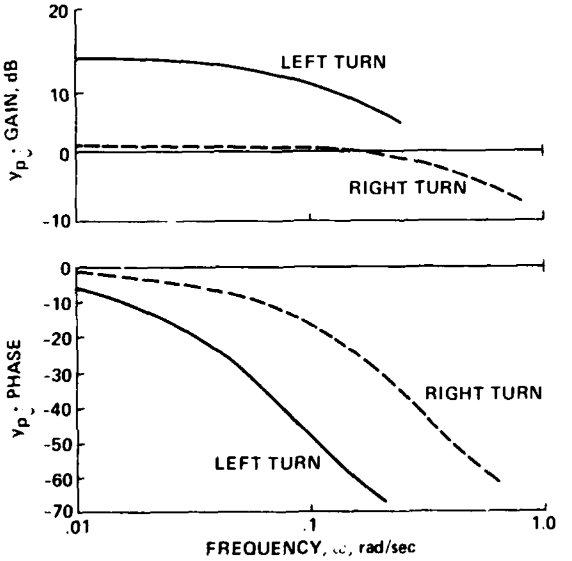

Figure 15. Frequency response for $Y_{p_{\dot{\psi}}}$ (initial part of turn).

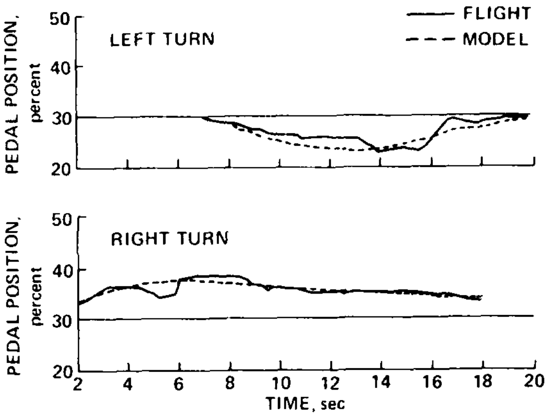

Figure 16. Control usage for initial part of the hovering turn.

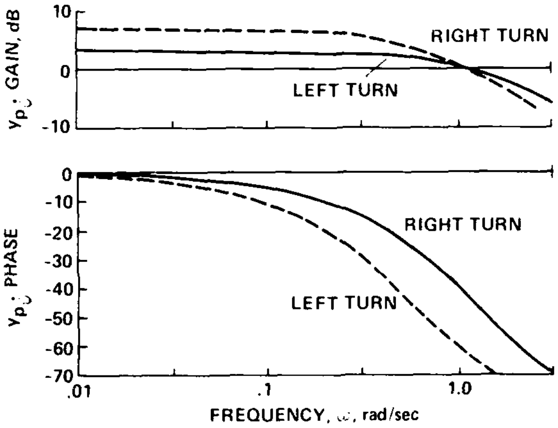

Figure 17. Frequency response for $Y_{p_{\dot{\psi}}}$ (second part of turn).

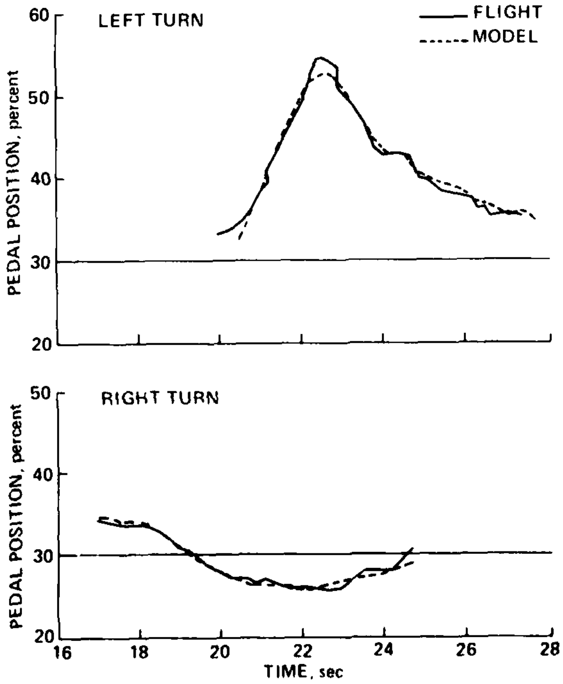

Figure 18. Control usage for second part of hovering turn.

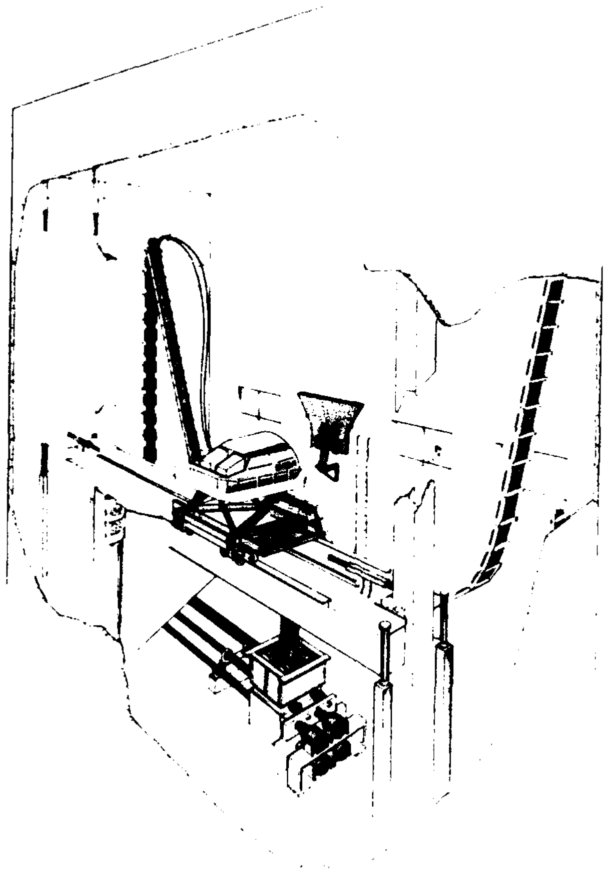

Figure 19. Vertical motion simulator (VMS).

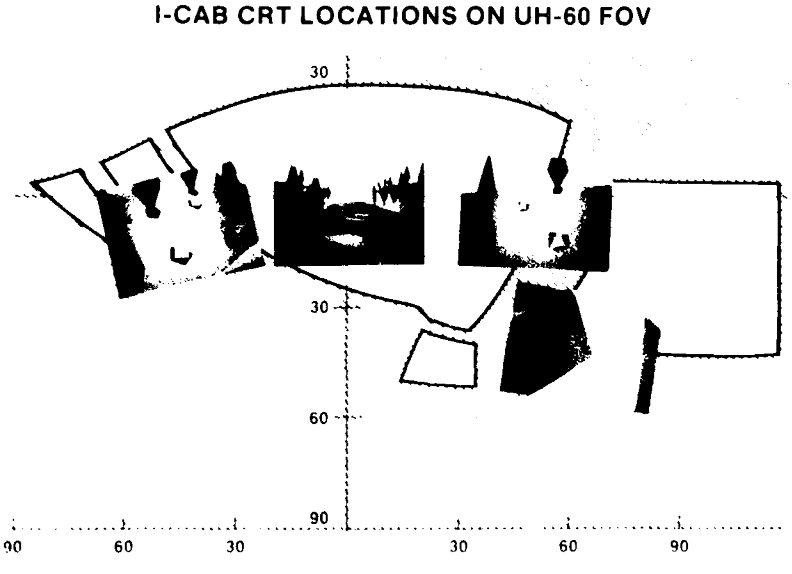

I-CAB CRT LOCATIONS ON UH-60 FOV

30
30
60
90
90
60
30
30
60
90

Figure 20. CGI four-window display.

CORRELATION ASPECTS OF ANALYTICAL, WIND TUNNEL AND FLIGHT TEST RESULTS FOR A HINGELESS ROTOR HELICOPTER

by

J. Kaletka and H.-J. Langer

Deutsche Forschungs- und Versuchsanstalt
für Luft- und Raumfahrt e.V. (DFVLR)
Braunschweig-Flughafen

SUMMARY

This paper discusses two approaches to develop and verify mathematical descriptions of rotorcraft characteristics: (1) wind tunnel experiments with a model rotor, and (2) parameter identification from flight test data.

The paper is divided into three parts. In the first part, the analysis of wind tunnel measurements is concentrated on. Then, the evaluation of flight test data is discussed, and, finally, results from both approaches are compared.

A rotor test stand with a Mach scaled BO 105 model rotor was used for measurements in two different large wind tunnels. After addressing rotor scaling aspects, emphasis is placed on wind tunnel influences and their corrections to provide the transferability of the results to the full-scale rotor. Specific tests to determine flight mechanical static derivatives are described.

BO 105 flight test data were used for the identification of mathematical models describing the dynamic behavior of the helicopter. After an introduction to system identification the paper concentrates on the system excitation problem and the verification of results. Examples showing both identified derivatives and time histories of the helicopter and identified model responses are given.

In the last part of the paper, derivatives extracted from wind tunnel and flight tests are discussed. For comparison theoretically calculated values are also presented.

1. INTRODUCTION

Accurate stability and control analyses and handling qualities evaluations are of keen interest for the improvement of today's helicopters and the development of future advanced rotorcraft. Consequently, there is a need for the determination of reliable mathematical models and system parameters as well as for the verification and extension of existing analytical calculation methods. For fixed wing aircraft investigations basically two experimental approaches to this problem area are used: (1) wind tunnel tests with scaled models have become standard and certainly can be considered as the classical approach, and (2) the extraction of system parameters from flight test data, known as parameter identification, has become another powerful tool during the last few years and is increasingly applied.

For rotary wing aircraft, however, these approaches are seldom utilized. This is mainly due to some specific problems not encountered in fixed wing aircraft:

The main difficulties for helicopter wind tunnel tests are proper scaling and fabrication of the rotor to achieve the transferability to full-scale helicopters. Fuselage models are usually scaled to have comparable aerodynamic characteristics. The scaling of the rotating rotor, however, must provide both aerodynamic and dynamic similarity, which has three important consequences:

- It is not possible to achieve complete similarity between model and full-scale rotor.
- The rotor blades must be manufactured with extremly high accuracy.
- The rotor should be as large as possible, which means that rotor tests must be conducted in large, costly wind tunnels.

Rotorcraft system identification is still a relatively complicated task because of three main problem areas:

- A large number of coupled degrees of freedom (DOF) necessitates a high order mathematical model (set of differential equations) to adequately describe helicopter dynamics. However, successful application of system identification techniques is limited by the size of the model, the number of unknowns that have to be identified, and the information content of the data.

- Inherent rotorcraft instabilities limit the time length for a data run because increasing amplitudes quickly invalidate small perturbation assumptions used for linear models. In addition they complicate the stabilization of the rotorcraft at defined steady state trim conditions and lead to large deviations from the steady state when gust disturbances are present.

- Data measurement quality is affected by the high vibration level of helicopters. Furthermore, some variables (like speed components for low speed flight conditions and hover and, in particular, rotor blade dynamics) are difficult to measure.

The advancement of both rotorcraft wind tunnel testing and rotorcraft identification are major research goals at the DFVLR Institute for Flight Mechanics. Therefore, a rotor test stand (Fig. 1) has been designed and built to investigate various problem areas like scaled rotor technology, transferability of results, higher harmonic control capability, etc.. Specific flight tests with the DFVLR BO 105 research helicopter (Fig. 2) provide the data base to develop and evaluate appropriate system identification procedures.

In the following two chapters of this paper, aspects of both wind tunnel experiments with the rotor test stand and rotorcraft identification from flight test data are presented. Finally, results obtained from theoretical calculations, wind tunnel measurements of the scaled BO 105 rotor and identification of the full-scale BO 105 helicopter are discussed.

2. EVALUATION OF WIND TUNNEL DATA

A rotor test stand was designed and developed by the DFVLR and the German industry (MBB and Dornier). It was sponsored by the German ministry of defense. The test support and the measurement system was designed to test different scaled rotors in large wind tunnels. The test stand is equipped with a hydraulic torque motor that provides a power of almost 70 kW. To control the rotor swashplate three hydraulic boosters are installed. The rotor shaft incidence angle can also be varied from -15 up to 13 degrees by a hydraulic booster.

Until now two different types of rotors were tested in wind tunnels, a 4-bladed hingeless rotor and a 2-bladed teetering rotor. The 2-bladed rotor can be operated by a combination of shaft and tip drive. This chapter will concentrate on measurements with the 4-bladed rotor. First, rotor scaling aspects and a brief description of the measurement system will be given. Then, emphasis will be placed on wind tunnel influences and their corrections and on rotor derivative measurements.

2.1 ROTOR SCALING

In order to obtain rotor measurements from the wind tunnel experiments that can be compared with BO 105 flight test data, the model rotor was scaled down from the BO 105 main rotor. It was decided to use Mach scaling as it has proved to be most appropriate to simulate helicopter rotor aerodynamic behavior. Maintaining the Mach number, however, implies that Reynolds scaling laws cannot be fulfilled. Consequently, the model should be as large as possible (Ref. 1). For a scaling factor of 2.5, wind tunnel measurements with the NACA 23012 profile have shown that the maximum lift coefficient decreases by 15 % (Ref. 2). The decrease in Reynolds number also results in a decrease in the lift gradient by 7.5 %. The blade force due to lift and drag would therefore be to small with respect to the mass forces and elastic forces of the blade. For this reason a slightly smaller scaling factor was used for the blade chord.

Ground and air resonance of a helicopter are influenced by the lagging frequency ratio and the lag damping. Therefore, the lagging frequency ratio of the BO 105 is $\omega_{\zeta}/\Omega_{Ro}$ =0.666 and the lag damping is 2 to 3 % of the critical damping to avoid resonance. As the fabrication of the small scaled blade fittings, for example, is relatively sophisticated, it cannot be guaranteed that for the model rotor the damping level of the BO 105 can be maintained. Therefore, the lagging frequency ratio of the model rotor was increased to $\omega_{\zeta}/\Omega_{Ro}$ = 0.7.

It was decided that it is not necessary to build a Froude scaled model because it is not required to provide the same inertia to gravity force ratio as in the full-scale rotor. In addition the influence of the gravity force can be neglected as the rotor is not operating vertically. Therefore, Froude scaling also is not required.

2.2 MEASUREMENT SYSTEM

Two 16-channel PCM systems were used to transfer and record the data from both the rotating system and the fixed system. In the rotating system strain gages are primarily used to measure stresses on pitch links and blades. Signals measured in the fixed system are hub loads, torque, rotor angle of attack, downwash data, and a reference signal to identify the blade position.

The hub loads are measured by a 5-component balance. The moments are in general measured with an accuracy of 5 % of the full scale. The accuracy is higher when there is no sign change in the moment measurements which usually can be achieved for the tests to determine derivatives. The thrust can be measured with an accuracy of 1 to 2 % of the maximum value of 7000 N.

The hydraulic boosters used to control the swashplate can be adjusted with an accuracy of 0.1 degree. It is, however, difficult to accurately define the resulting error because the relationship between thrust and collective contol settings is nonlinear with tunnel speed.

2.3 WIND TUNNEL COMPARISON

The BO 105 model rotor was tested in two different wind tunnels: The Daimler Benz tunnel (DB) is a so called "closed-on-bottom-only" wind tunnel. The maximum test section velocity is 70 m/s. The total length of the stream circuit is 126 m. The German-Netherlands wind tunnel (DNW) offers both open and closed test sections. Because the model rotor tests emphasized the high speed regime, a closed test section was selected. The maximum tunnel speed is 110 m/s and the stream circuit is 320 m long. A comparison of both test section sizes is shown in Fig. 3. Due to the short tunnel length of the Daimler Benz tunnel, rotor induced turbulences could be observed even before the flow reached the rotor plane. This is particularly true at high advance ratios and high thrust settings. The flow quality of the DNW seems to be significantly higher especially at high tunnel speeds. As it was expected, low tunnel speeds and high rotor thrust produce strong wall interferences and rotor vibrations in the DNW, due to the closed test section. In the practically open test section of the DB tunnel the flow has only small disturbances at low speed.

Fig. 4 shows differences of thrust and power at $\mu=0.2$ for both wind tunnels. This presentation was chosen since the thrust/power ratio is almost constant for a thrust higher than 2000 N, however it is dependent on cyclic control and rotor angle of attack. The comparison shows strong differences between the two wind tunnels. The results are highly dependent on the magnitude of the effective inflow angle at the rotor caused by different wall interferences. Fig. 5 presents the necessary wind tunnel correction angles that must be applied to obtain agreement with the BO 105 level flight condition. The DB and the DNW values were obtained from an interpolation of wind tunnel measurements. A comparison with Heyson's curves (Ref.3) yields considerable differences between measured and predicted correction factors, especially at low tunnel speeds.

2.4 THE WIND TUNNEL TEST PROGRAM

The objective of the test program was to evaluate the model rotor behavior for the main flight regime of the BO 105. Except of some rotor conditions in the low speed area and steep descent flight the flight regime is covered adequately by the wind tunnel tests (Fig. 6).

For the wind tunnel experiments the control angles of the model rotor were varied stepwise with two degrees for the collective, one degree for the longitudinal cyclic, and five degrees for the rotor angle of attack. These variations were made for five different advance ratios from 11 to 55 m/s in steps of 11 m/s. To compare the model rotor loads with the BO 105 hub loads interpolations had to be made because the control settings of the BO 105 do not correspond to the stepwise control angle variation of the rotor test stand.

BO 105 rotor derivatives were extracted from the test program by calculating the gradient of the force or moment change due to a change in the control (Fig. 7). As the above given stepsize turned out to be too large for an accurate determination of some derivatives a specific wind tunnel test program was conducted where the stepsizes were reduced to obtain more reliable results for the static stability and control derivatives. For the above given advance ratios the following stepsizes were defined:

- speed change between 1.4 and 2.8 m/s
- rotor angle of attack change $0.1/\mu$ degree
- longitudinal cyclic and collective pitch change 0.5 degree.

The steady state pitch and roll moments were scaled appropriately to the trim position of the BO 105 for level flight. The thrust was 3400 N which corresponds to a helicopter mass of 2200 kg.

Results presented in chapter 4 of this paper were extracted from these measurements. In addition rotor derivatives were theoretically calculated for comparison reasons. A detailed description of the calculation method is given in Ref. 4.

3. EVALUATION OF FLIGHT TESTS

In wind tunnel experiments forces and moments acting on the model are usually measured directly. For a flying aircraft, however, it is only possible to sense its reaction, in particular its accelerations, due to changes in forces and moments. For the derivative evaluation this fact has an important consequence: in wind tunnel tests static derivatives, e.g. force changes due to speed changes, can be determined from steady state conditions by directly measuring forces and moments at different constant speeds. When these derivatives have to be evaluated mainly from acceleration data of flight tests it is obvious that (1) dynamic tests are required because there are no accelerations in steady state flight conditions, and (2) in dynamic tests accelerations are also caused by various aircraft motion variables due to coupling effects. Therefore, the influence of an individual variable, like speed, on the total acceleration response still has to be determined.

Keeping this discussion in mind, the basic approach and principle of system identification can be explained quite easily (Fig. 8).

3.1 INTRODUCTION TO SYSTEM IDENTIFICATION

In flight tests the aircraft is stabilized at a defined steady state flight condition and its modes are excited by appropriate control inputs. Both input and system response are measured and recorded.

For the evaluation the aircraft behavior is assumed to be modeled by a set of differential equations describing the forces and moments acting on the aircraft in terms of acceleration, state and control variables. Most of the model coefficients, the derivatives, are unknown and substituted by estimated values. The model response due to the measured inputs is calculated and compared to the real aircraft response. The resulting differences are minimized by a mathematical algorithm, the identification method, by adjusting the model parameter values. Basically, this approach is quite straight forward. However, when the identification is applied to real systems, various complicating factors become obvious almost immediately:

- As the identification is based on the evaluation of the system input/output relationship a suitable input signal has to be defined to properly excite the modes of the system although the dynamic characteristics are more or less unknown. The input then has to be implemented, often by the pilot.

- The aircraft response not only results from the given input but also is influenced by unmeasurable external disturbances (e.g. turbulence) and aerodynamic interferences, (e.g. between helicopter rotor blades and fuselage). These effects are in general summarized as process noise.

- Measurement errors cannot be avoided. Although some variables can be measured with high accuracy, air data measurement, for example, is still problematic. This is particularly true for the helicopter low speed regime. Other sources of measurement errors are aircraft vibrations and structural modes as well as inaccuracies in CG position corrections and sensor calibrations.

- In general, relatively simple mathematical models, linearized for a steady state flight condition, are used to describe the aircraft characteristics. They have been used successfully for various applications. However, such models can only approximate the complex dynamics of an aircraft. Therefore, modeling errors also influence the identification results.

- Various identification methods have been developed. According to their characteristics and minimization criteria, slightly different results can be expected.

Although there are possibilities to reduce these complications, a verification of the obtained results is essential before the identified models can be used for further applications.

From the above discussion it can be visualized that major efforts have to be made to obtain high-quality flight test data. This requires not only carefully conducted flight tests and an accurate instrumentation system but also the application of techniques for determining and correcting data errors. However, main emphasis still has to be placed on approaches to increase the information content about the system under test for the identification algorithm. Therefore, this section concentrates on the design of appropriate input signals and their implementation. Then BO 105 identification results and an approach to verify these results are presented.

3.2 INPUT DESIGN AND IMPLEMENTATION

The main objective of optimized input signals is the appropriate excitation of all aircraft modes within the frequency range under consideration. In Ref. 5 various input signal design approaches and a comparison of the effectiveness of five different signals are presented to demonstrate the importance of input signal design. One of these signals, the DFVLR 3211 signal, has also been used extensively for the BO 105 identification. It is a multistep signal, optimized in the frequency domain to have a wide frequency range. Fig. 9 shows the power spectra of the basic 3211 signal and a modification of this signal. It can be seen that the multistep signals can effectively excite the aircraft modes within a frequency decade (factor between highest and lowest frequency at half power limit). The modified signal was designed to still sufficiently excite higher frequencies when filtering effects during the input implementation are present. By adjusting the pulse length the effective frequency band can be shifted to lower or higher frequencies and thus the signals can be adapted to specific system requirements.

In general, the control input signals have to be implemented by the pilot. Increasing complexity of the signal therefore requires that the pilot be given some help, e.g. using visual or audiovisual means. Based on the experience with a relatively simple two-needle instrument (Ref. 6), an improved device was developed for the helicopter tests (Fig. 10). On a small oscilloscope installed in the cockpit, both the desired and the actual movement of a selected control were shown versus time. The pilots quickly got used to the display and had no major difficulties in making the oscilloscope beam follow the given signal shape by moving the control. Fig. 11 demonstrates that both the basic and the modified 3211 signal could be implemented satisfactorily. This is particularly true for the collective control.

3.3 BO 105 IDENTIFICATION RESULTS

For the extraction of helicopter derivatives from flight test data a 6 DOF rigid body model with linear constant coefficients is generally used. In contrast to fixed wing aircraft, a reduction of the model size by considering longitudinal and lateral-directional motions separately usually is not possible because of the high coupling intensity of helicopter modes.

On the other hand, an extension of the model to more precisely describe helicopter characteristics by adding rotor DOF has only rarely been used successfully in the identification from flight test data. This is certainly primarily due to the fact that high quality rotor state measurements often are not available. In addition, there is still a need for techniques that can handle a large amount of data and estimate many unknowns within reasonable computation time and costs.

However, one has to be aware of the fact that in a rigid body model it is assumed that changes in control or state variables immediately influence the forces and moments acting on the helicopter. This means that the rotor dynamics are completely neglected and the rotor response due to a disturbance is an instantenous tilt to a new steady state position. In reality, however, there is an influence from the rotor dynamics when flight test data from dynamic tests are considered.

The present state of the art in rotorcraft identification is based on the assumption that effects of the rotor dynamics may be neglected when only the low frequency range of the rigid body is considered and higher frequencies are not excited. A new approach to more accurately model the helicopter without explicitly adding more DOF was published in Ref. 7. It has been validated using simulated data, however, it still has to be tested with flight test data.

It easily can be visualized that the identification of an increasing number of unknowns also requires an increase in the data information content. For a 6 DOF rigid body model of the BO 105 helicopter, Ref. 8 has shown that only poor identification results are obtained when a single run with an input to one control is evaluated. Although optimized signals were applied and there was significant coupling between the modes, the data information content about the lateral-directional motion was insufficient when a control input exciting primarily the longitudinal motion was used. The same was true for the lateral motion. In general, it is seldom possible to apply additional inputs within the same run because of helicopter dynamic instabilities. Therefore, the identification methods were extended to be able to use the information from different independent runs. Based on the 'concentrated' information one model is identified that is representative for the runs under consideration. This multiple run evaluation technique has meanwhile become standard for the DFVLR helicopter identification.

In the following, an identification example is presented that was obtained from flight test data (level flight, 60 knots) of the DFVLR BO 105 helicopter. The mathematical model representing the 6 DOF of the rigid body was

$$\begin{aligned} \dot{x} &= Ax + Bu \\ y &= Cx + Du \end{aligned}$$

with

state vector $x^T = [u, v, w, p, q, r, \Phi, \Theta]$
control vector $u^T = [\text{collective, long. stick, lat. stick, pedal}]$
measurement vector $y^T = [a_x, a_y, a_z, p, q, r, \Phi, \Theta, u, v, w]$

Basically this model is linear. However, nonlinear gravity and inertia terms have been included. Variables to be measured are defined by the vectors u and y so that the helicopter mainly was instrumented with linear accelerometers (a_x, a_y, a_z), rate gyros (p, q, r), a attitude reference gyro (Φ, Θ), a LASSIE low airspeed system (u, v, w), and potentiometers to measure collective, longitudinal and lateral stick as well as tail rotor pedal inputs.

For the identification, parameters found to be non-significant were neglected. Nevertheless, the matrices A, B, C and D still contained 37 state and control derivatives that had to be determined. In addition, drift and zero shift errors for each individual run had to be estimated so that altogether 94 unknowns had to be identified.

First estimates were obtained from a Least Squares identification technique. Then, a Maximum Likelihood (ML) method was applied, a method that is widely accepted as most suitable for aircraft parameter identification (Ref. 9 and 10). The time history comparison of measured data and ML identified model response demonstrates that a good agreement could be obtained (Fig. 12).

3.4 VERIFICATION OF IDENTIFICATION RESULTS

In the above example it has been shown that the response of the identified model satisfactorily fits the measured flight test data. It has to be taken into consideration, however, that the minimization of the time history differences was forced by the estimation method. Consequently, from a good curve fit between model output and data used for the identification it cannot necessarily be concluded that an accurate mathematical model was obtained. To verify the validity of the identified model it has to be proved that the model can predict the helicopter response due to arbitrary control inputs (simulation task) within a specified frequency range. Therefore, the control inputs from flight test data not used in the identification are treated as control variables of the model and the resulting calculated model response is compared with the measured data (Fig. 13).

As an example, a BO 105 flight test run with 40 seconds duration was selected, where collective, lateral, and longitudinal 3211 input signals were applied sequentially with pilot controlled retrims. The measured control inputs were fed to the identified 6 DOF model that was obtained from the ML evaluation of various multiple runs. Fig. 15 demonstrates that the model response agrees fairly well with the measured BO 105 time histories. Again, it has to be stressed that the model was identified from other data, different in both input signals and data length. From the satisfactory time history fit it can be concluded that the identified mathematical model has a high prediction capability and adequately represents the BO 105 dynamic behavior.

This result does not necessarily show that also the flight mechanical parameters were extracted accurately. Therefore, some data runs were evaluated using a different identification method, the Instrumental Variable technique. This method differs significantly from the Maximum Likelihood because its criterion is the minimization of the equation error where each equation is treated separately. Fig. 14 shows identification results obtained from both the Maximum Likelihood and the Instrumental Variable for some of the main parameters. Mean values and standard deviations were calculated from identification results of different data runs. It can be seen that most of the derivatives have almost the same value and that derivatives with larger differences, e.g. the q-derivatives, are still of the same order when the standard deviations are also taken into account.

In addition, it has to be considered that equation error methods, like the Instrumental Variable, are in general less powerful than the Maximum Likelihood. When the application of two significantly different identification methods leads to similar results, it can be assumed with high confidence that the identified values are representative for the BO 105 derivatives.

4. COMPARISON OF RESULTS

In the preceeding two sections tests conducted with the rotor test stand and the BO 105 helicopter were discussed in detail. Before results obtained from these experiments are compared two of the main differences in the evaluation shall be briefly summarized:

- The wind tunnel tests were conducted with a model rotor only. A streamline body was used to cover the balance and boosters. Except of fuselage/rotor interference influences this body did not affect the rotor measurements. The derivative evaluation is based on steady state conditions. As forces and moments can be measured directly it is possible to determine each static and control derivative separately. A definition of a mathematical model is not necessary.
- For the system identification from helicopter flight test data dynamic tests are required as derivatives have to be extracted from the measurement of the helicopter motion. All unknown derivatives must be determined simultaneously which is only possible when an appropriate mathematical model is used.

Fig. 16 presents BO 105 static stability and control derivatives obtained from theoretical calculations (rotor only), rotor measurements in two different wind tunnels, and system identifications of the helicopter. To obtain the confidence level of the identification results various data runs were evaluated. Therefore the mean values and the standard deviations of the identified derivatives are shown. As the data basis for the 20 m/s speed condition momentarily is too small to allow a meaningful statistical evaluation only one representative result is given. In the following these results will be discussed in detail.

4.1 STATIC STABILITY DERIVATIVES

The Z_u derivative represents the change of the vertical force due to a longitudinal speed change. Its primary contributor is the main rotor. Based on rotor inflow mass and angle of attack considerations it can be visualized that Z_u in general is negative in the low speed range and becomes positive for higher speed. It can be seen that a satisfactory agreement between calculated, measured, and identified values was obtained. Differences in the wind tunnel results are mainly due to the high sensitivity of Z_u to angle of attack changes and different rotor inflow angles in the wind tunnels, as already shown in Fig. 5. In contrast to flight tests the calculation and measurements were conducted for constant angle of attack. This certainly caused deviations from the identified values.

The velocity stability derivative M_u has a stabilizing influence when it is positive which means a nose up response of the helicopter with increasing speed. The rotor gives a positive contribution whereas the fuselage normally produces a destabilizing moment. The calculated and wind tunnel values agree almost perfectly up to a speed of about 30 m/s. Tests showed that differences in the higher speed regime could be significantly reduced by slightly varying the cyclic pitch and the angle of attack. It indicates that the deviations may result from wind tunnel induced effects. This assumption is confirmed by the DNW measurements. The identified derivatives are almost independent from speed. This is in good agreement with calculated and wind tunnel results. However, they are smaller which may be due to the influence of the fuselage.

The Z_w derivative is related to the slope of the lift curve (Z_{α}). It is often referred to as vertical damping and has a negative sign. Its main contribution arises from the rotor. In general, it slightly increases with speed because of a decreasing influence of the induced flow. The comparison of the results shows some discrepancies. Daimler Benz wind tunnel measurements are in good agreement with the calculation whereas the identified values show the same tendency as the DNW measurements.

The M_w derivative is related to the angle of attack stability M_{α}. A positive sign indicates static instability. Contributions to M_w arise from the rotor, the fuselage and the tail as well as from fuselage/rotor aerodynamic interferences. A destabilizing tendency is produced by the rotor and the fuselage, whereas the horizontal tail provides a negative (stable) value. The comparison of calculated and wind tunnel results shows some discrepancies expecially in the low speed regime. The identified derivatives also increase with speed and show almost perfectly the same tendency as the calculated data. However, they are significantly smaller which results from the stabilizing influence of the horizontal tail and stabilizer. In addition, downwash interferences may also contribute to these differences.

4.2 CONTROL DERIVATIVES

The derivative $Z_{\theta s}$ characterizes changes in lift due to longitudinal cyclic pitch. It can be seen that the wind tunnel results and the calculated values agree satisfactorily. As the DNW measurements have a high confidence level it can be concluded that the deviations of the Daimler Benz wind tunnel measurements result from tunnel induced effects. As the $Z_{\theta s}$ derivative has only minor influence in the lift equation of the mathematical model it cannot be identified with sufficient accuracy.

The change in pitch moments due to longitudinal cyclic pitch is described by the $M_{\theta s}$ derivative. The comparison of calculated and wind tunnel results shows a satisfactory agreement although there are some deviations in the higher speed regime. Mainly for two reasons the identified derivatives are significantly smaller: (1) The BO 105 control inputs were measured at the stick. Influences of the dynamic characteristics of the helicopter hydraulic system were supposed to be negligible within the frequency range under consideration, and (2) the mathematical 6 DOF model is based on the assumption that there is an instantenous rotor tip path plane response due to control inputs and that the rotor reaches its new steady state immediately. It means that the influence of rotor dynamics is neglected which only can be justified by the high frequency response of the rotor in comparison to the relatively low rigid body frequencies.

The $Z_{\theta o}$ derivative is the main collective control derivative. Wind tunnel measurements and identified derivatives agree fairly well. The calculation yields slightly higher values which may be caused by inaccuracies in the rotor downwash model and uncertainties in the blade torsion modes used in the computation.

The change in pitch moments due to collective, the $M_{\theta o}$ derivative, increases with speed. There is a good agreement between measurements and calculation. The identified derivatives are smaller for the same reasons that were discussed above for the $M_{\theta s}$ derivative.

5. CONCLUSIONS

Two different experimental approaches to determine BO 105 helicopter flight mechanical characteristics were discussed: measurements on a model rotor in two different wind tunnels and the evaluation of flight test data by system identification techniques. For the model rotor scaling aspects, wind tunnel influences and derivative measurements were addressed. Parameter identification aspects were presented where emphasis was placed on input signal implementation and the verification of identification results.

Static stability and control derivatives obtained from wind tunnel measurements, identification, and theoretical calculations were compared. Basic differences in these approaches were discussed. When deviations arising from these differences are taken into account it can be stated that a satisfactory agreement could be obtained for most of the derivatives. This is in particular true for the force derivatives. Higher deviations for some identified moment derivatives from calculated and wind tunnel results indicate that future rotorcraft modeling for the identification must also include the rotor dynamics.

Future DFVLR research activities will be directed to further investigate and improve the transferability of model rotor results to the full-scale helicopter and to extend rotorcraft mathematical models by including rotor degrees of freedom. Based on the present experience it is expected that the identification technology will be helpful to determine model rotor dynamic derivatives and, on the other hand, the helicopter identification will benefit from the wind tunnel results by using them as additional information in the parameter estimation.

6. REFERENCES

1. Gmelin, B., "A Model for Wind Tunnel Rotorcraft Research - Model Design and Test Objectives - ", 2nd European Rotorcraft and Powered Lift Aircraft Forum, Bückeburg, Germany, 1976.
2. Derschmitt, H., Weiß, H., "Auslegung eines Modellrotorblattes für ein gelenkloses Rotormodell mit 4 m Durchmesser", MBB TN-D125-1/75, 1975
3. Heyson, H., "Rapid Estimation of Wind Tunnel Corrections with Application to Wind Tunnel and Model Design", NASA TN D-6416, 1971
4. Langer, H.-J., Grünhagen, W. von, "Comparison of Rotor Analysis Results with Aerodynamic Wind Tunnel Data", AGARD-CCP-334, London, 1982
5. Plaetschke, E., Mulder, J.A., Breeman, J.H., "Flight Test Results of Five Input Signals for Aircraft Parameter Identification", 6th IFAC Symposium on Identification and Parameter Estimation, Arlington Va., USA, June 1982
6. Kaletka, J., Rix, O., "Aspects of System Identification of Helicopters", 3rd European Rotorcraft and Powered Lift Aircraft Forum, Aix-en-Provence, France, September 1977
7. Hansen, R.S., "Toward a Better Understanding of Helicopter Stability Derivatives", Lichten Award Paper, 8th European Rotorcraft Forum, Aix-en-Provence, France, September 1982
8. Kaletka, J., "Rotorcraft Identification Experience", AGARD-LS-104, October 1979
9. Klein, V., "Identification Evaluation Methods", AGARD-LS-104, October 1979
10. Iliff, K.W., "Aircraft Identification Experience", AGARD-LS-104, October 1979

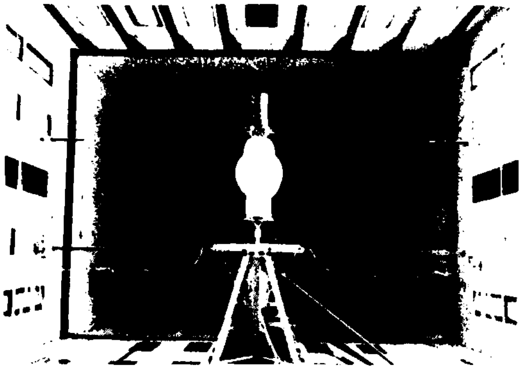

Fig. 1: Rotor test stand with BO 105 model rotor in the DNW wind tunnel

Fig. 2: DFVLR BO 105 research helicopter

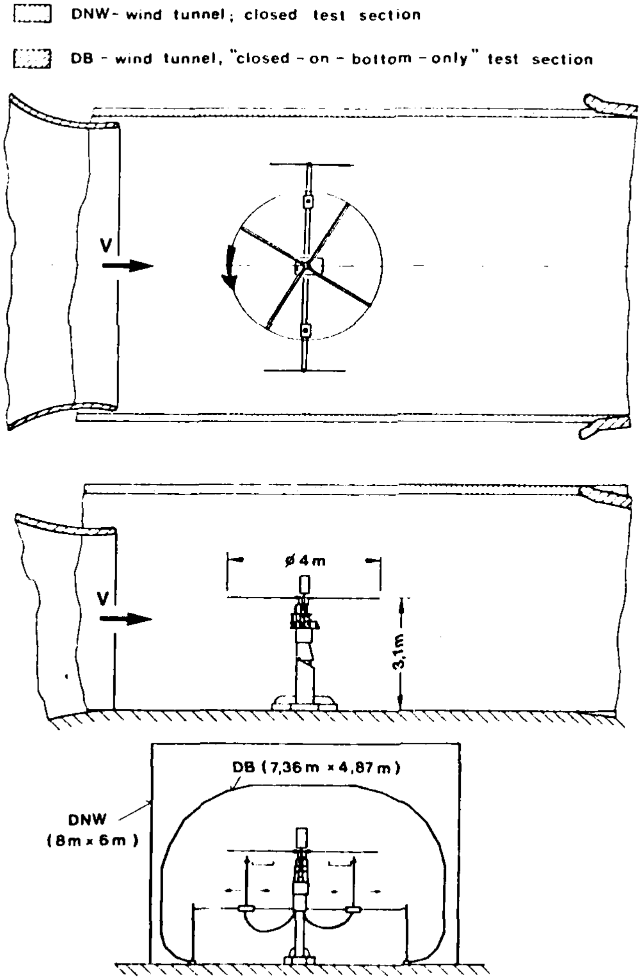
▭ DNW- wind tunnel; closed test section
▨ DB - wind tunnel, "closed - on - bottom - only" test section
V
V
ø 4m
3,1m
DB (7,36 m × 4,87 m)
DNW
(8m × 6m)

Fig. 3: Comparison of Daimler Benz (DB) and German-Netherlands (DNW) wind tunnel sizes

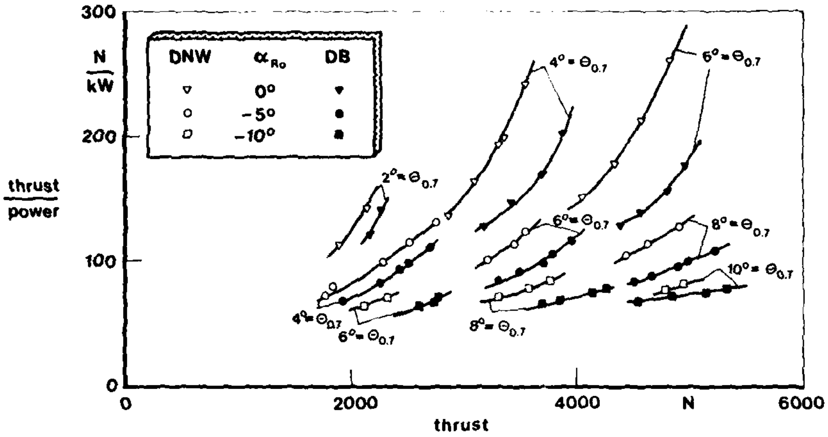

Fig. 4:

Thrust/Power ratio at different thrusts, measured in the DNW and DB wind tunnel ($2^{\circ} \leq \theta_{0,7} \leq 10^{\circ}$, $-4^{\circ} \leq \theta_{S} \leq 0^{\circ}$, $-10^{\circ} \leq \alpha_{Ro} \leq 0^{\circ}$)

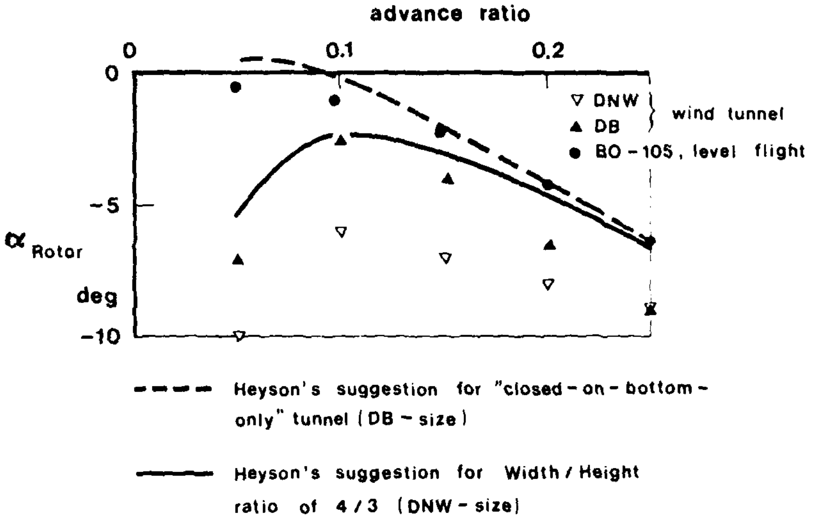

Fig. 5:

Angle of attack correction factors for the Daimler Benz (DB) and German-Netherlands (DNW) wind tunnel in comparison to Heyson's curves

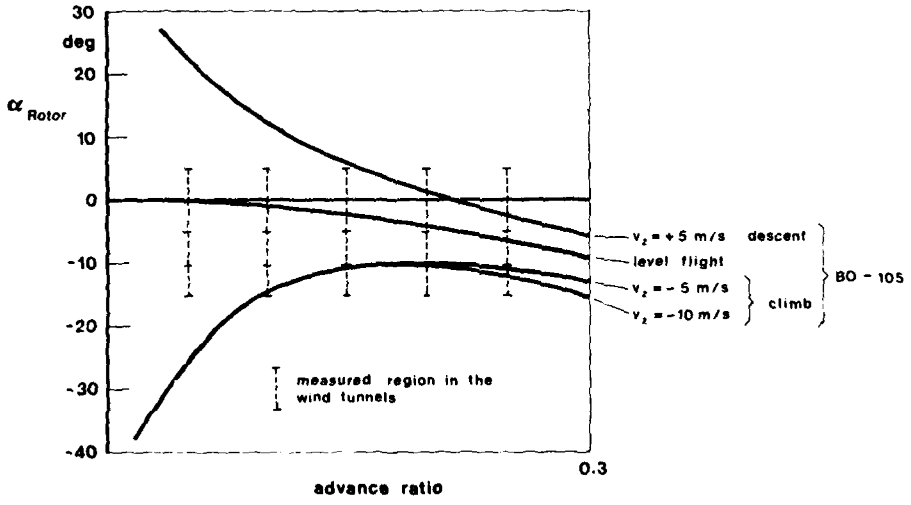

Fig. 6: Comparison of wind tunnel test regime and BO 105 flight regime

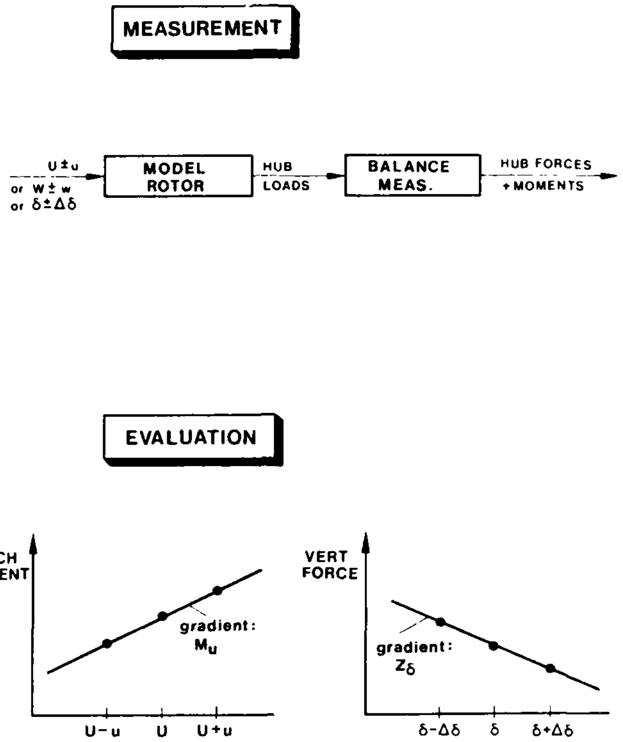
MEASUREMENT
U±u
or W±w
or δ±Δδ
MODEL ROTOR
HUB LOADS
BALANCE MEAS.
HUB FORCES +MOMENTS
EVALUATION
PITCH MOMENT
gradient: M_u
U−u
U
U+u
VERT FORCE
gradient: Z_δ
δ−Δδ
δ
δ+Δδ

Fig. 7: Principle of derivative evaluation from wind tunnel measurements

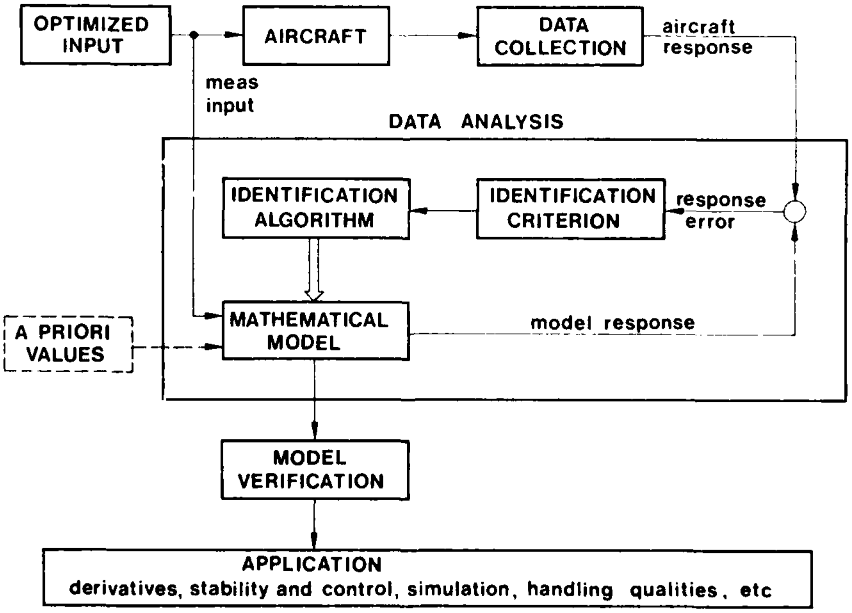
OPTIMIZED INPUT
AIRCRAFT
DATA COLLECTION
aircraft response
meas input
DATA ANALYSIS
IDENTIFICATION ALGORITHM
IDENTIFICATION CRITERION
response error
A PRIORI VALUES
MATHEMATICAL MODEL
model response
MODEL VERIFICATION
APPLICATION
derivatives, stability and control, simulation, handling qualities, etc

Fig. 8: System identification procedure

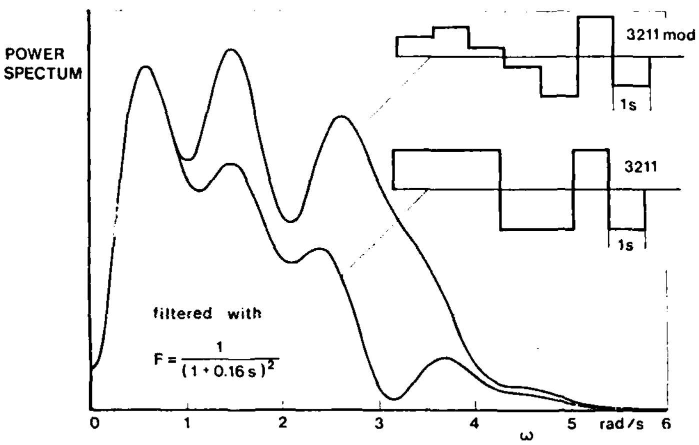

Fig. 9: Power spectra of DFVLR 3211 and modified 3211 input signals

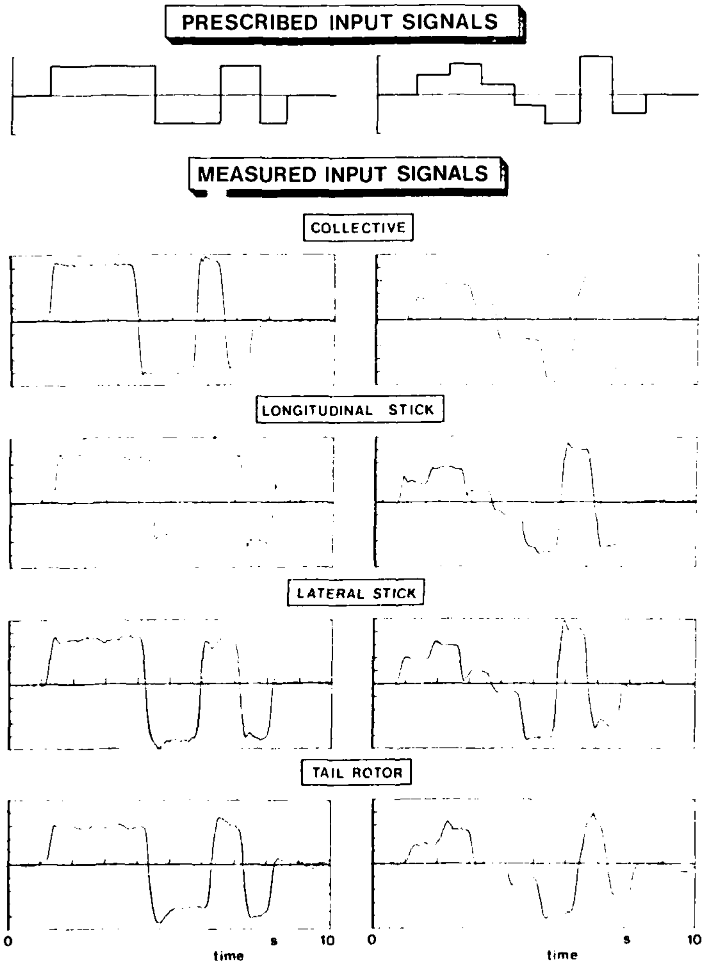

Fig. 11: Pilot implemented input signals

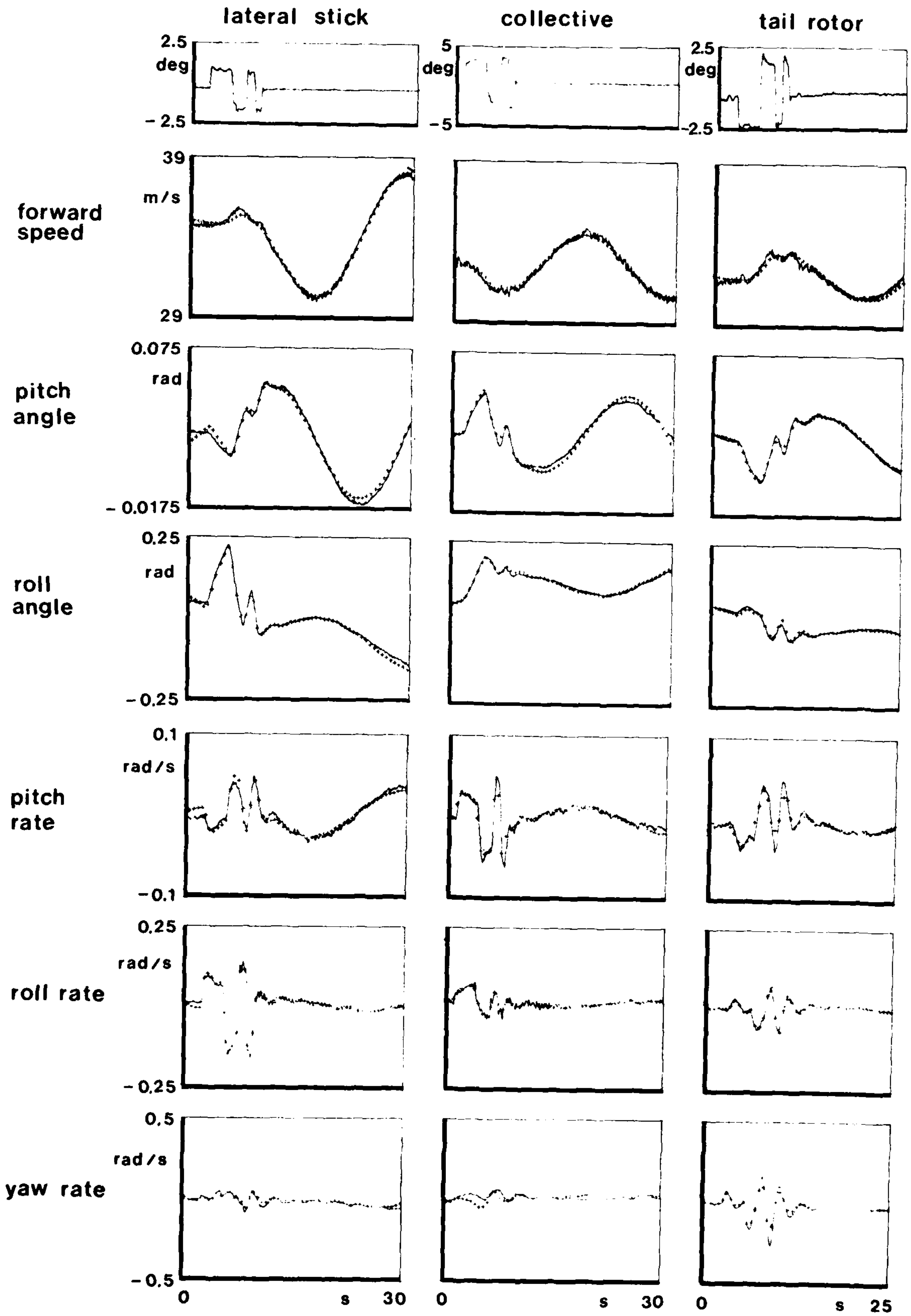

Fig. 12: Time history comparison of measured flight test data (-) and the identified model response (+++) (BO 105, [illegible] knots, level flight, [illegible] kg)

AD-A129 433 GROUND/FLIGHT TEST TECHNIQUES AND CORRELATION(U)
ADVISORY GROUP FOR AEROSPACE RESEARCH AND DEVELOPMENT
NEUILLY-SUR-SEINE (FRANCE) FEB 83 AGARD-CP-339

4/6

UNCLASSIFIED F/G 1/3 NL

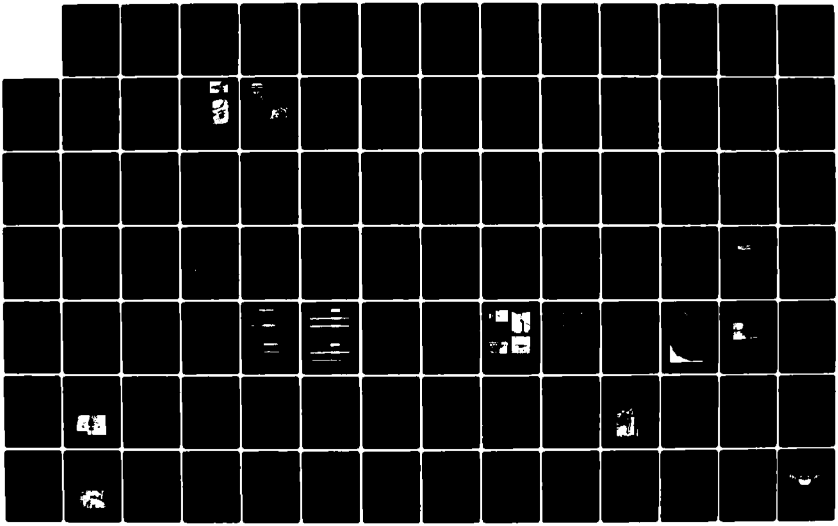

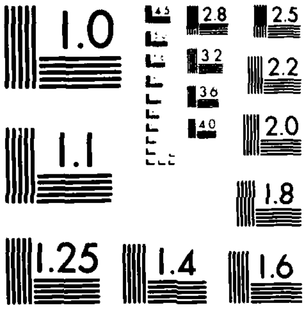
1.0
2.8
2.5
3.2
2.2
3.6
4.0
2.0
1.1
1.8
1.25
1.4
1.6

MICROCOPY RESOLUTION TEST CHART
NATIONAL BUREAU OF STANDARDS 1963-A

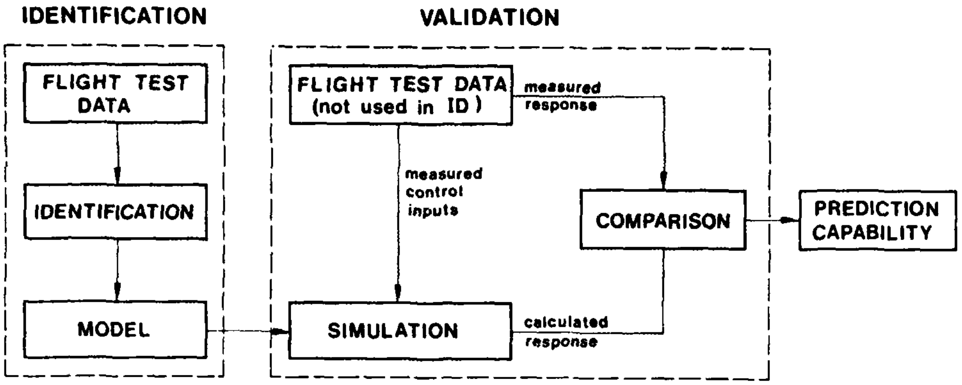
IDENTIFICATION
VALIDATION
FLIGHT TEST DATA
IDENTIFICATION
MODEL
FLIGHT TEST DATA (not used in ID)
measured response
measured control inputs
COMPARISON
PREDICTION CAPABILITY
SIMULATION
calculated response

Fig. 13: Principle of identified model verification

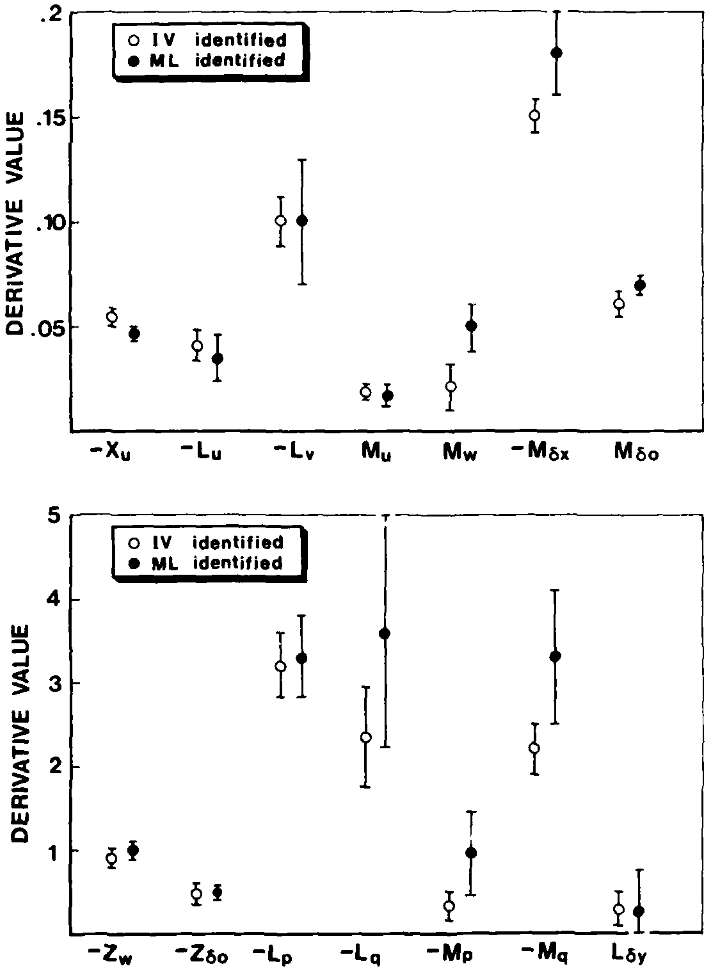

Fig. 14: Comparison of identified derivatives obtained from two different identification methods (BO 105, 80 knots, level flight, 2300 kg)

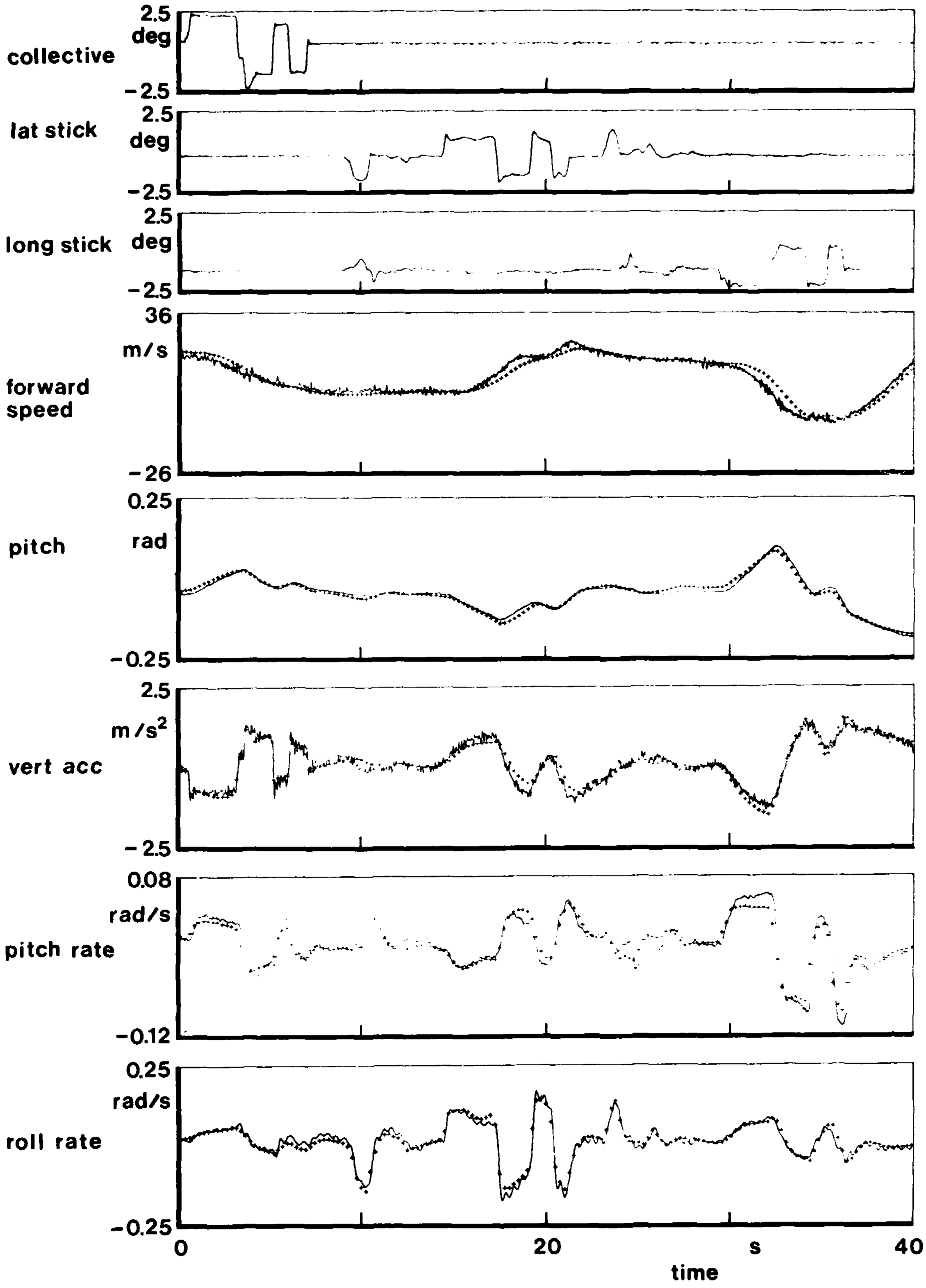

Fig. 15: Time history comparison of measured flight test data (-) and prediction of the identified model (+++). The identified model was evaluated from different flight test data (BO 105, 80 knots, level flight, 2300 kg)

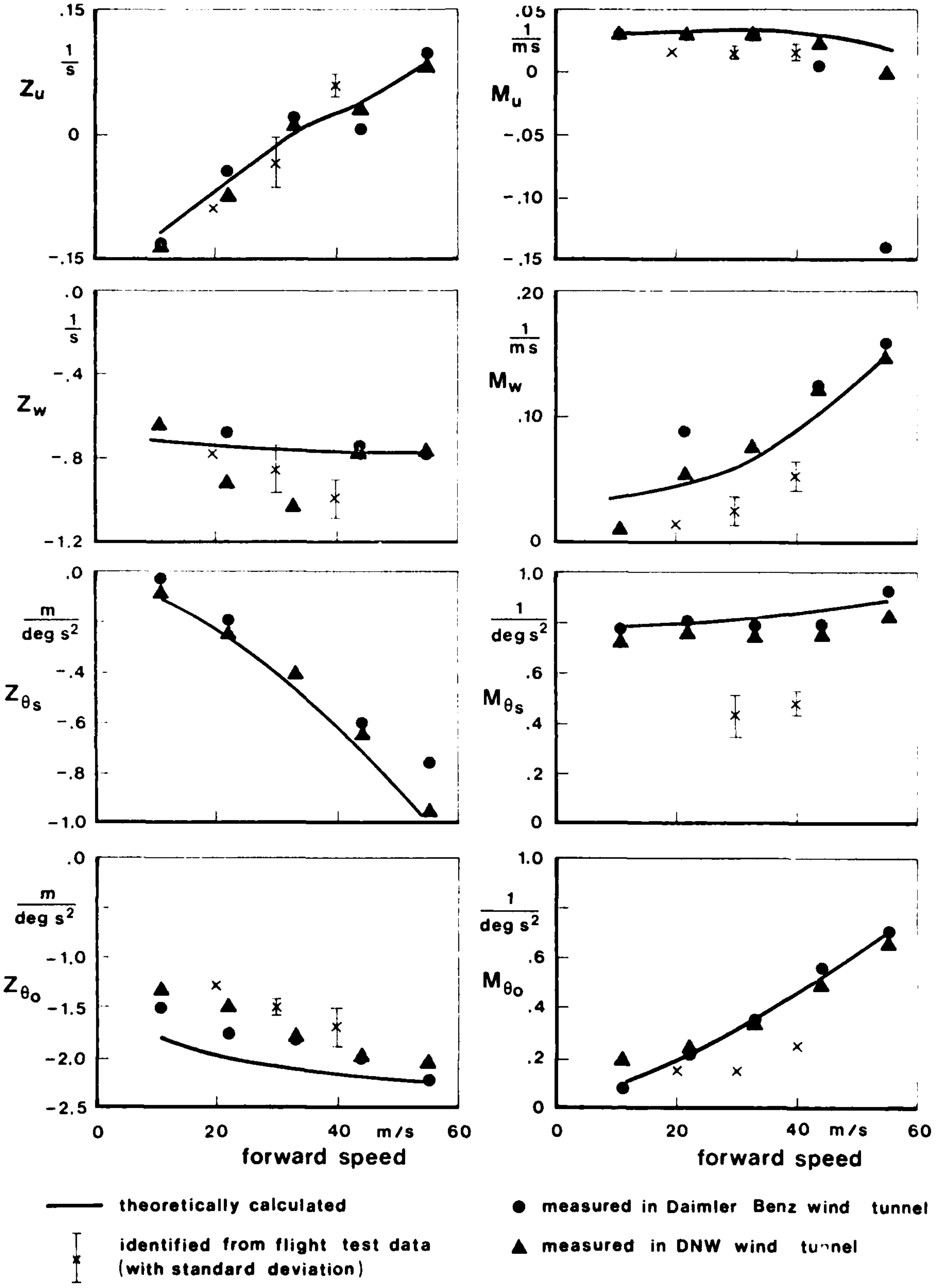

Fig. 16: Comparison of derivatives obtained from theoretical calculations, measurements in the Daimler Benz and German-Netherlands wind tunnels, and parameter identification from flight test data (BO 105, level flight, 2300 kg)

CORRELATION ASPECTS IN THE IDENTIFICATION OF DYNAMIC EFFECTS USING COMPLEMENTARY TECHNIQUES FLIGHT IN TURBULENCE - GUST ALLEVIATION

by

K. Wilhelm

Institut für Flugmechanik
Deutsche Forschungs- und Versuchsanstalt
für Luft- und Raumfahrt e.V. (DFVLR)
D 3300 Braunschweig-Flughafen, West Germany

and

R. Verbrugge

Institute de Mécanique des Fluides de Lille
F 59000 Lille, France

SUMMARY

This paper presents an overview of a common research program presently underway at DFVLR-Braunschweig (FRG) and IMF-Lille (France). The goals of this program are (1) the comparison of complementary techniques by correlating their results, and (2) the modeling of aerodynamic transient effects which must be considered for aircraft flying in turbulence situations in connection with a gust alleviation system.

The following techniques are applied in the program: theoretical prediction, static wind tunnel measurements, forced oscillation balance measurements, semi-free flight model tests (dynamic simulation in wind tunnel), catapult free-flight model tests, full-scale flight tests and system identification methods.

A brief description of the different facilities is given, advantages and special problems associated with the application of the different test techniques are shown. Test results are presented and compared.

Two alternate approaches for modeling aerodynamic transient effects are presented. The influence of the modeling of these effects on the efficiency of an open-loop gust alleviation system is shown.

1. INTRODUCTION

The increasing requirements imposed on aircraft performance and flight characteristics call for an extended use of automatic control systems by implementing active control systems. The use of active control technology however requires a detailed understanding of the influence of the anticipated external disturbances, aerodynamic characteristics and control system responses and requires considerable advances in the ability to describe and model such phenomena.

Active control systems can only be designed properly, if the mathematical models which represent the aircraft behaviour are accurate. While the estimation of *static* flight mechanics coefficients normally produces no difficulties, problems may arise in the experimental estimation of *dynamic* stability parameters. Even more difficult is the identification of those effects which are related to high frequency motions like in the case of flight in turbulence. These effects, called the *instationary aerodynamic transient effects*, can play an important role in the design of an active control system like a gust alleviation system.

2. SURVEY OF THE COMMON RESEARCH PROGRAM

Goal of Program

A common research program is underway at DFVLR-Braunschweig Research Center (Germany), and IMF-Lille (France). The research program has three goals:

(1) To compare the various ground test facilities by correlation of their results using an identical 1/8 scaled model of one specific aircraft in order to obtain more confidence in the results by involving several complementary test techniques and methods.

(2) To apply the system identification methods to different test techniques and to adjust these methods to the specific test technique.

(3) To come to a better understanding of dynamic effects which are important in conjunction with a gust alleviation system, i.e. modeling of the dynamic response due to quick acting flaps and high frequency gusts.

The present paper gives an overview of the different test facilities and the associated methods applied in this program and shows advantages and problems associated with the application of the different test techniques. Test results are presented and compared.

The program includes prediction method, stationary wind tunnel measurements, forced oscillation balance measurements, semi-free flight model tests (dynamic simulation in wind tunnels), catapult free-flight model tests, and full-scale flight tests. For all the ground tests a 1/8-scale model of the Do 28 was used. The model was realized in fiber material (glass and carbon) in order to represent rigid body conditions (first bending mode of wing is situated at 39 Hz).

Aircraft Configuration

The aircraft configuration used in the wind tunnel and flight tests is shown in Fig. 1. It is a Dornier Skyservant, which has been modified for use as a flying test bed for a new technology wing (TNT). The Do 28 TNT program is an application-oriented experimental development program sponsored by the German Federal Ministry of Research and Technology. The objective of the TNT-program is to design, engineer, build and test a representative wing for a twin-engine general aviation aircraft. As part of this program several types of gust alleviation system have been investigated and will be tested in the aircraft. Gust alleviation is of interest for small transport aircraft flying at medium altitudes where most of the turbulence is encountered. For these aircraft the improvement of passenger ride comfort is the main aim of gust alleviation.

3. BRIEF DESCRIPTION OF THE DIFFERENT FACILITIES AND TEST TECHNIQUES

Stationary Tests

A series of classical static wind tunnel tests were performed. These static wind tunnel test data formed the basis of all further investigations:

- provided the reference flight conditions,
- provided the necessary data for the simulation experiments,
- made possible advanced formulation of the test program.

Most of the static wind tunnel tests were performed in the DFVLR 3 m low speed wind tunnel in Braunschweig at a Reynolds number of $Re = 0.48 \cdot 10^6$. To investigate the Re-number effect measurements were also conducted at $Re = 0.26 \cdot 10^6$ and $Re = 1.18 \cdot 10^6$, but only minor Re-number effects were identified. To get confidence in the values different types of mountings were used for balance measurements, tests in open and closed test sections were performed. Fig. 2 shows as an example the Do 28 TNT model in the DFVLR wind tunnel.

The wind tunnel measurements at IMFL were conducted in a closed test section with a diameter of 2.4 m at $Re = 0.48 \cdot 10^6$. Additional, free-flight model tests were performed in the IMFL-laboratory catapult free-flight facility (see page 17A-4). These tests - realized with the same model and with the same Re-number - were permanent and stationary flights at different angle of attack and elevator deflection from which equilibrium conditions can be obtained. The test program had two goals (1) to define the reference flight conditions on which the various inputs could be superimposed for dynamic effects investigations and (2) to give additional information on the aerodynamic static characteristics.

On the basis of the USAF Stability and Control DATCOM (Ref. 1) some theoretical values were estimated.

Mobile Oscillatory Derivative Balance (MOD)

The technique of forced oscillation tests for the determination of the dynamic derivatives is well-known. In this technique an aircraft model is forced to oscillate at a constant amplitude and primarily in a single degree of freedom. That means the aerodynamic reaction only consistent with such a motion can be determined. There are various wind tunnel facilities currently available for such tests (Ref. 2). For the tests in various 3 m low speed wind tunnels in FRG a balance including data acquisition and evaluation system was constructed. Fig. 3 shows the principle of this so-called Mobile Oscillatory Derivative balance (MOD) (Ref. 3). The model is mounted on a moving head supported by a vertical strut. The oscillatory motion is induced by a mechanical drive system employing three geared driving motors, excentric discs and pushrods. Each motor is needed for a special motion. Maximum amplitude is $\pm 4^\circ$ for pitch, roll, yaw motion and $\pm$ 30 mm for heave motion. Frequency range is 0 to 3 Hz. The maximum angle of attack is about 35°, but this can be extended to about 50°, if the MOD is mounted on a special support. The reactions are measured by a five component internal strain-gauge balance.

Fig. 4 shows the model mounted on the MOD-balance in the DFVLR low speed wind tunnel.

The advantage of the MOD is the possibility of varying the reduced frequency and the amplitude independently.

However, two of the major problems encountered in performing captive-model dynamic experiments in wind tunnels also apply to the MOD:

(a) the inevitable interference associated with the suspension and its vibration,
(b) the inherent inability of any mechanical support to provide simulation of the unrestrained model motion.

Further, dynamic response investigations due to control inputs which are essential for active control technique are not possible.

All the effects of high frequency gust (gust length small in comparison to the aircraft length) cannot be investigated with the MOD-balance.

In the measurements, the wind tunnel speed was V = 28 to 50 m/s corresponding to a Reynolds number of $Re = 0.48 \cdot 10^6$ to $0.8 \cdot 10^6$. The reduced frequency range of the short period oscillation was $\omega_\alpha^* = 0.055$ to 0.096.

DFVLR-Installation for Dynamic Simulation in Wind Tunnels (DSW)

The installation for Dynamic Simulation in Wind Tunnels is an extension of a similar test technique, which is used for testing flutter-models but allows the simulation of a part of the rigid body motion.

The facility was designed for the estimation of the aircraft stability derivatives and for the testing of active control systems (Refs. 4, 5, 6). Within certain limitations, portions of the flight envelope can be simulated in the wind tunnel for a variety of aircraft. These constraints are given by the observance of the laws of similarity (Ref. 6) and by the limited freedom of movement in the wind tunnel. The installation for Dynamic Simulation consists of four main parts (Fig. 5):

- the suspension frame for the model
- the control/data processing station
- the gust generator system
- the model.

Suspension Frame

The suspension frame consists of a large tubular frame in combination with a vertical rod, which allows freedom of motion in pitch, yaw, heave and to some extent in roll. The frame surrounds the open test section of the 3 m-subsonic wind tunnel; the distance between frame and airflow is 0.5 m. The resonant frequency of the rod/frame system is about 14 Hz. This value is high enough to allow measurements up to frequencies of 10 Hz. The maximum pitch motion is ± 10 degrees, the model can heave ± 0.4 m.

A servo controlled vertical force generator can produce constant vertical forces independent of the model motion. This device is necessary due to the laws of similarity (Froude number) and in order to control the model in the airflow.

Control/Data Processing Station

The central control station is located in a container next to the test section. This container houses the model control devices, the measurement data processor, and various monitoring devices.

Gust Generator System

Two movable flaps are installed in the nozzle of the wind tunnel. They are driven by an electro-hydraulic actuator. This device allows a deflection of the airflow within the test section of up to 10 degrees. The gust generator can generate gusts in the frequency range from zero to 15 Hz. It is possible to generate various types of gust profiles, such as impulsive or stochastic gusts. The properties of the gust generator allow the simulation of a scaled stochastic gust field with a special characteristic (for example Dryden).

Model

The model (Fig. 6) is equipped with control surfaces (inner flaps, outer flaps, elevator) which are driven by fast acting servo actuators. Sensors such as accelerometers, rate gyros, pressure transducers, potentiometers for the control surfaces, various angle of attack probes are installed at different locations of the model to measure the motion and the disturbances. Power supply, control signals and measured data are transmitted to and from the model via cables.

The equation of the longitudinal motion of a suspended model in comparison with the equation of a free-flying model shows that due to the blockage of the x-degree of freedom the phugoid motion is fully suppressed. The short period mode, however, is not affected significantly because the corresponding terms in the equations are small. Figure 7 shows the Bode plot of the response of the suspended model and the free-flying model due to an elevator input (Ref. 7). There is good agreement between the motion of both models for frequencies equal or higher than the short period mode. In this frequency range good transferability of the results can be obtained. At frequencies lower than half the short period mode, the suppression of the phugoid mode results in major differences.

The Dynamic Simulation was performed at a Reynolds number of $Re = 0.48 \cdot 10^6$ corresponding to a wind tunnel speed of $V = 30$ m/s. This leads to a reduced frequency of the short period motion of $\omega^*_\alpha = 0.08$.

The wind tunnel experiments conducted show that due to the special suspension technique some additional influences exist which affect the movement of the model:

(1) The cables for data transmission to and from the model create small forces and moments which are dependent on the heave of the model (Ref. 8).

(2) Although it is outside the test section the large suspension frame produces a contraction of the airflow in the plane of the suspension frame, but leads to an expansion of the airflow behind the frame. This results in a gradient $\partial\alpha/\partial z$, which varies according to the position in the test section (Ref. 8).

(3) The two-dimensional gust field which is produced by the gust generator shows a non-linear propagation dependent on frequency and position (Ref. 9).

Thus the wind tunnel investigations began with extensive experiments for the identification of the model motion and all disturbing effects. The goal was to obtain a mathematical description which models all effects. Difficulties arose in arriving at a mathematical model of the gust field. But despite some deficiencies a good agreement now exists between the results of measured and computed gust field within the frequency range from 0.8 Hz to 5 Hz.

One of the main advantages of the DSW is the possibility of performing wind tunnel tests in a scaled turbulence field with various gust signals over an extended period of time and to perform parametric studies.

IMFL-Catapult Free Flight Model Tests (CFF)

The laboratory catapult free-flight model test technique has been developed in extension of similar techniques applied initially for spin research and based on free model tests in wind tunnel (Refs. 10, 11).

These techniques were especially developed to contribute in dynamic effects and unsteady phenomena investigations such as:

- dynamic stability parameter identification
- control efficiency
- gust effects (also ground effects)
- flight qualities studies integrating ACT concept.

The main specifications of the technique will be recalled here as far as they concern dynamic effect investigations. (More details can be found in Ref. 10).

Basically the test method is very simple:
Unpropelled models, dynamically scaled, are launched in free flight by means of a catapult system. The flight is performed over 50 meters in a laboratory and the model is recovered. A scheme of the facility is presented in Fig. 8. All initial conditions of the flight can be adjusted. The flights can be performed in still air including in board or ground based control loops. Gust generators can be introduced creating various gust profiles (intensity up to $\Delta\alpha_{gust} = 6^\circ$ and frequency range up to 15 Hz). An optical trajectography system delivers the coordinates of the CG and Euler angles during the flight. The accuracy is of .01 m on positions and $.05^\circ$ on angles. All the informations coming from in board transducers (accelerometers, gyro, pressure transducers ...) are transmitted to ground via PCM telemetry system (30 channels, word of 12 bytes, bandwidth of 250 Hz on each channel).

Fig. 9 shows the Do 28 TNT model in flight after crossing the vertical gust generator and the trajectory of optical reference points of the model. The free flight model was in Froude similarity.

The on board instrumentation for symmetric flights consisted of:

- accelerometers for longitudinal and vertical motion,
- pitch gyrometer,
- pressure probe situated on the nose for angle of attack and kinetic pressure measurements,
- actuators for symmetric deflection of the ailerons and horizontal tailplane,
- micro processor for a generation of predetermined control deflections and for open loop gust alleviation control laws,
- PCM-coder associated to telemetry system,
- opto-electronical system for speed and trajectography measurements.

The main characteristic of the equipment is the large bandwidth (pressure measurements: response to a step 15 ms, actuators 20 Hz with 30° phase angle for 5° amplitude ...).

For gust response tests the nature of the gust was chosen to be critical regarding to the penetration problem and the frequency range for alleviation. ($\Delta\alpha_{gust}$ from 3 to 5°, ΔT_{gust} = .1 sec so the gust length is about 1.5 length of the aircraft, impulsive type). The advantage of the test method is that the gust profile is well-known because generated by a closed-loop wind tunnel and the speed distribution of the gust can be easily adjusted and controlled.

On this aspect needs for complementary tests arise mainly because no harmonic or stochastic gust inputs can be created and actually only short gusts can be generated.

Some specific aspects of the CFF are shown in Fig. 10.

Full-Scale Flight Tests (FSA)

The full-scale flight tests were performed by the Dornier company with the Do 28 TNT experimental aircraft. Fig. 11 shows a picture of this aircraft. The aircraft was equipped with an instrumentation system permitting the measurement of all parameters necessary for system identification and some additional redundant parameters. The flight test program consisted of flights at different reference flight conditions. Different types of elevator inputs were used to excite the aircraft longitudinal motion.

System Identification Technique (SI)

To get detailed information about the dynamic behaviour, system identification techniques were applied extensively to the dynamic tests (DSW, CFF, FSA). More than other techniques, system identification provides the basis for flight/ground testing correlation by extracting as much information as possible from subscale dynamic wind tunnel investigations and full-scale free flight tests.

System identification includes the following three essential elements (see Fig. 12, Ref. 12):

(1) Proper input signals:
The input signals must excite all of the aircraft response modes. They have to be optimized to achieve accurate identifications.

(2) Adequate instrumentation:
This covers the entire data acquisition process and takes into account the effect of measurement noise and sensor dynamics. The extracted derivatives are a direct function of the accuracy of the instrumentation system.

(3) Identification procedure:
This describes the analysis of flight test data and includes
- the mathematical model of the dynamic behaviour of the aircraft,
- the iterative computational algorithm to minimize the response error and to identify the derivatives.

Detailed investigations were made to ensure compliance with all of these requirements.

Two methods of SI were applied.

(1) At DFVLR a maximum likelihood estimation method was used to determine the stability, control and dynamic derivatives from dynamic flight tests. The method used is an iterative technique that minimizes a weighted function of the difference between the aircraft's measured and computed response by adjusting the derivative values used in calculating the computed response. A modified Newton-Raphson method is used to attain the minimizations. After each iteration step, the weight factors are automatically updated according to the resulting output errors. The method also takes into account an unknown constant shift in each equation and for each measurement (bias). This method is described in Ref. 13. In addition this method provides uncertainty levels associated with each derivative. Uncertainty levels are proportional to the approximation of the Cramer-Rao bounds and are analogues to standard deviations of the estimated derivatives. The larger the uncertainty level, the greater is the uncertainty in the estimated derivative.

(2) At IMFL a conjugated gradient method is used to minimize the cost function in the identification algorithm. The cost function is calculated on the basis of weighted state vector components and its derivatives. Up to now no bias terms are introduced in the differential and observation equations which could be identified in the same process but could lead to some numerical difficulties if considering several flights all together in one identification run. The method doesn't give confidence level estimation on the identified parameters. To supply to this deficiency sensitivity tests were performed to define for any iteration, for any flight and unknown parameter the contribution to the gradient and each flight contribution to the cost function (s. Refs. 14, 15).

4. RESULTS AND DISCUSSION

An overview of the tests which were performed and the methods which were applied in the program is given in Fig. 13. This figure shows that, beside theoretical prediction, a series of static wind tunnel measurements were performed. The dynamic tests include semi- and free-flight model tests and full-scale flight tests.

Static Measurements

Classic static wind tunnel tests were performed. In this test program different mounting systems and test sections were used. DFVLR: open test section (wire mounting, vertical sting mounting), closed test section (vertical sting mounting). IMFL: closed test section (profiled pylons).

A comparison of the results of the different wind tunnel measurements shows a good agreement. As an example, C_{m_α} and C_{Z_α} are presented in Fig. 14. The small differences which occur in the slope may be due to the fact that the model was slightly changed during the different project steps. On the other hand, there are some small influences of the different mounting systems and of the different kind of test sections.

Some small discrepancy is observed on C_{mo} ($\Delta C_{mo} = 0.025$) which can be introduced by support effects, too.

To validate in another way the static wind tunnel measurements permanent free-flight tests were performed with the same model and Reynolds number. The main observations are:

- The trim conditions for equilibrium flights are slightly shifted (max value $\Delta\delta_e = .25^\circ$) mainly due to C_{mo} definition.
- The gain on $\Delta\alpha/\Delta\delta_e$ for equilibrium flights is quite similar for the free-flight and for the wind tunnel (1.8). A good confidence on C_{m_α} and $C_{m_{\delta e}}$ can be observed in this range of angle of attack taking into account some nonlinearities particularly in C_{m_α} characteristic.
- The wind tunnels drag measurements differ with a maximum of 1 % of C_{X_O}. C_{X_α} is in good agreement. From the free-flight the drag obtained has an intermediate value between the tunnel results.

In total, the results show that the confidence level of the values of the different wind tunnels is good and that the classical wind tunnel correction programs applied to each facility worked efficiently. Comparison with the theoretically obtained values shows that for a classical aircraft configuration the prediction is satisfactory.

Dynamic Tests

To get the usual set of derivatives including stability derivatives, control derivatives and dynamic derivatives, various complementary techniques were developed and applied. The techniques combine dynamic tests in different facilities with specific evaluation procedures:

(1) *Optimization of the test program* researching the most sensitive inputs for the determination of the dynamic terms,

(2) *Dynamic tests* performed in wind tunnels (MOD and Dynamic Simulation in Wind Tunnel), in laboratory (Catapult/Free Flight Tests) and on the real aircraft,

(3) *Extensive use of system identification technique.*

(1) Optimization of the test program

The importance of adequate design of flight test maneuvers for system identification purposes is well recognized (Ref. 16). The reliability of aircraft parameter extraction from dynamic test maneuvers depends heavily on the amount of information available in the response. Therefore, the shapes of the control inputs should be chosen such that they excite the aircraft dynamics as much as possible in the frequency region of interest.

For the determination of optimal input signals a procedure was applied which uses the Bode plot of the frequency responses (Ref. 17). In this procedure the magnitude of the frequency responses multiplied by the corresponding equation coefficient is plotted. For the Catapult Free-Flight tests in Fig. 15 the dependency of the terms of the pitching moment and vertical acceleration equations on the frequency is shown. If an input signal is introduced with a definite frequency, only these coefficients can be determined which have an essential influence at this frequency. Fig. 15 shows that for lower frequencies of the δ_e, δ_a-input the inertia term is of small importance. This leads to the fact that only ratios of coefficients can be determined in that frequency range. For high frequencies the α, q-terms are small compared with the other terms of the equation and therefore not identifiable.

In Fig. 16 the required frequency ranges of the input signals for the determination of a specific set of derivatives are shown. In these frequency ranges the magnitude of the coefficient term is not smaller than 10 % of the maximum term of the equation.

It can be seen that the best frequency for identifying the α, q, δ_e, δ_a derivatives is the short period oscillation frequency ($\sim$ 1 Hz). To identify instationary effects (derivatives due to flap deflections rate) input signals are necessary with frequencies higher than approximately 5 Hz.

Because a narrow band input is not sufficient for identifying more than two derivatives of the pitch equation a signal with a broad bandwidth (3-2-1-1-signal) was used in the tests. In both the dynamic simulation in wind tunnel and in free-flight tests (model and full-scale) the time-scaling of the input was defined in such a way that the maximum of the input power spectrum was located near the short period oscillation frequency.

(2) Dynamic Test Program

Fig. 17 gives an overview of the tests performed with the three facilities, i.e. the input types, the actuated controls and the measured parameters. It can be seen that in the DSW, in addition to the inputs to the three control surfaces (elevator, outer flaps, inner flaps) a vertical force input could be given using the weight compensation system. Also, well-known scaled gusts (harmonic, deterministic, stochastic) were applied.

In the CFF inputs were given to elevator and outer flaps. Also impulsive-type gusts could be generated which were well defined and exact measured.

In the flight test program with the full-scale aircraft only the elevator could be used to excite the aircraft motion. This resulted in a reduction in the information content and, therefore, a somewhat greater uncertainty in the determination of the z-derivative.

(3) System identification

For the data evaluation and the correlation of the results two approaches were used (Fig. 18).

The *first* approach starts from measurements of different dynamic test facilities and applies one identification method to the data from the different measurements. By using this approach it is possible to prevent, in the comparison, method specific effects from influencing the correlation aspects. The approach used was to apply the DFVLR-system identification method to the measurements of the Dynamic Simulation in Wind Tunnel, the Catapult Free-Flight Tests and the Full-Scale Aircraft Flight Tests.

In the identification process, nonlinearities have to be taken into account because the aerodynamics of the Do 28 TNT show some nonlinearities when considered over a range of angle of attack. For example, the pitching moment coefficient C_m as a function of α is quite nonlinear which can be seen on the derivative $C_{m\alpha}$ in Fig. 14.

In the DFVLR system identification method the nonlinear behaviour has been approximated by segments about the reference point where C_m is locally linearized over α. Because the flight tests were conducted in a certain region of angle of attack about the reference point this dependency on α has been taken into account in the identification procedure.

The results of the identification of the different measurements using the same identification method are presented in Fig. 19, 20 (No. 5, 6, 7). It can be seen that the overall agreement of the estimated values is good.

The identification results based on the DSW measurements show a generally higher degree of standard deviation in comparison with the results based on the CFF and FSA measurements. This can be attributed to the relatively high turbulence occuring in the wind tunnel. This turbulence is interpreted in the system identification algorithm as an additional measurement noise which leads to this higher values of standard deviation. By comparison, both the CFF and FSA measurements were performed in calm atmosphere.

In Fig. 19 it can be seen that the identification results for the FSA in the case of small values of angle-of-attack, corresponding to high speed, exhibit a high discrepancy in $C_{m\alpha}$ in comparison to all other wind tunnel and free flight model tests. Normally the identification values of the derivatives would overlap for segments of similar angle of attack. These discrepancies which only occur in the FSA measurements may have their cause in speed dependent aeroelastic effects due to fuselage bending. Another cause for these discrepancies may be the thrust influence. To investigate this influence additional wind tunnel measurements with model engines were performed. But in these measurements only minor thrust influences could be identified. It should be mentioned, however, that only the propeller diameter and the thrust coefficient were modeled. This effect has not yet been clarified and will be analyzed in the future.

It can be seen from Fig. 19/20 that the DSW can lead to values comparable with free-flight model tests though it is a semi-flight facility. Thus the influence of the model suspension (cable, rod, frame ...) on the aerodynamics is relatively small if a proper mathematical model of this influence has been integrated in the evaluation process and the identification method. In addition, the comparison shows that the blockage of the x-degree of freedom has only minor effects on the determination of the z and M derivatives.

A simpler mathematical model can be used in the evaluation of the measurements obtained in the CFF because there are no suspension effects. The mathematical model includes also the x-derivatives.

In the FSA tests only inputs to the elevator could be given. Therefore, no derivatives due to flap deflection could be estimated from these flight tests. This also reduces the information content with respect to the z-derivatives. Nevertheless, these measurements yielded relatively small standard deviations. This can be attributed to the long measurement time in comparison to the DSW and CFF (5 times that of CFF) which could be used in the identification process. This leads to an overall reduction in the computed standard deviation.

A principal source of inaccuracy in identifying aircraft parameters is the error in the flight test instrumentation and data reduction. The system identification accuracy is highly dependent on the quality of the measured data. Because all measurements were obtained with different instrumentation systems, extensive redundancy calculations for the measured signals of all instrumentation systems were performed to improve the confidence level of the measurements. From this, a corrected set of signals was computed and then applied to the identification process.

The *second* data evaluation approach begins with the measurement of only one facility and applies different identification algorithms to these data. This approach was done using the CFF tests and applying both DFVLR and IMFL system identification methods to these measurements. This can show specific effects and yields information about the performance of the system identification methods used.

The results of this approach can be seen in Fig. 19 and in Fig. 20 No. 7 and 8. No uncertainty levels could be given in the results of No. 8 due to the identification method used. Although the overall agreement is quite good some differences occur. To try to give reasons for the differences in the estimated values it should be mentioned that

(1) the IMFL mathematical model - as it was used in the program - does not take into account the nonlinearities in the aerodynamic characteristics which are observed for this aircraft,

(2) the IMFL identification procedure does not include an automatic weighting optimization algorithm of the state vector,

(3) no bias terms are introduced in the differential and observation equations.

This can lead to some different values, which in particular occur in the values which only have low importance, for example ($C_{zq} + C_{z\dot{\alpha}}$).

From the *MOD-balance* measurements, stability parameters were determined which lie within the limits of the static wind tunnel measurements and the dynamic tests (see Fig. 19). The somewhat higher value of $C_{m\alpha}$ may be attributed to the relatively thick vertical sting which has a small influence on the pitching moment behaviour. The dynamic derivatives can also be determined within the limits of the values of the other dynamic measurements (Fig. 20). Thus the MOD-balance measurements show that it is possible to determine reproducable dynamic derivatives with a relatively high confidence level. This can also be seen from the deviations of each individual measurement within one test run.

It is important to note that, similar to the other dynamic measurements, a separate determination of the dynamic pitch and heave derivatives is not possible. To demonstrate this situation some calculations have been made to show the degree of measurement error in the instationary force of the MOD-balance (Fig. 21). It can be seen that in the longitudinal motion the dynamic derivatives due to pitching can be measured accurately. The derivatives due to heave motion are not measurable because of their low importance in the instationary force.

5. AERODYNAMIC TRANSIENT EFFECTS

Problems to be considered for transport aircraft flying in turbulent situations in connection with a gust alleviation system are

(1) the modeling of the influence of high frequency control inputs used for gust alleviation,

(2) the measurement of the gust and, in particular, the modeling of the influence of short length gusts including penetration effects,

(3) the design and optimization of gust alleviation control laws using mathematical modeling.

All three areas were investigated in the program using both facilities the DSW and the CFF in a complementary manner.

(1) Modeling the non-steady downwash effect due to quick acting flaps

For the description of the aircraft behaviour, a linear mathematical model is normally used. This model takes into account only the effect of relatively low frequency changes of lift on the downwash at the elevator. Such a model does not take into account aerodynamic dependent phenomena. For high frequency flap inputs, required for gust alleviation system (GAS), this mathematical model is not applicable. This can be seen in a comparison of the identification results with measurements obtained from the DSW. Discrepancies occur in the response of the wind tunnel model and the computer model (see left side of Fig. 22) which are particularly evident in a time shift of the pitching motion. The reason for this is the nonstationary wing-tail interference: the variation in the flap position produces a variation in the lift on the wing and in this way a somewhat delayed onset in change of pitching moment as a result of the downwash variation on the elevator. Thus, an additional pitching moment occurs directly after the adjustment of the flap until the new stationary downwash is established on the elevator. The angle of attack change on the elevator due to flap deflection δ is a function of wing lift coefficient C_{Lw}

$$\Delta\alpha_e = \frac{\partial\alpha_e}{\partial C_{Lw}} C_{L\delta}\,\delta\,(t - t_L)$$

with t_L denotes the time required for the flow to travel from the wing to the elevator.

The relative error of the normal linearization by Taylor's series of first order for $\delta\,(t - t_L)$ will exceed 10 % if $\omega > 0.45 / t_L$. The flight tests were performed with a model with a distance from wing to tailplane of about 1 m and a speed of 30 m/sec which leads to $t_L = 0.033$ sec and $f_{Limit} = 2.2$ Hz. As the total flap movement took place within 1/60 sec the frequency of the flap actuation was so high that the Taylor's series expansion is not applicable here.

To avoid the discrepancy in modeling of quick flow changes, a new mathematical model was introduced (Ref. 18): In this model the steady values were separated from the non-steady values. The steady values proportional to $\delta(t)$ are already contained in the stationary derivatives. The non-stationary contributions were introduced by the differential signal

$$\delta_{LAG} = \delta(t) - \delta(t - t_L)$$

and the non-stationary flap derivatives $C_{L\delta LAG}$ and $C_{m\delta LAG}$. The use of this model, which takes the time lag of the downwash on the elevator into account, leads to a better curve fit in the pitching motion between measured and computed data as can be seen on the right side of Fig. 22.

(2) Modeling the Gust Response

The preceding section has shown that the description of the aircraft behaviour in the case of quick flow changes due to high frequency flap inputs by using only global derivatives is not sufficient. This is true in particular for the determination of the interaction of short gusts with the airframe. It is necessary to separate the effect into several components which produce a delayed influence on the major aerodynamic surfaces.

Two approaches for modeling such phenomena have been investigated.

The *first approach* (DFVLR), which was also used for the modeling of the non-steady downwash effect due to quick acting flaps, is based on the assumption that the entire aircraft is located in a stationary gust. The effect of the variation in turbulence along the aircraft will be described by additional dynamic correction factors. These are determined by the differences in turbulence angle of attack measurements on the forward fuselage, wing and horizontal tail (Refs. 8, 19). These terms become significant only at higher turbulence frequencies (shorter turbulence wave lengths).

Some results of system identification using this approach are presented in Fig. 23 and 24. Fig. 23a shows the results for the case where no time-shift was taken into account. Large discrepancies occur in both the heave and the pitching motion. As a first approximation, the delayed interaction of the measured gust on the wing was taken into account (Fig. 23b). The results show a better curve fit only in the heave motion. Taking the total time-shift of the measured gust signal into account, an overall good curve fit is received (Fig. 23c). In Figure 24 the influence of the different model structures on the estimated derivatives and the cost function of the system identification algorithm is presented. It can be seen that both the uncertainty level and the value of the cost function is reduced when changing from model A to model C.

In the *second approach* for the modeling of the gust response (IMFL), the effect of the turbulence is calculated separately for three positions on the aircraft (forward fuselage, wing, horizontal tail) from the local angles of attack and their derivatives. As a result, in contrast to the first method, it is necessary to superimpose the contributions from several positions even when turbulence along the aircraft is constant (Refs. 20, 21).

This approach is illustrated in Fig. 25 showing three segments of the aircraft with their local parameters and an example of the time histories of local angle of attack.

For each element, local state variables are defined at a reference point, taking into account aircraft motion, gust input and interactions such as wing to tailplane, and dynamic effects.

From the local state variables, three local contributions to the aerodynamic forces and moments are determined and introduced in the matrices A and C. This part of the model must be in accordance with the behaviour of the aircraft described by the global representative model (without gusts).

For the three elements, gust terms are introduced separately, considering $\Delta\alpha_{gust}$ and $\Delta\dot{\alpha}_{gust}$ vectors associated to the matrices D and E.

A control input vector is defined, taking into account time shifts for wing to tailplane interactions for aileron deflection and associating specific free flight inputs as steps in $\ddot{z}$ due to change of mass (Δm) and $\dot{q}$ due to change of c.g. position (Δx).

- For practical application a three element model needs more information about the aerodynamic characteristics of the separate elements. For this purpose, specific static wind tunnel tests were performed on these elements, separately or in combined configurations, in order to identify their individual characteristics and the interactions effects. The tests were performed in the IMFL horizontal wind tunnel. Global longitudinal characteristic measurements on the elements where associated to measurements on the tailplane through a local two components strain-gauges balance.

  From these characteristics (shown in Fig. 26) static coefficients and local derivatives were extracted and wing-fuselage / wing-tailplane interference was modeled.

- An example of Do 28 TNT gust test results compared with simulation results with the three elements mathematical model is given in Fig. 27 (left side).

  The gust is a short impulse of ΔT = .1 s, introducing significant frequencies up to 10 Hz. For comparison, the global math. model gives in this case a completely wrong solution (see q time history).

  In the second part of the figure an example is shown comparing simulation results of the three elements model and the global model (without gusts) to verify the identity of both models for the case without gusts and flap input.

- Some improvements will be added in the future, particularly concerning the choice of the reference points for each element and the direct identification of the aerodynamic characteristics from gust response tests.

(3) Gust Alleviation System

Gust alleviation is of interest for small transport aircraft flying at medium altitudes where most turbulence is encountered. For these aircraft the improvement of passenger ride comfort during cruise is the main aim of gust alleviation. For the Do 28 TNT the DFVLR chose an open loop system. This system has the advantage that the time which the gust needs to pass the distance from the angle of attack sensor to the major surfaces of the airframe can be used to compensate the actuator lag. Fig. 28 (Ref. 22) shows a block diagram of the open loop gust alleviation system.

The investigations in the DSW have shown that the efficiency of such a system is influenced by the gust angle of attack measurement and, in particular, by the complicated interaction of downwashes, dead-times, actuator lags, sensor positions and unsteady aerodynamic transient effects. This means that an optimized realization is only possible if the dynamic effects are fully understood and if they can be modeled properly.

In the following example, the influence of the modeling of the dynamic effects on the efficiency of an open loop gust alleviation system (OLGA) is shown.

Referring to the block diagram in Fig. 28, in the first case the computed gust signal was fed directly to the control surface actuators. No time shift of the measured gust signal and its influence on the dynamic reaction was taken into account. This case corresponds to model A in Fig. 23a and Fig. 24. Fig. 29 shows the efficiency of the OLGA. In this figure the frequency response measurements of the vertical acceleration due to gust inputs are plotted without OLGA and with OLGA engaged but using various aerodynamic models. It can be seen that the OLGA without considering a time shift leads to a 10 dB reduction of the acceleration amplitude for frequencies near the short period frequency. At higher gust frequencies, however, this type of OLGA begins to destabilize the model motion. The OLGA capability is rather limited because the phase conditions are not satisfied.

In the second case both the delayed interaction of the gust on the wing and the elevator and the delayed onset in change of the downwash on the elevator due to the quick acting flaps were taken into account. Fig. 29 shows that in this case, which corresponds to model C, the efficiency of the OLGA can be improved.

Fig. 30 shows the response of the model flying in a scaled gust field in the DSW. It can be seen that in the first case the plot shows a reduction of the vertical acceleration, while the pitching acceleration remains nearly unchanged. Using the model C for the design of the OLGA the efficiency of the system is significantly better.

6. CONCLUSIONS

A common research program is underway at IMFL and DFVLR. This program includes the application of complementary ground test facilities and methods.

In this paper the results obtained with the different techniques were compared and system identification aspects were presented. Two alternate approaches for modeling aerodynamic transient effects were given. The effect of modeling on an open loop gust alleviation system was discussed.

Although further analysis of the experimental data is required the following conclusions can be drawn:

(1) Each technique applied in the program has special advantages and problems. The combination of test results of complementary techniques makes it possible to identify and to compensate problem areas in each technique. The obtained results can be confirmed and the techniques can be improved.

(2) The possibilities of undertaking investigations in special research areas are gr improved through the availability of test data on complementary facilities.

(3) It is difficult to compare the results of different techniques, because each facility has specific influences which have to be included in the respective mathematical model. Failure to model these facility-specific effects can lead to differences in the derivatives.

(4) The results were influenced, in addition, by the evaluation method applied to the measurements, i.e. by the identification algorithm, by the weighting of the measured signals, by the choice of the time history.

(5) Even when the comparison of the results from the ground facilities is satisfactory, the correlation of these results to the full-scale aircraft remains problematic. It is therefore necessary to identify which additional effects are present in the behaviour of the full-scale aircraft and to integrate these effects in the mathematical model.

(6) For the investigation of aerodynamic transient effects, dynamic measurements under reproducable conditions are necessary (i.e. dynamic model tests in wind tunnels or laboratories). The determination of these effects is possible only if system identification techniques are applied to the measurements.

(7) The choice of suitable input signals is important for the performance of successful system identification.

(8) An ACT-system, such as an open-loop gust alleviation system, is very sensitive to incorrect modeling of the aircraft behaviour. An optimized realization of such a system is only possible if the dynamic effects can be modeled properly.

(9) In the case of sudden flow changes due to short length gusts or high frequency flap inputs, the description of the aircraft behaviour by using only global derivatives is not sufficient. It is necessary to separate the effect into several components which produce a delayed influence on the major aerodynamic surfaces.

(10) The two approaches for modeling aerodynamic transient effects have shown that they can lead to a good description of the non-stationary effects.

(11) Future research activities with regard to modeling aerodynamic transient effects will be directed toward:

   (1) further investigation of the two approaches to modeling aircraft gust response.

   (2) exact determination of gust inputs from flight test measurements.

7. REFERENCES

1. Hoak, D.E., Ellison, D.E., "USAF Stability and Control Datcom", McDonnell Douglas Corporation, 1960, Revised 1969.

2. Orlik-Rückemann, K., "Review of Techniques for Determination of Dynamic Stability Parameters in Wind Tunnels", AGARD-LS-114, 1981.

3. Hafer, X., "Wind Tunnel Testing of Dynamic Derivatives in West Germany", AGARD-FDP-Symposium on Dynamic Stability Parameters, Paper 5, 1978.

4. Subke, H., Krag, B., "Dynamic Simulation in Wind Tunnels, Part II", AGARD-CP-187, 1975.

5. Hamel, P., Krag, B., "Dynamic Wind Tunnel Simulation of Active Control Systems", AGARD-CP-260, 1978.

6. Wilhelm, K., Gmelin, B., "DFVLR-Dynamic Model Testing in Wind Tunnels for Active Controls Research", 12. ICAS Congress, Munich 1980.

7. Subke, H., "Test Installation to Investigate the Dynamic Behaviour of Aircraft with Scaled Models in Wind Tunnels", Symposium on Dynamic Analysis of Vehicle Ride and Manoeuvering Characteristics, London, 1978.

8. Rohlf, D., "Bewegungsgleichungen und modifiziertes Open-Loop-Böenabminderungssystem für das Do 28 TNT Windkanalmodell", DFVLR-IB 154-79/17, 1979.

9. Krag, B., "The Wind Tunnel Behaviour of a Scaled Model with a Gust Alleviation System in a Deterministic Gust Field", Symposium on Dynamic Analysis of Vehicle Ride and Manoeuvering Characteristics, London, 1978.

10. Charon, W., Verbrugge, R.A., "Nouvelle Technique d'essais sur Maquettes Libres en Laboratoire pour la Determination de Caracteristiques Aerodynamiques", AGARD-CP-235, 1978.

11. Cocquerez,S.L., "Etudes de Mécanique du Vol par Maquettes Catapultées en Laboratoire", Association Aeronautique et Astronautique de France, 16e Colloque, Lille, Novembre 1979.

12. Hamel, P., "Aircraft Parameter Identification Methods and their Applications - Survey and Future Aspects", AGARD-LS-104, 1979.

13. Plaetschke, E., "Parameter Identification Using Maximum-Likelihood-Methods", DFVLR-IB 154-74/20, 1975.

14. Verbrugge, R.A., Charon, W., Marchand, M., "Wind Tunnel and Free Flight Model Identification Experience", AGARD-LS-104, 1979.

15. Charon, W., Cotillon, T., "Methode du Gradient Conjugée en Identification en Mécanique du Vol, IMFL, Septembre 1978.

16. Plaetschke, E., Schulz, G., "Practical Input Signal Design", AGARD-LS-104, 1979.

17. Marchand, M., Koehler, R., "Determination of Aircraft Derivatives by Automatic Parameter Adjustment and Frequency Response Methods", AGARD-CP-172, 1975.

18. Marchand, M., "Bestimmung der Derivative eines Do-28-TNT-Modells aus Freiflugversuchen", DFVLR-FB 82-17, 1982.

19. Rohlf, D., "Zum Einfluß des Rumpfvorderteils auf eine Open-Loop-Böenabminderung", DFVLR-IB 154-79/29, 1979.

20. Coton, P., "Validation de Modèles de Representation du Compartiment des Aerodynes en Rafales Verticales", IMFL, Juin 1981.

21. Coton, P., "Application du Filtrage de Kalman a la Restitution des Trajectoires et des Attitudes de Maquettes d'avions Catapultées en Vol Libre en Laboratoire", IMFL, Septembre 1982.

22. Krag, B., Rohlf, D., Wünnenberg, H., "OLGA, a Gust Alleviation System for Improvement of Passenger Comfort of General Aviation Aircraft", ICAS Congress, Munich 1980.

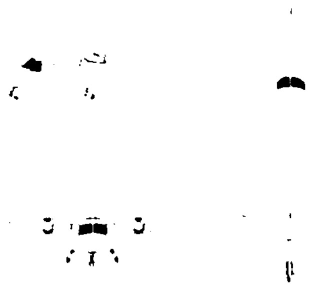

Fig. 1: Three-view drawing of Do 28 TNT aircraft configuration

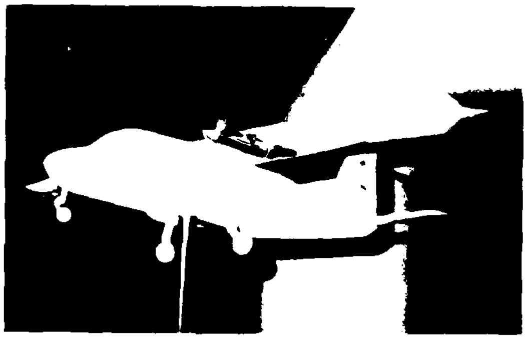

Fig. 2: Do 28 TNT 1/8-scale model in DFVLR wind tunnel

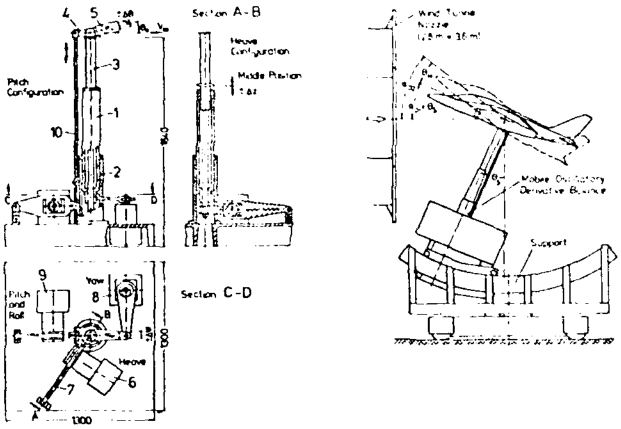
4
5
Section A-B
Heave Configuration
Middle Position
3
Pitch Configuration
1
10
2
C
D
9
Yaw
8
Pitch and Roll
B
Section C-D
Heave
6
7
A
1300
1300
Wind Tunnel Nozzle
Mobile Oscillatory Derivative Balance
Support

Fig. 3: DFVLR MOD-balance

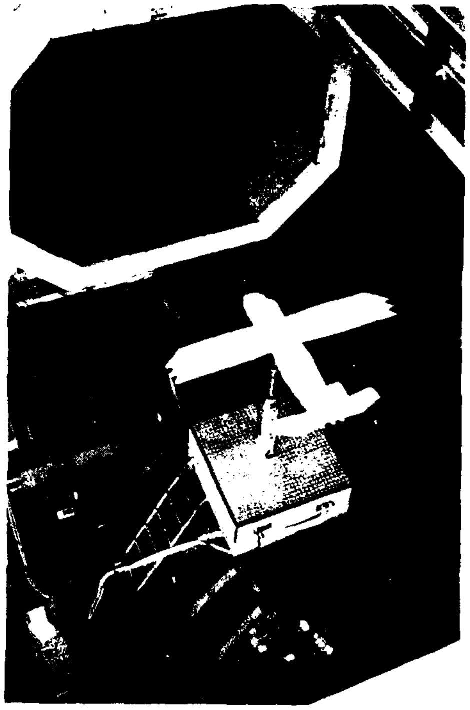

Fig. 4: Do 28 TNT 1/8-scale model installed on MOD-balance

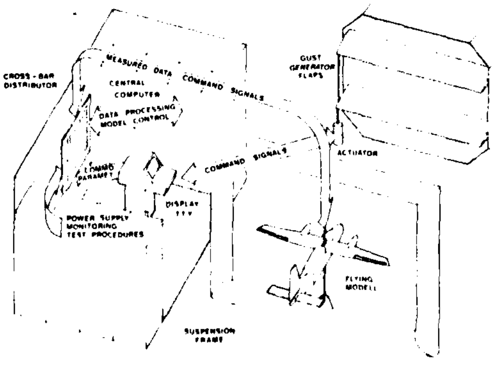
CROSS - BAR DISTRIBUTOR
MEASURED DATA
COMMAND SIGNALS
CENTRAL COMPUTER
DATA PROCESSING MODEL CONTROL
GUST GENERATOR FLAPS
ACTUATOR
COMMAND SIGNALS
DISPLAY TTY
POWER SUPPLY MONITORING TEST PROCEDURES
FLYING MODELL
SUSPENSION FRAME

Fig. 5: General view of the installation for dynamic simulation in wind tunnels

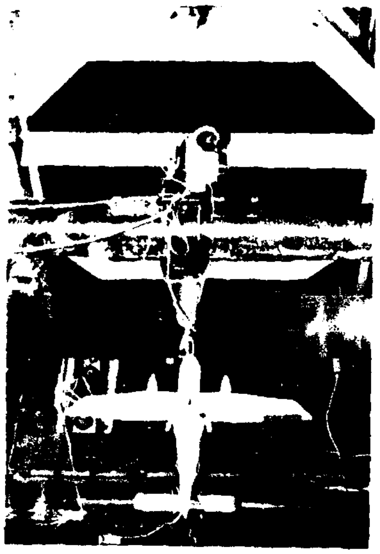

Fig. 6: Remotely controlled wind tunnel model of Do 28 TNT

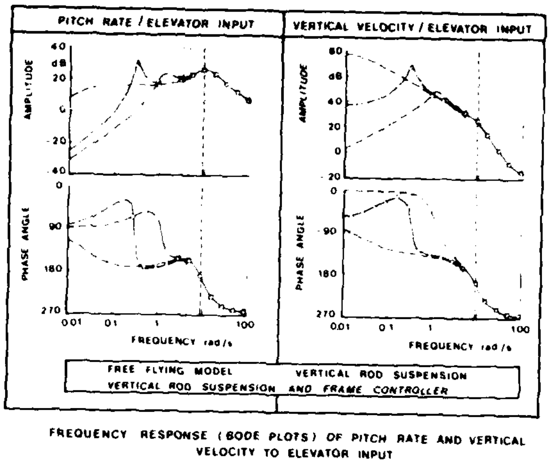

Fig. 7: Frequency response of pitch rate and vertical velocity to elevator input

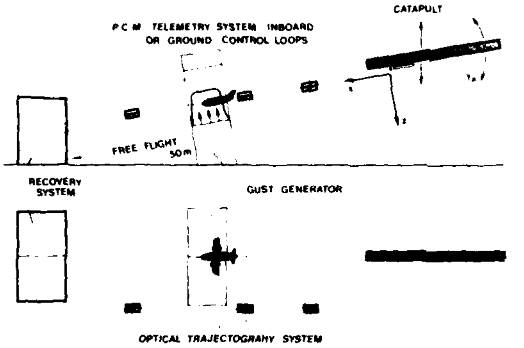
CATAPULT
PCM TELEMETRY SYSTEM INBOARD OR GROUND CONTROL LOOPS
FREE FLIGHT 50m
RECOVERY SYSTEM
GUST GENERATOR
OPTICAL TRAJECTOGRAPHY SYSTEM

Fig. 8: Schematic of the catapult free-flight facility

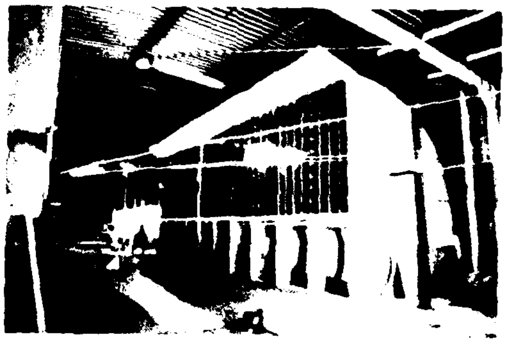

Fig. 9: Do 28 TNT model in the catapult free-flight facility

SPECIFIC ASPECTS

- ALL DEGREES OF FREEDOM REPRESENTED
- WELL KNOWN ENVIRONMENT LABORATORY CONDITIONS
- HIGH ACCURACY IN MASS INERTIA AND STRUCTURAL CHARACTERISTICS OF THE MODEL
- LARGE DIVERSITY OF ACCURATELY DEFINED INPUTS INITIAL CONDITIONS CONTROL AND EXTERNAL INPUTS GUST EFFECT
- EXTENSIVE AND HIGH PERFORMANCE INSTRUMENTATION INCLUDING IN BOARD OR GROUND BASED AUTOMATIC CONTROL LOOP
- APPLICATION OF PARAMETER IDENTIFICATION TECHNIQUES
- WIDELY COMPLEMENTARY WITH LOW SPEED WIND TUNNELS
- LOW SPEED TEST REYNOLDS NUMBER IN THE RANGE OF 10^6 (ON AMC)
- SHORT DURATION OF THE TEST (5 TO 15 SEC FULL SCALE)

Fig. 10: Specific aspects of the catapult free-flight facility

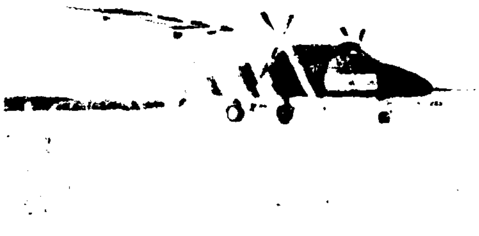

Fig. 11: Do 28 TNT full-scale experimental aircraft

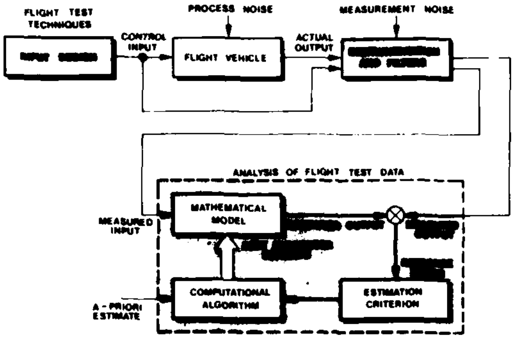
FLIGHT TEST TECHNIQUES
PROCESS NOISE
MEASUREMENT NOISE
CONTROL INPUT
FLIGHT VEHICLE
ACTUAL OUTPUT
ANALYSIS OF FLIGHT TEST DATA
MATHEMATICAL MODEL
MEASURED INPUT
COMPUTATIONAL ALGORITHM
ESTIMATION CRITERION
A - PRIORI ESTIMATE

Fig. 12: Basic system identification procedure

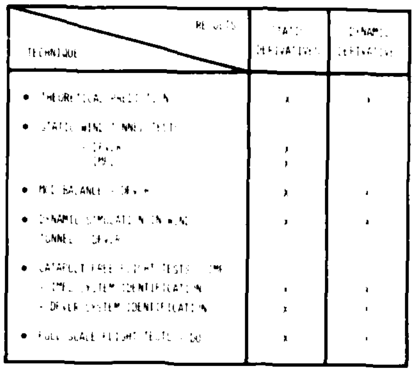

TECHNIQUE \ RESULTS	STATIC DERIVATIVES	DYNAMIC DERIVATIVES
• THEORETICAL PREDICTION	x	x
• STATIC WIND TUNNEL TESTS		
- DFVLR	x	
IMFL	x	
• MGC BALANCE - DFVLR	x	x
• DYNAMIC SIMULATION IN WIND TUNNEL - DFVLR	x	x
• CATAPULT FREE FLIGHT TESTS - IMFL		
- IMFL SYSTEM IDENTIFICATION	x	x
- DFVLR SYSTEM IDENTIFICATION	x	x
• FULL SCALE FLIGHT TESTS - DO	x	x

Fig. 13: Techniques applied in the program

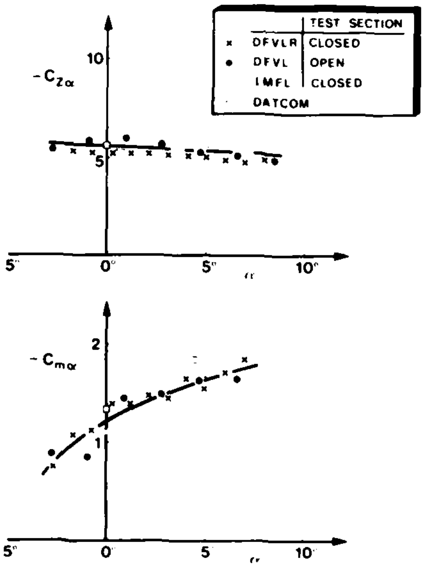

Fig. 14: Comparison of static test data of $C_{Z\alpha}$ and $C_{m\alpha}$ over angle of attack

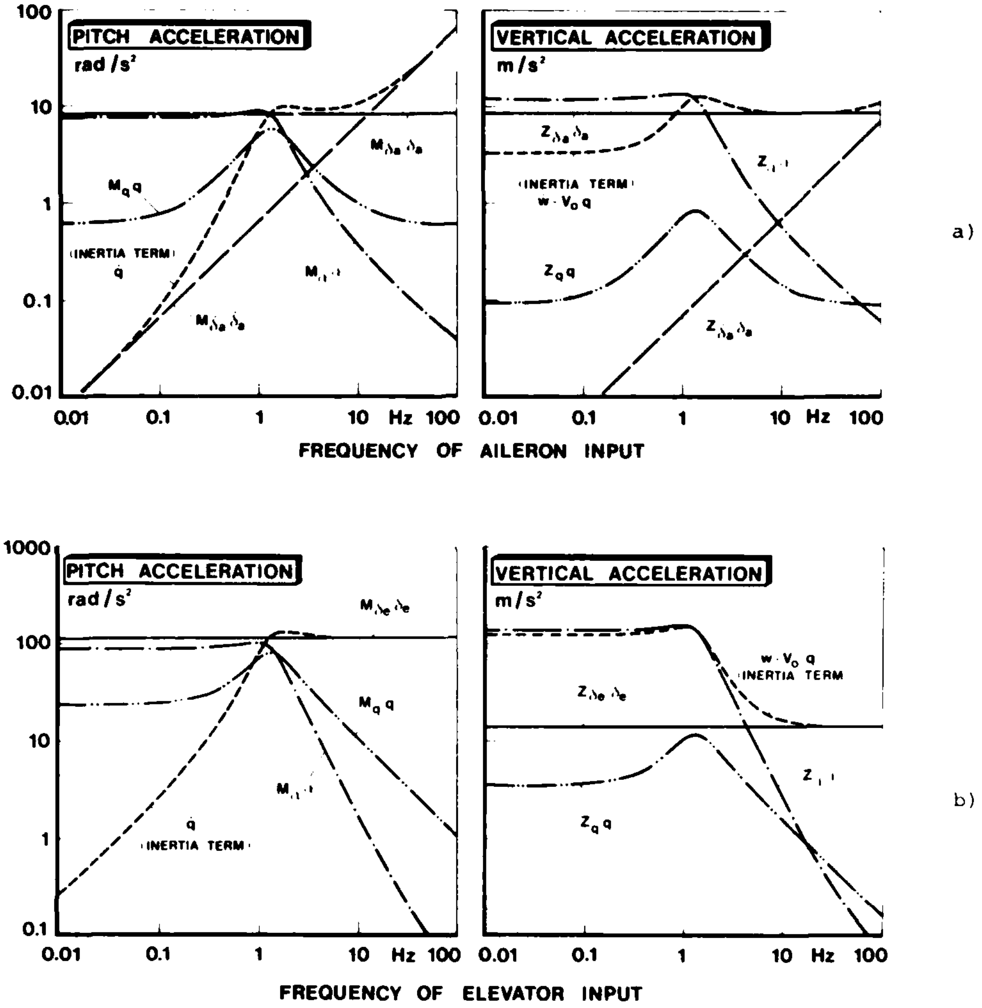

Fig. 15: Sensitivity investigation in frequency domain (Bode-plot of M/Z equation terms)

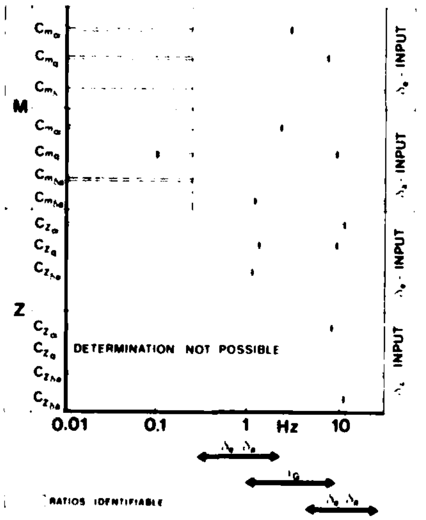

Fig. 16: Optimum frequency ranges of the input signals

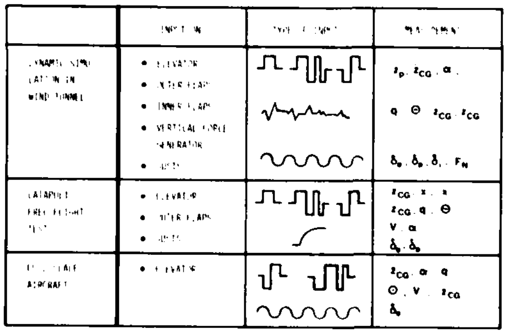

	INPUT ON	TYPE OF INPUT	MEASUREMENT
DYNAMIC SIMULATION IN WIND TUNNEL	• ELEVATOR • OUTER FLAPS • INNER FLAPS • VERTICAL FORCE GENERATOR • GUSTS		$\ddot z_p$, $\ddot z_{CG}$, α, q, Θ, $\dot z_{CG}$, z_{CG} δ_e, δ_a, δ_i, F_N
CATAPULT FREE FLIGHT TEST	• ELEVATOR • OUTER FLAPS • GUSTS		$\ddot z_{CG}$, $\ddot x$, $\ddot a$ $\dot z_{CG}$, q, Θ V, α δ_e, δ_a
FULL SCALE AIRCRAFT	• ELEVATOR		$\ddot z_{CG}$, α, q Θ, V, $\dot z_{CG}$ δ_e

Fig. 17: Overview of the test program

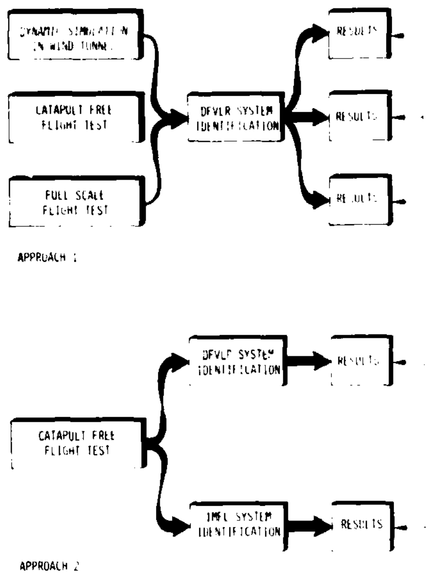
DYNAMIC SIMULATION IN WIND TUNNEL
CATAPULT FREE FLIGHT TEST
FULL SCALE FLIGHT TEST
DFVLR SYSTEM IDENTIFICATION
RESULTS
RESULTS
RESULTS
APPROACH 1
DFVLR SYSTEM IDENTIFICATION
RESULTS
CATAPULT FREE FLIGHT TEST
IMFL SYSTEM IDENTIFICATION
RESULTS
APPROACH 2

Fig. 18: Alternate approaches for data evaluation

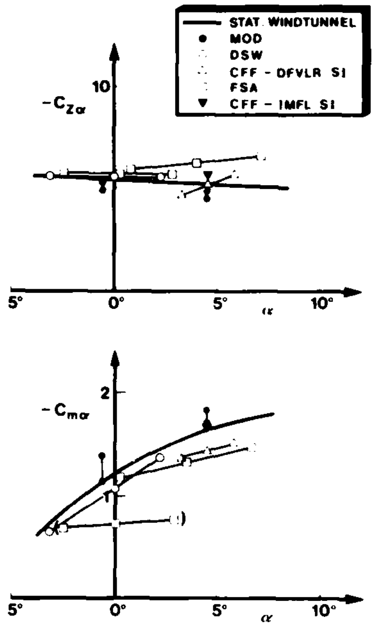

Fig. 19: $C_{m\alpha}$ and $C_{Z\alpha}$ estimated from flight tests

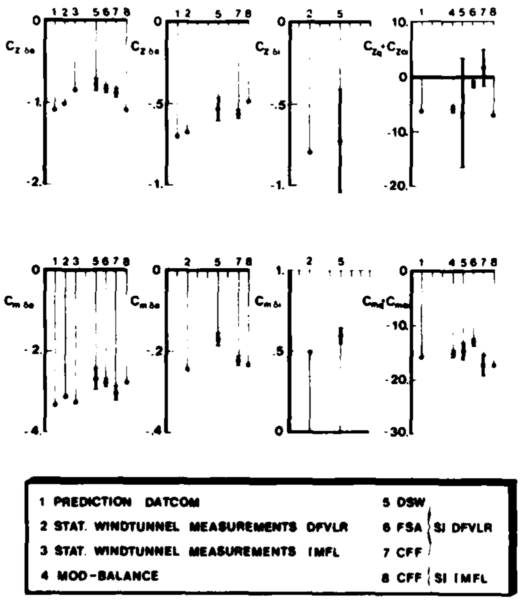

Fig. 20: Comparison of control and dynamic derivatives

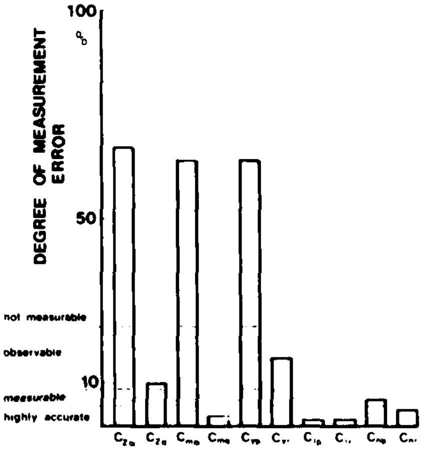

Fig. 21 MOD-balance measurements

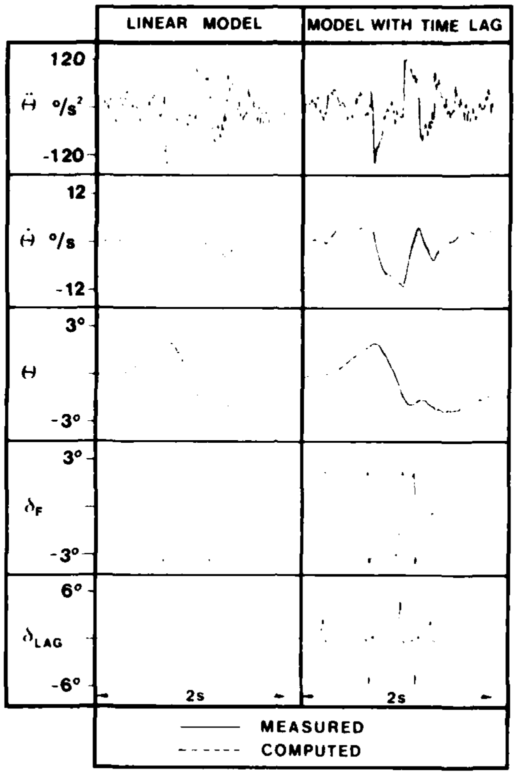

Fig. 22: Difficulties in wing tail interference modeling

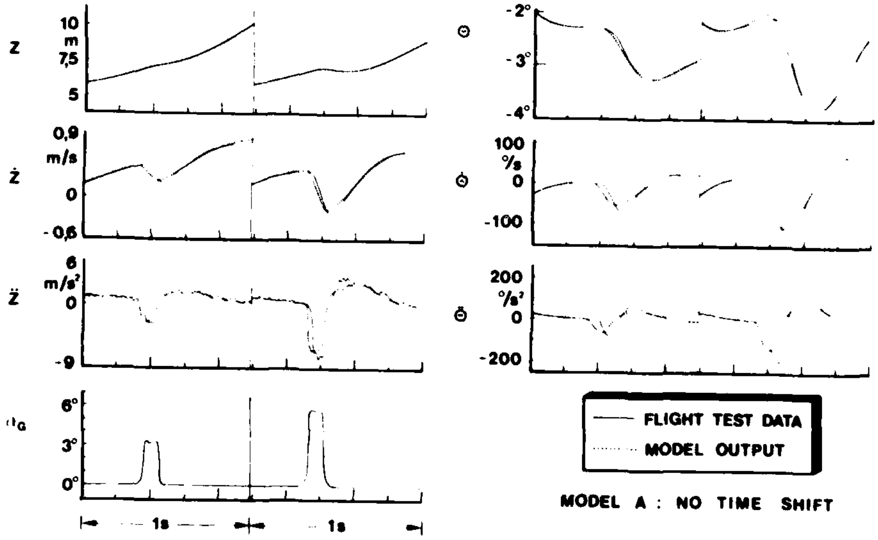

Fig. 23: Estimated model outputs compared with direct measurements

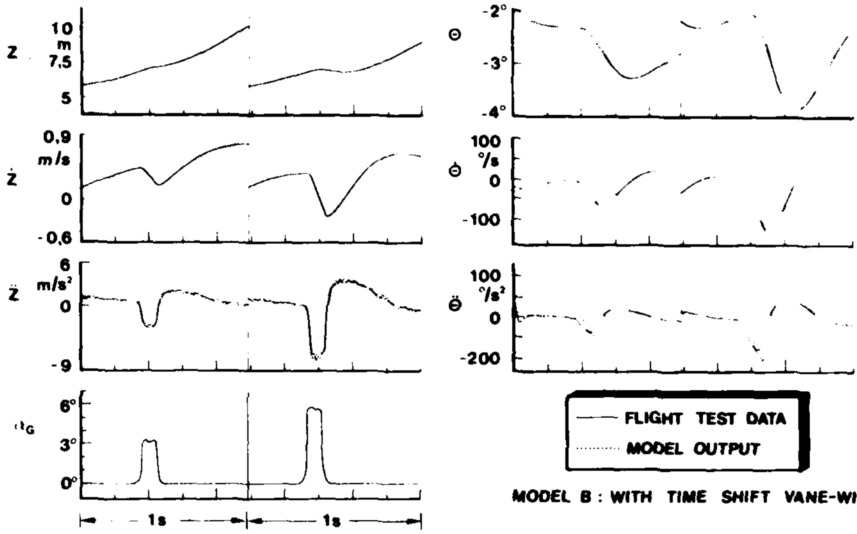

MODEL B : WITH TIME SHIFT VANE-WING

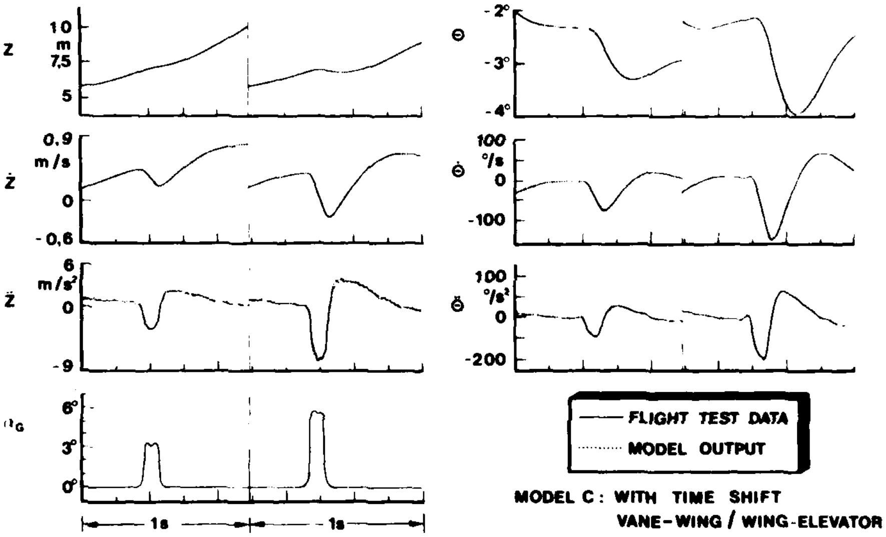

MODEL C : WITH TIME SHIFT
VANE-WING / WING-ELEVATOR

Fig. 23: Continued

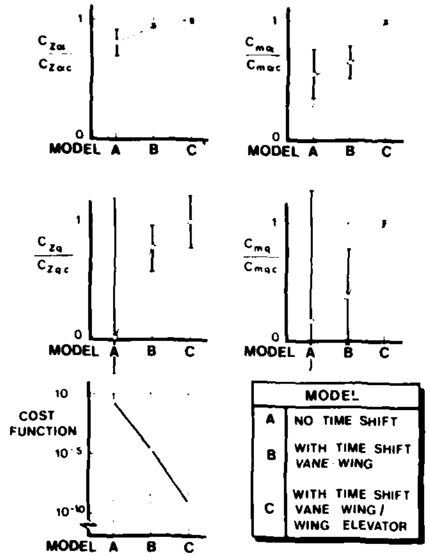

Fig. 24: Effect of time shift of the measured turbulence on the estimated coefficients

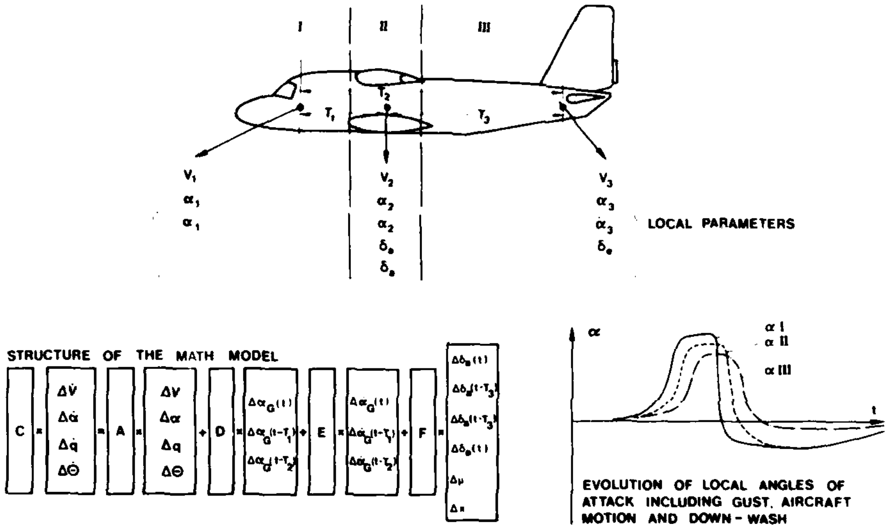

I
II
III
T_1
T_2
T_3
V_1 α_1 $\dot{\alpha}_1$
V_2 α_2 $\dot{\alpha}_2$ δ_a $\dot{\delta}_a$
V_3 α_3 $\dot{\alpha}_3$ δ_e
LOCAL PARAMETERS
STRUCTURE OF THE MATH MODEL
C
$\Delta\dot{V}$ $\Delta\dot{\alpha}$ $\Delta\dot{q}$ $\Delta\dot{\Theta}$
A
ΔV $\Delta\alpha$ Δq $\Delta\Theta$
D
$\Delta\alpha_G(t)$ $\Delta\alpha_G(t-T_1)$ $\Delta\alpha_G(t-T_2)$
E
$\Delta\dot{\alpha}_G(t)$ $\Delta\dot{\alpha}_G(t-T_1)$ $\Delta\dot{\alpha}_G(t-T_2)$
F
$\Delta\delta_a(t)$ $\Delta\delta_a(t-T_3)$ $\Delta\dot{\delta}_a(t-T_3)$ $\Delta\delta_e(t)$ $\Delta\mu$ Δx
α
α I
α II
α III
t
EVOLUTION OF LOCAL ANGLES OF ATTACK INCLUDING GUST, AIRCRAFT MOTION AND DOWN-WASH

Fig. 25: Schematic of the three-elements mathematical model

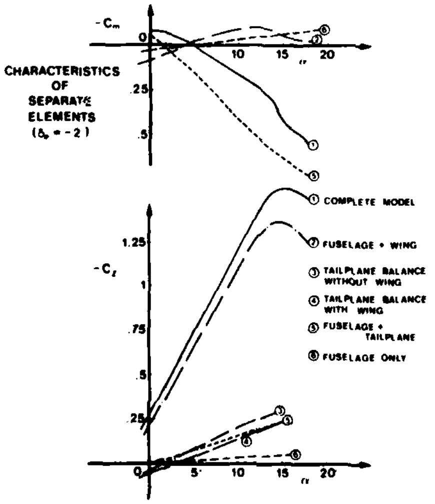

Fig. 26: Static wind tunnel measurements for separate elements

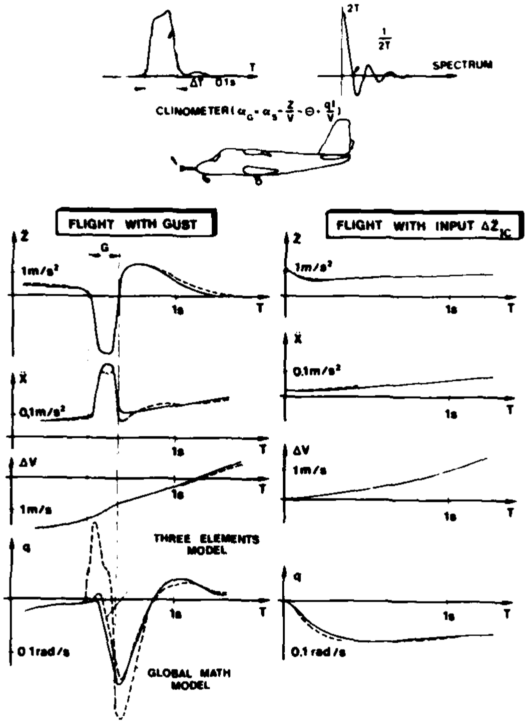

Fig. 27: Do 28 TNT flight test and simulation results

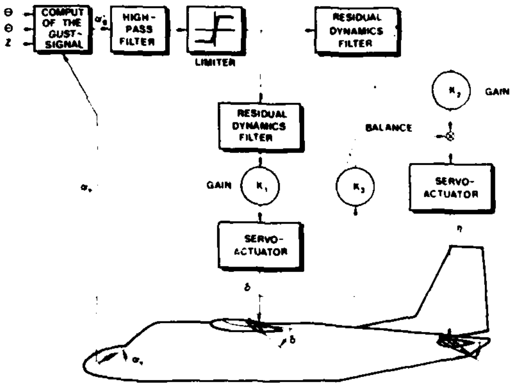

Θ
Θ
Z
COMPUT OF THE GUST-SIGNAL
α_G
HIGH-PASS FILTER
LIMITER
RESIDUAL DYNAMICS FILTER
RESIDUAL DYNAMICS FILTER
K₂
GAIN
BALANCE
GAIN
K₁
K₃
SERVO-ACTUATOR
SERVO-ACTUATOR
α_s
δ
η

Fig. 28: Block diagram of gust alleviation system

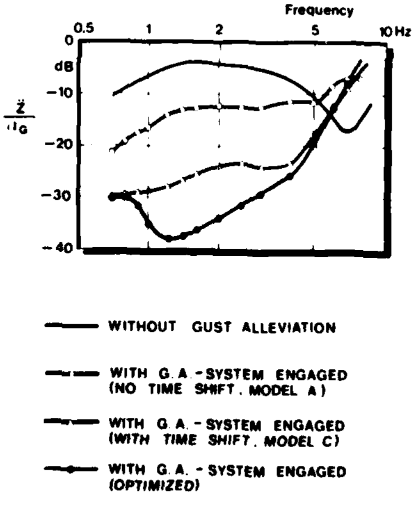

Fig. 29: Frequency response of the vertical acceleration. Effect of gust alleviation system

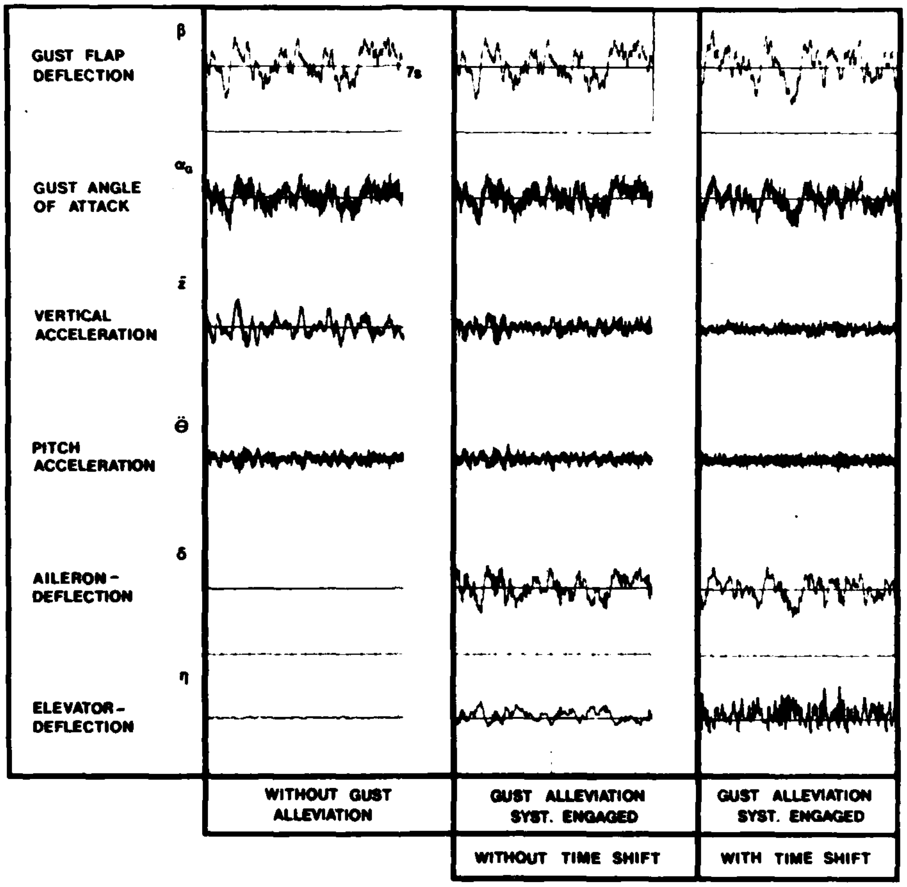

Fig. 30: Time histories of the model response during flight in a scaled turbulence field

ASPECTS DE LA CORRELATION DANS L'IDENTIFICATION D'EFFETS DYNAMIQUES A PARTIR DE TECHNIQUES COMPLEMENTAIRES

EVOLUTION AUX GRANDS ANGLES

D. Tristrant

Institut de Mécanique des Fluides
I.M.F.L.(France) 5 bd Painlevé, Lille

SUMMARY

The aim of this paper is to present some experimental or analytical methods which contribute to the comprehension and prediction of aircraft behaviour at high angles of attack and stall/spin.

To illustrate these different methods, we present three examples of recent works realized at IMFL on this subject :

A.Spin description method.

A combat aircraft can start a spin departure around an horizontal trajectory which becomes vertical after several spin turns. The comparison between such a spin and that observed in vertical wind tunnel on free flight model is not easy, particularly if these movements are agitated. We will suggest a representation of high angle motions visually giving the principal characteristics of the phenomena, independently of the trajectory. Such a representation allows the correlation of spin motions between the vertical wind tunnel and the full scale flight.

B.Spin correlation.

One of the basic parameters which could modify the quality of the correlation of spin tests realized in Froud similitude is the Reynolds number. We will show, with a typical example concerning a light aircraft, the important influence of Reynolds number on spin equilibrium state, and the test method which allows to understand and correlate the phenomena.

C.Modeling and Simulation.

With a typical example concerning a combat aircraft, we will expose some measurement results on a dynamic balance allowing the evaluation of the aerodynamic force system at high angle of attack, the modeling of aerodynamic effects and then spin simulations which can be compared with vertical wind tunnel results on free flight model.

INTRODUCTION

Ces dernières années ont vu l'apparition, dans l'aéronautique, de technologies nouvelles comme la CAG, les matériaux composites, les microprocesseurs embarqués ... Or ces progrès technologiques ont sensiblement influé sur l'architecture des avions, notamment des avions d'armes, et ont permis d'élargir considérablement leur domaine de vol. Ces plus grandes possibilités offertes au pilotage ont, par voie de conséquence, soulevé les problèmes liés à la manoeuvrabilité, aux qualités de vol et ont mis l'accent sur l'aspect sécurité.

Les avions de combat pouvant évoluer à des incidences de plus en plus élevées, effectuer des manoeuvres de plus en plus serrées, ont atteint un domaine de vol nécessitant pour sa maitrise des études et des recherches importantes, tant pour connaître son aérodynamique que pour comprendre les phénomènes observés et prédire ses mouvements.

Ces études passent notamment par des essais en soufflerie sur maquette, soufflerie où il est très difficile, pour ne pas dire impossible, de reproduire l'ensemble du domaine de vol. D'autant que beaucoup d'évolutions aux grands angles des avions modernes, en particulier les vrilles, sont devenues de plus en plus complexes et difficiles à décrire : les mouvements de l'avion de combat comportant bien souvent des agitations amples autour de trajectoires tendues, ne permettent pas la comparaison directe avec la soufflerie verticale où les maquettes sont testées en vrille autour de trajectoires verticales.

Par ailleurs, pour les avions légers essentiellement, peut intervenir un effet Reynolds rendant délicate la corrélation entre la soufflerie verticale et les essais en vol.

L'objectif de cet exposé est de présenter quelques méthodes expérimentales ou d'analyse contribuant à la compréhension et à la prédiction du comportement d'un avion dans le domaine décroché, de ses pertes de contrôle, de ses vrilles et évolutions diverses.

Afin d'illustrer ces différentes méthodes, nous presentons, dans ce papier, trois exemples de travaux récemment entrepris sur ce sujet à l'IMFL :

A - Figuration vrille - [illegible] en vol.

On montrera que les transpositions de mouvement entre la soufflerie verticale et les essais en vol de vrille ne peuvent se faire de façon directe. Nous proposons donc un mode de représentation des mouvements aux grands angles traduisant les principales caractéristiques de ces phénomènes indépendamment de la trajectoire de l'avion ou de la maquette. Une telle représentation permet ainsi la corrélation des mouvements de vrille en soufflerie verticale et en vol grandeur.

B – Corrélation maquette-avion relative à la vrille.

[illegible] parfois influé fortement sur la qualité de la corrélation [illegible] effectuées en similitude de Froude, est le [illegible], relatif [illegible] influence décisive sur l'état d'équilibre en vrille, [illegible] permettent [illegible].

C – Difficultés [illegible].

[illegible] d'armes, [illegible] de mesures [illegible] vrille [illegible] soufflerie verticale.

A – [illegible]

1) Généralités.

[illegible] mouvement hélicoïdal [illegible] verticale. [illegible] le mouvement de rotation fait défiler l'horizon [illegible].

Cependant, certains avions, notamment les avions d'armes modernes, peuvent engager une vrille autour d'une trajectoire initialement horizontale [illegible], et qui ne **devient** verticale qu'après plusieurs tours de vrille. [illegible] différentes [illegible].

Ainsi, pour une même vrille, les caractères "plat" ou "piqué", "calme" ou "agité", qui sont fondamentaux pour reconnaître une vrille et sa sévérité, pourront se traduire de façon très différente en vol et en soufflerie verticale. L'ingénieur d'essai en vol qui doit pouvoir identifier rapidement et sans [illegible] le mouvement de l'avion, n'en a pas la tâche simplifiée. Aussi nous-a-t-il semblé légitime de rechercher un mode de [illegible] permettant d'identifier rapidement un type de mouvement [illegible] et cela dès les premiers tours de vrille. Nous avons donc voulu trouver une représentation [illegible] des évolutions aux grands angles permettant d'identifier et de classifier les différents phénomènes. Cependant il convient que celle-ci soit la plus simple possible et la plus synthétique possible afin que l'ingénieur, suivant du sol les essais en vol, puisse d'un seul coup d'oeil en déduire le type et la nature du mouvement et en connaître la sévérité. Ceci nous a donc amenés à choisir trois variables de façon à pouvoir dégager, pour tous les principaux phénomènes, leurs caractéristiques essentielles et cela quelle que soit la trajectoire de l'avion ou de la maquette.

2) Caractères principaux.

Pour décrire à la fois les vrilles, les autotonneaux, le deep-stall, ... les trois caractères suivants nous ont semblé fondamentaux.

a. le caractère plat ou piqué : traduit par l'incidence. C'est un paramètre très important et bien souvent les consignes de sortie de vrille dépendent de sa valeur moyenne. D'autre part, lorsqu'une vrille est fortement agitée, l'évolution vers la sortie n'est pas toujours évidente pour le pilote, c'est la décroissance en moyenne de l'incidence qui peut en informer l'ingénieur suivant les essais au sol.

b. le caractère "lent ou rapide" : traduit par la composante du vecteur rotation instantanée suivant le vecteur vitesse ($\vec{\Omega} \cdot \vec{V}/V$). Ce facteur associé au caractère plat est significatif de la sévérité d'une vrille. Plus une vrille plate est rapide et plus la durée de sortie sera longue : certaines vrilles très rapides nécessitent d'appliquer sur les gouvernes la consigne de sortie pendant plusieurs tours avant de quitter la vrille. D'autre part, le signe de $(\vec{\Omega} \cdot \vec{V})$, c'est-à-dire le sens de la vrille, qui n'est pas toujours bien perçu par le pilote lors des vrilles très agitées, est fondamental pour appliquer la consigne sur la direction et le gauchissement.

c. le caractère "calme" ou "agité" : traduit par l'autre composante du vecteur $\vec{\Omega}$ située dans le plan perpendiculaire au vecteur vitesse ($\vec{\Omega} \wedge \vec{V} / V$). Comme nous l'avons signalé précédemment, il est bien souvent très difficile, pour un pilote, de distinguer les agitations du mouvement principal de l'avion.

Par contre, l'existence d'agitations, surtout lorsque celles-ci croissent dans le temps, est très souvent un facteur favorable à la récupération, ou tout au moins à une évolution vers un autre état d'équilibre. La connaissance de l'aspect agité ou calme est donc important pour l'ingénieur d'essai. Ces différentes grandeurs nous ont donc semblé essentielles pour caractériser un mouvement mais également pour traduire l'état aérodynamique de l'avion et permettre donc, à la lumière des résultats d'essais de vrille libre sur la maquette en soufflerie verticale, de donner la consigne correcte à effectuer sur les gouvernes pour sortir de vrille.

utilisant ces trois variables, nous avons donc réalisé une représentation tridimensionnelle de l'état de l'avion ou de la maquette.

3) Classification.

Reprenant la classification des différents types de vrille (3), nous pouvons avec notre méthode de figuration, représenter et identifier clairement les principaux phénomènes suivants :

- la vrille calme piquée : caractérisée par une incidence de l'ordre de 45° ou moins et un taux de rotation constant. Elle est le fait de nombreux avions légers,

- la vrille plate et rapide : l'incidence est supérieure à 60° et le taux de rotation est important (1 tour en moins de 2 secondes). Cette vrille est souvent considérée comme sévère car les sorties sont souvent longues (quand elles ne sont pas impossibles),

- la vrille dos : l'incidence est négative,

- le deep-stall : il ne s'agit pas de vrille proprement dite mais d'un phénomène sans rotation et à incidence de vrille.

Tous les mouvements précités sont des mouvements dits calmes, mais il existe également :

- les vrilles moyennement agitées : sont la superposition d'oscillations de tangage et de roulis sur une vrille calme. Les périodes ne sont généralement pas égales,

- les vrilles agitées ordonnées : comportent des oscillations sur les trois axes (y compris le lacet) et d'amplitudes importantes et cycliques. Ce mouvement peut être apparenté au mouvement d'Euler-Poinsot,

- les vrilles à agitations divergentes : ce sont des vrilles où l'amplitude des agitations est croissante jusqu'à ce que la vrille cesse pour laisser place à :
  - . un passage dos : qui s'effectue généralement par roulis,
  - . des autotonneaux : la vitesse de roulis est grande dans un tel mouvement et l'angle entre le vecteur vitesse et le vecteur rotation est important,

- les oscillations roulis-lacet : ce mouvement est rencontré sur des avions résistant à la vrille, il se caractérise par des oscillations périodiques en roulis et lacet, mais il ne s'agit pas de vrille,

- la vrille agitée désordonnée : les agitations n'ont pas de période régulière et les mouvements de l'avion semblent aléatoires : l'incidence peut changer de signe.

4) Mode de représentation.

A chaque instant, l'état de l'avion est donc représenté dans un trièdre comportant suivant x l'incidence, suivant y le taux de rotation autour du vecteur vitesse ($\vec{\Omega} \cdot \vec{V} / V$) et suivant z l'autre composante de $\vec{\Omega}$ située dans le plan perpendiculaire à $\vec{V}$: ($\vec{\Omega} \wedge \vec{V} / V$). La représentation peut être faite en temps réel sur un écran graphique lors des essais en vol instrumenté, le temps de calcul nécessaire pour retrouver ces quantités à partir de l'instrumentation étant relativement faible. De plus, afin de mettre en évidence l'aspect *"évolution du mouvement"*, on conserve sur l'écran de la représentation, l'image des 10 ou 15 états précédents. Cela permet ainsi de traduire une notion de la valeur des dérivées des différentes quantités. Dans le cas où il existe des agitations, par exemple, l'aspect dérivée permet de savoir si une vrille diverge, si l'avion est susceptible de quitter sa vrille.

Un exemple de représentation est donné planche 2.

Afin d'illustrer la méthode de représentation, nous presentons ici un film d'animation où sont simulés les principaux phénomènes grands angles précédemment décrits. On peut ainsi dégager dans l'espace de représentation des régions propres à une catégorie de mouvements donnés. D'ailleurs, comme nous le montre la planche 3, dans le plan (α, $\vec{\Omega} \cdot \vec{V} / V$) nous pouvons déjà y reconnaître des domaines relatifs à quelques mouvements bien typiques.

5) Conclusion.

En conclusion, nous dirons qu'une telle représentation n'a pas eu la pretention de pouvoir traduire, à l'aide uniquement des 3 variables précitées, tous les mouvements possibles de l'avion. Un tel dessein nécessiterait un nombre de grandeurs physiques bien plus important.

Elle n'a eu pour objectif que de donner, de façon synthétique, les caractéristiques du mouvement qui nous ont semblé essentielles afin d'identifier rapidement le mouvement, d'en déduire la sévérité ainsi que la consigne de gouvernes adéquate pour en sortir. Car, bien souvent, les consignes diffèrent selon les caractères plat ou piqué, dos ou ventre ou d'autres encore. De plus, l'évolution du phénomène peut être favorable selon l'aspect des agitations.

Pour le pilote soumis à un fort facteur de charge, voyant l'horizon défiler et basculer rapidement, l'identification du mouvement n'est pas simple. L'expérience a montré que la confusion peut se produire entre une vrille et un tonneau, une vrille ventre et une vrille dos et même entre une vrille à gauche et une vrille à droite.

Enfin, pour terminer, nous signalerons qu'une telle représentation peut concourir à une meilleure classification des différents phénomènes, à leur meilleure connaissance et permettre aussi à l'ingénieur d'essai en soufflerie de comparer directement les vrilles grandeur avec celles obtenues sur maquette lors des lancers manuels à la soufflerie verticale.

B - *CORRELATION MAQUETTE-AVION RELATIVE A LA VRILLE*

Exemple de prédiction incomplète des essais en soufflerie et possibilités de solutions.

1° Les essais de vrille à l'I.M.F.L.

C'est en 1948 que commencèrent les essais de vrille sur maquettes en soufflerie verticale à l'I.M.F.L.

A ce jour environ [illegible] maquettes d'avions de tous types (armes, légers, transport) ont été essayées. Le grand nombre d'études confiées à l'IMFL précise à lui seul la confiance accordée à de tels types d'essais par les constructeurs.

En effet, la prédiction de la soufflerie s'est avérée très souvent satisfaisante tant pour les avions d'armes que pour les avions légers (nous écartons ici les avions de transport, pour lesquels les possibilités de comparaison des vrilles maquette et avion ne peuvent être que très rares).

Ainsi, pour les avions d'armes, la (ou les) vrille (s) rencontrée (s) en grandeur, se trouve (nt) toujours parmi celles trouvées en soufflerie.

Les rares cas où la corrélation maquette-avion n'est pas bonne concernent surtout les avions légers. En effet, il arrive que pour un avion ayant plusieurs formes de vrille, toutes ne sont pas trouvées sur sa maquette. Or cette prédiction incomplète s'avère grave si la vrille non trouvée en soufflerie est un phénomène critique.

Le présent papier concerne un de ces cas récemment rencontré.

2° Avion concerné.

Il s'agit d'un moto-planeur, le RF 10, dont la géométrie est rappelée dans la figure 1.

Ne serait-ce que pour faciliter la construction du modèle, l'échelle choisie fut telle qu'il s'agissait d'une grande maquette ; en effet **son** envergure était de 1,[illegible] m, alors que celle des maquettes d'avions légers classiques est souvent de l'ordre de 0,8 m. Cependant, malgré la taille de la maquette, les dimensions de certains de ses éléments étaient encore faibles ; en particulier la corde en extrémité de voilure n'était que de 3,[illegible] cm.

Auparavant, une seule maquette de ce type d'avion avait été essayée en soufflerie ; il s'agissait du RF 8 (envergure maquette : 1,24 m) pour lequel l'accord entre les résultats maquette et avion fut bon.

3° Historique des essais avion et maquette.

Le tableau ci-après présente, selon leur ordre chronologique, les diverses campagnes d'essais relatives à la vrille du moto-planeur (essais grandeur et sur maquette). Dans ce tableau il apparaîtra que telle phase d'essais sur maquette est la conséquence directe de résultats obtenus dans la phase précédente d'essais sur avion. Le tableau se limite à donner un bref résumé des résultats ; ceux-ci seront repris en détail par la suite.

Campagne d'essais	Essais avion	Essais maquette
1	Essais "constructeurs" Après plusieurs vrilles saines, obtention d'une vrille non maîtrisée. Pas d'enregistrements d'où renseignements surtout qualitatifs	
2		Essais effectués pour tenter de retrouver la vrille critique trouvée en 1 ainsi que pour couvrir les futurs essais 3 . Les vrilles obtenues sont toujours parfaitement saines, sans aucun problème de récupération. Cependant, par sécurité, étude d'un moyen de secours qui serait installé sur l'avion pour la campagne 3 . Moyen retenu : fusée sous l'extrême arrière fuselage et agissant en tangage.
3	Essais au C.E.V. et donc avec enregistrements. . Environ 40 vrilles effectuées . Programme prévu inachevé . 90 % des phénomènes obtenus sont semblables à ceux de la soufflerie 2 donc aucun problème. Dans 10 % des cas la récupération est plus longue, parfois très longue. La dernière vrille refuse de s'arrêter. Utilisation, avec succès, de la fusée. Donc confirmation des possibilités de vrille critique trouvée lors des essais 1	
4		Etude orientée vers la recherche d'un éventuel effet Reynolds pour tenter de retrouver la vrille incontrôlable de l'avion. Géométrie de la maquette modifiée dans ce but. Avec la maquette "Reynolds" vrilles critiques 1 et 3 retrouvées.
5		Sur demande du constructeur, recherche d'une nouvelle géométrie de l'arrière susceptible de rendre toutes les vrilles saines. Solution retenue : empennages en T
	Essais futurs avec empennages en T	

Les prochains paragraphes reprendront en détail les résultats des diverses campagnes d'essais relatives à la vrille du RF 10.

4° Phase 1 : Première campagne d'essais avion.

Nous reproduisons ci-dessous quelques extraits du rapport du pilote.

- Plusieurs vrilles gauche et droite de 1 à 5 tours.
- Vrilles qualifiées de confortables et saines $\theta \simeq -45°$, $\Omega \simeq 4$ s/tour
- Sortie en 3/4 tour avec la consigne
  . Manche poussé (manoeuvre prépondérante)
  . Pied contre
  . Ailerons vers le neutre
- Poursuite des essais jusqu'à l'obtention d'une vrille initialement prévue à 3 tours et pour laquelle diverses manoeuvres de sortie n'ont eu aucun effet (bien que la vrille soit du même type que celle des essais précédents)
- Le pilote "saute" vers le 12ème tour
- "Sortie" de vrille de l'avion après abandon du pilote.

5) Phase 2 : Première étude en soufflerie.

Les tableaux de la planche 5 présentent les résultats de soufflerie.*

Dans cette planche nous voyons en premier lieu que la vrille maintenue est moyennement piquée ou piquée et peu rapide (3 à 3,5 s/t valeur avion).

La vrille se perpétue dans un domaine de gouvernes approximativement égal au 1/3 du domaine total. Par voie de conséquence le domaine des gouvernes favorables à la sortie est très étendu ; la récupération ne présente donc pas de difficultés particulières ; elle peut être obtenue avec une consigne simple telle que :

- direction Contre et profondeur au neutre ou à piquer voire même : toutes gouvernes recentrées.

En tout état de cause la consigne optimale de sortie définie dans la planche 5 n'est absolument pas indispensable pour obtenir une bonne sortie.

A noter que les résultats de la planche 5 ont été obtenus même dans des conditions à priori sévères vis-à-vis de la vrille (par exemple à un centrage anormalement arrière). Malgré cette sévérité nous n'avons jamais retrouvé la vrille critique de l'avion.

Cette première étude en soufflerie s'est terminée par la recherche d'un moyen de secours en vue de protéger l'avion pour sa future campagne de vrille. Nous avons étudié une fusée placée à l'extrême arrière du fuselage et agissant successivement en lacet et en tagage ; c'est la fusée "tangage" qui fut retenue.

La comparaison de ces résultats et des commentaires pilote de la phase d'essais 1 fait apparaître de nombreux points d'accord, notamment sur :

- le caractère des vrilles,
- l'efficacité de la profondeur,
- les consignes de sortie.

Mais il s'agit là de points de détail dans la mesure où, sur le point le plus important (risques de vrille incontrôlable), le désaccord reste total.

6) Phase 3 : Deuxième campagne d'essais avion.

6.1 - Programme d'essais.

Le programme d'essais prévoyait des vrilles :

- gauche et droite,
- moteur réduit ou coupé,
- de durées diverses (1 t , 2t, 3t et 5t)
- aérofreins rentrés ou sortis,
- 3 différents centrages.

En ce qui concerne les gouvernes, la vrille était lancée (puis maintenue) avec les manoeuvres classiques pour un avion léger, soit :

- Direction dans le sens souhaité,
- Manche tiré.

Les ailerons étaient :

- laissés au neutre
- ou mis Avec (soit pro-vrille
- parfois Contre (soit anti-vrille

selon la soufflerie et pour cet avion)

Pour la sortie la manoeuvre initiale fut toujours :

- Direction inversée
- Manche poussé.

La campagne d'essais fut interrompue à la 37ème vrille ; de ce fait l'étude de certains paramètres n'a pu être terminée.

6.2 - Les vrilles fréquentes.

Par vrilles fréquentes nous entendons les phénomènes qui furent obtenus dans ≃ 90 % des cas et qui peuvent être présentés en une seule et même description.

---

* Dans les tableaux de résultats, direction et ailerons sont dits "Avec" ou "Contre" lorsque ces gouvernes sont braquées pour ou contre un virage de même sens que la vrille.

Les résultats sont présentés dans la planche 6 ; ils peuvent être décrits comme suit :

Résultats	Accord avec la soufflerie
Caractère de la vrille : moyennement piquée peu rapide	Bon
Influence des ailerons durant la vrille : Vrille bien maintenue ailerons Neutre ou Avec Evolution vers un arrêt ailerons Contre	Très bon
Récupération Rapide (≤ 1 tour) avec la consigne Direction Contre Manche poussé	Très Bon

De ces résultats présentés jusqu'ici nous retiendrons la parfaite corrélation existant entre les vrilles maquette et avion.

6.3 - La vrille critique.

Pour environ 10 % des vrilles de l'avion, les résultats se sont donc écartés de ceux de la soufflerie en ce sens que la récupération fut plus longue, parfois très longue et enfin impossible (du moins par les gouvernes) pour la dernière vrille.

Le présent paragraphe concerne la vrille incontrôlable par les gouvernes (nous reviendrons ultérieurement sur les "longues" sorties).

De la planche 7, qui contient l'essentiel des résultats de cette vrille, nous pouvons faire quelques commentaires.

Au moment de la manoeuvre de sortie (à la fin du 2ème tour), la vrille était moyennement piquée et moyennement rapide (elle était légèrement plus rapide que les vrilles précédentes).

La première tentative de sortie (faite avec les manoeuvres qui, jusqu'ici, avaient été efficaces) n'amène pas la récupération ; au contraire la vrille s'aplatit légèrement. Les gouvernes ont été maintenues pendant 2 tours.

Lors de la deuxième tentative de sortie le pilote applique la consigne optimale préconisée par la soufflerie ; cette consigne est maintenue pendant 4 tours mais cela n'empêche pas la vrille de s'aggraver (vrille devenant plus plate et plus rapide). Le pilote a alors recours à la fusée et l'arrêt est immédiat.

Il est évident que cette description est en total désaccord (mise à part l'efficacité de la fusée) avec ce qui fut trouvé en soufflerie puisque au cours des tentatives de sortie, non seulement l'arrêt n'a pas été obtenu mais la vrille s'est aggravée (ce qui ne veut pas dire que ce sont les manoeuvres de sortie qui ont aggravé la vrille, car nous ignorons ce qu'elle serait devenue si les gouvernes avaient été laissées pro-vrille).

Mais si ce résultat est en désaccord avec la soufflerie il faut également remarquer que cette vrille (et surtout sa sortie) s'écarte aussi fortement des phénomènes précédemment trouvés sur cet avion. Il y a donc également une dispersion à l'intérieur même de la campagne d'essais avion, dispersion que nous avons tenté d'expliquer par une analyse approfondie de toutes les vrilles et que nous présentons dans le prochain paragraphe.

6.4 - Analyse de l'ensemble des vrilles.

Au cours de cette analyse nous avons recherché l'influence des divers paramètres (sens de la vrille, sa durée, le moteur ...). Et il est apparu que seule la durée de la vrille (1t, 2t, 3t ou 5t) avait une action marquée sur la durée de sortie.

En effet, et comme le montre la planche 8, les sorties sont systématiquement satisfaisantes, sauf lorsque la manoeuvre de sortie est tentée à la fin du 2ème tour ; dans ce cas la récupération peut être :

- encore satisfaisante (3s)
- acceptable (4s)
- très longue (7s)
- impossible (utilisation de la fusée)

Ces résultats sont pour le moins surprenants car, entre autres, nous pourrions en conclure que si toutes les vrilles de l'avion avaient été longues (> 3 tours) il n'y aurait jamais eu de problèmes.

Compte-tenu de ces premiers résultats nous avons poussé plus loin l'analyse des vrilles ; cela nous a conduits aux résultats inclus dans la planche 9 qui, dans une certaine mesure, pourraient fournir une explication aux difficultés de sortie rencontrées après 2 tours de vrille.

Dans la planche 9 nous voyons en effet qu'à la fin du 2ème tour la vrille est plus sévère, et ce pourrait être cette aggravation passagère de la vrille qui détériorerait les sorties.

Il faut cependant reconnaître que cette explication ne peut pas nous satisfaire totalement ; nous avons déjà précisé qu'il existait une certaine dispersion entre les résultats avion et cela apparaît nettement dans la planche 10 ; dans cette planche, deux essais lancés dans des conditions (sens, moteur, centrage ...) identiques ont donné des vrilles très voisines à partir desquelles la récupération a été satisfaisante pour l'une et très longue pour l'autre.

L'interruption prématurée des essais n'a pas permis d'apporter de nouveaux éclaircissements sur ce point et ce n'est pas des essais en soufflerie verticale qui peuvent le faire.

7) Phase 4 : Deuxième étude en soufflerie.

L'incident que nous venons de décrire a provoqué une étude complémentaire en soufflerie ; compte tenu de la géométrie de la maquette et notamment de la faible corde de l'aile en son extrêmité nous avons envisagé une influence du nombre de Reynolds sur la voilure ($\mathcal{R}$ avion = 3.10^6, $\mathcal{R}$ maquette = $0{,}06.10^6$; nos essais ont donc été orientés dans ce sens. Avant de présenter les résultats de cette phase d'essais, nous donnons quelques renseignements qui nous furent très utiles pour la conduite de l'étude.

7.1 - Résultats NASA.

La planche 11 présente quelques résultats de mesures qui furent effectués à la NASA.

Le premier graphique montre l'évolution des courbes $C_z = f(\alpha)$ en fonction de $\mathcal{R}$ (réf.1) ; nous voyons en particulier que :

a) pour un domaine d'incidence relativement étendu (de 10° à 40°) l'influence de $\mathcal{R}$ est bien marquée et se caractérise par :

- une modification de la valeur de l'incidence de décrochage
- une variation du C_z max
- des inversions du gradient de portance.

b) l'effet Reynolds disparaît pour $\alpha > 45°$.

Le second graphique montre les possibilités de modifier sur une maquette les caractéristiques aérodynamiques (pour se rapprocher de celles avion) en modifiant le profil de la voilure. Le remède consiste à ajouter un bec sur toute ou partie de l'envergure (réf. 2).

7.2 - Incidences locales durant une vrille.

Du premier graphique de la planche 11 nous pourrions conclure que l'effet Reynolds ne se manifeste pas dans le domaine d'incidence de vrille ; en effet au cours d'une vrille l'incidence atteint fréquemment 45° et peut même aller beaucoup plus loin, de l'ordre de 70° pour une vrille plate. Mais il ne s'agit là que d'incidences moyennes, celles concernant le plan de symétrie.

Or si nous prenons en compte les incidences locales, intéressant en particulier la voilure, nous constatons (voir planche 12) que, par exemple, en extrêmité de l'aile extérieure l'incidence est relativement faible (surtout pour un planeur) ; en tout état de cause, au vu de la planche 11, cette extrêmité d'aile peut très bien être concernée par l'effet Reynolds, ce qui peut remettre en question la représentativité des phases de vrille en soufflerie.

Certes il n'y a pas lieu de généraliser cette remarque à tous les avions légers, car l'on sait que l'effet Reynolds en vrille est très dépendant des caractéristiques de la voilure (profil, envergure ...).

7.3 - Essais préliminaires à l'IMFL.

Au vu des résultats NASA nous avons commencé la deuxième étude du moto-planeur par des mesures sur balance en équipant la voilure de becs de formes diverses (voir planche 13) et parfois de petits volets braqués. Par la suite, pour les essais de vrille libre, il suffisait alors de choisir la géométrie de voilure qui donnait des $C_z(\alpha)$ les plus proches de ceux de l'avion.

Un obstacle se présentait cependant car pour l'avion concerné (et c'est souvent le cas pour des avions légers) nous n'avions que très peu de renseignements sur ses caractéristiques aérodynamiques (seul le $C_z$max était connu). En l'absence de ces renseignements nous avons alors procédé ainsi :

La vrille critique de l'avion (que nous devions reproduire en soufflerie) était bien définie ; en particulier nous connaissions ses principales caractéristiques (assiette longitudinale, durée de 1 tour) et cela pour trois phases de vrille bien précises et correspondant chacune à une combinaison de braquage de gouvernes bien définie, soit :

a) maintien de la vrille :
Direction Avec + Manche tiré + Ailerons neutre
b) première tentative de sortie :
Direction Contre + Manche poussé + Ailerons neutre
c) deuxième tentative de sortie :
Direction Contre + Manche poussé + Ailerons contre

voir planche 7

Nous avons alors reproduit sur la maquette ces trois combinaisons de gouvernes et, pour chacune d'elles, nous avons tenté de retrouver la vrille de l'avion en utilisant successivement les différentes géométries de voilure mises à notre disposition par les mesures sur balance.

Le résultat escompté fut obtenu avec une géométrie de voilure qui, lors des mesures sur balance, a donné les résultats inclus dans la planche 14. Les résultats de vrille libre obtenus avec la nouvelle géométrie sont donnés dans la planche 15 (qu'il faut comparer à la planche 7) ; le seul écart bien marqué concerne le phénomène obtenu avec les gouvernes pro-vrille et pour lesquelles la vrille en soufflerie est plus plate ; mais cet écart peut être attribué au fait que sur l'avion, à la fin du 2ème tour, la vrille stabilisée n'était pas encore atteinte.

7.4 - Etude complète de vrille libre.

Après obtention de ces premiers résultats nous avons approfondi les essais de vrille libre avec la voilure "Reynolds".

Les résultats de cette investigation sont donnés dans la planche 16 à partir de laquelle trois constatations importantes peuvent être faites.

En premier lieu nous voyons que dans un domaine de gouvernes (d'ailleurs assez restreint), des vrilles très plates (θ = -10°) et très rapides (1 s/t avion) sont observées ; ces vrilles sont nettement plus sévères que celles de l'avion, mais cela ne constitue pas un désaccord car le domaine "pro vrille plate" trouvé en soufflerie n'a pas été exploré sur l'avion.

La deuxième remarque importante concerne l'étendue du domaine des gouvernes à l'intérieur duquel la vrille se perpétue ou se maintient longtemps ; ce domaine recouvre, ou presque, la totalité du domaine des gouvernes ; en d'autres termes les possibilités de sortie sont nulles ou faibles. Cela confirme les problèmes de l'avion.

Enfin troisième remarque, d'après la planche 16 les possibilités (faibles) de récupération n'existent que si :

a) La direction est mise contre et le manche est poussé	consigne identique à celle trouvée précédemment sur la maquette "origine" (et confirmée sur avion)
b) Et si, en plus les ailerons sont mis Avec	alors que la consigne préconisée avec la maquette origine était ailerons Contre (voir § 1.)

Nous nous trouvons ainsi devant un cas (qui n'est d'ailleurs pas unique) pour lequel le sens d'action d'une gouverne (et donc la consigne) change, pour un même avion, selon le caractère de la vrille à vaincre.

Ainsi, lors de la vrille critique de l'avion, le pilote, se fiant aux consignes préconisées par la soufflerie (trouvées sur la maquette "origine" et définies pour contrer une vrille piquée) n'a pas appliqué la consigne totale permettant de vaincre une vrille plate.

En conclusion, les essais en soufflerie avec la maquette "Reynolds" ont permis de retrouver la vrille incontrôlée de l'avion ; mais ces essais ont aussi montré que la soufflerie n'avait pas fourni au pilote la totalité des informations susceptibles de maîtriser la vrille ; ou plus exactement la soufflerie avait donné tous renseignements valables pour contrer une vrille piquée, mais non valables, dans leur totalité, pour vaincre une vrille plate.

Remarque : **Pour** les raisons bien compréhensibles, l'étude en soufflerie a porté sur les points les plus intéressants pour l'avion, à savoir : la vrille critique et les moyens d'y remédier (ce qui fera l'objet du paragraphe 8).

Cependant de quelques essais faits avec voilure Reynolds il semble que, avec cette nouvelle géométrie, nous pouvons également reproduire la vrille la plus fréquente de l'avion, c'est-à-dire la vrille piquée sans problème.

De ces quelques essais il semblerait donc ressortir qu'une géométrie de maquette, modifiée pour remédier à l'effet Reynolds, n'élimine pas pour autant en soufflerie, certaines formes de vrille que l'avion est susceptible de rencontrer.

8) Phase (5) : Troisième étude en soufflerie.

Sur demande du constructeur, nous avons étudié diverses modifications de maquette (bien entendu équipée de la voilure "Reynolds") afin d'éliminer tout risque de vrille incontrôlable.

Ce résultat a été obtenu avec —. les empennages en T (voir planche 17 qui, comparée à la planche 16, montre une nette amélioration).

9) Conclusion.

Le cas de mauvaise prédiction (ou plus exactement de prédiction incomplète) que nous venons de décrire s'est présenté rarement au cours des 30 années d'essais de soufflerie à l'IMFL.

Cependant, lorsqu'une mauvaise corrélation est constatée entre les vrilles maquette et avion, l'écart est très souvent dans le sens indésirable (du point de vue sécurité s'entend) dans la mesure où les résultats de soufflerie sont optimistes.

Ces écarts nous ont conduits à modifier progressivement notre méthode d'essais, ainsi d'ailleurs que notre façon d'interpréter les résultats de soufflerie. A titre d'exemple, et compte tenu des résultats du moto-planeur, les essais de vrille libre sont maintenant précédés de mesures sur balance et cela pour toutes les maquettes d'avions légers ; en effet si nous considérons que la vrille d'un planeur peut, le plus, être affecté par l'effet Reynolds, certains résultats NASA et IMFL ont montré que les avions légers classiques n'étaient pas à l'abri de tels problèmes.

C - MODELISATION ET SIMULATION DE LA VRILLE PLATE.

Au cours de ces dernières années, ont été effectués à l'IMFL sur une même maquette d'avion d'armes, à la fois des essais de vrille libre en soufflerie verticale et des mesures sur montages dynamiques du torseur aérodynamique global.

Or, sur cette maquette, on a retrouvé en vrille libre, une vrille plate et rapide. Sur la base des résultats de mesures obtenus sur balance en soufflerie, nous avons donc essayé d'écrire un modèle aérodynamique, d'en identifier les principaux coefficients et de retrouver en simulation la vrille plate et rapide reconnue lors des lancers manuels à la soufflerie verticale. Ceci dans l'objectif d'essayer de corréler, à travers un modèle aérodynamique limité et adapté au domaine de la vrille plate, les mesures expérimentales sur balance avec le mouvement retrouvé sur maquette en vol libre.

L'intérêt d'une recherche de compréhension des phénomènes liés à la vrille plate réside dans le fait que ces vrilles sont les plus critiques, souvent irrécupérables par le jeu des gouvernes conventionnelles.

Au cours de cet exposé, nous présenterons successivement :

1) Les résultats expérimentaux en soufflerie.
2) Le modèle aérodynamique.
3) Les résultats de simulation.

I - Résultats expérimentaux.

Montages dynamiques.

L'Institut de Mécanique des Fluides est doté de deux montages permettant d'effectuer des essais dynamiques jusqu'aux très grandes incidences dans le domaine incompressible.

Le premier présenté (pl.18) est un montage tournant installé dans la soufflerie verticale de 4 m. de diamètre et permettant d'effectuer des mesures de coefficients en rotation continue.

Ce montage est particulièrement adapté à simuler la vrille puisqu'il permet d'effectuer des taux de rotation importants autour du vecteur vitesse jusqu'aux très grandes incidences.

Le second présenté (pl.19) est un montage d'oscillations forcées installé dans la soufflerie horizontale de l'IMFL et qui permet notamment les oscillations en roulis et tangage jusqu'à 90° d'incidence.

Maquette.

La maquette utilisée est une maquette d'avion d'armes de type général, présentant notamment les caractéristiques géométriques suivantes : aile en flêche à profil mince, voilure basse et fond fuselage plat.

a) Essais sur montage tournant.

Les essais sur la balance rotative ont été effectués à une vitesse de 30 m/s, soit un nombre de Reynolds par rapport à la corde de 330 000. Le programme, réalisé pour d'autres objectifs, couvrait un large domaine de vol et ne comptait qu'un nombre d'essais limité : mesures par pas de dix degrés en incidence, celle-ci variant de 0 à 80 degrés. Des essais en dérapage ont également été effectués par pas de dix degrés. Pour chaque valeur du couple (α , β) les mesures ont été faites en statique et en rotation continue pour trois valeurs distinctes de $\Omega \ell / V$.

Pour des raisons de commodité, propres à la modélisation, les résultats expérimentaux fournis sont les valeurs des coefficients aérodynamiques en repère lié au vent (C_{xa}, C_{ya} , C_{za}) et les coefficients de moment en repère maquette (C_ℓ , C_m , C_n). Nous présentons les résultats d'essais en essayant de dégager l'influence de chaque variable, à savoir successivement l'incidence, le dérapage et la rotation continue.

▪ *Variations en fonction de l'incidence.*

La remarque la plus notoire en ce qui concerne la variation des coefficients vis-à-vis de est l'apparition d'une importante discontinuité des valeurs du moment de lacet et de la force latérale à $\beta = 0$, pour une valeur de l'incidence comprise entre 40 et 60 degrés (pl.20).

Au vu de nombreux résultats expérimentaux tant français (IMFL, CEAT ...) qu'étranger (NASA ...), cette discontinuité correspond à un effet bien connu de pointe avant :

- cette discontinuité semble apparaître simultanément sur C_{ya} et C_n
- les valeurs de C_{ya} et C_n sont de même signe
- le moment de roulis (C_ℓ) reste, quant à lui, de très faible amplitude. Cette asymétrie attribuée à l'existence de vortex dissymétriques au niveau du nez de l'avion (4). Cette structure d'écoulement crée une importante force de pression latérale dont le point d'application se trouve à proximité de l'axe longitudinal et à l'avant de la maquette.

Au-delà de cette dissymétrie, le moment de lacet redevient en module beaucoup plus faible.

Par contre, le moment de tangage reste quant à lui constamment négatif, décroissant en fonction de l'incidence, et de module très important comparé au moment de lacet.

Par ailleurs, nous donnons (pl.21) le tracé de la polaire de cette maquette qui, nous le verrons plus loin, jouera un rôle important dans la modélisation de la vrille plate.

■ *Variations en fonction du dérapage.*

Plusieurs principaux résultats d'expérience peuvent être résumés ainsi :

- Les paramètres longitudinaux (C_{xa}, C_{za}, C_m) se trouvent relativement peu influencés par le dérapage, tout au moins tant que celui-ci ne dépasse pas en module 10 degrés.

- Le moment de roulis, par contre, dépend fortement de la valeur du dérapage comme le montre la planche 22 où l'on peut voir que, jusqu'aux très grandes incidences, C_ℓ reste linéaire en fonction de β, la dérivée $C_{\ell\beta}$ conservant sur un large domaine d'incidence une valeur quasi-constante et restant de toute façon négative : l'effet "dièdre" est conservé jusqu'à 90 degrés d'incidence.

- Les coefficients C_{ya} et C_n sont, eux aussi, jusqu'aux très grandes incidences, fort dependants du dérapage comme nous le montrent les planches 23 et 24. D'ailleurs à ce sujet deux faits importants peuvent être notés.

. Les dérivées $C_{n\beta}$ et $C_{ya\beta}$ s'annulent et changent de signe simultanément pour une valeur de de l'ordre de 23 degrés. A partir de cette incidence, l'effet "girouette" disparaît et la maquette devient instable en dérapage.

. La discontinuité trouvée à β nul existe encore lorsqu'il y a du dérapage et agit dans le même sens que précédemment. On peut considérer que l'on a ici superposition de deux effets, l'effet de dérapage et celui de pointe avant. La courbe obtenue à $\beta = 0$ pouvant en première approximation être considérée comme la courbe moyenne de celle à $\beta = +10°$ et $\beta = -10°$. De plus, nous pouvons considérer que les coefficients aux très grands angles varient linéairement avec le dérapage.

■ *Variations en fonction de $\Omega \ell / V$.*

La rotation imposée à la maquette est une rotation centrée sur le centre d'inertie autour du vecteur vitesse. Au cours d'un tour incidence et dérapage sont donc constants. Sur la planche 25 nous pouvons noter la dépendance du moment de lacet vis-à-vis de la rotation. Sur cette figure, nous pouvons distinguer grossièrement trois zones d'incidence où le comportement du C_n semble différent :

. La zone où α est inférieur à 30 degrés d'incidence. Dans cette région, le comportement en lacet peut très bien se traduire grâce à un modèle linéaire comportant les dérivées de stabilité dynamiques classiques : C_{np} et C_{nr}.

. La zone comprise entre 30 et 60 degrés d'incidence où quelle que soit la valeur de $\Omega \ell / V$, on retrouve l'asymétrie de l'écoulement et la discontinuité trouvée en statique. Dans cette zone, C_n atteint un minimum aux alentours de 50° pour une valeur comprise entre .12 et .15.

. Enfin la zone des très grandes incidences où le moment revient en module à des valeurs beaucoup plus faibles. Dans cette région la dépendance vis-à-vis de $\Omega \ell / V$ apparaît complexe et surtout difficile à identifier car les moments de lacet correspondants sont petits, la détermination de dérivees dans un domaine de variation aussi étroit est très sensible aux bruits de mesure. Nous verrons d'ailleurs par la suite que, pour la vrille plate et rapide, le moment de lacet aérodynamique est en valeur absolue très faible. Mais sa variation, sa dépendance vis-à-vis des variables d'état, joue un rôle important dans l'équilibre de vrille.

b) Essais en oscillations forcées.

Le montage balance rotative favorise cinématiquement, dans le domaine de la vrille plate, la vitesse de lacet par rapport aux autres vitesses de rotation. Celles-ci ont des modules trop faibles pour permettre une bonne identification des coefficients de stabilité correspondants, en l'occurrence les coefficients d'amortissement C_{mq} et $C_{\ell p}$.

Nous disposions de résultats d'essais en oscillations forcées effectuées dans la soufflerie horizontale de 2 m de diamètre de l'IMFL. Ce montage permet d'effectuer, jusque dans le domaine des très grandes incidences, des oscillations de tangage et de roulis (pl. 19).

Le traitement de ces mesures nous permet d'identifier les coefficients dérivés de stabilité.

II - Modélisation de la vrille plate.

A partir des données aérodynamiques présentées précédemment, nous avons essayé d'écrire un modèle prenant en compte les principaux effets aérodynamiques dans le domaine de la vrille plate.

Mais l'objectif fixé était surtout d'essayer de dégager certains facteurs structurels importants dans un tel modèle aérodynamique. Ce modèle tente donc de traduire schématiquement les caractéristiques essentielles.

Nous avons donc été amenés à faire une série d'hypothèses, certaines d'entre elles tiennent aussi à la limitation du nombre de mesures effectuées et de la quantité d'informations disponibles.

Les efforts aérodynamiques sont supposés être la superposition de différents effets bien distincts :

. L'effet de l'incidence ; ce paramètre est fondamental. Les résultats de mesure obtenus en statique, en fonction de l'incidence, sont considérés comme des fonctions à part entière $C_{xi}(\alpha)$. Pour chaque coefficient les courbes $C_{xi}(\alpha)$ sont tabulées, mises en mémoire et utilisées comme une donnée aérodynamique de base.

. L'effet du dérapage.

Comme nous l'avons signalé précédemment, dans le domaine qui nous intéresse, l'effet du dérapage peut être considéré comme linéaire. Il intervient donc par l'intermédiaire d'une dérivée première.

. L'effet de la rotation de vrille.

Nous avons vu, à travers les courbes expérimentales de C_n (pl.25), qu'il était difficile de distinguer l'effet de la rotation aux très grandes incidences. Les différentes valeurs du coefficient de moment restant en module petites, empêchent une identification ou même une linéarisation. Il faudrait pour cela une très grande précision de mesure et quand bien même y arriverait-on que le problème du choix du modèle de représentation se poserait encore. Or, il est évidemment nécessaire de bien prendre en compte les caractéristiques du moment de lacet lorsque l'on veut pouvoir simuler une vrille plate et rapide stable, et l'introduction dans le modèle de simples termes dérivés par rapport à la rotation ne sont pas apparus satisfaisants pour simuler une vrille plate et rapide.

Nous avons donc essayé de modéliser l'effet de la rotation en partant de considérations physiques et en effectuant certaines hypothèses.

Tout d'abord l'effet de la rotation sur le moment de lacet est supposé être la superposition de deux phènomènes différents :

. Un effet d'amortissement dû notamment à la présence du fuselage et de la dérive, lequel peut en première approximation être considéré linéaire.

. Un effet dû à la variation d'incidence suivant l'envergure lorsque la voilure est en rotation. En effet, chaque section de l'aile avançante voit une incidence locale d'autant plus faible qu'elle se trouve près de l'extrêmité, tandis qu'inversement sur l'aile reculante l'incidence locale croît. Connaissant la polaire du profil on peut alors calculer les efforts aérodynamiques locaux et en déduire par intégration les couples résultants. Ceci revient à faire l'hypothèse de l'écoulement par tranches. Une méthode analogue a déjà, par le passé, été utilisée, notamment par Glauert et Knight afin d'expliquer les phénomènes d'autorotation d'aile seule.

Mais par ailleurs, faute de données aérodynamiques sur les profils, nous avons été amenés à utiliser pour ces calculs la polaire de la maquette mesurée en soufflerie, ce qui revient :

- d'une part à considérer que le 1/2 avion gauche et le 1/2 avion droit ont même polaire (une telle hypothèse serait plus délicate dans la région d'incidence où l'écoulement est apparu fortement dissymétrique),

- d'autre part à considérer que l'effet de la rotation peut être traduit en prenant pour chaque section la même polaire, celle mesurée globalement sur la maquette. Cette hypothèse est discutable mais n'a toutefois été utilisée que parce que l'on se trouvait dans le domaine des très grandes incidences, là où l'écoulement est complètement décroché.

Le modèle aérodynamique utilisé est présenté planche 26. Tous les termes de ce modèle correspondant à des coefficients dérivés ont été identifiés, à partir des mesures expérimentales, par la méthode des moindres carrés.

III - Simulation.

Avant de présenter les résultats de simulation, il convient de présenter un peu plus précisément les résultats expérimentaux obtenus sur la maquette en vrille libre.

Résultats de vrille libre.

Dans un grand domaine des gouvernes, on retrouve en vol libre dans la soufflerie verticale de l'IMFL deux principaux types de phénomènes.: - la vrille plate et rapide stable,
- des vrilles à agitations divergentes.

Pour une même condition de centrage et une même position des gouvernes, les deux phénomènes peuvent se retrouver en fonction des conditions initiales données lors du lancer manuel en vrille. Mais pour la vrille stable, l'incidence se situe toujours entre [illegible] et 85 degrés, le taux de rotation entre [illegible] et [illegible] tours par seconde, ceci en fonction des conditions de centrage et des gouvernes.

Simulation.

A partir du modèle du torseur des efforts aérodynamiques (pl.26), on peut intégrer les équations de la mécanique (pl.27) et obtenir l'évolution temporelle de toutes les variables. Ne possédant pas de résultats relatifs aux efficacités de gouvernes, nous n'avons étudié, que pour une même configuration : tout au neutre, l'influence des conditions initiales de lancer sur les états d'équilibre de vrille obtenus.

Résultats.

Dans les équations d'équilibre en roulis et lacet, les couples aérodynamiques dus à la variation d'incidence sur la voilure interviennent. Or ceux-ci sont calculés à partir de la donnée de polaire obtenue en statique. Mais, rappelons-le, cette polaire a été mesurée avec un grand pas d'incidence. De plus utiliser dans le modèle la même polaire en chaque section d'aile est une approximation schématique. Etant donné qu'il est nécessaire pour le calcul d'avoir pour chaque valeur précise de l'incidence une valeur du C_{xa} et du C_{za}, nous avons effectué la simulation pour deux types de polaire qui, comme on peut le voir sur la planche 21, tout en passant par les mêmes points de mesure, diffèrent dans la région des très grands angles.

Or, pour les deux cas, nous retrouvons en simulation un comportement fort différent :

. Dans le premier cas (polaire 1), quelles que soient les conditions initiales données à la maquette on ne retrouve pas de vrille stable.

. Dans le second cas (polaire 2) nous retrouvons tant pour un lancer à droite qu'à gauche un équilibre stable de vrille plate et rapide. De plus on note également en simulation une dépendance du mouvement obtenu vis-à-vis des conditions de lancer :

- pour un lancer plat et rapide, on retrouve une vrille plate ($\alpha \simeq$ [illegible]°), rapide ([illegible] tours/s) et stable. Cette vrille est bien calme comme le montre la planche 28.A et l'assiette latérale [illegible] est très faible, mais non nulle (de l'ordre de -1°). Cette caractéristique est très difficile à mesurer à partir des films de vrille libre, cela nécessiterait une instrumentation de la maquette appropriée,

- si le lancer est un peu moins plat et un peu moins rapide, la maquette atteint la même vrille, mais le mouvement comporte de légères agitations stables elles aussi (pl. 28.B),

- enfin, pour un lancer *encore moins* plat et moins rapide,la vrille comporte de fortes agitations de tangage et de roulis, lesquelles font diverger vers la sortie (pl. 28.C).

Ces résultats appellent quelques remarques :

- Une bonne définition de la polaire est nécessaire dans notre modèle pour prendre en compte correctement l'effet de la variation d'incidence due à la rotation et retrouver un équilibre stable de vrille plate et rapide.

- Dans les deux cas on peut, pour différentes valeurs de la rotation et de l'incidence au c.d.g., calculer les couples induits par la variation d'incidence en envergure. Nous donnons, à ce sujet, sur la planche 29 les valeurs en terme de coefficient du moment autour du vecteur vitesse (C_{ia}) dans les deux cas de polaire. En comparant les deux planches 29.A et 29.B, nous pouvons voir que pour le point d'équilibre de vrille plate retrouvé (75° d'incidence, 720°/s), les valeurs du couple ne sont pas sensiblement différentes, elles sont d'ailleurs dans les deux cas négatives. Par contre autour de ce point, la valeur du gradient par rapport à diffère complètement. L'obtention, dans le cas de la polaire 2 d'une dérivée locale $\partial C_{ia} / \partial \alpha$ de signe contraire au sens de la vrille, donc opposé à celui de Ω, jouant un rôle stabilisant sur la vrille.

D'ailleurs, nous montrons en annexe, que cette caractéristique peut être retrouvée en écrivant l'équation aux petits mouvements autour d'un état d'équilibre de vrille plate.

IV - Conclusion.

Cette étude n'est évidemment qu'un premier pas vers une modélisation et une simulation de la vrille plate et rapide prenant en compte le phénomène dans son intégralité. Cependant, le modèle décrit ici, bien que simplifié, a quand même permis de retrouver une vrille plate et rapide stable, et a d'autre part mis l'accent sur une caractéristique aérodynamique pouvant sensibiliser de façon importante la stabilité de la vrille plate.

Certaines hypothèses du modèle pourraient être levées en disposant d'une donnée aérodynamique plus riche, ce qui permettrait de mieux étudier la fiabilité du modèle et son domaine de validité. Si un tel modèle se révèle susceptible de représenter le phénomène de vrille plate, il est alors envisageable d'en tirer des enseignements très intéressants, d'autant que la vrille plate et rapide présente bien souvent un caractère dangereux pour la sécurité du pilote et de l'avion.

Ainsi par exemple, l'effet du gauchissement, qui se révèle très important sur une telle vrille, pourrait trouver son explication dans le modèle : un braquage des ailerons revenant à modifier sensiblement le profil, donc la polaire sur une section donnée de la voilure. De même, l'effet pro-agitations des ailerons, qui apparaît parfois en vrille plate et rapide, pourrait correspondre à un effet destabilisant dû à la modification du terme $\partial C_{l_a} / \partial\alpha$ autour du point d'équilibre. Ces agitations pouvant, par ailleurs, faire diverger la vrille et engager la sortie.

Enfin d'autres applications pratiques sont envisageables : souvent l'extrême sévérité de la vrille plate et rapide empêche toute sortie quelle que soit la position des gouvernes. Il convient donc de trouver en soufflerie verticale, une modification géométrique de la maquette permettant de rendre saine une telle vrille. Une telle modification pourrait alors être aiguillée par un modèle aérodynamique prenant suffisamment en compte les phénomènes physiques essentiels.

R E F E R E N C E S

(1) Overview of stall-spin technology
AIAA paper - J.R.Chambers - NASA 11-13 Août 1980.

(2) General aviation stall-spin workshop
NASA 3-4 Septembre 1980.

(3) La vrille et leurs essais
C.F.V. Istres - I.P.A. Lelaie - Février 1978.

(4) Recent experience with techniques for prediction of spin characteristics of fighter aircraft
Journal of Aircraft - J.R.Chambers - J.S.Bowman - Juillet 1971.

A N N E X E

On se place dans les conditions d'une vrille plate calme et où l'angle de gite ϕ sera supposé nul. On écrit alors les équations d'équilibre en tangage et autour du vecteur vitesse. Ceci nous donne le système :

$$\dot{\alpha} = q \qquad (1)$$

$$[A\dot{p} + (C-B)qr]\cos\alpha + [C\dot{r} + (B-A)pq\sin\alpha] = L_a(\alpha,\Omega) \qquad (2)$$

$$B\dot{q} = (C-A)pr + M(\alpha,q) \qquad (3)$$

On effectue une étude aux petits mouvements en introduisant les variations élémentaires $\delta\alpha$, $\delta\Omega$ et δq autour de l'état d'équilibre ($\alpha_0, \Omega_0, q_0 = 0$). Compte tenu de $p_0 = \Omega_0 \cos\alpha_0$, $r_0 = \Omega_0 \sin\alpha_0$ nous aboutissons au système linéaire :

$$\begin{pmatrix} \delta\dot{\alpha} \\ \delta\dot{\Omega} \\ \delta\dot{q} \end{pmatrix} = \begin{pmatrix} 0 & 0 & 1 \\ L_{a\alpha}/K & L_{a\Omega}/K & -J\Omega_0/K \\ I/B & J\Omega_0/B & M_q/B \end{pmatrix} \begin{pmatrix} \delta\alpha \\ \delta\Omega \\ \delta q \end{pmatrix}$$

où : $I = M_\alpha + \Omega_0^2 (C-A)\cos 2\alpha_0$

$J = (C-A)\sin 2\alpha_0$

$K = A\cos^2\alpha_0 + C\sin^2\alpha_0$

L'équation caractéristique de ce système s'écrit : $0 = \lambda^3 - \left(\frac{L_{a\Omega}}{K} + \frac{M_q}{B}\right)\lambda^2 + \left(\frac{L_{a\Omega}M_q}{B} - \frac{I}{B} + \frac{J^2\Omega_0^2}{KB}\right)\lambda + \frac{I L_{a\Omega} - J\Omega_0 L_{a\alpha}}{KB}$

Pour que l'équilibre soit stable il faut que le polynôme caractéristique ne possède pas de solution à partie réelle positive. Or pour que $\lambda^3 + b\lambda^2 + c\lambda + d$ ait ses solutions à partie réelle négative il faut que : $b > 0 \quad c > 0 \quad d > 0$

Soit

- $\left(\frac{L_{a\Omega}}{K} + \frac{M_q}{B}\right) < 0$
- $\left(\frac{L_{a\Omega} \cdot M_q}{KB} + \frac{J^2\Omega_0^2}{KB} - \frac{I}{B}\right) > 0$
- $\left(I L_{a\Omega} - J L_{a\alpha}\Omega_0\right) > 0$

Remarques : 1) La condition (I) est toujours vérifiée dans la mesure où $L_{\omega\Omega}$ et M_q, qui sont des termes d'amortissement, sont négatifs.

2) Pour une vrille à plus de 45 degrés d'incidence, la quantité I est négative si le M_α est négatif. Alors la condition (II) est également vérifiée.

3) La condition (III) peut s'écrire : $I L_{\omega\Omega} > J L_{\alpha\alpha} \Omega_o$. Le membre de gauche est positif, de plus J est positif. Nous voyons que si le $L_{\alpha\alpha}$ est de signe opposé à Ω_o, le membre de droite est négatif et la condition est vérifiée. Donc un terme $\partial C_{\ell\omega}/\partial\alpha$ de signe opposé à Ω_o est un facteur stabilisant sur la vrille (tout au moins sur la vrille plate). Inversement un $\partial C_{\ell\omega}/\partial\alpha$ de même signe que Ω_o, et suffisamment important en module, peut suffire à empêcher l'équilibre de vrille plate et rapide.

PLANCHES

VRILLE CALME
ATTITUDES LONGITUDINALES
SELON LA TRAJECTOIRE

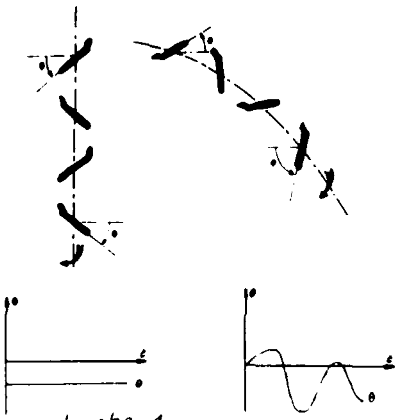

planche 1

FIGURATION VRILLE

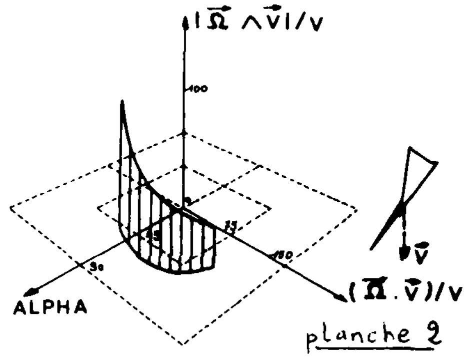

planche 2

RECONNAISSANCE DES PRINCIPAUX MOUVEMENTS, HORS AGITATIONS

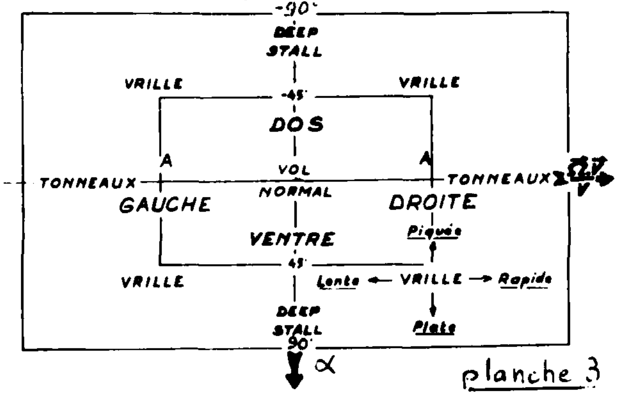
-90°
DEEP STALL
VRILLE
VRILLE
-45°
DOS
A
A
TONNEAUX
VOL NORMAL
TONNEAUX
Ω.V/V
GAUCHE
DROITE
VENTRE
Piqués
45°
VRILLE
Lente
VRILLE
Rapide
DEEP STALL
Plate
90°
α

planche 3

LE MOTO-PLANEUR R.F.10

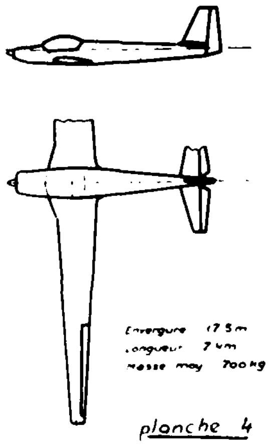
Envergure 17,5 m
Longueur 7 m
Masse moy 700 kg

planche 4

Planche 5

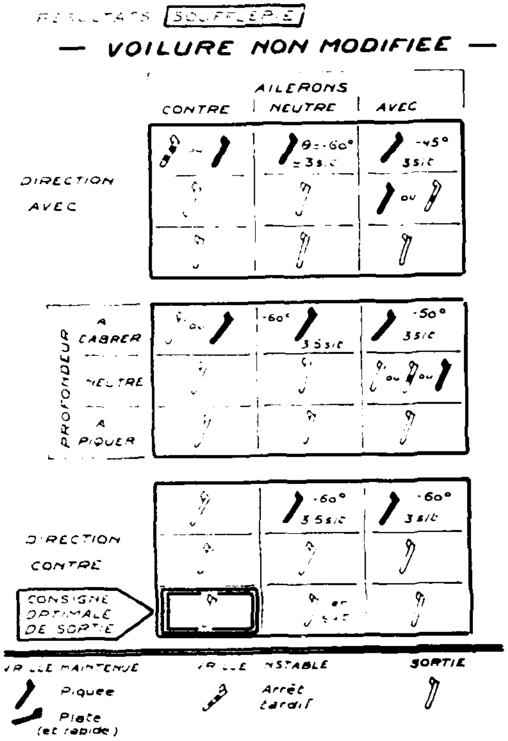
RESULTATS SOUFFLERIE
— VOILURE NON MODIFIEE —
AILERONS
CONTRE
NEUTRE
AVEC
DIRECTION AVEC
θ=-60°
≈3 s/t
-45°
3 s/t
ou
A CABRER
NEUTRE
A PIQUER
PROFONDEUR
ou
-60°
3,5 s/t
-50°
3 s/t
ou
ou
DIRECTION CONTRE
-60°
3,5 s/t
-60°
3 s/t
CONSIGNE OPTIMALE DE SORTIE
en
VRILLE MAINTENUE
Piquee
Plate (et rapide)
VRILLE INSTABLE
Arrêt tardif
SORTIE

Planche 6

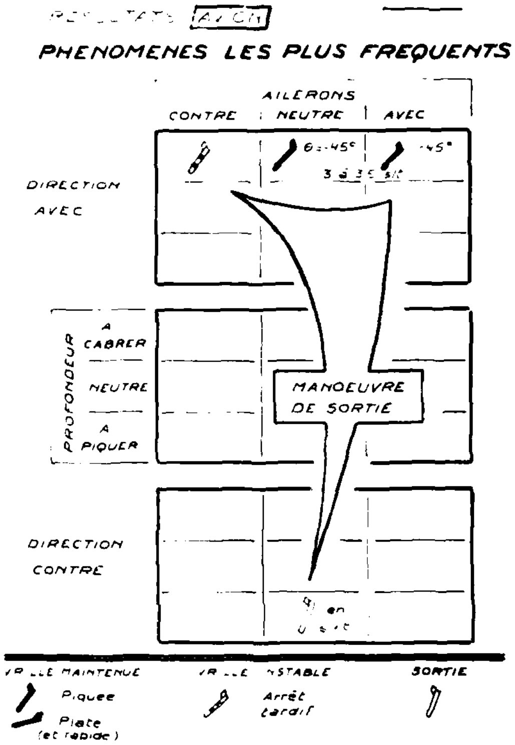
RESULTATS AVION
PHENOMENES LES PLUS FREQUENTS
AILERONS
CONTRE
NEUTRE
AVEC
DIRECTION AVEC
θ=-45°
-45°
3 à 3,5 s/t
A CABRER
NEUTRE
A PIQUER
PROFONDEUR
MANOEUVRE DE SORTIE
DIRECTION CONTRE
en
VRILLE MAINTENUE
Piquee
Plate (et rapide)
VRILLE INSTABLE
Arrêt tardif
SORTIE

Planche 7

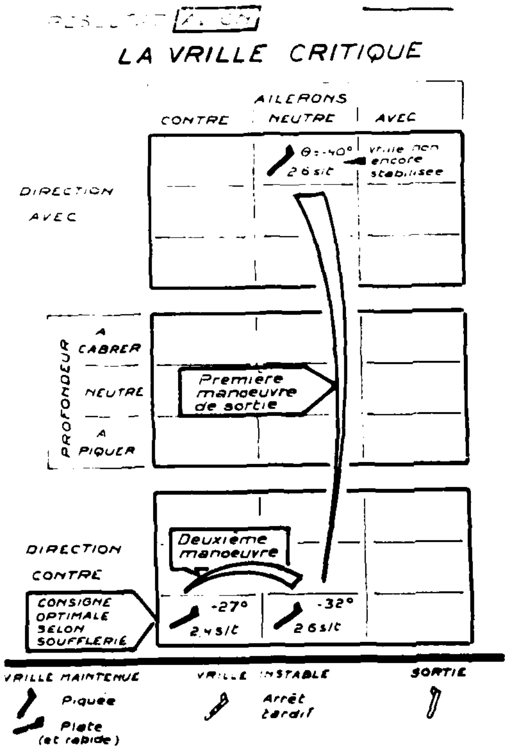
RESULTATS AVION
LA VRILLE CRITIQUE
AILERONS
CONTRE
NEUTRE
AVEC
DIRECTION AVEC
θ=-40°
2,6 s/t
vrille non encore stabilisee
A CABRER
NEUTRE
A PIQUER
PROFONDEUR
Première manoeuvre de sortie
DIRECTION CONTRE
Deuxième manoeuvre
CONSIGNE OPTIMALE SELON SOUFFLERIE
-27°
2,4 s/t
-32°
2,6 s/t
VRILLE MAINTENUE
Piquée
Plate (et rapide)
VRILLE INSTABLE
Arrêt tardif
SORTIE

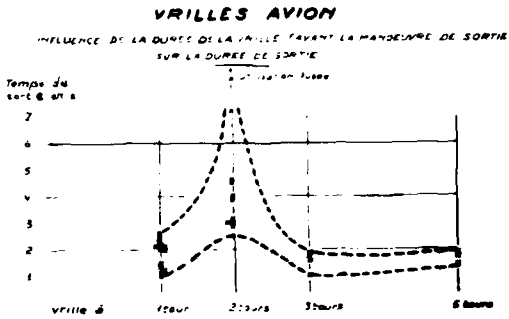

planche 8

VRILLES AVION Planche 9

EVOLUTION DE r POUR LES LONGUES VRILLES (3 et 5t)

AILERONS [NEUTRE OU AVEC]

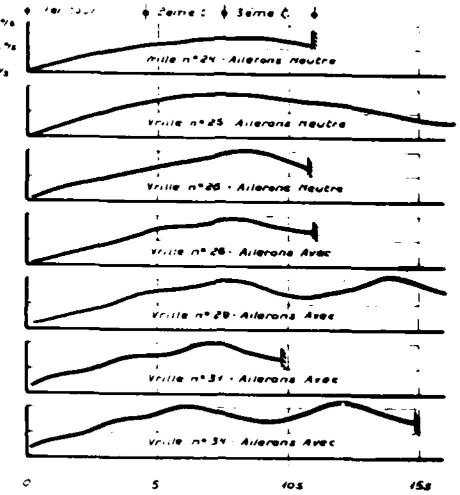

Date de manoeuvre de sortie sur les gouvernes

Note : en considerant que plus r est eleve plus la vrille est severe (plus plate) cette planche precise donc l'evolution dans le temps de la severite de la vrille

Planche 10 VRILLES AVION

EXEMPLES DE DISPERSION DES RESULTATS

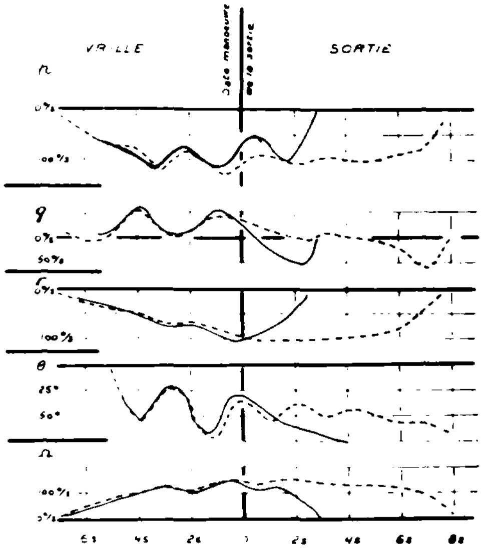

— Vrille n° 30
----- Vrille n°21

2 tours à Gauche ~ 33%
Ailerons Avec
Moteur coupé

Planche 11 RESULTATS NASA

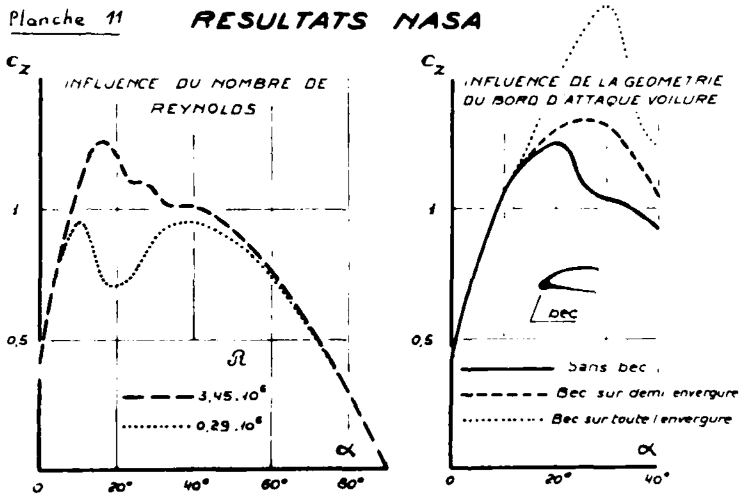

INCIDENCES LOCALES PENDANT LA VRILLE

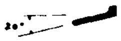

VRILLE PLATE ET RAPIDE
θ = -20° 2 s/t

AVION LEGER	≃ 45°	70°	≃ 95°
PLANEUR	≃ 30°	70°	≃ 110°

INCIDENCE	en extrémité d'aile extérieure	dans le plan de symétrie	en extrémité d'aile intérieure

AVION LEGER	≃ 30°	45°	≃ 60°
PLANEUR	≃ 20°	45°	≃ 70°

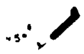

VRILLE MOYENNEMENT PIQUEE
θ = -45° 3 s/t

planche 12

Planche 13

RESULTATS IMFL

MESURES SUR BALANCE AVEC DIVERSES GEOMETRIES DE VOILURE

(Modifications du bord d'attaque seulement)

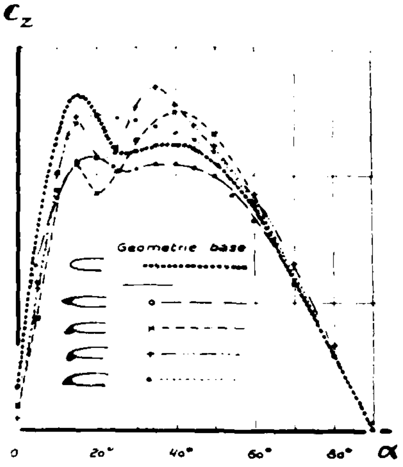

Planche 14

MESURES DE PORTANCE

sur maquette voilure origine et modifiée

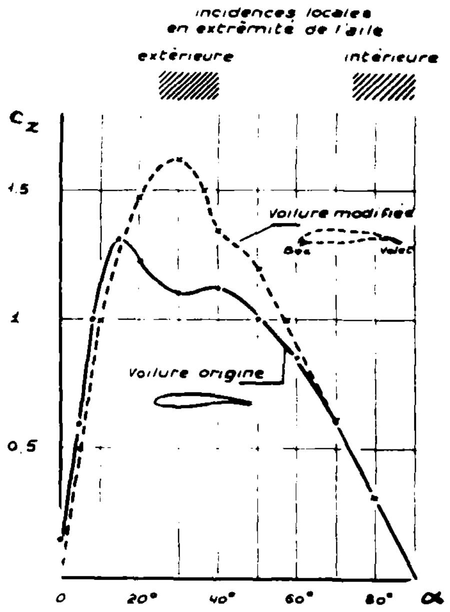

Planche 15

PREMIERS RESULTATS SOUFFLERIE

VOILURE "REYNOLDS"

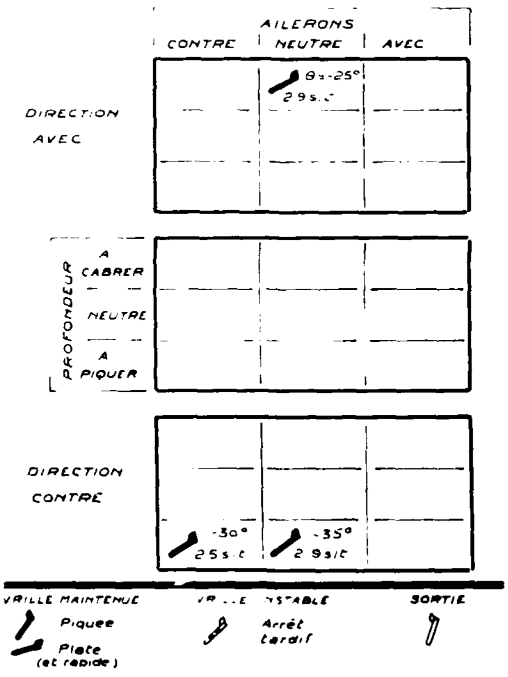

AILERONS
CONTRE
NEUTRE
AVEC
DIRECTION AVEC
θ = -25°
2.9 s/t
PROFONDEUR
A CABRER
NEUTRE
A PIQUER
DIRECTION CONTRE
-30°
2.5 s/t
-35°
2.9 s/t
VRILLE MAINTENUE
Piquee
Plate
(et rapide)
VRILLE INSTABLE
Arrêt tardif
SORTIE

Planche 16

RESULTATS COMPLETS SOUFFLERIE

VOILURE "REYNOLDS"

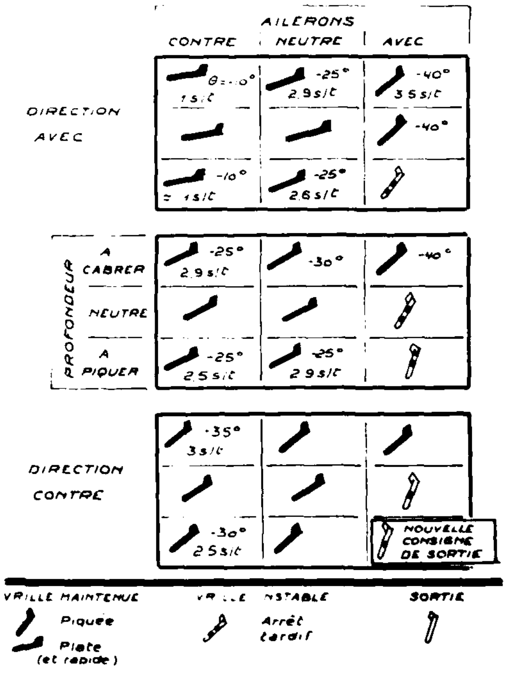

AILERONS
CONTRE
NEUTRE
AVEC
DIRECTION AVEC
θ = -10°
1 s/t
-25°
2.9 s/t
-40°
3.5 s/t
-40°
-10°
≃ 1 s/t
-25°
2.6 s/t
PROFONDEUR
A CABRER
NEUTRE
A PIQUER
-25°
2.9 s/t
-30°
-40°
-25°
2.5 s/t
-25°
2.9 s/t
DIRECTION CONTRE
-35°
3 s/t
-30°
2.5 s/t
NOUVELLE CONSIGNE DE SORTIE
VRILLE MAINTENUE
Piquee
Plate
(et rapide)
VRILLE INSTABLE
Arrêt tardif
SORTIE

RESULTATS SOUFFLERIE

Planche 17

EMPENNAGES EN T + VOILURE REYNOLDS

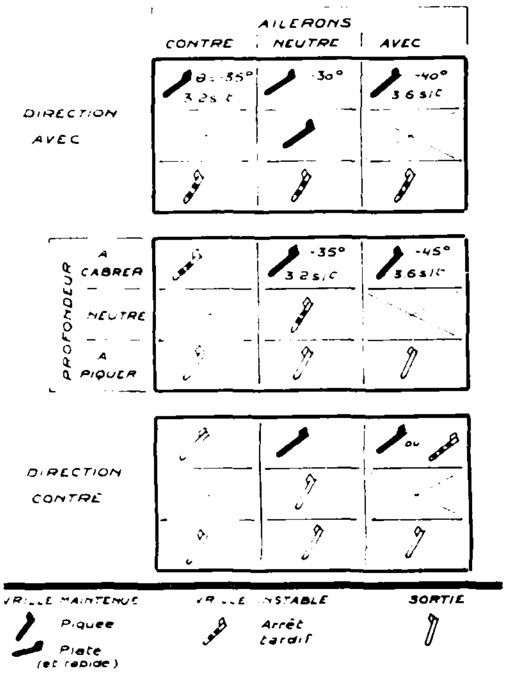

Planche 18

SCHEMA DU MONTAGE TOURNANT

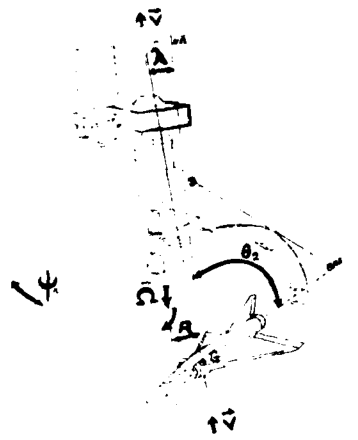
$\vec{V}$
λ
θ₂
ψ
Ω
R
G
$\vec{V}$

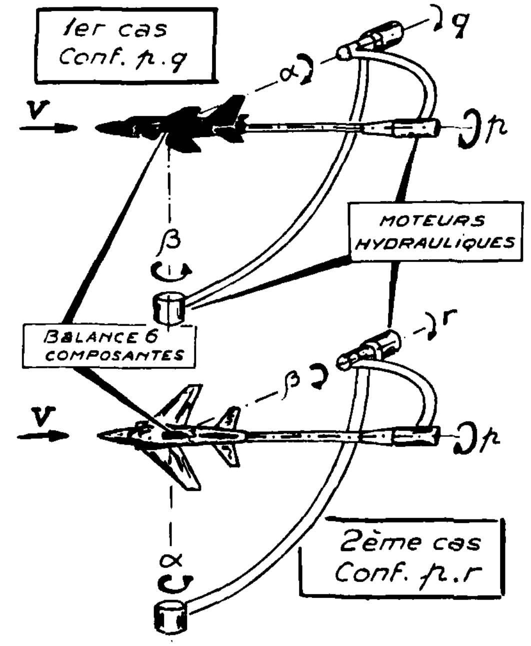
1er cas
Conf. p.q
q
α
V
p
β
MOTEURS HYDRAULIQUES
BALANCE 6 COMPOSANTES
r
β
V
p
α
2ème cas
Conf. p.r

Planche 19 . Montage oscillant

APPARITION DE L'ASYMETRIE D'ECOULEMENT A $\beta = 0$ SUR C_n ET C_{y_a}

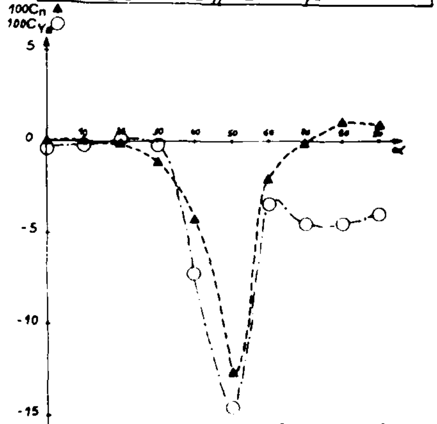

Planche 20

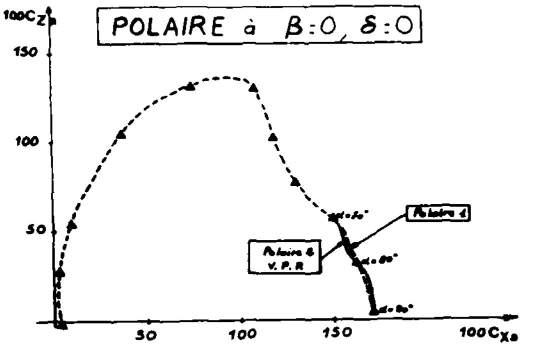

Planche 21

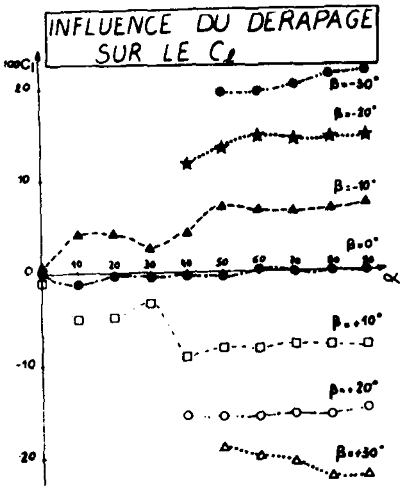

Planche 22

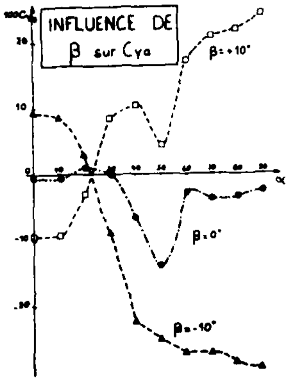

Planche 23

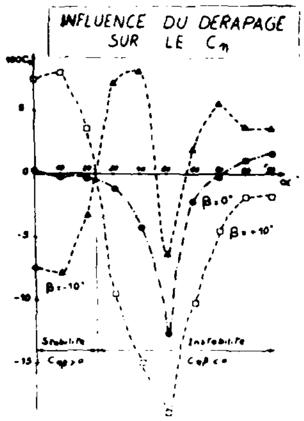

Planche 24

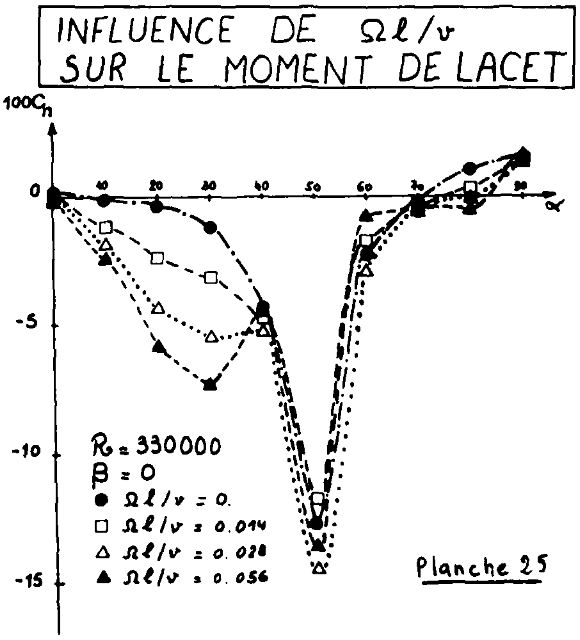

Planche 25

MODELE AERODYNAMIQUE
DE VRILLE PLATE
$\delta = 0°$

Planche 26

$$C_{x_0}(\alpha,\beta,p,q,r) = C_{x_0}(\alpha)$$

$$C_{y_0}(\alpha,\beta,p,q,r) = C_{y_0}(\alpha) + C_{y_0\beta}\cdot\beta + C_{y_0p}\cdot\frac{p\ell}{V}$$

$$C_{z_0}(\alpha,\beta,p,q,r) = C_{z_0}(\alpha) + C_{zq}\cdot\frac{q\ell}{V}$$

$$C_\ell(\alpha,\beta,p,q,r) = C_{\ell\beta}\cdot\beta + C_{\ell p}\cdot\frac{p\ell}{V}$$

$$C_m(\alpha,\beta,p,q,r) = C_m(\alpha) + C_{mq}\cdot\frac{q\ell}{V}$$

$$C_n(\alpha,\beta,p,q,r) = C_n(\alpha) + C_{n\beta}\cdot\beta + C_{nr}\cdot\frac{r\ell}{V}$$

$$\vec{m} = \frac{1}{2}\rho S\int_{aile} y\,v^2(y)\left[C_{x_0}(\alpha(y)).\vec{X}_0 + C_{z_0}(\alpha(y)).\vec{Z}_0\right]dy$$

$$\alpha(y) = \mathrm{Arctg}\left(\frac{w+py}{u-ry}\right)$$

$$v^2(y) = V^2 + y^2(p^2+r^2)$$

SIMULATION
EQUATIONS GENERALES

Planche 27

$$m\dot{u} = m(rv-qw) - mg\sin\theta + \frac{1}{2}\rho SV^2C_x$$

$$m\dot{v} = m(pw-ru) + mg\cos\theta\sin\phi + \frac{1}{2}\rho SV^2C_y$$

$$m\dot{w} = m(qu-pv) + mg\cos\theta\cos\phi + \frac{1}{2}\rho SV^2C_z$$

$$A\dot{p} - E\dot{r} = (B-C)qr + Epq + \frac{1}{2}\rho SV^2C_\ell + m_\ell$$

$$B\dot{q} = (C-A)pr + E(p^2-r^2) + \frac{1}{2}\rho SV^2C_m$$

$$C\dot{r} - E\dot{p} = (A-B)pq - Eqr + \frac{1}{2}\rho SV^2C_n + m_n$$

$$\dot{\Psi} = (q\sin\phi + r\cos\phi)/\cos\theta$$

$$\dot{\theta} = q\cos\phi - r\sin\phi$$

$$\dot{\phi} = p + (q\sin\phi + r\cos\phi)\,\mathrm{tg}\,\theta$$

Planche 28

RESULTATS de SIMULATION

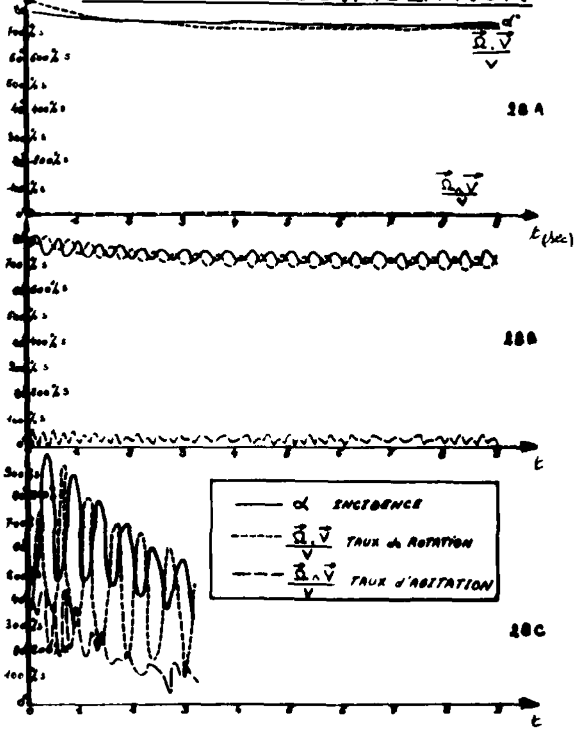

COUPLE INDUIT SUR LA VOILURE PAR LA ROTATION
(vrille a droite)

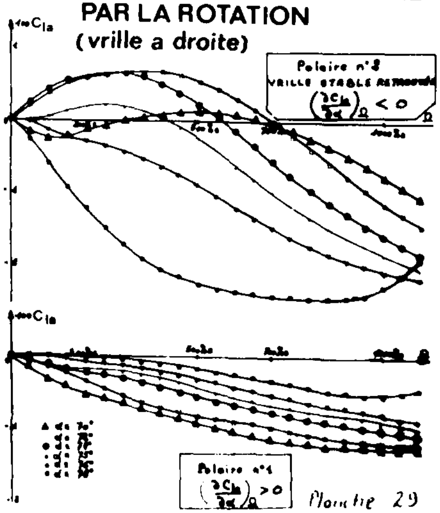

Planche 29

DYNAMIC STRUCTURAL AEROELASTIC STABILITY TESTING OF THE XV-15 TILT ROTOR RESEARCH AIRCRAFT

by

L. G. Schroers
Aeromechanics Laboratory
U.S. Army Aviation R&D Command
Ames Research Center
Moffett Field, California 94035, U.S.A.

ABSTRACT

For the past 20 years, a significant effort has been made to understand and predict the structural aeroelastic stability characteristics of the tilt rotor concept. Beginning with the rotor-pylon oscillation of the XV-3 aircraft, the problem was identified and then subjected to a series of theoretical studies, plus model and full-scale wind tunnel tests. From this data base, methods were developed to predict the structural aeroelastic stability characteristics of the XV-15 Tilt Rotor Research Aircraft. This paper examines the predicted aeroelastic characteristics in light of the major parameters effecting rotor-pylon-wing stability; describes flight test techniques used to obtain XV-15 aeroelastic stability; presents a summary of flight test results; compares the flight test results to the predicted values; and presents a limited comparison of wind tunnel results, flight test results, and their correlation with predicted values.

1. BACKGROUND - PROBLEM IDENTIFICATION

The XV-3 Tilt Rotor Aircraft, shown in Fig. 1, identified a problem of possible rotor-pylon-wing instability during maneuvers in the airplane mode. During the 1962 NASA Ames 40- by 80-Foot Wind Tunnel test of the XV-3 aircraft, a sustained rotor-pylon oscillation was encountered. An extensive program of analyses and model testing was begun to investigate the low frequency rotor-pylon oscillation phenomenon, and the results are reported in Refs. 1 and 2. The objectives of these investigations were to provide a physical understanding of rotor-pylon stability, and to establish means of assuring stable configurations for the XV-3 and future tilt rotor VTOL designs. The sustained oscillation (decreased damping) was generated by destabilizing rotor forces that, at high inflow angles, could become significant in determining the coupled rotor-pylon stability. Figure 2 illustrates the forces acting on a rotor and pylon system during steady pitching motion. A complete description of this phenomenon is described in Ref. 1, but, in brief, the destabilizing moment is generated by the H forces that add to produce a hub shear force in the direction of the pylon pitching rate. The destabilizing moment is directly proportional to blade inertia, the number of blades, mast length, airspeed, and is inversely proportional to rotor radius squared. The results of these analytical and model testing programs defined the major parameters that can affect rotor-pylon-wing stability. These major parameters, and their affects on aeroelastic stability, are outlined in Table 1.

TABLE 1. MAJOR PARAMETERS AFFECTING ROTOR-PYLON-WING AEROELASTIC STABILITY

Parameter	Affect	Comments
High pylon mounting stiffness	Stabilizing	Increasing the pylon stiffness increases the frequency of the pylon oscillation so that the rotor cannot follow, and the rotor mode of oscillation remains highly damped.
Swashplate/ pylon coupling	Destabilizing	Rotor controls must be isolated from pylon motion to prevent destabilizing forces that are generated when the rotor plane is disturbed.
Delta three control	Destabilizing	The use of negative delta three control reduces maneuvering induced rotor flapping, but has a destabilizing effect on rotor-pylon-wing stability
Rotor elastic flapping restraint	Stabilizing	Spring restraint on rotor flapping produces a stabilizing effect.
Wing mode effects	Destabilizing	Wing beam and torsional degrees-of-freedom produce a destabilizing effect by lowering the pylon stiffness and consequently the pylon natural frequency.
Increasing airspeed	Destabilizing	Increasing airspeed is destabilizing because it is accompanied by increasing destabilizing rotor forces at high in-flow angles.
Increasing rotor thrust	Stabilizing	Increasing rotor thrust has a stabilizing effect because it has the effect of increasing pylon stiffness.
Increasing rotor rpm	Destabilizing	Increasing rotor rpm is destabilizing because the increase in rotor angular momentum produces an increase in processional moments resulting in greater rotor destabilizing forces.

2. PREDICTED XV-15 STRUCTURAL AEROELASTIC STABILITY

The technology base derived from the earlier analytical and model testing programs made it possible to predict the structural aeroelastic stability of the XV-15 Rotor Research Aircraft with a high degree of confidence. The validity of these predictions were then evaluated by additional model and full-scale tests. The results of these tests are presented and discussed in a later section of this paper.

The XV-15 predictions produced by the Bell Helicopter Company were based on a linear analysis (BHC Proprotor Stability Analysis, DYN4), and a nonlinear analysis (BHC Proprotor Aerolastic Analysis, DYN5) techniques. The DYN4 and DYN5 analysis techniques are described in Ref. 3. The DYN5 program is an expanded version of a math model and computer program developed for the Air Force Flight Dynamic Laboratory and is described in Ref. 4.

The XV-15 predictions produced by the NASA-Ames Research Center are presented in Ref. 5, and updated predictions are presented in Ref. 6.

The predicted rotor-pylon-wing stability characteristics of the XV-15 in airplane mode are presented in the root locust format in Figs. 3, 4, 5, and 6. Bell predictions for the symmetric and asymmetric modes are presented in Fig. 3 and 4, respectively. The NASA-Ames predictions for the symmetric and asymmetric modes are presented in Figs. 5 and 6, respectively. They both show:

1. Low frequency, highly damped rotor modes.
2. High frequency, lightly damped pylon modes.
3. Low frequency, lightly damped wing modes.

These predictions are also compared to flight test results as a function of damping ratio (ζ) and airspeed.

Differences in the predicted damping levels for the various modes may result from differences in the analysis techniques. These differences are listed in Table 2.

TABLE 2. ANALYSIS DIFFERENCES

Bell Helicopter (linear analysis)	Government
Wing motion	
Discrete masses, inertias and springs which are coupled to match the 6 fundamental wing modes and pylon pitch and yaw modes	NASTRAN mode shapes (all six components)
Rotor blade lag motion	
Purely inplane, rigid body rotation about offset hinge with spring that represents first in-plane cyclic mode	Coupled inplane/out-of-plane bending modes of elastic blade
Rotor aerodynamics	
Analytical integration over rotor disk, using single lift-curve slope value (corrected for compressibility) (ideally twisted blade @ 3/4 radius)	Numerical integration over disk, using lift-curve slope based on local angle-of-attack and Mach number
Axial flow and high inflow only	Applicable to conversion and helicopter mode flight also
Rotor dynamics	
No blade torsion dynamics	Coupled blade bending and torsion
Pitch/lag coupling calculated from separate analysis	Pitch/lag coupling calculated automatically

3. AIRCRAFT DESCRIPTION

The XV-15 aircraft is powered by two Lycoming T-53 turboshaft engines, which have been uprated and modified for both vertical and horizontal operation. The three-blade proprotors are 7.62 m (25 ft) in diameter, and the blade twist is 45° from root to tip. The rotors are gimbal-mounted to the hub with an elastomeric spring for flapping restraint. The wing span is 9.75 m (32 ft) from spinner to spinner, and the aircraft is 12.8 m (42 ft) long, excluding the instrumentation boom. Aircraft dimensions are shown on the three-view drawing in Fig. 7. Wing loading is 3687 n/m^2 (77 lbs/ft^2), and disc loading at the design gross weight of 13,000 lbs. is 632 n/m^2 (13.2 lbs/ft^2). The XV-15 carries 669 kg (1,475 lbs) of fuel, which allows a research flight of about 1 hour. It is equipped with LW-3B rocket seats which provide a 0-altitude/0-airspeed recovery capability for the crew.

The key design features and the reason for selection in the XV-15 design are listed in Table 3.

The XV-15 flight control system includes exciter actuators in the right-hand flaperon and right-hand collective control systems to excite the modes shown in Fig. 8. Inflight structural aeroelastic stability investigations used the flaperon exciter actuator to excite the wing beam and torsional symmetrical, and

TABLE 3. KEY XV-15 DESIGN FEATURES

Design Feature	Reason for Selection
Torsionally stiff wing and stiff pylon-to-wing attachment	Ample stability margin at low technical risk
Forward-swept wing planform	Ample clearance (12 degrees) for flapping in severe maneuvers and gust encounters
Gimbaled, stiff-inplane, over-mass-balanced proprotor	Proprotor loads not sensitive to flapping
	Air and ground resonance problems avoided
	Blade pitch-flap-lag instabilities and stall flutter problems avoided
Large tail volume, H configuration	Good damping of Dutch roll and short-period flight modes

asymmetrical bending modes. The collective exciter actuator was used to excite the wing chord symmetric and asymmetric bending modes. Inflight use of these exciter actuators are shown and discussed in the following section.

4. FLIGHT TEST TECHNIQUES

Structural aeroelastic stability flight test evaluations were conducted at the contractor's Flight Research Facility in Arlington, Texas, and at the NASA Dryden Flight Research Center at Edwards AFB, California. These tests were conducted within the limits listed below:

1. Design gross weight of 5900 kg (13,000 lbs) and a neutral C.G. location.
2. At density altitudes of 1,500, 3,000, and 4,600 meters (5,000, 10,000, and 15,000 feet).
3. In airplane mode (pylons down and locked) within the true airspeed range of 170 to 296 knots.
4. At two rotor speeds of 98% (589 rpm) and 86% (517 rpm).

The XV-15 aircraft was predicted to have low frequency, lightly damped wing beam, chord and torsion bending modes. The three techniques used to excite these modes are:

1. Atmospheric turbulence.
2. Exciter frequency sweeps.
3. Exciter frequency dwell/decay.

Strain gages, mounted on the left and right wing, measured the beam, chord, and torsional bending response of the wing to the exciting force. The left and right gages were combined in a sum/difference network to separate the symmetric and asymmetric modes.

In the first technique, the aircraft was flown in moderate turbulence that provided a broad band excitation force. Continuous time history records of the wing gages were taken while the aircraft was flown in trimmed level flight in turbulence. The digital time history of the wing beam, chord, and torsional bending data were then analyzed to determine the natural (or resonant) frequencies of the wing structural modes, and to calculate the associated structural damping ratio for each mode. The method used to analyze this data is the Random Decrement Signatures (RANDOMDEC) program described in Ref. 7.

In the second technique, the aircraft was flown in trimmed level flight while a constant amplitude automatic frequency sweep from 1 to 10 Hz. was performed with either the flaperon or the collective exciter. Again, continuous time history records were taken during the frequency sweeps. The data were analyzed off-line using the RANDOMDEC program and/or a modal analysis technique developed by the Grumman Corporation.

The third method used the frequency dwell/decay technique. In this technique, the pilot flew the aircraft in trimmed level flight or descending wind-milling (power off) flight, and the copilot tuned the selected exciter to the desired frequency and amplitude as dictated by the on-line monitoring in the ground control room. Once the exciter was tuned to the desired wing bending mode, it was turned on and the mode excited at a constant amplitude and constant frequency. Once the desired mode was excited, the exciter was turned off, and the excitation decay was qualitatively evaluated in the control room before the test was repeated. These decays were later analyzed off-line using an interactive computer program to obtain frequency and damping values. This interactive program is discussed in Ref. 8 and described in detail in Bell Helicopter Company Report 299-099-898.

Figures 9 through 12 present examples of the dwell and decay technique for the symmetric and asymmetric modes, with and without the sum and difference on-line analysis technique. For example, Fig. 9 presents a frequency dwell at 3.3 Hz., and a decay response of the symmetric wing beam bending mode without using the sum-and-difference technique. As shown, both the right and left beam bending modes are excited. The right wing beam bending load is higher than the left, because the flaperon exciter is operating on the right wing only. From these traces, it is difficult to determine if the symmetric or asymmetric beam bending mode is excited.

Figure 10 is the same frequency dwell/decay record using the sum and difference technique. Comparison of the amplitude of the two traces makes it apparent that the symmetric wing mode has been excited. The positive damping of the symmetric wing beam bending mode is easily recognized by the shape of the decay envelope in Fig. 9 or 10. The sum and difference was only used to identify the wing bending mode. The dwell-and-decay technique worked very well on the beam bending mode for three reasons. First, the damping level is positive, but low, making it easy to excite the load. Second, the ambient noise level was low (nonturbulent flight conditions), and the signal-to-noise ratio is high without abusing the structure with excessively high exciter input forces. Third, the symmetric natural frequency of 3.4 Hz. was sufficiently separated from the asymmetric natural frequency of 6.7 Hz. to prevent coupling of the two modes.

An example of coupled symmetric and asymmetric response is shown in Figs. 11 and 12. Figure 11 presents a frequency dwell/decay record of the symmetrical wing torsion mode. Both the left and right wing loads have a "beat" type response caused by the coupling of the symmetric and asymmetric modes which have a natural frequency of 7.7 and 8.2, respectively, and are very close to the 1 per revolution frequency of the rotor which is 8.6 Hz. Figure 14 presents the same dwell/decay record using the sum and difference technique. Again, the sum and difference technique is used to identify which mode is excited, but the damping level is not easily recognized because of the "beat" type response that still exists in the "sum" trace.

The dwell and decay technique was the primary tool used to measure the aeroelastic stability of the XV-15 aircraft. Its advantages are:

1. It provides a point-by-point evaluation of the aeroelastic modes.

2. It provides, in most cases, the opportunity to qualitatively evaluate the damping level at each point.

3. Final calculations of natural frequency and damping are relatively easy using the analysis technique described in Ref. 8.

4. It is easy to abort a test (turn off exciter) if a problem is encountered.

Its disadvantages are:

1. It is time consuming to do a point-by-point evaluation.

2. It requires nonturbulent atmospheric conditions.

3. It requires extensive ground-to-air-to-ground coordination.

4. It was difficult to excite the desired symmetric or asymmetric modes because the flaperon and collective exciter actuators were mounted only on the right wing and right rotor. In the future, the exciters should be incorporated on both rotors and wings.

Data obtained by flying in moderate turbulence using the RANDOMDEC analysis method compared very well with data from the dwell/decay technique as shown in Ref. 8. The advantages of this method are:

1. Tests can be conducted in turbulent air.

2. It is time efficient in that data for all modes are collected simultaneously.

3. Very little ground-to-air-to-ground coordination is required.

4. It may identify an overlooked resonant frequency.

Its disadvantages are:

1. It does not provide an on-line point-by-point evaluation of individual aeroelastic modes.

2. Without this point-by-point evaluation capability, it is not as easy to detect stability augmentation/airframe coupling as was encountered during evaluations of the asymmetric wing beam bending mode. (This problem is discussed in Test Results section of this paper.)

3. If a problem is encountered, it is more difficult to abort the test, as it is harder to "turn off" the turbulence than it is to turn off the exciter in the dwell/decay technique.

4. It is difficult to get the right amount of turbulence at the higher altitudes.

5. The data is more difficult to analyze, because of the multiple mode content of the data.

The automatic frequency sweep technique was only used occasionally during these tests. Data obtained using the RANDOMDEC analysis compared favorably with other data, but the disadvantages of the technique outweighed the advantages. Its advantages are:

1. It can help to identify overlooked resonant frequencies in the range of the frequency sweep, 1 to 10 Hz.

2. Tests can be aborted easily if a problem is encountered.

Its disadvantages are:

1. Tests must be flown in nonturbulent atmospheric conditions.
2. It is time consuming, because it requires a point-by-point data collection process.
3. It does not provide a good point-by-point evaluation of individual modes.
4. Control system/airframe coupling is not easily recognized.
5. It requires considerable ground-to-air-to-ground coordination.
6. The data is difficult to analyze because of the multiple mode content of the data.

5. FLIGHT TEST RESULTS

The results of the structural aeroelastic stability tests conducted with the XV-15 Tilt Rotor Research Aircraft are summarized in Fig. 13. Natural frequency and damping ratio data is plotted as a function of calibrated airspeed.

The predicted natural frequencies of the six primary wing bending modes agree very well with those measured in flight as shown in Table 4. Both Bell Helicopter Company and NASA Ames used the NASA NASTRAN program to predict mode natural frequencies. NASA Ames and Bell Helicopter predicted curves of aeroelastic structural damping levels (as a function of airspeed) are also presented in Fig. 13. The largest discrepancy between the two prediction techniques is seen in the symmetric and asymmetric wing beam bending modes. The NASA Ames prediction appears to be correlated with the symmetric beam bending mode, whereas the Bell prediction has better correlation with the asymmetric beam bending mode. But the point of greatest interest in these predictions is the airspeed where the damping ratio approaches zero: neither of these prediction techniques have been tested in this area as airspeeds to date have not approached the stability boundary limits. Data presented in Fig. 13 represents data up to the maximum speed obtainable in level flight with maximum continuous power at 86% (517 rpm) rotor speed.

TABLE 4. COMPARISON OF PREDICTED AND MEASURED XV-15 WING MODE NATURAL FREQUENCIES

Wing Bending Modes	Natural Frequency Hz Predicted	Measured
Symmetric beam bending	3.1	3.3 to 3.4
Asymmetric beam bending	5.7	6.1 to 6.7
Symmetric chord bending	5.9	6.3 to 7.6
Asymmetric chord bending	5.7/8.1*	7.5 to 8.2
Symmetric torsional bending	7.9	7.5 to 8.6
Asymmetric torsional bending	7.5	7.1 to 8.3

*First NASTRAN model did not include a wing/fuselage shear tie member. Inclusion of this member increased stiffness and frequency.

The next point of interest is the large variation in measured damping ratios for a given mode and flight condition. The symmetric wing beam bending mode has the least amount of scatter. This is caused by two factors. First, it has low damping level and is easily excited by the flaperon. Second, its natural frequency (3.4 Hz.) is significantly lower than the other modes, and the absence of mode coupling makes it easier to analyze (see Figs. 9 and 10). Other modes, specifically the symmetric wing chord bending mode, have a high damping level at the airspeeds tested, and the modes are difficult to excite with only a right-hand exciter system. The greater the scatter in the data, the more difficult it is to detect trends in the data.

The third point of interest on this summary plot is the coupling of the roll stability and control augmentation system (SCAS) with the asymmetric wing beam bending mode. Coupling of the roll SCAS caused the oscillation to continue after the flaperon exciter was turned off, giving the appearance of low damping, see Fig. 14. Checks made with the roll SCAS turned off produced significantly higher levels of damping. Its permanent solution was the incorporation of a "notched" filter in the roll SCAS to prevent coupling at the natural frequency of 6.0 Hz.

6. COMPARISON OF WIND TUNNEL FLIGHT TEST RESULTS

Over the past 20 years, a significant theoretical and model testing effort has been made to understand and to predict the structural aeroelastic stability characteristics of the tilt rotor concept. Using only one mode, the symmetric wing beam bending mode, an attempt is made to show correlation between ground and flight test results. This mode was selected because it had a low predicted damping level, and therefore, it is used most often by those conducting model tests to evaluate prediction methods. Figure 15 is a composite photograph showing four major ground tests conducted prior to the flight tests. These tests are:

Fig. 15A - Wind tunnel test of the 1/5 scale semispan wing

Fig. 15B - Wind tunnel test of the full scale semispan wing

Fig. 15C - Wind tunnel tests of the 1/5 scale XV-15 aircraft

Fig. 15D - Wind tunnel test of the XV-15 aircraft

Figure 16 presents data from each of these tests with a comparison to flight test results. In general, there appears to be fairly good agreement between ground and flight tests results, with the model tests tending to be optimistic. Figure 17 presents the same data on a single plot and includes Bell Helicopter Company and NASA Ames prediction curves. The ground test results tend to confirm the Bell predictions, whereas the flight test results tend to confirm the NASA Ames predictions. It must, however, be pointed out again that it is this mode, the wing beam mode, where the greatest difference was noted between the two prediction techniques. Comparison with the ground tests results to the Bell prediction curve indicates that the Bell prediction methods are conservative. Flight test results have not been conducted at high enough speeds to determine if the NASA Ames curve is also conservative.

7. CONCLUSIONS

1. Within the airspeeds tested, the XV-15 is free of structural aeroelastic instabilities.

2. Resonant frequencies can be reliably predicted using the NASTRAN method.

3. The aeroelastic testing indicating that the theoretical and model testing effort resulted in prediction methods that are, in general, conservative and adequate for future development of the tilt rotor concept.

4. Flight test techniques need to be refined to lower the risk to the aircrew, decrease the time required for data collection, and permit better excitation of selected structural modes. (Exciters should be installed on both wings and rotors.)

5. Postflight off-line data analysis method should be refined, and if possible, moved to on-line data processing system.

ACKNOWLEDGEMENTS

The author wishes to express his appreciation to Messrs. J. Bilger and R. Marr of the Bell Helicopter Company for the efforts in the collection and analysis of data used in this paper. The author would also like to express his appreciation to Dr. J. Leung, of the NASA Ames Research Center, for his assistance in the reprocessing and analysis of selected data.

REFERENCES

1. Edenborough, H. K., "Investigation of Tilt Rotor VTOL Aircraft Rotor-Pylon Stability," 5th Aerospace Sciences Meeting, New York, N.Y., Jan. 23-26, 1967, AIAA Paper No. 67-17, January 1967.

2. Hall, W. Earl Jr., "Prop-Rotor Stability at High Hover Ratios," J. Am. Helicopter Soc., vol. 2, no. 2, April 1966, pp. 11-26.

3. Advancement of Proprotor Technology, Task II - Wind Tunnel Test Results, NASA Contractor Report CR-114363, September 1971.

4. Yen, Jing, Weber, G. E., Gaffey, T. M., "A Study of Folding Proprotor Dynamics," AFFDL-TR-71-7, February 1971.

5. Johnson, W., "Predicted Dynamic Characteristics of the XV-15 Tilting Proprotor Aircraft in Flight and in the 40- by 80-Foot Wind Tunnel," NASA TM X-73158, June 1976.

6. Johnson, W., "The Influence of Pitch-Log Coupling on the Predicted Aeroelastic Stability of the XV-15 Tilting Proprotor Aircraft," NASA TM X-73213.

7. Cole, H. A., Jr., "On-Line Failure Detection and Damping Measurement of Aerospace Structures by Random Decrement Signatures," NASA CR-2205, March 1973.

8. Bilger, J. M. and Marr, R. C., "Results of Structural Dynamic Testing of the XV-15 Tilt Rotor Research Aircraft," AHS Paper 81-53, May 1981.

Fig. 1. XV-3.

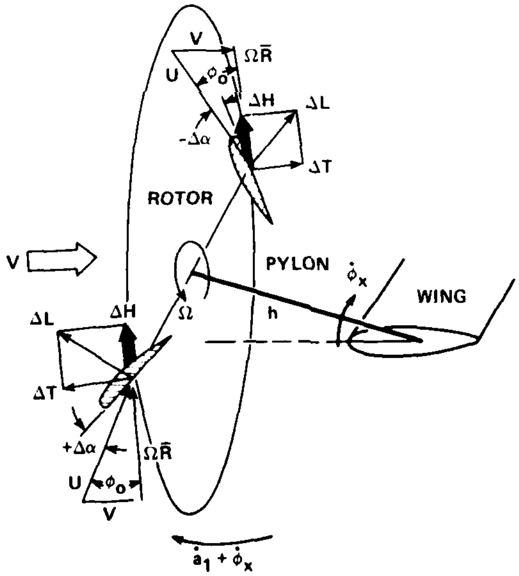
V
$\Omega\bar{R}$
U
ϕ_o
ΔH
ΔL
$-\Delta\alpha$
ΔT
ROTOR
V
PYLON
$\dot{\phi}_x$
WING
ΔL
ΔH
Ω
h
ΔT
$+\Delta\alpha$
$\Omega\bar{R}$
U
ϕ_o
V
$\dot{a}_1 + \dot{\phi}_x$

Fig. 2. Rotor tip path plane schematic showing origin of destabilizing forces.

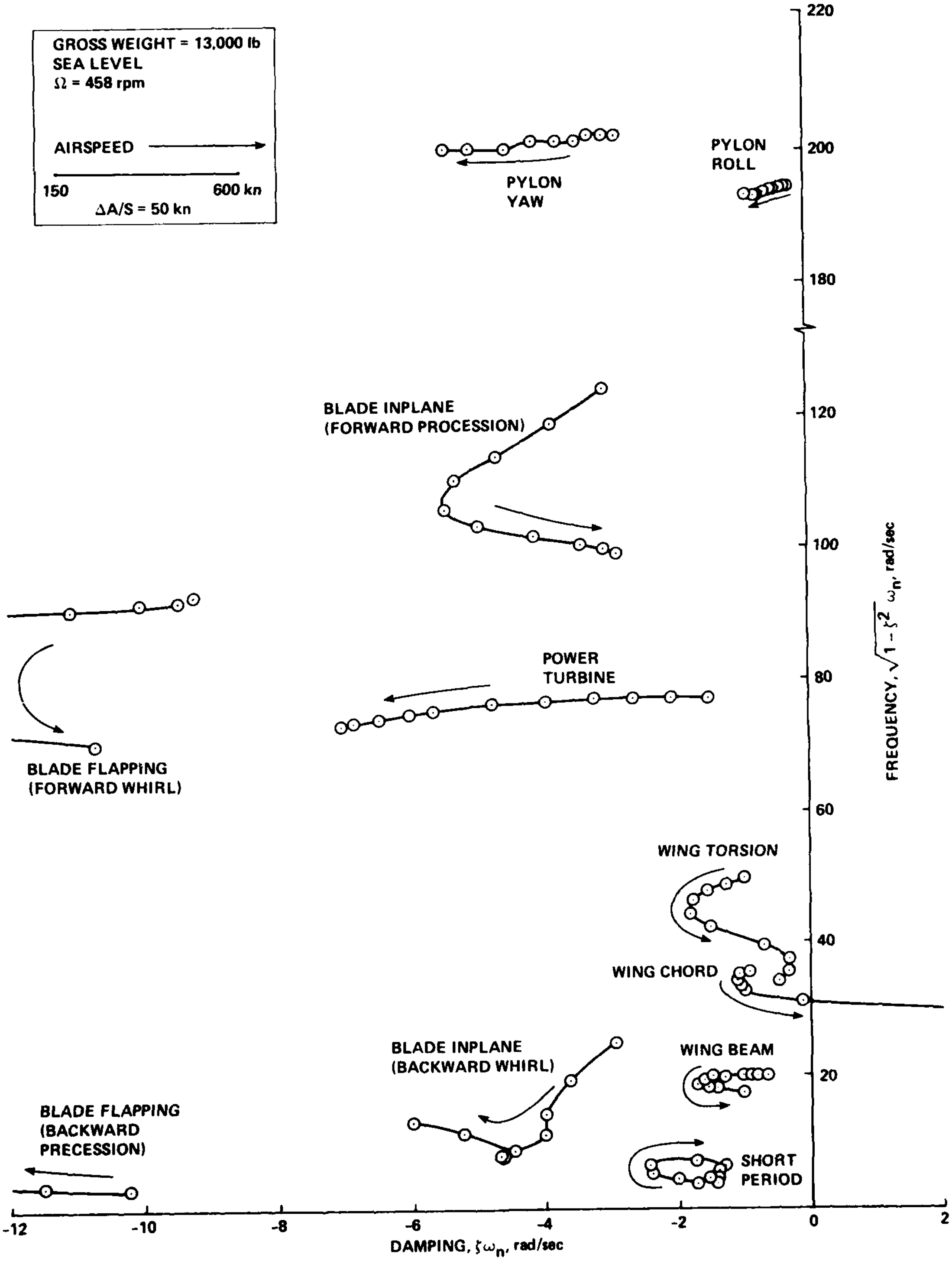

Fig. 3. Bell stability predictions of the XV-15 symmetric rotor-pylon-wing modes.

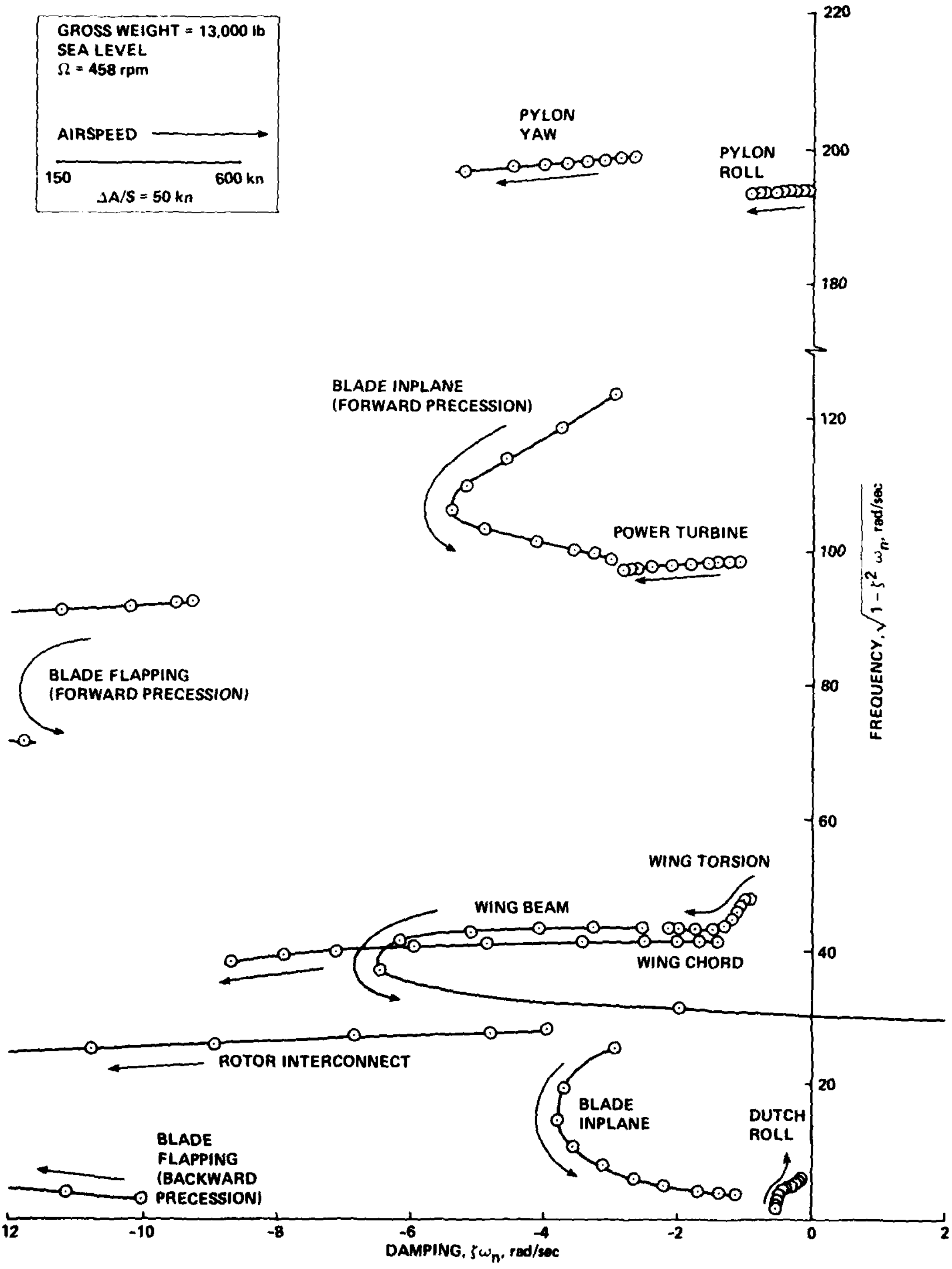

Fig. 4. Bell stability predictions of the XV-15 asymmetric rotor-pylon-wing modes.

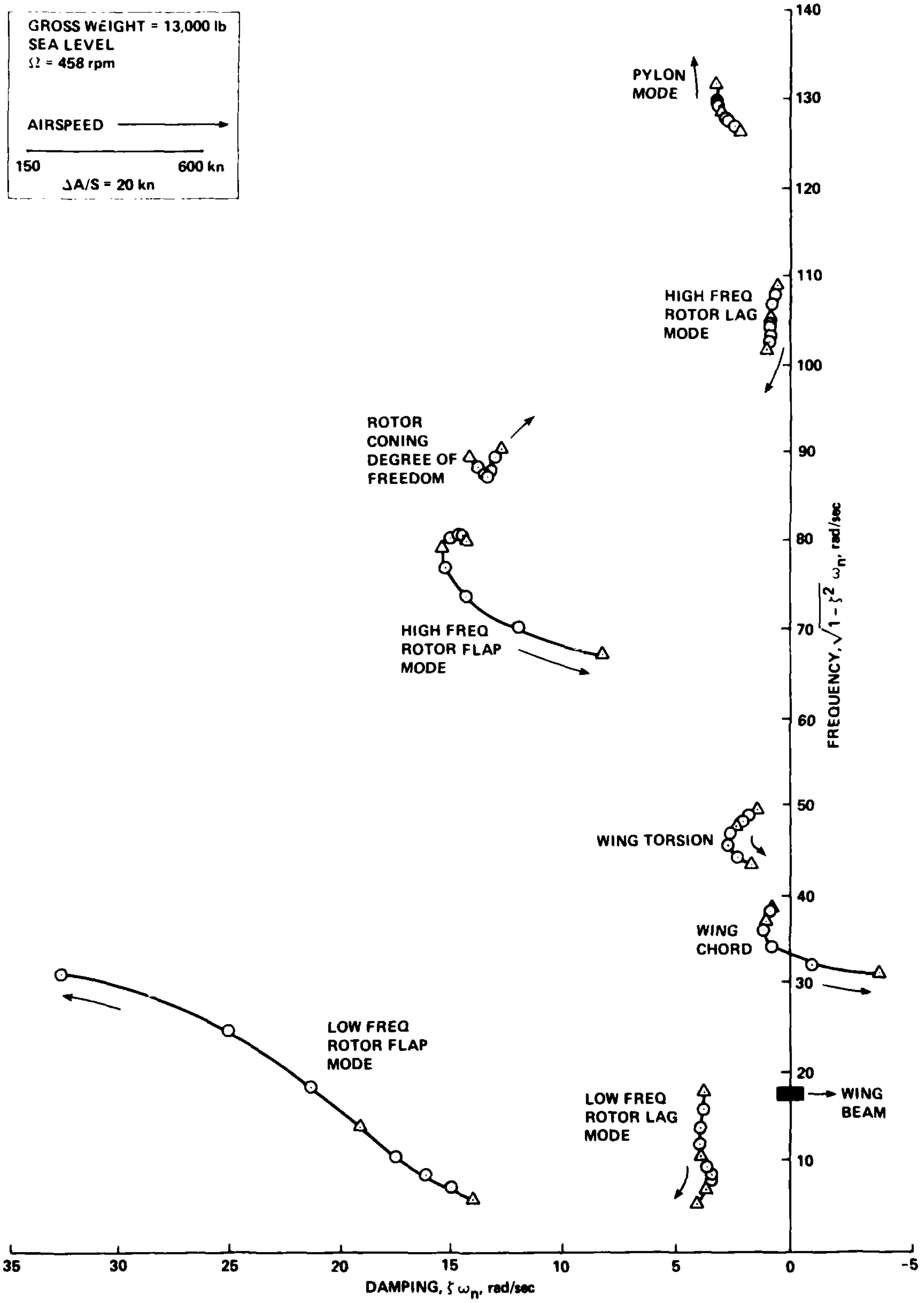

Fig. 5. NASA Ames stability predictions of the XV-15 symmetric rotor-pylon-wing modes.

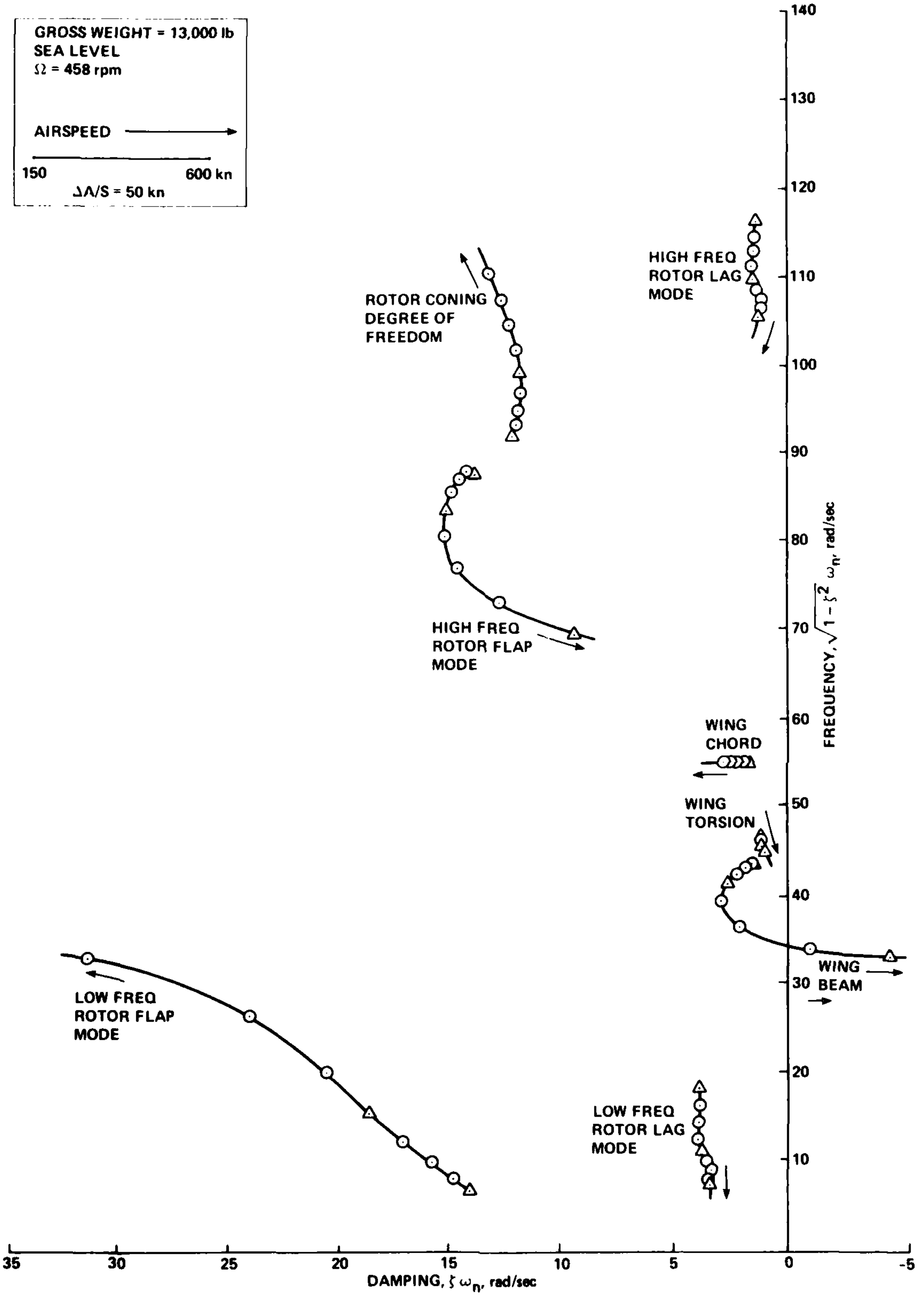

Fig. 6. NASA Ames stability predictions of the XV-15 asymmetric rotor-pylon-wing modes.

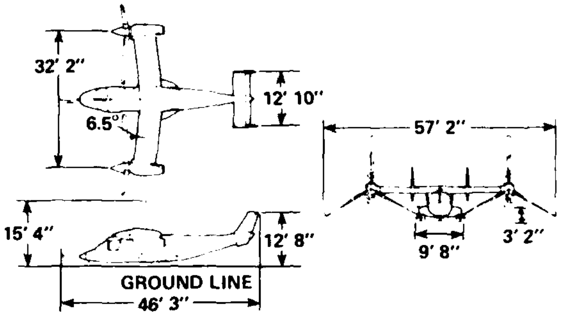
32' 2"
12' 10"
6.5°
57' 2"
15' 4"
12' 8"
GROUND LINE
46' 3"
9' 8"
3' 2"

Fig. 7. XV-15 dimensions.

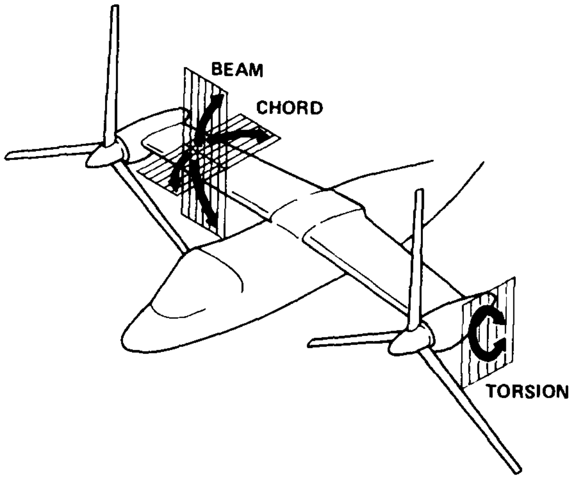
BEAM
CHORD
TORSION

Fig. 8. XV-15 rotor/pylon/wing aeroelastic modes.

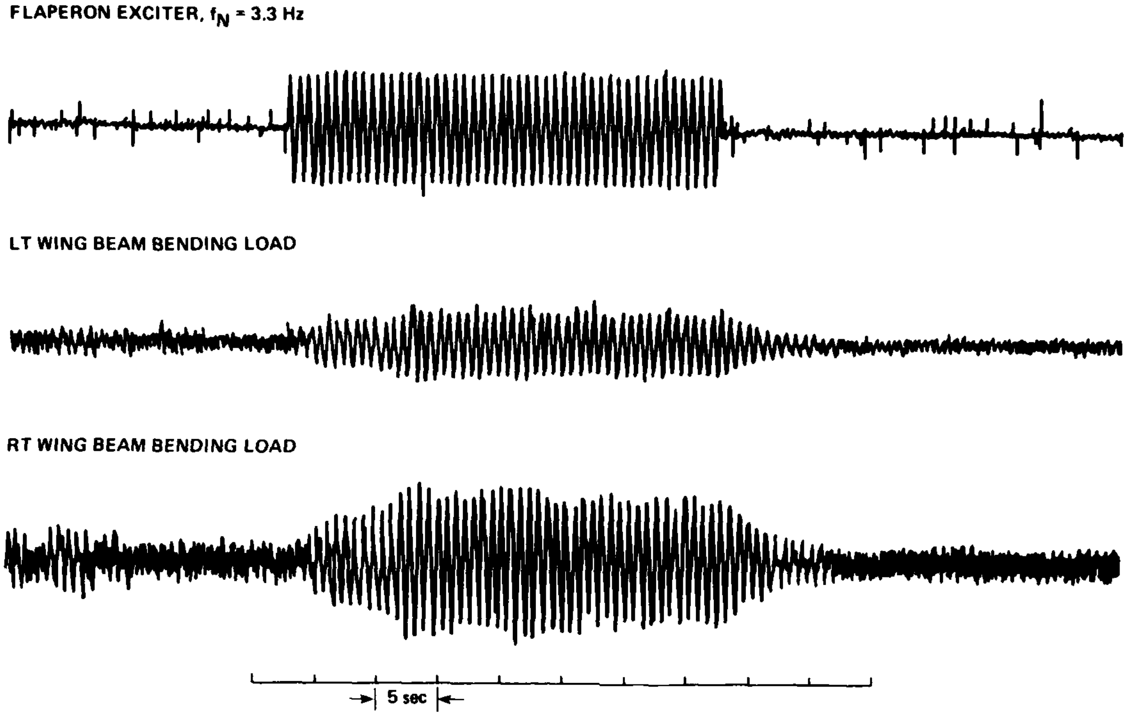

Fig. 9. Symmetric wing beam bending mode.

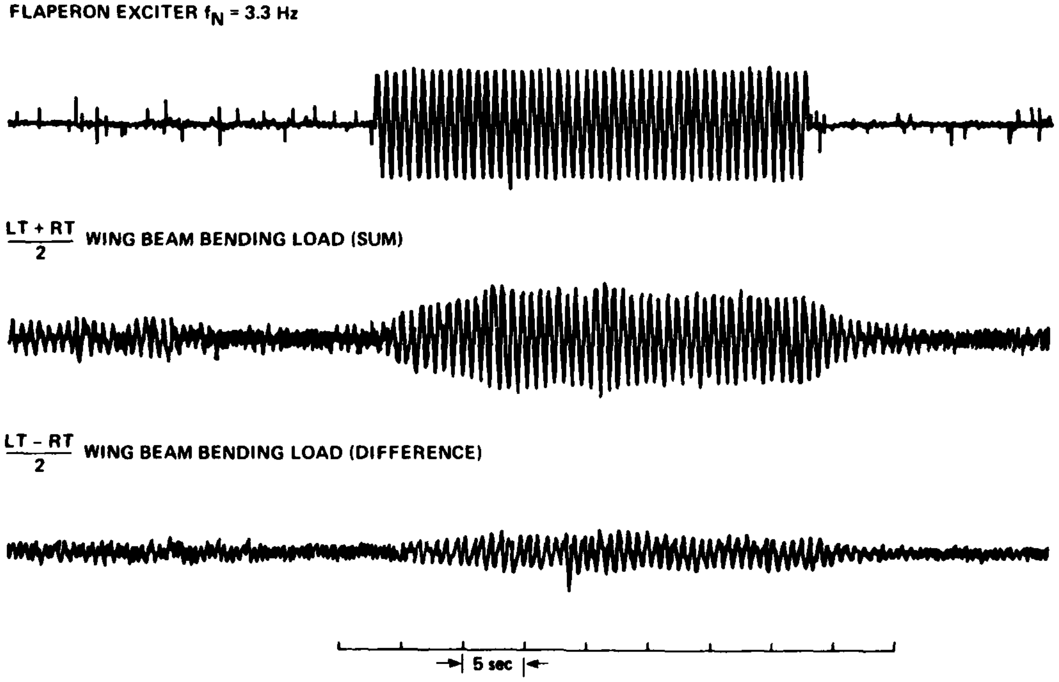

Fig. 10. Symmetric wing beam bending mode using the sym/difference technique.

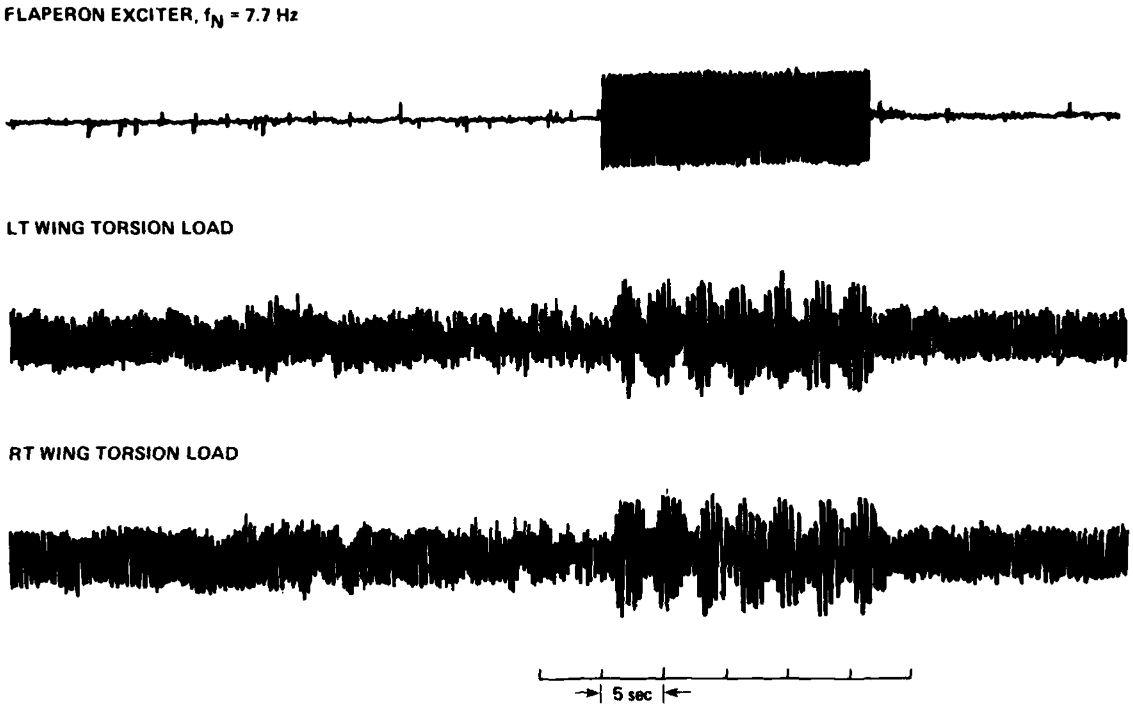

Fig. 11. Symmetric wing torsion mode.

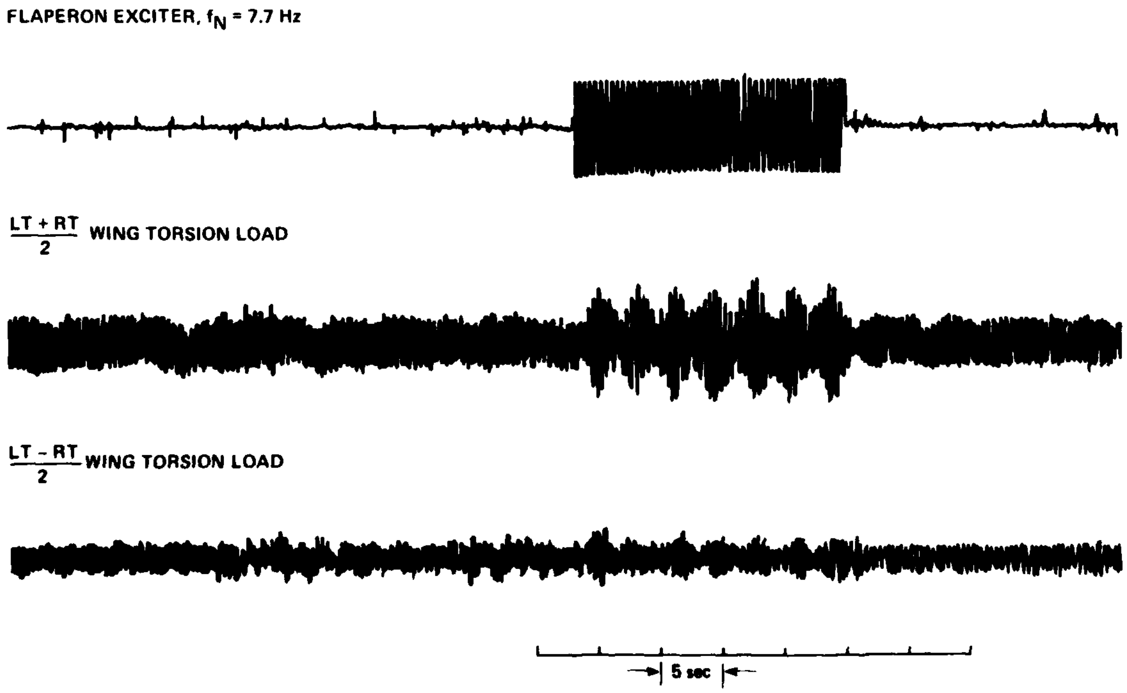

Fig. 12. Symmetric wing torsion mode using the sum/difference technique.

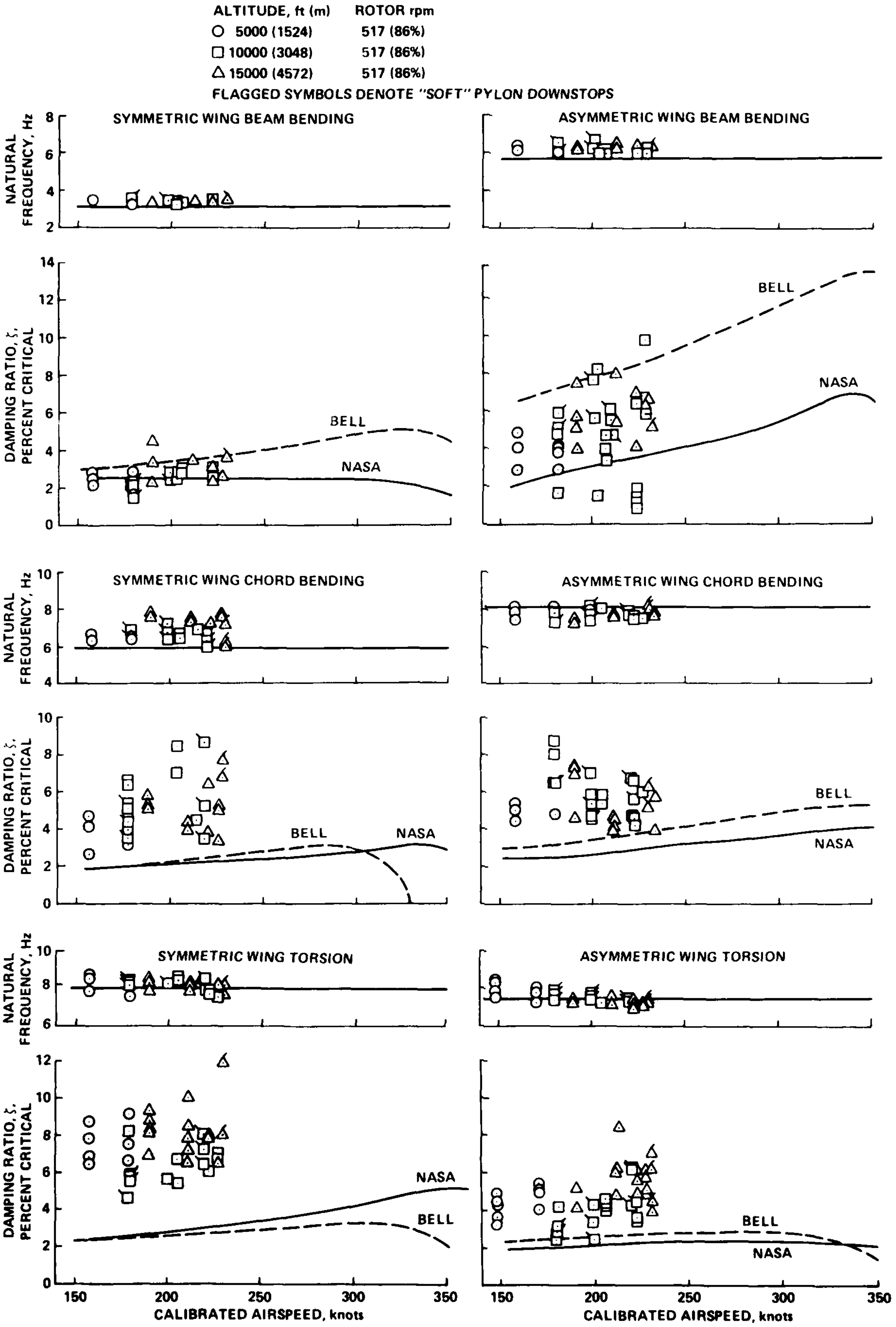

Fig. 13. Summary of aeroelastic stability data.

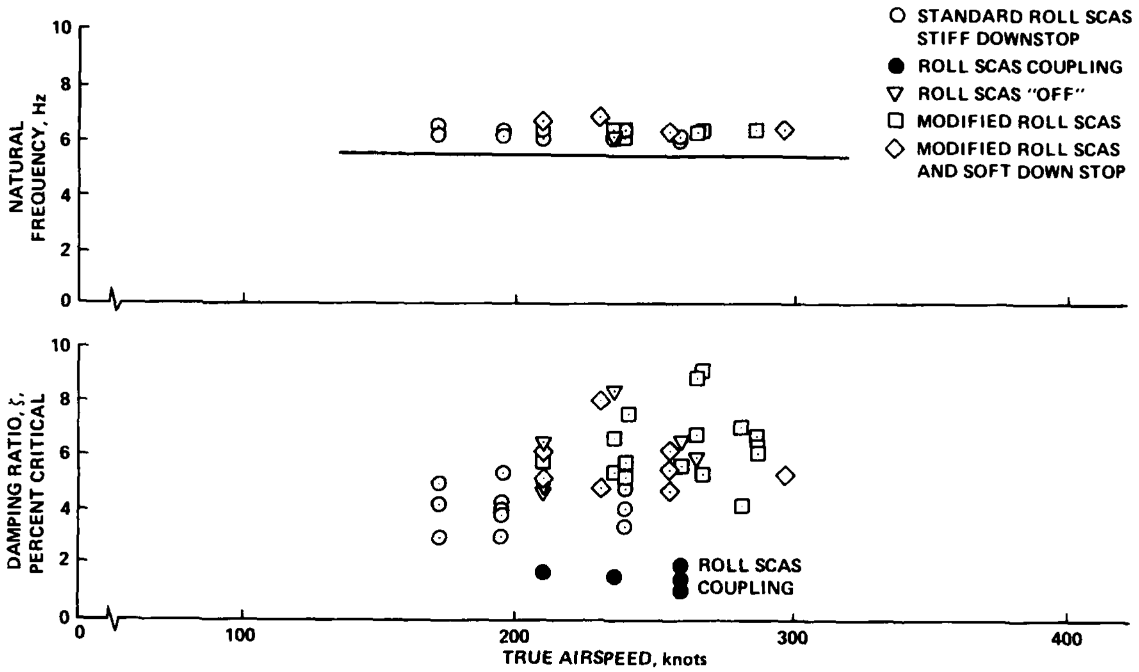

Fig. 14. Roll SCAS coupling.

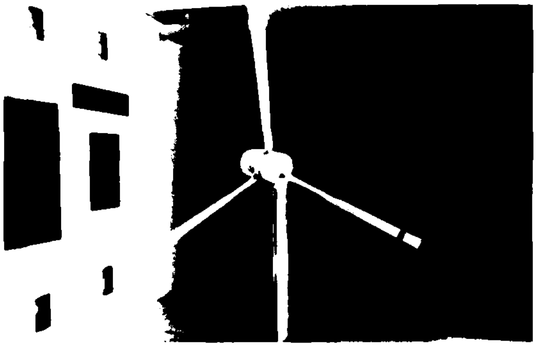

Fig. 15A. 1/5 scale semispan wing

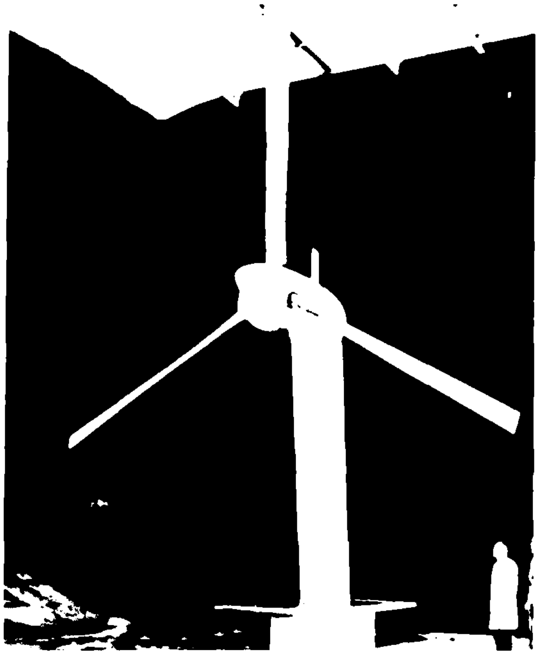

Fig. 15B. Full scale semispan wing

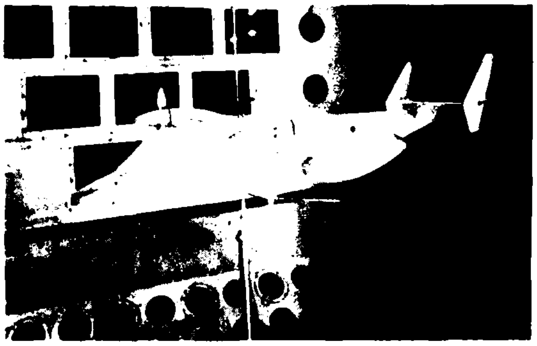

Fig. 15C. 1/5-scale aircraft model

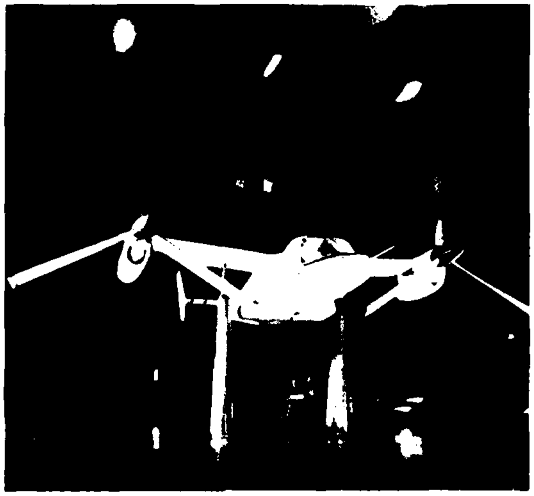

Fig. 15D XV-15 aircraft

Fig. 15. Composite photo of 4 major ground tests.

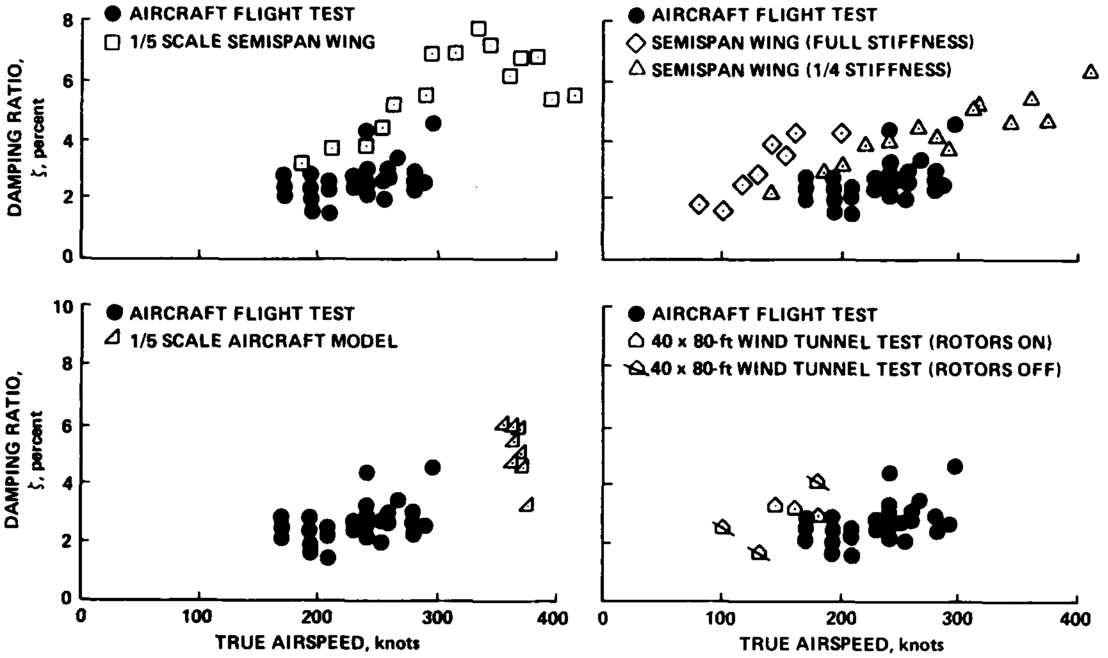

Fig. 16. Test data from 4 major tests.

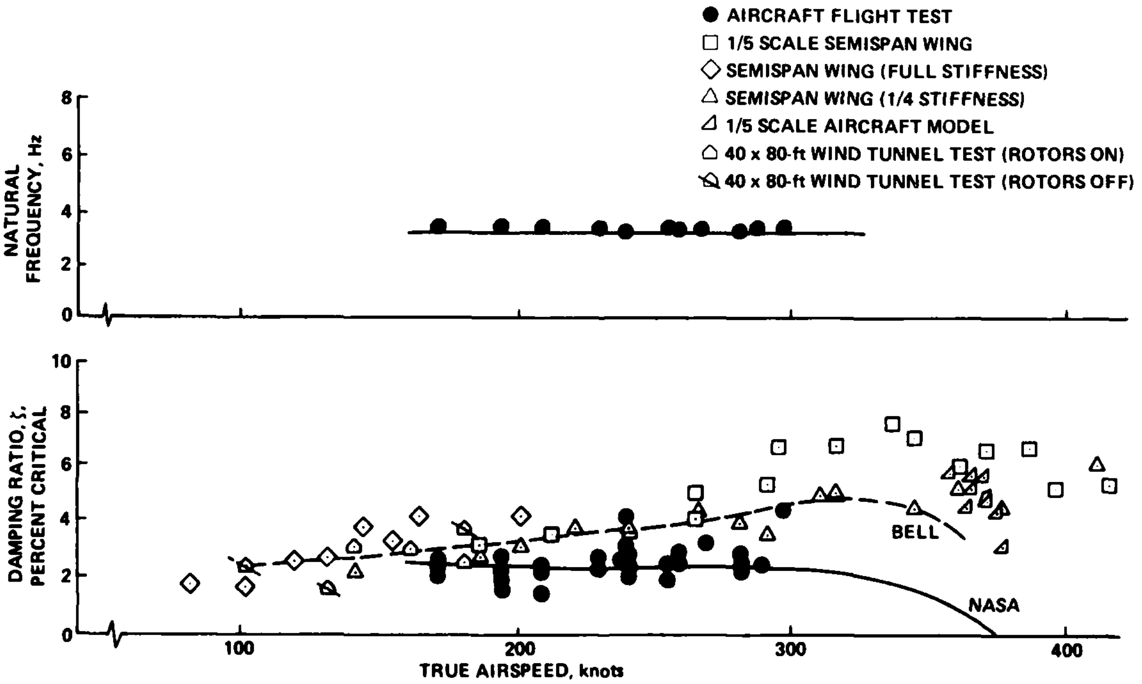

Fig. 17. Plot of all data from 4 major individual ground tests and flight tests.

GROUND AND FLIGHT TEST TECHNIQUES USED FOR PROOF OF STRUCTURAL INTEGRITY OF THE TORNADO COMBAT AIRCRAFT *

by

Karl Knauer
Director Technical Development

and

O. Sensburg
Deputy Chief Structures

Messerschmitt-Bölkow-Blohm GmbH.
Military Aircraft Division
P.O. Box 80 11 60, D - 8000 München 80

INTRODUCTION

The Tornado is a twin engine, two seater variable geometry aircraft. The wing sweep can be varied between 25 and 66 degree and is the feature which allows the Tornado to take off and land on short runways at very low speed and on the other extreme grants a considerable high speed, supersonic performance. Compared to aircraft with similar performance and weapon loading capability the Tornado is a very small aircraft (Fig. 1).

The development of this aircraft was started in early 1970. Since several nations and companies had left the consortium already in 1969, a trinational project was started and British Aerospace for the UK, Air Italia for IT and MBB for GE formed the managing body Panavia to develop, build and support the Weapon Systems. Some major milestones of the programme are mentioned: The development period up to 1973 was determined by 4 check points at which the nations decided on the continuation of the programme. The first prototype out of a fleet of nine prototype and six preseries A/C was flown by MBB in August 1974. End of 1975 the UK decided to develop part of their fleet as air defense versions (ADV), the flight testing of which started by the end of 1978. First flight of a production aircraft took place in early 1979 and initiated the series build of the Tornado. Currently more than 150 A/C have already been handed over to the customers and the introduction to the airforces did not present any major problems so far.

The operational requirement that initiated the development of the Tornado was dominated by the need for an aircraft which had low and high speed capabilities and simultaneously would show highest maneuverability and flight performance throughout the envelope. In order to achieve this goal for all aircraft configurations and loading cases an intelligent fly by wire-flight control system was designed, features of which are shown in Fig. 2. The primary and secondary flight control system consists of the differential tailerons, the rudder, air brakes, flaps, slats and spoilers which grant comfortable ride and good control of the A/C in all sweep conditions and for flights at lowest altitudes. The picture also shows the three spool Turbo Union engines which especially have been developed for the Tornado. Note the thrust reverser mechanism which is an important help to achieve short landing distances. An important feature of the aircraft is its terrain following capability (Fig. 3).

The aircraft is directed by a TF-radar detecting the terrain, monitored by a radar altimeter. The information is computed and an autopilot mechanizes the commands to the pilot for manual flights or directly to the CSAS for automatic flight. Thus the aircraft is capable of flying at very low altitudes and, due to the high performance engines even at supersonic speeds, close to the terrain overflown.

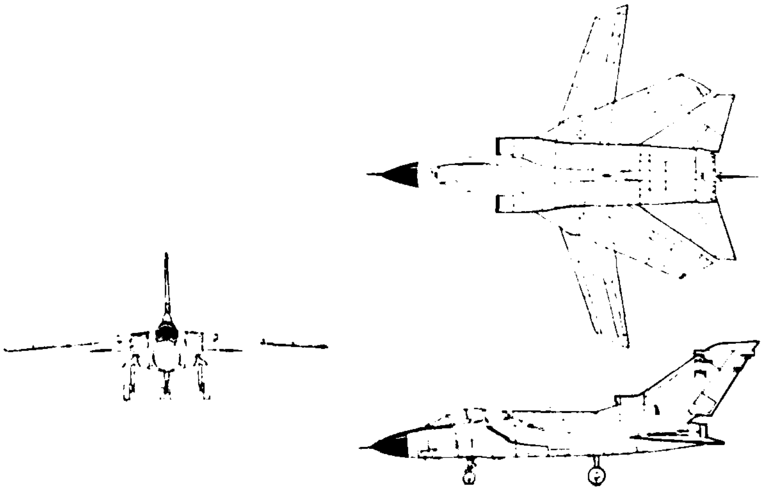

FIG. 1 TORNADO AIRCRAFT

---

* See page 19A-48 for Abstract of this paper.

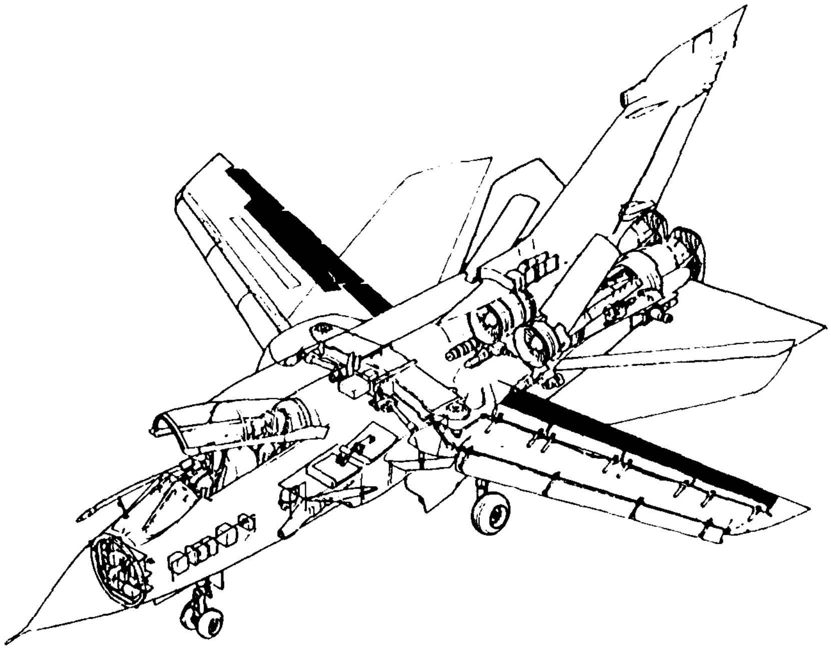

FIG. 2 PRIMARY AND SECONDARY FLIGHT CONTROL SYSTEM

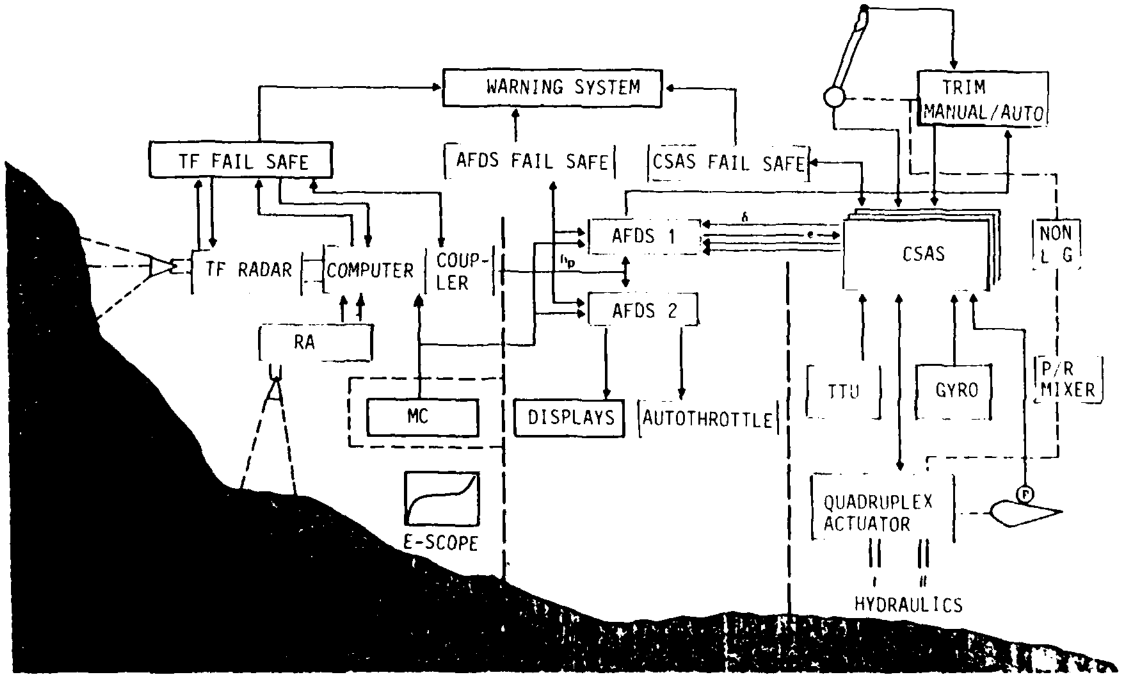
WARNING SYSTEM
TRIM MANUAL/AUTO
TF FAIL SAFE
AFDS FAIL SAFE
CSAS FAIL SAFE
AFDS 1
δ
CSAS
NON L G
TF RADAR
COMPUTER
COUP-LER
h_p
AFDS 2
RA
MC
DISPLAYS
AUTOTHROTTLE
TTU
GYRO
P/R MIXER
E-SCOPE
QUADRUPLEX ACTUATOR
P
I
II
HYDRAULICS

FIG. 3 TERRAIN FOLLOWING RADAR SYSTEM

In most cases the structural integrity is demonstrated successfully by the ground test program where component and element tests define or verify the basic allowables and major static and fatigue tests demonstrate that the aircraft is adequate for the different design load conditions.

The selection of these design load conditions however is a complicated and risk burdened iterative process which has to show that in the whole Mach-Altitude-Manoeuvre envelope no additional design conditions - beyond those already considered - are likely to be expected.

This is done by using progressively refined rational mathematical models representing the aerodynamic, inertia and dynamic behaviour of the aircraft incl. flight control and actuator systems

- to simulate c.g. responses (time histories) in design critical flight- and ground manoeuvres

and of the major aircraft components

- to cover their design loadings during this manoeuvering and in special cases their reaction on c.g. response (hinge moments and component dynamics).

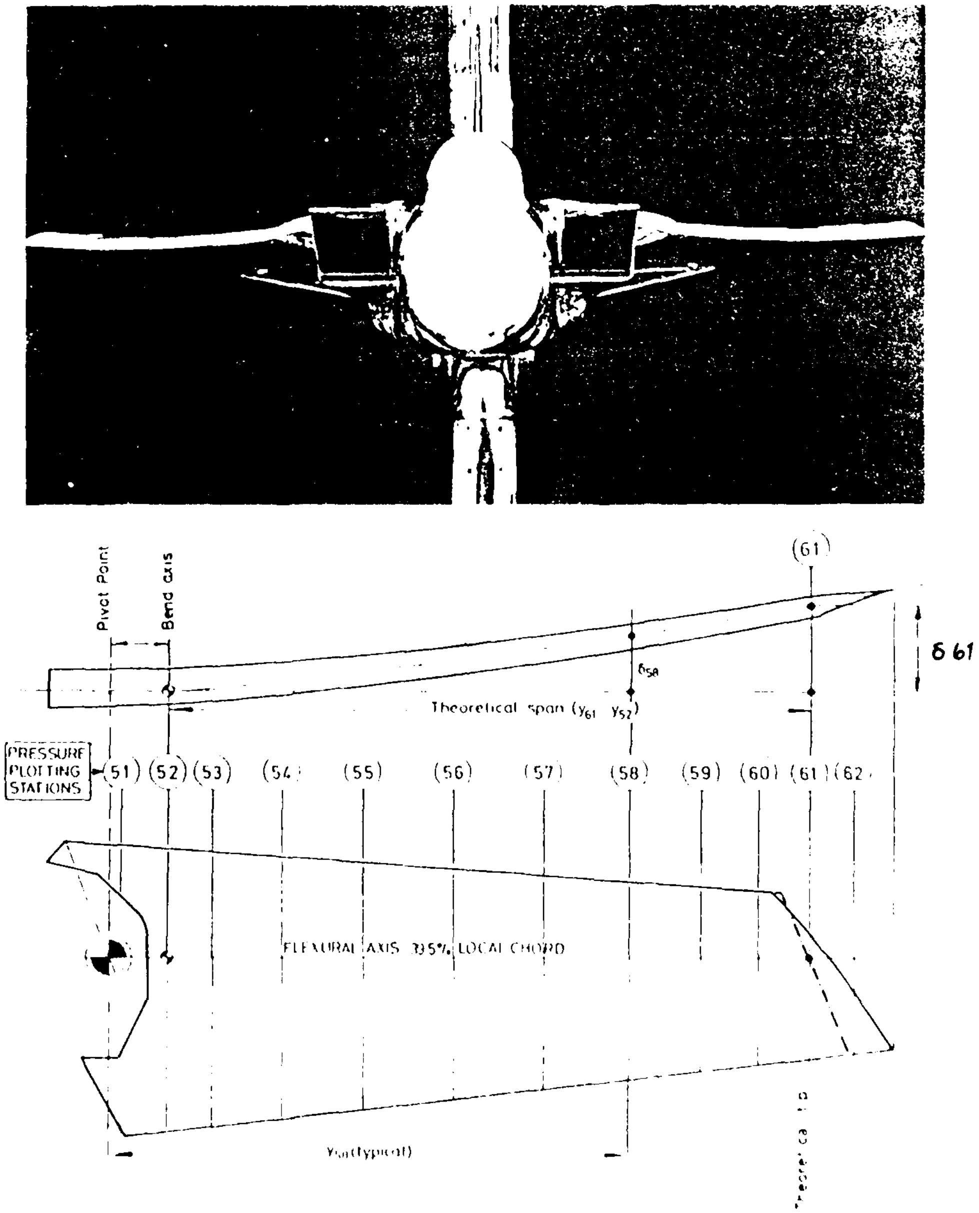
Pivot Point
Bend axis
(61)
δ 61
δ_{58}
Theoretical span (y_{61} y_{52})
PRESSURE PLOTTING STATIONS
(51)
(52)
(53)
(54)
(55)
(56)
(57)
(58)
(59)
(60)
(61)
(62)
FLEXURAL AXIS 33.5% LOCAL CHORD
y_{58} (typical)

FIG. 4 WINDTUNNEL – MODEL WITH BENT WING

This matching of mathematical models for advanced high performance aircraft naturally starts with the update of theoretical aerodynamic data by means of windtunnel test results. A special tool is the use of pressure plotting models, which turned out to be a relatively reliable means for covering major A/C components aerodynamic loading.

The pressure model (Fig. 4) for the Tornado aircraft consisted of a

wing with	251	pressure holes
tailplane with	150	pressure holes
fin with	79	pressure holes
nib with	32	pressure holes
and a fuselage incl. intakes with	205	pressure holes

The model was supplied with rigid unbent and bent wings (representing an 8g design condition) in order to demonstrate nonlinear aerodynamic effects in high 'g' conditions on components - especially on elastically corrected load distributions of wing and tailplane - and the interference effects on total aircraft aerodynamic coefficients.

Test results for unbent wing, corrected by static aeroelastic functions, have been used to define max. design cases (shear, bending, torque) and load predictions for the whole Mach-Altitude range.

Flight Load Survey

The design loads which are based on the predictions from wind tunnel models and on analytical predictions - which in recent years have made great progress - still can yield error based on uncertainties or unconsidered effects. Especially in the transonic regimes, where analysis and wind tunnel model cannot accurately represent the aircraft a flight load survey will help to overcome these uncertainties.

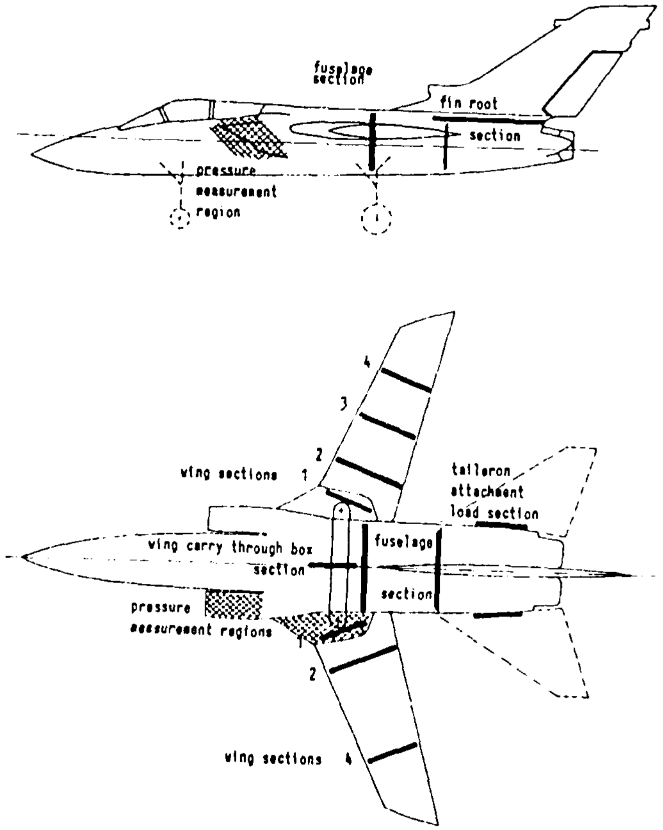
fuselage section
fin root
section
pressure measurement region
4
3
2
wing sections 1
tailleron attachment load section
wing carry through box section
fuselage section
pressure measurement regions
2
wing sections 4

FIG. 5 BASIC STRUCTURAL LOADS INSTRUMENTATION LOCATIONS

Therefore a comprehensive flight load survey has been planned as an integral part of the design and development of the Tornado and was conducted both for the aircraft without and with external stores.

The flight load survey was performed on two prototypes one of which was instrumented for the clean A/C load survey, the instrumentation of the other was tailored to the store loads measurement task.

The clean A/C survey prototype was instrumented to measure wing-bending, torque and - shear in 4 spanwise sections and fuselage loads in 2 sections. The wing carry through box as well as taileron fin and rudder had attachment loads instrumentation. So were instrumented for attachment loads other structural components as high lift devices, spoiler, airbrakes, arrestor hook, flight refueling probe, main and nose undercarriage and wing sweep-, Krueger flap - and intake ramp actuators. Loads in the area of air intake and fixed wing area have been determined by means of pressure distribution measurements.

Fig. 5 shows a schematic view of the instrumented airframe sections.

The A/C which was used for store loads measurements had a reduced airframe instrumentation, but additional pylon and store attachment loads instrumentation.

Calibration of the strain gauge instrumentation to the applied load was either done in a component rig, whenever the instrumented component could be removed from the A/C, or in a complete A/C ground loading rig providing enough loading to cover nonlinear effects.

Certain loads parameters as for example wing sweep or taileron actuator loads or for loads of nose or main undercarriage have been installed into some other prototypes and relevant data were additionally gathered during other test tasks than flight load survey.

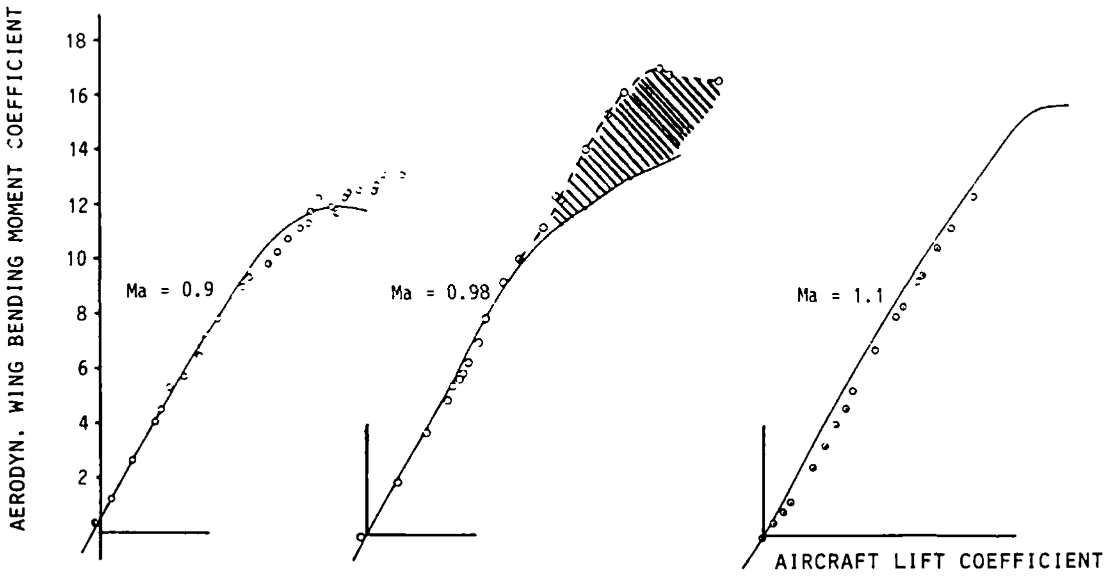

FIG. 6 COMPARISON OF MEASURED AND PREDICTED AERODYNAMIC TRANSONIC WING BENDING MOMENT (AT I/B STN)

The necessity of a flight load survey is best demonstrated by Fig. 6. This figure shows a comparison of measured and predicted aerodynamic wing bending moments versus A/C trimmed lift coefficient in the transonic region for 3 Mach numbers. Above the predicted linear region measurements show the linear loading relationship to be sustained to higher lift coefficients.

Especially at the near sonic Mach numbers this effect of bad correlation can only be explained by a combination of real Reynolds number and Mach effects being established at high incidence starting at a slightly lower Mach number inflight, than in the wind tunnel, resulting in higher wing and rear fuselage loads.

A few examples are presented now which show the interrelations of predictions and ground- and flight test data.

External Stores Design Loads and Rapid Rolling (RR) Clearance

External stores have been designed for manoeuvres from MIL-Spec. requirements based on initial response calculations and component loads monitoring with wind tunnel data.

The store loads data set has subsequently been matched in the mentioned flight load survey program performing the following test manoeuvres:

- roller coasters and wind up turns from 0 to high 'g' in order to cover the angle of attack effect
- steady heading sideslip at 1 g in order to cover the sideslip effect.

For these manoeuvres the store loads including pylon and inertia effects were measured at the spigot point. From flight parameter records the inertia loads were extracted in order to get the aerodynamic loads on the store/pylon combination. Fig. 7 shows the test set up and Fig. 8 and Fig. 9 show a direct comparison between windtunnel (WTT) and flight test data (FLS) for symmetric (alpha) and asymmetric (sideslip) manoeuvres respectively on an i/b wing mounted external tank. Fig. 10 presents the final comparison from the regression analysis of the FLS-data including windtunnel based extrapolations which now is used for check stress load calculations which may lead to redesign or limitations of prototype flying.

Just in context with the qualification of external stores configurations it seems worth-while to touch on the so-called "rapid rolling clearance procedure".

Rolling is an essential manoeuvre for a combat aircraft for which there are requirements on performance and handling qualities. Rapid rolling responses are complicated by inertial and aerodynamic coupling effects, which can produce large disturbances in sideslip and incidence when rolling an aircraft rapidly from manoeuvring flight.

As a result high structural loads and handling problems (e.g. tendency to autorotation) can arise. Consequently, adequate safety margins from critical conditions are essential when giving clearance for RR-manoeuvres. This implies a good knowledge of the aircraft's characteristics in flight to enable critical handling and loading areas to be defined. The aerodynamic coefficients required to predict rapid rolling characteristics have to be extrapolated from measurements of aircraft stability and control in small amplitude manoeuvres and of matched data from less severe entry conditions (entry g, pitch stick trim e.g.). Thus a gradual work up of the severity of entry conditions must be carried out with the safety of each stage being assessed by predictions (= response calculations) made between flights. It is essential to point out, that this final operating clearance may well be limited though the design conditions according to MIL-Spec. (e.g. - 1 g to 0.8 'g' max) are not exceeded. This can be seen on Fig. 11 where the steep gradients near -1g for load component 1 and at 5 g for load component 3 prohibit even small tolerances on design conditions - loads being very sensitive on those parameters.

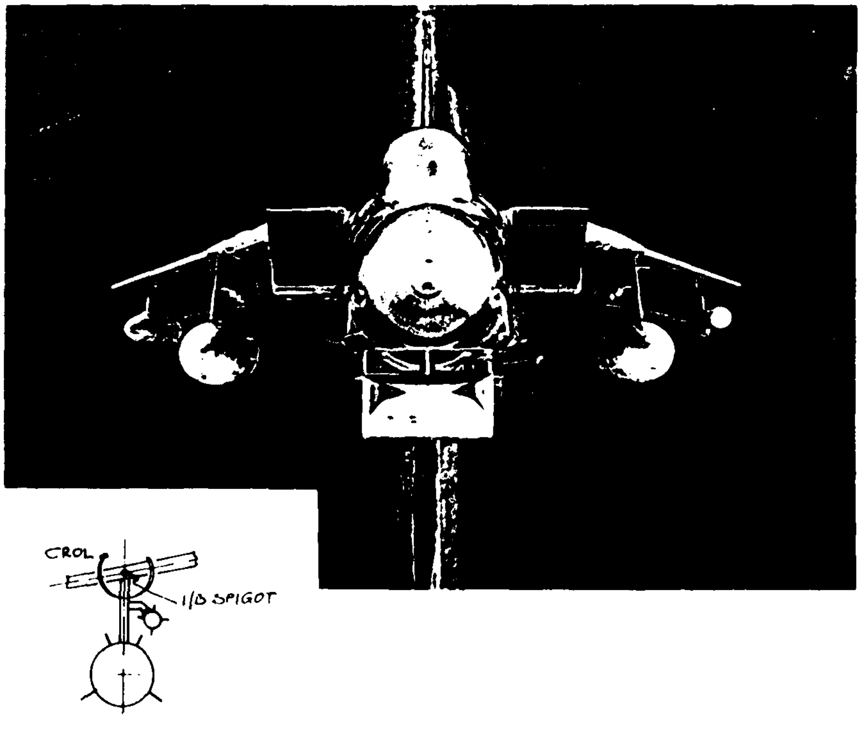

FIG. 7 WIND TUNNEL MODEL WITH STORES

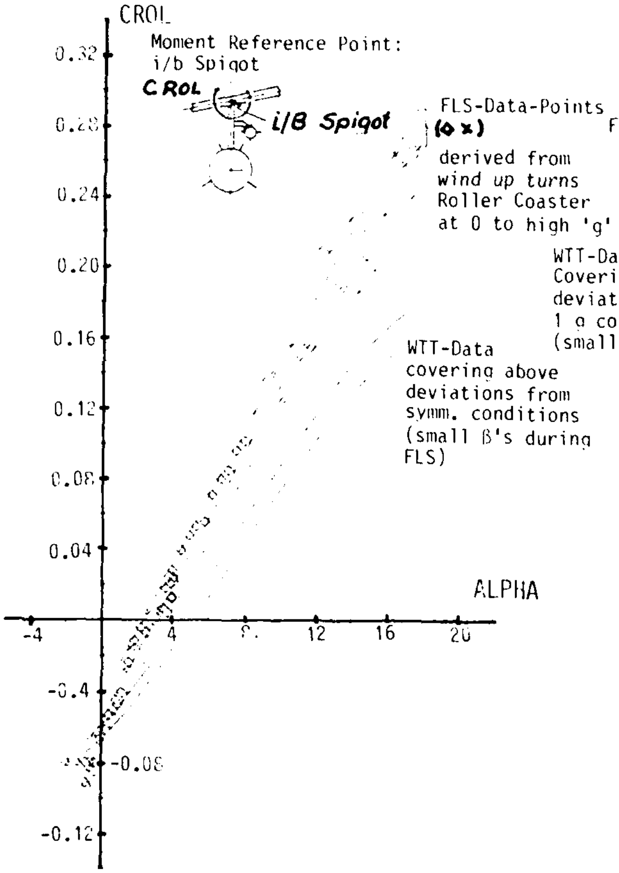

FIG. 8

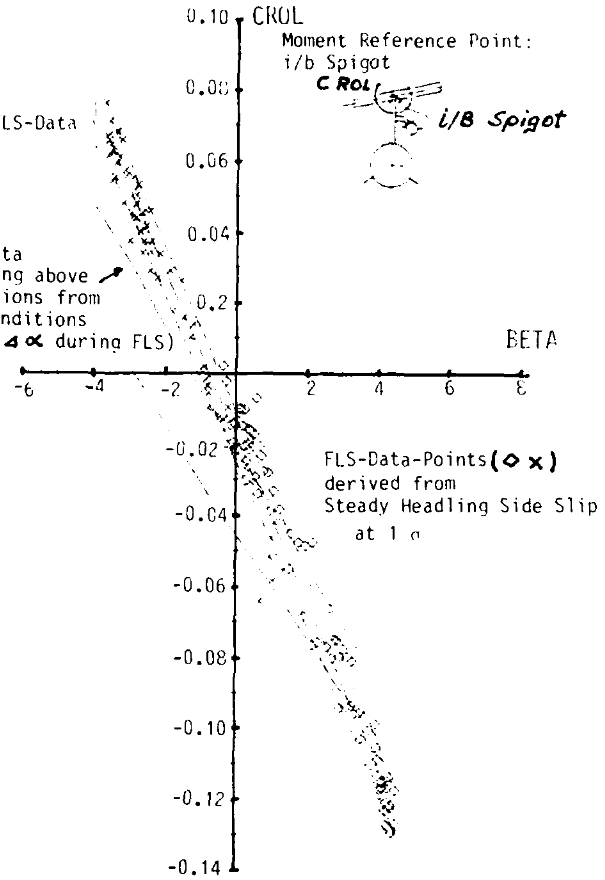

FIG. 9

ROLLING MOMENT COEFFICIENT VS. ALPHA

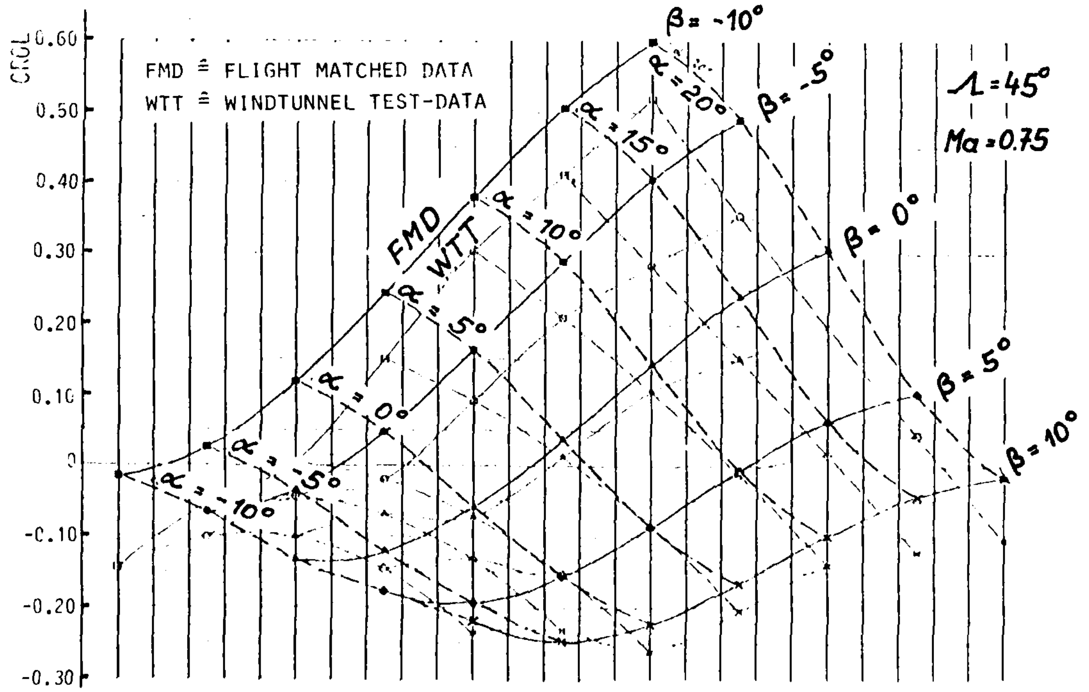

FIG. 10 FLIGHT MATCHED ROLLING MOMENT COEFFICIENT

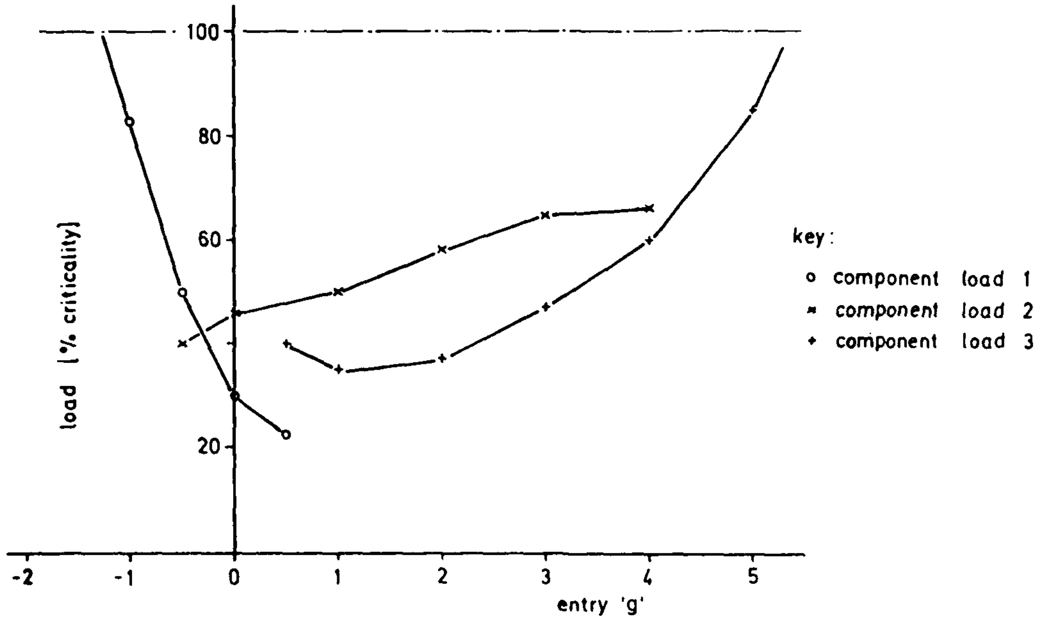

FIG. 11 LOAD CRITICALITY VS. ENTRY 'G' IN RAPID ROLLING MANOEUVRES

Hammershock Induced Loads in the Intake of the Tornado Aircraft

The Tornado propulsion system is equipped with two variable geometry two-dimensional three-shock intakes which are controlled by an electrohydraulic control system (see Fig. 12). It has three ramps. The first is fixed, the second one (supersonic ramp) is variable. The third ramp (subsonic ramp) is mechanically linked to the second and both are operated by a single actuator.

For engine air intake load assessment the occurrence of engine surges must be considered. An engine surge can be described as sudden reduction in flow in the compressor caused by abrupt flow breakdown or aerodynamic stalling of the blades in a portion of the compressor. This sudden reduction in flow creates a strong shock wave, with high peak pressures frequently referred to as a hammershock, which moves upstream of the intake duct.

An engine surge can be initiated either by engine related factors (overfuelling, control transients) or by intake induced flow distortions. Shape and propagation velocity of the shock wave are dependent on intake operating condition, flight altitude and flight Mach number. A typical example of the pressures at different intake positions is shown in Fig. 13. The associated load acts only over a very short time period, however, high peak levels can be experienced. For example, the incremental load on the subsonic ramp caused by a strong hammershock amounts to some 130 kN with a duration of only 0.0075 s.

The total load of the ramp system is the sum of a steady-state pressure under running conditions and the dynamic pressure caused by a hammershock. The final loads analysis corresponding to MIL-A-008860 requires, that

- limit loads shall neither cause plastic deformations nor inhibit or degrade the mechanical functioning
- ultimate loads shall not cause a failure of the structure (ultimate load generally will be obtained by multyplying the limit load by the factor of safety 1.5)
- the dynamic behaviour of the structure and load in amplitude and distribution must be considered when short-time processes occur.

The best possibility to accomplish a realistic loads assessment for all components of the air intake would be a dynamic load test. Such a test is not feasible.

Therefore a number of theoretical investigations had to be accomplished. Static tests of critical parts of the structure were carried out using the calculated loads.

The final loads proof analysis procedure was the following

- setup of a dynamic model with regard to the kinematic and dynamic properties
- calculation of the natural modes' frequencies

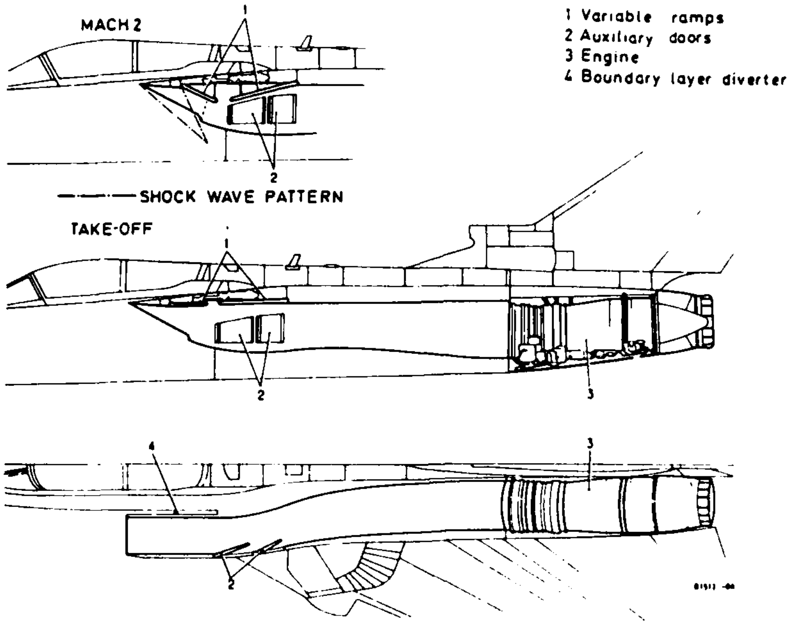
MACH 2
1 Variable ramps
2 Auxiliary doors
3 Engine
4 Boundary layer diverter
1
2
SHOCK WAVE PATTERN
TAKE-OFF
1
2
3
4
3
2

FIG. 12 TORNADO PROPULSION SYSTEM

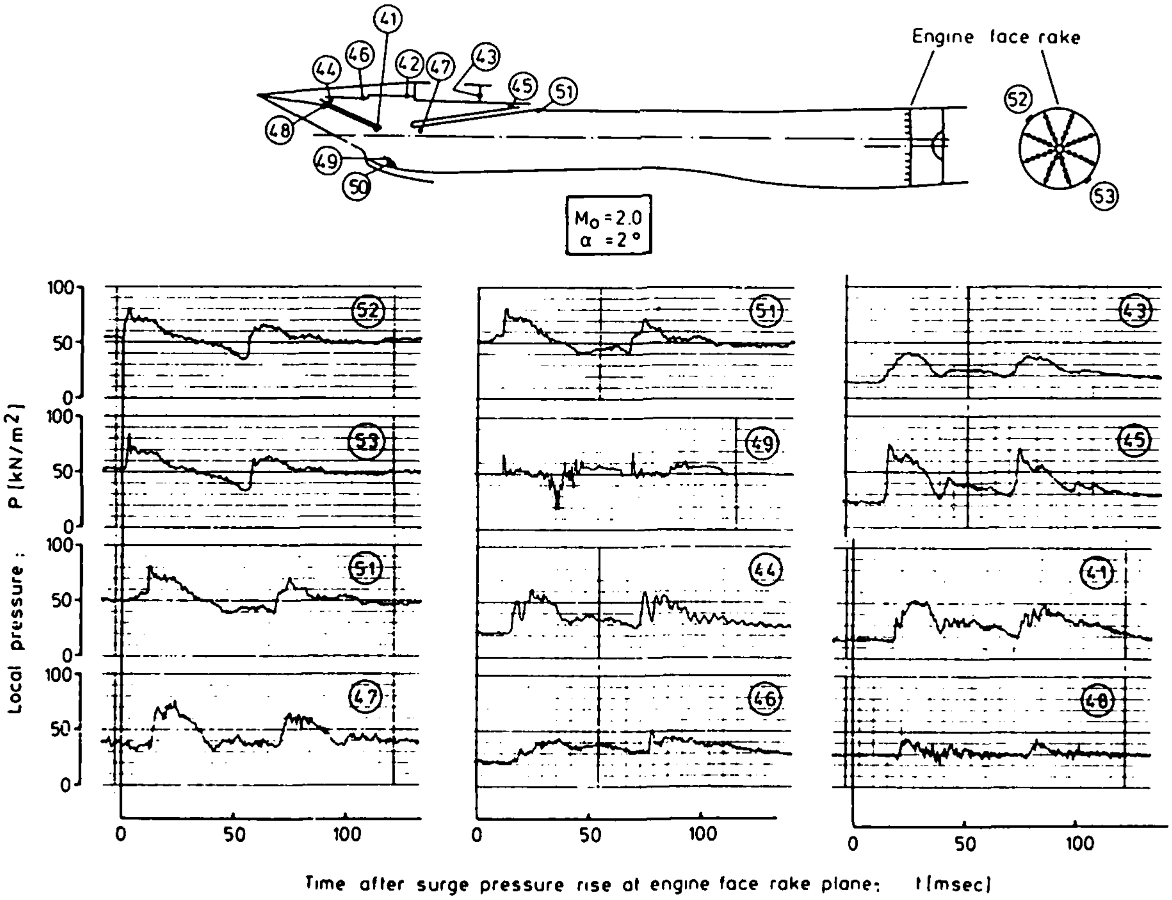

FIG. 13 SURGE PRESSURE HISTORIES IN INTAKE AND DUCT

Ramp-type	Mode	Frequencies depending on exciter force ampl.			Damp.
		~225 N	~150 N	~75 N	g[%]
Supersonic ramp	Bending	69 Hz			27 %
"	Pitch mode	103 Hz	102,4	102,4	24 %
"	1. Ramp torsion	143,7 Hz	151,7	156,99	-
"	1. Ramp bending	231,7 Hz	237,7	244,7	-
Subsonic ramp	Pitch mode	84,8 Hz	92,8	107,7	26 %
"	1. Ramp torsion	155,46 Hz	156,65	158,96	16 %
"	Ramp bending	190,97 Hz	193,37	198,16	16 %
"	2. Ramp torsion	344,97 Hz			-

FIG. 14 GROUND TEST RESULTS FOR RAMPS

- verification of the dynamic model in a ground vibration test and determination of damping (Fig. 14). This figure also shows the nonlinear behaviour of the ramps.
- calculation of gain-factors for maximum hammershocks and propagation velocities (Fig. 15)
- measured hammershock loads (Fig. 16) and comparison with calculated results (Fig. 17). Since correlation was good theoretical loads could be used for the stress analysis.

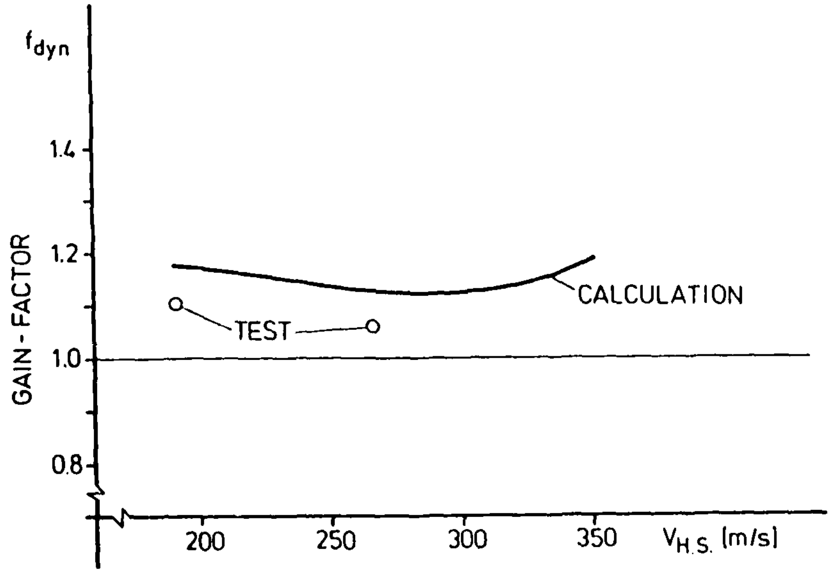

FIG. 15 GAIN FACTOR VERSUS HAMMERSHOCK PROGRESSION VELOCITY $V_{H.S.}$

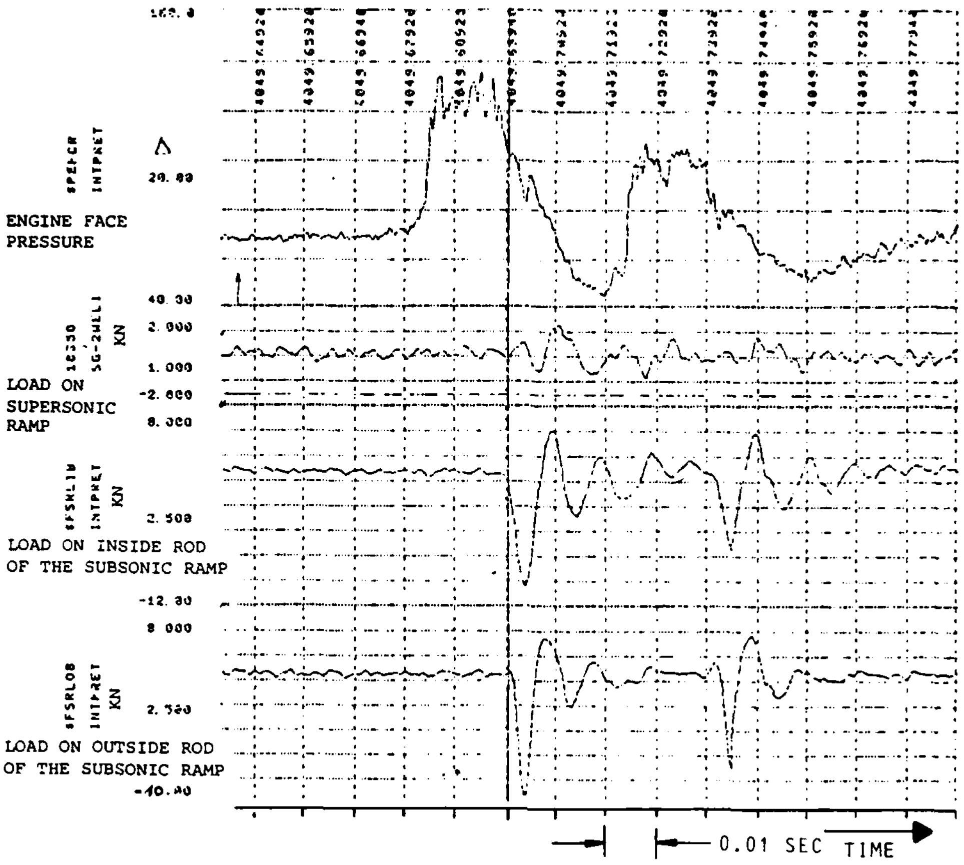

FIG. 16 LOADS CAUSED BY A HAMMERSHOCK DURING TAKE-OFF-PHASE (MAX. REHEAT)

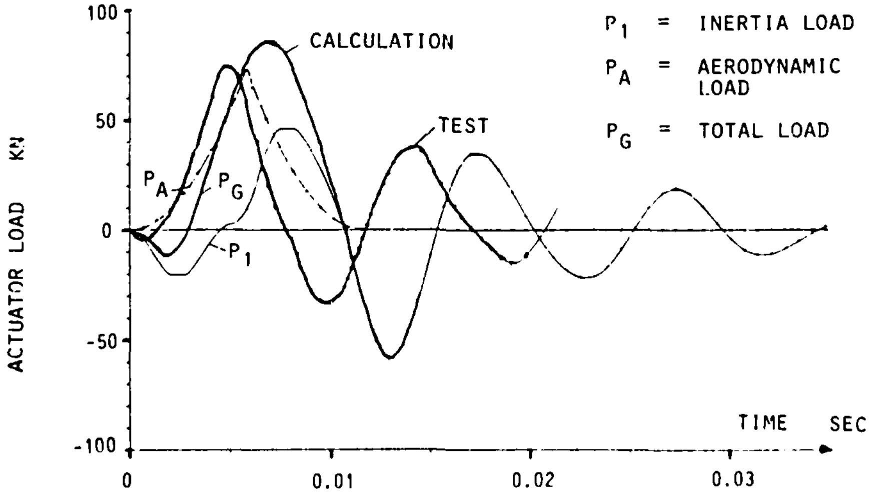

FIG. 17 DYN. ACTUATOR LOAD VERSUS TIME

Loads Induced by Dispenser Weapon Store Release and Emergency Store Release

The problem of a dispenser weapon system consisting of several single container will be discussed because of the strong dynamic excitations at the still attached containers during jettison within a very short programmed time sequence resulting in dynamic design load cases for the surrounding structure. The dispenser weapon system consists of four separate dispensers and is carried with two underfuselage pylons (Fig. 18).

Each pylon is attached to the fuselage by means of four spigots (FSS, FMS, AMS and ASS), each dispenser is suspended in one ERU at the left and right hand pylon. The dispenser weapon system is a comparatively heavy store (25 percent of the aircraft take-off-mass). (ERU = Ejection Release Unit)

Normally the empty dispensers are getting jettisoned, in the case of emergency the full dispensers also. For the required release behaviour strong jettison pulses (~150 kN for each dispenser, this corresponds with 3/4 of the take-off weight) and a release time of less than one second for all dispensers together are necessary.

The theoretical investigations carried out are of fundamental importance for the layout of dispensers, pylons, ERU's and underfuselage attachments as well as for the demonstration of the dynamic behaviour of the whole aircraft, and herewith for the flight clearance, which has to be based on the MIL-Spec. (A-8861 A) requirements:

§ 3.19.5 Emergency stores release

Emergency release of the most critical combination of required carriage stores shall not result in exceedance of limit strength of the airplane for the following conditions:

a) At speeds up to the maximum for such release with all values of vertical load factor between 0.5 and 2.0

b) At speeds up to V_{LF} with devices in their applicable position for take off with all values of vertical load factor between 1.0 and 1.5.

The model for dynamic investigations consists of the elastic components of pylons and dispensers connected to the aircraft center of gravity representing the kinematic behaviour and the short-time interaction of the jettison pulse (0.05 sec.) The distributed mass is replaced by a number of discrete mass points (Fig. 19). In preliminary calcs it could be demonstrated that it was sufficient to attach the elastic dispenser weapon to the rigid free-free aircraft rather than using the whole elastic aircraft. So a very cost efficient mathematical model could be generated.

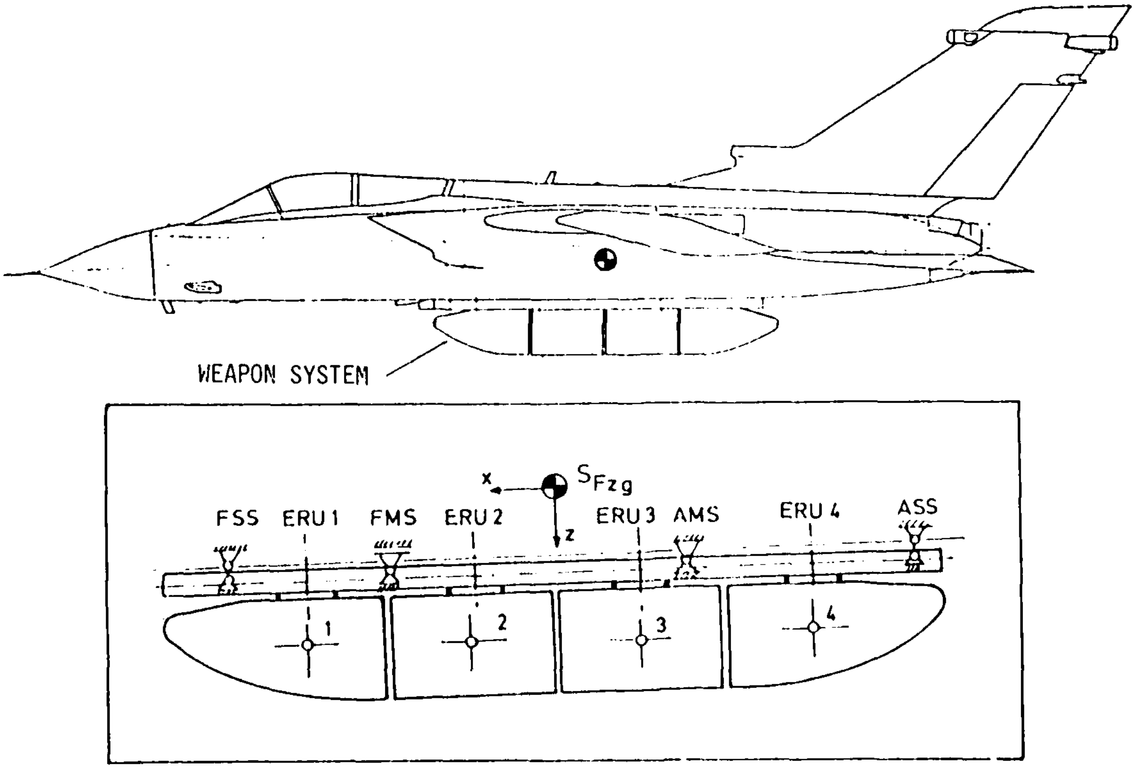

FIG. 18 DISPENSER WEAPON ON TORNADO

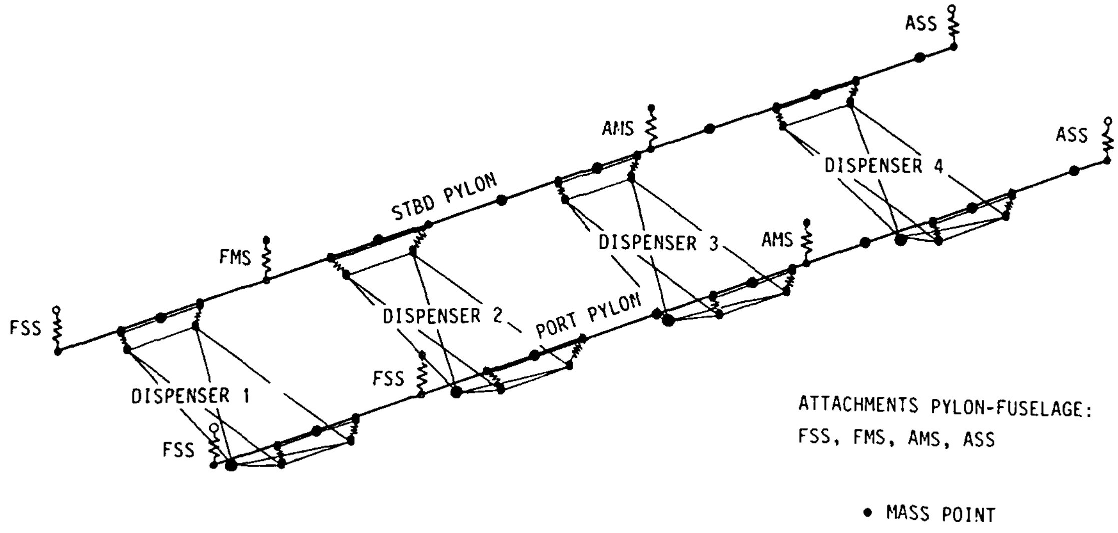
ASS
AMS
ASS
STBD PYLON
DISPENSER 4
FMS
DISPENSER 3
AMS
FSS
DISPENSER 2
PORT PYLON
FSS
DISPENSER 1
FSS
ATTACHMENTS PYLON-FUSELAGE:
FSS, FMS, AMS, ASS
• MASS POINT

FIG. 19 DYNAMIC MODEL DISPENSER WEAPON

In Fig. 20 two characteristical natural modes are shown. The highest mode considered for load calculations had a frequency of 120 Hz.

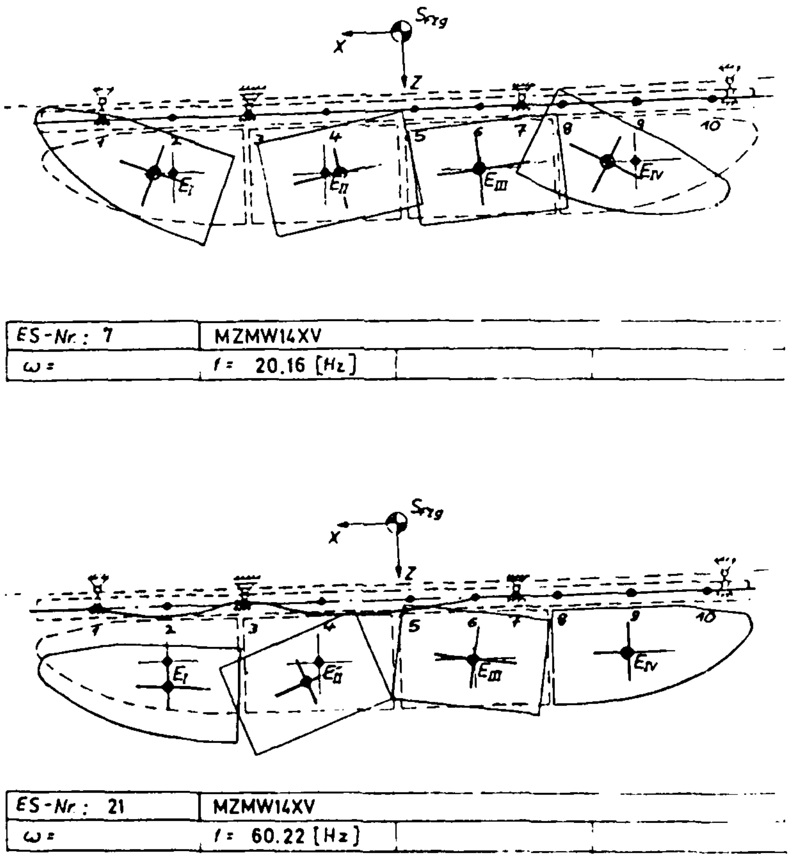
S_{Trg}
X
Z
1
2
3
4
5
6
7
8
9
10
E_I
E_{II}
E_{III}
E_{IV}

ES-Nr.: 7	MZMW14XV		
ω =	f = 20.16 [Hz]		

ES-Nr.: 21	MZMW14XV		
ω =	f = 60.22 [Hz]		

FIG. 20 CHARACTERISTIC NATURAL MODES

Representative for flight test results, Fig. 21 shows a sequential emergency release of the four empty dispensers at Ma = 0.92, Fig. 22 shows the comparison of measured and precalculated spigot loads during release of the first full dispenser. Good correlation was achieved.

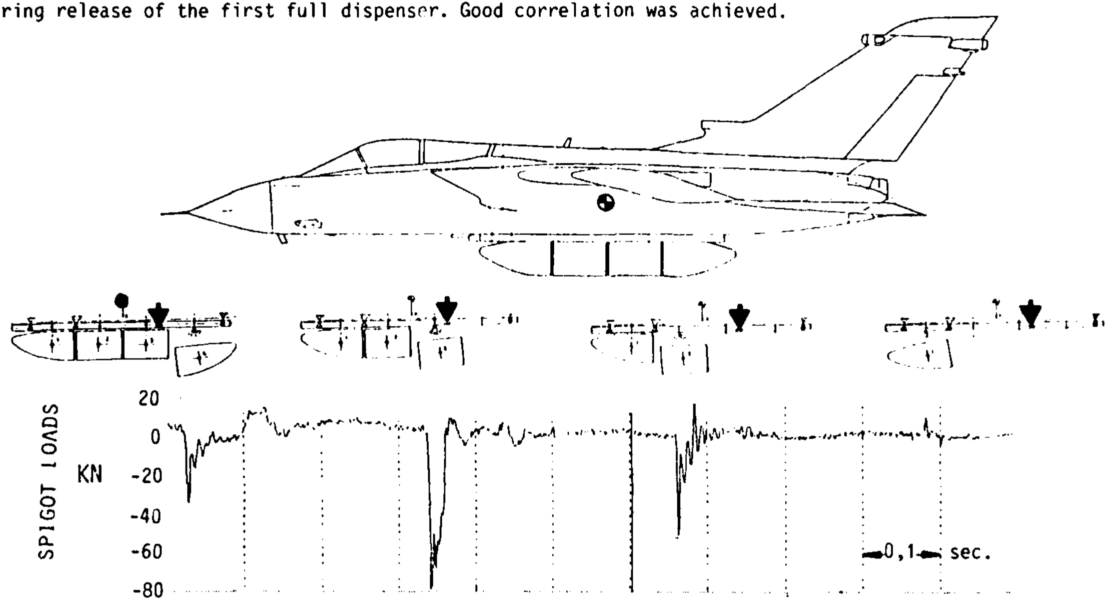

FIG. 21 EMERGENCY RELEASE DISPENSER WEAPON, EMPTY, SPIGOT LOAD ON AMS, Z-DIRECTION

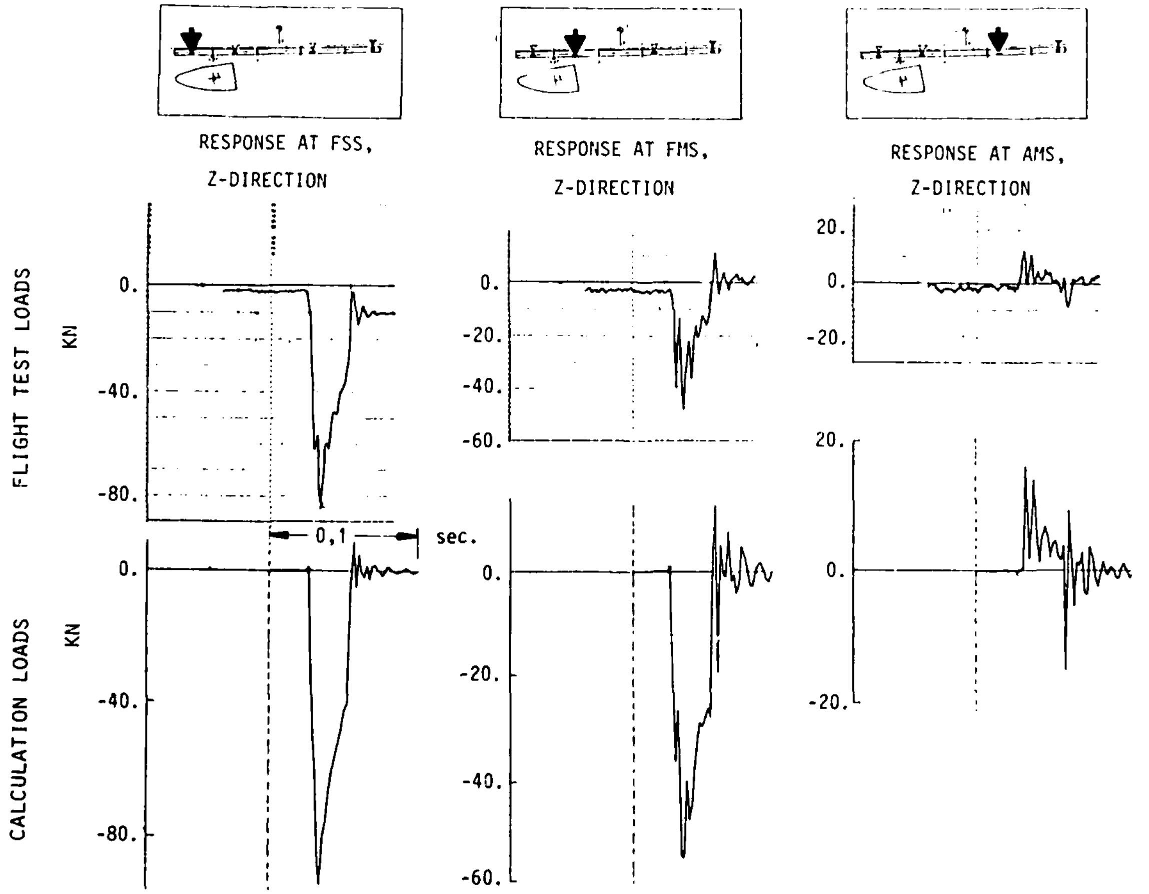

FIG. 22 DISPENSER WEAPON 1, FULL, EMERGENCY RELEASE, COMPARISON OF CALCULATED SPIGOT LOADS WITH FLIGHT TEST RESULTS, MA = 0.92

UNDERCARRIAGE

The Tornado undercarriage design was performed according to a tailored specification. After rig testing (drop test, strength test etc.) the undercarriage was cleared for prototype flying. During appropriate flight trials unsatisfactory torsional stiffness of the main U/C was discovered. The problem was solved mainly by stiffening the torque links in combination with the introduction of a slight wheel toe-in and a re-adjustment of the hydraulic damping.

Additionally the nose gear airspring was modified in order to cover unexpected high loads from thrust reverser operation.

Main U/C Drop Test

Wheel spin-up force at landing touchdown bends the U/C backwards. On Tornado main U/C, this bending is accompanied by leg twisting, since the single wheel is laterally offset from the leg. After spin-up, the circumferential tyre force reduces, which initiates both bending and twisting spring-back. At the same time, the tyre attains full side-force capability. Therefore, the twisting oscillation spurs a lateral oscillation as well.

Due to the many nonlinearities involved (especially with regard to tyre behaviour) a comprehensive drop test program was performed with a heavily instrumented main U/C attached to a quarter fuselage section (Fig. 23). Approximately 70 drops were performed onto a rotating drum, varying "forward speed", A/C mass, lift-to-weight ratio, sinkrate, pitch angle, bank angle, yaw angle as well as wheel toe-in angle and different stiff torque links. Tests were accompanied by computer simulations aiming mainly at dynamic correlation of the load triplet, vertical load, fore/aft load, and lateral load.

The results of the drop tests were introduced into a combined undercarriage/airplane simulation programme, which was very successfully applied to prediction and recalculation of U/C flight tests as well as for clearance of Tornado landing condition envelope (Fig. 24).

After this chain of rig and flight testing in combination with model improvements the full required undercarriage performance was achieved including a remarkable repaired runway capability of the aircraft.

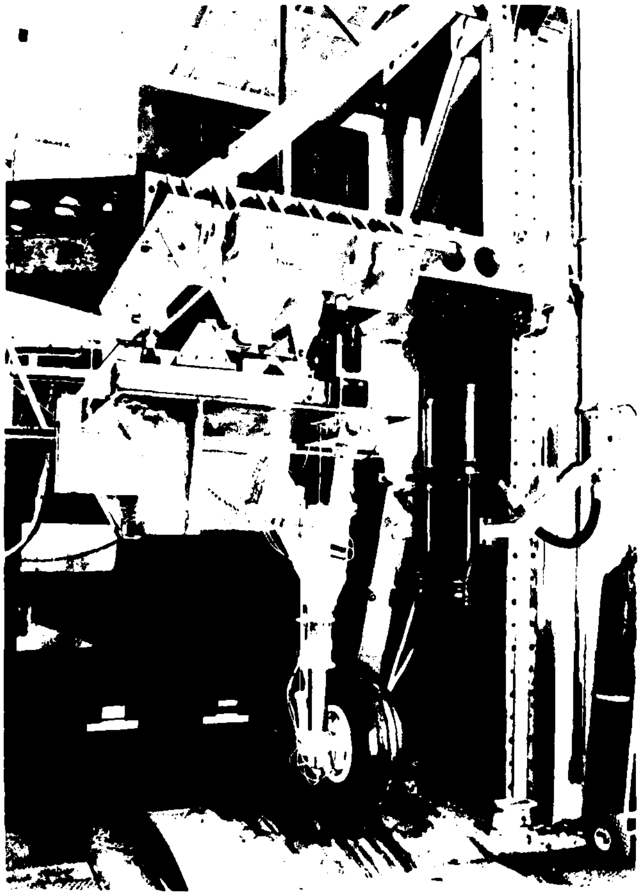

FIG. 23

MAIN UNDERCARRIAGE DROP TEST SETUP

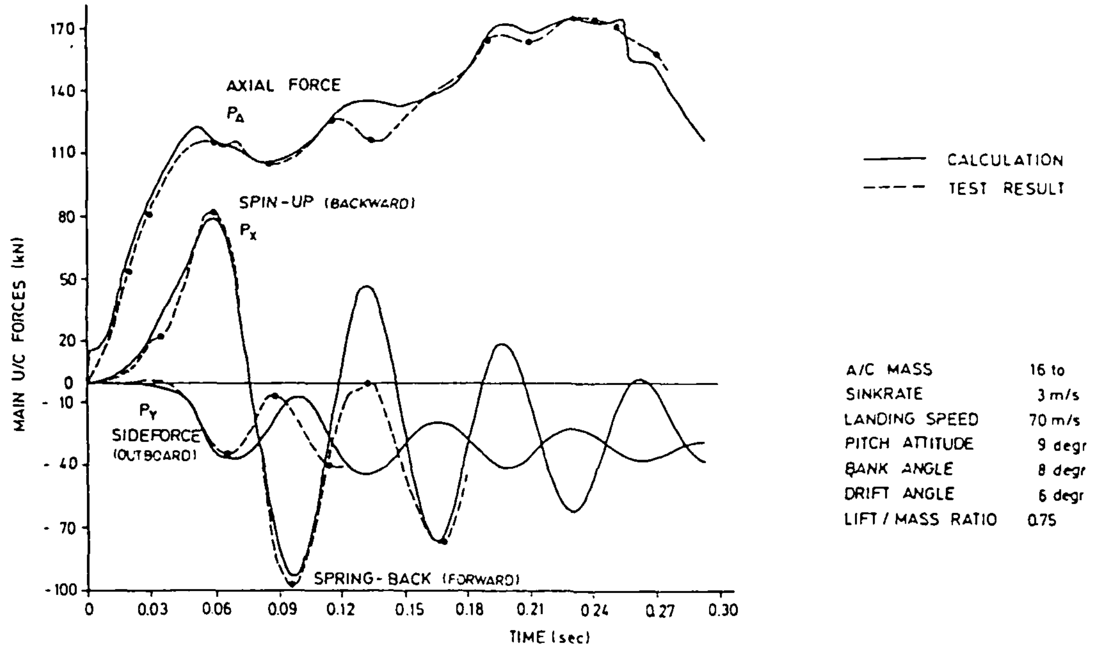

FIG. 24 DROP TEST – TRIPLE LOAD COMPARISON

Tornado U/C design copes with operation from bases with runway roughness equivalent to semiprepared fields. However, from an operational point of view the capability to operate from a regular runway which was bomb damaged and rapidly repaired is very interesting, too.

Therefore, "Repaired Runway Trials" have been planned and were carried out. AM 2 repair mats (3.8 cm thickness) were laid out on undamaged original pavement.

In contrast to usual flight loads, which mostly are of linear or degressive character (e.g. lift *versus angle of attack*), the airspring of an undercarriage exhibits a strongly progressive load/stroke characteristic. Therefore, "Repaired Runway Trials" are to be very carefully planned and monitored in order to keep the risk of inadvertently exceeding structural limits at an acceptable level.

Fig. 25 shows traces from a Tornado traverse of two AM 2 repair mats at Manching. The dots mark the respective extreme points of the corresponding computer simulation. Considering the U/C nonlinearities correlation is very good over a considerable time period.

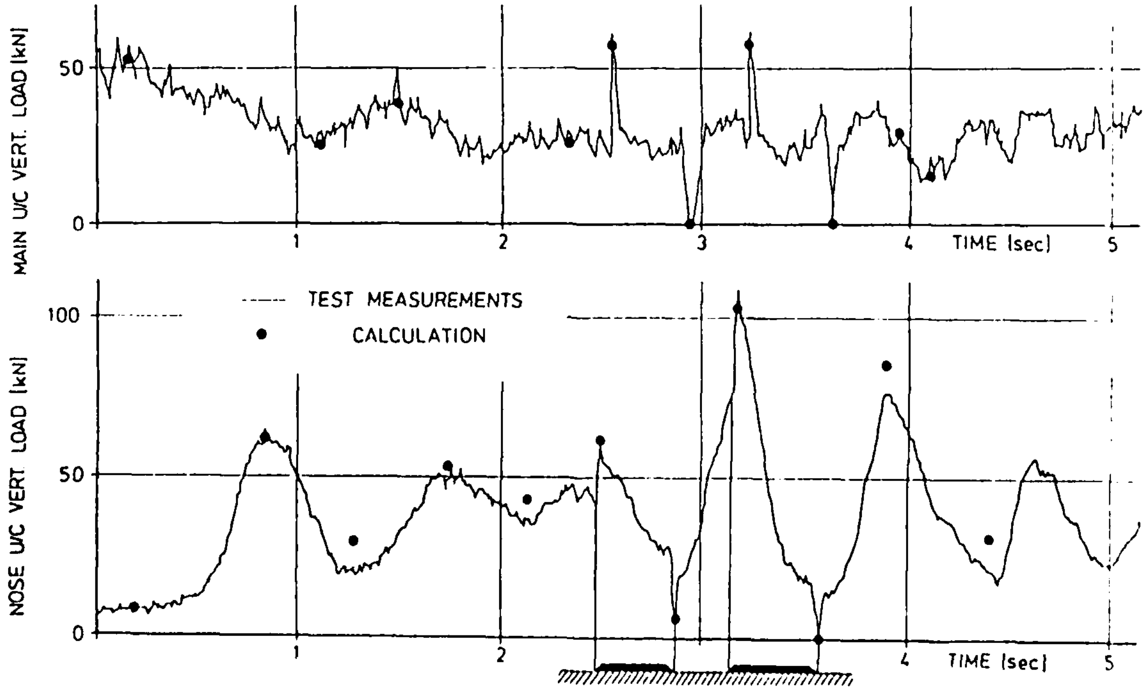

FIG. 25 TRAVERSE OF TWO AM-2 RUNWAY REPAIR MATS DURING A MAX. DECELERATING LANDING-RUN

STRESS ANALYSIS

Stress analysis is the key analysis needed for detail design. It uses the loads previously described and represents the structure by finite elements (deformation method). The basic airframe parts were idealized and then coupled together by substructure technique in order to check each part separately and save computer cost. As a typical example the stress analysis and manufacturing procedure for the Tornado wing box is illustrated.

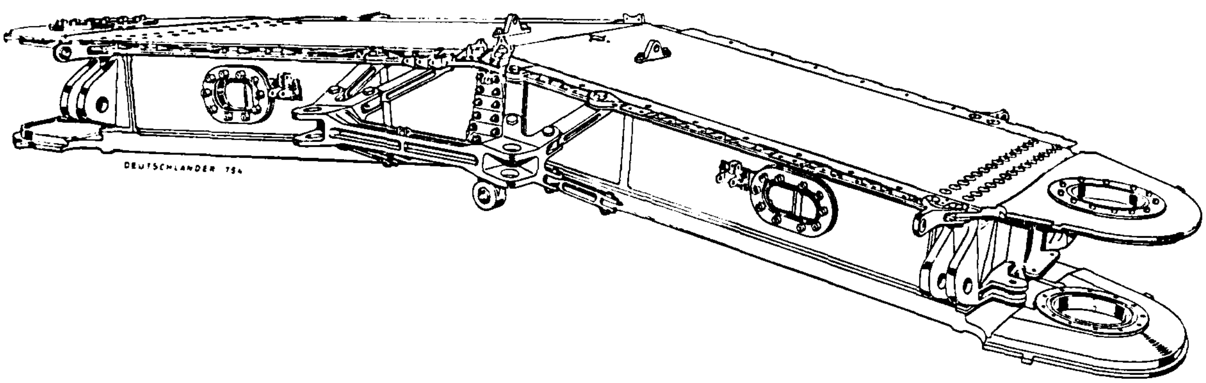

FIG. 26 WING CARRY THROUGH BOX

Tornado Wing Carry Through Box

The Tornado wing carry through box, the "heart of the aircraft", is a high strength safety class 1 type of structure (Fig. 26). Stress analysis of the wing carry through box was done using finite element methode. The finite element mesh is indicated by Fig. 27. High stress gradients, an example is given in Fig. 28, required a large number of finite elements. The total number of finite elements for half of the wing carry through box, i.e. on one side of the symmetry plane, is 3824 elements having 2370 nodal points. For this, the number of static undeterminates is 9700. Because of the large amount of finite elements it was necessary to use substructure technique for inclusion of the wing carry through box in the unified stress analysis of the whole aircraft structure. The computer program used was NASTRAN. Because of the very much refined structural schematization the computer results could be used directly for stress checking. Comparison of the computer results with strain gauge measurements from static tests on the wing carry through box have shown good correlation.

The material used for the wing carry through box is titanium alloy Ti6Al4V annealed, except the upper load plate which is made from Ti6Al6V2Sn. The assembly of the carry through box is mainly by electron beam welding. Only the upper plate is bolted to the box. With the welded concept a significant weight saving was achieved, because there are no holes for mechanical fasteners through the lower fatigue critical plate. Sealing problems are also substantially reduced. The lower load plate consists of two integral plates, NC machined and welded together in the symmetry plane of the box. The sidewalls and facewalls are dye forged components. The rigs are made from hot formed titanium sheets. The upper load plate is one piece integrally machined. Upper load plate and ribs are bolted against the lower part of the wing carry through box. The attachment of the upper load plate is being sealed because the wing carry through box is used as an integral tank too.

A lot of development work had been done in order to end up with a reliable welded construction. The result of this extensive work is, that the welded connection has the same static strength as the basic material and also the fatigue properties are very similar to those of the basic material. Just in order to cater for possible micro flaws in the welded area which could induce stress concentrations, the thickness of the joined components had been locally increased at the weld planes.

Due to large progress made by MBB in EB welding of titanium material it is now possible to allow EB welding repairs. For later production, the material of the upper load plate was changed to Ti6Al4V with the possibility to make this from two pieces welded together in the symmetry line.

After having done the EB welding process the wing carry through box is being annealed in order to relieve residual stresses. Glass ball shot peening is applied on the surfaces.

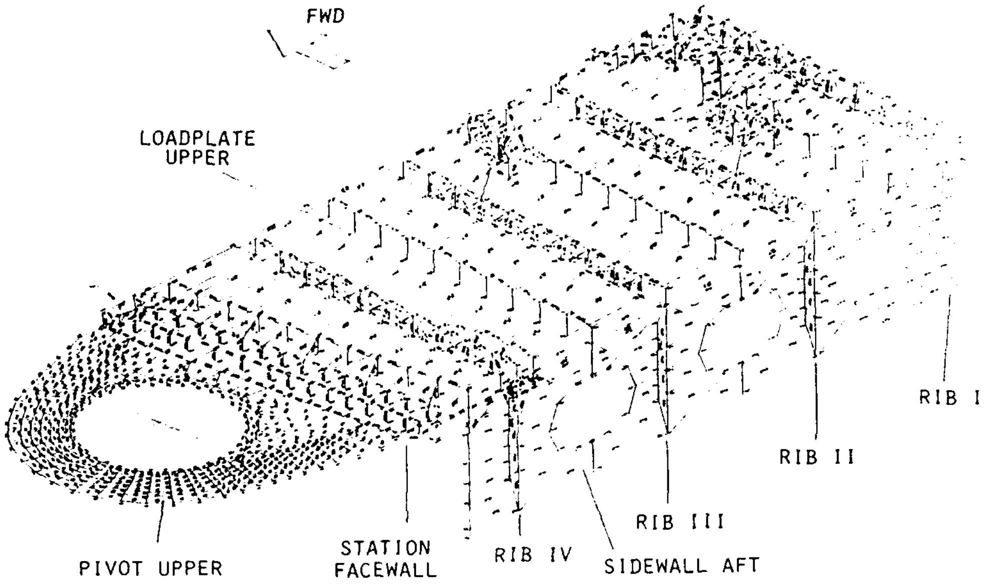
FWD
LOADPLATE UPPER
RIB I
RIB II
RIB III
PIVOT UPPER
STATION FACEWALL
RIB IV
SIDEWALL AFT

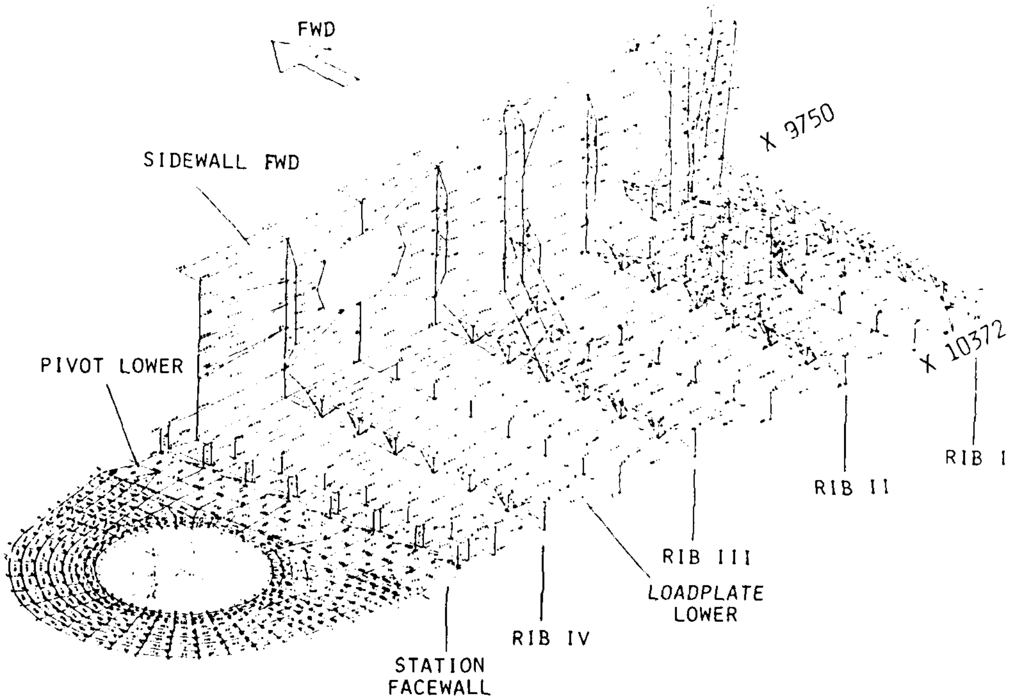
FWD
SIDEWALL FWD
X 9750
PIVOT LOWER
X 10372
RIB I
RIB II
RIB III
LOADPLATE LOWER
RIB IV
STATION FACEWALL

FIG. 27 FINITE ELEMENT GRID OF WING CARRY THROUGH BOX

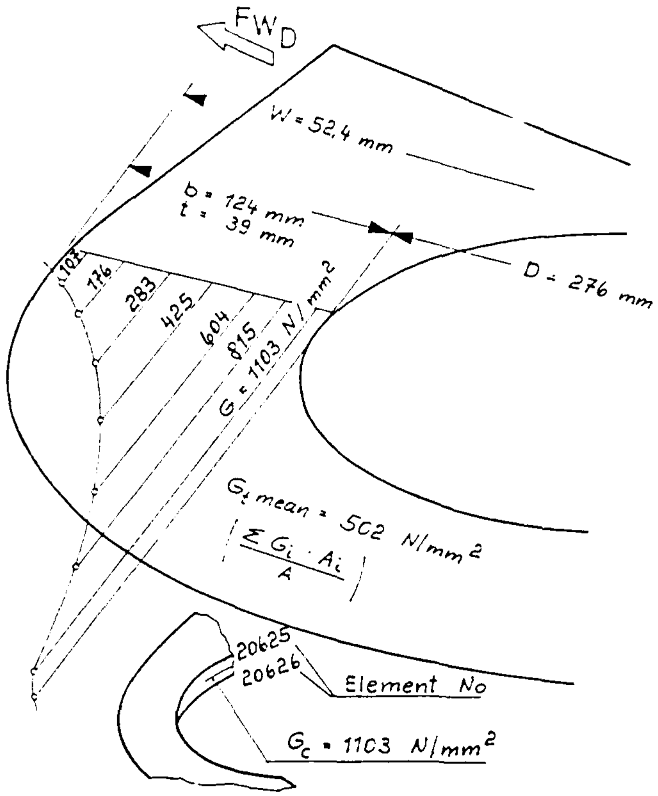

FIG. 28 STRESS DISTRIBUTION FOR LOWER PIVOT LUG

FATIGUE LIFE VERIFICATION

For modern fighter aircraft fatigue life of the structure is of great importance. Indeed the number of missions and provable life hours is considerable less than for commercial aircraft, however the number of load cycles per flight hour and the severity of the fatigue load spectrum is considerably higher. The basic design requirement for the Tornado structure was a pure fatigue life demonstration up to four times of the operational life. There was no requirement to demonstrate damage tolerance according to MIL 83444. However, damage tolerance was extensively applied to wing carry through box and wing sweep actuator support.

The basic load spectrum has been defined by the customer and was part of the Performance and Design Requirements (PDR). The customer has derived the spectrum from the experience of fighter aircraft still in service with the air forces of the Tornado partner countries and extrapolated it to the likely usage of the Tornado A/C.

Fatigue Life Analysis

Miner's Rule has been used as the basic method of calculating damage accumulation, with the assumption of failure occuring when damage accumulation equals 1.

For each component the most appropriate S-N curve has been chosen according to the experience of the particular company which in many cases has been gained from the analysis of test results on similar components.

Whenever possible the results of fatigue tests on the Tornado structure have been included in the analysis by the use of factors which correlate the S-N curve with the test results.

In certain cases the results of fatigue tests on coupon specimens with flight by flight loading have been read across to Tornado components by use of the relative Miner Rule.

To cover scatter in load spectra and fatigue endurance a safe fatigue life factor of 4 as required by the P.D.R. is used.

During the development and production phase a considerable number of fatigue tests on specimens and components besides the full scale airframe tests have been carried out.

The main objective for fatigue testing is to generate basic fatigue design data, to reduce the development risk e.g. for components with new production technique and to verify the fatigue life for the final structure.

In the following the most important fatigue life verification tests, namely, Full Scale Hinge Fatigue Test (FSHFT) and the Major Airframe Fatigue Test (MAFT) are described.

Full Scale Hinge Fatigue Test

The full Scale Hinge Fatigue Test was to demonstrate the fatigue behaviour of the most essential section of the Tornado structure during a reasonably early programme stage.

The test set-up (Fig. 29) comprised a fuselage centre section shortened on the rear end, together with a complete wing carry-through structure, a production wing box with both pylons, I/B - flap and discus on the RH side and a dummy wing with dummy I/B flap on the LH side. Front and rear fuselage sections, air intakes and main landing gear were replaced by appropriate dummy structures.

The loading system was made up by six rigid struts which kept the test specimen in position plus 22 hydraulic jacks which were distributed as follows: (Fig. 30).

6 at the RH original wing box

4 at the wing pylons (horizontal loads only)

3 at the LH dummy wing

2 at the air intake dummies

2 at the centre fuselage structure

1 at the MLG dummy

2 at the fuselage dummies (front and rear) and

2 for sweeping the slave wings which reacted the RH and LH wing loading jacks and also drove the RH wing box and the LH dummy wing by means of hinged struts attached to cantilevers.

A pneumatic system applied pressure to the air intake ducts by means of rubber bags and the wing slot sealing bags. Only symmetric load cases were simulated. The airframe was loaded according to a flight by flight load programme consisting of 42 flights of random sequence compiled of 542 load cases.

Strain gauge instrumentation comprised an overall coverage of critical areas at the beginning of the test with subsequent extension as damage and repair events demanded. (Maximum 725 strain gauges at a time). Inspection were performed in predetermined intervals (minimum 1000 hrs) and as triggered by damages.

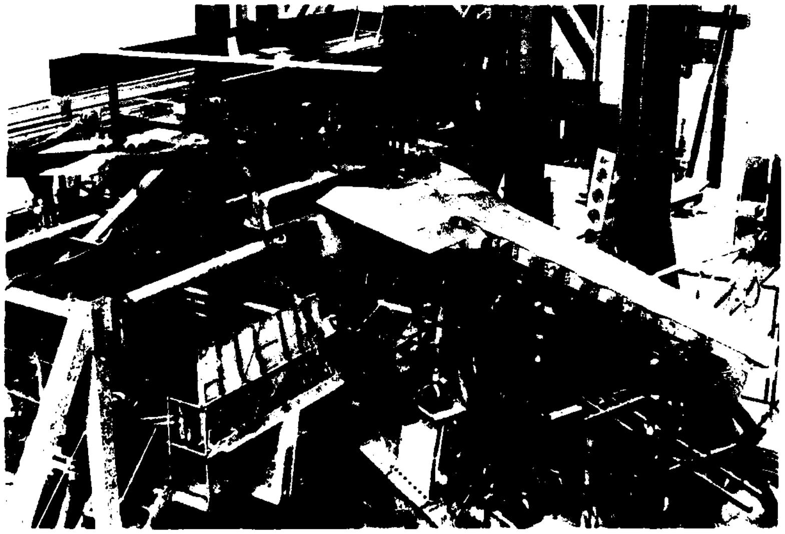

FIG. 29 FULL SCALE HINGE FATIGUE TEST

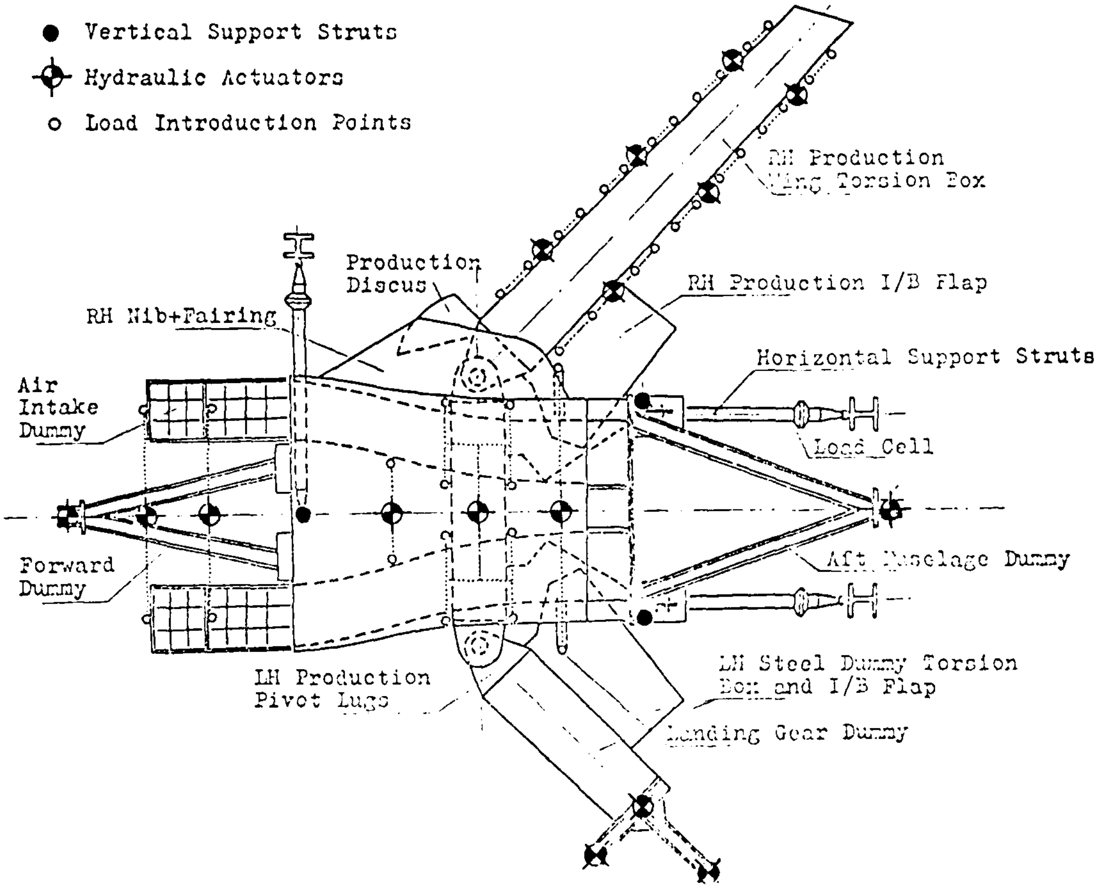
● Vertical Support Struts
Hydraulic Actuators
o Load Introduction Points
RH Production Wing Torsion Box
Production Discus
RH Nib+Fairing
RH Production I/B Flap
Horizontal Support Struts
Air Intake Dummy
Load Cell
Forward Dummy
Aft Fuselage Dummy
LH Steel Dummy Torsion Box and I/B Flap
LH Production Pivot Lugs
Landing Gear Dummy

FIG. 30 VIEW OF TEST SET UP

The Major Airframe Fatigue Test (MAFT) giving the final fatigue life proof for Tornado is unique in its extent with respect to the loading system and loading programme. The requirement is to demonstrate a safe airframe life of 4000 flight hours which with a scatter factor of 4 means, that 16 000 flight hours have to be simulated on the test.

The test specimen comprises a complete, unequipped airframe except for the following components which are dummies

- Engines
- Airbrakes
- Tailerons
- Rudder
- Radome
- Nose and Main Landing Gears
- O/B Flaps (2,3 and 4)
- Slats
- Movable intake ramps

All of which are tested separately. The dummies are designed in such a manner that correct loading can be introduced to the relevant attachment points.

A total of 79 servo-controlled hydraulic jacks, 6 statically determinate struts and 6 different pneumatic systems serve to simulate the required flight conditions. 68 of the jacks apply net aerodynamic/inertia loads (including stores), 1 applies thrust and reverse thrust to the dummy engines, 8 apply landing loads to the nose and main gear. The remaining two sweep the slave wings which in turn are attached to the aircraft wings by struts.

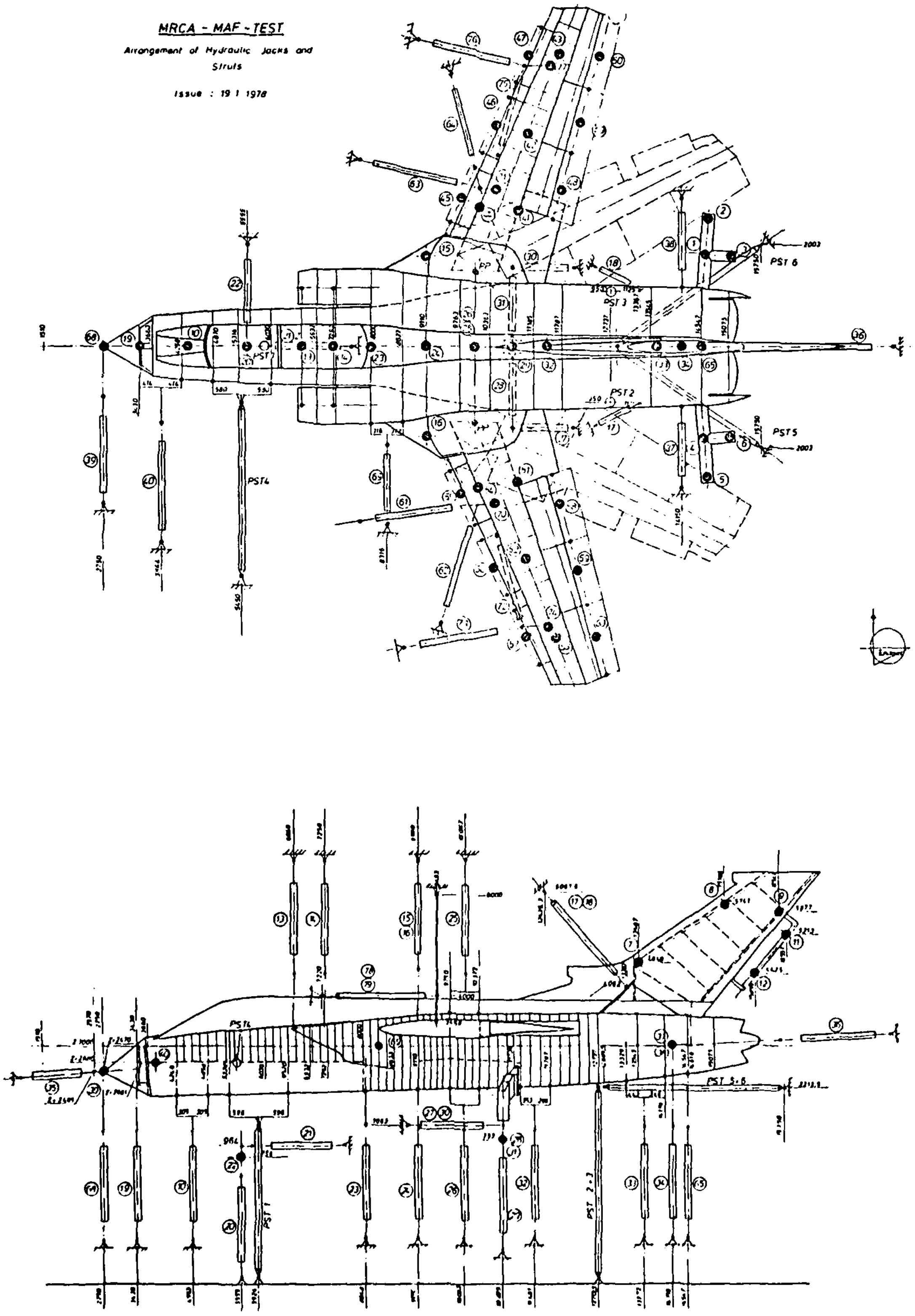
MRCA - MAF - TEST
Arrangement of Hydraulic Jacks and Struts
Issue : 19 1 1978
PST 1
PST 2
PST 3
PST 4
PST 5
PST 6
PST 7
PST 2-3
PST 5-6
PP

FIG. 31 'MRCA-MAF-TEST (ARRANGEMENT OF HYDRAULIC JACKS AND STRUTS)

The pneumatic systems apply pressure to the cockpit, cockpit seal, fuel tanks, intakes, bleed chamber, and wing slot seal. Fig. 31 shows the principal arrangement of the test and the jacks and struts.

A randomised flight-by-flight test programme is performed. 40 different flights are derived from 6 basic missions which have been defined by the Air Staffs. To cover all conditions a total of 1095 load cases have been evaluated comprising.

555	Symmetric Steady State manoeuvres
110	Symmetric response manoeuvres
330	Asymmetric Steady State manoeuvres
100	Landing Cases

85 000 different actuator loads are required to match the load cases. During the 16 000 hours there will be a total of 2.88 million load cycles and 112 000 wing sweeps.

Two computers are used for the control and monitoring systems. Jacks are operated through a closed loop servo-system to a guaranteed accuracy of 0.5 % of the maximum load.

To assure the safety of the test airframe against incorrect loading, several safety devices are installed. If the difference between demand values and actual values exceeds a pre-set threshold the test will be shut down immediately. The computer monitors also the load distribution and load sequence.

As a final safety device, mechanically acting load limiters are installed. A central control desk displays all information needed by the test engineer to survey and command the test.

The test specimen is fitted with 609 strain gauge channels and 61 deflection transducers. Recordings will be taken every 1000 test hours via a high speed data acquisition system which will simultaneously record the loading distribution.

In addition a number of crack detection wires are applied in areas suspected of being critical e.g. wing lower surface, fin and side skins.

Visual external inspections are carried out daily. On completion of every 1000 test hours the airframe will be inspected using visual, eddy-current magnetic and X-Ray techniques. After every 2000 test hours a major inspection will be carried out. In addition to the 1000 test hour inspection it will involve the removal of considerable parts of the rig and dummy components. At the end of 16 000 hours there will be a complete strip-down.

Fatigue Life Monitoring for Tornado

The fatigue life of the Tornado is monitored in phase I by a g-counter being installed in each A/C. The g-counter records the centre of gravity spectrum for each wing position. Besides the mission, configuration, fuel weight and the number of landings will be registered on a data sheet. The fatigue damage respectively the residual fatigue life will be determined for certain structural areas applying appropriate analytical functions which give a correlation between g-counting and data sheet at the one hand and the local stressing at the other hand. The fatigue life monitoring will be limited to such structural areas which meet the following requirements:

- through monitoring the structural area has to be expected to show a high degree of economic profit
- the structural area can be monitored with sufficient reliability.

Basically the structural areas which will be selected for fatigue life monitoring are potential fatigue life critical components within the primary wing and centre fuselage structure requiring a considerable inspection effort.

In phase II it is intended to install a statistically representative number of maintenance recorders in order to improve the accuracy of the residual fatigue life prediction and to increase the structural area for fatigue life monitoring. The maintenance recorder is intended to monitor both the structure and the engines. The following deals only with the monitoring of the structure.

The damage respectively residual fatigue life will be determined using the flight parameters measured and registered by the maintenance recorder. The correlation between flight parameters and local damage will be performed by regression analysis. The important parameters being recorded are listed below

- Pressure Altitude
- Calibrated Airspeed
- Normal Acceleration
- Angle of Attack
- Roll Rate
- Pitch Rate
- Yaw Rate
- Taileron Position Port
- Taileron Position Starboard
- Outboard Spoiler Position Port
- Inboard Spoiler Position Starboard
- Rudder Position
- Wing Sweep Angle

etc.

Before introducing the maintenance recorder in the production A/C a qualification programme has to be performed:

- in the first step it will be demonstrated that the MR together with its sensors and wiring is compatible with the Tornado and able to collect and to record the data with high fidelity
- in the second step the functioning of the complete system consisting of data acquisition data analysis and fatigue life analysis will be tested an a trade study of an operational structure and engine control by the MR will be carried out.

Referring to maintainability the introduction of the MR has the following aims:

- Fatigue life monitoring is an additional measure for the maintenance and inspection programme to increase the safety and to confirm the assumptions made for the design.
- Fatigue life monitoring is a measure to rationalize the maintenance i.e., reduction of the inspection effort by optimizing the inspection interval through damage equivalent inspection.

STRUCTURAL DYNAMICS

With the increased emphasis on high performance-multipurpose aircraft the role of structural dynamics in the design process has become much more important. Parameters that improve performance characteristics such as lower thickness to chord ratio, larger surface areas and higher aspect ratios are driven to near optimum values within the constraints of weight and structural dynamics limitations such as flutter, vibration environment (including accoustics), control surface effectiveness, buffet response. Because the Tornado features a powerful fly by wire Command and Stability Augmentation System aeroservoelastic analyses and tests had to be performed to avoid adverse coupling of the CSAS with the structure. Since the aircraft also carries a tremendous number of external stores on two underwing pylons for each wing and on the fuselage differing in weight and radius of gyration the problem of giving flutter clearances must be tackled with very careful selection of certain stores - for each wing sweep - to define corner points and a read across of the in between stores. The problem gets more complicated when tanks are considered and flutter free fuel emptying sequencies have to be defined. It should also be mentioned here that covering the supersonic flight regime almost doubles the analytical and test efforts compared to subsonic airplanes.

Buffet Investigations

The high maneuverability requirements for military aircraft necessitates predictions how much the pilots performance is affected by structural vibrations.

The central problem in predicting the buffet response of a full scale aircraft is the difficulty in estimating the excitation due to the separated flow over the wing. The unsteady component of the buffet pressures were measured on a rigid model by direct pressure transducers at a number of points on the wing.

The model as shown in Fig. 32 consisted of a half fuselage part without tail and a sweepable wing. Pressure pickups were located at three spanwise sections, at 0.87, 0.67 and 0.47 s in the 25° sweep position on the wing upper side, six at each section. In addition there were six accelerometers installed, to investigate the dynamic response of the model. The test program included the measurement of two sweep positions, 25° and 45°, the Mach numbers M = 0.75 and 0.8 for 25° and M = 0.7, 0.75, 0.8 and 0.825 for 45°. The incidence could be varied stepwise ($\Delta\alpha = 0.5^\circ$) in the region $4^\circ \leq \alpha \leq 13^\circ$. The wind tunnel tests were performed in ARA Bedford 8' x 9' transonic wind tunnel at 1 atm.

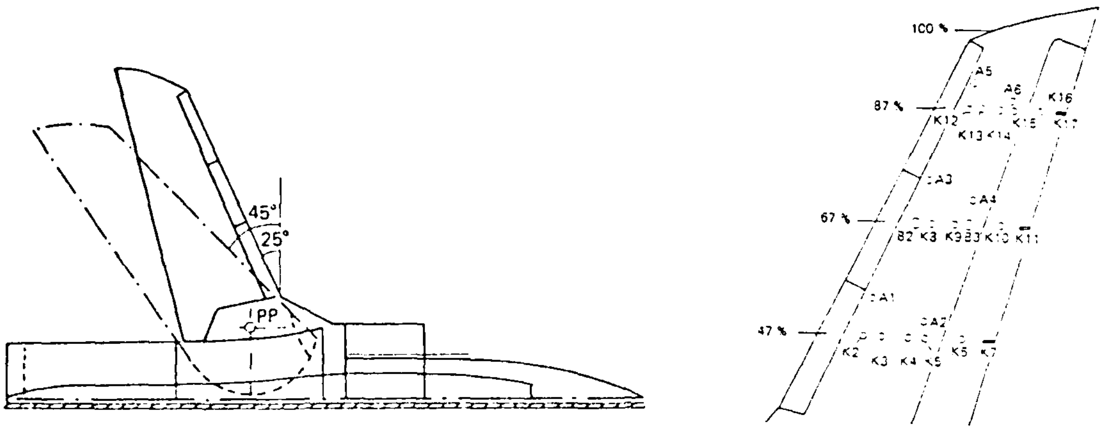

FIG. 32 GEOMETRY OF THE VARIABLE WING SWEEP MODEL AND LOCATION OF PRESSURE PICKUPS K, B AND OF ACCELEROMETERS A

Fig. 33 shows a typical example of rms pressures and accelerations. The buffet prediction method is shown in Fig. 34.

In order to prove the applicability of the method acceleration responses of the model were calculated and compared with test results (Fig. 35). Correlation is good for the two bending modes at 24 Hz and 95 Hz but the torsional modes response of the model is much higher than predicted.

Apparently the aerodynamic damping from linear theory is to high for this angle of attack. Considerable theoretical work has been done since to improve the buffet prediction method and the next MBB-fighter aircraft will show better correlation between test and analysis.

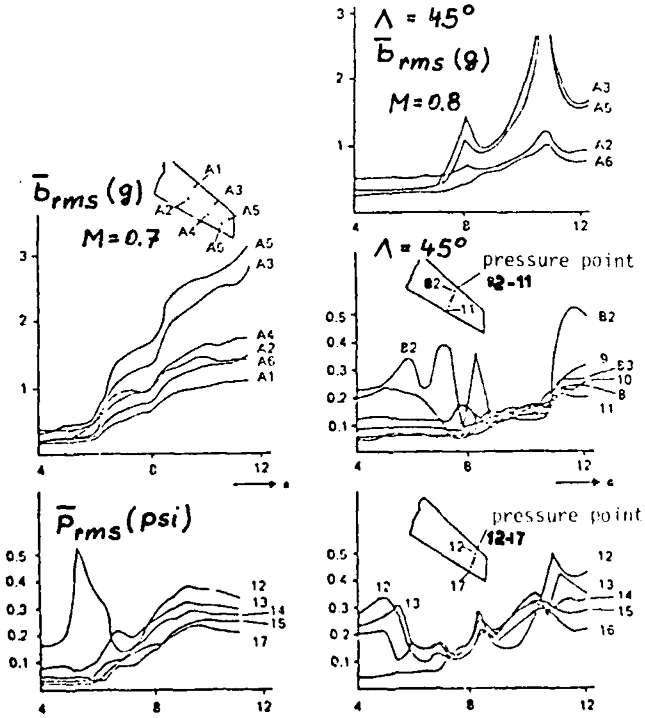

FIG. 33

INFLUENCE OF INCIDENCE AND MACH NUMBER ON THE RMS PRESSURES AND ACCELERATIONS ON THE WING AT $\Lambda_{LE} = 45°$

MODAL TRANSFERFUNCTION OF TOTAL AIRCRAFT

$H(i\omega) = [-\omega^{2} M + (1 + ig) K + L (i\omega)]^{-1}$

M, K, L = generalized inertia, stiffness and aerodynamic stiffness and damping

GENERALIZED SPECTRA OF THE EXCITATION FROM MODEL PRESSURE MEASUREMENTS

$S_M (i\omega) = \int_{-\infty}^{\infty} R(\tau) e^{-i\omega\tau} d\tau$

$R_{mn}(\tau) = \lim \frac{1}{T} \int_0^T [\sum_{j=1}^{J} \phi_{mj} \int_{F_j} p_j(t) dF] [\sum_{j=1}^{J} \phi_{nj} \int p_j(t + \tau) dF] dt$

R_{mn} = generalized cross correlation

CROSS POWER SPECTRA OF THE DYNAMIC RESPONSE

$S (i\omega) = \phi\, H (-i\omega)\, S_0 (i\omega)\, H (i\omega)\, \phi^T$

$S_0 (i\omega) = (\rho/\rho_M)^{2} (V/V_M)^{3} (S/\bar{s})^{5} S_M$

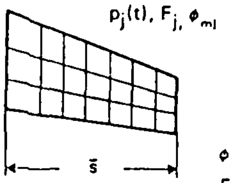

ϕ_{mj} eigenvector m

F_j panel area j

M = MODEL

FIG. 34 ILLUSTRATION OF THE BUFFET PREDICTION ANALYSIS

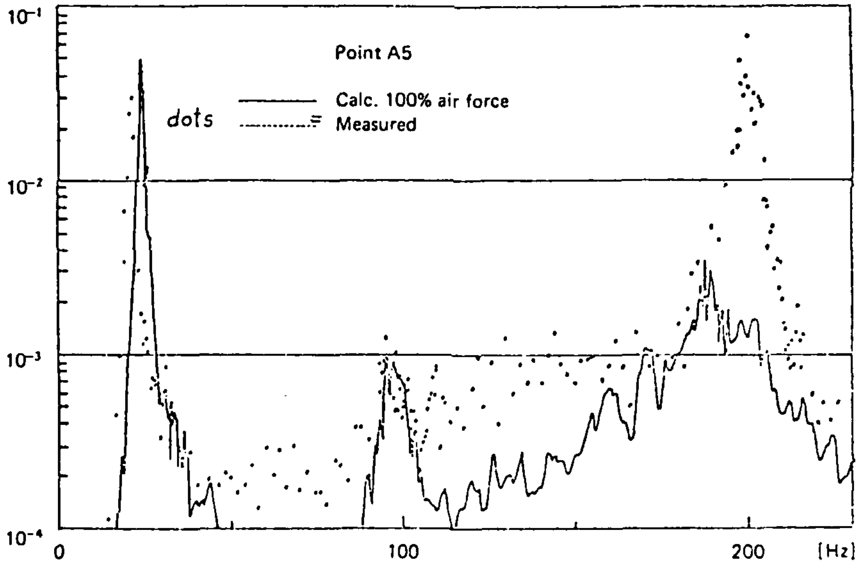

FIG. 35 PSD OF WING TIP ACCELERATIONS
$\alpha = 12°$, MA = 0.7, $\Lambda_{LE} = 45°$

Gust and Manouvre Load Analysis

In order to produce reliable gust and manouvre load predictions it is absolutely necessary to represent the elastic aircraft as well as the command and stability augmentation system in the mathematical model. The degree of refinement needed to give good results differs considerably varying from representing the aircraft aerodynamics and elastic properties with elastically corrected derivatives and the control system - including load dependent actuators - with lag functions up to a full elastic aircraft with all important structural modes and a highly sophisticated control system with all structural feedbacks. The elastic aircraft behaviour is tested in the "Ground Resonance Test". The control systems behaviour - at zero airspeed - can be checked and corrected using results of the so-called "Structural Mode Coupling Test" which is described later.

Fig. 36 shows the transfer function of the fin root shear force and of the lateral acceleration on the fin leading edge tip with and without CSAS.

It can be seen from this picture, that there is a big influence of CSAS on fin shear force because the power spectrum of turbulence has its maximum at low frequencies. Little influence of CSAS can be expected on the tip acceleration.

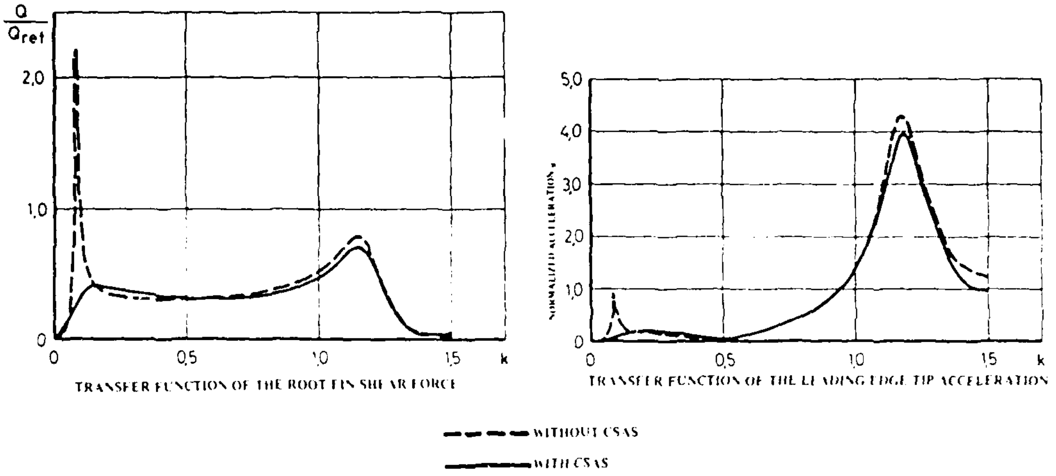

FIG. 36 FIN TRANSFER FUNCTIONS FOR LATERAL GUST

In Fig. 37 the frequency of exceedance of the wing root bending moment due to vertical stochastic gust excitation and the shear force on the fin root due to lateral stochastic gust excitation is shown. The constants used for this calculation were taken from the US-Airforce Military Specification 8861 A (May 1960). The influence of the CSAS on the fin root shear force is considerable.

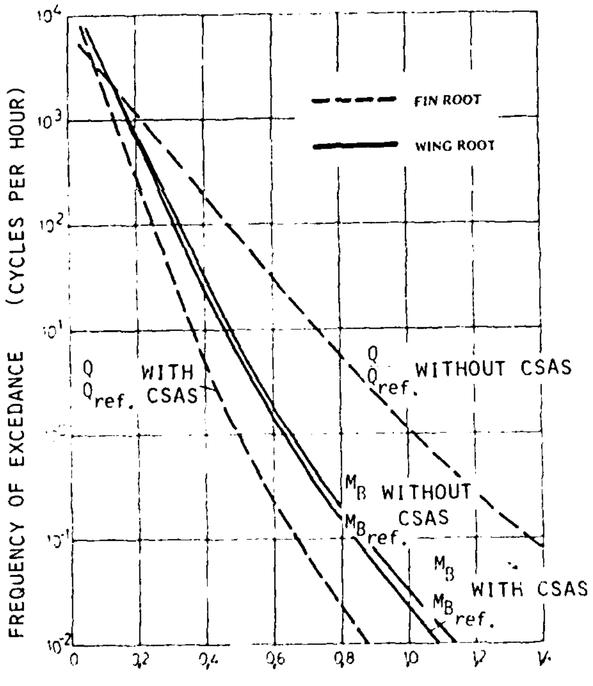

FIG. 37 FREQUENCY OF EXCEEDANCE OF WING ROOT BENDING MOMENT AND FIN ROOT SHEAR FORCE FOR GUST EXCITATION

The influence of CSAS on response calculations due to a normalized manoeuvre is shown in the next figures. In order to sort out the different influences three different kinds of tailplane movements were considered:

a) the theoretical trapezoidal tailplane movement

b) the trapezoidal tailplane movement multiplied with the actuator functions

c) the trapezoidal tailplane movement multiplied with the transfer function of the command augmentation system (CAS) and the actuator.

These three tailplane motions are presented in Fig. 38.

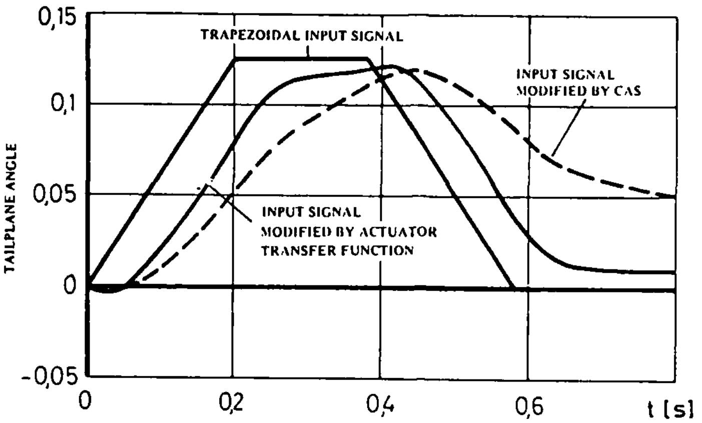

FIG. 38 TAILPLANE ANGLE INPUT SIGNAL

These three motions were introduced as tailplane manoeuvre input into the rigid and elastic mathematical model. In Fig. 39 the vertical acceleration of the center of gravity is depicted.

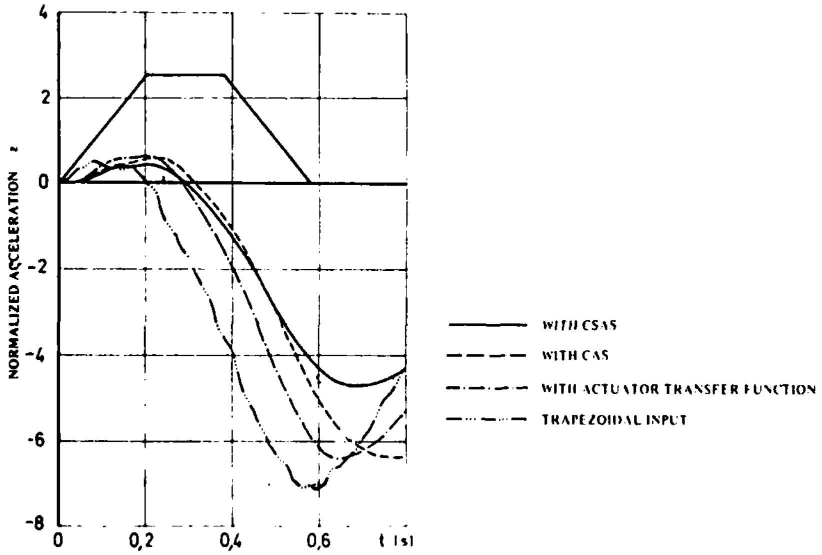

FIG. 39 A/C CENTER OF GRAVITY VERTICAL ACCELERATION DUE TO MANOEUVRE (ELASTIC A/C)

The corresponding vertical accelerations on the wing tip are presented in Fig. 40.

It should be pointed out, that design loads from gusts are altered considerably by inclusion of a CSAS. Design loads from manoeuvres however have always to be assigned to the same MIL-Spec. requirements (e.g. 'g' level), that means the pilot input has to be chosen in order to produce equivalent 'g' levels with and without CSAS respectively.

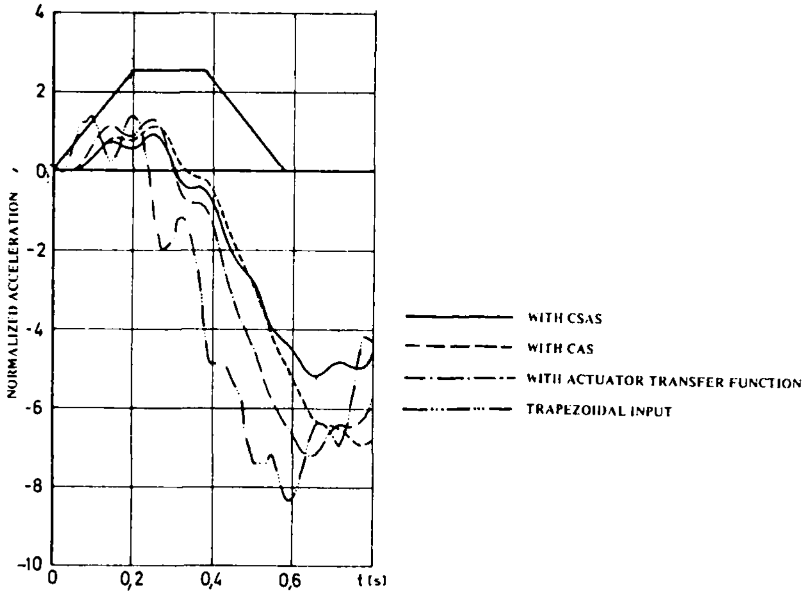

FIG. 40 WING TIP VERTICAL ACCELERATION DUE TO MANOEUVRE (ELASTIC A/C)

Flutter Investigations

Dynamically scaled models were used to predict the flutter behaviour of the Tornado A/C with and without underwing stores. Model test results were also used to check and correct analytical predictions. Unsteady pressure measurement were performed in the subsonic regime to check interference air forces between wing and tailplane and in the transonic regime to check rudder air forces against predictions. A rather exotic wind tunnel flutter test peculiar to the Tornado sweep wing aircraft was done on the wing slot seal bag.

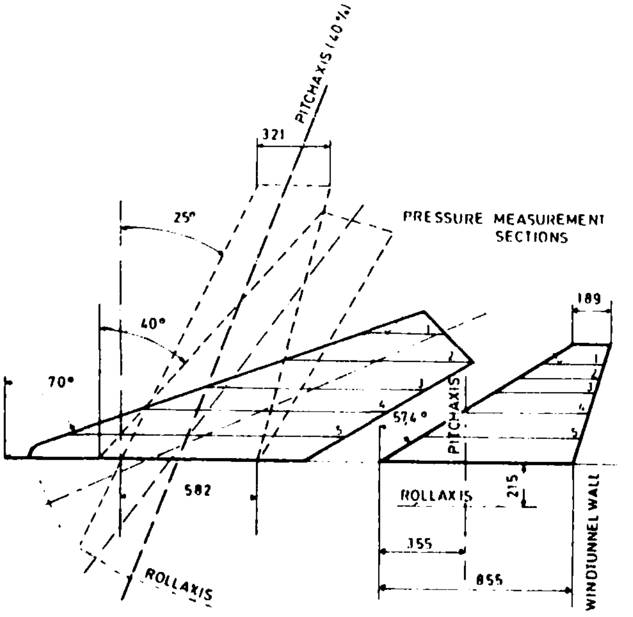

Test Program

Wing Sweep Angle	25°, 40°, 70°
Tail Aft Position	0.5s₁ < X < 1.4s₁ s₁ = wing semispan at 25°, 40° or 70°
Tail Vertical Position	-10 mm, +130 mm
Tail Dihedral	15°, 30°
Angle of Attack	= 0°, 6°
Wing Frequencies	5, 10, 15 Hz
Elevator Frequencies	5, 10, 15 Hz
Modes of Wing & Elevator Oscillations	Rolling and Pitching
Tunnel Speed	20, 30 and 40 m/s
Amplitude about Roll & Pitch Axis	0.3° < 1.5°

FIG. 41 WIND TUNNEL MODEL FOR UNSTEADY PRESSURE MEASUREMENT

Unsteady Aerodynamic Interference Airforces

During earlier wind tunnel test a flutter problem was detected which could not be predicted analytically because unsteady interference air forces were neglected. The flutter speed was highly dependant on vertical offset between wing and tail and on fuselage stiffness. A new unsteady air force theory was developed and its validity was proven with a rigid model (Fig. 41). Fig. 42 shows some results of the wind tunnel tests compared with predictions. Because correlation was very good the new air force theory was proven.

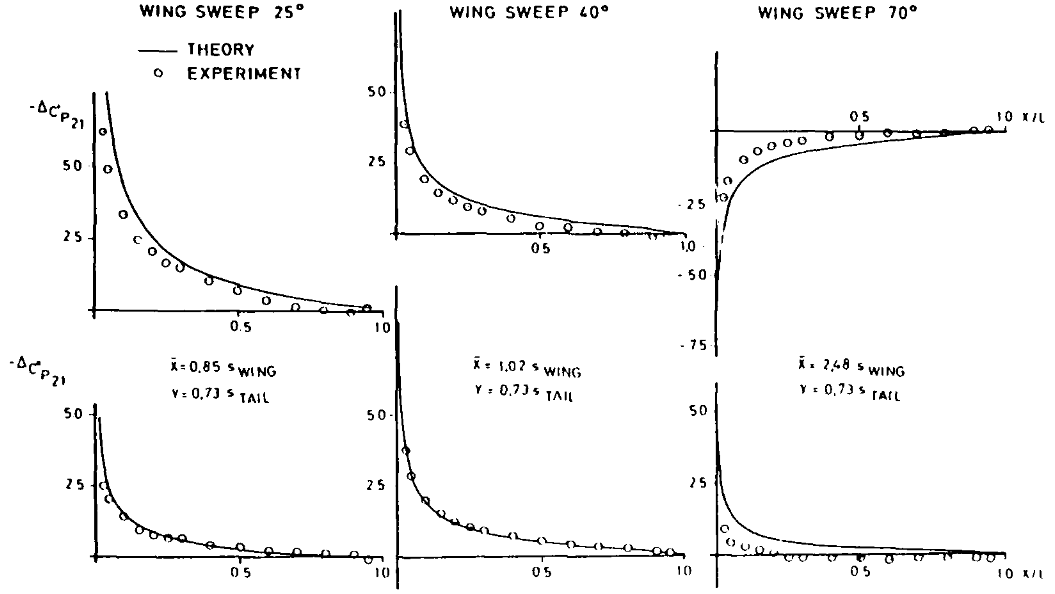

FIG. 42 INDUCED THEORETICAL AND EXPERIMENTAL PRESSURE DISTRIBUTION ON THE STEADY TAIL DUE TO WING PITCH REDUCED FREQUENCY K = 2.39; WING SWEEP 25°, 40°, 70°, PLANAR CONFIGURATION

Unsteady Pressures due to Control Surface Rotation at Low Supersonic Speed

The accuracy of control surface unsteady aerodynamics is particularly important on modern combat aircraft at low supersonic Mach number/high frequency parameter combinations. In order to assess the accuracy of current theories, a nominally rigid model has been designed, built and tested at NLR, Amsterdam, at Mach numbers up 1.3 and reduced frequencies, based on semispan, up to 1.6.

Geometry and the location of tube pressure holes is shown in Fig. 43 .

Rudder rotation was excited by an electrodynamic exciter in resonance condition. This resonance condition was fulfilled by attaching the rudder with various springs to the fin. To account for tube system dynamics with wind on some direct pressure transducers were installed and thereby a correct calibration could be established.

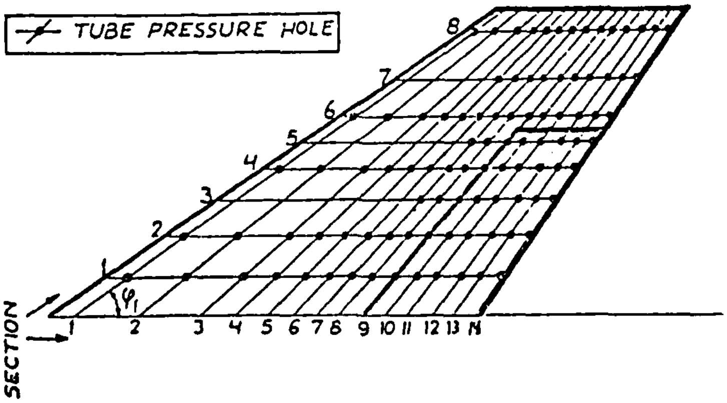

FIG. 43 LOCATION OF TUBE PRESSURE HOLES

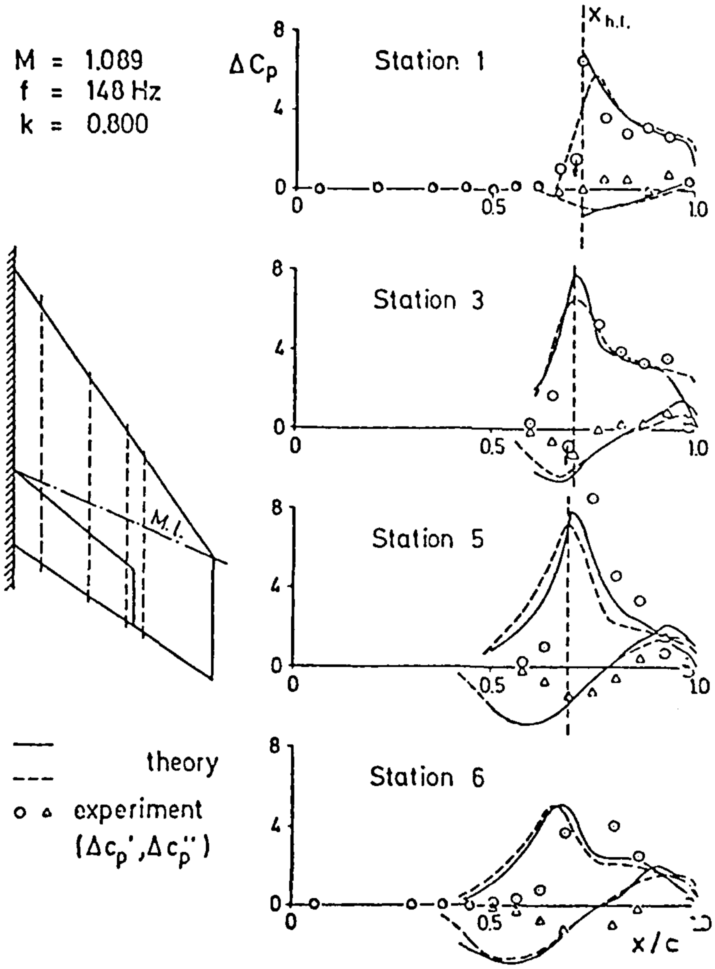

FIG. 44 EXPERIMENTAL AND THEORETICAL PRESSURES AT TEST STATIONS

Theory and experiment were compared for 4 stations in Fig. 44 . It can be stated that agreement is satisfactory.

A very interesting result is shown in Fig. 45 were rudder hinge moment is depicted versus Mach number. The imaginary part of the moment may drop below zero which means that one degree of freedom flutter could occur. This effect is also predicted by theory.

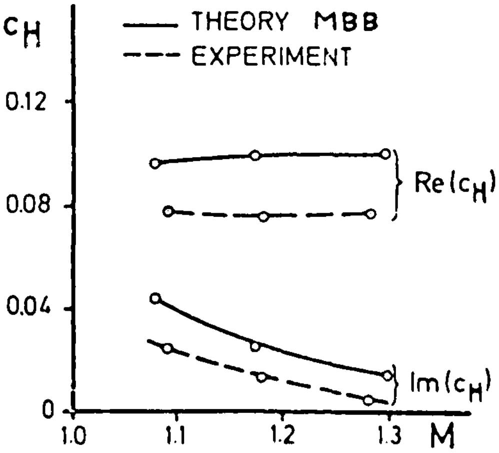

FIG. 45 HINGE MOMENT VS MACH NUMBER

Subsonic Flutter Model

Complete free-free flying flutter model were used to assess the A/C flutter behaviour. The model was used firstly to find appropriate measures to clear all surfaces to required speeds and define the sensitivity to parameters. Fig. 46 shows the model used.

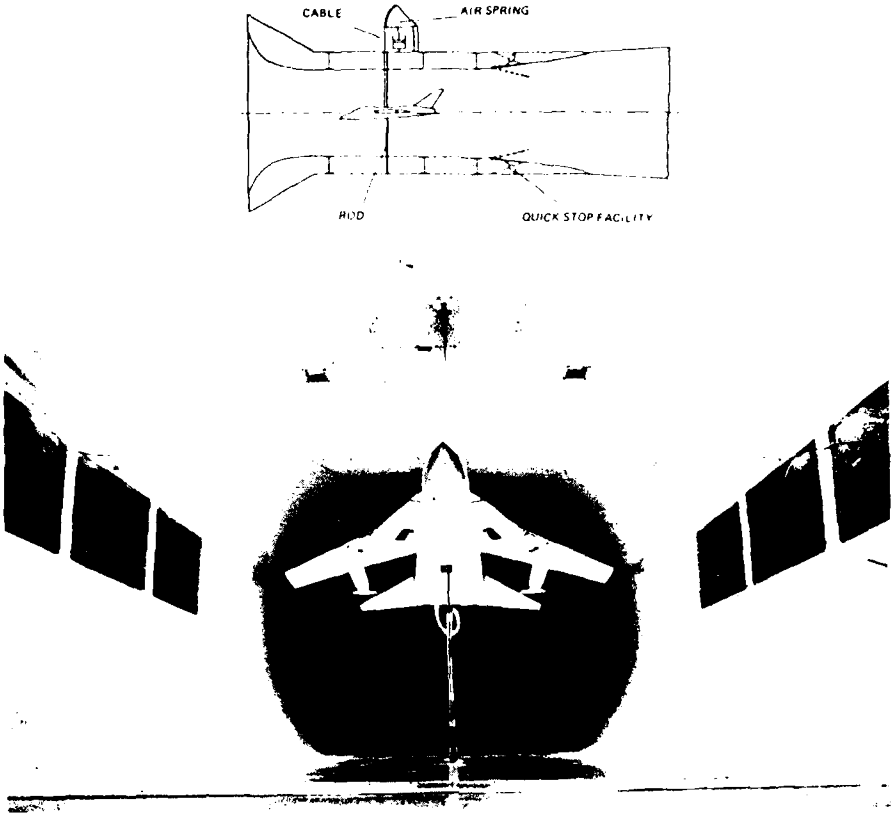

FIG. 46 SUBSONIC FLUTTER MODEL AND SUSPENSION SYSTEM

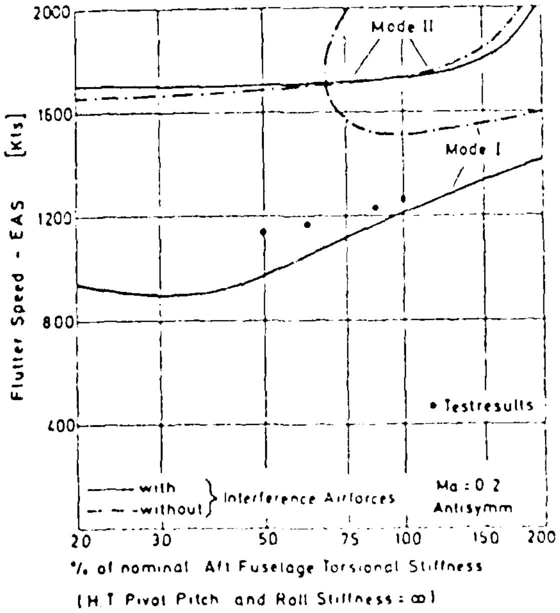

FIG. 47 FLUTTER SPEED VERSUS FUSELAGE TORSIONAL STIFFNESS

AD-A129 433   GROUND/FLIGHT TEST TECHNIQUES AND CORRELATION(U)
ADVISORY GROUP FOR AEROSPACE RESEARCH AND DEVELOPMENT
NEUILLY-SUR-SEINE (FRANCE) FEB 83 AGARD-CP-339

5/6

UNCLASSIFIED   F/G 1/3   NL

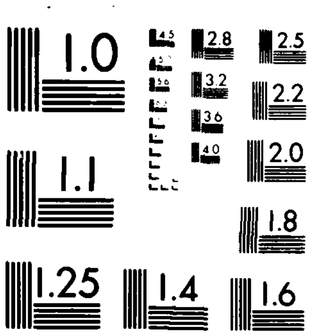
1.0
4.5
2.8
2.5
5.0
3.2
2.2
5.6
3.6
4.0
2.0
1.1
1.8
1.25
1.4
1.6

MICROCOPY RESOLUTION TEST CHART
NATIONAL BUREAU OF STANDARDS-1963-A

In Fig. 47 a flutter case is shown which is caused by aerodynamic interaction between the swept wing and the tailplane. The figure shows flutter speeds versus aft fuselage stiffness computed with and without interference air forces. Using conventional unsteady air forces the flutter speeds are completely different from the test results. By introducing interference air forces a good correlation between test and calculation was found. In Fig. 48 the trend of flutter speed versus tailplane mass balance is presented.

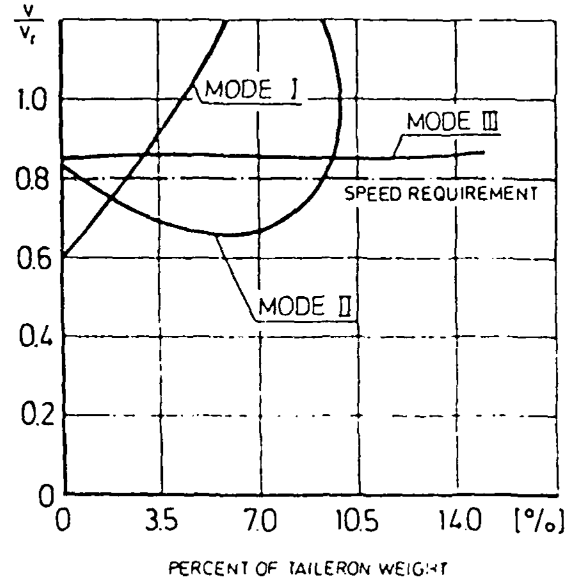

FIG. 48 FLUTTER SPEED VS TAILPLANE MASS BALANCE

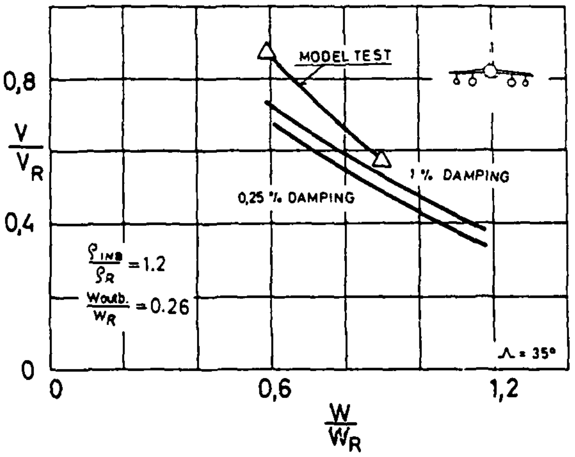

FIG. 49

FLUTTER SPEED VERSUS INBOARD STORE WEIGT FOR VARYING INBOARD STORES AND CONSTANT OUTBOARD STORE

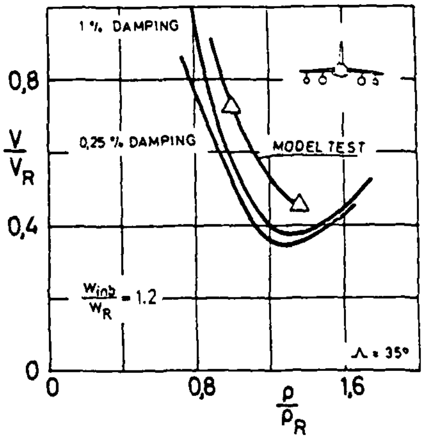

FIG. 50

FLUTTER SPEED VERSUS INBOARD STORE RADIUS OF GYRATION FOR VARYING INBOARD AND CONSTANT OUTBOARD STORE

The second purpose of the model was to find contour plots of flutter speeds for external stores carried on the wing for various parameters such as wing stiffness, pylon stiffness, etc. The flutter model testing described was found to be a powerful method for economical store flutter investigations. Typical results of store testing are depicted in the next figures. Fig. 49 shows a strong dependency of the flutter speed of two store inboard and outbaord on a wing with inboard store weight. Fig. 50 shows the variation of flutter speed of an airplane as a function of radius of gyration of the inboard store. These results were compared with predictions and good correlation was achieved. From the latter figures a contour plot as shown in Fig. 51 can be constructed.

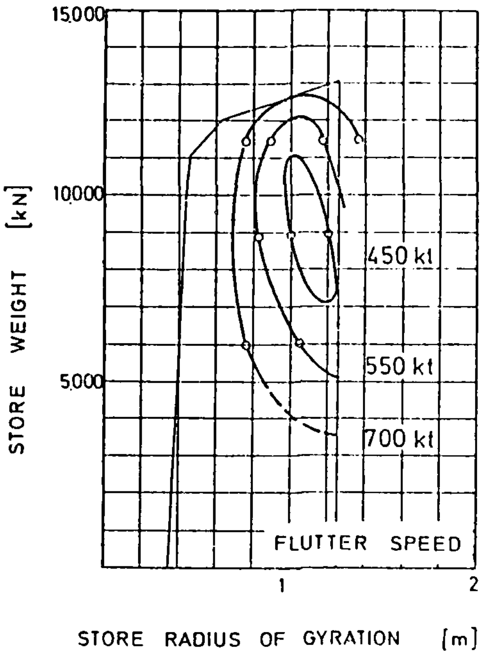

FIG. 51

STABILITY REGIONS FOR VARIOUS STORES

Transonic Flutter Model

A dynamically scaled model of the fin and rudder was built to investigate the transonic effects on the flutter speed (Fig. 52). Such a model requires a rather sophisticated design compared to a subsonic model. Frequencies and dampings were measured with autocorrelation techniques using the wind tunnel turbulence for excitation (Fig. 53). A result is shown for zero rudder jack stiffness which correlates quite well with predictions (Fig. 54).

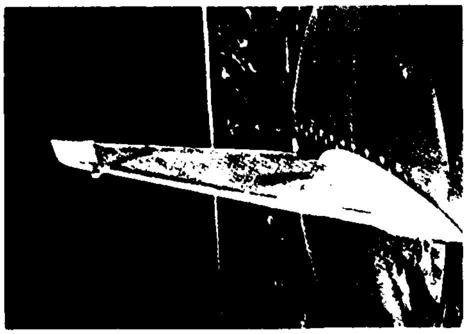

FIG. 52

TRANSONIC MODEL IN WIND TUNNEL

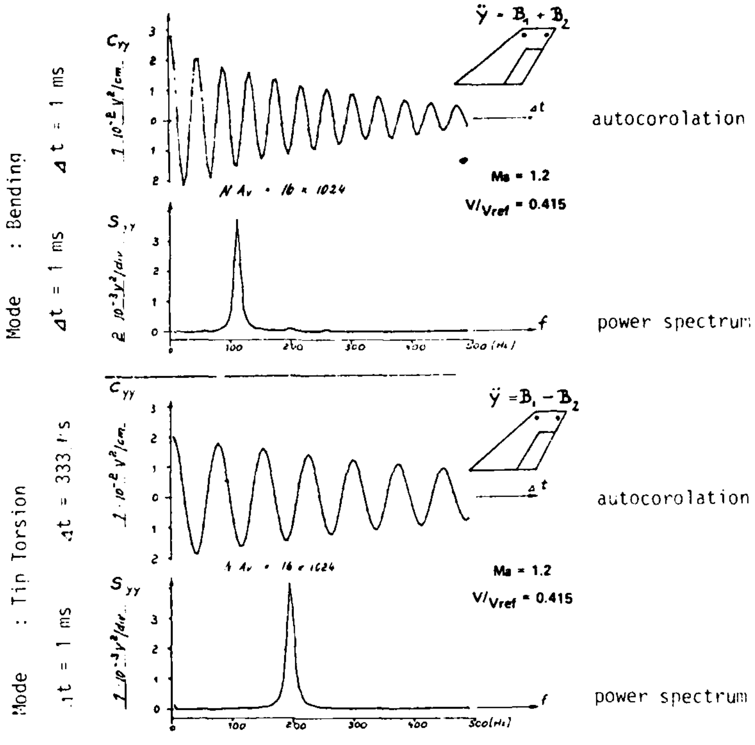

FIG. 53

AUTOCORRELATION FUNCTIONS AND POWERSPECTRA OF THE MODEL RESPONSE AT MA. = 1.2 AND V/V_{REF} = 0.415

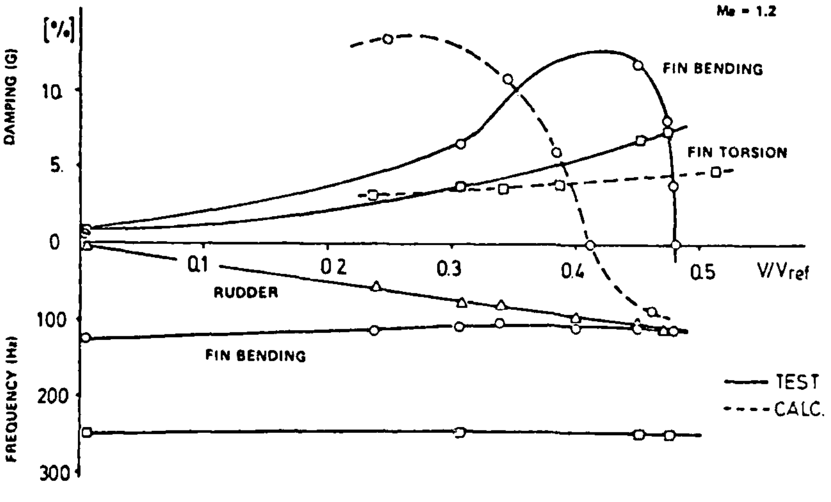

FIG. 54 FLUTTER SPEED VERSUS DAMPING AND FREQUENCY OF FIN WITH ZERO RUDDER JACK STIFFNESS

Wing Slot Seal Bag

The slot, which takes the movable part of the wing when it is swept back, is closed with an air-filled bag, consisting of an upper and lower section, providing an aerodynamically clean fuselage contour. Height of the wing slot seal have been dictated by the elastic deflection of the swept back wing under maneouver load.

The design made use of rubber sealed nylon fabric material with an outer teflon layer for wear reduction and previous experience indicated the tendency for flutter of the bag unless stabilized by sufficiently high internal overpressure.

In order to determine the minimum required system overpressure to reliably prevent flutter and thus rapid destruction of the bags, a wind tunnel test was performed with a slot seal system mounted flush into the wind tunnel wall of the Modane S2 tunnel (transonic and supersonic test section) and with a stub wing representing the wing trailing edge in relation to the slot seal. Conditions with compressed bags from the wing under load could be simulated by tilting the bags about the stub wing.

Through the test, the minimum required differential pressures to prevent bag flutter under all operational conditions could be determined, thus enabling a weight optimized wing slot seal and fuselage backup structure.

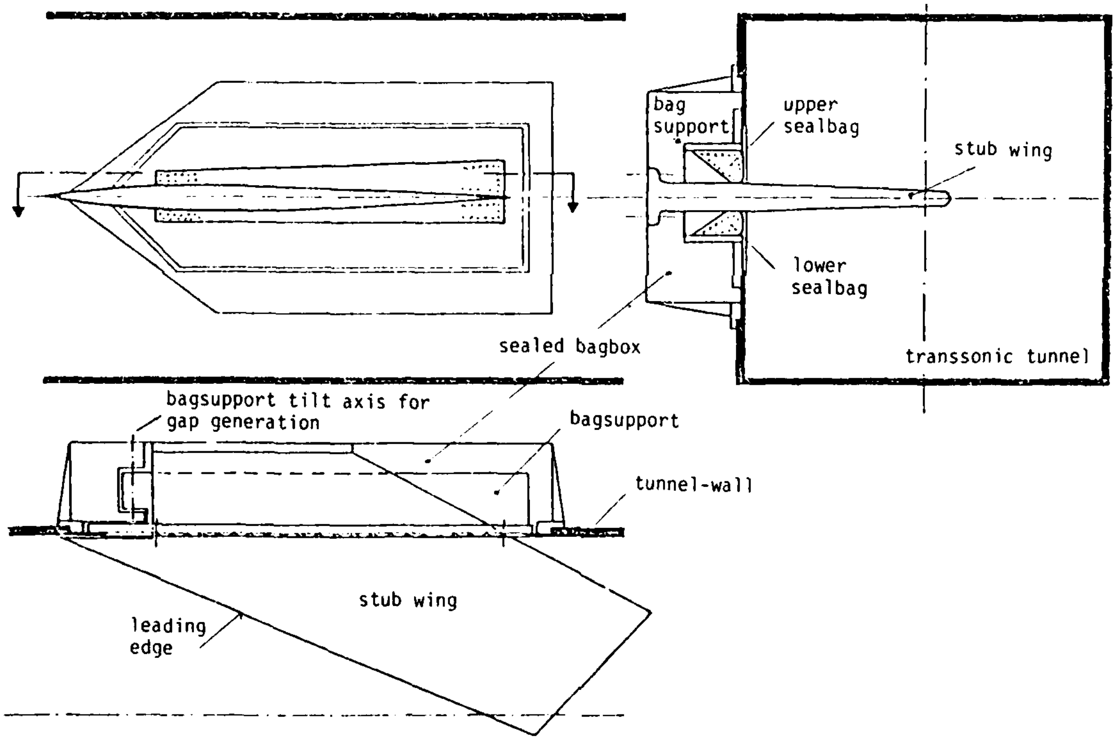
bag support
upper sealbag
stub wing
lower sealbag
sealed bagbox
transsonic tunnel
bagsupport tilt axis for gap generation
bagsupport
tunnel-wall
stub wing
leading edge

FIG. 55 WING SLOT SEAL – FLUTTER MODEL IN TRANSONIC WIND TUNNEL

INTERACTION BETWEEN AIRCRAFT STRUCTURE AND COMMAND AND STABILITY AUGMENTATION SYSTEM

As previously mentioned the CSAS must be introduced into the mathematical models for load prediction. It is also mandatory to consider its effects on the aeroelastic properties and to check predictions on ground and in air with relatively extensive tests.

During the ground testing of Tornado an instability was encountered involving symmetrical oscillations at about 13 Hz. This instability was created by detrimental coupling of the command and stability augmentation system - CSAS - with the elastic aircraft.

The surfaces controlled by the CSAS are a differentially moving tailplane (taileron), a rudder and wing mounted spoilers. These surfaces are actuated by hydraulic jacks. The aircraft motion is sensed and fed back by rate gyros. Fig. 56 shows a block diagram of the aircraft with CSAS.

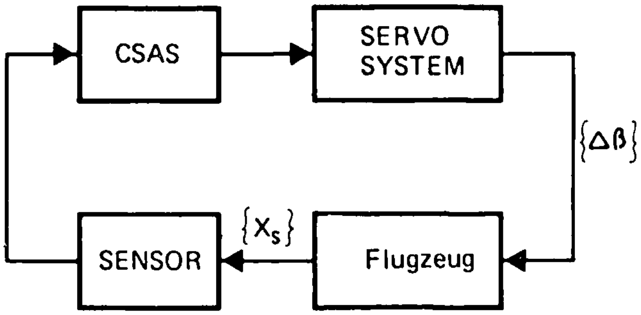
CSAS
SERVO SYSTEM
$\{\Delta\beta\}$
SENSOR
$\{X_s\}$
Flugzeug

FIG. 56

BLOCK DIAGRAM OF AIRCRAFT WITH CSAS

The airplane, being a combat aircraft, carries a huge amount of stores varying tremendously in mass and inertia properties at four sweepable stations on the wing and under the fuselage. Combining wing sweep with external stores a large number of configurations must be investigated. Thus it is absolutely necessary to have an analytical procedure which can predict the aeroelastic behaviour of the aircraft reliably so that test work can be restricted to a few check points. The mathematical model must be laid out in such a way that in can be easily adjusted to match test results.

The investigation method is shown in the block diagram of Fig. 57.

The first step was to calculate the vibration modes and frequencies based on theoretical stiffness and inertia information. These modes and frequencies were compared with ground resonance test results and the mathematical model was adjusted to match test results. Theoretical information about the CSAS was introduced into the mathematical model and later on replaced by test results (actuator impedance and transfer function measurements). Predictions gained from this theoretical model were compared with the CSAS-structural coupling test. Unsteady aerodynamic forces were fed into the mathematical model and the result of v-g plots were compared with flight flutter test results.

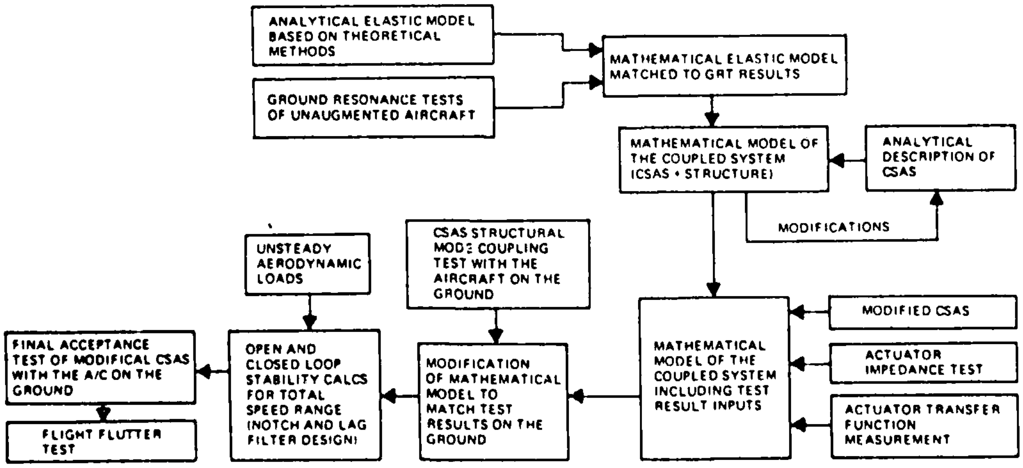
ANALYTICAL ELASTIC MODEL BASED ON THEORETICAL METHODS
GROUND RESONANCE TESTS OF UNAUGMENTED AIRCRAFT
MATHEMATICAL ELASTIC MODEL MATCHED TO GRT RESULTS
MATHEMATICAL MODEL OF THE COUPLED SYSTEM (CSAS + STRUCTURE)
ANALYTICAL DESCRIPTION OF CSAS
MODIFICATIONS
UNSTEADY AERODYNAMIC LOADS
CSAS STRUCTURAL MODE COUPLING TEST WITH THE AIRCRAFT ON THE GROUND
MODIFIED CSAS
MATHEMATICAL MODEL OF THE COUPLED SYSTEM INCLUDING TEST RESULT INPUTS
ACTUATOR IMPEDANCE TEST
ACTUATOR TRANSFER FUNCTION MEASUREMENT
FINAL ACCEPTANCE TEST OF MODIFICAL CSAS WITH THE A/C ON THE GROUND
OPEN AND CLOSED LOOP STABILITY CALCS FOR TOTAL SPEED RANGE (NOTCH AND LAG FILTER DESIGN)
MODIFICATION OF MATHEMATICAL MODEL TO MATCH TEST RESULTS ON THE GROUND
FLIGHT FLUTTER TEST

FIG. 57 BLOCK DIAGRAM OF CSAS-AEROELASTIC COUPLING INVESTIGATION

Flight Flutter Test Results

Tests were performed at a few air speeds with the unaugmented and augmented aircraft. First data evaluations show that differences in frequencies and dampings of these two conditions are within measuring accuracy. In Fig. 58 the measured and predicted frequencies and dampings versus airspeed are plotted for the most important mode.

Flight Flutter Test

Clean Aircraft:

Signals were telemetered to the ground station for quick look inspection. Post flight analysis was conducted with data stored on tape. Data evaluation was done with a special purpose digital computer using Fast Fourier Transform Techniques.

The philosophy underlying the flight flutter test phase was not only the rapid clearance of the flutter test aircraft (by tracing the most critical modes) but also the identification of the behaviour of the majority of the vibration modes. This has been undertaken in order to provide a comprehensive description of the aircraft's vibration characteristics, thus allowing more economic testing, in the future, of other prototype and production variants, even to the extent of clearance based only on calculations and simple demonstration flights.

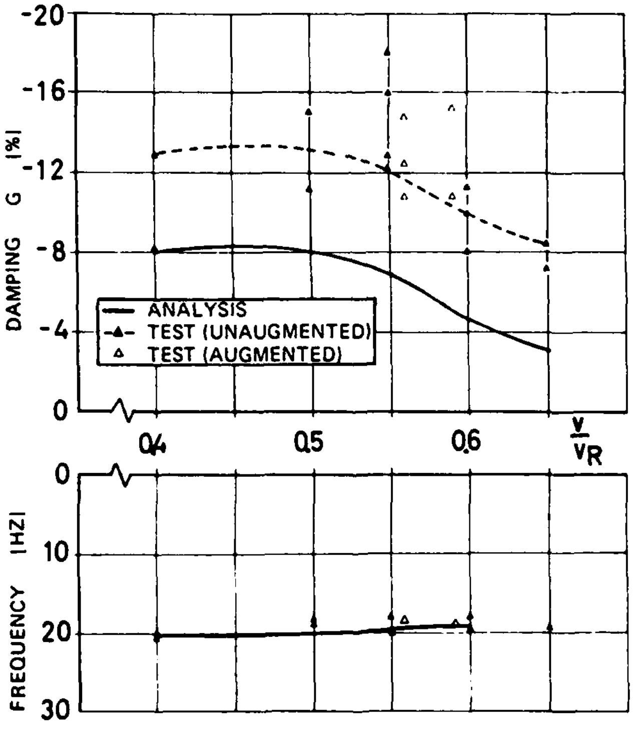

FIG. 58

COMPARISON OF ANALYSIS AND FLIGHT TEST RESULTS

Prior to flight flutter tests, clearance was given, based upon the previously-described calculations and ground tests, for flying within an envelope a little greater than half of the design envelope. Flutter testing then proceeded on a Mach Number and airspeed grid, covering the required range of Mach number at a particular airspeed before clearance to a higher airspeed was granted.

Following the identifications from the calculations that there was little effect of CSAS, and that this was slightly beneficial, the initial flutter test phase was conducted in the CSAS reversionary state, which possesses no autostabilization in the pitch and roll axes, and with the wings at the most critical sweep angle (full sweep, where interference flutter effects are greatest). Tests were then made with the CSAS engaged and at different wing sweep angles to establish the effect of these variables upon the vibration characteristics.

Following this phase, during which the entire subsonic envelope was cleared, the next phase adopted a similar approach initially, until further confidence was gained that the differences between the various configurations was not great. Following this specific excitation has been made at the most critical wing sweep angle and with the CSAS in its reversionary state, with pilot inputs sufficing in the other configurations.

It is worth noting that maximum level speed at minimum safe altitude was achieved seven months after the first flight of the flutter test aircraft.

Excitation and Instrumentation

It was planned from the outset of the project that two separate excitation systems should be provided in order to maximise the number of modes excited. This is consistent with the philosophy of identifying the maximum number of modes.

Bonkers are installed at the extremities of the taileron and fin and in a special pylon attached to the outer wing station. Inertia exciters (mass shakers) are installed in the taileron and fin. The location and force levels of the excitation equipment were defined by calculation - a compromise was achieved between excitation effectiveness and the effect upon the flutter characteristics.

The inertia exciters are electrohydraulic devices driving a heavy metal wedge by two small actuators working in a push-push fashion. Their force output is very close to the theoretical maximum achievable within the defined space limitations. The wedge angle is used as the control parameter, being scheduled against frequency to respect amplitude limits at low frequency and a force limit at higher frequencies. A maximum force of 1700 Newtons is obtained.

Correlation between Flight Test and Calculation

All modes of importance have been monitored throughout and predictions have so far been validated in every respect. It has proved necessary to increase apex mass from 60 % to 80 %, on completion of the subsonic envelope expansion, and from 80 % to 100 % during the supersonic clearance. Modal damping variations with airspeed are compared with prediction in Fig. 59 for supersonic airspeeds. The v-g plot shows measured and calculated results of the antisymmetrical taileron flutter mode for the test configuration with 60 % to 100 % taileron balance weight. 2.5 % structural damping are added to the calculated results according to the values measured in ground resonance test. The frequency of this flutter mode was predicted with 20 to 21 Hz whereas flight test results show frequencies between 19 and 20 Hz.

In agreement with experience the predictions are conservative but dependencies of the flutter trend upon flutter parameters are in line with flight test results and extrapolation of the flight test data seems to match the predicted flutter speed.

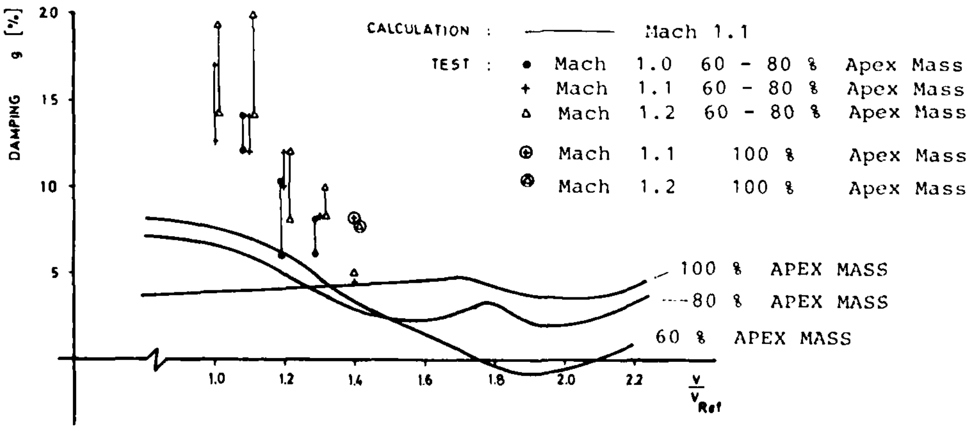

calculated Frequency : 20 - 21 Hz
measured Frequency : 19 - 20 Hz

FIG. 59 COMPARISON BETWEEN CALCULATION AND FLIGHT TEST AT SUPERSONIC AIRSPEEDS FOR DIFFERENT BALANCE WEIGHTS

Aircraft with Underwing Stores

System Description

In order to excite the vibration modes of the Tornado with stores during the flight flutter tests a special store (ig.60) was designed with the aerodynamic shape of a tank with the following possibilities:

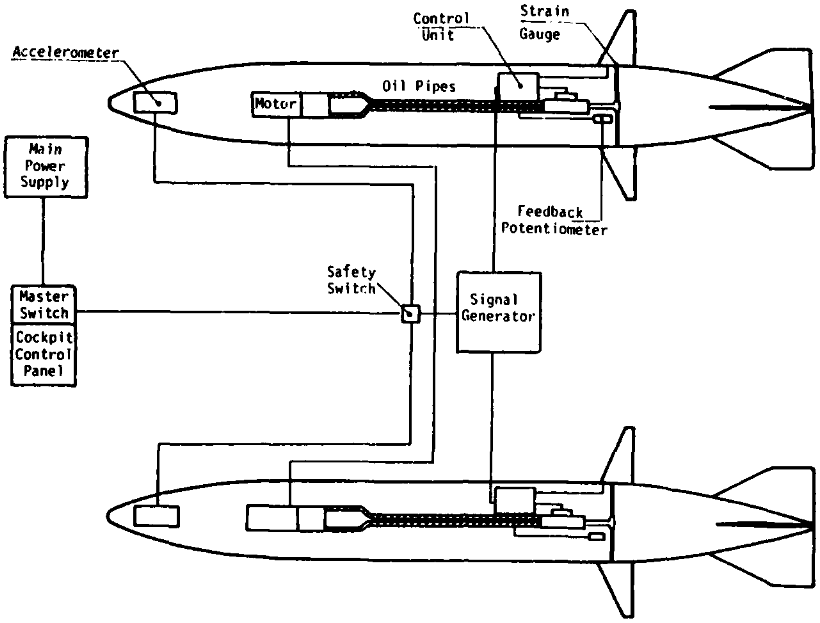

FIG. 60 FLUTTER FLIGHT EXCITATION SYSTEM

- to simulate a large variety of stores by operating on a set of ballast masses which could be added inside to change weight, inertia and C.G. position
- to excite the A/C during flight by means of a built-in electrohydraulically driven vanes excitation system.

Fitting two stores on underwing pylons both symmetric and antisymmetric excitations could be performed driving the two vanes coupled in phase or out of phase. Different sets of vanes could be fitted to cover subsonic - transonic - supersonic speed ranges.

The excitation system included:

a) Excitation signal generator, giving sinus (frequency sweep) random or pulse input signals, adjustable for amplitude, frequency range, sweep rate.

b) Actuator fed by the signal generator, driving the two vanes shaft.

c) Hydraulic power unit (motor + pump + reservoir) giving oil pressure to drive the actuator.

d) Pilot and/or Copilot control panels to choose the excitation kind and amplitude and to start/stop the system.

e) Electronic control unit which, accordingly to the control panel and signal generator setting, controls all functions. This unit included also the safety devices, which prevented operation with excess force or unsafe conditions.

During the flight flutter test the system was used for clearance of numerous stores and store combination and has worked very successfully.

Interpretation of Flight Flutter Test Results

Sometimes it is very difficult to understand flight test results and correlate it with the findings of analysis and previous ground and wind tunnel tests. If correlation is very bad one has to look for the different conditions of the various test. Usually the structural model and the unsteady aerodynamic forces are assumed to be linear. When large structural nonlinearities - friction and backlash for instance - exist then the flight test results depend on the excitation amplitudes and sometimes it is not possible to reach linear conditions in flight test because inputs are to large. As an example dampings of a store vibration mode are shown which give quite different results for lateral or longitudinal stick jerks (Fig. 61)

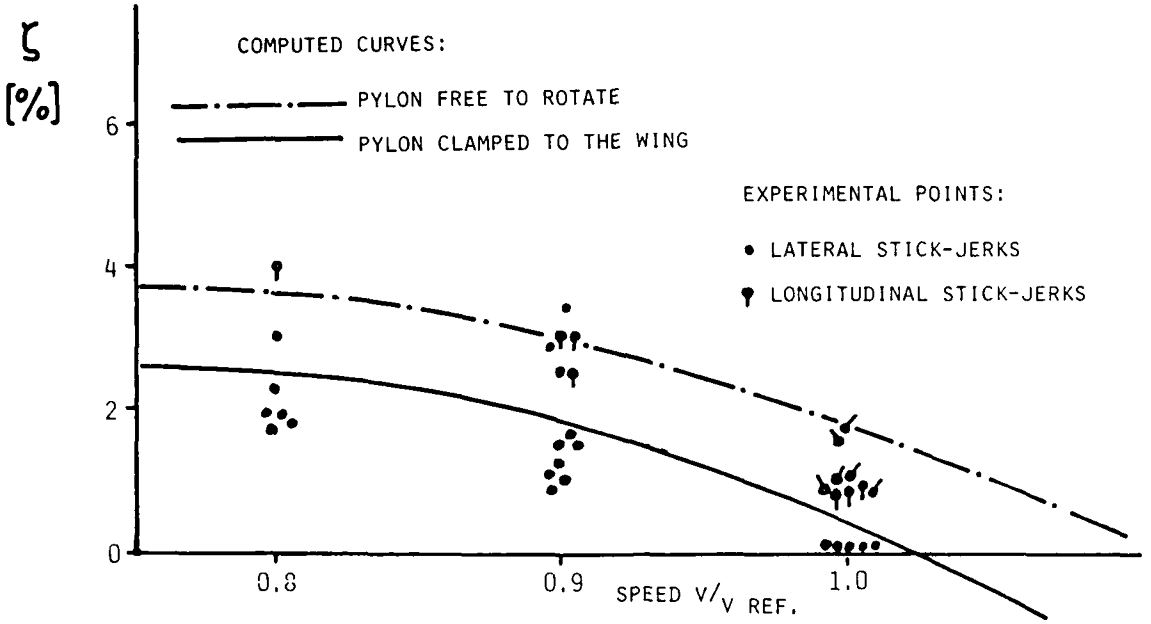

FIG. 61 IN FLIGHT MEASURED DAMPING VALUES OF INITIAL MODE COMPARED WITH COMPUTED CURVES

It is necessary to have an analytical method which can deal with those nonlinearities so required flight conditions can be defined.

Unsteady aerodynamic forces also can be very much dependent on stationary angle of attack when stall conditions are approached at high Mach numbers. Fig. 63 shows how the aerodynamic damping of the wing bending mode reduces with stationary angle of attack. Sometimes high buffet levels on the wing may occur which can be attributed to this phenomenon. For this reason it is required to have analysis methods available which can deal with these problems.

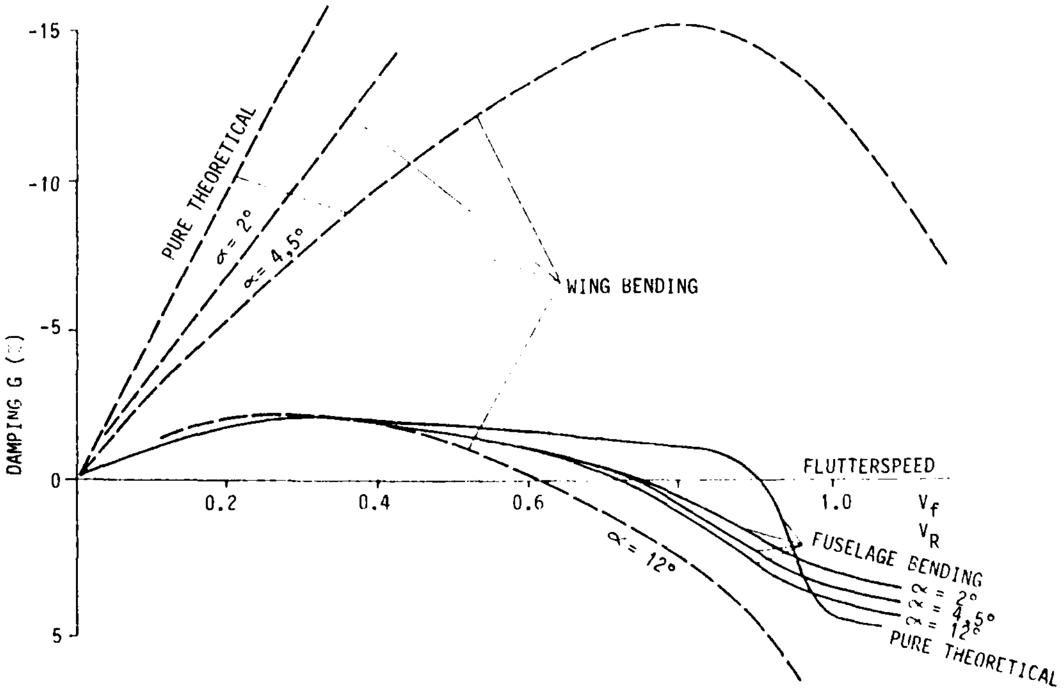

FIG. 62 VARIATION OF DAMPING WITH FLUTTERSPEED FOR CLEAN AIRCRAFT MACH = 0.9

Vibration Qualification

The vibration qualification procedure consists of several steps

- Analytical assessment of the vibration environment
- Vibration qualification using these predicted environments
- Verification flight for environment levels

This procedure applies for aerodynamic and engine noise produced general vibration environment as well as gunfire induced dynamic environmnent. Three typical examples are presented in the following.

Gunfire Environment

An example with characteristic acceleration time history is shown in Fig.63. This time history indicates the typical signal nature of such environment caused by gunblast- and mechanical induced excitation energy. The impulse response in the sequence of gun firing rate superimposed with broadband random can be clearly recognized. The corresponding accumulated exposure time of gunfire environment is relatively short but the levels in the vicinity of the guns are generally considerable above the general vibration environment.

To avoid overtesting and to provide realistic environmental test data a step by step approach was accomplished during gunrig firing tests, A/C ground firing- and A/C airfiring tests.

Preliminary gunfire vibration measurements were made on a gun rig, which represented the aircraft forward fuselage structure with left hand and right hand mounted gun and with simulated fuselage mass distribution.

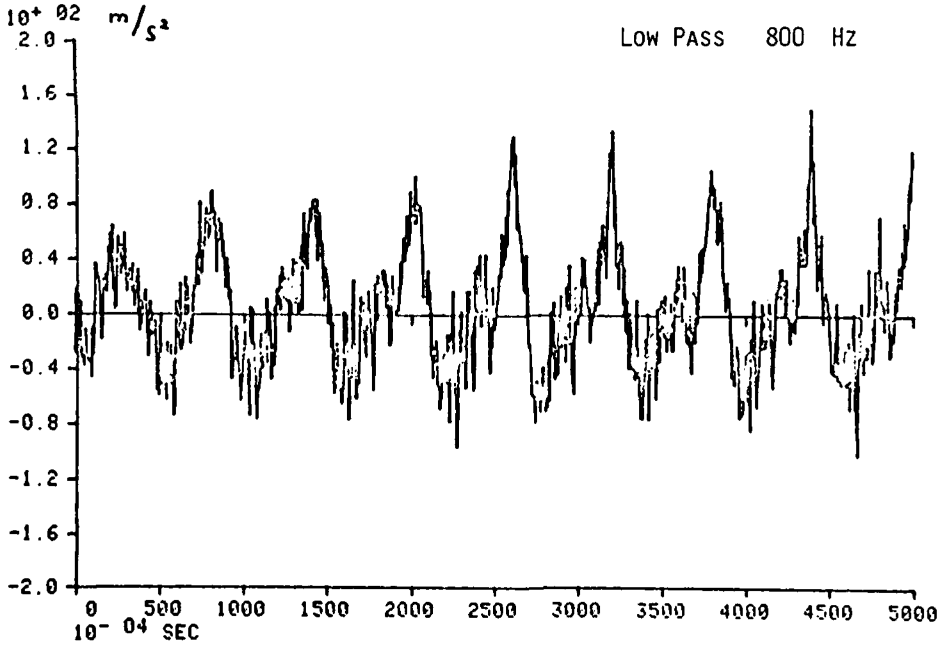

FIG. 63 TYPICAL GUNFIRE VIBRATION RESPONSE

Equipment gunfiring clearance was based on combined test spectra, derived from these gunrig tests, consisting of sinusoidal signals representing the gunfiring rate and up to 3 harmonics and with superimposed broadband random signal (Fig. 64).

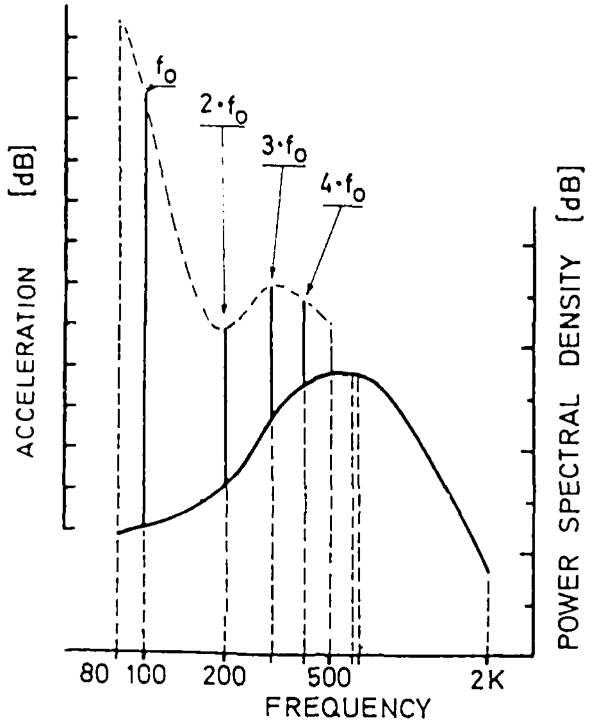
ACCELERATION [dB]
POWER SPECTRAL DENSITY [dB]
f_0
$2 \cdot f_0$
$3 \cdot f_0$
$4 \cdot f_0$
80
100
200
500
2K
FREQUENCY

FIG. 64 COMPOSITE SPECTRUM FOR GUNFIRE-QUALIFICATION

Further measurements during A/C ground firing trials were used to update the test spectra and equipment clearance. During A/C airfiring tests further gunfire vibration measurements were performed (Fig. 66) to provide the final inputs for equipment qualification comparable to Fig. 65.

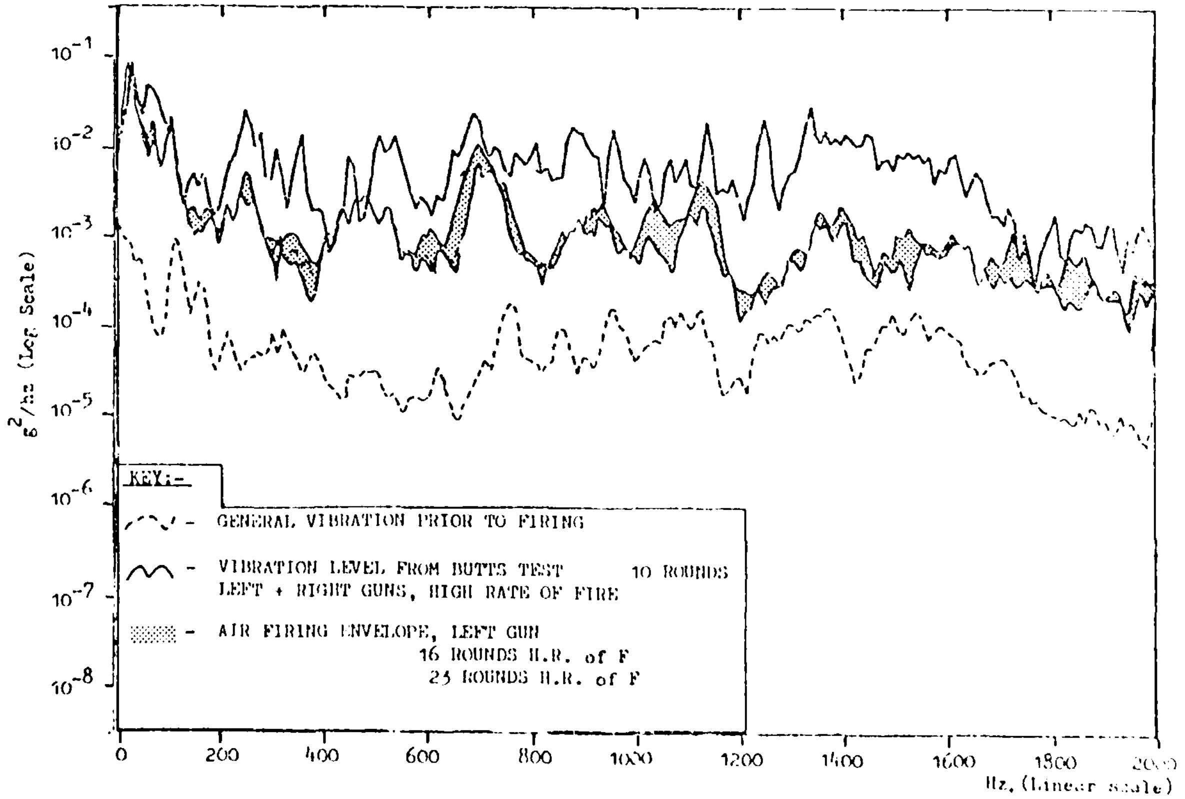

FIG. 65 MEASURED GUNFIRE VIBRATION SPECTRA

Special attention is required in case of large gun size with low firing frequency in the vicinity of fundamental A/C structural vibration modes and in case of shock mounted equipment. The use of measured gunfire vibration data proved as a realistic procedure to account for the real environment.

Similar procedures can be applied to cover the dynamic environment caused by firing of dispenser pods in the equipment qualification.

Dynamic A/C Component Tests

Ground resonance tests on rig mounted A/C components have been performed to define the vibration behaviour and to adjust the mathematical model used in vibration- and dynamic response calculations. Typical examples were GRT on rig mounted vertical fin and taileron as well as rig mounted pylons with single and with multiple store configurations.

Vibration Qualification of Assembled Stores

Instead of rigid shaker mounted stores rig mounted subsystems of store, ERU's and adapters or pylons have been used to simulate reasonable store environment. The test procedure was based on MIL-Std. 810 C, Method 514, Procedure II B. Key points of this procedure are the control of store response data in forward and rear store reference plane and direct excitation of the store by means of rod mounted shakers. The shaker attachment outside the store CG allows for instance also the excitation of important store yaw and pitch modes. Fig. 67 is an example of a subsystem test rig close to the mounting condition on the A/C. Good test experience has been gained with this new test procedure. Fig. 68 shows the determination of resonance peaks and the test spectrum for the functional test.

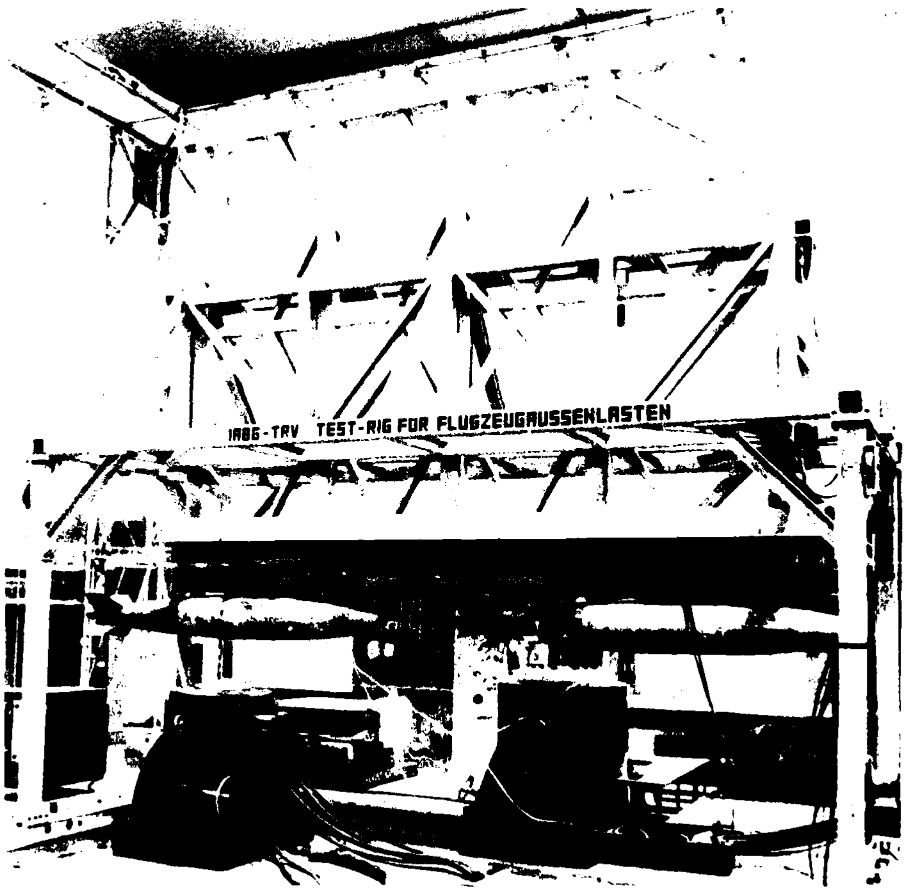

FIG. 66 STORE VIBRATION TEST RIG

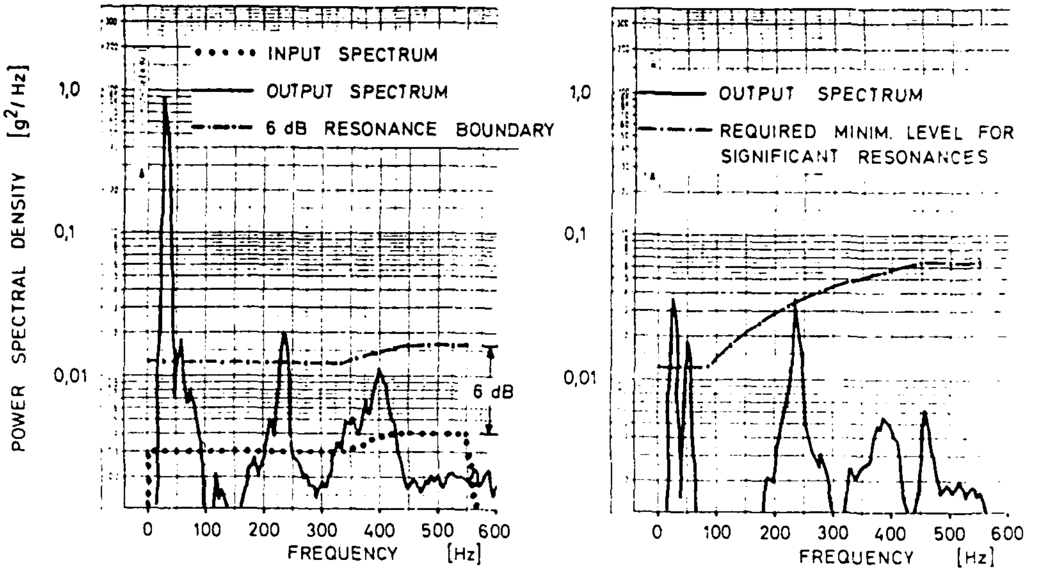

DETERMINATION OF RESONANCE PEAKS

VIBRATION TEST WITH "FUNCTIONAL LEVEL"

FIG. 67 VIBRATION QUALIFICATION FOR EXTERNAL STORES

Acknowledgement:

The authors want to acknowledge the contribution of the following MBB structural specialists whose findings were reported in this paper:

Seidel Wolfgang, Dr. Schreiner Eberhard, Scharold Helmuth, Dr. Geier Wolfgang, Krauss Arnulf, Kempf Gunther, Bartsch Otto, Schmidinger Gerhart, Pehl Manfred, Lotter Kurt, Dr. Lamatsch Hagen.

LIST OF REFERENCES

/1/ Laschka, B.
Zur Theorie der harmonisch schwingenden tragenden Fläche bei Unterschallströmung
Zeitschrift für Flugwissenschaften, Vol. 11, 1963, p. 265

/2/ Laschka, B.
Schmid, H.
Unsteady aerodynamic forces on coplaner lifting surfaces in subsonic flow (wing-horizontal tail interference)
AGARD Structures and Materials Panel Meeting, Ottawa/Canada Sept. 25-27, 1967; also Jahrbuch 1967 der Wissenschaftlichen Gesellschaft für Luft- und Raumfahrt, pp. 211-222

/3/ Sensburg, O.
Laschka, B.
Flutter induced by aerodynamic Interference between wing and tail
Journal of Aircraft, Vol. 7, Number 4, July-August 1970

/4/ Hönlinger, H.
Sensburg, O.
Dynamic Simulation in Wind Tunnels, Part 1
AGARD-Conference Proceedings No. 187 on Flight/Ground Testing Facilities Correlation

/5/ Becker, J.
Interfering Lifting Surfaces in unsteady Subsonic Flow Comparison between Theory and Experiment
AGARD-Report No. 614

/6/ Lotter, K.W.
Bissinger, N.C.
Dynamic Pressure Loads in the Air Induction System of the Tornado Fighter Aircraft
52nd Meeting of the AGARD Propulsion and Energetics Panel, Cleveland/Ohio, U.S.A., 23-27 October 1978
AGARD-Paper No. 21

/7/ Steininger, M.
Haidl, G.
Vibration Qualification of External A/C Stores and Equipment
53rd Meeting of the AGARD Structures and Materials Panel, Noordwijkerhout/Netherlands, 27 Sept. - 2 Oct. 1981
AGARD-Conference Proceedings No. 318

/8/ DeFerrari, G.
Chesta, L.
Sensburg, O.
Lotze, A.
Effects of Nonlinearities on Wing Store Flutter
50th Meeting of the AGARD Structures and Materials Panel, Athens/Greece, 13-18 April 1980
AGARD-Report No. 687 (1980)

/9/ Luber, W.
Schmid, H.
Flutter Investigations in the Transonic Flow Regime for a Fighter Type Aircraft
55th Meeting of the AGARD Structures and Materials Panel, Toronto/Canada, 19-24 September 1982
MBB-Report No. S/PUB/81

/10/ Haidl, G.
Lodge, C.
Zimmermann, H.
Dynamic Environments and Test Simulation for Qualification of Aircraft Equipment and External Stores
48th Meeting of the AGARD Structures and Materials Panel, Williamsburg/Virg. U.S.A., 1-6 April 1979
MBB-Report No. S/PUB/2

/11/ Krauss, A.
Bartsch, O.
Kempf, G.
Parameters Affecting Aircraft Performance on Runways in Bad Condition
49th Meeting of the AGARD Structures and Materials Panel, Porz-Wahn/Germany, Oct. 1979
AGARD-Report No. 685

/12/ Haidl, G.
Steininger, M.
Excitation and Analysis Technique for Flight Flutter Tests
47th Meeting of the AGARD Structures and Materials Panel, Florence/Italy, 24-29 September 1978
MBB-Report No. UF 1446 (Ö)

LIST OF REFERENCES (Cont'd)

/13/	Becker, J. Dau, K.	Evaluation of Vibration Levels at the Pilot Seat AGARD-Conference Proceedings No. 226
/14/	Collmann, K.D. Sensburg, O.	Impact of a Command and Stability Augmentation System on Gust Response of a Combat Aircraft 44th Meeting of the AGARD Structures and Materials Panel, Lisbon/Portugal, 17-22 April 1977 MBB-Report No. UFE1328 (Ü)
/15/	Altham, D.W. Nuscheler, J. Potter, D.K. Seidel, W.	Tornado Flight Loads Survey Symposium on Flight Test Techniques of the Flight Mechanics Panel of AGARD; Porz-Wahn/Germany, 11-14 October 1976 MBB-Report No. M/FE22/1331
/16/	Potter, D.K. Lotze, A.	Inflight Flutter Identification of the MRCA 42nd Meeting of the AGARD Structures and Materials Panel, Ottawa/Canada, 4-9 April 1976 MBB-Report No. M/FE17/1325
/17/	Lodge, C. Schmid, H.	Unsteady Pressures due to Control Surface Rotation at Low Supersonic Speed - Comparison between Theory and Experiment 42nd Meeting of the AGARD Structures and Materials Panel, Ottawa/Canada, 4-9 April 1976 MBB-Report No. M/FE126/1327
/18/	Lotze, A. Sensburg, O. Kühn, M.	Flutter Investigations on a Combat Aircraft with a Command and Stability Augmentation System AIAA Aircraft Systems and Technology Meeting, Los Angeles, Calif., U.S.A., 4-6 August 1975 MBB-Report No. UFE1189 (Ü)
/19/	Sensburg, O. Lotze, A. Haidl, G.	Wing with Stores Flutter on Variable Sweep Wing Aircraft 39th Meeting of the AGARD Structures and Materials Panel, Munich/Germany, 6-12 October 1974 MBB-Report No. UFE1118 (Ü)
/20/	Krauss, A. Bartsch, O. Kempf, G.	Influence of Mathematical Modelling of Undercarriage on the Prediction of Aircraft Loads due to Damaged and Repaired Runways AGARD - Aircraft Dynamic Response to Damaged Runways AGARD-CP-326 (1982)

Abstract

The paper starts with a short description of the Tornado program. The complex requirements for this all-weather combat aircraft resulted in an optimal concept including features like

- highly loaded swing wing in combination with a sophisticated high lift system
- fly-by-wire and automatic terrain following
- supersonic inlet
- 2 three spool engines with integrated thrust reverser

To accomodate all the mentioned features in a minimum size/weight aircraft, it is necessary to give special attention to the structural aspects.

A description of some typical examples for structural certification is presented:

- load and flutter models
- structural component tests
- design verification tests, especially for the wing suspension and pivot system
- proof and ultimate load testing
- fatigue life assessment

Comparisons of selected predictions with ground and flight test results will be *presented for the important structural disciplines:*

- stresses and deflections of important components
- loads
- aeroelastics

Some examples of bad correlation between theory and test will be discussed together with possible explanations.

The merits and disadvantages of the most important theoretical methods will be highlighted

COMPARISON OF FLIGHT LOADS MEASUREMENTS RESULTS AND PREDICTION FOR TORNADO

J. R. J. DOVEY

G. MORETTI

BRITISH AEROSPACE PLC
AIRCRAFT GROUP
WARTON DIVISION
WARTON AERODROME
PRESTON, LANCS
PR4 1AX

Summary

An extensive programme of flight loads measurements has been made on Tornado to contribute to service clearance as required by the American Mil Spec.

A brief resume is presented of the purpose of flight load measurements, the overall programme, the calibration of the load measurement devices, the data reduction facilities, the flying techniques and of the methods used for detailed analysis of the results.

Comparisons are made between flight measurements and predictions for several aircraft components for specific manoeuvres and for rates of change of load with change of aircraft parameters. The contribution of flight load measurements to the extension of the flight envelope in rapid roll manoeuvres is discussed and the usefulness to the final Tornado flight clearance is also assessed.

1. Introduction

At the FMP Symposium in 1976 a paper (ref 1) was presented which described the ongoing flight load measurement programme on Tornado. Few results had been obtained at that time and the emphasis of the paper was on the programme of preparation, calibration and aquisition of data. This paper recaps on the overall load measurement programme. calibration, preparation and analysis methods and gives the technical background to the requirement for the flight measurement programme.

Examples are given of comparison between flight load measurement and prediction. Taileron torques are shown to be less than those based on wind tunnel data and within the actuator capability, rear fuselage bending loads in a heavy store configuration are shown to be far greater than predicted. A large increase in the available manoeuvre envelope with manoeuvre devices has resulted from flight loads measurement analysis and for the clean aircraft some strengthening and small reduction in the transonic flight envelope has been shown to be necessary. Some of the methods used to resolve discrepancies in measurements are discussed.

2. Background to Flight Measurement Programme

Confidence in the structural integrity of an aircraft is dependent on demonstration that the structure can withstand the design loads and that the actual loads experienced throughout the flight envelope do not exceed the limit strength of the structure. The ability of the structure to withstand the design loads has traditionally been demonstrated by component and whole aircraft static ground tests to limit load, ultimate load, and testing to fatigue duty cycles.

Flight load measurments need to be made to demonstrate integrity of the load estimates. In Britain it has been traditional not to carry out comprehensive flight load measurements but to identify only components of major concern, such as the T tail of BAC 111, for flight load measurement. For aircraft which have a low g (wing) loading (i.e. where nW/Sa_1 is low) and do not penetrate transonic flight conditions high loads occur almost exclusively in conditions of linearity of the aerodynamic characteristics, where estimates of aerodynamic loading are at their most reliable and differences due to scale effect between wind tunnel model results and flight are likely to be small. It is not unreasonable therefore to have adopted this approach.

For Tornado the g loading is several times greater than for Civil Airliners, resulting in flight at much greater incidences as shown in figure 2.1, so that design loads occur almost exclusively in conditions of non linearity of the aerodynamic characteristics resulting from flow breakdown, shock separation, etc. In many instances this results in loads smaller than would result from attached flow conditions and hence smaller than would be predicted by available theoretical methods. Use of the lower loads will result in a minimum weight structure. In other cases the loads are greater than predicted by theoretical methods. Also for Tornado large static aeroelastic effects were predicted, but the only methods available for the calculation of aeroelastic effects assume attached flow. How relevant are these results in conditions where the flow is partially separated? Wind Tunnel data can provide data only at relatively low Reynolds number. Significant scale effects have been recorded elsewhere.

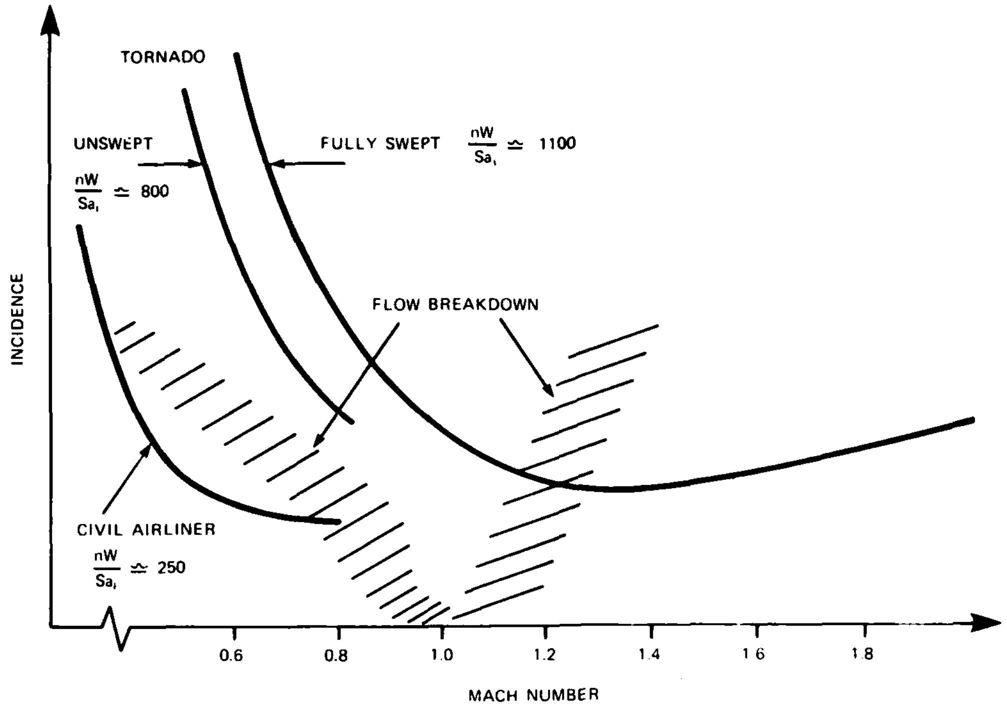

Figure 2.1: Comparison of Incidence for Maximum Normal Acceleration at Maximum Speed and for Flow Breakdown

Consideration may be given to the possibility of over designing the structure either by the use of an arbitrary factor or by careful consideration of the likely tolerances on available data for each aircraft component. This procedure inevitably leads to some structural weight increase which was decided to be unacceptable on Tornado. For these reasons it was chosen to base flight load measurements on the Mil Spec requirements.

3. Flight Testing

Two prototype aircraft were instrumented to measure in-flight loads, the instrumentation being calibrated on ground.

An extensive flight load survey was performed on the clean and external stores configuration throughout the whole of the flight envelope, for comparison with prediction.

The manoeuvres involved for the testing were basically,

- roller coasters, a gentle push to 0g and pull to 3-4g
- wind up turns
- constant alpha (under g) slowdown
- steady heading sideslip at 1g
- rapid rolling manoeuvres

For the last of these a particular method of analysis has been developed and will be later described.

During the flight of the two prototypes load measurements were continuously monitored in most of the cases by a telemetry link, so as to safeguard the structural integrity of the aircraft, to gather more data outside the expected critical areas and to assess the high frequency loading characteristics throughout the flight envelope.

3.1 Instrumentation

Various methods of measuring in-flight loads were used i.e. pressure transducers, accelerometers, acoustic pickups and strain gauges. The last method is the most generally useful since it produces directly the loading characteristics in terms of shear, bending and torsion acting on an aircraft component, as well as local stress distribution.

Both wings, taileron and fin were instrumented with strain gauges to give loading characteristics and, in the case of the wing, loading distribution by means of measuring loads at four wing stations (root, adjacent to inboard and outboard pylons and an outboard station) - see fig 3.1.

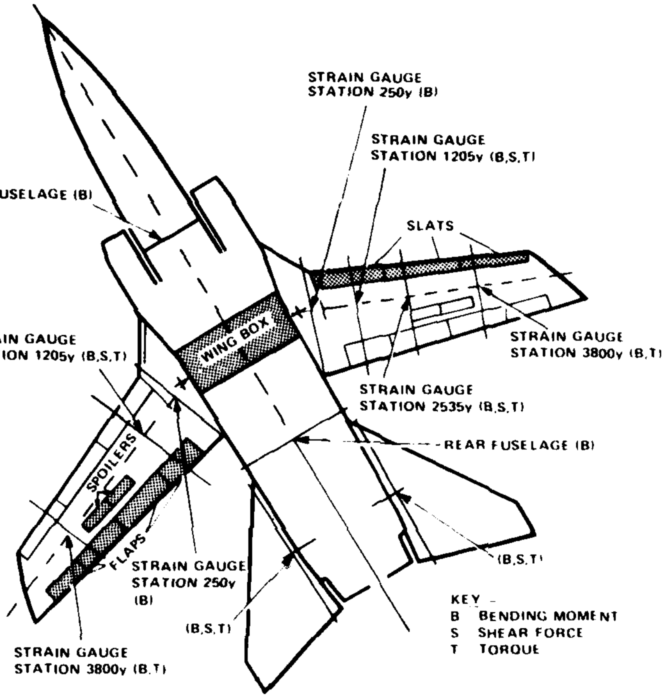
STRAIN GAUGE STATION 250y (B)
STRAIN GAUGE STATION 1205y (B,S,T)
FRONT FUSELAGE (B)
SLATS
STRAIN GAUGE STATION 1205y (B,S,T)
WING BOX
STRAIN GAUGE STATION 3800y (B,T)
STRAIN GAUGE STATION 2535y (B,S,T)
REAR FUSELAGE (B)
SPOILERS
FLAPS
(B,S,T)
STRAIN GAUGE STATION 250y (B)
(B,S,T)
STRAIN GAUGE STATION 3800y (B,T)
KEY -
B BENDING MOMENT
S SHEAR FORCE
T TORQUE

Figure 3.1: Tornado P03 Flight Loads Instrumentation Scheme

Three shear bridges and two bending bridges were installed on each spar at each wing station. Because of the complexity of the structure each of these bridges became responsive to shear and bending and torsion, although it was possible to establish the main sensitivity to one of these characteristics. An electrical combination of the bridges was carried out (using Skopinsky method, see reference 2) in order to compensate the main bridges for the secondary load effect and to reduce the number of channels to be recorded.

An alternative method of recording the output of each bridge to cure secondary effects was used on the fin and taileron instrumentation. Both methods proved reliable, the choice being subject to individual preferences and local constraints.

In addition to the main lifting surface instrumentation various areas of the aircraft structure were instrumented,

- wing carry through box
- leading edge slat
- trailing edge flap
- spoilers
- rudder
- airbrake
- wing pylons (store + pylon loads)
- store attachment and release unit (store loads)
- rear fuselage transport joint
- front fuselage transport joint

All these measurements were recorded in flight using PCM (Pulse Code Modulation) in order to obtain quasi steady loads. Continuous recording of some of these parameters was also done via FM (frequency modulation) in order to assess "buffet" loads.

All parameters prior to the recording were connected to filters and amplifier circuits to precondition the electrical signals and make them compatible with the recording system.

3.2 Calibration

Instrumentation was calibrated up to 60% of the limit load. This level of load was believed to be high enough to detect all non-linearities and to have sufficient safety margins in the extrapolations to limit loads. Calibration was extended from 60% up to 90% in some instances, after examination of the original calibration data showed non-linearities.

Calibration involved the application of point loading in various areas of the aircraft structure to cover the possible theoretical excursion of the centres of pressure. The aircraft was loaded in a complex loading rig and all the applied loads were reacted via the undercarriage, the nose undercarriage being modified for the job.

When possible aircraft components, mainly actuators, were calibrated off the aircraft in a much smaller rig.

The intent of the calibration was derivation of the equation relating the bridge responses to the combination of shear, bending and torsion applied. Where possible the bridges were electrically combined to directly measure shear or bending or torsion using the Skopinsky method.

Some complex areas of the structure i.e. wing box and rear transport joint, proved very difficult to instrument and calibrate and alternative methods have been derived in flight to provide cross checks of the instrumentation.

3.2.1 Thermal drift calibration

As an integral part of the calibration a flight was dedicated to the derivation of temperature effect on the instrumentation (i.e. thermal effect on a bridge or thermal stress on the structure). A roller coaster and a sideslip at the same flight conditions were performed before and after a hot soak (i.e. cruise for say 15 minutes at low altitude) and a cold soak (i.e. cruise for say 15 minutes at high altitude). Different levels of loads were encountered in the taileron instrumentation and the instrumentation scheme was subsequently successfully revised and re-calibrated.

3.2.2 Calibration accuracy

Taking into account the scatter of the calibration data used to derive the calibration equation, it can be said that an accuracy of better than ± 2% of the limit load can be expected. Together with the rigging, geometry, applied load, electrical amplifiers errors, the overall accuracy of all the measurements is believed to be within ± 5% of the full scale.

Although bridge non-linearities, when present, can be analytically accounted for, they do penalise the overall accuracy of the data to a level which in some cases made the measurement unacceptable.

Although the calibration errors can be established, much effort was necessary to monitor and maintain the integrity of the electrical aspects of the instrumentation.

3.3 Flight Loads Programme

The flight programme carried out on Tornado could be split as follows:

- Flight loads survey,where essentially roller coasters and sideslip manoeuvres were performed at 60-80% of the strength envelope. The flight manoeuvres covered an intensive range of Mach and altitude, as well as sweep, flap and stores configuration.
- In order to reduce extrapolation, especially in areas of non-linearities, a set of wind up turns and negative g pulls was performed, reaching 90% of the limit strength. In addition, slow downs at constant incidence (high g) were performed in the transonic region to further assess the Mach effect on the aircraft structure.
- Following the subsequent data analysis, the aircraft demonstrated the structural capability in two manoeuvres predicted from the previous flight data to be the worst loading cases for different aircraft components. These two "demonstration" manouevres were performed in two separate flights and structural and geometry inspections were performed between the flights to safeguard the overall structural integrity.

- In parallel to the above the aircraft started a comprehensive testing of "rapid rolling" manoeuvres. These tests, being dynamic, do not really allow for simple extrapolation. A process of prediction - flight data matching and prediction of next most severe condition was used to extend the flight envelope for rapid rolling to the boundaries of the manoeuvre envelope. This phase covered various external stores configurations and although it required an extensive use of computer and man power it maximised the aircraft flight envelope and at the same time reduced the risk involved in progressing the flight testing.

- Datum manouvres; each loads flight was initiated and terminated with:

  - a ground datum manoeuvre to zero the load measurement when the aircraft is stationary on ground in a particular engine and control surface setting.

  - an in-flight datum manouevre i.e. roller coaster and sideslip at fixed condition to assess the consistency. The 0g point is of particular significance in this datum manoeuvre.

3.4 Points to Consider

The Tornado flight programme emphasised the need to consider the following points:

Instrumentation:

- strain gauges method can give good results
- use electrical gauges combination, if possible
- a bad instrumentation scheme will ruin the whole of the exercise, therefore
- minimise thermal effect on the gauges responses
- select accurately the positioning of the gauges, avoid areas of stress concentration, aim to find linearities in the gauge response versus applied load

Calibration:

- apply enough cases to cover the possible range of load distribution in flight
- apply loads up to 60% of the limit loads
- discard gauges which do not respond linearly to applied loads

Flight Programme:

- test for thermal effect on the gauges
- perform datum manoeuvres at each flight
- perform symmetric and asymmetric manoeuvres at various combinations of Mach and altitude to cover the area of the flight envelope surrounding the design points.

4. Data Analysis

The vast amount of data acquired from Tornado flights was analysed at various levels. An in-flight monitor and between flight analysis of data were carried out to ensure safety during the flight trials. This was followed by a more detailed analysis, the methods of which are explained.

4.1 In-flight monitor

All load measurements and flight condition parameters recorded on the airborne magnetic tape were also transmitted via telemetry to a ground station which displayed some selected parameters on digital analogue displays and paper recorders. It was thus possible to,

- monitor the aircraft structural safety presenting to the engineer the structural behaviour of the aircraft during the whole of the flight.

- assist the pilot to set up the correct conditions for each test point and check the correct execution of the requested manoeuvre.

- monitor the instrumentation behaviour, in order to produce good quality data from each flight.

It is obviously difficult to directly quantify the advantages of the telemetry system but in comparison with previous projects it is believed that the number of flights required to complete the flight programme has been significantly reduced.

4.2 Between flight analysis

4.2.1 Symmetric/quasi static manoeuvres

Although an assessment of the data was already performed during telemetry subsequent to each flight a more detailed analysis was required. It consisted of,

- max min monitor, a summary of the maximum load achieved on each component during each manoeuvre. These total loads were compared against limit strength envelopes.
- total loads plots; all loads parameters were plotted versus the product of normal acceleration times mass (NZW) on summary plots to confirm general load trends and data consistency. The apparent scatter was largely due to the Mach and altitude spread of the manoeuvres (see figure 4.1).
- detailed analysis of the problems, when encountered, during particular flights to assess the implication for the future flights.
- instrumentation checks on the serviceability for the next flight.

A selection of the data was then transferred to the main computer to provide permanent storage of selected manoeuvres for detailed analysis.

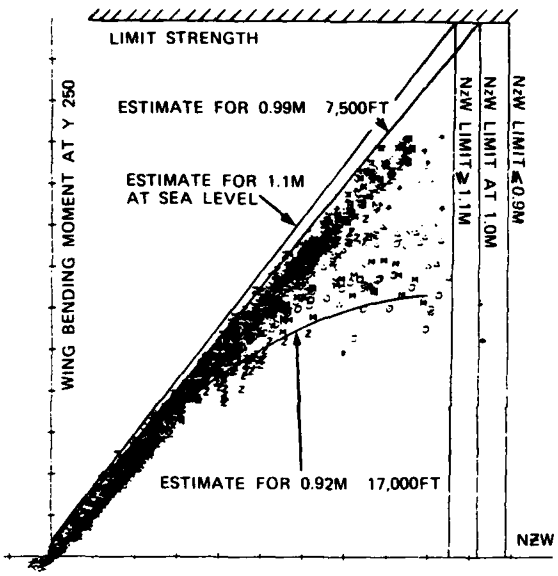

Figure 4.1: Total Loads – Summary Plot

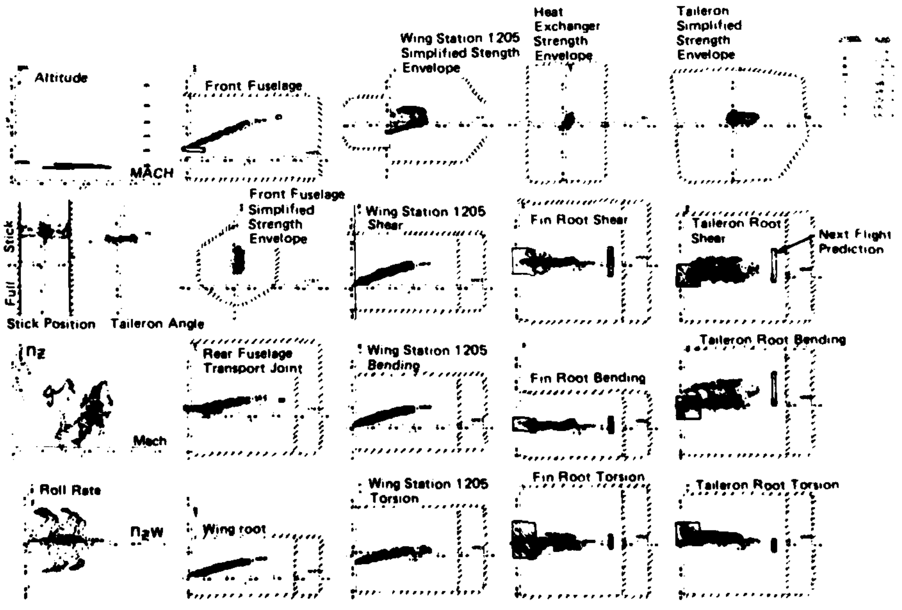

Figure 4.2: Summary of Load Measurements During Rapid Rolls

4.2.2 Rapid Rolling

In view of the potentially hazardous nature of rapid rolling manoeuvres a special procedure was used to expand the flight envelope as indicated in para 3.3. Special attention was paid to the presentation of measured loads during this flying. A summary of the total loads achieved during the rapid rolling testing of each particular test condition was produced (see figure 4.2). Measured loads were plotted against the NZW product to establish general load trends. Although the rapid rolling manoeuvres were analysed individually this presentation assisted the engineer to confidently accept the extrapolations to the next entry g, see boxes in the figure.

4.3 Detailed Analysis

The detailed analysis has been carried out for symmetric quasi-static manoeuvres and for dynamic manoeuvres. The two types of manoeuvre require very different methods of analysis.

4.3.1 Symmetrical Quasi Static Manoeuvres

For quasi steady conditions the equation for any load on the aircraft in flight takes the general form:

$$L = \text{Aerodynamic Load} + \text{Inertia Load} \qquad (1)$$

The inertia load is simply a product of mass and normal acceleration and does not require derivation from flight. The aerodynamic contribution may be written:

$$L_{AERO} = \underset{\text{at } n = 0}{L_{AERO}} + L_{AERO}\; f\,(n) \qquad (2)$$

These terms vary with aircraft mass and centre of gravity and due to aeroelastic effects and with wing fuel state; both terms vary with Mach number.

- Rigid Aircraft

For a given mass, c.g., wing fuel state and Mach and for a rigid aircraft with linear characteristics, equation (2) becomes:

$$L_{AERO} = \frac{q\,(dL_A)}{(dq\;)}\;{}_{n\,=\,CONST} + \frac{n\,W \times (dL_A)}{(d\;nW)}\;{}_{q\,=\,CONST} \qquad (3)$$

where q is dynamic pressure
n is normal acceleration
W is aircraft mass

Subscript A denotes aerodynamic load

The aerodynamic load may be plotted as a carpet versus q and nW and as a carpet of 'semi non-dimensional' load versus q and nW/q shown in figures 4.3 and 4.4.

It can be seen that $\frac{L_A}{q} = \text{const} + f\left(\frac{nW}{q}\right)$ (4)

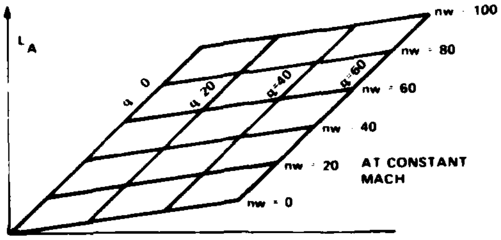

Figure 4.3: Variation of Aerodynamic Load with Dynamic Pressure and Normal Acceleration for Rigid Data

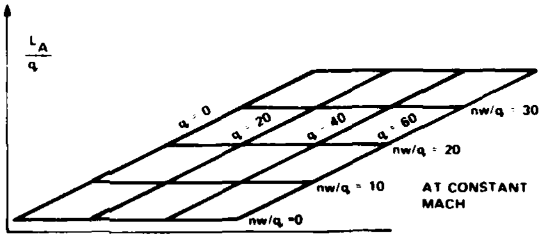

Figure 4.4: Variation of Load Coefficient with Dynamic Pressure and Lift Coefficient for Rigid Data

- Aeroelastics and Non Linear Characteristics

If we consider a flexible aeroplane in which the aerodynamic characteristics are affected by the structural deformation resulting from application of load, the load at n = 0 and the load due to normal acceleration become separate functions of dynamic pressure. *Ignoring the relatively small effect of the distortion due to inertia, equation (3) becomes:*

$$L_{AERO} = q \frac{dLA}{dq}_{(n = 0)} f(q) + nW \times \frac{dLA}{dnW} f(q) \qquad (5)$$

At high lift coefficients the wing flow starts to break down. This phenomenon is very dependent on Mach number and the development of the shock system, culminating in separation. *This affects loads on other parts of the airframe. For example the rear* fuselage bending results from aerodynamic loading on tails and rear fuselage which balances the moments created by forward fuselage, intake, nib and wing - hence changes of the wing flow conditions will result in changes to the rear fuselage bending.

Due to these changes in wing distributions the structural deformation resulting from applied loading will be different from that in the attached flow (linear) situation. The combined effects of aeroelastics and non-linearity will *result in a modification* to the rigid aircraft, shown in Figs. 4.3 and 4.4, to give the characteristics shown in Figs. 4.5 and 4.6.

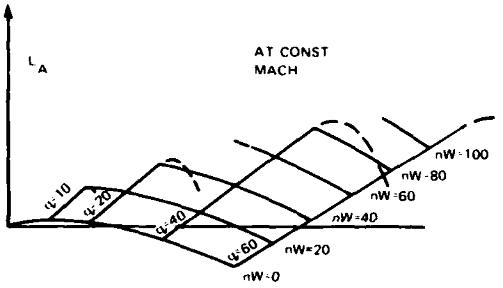

Figure. 4.5: Variation of Aerodynamic Load with Dynamic Pressure and Normal Acceleration for Flexible Aircraft Including Conditions of Flow Breakdown

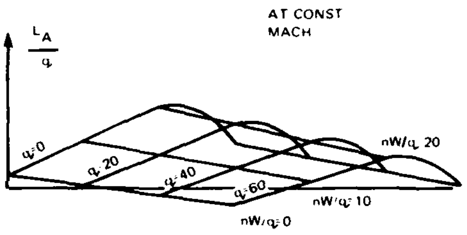

Figure 4.6: Variation of Load Coefficient with Dynamic Pressure and Lift Coefficient for Flexible Aircraft Including Conditions of Flow Breakdown

In order to analyse the flight data within this analysis framework, conditions of near constant Mach must be selected and the estimated contribution of inertia must be *subtracted from the measurements.* "Worm plots" (figure 4.7) were also produced, to show the variation of load factors superposed on a presentation of altitude, to allow the engineer to establish the accuracy of the manoeuvre and a useful visual record of the availability of flight data.

4.3.2 Dynamic Manoeuvres

The detailed analysis concentrates not only on the more precise definition of quasi static loading derivatives, taking into account the secondary control variables, but also on the analysis of the dynamic manoeuvres since these cannot be analysed by quasi static techniques. In the case of the dynamic manoeuvres, predictions have been made for standard control inputs, to provide flight clearances and a guide to upper bounds for monitoring purposes. These predictions are of little help in making a quick analysis of measured loads because the aircraft *response and resultant loads depend* upon the individual control inputs. This can be illustrated by considering a pitch stick jerk. The taileron load is a function of the direct loading derivatives due to aircraft angle of attack, taileron angle and pitch rate and the aerodynamics due to the distortion of the structure under normal and pitch acceleration inertia loads.

For detailed analysis one technique used is to predict loads from the representation;

$$\text{LOAD (L)} = \frac{\partial L}{\partial \eta} \eta + \frac{\partial L}{\partial p} p + \ldots.$$

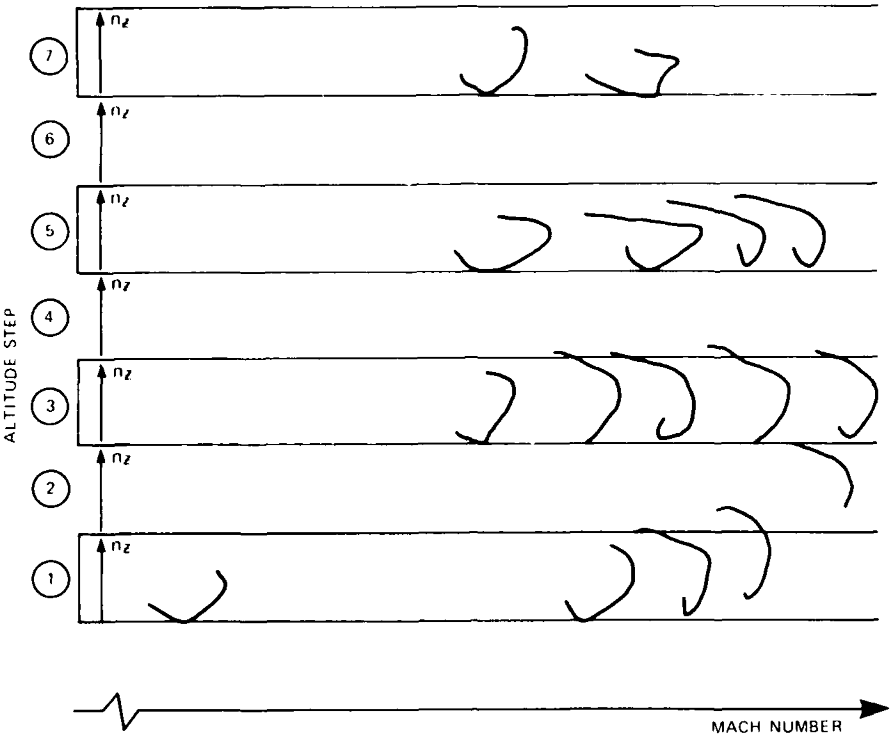

Figure 4.7: Load Factors Versus Mach and Altitude. (" Worm Plots ")

by (1) interpolating loading derivatives such as $\partial L/\partial \eta$ to the measured flight condition - the loading derivatives being represented at a discreet set of sweeps, Mach numbers, speeds, incidences, control angles and aircraft configurations - interpolation is by splined hypercubes,

(2) scaling these interpolated loading derivatives by the measured aircraft control input and response parameters such as taileron angle (η) and roll rate (p), etc., extracted from the data base,

and (3) summing the scaled contributions

Because of the volume of data to be handled the scheme is computerised but with a large involvement of the engineer. The predicted and measured loads and their difference can be machine plotted in a variety of forms; and if the engineer considers the comparison inadequate he can instruct the computer to "match" the difference by a range of functions which he selects. The results of such analyses over the flown flight envelope are assessed as a whole and are used to refine the computer stored representation of the predicted loading derivatives. In parallel, analyses are made of measured prototype responses to refine the predicted aircraft stability derivatives. This data, with extrapolations if necessary, is then used to predict aircraft responses and loads for standard control inputs and these form the basis for:

- clearance for future high load level flights and

- structural re-assessment at design conditions.

The following example illustrates the matching procedure used.

Fig 4.8 shows taileron bending moment coefficient versus time in a rapid roll manoeuvre. Comparison is made between the flight measured data and values predicted using measured flight mechanics parameters with wind tunnel based loading derivatives. The differences shown imply that one or more of the loading derivatives is different in flight. To establish whether a linear correlation exists between the load difference and one or more response parameters the difference is plotted against relevant response parameters.

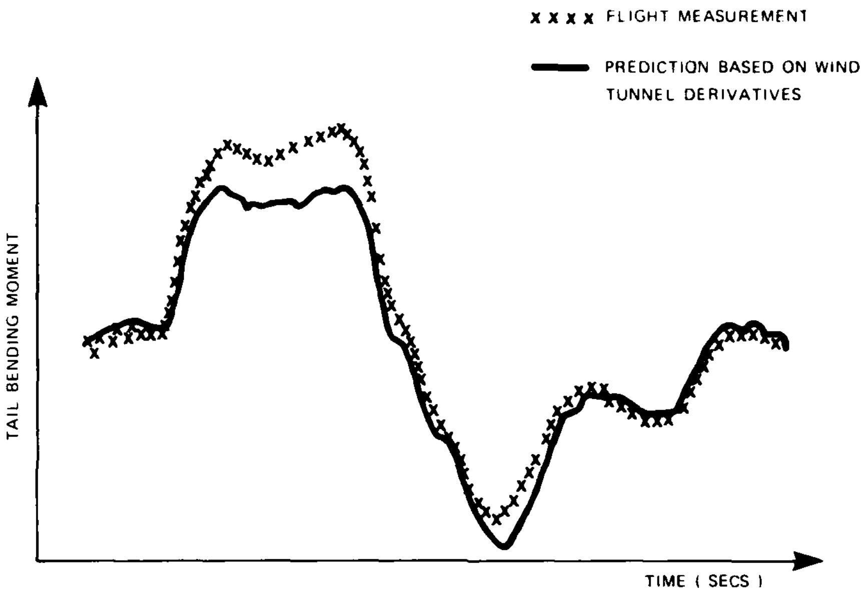

Figure 4.8: Comparison of Wind Tunnel Prediction and Flight Measured Tail Bending During a Rapid Roll Manoeuvre.

Fig 4.9 shows a good correlation against differential tail whilst fig 4.10 shows no correlation against roll rate for the same manoeuvre. Hence a changed derivative due to differential tail angle is indicated. Having established which loading derivatives are likely to be different the automatic matching technique is used, with freedom to vary these loading derivatives to obtain a minimum difference between predicted and flight measured loads.

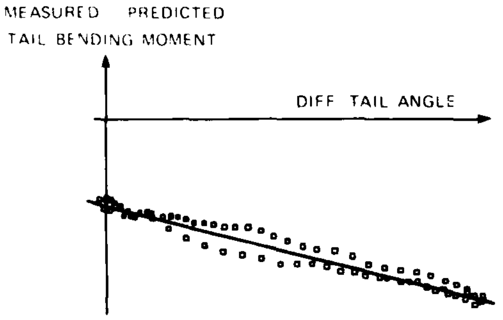

Figure 4.9 Comparison of the Difference Between Flight Measured and Wind Tunnel Predicted Tail Bending Moment Versus Differential Tail Angle.

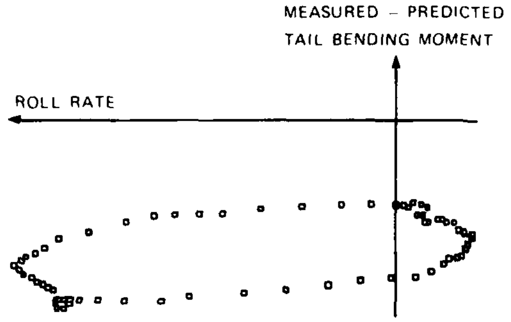

Figure 4.10: Comparison of the Difference Between Flight Measured and Predicted Tail Bending Moment Versus Roll Rate.

Fig 4.11 shows the comparison of the flight data and the new prediction which resulted in this case from a 15% change to the taileron bending moment derivative due to differential tail angle.

Completion of the detailed analysis resulted in a revised loading derivative data set. This data set is being used as the basis for final service clearance, and will be used for further fatigue assessment.

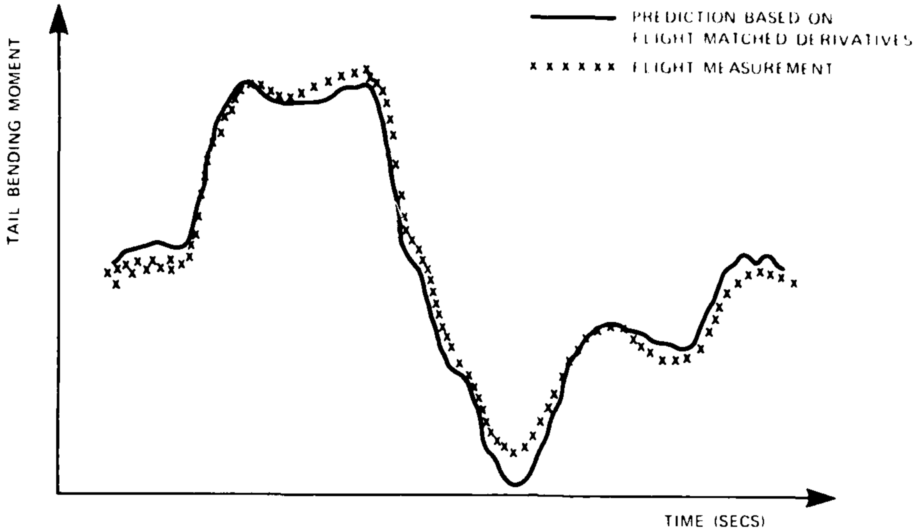

Figure 4.11: **Comparison of Flight Based Prediction and Flight Measured Tail Bending During a Rapid Roll Manoeuvre**

5. Discussion of selected results

5.1 Taileron Torques

The results of wind tunnel testing of two Tornado models indicated that taileron torques in excess of the actuator capability could be encountered. However, the two models generated very different torque characteristics with respect to Mach number, leading to doubts as to the validity of either set of data. Figure 5.1 shows the variation with Mach number of the maximum positive and negative torques, for steady flight conditions at the maximum and minimum normal acceleration. Comparison with the single system actuator capability shows that from both models excessive values were predicted. Doubts about the validity of these predictions were increased by the fact that the taileron torques are very dependent on the theoretically estimated aeroelastic characteristics of both the taileron panel and the downwash field behind the flexible wing.

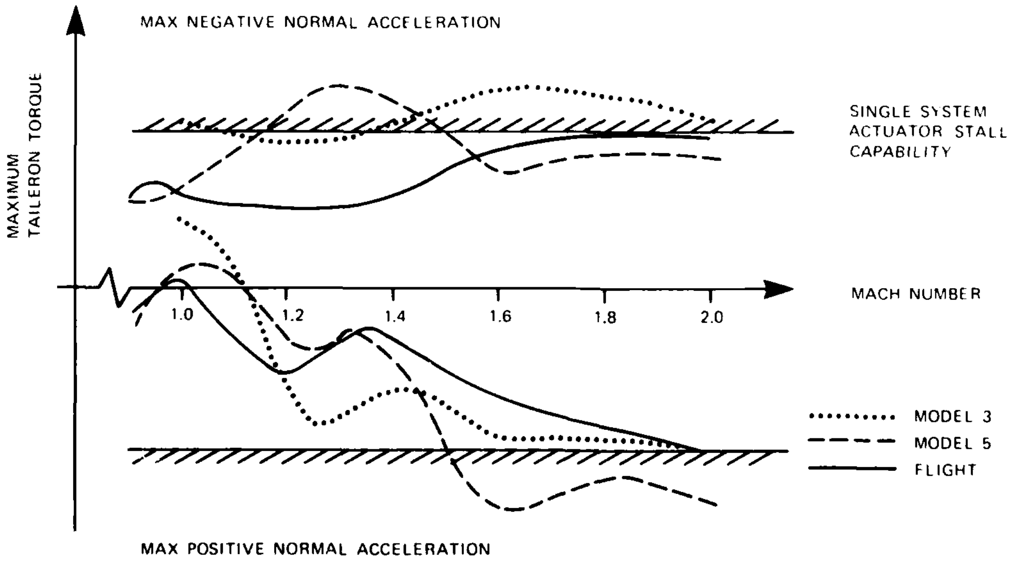

Figure 5.1: **Variation with Mach Number of Maximum Positive and Negative Torques, for Steady Flight Conditions at the Maximum and Minimum Normal Acceleration**

This led to the initial prototype trials being flown within a restricted flight envelope to allow detailed analysis of flight data, but the measured flight data was found to be significantly different from the wind tunnel based results and it can be seen from fig 5.1 that the taileron torques do not exceed the actuator capability.

Detailed examination of the results shows a broad similarity with the Model 3 data except that values at low incidences are consistently less positive than for the model (a difference in C_{m_0}) and where both models indicated a consistent increase in negative torque with increase in incidence, the flight data indicated a levelling off at higher incidences. Comparisons of the variation with incidence between model 5 and flight can be seen in figure 5.2. Figure 5.3 shows the comparison between flight and model 5 based prediction of taileron torque in a rapid roll at 4g at Mach 0.95 and the comparison, after a change of the torque derivatives with incidence and with differential tail setting derived from matching, is shown in figure 5.4.

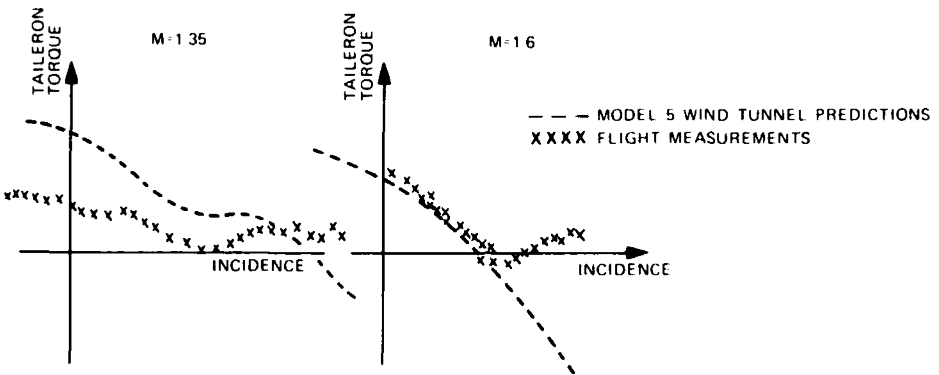

Figure 5.2: Variation of Taileron Torque with Incidence for Model 5 and Flight Measurements.

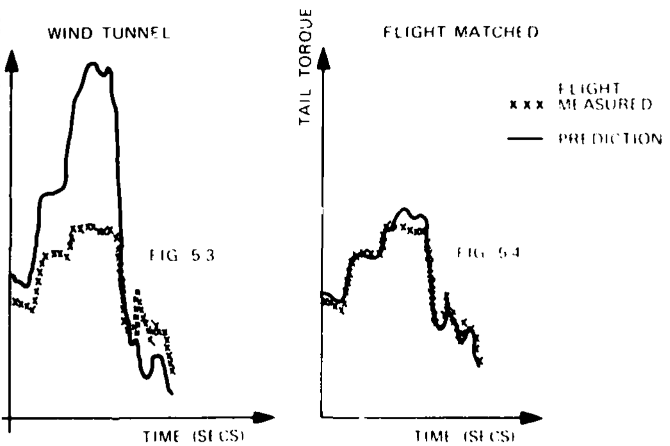

Figures 5.3 and 5.4: Comparisons of Predicted and Flight Measured Tail Torque During a Rapid Roll Manoeuvre

Model 5 was a final prototype check out model and most closely represented the lines of the actual aircraft.All early flight clearance work was based on this model data. The data from Model 5 however does not exhibit consistent trends in comparison with the flight data. It is not possible to be certain but this leads to the tentative conclusion that the Model 5 wind tunnel results were inaccurate due to strain gauge balance inadequacy rather than differing aerodynamic characteristics model to flight. A drift of the balance zero for different Mach numbers is the most likely explanation. A reasonable match between the Model 3 results and flight can be obtained by modifying the estimated aeroelastic contributions.

Further examination of the wind tunnel data has shown that at high speed the maximum allowable torque is compatible with less than 10% of the full range capability of the wind tunnel model strain gauge balance. The difference between the two models or between model and flight represents only about 3 or 4% of model capability in these conditions. The need for high model capability results from the fact that the full incidence range needs to be tested at maximum dynamic pressure to obtain data appropriate to high altitude and therefore low dynamic pressure in flight. It is apparent therefore that an order of magnitude improvement in the accuracy of the wind tunnel model balance was necessary.

For the trim conditions presented here the taileron shear is very small, the effect of incidence being offset by taileron setting to maintain trim. The torque at negative normal acceleration results mainly from the camber shape of the taileron. The rapid variation with normal acceleration supersonically results primarily from the fact that the centres of pressure due to incidence and due to taileron angle are in very different places due to the effects of a vortex from the side intakes and due to proximity of the taileron to the wing trailing edge, involving shock interactions between the two surfaces. The camber shape of the taileron was chosen so as to equalise the maximum positive and negative torques. Theoretical methods available at the time gave values due to camber similar to those measured but the predicted variation with normal acceleration was very much smaller. The theoretical results underestimated the required size of the actuator by a factor of 2.5.

In conclusion:

- The use of flight load measurements has avoided the need to increase actuator size or restrict the flight envelope.
- A high level of accuracy is required of wind tunnel measurements.

5.2 Effect of Heavy Store Configuration on rear fuselage bending

For a configuration with heavy stores underwing and underfuselage, depicted in fig 5.5 it was found at Mach 0.92 from monitoring that trim taileron angles and incidence were greatly different from those predicted (Figures 5.6 and 5.7). A calculation assuming the wind tunnel based loading 'derivatives' in combination with flight measured incidence and taileron setting implied rear fuselage loads far in excess of the aircraft strength (fig 5.8). This result appeared to be compatible with the high measured taileron bending moments, if the centre of pressure of the taileron load was assumed to be as for the clean aircraft. Unacceptable restrictions on the flight envelope in this configuration were indicated.

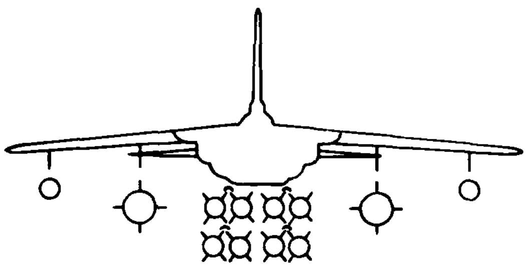

Figure 5.5

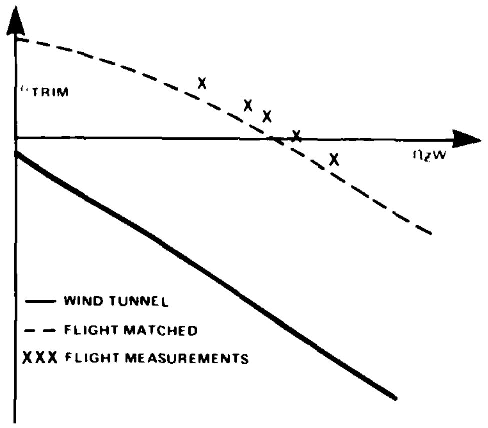

Figure 5.6: Comparison of Tail Angle to Trim for Wind Tunnel and Flight

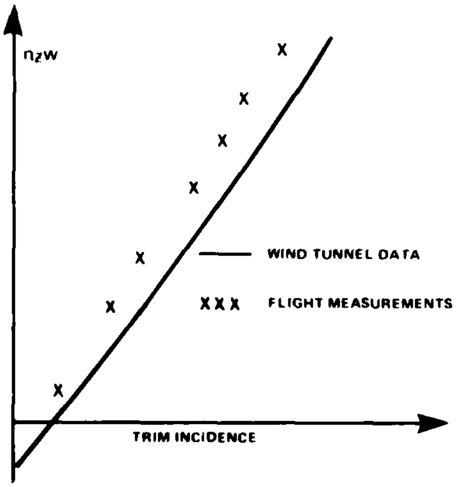

Figure 5.7: Comparison of Trim Incidence for Wind Tunnel and Flight

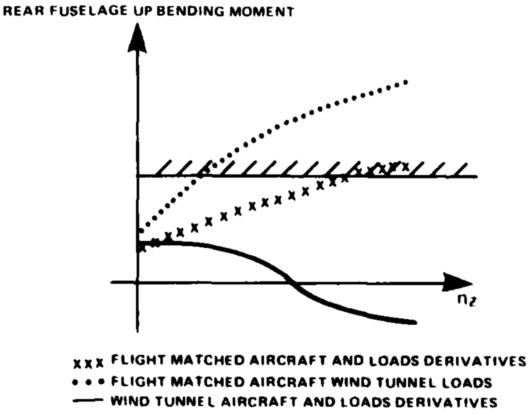

Figure 5.8: Variation of Rear Fuselage up Bending Moment with Normal Acceleration

The fact that the tail angle to trim was different from wind tunnel data indicates either a difference in the wing and fuselage characteristics requiring a change of tail load to balance the aircraft, or a difference in downwash, requiring a change of tail setting with no change of tail load. It is most likely to be a combination of these. It is not possible therefore to be certain whether the different trim angles result in the load change indicated.

Detailed analysis of flight load measurements for this configuration showed that the variation of taileron shear with incidence and at zero tail setting was very different from that found in the wind tunnel, as shown in fig 5.9. The similarity of bending moment indicates a different centre of pressure on the taileron.

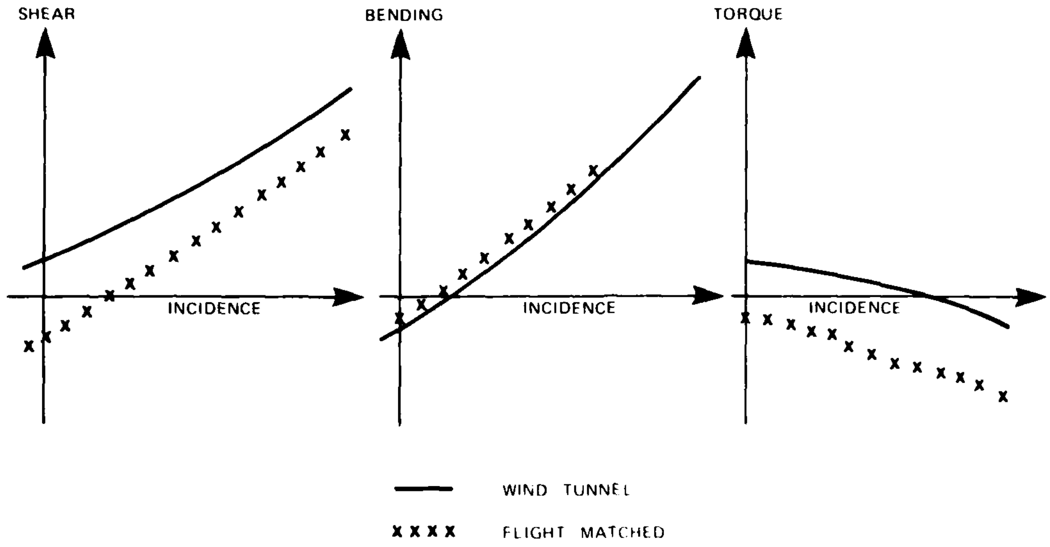

Figure 5.9: Variation of Taileron Loading with Incidence

The resulting flight measured loads are seen in fig 5.8 to be greatly below those implied by the simple expedient of using flight trim angles with wind tunnel loads data, although they are greater than the pure wind tunnel based values for this configuration, which by prediction was not a critical design case for the structure. However, they are greater than the original design loads, albeit less than the actual strength established by check stress. In the event no restrictions were necessary.

Several lessons emerge:

- The use of flight measured flight parameters with wind tunnel predicted loads derivatives can be misleading.
- The use of incomplete flight load measurements can be misleading.
- Care must be taken to monitor a broad spectrum of configurations and flight conditions - not just those predicted to be critical.

5.3 Expansion of Flight Envelope with Manoeuvre devices deployed

The structure of Tornado was designed to withstand the loads resulting from flight throughout the full flight envelope without flaps deployed. The "fallout" flight envelope available within the strength, with the flaps deployed to manoeuvre setting was determined from wind tunnel data. Although this resulted in acceptable symmetric g capability, full stick (rapid) rolls were severely limited. Fig 5.10 shows the variation of roll rate with normal acceleration resulting from a full pilot roll control application compared with the boundary for which 100% design load on the wing results from calculations using wind tunnel based data.

Progressive flight envelope expansion involving detailed analysis of flight measured data established that loads at higher incidences were lower than predicted allowing a clearance for full stick rolls up to 80% of the symmetric limit. The comparison of predicted wing bending moment in rapid roll manoeuvres between prediction and flight measurements is shown in figure 5.11 in which it can be seen that the flight values are significantly less than the predicted values.

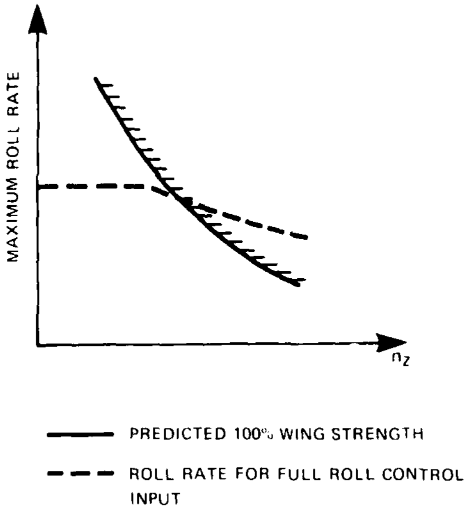

Figure 5.10: Variation of Maximum Roll Rate with Normal Acceleration

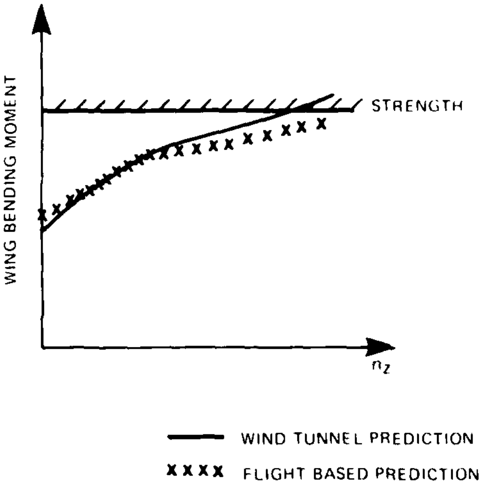

Figure 5.11: Variation of Wing Bending Moment with Normal Acceleration

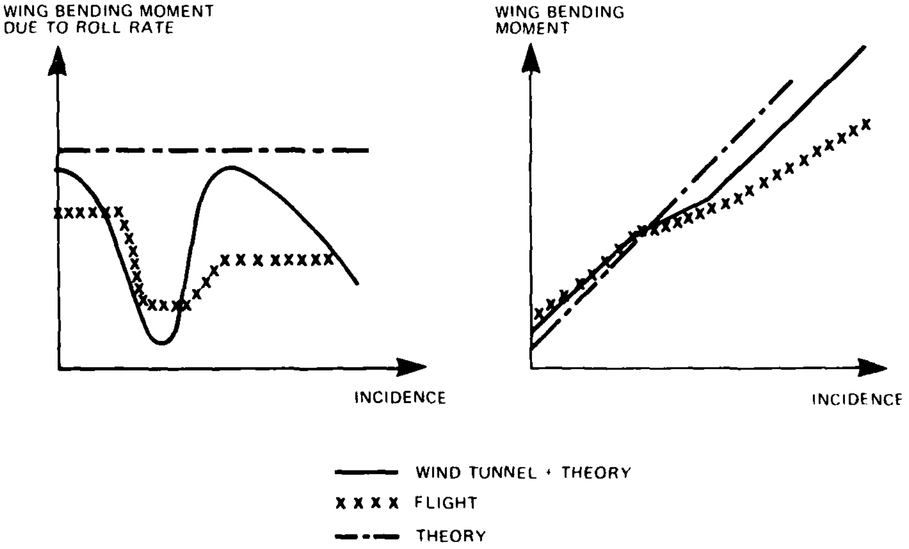

Figure 5.12: Wing Loading Characteristics Due to Roll Rate and Incidence

Fig 5.12 shows the comparison of wind tunnel, theoretical estimates and flight data of the variation of wing bending moment due to roll rate and of wing bending moment due to incidence (symmetric contribution). Although the three are similar at low incidence the high incidence characteristics are seen to differ greatly, the reduction of symmetric bending moment at moderate incidences being reflected in the variation of bending moment due to roll rate. The combination of these two effects, which are associated with the development of shocks as transonic conditions are encountered, results in smaller loads which allow clearance to a larger flight envelope.

* The availability of a means of flight load measurement has clearly been of great benefit in this instance in providing a far better service clearance than would otherwise have been possible.

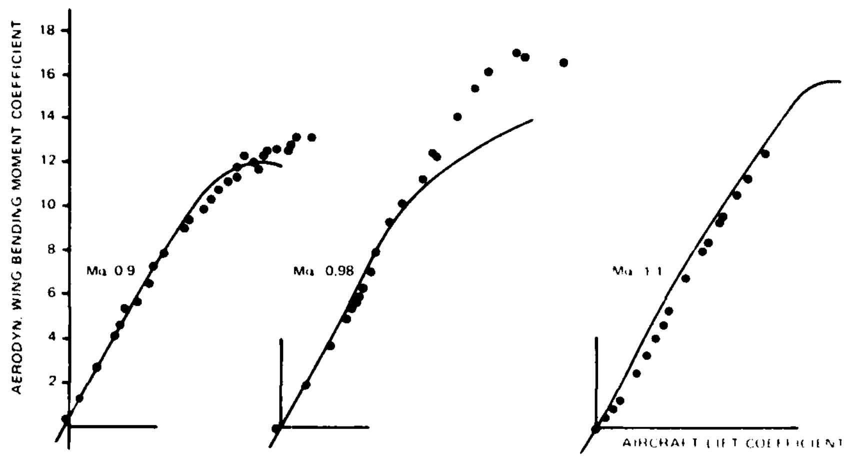

Figure 5.13: Comparison of Measured and Predicted Aerodynamic Wing Bending Moment (at STN. y1205) in tne Transonic Region

5.4 Transonic Effects on Flight Clearance

Flight load measurements for mid sweep have shown a rapid variation of wing bending moment as mach number is varied. Figure 5.13 shows a typical example at 25000 feet of the variation of wing bending moment co-efficient versus lift coefficient for a selection of mach numbers. At low incidences where the wind tunnel data is linear the agreement with flight is good. At transonic mach numbers, above the predicted linear region the flight measurements show the linear loading relationship to be sustained to higher lift coefficients.

Examination of the wing shear measurements has shown that the main non linearity results from an inboard movement of the wing centre of pressure which is delayed to higher incidences in the case of the flight data. Since the wing is swept this results in greater nose down pitching moments at the higher incidences which need to be balanced by greater down tail load. The flight tail load measurements confirm this effect.

These transonic effects can only be explained by a combination of full scale Reynolds numbers and mach effects resulting in "supersonic" type flow being established at high incidence at a slightly lower mach number in flight than in the tunnel. This has given better high incidence handling and manoeuvrability, at the expense of slightly higher wing and fuselage loads in this small transonic region.

Detailed analysis of the flight data has shown that for the original design flight envelope the maximum wing bending moment is greater than the wing design loads. A small change to the cleared flight envelope in the transonic region as shown in figure 5.14 results in a variation of maximum wing bending moment versus mach as shown in fig 5.15.

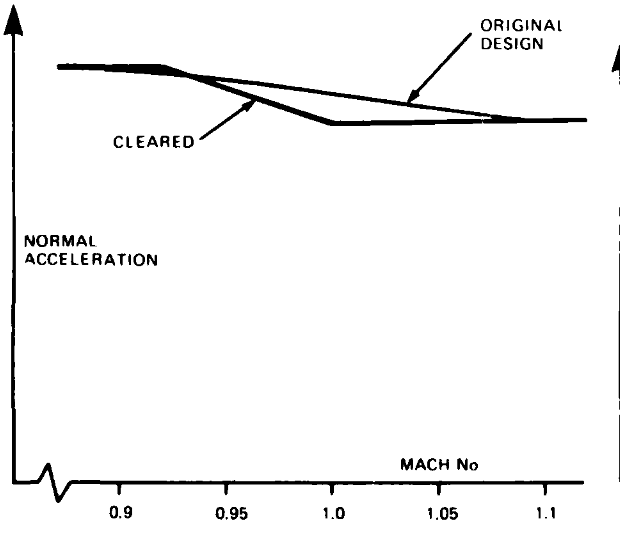

Figure 5.14: Limit Normal Manoeuvre Envelope

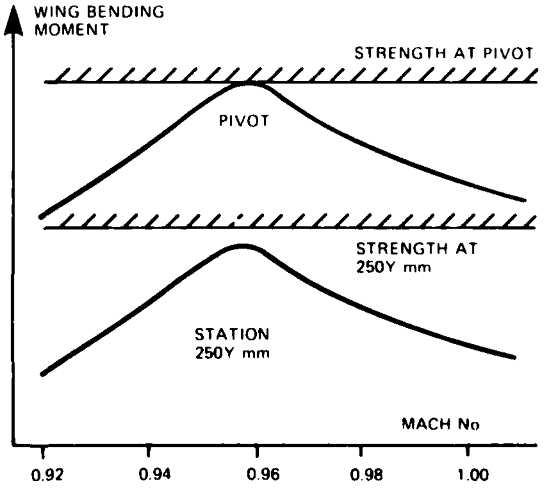

Figure 5.15: Variation of Maximum Wing Bending Moment with Mach Number

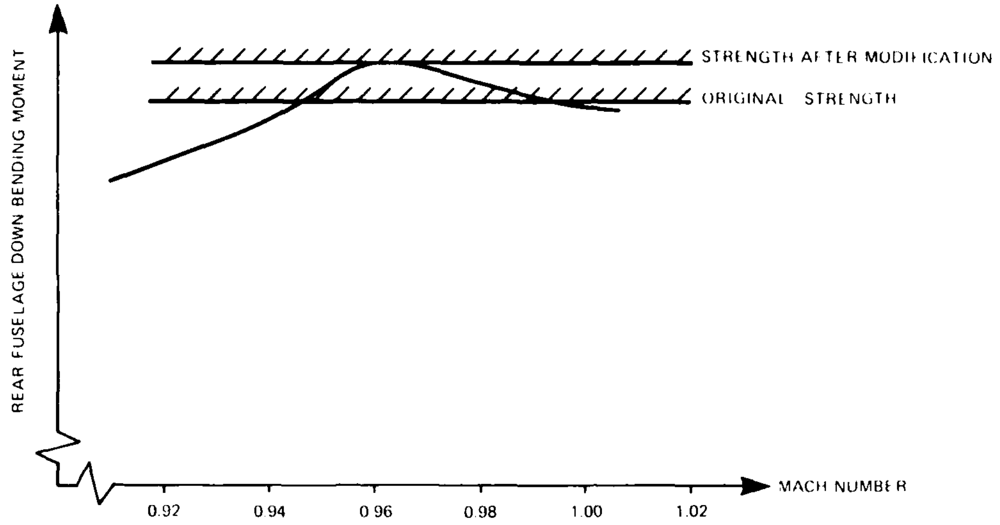

Figure 5.16: Variation of Maximum Rear Fuselage Down Bending Moment with Mach Number.

The increase in down tail loads to trim the changed wing distribution adds to the rear fuselage bending moment. As a result it has been necessary to increase the strength of the rear fuselage as show in figure 5.16. The small change to the cleared flight envelope avoided the need for greater strengthening.

* Flight load measurements have shown that in the transonic region wind tunnel data cannot be relied upon to provide sufficiently good results for full flight clearance.

6. Resolution of difficulties encountered

The usefulness of a flight load measurement programme must be judged on many factors. The most important of these is possibly the extent to which one can rely on the accuracy of the data measured. There is no absolute means of determination of the accuracy of the data but various methods are available which can provide a high level of confidence. Experience in the Tornado programme has shown that a high percentage of the data has at one time or other been suspect and a large proportion of the total time used in the analysis of the data has been used in the identification of discrepancies in the data and their resolution. Some examples are discussed here.

During early flying it was found that the variation of the taileron torques between the pre and post flight on ground datums and the in flight datums was outside the values expected. The taileron shear also exhibited inconsistencies. The hot soak flight established large temperature drift effects. Examination of the installation for the measurement of taileron torque showed that the bridge temperature compensation gauges had been mounted too far away from the active gauges. In the case of the taileron shear the problem was far more subtle and resulted from temperature stresses in the structure to which the strain gauges were mounted. The effects were large and made a nonsense of the measurements. After developing several different strain gauge installations to try to establish a reliable measurement a satisfactory solution was found.

The datum manoeuvre results were also used to identify a small apparent discrepancy in the wing bending moments. After much investigation it was established that the error lay not in wing strain gauge measurements but that the normal accelerometer reading had a datum error. Such findings give great confidence in the accuracy of the load measurements but make one very wary of flight parameter measurements. The accuracy of the interpreted loads is dependent on both the accuracy of the load measurement and the flight parameters.

A further source of difficulty in matching flight data resulted from inconsistent record of incidence. The need to fully calibrate the incidence measurement prior to flight load measurement cannot be over emphasised.

Comparison of port and starboard results may be sufficient to identify the differences but not to establish which (if either) is the correct measurement. On Tornado wing bending moment is measured at 4 spanwise stations. Port and starboard results for the second station from the root consistently showed 15% difference in value. All other stations were within 2%. No fundamental instrumentation checks had resolved this difference. A double differentiation of the variation of bending moment with span results in a loading diagram and although this exercise cannot be carried out precisely it was sufficiently good to establish that the rogue measurement was the lower value.

In several areas the calibration was limited in order to reduce time on the ground or because of difficulty in establishing sufficient load application points on the aircraft. An example of this is the front fuselage on which bending moments were made by means of strain gauged straps at the front transport joint. Analysis of the results showed variation with Mach number different from the Tornado wind tunnel data and any available literature on forebodies. This was believed to be due to inadequate calibration since loads were applied at a single point and the response of the gauges to vertical shear had not been established, neither had the response to lateral loads on the forebody.

7. Contribution of flight loads measurements to clearance to service

Final clearance to service of the aircraft in respect of structural loads has been achieved in a composite manner, following the test to ultimate load on the static test airframe. Quasi-static symmetric manoeuvres were demonstrated in the most critical conditions by roller-coasters and wind up turns, based upon the results of the survey to 80% limit load. Symmetric dynamic manoeuvres have been cleared by calculation using the flight based loading derivative and aircraft derivative data sets. Asymmetric manoeuvres have been cleared partly by the rapid rolling flight envelope expansion process and partly by calculation of the checked asymmetric manoeuvres required by the Mil Specs using the flight based data sets.

Loads measurement has allowed the rapid roll flight envelope expansion programme to be progressed with a greater assurance of safety, than would otherwise have been the case. In some areas the rapid roll flight envelope has been extended beyond that predicted by the use of wind tunnel data, greatly increasing the aircraft operational capability with manoeuvre devices.

In addition to the overall contribution outlined above, there have been several areas in which the flight load measurements made a special contribution to the service clearance,

* the taileron actuator size was established to be adequate despite indications to the contrary from wind tunnel.

* the availability of load measurement data in heavy stores configurations avoided unnecessary restrictions on the manoeuvre envelope which would have resulted if only flight parameters had been available.

* the use of flight measurements has resulted in a clearance for rapid rolling in the manoeuvre wing configuration up to 80% of the symmetric limit, compared with a 2g limit based on wind tunnel and theoretical prediction.

* flight loads measurements identified excessive wing and fuselage loads for transonic conditions of the clean aircraft, allowing the determination of a satisfactory safe manoeuvre envelope with a minimum of strengthening. The maximum available manoeuvre envelope has been determined with a minimum of risk from excessive loads, within the minimum weight philosophy adopted for design.

* The confidence with which service clearance can be given has been enhanced by the knowledge, based on flight loads measurement that the structural strength matches the maximum loads expected in service.

* In the longer term greater assurance of safety will result from the use of the flight based loads data sets in combination with in service flight parameter measurements to determine usage of fatigue life.

8. Conclusions

- Flight load measurements have made a significant contribution to the Tornado service clearance.
- Care is needed, in defining the instrumentation, gauge positioning to ensure linear responses, avoiding extraneous effects.
- Adequate calibration of strain gauges must be provided, including in-flight datum and calibration checks.
- The flight programme must cover a broad distribution of flight conditions in addition to areas where critical cases are predicted to occur.
- Adequate facilities must be provided to allow monitoring, easy data acquisition, storage and retrieval and to carry out detailed analysis.
- Flight load measurements in the linear range for the clean aircraft have generally been in close agreement with predictions.
- Wind tunnel data has, in some instances, for example taileron torque, been found to be unreliable, possibly due to inadequacy in the measurement techniques. In similar circumstances theoretical methods grossly underestimated the loads.
- For transonic conditions, where theoretical methods were not available, the wind tunnel data was found to be inadequate, leading to greater wing and rear fuselage loads in flight than those predicted.
- Small differences, between wind tunnel and flight, in the behaviour of the wing aerodynamics in the manoeuvre flap configuration at high incidence, were sufficiently great to make a significant difference to the flight envelope cleared.
- Within the context of the minimum weight philosophy, and hence untoleranced loads, used for Tornado design the flight measurements have been shown to be an essential means to establish flight clearance, since some measured loads were found to be different from prediction.
- Careful consideration should be given to the need for comprehensive flight load measurements based on the requirement of the particular project. The magnitude of the wing loading affects the extent to which prediction and flight are likely to disagree, tolerances on prediction may result in acceptable weight penalties dependent on the requirement of the aircraft.

References

1.	D. W. Altham J. Nuscheler D. K. Potter W. Seidel	Tornado flight Loads Survey AGARD - Conference Proceedings No. 223 ref 4 April 1977
2.	Skopinsky, T.H. Aiken, W.S. jr. Huston, W.B.	Calibration of Strain Gauge *Installation in Aircraft Structures* for the Measurement of Flight Loads NACA Report 1178 (1954)

Acknowledgement

The authors acknowledge the work undertaken by the BAe team involved in the flight load measurement programme, and analysis of the results, and especially to Miss A. J. McNish for help in relation to preparation of this paper.

CORRELATION PROBLEMS BETWEEN FLUTTER FLIGHT TEST DATA AND GROUND TESTS/ CALCULATION RESULTS FOR A VARIABLE SWEEP WING AIRCRAFT

by

G. De Ferrari

AERITALIA
Gruppo Velivoli Da Combattimento
Corso Marche 41, 10146 Torino
Italy

and

A. Lotze

MESSERSCHMITT-BÖLKOW-BLOHM GMBH
Airplane Division
P.O.Box 80 11 60, 8000 München 80
W.-Germany

and

R. Pyrah

British Aerospace Aircraft Group
Warton Division
Warton Aerodrome
Preston, Lancs. PR4 1AX
United Kingdom

ABSTRACT

The large variety of external stores carried on underwing pylons of modern combat aircraft requires a large amount of prediction work to assess the flutter behaviour.
This work, based on calculations, wind tunnel and A/C ground testing, is to be matched with flight test data for final qualification.
This paper reports the various problems encountered in this matching work, e.g.:

- structural nonlinearities, particularly due to variable sweep wing and related pivot arrangements

- effects of excitation techniques

- control system interaction with structural modes

- transonic aerodynamics

The probable causes of these problems are discussed and the trends in which both theoretical and test techniques should be improved are highlighted.

INTRODUCTION

During early development stages of a variable sweep wing combat aircraft extended wind tunnel testing of wing store configurations on subsonic flutter models were performed. Ground resonance tests on aircraft components,clean A/C and A/C with stores were conducted and the results were incorporated into the analytical model. Flight Tests of the clean aircraft and of the aircraft with stores followed, concentrating only on key configurations.
This paper deals with the difficulties the dynamicists had to face in correlating results with analytical simulation in the final flight test period . Particular reference is made to the aircraft with underwing stores, the clean aircraft development is being dealt with in ref. 5.

STRUCTURAL NONLINEARITIES

The problem of structural nonlinearities involves two fundamental aspects:

- the interpretation of flutter flight test results, which implies an assessment of how nonlinear the behaviour of flying prototypes was during individual measurements

- the prediction of production aircraft non-linear behaviour during all service life, in which any inspection or replacement of parts must be kept to a minimum.

The procedure leading to the flutter clearance for each external store configuration must of course be based on the understanding of both aspects.
A typical case of such a procedure in which the correlation problem was succesfully managed is now presented.

Reference 1 discussed both the usual slight nonlinearities of any aircraft structure and the large one concentrated in the variable sweep-underwing pylons alignment system. Figures 1 and 2 presented here show this case, leading to the two different kinematic behaviours:

- pylon clamped to the wing by static friction in the bearings (yaw loads are transmitted to the wing itself and the control rod is not giving significant contribution; this condition is referred to as "rigid control rod")
- pylon free to rotate relative to the wing (when friction forces are exceeded by yaw oscillation inertia forces; the yaw moment is transmitted to the control rod which is therefore treated as "elastic").

For the store configuration considered (large tank on i/b pylons) the flutter mechanism is different for the two kinematic states. In the first case the store yaw mode frequency lies in the range of the two modes giving the critical coupling (first wing bending and store pitch). This improves the flutter behaviour as it is shown in fig. 3 in which the computed flutter speed is presented versus the pylon yaw flexibility. Any uncertainty in the definition of this important parameter (affected by the usual slight nonlinearities above mentioned) leads to the shown considerable differences in flutter speed. The trend can be explained easily: increasing the yaw flexibility, the yaw frequency, formerly higher than those of wing bending and store pitch, reduces and crosses this range causing energy absorbtion (yaw of a heavy store) and a yaw-pitch modal exchange, which, by raising the pitch, decouples the critical modes and therefore raises the flutter speed drastically (figures 3, 4). When the yaw flexibility is further increased, the flutter speed again decreases as the yaw mode disappears downward from the coupling area.
If the elastic control rod is considered, the pylon yaw flexibility is drastically increased by the rod flexibility added in series and the total value is high enough to decouple the yaw mode completely, being now at very low frequency.
Therefore the flutter speed is practically constant in the whole plot range (figure 3).
For the nominal value of the pylon yaw flexibility the elastic control rod case is more critical and this unfavourable difference could be significantly larger if the possible effective flexibility range, due to slight nonlinearities and normal differences between various production aircrafts,is taken into account. Therefore the problem of correlation, having a considerable impact on final clearance, was solved with the following approach.
The first logical suggestion was of course to try to excite the store yaw mode at high amplitude in order to generate the more critical elastic control rod case as the starting condition for the aircraft flutter mode evolution to be measured. This was difficult to do as all excitation devices were as usual designed to provide a vertical bending-pitch excitation. On the other hand it must be noted that the flutter mode related to the elastic control rod case does not contain a significant store yaw component as for the rigid case (see figure 5). It is decoupled, at lower frequency as shown above. As a consequence, it can be stated that the flutter mode itself is showing the nature of the kinematic condition.

A proper indication of this condition can therefore be built up taking the ratio of store yaw to pitch motion Ψ/Θ for the critical mode which is easy to excite during flight tests. The important feature of this parameter is that its trend versus the yaw flexibility and versus the kinematic condition follows the flutter speed trend quite well (see figures 6 and 3).

At this point the procedure is clear:

1. - compute the plots of figures 3 and 6 for prototype A/C taking into account for important modes the structural damping measured during ground resonance tests (performed over wide amplitude range) at the amplitude normally achieved during flight tests

2. - take from inflight measured mode shapes the value of Ψ/Θ

3. - compare this value with the computed plot of fig. 6. This will show which kinematic behaviour (rigid or elastic control rod) has been achieved and, in the rigid rod case, also the proper value of the yaw flexibility $C_{\psi\psi}$ "operating" during the test

4. - take the corresponding computed flutter speed from the plot of figure 3 and compare this with the values extrapolated from test results; build up if necessary a correcting factor

5. - apply this correcting factor to the flutter speed computed for service aircraft using for critical modes the structural damping factors considered reliable for both large amplitude of oscillations (where the friction part of damping tends to disappear) and for all service life. Figure 7 shows the pitch mode damping measured during ground resonance test of a prototype after a considerable amount of flying hours. From this plot a reliable damping value of 6% was taken. For those calculations of course the elastic control rod case must be considered as this is sooner or later reached for both increasing oscillations and wear of the pylon to wing connection.

6. - define flutter clearance on the basis of the flutter speed obtained above corrected by the usual 15% safety factor.

The comparison of flutter speed of point 4 is particularly useful in defining the correcting factor if excitation during flight tests indicates both elastic and rigid control rod behaviours.
This was the case for the referenced configuration where a first set of flight tests showed the rigid rod case only (figure 5 c) and a second set performed with the same prototype in a 2nd test stage (having more flown hours and coupling wear) showed also the elastic rod case (figure 5 b). It can be noted from figure 6 that the experimental values of Ψ/Θ correlate quite well with the calculated values.
If the flutter clearance had been given on the basis of the first set of flight tests only, without this specific correlation study confirmed by the second set, a dangerous situation for in service aircraft could have been created.

EFFECTS OF EXCITATION TECHNIQUES

The particular requirement for this aircraft was to obtain sufficient excitation and hence signal to noise ratio to achieve the free or large amplitude kinematic state described previously. This was furthermore required for a large number of underwing store configurations.

Both inertia exciter and bonker excitation (rocket motors) were discarded at the outset as means of excitation since with the low wing-store frequencies expected for this aircraft, high energy levels would be required. This would entail fairly large and massive installation which would substantially effect the flutter characteristics under investigation.

Turbulence as a means of excitation was similarly rejected since levels encountered were not expected to be sufficient to obtain elastic control rod kinematic conditions.

In view of the number of stores to be cleared, the decision was made to develop a dedicated flutter store, based on an underwing fuel tank from the stores list, with hydraulically operated vanes providing the excitation force. This was arranged to accept variable ballast masses to simulate the mass, centre of gravity and radius of gyration of the critical stores to be cleared. The principal excitation used was frequency sweep although psuedo random binary noise and selected pulse excitations were available. Since the flight envelope to be explored was readily achievable in straight and level flight, a slow sweep rate was preferred to maximise the wing-store response for the available excitation force. A facility for varying the excitation amplitude was included.
The response of the aircraft was measured by means of vertical and longitudinal accelerometers positioned on the wing tip and triaxial accelerometers on the nose and tail of the flutter store and other outboard underwing stores when present.

The results were analysed using cross correlation techniques to obtain an equivalent impulsive response, followed by a process of filtering in the frequency domain and subtraction in the time domain to obtain the dominant and sub-dominant modes of interest. This process was performed on an HP5451C Fourier Analyser using the programs detailed in ref. 5

The results obtained were to be supplemented by manual analysis of the response due to stick jerks and wing sweep start and stop inputs.

Since the critical flutter couplings under investigation were symmetric the obvious form of stick jerk excitation was longitudinal. This, however, in practice proved to give only poor excitation since at the taileron the displacements are generally low for the wing store modes and therefore only a limited amount of energy can be introduced. Wing sweeps were also found to give only a very limited amplitude of excitation again due to the limitations of the sweep rate. It was discovered however that lateral stick jerks, using the wing spoilers as the main excitation device, could attain reasonable amplitudes of response. Initially an asymmetric motion was excited which settled down to a symmetric response. This led to the special dynamic manoeuvres used during the flight programme where, in order to maximise the response, the pilot initiated a roll, reversed it, and stopped the roll by using rapid lateral stick inputs.

This method of excitation achieved fairly consistent results with some stores (e.g. for the above mentioned tank cofiguration) One problem encountered was that the duration of the stick jerk, and therefore its frequency components, was variable - needing several manoeuvres to obtain a few test points with adequate excitation. This problem could be overcome by injecting a preprogrammed electrical signal into the control system giving a known, and repeatable excitation source. Being impulsive in form such a system would have to have a fairly large degree of authority over the control surface to generate sufficient response and it follows that there is a need for it to be fail-safe in performance.

A further problem was that by the time fully symmetric behaviour was estabished the signal had often decayed to fairly low signal noise ratios. These problems were compounded by the limited separation of the two critical modes (e.g. approx 0.4 Hz) which meant that beating between the modes could well affect the results without being readily apparent from the short time history available.

The flutter store, using frequency sweep excitation, proved to be quite effective at exciting the lower damped critical flutter mode, and, by concentrating on accelerometers which displayed the least distortion or contamination by the adjacent higher damped mode, gave a reasonably consistent set of results. These agreed well with the trends predicted by theoretical means for the rigid control rod case. Reliance on detailed studies of critical parameter variations and their possible influences was therefore necessary to define safe flutter clearances for use in service.

Neither of the principal methods used (flutter store frequency sweep or special dynamic manoeuvres) could reliably extract good quality results for the higher damped mode of the flutter coupling or for the pylon yaw mode. For future work it has been proposed that the flutter store facilities should be extended to provide a means for specific independent yaw axis excitation. This would ensure that the free kinematic state was present during even moderate store pitch - wing bending excitation and give added confidence to the final production flutter clearances.

INVESTIGATION OF STRUCTURAL MODE COUPLING WITH THE FLIGHT CONTROL SYSTEM

Modern aircrafts are using sophisticated power control and automatic control systems, which basically are designed to maneuver the aircraft and to provide sufficient damping for the rigid body modes. Since the sensors are attached to a flexible structure, motions of the elastic aircraft also are picked up and may be modified by the system. Tactical requirements lead to the use of fast responding pressure feedback actuators capable of producing large forces at structural mode frequencies. In order to avoid instabilities it is necessary to predict the response of the airplane with the control system and to correlate with test data. An analytical approach for the complete system including unsteady aerodynamic forces was developed in which the elastic structure is described by normal modes modified by results of a ground resonance survey (Ref. 6).

A block diagram of the fully operative CSAS (Command and Stability Augmentation System) for the high speed range is shown in Fig. 8. The pitch, roll and yaw rate signals are picked up by gyros and filtered and shaped to provide pitch, roll and yaw control by means of an all-moving tailplane (taileron) and a conventional rudder. The possible implementation of a structural mode filter must be provided in the design of the CSAS to suppress unfavourable coupling effects of structural modes. The actuator dynamics are highly nonlinear depending on preloading, amplitude, input, and service conditions. One must be sure, therefore, that the transfer function of the worst possible case is introduced into the analysis.

Whereas transfer functions of all of the electrical blocks in the CSAS can be predicted analytically with sufficient accuracy, the actuator impedance and frequency response functions must be measured. Open loop calculations have been performed considering the dynamics of the aircraft structure, the complete CSAS and servo system. The excitation is represented by a harmonic oscillating electrical input signal, fed into the system which was cut off behind the rate gyros. The results of these calculations are demonstrated by Nyquist diagrams. Open loop tests were conducted with the aircraft standing on inflated and deflated tires for various fuel conditions and wing sweep angles. The purpose of this test was to measure the transfer function of elastic aircraft with CSAS and close the loops whenever stability was assured. In the first test series this was only possible for the yaw loop because the pitch and roll loops were unstable. After introducing a lag filter into the actuator circuit, the aircraft was stable but did not yet fulfill our requirements for safety margins.

The Nyquist plot of Fig. 9 comparing test with analytical results for a system without structural mode filters (notch filters) but with the lag filter introduced into the taileron actuator circuit shows good correlation for the pitch axis. The structural model had to be adjusted to reflect the test condition of the aircraft standing on tyres and structural damping g = 0.02 was introduced for every vibration mode. Fig. 9 shows considerable responses in the three symmetrical vibration modes: First symmetrical wing bending at 6.1 Hz, first fuselage vertical bending at 9.9 Hz and first symmetrical tailplane bending at 13.0 Hz.

The aircraft is stable because the response does not encircle the point (-1) on the real axis. Similar results have been obtained for the roll axis. The phase lag introduced into the low-frequency area by a notch filter was expected to be detrimental to the stability of flight mechanical-CSAS coupled modes. Since this phase lag increases with higher notch filter attenuation, there was the requirement to keep the attenuation to a minimum. On the other hand, it is necessary to cover frequency and amplitude shifts of structural modes (generated by flight flutter test excitation equipment, wing and fuselage fuel contents, wing sweep), and gain and phase variation of actuators by reasonable margins.

In difference to the requirement for stability of MIL-Spec. A-008870 A, asking for a gain margin of at least 6 dB and separately for a phase margin of at least + 60° we required a 6 dB margin on the amplitude of each structural mode and applied MIL-Spec philosophy only for failure cases. This approach seems to be more advisable for modern aircraft using very sophisticated control systems and fast responding pressure feedback actuators.

On the basis of a 6 dB margin for all amplitudes, a notch filter was designed for the pitch and roll axis, considering various configurations and fuel conditions. Fig.10 shows the notch filter characteristic for the pitch axis, providing an attenuation of -30 dB at about 11 Hz. The calculated and measured open loop diagram for the pitch axis with the notch filter implemented is presented in Fig. 11.

Open loop tests in various configurations have been performed also on production aircraft. It is worth mentioning that the attenuation of the structural filters was proved to be sufficient throughout all aircraft development stages. To avoid unfavourable phase effects on the flight mechanical modes, the deletion of actuator lag filters is in consideration which has been made possible by improvements of the actuator frequency characteristic.

When the aircraft was proved to be stable on the ground and reasonable agreement was achieved between test and analysis, the stability of the CSAS-structural mode coupling behaviour in flight had to be investigated by analyses. Only a few check points had to be tested with fully engaged CSAS during normal flutter test flights.

The open loop diagrams of the pitch response, as shown in Fig.12 for two different flight conditions, demonstrate (in comparison with the results obtained on the ground) the attenuating effect of unsteady aerodynamic forces. Close loop calculations indicated that there is practically no influence of the CSAS on the flutter behaviour. The small effect of the CSAS on the flutter behaviour has been confirmed by check points during flight flutter testing of various clean aircraft and wing store configurations. A possible exception of the general validity of this result will be discussed in the following chapter which deals with the influence of the stick pitch circuit on wing store flutter by coupling with the flutter mode.

STICK PITCH COUPLING WITH STRUCTURAL MODES

Approaching transonic speeds during flutter flight testing of an inboard and outboard wing store configuration at 45 degree wing sweep, apparant zero damping was indicated by constant wing bending and store pitch oscillations at 4 Hz after excitation by lateral stick jerks. On the inboard wing pylons flutter stores were carried, simulating the full external tank. The oscillations could be stopped by sweeping the wing to the back position. The flutter case was predicted by conventional flutter calculations but the flutter speed was higher than measured in flight test. During the amplitude limited wing and store oscillations significant responses in stick pitch and taileron pitch were shown by the stick and taileron instrumentation. Therefore a contribution of the control system to the aeroelastic behaviour of the aircraft structure seems to be likely and a careful investigation was initiated including ground testing, coupled stick pitch - structural mode calculations and further flight flutter testing.

In Figure 13 the results of a conventional flutter analysis for the inboard and outboard wing store configuration considered are plotted, showing an inboard store pitch - wing bending flutter at about 4 Hz. Because in this calculation free yaw displacements of the pylons relative to the wing are represented, the inboard store yaw frequency is separated and contributes only little to the flutter mode. For the calculations a conservative assumption of 2 has been made for the damping of each structural mode on the ground. In spite of this fact the flight test measurements indicate a flutter speed which is about 8 lower than the calculated speed. The results of the flight flutter test are also depicted in this figure.

The mathematical model, developed to represent the CSAS/structural mode coupling behaviour could also be used for this investigation after introduction of an additional degree of freedom for the stick pitch feel system dynamics and after completion of the control system representation by the electrical connection between the stick pitch pick up and the taileron. The mechanism of the mechanical and electrical stick pitch circuit are demonstrated by the flow diagram in figure 14.

The stick pitch sensor which is used in the electrical (CSAS or direct link) mode is fixed to the fuselage structure, measuring the stick pitch angle relative to this fuselage station. The signal, therefore, also includes structural motions of the fuselage excited by the taileron.

Secondly, the mechanical parts of the pitch control line, including stick, feel jack, links and control rods up to the clutches (connected to the taileron actuators if the aircraft is controlled mechanically) can be excited by fuselage oscillations at fuselage attachment points.

Both effects are able to close the stick pitch loop by means of structural feedback.

In figure 15 a frequency response curve of the pitch control line operating in "Direct link" is shown, being available from rig testing for various flight conditions, different amplitudes and for flight simulation of the "direct link" or the full CSAS condition.

According to the nonlinear characteristic of the pitch feel spring system, amplitudes and resonance frequency are highly dependent on the excitation. Due to a nearly 180° phase shift at the resonance frequency, the control line could be represented by a single mass-spring-damper system with a resonance frequency between 3 and 4 Hz and a structural damping of about 15 . Using these data for first analytical investigations of the full dynamical system including the unbalanced pitch control line results in flutter trends which are demonstrated by figure 16.

For general illustration of nonlinear feel system effects on flutter, the damping of the critical flutter mode is depicted for different resonance frequencies of the stick pitch mode. Due to the rapid phase change at the stick pitch resonance frequency the coupling of the flutter mode with the stick pitch mode can reduce the flutter speed for about [illegible] if the feel system resonance frequency is equal or lower than the critical flutter mode frequency.

If the feel system frequency is higher than the flutter mode frequency, then the effect on flutter can be beneficial. New frequency response measurements of the control circuit were performed on prototype as well as on production standard aircraft. Similar characteristics were obtained for the different flight mechanical operation modes, but the mechanical mode exhibited much lower amplitude responses. Therefore further investigations were concentrated on the "Direct Link" and the CSAS mode.

Stick pitch frequency responses measured on prototype aircraft in "Direct Link" operation are presented in figure 17. The resonance frequency drops from about 5.3 Hz at small excitation to 4 Hz at large excitation due to the nonlinear characteristic of the feel actuator. A reduction in resonance frequency is also obvious when the resonance conditions are approached from higher frequencies. Further tests at different trimm positions extended the range of possible resonance frequencies which had to be considered by calculation between 6 and 3.5 Hz. In contrast to the rig test results the phase change at the resonance frequency was not higher than 90° for all aircraft measurements which is matched by calculations just for the resonance conditions. Although some design changes had been applied to the feel spring system, the measurements on the production aircraft reveals similar results, but the pitch feel system damping was reduced from 15 , measured on prototype aircraft, to about 5 . Final determination of the mass and inertia properties of the complete pitch control line confirmed that the system is suitably balanced for aircraft pitch, fore and aft and vertical accelerations. Using this data in a coupled "aircraft structure-control system" analysis and investigating the effect of the frequency and mass parameters of the control line yielded the following results:

The effects of mass coupling between pitch control and aircraft x and z are negligible. The influence of the mass coupling between pitch control and aircraft pitch is evident but relatively small. The largest effects are generated by the variation of control line resonance frequency and the control line pitch inertia as represented by figure 18 and figure 19. However, the calculation indicates a detrimental effect of the pitch control resonance frequency only for the unbalanced system whereas for the balanced system values of pitch control resonance frequencies higher or lower than the flutter frequency lead to flutter speeds higher than the speeds obtained by conventional flutter calculations. It should be mentioned that by adding the balance weights to the control line, the pitch control inertia was increased by about 40%. But, as shown in figure 19, the control line pitch inertia was also proved to have large influences on the flutter speed only for values smaller than relevant aircraft data.

Comparing the fully operational CSAS mode with the "direct link" mode reveals a slightly benefical effect of the CSAS which is presumably caused less by the feedback of fuselage motions via the pitch rate gyro than by the changes of circuit gain and phase in full CSAS.

The analytical results have indicated a possible reduction in flutter speed if certain conditions are met. Considering the complexity of the problem and the large number of possible parameter constellations due to nonlinearities of the control system and aircraft structure, nonlinear calculations may be necessary to cover the most critical case.

As already shown by analytical investigations of the linearized problem, the possible reduction in flutter speed seems not to be dramatic but it was proved that in some cases realistic flutter speeds can not be predicted without considering the fully coupled dynamical and flight mechanical system.

TRANSONIC EFFECTS

Another difficult problem which can hardly be predicted if no transonic flutter model or unsteady pressure distribution model is available, is the influence of transonic aerodynamics on store flutter.

Carrying stores on the outboard wing pylons, decreasing damping of the wing bending mode has been measured in first flight flutter tests. According to analytical predictions the mass and inertia properties of the stores were not flutter critical. As demonstrated by figure 20 and 21 the flight flutter test was interrupted after a first test series, when low dampings in the wing bending mode were indicated which were confirmed by repeated flight measurements. The large scatter in measured dampings could be explained by transonic effects, being different for slightly changed flight conditions as well as by the strong coupling between wing bending and store yaw which generates two modes, both showing large wing bending motions but different modal dampings.

Before having solved the problem, the outboard store configurations for the transonic speed range had to be limited to high altitudes.

A combined experimental - analytical study was initiated involving flow pattern measurements on an aeroelastic research model at RAE as well as flutter analyses including transonic effects. Since neither a transonic flutter model nor an unsteady pressure distribution model was available, the calculation had to be based upon steady pressure distributions measured on a buffet model in the transonic range. The doublet lattice method was used to apply so called additive corrections to the theoretical pressure distribution of each individual panel. (For detailed information, see Ref. 7). Representing a typical example for necessary transonic corrections on outboard store configurations, figure 22 demonstrates the effect of this additive correction for the first wing bending mode at a Mach number of 0.9. As expected the correction is most effective at the outboard wing.

Results of flutter calculations with modified aerodynamic data are plotted in figure 23 showing only the two important modes wing bending and store yaw for Mach numbers 0.9 and 0.95. To compare calculated results of figure 23 with flight test results of figure 20 and 21, about 3% structural damping as measured in ground resonance test for the wing bending mode have to be added to analytical results. It is proved that there is a pronounced transonic effect on the damping of the wing bending mode, increasing with Mach number and angle of incidence, but generating an unstability only at very high, non realistic airspeeds.

Step by step flutter flight testing was continued, trying to achieve amplitudes of excitation as large as possible to overcome structural nonlinearities. The results are demonstrated by the second test series data in figure 20 and figure 21 which confirmed the predictions by recovering damping values with increasing Mach numbers and airspeed.

CONCLUSION

It has been shown that especially in connection with nonlinearities, either generated by structural, control system or aerodynamic transonic effects, flutter clearance can not be based exclusively on flight testing nor on conventional flutter calculations. Flutter flight testing is a useful and required tool for flight clearance purposes but approaching areas with low flutter margins, good correlation with analytical investigations confirmed by ground resonance tests is vitally necessary, to be able to explain the physical behaviour of the flutter case and to avoid unsafe conditions during flutter flight testing. If correlation between flight test and analysis is poor, possible nonlinear effects must be incorporated into the analysis. Having proven good correlation with flight testing for special test conditions, the clearance according to the most critical case during whole service life and considering all possible amplitudes has to be provided by analysis if this condition can not be reached by flight testing.

REFERENCES

/1/ DE FERRARI; G.; CHESTA, L.; SENSBURG, O.; LOTZE, A.
Effects of Nonlinearities on Wing-Store Flutter
AGARD Report 687 (1980)

/2/ MATTEA, G.; DE FERRARI, G.
Wing with stores flutter
Calculation-flight test comparison for subsonic tanks configuration
AERITALIA Report 82144

/3/ HAIDL, G.
Nonlinear Effects in Aircraft Ground and Flight Vibration Tests
AGARD Report 652 (1976)

/4/ SENSBURG, O.; SCHOEN, B.
Schwingungs- und Flatteranalyse von Flugzeugen mit besonderen nichtlinearen Struktureigenschaften.
Zeitschrift f. Flugwissenschaften und Weltraumforschung No. 2 (1978) Heft 6

/5/ POTTER, D.K.; LOTZE, A.
Inflight Flutter Identification of the MRCA
AGARD Report 646 (1976)

/6/ LOTZE, A.; SENSBURG, O.; KUEHN, M.
Flutter Investigation of a Combat Aircraft with a Command and Stability Augmentation System
JOURNAL OF AIRCRAFT Vol 14, No. 4 April 1977, pp 368-374

/7/ LUBER; W.; SCHMID, H.
Flutter Investigations in the Transonic Flow Regime for a Fighter Type Aircraft
55th Meeting of the
AGARD Structures and Materials
Panel, Sept. 1982

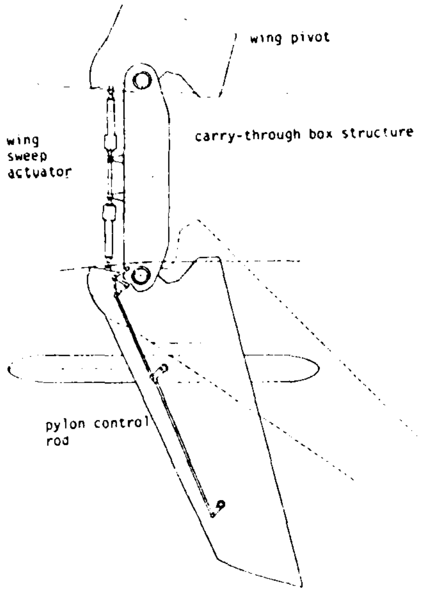
wing pivot
carry-through box structure
wing sweep actuator
pylon control rod

FIG. 1 SCHEMATIC VIEW OF THE WING SWEEP – UNDERWING STORES ALIGMENT SYSTEM

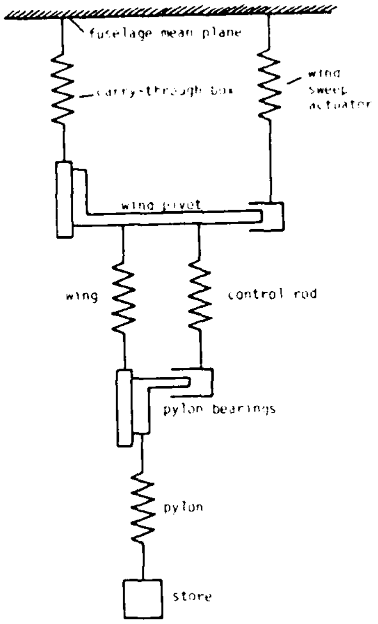
fuselage mean plane
carry-through box
wing sweep actuator
wing pivot
wing
control rod
pylon bearings
pylon
store

FIG. 2 IDEALIZED SYSTEM FOR WING AND STORE YAW MOTION

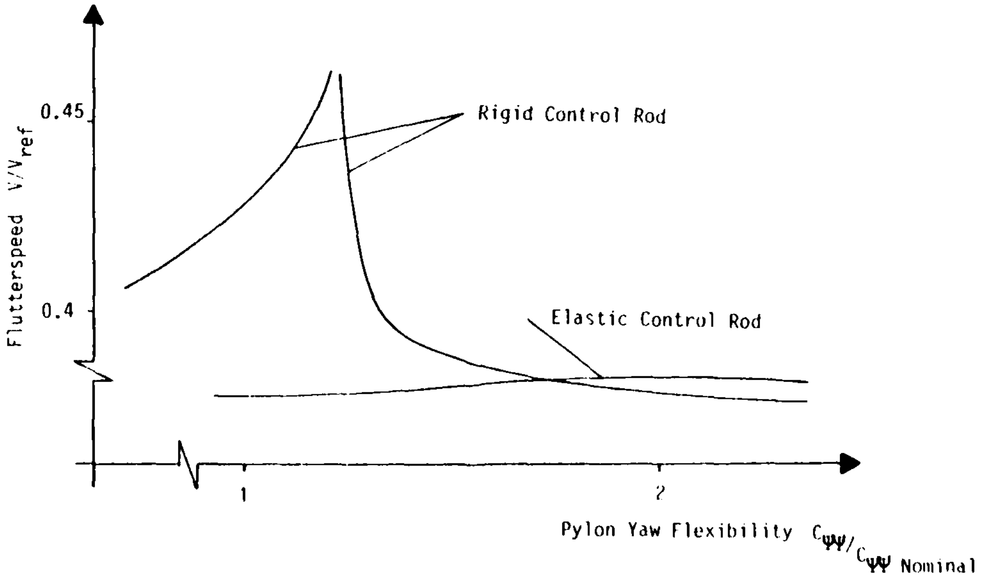

FIG. 3 COMPUTED FLUTTER SPEED VERSUS PYLON YAW FLEXIBILITY FOR RIGID AND ELASTIC CONTROL ROD CASES

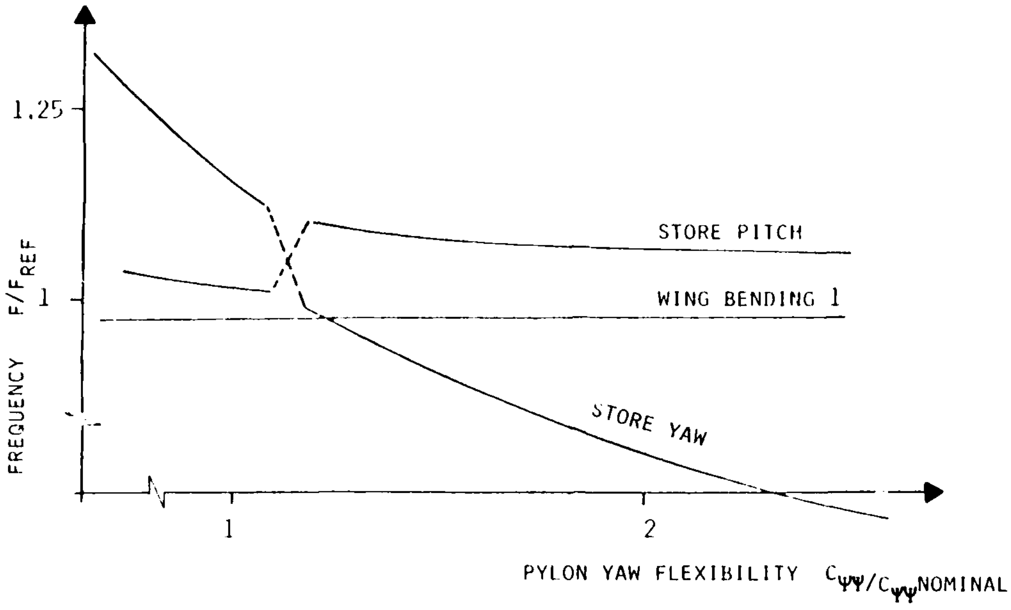

FIG. 4 CRITICAL MODE COUPLING VERSUS PYLON YAW FLEXIBILITY FOR THE RIGID CONTROL ROD CASE

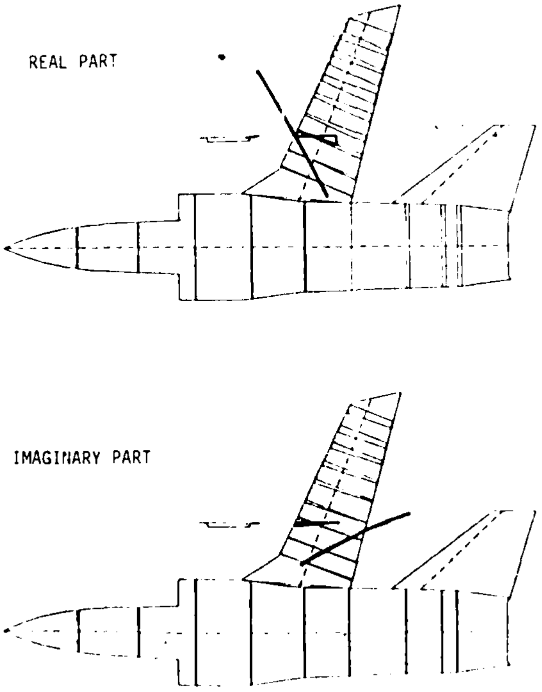
REAL PART
IMAGINARY PART

FIG. 5 A) COMPUTED CRITICAL MODE FOR THE ELASTIC CONTROL ROD CASE

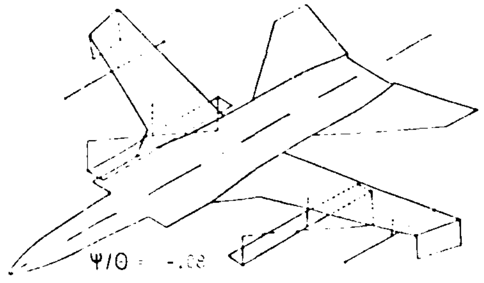

FIG. 5 B) EXPERIMENTAL CRITICAL MODE FOR THE ELASTIC CONTROL ROD CASE

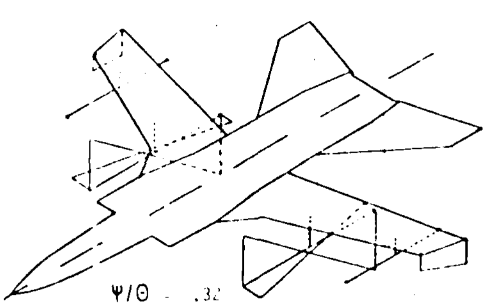

FIG. 5 C) EXPERIMENTAL CRITICAL MODE FOR THE RIGID CONTROL ROD CASE

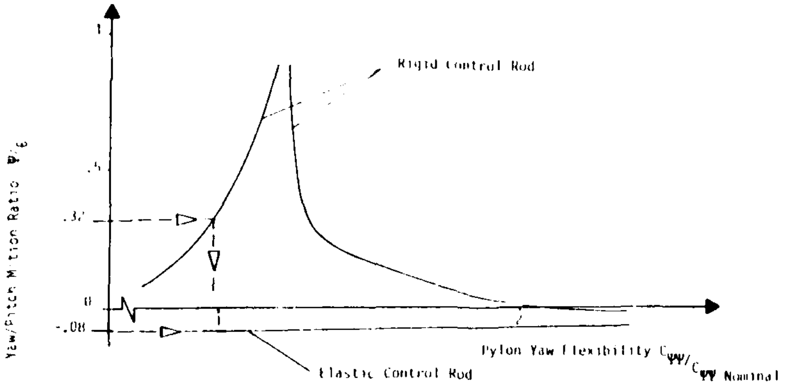

FIG. 6 COMPUTED RATIO OF THE STORE YAW TO PITCH MOTIONS FOR THE CRITICAL MODE (RIGID AND ELASTIC CONTROL ROD CASES)

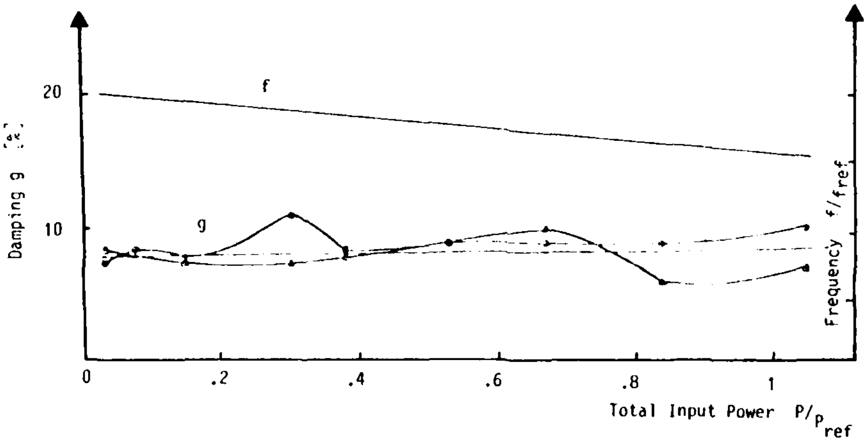

FIG. 7 DAMPING RATIO MEASURED DURING GROUND RESONANCE TEST FOR THE PITCH MODE

CSAS-CONTROL SYSTEM

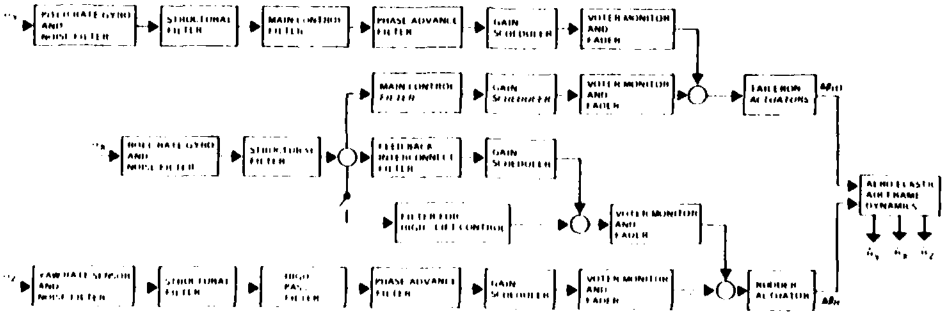
PITCH RATE GYRO AND NOISE FILTER
STRUCTURAL FILTER
MAIN CONTROL FILTER
PHASE ADVANCE FILTER
GAIN SCHEDULER
VOTER MONITOR AND FADER
MAIN CONTROL FILTER
GAIN SCHEDULER
VOTER MONITOR AND FADER
TAILERON ACTUATORS
ROLL RATE GYRO AND NOISE FILTER
STRUCTURAL FILTER
FEEDBACK INTERCONNECT FILTER
GAIN SCHEDULER
FILTER FOR HIGH LIFT CONTROL
VOTER MONITOR AND FADER
AEROELASTIC AIRFRAME DYNAMICS
YAW RATE SENSOR AND NOISE FILTER
STRUCTURAL FILTER
HIGH PASS FILTER
PHASE ADVANCE FILTER
GAIN SCHEDULER
VOTER MONITOR AND FADER
RUDDER ACTUATOR

FIG. 8 MAIN ELEMENTS OF THE CSAS-CONTROL SYSTEM.

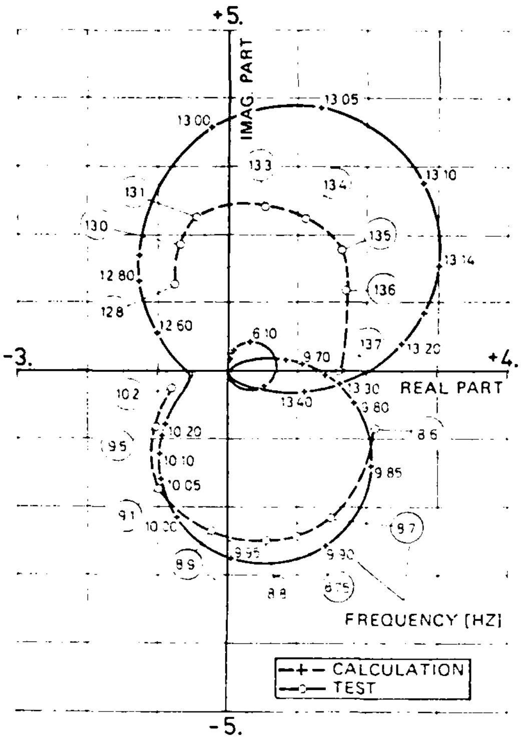

FIG. 9 OPEN LOOP DIAGRAM OF THE PITCH AXIS AT ZERO AIRSPEED (WITHOUT NOTCH FILTER).

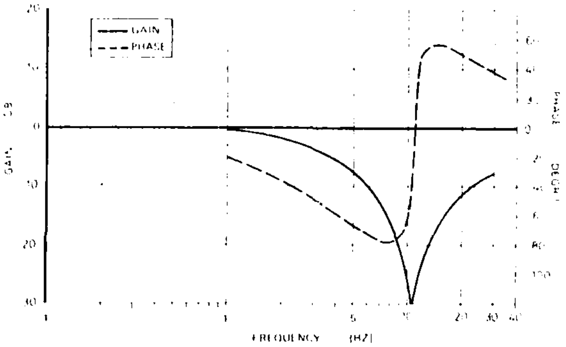

FIG. 10 PITCH AXIS STRUCTURAL MODE FILTER CHARACTERISTICS.

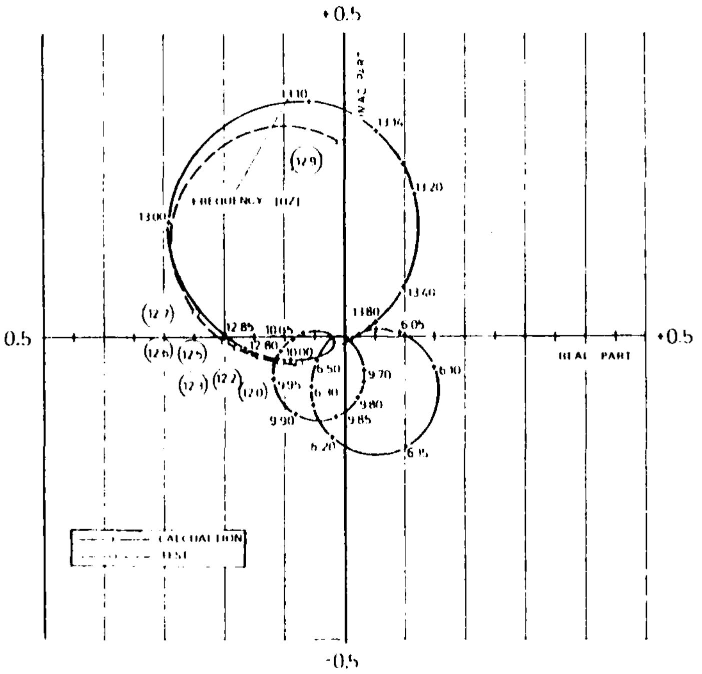

FIG. 11 OPEN LOOP DIAGRAM OF THE PITCH AXIS WITH NOTCH FILTER ENGAGED AT ZERO AIRSPEED.

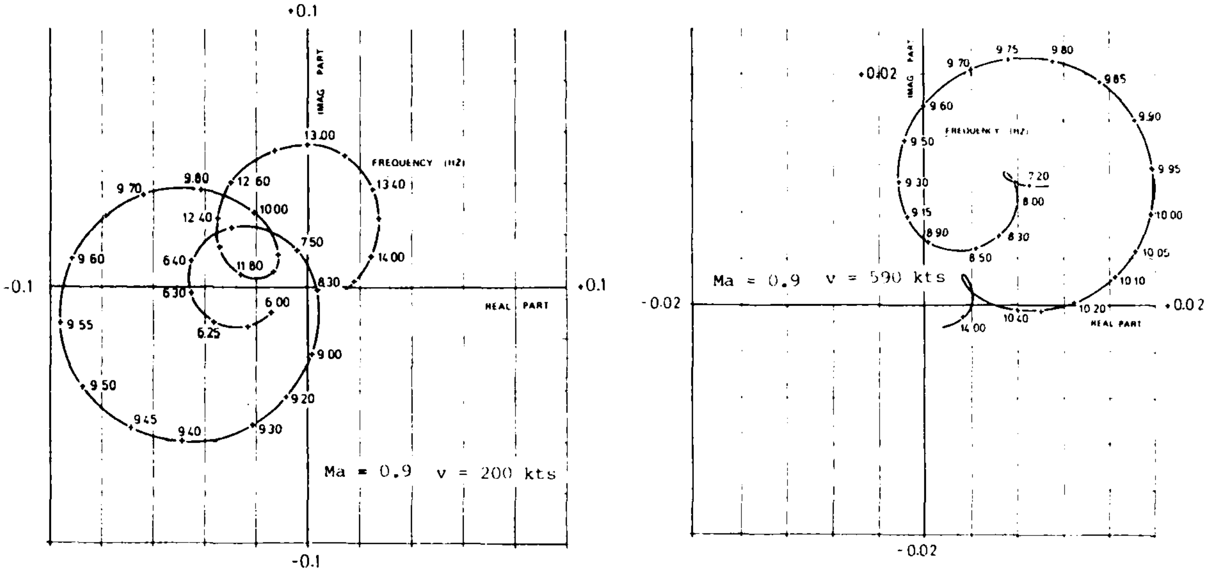

FIG. 12 EFFECTS OF UNSTEADY AERODYNAMIC FORCES AT VARIOUS AIRSPEEDS FOR THE PITCH AXIS.

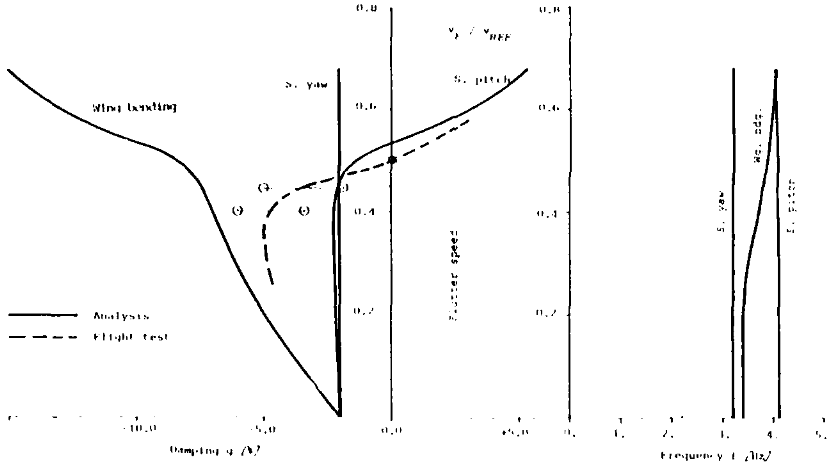

FIG. 13 RESULTS OF CONVENTIONAL FLUTTER ANALYSIS COMPARED WITH FLIGHT TEST RESULTS. INBOARD AND OUTBOARD STORE CARRIAGE.

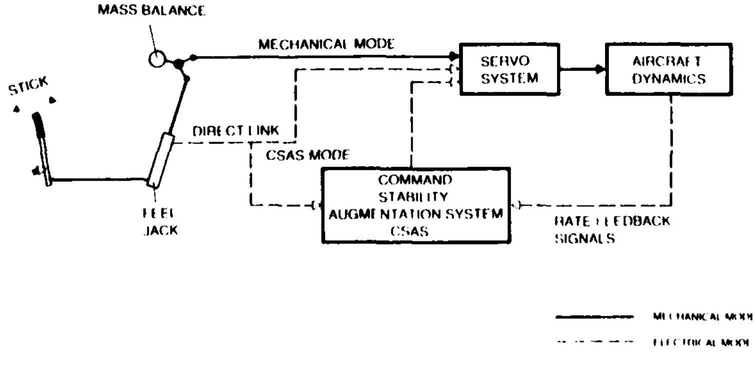
MASS BALANCE
MECHANICAL MODE
SERVO SYSTEM
AIRCRAFT DYNAMICS
STICK
DIRECT LINK
CSAS MODE
COMMAND STABILITY AUGMENTATION SYSTEM CSAS
FEEL JACK
RATE FEEDBACK SIGNALS
MECHANICAL MODE
ELECTRICAL MODE

FIG. 14 PRINCIPLE FLOW DIAGRAM OF THE PITCH CONTROL LINE.

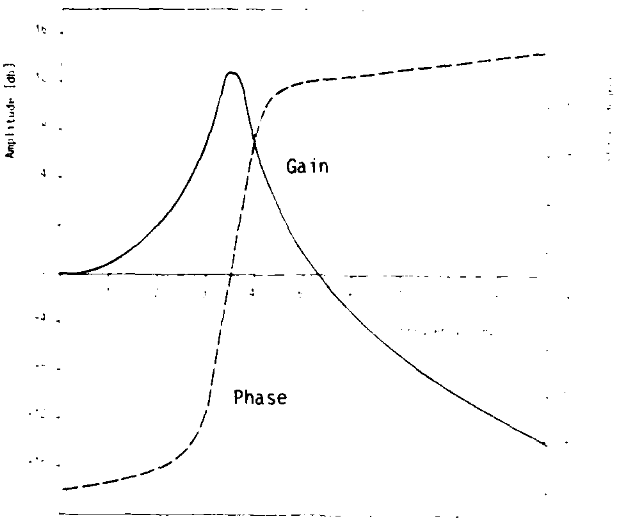

FIG. 15 FREQUENCY RESPONSES MEASURED ON THE RIG MOUNTED PITCH CONTROL LINE IN DIRECT LINK.

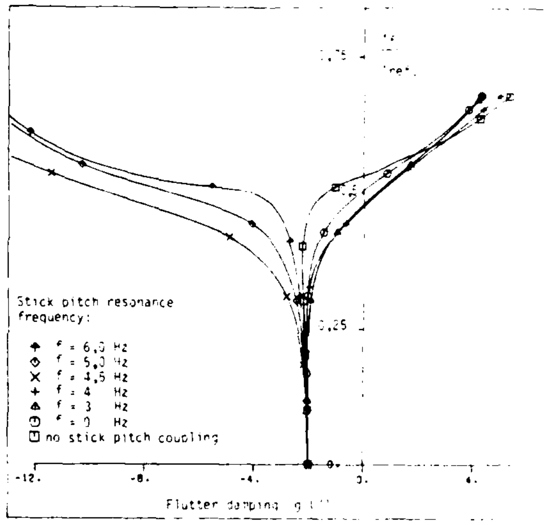

FIG. 16 VARIATION OF CALCULATED FLUTTER DAMPING WITH STICK PITCH RESONANCE FREQUENCY. UNBALANCED CONTROL LINE. CSAS MODE: DIRECT LINK.

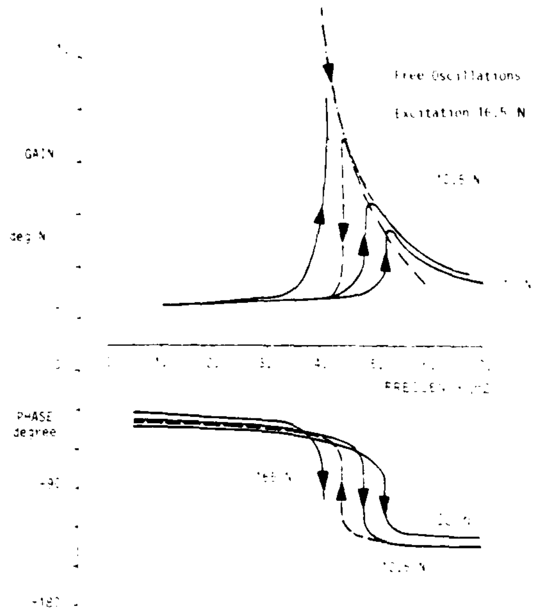

FIG. 17 FREQUENCY RESPONSES OF THE PITCH CONTROL LINE MEASURED ON THE AIRCRAFT.

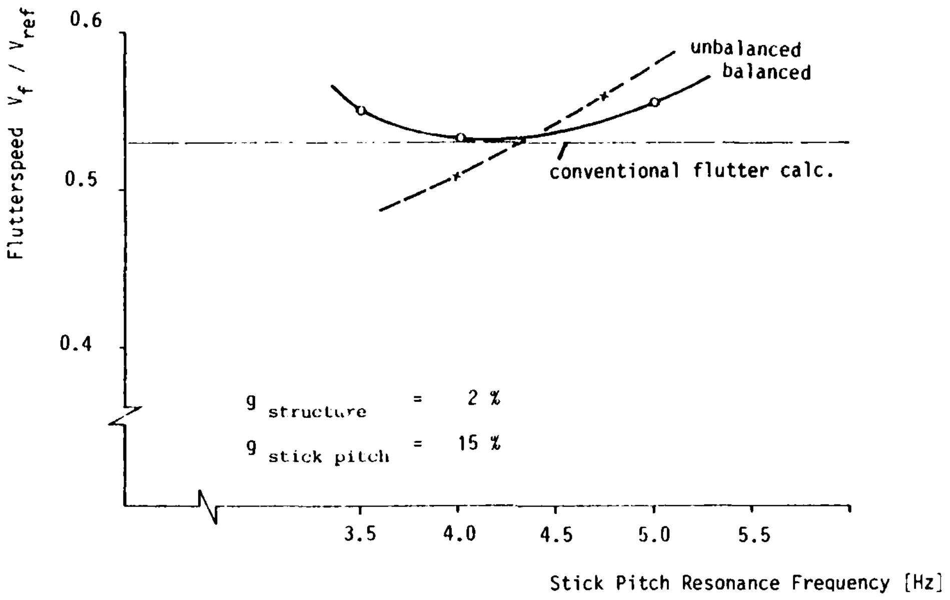

FIG. 18 VARIATION OF CALCULATED FLUTTER SPEED WITH STICK PITCH RESONANCE FREQUENCY FOR DIFFERENT BALANCE CONDITIONS.

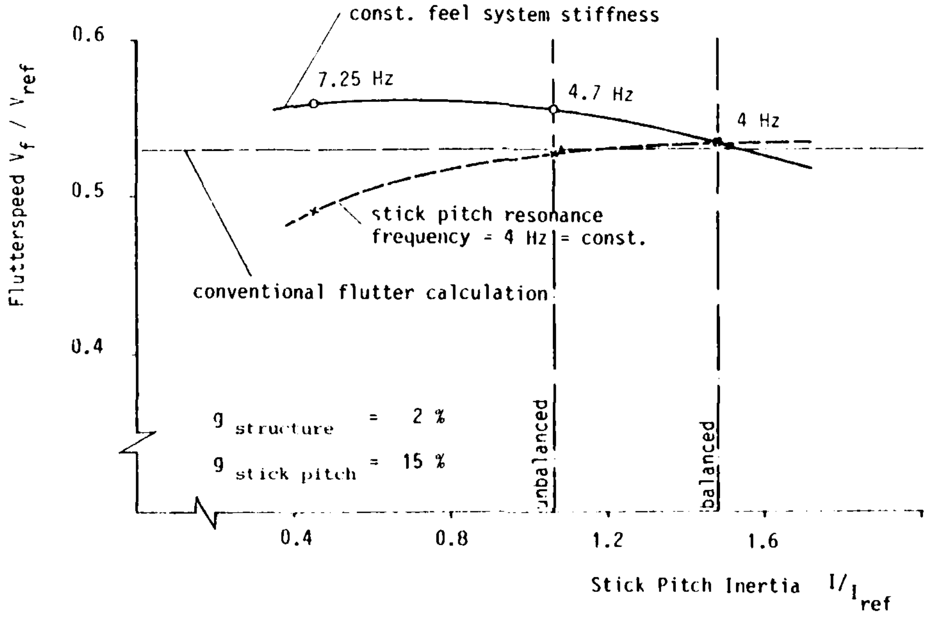

FIG. 19 INFLUENCE OF CONTROL LINE PITCH INERTIA ON CALCULATED FLUTTER SPEEDS.

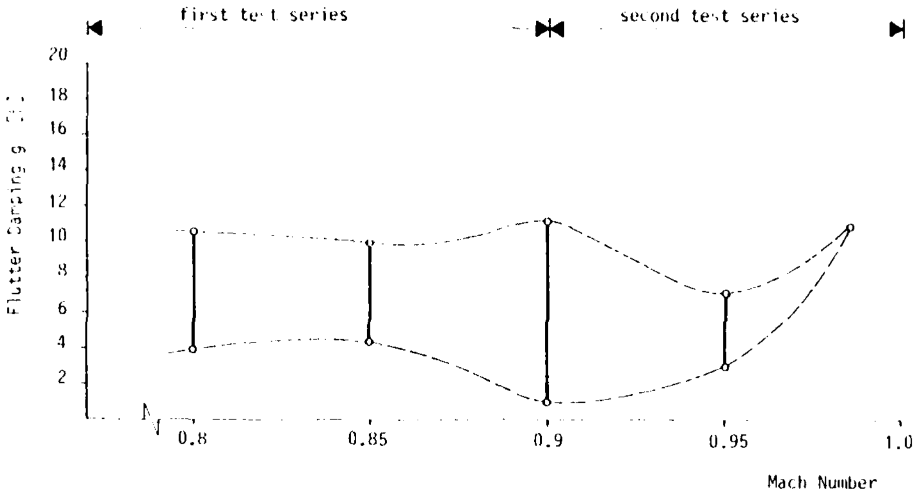

FIG. 20 IN FLIGHT MEASUREMENTS OF WING BENDING DAMPING FOR OUTBOARD STORE CARRIAGE VERSUS MACH NUMBER.

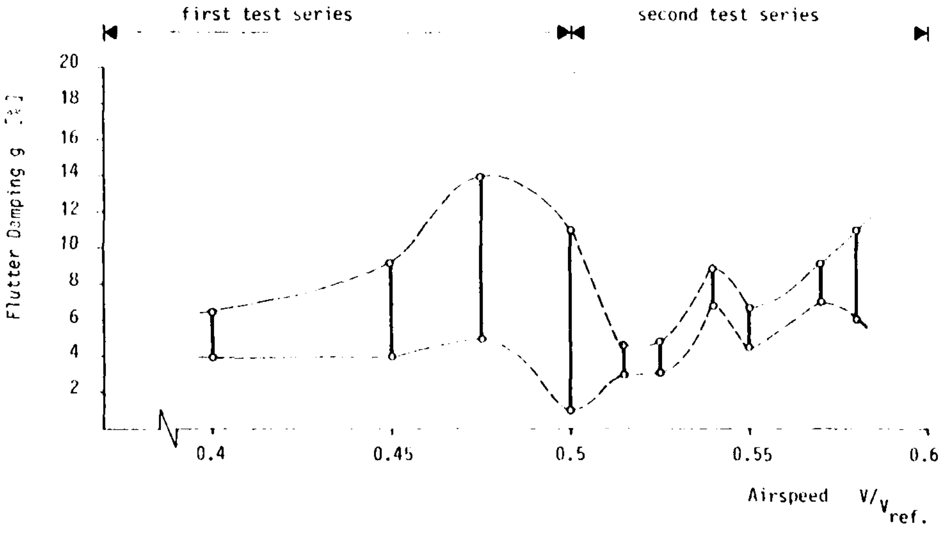

FIG. 21 IN FLIGHT MEASUREMENTS OF WING BENDING DAMPING FOR OUTBOARD STORE CARRIAGE VERSUS AIRSPEED.

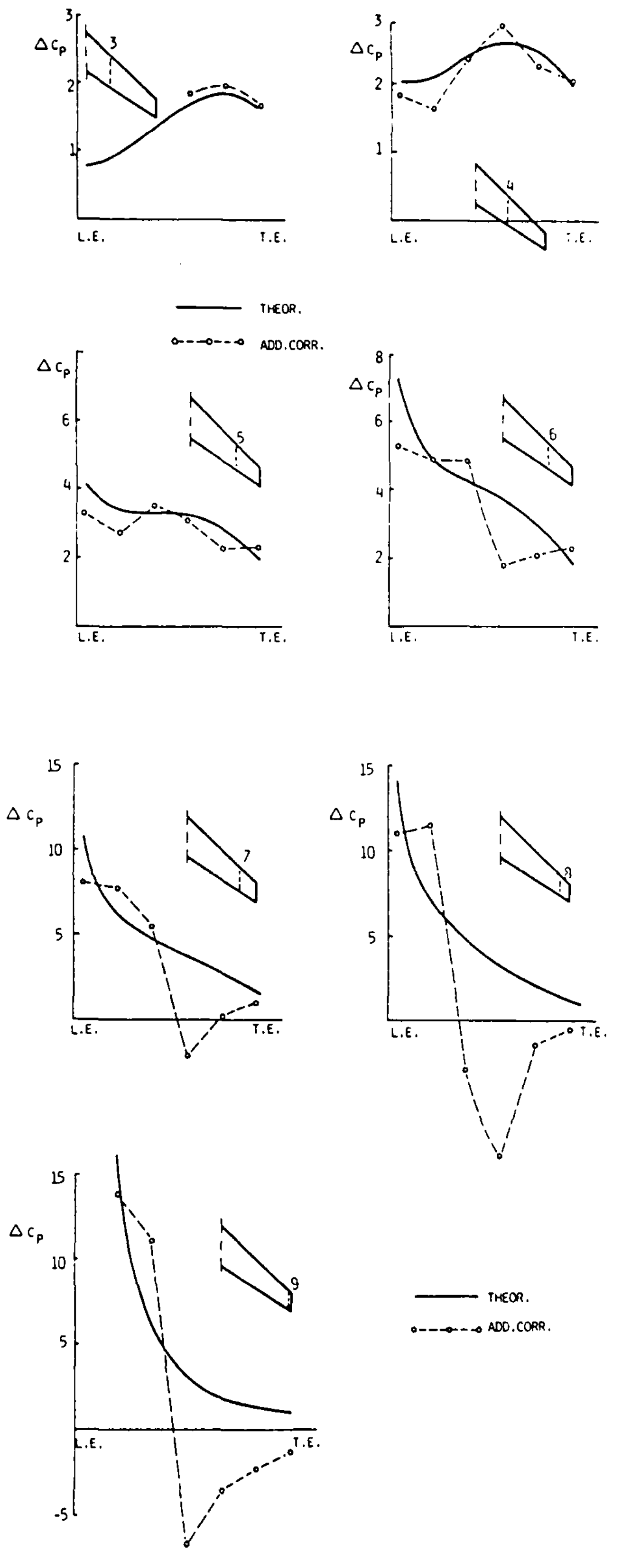

FIG. 22 THEORETICAL AND CORRECTED CHORDWISE PRESSURE DISTRIBUTIONS AT M = 0.9.

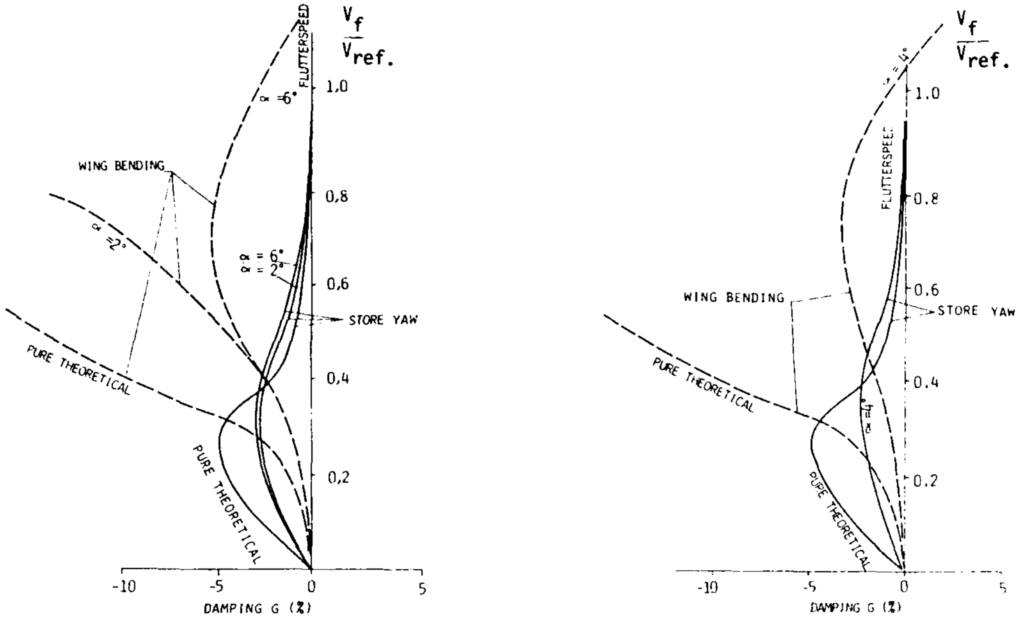

MACH = 0.9 **MACH = 0.95**

FIG. 23 VARIATION OF DAMPING WITH FLUTTER SPEED FOR OUTBOARD STORE CARRIAGE.

REAL-TIME FLUTTER ANALYSIS OF AN ACTIVE FLUTTER-SUPPRESSION SYSTEM ON A REMOTELY PILOTED RESEARCH AIRCRAFT

Glenn B. Gilyard
NASA Ames Research Center
Dryden Flight Research Facility
P.O. Box 273
Edwards, California 93523, U.S.A.

John W. Edwards
NASA Langley Research Center
Hampton, Virginia 23665, U.S.A.

SUMMARY

Flight flutter-test results of the first aeroelastic research wing (ARW-1) of NASA's drones for aerodynamic and structural testing (DAST) program are presented. The flight-test operation and the implementation of the active flutter-suppression system are described. The software techniques used to obtain real-time damping estimates and the actual flutter testing procedure are also described in detail. Real-time analysis of fast-frequency aileron excitation sweeps provided reliable damping estimates. The open-loop flutter boundary was well defined at two altitudes; a maximum Mach number of 0.91 was obtained. Both open-loop and closed-loop data have been of exceptionally high quality. Although the flutter-suppression system provided augmented damping at speeds below the flutter boundary, an error in the implementation of the system resulted in the system being less stable than predicted. The vehicle encountered system-on flutter shortly after crossing the open-loop flutter boundary on the third flight and was lost. The aircraft has been rebuilt, and initial testing is scheduled for the fall of 1982. Changes made in real-time test techniques are included.

SYMBOLS AND ABBREVIATIONS

ARW-1	advanced research wing no. 1
ARW-1R	advanced research wing no. 1, rebuilt
a_z	normal acceleration, g
CMP	control and monitor panel
$d\varphi/d\omega$	rate of change of phase, deg/deg
DAST	drones for aerodynamic and structural testing
f	frequency, Hz
F	Fourier transform
FSS	flutter-suppression system
G_c	common filter-transfer function
G_s, G_a	symmetric and antisymmetric filter-transfer functions
GVT	ground vibration test
H	altitude, m (ft)
$H(s)$	single-degree-of-freedom transfer function
i	$\sqrt{-1}$
K	FSS gain
M	Mach number
M_f	flutter Mach number
PCM	pulse code modulation
RPRV	remotely piloted research vehicle
s	Laplace transform variable, rad/sec
S_{xx}	auto-spectrum of x
S_{xy}	cross-spectrum between x and y
t, T	time, sec
u	intermediate FSS variable
α	angle of attack, deg
δ, δ_a	aileron position, deg
ζ	damping ratio
σ	$\zeta\omega$
$\ddot{\varphi}$	center-of-gravity roll acceleration, rad/sec^2
ω	frequency, rad/sec
Subscripts:	
c	command variable
cg	center of gravity
l, r	left, right
s, a	symmetric, antisymmetric
tm	tip mass

1.0 INTRODUCTION

Correlation of theoretical predictions and experimental flight-test results of aeroelastic effects in the high subsonic to transonic speed range are of great interest because aeroelastic effects frequently are critical in aircraft design. An objective of NASA's drones for aerodynamic and structural testing (DAST) program (Ref. 1) is to pursue investigations within this speed range, using a series of aeroelastic research wings (ARW) which will be flight tested in combination with a modified Firebee II target drone vehicle fuselage utilizing the remotely piloted research vehicle (RPRV) technique (Ref. 2). DAST is a joint program of Langley Research Center and the

Dryden Flight Research Facility, Ames Research Center. The flight tests described in this paper were supported under contract by the Boeing Military Aircraft Company, Wichita Division. The first wing to be tested in the DAST program, denoted the ARW-1, is a sweptback, supercritical airfoil, transport-type wing with a performance design point of $M = 0.98$ at 13.72 km (45,000 ft).

The primary research objective of the ARW-1 is to investigate, through flight test, those systems synthesis and analysis techniques applicable to active control of flutter, utilizing an on-board analog flutter-suppression system (FSS). A secondary objective is to use flight test to validate analysis techniques for aerodynamic loads predictions. The use of the RPRV technique poses special considerations in the conduct of the flight testing, because test time per flight is quite limited and a higher probability of vehicle loss can be an accepted risk. As such, the flight testing of the ARW-1 had the additional objective of developing flutter-test techniques for use under these conditions.

This paper presents details of the flutter-test technique development and of the implementation of the FSS on the vehicle. Frequency and damping estimates obtained from flight tests using this real-time estimation technique are compared with predictions from Ref. 3. Newsom and Pototsky (Ref. 3) present details of the mathematical modeling and FSS design, and Bennett and Abel (Ref. 4) present more detailed frequency and damping estimates obtained using a postflight parameter-estimation technique. Three operational flights of the ARW-1 were conducted.

Because of an error in the implementation of a gain in the FSS, the vehicle experienced flutter on the third flight; the flutter caused the right wing to separate and there was further damage caused by ground impact. The aircraft has been rebuilt and is approaching a new phase of flight testing. Improvements made in the real-time flutter-test techniques are included in this paper.

2.0 DAST SYSTEM DESCRIPTION

The first wing to be tested in the DAST program is a 6.8 aspect ratio, sweptback, transport-type wing with a supercritical airfoil shape. Design of this wing and the active flutter-suppression system is described in Refs. 1 and 5. Although the supercritical wing design point was at $M = 0.98$ and $H = 13.72$ km (45,000 ft), the achievement of the active flutter-suppression experiment goal of a 20% increase over the unaugmented flutter speed was to be accomplished at altitudes of only 3.05-4.57 km (10,000-15,000 ft). The basic Firebee drone has no wing control surfaces; it is controlled by deflections of the collective and differential horizontal stabilizer and rudder. The ARW-1 retained this method of flight control, thus leaving the wing ailerons free to perform the flutter-suppression fuction.

Figure 1 shows the overall planform of the vehicle. The wing was constructed with front and rear steel spars, with torsional stiffness provided by fiberglass skins. The wing leading and trailing edges are constructed of fiberglass; the wing span is 4.30 m (14 ft). To produce wing flutter within the operational envelope of the vehicle, torsional stiffness was intentionally reduced by orienting the fiberglass filaments at 0° and 90° to the front spar. During wing fabrication, it became apparent that the torsional stiffness was higher than predicted, resulting in a predicted flutter boundary at a higher Mach number than desired. To reduce the flutter Mach number, 0.91 kg (2 lb) of wingtip ballast (encapsulated lead shot) was added.

2.1 Tip-Mass Release System

Automatic or manual jettison of the tip masses was viewed as a desirable feature in order to aid recovery from inadvertent large-amplitude wing oscillations. This was accomplished on the ARW-1 by sensing wingtip accelerations and firing a pyrotechnic device to allow the lead-shot ballast to be thrown out of its container. The automatic firing sequence was initiated when the rms wingtip acceleration exceeded a 10.6-g threshold, with the actual firing occurring after a delay determined by the rms acceleration level in excess of the threshold. For instance, a sinusoidal wingtip oscillation of ±15 g's (10.6 g's rms) at 20 Hz would cause tip mass firing after 12 cycles of oscillation, and an amplitude of ±30 g's would release the masses after 3 cycles. The threshold g-level was selected based on the acceleration causing saturation of the FSS compensator. It was predicted that structural failure of the wing would not occur until wingtip accelerations reached 64 g's and that compressive stress of the wing skin along the 25% chord line was the critical stress. It was anticipated that this automatic tip-mass release system could save the wing structure in event of mildly divergent wing oscillations. A backup manual tip-mass release capability was provided for the flutter-test experimenters for activation at their discretion. Reference 1 describes a wind-tunnel test of this tip-mass release technique in which a solid weight was manually released at the open-loop flutter boundary when mildly divergent oscillations were observed. The wing response changed quickly to stable convergent oscillations, indicating an incremental increase in damping.

2.2 Mathematical Model

A NASTRAN finite-element model of the ARW-1 and Firebee fuselage-empennage was constructed and ground vibration tests (GVT) were performed on the vehicle. Table 1 presents comparisons of the frequencies obtained by NASTRAN and GVT; the results show fair to good agreement between the two. The differences between NASTRAN and GVT in first wing-bending-mode frequencies (0.5 Hz for symmetric and 1.2 Hz for antisymmetric) are larger than desirable; however, attempts to refine the NASTRAN model did not significantly improve the agreement with the GVT results.

Aeroelastic analysis, using a doublet lattice computer program, predicted classical wing bending-torsion flutter in both symmetrical and antisymmetrical modes at nearly identical altitude/Mach number conditions. In both cases, the lower frequency first wing-bending modes near 10 Hz combined with the bending-torsion modes near 30 Hz to produce flutter modes in the range of 15-20 Hz, with the lower frequency bending modes becoming the unstable flutter modes.

2.3 Instrumentation

All on-board data measurements were telemetered to the ground via two pulse-code modulation (PCM) telemetry systems; there was no on-board recording capability. The critical flutter parameters, such as accelerations, aileron deflections, excitation signal, and servo commands, were transmitted at the maximum rate of 500 sps. All of these signals were analog-prefiltered to prevent aliasing, with most channels incorporating 70-Hz, sixth-order filters. The remaining primary PCM system parameters consisted of 46 signals sampled at 50, 100, and 250 sps comprising a standard flight-test instrumentation lineup. The secondary PCM system (Ref. 6) monitored sensors, installed in the wing, that were devoted to the loads experiment. There were 86 static upper and lower surface pressure sensors and 16 strain gages.

3.0 FLUTTER-SUPPRESSION SYSTEM

The flutter-suppression system (FSS) was designed and fabricated under contract (Ref. 5) and was implemented as an on-board analog system, as shown in Fig. 1. No redundancy was provided for any of the systems' sensors, electronics, or actuators. The 23%-chord ailerons have a 0.254 m (10 in) span and are located just inboard of the wing closure rib. During the FSS design study, combinations of two accelerometers on each wingtip were considered for sensing wing motion, but a single accelerometer mounted on the rear spar at the outboard aileron edge was chosen.

Miniaturized rotary-vane hydraulic actuators (Ref. 7) were used to control the aileron motion. Figure 1 shows the location of the hydraulic pump and accumulator and the electrohydraulic servovalves which were separated from the actuators by 2.14 m (7 ft) of hydraulic tubing. The control surfaces were stabilized with position and differential pressure feedback. The bandwidth of these control surfaces proved to be a critical variable in the FSS design. Preliminary design of the FSS was accomplished assuming a mathematical model of the controls with a bandwidth of 100 Hz. When the controls were fabricated and bench tested, a 70-Hz bandwidth was achieved; when the control surfaces were installed in the wing, the final bandwidth was 50 Hz. The resulting phase lag (≈30° at 20 Hz) severely compromised the original FSS compensator design.

Since suppression of both symmetrical and antisymmetrical flutter modes was required, the FSS compensator was implemented by means of the summing and differencing networks shown schematically in Fig. 2. The left and right wingtip accelerations, a_{z_l} and a_{z_r}, were passed through common filters, G_c, and then summed to yield the symmetric intermediate signal, u_s, and differenced to yield the antisymmetric intermediate signal, u_a. In order to isolate the FSS dynamics from the lower-frequency rigid-body dynamics, the center-of-gravity acceleration, $a_{z_{cg}}$, was subtracted from each signal and the fuselage roll acceleration, $\ddot{\phi}$, was added to a_{z_l} and subtracted from a_{z_r}. The intermediate signals, u_s and u_a, were filtered by G_s and G_a, and the resulting signals summed, differenced, and multiplied by the gain, K, to yield the left and right aileron servo commands δ_{l_c} and δ_{r_c}.

Although predictions indicated that the reduced control-surface bandwidth previously mentioned would not allow achievement of a 20% increase in flutter speed, it was adequate for flutter suppression at speeds moderately above the flutter boundary, and it was retained for the first two flight operations. During this time period, the FSS was redesigned incorporating the reduced bandwidth characteristics of the servoactuator system. This redesigned system was used for the third flight but because of an implementation error, the flight system had one-half the nominal design gain.

Figure 3 presents the predicted performance of the above defined symmetrical FSS, showing the loci of the open-loop bending and bending-torsion modes versus Mach number. The open-loop bending mode goes unstable (flutters) at approximately $M = 0.83$ at a frequency of 100 rad/sec (16 Hz), and the open-loop torsion mode becomes heavily damped as Mach number increases. Also shown, near $\omega = 100$ rad/sec is the locus of the first fuselage bending mode, which indicates considerable coupling with the bending mode near M_f. The effect of increasing the gain from 0.0 to 1.0 is shown for $M = 0.75$, 0.85, and 0.90. Acceptable damping is achieved at all Mach numbers for nominal gain ($K = 1.0$), but the bending mode is predicted to be unstable above $M = 0.85$ at one-half nominal gain. The torsion mode is heavily damped by the FSS at all Mach numbers.

4.0 DAST OPERATIONAL TECHNIQUE

The flight-test operations of the DAST program utilize the RPRV technique developed by Dryden Flight Research Facility (Ref. 2). The Firebee II vehicle with the ARW-1 wing was air-launched from a B-52 aircraft, flew a preplanned flight track and test points, and was recovered in midair by an Air Force helicopter crew. With the ARW-1 wing installed, flight-test time for each flight varied between 15 and 30 min, depending on the flight conditions chosen. The vehicle was remotely controlled from a ground-based RPRV facility consisting of (1) a PCM telemetry downlink receiver and uplink transmitter, (2) a dedicated, simulation-type cockpit from which the test pilot controls the aircraft, and (3) a ground-based computer interfacing the telemetry links and the cockpit and also providing closed-loop remote control augmentation. In the event of loss of the command signal from the ground, a backup controller in an F-104 chase aircraft provides basic attitude control capability via an air-to-air telemetry link.

The telemetry downlink receives the signal from the primary PCM system described earlier, and the telemetry uplink transmits proportional PCM-coded stabilator, rudder, and throttle commands. The computer was programmed to provide the pilot with selectable augmentation modes in the pitch, roll, and yaw axes. Rate-damper, altitude-hold, and attitude-hold modes were provided in the pitch axis. The roll-axis augmentation consisted of roll-damper and bank-angle hold modes, and the yaw-axis augmentation consisted of a yaw damper. These modes were additive and, when flying straight and level, were all engaged. To perform turns, the pilot disengaged the bank-angle hold and selected roll-rate damping. The intent of these augmented modes was to allow the DAST pilot to control the small, highly responsive Firebee II vehicle and to concentrate maximum attention on Mach number and altitude so that the flutter-test points could be flown with precision. During the flight tests, the pilot was able to maintain the vehicle to within ±0.01 Mach number of the desired test-point conditions.

5.0 FLUTTER-TEST TECHNIQUE

There are two additional ground-based facilities for monitoring and controlling the progress of the flight test: the control room and the spectral analysis facility. The control room contains strip charts for monitoring the vehicle rigid-body stability and control functions and operational functions, radar plot boards for monitoring vehicle flightpath, and communication equipment required to coordinate the aircraft involved in the test. During flight tests, a test pilot is stationed in the control room to serve as flight director. In the past, the flight director was the only person to communicate directly with the test pilot, but this procedure has been modified for the DAST flutter-test operations. Because of the hazardous nature of active flutter control testing, it was recognized that direct communication between the flutter-test engineers and the test pilot was required. The flutter test monitoring was performed in a separate location, the spectral analysis facility (SAF).

5.1 Spectral Analysis Facility

The spectral analysis facility (SAF) is a dedicated facility designed to perform spectral analysis of a wide range of experiments as well as flutter testing. Figure 4 is a photograph of the SAF as it is configured for testing of the rebuilt ARW-1. The main elements consist of (1) a dedicated PCM decommutation station and patch panel, (2) a minicomputer-based fast Fourier analyzer (HP-5451C), (3) two x-y plotters, (4) a real-time spectral analysis display (SD-335, referred to as a Spectrascope), (5) the DAST control and monitor panel (CMP), (6) strip charts, (7) video cathode ray tube (CRT) displays, and (8) a plotter computer (TI-990).

Six flutter-test engineers are required for real-time flutter clearance: (1) flutter-test conductor, (2) primary FSS analyst, (3) Spectrascope operator, (4) control and monitor panel operator, (5) primary flutter strip-chart observer, and (6) FSS system health monitor. The flutter-test conductor oversees the conduct of the flutter testing and as such is also in direct communication with the RPRV pilot.

The capabilities of the control and monitor panel are (1) FSS on or off, (2) frequency sweep or pulse excitation, (3) symmetric or antisymmetric excitation, (4) low or high excitation, (5) auxiliary filter in or out switch, and (6) tip-mass release switch. In addition, the primary flutter strip-chart observer is provided a pickle switch to remotely jettison the tip masses.

The Spectrascope is used as a "quick-look" instrument, capable of providing real-time spectral estimates of one of 12 preselected parameters. The Spectrascope has selectable bandwidths and is used primarily to look for problem areas other than those associated with the primary flutter frequencies. In this respect, it augments the Fourier analyzer, which is dedicated to the estimation of frequency and damping of the anticipated flutter modes.

Six channels of high-sample-rate data were input to the Fourier analyzer from the PCM station located in the SAF, using the multiplexer preprocessor. The data channels for ARW-1 were three wingtip accelerations, two aileron deflections, and the FSS excitation signal. The Fourier analyzer computes transfer-function responses of the aileron sweep maneuvers from which frequency and damping are estimated. These results are displayed on the CRT unit. The frequency and damping estimates are also summarized on the x-y plotters: one for symmetric modes and one for antisymmetric modes.

The procedure has been automated such that the Fourier analyzer lights a ready light on the CMP. At this point the CMP operator can initiate the next maneuver command, providing flutter clearance has been granted and the aircraft is at proper flight conditions. Once the maneuver is commanded, a trigger signal is sent to the Fourier analyzer to initiate data gathering.

5.2 FSS Excitation

Flight flutter-test techniques (Refs. 8 and 9) have traditionally relied heavily on long-duration testing to obtain random turbulence excited response or on slow-frequency sweeps to obtain quasi-steady-state forced response. The goal in any case is to obtain reliable estimates of critical mode damping to allow flight testing to proceed. The introduction of minicomputer-based Fourier analyzers utilizing fast-Fourier-transform techniques, coupled with the measurement of both the input forcing function (control-surface displacement) and the response (wing acceleration), allows the use of the transfer-function analysis and greatly reduces test time. Quasi-steady-state test methods are no longer necessary, and fast-frequency sweeps were chosen as the preferred method of excitation. The excitation was summed with the FSS feedback signals, allowing the ailerons to be used both to excite the wing and to control the flutter mode. A logarithmic frequency sweep function was implemented as

$$\delta_{a_c} = A \times \sin\left[a \times \omega_0 \times ln\ (a - t)\right]$$

where $a = \omega_1 \times T/(\omega_1 - \omega_0)$ with ω_0 and ω_1 the starting and stopping fequencies and T the sweep duration. Sweep amplitudes, A, of 1° and 2° were available. Since the predicted flutter frequency was near 20 Hz, the starting and stopping frequencies were chosen to be 10 and 40 Hz. A sweep duration of 7 sec was chosen, based on an 8-sec period required for the Fourier analyzer to take 4,096 data points at the maximum rate of 500 samples per second. This allowed 0.5 sec settling time at the start and end of the sweeps for transients to die out. In addition, the sweep-command amplitude was tapered at the beginning and end to eliminate transients (Ref. 10). In addition to the sweeps, a capability to pulse the ailerons was included so that the test engineers could monitor transient reponses. The pulse consisted of a single cycle of a 20-Hz sine wave with an amplitude of either 1.7° or 3.4°. The primary benefit of the pulsing command was to monitor structural damping during periods when changing flight conditions.

5.3 Transfer-Function Smoothing

Because of the limited flight time available for a given flight, as well as the possibility of losing the aircraft during the midair recovery process, efficient use of flight time was critical. Considerable effort was devoted to minimizing the time required for single-mode frequency and damping estimates, thereby minimizing operator interaction.

The real-time method arrived at is diagrammed in Fig. 5 for open-loop analysis. The raw transfer-function estimate of acceleration response to aileron deflection was obtained as the cross-spectrum, $S_{a_z\delta_a}$, divided by the input autospectrum, $S_{\delta_a\delta_a}$. Minimal input power existed outside the range of the frequency sweep; therefore, the transfer function was set to zero below 10 Hz and above 40 Hz. For closed-loop analysis, the FSS excitation is used in place of the aileron deflection.

Normally it is desirable to obtain multiple maneuvers and perform averaging in order to produce reliable transfer-function estimates. A single raw transfer-function estimate quite often will produce poor results because of noise, truncation, and unknown (i.e., turbulence) forcing functions. When averaging is not feasible, ad hoc smoothing techniques are quite often required to enhance the usefulness of the data. In the DAST program, the luxury of multiple maneuvers was not available and therefore, the raw transfer-functions produced were quite rough.

A number of techniques have been investigated for smoothing the raw transfer function, the first of which was application of an exponential window (Ref. 11). Benefits of the exponential window are ease of application and the simple damping correction factor at resonant frequencies. The inverse Fourier transform of the transfer function, F^{-1}, yields an estimate of the impulse-response function. Block multiplication of the impulse response by e^{-t} forces the function to zero and minimizes extraneous effects for large values of t. The Fourier transform of the smoothed impulse response yields the smooth transfer function. The frequency and damping estimates are then made from this transfer function. The exponential window effects representing the raw and smoothed transfer functions of a_z/δ_a from a symmetrical FSS OFF sweep at $M = 0.74$ and an altitude of 4.57 km (15,000 ft) are presented in Figs. 6 and 7. The magnitude and phase of the raw transfer function are presented in Fig. 6; the results of smoothing with the window e^{-t} are in Fig. 7. The lightly damped mode at $f = 13.3$ Hz is wing bending, and the smaller mode near 16 Hz is first vertical fuselage bending. This window was used during the initial ARW-1 testing.

5.4 Damping Estimation

The smooth transfer function is used to estimate the frequency and damping of the dominant resonant peak. Although many techniques for extracting resonant mode characteristics are available, a primary requirement was for a relatively simple, automated, real-time procedure. The technique selected consisted of searching for the peak magnitude of the transfer function and then, at that frequency, determining a damping estimate from the slope of the phase curve. Damping of a single-degree-of-freedom transfer function $H(s)$ where

$$H(s) = \frac{\omega^2}{s^2 + 2\zeta\omega s + \omega^2}$$

is given by

$$\zeta = \frac{-1.0}{\omega(d\varphi/d\omega)}$$

where $d\varphi/d\omega$ is the slope of the phase curve at resonance. The frequency of the peak resonance was estimated by means of a least-squares curve fit of a quadratic function to the five points nearest the peak magnitude. For the first three ARW-1 flights, a five-point least-squares curve fit of a cubic function to the phase curve was used. The derivative of the function was then taken to obtain the slope. For well-defined resonances, this five-point cubic fit provided good damping estimates. The real-time frequency and damping estimates are implemented in the Fourier analyzer in a fully automatic mode.

The first two flights of ARW-1 utilized the program with the maximum data block size available in order to obtain the best results possible (block size of 4096, 500 sps). This block size required 15 sec to process each transfer-function estimate and obtain frequency and damping estimates. Postflight data processing indicated that equivalent results could be obtained with a smaller block size and the third flight utilized the program with a block size of 1024 and a sample rate of 100 sps. This reduced the processing time to 5 sec.

The ARW-1 flight testing was accomplished at constant altitude, using preplanned Mach number increments of 0.050 and 0.025. The test procedure at each flight condition depended on whether the flight condition was above or below the predicted open-loop flutter Mach number. At conditions below the flutter boundary, a sequence of four sweeps was used: (1) symmetric, FSS OFF, (2) antisymmetric, FSS OFF, (3) antisymmetric, FSS ON, and (4) symmetric, FSS ON. Beyond the open-loop flutter boundary, the FSS could obviously not be turned off and only the two FSS ON sweeps were to be obtained.

The left and right wing aileron positions and accelerations were summed and differenced to provide signals for symmetric and antisymmetric processing. For FSS OFF tests, transfer functions of acceleration due to aileron motion provided open-loop damping estimates, and transfer functions of acceleration due to the excitation signal provided closed-loop damping estimates for the FSS ON tests. For the FSS ON sweeps, transfer-function estimates were also obtained for wing acceleration due to aileron motion in an attempt to determine the open loop damping from closed-loop data. This technique requires that the data be relatively noise free and also free from extraneous inputs such as atmospheric turbulence.

6.0 FLIGHT TEST RESULTS

It was anticipated that the objectives of the flutter-suppression tests could be accomplished in six flights (Ref. 1). Testing was planned at low, medium, and high altitudes, with the FSS design point to be reached on the fourth flight at 3.05 km (10,000 ft). The first flight was to be devoted to subcritical testing, exercising the FSS at Mach numbers no closer than 0.1 M to the predicted flutter boundary. The second flight was to test 0.05 M past M_f with the FSS engaged. Figure 8 shows the test points that were achieved on the three flights of the ARW-1 and gives the predicted flutter boundaries that were used to plan the third flight. Boundaries are shown for FSS OFF and ON and for the tip masses ON and OFF. The open symbols in Fig. 8 denote test points at which only FSS OFF testing was accomplished, and the half-open symbols indicate test points for both FSS OFF and FSS ON testing. Solid symbols indicate those points that were predicted to be at or above the flutter Mach number, and thus only FSS ON testing was done.

There were several difficulties during the first flight, including failure of the FSS hydraulic pump and intermittent loss of the telemetry uplink command signal; the latter resulted in a premature flight termination.

At the first test point on the second flight ($M = 0.7$ at 6.10 km (20,000 ft)) a 200-Hz, limited amplitude instability was observed when the FSS was engaged. Similar instabilities had been encountered during ground testing; they were caused by the interaction of the high-bandwidth aileron control systems with the structure. These hydraulic resonances observed during ground testing were controlled with notch filters, and when they were observed in flight it was decided to terminate FSS ON testing for the remainder of the flight, even though the FSS was providing excellent control of the bending modes at the first test point. The flight lasted 25 min and test data were obtained from 14 frequency sweeps and 177 pulses. The flight resulted in a very good definition of the flutter boundary at approximately $M = 0.92$ and 7.62 km (25,000 ft) (Fig. 8), whereas analysis had predicted $M_f = 0.95$ at this altitude. This led to the incorporation of a correction factor (Ref. 3) into the unsteady airloads; this factor was based on the ratio of the static rigid-body lift-curve slope measured during a wind-tunnel test to its predicted value. This correction factor was included in the predictions used in the planning of the third flight.

The objective of the third flight was to test 0.05 M past the open-loop flutter boundary at 4.57 km (15,000 ft) and 6.10 km (20,000 ft). Flight planning was based on the more conservative flutter boundary estimated from the first two flights (Fig. 8) rather than the predicted flutter boundary, and $M = 0.825$ was the highest Mach number to be tested at 4.57 km (15,000 ft). Flight three continued for 10 min before the flutter incident, during which time four test points were achieved and data were obtained from 12 frequency sweeps and 75 pulses.

6.1 Frequency-Sweep Data Analysis

The quality of the flight-test data obtained from the ARW-1 was extremely good. The average rms background acceleration level was approximately 0.25 g's, and responses due to FSS excitation signals ranged up to 10 g's. Consequently, the signal-to-noise ratio was very high. Figure 9 shows time histories of symmetric aileron sweep maneuvers with FSS OFF and FSS ON (low amplitude) at $M = 0.74$ and at 4.57 km (15,000 ft). Left and right wing tip accelerations and aileron deflections are presented along with the frequency-sweep excitation. The resonance of the bending mode is clearly seen in the FSS OFF sweep of Fig. 9(a), whereas this mode is heavily damped in the FSS ON sweep of Fig. 9(b). Figure 10 gives the frequencies and dampings obtained during the second flight at 7.62 km (25,000 ft) by the real-time damping estimation technique. The frequencies near 25 Hz are from the more highly damped torsion modes and were determined from postflight analysis. The faired curves through the data points give very good indications of the FSS OFF flutter boundaries between $M = 0.91$ and 0.92 for both symmetric and antisymmetric modes. Although the solid lines in Fig. 10 are fairings of the real-time data, during the flight the frequency and damping estimates were plotted on graphs containing preplotted predictions.

The elimination of FSS ON testing due to the 200-Hz instability during the second flight left ample flight time for repeat testing at $M = 0.85$, 0.875, and 0.90; Fig. 10 indicates good repeatability of the damping estimates at these Mach numbers. Also, at $M = 0.85$, data were obtained from high-amplitude (±2°) frequency sweeps, and the resulting damping estimates shown in Fig. 10 indicate no appreciable amplitude effect at this Mach number. Between the second and third flights, the modified FSS compensator was implemented, including the one-half gain error described earlier. Figure 8 indicates test points at 4.57 km (15,000 ft) and at $M = 0.70$, 0.75, 0.775, and 0.80, which were achieved before the flutter incident at $M = 0.825$. The FSS ON nominal gain flutter boundary was predicted to be $M_f = 1.06$ at this altitude (Fig. 8).

The results of the real-time damping estimates obtained from sweeps on the third flight are presented in Figs. 11 and 12 (root locus plots were not maintained during the actual flutter testing). Comparisons of predictions and flight-test results are shown as s-plane root loci to better explain the effects of FSS OFF and ON and one-half nominal gain. Figure 11 presents the antisymmetric results. The predicted FSS OFF root loci of the bending and torsion modes are shown for $0.70 \leq M < 0.90$. Also shown are the predictions of the FSS ON dominant mode root loci for nominal and one-half gain. The effect of the FSS on the bending mode is to heavily damp the mode and lower its frequency for Mach numbers less than M_f; the torsion mode is slightly destabilized. Figure 11 indicates that the antisymmetric mode is predicted to be stable, even at one-half gain for Mach numbers up to 0.90. The flight-test frequency and damping estimates are indicated by solid symbols; good agreement with these predictions is apparent. The flight test open-loop bending mode frequencies shown near 100 rad/sec agree well with predictions, although the damping is overpredicted. The flight-test results appear to project to an open loop flutter boundary at a lower Mach number and frequency than those predicted. The results from the third test point at $M = 0.775$ are believed to be less reliable than the others, since extraneous wing responses, possibly because of atmospheric turbulence, were observed at this test point. The FSS was kept on for the $M = 0.775$ and 0.80 cases; therefore, FSS OFF data were calculated from the FSS ON sweep data.

The FSS ON antisymmetric response of the wing correlates well with predictions, as shown by the closed symbols near 160 rad/sec in Fig. 11. Again the $M = 0.775$ result appears to be erratic, and the other three estimates are close to their predicted values, especially at $M = 0.80$. Reference 4 presents frequency and damping estimates of both the bending and torsion modes obtained from postflight analysis, and Ref. 3 gives more details of the predicted response.

Similar information for the symmetric case is presented in Fig. 12. The estimated FSS OFF frequencies and dampings near 80 rad/sec are lower than predicted and project to an open-loop flutter Mach number lower than that predicted. The trend toward instability is in reasonable agreement. As with the antisymmetric case, the results from $M = 0.775$ appear erratic. The effect of the one-half gain error is much more severe in this case, with instability predicted above $M = 0.85$ with FSS ON. Also, the rate of change of damping of the one-half gain locus between $M = 0.825$ and 0.850 indicates a very violent flutter onset, whereas the nominal-gain locus, which was anticipated during the flight, indicates increased damping above $M = 0.825$. The nominal and one-half gain locus have been shown only for the most critical structural mode.

The real-time FSS ON damping estimates for $M = 0.70$ and 0.75 were off scale and are not shown. The more accurate postflight damping estimates of Ref. 4 for these Mach numbers give values of $\zeta \approx 0.13$ and of $\omega \approx 125$ rad/sec, corresponding to a root location at $s \approx 16 \pm i125$ rad/sec, close to the predicted location. Thus, the real-time damping estimation appears to be suspect for damping ratios greater than 0.10. The frequency and damping estimate obtained from the sweep data at $M = 0.80$ and the frequency of the flutter mode at $M = 0.825$ correlate very well with the trend of the predicted one-half gain locus. Particularly interesting is the fact that the doublet-lattice aerodynamic theory predicted the control-surface effectiveness very well. The mathematical model predicted an increase of bending-mode frequency from $\omega = 95$ rad/sec to 131 rad/sec for the one-half gain FSS at $M = 0.80$, whereas the flight data show an increase from 87 rad/sec to 125 rad/sec.

6.2 Pulse Data

Pulse-response data were, in general, obtained at all times except when sweep responses were being measured. Pulse responses were performed in all four possible configurations of FSS OFF or ON and symmetric or antisymmetric; amplitude was also selectable as low or high. The basic requirement for the pulses was to monitor structural damping characteristics by means of the strip chart. Figure 13 is a representative pulse response as observable on the strip chart and was obtained at a symmetric, open-loop configuration of $M = 0.907$ and at 7.62 km (25,000 ft). The pulse data have been analyzed, using postflight techniques to determine their usefulness for providing damping estimates and to study possible angle-of-attack effects on damping at transonic Mach numbers. For the antisymmetric mode, an increase in damping with increasing angle of attack is apparent, as reported in Ref. 12.

6.3 Nyquist Analysis

To gain insight into FSS degradation during the third flight, a postflight Nyquist analysis was performed on the eight FSS ON maneuvers. The maneuvers analyzed consisted of both symmetric and antisymmetric sweeps obtained at Mach numbers of 0.70, 0.74, 0.775, and 0.80. (The Nyquist analysis procedure used is discussed later.) The phase-margin results are presented in Fig. 14; gain-margin results are not presented, because they were not defined over the 10-40-Hz frequency range of interest. The phase-margin results appear to present a clear indication of FSS ON degradation for the symmetric mode. The system design goal had been to provide a minimum 30° margin over the entire FSS ON range. Although preflight predictions indicated the 30° minimum could not be obtained over the entire FSS ON range, the phase-margin results for the symmetric mode at $M = 0.80$ are significantly lower than expected. Although the trends are smooth, the Nyquist analysis of the symmetric sweep at $M = 0.775$ did produce a poor estimate and is the same maneuver referred to earlier as providing a poor (high) damping estimate, which in turn led to the impression the FSS was functioning normally. It should be noted that the Nyquist display of the suspect maneuver was very erratic and, as such, appears to provide a good indication of sweep-response quality.

6.4 Flutter Incident

As the third flight progressed, there was no indication of problems in the operation of the FSS and no warning evident to the flutter-test engineers that the FSS was operating at one-half nominal gain. The FSS ON test results for $M = 0.775$ and 0.80 shown in Figs. 11 and 12 are similar to those anticipated for the full-gain FSS. In particular, the symmetric damping estimate at $M = 0.775$ was misleading, as described above, and had a better estimate been obtained at this Mach number, the trend toward a violent flutter condition would have been apparent at $M = 0.80$. Since the results appeared to agree with the nominal-gain predictions, which indicated a minimum damping condition near $M = 0.80$, clearance was given to $M = 0.825$.

Typical accelerations for Mach increments of 0.025 required from 12 to 15 sec. During the acceleration from $M = 0.80$ to 0.825, several pulse responses were obtained showing increasingly lighter damping. The final pulse that preceded the flutter incident is shown in Fig. 15. Shown are the wingtip FSS accelerometer signals, the wingtip-mass release accelerometer signals, the aileron-position signals, angle of attack, and Mach number. As this pulse response was observed, the test pilot was instructed to terminate the test. The throttle was retarded at the 2.5-sec point, and the motion on the angle-of-attack trace at 3 sec is the result of pilot commands. In the remaining seconds before the flutter incident, however, the Mach number continued to increase. Mildly divergent oscillations at 20 Hz are seen at 3 sec where $M = 0.82$, and rapidly divergent oscillations occur at 4.5 sec where $M = 0.825$. Before the 5-sec point, where the FSS accelerometers go off scale, the oscillations doubled in amplitude in six cycles, corresponding to a negative damping of $\zeta = -0.02$. The ailerons saturated in amplitude two cycles later, followed by the firing of the tip-mass release pyrotechnics at 5.2 sec. (The automatic and manual tip-mass release commands occurred nearly simultaneously.) The saturation of the ailerons resulted in an effective gain reduction and the effect on the wing stability is shown in the $M = 0.85$ gain root locus of Fig. 3. The flutter mode frequency decreased from 20 Hz to 15 Hz, and the coupling with the 16-Hz fuselage bending mode is apparent in the oscillations seen in the angle-of-attack trace. The rate of growth of the oscillations was so large at the time of the operation of the tip-mass release system that the oscillations were not arrested. Structural failure of the right wing tip and aileron occurred at 5.4 sec followed by failure of the structural attachment of the right wing to the fuselage carrythrough structure at 5.6 sec. The resulting rolling gyrations at large angle of attack and sideslip caused subsequent partial failure of the parachute recovery system and the vehicle hit the ground.

It has been concluded that the primary cause of the flutter incident was the one-half gain setting error in the FSS.

7.0 REBUILT ARW-1

Because of an error in the implementation of the on-board FSS, the ARW-1 encountered flutter on the third test flight and was subsequently lost. At the time of the incident, all systems were functioning and the flutter suppression techniques applied to the ARW-1 appeared capable of achieving the design goals. Following the incident, a decision was made to rebuild the ARW-1 and complete the flutter-test series to verify the design goals. Although the fuselage structure of the Firebee drone was damaged beyond repair, the wing spars and many of the avionics systems were reusable. The vehicle (referred to hereinafter as ARW-1R) has been rebuilt with some small but important changes.

7.1 Aircraft and Systems Modification

The fiberglass skin of ARW-1 had a significant variation of stiffness versus stress characteristic because of the ply orientation of 0° and 90°. For ARW-1R, some plys are oriented at 45° which produces an improved stiffness versus stress relation (Ref. 13).

An improved tip-mass release system has been designed and implemented for ARW-1R testing. The redesign was required to provide a system that would react to a much more rapid flutter divergence than the previous system. In the new system, there are three ways in which the tip-mass release can be automatically activated: (1) if 2/3 control-surface authority is exceeded, (2) by a 12-g rms level over two cycles, or (3) by a 21-g peak value. Timing windows are used in the logic to minimize any spurious triggering.

An external centerline fuel tank has been added to the vehicle and will at least double flight-test time available. This will also permit a less aggressive testing procedure than was required for the initial vehicle.

The FSS system is being redesigned by Langley Research Center, and the same accelerometer locations and control surfaces will be used. The FSS compensator will require less high-frequency gain than the original system. New actuators have been fabricated which have improved frequency-response characteristics.

7.2 Real-Time Analysis Modifications

In preparing for ARW-1R flight testing, real-time Nyquist plot displays were investigated as a means of providing closed-loop gain and phase-margin information. For this type of data display, the exponential window has a significant shortcoming, in that the phase curve of the smoothed transfer function has a significant negative skew. This effect is observed by comparing the raw phase curve of Fig. 6 with the smooth phase curve of Fig. 7. The result is a rotation of the Nyquist plot which affects gain and phase-margin determination. This effect is due to the asymmetry of the exponential window. Inspection of the impulse response function shows significant (unphysical) information contained in the last half of the record which the exponential window suppresses.

An early ad hoc approach to correcting the dominant effect of this problem requires the addition of a unity pulse at the end of the exponential window (Ref. 10). Although this modified window approach does improve the phase skewing effect, it is not readily applicable in a real-time process, since selection of the unity pulse width is highly data-dependent.

The final smoothing technique arrived at for real-time ARW-1R testing consists of a further refinement in the window modification process. Instead of using a unity pulse at the end of the window, a time-reversed exponential is used. The net window then consists of e^{-t} over the region $t = 0$ to $t = T/2$, and the region from $t = T/2$ to T is a mirror image of the first half. Application of this window eliminates the phase-skew effect of the one-sided exponential window. The effect of this window is illustrated in Fig. 16 for the same a_z/δ_a transfer function of Figs. 6 and 7. The Nyquist analysis requires input of the left and right aileron servovalve position commands to the Fourier analyzer.

For ARW-1R testing, Nyquist results will be displayed in real time and comparisons made with predictions. Maneuver quality will also be evaluated from the Nyquist display.

For well-defined resonances, the five-point cubic fit of the phase curve provided good damping estimates; however, for more poorly defined (i.e., rough) transfer functions, it may produce poor damping estimates, even in some cases with the wrong sign. The main problem is that the curve fit is very sensitive to the data points; this in turn affects the slope determination. For ARW-1R testing, the slope will be determined by a linear fit of the data. This produces a slope less sensitive to any particular data point; however, it will in general produce an unconservative, higher damping estimate, as shown in Fig. 17. The slope estimate will be increasingly unconservative as the number of points used in the curve fit increases. To compensate for the unconservative nature of the estimate, an empirical formula based on a single-degree-of-freedom model, is applied to the damping estimate. It should be noted that the single-sided exponential window will produce a conservative estimate because of the negative phase bias mentioned previously.

8.0 CONCLUDING REMARKS

Flight-test results of the first three flights of an aeroelastic research wing have been described. The flight flutter-test technique used to obtain real-time damping estimates from fast-frequency sweep data was obtained and the open-loop flutter boundary determined. Nyquist analyses of sweep maneuvers appear to provide additional valuable information about FSS operation, both in terms of phase-margin estimates and as a means of evaluating maneuver quality. An error in implementing the flutter-suppression system resulted in a one-half nominal gain configuration, which caused the wing to be unstable at lower Mach numbers than anticipated, and the vehicle experienced closed-loop flutter on its third flight. Real-time flutter-testing procedures have been improved, and ARW-1R testing is scheduled to begin in the fall of 1982.

REFERENCES

1. Murrow, H. N.; and Eckstrom, C. V.: Drones for Aerodynamic and Structural Testing (DAST)—A Status Report. J. Aircraft, vol. 16, Aug. 1979, pp. 521-526.
2. Edwards, J. W.; and Deets, D. A.: Development of a Remote Digital Augmentation System and Application to a Remotely Piloted Research Vehicle. NASA TN D-7941, 1975.
3. Newsom, J. R.; and Pototsky, A. S.: Comparison of Analysis and Flight Test Data for a Drone Aircraft with Active Flutter Suppression. AIAA Paper 81-0640, Atlanta, Ga., 1981.
4. Bennett, R. M.; and Abel, I.: Application of a Flight Test and Data Analysis Technique to Flutter of a Drone Aircraft. AIAA Paper 81-0652, Atlanta, Ga., 1981.
5. Visor, O. W.; and Sevart, F. D.: Preliminary Design Study of Flutter Suppression Control System for BOM-34E/F Drone Aircraft With a Supercritical Wing—Final Report. NASA CR-14508, 1977.
6. Eckstrom, C. V.: Loads Calibration of Strain Gage Bridges on the DAST Project Aeroelastic Research Wing (ARW-1). NASA TM-81889, 1980.
7. Bergmann, G. E.; and Sevart, F. D.: Design and Evaluation of Miniature Control Surface Actuation Systems for Aeroelastic Models. J. Aircraft, vol. 12, Mar. 1975, pp. 129-134.
8. Flutter Testing Techniques. NASA SP-415, 1976.
9. van Nunen, J. W. G.; and Piazzoli, G.: Aeroelastic Flight Test Techniques and Instrumentation, Vol. 9. AGARD Flight Test Instrumentation Series, AGARD-AG-160, Feb. 1979.
10. Jennings, W. P.; Olsen, N. L.; and Walter, M. J.: Transient Excitation and Data Processing Techniques Employing the Fast Fourier Transform for Aeroelastic Testing. Flutter Testing Techniques, NASA SP-415, 1976.
11. Newman, K. W.; Skingle, C. W.; and Gaukroger, D. R.: The Development of Rapid-Testing Techniques for Flutter Experiments. ARC CP No. 1274, 1974.
12. Edwards, John W.: Flight Test Results of an Active Flutter Suppression System Installed on a Remotely Piloted Research Vehicle. AIAA Paper 81-0655, Atlanta, Ga., 1981.
13. Eckstrom, C. V.; and Spin, V.: Design Considerations and Experiences in the Use of Composite Material for an Aeroelastic Research Wing. NASA TM-83291, 1982.

TABLE 1. -NORMAL MODE FREQUENCIES PREDICTED BY NASTRAN ANALYSIS AND MEASURED DURING GROUND VIBRATION TEST

Mode	Frequency, Hz	
	NASTRAN	GVT
Symmetric—		
First wing bending	9.1	9.6
First fuselage bending	16.5	16.2
Wing bending-torsion	29.6	29.1
Antisymmetric—		
First wing bending	12.3	13.5
First fuselage yaw	21.7	19.3
Wing bending-torsion	30.0	27.0

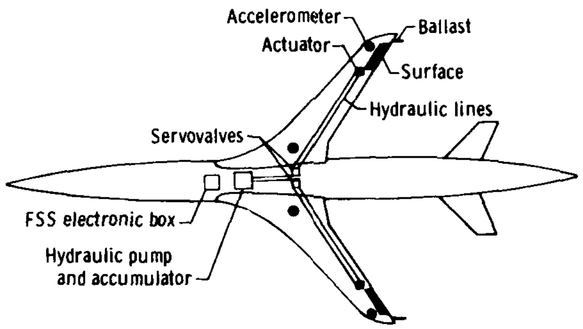
Accelerometer
Ballast
Actuator
Surface
Hydraulic lines
Servovalves
FSS electronic box
Hydraulic pump
and accumulator

Figure 1. DAST ARW-1/1R planform illustrating the flutter-suppression system layout.

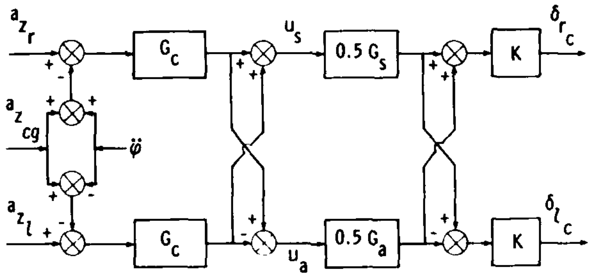
a_{z_r}
G_c
u_s
$0.5\,G_s$
K
δ_{r_c}
$a_{z_{cg}}$
$\ddot{\varphi}$
a_{z_l}
G_c
u_a
$0.5\,G_a$
K
δ_{l_c}

Figure 2. Flutter-suppression system block diagram.

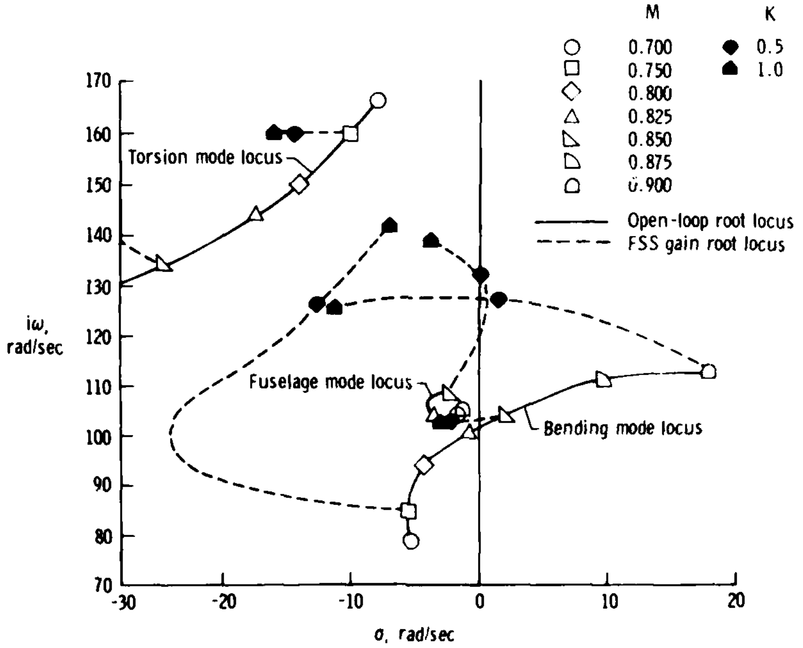

Figure 3. Predicted open-loop flutter-mode root locus and flutter-suppression system gain root locus at H = 4.57 km (15,000 ft).

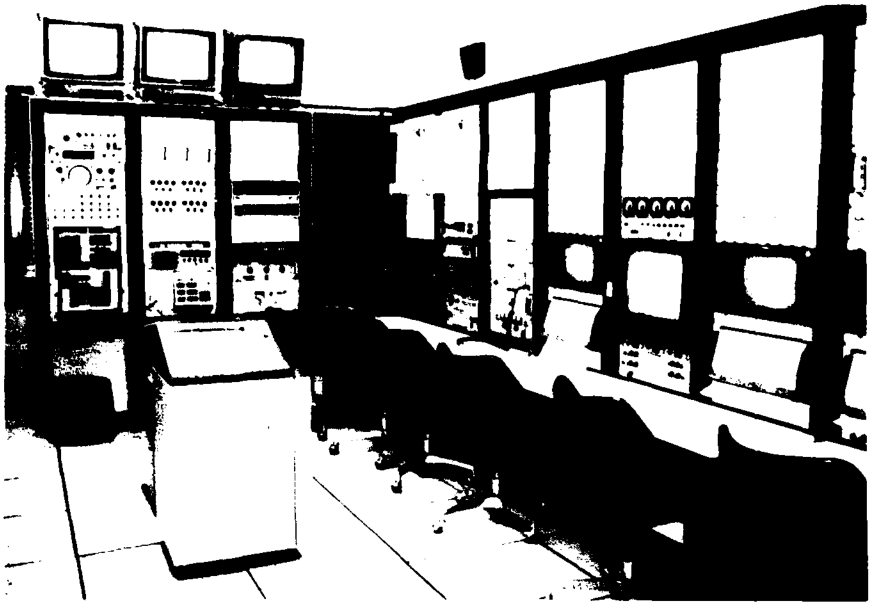

ECN 18946

Figure 4. Spectral analysis facility.

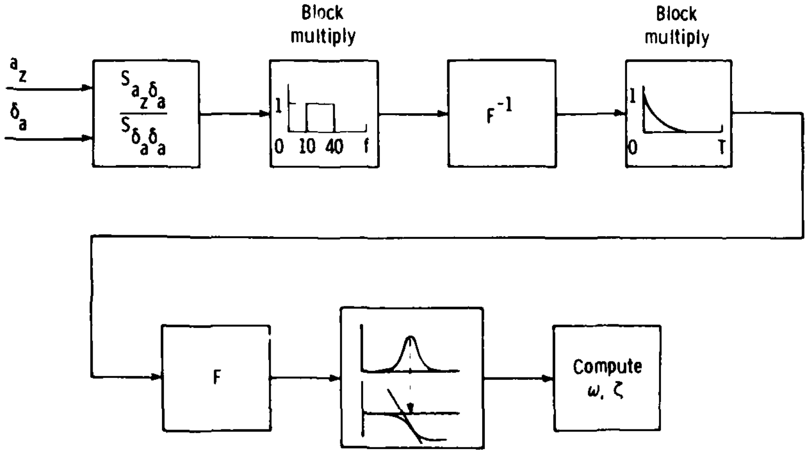
Block multiply
Block multiply
a_z
δ_a
$\frac{S_{a_z\delta_a}}{S_{\delta_a\delta_a}}$
1
0 10 40 f
F^{-1}
1
0
T
F
Compute
ω, ζ

Figure 5. Functional diagram of the real-time transfer-function and damping-ratio estimation algorithm.

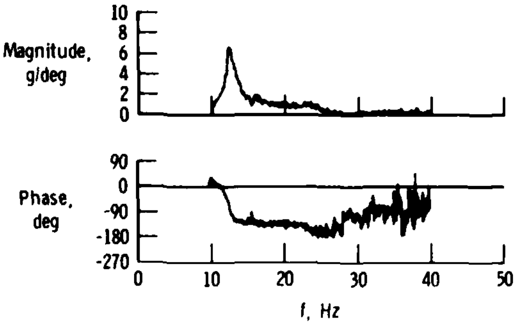

Figure 6. Raw transfer-function estimate of a_z due to δ_a for a symmetrical frequency sweep: M = 0.74 and H = 4.57 km (15,000 ft).

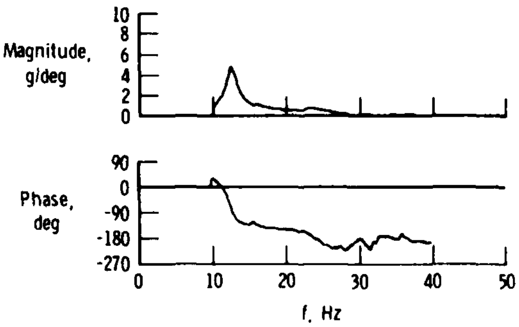

Figure 7. Smoothed transfer-function estimate of a_z due to δ_a for a symmetrical frequency sweep using an exponential window: M = 0.74 and H = 4.57 km (15,000 ft).

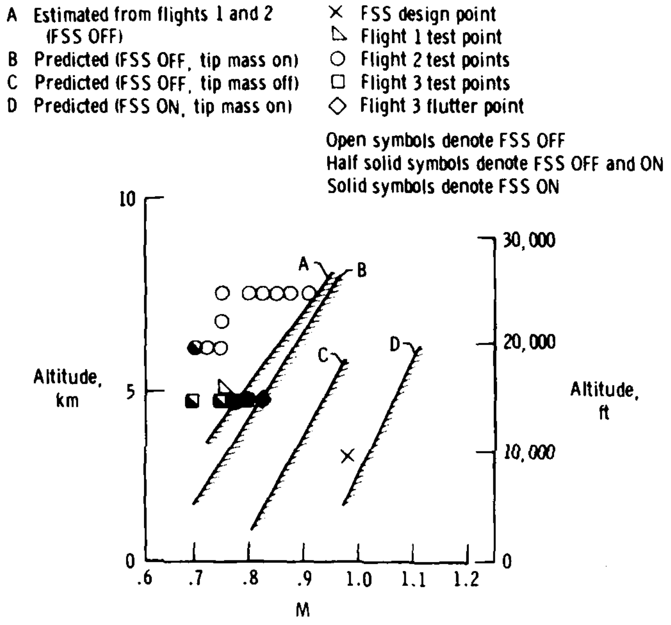

Figure 8. Flight envelope of the ARW-1 showing predicted flutter boundaries and flight-test points.

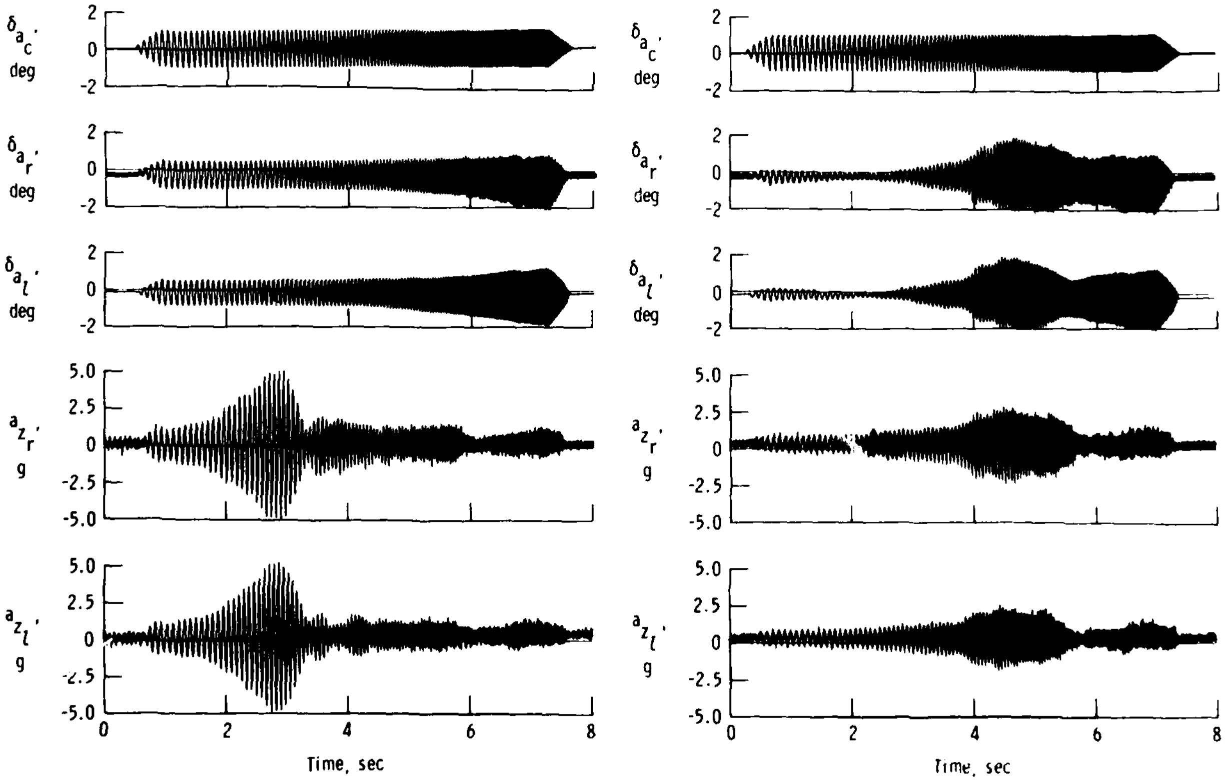

(a) FSS OFF.

(b) FSS ON.

Figure 9. Response to symmetrical frequency sweep excitation at M = 0.74 and H = 4.57 km (15,000 ft) during flight 3.

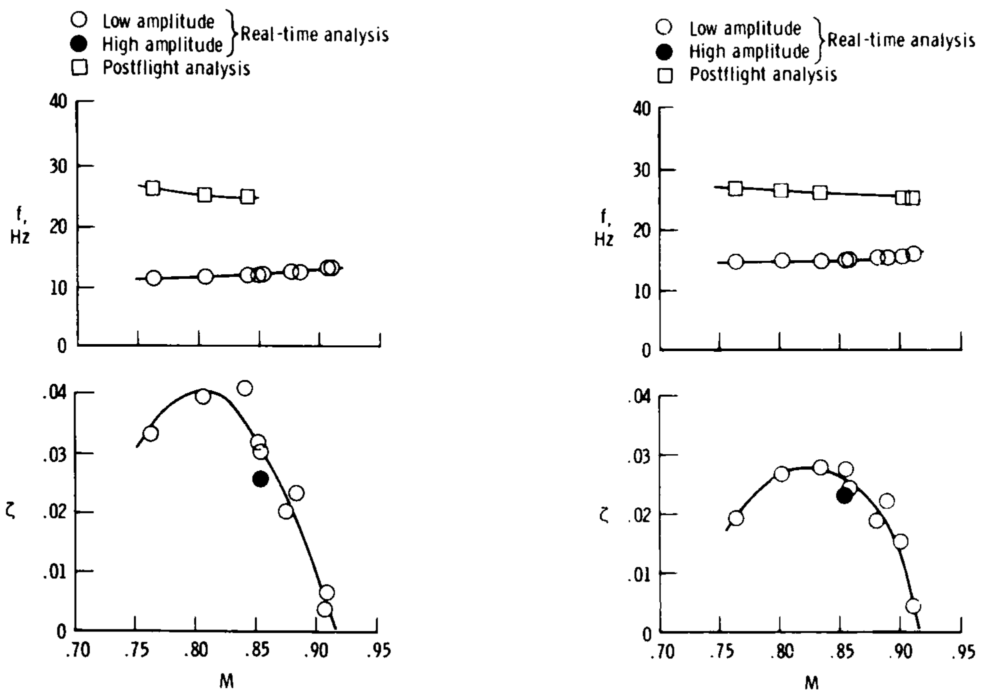

(a) Symmetric.

(b) Antisymmetric.

Figure 10. Bending-mode frequency and damping at H = 7.62 km (25,000 ft).

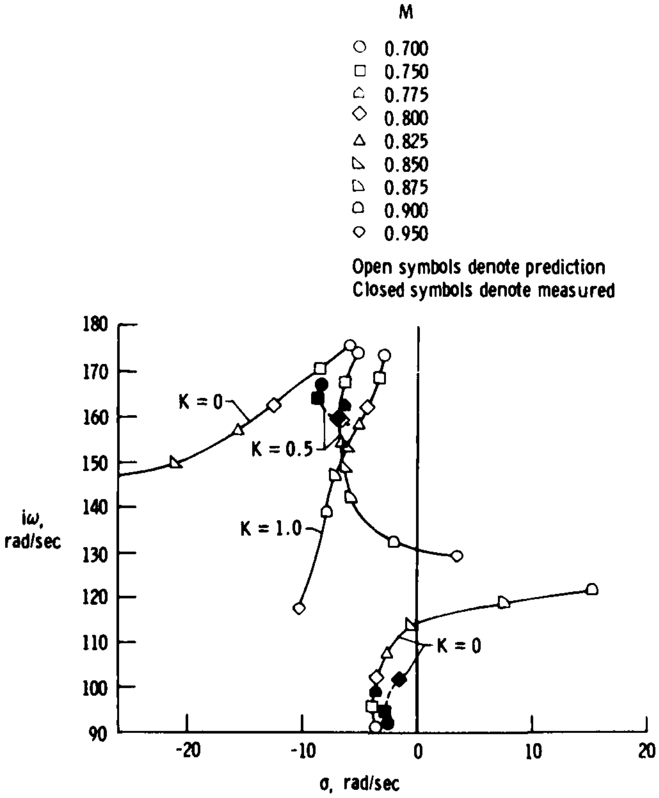

Figure 11. Comparison of predicted and measured antisymmetrical root loci versus Mach number at H = 4.57 km (15,000 ft).

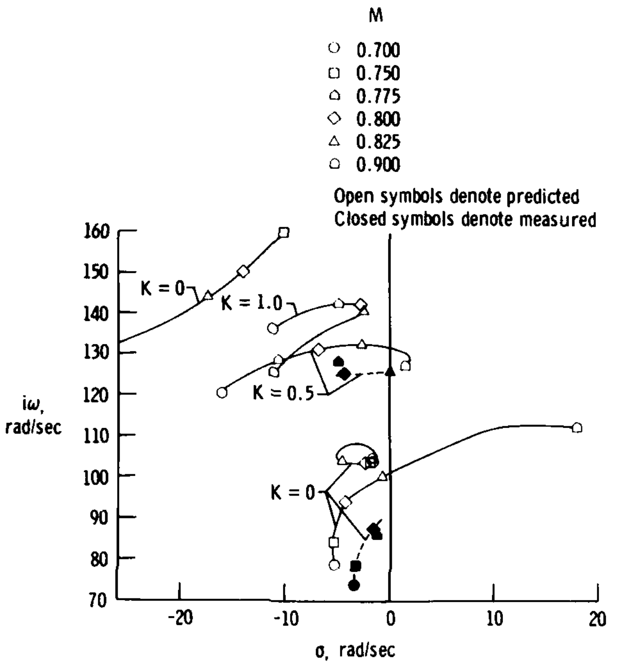

Figure 12. Comparison of predicted and measured symmetrical root loci versus Mach number at H = 4.57 km (15,000 ft).

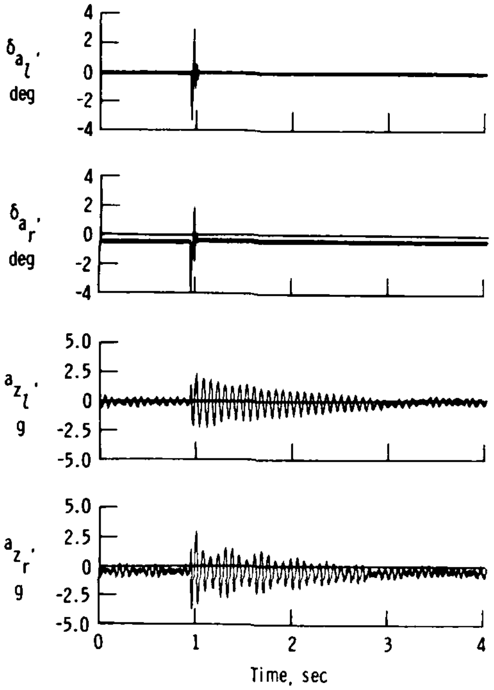

Figure 13. Symmetric, open-loop response to pulse excitation at M = 0.907 and H = 7.62 km (25,000 ft).

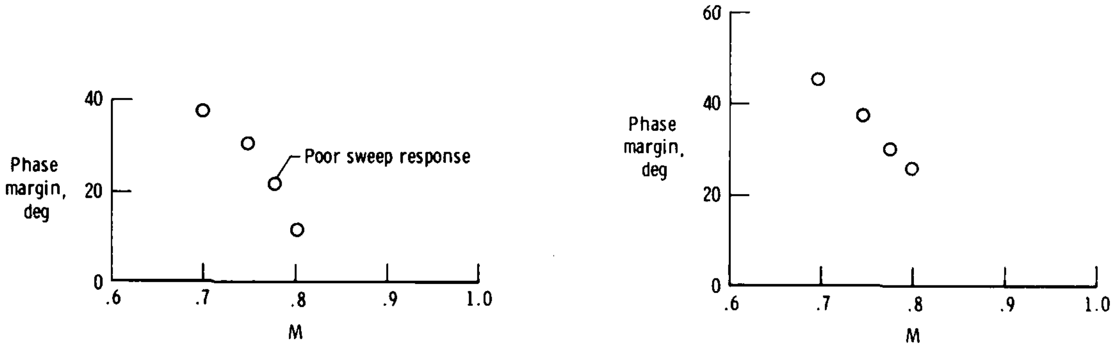

(a) Symmetric.

(b) Antisymmetric.

Figure 14. Phase margins obtained from flight 3 FSS ON sweeps (H = 4.57 km (15,000 ft)).

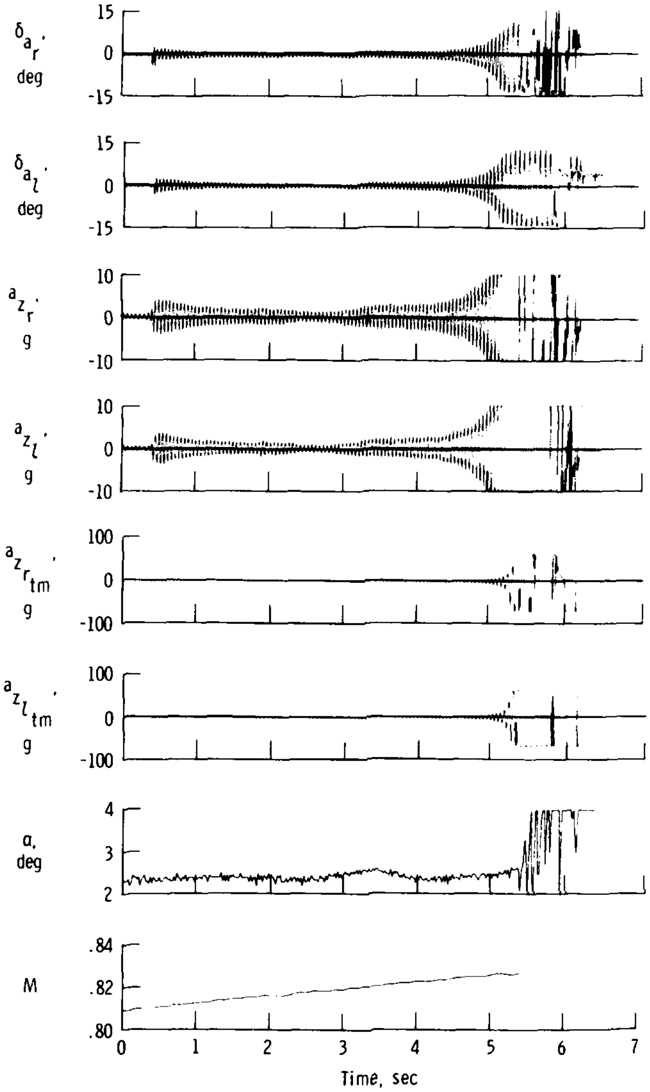

Figure 15. Response following symmetric, FSS ON pulse excitation at M ≈ 0.825 and H = 4.57 km (15,000 ft).

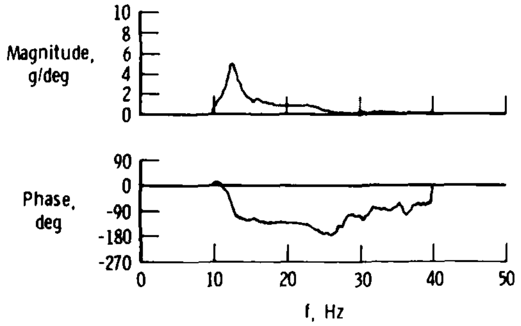

Figure 16. Smoothed transfer-function estimate of a_z due to δ_a for a symmetrical frequency sweep using a symmetrical exponential window: M = 0.74 and H = 4.57 km (15,000 ft).

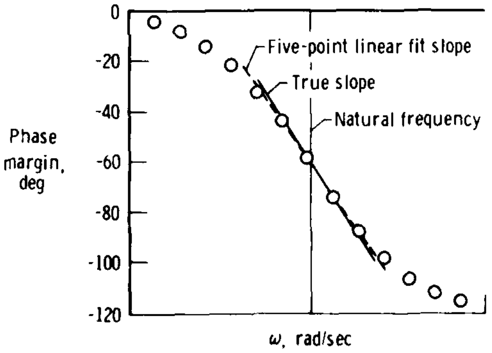

Figure 17. Phase curve slope determination (five-point linear least squares fit of slope).

FLIGHT FLUTTER TESTING WITH EMPHASIS ON THE TIP VANE METHOD

by
Helmut Zimmermann
Vereinigte Flugtechnische Werke GmbH, D-2800 Bremen,
Germany

and
Roger Destuynder
Office National D'Etûdes et de Recherches Aerospatiales
29, Avenue de la Division Leclerc - 92320 Chatillon
France

SUMMARY

Flight vibration testing is an important means for studying the flutter behaviour of an aircraft. The paper gives a short summary of the most important flight excitation systems developed and used in the last twenty years. Special emphasis is put on the vane excitation system. This system was developed for the flight vibration tests of the A 310 intermediate-range transport aircraft. The general, functional, and safety requirements for this system are described. Also the preliminary tests, and the set-up and handling of such a system are reported. Because the vane excitation can be measured precisely, the tip vane method offers the advantage of representing aircraft response in terms of transfer functions rather than only autospectra. The transfer function so derived together with a multi-mode matching technique were then used to determine the frequencies and damping of the aircraft modes. The multi-mode matching technique is also described. The paper also reports some results obtained by flight vibration testing of the A 300 and A 310 aircraft.

1. INTRODUCTION

During the development of commercial or military aircraft it is standard procedure to perform flight flutter tests to show that the aircraft is free of flutter within its flight envelope. To determine the flutter behaviour of the aircraft, the frequency and damping values of the appropriate flight vibration degrees of freedom must be measured for various speeds and Mach numbers within the flight envelope. This is usually done by installing transducers, such as accelerometers, gyros, potentiometers, goniometers and strain gauges at various points on the aircraft; then inducing vibrations in the airframe by various natural or artificial means; and recording the resulting oscillation amplitudes and phase relations. The data are recorded on magnetic tape on board the aircraft or transmitted by telemetry (PCM, pulse code modulation) to ground recording equipment, or both.

As a means of exciting flight vibration modes control surfaces, auxiliary flaps, natural or artificial turbulence, hydraulic or electrodynamic exciters, or bonkers have all been used in the past. The excitation process may be harmonic, impulsive or random, depending on the excitation system. Whenever possible the excitation force is also recorded and processed. On the ground the data are usually filtered, digitized and transmitted to a ground computer, which calculates power spectra, correlation, coherence, and transfer functions, if possible. By matching these functions to appropriate mathematical models the frequency and damping of each mode may be obtained. Figure 1 gives a schematic view of the excitation, measurement, and evaluation systems for flight vibration testing. Flight flutter tests are usually carried out by advancing flight speed and Mach number in discrete steps. During each speed advance the test data is telemetered to the ground for preliminary assessment to permit the aircraft to advance to the next higher speed. Since each speed increase entails a certain risk for aircraft and crew, the quick-look capability of telemetry has become a valuable tool in flight flutter testing.

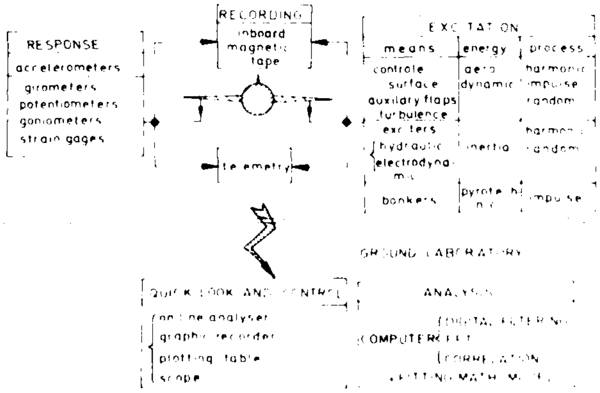
RECORDING
inboard magnetic tape
RESPONSE
accelerometers
girometers
potentiometers
goniometers
strain gages
telemetry
EXCITATION
means
energy
process
controle surface
aero dynamic
harmonic
impulse
random
auxilary flaps
turbulence
exciters
hydraulic
electrodynamic
inertia
harmonic
random
bonkers
pyrotechnic
impulse
GROUND LABORATORY
QUICK LOOK AND CONTROL
on line analyser
graphic recorder
plotting table
scope
ANALYSIS
COMPUTER
DIGITAL FILTERING
FFT
CORRELATION
FITTING MATH. MODEL

FIG 1 FLIGHT VIBRATION TEST EQUIPMENT FOR EXCITATION MEASUREMENT AND EVALUATION

2. EXISTING METHODS TO EXCITE AN AIRCRAFT IN FLIGHT [1]

To excite an aircraft in flight, various methods have been used in the past and today. These methods may be divided into roughly two groups: those for which the determination of excitation force is impossible or unreasonable, and those for which these forces can be determined, and where it makes sense to correlate them to the aircraft response. For the following methods it is difficult or inappropriate to measure the input forces:

2.1 EXCITATION BY ATMOSPHERIC TURBULENCE

Except for the rigid-body modes of the aircraft (which are mainly relevant to flight dynamics), where knowledge of the turbulence at one location is available by vane measurement, it is not possible to correlate incident turbulence with aircraft response easily. The disadvantages of this method are thus as follows:

- no discrimination between symmetric and antisymmetric modes
- many flights are necessary to find turbulence of sufficient intensity
- poor statistical stationarity of turbulence in time and space
- input forces unknown
- no choice of excitation level at selected frequencies

On the other hand the advantages of the method are the simplicity of the equipment, and the capability of attaining a high level of low-frequency energy as predicted by the theoretical von Karman spectrum of atmospheric turbulence.

2.2 EXCITATION BY AVAILABLE CONTROL SURFACES

Excitation by actuating the control surfaces that are part of the standard aircraft equipment offers a more selective choice than the previous method, because symmetric and antisymmetric modes can be excited at will. The inputs are the unsteady aerodynamic forces induced on the wing by control surface motion, which, however, cannot be measured in flight. It is also necessary to modify the electrical or hydraulic control surface actuators. The method is basically limited to low frequencies because of the low-pass characteristics of the actuator transfer functions. This disadvantage can be removed by exchanging the regular valves for other valves with higher control velocities, but this exchange will alter the flight dynamic behaviour of the aircraft. In any case the interference between the excitation loop and the pilot authority must be suppressed.

2.3 EXCITATION BY BONKERS [2]

This kind of excitation is probably one of the oldest and most successful methods developed for dynamic flight testing. Small solid-fuel rockets (bonkers) are attached to the aircraft at various points, which on ignition impart a short-duration impulse to the aircraft structure, thereby exciting a certain number of aircraft eigen modes. Figure 2 shows a number of bonkers for various thrust levels and durations. The variation of thrust with time produced by the bonker is roughly trapezoidal, and is shown in Fig. 3 for a typical bonker. Although the thrust cannot be measured directly in flight, bonkers may be easily calibrated on the ground, and selected to furnish the desired thrust history. The level of thrust depends on the nozzle diameter and propellant area, while the duration of the thrust is governed by the length of the propellant charge. The duration of the thrust determines what range of frequencies are going to be excited. In Fig. 4 the thrust is plotted against frequency for two propellant areas.

Because the bonker system can be installed easily at a relatively low price, the system is used widely for commercial and military aircraft. The drawbacks of the method are as follows:

- Interpretation of the results is difficult, because there is no easy way of identifying the individual vibration modes from the transient response curves.
- Degrees of freedom with small frequencies and large generalized masses cannot be excited by bonkers
- The number of impulses per flight is limited

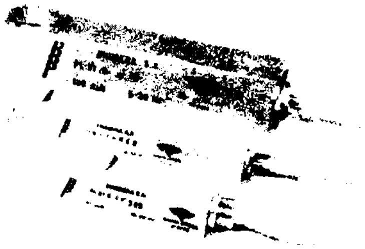

FIG 2 FLAT BONKERS

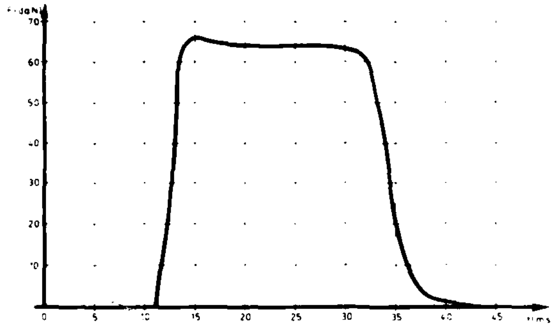

FIG 3 THRUST VERSUS TIME

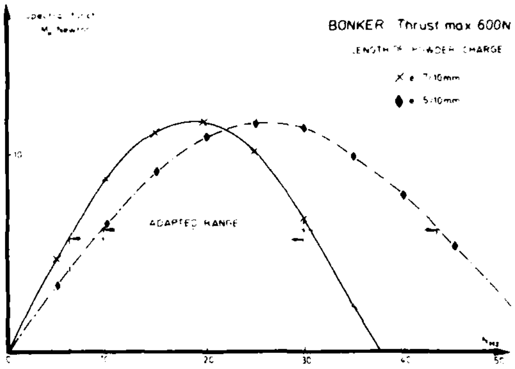

FIG 4 FLAT BONKER Thrust

In the methods described below the input forces can be measured for correlation with the response.

2.4 EXCITATION BY INERTIAL SHAKERS

Another means of imparting vibrations to aircraft in flight is given by inertial shakers, which exploit the acceleration of a more or less freely oscillating mass to exert a reaction force on the aircraft structure. The magnitude of the excitation force which is supplied by this system is proportional to the oscillation amplitude and the square of the excitation frequency. The suspension of the mass is usually given a low stiffness in the manner of a seismic platform to reduce elastic coupling with the aircraft structure as much as possible.

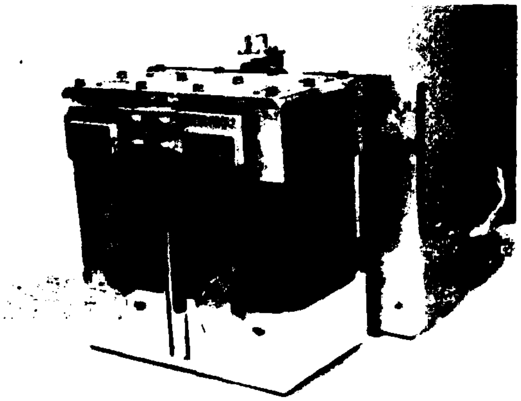

FIG 5 ELECTRODYNAMIC SHAKER

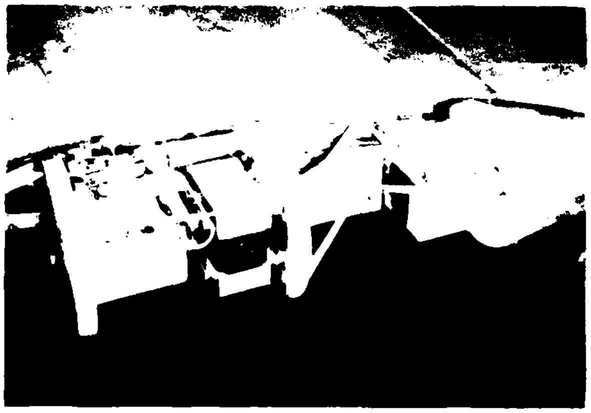

FIG 6 ELECTRODYNAMIC SHAKERS ATTACHED TO THE AIRCRAFT

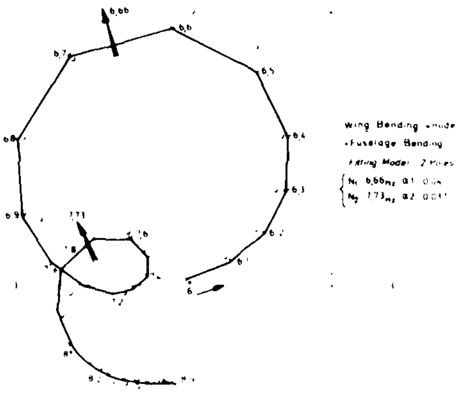

FIG 7 NYQUIST DIAGRAM OF AIRCRAFT RESPONSE TO ELECTRODYNAMIC SHAKER EXCITATION

Fig. 5 shows an inertial shaker of the electrodynamic type, and Fig. 6 shows the attachment system of the shaker to the aircraft. The electrodynamic type has a coil oscillating between two heavy U-shaped magnets. This arrangement is capable of producing appreciable forces in the 4-15 Hz range; but its effectiveness decreases rapidly for lower frequencies because of the amplitude limitations of the arrangement. Figure 7 shows a Nyquist curve obtained by electrodynamic excitation for the purpose of determining aircraft eigenfrequencies.

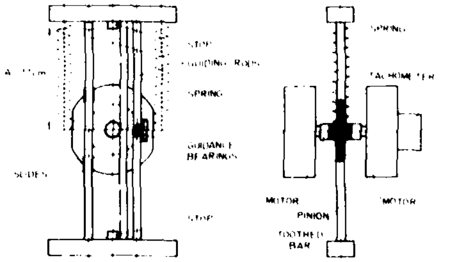

FIG 8 ELECTROMECHANICAL EXCITER WITH LARGE STROKE

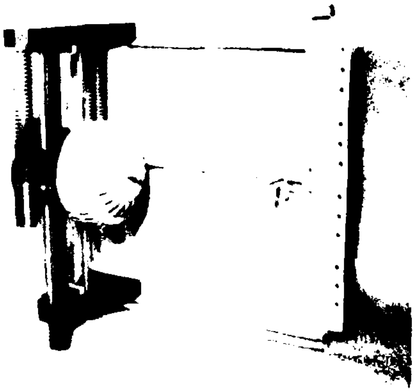

FIG 9 MOUNTING OF AN ELECTROMECHANIC SHAKER AT THE WING TIP CAP

A second type of inertial exciter, the electromechanic shaker, performs somewhat better at low frequencies, achieving typically 200 N at 2 Hz (see Fig. 8 and 9). There a torque motor and an eccentric mass, instead of magnet and coil, produce the desired forces. This arrangement allows larger amplitude at low frequencies, but is bulkier than the electrodynamics type, and thus more difficult to instal in confined spaces (external stores, tail, etc).

The salient features of this system are thus:

- amplitude and phase of the excitation forces are easily determined and controlled
- performs well except at low frequencies
- does not alter the elastic properties of the aircraft, but changes its inertial properties
- difficult to instal in confined spaces because of its bulkiness

2.5 VANE EXCITATION SYSTEM

Recently the choice of methods at the disposal of flight vibration testing has been expanded by the development of vane excitation systems, which utilize a power driven vane installed especially for this purpose at a suitable point on the aircraft, to provide the oscillatory forces necessary for flight vibration tests. Such systems have been developed in a number of countries, particularly by the Boeing and Lockheed corporations in the U.S..

By proper design the following characteristics may be realized by a vane system:

- The elasto-dynamic behaviour of the aircraft is not altered by the vane installation, except for its additional masses
- The excitation forces are well defined and can be measured and controlled easily, and also correlated with the induced vibration.
- If the vane chord is much smaller than the aircraft surface under investigation (e.g. the wing) the reduced frequency of the vane is much smaller than the reduced wing frequencies. This makes the unsteady vane airforces practically constant over the range of aircraft frequencies.
- Undesirable moment and force reactions can be reduced by vane mass balanced design and a suitable choice of the torque motor axis location near the vane aerodynamic centre.

3. THE TIP-VANE SYSTEM

3.1 GENERAL

For the development of a tip-vane excitation for aircraft, results of two independent wind tunnel tests in the transonic speed range were used. One test series was conducted with a movable tip vane driven by a mechanism similar to that on the aircraft. However, only the tip part of the wing (scale 1), was attached to the tunnel wall. In this test the lift of a vane with an area of 0.163 m^2 was measured for a constant altitude as given in the following table:

M	0.75	0.8	0.84
Lift (N)	415	487	558

I.e. the lift coefficient L/M^2 is nearly constant. The limitation of the dynamic amplitude is due to two parameters:

- the flow rate
- the shaft torsion induced by the inertial moment

In the other test series the vane and its position relative to the wing was optimized. The following results were obtained:

- The relative steady angle between the vane and the wing tip does not change the lift curve slope (Fig. 10) for a large range of wing incidence.
- The gap between vane and wing tip was varied from 7.9 % to 15.7 % of vane semispan (with end plate), see Fig. 11. At the same time the wing incidence was varied from -4° to 6°, which took care of virtually all flight conditions. It is evident that the lift curve slope is not sensitive to this parameter.
- Adding an end plate to the vane root is a possibility to improve the lift curve slope slightly (Fig. 12). The rate of improvement is sufficient for a relatively small plate. To reduce the moment of inertia of the vane it is advantageous to keep the size of the end plate down.

The aim was to get a large lift for a vane with a small area. To prevent flow separation for small vane incidences due to the high flow angle gradient of the tip vortex the vane was twisted.

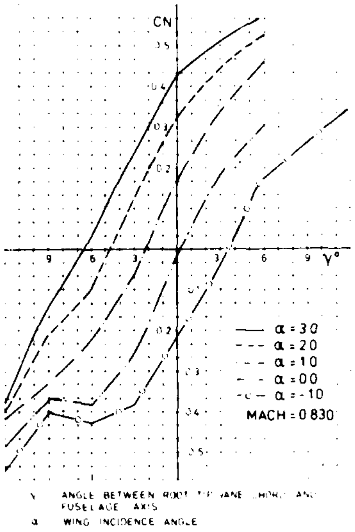

FIG 10 VANE LIFT VERSUS RELATIVE VANE INCIDENCE FOR VARIOUS WING INCIDENCES

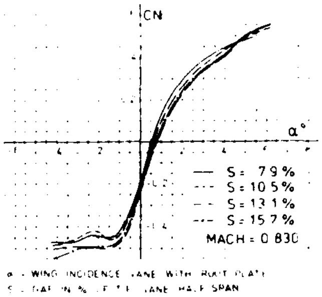

FIG 11 INFLUENCE ON THE LIFT OF THE GAP WIDTH BETWEEN THE TIP OF THE WING AND VANE

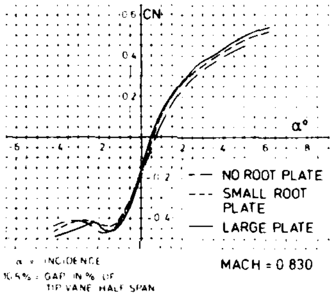

FIG 12 INFLUENCE OF VANE ROOT END-PLATE ON VANE LIFT

3.2 GENERAL REQUIREMENTS [3]

Without doubt, the optimum type of excitation for a tip vane, by which the largest magnification factors may be obtained between excitation and response, is harmonic excitation at resonance. Nevertheless, magnification factors close to those of harmonic excitation can also be attained by "frequency sweeps". The only prerequisite for this is that a suitable frequency sweep bandwidth is selected, and that the duration of excitation is large enough compared with the period of the eigenmode. The vibration levels to be generated in flight should be larger than the expected natural disturbance level (approx. 0.15 g), but should not be higher than the strength limit (2.5 g rigid-body acceleration by gusts). The frequency range of the vibrations should include enough eigenfrequencies to characterize the dynamic behaviour of the wing. It will not be possible in general to achieve these performance requirements equally well for all aircraft eigenmodes, since the magnitude of the excitation acceleration depends on:

- the point of application of force
- the place of measurement
- the damping to be overcome
- the mass to be accelerated
- the available excitation force

The optimum position for excitation and measurement is without any doubt the place of maximum modal deformation. This has a different location for every mode and the mode can change with speed and M-number. If only one excitation system is to be used, the best compromise is to arrange the aerodynamically effective surfaces at the wing tips. This is where most of the modes have their maximum deformation. For technical reasons, the system must be installed approximately halfway between front and rear spar. In contrast, the pick-ups can be positioned optimally without exception. Their dimensions are small, and several pick-ups have to be fitted in the aircraft anyway.

As a compromise regarding the performance requirements for the A 310 tip vane, it was required that at least ± 1000 N must be achieved with a steady incidence of ± 3° at VMO/MMO, and that a frequency sweep of up to 20 Hz should be possible. In this way, most of the modes can be excited to measurable accelerations.

3.3 FUNCTIONAL REQUIREMENTS AND SECONDARY CONDITIONS

- A vane is installed at each wing tip.
- Each vane is fitted to a torque shaft.
- The axis of the shaft is in the wing plane and perpendicular to the flow.
- A static angle of incidence of ± 12° with reference to the last wing rib can be set.
- A dynamic angle which can be changed as a function of time, with a possible maximum amplitude of 7° can be superimposed over the static angle.
- On option, the superimposition of the dynamic angle can either be symmetrical or anti-symmetrical for both vanes.
- The dynamic angle can be controlled by a frequency generator in such a way that harmonic vibrations and vibrations with a frequency sweep can be generated. The amplitudes of these vibrations are continously adjustable between 0° and 7°. The frequencies for harmonic motion are continously selectable between 0 and 20 Hz. As regards the sweep, the frequency can be varied linearly as a function of time. The initial and final frequencies can be selected independently from one another with values of 1.4; 2.8; 4; 5.6; 8; 11.2; 16; 22.4 Hz. The rate of frequency change can be selected with 12; 15; 20; 30; 40; 60; 180 sec/octave. The motion always starts and finishes at an angle of 0°, to avoid the overlap in the FFT. When the selected maximum frequency has been reached, the motion is continued with a decreasing frequency until the initial frequency is reached. Subsequently, the procedure is repeated cyclically. In addition the purchased frequency generator has a possibility of exciting a random vibration. In this case, step functions with a constant amplitude are statistically distributed over time. The frequency bandwidth and the sequence length are selectable. The accuracy of the setting for all types of motion is better than ± 0.01° and ± 0.01 Hz.

- The motion is generated by a hydraulic swivel motor, furnishing a pure torque.
- The lift force of the vane is equally large for positive and negative angles of attack (symmetrical profile).
- The centre of force application is approximately on the extended axis of rotation, resulting in the minimum drive moment for vane motion. The unavoidable wanderings of the center of force application due to changing flight conditions mainly take place in the downstream area of the axis of rotation.
- Buffeting only occurs at angles of attack exceeding 7°.
- All other components were designed as light as possible to keep the additional weight and thus any influence on the vibrational behaviour of the aircraft as small as possible.
- The stiffness of the components was selected to be as large as possible.
- The vane can be installed on, and dismounted from the aircraft from the outside.
- The spatial conditions in the wing tip cap had to be taken into account when deciding on the geometrical design and arrangement of the components. Attachment is at the last wing rib.
- The system is controlled from a console in the aircraft. This console also incorporates a digital indication for the lift forces, the static angle and the maximum amplitudes of the dynamic angles at both vanes.

3.4 SAFETY REQUIREMENTS

In addition to the actual requirements concerning the function, various conditions that are of relevance to the safety have had to be fulfilled.

- Neither through its existence as such nor through its operation shall the excitation system be detrimental to the flight properties of the aircraft.
- When not in operation, the tip vane is blocked in its defined zero position by a brake, thereby precluding that uncontrolled vane movements aggravate flight conditions.
- A self-monitoring feature with an emergency-off function when a limit value is exceeded is provided for 8 selectable pick ups.

The monitored signals at each vane are as follows:

-- wing acceleration, vertical
-- engine acceleration, vertical
-- vane angle measured signal
-- reduced hydraulic pressure at motor inlet.

- The hydraulic supply is automatically switched off when the electrical power supply fails.
- Emergency-off switches are provided for the pilot and flight test engineers.
- The installation of a pressure relief valve serves to prevent any excessive loading of the vanes torque shaft through the drive motor in the event of a failure.
- lift is measured by a linear combination of two unsteady bending moments measured by strain gauge bridges fixed on the rotation axis.

3.5 SET-UP AND HANDLING

For design and requirements reasons the tip vane excitation system consists of

- the aerodynamically effective surfaces, namely the tip vanes
- the support and fixtures
- the hydraulic drive
- and the control system including control circuits, monitoring circuits, and the frequency generator.

The tip vane itself is an aluminium sheet contruction. Fig. 13 shows the arrangement on the aircraft and Fig. 14 illustrates the drive system and system components.

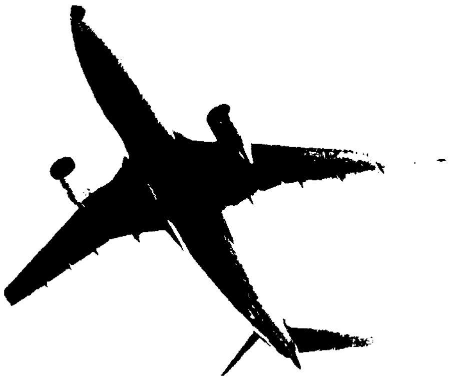

FIG 13 TIP VANE ON A310 AIRCRAFT

FIG 14 TIP VANE DRIVE

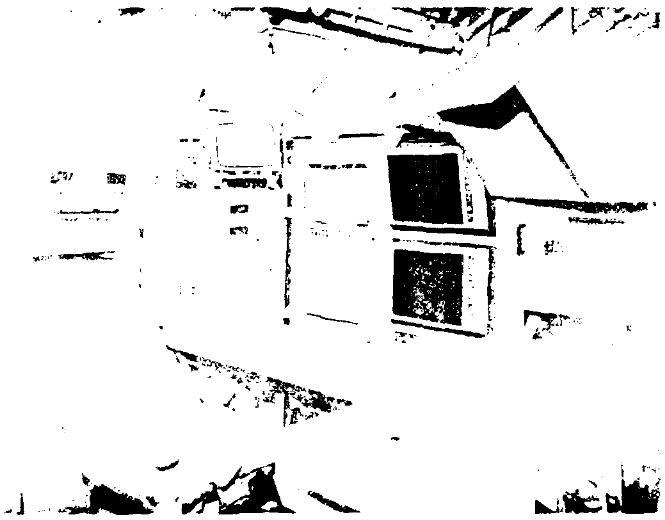

FIG 15 AIRBORNE FLIGHT TEST WORK SPACE

The

- torque shaft with its bearings
- brakes
- hydraulic motor

are apparent. Attachment is via a bracket to the last end rib.

The system is controlled from a control unit arranged in the fuselage of the aircraft.

Fig. 15 shows the airborne flight test work space: the limit value monitors; the so called "operator control panels"; the frequency generator and the recorder for monitoring the measured values.

4. TEST DATA REDUCTION

4.1 GENERAL

During the flight flutter tests, the lift of the port and starboard vanes, and the torque was measured and recorded on tape. With the lift of the vanes, the excitation forces are known. Together with the signals of the acceleration pick-ups distributed over the aircraft all functions necessary for good data evaluation can be calculated, such as power spectra, cross power spectra, transfer and coherence functions. To determine the frequency and damping values for the various flight vibration modes the transfer function was used. Although the transfer function contains all the information necessary to calculate the frequency and damping values as well as the complex modes, the coherence function indicates, how far the measured response of the airplane is due to the vane excitation or an extraneous input. One of the most troublesome of these is atmospheric turbulence. Therefore the flight tests with a vane excitation or another excitation which do not use atmospheric turbulence as an excitation must be carried out at small turbulence. Nevertheless it is reasonable to determine the coherence function in any case, to be sure that the response is mainly produced by the installed excitation mechanism. The values of frequency and damping for the various degrees of freedom can be obtained by matching the theoretical transfer function with unknown values for frequency and damping with the measured one. Taking into account the following aspects, that

a) The measured transfer function is only an estimate of the actual transfer function

b) The matching of the theoretical transfer function with the measured one will be done by a least square error method within a certain frequency range.

c) The theoretical transfer function does not represent the real one,

then it is clear that the values for damping and frequency obtained by the fitting method are estimates with more or less large errors. The most difficult problem is to determine these errors or, in other words, the confidence intervals for these calculated values. The coherence function alone is not sufficient to furnish an error estimate for this kind of output.

4.2 METHODS USED FOR MATCHING

Before showing some results we will explain details of the method used. The transfer function of a structure capable of oscillation with n degrees of freedom can be expressed quite generally as a polynomial of 2-nth order in iω :

$$H = \frac{\sum_{0}^{2n} a_{2n} \cdot (i\omega)^{2n}}{\sum_{0}^{2n} b_{2n} \cdot (i\omega)^{2n}}$$

The zeros of the denominator polynomial are the complex eigenvalues of the system. The functional of analysis was formulated as a linear equation of the polynomial coefficients, i.e.

$$H \cdot \sum_{0}^{2n} b_{2n} \cdot (i\omega)^{2n} - \sum_{0}^{2n} a_{2n} \cdot (i\omega)^{2n} = 0$$

If approximate values for the polynomial coefficients are inserted into the functional, the result deviates from the exact value of zero. This deviation is called residue. Extremum values, including the minimum, of the sum of the squares of the residues for a number of frequencies can be found where the first derivative of the sum of the error squares goes to zero. These considerations lead to a directly solvable system of 2 x 2 + 1 linear equations for the polynomial coefficients. With the known coefficients the eigenvalues of the structure as the zeros of the polynomial are calculated by one of the known methods, e.g. by Rosenbrock [4] . Since it must be assumed in general that measured transfer functions contain errors, or contain mode components that lie outside the frequency range of interest, an iterative correction may be superposed, if necessary, on the direct calculation of the eigenvalues.

For this purpose "offset" corrections, which are constant or vary linearly with frequency, are added to the real and imaginary parts of the measured transfer function. Their absolute values are changed in such a way that the sum of the residue squares of the polynomial coefficients, which itself is already a minimum, is further minimized. This analytical method may be applied without limitations to arbitrary structures. The lowest number of complex values of the transfer function necessary to calculate n complex eigenvalue is 2n + 1. The maximum number is arbitrary. It can be shown, however, that the effects of errors, or the extraneous components of the transfer function are lowest, when the values that are used are taken from the immediate neighborhood of the eigenfrequencies of interest. The formulation for this method was made by König, VFW, details of which have not yet been published, but it appears that this method is similar to the method of Dat and Meurzec [5] . Furthermore, two other methods using a Hewlett-Packard 2100 and a Nicolet computer should be mentioned. According to J.C. Copley[6] we can in principle distinguish between two methods, the one described above, and another method, which uses a functional formulated in terms of the eigenfrequencies and the damping of the flight vibration degrees of freedom, with a partial fraction representation of the transfer function for each degree of freedom. If the latter functional is used in a least square method it leads to equations nonlinear in the frequency and damping values which must be solved iteratively.

5. FLIGHT TEST AND TEST RESULTS

5.1

A series of tests were performed with the system described above aboard two aircraft. One test series was conducted on the A 300 Nr. 3 aircraft to check the effectiveness of the excitation system, to acquire experience in handling the system, and to decrease its susceptibility to malfunction. The second test series was conducted with the A 310 Nr. 162 aircraft. This test series was conducted to show that the A 310 was free of flutter in its entire flight envelope. The two test series showed that the effectiveness of the vane was higher than indicated by the wind tunnel tests, i.e. the lift obtained for a given amplitude was higher than the estimated value; and that buffeting appears at a larger angle than expected.

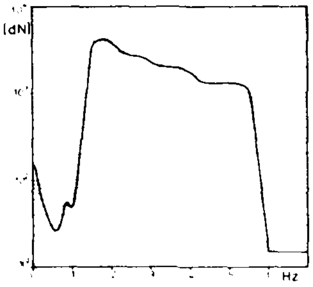

FIG 16 AUTOSPECTRUM OF VANE LIFT FOR LINEAR FREQUENCY SWEEP

Fig 16 shows the autospectrum of the lift for a sweep between 1,4 and 5,6 Hz. Theoretically the autospectrum of the lift must be rectangular. But this spectrum drops with rising frequency. The reason for this decrease comes from the fact that the vane angle decreases slowly with rising frequency as seen in fig. 18.

Tests with different sweep times per octave show the optimum sweep rate to be 30 s/oct. for a complete sweep cycle. The autospectra and transfer functions that were obtained were not improved for higher sweep times, and the response of the aircraft was nearly the same as that for a harmonic excitation. Therefore this sweep time was used in general, i.e. for horizontal flight conditions. In both test series, it could be shown that nearly all modes with non-vanishing amplitudes on the wing in the measured frequency range could be matched to those found in ground resonance test, and their type could be identified.

5.2 VIBRATION MEASUREMENTS ON THE A 310

Fig. 17 gives a general view of the connected pick-ups. Most of them are acceleration pick-ups, and position-, lift- and torque pick-ups for the vane. The view shows that the pick-ups are well distributed over the aircraft, so that it was possible to measure the maximum amplitude of all modes, and to identify the type of the mode. In each case the signals of half the pick-ups were stored on magnetic tape and the signals of ten of them were transmitted by PCM telemetry to the ground laboratory.

Fig. 18 gives a view of measured excitation and response signals for a Mach number of 0.78 and 330 KCAS. The lift force, the torque and the position of the vane are presented in sequence followed by the acceleration at the wing tip, at the engine in the z-direction, and at the engine in a lateral direction. The entire sweep-time is nearly 2,10 minutes. The frequency range is between 1,4 and 5,6 Hz, and the sweep rate is 30s/octave. That means that the frequency started from 1,4 Hz, went up to 5,6 Hz, down to 1,4 Hz, and up again to a stop.

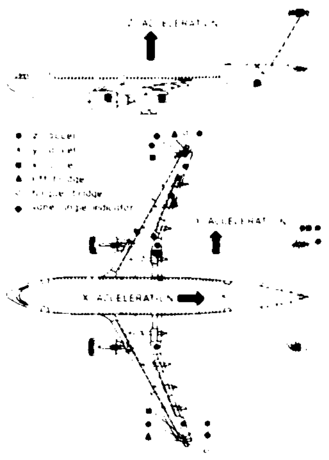

FIG 17 LOCATION OF TRANSDUCERS

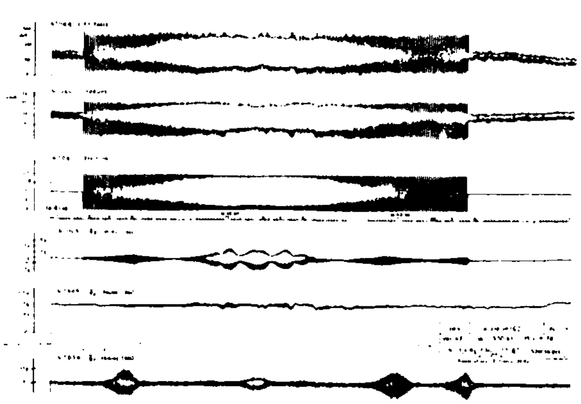

FIG 18 TIME RECORDS OF EXCITATION AND RESPONSE

In Fig. 19 to 23 we find transfer functions in the frequency range from 1,4 to 5,6 Hz, calculated for the lift of the vane and the responses due to the vane excitation at different positions on the plane, for a speed of 360 KCAS and a Mach number of 0.78. The dynamic angle of the vane was ± 4°. The first four transfer functions are for a symmetrical excitation, the last for antisymmetrical excitation.

Fig. 19 shows the transfer function obtained at the wing tip in the z-direction

Fig. 20 shows the transfer function obtained at the engine in z-direction

Fig. 21 shows the transfer function obtained at the engine in y-direction.

Frequency Interval	Frequency	Damping
1 90 - 2 30	2 22	0 1148
4 50 - 4 80	4 75	0 0526

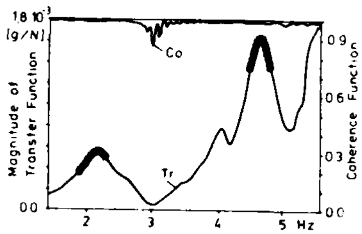

FIG 19 TRANSFER FUNCTION FOR WING TIP ACCELERATION, SYM EXCITATION

Frequency Interval	Frequency	Damping
3 30 - 3 45	3 44	0 0308
4 60 - 4 80	4 75	0 0423

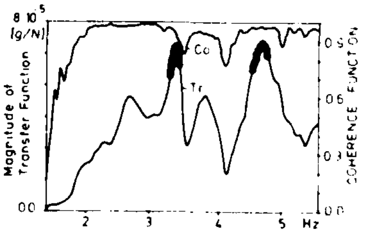

FIG 20 TRANSFER FUNCTION FOR ENGINE Z-ACCELERATION, SYM EXCITATION

Frequency Interval	Frequency	Damping
1 70 - 2 10	1 85	0 0608
1 70 - 2 10	2 03	0 0647

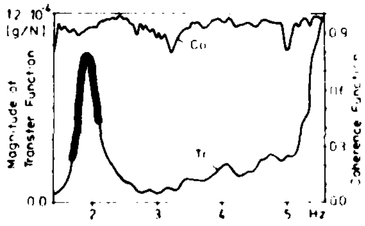

FIG 21 TRANSFER FUNCTION FOR ENGINE Y ACCELERATION, SYM EXCITATION

Note that in figure 21 the peak contains two degrees of freedom, the symmetrical and antisymmetrical lateral bending of the engine, which can be seen in the table above the figure. Fig. 22 shows the transfer function obtained at the horizontal tail in the z-direction, and we can notice frequencies on the tail not below 3,5 Hz in contrast to the wing motion. Fig. 23 shows the transfer function obtained at the vertical tail in the y-direction. It is remarkable that with the vane excitation on the wing, tail-modes are excited. At the top of all pictures except fig. 23 we see the coherence-functions. The heavy solid lines are the fitted curves. The excitation is nearly without extraneous inputs.

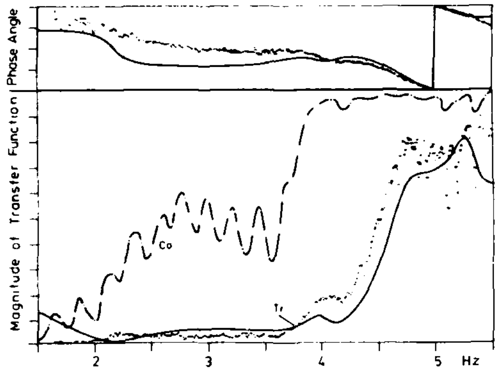

FIG. 22 TRANSFER FUNCTION FOR Z-ACCELERATION OF HORIZONTAL TAIL, SYM. EXCITATION

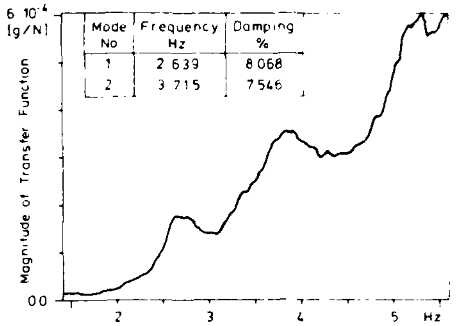

Mode No	Frequency Hz	Damping %
1	2 639	8 068
2	3 715	7 546

FIG 23 TRANSFER FUNCTION OF Y- ACCELERATION OF VERTICAL TAIL ANTISYMMETRICAL EXCITATION

In the next figure 24 we see in one figure transfer functions of the same pick-up obtained for different speeds but for one Mach number 0,78. The remarkable feature of these pictures is the shift of the peaks with speed. That means the frequencies decrease or increase with increasing speed. Figure 25 shows for M = 0,78 the frequencies for the symmetrical degrees of freedom: 2-node wing bending, lateral engine bending and engine *pitching versus speed. The solid lines are the calculated frequency; the symbols represent* frequency values obtained by the flight vibration test. The calculation results are based on a finite-element model for the structure and the doublet-lattice method corrected for transonic effects for the unsteady aerodynamics. Airforces are included for the vertical and lateral motion of the engine.

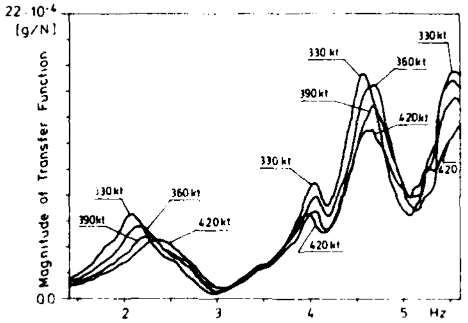

FIG 24 TRANSFER FUNCTION OF WING TIP ACCELERATION FOR VARIOUS SPEEDS SYMMETRICAL EXCITATION

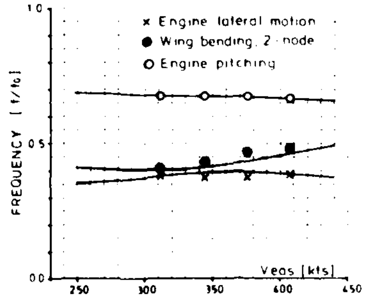

FIG 25 FREQUENCY VALUES VERSUS SPEED FOR M = 0.78

A comparison was made between the flight test results and the calculation of the unsteady transfer function. This was done by solving the flutter equation in which the right side of the equation respresented the vane excitation at various frequencies. Sweeps were made from 1 to 4.5 Hz, with a frequency increment of 0.02 Hz, 13 modes were included. The theoretical unsteady force was applied at the same point on which the vane lift acted, and the point at which response was measured was at the top of the wing very close to the vane. The results correspond to a z-displacement transfer function. It is necessary to multiply these values by ω^2 before comparing them to the flight test acceleration results.

Fig. 26 shows the calculated Nyquist-Diagrams for speeds 330, 360, 390 and 420 KCAS, M = 0.84. The change in the mode coupling for the first three degrees of freedom is clearly recognizable. Fig. 27 shows the calculated transfer-functions for 330 and 420 KCAS, M = 0.84. It is easy to interprete the coupling as the transfer of energy between the different modes.

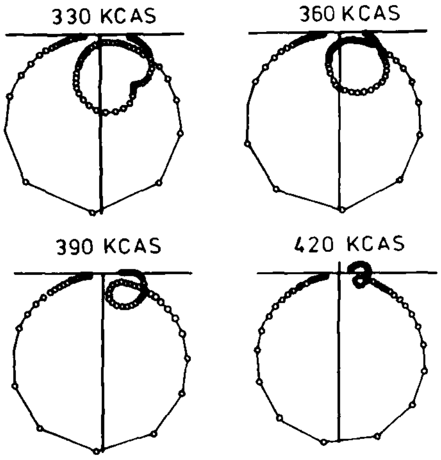

FIG. 26 CALCULATED NYQUIST PLOTS OF WING TIP RESPONSE FOR SEVERAL FLIGHT SPEEDS AT M = 0,84

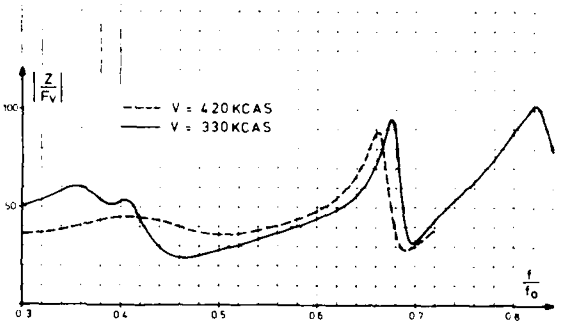

FIG. 27 CALCULATED WING TIP TRANSFER FUNCTIONS FOR TWO FLIGHT SPEEDS AT M = 0,84

CONCLUSIONS

The vane excitation method developed by Airbus Industrie for the flight vibration tests of the A 310 aircraft proved to be sucessful, and resulted in considerable savings of time and expense in the flight test stage.

It seems appropriate to recall the advantages offered by this method. Its salient features are:

- excitation amplitude and phase can be easily controlled and measured
- performs well at all frequencies
- does not alter the relevant properties of the aircraft
- easily installed and dismounted according to need
- excitation force is largely independent of frequency
- may be easily adapted to aircraft of different sizes.

REFERENCES:

[1] Methods et techniques de l'essai de vibration en vol
G. Piazzoli, Agard Symposium: Flight test technique.
Porz-Wahn, 11. - 15. October 1976

[2] Impulseur Pyrotechnique - Pyrotechnic bonkers
Fiche Technique ONERA, October 1976

[3] Experience from flight flutter testing with tip-vanes on Airbus
K. König, International Symposium on Aeroelasticity, Nuremberg, Germany
October 5. - 7. 1981

[4] An automatic method for finding the greatest or least value of function.
Rosenbrock
Computer Journal 3 (1960), 175 - 184.

[5] Exploitation par lissage mathematique des mesures admittance d'un systéme linearisé.
R. Dat - J.L. Meurzec
Recherche Aerospatiale 1972 -4

[6] Numerical Analysis of vector response
J.C. Copley, Royal Aircraft
Establishment, Technical Report 80135
November 1980

A THEORETICAL/EXPERIMENTAL TECHNIQUE
TO EVALUATE STORE SEPARATION CHARACTERISTICS

by

F. PORRATO and V. MO
AERITALIA - Società Aerospaziale Italiana
Gruppo Velivoli da Combattimento
Corso Marche 41
10146 Torino
Italy

SUMMARY

This paper describes the methodology developed in AERITALIA for a few years and currently adopted to clear the separation of external stores from the parent aircraft. The tools used in this process, i.e. mathematical model, wind tunnel testings, ground and flight trials, are presented and their advantages and disadvantages briefly discussed.

Particularly, the role of the matching phase between data gathered by the different techniques mentioned above to increase the reliability on store separation predictions, and hence to clear the separation of stores from the parent aircraft, is presented and discussed with a brief assessment of the method used.

1. INTRODUCTION

The development of modern combat aircraft in relation to the complexity of the weapon system, i.e. the capability to carry and release a wide range of external stores and with different loading configurations, has led to extensive requirements for investigation of separation characteristics with a large share in the overall design effort. Two aspects converge in this design effort with regard to external stores: safe separation as the aircraft has to be safely cleared from all stores in case of emergency, and release accuracy, to satisfy the operational requisites, for which all parameters affecting the store trajectory to the target have to be carefully appraised.

The present trend is to design the combat aircraft as a whole weapon system instead, as in the past, of designing the aircraft in isolation and adding at a later stage the external stores, with the consequence of having to accept either compromising features or expensive and lengthy studies to optimise the matching between store configurations and parent aircraft.

The capability to define design criteria of such a weapon system in relation to store separation characteristics depends upon the development and the proper use of different prediction and investigation tools and upon their integration. Experience has shown that the proper use of accurate predictive methods will not only result in increased delivery capability and enhance the safety of weapon delivery and jettison during flight testing and in service operation, but considerable savings of time and money can also be achieved. This technique gives in addition evidence of potential problem areas which could lead to shape modification of the aircraft/store interface and/or to the optimization of store release sequences and intervals in the early stage of aircraft design.

A further convenience of this technique is the possibility to investigate and to clear areas of the release envelope which are not flight tested or to limit the extent of flight trials to a selected number of test cases, having identified in advance possible critical areas in the envelope to be cleared.

2. TECHNIQUE TO PRODUCE A STORE SEPARATION CLEARANCE

For the reasons discussed in paragraph 1 a theoretical and experimental technique has been developed since several years ago and continuously refined by AERITALIA - Gruppo Velivoli da Combattimento, to assess the characteristics of separation of external stores from the parent aircraft.

The method (see fig. 1) is set up in three successive phases, so that at the end of each individual step, the following milestones are achieved:

- Build up of "the best" theoretical model
- Completion of flight trials and matching to experimental results
- Final updating of the model and theoretical extrapolation

2.1 - First phase: build up of the mathematical model.

This phase begins with the gathering of all data that have to be fed into the mathematical model.

They have to be analysed respecting accuracy and compatibility and further to gain some insight into the problems which might be encountered along the clearance process, and obviously have in addition to be made congruent to the mathematical model input data format.

The data are of different type and come from different sources as detailed in paragraph 3.1.

The mathematical model, having been fed with the input data, is then used to calculate the store trajectories for the given flight conditions.

At the same time, by means of a properly dynamically scaled model, a series of wind tunnel jettison tests is carried out to simulate store separation trajectories at given flight conditions.

This new set of trajectories is compared to those theoretically derived , and, if necessary, the mathematical model is updated until a good agreement between wind tunnel and theoretical trajectories is obtained.

The refining of the model is attempted upon those entry data which, by past experience, are guessed to be less reliable.

At the end of this process, an "optimum" model becomes available to predict store separation characteristics and to conform a flight test programme by selecting the test points in the significant areas of the flight envelope to be cleared.

The flight test programme is formulated to start at the flight conditions which have been predicted to be less critical and/or where the data, on which the theoretical predictions are based, are more reliable; further steps are stated on the básis of parametric studies to evaluate the influence of variables, like speed, incidence, sideslip, gun thrust etc., on store trajectory.

Therefore, the flight test programme as defined above is backed up by store trajectory predictions, which also include appraisals of the deviation from the standard trajectory due to tolerances on certain parameters such as sideslip, load factor, ERU performance, etc.

2.2 - Second phase: flight trials and matching to experimental results

During flight the store initial trajectory is filmed by means of on-board cameras, and additionally, in case of stores such as bombs, for which the entire ballistic is requested, by range kinetheodolites.

After flight, the films are analysed and the store separation trajetory is reduced to its six components vs. time, and therefore in a format which is directly comparable with the predictions.

The analysis of the deviations between the two trajectories allows identification of which input data of the mathematical model have to be rectified, with an iterative loop, to obtain a good agreement between the two trajectories.

Having updated in this way the model, the new predictions for the next flight test step are computed.

At this point, the process (flight test, analysis and matching) is started and repeated again, until the test programme is carried out and the model is validated throughout the required flight envelope.

In addition to this excercise, the flight trials allow also an assessment of the functioning of the armament system, e.g. arming sequences, mechanical and electrical interfaces etc. and an assessment of the air craft handling and structural response during the ejection phase.

2.3 - Third phase: theoretical extrapolation and envelope clearance

During the third phase, which begins after the completion of the armament trials, the flight tested jettison envelope is theoretically extrapolated, by means of the mathematical model, now matched to flight data to clear the jettison envelope requested by the customer, or, when limiting factors are found, to specify the jettison envelope boundaries whithin which safe separation can be guaranteed.

Aim of the extrapolation is:

a. To save flight trials, which being money and time consuming, have to be devoted to investigate only some selected key points, as mentioned above.

b. To investigate the jettison behaviour at those conditions which might not be flight tested pending current limitations on the test aircraft, which often is a prototype aircraft.

c. To produce a complete set of deviations from standard trajectories due to tolerances on separation parameters and flight conditions to add a safe margin to the clearance.

In the light of the brief description of the three phases, it is evident that the results which build up during the process allow for a timely intervention for modifications such as:

a. store configuration (e.g. fins)

b. store aircraft interface (e.g. ERU characteristics and throttle settings)

c. release sequences and intervals

which might be necessary to improve separation.

Though the process is mainly devoted to define safe separation clearances, for those stores, such as bombs, for which it is of relevance, an effort is also made during the three phases to identify parameters affecting the separation accuracy in respect of ballistics.

3. INSTRUMENTS TO PRODUCE STORE SEPARATION TRAJECTORIES

The definition of store separation trajectories from the parent aircraft and of the consequent safe separation envelope are the result of the matching and of the integration of results obtained from different sources: mathematical model, dynamically scaled jettison tests and flight trials. A brief description of these three instruments, as well as an analysis of their advantages and disadvantages is given below.

3.1 - Input data of the mathematical model

To allow a better understanding of the meaning of the various input data of the mathematical model and of their mutual relations, it is convenient to give a picture of the aerodynamic flow field with which the store interacts along its separation trajectory. It can be schematically divided into the zones which follow one after the other along the trajectory:

- Interference field: in this zone, which is close to the aircraft, the aerodynamic flow field is affected by the mutual aerodynamic interference exerted among the different external stores and between them and the aircraft. The consequent flow field is strongly distorted with non-stationary components which can not always be neglected and which is dominated by viscous and compressibility effects. Furthermore, bearing in mind that the extreme proximity of the external stores causes the formation of several reflected shock waves, especially in the speed range in which the modern combat aircraft operate, it is evident how the flow-flied is difficult to be theoretically simulated and how the analysis of wind tunnel results should be cautious as well as matching, for example, data coming from different sources: i.e. store balance components and oil flow visualizations (fig. 2) to avoid misleading interpretations of the latter.

Nevertheless the knowledge of this zone of aerodynamic flow-field is of paramount importance in predicting store separation trajectories, because the weapon release disturbance, which acts on the store in this zone, influences the outer trajectory, particularly when the store has low density or when it has a small aerodynamic stability margin.

- Near field: in this zone, which extends from about 1 meter down to 4 + 5 metres below the aircraft, the effect of the mutual aerodynamic interference among external stores is practically negligible, and the aerodynamic flow-field is disturbed only by the presence of the aircraft. Therefore the aerodynamic load acting on the released store in a fixed point can be determined by superposition of store free air aerodynamics and aircraft flow-field characteristics (expressed in terms of local incidence, sideslip, Mach number etc.) at that point in absence of the store.

  It is clear that, being the flow-field perturbed, i.e. with its characteristic parameters varying from point to point and then also along the store, the aerodynamic forces and moments acting on it are the sum of the contributions of the different sections in which the store is divided and around which the aerodynamic flow-field can be reasonably assumed constant.
- Far field: in this zone, because of its fairly large distance from the aircraft, the flow-field can be assumed to be free stream and hence the aerodynamic force acting on the store is calculated by superposition of store free air aerodynamics and free stream characteristics.

  If the purpose of the prediction of jettison trajectories is limited to the check of store safe separation, this zone is the less critical both because the flow-field can be assumed to be free stream and hence constant, and because, being this zone quite far from the aircraft, it has a minor influence on jettison safety for which the first part of the trajectory is determinant.

  On the contrary, if the purpose includes the extrapolation of flight trials results with regard to the ballistics of the stores, this zone is perhaps the most important because it influences for longer time the store trajectory and, hence assuming the flow-field as constant, it might no longer lead to satisfactory predictions. Therefore more detailed informations about flow field characteristics versus altitude (velocity profiles) are needed.

3.1.1 - Store free air aerodynamics

The aerodynamic force acting on a store along its separation trajectory plays a fundamental, and in some case decisive, role in determining the jettison safety: a fundamental role, because among the forces of different nature acting on a store when dropped, the aerodynamic action is never secondary; a decisive role when low density stores (empty fuel tanks, multiple store carriers, etc. are jettisoned as the aerodynamic force is by far predominant over others.

It is therefore evident the primary importance of the knowledge of the static aerodynamic forces and moments acting on the isolated store and the accuracy required to measure them. Much care has to be taken, and a certain experience is also required, for example, in positioning transition bands on models (fig. 3 shows a tipical arrangement) with the aim of approaching in the best possible way the flow-field around the full scale body. Another critical problem is to minimize or in any case to quantify the aerodynamic interference of the model support, particularly on the normal force and on the pitching moment for a suspension from the floor and on the axial force using a rear sting. A well known technique to quantify this interference consists of using a dual sting (fig. 4), with which it is possible to calculate the interference of the dummy sting by difference. This problem is however made worse by the particular incidence range required for some external stores (in a case it has been necessary to measure the aerodynamic force for an incidence traverse from 0° to 360° and a sideslip range from 0° to 180°). This implies that the information about the sting/wall aerodynamic interference obtained by means of the usual wind tunnel calibration models is often not sufficient to solve the problem. A valid help sometimes comes from aerodynamic numerical codes (panel method), which for selected speed/incidence ranges allows the simulation of the effects of the supporting strut and then to quantify its interference on model aerodynamics.

Another important set of input data of the mathematical model are aerordynamic damping derivatives, whose knowledge is very useful to have a complete appraisal of store aerodynamics. These coefficients are normally obtained by wind tunnel tests using the forced oscillations method (a pilot-plant has been tested at AERITALIA), but sometimes they are theoretically calculated using standard methods such as Datcom. The theoretical evaluation of aerodynamic damping derivatives, which at high incidence is little reliable, implies however an increase of the subsequent matching activity at least for the first drops.

3.1.2 - Aircraft aerodynamic flow-field

The jettisoned store crosses along its trajectory a region of highly perturbed flow, mainly due to the presence of the parent aircraft; it is therefore of paramount importance to know in each point of this region the characteristics of the flow.

It would be necessary, to carry out this research in the best way, to measure the flow-field for all the external store configurations or at least for some selected key configurations and to read across the others. As this approach is extremely expensive, it is preferred to measure, or in some cases to calculate theoreretically (panel method) but with results not always satisfactory, the flow field relevant to the clean air

craft (fig. 5) and to delegate to other types of wind tunnel tests the measure of the mutual aerodynamic interference among stores and between them and the aircraft.
During the MRCA Tornado project the flow-field was measured in the A.R.A. transonic wind tunnel utilizing a rake of 16 five hole pressure measuring probes which swept the region beneath the aircraft model. In each measuring station (10 underwing and 8 underfuselage) the local characteristics of flow-field were tape-recorded and then, by means of a reduction program, the local values of incidence, sideslip, Mach number, total and dynamic pressures were obtained for different flight conditions (α_∞ ,β_∞ ,M_∞) and for two values of tailplane setting. These data were then cross plotted to allow a check of the congruence among them, especially on the overlap regions of the measure points, and afterwards they were stored in order to permit an easy read-across by the mathematical model. The greatest difficulties experienced during these tests were the correct positioning of the rake close to the model due to the geometrical interference, as well as the measure of the aerodynamic disturbance caused by the rake itself.

3.1.3 - Installed store loads

This kind of wind tunnel tests, together with store trajectory load measurements, which will be described in the following paragraph, is the most effective tool to derive the mutual aerodynamic interference among external stores and between them and parent aircraft. In fact with this technique it is possible to measure, for different flight conditions and external store configurations, the aerodynamic forces and moments acting on a certain store when it is installed on the aircraft. The advantage of these wind tunnel tests is that they allow a fairly accurate measurement of the forces and moments, because there are no problems of sting interference, being the balance mounted inside the store consequently being able to simulate correctly the configuration geometry. On the other hand they are rather expensive because of the great number of configurations to be tested. In fact their number is the product of the number of key configurations times the number of possible configurational variants (which come out from the release sequence combinations allowed by the Store Management System) and times the number of selected aircraft configurations and flight conditions (wing sweep angle, tailplane setting, Mach number etc.). In addition the results obtained from these wind tunnel tests can be misleading, if not used with caution, in the theoretical prediction of separation trajectories, because the aerodynamic force acting on the store just jettisoned can be different from that acting on the installed store. A typical example is the case of two bombs carried on a twin carrier and flying at transonic speed (fig. 2). In all probability the channel between bombs will be choked with a consequent increase of pressure on stores forebody, and this blockage effect will persist for reasonable variations of upstream flow. On the contrary, when one bomb is dropped, the blockage effect vanishes and hence the longitudinal components of the aerodynamic force acting on the store change very quickly, as well as the lateral ones due to the mutual suction.
Consequently the informations obtained from store installed load measurements can be usefull input data in producing separation trajectory predictions only if very carefully analysed and when possible matched to results coming from other sources.

3.1.4 - Store trajectory loads

These wind tunnel tests are a generalization of the previous tests, in that they allow the measure of the aerodynamic load acting on a store not only in the installed position but also along the separation trajectory. The facility used is the same as the one employed for the Captive Trajectory System, i.e. utilizing a dual sting (fig. 6). In this case however position and attitude of the store model are not controlled by the computer solving the motion equations, but they are varied with a grid scheme through the volume expected to be crossed by separation trajectories of that store.
The advantage of these tests is to provide a rather accurate measure of the mutual aerodynamic interference between jettisoned store and aircraft or other weapons, providing therefore an usefull term of comparison for results obtained from the matching of the previous wind tunnel tests. On the contrary, besides the disadvantage of having to test many configurations, similarly to the tests described before, and here made worse by the need to sweep several positions and attitudes for each external store, this technique presents additional disadvantages:

- dual support method may require alteration to the store afterbody to accomodate the sting and also raises the question of sting effect on the store loads
- the possibility to reach high store attitudes due to the geometric interference between secondary sting and aircraft model
- the possibility to measure the aerodynamic forces and moments of one store at the time only
- weapon trajectories are often relatively short in duration because of the geometrical constraints of the support.

3.1.5 - Store inertial characteristics

Store inertial characteristics, expressed in terms of mass, center of gravity position and moments of inertia along the three principal axes, are important input parameters in predicting separation trajectories. Particularly, for low density stores and/or with narrow aerodynamic stability margins, the center of gravity position with respect to the centreline of the ejection release unit is determinant for jettison safety, because it produces the initial pitching moment on the store (nose up or down) from which the course of the trajectory depends. For this reason, while for non critical stores with regard to safe separation (high density stores or with a large separation velocity) it is sufficient to know the inertial characteristics meas sured on some standard samples, for critical stores it is necessary to measure with the highest accuracy the inertial characteristics of each store to be released.

3.1.6 - ERU performances and missile booster thrust

There are basically two types of bomb ejection racks in common use, those with single ejection piston and those with dual ejection piston. The latter (a typical impulse performance is shown in fig. 7A) usually have orifices which are ground adjustable to meter the flow of ballistic gas from the cartridges to the ejection pistons. This feature permits the force of each ejection piston to be indipendently varied from completely closed to fully open. Thus the ejection forces and moments imparted to the store can be controlled over a wide range. The knowledge of the ERU performances versus different parameters like throttle setting, atmospheric temperature, rack supporting structure flexibility etc., is of paramount importance in predicting store separation behaviour. Performance curves (as shown in fig. 7B) are determined during a ground rig test and are normally provided by the ERU's manufacturer without calibrations for temperature and corrections for store aerodynamics loading or dynamic and elastic effect of rack/store carrier/ pylon/ wing. Adequate guidelines do not exist for correcting static bomb rack ejection data. The only known procedure to evaluate dynamic and elastic effect of rack supporting structure on ERU's performances are pit drop tests which are detailed in the next paragraph.
As far as the propelled weapon is concerned, the necessary input data for a correct trajectory simulation regard the state of booster thrust versus time, of which figure 8 shows a typical trend, and its changes with atmospheric temperature, as well as some information about launcher/missile mechanical constraints and intervals/sequence of booster ignition.
These data are normally provided by the missile suppliers.

3.1.7 - Pit drop tests

The information which is gathered from pit trials is ERU performances (in terms of ejection force, ejection velocity and initial store trajectory). The advantage of the pit drop trials is that several cases can be tested, at low cost, when applicable, for different wing sweep, ERU throttle setting, store centre of gravity positions etc.
The separation data obtained from pit drop tests are fed into the mathematical model during the first phase (see paragraph 2.1).
The separation data are obtained by processing and analysing the film records of the cameras which have been run during the separation of stores from the aircraft. For this purpose, cameras are installed both in the aircraft (fuselage fairings and camera pods) at the same locations which are used for the flight trials and externally at suitable positions to obtain the best camera coverage. The cameras are run at high speed (200 + 500 frames per second) and the pictures from the different cameras are correlated between them and with the aircraft on-board instrumentation, which normally records the armament events as release button press and weapon gone's, to allow the triangulation analysis to output the store trajectory and attitudes in the aircraft axis reference system.
The most accurate analysis is on the very initial trajectory. i.e. up to the end of the ERU gun stroke (normally 0.1m), which provides, after further analysis, the actual ERU performance data.
The camera film readings are made by means of a film analyser, which outputs store and reference points position, recorded on cassettes, which are then processed at the Data Processing Center.
Details of the film analysis are given, being similar to the flight trials analysis, in the paragraph 3.4.
Beyond the separation analysis, the pit drop tests are envisaged to provide an assessment of the armament loading procedures armament ancillaries operation and the evaluation of the aircraft structural response when jettisoning external stores, as reference to the flight trials data.

3.2 - Mathematical model

The definition "mathematical model", whose lay out is shown if fig. 9, does not include just the computer program which solves store motion equations and then calculates store jettison trajectories from the parent aircraft, but also comprises all input data which define store aerodynamic/inertial characteristics, ejection rack performances, aircraft flow-field to allow the numerical simulation of separation trajectories. Therefore, after having described in the previous paragraphs the mathematical model "data bank" itself stored in the computed memory, the numerical code and its outputs are briefly illustrated. Knowing the flight conditions at which the drop will be performed (and they can be the most various as the numerical code allows a representation of aircraft manoeuvres), aerodynamic forces and moments acting on store are calculated by superposition of store aerodynamic characteristics and aircraft flow-field. Installed store loads, which are reduced from the installed position to zero at a depth where it is considered that interference effects are negligible, are then summed up to the previous aerodynamic loads, which, on the contrary, are increased from zero to their actual values at the same depth and the results of the sum are matched to store trajectory loads, when they are available.

$$F_{TOTAL} = K_1 \; F_{A/C\ flow\text{-}field} + K_2 \; F_{interference}$$

Aerodynamic forces are combined with physical forces such as store mass, ejection forces or missile thrust etc., and then the store velocity and displacement components are computed solving the Euler equations of motion for a body with six degrees of freedom. The differential equations of motion are transformed in finite difference equations and then integrated by means of an iterative loop whose formulas are listed in figure 10.

The output of the mathematical model is:

- position and attitude of the store versus time referred both to a ground frame and to a frame fixed to the aircraft which of course during separation can be manoeuvering
- six component store velocity versus time referred to a body frame
- components of forces and moments acting on store versus time referred to the same reference frame
- plots of the three orthogonal projections of store trajectory referred to a reference frame fixed to the aircraft. A typical example of these plots is shown in figure 11.

The experience gained till now, mainly from the Tornado project, has proved that the use of the mathematical model to co-ordinate different types of wind tunnel test data and to match flight trial results is in general very reliable (fig. 12).

In addition, the mathematical model is an instrument to predict separation behaviours of a store from parent aircraft much more flexible, quick and cheap than dynamically scaled jettison tests and even more so than flight trials.

Therefore, thanks to the good simulation that can be obtained with this tool after an adequate matching with experimental results, the basic study has to be performed with the mathematical model, delegating to experimentation, especially in flight, only the check of the most critical conditions or at least of the most meaningful ones. Moreover the flexibility of the mathematical model permits the study, in relatively short time and cheaply, of the possible variants of store shape and/or aircraft-weapon interface as well as changes in release intervals/sequences and then to test only the solution found to be the most convenient.

On the other hand the mathematical model is not an instrument which can straight fordwardly predict or match the jettison trajectory for whatever flight condition or load configuration. Often instead, for transonic flight conditions or for critical stores regarding safe separation, where compressibility or aerodynamic interference effects are dominant, a considerable amount of analysis of the mathematical model input/output and of matching to experimental results is necessary to understand in depth aerodynamic interference mechanisms and their effects on store jettison trajectory behaviour.

3.3 - Dynamically scaled jettison tests

The aim of these wind tunnel tests is to gain a better insight into store separation behaviour and to obtain some experimental results with which to calibrate the mathematical model. In particular in the early stage of a project the complete set of mathematical model input data is sometimes not available, or at least some data have been guessed or theoretically derived (especially store aerodynamic damping derivatives) and the effect of the aerodynamic interference is not quite clear; in these conditions an accurate analysis of wind tunnel jettison test results can provide an useful key to identify the typical characteristics of store separation in a certain configuration and the relationships which link them with the flight conditions at which the jettison has been performed.

The geometry similarity between separation trajectories obtained both from flight and wind tunnel test requires that, besides the obvious geometrical similarity between full and model scale stores configuration, also the dynamic similarity (i.e. involved forces and moments are in the same ratio both at full and model scale) be complied. Three dynamic similarity laws are normally used in this kind of tests: heavy body, light body and Froude's; each of them do not allow to duplicate all the involved parameters, so the choice depends upon the problem to be solved, the gained experience and wind tunnel facilities. At Aeritalia, Froude's similarity law (seldom light body law), is normally used, and the ratios between full and model-scale quantities are enlisted in fig. 13. This law, as known, does not permit to duplicate Mach number, so the simulation is limited to moderate speeds where compressibility effects can be neglected.

A dynamically scaled jettison test is set up in the following steps (fig. 14):

- the model of external store to be dropped is hung to the aircraft model, respecting the full scale loading configuration
- the flight conditions at which the jettison has to be performed are reached in similarity
- the store, pushed by two pneumatically driven pistons, leaves the aircraft
- the store positions along the separation trajectory are photographed by two cameras mounted in front and laterally to the aircraft model. Multiple exposures on the same frame are obtained by means of a stroboscope
- from the front and side views of the store trajectory so obtained, the six components of store motion versus time are derived.

A typical output of wind tunnel jettison tests is illustrated in figure 15 which shows also the comparison with theoretical results.

The main advantages of free-drop tests are the following:

- the possibility of simulating correctly store jettison trajectory from the parent aircraft, being able to duplicate the full scale store configurations, because there are no problems of sting aerodynamic interference
- the possibility to perform multiple releases
- the wind tunnel facilities necessary to carry out these tests are not so sophisticated as those required by other techniques

On the contrary dynamically scaled jettison tests presents typical disadvantages:

- the possibility to simulate store releases only at straight and level flight conditions
- weapon trajectories are often relatively short in duration because of the geometrical interference of wind tunnel walls
- the difficulty encountered in some cases in manufacturing dynamically scaled models (expecially those representing low density stores) which implies the use of various materials to respect the required inertial characteristics
- the necessity to built many store models, being these damaged and therefore not re-usable, in general, after every three or four drops.

3.4 - Flight trials

3.4.1 Preflight activity

Before armament flight trials commence, a certain amount of work has to be carried out on ground to make the acquisition system able to acquire with the necessary accuracy all the trajectory data needed to properly match the mathematical model results to flight data. This work is illustrated below.

- As the appraisal of the store trajectories is made by means of cameras installed in the aircraft (fig. 16 - fuselage fairings and camera pods), the first step is the selection of the cameras to be used for every planned drop. The selection is made on the basis of the camera coverage, which should be at least 8 metres of vertical trajectory, taking into account the aircraft configuration (e.g. wing sweep), the obscurations which may occur from other stores and/or pylons and the expected store trajectory. At least two cameras are needed, to allow triangulation, but in general up to five cameras are used for each drop.
- Special markers have to be painted, at suitable positions relative to the cameras, on the aircraft fuselage and pylons.
  The X, Y, Z coordinates of the markers have then to be accurately measured, as they will be used as fixed reference for the store trajectory analysis.
- In the case of a forward trajectory (missile firing trajectory analysis), the forward looking cameras have to be "harmonized", i.e. the camera optical axis orientations have to be determined using a board with markers at known positions in respect to the aircraft axes reference system. The board is positioned at right angles to the aircraft axis, at a distance from the cameras of about 30 metres.
- The stores should have a special painting, to ease the measurements of the pitch, yaw and roll motions: special markers will be therefore painted at every 30 deg. around the store circumference at relevant sections (e.g. centre of gravity). The coordinates of the markers have to be measured.
- The stores to be dropped must have the weight, centre of gravity position and moments of inertia determined.

3.4.2 Flight testing

The flight trials, for each external store configuration, are then started, at the test conditions predicted by means of the mathematical model, to be significant or less critical.

After flight the trajectory data are analyzed (fig. 17) and compared to the predictions. The mathematical model will then be updated, if necessary, so that an agreement is obtained between experimental and theoretical results.

The flight trials then progress, with a matching phase at every step, till the mathematical model is confidently validated.

3.4.3 Postflight analysis

The store trajectory is obtained by reading out the camera films from a film analyser whose output is processed through a computer programme (fig. 18). Basically two programmes are currently in use for the analysis, in order to have some flexibility depending on the type of store and the expected trajectory.

The two programmes care for the following store separations:

a - vertical separation of light and large stores.
b - vertical separation of heavy stores and light/small stores.
c - horizontal separation (missiles and rockets).

The programme for the separation of light and large stores (e.g. empty tanks) works on the concept of overimposion (form fitting) of sequential store positions in the space (with six degrees of freedom): it compares the initial position of the store with those resulting during separations, and the accuracy, even in the case of large lateral movements coupled to roll motions, is very high.

The trajectories produced are computed individually from each camera (from 1 to 5) and then compared; the output will be a minimum deviation calculated trajectory. Each individual camera trajectory can also be printed out to monitor the dispersion and hence the accuracy of the analysis.

The other programme (fig. 19), for the separation of heavy stores (e.g. bombs), light/small stores and missiles has several loops for computation; it is based on a triangulations concept and the positions of each store marker, during separation, is calculated simultaneously from two selected cameras, which have to be perfectly syncronised and correlated. The motion of the store is obtained by measuring from the film frame the coordinates of 3 store markers; the markers have to be the same for both cameras. From ground harmonisations, the coordinates of the markers are known in the aircraft axis reference system, and therefore the motion can be referred to this system. This process requires the in-flight harmonisation of the two cameras,

i.e. the alignement of the cameras in respect of the aircraft axis system: for this purpose at least two aircraft fuselage markers have to be visible from both cameras (fig. 20).
During the film reading, the store markers, whose coordinates are measured, can be changed (this is obviously necessary in presence of large yaw and roll motions), provided that the markers are always the same for both cameras.

4. GROUND/FLIGHT TEST RESULTS CORRELATION

The ground/flight test results correlation is presented here in two sections: the first will show the technique to match the theoretical predicitions to the experimental results from both wind tunnel and flight trials; the second section will present a case history to demonstrate how that technique was capable of evidentiating the characteristic separation behaviour of a store from the parent aircraft and hence to clear the separation envelope.

4.1 - Matching technique

The correlation process which is carried out after every in-flight test has three purposes:
- To evidentiate, on the basis of the accurate analysis of the time-histories of the six motion components, the peculiar characteristics of the store separation trajectories.
- To correlate those characteristics to the parameters which may affect them (flight conditions at release, store aerodynamics, ejection force etc.)
- To update accordingly the mathematical model input data in order to duplicate the experimental trajectories.

At the end of the trials, and having fulfilled entirely the above purposes, beyond the validation of the mathematical model a further important result has been achieved, i.e. the knowledge of the "weight" of each parameter in determining the store separation characteristics.
The matching process begins with the re-computation of the trajectory theoretical prediction, but with the flight conditions corresponding to the actual experimental release conditions. This is obviously necessary as in fligth the release conditions may slightly differ from those for which the theoretical prediction was computed. Though little changes to some of the flight test conditions (e.g. ± 5 ÷ 10 KCAS, ± 2000 ft height) do not produce noticeable effects on the trajectories, even little deviations from the nominal data of other flight conditions (e.g. ± 0.5 deg. incidence or sideslip) cannot be neglected as they might heavily influence the store trajectory.
The second step of the matching process is the comparison between the theoretical predictions and the experimental results. The comparison is made at the same time over the store six motion components time histories, as in greater or less extent there is always a connection between the six components.
A typical example of this behaviour is given by a large empty external fuel tank which, because of a great difference between lateral and pitch stability caused by the asymmetry of the tail fins, shows a nose up tendency when rolled of about 90 degrees. Another typical characteristic of the motion of this tank is that it couples an inner fin down rolling movement with a nose out yawing rotation and viceversa.
Therefore, when analysing the differences between the individual theoretical and experimental motion components, one ought to be very cautious and able to put in evidence those indipendent variables on which the greatest part of the matching process is centered. In the typical case indicated above it was shown that, by matching correctly the tank roll motion, the deviations between the theoretical and the experimental results of tank pitch attitude and of vertical displacement were largely reduced. It is clear that the greatest care should be applied when matching the early flight test results as, after having gathered confidence on the separation characteristics of a store in a given configuration during trials progress, the matching process becomes generally straight forward.
The third step of the matching process consists in the investigation of the reasons for the deviations between the theoretical and experimental six motion components, i.e. to find the correlation of each typical separation trajectory behaviour with one or more mathematical model input parameter. As every individual effect on trajetory may be apparently produced by several causes, as shown in fig. 21, it is necessary to proceed during this phase with a comparative analysis of the input data of the model to individuate the parameter, or sometimes those parameters, which really determines the deviation.
Also in this phase of the analysis it is of paramount importance to examin the entire trajectory set because, as a pattern might be produced by different causes, in the same way the variation of a given input parameter to the model might end with several different effects on as much different motion components; it is therefore necessary to correlate the deviations between theoretical and experimental results to discriminate the one, or more, input data responsible for the deviation.
A further rule for the selection of the input parameters to be changed into the mathematical model is based on the level of their reliability, i.e. whether they have been valued theoretically only, or measured experimentally (e.g. during wind tunnel and pit drop tests) and, in the latter case, with which level of accuracy (number of test points etc.). Again this analysis work might be rather extensive in the early stage of the experimental phase, but, as trials progress, even towards the critical areas of the flight envelope where the effects produced by the different input data are more remarkable, the matching activity and the corresponding updating of the mathematical model become straight forward and less difficult because of the experience gained on the role played by the several input parameters.

4.2 - A typical case history

The value of using the matching process and a wide range of information inputs to the mathematical model can best be demonstrated by describing a typical case history for a practice weapon dispenser. The reason for which this store has been selected among the many that have been cleared for the TORNADO aircraft is that the dispenser has shown to be critical and has required a relevant matching activity.

It would be little significant to present a case history for a body non-critical from a separation point of view (and fortunately most of stores were non-critical), as the relation between theoretical prediction activity and envelope clearance is purely a straight forward matching activity because of the good agreement between predicted and experimental trajectories.

The practice weapon dispenser, in spite of the limited required jettison envelope, was a rather difficult body to be cleared for separation because of the following reasons:

- it had to be cleared with different practice bomb loading configurations, including the asymmetric ones.
- in some of above configurations it is a low density store with a tendency to float in the air
- in some attitude ranges the dispenser becomes aerodynamically unstable being without tail fins
- the dispenser longitudinal centre of gravity position in respect to the ejection release unit centre-line does not permit to achieve the necessary nose down pitching moment.

In addition, the theoretical prediction itself was made more difficult because of the lack of some input data as:

- store installed/trajectory loads;
- store aerodynamic damping derivatives;
- ejection release thrust reduction due to wing and pylon flexibility;
- actual data on ERU performance when asymmetric throttle setting is applied (for the dispenser the nominal thrust was 100% for the forward ERU gun and 20% for the rear one);
- the limited range of attitudes ($+ 60 \leqslant \alpha \leqslant - 60$ deg, $+ 30 \leqslant \beta \leqslant - 30$ deg) for which the store free air aerodynamics were measured. In general this range of attitueds is adequate to cover all attitudes of a store along its trajectory, but not for the dispenser which, being aerodynamically unstable, separates from the aircraft rolling mainly in the longitudinal plane.

Having therefore estimated theoretically the missing input data for the mathematical model, the safe separation envelope of the dispenser was predicted. Already from the preliminary prediction work it became clear the need to change the throttle setting of the ejection release unit, that was originally planned to be full thrust, to improve the separation characteristics of the dispenser in some loading configurations (i.e. empty or with two forward practice bombs, with the consequent advance of centre of gravity in respect of the ejection release unit centre-line which produced the dispenser nose up pitching moment at release - see fig. 22).

A parametric study indicated that, by applying an asymmetric ejection thrust (100% forward and 20% rear), the separation characteristics for the above loading configurations were largely improved (fig. 23), but with detrimental effects, when the dispenser was loaded with only two rear practice bombs: in this case the dispenser afterbody showed a tendency "to lean" on the aircraft pylon, obviously because of the greater pitch down moment produced by the ejection release unit in addition to that one developed because of the dispenser rear centre of gravity position.

Several proposals were made to overcome the problem, as:

- to find an average throttle setting suitable for the different loading configurations
- to fit a rubber fairing to the rear end of the dispenser.

At the end, the Customer recognized that the emergency jettison of the dispenser with two rear bombs represented only a consecutive double failure case and the requisite to clear that particular loading configuration was dropped.

The results obtained with the dynamically scaled jettison tests had confirmed, in general, the theoretical predictions both with regard to the safe separation envelope and to the need of an asymmetric throttle setting (compare fig. 23 with 24).

The analysis of the deviations between theoretical and experimental trajectories further revealed some information on the mutual aerodynamic interference between the dispenser and the aircraft thus allowing the updating of the mathematical model input data. No data was, in the other hand, achievable on the actual ERU performance with asymmetric throttle setting and on the effect of flexibility of the wing/pylon structure as they are input data for the wind tunnel jettison tests.

Having the Customer dropped the requirement for the dispenser side rocket panniers, the mathematical model had to be set up again in relation to the store aerodynamics and a new safe separation envelope had to be recalculated. The results which have been obtained revealed an improvement of the separation characteristics of the dispenser for all practice bomb loading configurations, because of the reduced lifting area. Similarly to the previous tests, from the analysis of the results of the dynamically scaled jettison tests, in agreement with the theoretical predictions, some usefull data on store and aircraft mutual interference have been derived to update the mathematical model. At the end of the process, the most reliable model has become available and it has been possible to conform the relevant flight test programme by selecting key tests points in the significant areas of the jettison envelope and some loading configurations, starting of course from those predicted to be less critical.

As flight trials progressed, the comparison between theoretical and experimental trajectories evidentiated the need to modify same of the mathematical model input data to achieve a good agreement between the trajectories. At first, it became clearly evident that the ERU ejection forces were higher than expected, due to the excessive reduction to the nominal thrust envisaged to take into account the wing and pylon flexibility which in turn was lower than expected. An early sign of this problem had in fact already been given

from the previous trials on other stores and because of this, the ejection force input data had to be increased, almost zeroing the reduction estimated for the flexibility. In the practice weapon dispenser case this reduction had to be almost totally neglected because of the low mass of the store.
A further source of problems came from the selection of differential throttle settings due to the non-linearity between ejection release forces and throttle size.
The analysis of the flight trial results also provided some indications on the mutual aerodynamic interference between the dispenser and the parent aircraft, and on the modifications to be applied to the estimated damping derivatives, which allowed for a further updating of the mathematical model.
The preliminary flight trial results also put in evidence the poor reliability of the store free air aerodynamic data fed into the mathematical model, which where measured in a relatively limited α and β range and than theoretically extrapolated. The evidence of this problem came out from the difficulty to match the experimental trajectory trend and in particular the vertical displacement and the picth attitude so that, for example, the typical rotation in the longitudinal plane could not be theoretically reproduced (fig. 25). This behaviour was not revealed by the dynamically scaled jettison tests because of the relatively short duration of the trajectories. For this reason the dispenser free air aerodynamics has been further measured for an α traverse of 360° and β traverse of ± 90°. Having updated the model with the new store aerodynamics a good matching was finally achieved (compare fig. 25 with fig. 26) thus allowing the extrapolation of the flight tested jettison envelope to clear the required dispenser jettison zone of operation, with an adequate level of reliability and with a sufficient set of data to cover the tolerance cases.

5. CONCLUSIONS

From the discussions and the case history presented above it appears convenient to integrate theoretical and experimental work in the exercise of clearing the safe separation of a large range of external stores from the parent aircraft. The achievement of the theoretical and experimental joint work will be, besides the saving in terms of number of flights and time to provide the clearance, a thorough knowledge of the various items governing the separation pattern of different stores and from that the background for further developments.

ACKNOWLEDGEMENTS

The authors wish to acknowledge Aeritalia's permission to present this paper. They also express their appreciation to Mrs. L. Marietti and Mrs. L. Neri for the contribution in typewriting and drawing.
The activity presented in this paper is the result of team work and for this reason the authors thank Mr. E. Barbantini (Wind Tunnel), Mr. F.P. Laurino (Flight Test) and Mr. S.Barbero (Aerodynamics).

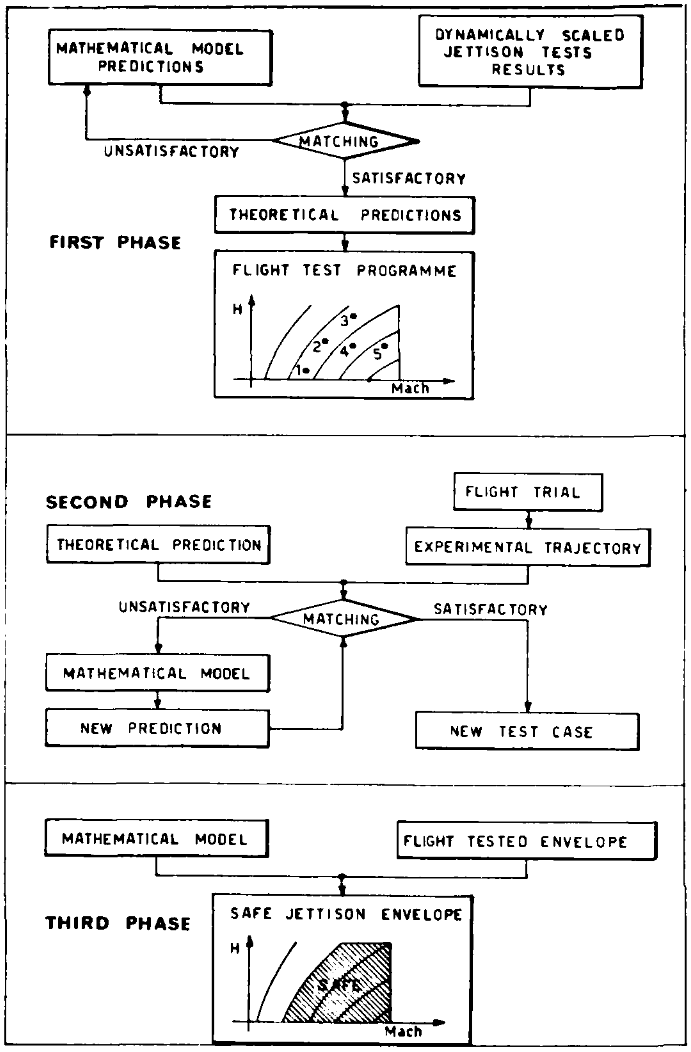
MATHEMATICAL MODEL PREDICTIONS
DYNAMICALLY SCALED JETTISON TESTS RESULTS
UNSATISFACTORY
MATCHING
SATISFACTORY
THEORETICAL PREDICTIONS
FIRST PHASE
FLIGHT TEST PROGRAMME
H
1
2
3
4
5
Mach
SECOND PHASE
FLIGHT TRIAL
THEORETICAL PREDICTION
EXPERIMENTAL TRAJECTORY
UNSATISFACTORY
MATCHING
SATISFACTORY
MATHEMATICAL MODEL
NEW PREDICTION
NEW TEST CASE
MATHEMATICAL MODEL
FLIGHT TESTED ENVELOPE
THIRD PHASE
SAFE JETTISON ENVELOPE
H
SAFE
Mach

FIG. 1 - Method scheme

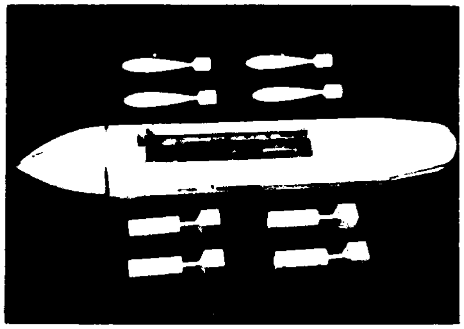

FIG. 3 - Transition bands positioning

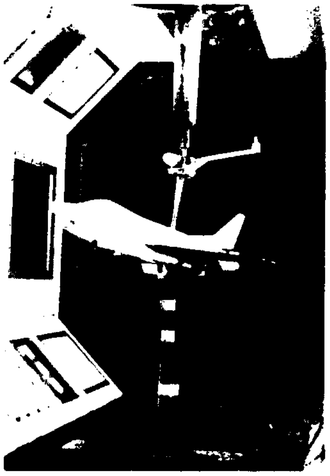

FIG. 4 - Dual sting support

FIG. 2 - Flow visualization

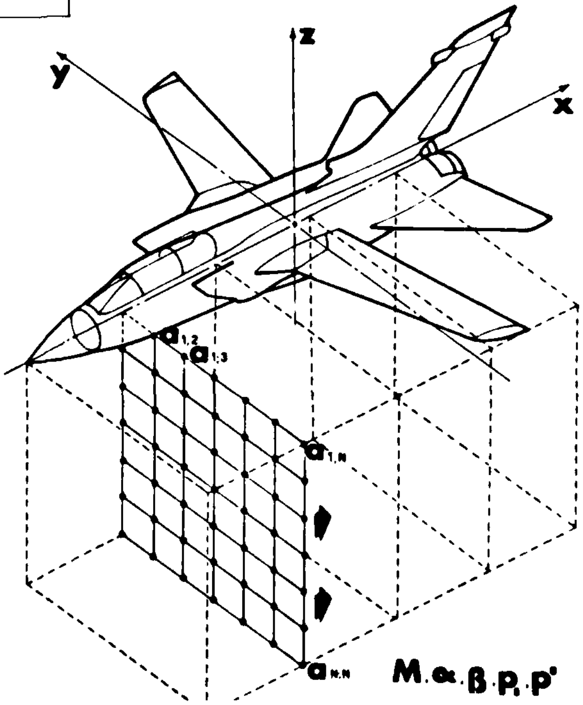
z
y
x
$a_{1,2}$
$a_{1,3}$
$a_{1,N}$
$a_{N,N}$
M.α.β.p.p'

FIG. 5 - Matrix of A/C flow field measurement points

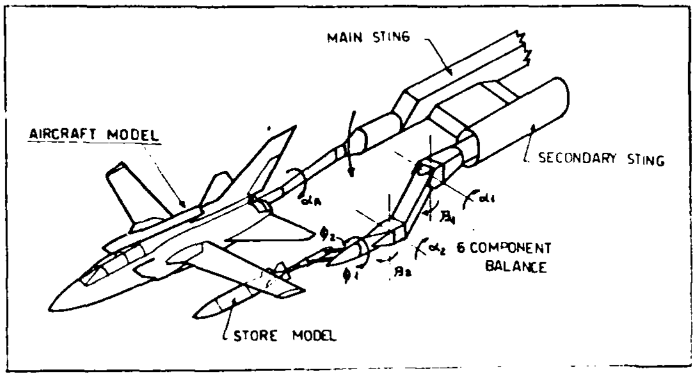
MAIN STING
AIRCRAFT MODEL
SECONDARY STING
α_A
α_1
ϕ_2
β_1
α_2
6 COMPONENT BALANCE
ϕ_1
β_2
STORE MODEL

FIG. 6 - Store trajectory loads measuring facility

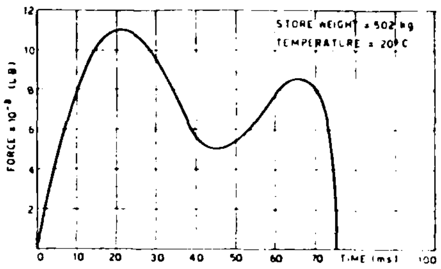

FIG. 7A - ERU ejection thrust

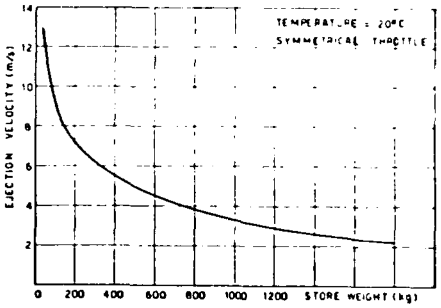

FIG. 7B - End of stroke ejection velocity vs. store weight

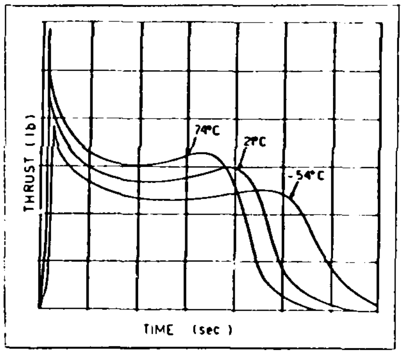

FIG. 8 - Missile thrust vs. time

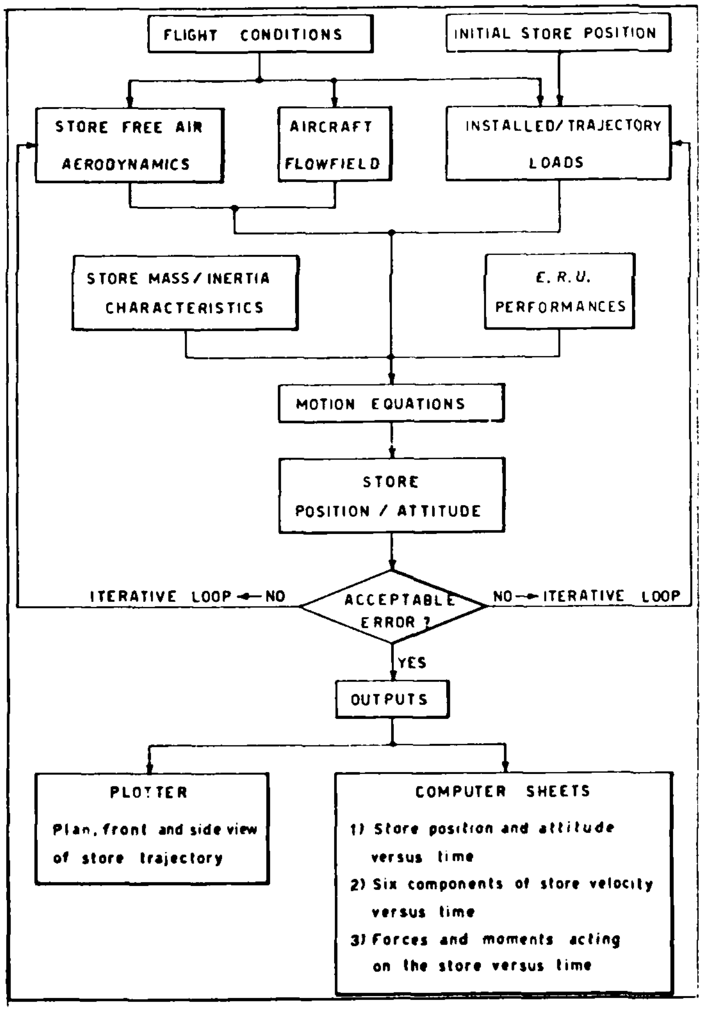
FLIGHT CONDITIONS
INITIAL STORE POSITION
STORE FREE AIR AERODYNAMICS
AIRCRAFT FLOWFIELD
INSTALLED/TRAJECTORY LOADS
STORE MASS/INERTIA CHARACTERISTICS
E.R.U. PERFORMANCES
MOTION EQUATIONS
STORE POSITION / ATTITUDE
ITERATIVE LOOP ← NO
ACCEPTABLE ERROR ?
NO → ITERATIVE LOOP
YES
OUTPUTS
PLOTTER
Plan, front and side view of store trajectory
COMPUTER SHEETS
1) Store position and attitude versus time
2) Six components of store velocity versus time
3) Forces and moments acting on the store versus time

FIG. 9 - Mathematical model layout

$$Z^{(0)}_{n+1} = Z^{(0)}_{n} + \Delta t \cdot f(t_n, Z^{(0)}_n)$$

$$Z^{(1)}_{n+1} = Z^{(0)}_{n+1} + \frac{\Delta t}{2} \left[f(t_{n+1}, Z^{(0)}_{n+1}) - f(t_n, Z^{(0)}_n) \right]$$

$$Z^{(i+1)}_{n+1} = Z^{(i)}_{n+1} + \frac{\Delta t}{2} \left[f(t_{n+1}, Z^{(i)}_{n+1}) - f(t_{n+1}, Z^{(i-1)}_{n+1}) \right]$$

CONVERGENCE WHEN:

$$\left| f(t_{n+1}, Z^{(i)}_{n+1}) - f(t_{n+1}, Z^{(i-1)}_{n+1}) \right| \leq 10^{-3}$$

FIG. 10 - Iterative loop solving motion equations

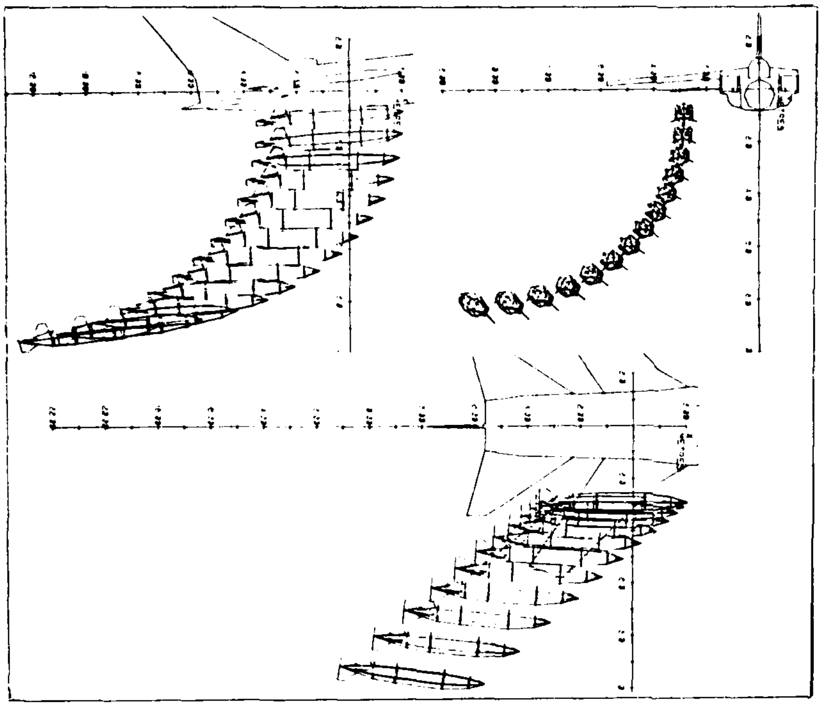

FIG. 11 - Mathematical model output

PARAMETERS (full / model scale)	SIMILARITY	
	TOTAL	PARTIAL
AIR DENSITY	δ	–
LENGTHS	λ	λ
TIMES	$\sqrt{\lambda}$	$\sqrt{\lambda}$
BODY SPEED	$\sqrt{\lambda}$	$\sqrt{\lambda}$
AIR SPEED	$\sqrt{\lambda}$	$\sqrt{\sigma/\delta}$
ACCELERATIONS	1	–
ANGLES	1	–
ANGULAR VELOCITY	$1/\sqrt{\lambda}$	$1/\sqrt{\lambda}$
ANGULAR ACCELERATIONS	$1/\sqrt{\lambda}$	$1/\sqrt{\lambda}$
BODY DENSITY	δ	σ/λ
DYNAMIC PRESSURE	$\delta\lambda$	σ
FORCES	$\delta \cdot \lambda^3$	$\sigma \cdot \lambda^2$
MOMENTS	$\delta \cdot \lambda^4$	$\sigma \cdot \lambda^3$
MOMENTS OF INERTIA	$\delta \cdot \lambda^5$	$\sigma \cdot \lambda^4$

FIG. 13 - Model scaling ratios

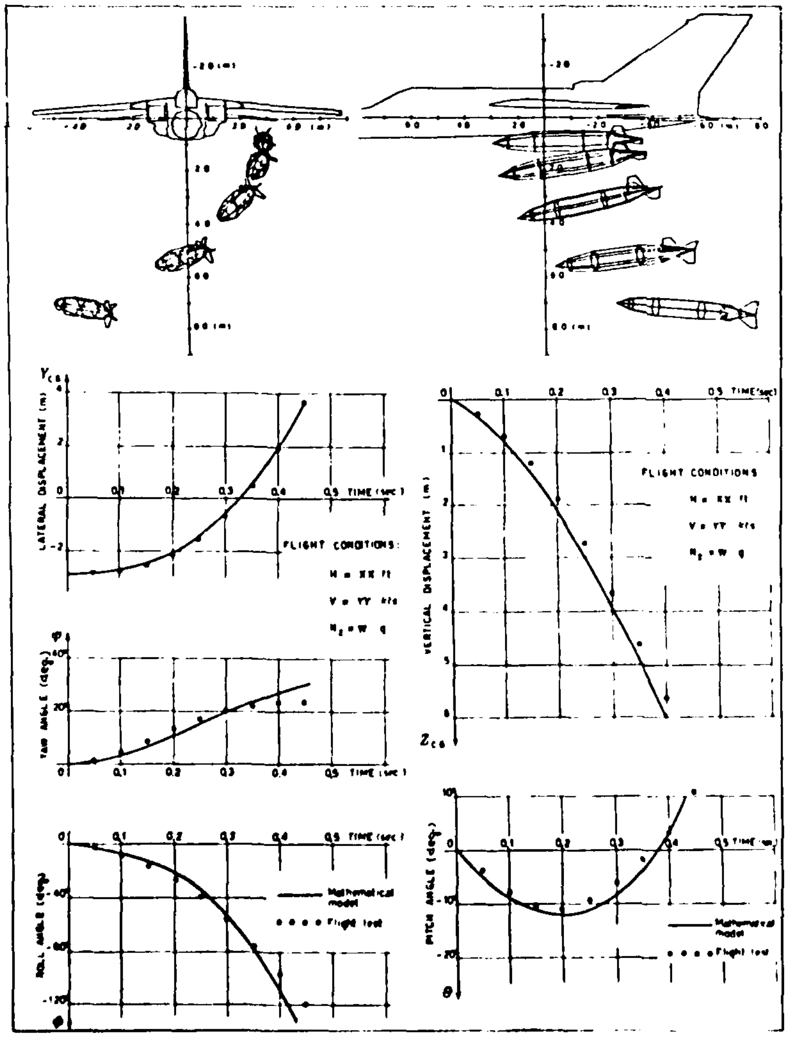

FIG. 12 - Comparison between model and flight test trajectories

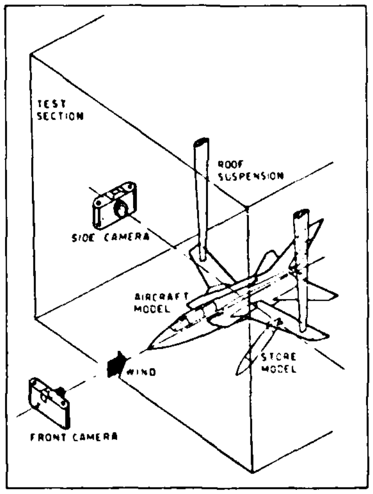

TEST SECTION
ROOF SUSPENSION
SIDE CAMERA
AIRCRAFT MODEL
STORE MODEL
WIND
FRONT CAMERA

FIG. 14 - Dynamically scaled jettison test layout

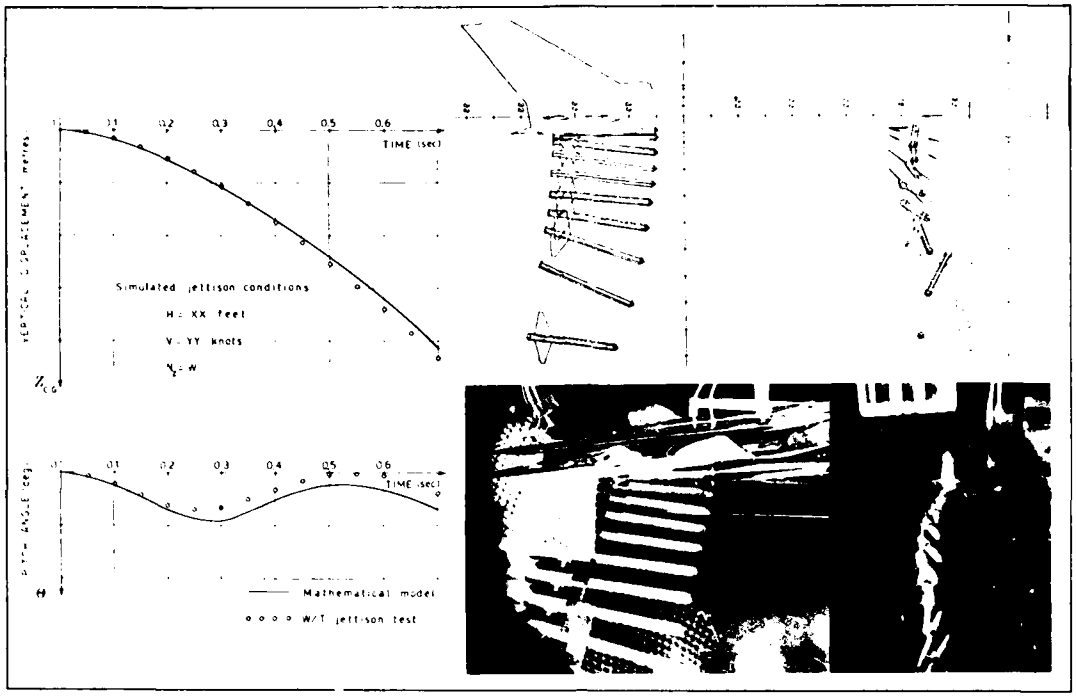

FIG. 15 - Comparison between theoretical predictions and wind tunnel results

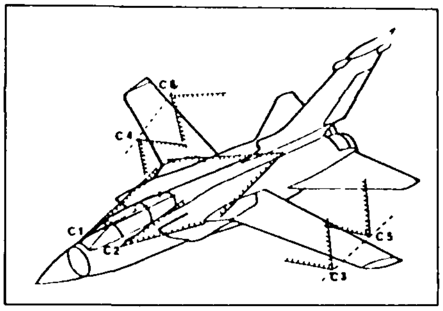

C1
C2
C3
C4
C5
C6

FIG. 16 - On-board camera lay-out

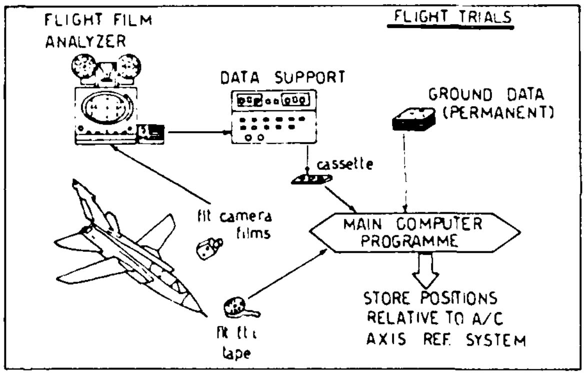

FLIGHT FILM ANALYZER
FLIGHT TRIALS
DATA SUPPORT
GROUND DATA (PERMANENT)
cassette
flt camera films
MAIN COMPUTER PROGRAMME
flt tape
STORE POSITIONS RELATIVE TO A/C AXIS REF. SYSTEM

FIG. 18 - Flight trials data collection

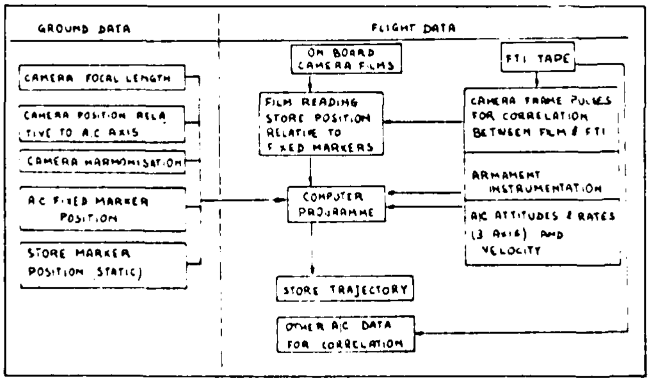

GROUND DATA
FLIGHT DATA
CAMERA FOCAL LENGTH
CAMERA POSITION RELATIVE TO A.C AXIS
CAMERA HARMONISATION
A.C FIXED MARKER POSITION
STORE MARKER POSITION (STATIC)
ON BOARD CAMERA FILMS
FTI TAPE
FILM READING STORE POSITION RELATIVE TO FIXED MARKERS
CAMERA FRAME PULSES FOR CORRELATION BETWEEN FILM & FTI
ARMAMENT INSTRUMENTATION
A/C ATTITUDES & RATES (3 AXIS) AND VELOCITY
COMPUTER PROGRAMME
STORE TRAJECTORY
OTHER A/C DATA FOR CORRELATION

FIG. 17 - Determination of store trajectory from flight trials

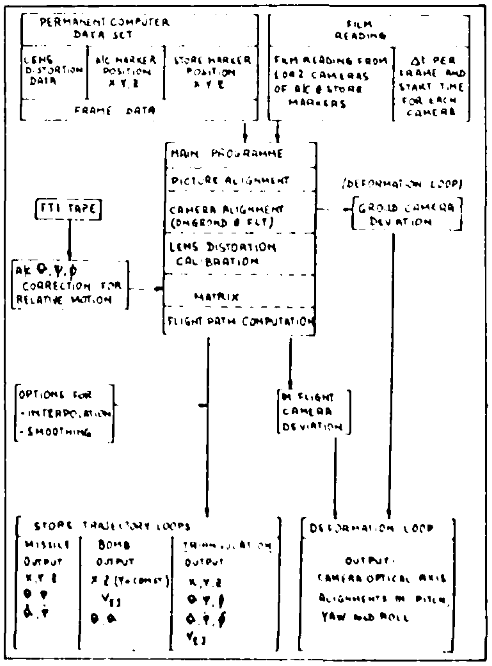

PERMANENT COMPUTER DATA SET
LENS DISTORTION DATA
A/C MARKER POSITION X Y Z
STORE MARKER POSITION X Y Z
FRAME DATA
FILM READING
FILM READING FROM 1 OR 2 CAMERAS OF A/C & STORE MARKERS
Δt PER FRAME AND START TIME FOR EACH CAMERA
MAIN PROGRAMME
PICTURE ALIGNMENT
CAMERA ALIGNMENT (ON GROUND & FLT)
LENS DISTORTION CALIBRATION
MATRIX
FLIGHT PATH COMPUTATION
(DEFORMATION LOOP)
GROUND CAMERA DEVIATION
FTI TAPE
A/C Θ, Ψ, Φ CORRECTION FOR RELATIVE MOTION
OPTIONS FOR - INTERPOLATION - SMOOTHING
IN FLIGHT CAMERA DEVIATION
STORE TRAJECTORY LOOPS
MISSILE OUTPUT X, Y, Z Θ Ψ Θ̇ Ψ̇
BOMB OUTPUT X Z (Y = CONST) V_E3 Θ Θ̇
TRIANGULATION OUTPUT X, Y, Z Θ Ψ Φ Θ̇ Ψ̇ Φ̇ V_E3
DEFORMATION LOOP
OUTPUT: CAMERA OPTICAL AXIS ALIGNMENTS IN PITCH, YAW AND ROLL

FIG. 19 - Trajectory analysis programme

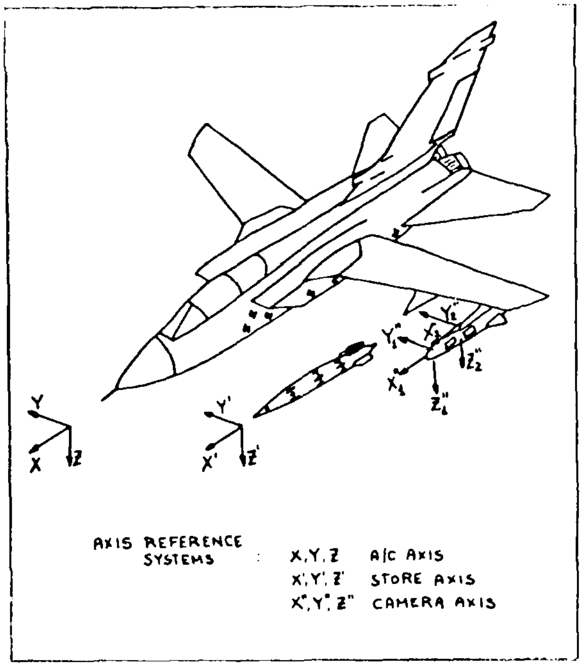
Y
X
Z
Y'
X'
Z'
Y_1''
Y_2''
X_2''
Z_2''
X_1''
Z_1''
AXIS REFERENCE SYSTEMS :
X,Y,Z A/C AXIS
X',Y',Z' STORE AXIS
X",Y",Z" CAMERA AXIS

FIG. 20 - Axis reference systems

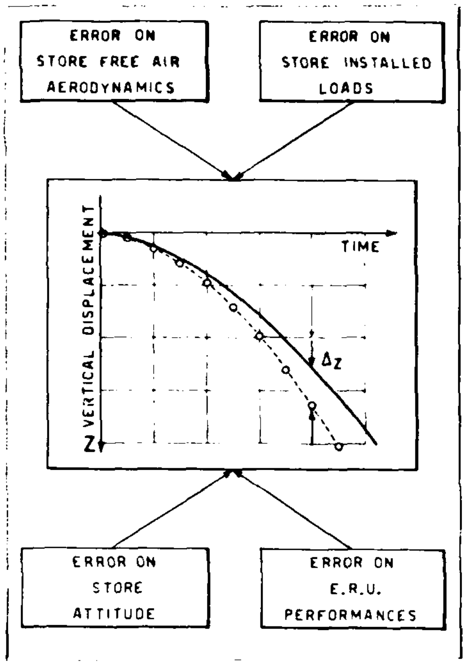
ERROR ON STORE FREE AIR AERODYNAMICS
ERROR ON STORE INSTALLED LOADS
VERTICAL DISPLACEMENT
Z
TIME
Δz
ERROR ON STORE ATTITUDE
ERROR ON E.R.U. PERFORMANCES

FIG. 21 - Possible causes for a vertical displacement mismatching

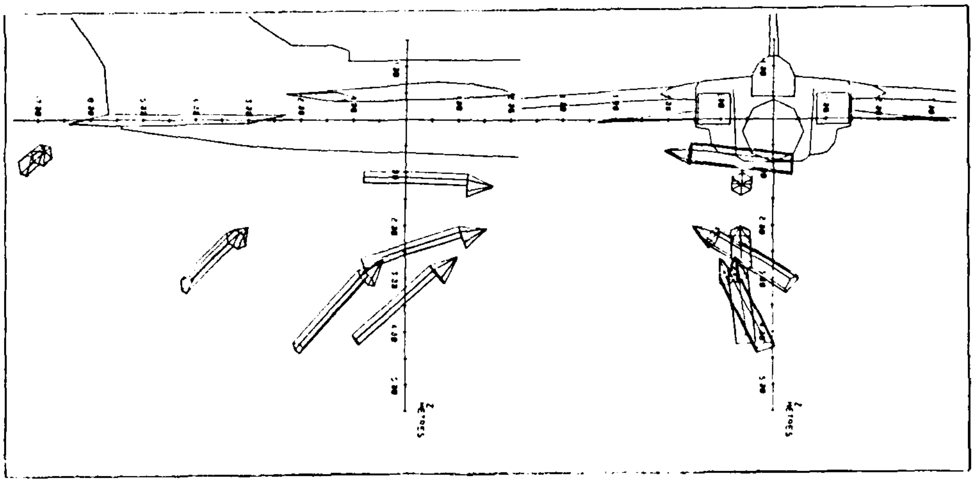

FIG. 22 - Theoretical dispenser trajectory with full gun thrust

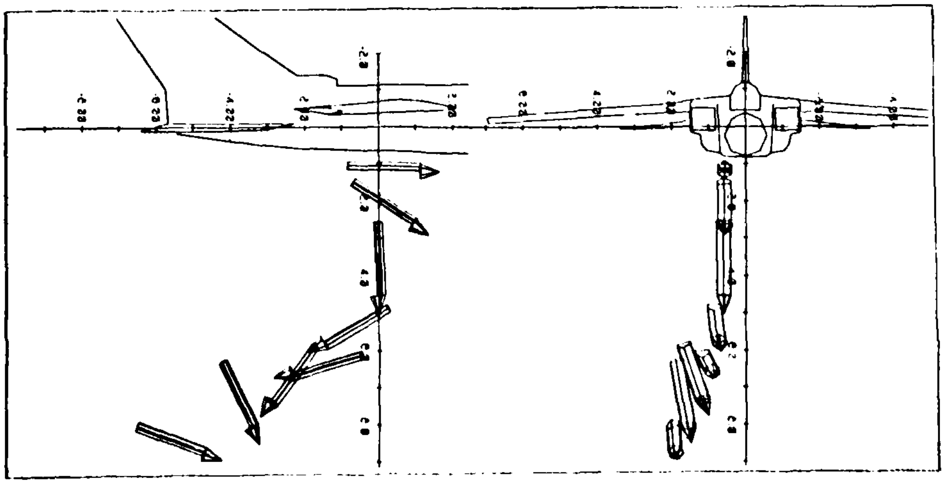

FIG. 23 - Theoretical dispenser trajectory with asymmetric gun thrust

AD-A129 433 GROUND/FLIGHT TEST TECHNIQUES AND CORRELATION(U) 6/6
ADVISORY GROUP FOR AEROSPACE RESEARCH AND DEVELOPMENT
NEUILLY-SUR-SEINE (FRANCE) FEB 83 AGARD-CP-339
UNCLASSIFIED F/G 1/3 NL

END
DATE
FILMED
7-83
DTIC

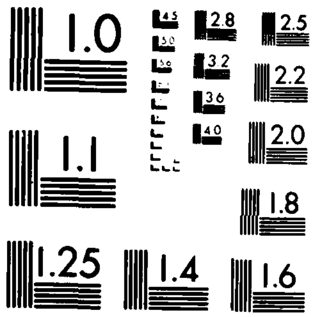
1.0
1.1
1.25
1.4
1.6
1.8
2.0
2.2
2.5
2.8
3.2
3.6
4.0
4.5
5.0
5.6

MICROCOPY RESOLUTION TEST CHART
NATIONAL BUREAU OF STANDARDS-1963-A

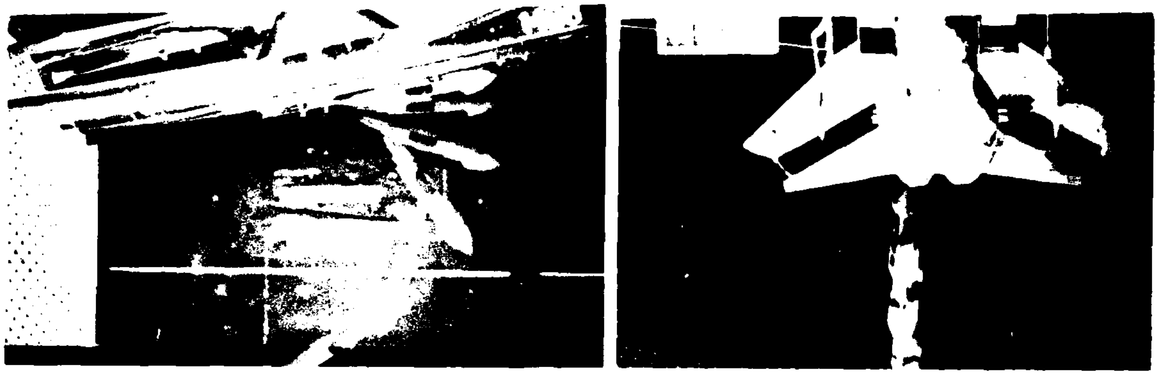

FIG. 24 - Experimental dispenser trajectory with asymmetric throttle setting

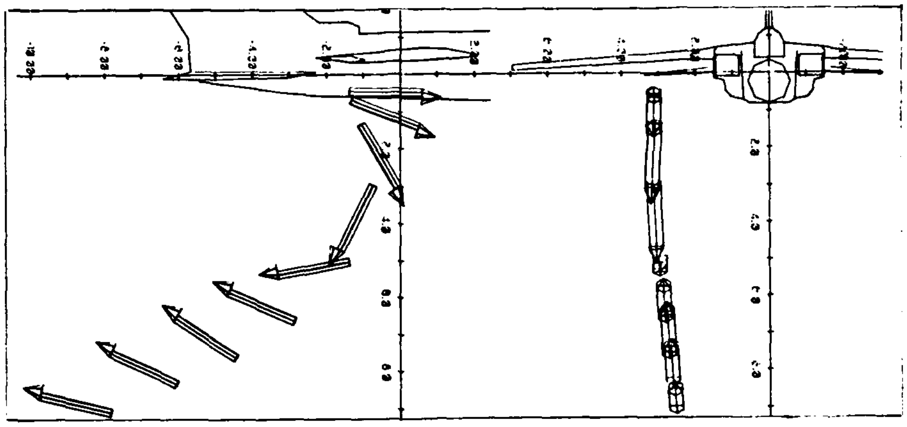

FIG. 25 - Dispenser trajectory prediction with early store free air aerodynamics

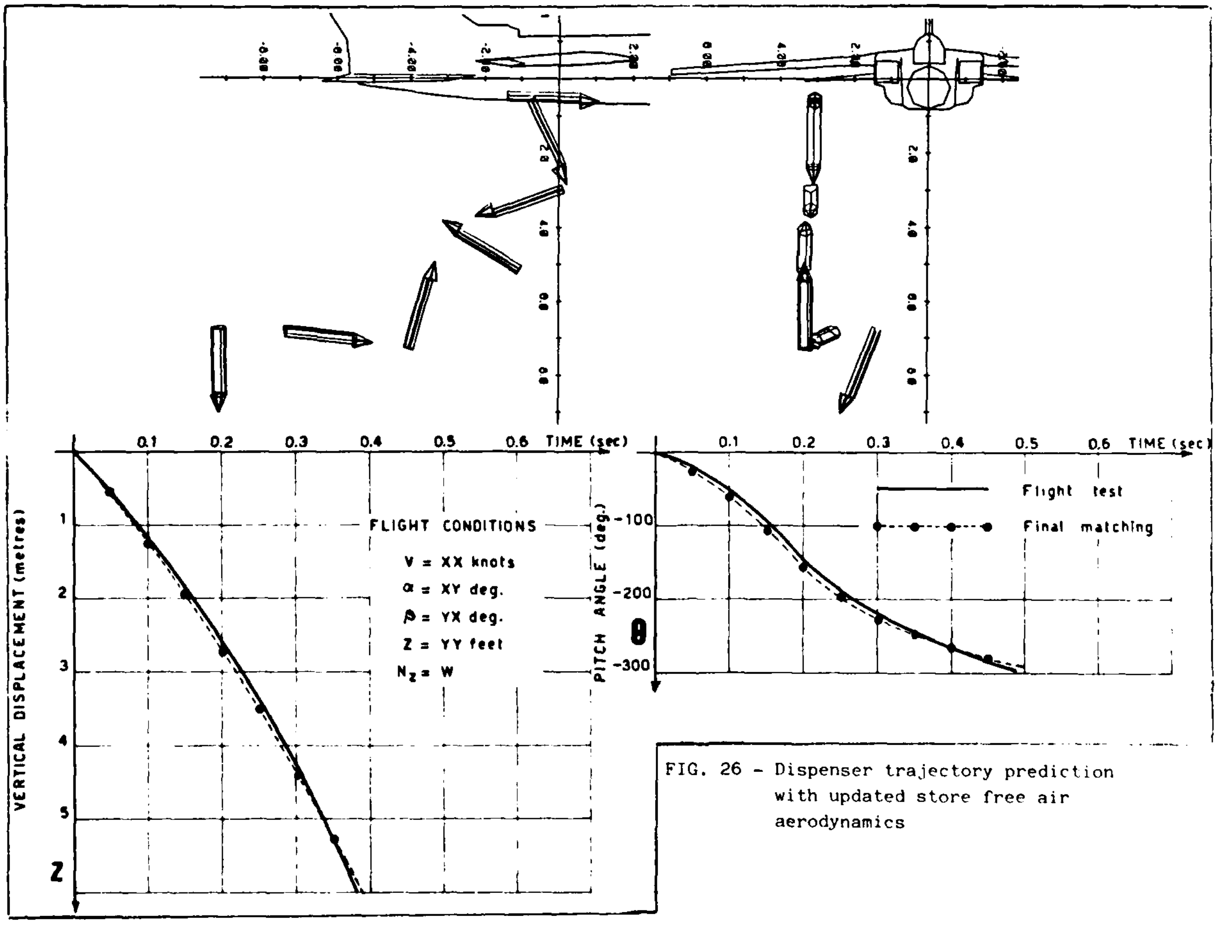

FIG. 26 - Dispenser trajectory prediction with updated store free air aerodynamics

HELICOPTER AIR INLETS :

DESIGN PROCESS, WIND TUNNEL TESTING AND CORRELATIONS WITH FLIGHT DATA

by

F. TOULMAY
AEROSPATIALE (FRANCE)

ABSTRACT

The increasing demand for fuel efficient, high speed helicopters has triggered considerable research on engine air inlet design in the past five years at AEROSPATIALE. Wind tunnel testing was found to be the most flexible and powerful tool in the long iterative process that leads from the very first project drawings to certification.

This paper emphasizes major inlet design problems and ways of solving them through down-scaled models :

- pressure loss
- dynamic pressure recovery
- pressure distortion
- hot air re-ingestion
- compatibility with FOD, sand and icing protection
- external drag
- constraints due to engine and/or aircraft architecture.

Indications are given concerning the selection of model parameters, test procedure and real-time processing. Pending or unsolved questions are be mentioned along with future developments.

ENTREES D'AIR D'HELICOPTERES :

CONCEPTION, ESSAIS EN SOUFFLERIE, CORRELATIONS AVEC LES RESULTATS DE VOL

par

F. TOULMAY
AEROSPATIALE (FRANCE)

RESUME

La demande croissante pour des hélicoptères rapides et consommant peu a déclenché un important effort de recherche sur les entrées d'air depuis cinq ans. Les essais en soufflerie sont considérés comme l'outil, le plus souple et le plus puissant dans le long processus itératif qui conduit de l'avant-projet à la certification.

Cet article insiste sur les problèmes majeurs de conception et les moyens de les résoudre à l'aide de maquette à échelle réduite :

- pertes de charge
- récupération de pression dynamique
- distorsion de pression
- réingestion d'air chaud
- compatibilité avec les protections contre les corps étrangers, le sable, le givre
- trainée
- contraintes d'architecture du moteur et/ou de l'appareil.

Des indications sont fournies concernant le choix des paramètres de la maquette, la conduite d'essai et le dépouillement en temps réel. Les problèmes non résolus sont mentionnés, ainsi que les développements envisagés.

1. INTRODUCTION

Au début de la courte histoire des hélicoptères, les entrées d'air des moteurs ne faisaient pas l'objet de beaucoup d'attention dans les bureaux d'étude. Ceci tenait à deux raisons : d'une part, tous les efforts étaient focalisés sur les problèmes cruciaux propres à ce type d'appareil (endurance des pièces mécaniques, vibrations, pilotage du rotor) ; d'autre part, les moteurs à pistons, alors utilisés exclusivement, nécessitaient des débits d'air faibles et montraient une tolérance relativement grande aux mauvaises conditions d'alimentation. Aucun problème de fonctionnement comparable au pompage n'était à craindre et l'influence des pertes de charge sur la puissance délivrée restait limitée.

Avec l'introduction des turbines (1955 - Alouette II), certaines précautions élémentaires devinrent nécessaires afin d'assurer le fonctionnement correct des compresseurs : adapter un pavillon d'entrée pour réduire les pertes de charge et éviter les décollements s'assurer que les gaz d'échappement ne sont pas réingérés par le moteur. Ces précautions étant prises, le fonctionnement était assuré. Les performances en vol de translation restaient cependant médiocres. Le jeu de la concurrence a alors poussé les fabricants à améliorer les performances de leurs hélicoptères : les vitesses de croisière passèrent progressivement de 80 à 140 noeuds.

A forte vitesse, les entrées d'air simples qui donnaient jusqu'alors satisfaction commencèrent à créer des problèmes de pompage. Ceux-ci étaient d'autant plus à craindre que les marges au pompage des moteurs avaient parfois tendance à diminuer, du fait de la recherche de consommations spécifiques plus faibles.

Avec l'augmentation brutale du prix du pétrole, l'objectif d'économie sur le carburant s'imposa également pour l'hélicoptère lui-même (ref. 1 et 2). Tandis que l'on s'efforcait d'améliorer l'aérodynamique des rotors et des fuselages, il devint évident que des gains importants pouvaient aussi être obtenus par l'amélioration des entrées d'air. A l'AEROSPATIALE, un effort de recherche lancé en 1977 s'est poursuivi jusqu'à ce jour, apportant des résultats très significatifs. Parmi les moyens mis en oeuvre, la soufflerie de Marignane intégrée au Bureau d'Etude offrait une souplesse d'emploi qui en a fait un instrument privilégié .

Parallèlement à la recherche proprement dite et grâce à celle-ci, une méthodologie moderne de conception et d'essai vit le jour et s'inséra au fur et à mesure des progrès enregistrés dans le cycle normal de développement des appareils. Mais le temps étant un élément déterminant pour la réussite d'un programme, il fallait d'urgence améliorer la conduite d'essai afin de respecter les délais imposés tout en minimisant les risques d'échec. L'automatisation des essais et du dépouillement a permis d'approcher ce but, si bien qu'en retour, la tâche du personnel des essais en vol a été considérablement allégée : la mise au point en vol, empirique, coûteuse parfois fort longue, a pu être évitée pour plusieurs appareils récents. Le travail effectué en vol s'est limité à un simple contrôle de conformité aux normes du manuel d'installation du moteur. Les essais de soufflerie, effectués sur maquette à échelle réduite, donc peu coûteux ont, de même, permis d'éviter le recours à un bon nombre d'essais au sol classiques. C'est seulement lorsque la réalisation technologique des pièces (étanchéité des joints, par exemple) pose des problèmes que les essais sol sont strictement indispensables et c'est là l'occasion de pratiquer des corrélations intéressantes.

Cet exposé a pour but de décrire l'ensemble des méthodes utilisées à l'AEROSPATIALE dans la conception et la mise au point en soufflerie des entrées d'air d'hélicoptères.

2. HISTORIQUE

L'originalité et l'avantage déterminant de l'hélicoptère par rapport aux autres aérodynes résident dans son aptitude au vol stationnaire. Pour profiter de cette caractéristique unique, les premiers utilisateurs (secours en mer, en montagne, police, transport de troupes) s'accomodèrent de performances modestes en vol de translation. Les missions s'effectuaient sur de courtes distances si bien que le but dans l'étude des appareils de cette époque était essentiellement d'augmenter la charge payante décollable afin de rentabiliser le coût énorme représenté par l'achat et la maintenance de ce matériel. On gagnait de la masse en éliminant tout carénage, ce qui n'avait guère de conséquences sur la vitesse, laquelle était plutôt limitée par les vibrations et la mécanique du rotor.

Dans ce contexte, les entrées d'air devaient être adaptées au vol stationnaire, et rester légères. Les premiers appareils (Djinn, Alouette II et III) furent dotés d'un simple pavillon en tôle (Fig. 1) dont le fonctionnement est parfait en vol stationnaire : l'accélération progressive de l'air grâce à un rapport R/D très grand (≈ 1) réduit les pertes par frottement à une valeur tellement faible (< 1 mb) que les performances du moteur ne sont pas sensiblement modifiées par rapport au fonctionnement au banc d'essai. En translation, l'écoulement dans tel pavillon se dégrade considérablement mais les conséquences étaient limitées par la faible vitesse de croisière de ces appareils.

Sur les appareils plus lourds (exemple : Puma), l'architecture générale facilite naturellement la conception des entrées d'air : les moteurs situés devant la BTP * permettent de placer les entrées à l'avant du fuselage (Fig. 2). Elles sont bien orientées, dégagées de tout sillage, et les pavillons se raccordent sans discontinuité au profil des capotages GTM ‡. Dans ces conditions, l'alimentation des moteurs est quasiment parfaite aussi bien en translation qu'en vol stationnaire. Toutefois, la trainée aérodynamique peut varier très sensiblement suivant le soin apporté à la forme du raccord entrée d'air - capot. La réingestion de gaz chauds qui paraît intuitivement improbable étant donné la position avancée des entrées, peut, paradoxalement, créer des problèmes sous l'effet du champ des vitesses induites par le rotor en effet de sol. Ce phénomène identifié sur le Super-Puma, a également été signalé par d'autres hélicoptéristes dans des cas analogues (Ref. 3, 4, 5).

---

* Boîte de Transmission Principale

‡ Groupe Turbo-Moteur

Plus récemment, une nouvelle génération de petits appareils (Ecureuil - Astar) a vu le jour, pour lesquels l'analyse de la valeur (design to cost) fut appliquée avec rigueur. Le moteur étant placé à l'arrière, l'entrée est constituée par une simple découpe rectangulaire dans la face supérieure du capot derrière le mât rotor. Cette découpe vient se raccorder au conduit d'amenée du moteur lors de la fermeture du capot. La surface de cette entrée est choisie suffisamment large pour que les décollements prenant naissance sur les arêtes vives soient rapidement éliminés par le gradient de vitesse positif dans le conduit (Fig. 3a). Ce dessin, satisfaisant en vol stationnaire, conduit à un type d'écoulement très défavorable en translation. Une large zone décollée obstrue les 2/3 de l'entrée en translation rapide, avec des pertes de charge et des fluctuations de pression importantes. A ce problème s'ajoute la réingestion d'air chaud du compartiment BTP qui s'échappe par la large ouverture autour du mât et des bielles de commande. Les moteurs des deux versions (Arriel 1A et LTS 101.600) disposent de marges suffisantes pour accepter ces conditions de fonctionnement médiocres au prix toutefois de pertes d'avionnage importantes.

Un appareil bimoteur (Twinstar SA 355) a été dérivé de cette famille. L'augmentation de consommation résultant de la configuration bimoteur est partiellement compensée par la réduction des pertes d'entrée en vol de translation, ceci dans le but de sauvegarder un rayon d'action suffisant. A cette fin, les entrées sont montées latéralement (Fig. 4), hors des perturbations du mât rotor et orientées vers l'avant. Le flux d'air chaud issu des radiateurs d'huile est éjecté à l'arrière.

Pour les appareils de taille moyenne (3000 à 4000 kg de masse maximale au décollage), les exigences du marché civil ont poussé l'AEROSPATIALE à rechercher le meilleur compromis entre les objectifs de rapidité, grande distance franchissable et économie de carburant. Ces objectifs exigent un fonctionnement d'entrée d'air optimisé pour le vol de croisière. Dans ce but, les entrées du Dauphin 365 N (Fig. 5) sont placées à l'avant des capotages et reliées aux moteurs situés derrière la BTP par des conduits longs d'un mètre environ. La perte de charge propre aux conduits est compensée par l'absence de sillage, de couche limite et de recirculation de gaz chauds. Ce concept s'est révélé globalement plus performant que celui du Dauphin 365 C, version antérieure dont les entrées d'air dites «statiques» affleurent le profil du capot derrière le mât rotor.

Enfin, il convient de rappeler que les hélicoptères volent fréquemment dans des conditions d'environnement très sévères telles que :

- vol à basse altitude avec risque d'ingestion d'oiseaux
- atmosphère givrante
- atmosphère chargée de sable ou poussière.

Très tôt, s'est imposée la nécessité de protéger les moteurs par des dispositifs appropriés : grilles sur les appareils au standard série et filtres anti-sables sur option. L'adaptation des filtres anti-sable , en particulier, génère des contraintes supplémentaires sur la conception de la cellule de base. Leur mise au point souleva des problèmes sur de nombreux appareils du fait de pertes de charge aux conséquences indésirables sur les performances, et surtout de la difficulté d'obtenir une efficacité de filtrage suffisante.

3. CONCEPTION

3.1. Section d'entrée

Comme illustré précédemment, le choix d'une configuration d'entrée d'air relève d'un compromis entre de nombreux facteurs dont certains sortent des compétences de l'aérodynamicien :

- étendue du domaine de vol (vitesse)
- qualités dominantes recherchées
- architecture de l'hélicoptère
- architecture du moteur.

Ce choix étant effectué, l'aérodynamicien a pour mission d'optimiser le fonctionnement en précisant les paramètres géométriques: surface de l'entrée, forme des lèvres, géométrie du conduit .....

Deux cas sont à distinguer :

- le plan d'entrée du conduit est parallèle à la direction générale de l'écoulement, on parle alors d'entrée d'air «statique»
- il fait face à l'écoulement, on parle alors d'entrée d'air «dynamique».

Les appareils les plus récents étant tous équipés d'entrées dynamiques, les méthodes décrites dans la suite s'appliquent directement à celles-ci, toutefois elles pourraient facilement être adaptées aux entrées statiques.

En vol stationnaire, l'air brassé par le rotor est animé d'une vitesse qui peut toujours être considérée comme négligeable par rapport à la vitesse de l'écoulement dans l'entrée. L'air est aspiré, dans toutes les directions, par l'entrée d'air comme par un puits, si bien que la vitesse ne s'accroît notablement qu'au voisinage immédiat de celle-ci. (Fig. 6a).

Les lignes de courant provenant de l'avant aboutissent au centre de l'entrée, avec une accélération uniforme de l'air de $V = 0$ à $V = V_I$. Celles provenant de l'arrière aboutissent près des parois en suivant leur courbure. L'accélération centripète due à la courbure est obtenue grâce à une dépression, donc à une accélération autour des lèvres, jusqu'à une certaine vitesse V_M
Le ralentissement de V_M à V_I s'accompagne d'une recompression qui peut conduire à un décollement si le gradient de pression est trop fort. La survitesse V_M / V_I est d'autant plus réduite que le rapport e/h est plus grand. Le décollement peut donc être évité en augmentant l'épaisseur relative des lèvres. De plus, la forme des lèvres influe également sur la vitesse maximale V_M et sur le gradient. Pour une même épaisseur, certains profils donnent une pointe de vitesse V_M importante sur une courte

distance, tandis que d'autres donnent une vitesse V_M plus faible sur une distance plus longue avec une recompression également plus douce. Ce dernier cas est préférable afin d'éviter le décollement.

En vol de translation, le champ de vitesse autour de l'entrée d'air est déterminé par la valeur du coefficient de débit :

$$\varepsilon = \frac{A_0}{A_1} = \frac{Q}{\rho_0 V_0 A_1} \qquad \left(= \frac{V_1}{V_0} \text{ en écoulement incompressible}\right)$$

A faible vitesse, ε est grand et le point d'arrêt se situe sur la partie extérieure de la lèvre comme en vol stationnaire, une survitesse apparaît à l'intérieur. A grande vitesse, ε diminue et le point d'arrêt se situe sur la partie intérieure de la lèvre. Une survitesse apparaît cette fois sur la partie extérieure. Le décollement qui peut survenir dans ce cas n'affecte pas le moteur, mais augmente la traînée parasite du fuselage. L'optimum consisterait à choisir A_1 de telle façon que $\varepsilon = 1$ à la vitesse de croisière. Toutefois, avec la vitesse élevée des appareils actuels, ce calcul conduit à une surface A_1 faible, ce qui augmenterait excessivement les pertes de charge en vol stationnaire. Le compromis actuellement en usage consiste à choisir A_1 de telle sorte que $\varepsilon = 0{,}8$.

Pour le dessin de projet d'une nouvelle entrée d'air, nous utilisons une méthode de calcul par transformation conforme (méthode de l'hodographe- Ref. 6) qui permet de spécifier l'évolution du vecteur vitesse le long des parois et fournit la forme de la lèvre. Cette méthode bi-dimensionnelle (2D) en écoulement plan, nécessite une interprétation délicate des données et des résultats car l'écoulement réel est toujours fortement tri-dimensionnel.

Diverses méthodes directes 3D et 2D - axisymétriques permettent de vérifier que le dessin choisi ne conduit pas à une survitesse excessive. Le critère utilisé est le suivant :

$\frac{V_2}{V_1} < 1{,}4$: pas de risque de décollement

$1{,}4 \leqslant \frac{V_2}{V_1} \leqslant 2$: risque de décollement. Investigations supplémentaires nécessaires

$\frac{V_2}{V_1} > 2$: décollement quasi-certain. Modifications du dessin nécessaires

Un calcul couplé de couche limite 3D permettra d'affiner considérablement la prédiction des décollements, dès qu'une telle méthode se sera montrée suffisamment souple pour une utilisation opérationnelle.

3.2. Conduit

Le dessin du conduit dépend de la position relative de l'entrée et du plan de raccordement au moteur, de l'orientation de ces deux sections et de leurs surfaces. L'architecture moteur peut conduire à deux cas très différents (Fig. 7).

Si le compresseur est situé à l'avant du moteur, l'arrivée de l'air est axiale et le diamètre de l'extrémité du conduit correspond au diamètre du premier étage. Cette section A_2, toujours plus réduite que A_1 permet à l'écoulement d'accélérer dans le conduit. Le gradient de pression négatif qui en résulte évite tout décollement et amortit considérablement les perturbations présentes à l'entrée. Pour réduire les pertes de charge, il est possible de garder une section constante et égale à A_1 sur la plus grande partie du conduit, et de réduire rapidement la section de A_1 à A_2 sur une courte distance devant le compresseur (Fig. 8). Le désalignement des extrémités du conduit et l'encombrement des organes mécaniques obligent souvent à courber son profil mais cela n'entraîne pas d'inconvénient tant que la section est constante ou convergente et que le rapport R/D est supérieur à 2 (Fig. 9).

Si le compresseur n'est pas situé à l'avant du moteur, l'alimentation ne peut être que radiale. L'air est puisé dans une chambre qui entoure le carter d'entrée. Plus le volume de cette chambre est important, plus l'alimentation a des chances de se répartir uniformément à l'entrée du carter. Encore faut-il pour cela que la vitesse à l'entrée de cette chambre soit suffisamment faible. Le motoriste propose donc généralement une section A_2 très large et orientée perpendiculairement à l'axe de rotation du compresseur. (Fig. 10). Le conduit reliant A_1 à A_2 sera donc divergent et comportera un coude à 90°. L'encombrement de ce coude devra la plupart du temps être réduit au minimum, ce qui nécessite un rayon de courbure très faible (R/D de l'ordre de 1). Dans un coude, si prononcé, l'évolution des sections ne peut en aucun cas être divergente. On retrouve donc à l'entrée du coude une section A'_2 supérieure ou égale à A_2. Entre l'entrée A_1 et le coude A'_2, l'évolution des sections diverge. Ceci favorise de faibles pertes de charge mais destabilise l'écoulement. Pour un divergent rectiligne dont la forme des sections évolue peu, l'angle de divergence moyen :

$$\alpha_S = 2\tan^{-1}\left[\frac{1}{L\sqrt{\pi}}\left(\sqrt{A'_2} - \sqrt{A_1}\right)\right]$$

ne devra pas excéder 6 à 7°. Si les données A_1, A'_2, L conduisent à une valeur de α_S supérieure à 7°, on peut envisager les actions suivantes :

1) augmenter la longueur L en avançant le plan d'entrée A_1

2) choisir une surface A_1 plus grande en enfreignant la règle du $\varepsilon = 0{,}8$.

La première solution implique une augmentation de masse et de complexité technique, la seconde a l'avantage de réduire les pertes de charges mais conduit à épaissir fortement les lèvres pour éviter un décollement externe en vol de translation et l'augmentation de trainée qui lui est liée.

Si de plus, les extrémités du conduit ne sont pas alignées ou si la forme des sections évolue fortement, l'angle α_S maximum devra être nettement inférieur à 6°, ce qui complique encore la décision de l'aérodynamicien. Dans ce cas, le recours à des essais au sol, ou en soufflerie devient impératif avant de figer les plans de définition de l'appareil. En effet, aucune méthode de prévision n'est aujourd'hui suffisamment sûre pour s'en dispenser.

4. ESSAIS EN SOUFFLERIE

4.1. Moyens matériels

Le Bureau d'Etude de l'AEROSPATIALE dispose dans l'enceinte de l'usine, d'une soufflerie basse vitesse (V_{max} = 50 m/s) à retour non guidé de type Eiffel. La veine cylindrique non guidée a un diamètre de 3 mètres.

L'échelle des maquettes utilisées pour les études d'entrées d'air varie de 1/2 à 1/3 suivant la taille de l'appareil à représenter. La partie haute du fuselage, les capots supérieurs, le moyeu rotor et le circuit d'entrée d'air sont conformes à l'appareil ; par contre, la partie inférieure du fuselage et la poutre de queue sont supprimées afin de limiter le blocage de la veine. Le débit des ventilateurs qui simulent le flux moteur varie de 0,2 à 0,3 kg/s suivant les pertes de charge, ce qui concorde bien avec la dimension des entrées et la vitesse du vent. Le débit peut être mesuré à tout instant grâce à un venturi situé dans le circuit de refoulement. L'instrumentation permettant de mesurer les performances de l'entrée d'air est regroupée dans un plan appelé section de mesure et qui coïncide le plus souvent avec l'entrée du premier étage du compresseur à simuler. Elle se compose de prises de pressions statiques pariétales et de plusieurs (6 ou 8) peignes comportant chacun 4 à 6 prises de pressions totales. Elle est conforme à l'installation préconisée par le motoriste pour les essais en vol lorsque celà semble souhaitable, ou bien elle peut être remplacée par un peigne tournant qui offre l'avantage d'augmenter considérablement la finesse du sondage en permettant le tracé de cartes de pression, vitesse, Mach . . .

Le nombre de pressions à mesurer étant élevé, on utilise un commutateur de pressions automatisé et un unique capteur pour toutes les pressions, y compris la mesure du débit ventilateur, et du vent soufflerie. Cette méthode permet d'annuler pratiquement l'influence d'une erreur d'étalonnage ou d'une dérive du coefficient de sensibilité du capteur. En effet, le dépouillement des résultats passe toujours, de manière explicite ou non, par le calcul de coefficients de pression :

$$Cp = \frac{P - P_{ref.\,1}}{P_{ref.2} - P_{ref.\,1}}$$ où $P_{ref.\,1}$, $P_{ref.\,2}$ sont des pressions en deux points de référence de l'écoulement

On constate aisément qu'une erreur d'étalonnage du capteur unique se répercute de façon identique sur le numérateur et le dominateur, si bien que C_p reste inchangé. A la limite, on peut totalement ignorer le coefficient d'étalonnage et cependant fournir des résultats exacts ! On doit toutefois s'assurer de la linéarité de la chaine de mesure et connaître à chaque instant la dérive du zéro électrique (tension d'offset) qui sont sources d'erreurs.

Outre les mesures de pression, on mesure quelquefois la traînée de la maquette. Ces mesures ne sont significatives que par comparaison avec d'autres entrées d'air montées sur la même maquette, puisque les formes du fuselage ne sont que partiellement représentées.

4.2. Règles de similitude

Entre autres nombres sans dimension, il est bien connu que le nombre de Mach et le nombre de Reynolds sont les deux paramètres fondamentaux à respecter pour s'assurer de la similitude de l'écoulement soufflerie par rapport à l'écoulement autour de l'hélicoptère.

4.2.1. Nombre de Mach

Dans le cas particulier des entrées d'air, la compressibilité intervient très peu dans le champ étudié sauf au voisinage immédiat du compresseur où l'écoulement accélère rapidement jusqu'à Mach $M \simeq 0{,}5$ à 0,6 (Fig. 12).

On peut partager fictivement le champ aérodynamique en deux zones :

- une zone «compressible» au voisinage immédiat du compresseur
- une zone «incompressible» englobant tout le reste.

Les phénomènes étudiés (décollements, tourbillons, pertes de charge, turbulence) trouvent tous leur origine dans la zone incompressible. En effet, dans la zone compressible, l'accélération assure un gradient de pression favorable qui ne risque pas de provoquer de tels problèmes. La partie intéressante de l'écoulement se situe donc entièrement dans l'écoulement incompressible, pour lequel le nombre de Mach n'a pas d'influence sensible. Toutefois, il est nécessaire d'effectuer des corrections de compressibilité sur les pressions statiques dans la zone compressible en utilisant pour cela les formules des écoulements isentropiques.

Les coefficients de pressions totales sont considérés comme indépendants du nombre de Mach. L'impossibilité de respecter le nombre de Mach découle du fait que la vitesse soufflerie ne peut pas atteindre les 80 m/s des hélicoptères modernes.

4.2.2. Nombre de Reynolds

Le respect du nombre de Reynolds sur des maquettes à échelle réduite ne peut pas être observé en soufflerie, sauf dans les souffleries cryogéniques ou pressurisées. On opère donc à un nombre de Reynolds réduit dans un rapport de 4 à 10.

En atmosphère non turbulente, il devrait en résulter un recul (vers l'aval) de la transition de la couche limite dans les zones non décollées, ainsi qu'une augmentation des coefficients de perte de charge. Or, ces variations ne sont généralement pas observées lorsque l'on fait varier le nombre de Reynolds sur une maquette de soufflerie ou lorsqu'on compare les essais sur maquette avec des essais en vol. Cette constatation surprenante peut s'expliquer par de nombreuses causes, qui sont toutes liées à l'effet de la turbulence :

- la soufflerie de Marignane présente un taux de turbulence particulièrement élevé : 1,8 %
- l'état de surface des maquettes n'est pas parfait : leur fabrication par moulage d'un stratifié de résine et tissu de verre sur un moule perdu en mousse synthétique laisse de légères ondulations dont l'amplitude est de quelques centièmes de millimètres. Les raccordements entre les pièces peuvent donner lieu à des discontinuités de surfaces de quelques dixièmes de millimètres.
- la plupart des essais sont effectués avec une grille de protection sur l'entrée d'air qui génère une turbulence supplémentaire.

La représentation correcte de la grille à échelle réduite pose des difficultés particulières : la réduction géométrique dans le même rapport (1/2) que les autres dimensions conduit à un Reynolds (rapporté au diamètre du fil) inférieur au Reynolds critique de 2000 (Fig. 17), donc à une augmentation des pertes de charge : + 15 %. L'augmentation de la maille de façon à conserver le même Reynolds qu'en vol conduit à une disproportion entre la maille et l'entrée, avec des interactions modifiées et des problèmes de réalisation des pièces de fixation. Des mesures comparatives ont permis de conclure que la solution intermédiaire consistant à conserver sur la maquette la même maille que sur l'appareil donne les meilleures corrélations.

4.2.3. Angles d'incidence et de dérapage

L'attitude de la maquette peut être réglée à volonté dans les limites suivantes :

Incidence : $\pm 10^{o}$
Dérapage : $\pm 10^{o}$

Des écarts supérieurs sont techniquement possibles, mais l'augmentation importante du blocage de la veine d'essai conduit à des résultats peu significatifs.

La dissymétrie d'écoulement résultant du souffle rotor sur le fuselage apparaît de manière flagrante sur de nombreux résultats d'essai en vol (Fig. 19). Le rotor de la maquette ne comprenant pas de pales, les essais soufflerie effectués à dérapage nul fournissent des résultats symétriques, donc incorrects. C'est pourquoi un dérapage calculé d'après les caractéristiques du rotor peut être appliqué à la maquette de façon à simuler la dissymétrie du vol. Cette technique n'est pas utilisée systématiquement du fait de sa validité approximative.

4.2.4. Coefficient de débit

La condition de similitude fondamentale est le respect du coefficient de débit ε qui fixe la frontière du tube de courant pénétrant dans l'entrée d'air. Chaque point du domaine de vol à simuler est caractérisé par un coefficient de débit qu'il convient de restituer en soufflerie. Au début de chaque essai, le réglage de ε peut se faire de la manière suivante :

a) mesure du débit

b) calcul de la vitesse vent nécessaire

c) réglage du vent

d) mesure du débit

e) si le débit a varié, recommencer à l'étape b).

Le couplage vent - débit rend cette opération délicate et longue. Les conditions ambiantes variant d'un essai à l'autre, les réglages obtenus doivent être repris souvent.

On préfère généralement régler l'alimentation des ventilateurs une fois pour toute et effectuer plusieurs essais à vitesse croissante sans chercher à ajuster ε à une valeur déterminée. On trace alors les résultats en fonction de ε, ce qui permet d'apprécier la cohérence et la précision des mesures au vu de l'écart des points par rapport à une courbe lissée statistiquement.

Les résultats correspondant à un cas de vol précis, sont obtenus sur la courbe avec une fiabilité bien supérieure à la première méthode.

4.3. Conduite des essais et exploitation

Le but des essais soufflerie consiste à mesurer les performances d'une entrée d'air et à les comparer avec les performances prévues lors de la conception et avec celles des autres entrées connues. On doit en particulier, s'assurer que la distorsion reste dans les limites fixées par le motoriste, ceci dans tout le domaine de vol.

Il y a une dizaine d'années, les moyens informatiques limités et centralisés ne permettaient pas de dépouiller rapidement les résultats. Ceux-ci étaient enregistrés sur bande magnétique sous forme analogique ou numérique et traités en temps différé avec un délai atteignant parfois plusieurs jours. On ne disposait en temps réel, que de mesures brutes difficilement exploitables.

L'arrivée des micro-calculateurs, souples et autonomes, a considérablement diminué les délais d'exploitation en réunissant sur une même machine les fonctions suivantes (Fig. 13) :

- contrôle des conditions d'essais : calcul et affichage de la masse volumique de l'air, des débits, de la vitesse du vent
- acquisition des mesures (valeurs électriques en Volt)
- pré-dépouillement et édition des résultats en valeurs physiques

  stockage sur cartouche magnétique des résultats en valeurs physiques
- conversion des résultats à l'échelle appareil, calcul des paramètres globaux : perte de charge, indice de distorsion
- édition des résultats numériques et de courbes directement au format du rapport d'essai dans les 3 minutes suivant la fin de l'essai.

La manière dont sont présentées les informations finales revêt une grande importance. Elles s'adressent en effet à des spécialistes des turbomachines et des responsables de projet qui préfèrent des nombres relatifs à l'appareil lui-même plutôt qu'à une maquette à échelle réduite. L'interprétation des coefficients de pression, par exemple, nécessite des calculs et la connaissance de conventions relatives à la maquette qui deviennent superflus si ce travail d'interprétation est déjà inclus dans le traitement des données. C'est pourquoi une philosophie a été adoptée au service Aérodynamique de l'AEROSPATIALE. Elle s'exprime de la façon suivante :

- les essais soufflerie **simulent des essais en vol**

  donc, toutes les grandeurs doivent être exprimées comme si elles étaient le résultat de mesures sur appareil réel ou d'essais en vol (dimensions géométriques, vitesse, débit, pressions, . . .)
- afin d'éliminer toute confusion, aucun résultat à l'échelle de la maquette ne figure dans les documents d'exploitation (sauf mention contraire clairement indiquée). Y figurent par contre les limites de validité de la simulation : échelle réduite, non respect du Mach et du Reynolds, maquette partielle . . .

Les grandeurs suivantes sont généralement fournies (voir Fig. 14 - 15 - 16 et Annexe 1) :

- les conditions altitude-pression et température : toujours le standard sol
- le débit réduit du moteur : ce paramètre équivalent à un nombre de Mach, intervient directement dans le calcul des performances du moteur
- la vitesse de vol réduite : elle équivaut à un nombre de Mach et ne correspond à la vitesse propre et à la vitesse équivalente indiquée par l'anémomètre que dans les conditions standard sol
- la récupération de pression dynamique (ou perte de charge en vol stationnaire) : $r = \frac{P_1 - P_0}{P_0}$ en %, P_1 : pression totale devant compresseur

  Ce paramètre intervient directement dans le calcul des performances du moteur
- l'indice de distorsion : selon la définition fixée par le motoriste
- une carte de pression totale au niveau de la section de mesure.

Naturellement, les résultats archivés sur bande magnétique sont les mesures brutes à l'échelle maquette et ils peuvent être consultés à tout moment afin de vérifier la validité du dépouillement.

5. CORRELATIONS SOUFFLERIE / VOL

La comparaison se trouve facilitée par la présentation adoptée pour les résultats soufflerie : il suffit de reporter les points d'essais en vol sur le même graphique (après corrections pour les conditions atmosphériques si celles-ci diffèrent sensiblement du standard sol). On a ainsi constaté plusieurs cas de très bonne corrélation sur l'indice de distorsion, la perte de charge en vol stationnaire et la récupération de pression dynamique en vol de translation. On a également pu comparer des cartes de pression totale relevées grâce à des instrumentations parfaitement semblables (Fig. 20 - 21 - 22).

Ces cas sont naturellement précieux puisqu'ils permettent d'évaluer la validité des hypothèses et approximations diverses postulées lors des essais soufflerie et de leur interprétation. Ces recoupements positifs ayant été constatés, la soufflerie est couramment utilisée sans que de telles corrélations soient systématiquement établies, ceci pour deux raisons :

a) soit que les essais sur maquette soient considérés comme un simple outil de recherche dans le but de compléter les moyens de calcul encore insuffisants, auquel cas il n'y a, bien sûr, aucun essai en vol correspondant.

b) soit, à l'inverse, que ces essais remplacent purement et simplement des mesures impossibles ou très difficiles à pratiquer correctement dans l'environnement du vol : sondage dans le plan d'entrée du compresseur, peigne tournant, ou prises de pression très nombreuses. La qualité des résultats que permet le calme et la sécurité de la terre ferme, compense alors largement les imperfections de similitude. Ces motifs ont permis de justifier la qualité de l'installation motrice pour la certification de plusieurs appareils sur la seule foi de résultats de soufflerie (et en l'absence de problèmes de fonctionnement en vol).

Une étude systématique et rigoureuse des corrélations entre les différents moyens d'essai nécessiterait des essais spécifiques au sol simulant des essais en vol effectués **antérieurement** et dans des **conditions parfaitement identifiées**. Or, il est évident que si l'on dispose déjà de tels résultats de vol, les essais soufflerie deviennent superflus du point de vue du développement de l'appareil. C'est pourquoi les corrélations soufflerie / vol ne concernent qu'une faible proportion des travaux effectués.

6. RESULTATS

L'amélioration des méthodes de conception et d'essai a débouché sur des gains importants de performance, mesurés en soufflerie et confirmés en vol :

1) Perte de puissance à l'avionnage des moteurs.

Exemple :

vol stationnaire
SA 365 C (1974*) ——————→ 8 %
SA 365 N (1978) ——————→ 3 %

2) Distorsion

Exemple :

réduite par un facteur 3 sur SA 365 N par rapport au SA 365 C

3) Traînée parasite

Exemple :

réduction de 10 % de la traînée du fuselage du AS 332 par affinement des entrées d'air

Il semble que la poursuite de ces efforts permette prochainement de réduire la perte de puissance à moins de 1,5 % en vol stationnaire, avec une récupération de pression dynamique en croisière de l'ordre de 2 %.

7. CONCLUSION

Les essais de soufflerie constituent le complément idéal des méthodes de conception dans la recherche de performances toujours accrues pour les entrées d'air. L'introduction de la micro-informatique dans la conduite d'essai, l'acquisition et le dépouillement permet de réduire les délais et de présenter des résultats directement comparables aux essais en vol et exploitables aisément pour le calcul des performances moteur. Les essais en vol réels confirment globalement les progrès enregistrés en soufflerie mais les cas où l'on dispose simultanément de résultats de vol et de soufflerie dans des configurations rigoureusement semblables ne représentent qu'une faible proportion du travail effectué au sol et en vol.

---

* *Année de conception*

ANNEXE 1

Passage des variables maquette aux variables appareil

Introduisons d'abord les notations suivantes :

x_m = valeur de la variable x mesurée sur la maquette

x_a = valeur de la variable x au point homologue de l'appareil

$\dot{x} = \frac{x_a}{x_m}$ = facteur d'échelle sur la grandeur x

x_s = valeur standard sol de la variable x

La similitude du coefficient de débit s'écrit :

$$\varepsilon a = \left(\frac{Q}{\varrho V\ A_1}\right)_a = \left(\frac{Q}{\varrho V\ A_1}\right)_m = \varepsilon m$$

$$\Rightarrow \boxed{V'_a = V_m \cdot \frac{Q'_a}{Q_m} \cdot E^2 \cdot \frac{\varrho m}{\varrho s}} \qquad (1)$$

où :

$Q'_a = Q_a \sqrt{\frac{T_a}{T_s}} \cdot \frac{p_s}{p_a}$ = débit réduit du moteur

$V'_a = V_a \sqrt{\frac{T_s}{T_a}}$ = vitesse réduite de l'appareil

E = échelle de la maquette

Cette relation permet de calculer la vitesse de l'appareil pour un débit donné du moteur dans le cas de vol correspondant à un essai soufflerie donné.

Les pressions sont converties à l'échelle de l'appareil en utilisant la relation de conservation du coefficient de pression :

$$\left(\frac{p - p_0}{q_0}\right)_a = \left(\frac{p - p_0}{q_0}\right)_m$$

$$\frac{p - p_0}{p_0}\ _a = (p - p_0)_m \cdot \frac{\hat{q_0}}{(p_0)_a}$$

Or, d'après la similitude du coefficient de débit :

$$\frac{\hat{q_0}}{p_0}\ _a = \frac{1}{p_s} \cdot \frac{\varrho m}{\varrho s} \cdot \left(\frac{Q'_a}{Q_m}\right)^2 E^4$$

d'où :

$$\boxed{\left(\frac{p - p_0}{p_0}\right)_a = (p - p_0)_m \cdot \frac{1}{p_s}\ \frac{\varrho m}{\varrho s}\ \left(\frac{Q'_a}{Q_m}\right)^2 E^4} \qquad (2)$$

Cette relation est valable pour toute pression p (totale ou statique) mesurée dans la zone incompressible. Elle reste applicable dans la zone compressible pour les pressions totales. Il n'existe pas de méthode générale permettant de corriger les pressions statiques pour les effets de compressibilité. Toutefois, dans le cas où les pressions statiques et totales sont regroupées dans une même section de mesure, il est possible d'appliquer la procédure suivante :

a) calculer la pression statique moyenne $(\overline{p_1})_{\text{comp.}}$ connaissant le débit, la section, la température totale (égale à la température amont), la pression totale moyenne.

b) calculer les pressions statiques en chaque point par la formule (2), (donc sans tenir compte de la compressibilité) et leur moyenne $(\overline{p_1})_{\text{incomp.}}$

c) corriger les valeurs incompressibles par le fac : $\frac{(\overline{p_1})_{\text{co}}}{(\overline{p_1})_{\text{.omp.}}}$

BIBLIOGRAPHIE

[1] Les hélicoptères et les économies d'énergie
G. PETIT – 13ème Congrès International Aéronautique – Paris - 2 et 3 Juin 1977

[2] Amélioration du bilan propulsif d'un hélicoptère
J. GALLOT – 17ème Colloque d'Aérodynamique Appliquée – Grenoble - 12, 13, 14 Novembre 1980

[3] Aerodynamics of Helicopter Flight near the Ground
M. SHERIDAN – AHS n° 77.33.04

[4] Exhaust Gas Reingestion During Hover in Ground Effect
M.E. JACKSON - R.L. HOUSE – 37è. Forum of AHS – New Orléans, La. May 1981

[5] Exhaust Gas Reingestion Measurements
B. TURCZENIUK – Propulsion Specialist's Meeting – Williamsburg, Va. Nov. 1979

[6] La transformation de l'hodographe pour les écoulements plans incompressibles de fluide parfait
P. SOURIAU – Nord Aviation - NT 1798/STS - Mars 1962

[7] Aerodynamic Design of Engine Air Intakes for Improved Performance
A. VUILLET – 6è. European Rotorcraft & Powered Lift Forum – Bristol, England - Septembre 1980

[8] Entrées d'air moteur – Synthèse des connaissances acquises en aérodynamique
A. VUILLET – Aérospatiale Marignane - H/DE.EC 127/79

[9] Théorème d'Euler – Utilisation en aérodynamique
M. LAZAREFF – Aérospatiale Chatillon - Septembre 1971

[10] Perte de charge dans une entrée d'air à parois minces – Estimation théorique
M. LAZAREFF – Aérospatiale Suresnes - n° 81.559/76

[11] Improved Analytical Design Technique for Low Power-Loss Engine Inlets
E.H. STAUDT – F.B. WAGNER – 33è. Forum – AHS Washington DC - May 1977

[12] Essais d'entrée d'air en soufflerie
J. LAVERRE - M. BAZIN - J.P. LEDY – Revue Aéronautique & Astronautique n° 48 - pages 77 - 88

[13] Parabolic Procedure for Flows in Ducts with Arbitrary Cross Sections
D.W. ROBERTS - C.K. FORESTER – AIAA Journal - Vol. 17, No. 1 - Jan. 1979

[14] Unified Inlet/Diffuser Design by an Inverse Method
G.J. Hokenson - F.Y. Su – AIAA Journal, Vol 15, No. 1 - Jan. 1977

[15] Interaction Entrée d'air – Moteur
R. SCHLEGEL - P. SAGNES – Société Bertin - NT 82 CC 01

[16] Prise d'air de l'Ecureuil – Ecoulement interne avec échappement tourbillonnaire sur les arêtes
J. MARECHAL - C. REHBACH – Rapport ONERA n° 3/4349 AV 00-0 - Janvier 1982

[17] Calcul de l'écoulement turbulent dans une prise d'air bidimensionnelle à grande incidence
M. STANISLAS – Rapport IMFL n° 82/04 - Opération n° 0186 - Mars 1982

[18] Calcul de l'écoulement tridimensionnel dans une prise d'air Dauphin
B. BOIZART – Rapport ONERA n° 2/4349 AY 004 - Mars 1982

[19] Visualisation hydrodynamique de l'écoulement dans une maquette de prise d'air Ecureuil
H. WERLE – Rapport ONERA n° 1/4349 AY - Mars 1982

[20] Three-Dimensional Calculations of the Flow in Helicopter Air Intakes
B. BOIZART – 8è. European Rotorcraft Forum - AAAF - Sept. 1982 - Aix-en-Provence

[21] Distortion Induced Engine Instability
AGARD - Lecture Series n° 72

[22] Aerodynamics of Power Plant Installation
AGARD - Advisory Report n° 173

[23] Aerodynamics of Propulsion
KUCHEMAN & WEBER - Mac Graw-Hill - New-York 1979

[24] Relaxation methods for solution of elliptic problems in domains with arbitrary boundary. Applications to computation of subcritical flows
M. FENAIN Journal of Applied Mechanics, Vol 1 No. 1 - 1977, p. 27-67

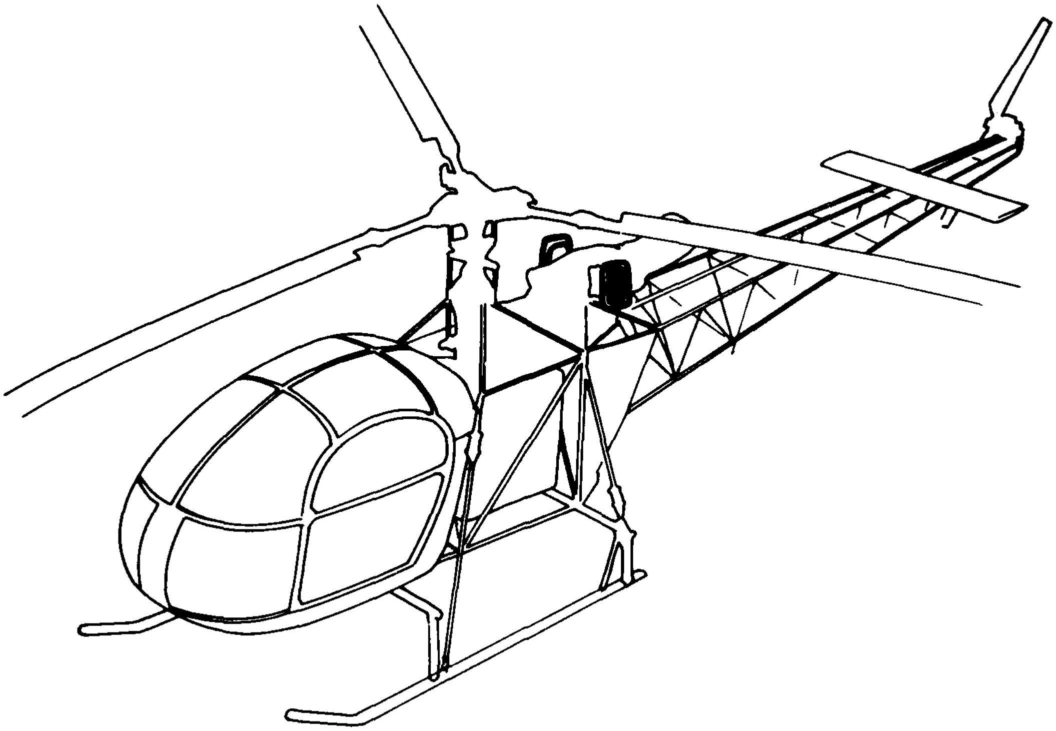

Fig. 1 : ENTREE D'AIR PAVILLON (ALOUETTE II)

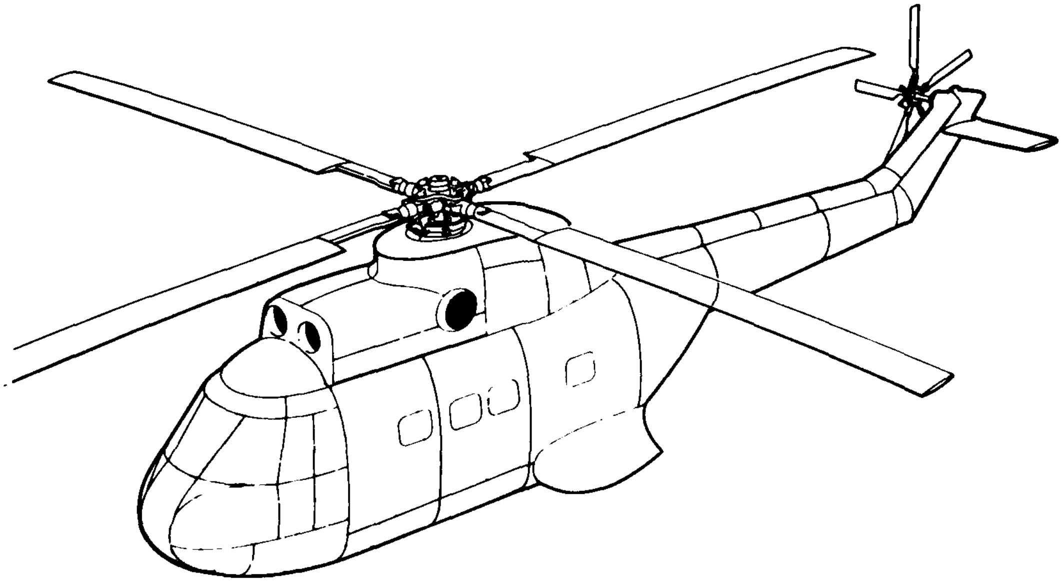

Fig. 2 : ENTREES D'AIR FRONTALES (PUMA)

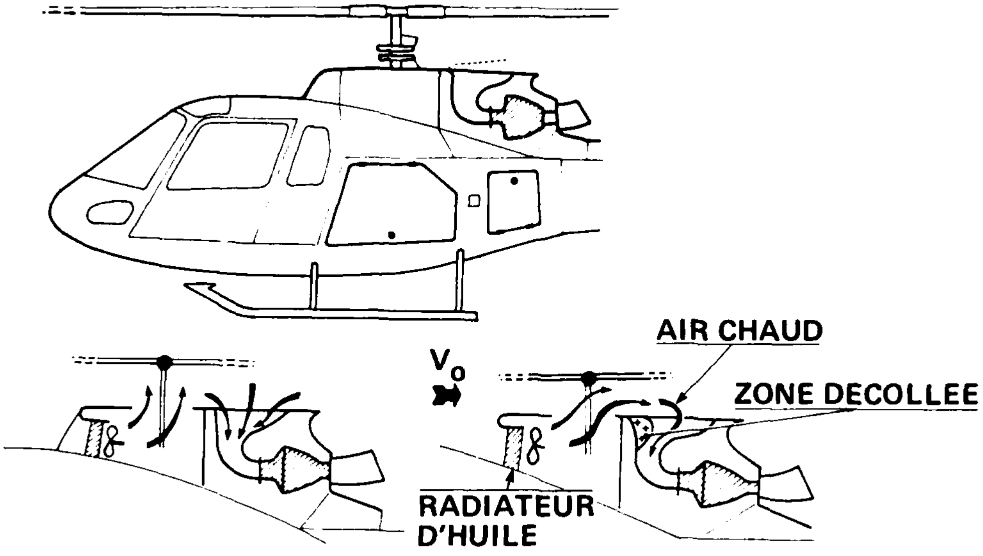
AIR CHAUD
V_o
ZONE DECOLLEE
RADIATEUR D'HUILE

3a. VOL STATIONNAIRE

3b. TRANSLATION

Fig. 3 : ENTREE D'AIR STATIQUE (ECUREUIL SA 350)

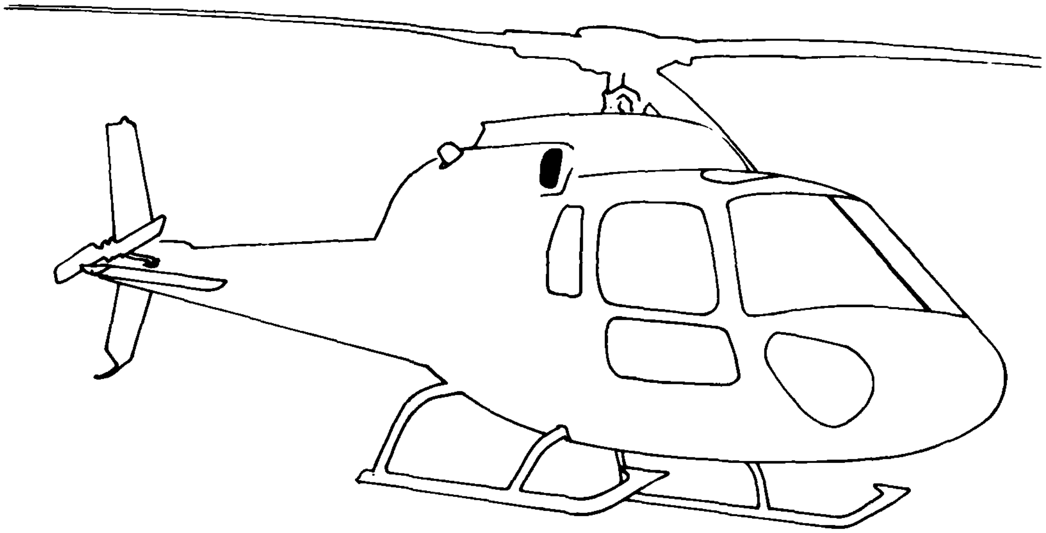

Fig. 4 : ENTREES D'AIR LATERALES (TWINSTAR AS 355)

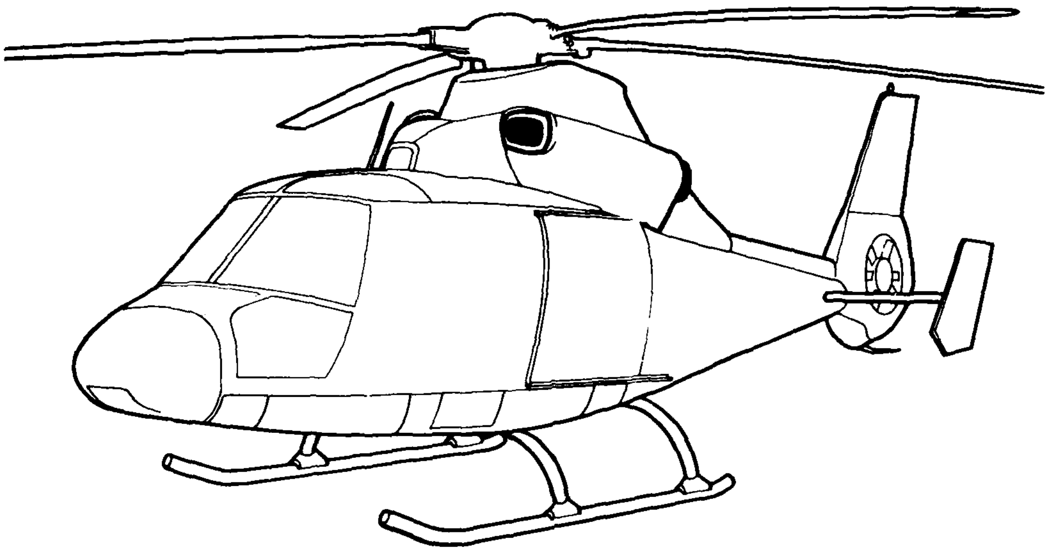

Fig. 5a : ENTREES D'AIR FRONTALES (DAUPHIN II – SA 365 N)

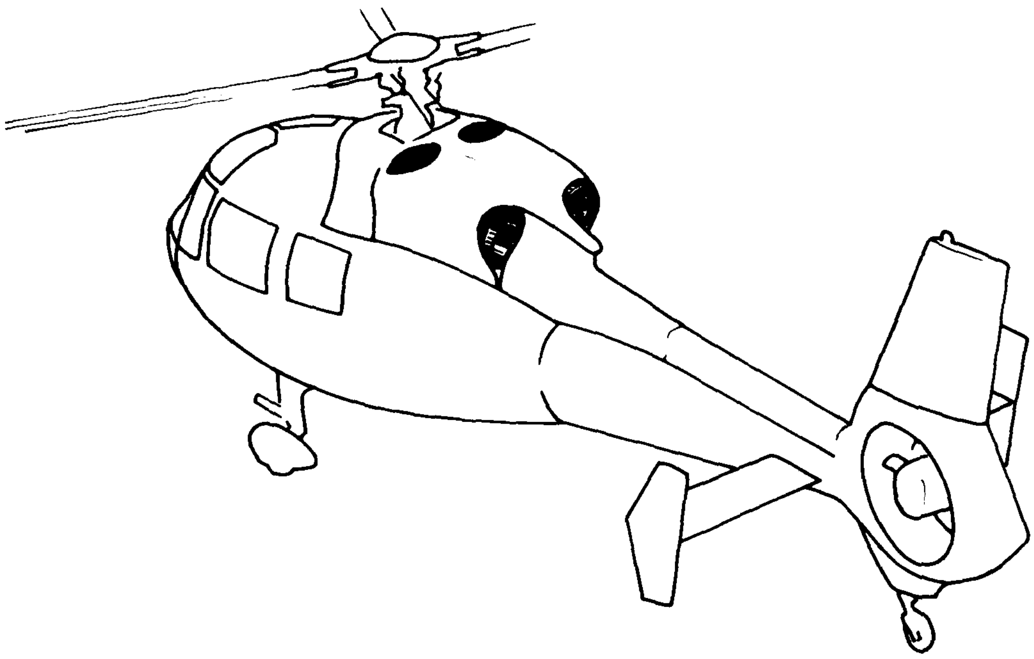

Fig. 5b : ENTREES D'AIR STATIQUES (DAUPHIN SA 365 C)

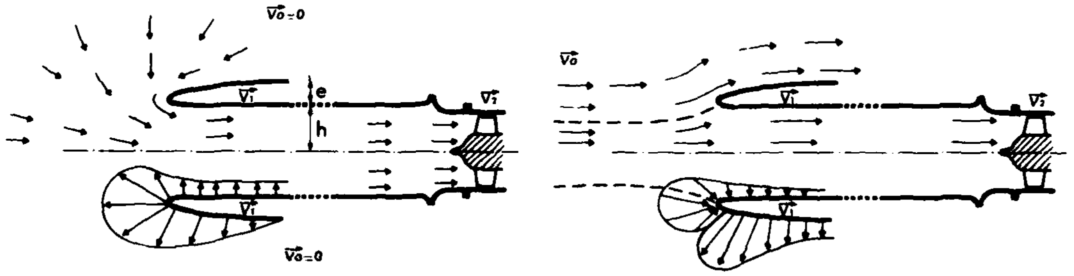
$\vec{V_0}=0$
$\vec{V_1}$
e
h
$\vec{V_2}$
$\vec{V_1}$
$\vec{V_0}=0$
$\vec{V_0}$
$\vec{V_1}$
$\vec{V_2}$
$\vec{V_1}$

Fig. 6 : DISTRIBUTION DE VITESSE SUR LES LEVRES

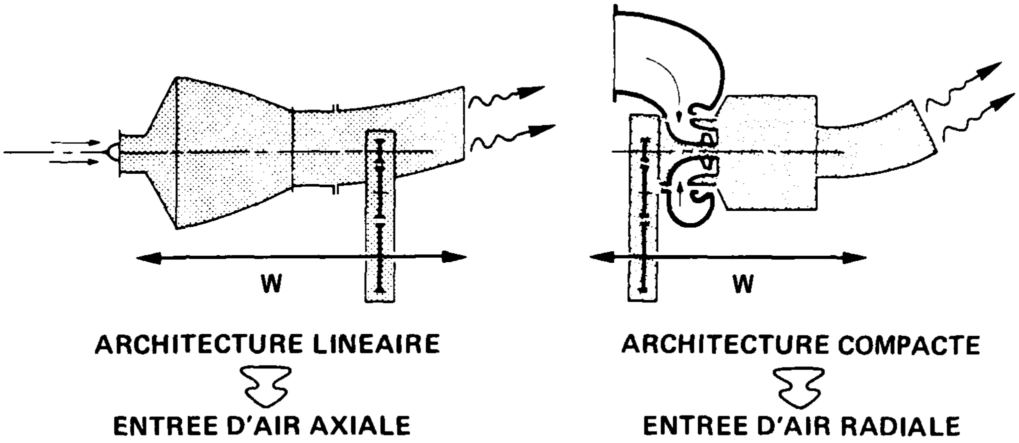
W
W
ARCHITECTURE LINEAIRE
ENTREE D'AIR AXIALE
ARCHITECTURE COMPACTE
ENTREE D'AIR RADIALE

Fig. 7 : ARCHITECTURE DES MOTEURS

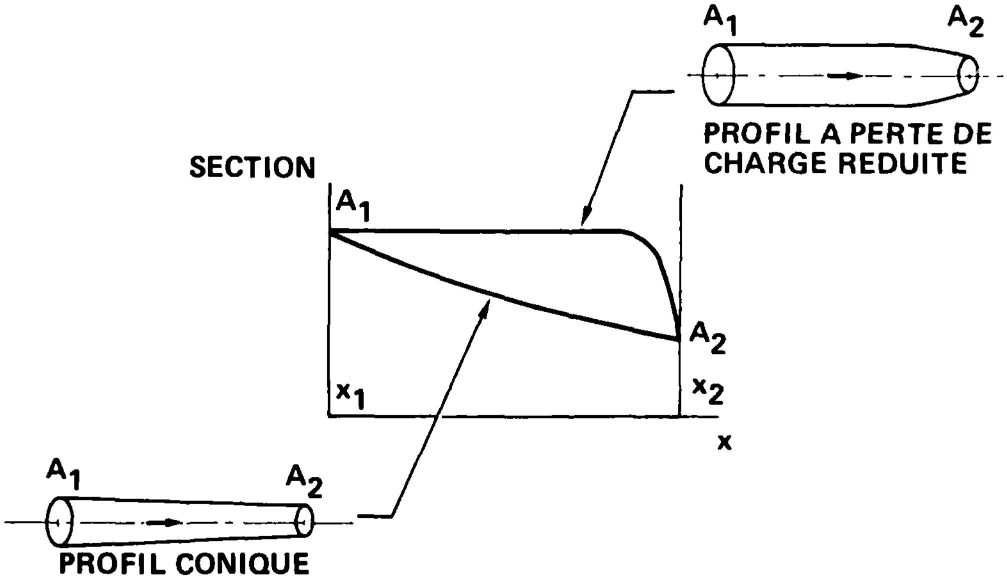
A1
A2
PROFIL A PERTE DE CHARGE REDUITE
SECTION
A1
A2
x1
x2
x
A1
A2
PROFIL CONIQUE

Fig. 8 : CONDUIT CONVERGENT

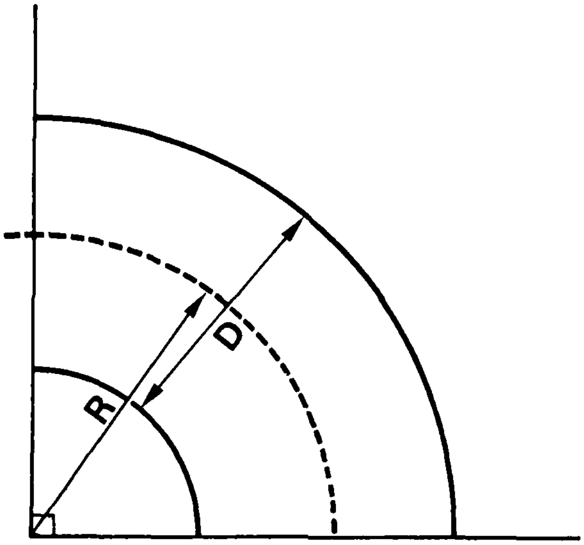

CRITERE PRATIQUE DE DIMENSIONNEMENT :

$\frac{R}{D} \geqslant 2$ **SECTION CONSTANTE OU CONVERGENTE**

Fig. 9 : CONDUIT COUDE A 90°

FONCTION DE POTENTIEL :

$$F(z) = Q \left(\frac{z}{A_2} - \frac{1}{2\Pi} . \text{ Log } z \right)$$

VITESSE COMPLEXE :

$$W(z) = Q \left(\frac{1}{A_2} - \frac{1}{2\Pi z} \right)$$

$$\begin{cases} V_n = \frac{Q}{A_2} \left(\cos\theta - \frac{1}{2\Pi} . \frac{A_2}{R} \right) \\ V_t = - \frac{Q}{A_2} \sin\theta \end{cases}$$

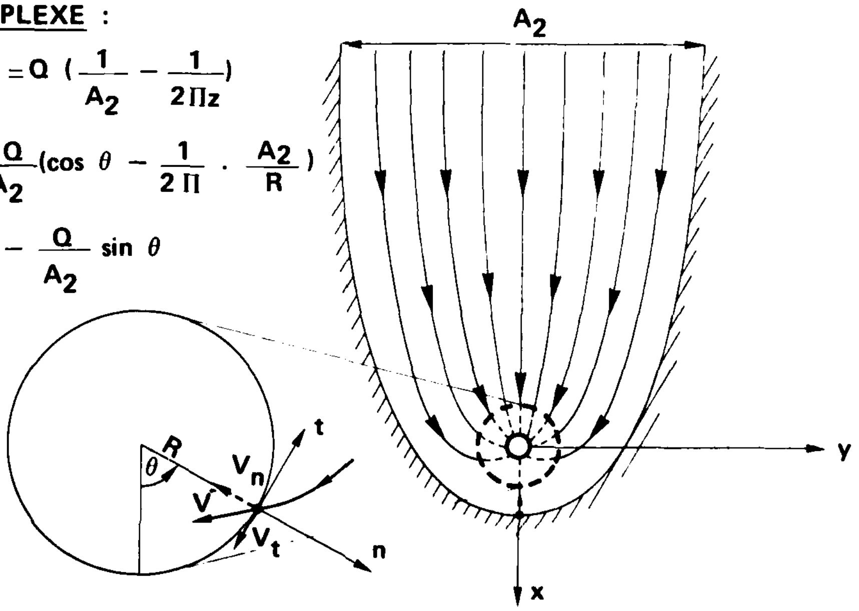

Fig. 10 : ECOULEMENT PLAN POTENTIEL DANS UNE ENTREE RADIALE AVEC CHAMBRE

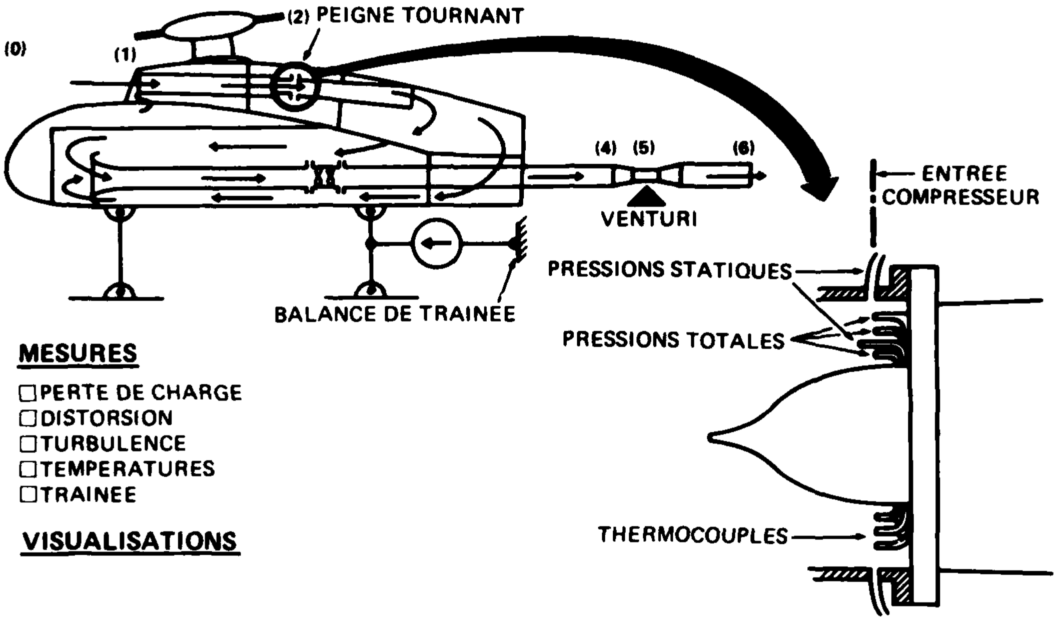
(0)
(1)
(2) PEIGNE TOURNANT
(4) (5) (6)
VENTURI
BALANCE DE TRAINEE
ENTREE COMPRESSEUR
PRESSIONS STATIQUES
PRESSIONS TOTALES
THERMOCOUPLES
MESURES
☐PERTE DE CHARGE
☐DISTORSION
☐TURBULENCE
☐TEMPERATURES
☐TRAINEE
VISUALISATIONS

Fig. 11 : ARRANGEMENT INTERNE D'UNE MAQUETTE A ECHELLE 1/2

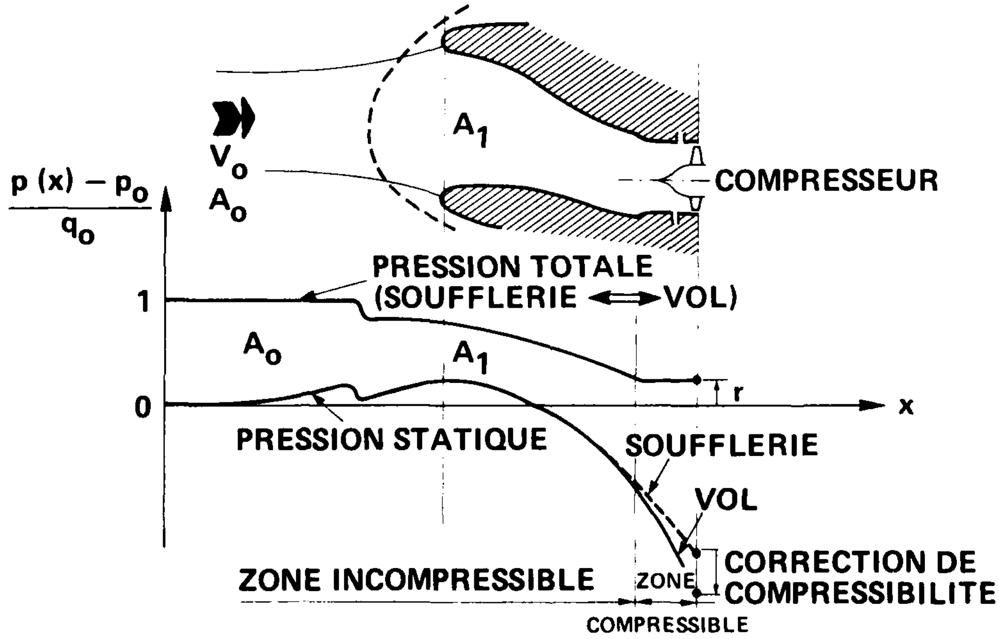

Fig. 12 : ZONES D'ECOULEMENT

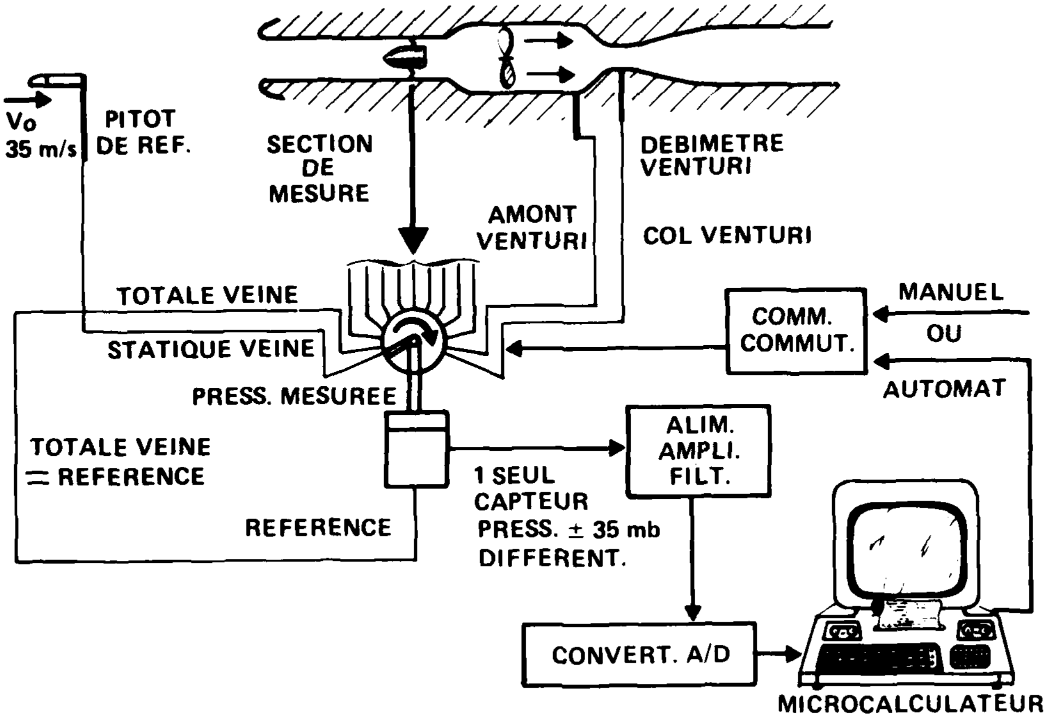

Vo
35 m/s
PITOT
DE REF.
SECTION
DE
MESURE
DEBIMETRE
VENTURI
AMONT
VENTURI
COL VENTURI
TOTALE VEINE
STATIQUE VEINE
PRESS. MESUREE
COMM.
COMMUT.
MANUEL
OU
AUTOMAT
TOTALE VEINE
= REFERENCE
ALIM.
AMPLI.
FILT.
1 SEUL
CAPTEUR
PRESS. ± 35 mb
DIFFERENT.
REFERENCE
CONVERT. A/D
MICROCALCULATEUR

Fig. 13 : SYNOPTIQUE DES MOYENS DE MESURE

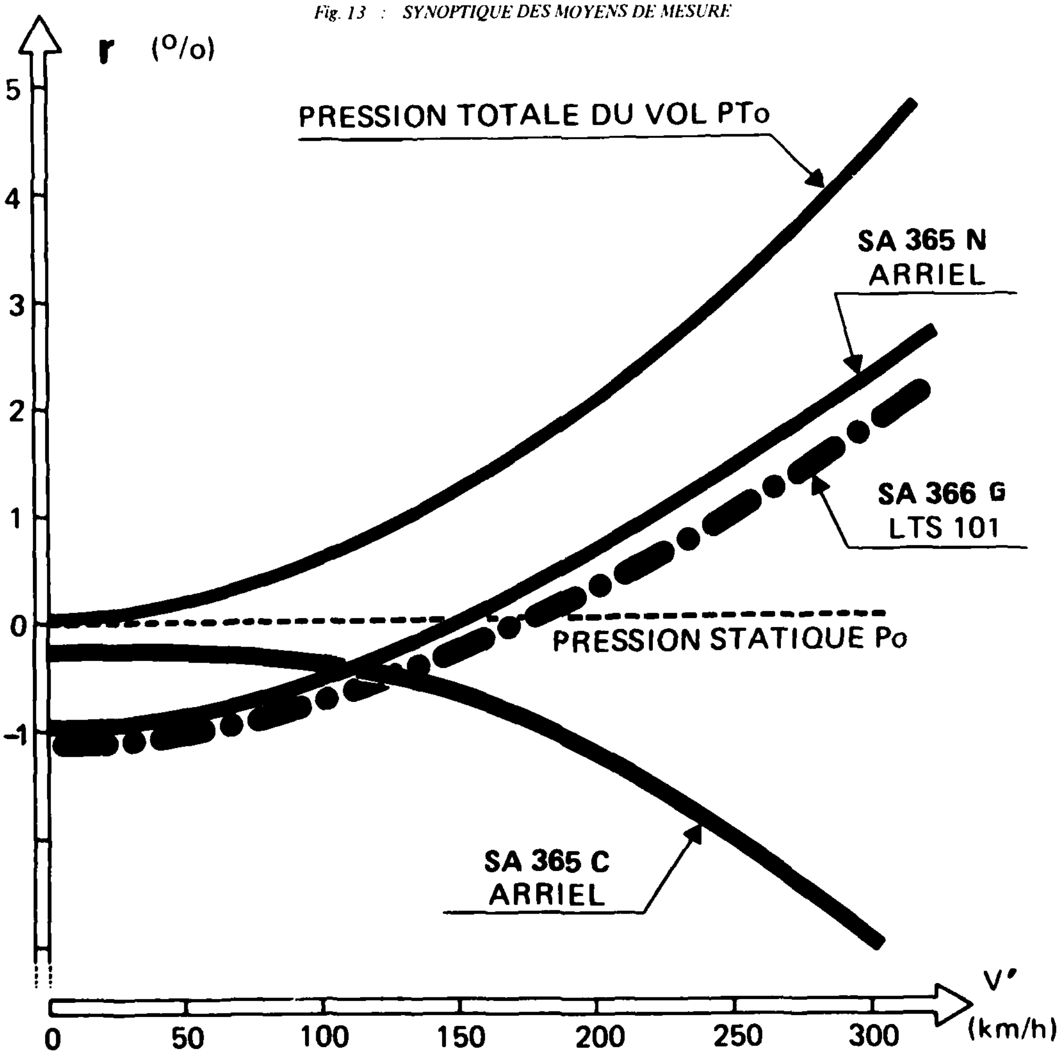

Fig. 14 : RECUPERATION DE PRESSION DYNAMIQUE

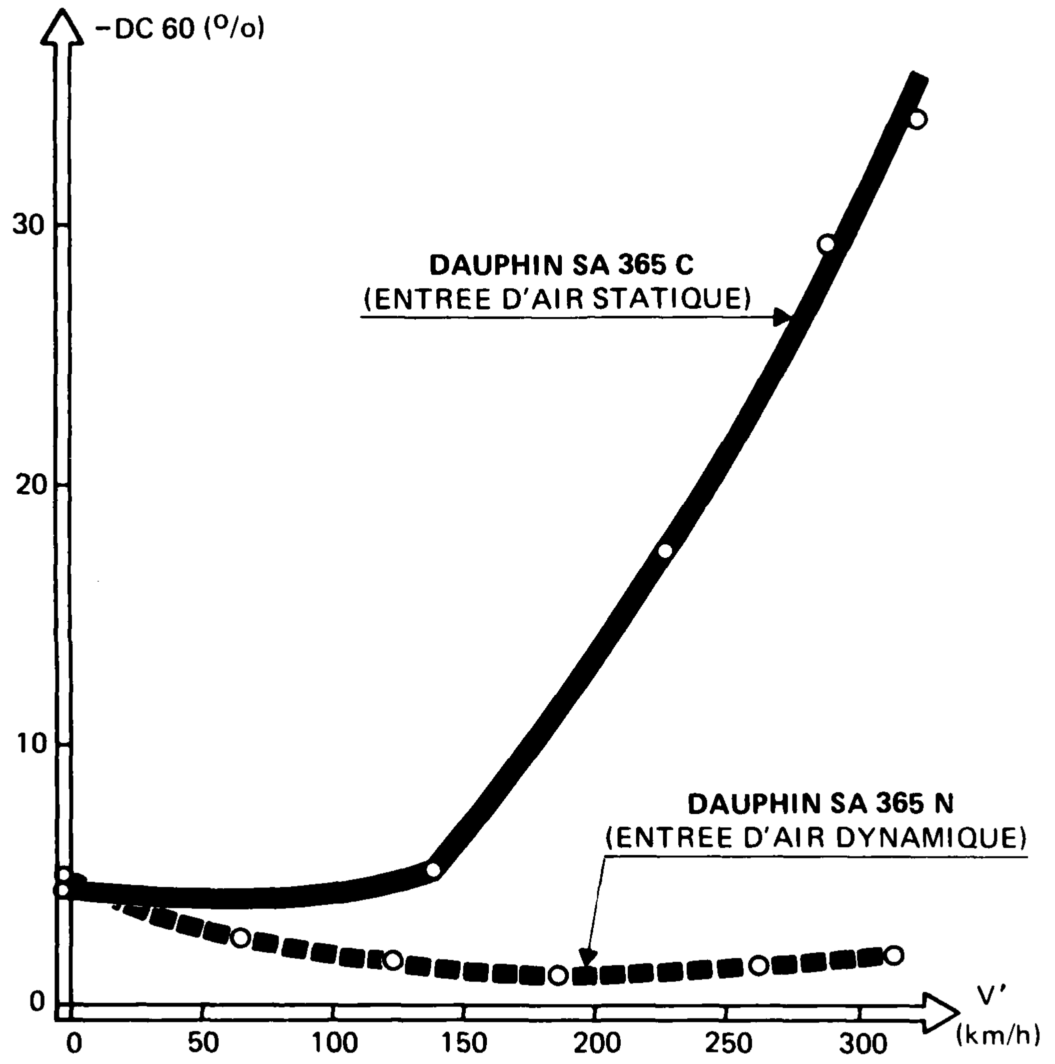

Fig. 15 : CRITERE DE DISTORSION (DC_{60})

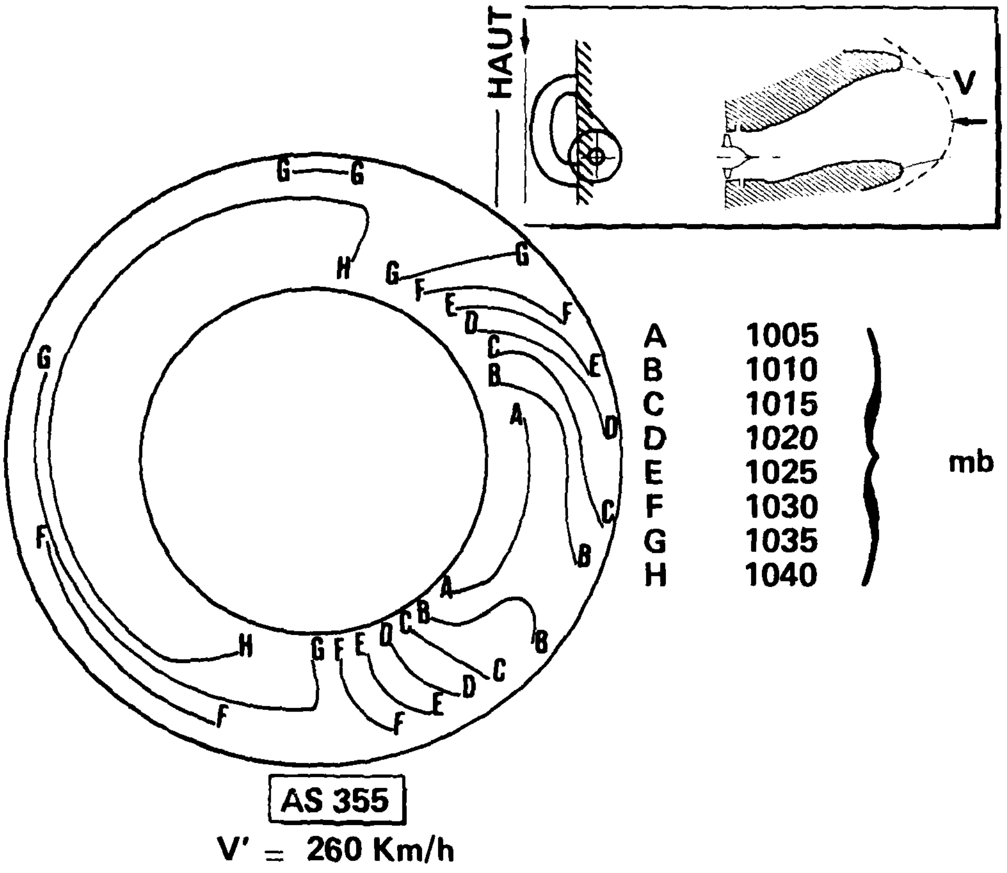
HAUT
V
G G
H G G
F F
E E
D D
C C
B B
A A
G F
H G F E D C B B C D E F
A 1005
B 1010
C 1015
D 1020
E 1025
F 1030
G 1035
H 1040
mb
AS 355
V' = 260 Km/h

Fig. 16 : CARTE DE PRESSION TOTALE

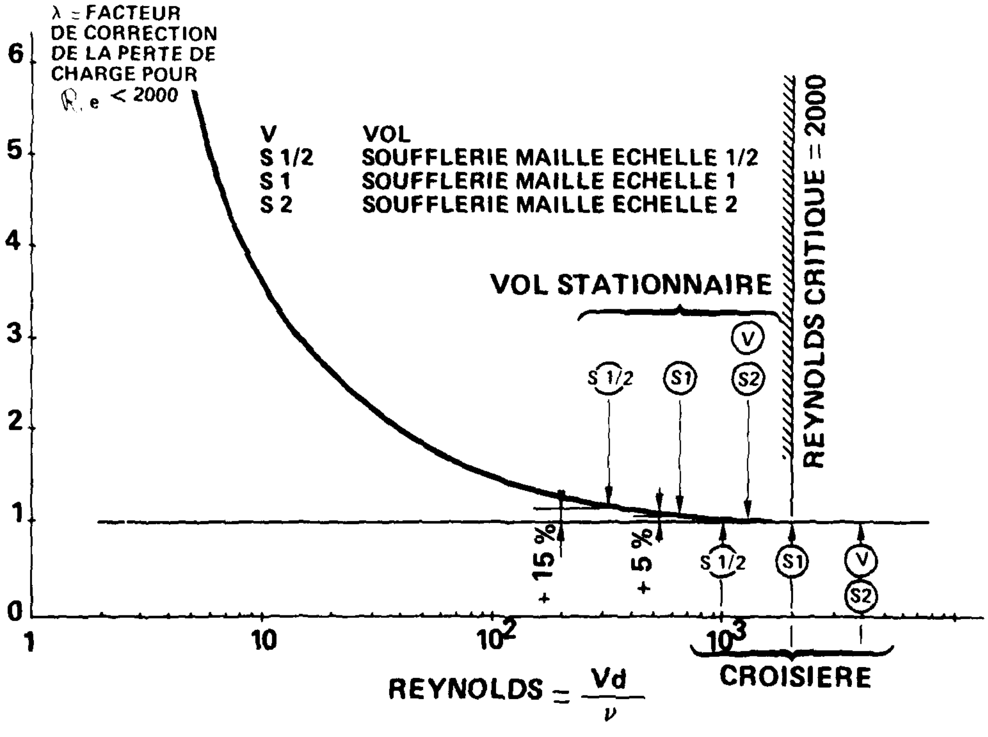

Fig. 17 : INFLUENCE DU REYNOLDS SUR LA PERTE DE CHARGE DE LA GRILLE

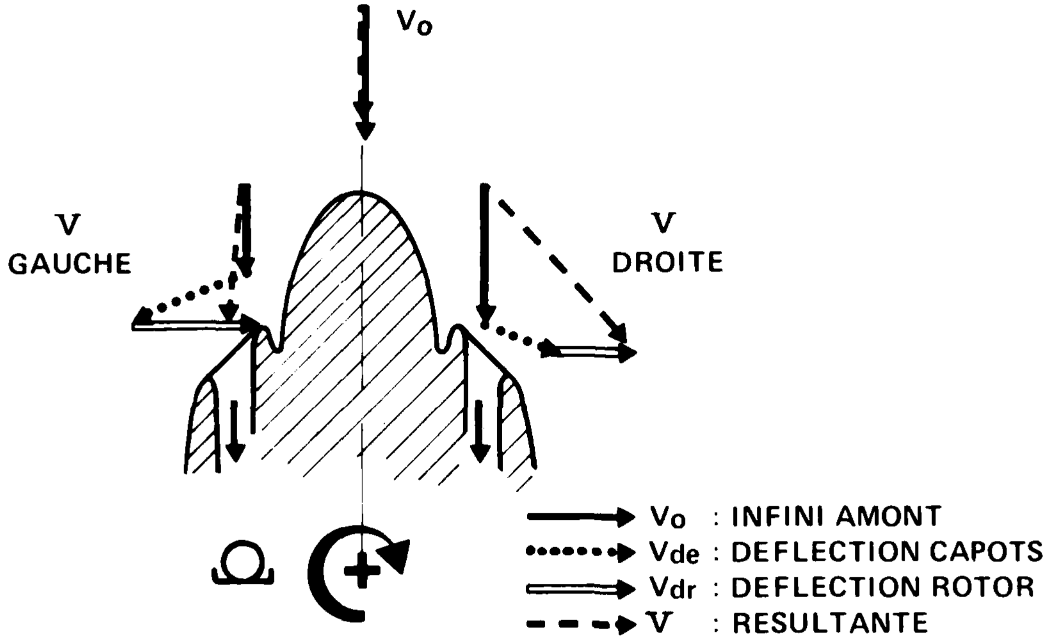
Vo
V
GAUCHE
V
DROITE
Ω
Vo : INFINI AMONT
Vde : DEFLECTION CAPOTS
Vdr : DEFLECTION ROTOR
V : RESULTANTE

Fig. 18 : DISSYMETRIE INDUITE PAR LE ROTOR

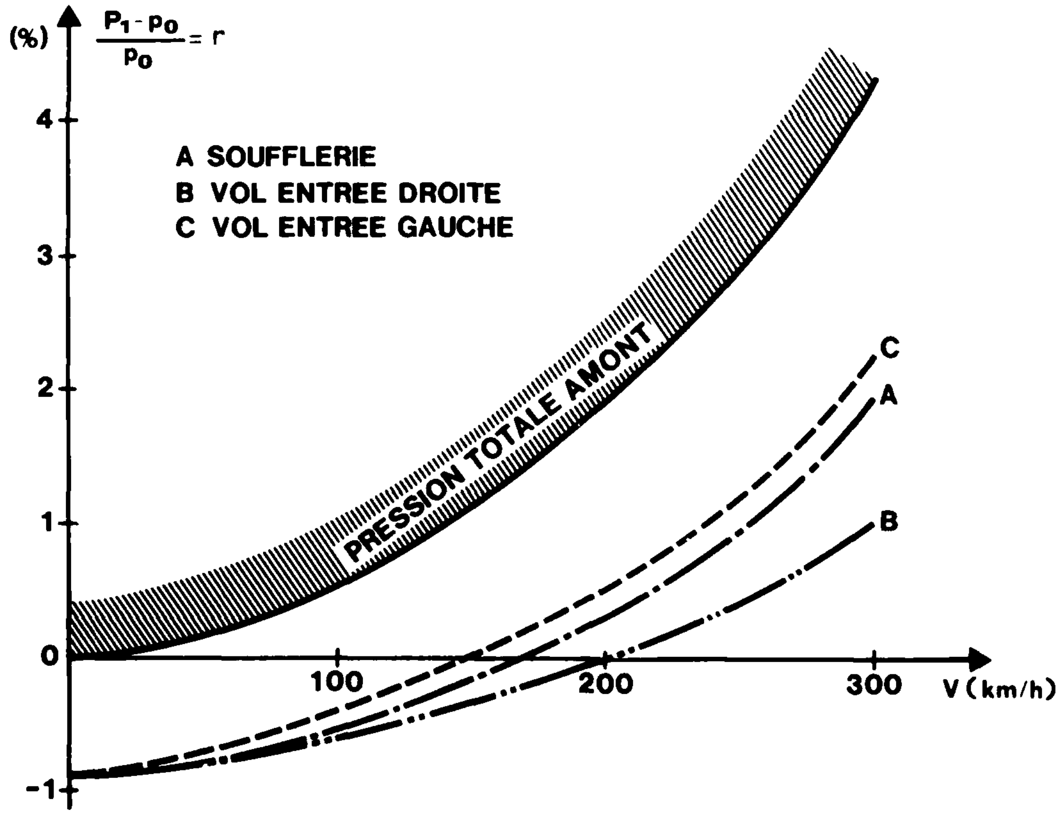

Fig. 19 : CORRELATION SOUFFLERIE / VOL (AS 366 G)

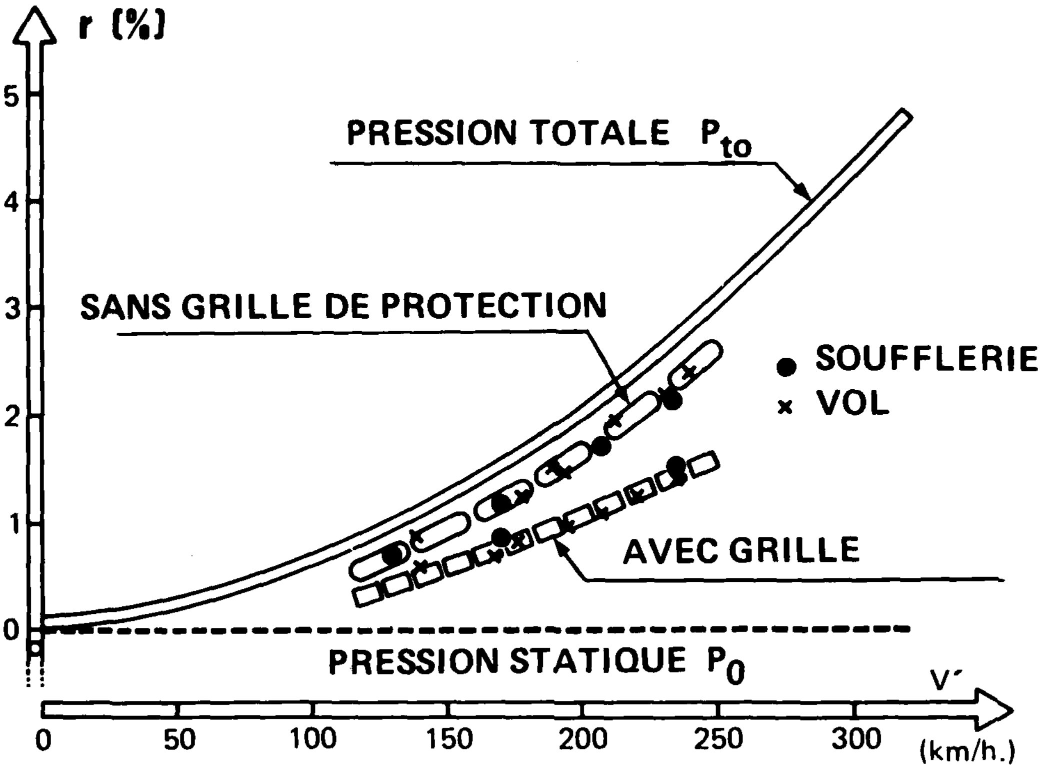

Fig. 20 : CORRELATION SOUFFLERIE / VOL (AS 355)

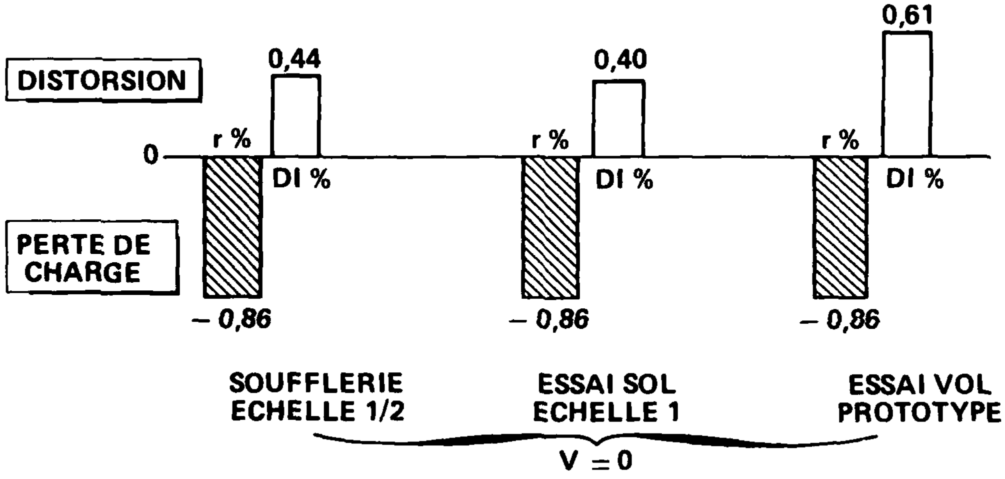

Fig. 21 : CORRELATION SOUFFLERIE / SOL / VOL (SA 366 G)

VUES DE FACE

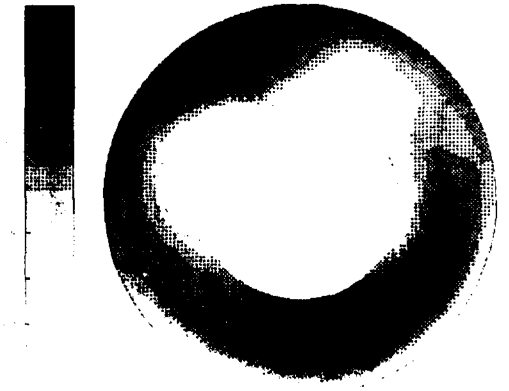

ENTREE DROITE : SOUFFLERIE

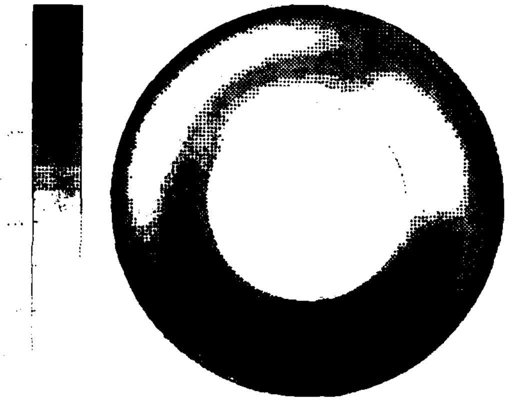

ENTREE GAUCHE : VOL

Fig. 22 : CORRELATION SOUFFLERIE / VOL CARTE DE PRESSION TOTALE EN VOL STATIONNAIRE

SYNTHESIS OF RESPONSES TO AGARD-FMP QUESTIONNAIRE ON "PREDICTION TECHNIQUES AND FLIGHT CORRELATION"

John Williams*
Formerly of Aerodynamics Department,
Royal Aircraft Establishment, U. K.

SUMMARY

In connection with the Symposium of the AGARD Flight Mechanics Panel on "Ground/Flight Test Techniques and Correlation" (Turkey, October 1982), the FMP Technical Program Committee issued a five-item questionnaire about prediction techniques and flight correlation. Part A of this paper introduces the basis of the FMP questionnaire, the key to the origins of the responses received from nationally selected experts, and the broad scope of aircraft design/prediction needs. Part B collates the detailed written responses received during the period end-June to late-September 1982, with minor technical editing, but with essential re-arrangements and translation for consistency of presentation. This paper was initially prepared to stimulate contributions to the 'Round-Table Discussion' at the FMP Symposium. Part C now also presents further edited comments based on some 'Contributors' Notes' received soon after the Symposium.

PART A - INTRODUCTION

1. NATURE OF FMP QUESTIONNAIRE AND RESPONSES

In connection with the Symposium of the AGARD Flight Mechanics Panel on "Ground/Flight Test Techniques and Correlation" (Turkey, October 1982), the appointed Technical Program Committee (Ph. Poisson-Quinton and F. N. Stoliker) issued a five-item questionnaire concerning the status and prospects of prediction techniques and correlation against aircraft flight results. An immediate synthesis of written comments received in the period July/August/September 1982, from the experts selected nationally by six NATO Countries (US, UK, NE, IT, GE , FR) was prepared initially as an up-to-date overview to stimulate the 'Round-Table Discussion' towards the end of the Symposium. Subsequently the further inclusion of some constructive written comments, received from Round-Table Members and one other participant after the Symposium, proved possible in time for publication as part of the Symposium Proceedings.

The five specific questions were phrased as follows by the FMP Technical Program Committee.
1. What are the advantages/disadvantages of different prediction techniques?
2. What portions of the flight regime cannot/should-not be addressed by ground-based techniques?
3. Are there areas where analytical prediction can be better than windtunnel and/or simulation results; or vice-versa?
4. Are there methods of reducing differences between prediction and flight-test results?
5. Are there any new prediction techniques that should be emphasised?

A Key to the various Respondents is provided by the next Section (Part A, § 2), taking the nations for convenience in reverse alphabetical order, which fortuitously correlates with the time-sequence in which most of the replies were received, ranging from the end-June deadline to late September! The remaining Section of this Introduction (Part A, § 3) broadly serves to stress

- The interdependency of aircraft design factors and the variation of allied prediction requirements according to the character and time-scale of the particular project.
- The variation in levels of sophistication and reliability of the required prediction methodology according to the stages reached in the development of the particular project.
- The complementary nature of the prediction tools available to the aircraft designers and the potential operators.

In posing the questions, no special guidance appears to have been given to the recipients concerning the intended scope or precise meaning of the particular technical terms used. Perhaps this freedom has led to somewhat differing interpretations of the questions, but probably has allowed wider and stronger expressions of personal interests and opinions. Indeed, the informal nature of the responses has been very gratifying; while, in the short time available for synthesis, the extent has been literally overwhelming - comprising over 10,000 words even without some supporting published papers.

The collated detailed responses are provided for the Questions 1 to 5 in Sections 1 to 5 respectively of Part B; for each question, the responses are taken in the same order as listed in the 'Key to Respondents'. My editing there has been properly restricted to some points of clarification/translation without introducing any intentional bias on my part, though some re-arrangement of the material has been at times necessary to attempt consistency of presentation. Likewise, Part C presents some edited comments based on 'Contributors notes' received soon after the Round-Table Discussion. The primary areas of interest and views expressed during the whole Symposium will of course be summarised and analysed further in the Technical Evaluation Report, to follow up publication of the Symposium Proceedings.

---

*Visiting Professor (part-time), Aeronautics and Astronautics Department, Southampton University, Southampton, Hants SO9 5NH, U. K.

2. KEY TO RESPONDEES

2.1 United States

- US/NASA - Prepared by NASA Ames Research Center; Langley Research Center elected not to respond, but to allow the Ames comments to represent NASA's views on the questions. Received through G. G. Kayten of NASA HQ (Washington DC).
- US/AFFTC - Provided by R. G. Hoey, Chief of Office of Manned Vehicles, Air Force Flight Test Center (Edwards AFB).
- US/NATC - Prepared by the Naval Air Test Center (Patuxent River, Mary.). Received through R. C. A'Harrah of Naval Air Development Center (Warminster, Pa.).
- US/NAVAIR - Prepared by E. C. Rooney of Naval Air Systems Command (Washington DC). Received through R. C. A'Harrah of NADC.
- US/AVRADCOM - Prepared by I. C. Statler of Army R&T Labs, to represent current opinions of both the Aeromechanics Lab. (Ames Research Center) and AEFMA with respect to rotary-wing aircraft.
- US/Bell Hel - Prepared by T. Wood (Aerodynamics) of Bell Helicopter Textron (Fort Worth).
- US/AFWAL - Provided by R. G. Anderson of Wright-Patterson Air Force Base (Dayton), comprising three separate inputs on Stability and Control, Handling qualities, and Ground-based Simulators.

Note that F. N. Stoliker of Computer Sciences Corp (Oxnard, Ca) stimulated and coordinated these US actions.

2.2 United Kingdom

- UK/BAe - Provided by T. B. Saunders of British Aerospace (Warton Division): comprising separate inputs from D. C. Leyland (Propulsion/Performance), J. R. Dovey (Aerodynamic loading), D. Booker (Stability and Control), M. Ormerod (Dynamics) and A. F. Darroch (Store release).
- UK/RAE - Prepared by A. J. Ross of Royal Aircraft Establishment, and relating specifically to Flight Dynamics.

2.3 Netherlands

- NE/Fokker - Prepared by E. Obert (Aerodynamics) of Fokker BV (Schipol, Amsterdam).
- NE/NLR - Prepared by A. Elsenaar of NLR High Speed Tunnel (Amsterdam).

Note that both these contributions were received through H. A. Mooij of NLR (Amsterdam).

2.4 Italy

- IT/AERIT - Prepared by J. Mautino and A. Filisetti of Aeritalia (Napoli).
- IT/MdD - Prepared by G. P. Marconi of the 'Ministero della Difesa' (Roma).

2.5 Germany

- GE/DFVLR - Prepared by P. Hamel (Flight Mechanics) of DFVLR (Braunschweig).

2.6 France

- FR/SNIAS.M - Prepared by Ph Roesce (Aerodynamics) of Aerospatiale/Helicopters (Marignane).
- FR/SNIAS.T - Provided by Aerospatiale/Aircraft (Toulouse).
- FR/SNECMA - Prepared by J. M. Hardy of SNECMA (Villaroche).
- FR/MDBA - Provided by J. Czinczenheim of Marcel Dassault-Breguet Aviation (Saint-Cloud).

Note that these four contributions were received through Ph. Poisson-Quinton of ONERA (Chatillon), the first three being originally in French.

3 BACKGROUND TO PREDICTION/DESIGN NEEDS

3.1 Increasing Technical Demands

Apart from the problems arising due to limitations of knowledge in particular disciplines (eg aerodynamics, structures), the aircraft engineer is continually faced with enormous difficulties in predicting and guaranteeing the flight characteristics of new projects to the definition levels and time-scales demanded, and of course in specifying optimum aircraft configurations. His problems are usually aggravated by a variety of complementary factors over some of which he has no direct control. For example:

i Estimates of performance and dynamics for conventional configurations at least, are usually expected to be given to much higher levels of accuracy and confidence than previously, to reduce any shortfall in ultimate aircraft performance and minimise development costs, or comply with more complex or more severe certification requirements.

ii Improvements in aircraft performance or mission effectiveness are invariably required, often with reduced or only small increase in operational costs, to ensure aircraft competitiveness on entry into service and throughout subsequent developments.

iii There is often a tendency towards introducing a wider range of speed/altitude maneouvre requirements for greater mission effectiveness or flexibility; thus the aircraft design cannot be biased so heavily towards one or two predominant aerodynamic conditions, or estimations for off-design conditions allowing extensive flow separations or/and severe shocks become important.

iv From time-to-time, new engine/airframe concepts have to be explored and optimised, simultaneously taking into account possible new operational capabilities and novel aircraft control techniques. Here, the possible significant errors in accuracy of prediction need to be well appreciated, particularly for comparative assessments with competitive conventional designs.

v The interplay between an increasingly large number of design parameters and diverse flight requirements necessitates even more careful studies in more widely-ranging disciplines, not only with a view to optimisation for operational cost effectiveness, but also in order to assess sensitivities to possible later deviations in practice from the original technical assumptions and the mission specification.

vi The available prediction and design capabilities which can be exploited for aircraft project work will differ significantly according to the revolutionary or evolutionary nature of the particular aircraft project. Correspondingly, there may be great differences in the R&D time-scales and in the related efforts required to ensure reliable estimates for the different design philosophies.

The foregoing list does not represent more than a few of the general constraints and needs of project studies, but it is important that their existence and nature should be appreciated, not merely by those directly engaged on specific project estimates, but equally by any research worker desiring practical application of his results.

3.2 Influence of Project Design Stage

The levels of sophistication and reliability of the prediction methodology needed will also vary significantly according to the stage reached in the design/development of the particular aircraft project/construction and in the associated military (or civil) requirement/application. Using simplified illustrative terminology for brevity here, I shall recall only that the technical design stages may progress from preliminary assessments, through feasibility studies, detailed project definition, engineering development, to 'prototype-batch' construction. Simultaneously, the related 'operational stages may proceed from outline concepts, through declared operational targets, definitive operational requirements, aircraft system specification, to flight-proving trials. Moreover, even before full production capability and in-service allocation have been established, improvements to the original aircraft design and operation may already be sought; demanding refined prediction techniques in the light of the updated experience from ground-based and flight research - including that from prototype testing.

3.3 Scope of Technical Considerations

The interdependent elements of aircraft flight prediction falling within the province of the AGARD Flight Mechanics Panel naturally relate to:

- Aircraft Performance; eg airfield, range/radius/loiter, climb/combat.
- Aircraft Dynamics; eg handling qualities, manoeuvre limitations, spin and recovery.
- Store Behaviour; eg carriage, release, delivery.

In setting up a particular prediction capability, a variety of practical considerations must be borne in mind, for example:

- Primary prediction goals and technical outputs required.
- Flight conditions to be examined and relative importance.
- Accuracy desired and error implications.
- Relevant prediction tools available or needed.
- Time scale and effort/funding allowed.
- Possible follow-on prediction demands and probability.

Specialised prediction techniques separately involving theoretical calculations, windtunnels, flight or simulators can profit often from a measure of direct competitiveness. Moreover, their relative priority will vary in the preferred treatments for different practical problems of performance or dynamics. Nevertheless, the complementary nature of all these prediction/design tools now available to the aircraft designer and the potential operators should be emphasised (see Figure A.1). The profitability of their joint improvement as well as individual advances must frequently be re-assessed, so that prediction efforts can continually be directed towards their better integration and interdependent usage.

PART B - COLLATED DETAILED RESPONSES TO QUESTIONNAIRE

ORGANISATIONAL NOTE

The detailed responses on the FMP Questions 1 to 5 are presented with some editing in this Part B, Sections 1 to 5 respectively. Under each Question/Section Heading, the responses are taken in the same order (country by country) as listed in the 'Key to Respondents' of Part A. For example, Section 4.1 here contains the responses received from the USA, while a typical designation US/NASA (4) then reveals the particular US source and the bracketed digit confirms the relevant question number. Two Respondents preferred to ignore the direct questions, so for convenience their comments are included here under Section 1, where they are indicated without a bracketed number, ie by (-).

1. ADVANTAGES/DISADVANTAGES OF DIFFERENT PREDICTION TECHNIQUES

1.1 United States (1)

US/NASA (1)

Prediction of flight motions depends on knowing the correct mathematical representation or model of the aerodynamic terms in the equations of motion and an accurate assessment of the values of the various static and dynamic aerodynamic coefficients which make up the math model. There are a number of ways to obtain some of the aerodynamic coefficients, including both computational and experimental techniques. Some of the aerodynamic coefficients are impossible to compute, and some of the dynamic coefficients are presently impossible to determine experimentally. Flight manoeuvres of modern day fighters, for example, require large angles-of-attack, which are accompanied by highly separated and complicated interactive vortex flows. We are only beginning to understand experimentally the fluid mechanics phenomena which produce these complex flows, and it will be some time before they can be calculated. We are in an even earlier stage of being able to predict the full flight dynamics of vehicles whose flight is governed by complex flows, and the total data base is inadequate to assess the advantages/disadvantages of different techniques.

During our experience with the Upper Surface Blowing Concept (QSRA) and the Augmentor Wing Jet STOL Concept (AWJSRA), we have not evaluated different prediction techniques. We put windtunnel data and, where necessary, estimated data into standard math models for both simulation and prediction of performance. In general, agreement of flight results with predictions has been good, but a significant amount of flight development was required to achieve predicted values of parameters such as lift coefficient.

US/AFFTC (1)

Windtunnels

Advantages - very effective provided proper attention is given to:

a. matching all potential flight conditions and control positions, and
b. ensuring that the model configuration truly represents the vehicle "as built", not "as designed".

Disadvantages - very expensive for certain flight regimes (eg, high Mach or high angle-of-attack). Could be traded off in many cases with conservative flight test approach. Long lead time for last minute model updates, scheduling, setup, rerun and analysis often result in correct windtunnel data being unavailable prior to first flights. Transonic data (0.9 to 1.7 Mach number) not consistently correct for all vehicles, all configurations. Inability to simultaneously duplicate all important flight environment parameters (Mach, Reynolds number, density, real gas, viscosity, etc). Caution/Conservatism still required in use of windtunnel results.

Simulation (as prediction technique)

Advantages - combines several prediction techniques to predict total outcome. Effective in uncovering system integration problems (eg, deficiencies that result from interaction of several subsystems or technical disciplines). Real time simulations can involve man-in-the-loop and are becoming invaluable for crew training.

Disadvantages - only as good as math models used. Potential for generating higher level of confidence than really warranted. Complex, full-mission simulators are expensive and usually become work-saturated thus forcing a fall-back to part task simulations or other prediction techniques for lower priority simulator work.

Theory (excluding computational aerodynamics)

Advantages - related to design parameters and is therefore useful in design phase. Only practical source for rotary derivatives.

Disadvantages - not precise for complex configurations. Interaction, other local effects often missed.

In-flight Simulation

Advantages - real world environment for man-machine interface predictions. Still best approach for landing, other high-pilot-gain tasks. Valuable as final proof-of-concept before flight.

Disadvantages - relatively expensive. Only as good as math models of aerodynamics and flight control system (thus sensitive to all supporting prediction schemes). May be limited in ability to simulate all aspects of flight (visibility, side force, etc).

USA/NATC (1)

Parameter identification prediction techniques can be categorized by two criteria - the computational method and generalized systems approach. Computational methods can be subdivided into three areas - the equation error methods, output error methods, and advanced methods. Equation error methods assume perfect measurements and optimize cost functions that are based on an assumed form of modelling error (process noise). Output error techniques assume that the model of the system is correct and optimize cost functions that are based on measurement system error models. Advanced methods are those that account for both process and measurement noise. Examples of equation error, output error and advanced methods are least-squares, Newton-Raphson, and maximum-likelihood/Kalman-Filtering techniques, respectively. If either process or measurement noise is present, then one of the first two methods can be in error; however, when using the advanced methods these error sources are taken into account and unbiased estimates can theoretically be obtained.

Any of these three techniques can be adapted into a generalized systematic approach to system identification. A generalized approach used at NAVAIRTESTCEN is a unique integrated system identification procedure. This integrated approach to system identification is composed of the following steps:

- Test input design. Flight data processing and analysis. Model structure determination. Parameter identification. Model verification.

Any system identification or parameter identification approach that does not use this five step process will be less successful than the approach outlined. For example, if care is not used in input design, the flight test measurement set generated will not have the information content required to estimate or predict critical parameters.

In the approach used at NAVAIRTESTCEN a maximum likelihood parameter identification algorithm has been modified to perform flight data processing prior to the estimation of model parameters. This step involves estimating scale factor errors and biases and obtaining a kinematically consistent set of measurements. Any prediction technique that does not have this feature will introduce errors into model parameter estimates.

Model structure determination is the next step in this process and its major purpose is to identify significant terms of a math model. Optional subset regression is the model structure approach used at NAVAIRTESTCEN. This type of approach is necessary in order to have a systematic method of defining the significant parameters of nonlinear aerodynamic models. If the model structure phase is ignored in the identification process, then the model will be over or under parameterized and errors will be introduced into the final model parameter estimates.

Parameter identification is the final data processing step and provides the refined estimates of the model parameters. A maximum likelihood algorithm is the parameter identification technique used at NAVAIRTESTCEN and is the technique most widely used in flight test applications in the United States. Failure to use an advanced parameter identification technique like the maximum likelihood method will result in biased estimates if both process and measurement noise are present.

The final step is the verification of the model and parameter estimates and involves the use of estimation uncertainty bounds and the prediction of aircraft responses. Engineering judgement also plays a role in the verification process.

This five-step approach to integrated system identification is extremely critical when attempting to predict the model and parameters of a highly nonlinear system. This approach has been successfully demonstrated on predicting the nonlinear model parameters of the VAK-191B vertical short takeoff and landing (VSTOL) aircraft and the F-4S fighter aircraft. In the VAK-191B application the problem was to model the nonlinear aerodynamic, engine thrust and reaction control system during conventional, transition, and hover flight. Data reconstruction, model structure determination, and parameter identification were applied to this problem and a sample of final parameter estimates is available.

The application of this technology in the F-4S program was specifically aimed at the nonlinear high angle-of-attack flight regime. During this program high angle-of-attack stall and departure manoeuvres were analyzed. Results from the instrumentation system analysis, model structure determination parameter identification and verification process are available.

US/NAVAIR (1)

All five FMP questions could relate to many aspects of aircraft ground/flight test techniques and correlations; ie, aerodynamics, structures, propulsion, flying qualities, etc. The US/NAVAIR responses are based on the particular area of experience in the prediction and flight documentation process of air vehicle performance for US Navy aircraft.

Analytical prediction procedures vary greatly in degree of complexity, accuracy and cost. The accuracy of the results is dependent on the applicability of the method of the aerodynamic configuration being analyzed. The simpler, less costly methods are based on the component build-up process using geometric information. These procedures may not account for (at least adequately) important interactions (ie airframe/inlet and exhaust or rotor-inflow and rotor-blade/tip-vortex interference). These procedures *may be adequate, however,* for less complex *aerodynamic/propulsion* configurations where interactions are expected to be small. When interactions must be considered, more sophisticated analytical programs exist but require judgment in modelling the interactions and are more costly. Errors in modelling the interactions may result in large errors in the result. Windtunnel based prediction processes are very expensive but have the advantage, at least potentially, of evaluating the exact aerodynamic configuration including interactions. The accuracy of the windtunnel based prediction may be affected by the windtunnel test techniques, the effort expended to isolate and account for all aerodynamic and propulsion forces, the scale effects adjustment to full-scale Reynolds number and the accountability for items not represented on the windtunnel model.

US/AVRADCOM (1)

In general, all of the prediction techniques for rotary-wing aircraft (whether they be for rotor-blade aerodynamic characteristics, aerodynamic interference effects, or rotor airloads prediction) are all empirical or at least semi-empirical. Each US helicopter company has its own prediction technique based on its own set of experimental data that is usually somewhat uniquely oriented to the rotorcraft configurations developed by that company. It is impossible to discuss in any generality the advantages and disadvantages of the prediction methods that are employed by the helicopter industry. Mostly, the differences relate to the modelling of the rotor wake and these range from very simple uniform inflow to highly complex free-wake analyses. Even the uniform inflow model is adequate for some prediction, but even the most sophisticated free wake is still inadequate for other applications.

US/Bell Hel (1)

For rotary-wing aircraft, prediction techniques depend largely upon empirical factors to achieve satisfactory results. Some techniques depend upon theory until the limits of the mathematical model are reached. After that point, the difference is made up with empirical corrections. These correction factors tend to make the analysis good for configurations that do not vary too far from the configurations used to determine the correction factors. An example of such corrections is the interference of the rotor wake on the fuselage, tail rotor, elevator, and vertical fin. This interference can produce significant handling qualities effects which would be missed in most prediction techniques. The advantage/disadvantages of different prediction techniques then becomes a judgment call on the part of the engineer based on the stated problem.

US/AFWAL (1)

As regards Stability and Control prediction techniques, the comments are as follows:

- Empirical - Accurate over data base range. Very limited in application.
- Semi-empirical - Generally a little less accurate. More widely applicable especially ref configuration geometry.
- Theoretical - Within range of restrictive assumptions can handle completely arbitrary geometry. Can handle limited complexity; no separation, no high-α, etc. (At the present time, some of these limitations may disappear as computers continue to "improve".)

For Handling Qualities the various short-period handling parameters we investigated (for MIL-F-8785C) are discussed in AFWAL-TR-81-3109, the forthcoming back-up document for 8785C. Calspan (in AFFDL-TR-72-41) and STI (in AFFDL-TR-73-76) had each proposed different roll-yaw coupling requirements, but we adopted neither. While they should be useful for design guidance, Calspan's revised definitions and boundaries and STI's rudder coordination parameter are still complicated and seem to be no more adequate than the present requirements for specification use. Of complementary interest is Mooij and van Gool's discussion of a number of alternative longitudinal and lateral-directional flying qualities parameters in NLR TRs 79127U and 80103L.

Ground-based Simulation fills the gap between paper/off-line computer analysis and flight testing. Its advantage is to introduce the human factor elements early in the aircraft/subsystem design phase to determine flying qualities, crew station design capabilities, to validate digital flight control laws and software, to establish redundancy management logic under a multitude of single and combination failures and to explore the boundaries of departure and flight envelope which would be high risk in flight. Its primary disadvantages are perceptual limits in visual and motion cues which may lead to loss of fidelity and the introduction of false cues. Computational and transport lags can also introduce unrealistic dynamic effects. However, the advantages of ground-based simulation far outweigh the disadvantages. Thorough paper analysis is necessary to validate and understand the limits of the simulation. Also, the simulation model should be updated to correlate with early flight test results to provide fidelity for expanded simulation investigation. Simulation is a cost effective method to investigate large numbers of mission sorties, to conduct parameter variation sensitivity studies, and to obtain statistical results from a variety of experienced or inexperienced crew members. Flight test costs are prohibitive for obtaining large sample testing.

1.2 United Kingdom (1)

UK/BAe (1)

From Propulsion/Performance viewpoints, it is considered that:

- Theory is usually quicker and cheaper than testing, at least for changes; therefore good for design studies; but test needed to give spot confirmation and overall answer.
- Windtunnel offers a controlled environment and is good for covering range of parameters; needs model design for convenient early configuration development.
- Flight testing appears nominally good because it is a real aircraft; but there are difficulties in obtaining accuracy and conditions relatable to a useful mathematical model. Such work requires concentration on reliable rather than many results.

For Aerodynamic Loadings, the relevance or otherwise of theoretical predictions is dependent on the range of incidence and Mach number to which the aircraft will be subjected at high dynamic pressures. Theoretical methods are inadequate for high values of (nW/Sa_1).

From Stability and Control experience comes the fundamental point that a sound data base and application model is essential for correct interpretation of flight measurements. The range of flight measurements which can be taken is usually restricted by cost and timescales, also possibly by safety considerations. The latter implies a good framework is needed on which to base extension of clearances to corner points. Care with instrumentation and flight-testing pays dividends in avoiding need for repeat testing. The pros/cons in respect of different prediction techniques include:

- Data-Sheet Methods - Restricted in applicability (although cheap) because of the information on which they are based.
- Computational Fluid Mechanics - Limited generally to potential attached flow.
- Windtunnel testing - Restricted by tunnel interference, support system interference (except free-flight), model distortion to fit support, usually low Reynolds number, and difficult representation of intake/nozzle flow.
- Free-Flight Models - Limited usually to low speed, while Reynolds number needs to be watched and internal flow representation difficult.

For Dynamics prediction the status of structure and aerodynamics treatments are respectively:

- Basic linear dynamic behaviour of the Structure is well understood and can be accurately modelled, while simple nonlinearities (backlash etc) can be represented and assessed. But structural damping (crucial in the clearance of heavy underwing stores) is not well understood and at present is arbitrarily treated. Ground Resonance Test (GRT) measured values are suspect because of deficiencies in modal excitation, unrepresentative a/c suspension and complex modal interaction.
- Current Aerodynamic lifting-surface theories are adequate for isolated wing/tail/fin in pure attached subsonic and supersonic flows. Predictions are very poor transonically and very careful flight flutter testing is required. Windtunnel tests help here but there are severe difficulties in designing and building a sufficiently accurate (and strong) dynamically-scaled model.

From Store-release considerations purely theoretical methods are not really adequate for store load estimation since non-linear effects due to separation at incidence are needed for most calculations. They can be used for aircraft flowfield in some configurations at low incidence and sub-critical Mach numbers. But potential flow methods give poor answers in the wing downwash and upwash fields close to the leading and trailing edges. Some of these methods are also very expensive to use. Empirically-based methods with non-linear effects represented are better for store load prediction.

Windtunnel tests are currently the most reliable source of data for trajectory calculations especially if used in combination to build up and validate a mathematical model, as in the Warton "broad-based" technique. Windtunnel tests are considered essential prior to flight releases unless the store is "heavy" and stable, eg a fixed geometry bomb. Disadvantages of windtunnel tests on stores, in addition to the usual scale worries, are:

- Cost.
- Sting interference/distortion in Two-sting testing in the presence of the aircraft or in isolated store testing.
- Gravity deficiency in "light model" jettison testing.
- Repeatability and accurate trajectory measurement in jettison testing.

UK/RAE (1)

This response relates to prediction of flight dynamics behaviour and is provided as Tables I and II at end of text (pages 29 and 30).

1.3 Netherlands (1)

NE/Fokker (1)

These remarks concern primarily Subsonic Transport aircraft, as is also true for Fokker responses to the complementary questions.

'Zero-Lift' drag coefficient - The only useful method is the "flat-plate drag times shape factor" method ($K_F \times C_f \times S_{wet}$) with shape factor either from model tests on particular configuration or from generalized data. The really difficult item remains "roughness and miscellaneous" drag. Furthermore shape factors are less well defined than one would expect. (Fairly large variations exist between different data sources.)

Induced drag factor ("e") - For modern jet transports with high wing loading, induced drag forms an important contribution to total climb and cruise drag. The induced drag factor can be taken both from generalized data and from windtunnel tests. Both have lower accuracy than is desirable. For low-speed high-lift configurations the windtunnel seems to be the only useful tool up to now.

Low-speed $C_{L_{max}}$ and stall characteristics - High Reynolds number tests ($Re_c \geq 5 \times 10^6$) produce the most accurate results. Often not available for initial design studies. 2-D theory may produce useful data on trends.

High-speed drag - Re-capability of present windtunnels is insufficient for accurate determination of drag creep and drag rise.

Simulation of high-Re conditions in present-day windtunnels by varying the location of the transition band is questionable. Programmes such as FLO22 seem to give useful indications on the effect of Re on drag creep and drag divergence Mach numbers. ETW should give an improvement. Induced drag at high C_L may remain a problem (tunnel wall effects).

Buffet onset boundary - As buffet onset is a combination of flow phenomena and structural damping its determination prior to first flight will always be approximate. At present the emphasis in any analysis lies on the aerodynamic component. The same can then be said about buffet onset as about high-speed drag. Again at present, modern transonic computer codes seem to give the only indication of Reynolds number effects up to flight Re-numbers.

Flight characteristics at conditions beyond the onset of flow separation - Unless the attention is focussed on controlled flow separation (vortex flow), this subject lies still largely outside the capabilities of our theoretical methods. For the determination of flying characteristics beyond buffet onset, both at cruise Mach numbers and between M_{MO} and M_D the windtunnel seems to be the most useful tool although an increase in Re-numbers capability is highly desirable.

Stability and control characteristics in the normal flight regime - Apart from handbook methods, the estimation of lateral and directional stability and control derivatives on a theoretical basis is practically non-existent, in particular angular-rate derivatives for take-off and landing configurations. Although various windtunnel facilities are nowadays equipped with dynamic test rigs the Reynolds number in tests on these rigs is by necessity very low except perhaps with the new test rig in the ONERA S1 tunnel at Modane. In particular, in view of the increasing interest in active control technology and in flight simulation, a much larger interest exists nowadays for an accurate knowledge of all stability and control derivatives. It would be worthwhile if, on this new test rig in the ONERA S1, a few configurations representative for modern transport aircraft could be investigated as a check and an extension of the present handbook methods.

Propeller/slipstream effects - In terms of required accuracy for design purposes the present theoretical methods do not go further than the preliminary design stage. Although the windtunnel is here a much more effective tool a limitation can be the scale of the model. This may severely limit the power output of the propulsion unit and therefore the achievable Reynolds number, in particular when high thrust coefficients have to be simulated.

NE/NLR (1)

The NLR note that their answers are based on experience in windtunnel testing and close contact with computational aerodynamics. Also that unfortunately, windtunnel engineers have only a very limited insight in the subsequent processing of windtunnel data and a comparison with flight tests by the aircraft factories.

"Trendology" - In this technique, (well) established trends in the variation of different aircraft characteristics are used to extrapolate windtunnel data. Examples are the variation of C_L-buffet with Reynolds number, profile drag with airfoil thickness, etc. These trends can be based on "data-sheets", windtunnel tests or "in-house" windtunnel/flight-test comparisons. A typical example is the Δ-approach: the observed difference between windtunnel and flight for a particular aircraft (and a particular windtunnel!) is added to the windtunnel results for the new designed aircraft. The advantages of this technique are that it is (most often) straight forward. It is very re-assuring to use well-established techniques based on "integrated" experience. A main objection is that it is (very often) based on poor physical modelling. For that reason it does not exploit the full limits of present day knowledge. This might be risky in the extrapolation of windtunnel data of designs that make use of new technologies. A classical example is the prediction of Reynolds effects for supercritical airfoils.

"Boundary-layer fixation manipulation" - The state of the boundary layer (laminar or turbulent) has a great influence on the aerodynamic characteristics. This is generally considered as a problem but in some cases it has become practice to select by artificial tripping such a boundary layer development that "full-scale" results are obtained in the windtunnel. A typical example is "shock-fixation" to determine buffet boundaries. The great advantage is that full scale results are measured directly. Objections are that it is difficult to select the proper transition location (based on windtunnel/flight correlation or computational aerodynamics) and that each point in the flight envelope requires a different fixation location (making windtunnel measurements more expensive). In principle, one might argue if the method is justified at all on theoretical grounds. This technique is not recommended, unless it is used as an additional tool to investigate the sensitivity to changes in boundary layer development.

"Computational aerodynamics" - At present the mathematical modelling of flow around aircraft configurations has not reached the state where computational aerodynamics alone are able to predict flight test results. However, when used on a relative basis and only for specific characteristics (eg drag) they might be useful or even essential to complement experiments, especially where the experiment is limited by accuracy or model design considerations.

"Physical modelling" - Understanding of the problem should be the basis for flight prediction. This can be achieved by careful designed experiments, phenomenological studies and subsequent (improvement of) mathematical modelling. A typical example is the prediction of buffet boundaries based on an empirical correlation of shock Mach number and local boundary conditions, rather than a C_L-buffet vs Re-trend. In fact this technique should be viewed as a "marriage" between windtunnel testing and computational aerodynamics. Its main disadvantage is that the time scale for this type of research is much larger than the available time for aircraft development. Therefore a combination of "trendology" methods with special attention to problem areas, in conjunction with "physical modelling", represents probably the most appropriate technique.

1.4 Italy (1)

IT/AERIT (1)

Computational Fluid Dynamics is a fundamental tool for design when used appropriately; offering both rapid flexible methods for preliminary evaluations, and most complete modes for final evaluations.

- Advantages: Quick analysis and possibilities to carry out a number of trade-offs for different configurations.
- Disadvantages: Impossibility at present to simulate separated flow conditions or to duplicate correctly detailed vortex flows. Also difficulty for data evaluation of complete and complex configurations.

Windtunnel tests provide an essential tool for aerodynamic configuration analysis and for data collection.

- Advantages: Possibility to simulate with good approximation the complete aerodynamic behaviour of an aircraft configuration including mutual interference, vortex detachments, non-linear resulting effects; then can collect all the data required in aerodynamic design, flight mechanics and loads analysis.
- Disadvantages: Long time for model design and manufacturing, high cost of transonic test, sophisticated facilities for simulation of Mach and Reynolds numbers.

For Dynamics studies (aerodynamic/structural), 2D Theoretical calculations are cost effective in parametric studies for preliminary design and development. 3D theoretical calculations are more accurate but limited to checks of frozen configurations because of high cost, but not sufficient to give the final clearances with the required approximation without matching against flight results. While theoretical unsteady aerodynamics is effective for analysis of subsonic and supersonic fields, it is very expensive and inaccurate in transonic - where windtunnel models (complete or partial) are preferred, even if expensive and not flexible in usage. High-incidence conditions may be tested on specialised windtunnel models, now constructed in carbon fibre ensuring accurate definition of the profile.

IT/MdD (1)

The main ground-prediction techniques are windtunnel and digital-computer calculations. Overall, the aeronautical industries are still compelled to use windtunnel tests widely when non-linear effects are involved. Digital computer calculations, nevertheless, have the advantage of a low cost of CPU, a low cost/effectiveness ratio, and a higher flexibility. Thus, with the computers used to reduce the number of windtunnel test programmes, an attractive solution of the problem can be the coupled use of windtunnel and computers.

1.5 Germany (1)

GE/DFVLR (1)

There are two kinds of prediction techniques. Firstly, those which predict the flight dynamics and flight performance and, secondly, methods which predict flight critical behaviour (PIO, instabilities). The first kind of prediction objectives is heavily related to simulation procedures (dynamics) as well as windtunnel and analytical tools (performance). The latter kind need criteria which have to be derived from equations of motion or windtunnel measurements.

If prediction techniques are understood as various different experimental investigation methods (eg static and dynamic windtunnel measurements, flow visualisation, model flight testing), the final results obtained yield more confidence the more of these techniques have been applied.

1.6 France (1)

FR/SNIAS.M (1)

We share entirely the opinion expressed in the Response US/AVRADCOM (1) concerning the empirical character (or at least semi-empirical) of the prediction techniques for helicopter load calculations currently used by the Firms. We agree equally to the comments made about the tailoring of the theoretical model used to the nature of the problem posed; very often, a simple physical model correctly tuned to experimental results is better for prediction than a complex mathematical model whose application would prove too long and costly for some complete parametric studies.

FR/SNIAS.T (1)

These remarks relate only to the flying qualities and the aerodynamics of transport aircraft. To predict the behaviour of an aircraft in flight, three principal complementary techniques are employed:

- Theoretical calculation by computer; model testing in windtunnels; simulator studies.

a. Flying qualities and piloting constraints -

Calculation is very efficient and not costly. Nevertheless, it is incapable of representing the 'behaviour' of a human pilot, while its reliability is tied to the quality of the aerodynamic coefficients and structural (aeroelasticity) coefficients which are used for calculation. Simulation is fundamentally essential to take into account the behaviour and judgement of the human pilot.

b. Aerodynamics -

Theoretical calculation permits a first choice of 'interesting configurations' without however furnishing reliable values for the set of aerodynamic coefficients needed in the prediction of flying qualities and performance. By contrast, it permits in most cases a good prediction of the aerodynamic loads necessary for structural calculations (including aeroelastic effects). It remains deficient for the treatment of transonic viscous flows and of strongly separated flows. Its improvement and reliability are tied to the augmentation of computer power; nevertheless, it is never likely to provide a complete set of aerodynamic coefficients which are reliable throughout the entire flight domain.

Windtunnel testing is the necessary indispensable complement to specify the aerodynamic characteristics of an aircraft before its first flight. Existing low-speed windtunnels capable of high Reynolds numbers (F 1/ONERA, 5m/RAE) permit good predictions, though without currently taking proper account of engine efflux effects (in contrast helicopter rotor flow can be simulated). Transonic windtunnels still remain deficient for corrections in respect of Reynolds numbers effects, wall constraints and model supports; in contrast they do permit satisfactory account to be taken of engine efflux (by compressed air, or air-turbines TPS). The improvement of results obtained in windtunnels is inherently dependent on reduction of the following deficiencies - much better knowledge of the actual model forms under high aerodynamic loads (taking into account model deformations) and the future development of a transonic cryogenic tunnel. In conclusion, the windtunnel will remain for a long time the best means of providing a complete set of reliable aerodynamic coefficients close to those of the real aircraft in flight.

FR/SNECMA (1)

For propulsion studies, windtunnel tests and numerical simulation of the flows are complementary. Numerical simulation, being less onerous than windtunnel testing, permits definition and refinement of shapes; the windtunnel experiments may then be made on optimised geometries to verify their performance. The windtunnel test usefully gives propulsion nozzle coefficients in a directly integrated form, from direct measurement of airflow and forces; by contrast it gives only an approximate knowledge of the aerodynamic field. Thus numerical simulation of the test can lead to a very profound knowledge of the aerodynamic field; comparisons of theory and experiment in respect of surface pressures permits identification of aerodynamic phenomena. However, when three-dimensional characteristics are especially marked because of jet-entrainment effects such as wing-engine integration with civil aircraft, or when flight conditions lead to transonic mixed flows with flow-reversal such as rear-fuselage conditions with a combat aircraft near M=1, then the current state of calculation methods does not lead to valid predictions. Windtunnel testing allows the better approach to the problem.

FR/MDBA (-)

Performance and flight characteristics prediction is an absolute necessity before the flight-testing of any air-vehicle. Therefore, in our opinion, the main problem is not to list the advantages and disadvantages but to improve and refine our prediction techniques for every new aircraft. On the same grounds, both windtunnel testing and analytical predictions must be done and combined together to solve adequately most of the aerodynamic problems.

It can also be stated that, up to now, there is not an absolute confidence in the results obtained by each individual prediction procedure. Our experience, based on comprehensive flight test results of many different prototypes, indicates that some prediction methods - which seemed sufficiently valid for one prototype - were not adequate for another one although belonging to the same aircraft family. The same experience indicates also that, by using both sources of information, risks of prediction errors are significantly reduced.

There is a definite need and possibility of improvement in both prediction procedures; for example more information must be extracted from unsteady flow measurements in windtunnels and more detailed flow information must be derived from computations based on a more precise mesh system or on a better viscous flow model.

In conclusion, for any flight regime and whatever the configuration, a maximum effort to obtain an accurate prediction must be made; while the feel for constant improvement of prediction methods and also of the quality of the flight test data must be showed by all engineers involved in air-vehicle development. Minimisation of prediction errors is vital, because any significant modification required after the first flights of a prototype has now too dramatic consequences on programme cost and time schedule. Finally, it should be mentioned that the foregoing discussion, limited here to computational aerodynamics and windtunnel prediction techniques, is also relevant to techniques based on simulators (ground-based or in-flight) and flying models, as well as on structural analysis and testing, etc.

2 PORTIONS OF THE FLIGHT REGIME NOT ADDRESSABLE BY GROUND-BASED TECHNIQUES

2.1 United States

US/NASA (2)

There is no part of the flight regime that should not be a candidate for improved ground-based techniques. However, there are flight characteristics and phenomena which, at the present time, cannot be adequately predicted using ground-based techniques. Flight motions that are governed by aerodynamic inputs which are highly nonlinear with rotational rates or which have strong dynamic cross-coupling between longitudinal and later-directional modes of motion cannot be properly addressed either experimentally or computationally yet.

Some of the other problem areas are:

- High angle-of-attack dynamics in controlled and uncontrolled flight.
- Total vehicle performance (eg L/D).
- Flying qualities of superaugmented aircraft whose dynamics are dominated by the flight control system, especially in high pilot gain tasks.
- Aeroservoelastic characteristics, especially for aeroelastically tailored composite structure and especially in the transonic regime.
- Static flexibility corrections.

For a propulsive-lift airplane, such as the QSRA and QWJSRA, it appears that all parts of the flight regime are appropriate for evaluation with ground-based facilities as a prelude to a flight programme. Limitations relative to Flight Dynamics and Performance and manoeuvre loads are in evidence, but the predictive accuracy based on ground testing is sufficient to make this a cost effective endeavour prior to flight, or as a prelude to extensive design changes. Measurement of ground effect appears to be the only area where windtunnel results have been significantly at variance with flight data. It also seems that simulation of the landing-flare and touchdown is not as good as we would desire.

Rotorcraft manoeuvre and transient loads cannot be adequately determined by ground-based techniques. The detailed flight dynamics and performance limits during manoeuvres are not yet predicted with sufficient accuracy to be duplicated on a flight simulator. Furthermore, gust loads and manoeuvres are not adequately simulated in a windtunnel because thetotal vehicle dynamics involved in flight control cannot be duplicated in the windtunnel. The significance of this premise is often overlooked. Further, rotorcraft vibration cannot be adequately assessed from ground-based testing, because the total coupled rotor airframe response cannot be simulated in a windtunnel.

US/AFFTC (2)

- The high altitude, high Mach number regime is very costly to duplicate even partially. Parameters of importance cannot be simulated simultaneously.
- Zero pressure, weightless (space) environment cannot be duplicated adequately. Exotic, integrated test setups often create questionable results.
- Stall/spin regime beyond the initial departure. Key drivers are time/expense not necessarily feasibility. Subscale test vehicles, manned or unmanned, often cheaper.
- Lee-side aerothermodynamics at high Mach number are poorly handled by all ground prediction techniques.
- Ground based simulators are often inadequate for assessing handling characteristics in a high pilot stress environment (such as landing, air-to-air combat). Pilot induced oscillations are occasionally experienced which were not predicted. Combined motion and visual cues are required. High fidelity, large amplitude, motion simulators appear to be essential to evaluate these particular tasks, but in-flight simulation appears best.

All flight regimes should be addressed for ground-based techniques but an objective trade-off regarding costs of ground vs flight options, should be made. There are many areas where ground and flight testing can complement each other (ie simple ground test to verify a safe starting point for flight test to proceed). Cost of aviation fuel is increasing, but so is the windtunnel electric bill!

US/NATC (2)

Recent experience in a high performance Navy fighter development programme has shown that significant problems still exist in predicting the angle-of-attack stall/departure/spin characteristics. Groundbased simulation techniques using analytical and model test results at the data base failed to predict all of the spin modes of this high performance fighter. However, following several incidents in the flight programme, additional windtunnel and drop model tests were used to update the simulation data base with some improvement in the ability to predict all of the spin modes. The lesson learned in this programme was that the high angle-of-attack response characteristics of modern fighter aircraft are still difficult to predict.

US/NAVAIR (2)

Available correlations between groundbased and flight data indicate problems associated with some windtunnel derived aerodynamic characteristics in the transonic and supersonic flight regimes. The lack of windtunnel/flight correlation in these areas is most likely caused by windtunnel wall/model interference effects. Correlation of helicopter computer programs with flight data is degraded as rotor blade stall is approached. The lack of correlation of these items should not imply that they should not be addressed in the particular prediction method, but that the results must be interpreted or modified based on actual flight experience of prior aircrafts.

US/AVRADCOM (2)

In general, windtunnels do not work very well for rotary-wing aircraft at very low forward speeds because of the recirculation of the rotor wake. For appropriately sized rotors in the Ames 40 x 80 ft windtunnel, this minimum speed is about 60 knots. A similar rotor in the new 80 x 120 ft windtunnel can be tested to about 20 knots. Static performance, ie hover of a rotor is particularly difficult to measure accurately. Most whirl tower facilities are hampered by varying ambient conditions and irregular surroundings structures including (and, in some cases, especially) the rotor stand and drive system. Testing in a hover chamber is limited by recirculation effects. This has been avoided in the unique hover test facility of the Aeromechanics Laboratory at Ames by using a self-energized diffuser to capture the wake and exhaust it through openings in the walls, thereby minimizing the recirculation problem.

Nevertheless, it still remains that it is extremely difficult to obtain highly accurate measurements of rotor performance at low speeds in ground-based facilities. Until recently, it was impossible to obtain such data in flight as well because the instrumentation was inadequate to separate the effects of the rotor from the fuselage. This problem is addressed by the new Rotor Systems Research Aircraft at the Ames Research Center in which all components of the aircraft are joined through balance systems. Of course, just as in the case of fixed-wing aircraft, it is impossible to obtain accurate measurements of manoeuvring loads in ground-based techniques.

US/Bell Hel (2)

For Rotary-wing aircraft, highly transient manoeuvres are difficult to be addressed by ground-based techniques. Such manoeuvres include high-g manoeuvres where the rotor is close to stall and reacting to unsteady aerodynamics. The limitations of the mathematical model begin to be very apparent in this area resulting in poor agreement between ground-based and flight results. In-ground-effect manoeuvres require special attention to properly account for the ground vortex and the non-uniform downwash of the rotor. If these areas are properly represented, then manoeuvres in this area may be satisfactory. In any manoeuvre where the interference effects of the rotor on the fuselage has a significant effect, the ground-based technique will differ from the flight data.

US/AFWAL (2)

As regards Stability and Control, there are of course areas where 'ground-based' results are less accurate, more difficult; eg, high-α (difficult to get correct flow fields at ground-test Re). Prediction is far more limited than ground-test. Cost is a factor, however, and may be prohibitive in some cases.

Manned simulators remain deficient in motion cues (fixed-base is sometimes better to spurious motion) and, at low altitude at least, outside visual cues. While high-gain tasks such as landing should be addressed in simulators, account must be taken of these inadequacies. We would also be somewhat sceptical of aerodynamics at extreme angles-of-attack and in ground effect - although of course these factors must be addressed in the windtunnel.

Additional comments are that:

- Automatic terrain following, landing systems, fire control systems, etc, must be validated in a variety of weather conditions, mission tasks, and combined environmental conditions to validate effects on sensors. Sensor modelling effects under these adverse conditions are not sufficiently adequate to depend entirely on simulation.
- Stall/departure/spin characteristics - Model methods are inadequate to totally define highly nonlinear aerodynamic effects under very large angles-of-attack and sideslip flight. Certain modes can be predicted, but it is essential to fly in these adverse conditions with a spin chute to positively identify all modes of departure and to determine recovery control methods (if they exist).
- It is widely recognized that ground-based simulators can not totally predict flying qualities with 100 percent assurance. Better simulation equipment (primarily wider field-of-view visual systems) and improved experimental test processes can provide higher fidelity results. In-flight simulators have had much greater success in predicting PIO effects and actual stress conditions than ground-based simulators.

2.2 United Kingdom

UK/BAe (2)

For Aerodynamic Loadings an attempt must be made to predict all portions of the flight regime achieveable by an aircraft. Such predictions must be based on any available means and, where those means are believed to have shortcomings, tolerances must be applied to ensure safety before committing an aircraft to such conditions. When safety is involved predictions must be backed up by progressive flight data analysis and extrapolative re-prediction.

For Dynamics, transonic predictions are especially poor. In general, all flutters can be identified by calculations/GRT but need to be quantified in flight.

For Store-release given appropriate-windtunnel-testing and trajectory modelling, it is considered that all parts of the flight envelope can be addressed. However, the accuracy of the prediction will be reduced in the transonic regime, or where flow separations are affecting the release (eg high incidence), or where behaviour is strongly influenced by close store-to-store or store-to-aircraft interference.

UK/RAE (2)

Piloted simulators cannot adequately represent some critical aspects of the aerodynamic characteristics in the mathematical model used and cannot fully present all the necessary physical cockpit cues to the pilot.

The determination of handling qualities at and near manoeuvre boundaries therefore cannot be addressed properly by ground-based techniques.

2.3 Netherlands

NE/Fokker (2)

The behaviour of the aircraft, once separation starts, ie at or beyond the low-speed stall, or at or beyond high-speed buffet onset, will always be an area where a detailed flight test analysis will be required because of the interrelations between:

- Reynolds number effects: The dynamic characteristics of the aircraft: The pilot's reactions: Static and dynamic aero-elastic effects.

Furthermore high and low-speed performance (single and multi-engined climb, cruise flight) will always be a critical period in the flight testing of any aircraft, because of the complicated relations between aerodynamics and propulsion on one hand and an increasing tightening of performance guarantees on the other hand.

NE/NLR (2)

No comment.

2.4 Italy

IT/AERIT (2)

In Aerodynamics, the real problem is not the possibility or convenience of investigating flight-envelope portions by ground-based techniques, but the reliability of the results. The most difficult areas to predict with ground techniques, including computational fluid dynamics and windtunnel methods are:

- High incidence characteristics, including problems of incipient spin or spin resistant parameters.
- Interference between propulsion and external aerodynamics; eg induced effects of air-intakes flow on C_{n_β} of Tornado at high M, on AMX longitudinal control at low speed, and Tornado jet effects on afterbody.
- Combinations of high Mach numbers and high C_L and the relevant limitations; eg flow characteristics and loads of Tornado.

Moreover, the reliability of aerodynamic load evaluation in the transonic field may be quite poor - even with windtunnel data, owing to frequent different behaviour of the flows on windtunnel models and on the real aircraft, due to Reynolds number effects, and possibly from non-linear high α/M conditions.

Again for Dynamics, the transonic field is very difficult and expensive to deal with, either by theoretical calculations or by windtunnel tests, and therefore flight tests are necessary in this case.

IT/MoD (2)

There are a number of flight conditions, ie high angles-of-attack and transonic Mach number, that exhibit large deviations from flight test results if studied with ground prediction techniques only.

2.5 Germany (2)

GE/DFVLR (2)

It is highly recommended that all portions of the flight regime should be addressed by ground-based techniques. Otherwise technical risks remain until the actual evaluation of the full-scale flight vehicle can be approached. Technical problem areas like insufficient control power may then be cured only by high cost solutions. If there are gaps in the application of ground-based techniques, these techniques have to be improved.

2.6 France

FR/SNIAS.H (2)

To the specific problems already raised in the response FR/AMD/CEV (2) concerning windtunnel testing of helicopters in stationary and low-speed flight, we will add those posed for the precise determination of manoeuvre loads on the rotor in turning and pull-up motions. Equally there are the problems relating to the dynamic studies about wake stability and vibrations of aerodynamic origin, where aeroelastic couplings play an important role and for which the similarity laws are either poorly understood or difficult to comply with.

FR/SNECMA (2)

If for the 'internal' flows of rear bodies (generally of revolution), one acknowledges that neither windtunnel testing nor numerical simulation have particular dominance, this is not so for external flows. In the transonic domain, with the boundary-layer significant due to boundary-layer/shock-wave interaction, or for flows below a free or forced separation, numerical simulation is currently insufficient, indeed inapplicable.

5 AREAS WHERE ANALYTICAL PREDICTION BETTER THAN WINDTUNNEL AND/OR SIMULATION RESULTS, OR VICE VERSA

5.1 United States (3)

US/NASA (3)

Analytical prediction methods are useful where the aerodynamics are reasonably linear with attitude and where the flight vehicle is a fairly simple shape. Complicated configurations, flight-attitudes where the configuration experiences highly separated or interactive flows, manoeuvres at high rotational rates, etc all tend to drive the means of assessing the aerodynamics to depend heavily on windtunnel experiments. Analytical predictions should be used in conjunction with experiments when possible on an interactive basis to optimize the value of the results and to minimize the test matrix.

US/AFFTC (3)

- Only analytical predictions are available for real gas effects at high altitude and Mach number.
- Rotary derivatives are best obtained from analytical sources although windtunnels have been effective in obtaining some of the rotary derivatives ($C_{m_Q} + C_{m_{\dot{\alpha}}}$, etc).
- It is too early to assess the role of computational aerodynamics, but it is expected to provide some powerful tools to ground prediction capability.

US/NATC (3)

Assuming that the analytical prediction techniques are parameter or system identification methods, then significant improvements can be achieved in prediction capability. These methods are used in conjunction with flight test data to calibrate windtunnel or analytical predictions. These techniques could also be used directly on windtunnel data to provide a more consistent and accurate set of aerodynamic estimates.

US/NAVAIR (3)

Analytical predictions may be better than windtunnel predictions when propulsion interactions are small but a very small scale model is employed for the windtunnel tests. In this case the windtunnel results could be misleading, because the fidelity of the model may have to be compromised and very large scale effects (of questionable magnitude) must be applied to the results. For optimum configurations, windtunnel testing is required.

US/AVRADCOM (3)

For Rotary-wing aircraft, the prediction methods rely to a large extent on flight or windtunnel test data because, as stated previously, all of the prediction methods are at least semiempirical. Well designed and executed windtunnel tests can provide accurate results for many flight conditions. If by simulation we mean man-in-loop flight simulation, then of course there are no adequate mathematical models for the human, and so we must rely on man-in-loop simulation (be it ground-based or in-flight).

US/Bell Hel (3)

For Rotary-wing aircraft, care must be exercised in using all three approaches. Windtunnel testing can indicate some problems which do not exist in flight. Therefore, a carefully constructed windtunnel programme must be run. The simulation results really depend on the math model and the method by which the inputs were generated. Generally, these come from a combination of windtunnel and analytical results. In conclusion, it takes a combination of all three rather than depending on any one area. Paper 16 of AGARD CP-187 is relevant, by J. M. Drees on 'The Art and Science of Rotary-Wing Data Correlation'.

US/AFWAL (3)

For Stability and Control, the windtunnel is generally better than analytical predictions. Even so, windtunnel results can be misapplied or misinterpreted, ie, poor results can be used (and not recognised). Ref Simulation, there may be situations where PIO can be predicted but not found in simulation because of fixed based and/or motion washout, etc. Again, analytical results may be "better" for some applications if cost is a factor.

We know of pilot-induced oscillations in flight which had not been seen in ground-based simulation. Yet we know of several analytical methods which should be able to predict many such PIOs: McRuer and Ashkenas' pilot-vehicle analysis, Neal and Smith's peak resonance and pilot lead, equivalent or effective time delay, Gibson's θ/δ attenuation around -180° phase, and Ralph Smith's n_z/δ phase at the frequency of a closed-loop pitch-control oscillation, for example.

Analytical design analysis is essential to fully understand the bounds of stability (gain and phase margins) and the sensitivity to parameter variations. There have been numerous cases of simulation experimental designs which had major deficiencies that adequate analysis and comparison with existing flying quality criteria would have quickly identified before flight testing.

3.2 United Kingdom

UK/BAe (3)

For performance prediction, the comment is made that:

"Theory good for local shape change; but test for complex geometry and/or viscous flow dependence, eg external stores, controls, afterbodies."

For aerodynamic loading considerations at least, a comprehensive analytical prediction is a pre-requisite for any aircraft design, partly as a basic model in which to fit data from other sources and partly because not all required information is obtainable from windtunnel models, so that recourse to theoretical methods is inevitable. Therefore for data which is obtainable from windtunnel models, the most vulnerable areas are those associated with inadequate scale representation and transonic conditions. More attention is required for the correlation of flight data versus windtunnel results in these areas to evolve empirical methods, or empirical corrections to windtunnel data. Theoretical methods in the areas most affected by scale or transonic conditions are totally inappropriate. More generally, there are numerous areas where theory may be used as a guide or tool, and indeed some small effects can later be predicted using (simple) theoretical methods rather than by windtunnel results where the resolution accuracy of the windtunnel balance may be inadequate.

In S&C/Dynamics, it is noted that:

- Simulation results are only as good as the mathematical model on which it is based.
- Pure subsonic and supersonic flutter predictions are probably more accurate and certainly more flexible and economic than windtunnel tests.

For Store-release predictions, windtunnel testing is considered to be the most reliable basis currently.

UK/RAE (3)

In manoeuvring flight, a purely analytical approach can never be as reliable as experimental methods (to the same level of sophistication).

3.3 Netherlands

NE/Fokker (3)

Comment covered by Response NE/Fokker (1).

NE/NLR (3)

The question really is to what extent computational and experimental aerodynamics are complementary with respect fo flight prediction. (There is no doubt that they are with respect to aircraft design!) In general experimental aerodynamics will have "the lead", especially for those flight conditions where separations are involved (most off-design boundaries buffet-intensity and so on), or for complex configurations (stability and control). However, there are some areas where the experiment is severely limited by accuracy or model design considerations. In those cases computational aerodynamics are not only complementary but essential. Typical examples are drag-predictions (and drag breakdown) and more complex flutter testing (where 2-D experimental results may be used as an input to a 3-D calculation method to predict flight characteristics).

3.4 Italy

IT/AERIT (3)

For Aerodynamic loads prediction by windtunnel measurements, aeroelastic factors simulation requires very complicated and expensive models. Therefore in such cases analytical prediction could give cost and time advantages, valuable at least in the preliminary design phases.

For Dynamics, analytical prediction can give better results when studying the influence of structural damping factors, difficult to simulate in a model. The same applies to the effects of the control systems kinematics. Present analytical methods find their limitations in dealing with non-linear behaviour, both structural and aerodynamic. Typical cases are free-play, friction, variable stiffness, etc.

Another particular case where analytical prediction can be better than windtunnel results is the external-stores drop or ejection test, where the effects can be introduced of the manoeuvring load factor at the ejection point and the correct correlation between flight Mach and Froude numbers. An opposite case, in critical flight conditions, is the PIO evaluation, when theoretical/empirical criteria are existing, based on previous research; from these it is possible to obtain a better evaluation of aircraft flying qualities compared to what can be developed with ground simulation where the PIO is difficult to reproduce.

IT/MdD (3)

If analytical prediction does not include numerical calculations, then it cannot be better than windtunnel and/or simulation results, unless very particular problems not concerning the aircraft "as a whole" are considered.

3.5 Germany (3)

GE/DFVLR (3)

Analytical predictions are based on the available methods of computational fluid dynamics. Panel methods in general take only 'potential theory' into account. Friction effects may nowadays be included only for simple mathematical 'bodies' and, hence, applicable in the preliminary design phase. Nevertheless, design parameter changes are more easily implemented on a computer.

3.6 France

FR/SNIAS.M (3)

As regards the aerodynamic characteristics of helicopter airframes, the windtunnel certainly still constitutes today a test method irreplacable as much for the quality of the measurements achievable as for the detailed knowledge of the complete aerodynamic field which it permits; current analytical techniques, even the most developed, are still far from its equal. By way of example, we would cite the fundamental but relatively banal problem of the calculation of the aerodynamic drag of a helicopter fuselage, which even the most developed of analytical methods are still incapable of resolving in a satisfactory manner, although such methods have been classically in use for conventional aircraft for a long time. This relates in a large part to the particular 'architecture' of helicopters, whose 'tormented' shapes engender difficulties in the modelling of their wakes (even without introducing the interactions with the rotor wake).

As regards the means of simulating the helicopter in real time, we still do not have at our disposal in Aerospatiale such an operational testing method, although such a study simulator is currently under development. Our experience is limited today to simulation methods in 'non-real' time, to help with the conception and development of our equipment and onboard systems.

FR/SNECMA (3)

Comment covered by Response FR/SNECMA (1).

4 METHODS OF REDUCING DIFFERENCES BETWEEN PREDICTION AND FLIGHT TEST RESULTS

4.1 United States

US/NASA (4)

Differences between flight test results and prediction will be reduced only if the aerodynamics of the flight vehicle are properly represented mathematically, and if the quantitative values of the aerodynamic coefficients can be accurately assessed either through experiments or from computations. It is also important that the determination of the aerodynamic parameters be made in the same Reynolds number range as flight, or that the data can be extrapolated to full-scale Reynolds numbers with high confidence.

The purpose of prediction is to know (or attempt to know), a priori, what flight test results will be. Obviously, improved prediction techniques will reduce the differences between predictions and flight test results. The essential step in improving prediction techniques is validation, through ground and flight tests. Ultimately, flight testing must be used to validate the prediction techniques. The data gained from testing must be correlated with predicted results to see where the predictions fail.

One way to reduce differences between prediction and flight test would be with more accurate large-scale windtunnel models. In the case of the Augmentor Wing and QSRA, the difference in characteristics of the large-scale model engines and the airplane engines resulted in significant differences which had to be resolved in a flight development programme. The 80- by 120-ft windtunnel would permit full-scale testing with flight engines. In the case of the relatively small OV-10 Rotating Cylinder Research Aircraft and the XV-15 Tilt Rotor Research Aircraft, the actual vehicles were tested in the 40- by 80-ft windtunnel.

Another aspect of this question is the ability to measure and analyse flight-test data for correlation with predicted results. While it is easy to predict component and model element results, it is not always easy to measure them. This is why a flight test vehicle, such as the Rotor Systems Research Aircraft with its unique force and moment balance systems, is essential to this validation cycle. Additionally, new flight test data analysis techniques, such as parameter identification, are starting to be effectively used to glean results from flight-test data which were not previously obtainable with standard data reduction methods.

US/AFFTC (4)

An energetic windtunnel model configuration control programme should be implemented and maintained through the early developmental phase of a new vehicle.

Special emphasis should be placed on fine-cut windtunnel tests and complete coverage over the expected flight spectrum and beyond.

A better closed-loop exchange of information between the windtunnel and flight-test technical disciplines should be encouraged. After-the-fact-windtunnel tests could be very beneficial to a better understanding of differences but they are usually not performed.

US/NATC (4)

Using the system identification technique outlined in Response US/NATC (1), this problem can be directly addressed. The flight test aerodynamic estimates obtained using system identification can be compared to analytical or windtunnel predictions to develop an empirical or systematic approach to including the calibration factors in the analytical prediction method.

US/NAVAIR (4)

When the opportunity exists in flight research or new aircraft development programmes, an assessment of the prediction/flight documentation processes should be made for the purpose of isolating any error sources in the prediction process. An improved prediction procedure, whether based on analytical calculations or windtunnel data, is then available for future application. The important elements and details of any research or development programme which include this objective are as follows:–

Prediction Process. Attention to detail is required in the techniques and procedures used in the prediction process. For windtunnel based predictions, these details include a thorough understanding of the windtunnel test-section flow field; the fidelity of the model; proper accountability for tares (support system and incremental balance force measurements not applicable to the aerodynamic configuration); number of models and location of metric split lines required for evaluation of all aerodynamic forces and propulsion system related force increments (may require separate and/or combined force and pressure measurements), and accountability for boundary-layer transition, scale effects and items applicable to the full-scale vehicle which are not incorporated on the model (leakage, ventilation, protruberences, excrescences, roughness, etc).

Flight Documentation Process. Accurate measurement of vehicle excess thrust, propulsive force and throttle related force increments is required for definition of the full-scale aerodynamic characteristics. State-of-the-art improvements in accelerometer measurement capabilities have enhanced the accuracy of vehicle excess thrust measurement. Measurement of power output for shaft engines is straightforward; but the adequacy of propeller and rotor data, required for the conversion of engine power output to propulsive thrust, may cause problems. For turbojet and turbofan powered aircraft, in-flight thrust currently must be deduced from in-flight engine measurements (such as temperature, pressure, RPM, etc) and correlation of these measurements with load cell force measurements in an Altitude Test Facility (ATF). The accuracy of this procedure may be affected by the engine test cell/flight instrumentation and data transmission (the data system resolution and predefined through use of uncertainty and error propagation analysis procedures); the degree of coverage of the vehicle Mach/altitude envelope in the ATF; and the accountability for any environmental effects between flight and the ATF on instrumentation measurements and the propulsion system performance (required because engine performance is evaluated in quiescent air in the ATF, without flow around the propulsion system). Because of these problems, redundancy of in-flight thrust measurement methods and iterative testing of engines between the ATF and flight may be required to isolate and correct any bias errors in the in-flight thrust measurement process.

Thrust/Drag Accounting. A useable thrust/drag bookkeeping procedure must be employed which is consistent between the prediction and flight documentation processes. This procedure must be capable of isolating all forces which are desired for comparison between the prediction and flight documentation processes.

Prediction/Flight Documentation Correlations. As many elements as possible, consistent with the chosen thrust/drag accounting system and detail capability incorporated in the combined prediction and flight documentation processes, should be compared. Suggested comparisons, as developed from prior programs, are as follows:

- Minimum drag variation with Mach number (level and trends in the subsonic, transonic and supersonic flight regimes).
- Induced drag (variation with lift coefficient and Mach number).
- Lift variation with angle-of-attack (lift-curve slope, Mach and Reynolds number effects, onset of buffet and maximum lift).
- Skin friction drag variation with Reynolds number (laminar or turbulent boundary layer theory? Flat plate or curved surface?)

- Throttle dependent inlet spillage drag variation with inlet mass flow ratio.
- Throttle dependent nozzle/nacelle or nozzle/airframe interference as affected by nozzle pressure ratio and nozzle geometry (if variable).
- Trim drag increments due to variations in vehicle center-of-gravity.
- Accountability for the effects of items not included on the windtunnel model (leakage, ventilation, protruberences, excrescences, roughness, etc).

US/AVRADCOM (4)

After the flight test, the data obtained can be used of course to modify the empirical constants, and this has invariably shown an improvement in the accuracy of prediction.

US/Bell Hel (4)

Provide more detailed measurements from flight test on the areas where prediction techniques are the most empirical. This will allow better empirical factors while the physics of the problems are being understood and the mathematical model developed.

US/AFWAL (4)

This is a good question since it acknowledges that differences do exist.

As regards Stability and Control considerations:

- There are means of reducing differences between prediction and flight-test results. Improvements can be made in both predictions of flight characteristics and in the extraction of information from flight-test data.
- These methods basically involve very careful attention to detail, not making simplifying assumptions without understanding the impact of the simplification and understanding past discrepancies so they are not repeated.
- Should note that for various reasons some differences are significant and others are not. For example, stability and control derivations (eg, moment due to [illegible]) extracted from flight data typically have scatter, which is usually inversely proportional to their importance in defining the aircraft dynamics. Of course, a larger amount of scatter in data extracted from flight makes it difficult to compare with predictions and reduces the confidence in the data base.

- The repeatability of flight-extracted parameters can be improved by using several methods: (1) using manoeuvres that excite all the significant parameters that are to be extracted, (2) using an extraction program that models the flexible body equations instead of rigid body equations and (3) using semi-empirical weighting factors based on the importance a parameter has on the aircraft dynamics versus the confidence (relative accuracy) of estimating that parameter.
- A significant discrepancy occurred during a recent fighter development in that a deep stall trim point was obtained that was not predicted. Factors that contributed to the pitching moment discrepancy ($\Delta C_m \approx 0.1$ at $\alpha \approx 60^\circ$) were Reynolds number corrections, windtunnel model discrepancy (engine nozzle position) and windtunnel model support interference.
- During the development of another fighter, a discrepancy appeared between simulation and flight time histories of abrupt, high-rate manoeuvres. This discrepancy could be reduced (but not eliminated) by reducing the horizontal tail pitching-moment effectiveness. Subsequent studies resolved this discrepancy by including inertial effects in the flexibility corrections to horizontal tail effects and by including an aerodynamic lag factor to the tail effectiveness. Studies also showed that the aerodynamic lag is very important for highly augmented, statically unstable aircraft.

For Handling Qualities in some areas, calibration factors can be applied with some confidence: touchdown rate of sink a few feet per second less in flight, best roll sensitivity half or less the optimum simulator valve (see Fort Worth paper by Roger Smith). Generally, attention to setting up a rigorous task, well defined and aggressively performed, will improve correlation.

Increased fidelity in ground-based simulation can be obtained through better wide field-of-view visual systems, more accurate motion-base systems, and carefully validated nonlinear computer modelling techniques. The engineer must carefully validate the simulation in bandwidth, physical effects and environmental modelling. Experimental processes and performance metrics must be carefully selected within a reasonable size test matrix to scientifically extract the results desired. Experimental procedures should be sufficiently severe to identify any "cliffs" or regions of instability in flying qualities for a variety of weather conditions and manoeuvres. Increase emphasis on flight testing procedures for improved parameter identification for improved correlation with windtunnel and ground-based simulations. Document flight test results thoroughly and distribute results.

4.2 United Kingdom

UK/RAe (4)

In Propulsion/Performance prediction, it is advantageous to include as much detail as possible in a mathematical model, even if some values must be assumed, or include all engine-dependent terms in thrust account and allowance for all known items in a drag account. Similarly, apply comprehensive corrections to Flight Test data even if they may be significant only in extreme areas. Adopt agreed datum conditions and datum methods so that differences in increments can be studied wherever possible. Equally, arrange measurement of increments and request a datum condition regularly. Measurement of afterbody drag rather than thrust-minus-drag is much preferable, even with some compromise on nozzle simulation. Adopt 'mistakes' analysis, on-line in a particular test and post-test before proceeding to further stage. Pre-test analysis for mistakes is worth more than post-test analysis of uncertainty.

For S&C/Dynamics in particular, predictions must always include sufficient parameter variation to cover the tolerances associated with unknown or badly described elements and local non-linearities. These uncertainties must be identified and sufficient flight test instrumentation specified to enable the effects to be assessed in flight. Moreover, make sure any Ground/Flight differences are real, take care in gathering information from both sources, and make sure that comparisons are justifiable.

For Store-release, a comprehensive series of windtunnel tests can lead to very accurate trajectory predictions using a "broad-based" prediction method. In all but a few cases, however, the cost of this approach cannot be justified. The degree of accuracy required and hence the level of windtunnel testing is usually defined on the basis of engineering judgement of the difficulty of the task; ie a compromise between cost and accuracy, culminating in a balance between cost and risk. A further source of differences between prediction and flight is the definition of ERU performance. Pit drop testing to define performance losses due to aircraft structural flexibility plus development work by manufacturers to reduce the scatter in ERU performance are both needed to improve the accuracy of predictions and reduce the scatter in store behaviour in flight.

UK/RAE (4)

To reduce differences between prediction and flight test results with respect to flight dynamic behaviour, we need to improve:

- The standard of mathematical models used, especially at high angles-of-attack.
- Estimation methods, especially for changes in aerodynamics due to changes in configurations.
- The ability to measure angle-of-attack and sideslip in flight, and to adopt better calibration standards for flight instruments.
- The accuracy of estimation of inertia characteristics.

4.3 Netherlands (4)

NE/Fokker (4)

Comment covered by Response NE/Fokker (1) and (5).

NE/NLR (4)

No comment.

4.4 Italy (4)

IT/AERIT (4)

Aerodynamic Load prediction could be improved possibly by adopting sophisticated computational-fluid-dynamics data, but there could be an unacceptable increase of cost to evaluate the large number of flight cases which need analysing for selecting the critical loads. Another possible approach is to set up a large file of test results, as available in the Tornado aircraft programme, and to then use it for the definition of 'adjusting parameters' to the theoretical calculation procedures.

For Flutter predictability improvement, it is essential to increase the accuracy and flexibility of the theoretical unsteady transonic methods, and to reduce their cost and computing time. Allied improvements are also required in the structural representation, to account for control laws of actuators, dampers control loops and any kind of non-linearities.

IT/MdD (4)

The lowest and acceptable differences between the predicted and flight test results can be obtained if the accuracy of the evaluation of aerodynamic, propulsive and inertial coefficients are improved for any test condition.

4.5 Germany

GE/DFVLR

The accuracy of a mathematical model can only be verified by flight tests; but the results of flight test programmes are flight test data which have to be analysed critically. If all aspects of the flight test aircraft are not well documented (weight, inertias, CG position, sensor positions and dynamics, filter dynamics, etc), then the danger of identifying erroneous aircraft parameters from flight tests is high. Especially, more importance should be paid to improved instrumentation including documentation as well as manoeuvres for aircraft parameter estimation methods. Not only the aircraft model parameters but also the model structure has to be verified. The last viewpoint is especially important for highly augmented aircraft.

In order to improve the quality and reliability of windtunnel data, it is highly recommended to use more redundant measuring techniques. It should become a standard practice to measure not only standard strain gauge 6-component windtunnel data, but to acquire and analyse also all signal-time histories from tapes.

Also, for redundancy reasons, dynamic model testing for the estimation of standard rotary derivatives from dynamic balances should include the measurement of the model motions by accelerometers. In addition, control surface inputs and simulated gust inputs can improve the information content of dynamic model testing in windtunnels. Finally so-called confidence levels should be superposed on measured data in order to give the analyst a better means of evaluating the correlation of windtunnel vs flight data.

4.6 France

FR/SNIAS.M (4)

As a general rule, the helicopter calculation models (semi-empirical) are re-adjusted each time that extra measurements from flight will permit. The prediction models are therefore under continual refinement and the correlation of calculation/experiment are constantly being improved. The organisation of data banks, which is taking place currently, should facilitate such revisions thanks to the systematic utilisation of statistical exploitation procedures. It is nevertheless important to stress here the difficulties which are sometimes presented in the interpretation of certain flight measurements, notably the correlations of calculation/experiment for the torsional loads of the blades. To the poor knowledge of the elastic behaviour of the materials, and to the imperfections related to the modelling of the aerodynamic moments of the profiles, above all in stalling and in the unsteady domain, may be added the special difficulties of flight measurement of the torsional deformations of the blades, which greatly impede the cross-checking between calculations and experiments.

FR/SNECMA (4)

One of the important sources of error in the prediction of flight performance can arise, unless special care is taken, in the use of propulsion nozzle coefficients deduced from model tests. Apart from scale effects, hot gases, and technological losses which can be evaluated, an uncertainty remains associated with the determination of the 'mean' generating quantities of the engine. In practice there exists a heterogenity of pressure and of temperature, radial and circumferential, to which are added fluctuations of pressure and temperature. The knowledge of the 'mean quantities' at a limited number of points (comb traverse) in the flow at the gas-generator exit is insufficient to completely characterise the flow.

The method which seems to us the most efficient is to adapt the model coefficients to the engine by re-adjustment of the generating conditions. The ground-test of the engine with flight rear-body and flight instrumentation permits not only knowledge of the reference generating conditions, but also of the thrust and flow-rate. In bringing together these elements and the nozzle coefficients obtained during model tests, one can determine two adjustment coefficients of upstream conditions, one relating to the grouping (D$\sqrt{T}$), the other to the rate of expansion.

5 NEW PREDICTION TECHNIQUES THAT SHOULD BE EMPHASISED

5.1 United States (5)

US/NASA (5)

Since the success of predicting flight depends on knowing the proper aero-math model and determining the numerical values of the model's coefficients, the emphasis for improvement in the prediction of flight histories should be in the derivation and validation of proper aero-math models and the means to determine the appropriate coefficients.

US/AFFTC (5)

Computational aerodynamics offers a potentially powerful tool to fill the gap between windtunnels and the flight environment. It could eventually replace all but very basic windtunnel testing! It currently requires extensive computer capacity, thus high cost in today's environment. Computational aero is relatively unproven and will require parallel, alternate predictions until well established.

US/NATC (5)

The integrated system identification approach, as discussed in the Response US/NATC (1), should be emphasised.

US/NAVAIR (5)

No new techniques that would enhance the accuracy of the prediction processes are known. Development and improvement of existing techniques through predictions versus flight comparisons, as discussed under Response US/NAVAIR (4), should be emphasised.

US/AVRADCOM (5)

Perhaps it is not clear what the term "prediction techniques" means in this general connotation. It would seem that a prediction technique for air-loads or aircraft performance is either purely analytical, semi-empirical, or empirical. These are the only categories, unless one becomes concerned with the details of the mathematical models themselves as they affect the computer codes. As stated previously, all of the prediction techniques for rotary-wing aircraft currently used are at least semi-empirical. What is badly needed is the development of reliable and generally applicable analytical methods that are not dependent on experimental data. A concerted effort needs to be made to establish the experimental data base that is needed in order to develop the reliable mathematical models. This is particularly evident in the case of modelling the rotor wake, where there has been a great deal of effort in developing highly sophisticated computer codes but where there are very few good experimental data that can be used for validation. Some of the new experimental facilities such as the RSRA, the 40 x 80 x 120 ft windtunnel, and the anechoic hover test chamber will be oriented to this problem.

Efforts should be made to incorporate some of the new fundamental aerodynamic developments into the future prediction codes for rotor airloads. However, these must be simplified because already the rotor computer programs are very elaborate. While significant advances have been made in recent years towards understanding and predicting individual aerodynamic events such as rotor blade aerodynamic characteristics and aerodynamic interference effects, much of this new information has yet to be incorporated into the large prediction codes for rotor airloads. Moreover, as stated previously, the comprehensive and sophisticated analyses have generally not been tested rigorously against the most complete and advanced sets of experimental data. Furthermore, none of the data sets appears to include all of the information that would be needed to completely validate the latest global computer models. While additional and more comprehensive data are needed, we should also point out that even the existing measurements tend to be under-utilized. With the increasing complexity in the computer codes, emphasis must also be given to structuring and managing these codes in a more unified and organized manner. A current program sponsored by the US Army Aviation R&D Command called Second Generation Comprehensive Helicopter Analysis System (2GCHAS) is directed to a concept that will consist of modular subsystems that can be individually modified to allow new technology to be introduced or corrections to be made with minimum effort and expense. The greatest limitation to the current generation of helicopter airloads prediction programs seems to be in extrapolating a given program to a new or unrelated rotor design.

US/Bell Hel (5)

For rotary-wing aircraft, the prediction of the rotor wake in all flight regimes especially during non-steady manoeuvres should be emphasised. A reliable math model would then allow the proper interference effects to be predicted. Thus, improvements in predicting handling qualities would allow better design prior to flight evaluation. Another area of interest is that of the tip region of the rotor from a performance and noise point of view.

US/AFWAL (5)

As regards Stability and Control, recommendations are:

- More Euler code solutions to reduce the amount of empiricism in some engineering methods. Missile Datcom will be a new tool that should be of some value.
- A fast, efficient, interactive panel-type aerodynamic prediction program that will predict a complete set of stability and control parameters.

For Handling Qualities we would recommend our current specification, MIL-F-8785C. We are working on a complete review and a 're-do', and shortly will be recommending that; see Fort Worth paper by Moorhouse and Woodcock.

Also require emphasis on.

- Analysis of digital effects (w'domain analysis).
- Flying quality criteria for higher order systems.
- Atmospheric effects models (turbulence, wind shear, wake, etc).
- Non-linear modelling.

5.2 United Kingdom

UK/BAe (5)

For Propulsion/Performance predictions there is a need for implementation of new CFM techniques for easier and therefore more frequent use by the engineer. Also more use of high-response pressure instrumentation in windtunnel and flight testing to monitor for buffet, buzz, vibration, intake flow distortion, at least to provide figure of merit if not absolute measurements.

S&C/Dynamics need in particular better treatment of unsteady transonic aerodynamics using semi-empirical techniques, and of high angle-of-attack aerodynamics probably by increasing use of free-flight models.

Store-release predictions require:

- Incorporation of non-linear effects and the effects of viscosity in theoretical methods so that they can be used with more confidence in a typical store release environment.
- Development of supersonic and transonic theoretical methods for off-body flow-field predictions and mutual interference effects.
- Development of windtunnel techniques for accurate and repeatable jettison testing and simulated gravity.
- Development of in-flight trajectory recording to increase accuracy and allow real-time transfer of the recorded trajectory to the ground.
- Development of fast, accurate trajectory analysis to complement real-time transfer of recording and allow the possibility of multiple releases in one flight with clearance for envelope expansion between releases.

UK/RAE (5)

As regards the prediction of flight dynamics characteristics, the new higher standards of Re now available in windtunnels should be used for stability and control measurements, particularly to predict the boundaries at high angles-of-attack. The use of dynamic rigs for directive measurements should be extended into these high Re tunnels and free-flight models which employ active control systems should be used wherever possible to take the prediction process further. This is particularly important for projects having relaxed levels of static stability which rely on the design of such systems critically.

5.3 Netherlands

NE/Fokker (5)

Possibly a more intensive use of dynamic rigs with large models in windtunnels.

Perform much more repeat runs in windtunnel tests on a routine basis in order to introduce an element of statistics into the test data.

NE/NLR (5)

The emphasis should be towards the improvement of mathematical modelling through better physical understanding - supported by specially-designed experiments. Quote also J. D. Whitfield (AIAA-paper 81-2474): "However, careful studies of Reynolds number trends, wall temperature effects, Mach number trends, configuration changes and turbulent effects are not as common today as they were years ago. This could be dangerous for future systems that require fundamental knowledge in the development cycle".

We are heading for more integration, not only of basic experimental and computational aerodynamics but also of the analyses of windtunnel and flight test results. An effort should be made to close the present gap between flight test evaluation and analysis of windtunnel data.

5.4 Italy

IT/AERIT (5)

Most of the remarks made in respect of "Methods of reducing differences between prediction and flight test results" inherently imply which new prediction techniques should be emphasised.

IT/MdD (5)

The areas to be emphasised are:

- The non-linear optimisation techniques.
- Any fast and correct computer simulation technique of aircraft kinematics and dynamics, with special reference to the non-linear range of the aircraft 'as a whole'.

Special mention is made of a 'Real-Time Flight Dynamic Simulator' envisaged in the context of the AGUSTA helicopter programme, to be utilised in both the design-development phase and the operational-development phase of a prototype.

5.5 Germany (5)

GE/DFVLR (5)

Absolutely new prediction techniques cannot be emphasised. The experimental techniques can be improved by fully using the application potential of modern micro-digital electronics and instrumentation.

5.6 France

FR/SNIAS.H (5)

We believe that an important effort should be made to develop the tools of statistical treatment for measurements effected in flight. This can take place through establishing data banks which will permit a systematic exploitation of all the existing test results, results which up till now remain under utilised, in the absence of use of an adequate system of information acquisition, of data management, and of treatment of the appropriate parameters. As regards the exploitation of tests on flying qualities (where much remains to be done), it would be necessary to develop the application of modern techniques of parametric identification to the determination of the aerodynamic characteristics of helicopters (obtainment of stability coefficients).

These analysis tools are cruelly absent for the stage of aircraft development and would be particularly useful for refining simulation models. Finally, it is undeniable that an important theoretical effort remains to be made in order to improve the reliability of pure analytical models and to set up the experimental data banks necessary for the elaboration and qualification of these models.

FR/SNECMA (5)

The introduction of heterogenity considerations into the methods of calculation for the engine efflux (gas-turbines) should permit quantification of these effects. Additionally, the utilisation of a unique algorithm to exploit the results of theoretical calculation, windtunnel test, engine tests, and flight tests should lead to a reduction of prediction errors.

PART C - EXTRACT FROM ROUND TABLE DISCUSSION

1. LIST OF ROUND-TABLE CONTRIBUTIONS

The final half-day session of the FMP Symposium began with a 40-minute survey of the background and national responses to the FMP Questionnaire concerning prediction techniques and correlation against aircraft flight results; see Parts A and B of this paper. Prepared overviews were next given on pre-selected topics by the 'Round-Table' members in the order shown below, and complemented by relevant comments expressed by other participants (as also listed).

1. Ph Poisson-Quinton (ONERA, Chatillon/FR) - 'Chairman's Introduction' of Round-Table Members and the chosen topics.

2. F. N. Stoliker (CSC, Oxnard/US) - 'Flight test technique developments'.

3. I. Czinczenheim MDBA, St Cloud/FR) - 'Performance prediction techniques'.

Extra comment by C de la Foye (STPA, Paris/FR).

4. H. Wunnenberg (Dornier, Friedrichshafen/GE) - 'How to cope with restrictions on time and money'.

Extra comment by E. Obert (Fokker, Amsterdam/NE).

5. A. Filisetti (Aeritalia, Torino/IT) - 'New aspects of structural design'.

Extra comment by A. Lotze (MBB, München/GE).

6. C. Bore (BAe, Kingston/UK) - 'Fluid Dynamics Panel aspects'.

7. H Mooij (NLR, Amsterdam/NE) - 'Modelling and measurement in ground effect dynamics'.

Extra comment by I. C. Statler (USAR & TL, Ames RC/US).

8. J. Williams (SU, Southampton/UK) - 'Supplementary remarks'.

Extra comments by J. Renaudi (CEV, Bretigny/FR), J. W. Britton and D. G. Mabey (RAE, Bedford/UK) and P. C. Leyland (BAe, Warton/UK).

Shortly after the Round-Table some 'Contributor's Notes' were received for the foregoing Items 2, 4, 5, 6 and 8. Corresponding edited comments could therefore be added here as the following Sections 2 to 6 respectively, in time for publication with the Symposium Proceedings; Section 7 relates likewise to another written Note received from R. R. Lynn (Bell Hel, Fort Worth/US). Later, these and other expressed views during the whole Symposium will be analysed (from tape-recordings) for the preparation of the final Technical Evaluation Report.

2 FLIGHT TEST TECHNIQUE DEVELOPMENTS (F. N. Stoliker)

Both Flight and Ground Test Techniques have certainly changed since I (FNS) started in flight test in 1950. The standard instrumentation system at that time was a photo-panel and the standard means of processing data was a slide rule. Correlation of data just from flight-to-flight was often a difficult task, while the correlation of ground and flight data was primarily for performance. Handling qualities flight-test results were largely qualitative and based heavily on pilot comments. System tests were almost totally qualitative; you flew the system till it would not work and then tried to find out why it broke and how to fix it!

As this Symposium has noted, flight and ground test techniques have become vastly more sophisticated, and more sophistication is coming with cryogenic windtunnels and new computer techniques. We now perform dynamic manoeuvres to gather performance data, much more data is gathered per flying hour with greatly improved instrumentation and systems, and the data repeatibility is much better. With the advent of the better instrumentation, high capacity computers, and powerful software tools such as MMLE, we can now routinely extract S&C derivatives from flight test. This in turn allows us to utilise simulators more confidently and thereby to support handling qualities tests in areas of high hazard. For example, in the F-16 high angle-of-attack tests, the simulator was updated with flight test derivatives on an almost daily basis to ensure the best match between flight and simulator. Test pilots would then spend as much as four hours in the simulator to prepare for a one-hour flight.

Since the mid-60's, there has been an immense increase in the on-board avionics capability that is combined with a computer. Of course, this can lead to large amounts of on-board software that must be evaluated, often under adverse conditions. Avionics simulators are in use or under construction in several AGARD countries to improve test capability. Overall, flight-test engineers are nowadays much better prepared for avionics and computer applications, while data reduction is now often possible at the flight-test centre itself and even in real flight time - at least for programme guidance.

Unfortunately, as R Wood pointed out, more sophisticated ground and flight test techniques have not necessarily improved our prediction capabilities even for up-and-away flight. In part, poor correlation of predicted data to flight test data can result from the various data evaluators not properly knowing all the assumptions made by another in preparing data for presentation. Additionally, in areas where pilot technique is a large factor in determining aircraft ability, prediction becomes less certain. For example, R Wood has mentioned that with a recent attack aircraft a 10% increase in take-off roll could result if the pilot over-rotated by 1° rather than being able to rotate precisely to 10° pitch attitude.

Capabilities for obtaining ground and flight test data have certainly improved dramatically in the past thirty years. In some cases predicted and flight data have been shown to match very well. In other cases there is still room for improvement, some of which hopefully can come from the discussions at this meeting and similar future meetings.

3 HOW TO COPE WITH RESTRICTIONS ON TIME AND MONEY (H. Wunnenberg)

This question will be discussed in the following from the manufacturers point of view. What are the main tasks a manufacturer has to fulfill concerning aerodynamic data within the development phase of a new aircraft project.

- To get all necessary Performance Data to be able to guarantee the required Performance values.

- To get all necessary stability and control coefficients and derivatives to be able to design the control system, define the trim and control effectiveness, and with that fulfill the required HQ Criteria or Specifications.

The required accuracy of the Performance Data depends on the allowed scatter range, plus and minus values, which may be part of the contract. The required accuracy of the stability and control data may depend on the flexibility of the design to changes during the flight tests or due to the insensitivity of the Stability System Design.

To illustrate this a little bit, the design procedure for a simpler aircraft project for which the time scale for the development and the budget to be spent is limited, is discussed roughly:

- Fast evaluation of a first set of performance data without HQ constraints by Handbook Methods and Sizing Computer Programs based on own experience and available knowledge to define a first low-speed WT Model.
- Low Speed WT Tests to update the data. Checking of the performance and evaluating the HQ problem areas.
- Revised aircraft configuration and definition of a high-speed WT Model. In this phase already the project office will try to mainly freeze the aircraft geometry for starting the structure design.
- High Speed and engine interference tests and parallel theoretical calculations to define problem areas and possible solutions in the non-linear high angle-of-attack and the transonic flight regime.
- The geometry will be frozen during this phase with minor changes open to improve further problems.
- Repetition or additional WT tests if necessary, eg high Re-number tests.
- Data collection and basic definition of Performance and Handling Qualities before the first flight.

The procedure leads to an extreme pressure on the aerodynamic design engineer to find a proper configuration as early as possible with usually a fixed amount of money to be spent within this process. The prediction methods to be used have to be selected therefore according to the answers of the following questions:

- What is the amount of time for preparation, and how accurate the geometry and overall definition has to be for a successful use of the different prediction methods?
- Is the information and its accuracy level worth the amount of time and money to be spent on them?
- Does the accuracy level of the prediction methods for the requested Performance and Handling Characteristics correspond to the accuracy of the flight test equipment.

In answering these questions the following requirements for further improvements of the presented state of the art in numerical methods, WT test techniques and Flight test techniques can be given.

- Further improvements of the Handbook methods as DATCOM, DATA Sheets, ESDU ... and its computerized versions, for more precise definition of a reasonable first configuration based on the given geometry.
- Improvements of the numerical methods to solve the Navier-Stokes equations for high angles-of-attack and the transonic Potential/Euler equation at lower data preparing andcomputer cost for a fast and precise finding of the problem areas and its possible solutions.
- Improvements of the WT techniques in respect to WT error reduction, interference effects of the propulsion system, faster data reduction and data plotting.
- More comparison between prediction and flight test results.
- Further improvements of the Parametric Identification Methods and perhaps a standardisation of the adequate accuracy of the flight test equipment in relation to the WT accuracy. Maybe the latter could be a task for AGARD.

4. NEW ASPECTS OF STRUCTURAL DESIGN (A. Filisetti)

Trying to summarize the results of the Session IV on 'Structure Design and Test', we can stress the following points:

- There is the capability to develop an aircraft to the limits of its true envelope with no margins left and no associated costs.
  This is accomplished through a process of theoretical prediction, ground tests (W/T + static tests + GRT + load calibration) and flight tests.
- Such a process is based on the common reference of mathematical models, used from prediction up to extrapolation of flight test results. These models are updated by matching the experimental results. Static and dynamic loads, flutter and stresses can follow this technique. A clear example has been given for rapid rolling testing in flight, where interpretation of the previous results is done by matching the mathematical model with them, to enable the subsequent flight test predictions.
- **The prediction capability of the aeroelastic stability of a tilt-rotor aircraft is encouraging.**

Major shortcomings which appear in the state of the art may be recalled as.

- Poor reliability in prediction of structural loads in transonic region, owing to Reynolds effects and structural deformations.
- Difficulty in flutter analysis to account for non-linearities both structural (friction, free-play), and aerodynamics (M and α effects).

- Interpretation of flutter flight-test results in critical conditions.
- Not achievement of a satisfactory integration in the flutter theoretical analysis of the control system characteristics.
- Obvious consideration for the future is to propose improvement of the bad things through improved analysis and test methods, taking advantage of the present and future-generation electronic-computer capabilities; in any case engineering judgement will be always a basic requirement.

But future operational requirements for military aircraft and the technological advances will demand the design of the new weapon systems by an integrated view, as illustrated by the following examples:

- The speed and manoeuvre performance of an interceptor and the radar detection performance must be defined in connection with the range capabilities of the SR missiles to maximize combat effectiveness.
- The Fire and the Propulsion control systems will be integrated in the Flight Control System to improve survivability and reduce pilot workload.
- Active Control Technology will alleviate the conventional requirements for aerodynamics design (relaxed stability) and structural design (load alleviation, flutter suppression, etc) to reduce weight and cost of the aircraft.

Cross feeding of the new technologies is in fact an outstanding way to improve cost/effectiveness.

Having set the general requirements, the structural design of a new aircraft must follow an automatic iteration process on the computer, following the subsequent steps; load analysis, stressing, weight and stiffness computation, aeroelastic deformations, aeroelastic loads; and with the constraints of flutter and static aeroelastic requirements. Here the problem is now stressed by the fact that we have to cope with a new kind of structures, made of advanced composite materials. We all know that we are living through a technological jump in the structural design and manufacturing, paramount for the aeronautical future.

The new composite structures are characterized by high specific resistant anisotropic material, able to be tailored to the load path, with potential saving in weight and cost of about 25 to 30%. The allowable may be of the order of the best aluminium alloys, but with specific weight remarkably lower. The design criteria must really take into account at first the manufacturing techniques, the possibility to qualify hybrid structures, the non-destructive tests methods, the known allowable defined by the non-linearity of the strain versus stress and by the hot and wet conditions, which could be quite severe in a supersonic combat aircraft. There is plenty of work to be done in order to effectively exploit the new material and part of that could be solved by a structural optimization process. A more detailed presentation of an optimization programme can now be given by Mr Albert Petre.

5. FLUID DYNAMICS PANEL ASPECTS (C. L. Bore)

5.1 Introduction

What excuse do I (CLB) have for being here? I am an interloper - a member of the Fluid Dynamics Panel - sent to ensure fair play for fluid dynamics interests - but as usual I will discuss whatever I fancy! What have we learnt from 30 or so papers by experts from all over NATO? Quite a lot: so much that I need some way of putting the many different points into some order. I will try to set up a framework appropriate for aircraft designers, rather than specialists. Let us consider the aircraft design background for a minute.

The cost of every new design tends to double (after allowing for inflation) relative to the previous one, and the time intervals are lengthening. Civil airlines are losing money, and governments are reluctant to pour much money into new military aircraft, or the R&D necessary. So our most basic objective is to provide more value for money in future aircraft. That, I believe, is the "name of the game". Civil aircraft fly for so long every year that fuel consumption and maintenance costs are dominant. So we have strong incentives to reduce drag and to reduce fatigue loading actions, and to increase confidence in performance estimates.

Military aircraft, however, fly perhaps only about 1/10 as long each year as the civil machines, and therefore fuel consumption affects costs less. Even the cost of buying the aircraft amounts to only perhaps 20% of the lifetime cost of an airforce - so our scope for giving better value for money lies far more in increasing the value (or effectiveness) of the airforce than in reducing the costs. Thus a 25% increase in effectiveness gives just as much improvement in effectiveness/cost as giving the aircraft to the airforce free. Now the military value or effectiveness is proportional to a number of factors, related to: load transport capability; accuracy of delivery; and availability (including all-weathers, the availability of take-off pads after runway denial weapons have been used; and vulnerability on the ground and in air). All these capabilities are competitive, so they have to be assessed in relation to the capabilities of the enemy, or perhaps an allied competitor. Our risks include not only the uncertainties of the enemy (in 10 years time) but also our own uncertainties about the precise capabilities we will actually deliver.

In our present context, we can pick out some areas where there is still room for improvement, namely:

- High L/D, better engine sfc and lower weight of aircraft are always welcome.
- For military aircraft, better controllability, more accurate weapon delivery and more agility are primary aims. Here, buffet and post-stall behaviour enters.
- For all aircraft, better knowledge of loading actions, closer prediction of performance and more reliable aeroelastic calculations; all add up to fewer mistakes. In this group, fatigue loading actions are important (and I do not believe we yet have full confidence on the relationship between load spectra and service endurance of structures of all kinds).

5.2 What we have learnt here

Windtunnel

The windtunnel data production rate has gone up by a factor of 10 in 10 years, and windtunnel repeatability is better. Optimisation of configurations in the windtunnel has been demonstrated. Reynolds number uncertainties are being reduced with great determination, by means of high Reynolds number windtunnels, and improved understanding of boundary layers. We know adaptable-wall windtunnels are being developed. Turbine power units for windtunnel models are in regular use.

BUT I have some reservations: firstly the high Reynolds windtunnels will not be magic - especially the cryogenic windtunnels. There will be problems to solve: involving the effects on boundary layer of heat transfer, aircraft waviness and skin joints, and excrescences. Support interferences will not disappear. The models will be expensive, and will take a long time to make and to alter. I have high hopes of adaptable wall windtunnels, when they come into regular use. We should hear a good deal more about all this in next year's FDP Symposium on 'Windtunnels and Testing Techniques' to be held at CESME (Turkey) 26-29 September 1983.

Computers

We all know how these are making enormous advances - invading windtunnels, design itself (through optimisation and CAD), and the cockpit itself (through active control). More and more of the design process - and eventually the flight operations - will integrate computers. Here it is worth looking again at Rubbert's diagram (Paper No 1). But, for a long time to come, the engineer will have to be vigilant to watch out for all the things that can cause trouble and yet are not yet computable. For example, many sorts of flow separations, buffet, shockwaves, gross separations such as occur in the narrow spaces near close-spaced stores, or those that attend military stores attaining high incidences when released.

Remotely Piloted Research Vehicles

It is interesting to find positive discussions of remotely piloted research aircraft, to investigate problems not adequately addressed by windtunnel, or computer, or flight on full-scale aircraft. They are clear of support interferences and wall constraints, and they can undertake researches which might take far too long on a piloted aircraft, and some researches which might be hazardous - such as flight buffet or flutter work. If these can be made much quicker and less expensive, they seem likely to come into more general use.

5.3 Miscellaneous Points

Handbook/Chart Production

Despite all the progress made on major new techniques, like computer programs and major windtunnels, there remains a need to present concise concentrated data - such as design charts and tables and handbooks - to guide the early stages of designs and to help assess the effects of proposed variations in design. Here the ESDU is a valuable example, and some of the AGARD Working Groups also play a useful role.

Buffet and Wing Rock

Despite extra glimmerings of understanding on buffet, I suspect we have a long way to go before we can predict the magnitudes to be expected in flight with full understanding. Indeed, other post-stall behaviours remain to be understood thoroughly.

Spin

We have heard interesting observations on spin recovery - but I wonder why so little is said of spin prevention? In the design of the Harrier wing, I went to a lot of care to ensure that the spread of boundary layer separation across the wings was slow, and was the same on both wings. This was to avoid the phenomenon of wing rock (in our case this was an unsteady aerodynamic forcing motion) and was achieved by a carefully evaluated set of leading-edge wing fences, sawteeth and vortex generators. However, the flow remains symmetrical to high incidence - so much so that one can only spin the Harrier deliberately, by pitching up rapidly to 30° or more and putting on full pro-spin controls. It then spins gently, and comes out immediately on centring the controls. So I ask again: why accept spin? Why not make the flow stay symmetrical?

Store Release

Finally, you will expect me to comment on store release. After all, for military aircraft, accurate delivery is the whole aim of the airforce. There is no point in having aircraft which manoeuvre marvellously all the way to the target and then spew their weapons in a wide scatter (or damage the parent aircraft on releasing stores). Progress has been made, of course, but this is a very big subject, on which I have been trying to get an FDP symposium to itself - if only I can persuade the smaller NATO countries without military aircraft industries to support this subject of such practical importance.

6. SUPPLEMENTARY REMARKS (J. Williams)

In advance of the Technical Evaluation Report, I will add only three major comments of personal concern from my synthesis presented earlier.

1. The individual prediction tools available (Figure A.1) must be continually revised, and employed as complementary techniques towards minimisation of overall flight prediction errors. As part of this continual process, it is nevertheless revealing to analyse and assess the relative advantages and disadvantages (merits and demerits) of the individual prediction tools and of their cost-effective bias in combination.

2. Wider appreciation and use must now be made of parametric identification techniques for data analysis in windtunnels as well as in flight. At the same time we must continue to improve our physical understanding, as a sound basis for theoretical framworks and calculations, even to the extent of testing special experimental and mathematical models for this purpose. Moreover, particularly in flight, we need better information as to detailed airframe and propulsor behaviour under flight load conditions. For reliable comparisons, a realistic framework for modelling the specific aircraft in flight is essential.

3. There is a regrettable absence here of any paper on the implication of lower noise requirements/prediction as regards aircraft performance and design considerations, including both aeroplanes and helicopters. Externally propagated noise can cause not only civil annoyance at ground level, but can also promote the military risks of early acoustic detection - particularly if the radar/infra-red/visual signatures have been reduced already. Internal noise and high-frequency vibration is important in both civil and military operations from ride-comfort and communication aspects, while also affecting flight operational effectiveness in respect of aircraft combat and weapon delivery. Indeed aircraft noise/vibration now presents an inherent prediction problem in aircraft flight performance and dynamics.

7. A HELICOPTER RESEARCH ENGINEERING VIEWPOINT (R. R. Lynn)

Although a variety of interesting and informative topics have been covered here by well-prepared papers, there has been no hard look as to how we really stand in our ability to calculate performance, stability, structural loading, and the host of other parameters involved in developing new aircraft and weapon systems; this is true irrespective of aircraft type. Consequently, we may have painted an aura of capability that is incorrect, leading our governments to expect system developments to go exactly as predicted, and thus exposing ourselves to unmerciful castigation when we carry out the normal development activities associated with problems which are expected in all programmes.

Here are some examples of where I (RRL) believe the helicopter industry stands in respect of test correlations with prediction.

- Hovering out of Ground Effect: ±3% gross weight based on engine limit.

- OEI Service Ceiling: Minimum power requirement ±6% (HP). Service ceiling ±25% (ft).

- Vmax. ±6%.

- Noise: Flyover ±3db. Approach ±5db. Take-off ±5dB. The last two totally empirical.

- Oscillatory loads at V_{max}: Prediction area is about 30% at design stage. Usually underpredict blade inplane loads. The area is reduced to about 10% when prediction is made of changes from a baseline blade.

- Maximum Vibration Level: With a good model, about 30% to 50%. Using full-scale shake tests for modifications, about 30%.

- Aeroelastic Stability: Damping predictions are within about 1% of critical. For air and ground resonance, predicted damping is about 1% conservative at the least damped condition.

- NASTRAN Analysis (simple, tailboom): About 3% error in frequencies for low frequency modes. Frequency range of 6 to 20 Hz - error about 8%. Higher frequency modes vary depending on representation of damping and input force.

- Handling Qualities: Flight mode stability, very poor correlation due to rotor fuselage interference effects and pylon control system coupling.

- Engine Compressor Stall - Altitude effects, trend data only. Rearward flight, no analytical techniques available.

Overall, if we are faced with having to carry out such predictions for a new vehicle, then an understanding of where we are analytically is essential. This subject should have been debated much more at the meeting.

CONCLUDING NOTE

Firstly, I (JW) wish to express my appreciation to all the named Contributors and their Establishments, for their efforts and cooperation in preparing and transmitting the many responses to the FMP Questionnaire and the aide-memoires on their Round-Table observations. Here, for consistency of presentation, these contributions have been subjected to some re-writing, re-arrangement, free-translation and expurgation. Secondly therefore I would apologise if, lacking adequate time for checking with the particular originators, I may have unwittingly misrepresented or omitted any major opinions or essential arguments. Finally, I would recall that the forthcoming Technical Evaluation Report is intended to draw conclusions and recommendations, not only from the present Synthesis (Questionnaire and Round-Table), but also from the views expressed in the Papers and ensuing discussions of the whole Symposium.

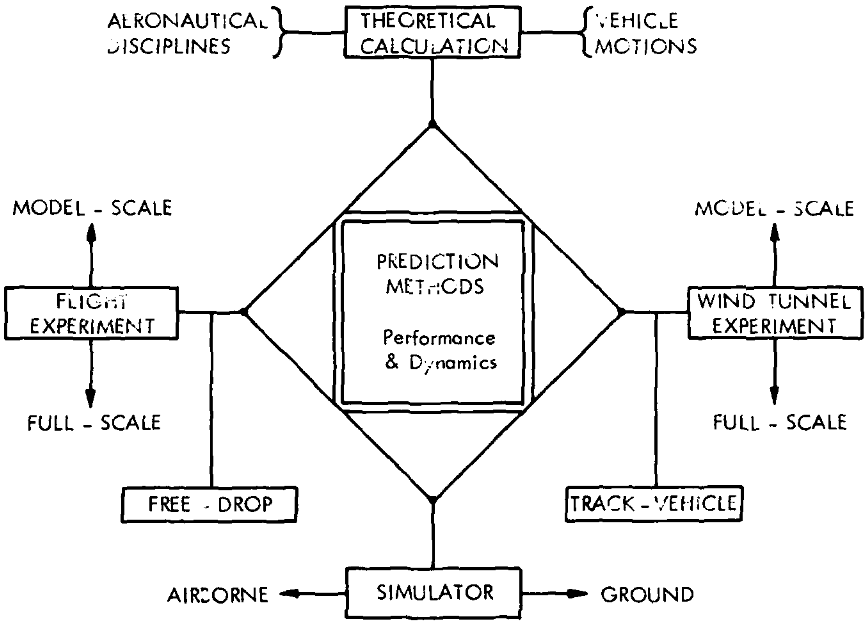
AERONAUTICAL DISCIPLINES
THEORETICAL CALCULATION
VEHICLE MOTIONS
MODEL - SCALE
FLIGHT EXPERIMENT
FULL - SCALE
PREDICTION METHODS
Performance & Dynamics
MODEL - SCALE
WIND TUNNEL EXPERIMENT
FULL - SCALE
FREE - DROP
TRACK - VEHICLE
AIRBORNE
SIMULATOR
GROUND

COMPLEMENTARY PREDICTION/DESIGN TOOLS

TABLE I: WHAT ARE THE PROS AND CONS OF DIFFERENT PREDICTION TECHNIQUES? : SOURCES OF AERODYNAMIC DATA FOR FLIGHT DYNAMICS PREDICTIONS

Type of Assessment / Source of Aerodynamic Data	Performance	Handling Qualities (Stability and Control Near 1-*g* Flight)	Manoeuvre Limitations
Theoretical Estimates	A. Useful for "paper" aircraft. Useful for extrapolation of experimental data on similar layouts. D. Needs engine data. Sensitivity studies required.	A. Useful for "paper" aircraft. D. Needs inertia estimates. Sensitivity studies required.	A. Some are as a first indication. D. "Guesstimates" can be misleading. No theoretical methods established.
Static Windtunnel Tests	A. Basis for design of lay-out etc. D. Needs engine data. The timescale for definitive model data can be long.	A. Basis for design of control surfaces, fin size etc. D. Needs inertia estimates. Sensitivity studies required.	A. Data can give likely trends in departure characteristics, and guidance on alleviation methods. D. Difficult to extrapolate to fullscale Re.
Dynamic Windtunnel Tests (Oscillatory Rigs, Rotary Rigs)	Not needed, unless performance impaired by manoeuvre limitations related to dampings.	A. Useful for design of Stability-Augmentation and Departure-Prevention Systems. D. The design process is delayed because of special windtunnel models needed.	A. Data can give likely trends in departure characteristics and guidance on alleviation methods. D. Effect of Re not known on the dynamic characteristics of flow-separation.

Notes: A = Advantages D = Disadvantages ACS = Active Control Systems

Disadvantages for all: (1) Open-loop responses. (2) Estimated corrections for aeroelasticity etc. (3) Simple representation of ACS.

TABLE II: WHAT ARE THE PROS AND CONS OF DIFFERENT PREDICTION TECHNIQUES? : EXPERIMENTAL PREDICTION TECHNIQUES USED IN FLIGHT DYNAMICS

Type of Assessment / Technique	Handling Qualities (Stability and Control Near 1-g Flight)	Manoeuvre Limitations	Spin and Recovery
(1) Piloted Simulator	A. Closed loop simulation. D. Depends on accuracy of mathematical models, motion cues and the tasks given to pilot.	A. Closed loop simulation. D. Not reliable because modelling of non-linear effects is difficult.	- -
(2) Spin Tunnel	- -	- D. Re not representative for departure.	A. Simple models, early prediction of spin modes. D. Difficult with ACS employed "Trial & Error" experimental process.
(3) Models "flying" in Wind-Tunnels	A. Dynamic responses representative of full-scale. D. Pilots needed for each control. No ACS.	- -	- -
(4) Free-flight Drop Models	A. Can give aerodynamic data at high Re. Can test ACS. D. Open loop limitation.	A. Can establish departure boundaries. Can test DPS in safety. D. Open loop limitation.	A. Can explore spin modes and recovery actions. Can include ACS. D. Open loop limitation.
(5) Remotely Piloted Vehicles.	A. As (4). Some pilot input and assessment. High speed flight possible. D. Restricted cues to the pilot.	A. As (4). Some pilot input possible. D. Restricted cues to the pilot.	A. As (4). Some pilot input possible. D. Restricted cues to the pilot.
(6) Full-scale	A. Final Answer. D. May be too late to rectify mistakes in design.	A. Final Answer. D. Risk to pilot and aircraft.	A. Not necessarily tested, if (2), (4) or (5) included in work-up. D. Risk to pilot and aircraft.

Note: Disadvantage of increasing cost and of lengthening time-scale from (1) to (6).

REPORT DOCUMENTATION PAGE

1. Recipient's Reference	**2. Originator's Reference**	**3. Further Reference**	**4. Security Classification of Document**
	AGARD-CP-339	ISBN 92-835-0328-7	UNCLASSIFIED

5. Originator Advisory Group for Aerospace Research and Development
North Atlantic Treaty Organization
7 rue Ancelle, 92200 Neuilly sur Seine, France

6. Title GROUND/FLIGHT TEST TECHNIQUES AND CORRELATION

7. Presented at the Flight Mechanics Panel Symposium on Ground/Flight Test Techniques and Correlation held in Çeşme, Turkey, 11–14 October 1982.

8. Author(s)/Editor(s)	**9. Date**
Various	February 1983
10. Author's/Editor's Address	**11. Pages**
Various	550

12. Distribution Statement This document is distributed in accordance with AGARD policies and regulations, which are outlined in the Outside Back Covers of all AGARD publications.

13. Keywords/Descriptors

Flight tests
Flight simulation
Wind tunnels
Mathematical prediction
Correlation
Comparison
Performance
Flight characteristics
Aeroelasticity
Aerodynamics

14. Abstract

These Proceedings contain the papers presented at the AGARD Flight Mechanics Panel Symposium on Ground/Flight Test Techniques and Correlation, held at Çeşme, Turkey, 11–14 October 1982. Topics covered include correlation between flight results and wind tunnel, analytical prediction, free-flight model, and simulation methods, for performance, flying qualities, aeroelastic effects and subsystems such as store separation and inlets.

AGARD Conference Proceedings No.339
Advisory Group for Aerospace Research and Development, NATO
GROUND/FLIGHT TEST TECHNIQUES AND CORRELATION
Published February 1983
550 pages

These Proceedings contain the papers presented at the AGARD Flight Mechanics Panel Symposium on Ground/Flight Test Techniques and Correlation, held at Çeşme, Turkey, 11–14 October 1982. Topics covered include correlation between flight results and wind tunnel, analytical prediction, free-flight model, and simulation methods, for performance, flying qualities, aeroelastic effects and subsystems such as store separation and inlets.

ISBN 92-835-0328-7

AGARD-CP-339

Flight tests
Flight simulation
Wind tunnels
Mathematical prediction
Correlation
Comparison
Performance
Flight characteristics
Aeroelasticity
Aerodynamics

AGARD Conference Proceedings No.339
Advisory Group for Aerospace Research and Development, NATO
GROUND/FLIGHT TEST TECHNIQUES AND CORRELATION
Published February 1983
550 pages

These Proceedings contain the papers presented at the AGARD Flight Mechanics Panel Symposium on Ground/Flight Test Techniques and Correlation, held at Çeşme, Turkey, 11 14 October 1982. Topics covered include correlation between flight results and wind tunnel, analytical prediction, free-flight model, and simulation methods, for performance, flying qualities, aeroelastic effects and subsystems such as store separation and inlets.

ISBN 92-835-0328-7

AGARD-CP-339

Flight tests
Flight simulation
Wind tunnels
Mathematical prediction
Correlation
Comparison
Performance
Flight characteristics
Aeroelasticity
Aerodynamics

AGARD Conference Proceedings No.339
Advisory Group for Aerospace Research and Development, NATO
GROUND/FLIGHT TEST TECHNIQUES AND CORRELATION
Published February 1983
550 pages

These Proceedings contain the papers presented at the AGARD Flight Mechanics Panel Symposium on Ground/Flight Test Techniques and Correlation, held at Çeşme, Turkey, 11 14 October 1982. Topics covered include correlation between flight results and wind tunnel, analytical prediction, free-flight model, and simulation methods, for performance, flying qualities, aeroelastic effects and subsystems such as store separation and inlets.

ISBN 92-835-0328-7

AGARD-CP-339

Flight tests
Flight simulation
Wind tunnels
Mathematical prediction
Correlation
Comparison
Performance
Flight characteristics
Aeroelasticity
Aerodynamics

AGARD Conference Proceedings No.339
Advisory Group for Aerospace Research and Development, NATO
GROUND/FLIGHT TEST TECHNIQUES AND CORRELATION
Published February 1983
550 pages

These Proceedings contain the papers presented at the AGARD Flight Mechanics Panel Symposium on Ground/Flight Test Techniques and Correlation, held at Çeşme, Turkey, 11 14 October 1982. Topics covered include correlation between flight results and wind tunnel, analytical prediction, free-flight model, and simulation methods, for performance, flying qualities, aeroelastic effects and subsystems such as store separation and inlets.

ISBN 92-835-0328-7

AGARD-CP-339

Flight tests
Flight simulation
Wind tunnels
Mathematical prediction
Correlation
Comparison
Performance
Flight characteristics
Aeroelasticity
Aerodynamics

ME

8